

PIPELINE PUMPING AND COMPRESSION SYSTEMS— A PRACTICAL APPROACH THIRD EDITION

Kamal K. Botros
Thomas Van Hardeveld



© 2018, ASME, 2 Park Avenue, New York, NY 10016, USA (www.asme.org)

All rights reserved. Printed in the United States of America. Except as permitted under the United States Copyright Act of 1976, no part of this publication may be reproduced or distributed in any form or by any means, or stored in a database or retrieval system, without the prior written permission of the publisher.

INFORMATION CONTAINED IN THIS WORK HAS BEEN OBTAINED BY THE AMERICAN SOCIETY OF MECHANICAL ENGINEERS FROM SOURCES BELIEVED TO BE RELIABLE. HOWEVER, NEITHER ASME NOR ITS AUTHORS OR EDITORS GUARANTEE THE ACCURACY OR COMPLETENESS OF ANY INFORMATION PUBLISHED IN THIS WORK. NEITHER ASME NOR ITS AUTHORS AND EDITORS SHALL BE RESPONSIBLE FOR ANY ERRORS, OMISSIONS, OR DAMAGES ARISING OUT OF THE USE OF THIS INFORMATION. THE WORK IS PUBLISHED WITH THE UNDERSTANDING THAT ASME AND ITS AUTHORS AND EDITORS ARE SUPPLYING INFORMATION BUT ARE NOT ATTEMPTING TO RENDER ENGINEERING OR OTHER PROFESSIONAL SERVICES. IF SUCH ENGINEERING OR PROFESSIONAL SERVICES ARE REQUIRED, THE ASSISTANCE OF AN APPROPRIATE PROFESSIONAL SHOULD BE SOUGHT.

ASME shall not be responsible for statements or opinions advanced in papers or . . . printed in its publications [Statement from the Bylaws (B7.1.3)].

For authorization to photocopy material for internal or personal use under those circumstances not falling within the fair use provisions of the Copyright Act, contact the Copyright Clearance Center (CCC), 222 Rosewood Drive, Danvers, MA 01923, tel: 978-750-8400, www.copyright.com.

Requests for special permission or bulk reproduction should be addressed to the ASME Publishing Department, or submitted online at: <http://tinyurl.com/p72hgfu>

ASME Press books are available at special quantity discounts to use as premiums or for use in corporate training programs. For more information, contact Special Sales at customer-care@asme.org

Library of Congress Cataloging-in-Publication Data

Names: Botros, Kamal Kamel, author. | Van Hardeveld, Thomas, author.

Title: Pipeline pumping and compression systems: a practical approach / Kamal K. Botros, Thomas Van Hardeveld

Description: Third edition. | New York: ASME Press, 2018. | Includes bibliographical references and index.

Identifiers: LCCN 2018022199 | ISBN 9780791861783

Subjects: LCSH: Pumping machinery. | Pipelines.

Classification: LCC TJ901 .M57 2018 | DDC 621.6/9--dc23 LC record available at <https://lccn.loc.gov/2018022199>

DEDICATION

We dedicate this third edition again to the memory of our dear friend and colleague, Dr. Mo Mohitpour, who continues to inspire the two authors of this book to share their knowledge and experience in the pipeline industry.

TABLE OF CONTENTS

Dedication	iii
Preface	xiii
Forewords	xv
<hr/>	
Chapter 1 Introduction to Pipeline Systems	1
1.1 Introduction	1
1.2 Liquid Pipelines System	2
1.3 Gas Pipeline System	4
1.4 Pipeline Safety	6
1.4.1 Process Safety	6
1.4.2 Dependability of Pipeline Systems	11
References	17
<hr/>	
Chapter 2 Liquid Pipeline Pumping System Design	19
2.1 Liquid Pipeline Design	19
2.1.1 Liquid Pipeline Hydraulics	19
2.1.2 Pipe Size and Pump Selection	19
2.1.3 Pipeline System Head Curve	24
2.1.4 Pipeline System Curve Development Example	26
2.1.5 Considerations for System Curves	27
2.2 Pump Station Configuration	28
2.2.1 General	28
2.2.2 Pumps in Series	29
2.2.3 Pumps in Parallel	29
2.2.4 Number of Units	30
2.3 Pump Station Piping Design	34
2.3.1 General Station Design	34
2.3.2 Station Piping Design	38
2.4 Contamination in Liquid Pipelines	44
2.4.1 Contamination Between Products	44
2.4.2 Erosion Due to Solid Contamination	48
2.4.3 DNV RP O501 Erosion Model for a 90 deg Elbow	50

2.5 Terminal Design	52
2.5.1 Terminal Piping Design	52
2.5.2 Overpressure Protection and Surge Relief	55
References	61

Chapter 3 Gas Pipeline Compression System Design	65
3.1 Gas Pipeline Design	65
3.1.1 Gas Pipeline Hydraulics	65
3.1.2 Pipeline Optimization with Respect to Compression	65
3.1.3 Pipeline Looping and Compression (Location and Spacing)	69
3.1.4 Hydraulic Simulation	70
3.1.5 Cost of Compressor Operation	73
3.2 Compressor Station Configuration	74
3.2.1 Operating Considerations	74
3.2.2 Types of Compression Equipment	75
3.2.3 Parallel and Series Configuration	76
3.2.4 Number of Units	76
3.2.5 Case Study: NPV Comparison Between Immediate and Deferred Unit Installation	77
3.2.6 Standby Units	78
3.2.7 Environmental Considerations	80
3.2.8 Case Study: Comparison of Different Usage Scenarios for Pipeline Station	81
3.2.9 Compressor Requirements	85
3.2.10 Driver Requirements	86
3.3 Station Layout and Facilities	87
3.3.1 Station Layout	87
3.3.2 Station Piping Layout	87
3.3.3 Scrubbers and Filters	90
3.3.4 Gas Coolers	91
3.3.5 Station and Unit Auxiliary Systems	92
3.3.6 Station and Unit Control Systems	92
3.3.7 Buildings and Weather Protection	95
3.3.8 Safety Systems and Environmental Controls	96
3.3.9 Codes and Standards	96
References	97

Chapter 4 Design and Operation of Pumps	99
4.1 Pumps for Liquid Pipeline Stations	99
4.2 Pump History	100
4.3 Centrifugal Pumps	104
4.3.1 Types of Centrifugal Pumps	104
4.3.2 Centrifugal Pump Design	106
4.3.3 Centrifugal Pump Mechanical Seals	109
4.3.4 Centrifugal Pump Nozzle Loading	114

4.4 Positive Displacement Pumps	119
4.4.1 Rotary Pumps	119
4.4.2 Reciprocating Pumps	121
4.4.3 Pulsation Dampeners	124
4.4.4 Other Pump Design Considerations	126
References	129

Chapter 5 Performance of Pumps	131
5.1 Introduction to Pump Performance	131
5.2 System Head	131
5.3 American Petroleum Institute Gravity and SG Relationship	133
5.4 Performance of Centrifugal Pumps	137
5.4.1 Pump Performance Curves	137
5.4.2 Centrifugal Pump Coverage Chart	138
5.4.3 Impeller Selection	138
5.4.4 Pump Head-Flow and System Head Flow Curves	140
5.4.5 Centrifugal Impeller Design Theory	141
5.4.6 Specific Speed	143
5.4.7 Impeller Curve Characteristics	145
5.4.8 Affinity Laws	148
5.4.9 Pipeline-Pump Operational Control	148
5.4.10 Pump Power and Efficiency	150
5.4.11 Performance Modifications	150
5.5 Cavitation in Centrifugal Pumps	154
5.5.1 Cavitation Phenomenon	154
5.5.2 Net Positive Suction Head	157
5.5.3 Net Positive Suction Head Available	158
5.5.4 Net Positive Suction Head Required	158
5.6 Centrifugal Pumps and Viscous Liquids	160
5.7 Centrifugal Pump Limits	163
5.7.1 Minimum Flow	163
5.7.2 Temperature Rise	163
5.7.3 Re-Circulation in Centrifugal Pumps	164
5.8 Pump Surge in System Operation	166
5.9 Performance of Positive Displacement Pumps	167
5.9.1 Rotary Pump Performance Chart	167
5.9.2 Pump Power and Efficiency	169
5.9.3 Rotary Pump Slip and Clearance	170
5.9.4 System Head Curves and Rotary Pump Curve	170
5.9.5 Reciprocating Pump Flow Characteristics	171
5.9.6 Reciprocating Pump Acceleration Head	171
5.9.7 Net Positive Pressures	172
5.9.8 Reciprocating Pump Selection	173
5.10 Measurement Units and Conversion Factors for Pumps	175
5.11 Pump and System Design Standards	177
References	178

Chapter 6 Design and Operation of Compressors	179
6.1 Introduction to Pipeline Compressors	179
6.2 Reciprocating Compressors	179
6.2.1 General Design	179
6.2.2 Running Gear	181
6.2.3 Frame and Cylinders	183
6.2.4 Capacity Control	187
6.2.5 Valves	187
6.2.6 Packings	193
6.2.7 Bearings and Lubrication Systems	193
6.2.8 Controls and Monitoring	196
6.2.9 Gas Cooling	198
6.2.10 Operation and Optimization	198
6.2.11 Design Standards	203
6.3 Centrifugal Compressors	203
6.3.1 General Design	203
6.3.2 Compressor Internals and Sealing	205
6.3.3 Bearings and Lubrication Systems	209
6.3.4 Sealing System	213
6.3.5 Controls and Monitoring	220
6.3.6 Physical Operation	223
6.3.7 Design Standards	228
6.4 Screw Compressors	229
6.4.1 Screw Compressor Design	229
6.4.2 Screw Compressor Operation	230
6.5 Integrally-Geared Compressors	231
6.5.1 Compressor Design	231
6.5.2 Bearings, Seals and Gears	233
References	234
 Chapter 7 Performance of Compressors	 237
7.1 Introduction to Compressor Performance	237
7.2 Basic Aspects of Performance	237
7.2.1 General	237
7.2.2 Nomenclature	237
7.2.3 Gas Properties	237
7.2.4 Compression Behavior	243
7.2.5 Head	244
7.2.6 Efficiency	244
7.2.7 Flow	245
7.2.8 Power	245
7.3 Performance of Reciprocating Compressors	247
7.3.1 General	247
7.3.2 Flow	247
7.3.3 Power	249
7.3.4 Discharge Temperature	251
7.3.5 Performance Maps	251
7.3.6 Piston Speed	254
7.4 Performance of Centrifugal Compressors	254
7.4.1 General	254
7.4.2 Dynamic Performance Characteristics	254

7.4.3	Selection and Sizing	260
7.4.4	Performance Testing	261
7.4.5	Effects of Mixture Composition on Compressor Performance	262
7.4.6	Compressor Performance Degradation Monitoring	264
7.5	System Characteristics	267
7.5.1	General	267
7.5.2	System Curves	267
7.5.3	Compressor Performance Comparison	270
7.5.4	Operating Limitations	271
7.5.5	Compressor Performance Adjustments	272
7.5.6	Operating Considerations	274
	References	276

Chapter 8	Pump and Compressor Drivers	279
8.1	Introduction to Drivers	279
8.2	Gas Turbines	280
8.2.1	Types of Gas Turbines	280
8.2.2	Basic Design of a Gas Turbine	283
8.2.3	Air Intake System	286
8.2.4	Air Compressor Surge	286
8.2.5	Variable Compressor Geometry	287
8.2.6	Anti-icing Systems	288
8.2.7	Exhaust System	289
8.2.8	Bearings and Lubrication System	289
8.2.9	Fuel System	292
8.2.10	Gas Turbine Performance	299
8.2.11	Design Standards	305
8.2.12	Waste Heat Recovery	306
8.3	Electric Motors	307
8.3.1	General	307
8.3.2	Types of Motors	307
8.3.3	Motor Design Considerations	310
8.3.4	Variable Speed Motors	310
8.3.5	Hermetic Compressors	315
8.3.6	Driver Economics	317
8.4	Internal Combustion Engines	320
8.4.1	General	320
8.4.2	Internal Combustion Engine Design	320
8.4.3	Integral Engine/Compressors	322
8.5	Couplings	323
8.5.1	Functions of Couplings	323
8.5.2	Coupling Selection	323
8.5.3	Gear Couplings	325
8.5.4	Flexible Couplings	325
8.5.5	Elastomeric Soft Couplings	327
8.5.6	Steel-Spring Soft Couplings	327
8.5.7	Coupling Standards	329
8.6	Comparison Between Drivers and Driven Equipment	330
8.6.1	General Factors	330
8.6.2	Advantages and Disadvantages of Gas Turbines	330

8.6.3 Advantages and Disadvantages of Electric Motors	332
8.6.4 Advantages and Disadvantages of Internal Combustion Engines	333
8.6.5 Advantages and Disadvantages of Centrifugal Compressors	334
8.6.6 Advantages and Disadvantages of Reciprocating Compressors	335
References	335

Chapter 9 Dynamic Behavior of Pumping Systems	339
9.1 Introduction	339
9.2 Unsteady Governing Equations and Solution Techniques	339
9.2.1 Governing Equation for Constant Area Pipes	339
9.2.2 Solution Techniques	341
9.3 Boundary Conditions	342
9.3.1 Flow Transients Across Other Elements	343
9.3.2 Flow Transients of an Accumulator	344
9.4 Dynamics Behaviour of Centrifugal Pumps	346
9.4.1 Homologous Relations	347
9.4.2 Full Pump Characteristics	347
9.4.3 Dynamic Equation	348
9.4.4 Pump and Motor Inertias	352
9.5 Other Useful Representations of Pump Four Quadrants	354
9.5.1 Application Examples of the Use of Pump Four Quadrant Charts	354
9.6 Water Hammer, Cavitation, and Column Separation	357
9.6.1 Water Hammer	357
9.6.2 Cavitation and Column Separation	358
9.6.3 Steam Condensation-Induced Water Hammer	359
9.7 Examples and Case Studies	361
9.7.1 Styrene Transfer System	361
9.7.2 Ethylene Pump	365
References	369
Other Bibliography	370

Chapter 10 Dynamics of Centrifugal Compression Systems	371
10.1 Introduction	371
10.2 Fundamentals of Dynamic Instabilities of Compression Systems	372
10.2.1 Simple Compression Systems	372
10.2.2 Complex Compression Systems	375
10.2.3 Control Dynamics	379
10.2.4 Solution Techniques	382
10.3 Emergency Shut Down	386
10.3.1 Effects of Compressor Performance Characteristics	389
10.3.2 Effects of Rotor Inertia	393
10.3.3 Example of Dynamic Instabilities in an Industrial Compression System	394
10.3.4 Integrally-Geared Compression Systems	402
10.3.5 Concept of Inertia Number	405
10.3.6 Recycle System around Compressors Arranged in Series	409
10.4 Check Valve Dynamics	411
10.4.1 Dynamics of Swing Type Check Valves	413
10.4.2 Slamming Characteristics of Swing Check Valves	417

10.4.3 Effects of Counterbalance on Maximum Reverse Velocity	421
10.4.4 Dynamics of Piston Type Check Valves	422
10.4.5 Dynamics of Wafer Type Check Valves	424
10.4.6 Effects of Check Valves of Compression Recycle System	425
10.5 Relief Valve Dynamics	427
10.5.1 Dynamics of Pilot-Operated Relief Valves	429
10.5.2 Solution Technique	434
10.5.3 Example	436
10.5.4 Field Tests	441
10.6 Station and Gas Pipeline Blowdown	444
10.6.1 Volume Model	446
10.6.2 Pipe Model	449
10.6.3 Comparison Between Models	450
10.6.4 Non-Isothermal Blowdown	453
References	457

Chapter 11 Pulsation and Vibration Analysis of Compression and Pumping Systems	463
11.1 Introduction	463
11.2 Pulsation Transmission Through Piping Elements	463
11.2.1 Acoustic Transfer Matrix for a Pipe Element	464
11.2.2 Acoustic Transfer Matrix for a Throttle Element	472
11.2.3 Acoustic Transfer Matrix for a Volume Element	478
11.2.4 Acoustic Transfer Matrix for a Centrifugal Compressor	479
11.3 Pulsation Generation	480
11.3.1 Flow-Generated Pulsation from Throttling Elements	480
11.3.2 Flow-Generated Single-Tone Pulsation from Closed End Side Branch	482
11.3.3 Pulsation Generated by Reciprocating Compressors and Pumps	485
11.4 Solution Techniques	487
11.5 Acoustic Boundary Conditions and Resonance	488
11.6 Techniques for Pulsation Suppression	490
11.6.1 Reactive Silencers	490
11.6.2 Spoilers for Pulsation Suppression at Source	493
11.6.3 Suppression of Noise From Blowdown Stacks	496
11.7 Liquid versus Gas Applications	499
11.8 Standards and Guidelines	502
11.8.1 API 618 Standard	502
11.8.2 API 674 Standard	510
11.8.3 Shaking Forces Arising from Pressure Pulsation	512
11.8.4 GMRC Design Guideline for High Speed Reciprocating Compressor Packages for Natural Gas Transmission & Storage Applications	513
11.8.5 API 610 and ANSI/HI 9.6.8	516
11.9 Case Study Examples	518
11.9.1 Case Study #1: Single-Source Pulsation	520
11.9.2 Case Study #2: Multiple Source Pulsation	521
11.9.3 Case Study #3: Pulsation Generated by a Reciprocating Compressor	523
11.10 Instability Criteria of Pressure Relief Valves	525
References	530

Chapter 12 Mechanical Analysis	533
12.1 Introduction To Mechanical Analysis	533
12.2 Basic Aspects Of Vibration	533
12.2.1 General	533
12.2.2 Mechanical Natural Frequency and Resonance	535
12.3 Mechanical Analysis of Rotating Equipment	536
12.3.1 General	536
12.3.2 Lateral Rotordynamics	537
12.3.3 Stability	540
12.3.4 Torsional Rotordynamics	541
12.3.5 Specific Machinery Considerations for Rotordynamics	551
12.3.6 Balancing	561
12.4 Mechanical Analysis of Piping Systems	563
12.4.1 Excitation Mechanisms	563
12.4.2 Vibration and Stress	564
12.4.3 Unbalanced Forces	566
12.4.4 Small-Bore Connections	569
12.4.5 Forced Response Analysis	572
12.4.6 Adding Damping to Mechanically Resonant Systems	577
12.4.7 Thermal Analysis	583
12.4.8 Centrifugal Compressors	584
References	588
Chapter 13 Environmental Issues Related to Compressor and Pump Stations	591
13.1 Introduction	591
13.2 Environmental Issues	591
13.2.1 Summary	591
13.2.2 Designing for Environmental Requirements	593
13.3 Noise Measurement	594
13.3.1 Noise Level Parameters	594
13.3.2 Noise Criteria Limits	595
13.3.3 Predictions of Noise Level from Compressor Stations	601
13.4 Noise Surveys	608
13.4.1 Noise Mapping Methodology	608
13.4.2 Example Application on a Compressor Station	610
13.5 NO _x Emissions from Gas Turbines	612
13.5.1 AP-42 Emission Factors	613
13.5.2 CEM Measurements	613
13.5.3 Neural Network Based PEM Models	615
13.5.4 PEM Implementation	620
13.6 Innovations in Capturing Vent Gas from Dry Gas Seals	624
13.6.1 Dry Gas Seal Leakage Rates	625
13.6.2 Primary Challenges of Supersonic Ejectors	625
13.6.3 Description of the Two Stages of the Ejector	626
13.6.4 Performance of the Integrated Two-Stage Supersonic Ejector	629
13.6.5 Supersonic Ejector in Operation	631
References	635
Index	639

PREFACE

The technology of pipeline pumping and compression continues to change, so we decided that it was worthwhile to again spend the time and effort to produce this third edition. In the end, the improvements turned out to be substantial, which makes us grateful to again share our knowledge and experience and that of the industry at large. The reader will find a wide range of topics that are both practical in nature and ones that delve more deeply into the science and engineering basis behind pumping and compression processes.

One of the drivers for this edition was its use as the textbook by one of the authors (Tom) for a graduate course in Mechanical Engineering at the University of Calgary called Pipeline Pump and Compressor Stations, a part of the Pipeline Engineering Center. In particular, a number of additions were made to enhance the content for this course.

There are no new chapters this time but significant additions include updated information on the pipeline industry, pipeline safety, contamination between batches, design of terminals, booster pumps, pump station design, monitoring of centrifugal compressor degradation, equations of state for gas mixtures, gas turbine auxiliary systems, cold vs. hot recycle surge protection, PSV instability, integrally geared compressors, pulsation and vibration control for reciprocating compressors, damping of mechanically resonant systems, transient analysis of liquid pipeline systems, a more comprehensive introduction to environmental issues and many more topics. We must admit to removing some sections related to gas and liquid hydraulics since these topics are already well covered in a similar publication from ASME, Pipeline Design and Construction – A Practical Approach, as well as other industry publications. This enabled the addition of other, more relevant advances in this area.

We have again reached out to colleagues and contacts in the industry and want to specifically recognize the following for their contributions and assistance:

John Sears – Flowserve
Matthew Piripavel – Flowserve
Wally Bratek – Wood.
Russ Barss – Wood.
Suzanne Wilton – Enbridge Inc.
Drew Devitt – New Way Air Bearings
Bill Forbes – Enbridge Inc.
Vik Kohli – Enbridge Inc.
Steve McNair – Windrock
Dr. Ron Hugo – University of Calgary.

Another improvement that was made was to provide many of the figures in color for the digital edition. Unfortunately, the printed book will still be in B&W so as not to drastically increase its cost but as compensation, many of the figures have been improved in quality.

Without ASME, this edition would not have been possible, so we want to particularly acknowledge the continuing support and encouragement of Mary Grace Stefanchik and Tara Collins Smith of ASME Press.

Again, we deeply appreciate the opportunity to contribute to this important field of engineering and restate that “This is the book I wish I had when I was a young engineer wanting to learn about pipeline pumping and compression.”

Kamal K. Botros

Thomas Van Hardeveld

FOREWORDS

Foreword to the first and second editions from TransCanada Pipelines

Pumping and Compression facilities are critical components of pipeline systems and *Pipeline Pumping and Compression Systems—A Practical Approach* is a tremendous resource that marks another milestone of excellence and achievement for the pipeline industry.

ASME Press initiated the development and publication of the pipeline series in 2000 with *Pipeline Design & Construction—A Practical Approach* and a number of excellently detailed and comprehensive pipeline titles since then. This book is in response to the needs of the industry and the community to further augment this series.

The book is a wide-ranging professional reference, training tool, and text covering all aspects of pipeline pumping and compression system design, configuration optimization, installation, commissioning, and operation. It provides practical solutions for dynamic situations encountered in designing pipeline systems to support reliable operation.

The content of this book reflects the considerable knowledge and expertise of the authors. Their learnings through eight decades of collective industry experience is supplemented by research and development as well as industry-generated data.

We are very pleased to continue with our support for this series of the ASME books and related efforts made in capturing the knowledge important to our industry.

Andrew Jenkins

Vice President, TransCanada PipeLines Limited



Foreword to the first and second editions from GE Oil & Gas

GE Oil & Gas has supported the preparation, review, and publication of the ASME book *Pipeline Pumping and Compressions Systems—A Practical Approach*. This timely publication completes the pipeline system design, construction, operation, and maintenance series of books, which ASME initiated in 2000.

Pumps and compressors are key elements in any pipeline transmission project. Today, a total of almost 50 million horsepower is used to service natural gas pipeline compression needs; a similar amount of power is used in pumping hydrocarbon liquids through transmission pipelines. Pump and compression units power range roughly between 500 and 45,000 hp, and new designs are increasing this power. There is no doubt that these units' capability have substantially contributed to increase the size, length, and grade of pipeline networks worldwide.

In the early 1900s, the throughput-to-fuel gas ratio was almost 50:50, whereas for modern day gas compression, the ratio is 94:6. Much of this development has been driven by environmental, operational, and cost implications. These demands for stricter emission controls, lower fuel costs, and higher availability are impacting new equipment purchase and also the decisions to replace older units.

Pipeline Pumping and Compressions Systems—A Practical Approach represents a thorough evaluation and presentation of pipeline pumping and compression needs and development. It serves as a useful guide for the design of such facilities in liquid and gas pipeline transmission systems, as well as a guide to various installation options.

The authors have used their considerable knowledge and experience of the pipeline industry to provide a very useful and practical document not only to augment the knowledge of professionals but also to help to convey the knowledge to new entrants in the industry.

I am pleased that such a comprehensive training and reference tool, covering all aspects of pipeline pumping and compression systems, is available to the industry.

Patrick Campbell, P.Eng.
General Manager,



Foreword to the third edition from Dr. Ron J. Hugo

Pipeline Pumping and Compression Systems – A Practical Approach was first published in 2008 in advance of the ASME International Pipeline Conference in Calgary, Alberta, CANADA. The second edition of this book was published in 2013.

Since the first edition of this book was first published in 2008, the industry has seen the retirement of a generation of experienced pipeline engineers who honed their skills working on complex projects with companies that performed the full lifecycle of an engineering project in-house, beginning with feasibility studies, to design, followed by construction and operation. Through the retirement of this experienced generation comes an apparent void. In response, this most recent edition by Botros and Van Hardeveld offers a critical and effective transfer of knowledge. This book provides the new generation of pipeline engineers with a solid foundation upon which they can build their careers.

The evolution of this third edition came about through its use in a graduate course taught by the second author, Thomas Van Hardeveld, and offered through the Pipeline Engineering Centre at the University of Calgary. With this in mind, the book will prove to be equally useful for both the engineering graduate student and the working professional. The collective years of experience of the two co-authors and the founding author in both gas and liquid transmission systems is unmatched, providing the reader with valuable knowledge and insight that has been gained through years of professional practice.

On behalf of the pipeline engineering community, I am grateful to the authors for investing so much of their time to share and give back to their profession. Their work provides an inspiration for all professional engineers.

Ron J. Hugo, Ph.D., P.Eng.
Director, Pipeline Engineering Centre
Li Ka Shing Foundation Chair in Engineering Education Innovation
Department of Mechanical & Manufacturing Engineering
Schulich School of Engineering
University of Calgary, 2500 University Dr NW
Calgary Alberta Canada T2N 1N4

INTRODUCTION TO PIPELINE SYSTEMS

1.1 INTRODUCTION

Pipelines affect the daily lives of people in most parts of the world. Modern-day life is based on structures in which energy fulfills a prevailing role. Oil and gas are major participants in this energy supply [1]. The ever shifting trends in forms of energy [2], such as coal, nuclear, hydro-electric, gas, oil and renewables (Fig. 1-1) will continue to dominate energy usage in the future, depending on acceptability, safety, technical, environmental, and economic issues. The rise of renewable types of energy replacing other forms of energy means that hydrocarbons will also be affected although this will be at least partially offset by increasing demand.

However, pipelines are the means by which many hydrocarbon-based forms of energy are transported. It is no coincidence that wherever there is the largest pipeline network, there is also the highest standard of living and technological progress. Compared with other forms of transport, pipelines allow a safer, more continuous, stable, and high-capacity supply of hydrocarbons to reach end-users. Pipeline transportation has the advantages of being well established, efficient, cost-effective, and readily expandable. In spite of claims that pipelines are not safe and environmentally damaging, pipelines have consistently maintained a very high safety record that is superior to other types of hydrocarbon transportation.

Pipeline technology is mature and well understood. The capital cost of a pipeline project is largely a function of its diameter and length, although other factors, such as geography and topography, are also significant. Operating expenditures and self-consumption of product are relatively minor and predictable. Economic feasibility of a pipeline is limited by variables, such as volumes to be transported, supply–demand distance relationships, operating pressure, projected reserve life, and various risk factors. These limitations are more restrictive offshore than onshore.

The relative transportation cost for various petroleum products is depicted in Fig. 1-2. Although pipelines have been the most cost-effective mode of energy transportation, it can be inferred from Fig. 1-2 that cost of energy transportation by pipeline is distance- and location- (offshore versus onshore) dependent [3].

Pipelines are mostly buried. In virtual silence, pipelines supported by pump and compressor stations that carry billions of cubic meters of our energy needs. Unattended pump stations push oil and petroleum products in large volumes and under high pressure. Similarly, natural gas transmission systems supported by compressor stations move large volumes of gas to multiple destinations.

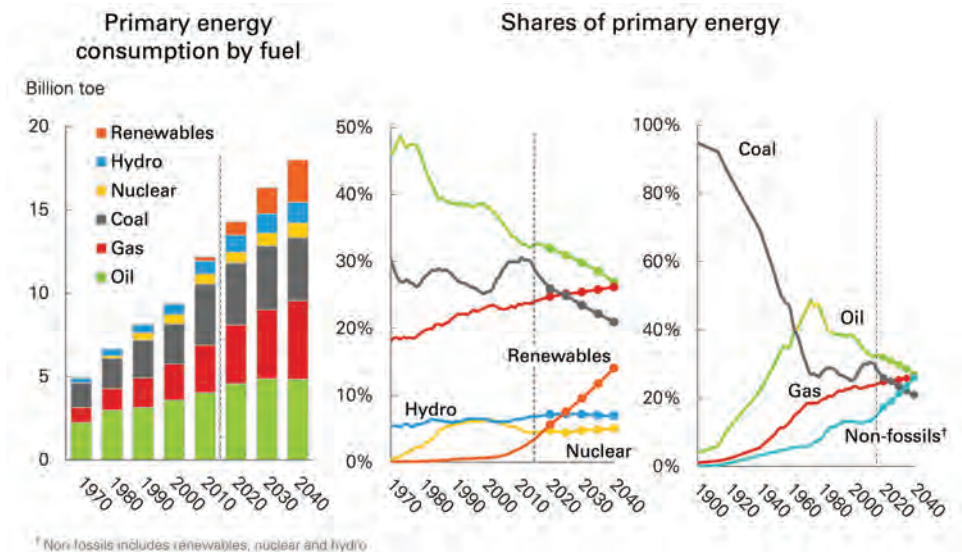


Figure 1-1. Trends in primary energy consumption [2].

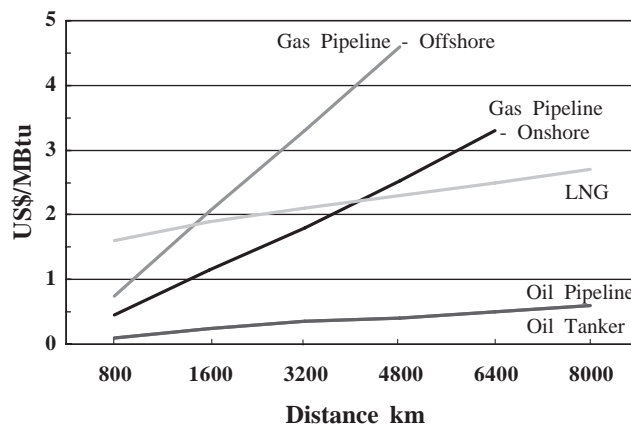


Figure 1-2. Representative costs of oil and gas transportation (US\$/MBTU) (Mohitpour et al. [3]).

1.2 LIQUID PIPELINE SYSTEM

The liquid pipeline transportation system applies to a variety of liquid hydrocarbons, including crude oil, refined petroleum products, liquid petroleum gas, gas to liquids, anhydrous ammonia, alcohols, and carbon dioxide. Liquid pipelines, including generally consist of laterals and mainlines which include tank farms, measurement facilities, pumping systems, pressure reduction, control systems, and pipeline appurtenances (scraper traps, valves, etc.). As can be seen from Fig. 1-3, pump stations are an integral component of this very extensive network.

Liquid pipelines are used to transport liquids, such as crude and refined oil, from the source of supply, such as a production area, to the market/demand locations, an export-loading terminal, or to a processing unit (a refinery). Mainline pump stations are installed

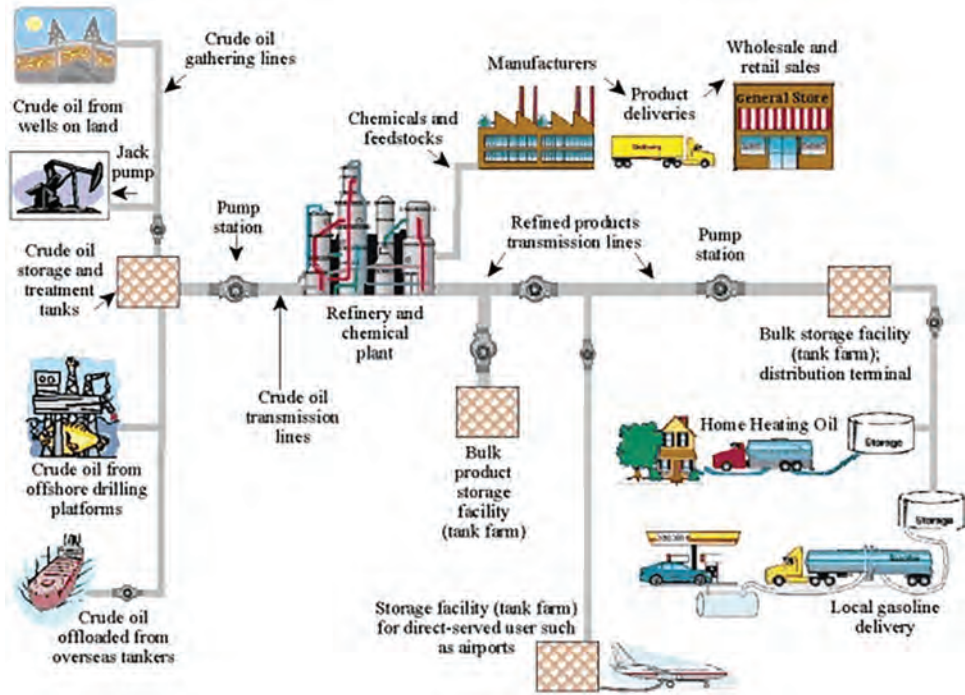


Figure 1-3. Liquid petroleum systems from the wellhead to the consumer [4].

along the transmission pipelines at variable distances to compensate for the pipeline pressure losses and elevation changes and to ensure a constant flow of liquid.

Scopes defining the limit of the pipeline system are well defined by applicable codes, an example of which is shown in Fig. 1-4 [5]. Also included within the scope of the system are:

- primary and associated auxiliary liquid petroleum and liquid anhydrous ammonia piping at pipeline terminals (marine, rail, and truck), tank farms, pump stations, pressure-reducing stations, and metering stations, including scraper traps, strainers, and prover loops;
- storage and working tanks, including pipe-type storage fabricated from pipe and fittings, and piping interconnecting these facilities;
- liquid petroleum and liquid anhydrous ammonia piping located on property which has been set aside for such piping within petroleum refinery, natural gasoline, gas processing, ammonia, and bulk plants; and
- those aspects of operation and maintenance of liquid pipeline systems relating to the safety and protection of the general public, operating company personnel, environment, property, and the piping systems.

Pipeline pumps are used for boosting pressures and for transferring product in both gathering and mainline transmission systems. Centrifugal, reciprocating, and rotary-positive displacement pumps are generally used for such pipeline applications.

In a pump station located on larger transmission lines, usually one or more high-capacity, single, or multi-stage centrifugal pumps are installed. They can be driven most commonly by electric motors usually in the 2–6 MW range but also sometimes by a gas turbine or diesel engine.

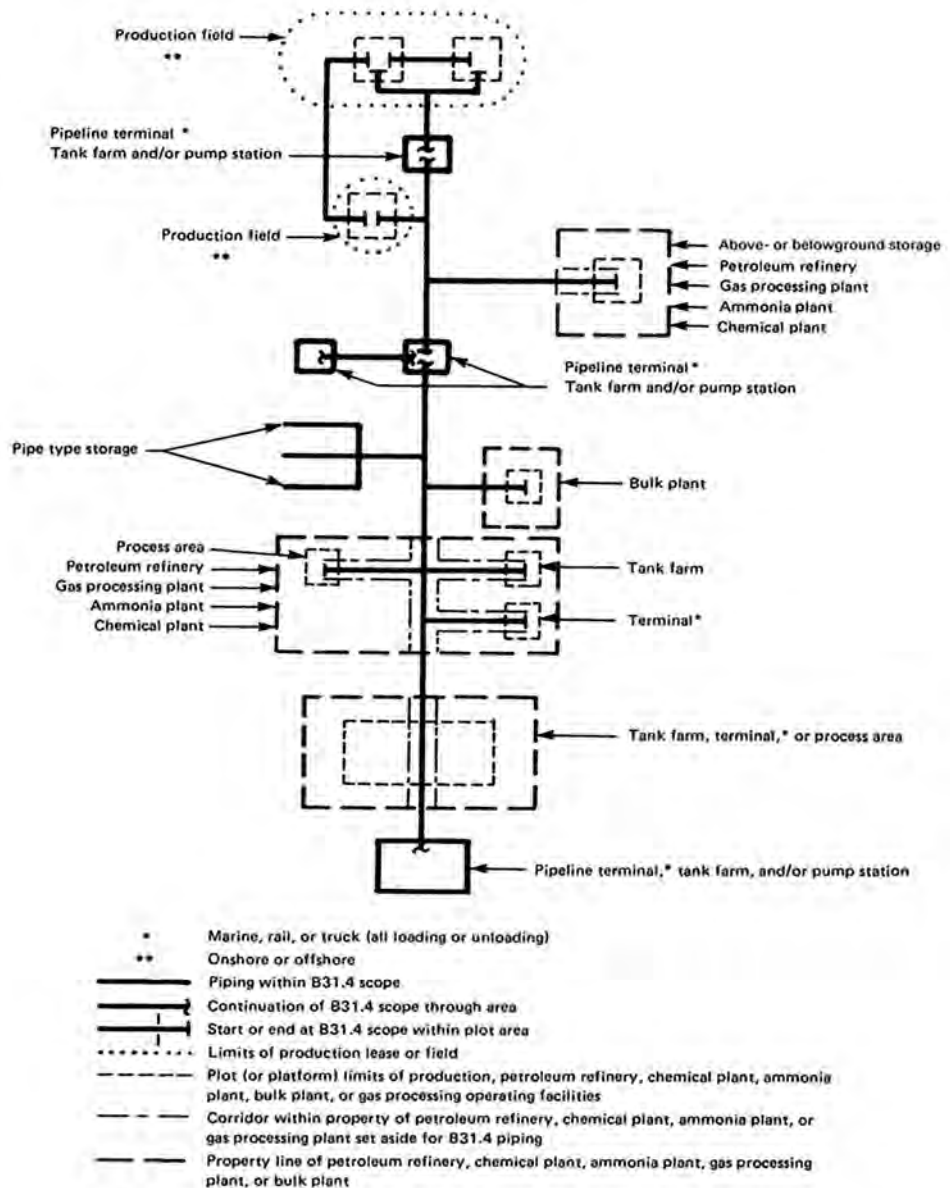


Figure 1-4. Liquid pipeline system definitions [5].

A unique aspect of a liquid pipeline system is that the product is pumped from the wellhead into a storage tank. From there, the liquid is carried by a gathering system pipeline (or flowline) to a larger set of storage tanks, also referred to as a terminal. The liquid is then pumped to the next terminal. This process continues all along the pipeline system, a necessary result of the fact that liquids are essentially incompressible.

1.3 GAS PIPELINE SYSTEM

Gas is usually considered to be any hydrocarbon-based gas or mixture of gases suitable for domestic or industrial fuel that is transmitted or distributed to the user by a pipeline/piping

system. The most common types are various compositions of natural gas but other gases such as hydrogen and carbon dioxide are becoming more prevalent. A gas transmission and distribution system (Fig. 1-5) consists of the following components:

- gas processing and treatment facilities to remove objectionable materials and constituents
- gathering pipeline facilities
- production plants/compression
- receipt meter stations
- lateral lines
- mainlines
- mainline control valves to regulate pressure or flow
- mainline compression facilities
- delivery meter stations/custody transfer/city gate stations
- storage facilities used for peaking requirements (usually the pipeline itself)

The components include production wells, gathering lines within the production wells, processing plants, transmission pipelines, compressor stations (periodically along the transmission pipelines), storage wells and associated gathering pipelines, metering stations and city gate at distribution centers, distribution piping, and meters at distribution sites (residential or industrial).

Compression facilities are the heart of gas pipeline systems. Compressor stations transmit natural gas through a pipeline by compressing the gas at intervals along the system. Compressing gas increases the mass flow and increased pressure is necessary to overcome friction and elevation. Gas flows by expanding in the pipe from the discharge side (high pressure point) from one station to the suction side (low pressure point) of the next.

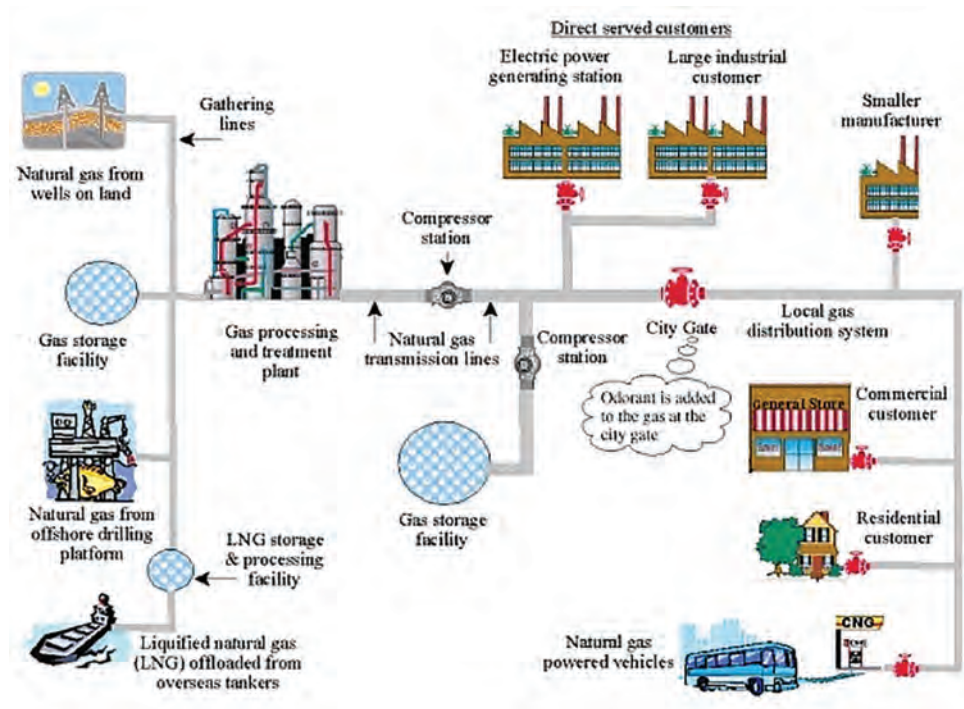


Figure 1-5. Natural gas pipeline systems from the wellhead to the consumer [4].

The use of compression equipment on or related to pipelines covers a wide field, ranging from a small manually operated field compressor up to a large computer-controlled installation involving many thousands of kilowatts. Compression equipment performs one or more of the following major functions with respect to the gas pipeline industry in general:

Transmission. Long-distance mainline transmission is designed with compressor stations spaced at intervals along the pipeline. The compression ratio across a station, resulting from pipeline friction losses and typically ranging from 1.2–1.7, is established by the compressor units as they are placed into operation or varied in load. These stations are usually designed for fully automatic, remotely controlled operation to enable a complete pipeline system to be operated from a central location.

Lateral Compression. Lateral pipeline transmission is designed to carry gas from one or more sources to a main pipeline, or from a pipeline to a sales point or distribution system. Operation varies from base load to “on–off” depending on the situation and can be subject to large changes. Compression ratios are often higher than for a main line station, with flows and power requirements being much less.

Field Compression. Field compression and gas gathering stations involve the boosting of gas field well-head pressures up to a required plant inlet pressure or directly to a pipeline-operating pressure. Compression ratios are often high, with a slowly declining suction pressure (and therefore increasing pressure ratio) as the gas field becomes depleted.

Interchange Compression. Interchange compression is often required to transfer gas between different pipeline systems. The operating conditions include variable suction and discharge pressures, which may vary at random, unaffected by the compressor operation.

Gas Storage Compression. Gas storage compression is designed for injection and withdrawal of gas from peak shaving or storage reservoirs. These compressor units operate under a continually changing compression ratio, both on injection and withdrawal, and would be considered as high-ratio, high-flow, and high-power units.

Booster Compression. Booster compression is designed to raise the pressure from a low pressure transmission line, for example, to a high pressure line. The units would basically be considered as transmission units but operating under higher compression ratios.

Gas Recovery Compression. Gas recovery compression is used to raise associated gas (gas in solution with crude oil) from very low pressures (down to almost atmospheric pressure) up to pipeline transmission pressure. This is a very high-ratio service.

1.4 PIPELINE SAFETY

1.4.1 Process Safety

1.4.1.1 Process Safety Management (PSM)

Pipeline facilities have an enviable safety record, particularly considering the hazardous products at pump and compressor stations. Accidents or incidents that do occur are usually contained within the facility perimeter with no or limited consequences to the public. In spite of the very low level of risk, pipeline transportation companies are increasingly adopting the process safety management systems that are common in the highly hazardous industries such as petrochemicals and process plants.

Process Safety is a disciplined management approach applied to systems containing hazardous materials. It focuses on the prevention, detection, control and mitigation of catastrophic incidents that have the potential to injure people or could have far-reaching and long-lasting consequences. Process safety is about preventing loss of primary containment (LOPC) of a hazardous commodity and mitigating subsequent impacts to people, environment, assets and reputation. Process safety incidents are extremely rare.

However, their consequences have the potential to be severe (large releases), up to and including company or industry ending impacts. Worker Safety incidents are much more frequent but minor in comparison. Both are important, and all safety incidents must be prevented.

More emphasis on Process Safety Management (as opposed to personal or occupational safety) is being placed with respect to managing risk and hazards in regulations such as OSHA 1910.119 Process safety management of highly hazardous chemicals in the US and the National Energy Board Regulations SOR/99-294 in Canada. While these regulations require programs to be set up for managing risks and hazards, they are not prescriptive as to how this should be accomplished.

To meet this need, the pipeline industry has published more specific guidance in API RP1173 [6] that applies to both pipelines and facilities. The major topics it covers are:

- Leadership and Management Commitment
- Stakeholder Engagement
- Risk Management
- Operational Controls
- Incident Investigation, Evaluation, and Lessons Learned
- Safety Assurance
- Management Review and Continuous Improvement
- Emergency Preparedness and Response
- Competence, Awareness, and Training
- Documentation and Record Keeping

Further guidance is provided in national standards such as CAN/CSA Z662 [7] and CAN/CSA Z767-17 [8]. There are also industry documents such as the recommended practice on facility integrity [9] by the Canadian Energy Pipeline Association (CEPA). The CEPA Recommended Practice provides a management systems approach in defining a Facility Integrity Management Program (FIMP) with more detail on implementing a practical framework [10]. The main challenge in developing a framework for a FIMP lies in the broad range of equipment and system types that the management system must encompass. Equipment, in the context of Facilities Integrity Management, must encompass not only station equipment (such as rotating equipment, valves, meters etc.) but also categories such as high pressure station piping and fuel lines.

The broad range of equipment types gives rise to three main parameters that needed to be addressed [9]:

- Equipment specific considerations: while fundamental concepts for managing integrity are essentially the same across all equipment types, the specific analysis methodologies and tactics will vary widely.
- Differing levels of criticality, or risk levels, associated with various equipment types: the criticality of different equipment types should correlate to the resources (both time and budget) dedicated to managing the integrity of the equipment.
- Widely varying asset life: longer asset life would be expected to correlate with maintenance dollars. Thus, in addition to potentially different time horizons for analysis, an Operator would expect to spend more effort in managing aspects of its system that have more significant cost implications.

1.4.1.2 Risk Assessment

A key component of applying Process Safety Management is identifying hazards and analyzing and evaluating risk or risk assessment. Many techniques are available for risk assessment [11] with the most common techniques being:

- Hazard and operability (HAZOP) studies [12]
- What If/Checklists [11]
- Failure Modes and Effects Analysis [13]
- Fault Tree Analysis [14]
- bowtie diagrams [15]

A very effective method is the use of bowtie diagrams. Bowtie diagrams are a widely used method for demonstrating the relationship between the causes and consequences of hazardous events. They are particularly useful for illustrating how safeguarding measures protect against particular threats or mitigate the various consequences of an incident. Figure 1-6 presents an example of a bowtie for a leaking flange at a pump station by showing its key features:

- Hazard – a potential source of danger. For a pump station, this would be oil in the pipe and for a compressor station, the high pressure natural gas in the main piping. Existence of a hazard does not necessarily imply that an incident will occur.
- Top Event – the hazardous event at the center of the diagram. The normal top event for a pump station would be a Loss of Primary Containment (LOPC), in this case a flange leak.
- Threats – potential causes of the top event, on the left-hand side. One threat for a flange leak could be a defective flange connection.
- Causes – the means by which a threat could result in a top event. For a defective connection, causes could be a manufacturing defect in the flange or gasket or improper installation.
- Prevention barriers – measures in place to prevent threats leading to the top event. Quality inspections at the vendor or during installation could be barriers that would prevent a cause from leading to a flange leak. There is the likelihood of gasket deterioration as a barrier decay mechanism that would suggest regular replacement or monitoring would be appropriate, especially for corrosive liquids.
- Mitigation barriers – measures in place to prevent the top event from leading to a more serious consequence. Quick emergency response would be a mitigation barrier and a barrier decay mechanism that would need to be considered is a storage issue with the emergency response equipment.

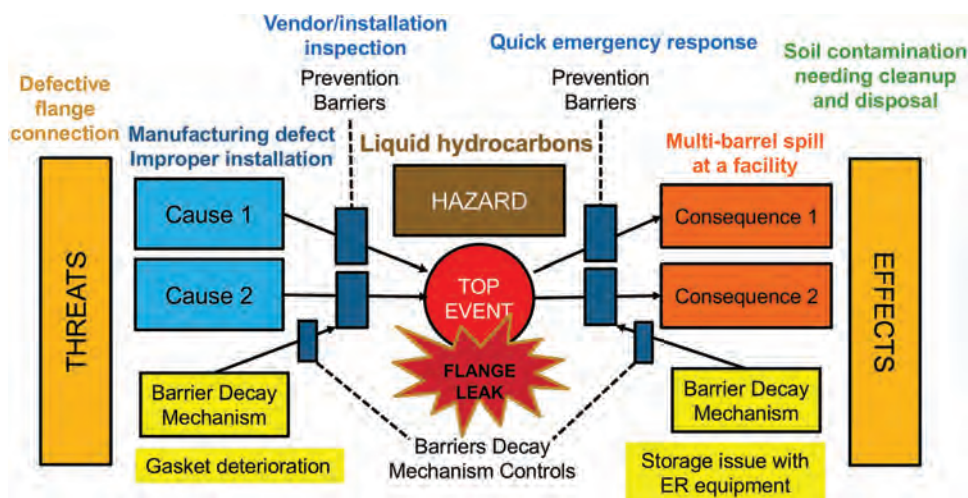


Figure 1-6. Example of a bowtie diagram for a flange leak at a pump station.

- Consequences – potential outcomes of the top event, on the right-hand side. For a leaking flange, this would be an oil spill, usually contained within the facility perimeter.
- Effects – actions that would have to be taken to deal with the consequences. In this case, oil contamination would result and would have to be cleaned up.

1.4.1.3 Operational Hazards and Risk

Operational hazards at pump and compressor stations are similar in some cases and vary for others, mainly due to the nature of the fluid being transported. Liquids may be volatile and present the risk of contamination and explosion. Gas may catch fire although it does not normally contaminate since it dissipates easily into the atmosphere.

Centrifugal pumps mostly used in the pipeline industry are for transportation of crude (including heavy) oil—a mixture of liquid hydrocarbons, some with volatile at atmospheric conditions such as condensate. Crude (particularly heavy oil) can be also warm (60–80°C).

Crude oil can also contain contaminants, some toxic such as hydrogen sulfide, radioactive such as strontium salts, or just water or grit. Additives may be introduced which have toxic properties, although these would normally be only in low concentrations. Therefore, hazard and risks associated with the pump operations must be considered and taken care of in the design and selection stage as much as possible.

The hazards associated with a large centrifugal pump must be considered over its complete operating/maintenance cycle. Operating range includes any abnormal and transient situations and loads. Poor operation/excursions/drive system failures and emergencies also are required to be covered.

The majority of hazards relate to the liquid being handled, either by a direct release, or by the consequent effects on upstream and downstream systems from a pump failure:

- failure of static components through fatigue, erosion, or corrosion
- failure of dynamic components leading to high fatigue loads on other components with potentially rapid catastrophic deterioration of seal or nozzles
- failure of the piping system due to extreme pressures or temperatures—either externally applied or generated by the operating pump or system, resulting from events such as pressure surges, process density, or liquid property changes

The direct threats to personnel from a release can arise from:

- the possible flammable nature of fluid released—volatile/high vapor pressure components, which would form a gas cloud with potential for explosion, or fire
- physical injury from a jet of fluid, or slips/falls from contaminated floor surfaces
- liquid which may well be hot, giving a scalding risk above 60–70°C range
- the liquid which may also evolve asphyxiating gases:
 - the toxic nature of components or additives within process material (liquids containing hydrogen sulfides are highly toxic)
 - small traces of radioactive salts within the process material can accumulate within a pump requiring appropriate handling precautions
 - inappropriate operation of the pump can induce high temperatures and pressures within a pump, giving rise to hazards from mechanical disintegration of the pump
 - handling material with higher concentrations of water or solids which can lead to higher pressure generation due to the effective increase in density

Hazards for compressors are due mainly to high pressure and the potential for fire when in a confined space such as the unit building. Piping components are also critical to safety as the weld

failure of a flange on a station gate valve at Princess Compressor Station in Alberta, Canada on February 23, 1980 showed (Fig. 1-7). High voltage electrical components are a hazard for electric units. Hermetic compressors are fundamentally very safe due to their sealed design but, as an incident revealed, the weak point is where the cable supplying the motor is not properly sealed and process gas can leak back into the control building where it can explode as Fig. 1-8 illustrates [16]. It must be remembered, however, that these types of incidents are very rare.

Mechanical hazards from improper pump or compressor operation could include:

- dynamic instability—vibration leading to bearing and pump component damage
- liquid induced vibration—running outside best efficiency point
- over-speed and reverse rotation—mechanically or process-induced
- internal clearances
- bearing failure/lubrication
- seal failure



Figure 1-7. Compressor station fire.



Figure 1-8. Compressor station explosion [16].

- joint failure
- loss of piping and pump restraints
- corrosion
- erosion
- failure of connections—overload and fatigue issues
- entrapment from contact with rotating shaft or other similar components

1.4.2 Dependability of Pipeline Systems

1.4.2.1 Dependability

In today's competitive and changing environment, it is crucial that pipelines and associated facilities create and sustain value for their stakeholders. This value can only be achieved by incorporating dependability into the pipeline system, in whole or in part. Dependability characteristics address not just availability and reliability as the probability of successful performance, but also identify other potential risk exposures such as degradation and wear-out that advocate the need for maintenance and logistic support to sustain "problem free" pipeline and facility operation. Dependability engineering [17] provides practical means and measurable targets for achieving value, which are then implemented by sound operational risk assessment practices.

The term "reliability" has the specific meaning as the probability that something may fail within a certain time period but is also commonly used in a broader sense for the combined and related concepts of availability, maintainability, supportability, maintenance, safety, integrity, and a host of other terms. This has led to a proliferation of aggregate terms such as R&M (Reliability and Maintainability), RAM (Reliability, Availability and Maintainability), RAMS where the additional "S" is safety, and Dependability, which is used by international standards.

On the international scene, the IEC (International Electrotechnical Commission) established a TC (Technical Committee) 56 in 1967 to address reliability standardization. The initial title of IEC/TC56 was "Reliability of electronic components and equipment." In 1980, the title was amended to "Reliability and Maintainability" to address reliability and associated characteristics applicable to products. In 1989, the title was changed to "Dependability" to better reflect the technological evolution and business needs on a broader scope of applications based on the concept of dependability as an umbrella term. In 1990, following consultations with ISO (International Organization for Standardization), it was agreed that the scope of TC56's work should no longer be limited to the electrotechnical field, but should address generic dependability issues across all disciplines. The scope of IEC/TC56 covers the generic aspects on dependability program management, testing and analytical techniques, software and system dependability, life cycle costing and technical risk assessment. This includes standards related to product issues from component reliability to guidance for engineering dependability of systems, standards related to process issues from technical risk assessment to integrated logistics support and standards related to management issues from dependability management to managing for obsolescence.

Dependability provides critical value at the pipeline system level by ensuring that the combination of pipe and pump/compressor stations can provide the capacity and availability to satisfy contractual requirements. For the pipe portion, dependability is normally couched in terms of risk management or integrity management with the objective of public, employee and contractor safety, avoidance of environmental damage, satisfying regulatory requirements and managing cost. For facilities, dependability value is obtained by high availability and reliability and low life cycle costs.

Due to fundamental differences in these assets—pipe being a structure and facilities consisting of many types of equipment—it is natural that different approaches and techniques are needed to ensure effective and dependable operation over their life cycle.

Dependability is the ability to perform as and when required. It applies to any physical asset such as a system, product, process, or service and may involve hardware, software and

human aspects. Dependability is a collective set of time-related performance characteristics that coexist with other requirements such as output, efficiency, quality, safety, and integrity. The main dependability characteristics of a system consist of:

- availability for readiness of operation
- reliability for continuity of service provision
- maintainability for ease of preventive and corrective maintenance actions
- supportability for provision of maintenance support and logistics to perform maintenance tasks

The interrelationship between these characteristics is shown in Fig. 1-9. Availability is the operational result of a combination of reliability, maintainability, and supportability. It is directly related to production capability and assurance in the oil and gas industry [18]. Reliability is inherent in the system design and must be sustained through the manufacturing and installation to provide dependable operation. Maintainability is dependent on the system design architecture and technology implementation guided by the maintenance strategies to enhance reliable operation. Supportability is enabled by available maintenance support resources to permit flexibility in logistic support management and outsourcing provision.

Performance requirements of equipment or a system can be divided into functional and non-functional components where the functional requirements denote fundamental objectives of the system and the non-functional ones are essential criteria needed to establish other requirements, such as safety, dependability, and usability. Dependability is associated with the time-dependent aspect of the requirements of a system. For example, the compression of natural gas is based on certain conditions of use to provide dependable compression capacity, safely and with minimum environmental impact. The resultant functional requirements become performance specifications, such as head, flow, and efficiency at a certain design point and operating range with the design carried out according to specified standards. Non-functional requirements relate to safety requirements and local and national regulations. The dependability characteristics relate to how this performance can be maintained over time, such as a pump producing the required pressure for a regulated flow to sustain operation without interruption or degradation with minimum downtime. A system configuration and design example is shown in Fig. 1-10.

1.4.2.2 The Value of Dependability for Pipelines

The general value of dependability is related to the ability of functional requirements to be satisfied from a time perspective. The value created by dependable operation is both

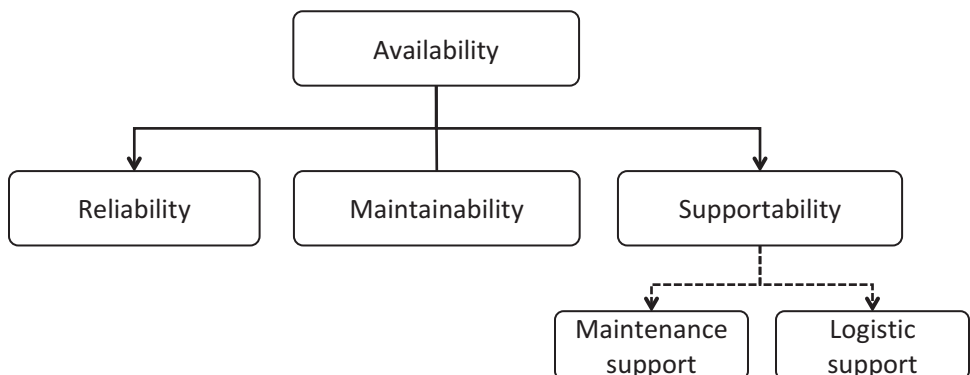


Figure 1-9. Interrelationship between dependability characteristics [19].

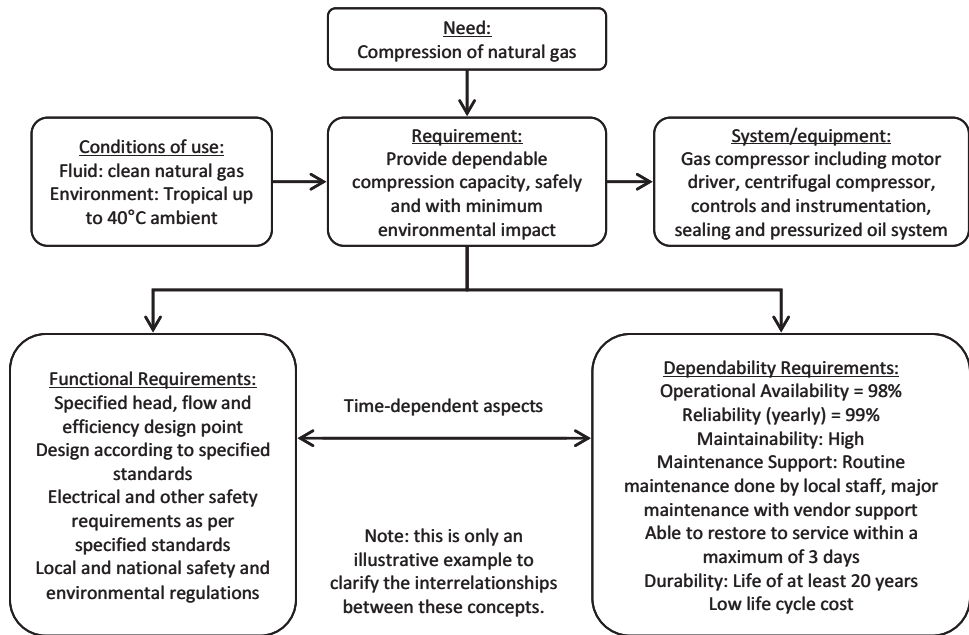


Figure 1-10. Functional and non-functional requirements [19].

positive in enhancing availability and reliability but also negative in the sense of avoidance of the consequences caused by cessation of required functions.

In general, dependability value can be expressed in the following ways:

1. **Safety is enhanced:** In many industries such as transportation, safe execution of the service is of paramount importance. Great lengths are taken to ensure no injuries or deaths are incurred although hopefully no one is under the illusion that all risk is eliminated. Moreover, there may be different acceptable safety levels for the public as opposed to employees.
2. **Customer or user satisfaction is achieved:** In particular for customer products and services, satisfaction is the measure of success even though likely not everyone will be equally satisfied. This satisfaction will be linked to the performance of the product or the service and whether any product failures or service interruptions are experienced. Availability upon demand is also important to the user or customer.
3. **Life cycle cost is minimized:** Life cycle cost is influenced by initial acquisition costs and the cost of operation and downtime or unavailability due to failures and the need for maintenance. Some costs may be inherent to the design while others can be minimized by good operating and maintenance practices. Sometimes long-term life cycle cost is compromised in the short term to achieve objectives. Costs and benefits may include not only those of the actual asset but ones related to achieved or lost production.
4. **Maximum asset life can be attained:** Dependable products and systems are much more likely to have a long life, something that is most important for infrastructure and very expensive assets. As long as the failure rate is not increasing dramatically, longer operation reduces life cycle costs.
5. **Environmental impact is minimized:** Failures can seriously impact emissions and environmental damage due to loss of containment of hazardous substances.
6. **Reputation is maintained or enhanced:** This is more problematic to quantify but a loss of reputation can impact business value such as the stock price and may result in a loss of market for products that could even lead to the end of an organization.

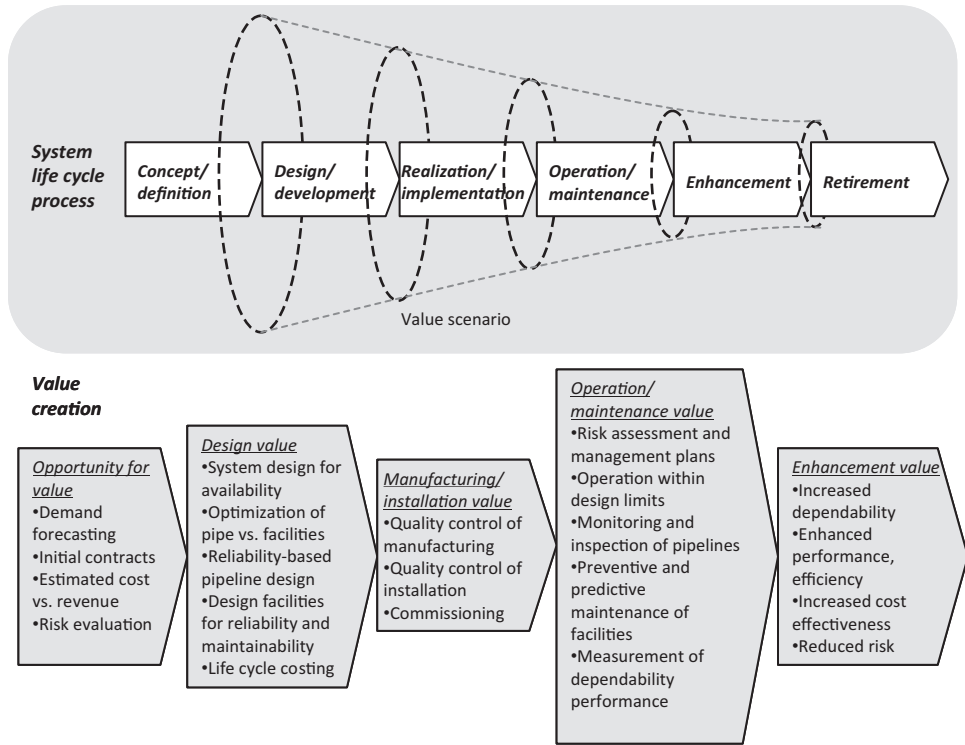


Figure 1-11. Dependability framework over the life cycle for pipelines [19].

The value of pipelines can be represented by the sequence of life cycle stages, which constitutes the primary process for value creation. Each life cycle stage from concept initiation to in-service operation adds value to the process. Figure 1-11 illustrates the general value creation framework for the system life cycle as applied to pipelines and facilities.

1.4.2.3 Dependability for Pumping and Compression

Satisfying dependability performance for a pipeline happens at several levels, starting with the pipeline system as a whole and being supported by specific and different approaches for the pipe portion and the compression or pumping facilities. The pipeline system level is essentially a network consisting of pipe and facilities with input and delivery points. The delivery is naturally also dependent on adequate supply volumes but this has to be assumed so it will not be considered further.

Delivery from a pipeline system is measured by availability as a function of flow with expectation by the customer that contracted volumes will be met. For a gas pipeline, even with loss of compression, expected volumes can often be made up due to changeable linepack and delivery requirements satisfied unless downtime is extensive. For oil pipelines, unless it is operating well below capacity, this may not be possible. For this reason, redundancy for pumping is more crucial than for compression.

Compared to pipe, compressors are less reliable and require downtime for maintenance. This would argue for less compression and larger pipe diameters except for the fact that installing pipe is considerably more costly than compression. Determining the most effective tradeoff options can be conducted by dependability analyses.

For pumping and compression facilities, the major dependability-related features are that:

- equipment consists of many different types of components with differing failure modes and failure rates
- failure rates are relatively higher
- consequences are generally from low to medium
- regular preventive maintenance is needed along with condition-based maintenance
- public safety or environmental damage is a not primary concern
- regulatory requirements are less stringent
- maintenance and replacement are technology driven and are continuously being improved

During the design phase, considering reliability and maintainability are particularly important and quite a few techniques exist to facilitate these as well as extensive standards, including international ones by IEC/TC56 [20].

Detailed pipeline system operational capability, reliability, and availability assessment of a system are described by Mohitpour et al. [21]. In this reference, applicable codes and standards providing guidelines for assessment of pipeline systems reliability, and availability/dependability are provided. Fundamentals and techniques are described, and typical pipeline component failure data are provided. Reliability/availability assessment application is then detailed.

Creating value from dependability for compression or pumping facilities leads primarily to these benefits: improved safety, high availability, and reduced costs. Improved safety applies mainly to employees and contractors and not so much the public so it is less critical than for pipelines.

Availability is linked to meeting delivery contract requirements and providing customer satisfaction. The impact of compressor/pump downtime is very dependent on the number of stand-by units installed and, especially for gas pipelines, the flexibility of the pipeline itself in handling short term downtime which will guide the tradeoff between availability and capital and operating costs.

Reduced costs may range from short-term cost comparisons to long-term life cycle costing (LCC is also known as TCO or total cost of ownership). LCC studies are best done during equipment acquisition and used to compare alternatives.

The major steps in a LCC analysis are:

- preparing a breakdown structure for applicable costs
- determining costs for each breakdown element
- collecting failure and repair data (MTBF/MTTR or Weibull) from industry sources
- actual experience
- analyzing system availability and reliability
- selecting an LCC model (e.g. $LCC = \text{Acquisition cost} + \text{Operating cost} + \text{Failure cost} + \text{Support cost} - \text{Net disposal value}$)
- estimating costs for each component of the LCC model
- applying discounting over the time period of the study
- determining the final LCC based on Net Present Value (NPV)
- comparing alternatives

1.4.2.4 Reliability, Availability and Maintainability Models in Pipeline Systems

Reliability, Availability and Maintainability (RAM) models have contributed to capital cost avoidance while maintaining or improving the reliable design and operation of the pipeline system [22]. These models constitute a very effective, factual and dependable tool to assess the throughput performance of a pipeline system over its entire life cycle or a specified time of interest. In addition, the RAM model cost is a small fraction of the overall monetary benefit, in the order of 1%, hence making RAM models a highly leveraged activity.

The concept of a RAM model stems from Reliability Block Diagram methods [23]. Interaction of large, complex and multi layered systems can then be analyzed using the Monte Carlo simulation methods (or Stochastic Discrete Event Simulation) hence quantifying the output of the entire system with greater accuracy than other estimating tools or methods. Over 10 years, the company has developed its own failure database for equipment and operational events, so consequently almost all model inputs are based on in-house data rather than industry generic data, making the model output more robust, accurate and appropriate for internal use [22].

Initially, RAM models were mainly built to assess and confirm the design capabilities of future pipeline designs and assist in the optimal selection of specific design options. Because of the effectiveness of the tool combined with the current cost constrained business environment, the company is moving towards building RAM models for assets already in operation in order to optimize their performance. This is proving to be an extremely cost effective addition to internal decision making processes. The approach has been used in risk-based budgeting, asset maintenance, design modifications and throughput optimization initiatives.

RAM models are usually built for two types of systems depending on size and complexity:

- simple sub-systems, which typically include a subset of a pumping facility or a terminal, typically including from 50 to 200 blocks with fixed flows.
- complex systems such as an entire pipeline can reach 5,000 blocks because they include terminals, pump stations as well as injections and delivery points with mechanical, electrical and control systems. These models include hydraulic capabilities of the pipeline under different pump or station outage states. Each state needs to be calculated using an external hydraulic model that feeds into the model.

The RAM process model for a complex system with inputs and outputs usually required is shown in Fig. 1-12. Not all inputs or outputs may be required. Also, if they are required, they may be quite simple. For example, flow inputs for one booster pump model may only have 3 states i.e. off, nominal or design flow. Whereas a 1,000 km pipeline may have 150-200 states, one for each combination of pump or station outage on the pipeline.

Outputs from the model can be customized both in types of data and formats. As an example, Fig. 1-13 shows overall throughput performance and the probability distribution of achievement.

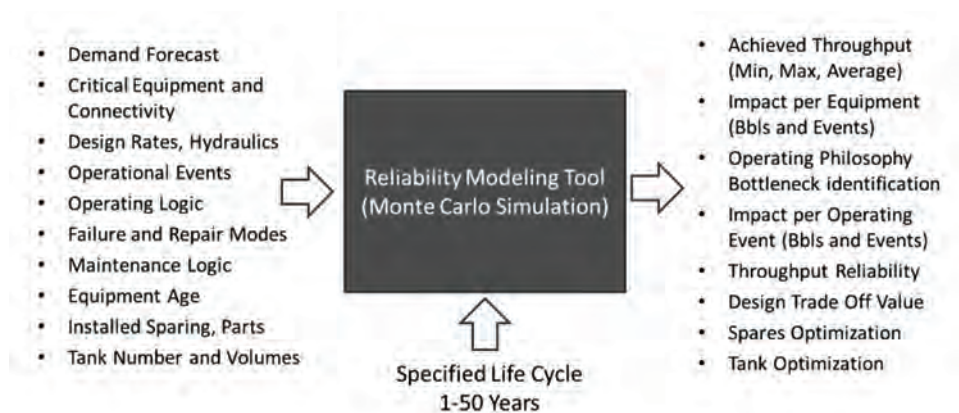


Figure 1-12. RAM process flow model [22].

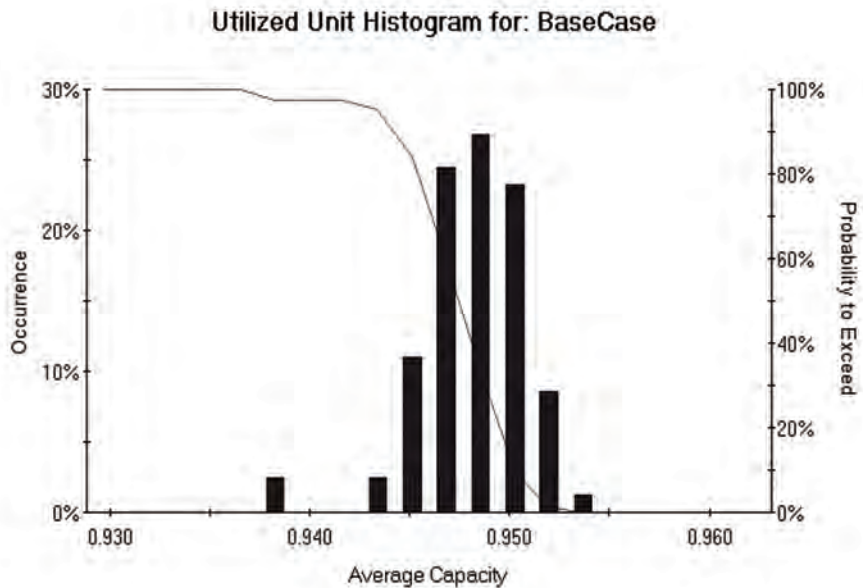


Figure 1-13. RAM process flow model [22].

REFERENCES

- [1] Mohitpour, M., 2008. *Energy Supply and Pipeline Transportation—Challenges and Opportunities*, ASME Press, New York.
- [2] BP Energy Outlook, 2018. BP p.l.c. 2018, <https://www.bp.com/en/global/corporate/energy-economics/energy-outlook.html>, p. 68.
- [3] Mohitpour, M., Dawson, J., Babuk, T. and Jenkins, A., 2000. “Concepts for Increased Natural Gas Supply—a Pipeline Perspective,” Presented at Forum 11, 16th World Petroleum Congress, June 11–15, Calgary, AB, Canada.
- [4] Pipeline & Hazardous Materials Safety Administration, U.S. Department of Transportation, “About Pipelines,” <https://primis.phmsa.dot.gov>.
- [5] ASME (American Society of Mechanical Engineers), 2016. “Pipeline Transportation Systems for Liquid Hydrocarbons and Slurries,” ASME Code for Pressure Piping, B31.4, An American National Standard.
- [6] API Recommended Practice 1173, 2015. “Pipeline Safety Management Systems,” American Petroleum Institute, First Edition, 27 pages.
- [7] CAN/CSA Z662-15, 2015. “Oil and Gas Pipeline Systems,” Canadian Standards Association, 868 pages.
- [8] CAN/CSA-Z767-17, 2017. “Process safety management,” Canadian Standards Association, 48 pages.
- [9] Canadian Energy Pipeline Association, 2013. “Facilities Integrity Management Program Recommended Practice,” 1st Edition, May 2013 (www.cepa.com).
- [10] Sahney, R., Reed, M. and Skibinsky, D., 2014. “The Development of a Facilities Integrity Management Program Recommended Practice for Canadian Energy Pipelines,” Proceedings of the 10th International Pipeline Conference, IPC2014-33746, Sept. 29–Oct. 3, 2014, Calgary, Alberta, Canada, 9 pages.
- [11] IEC/ISO 31010:2009. “Risk management - Risk assessment techniques,” Edition 1.0, 2009-11-27, 188 pages.
- [12] IEC 61882:2016. “Hazard and operability studies (HAZOP studies)—Application guide,” Edition 2.0, International Electrotechnical Committee, 2016-03-10, 124 pages.

- [13] IEC 60812:2006. “Analysis techniques for system reliability—Procedure for failure mode and effects analysis (FMEA),” International Electrotechnical Committee, 2006-01-25, 93 pages.
- [14] IEC 61025:2006. “Fault tree analysis (FTA),” Edition 2.0, International Electrotechnical Committee, 2006-12-13, 103 pages.
- [15] Pettitt, G. and Pennicott, P., 2016. “Use of Bowties for Pipeline Safety Management,” Proceedings of the 10th International Pipeline Conference, IPC2016-64243, Sept. 26–30, 2016, Calgary, Alberta, Canada, 9 pages.
- [16] Pipeline Investigation Report P00H0061, 2000. “Natural Gas Compressor Station Occurrence,” Transportation Safety Board of Canada, 71 pages.
- [17] Van Hardeveld, T. and Kiang, T.D., 2012. “Practical Application of Dependability Engineering,” ASME Press, New York.
- [18] ISO 20815:2008. “Petroleum, petrochemical and natural gas industries—Production assurance and reliability management,” First Edition, 2008-06-01.
- [19] Van Hardeveld, T. and Kiang, T.D., 2012. “Achieving Dependability Value for Pipelines and Facilities,” Proceedings of the 9th International Pipeline Conference, IPC 2012, September 24–28, 2012, Calgary, Alberta, Canada.
- [20] IEC/TC56 website, <http://tc56.iec.ch/index-tc56.html>, accessed March 9, 2018.
- [21] Mohitpour, M., Szabo, J. and Van Hardeveld, T., 2004. Pipeline Operation and Maintenance—A Practical Approach, ASME Press, New York, pp. 565–606.
- [22] Jones, B.M. and Ferrari, A.-M., 2016. “Reliability, Availability and Maintainability (RAM) Simulation Models in Pipeline Systems,” Proceedings of the 10th International Pipeline Conference, IPC2016-64205, Sept. 26–30, 2016, Calgary, Alberta, Canada, 10 pages.
- [23] IEC 61078:2016. “Reliability block diagrams,” Edition 3.0, International Electrotechnical Committee, 2016-08-12, 250 pages.

LIQUID PIPELINE PUMPING SYSTEM DESIGN

2.1 LIQUID PIPELINE DESIGN

2.1.1 Liquid Pipeline Hydraulics

As pumping requirements must match pipeline characteristics, the first step in liquid pipeline pump station design is the analysis of the pipeline hydraulic gradient for varying flow conditions for the particular route elevation profile. This defines the length and elevation change of the pipeline and is used to establish pipeline pressure, pipeline pumping power, number and location of stations, number of pumps, and appropriate mode of operation.

For a non-isothermal situation when the temperature gradient between the pipe and the surrounding environment is significant, heat transfer between the pipe and environment must be considered. Any hydraulics calculations must consider not only elevation change, supply and delivery pressures, and volume built ups, but also correctly allow for heat transfers between the fluid within the pipe through pipewall/coating and the surrounding environment such as ground.

Typical hydraulics profiles considering all factors of elevation change, thermal heat loss/gain to and from the surrounding environment, and frictional heat generation are shown in Fig. 2-1. From Fig. 2-1, it may be noted that the minimum flow for one initiating station operating will be about 52,000 Barrels Per Day (BBLSD). If a midpoint pump station is brought online [to the same discharge pressure (head) as the initiating station], then maximum flow of the pipeline can be restored as though the pipeline is operating with one station at maximum operating pressure.

The choice of pump type is usually made when the total flow and the required pressure (head) at various locations/stations along a pipeline route is established although centrifugal pumps are the common choice.

Pumping stations can consist of a multiple pump arrangement. In such cases, pumps can be connected either in parallel or in series. Parallel arrangement of the pumps has typically been applied along mountainous pipeline routes, where a significant pressure head is needed at each pumping station, as illustrated in Fig. 2-2. This is especially applicable since fixed speed pumps in parallel are easier to start than ones in series. VFD technology now enables a series pump to be started quickly and safely ramped up to full flow [1] so this arrangement is now also possible. Series arrangement is common for pipeline routes with little or moderate elevation changes, where the pressure head consists mainly of friction losses. In the end, a hydraulic analysis of the pressure and flow ranges required of the pump station is needed to determine the most efficient solution.

2.1.2 Pipe Size and Pump Selection

Pipe size is an important consideration. Pipeline costs are a direct function of diameter, and large distances are usually involved. They can be the highest cost component of the pipeline system, so the smallest diameter pipe is preferred from a capital investment point of view.

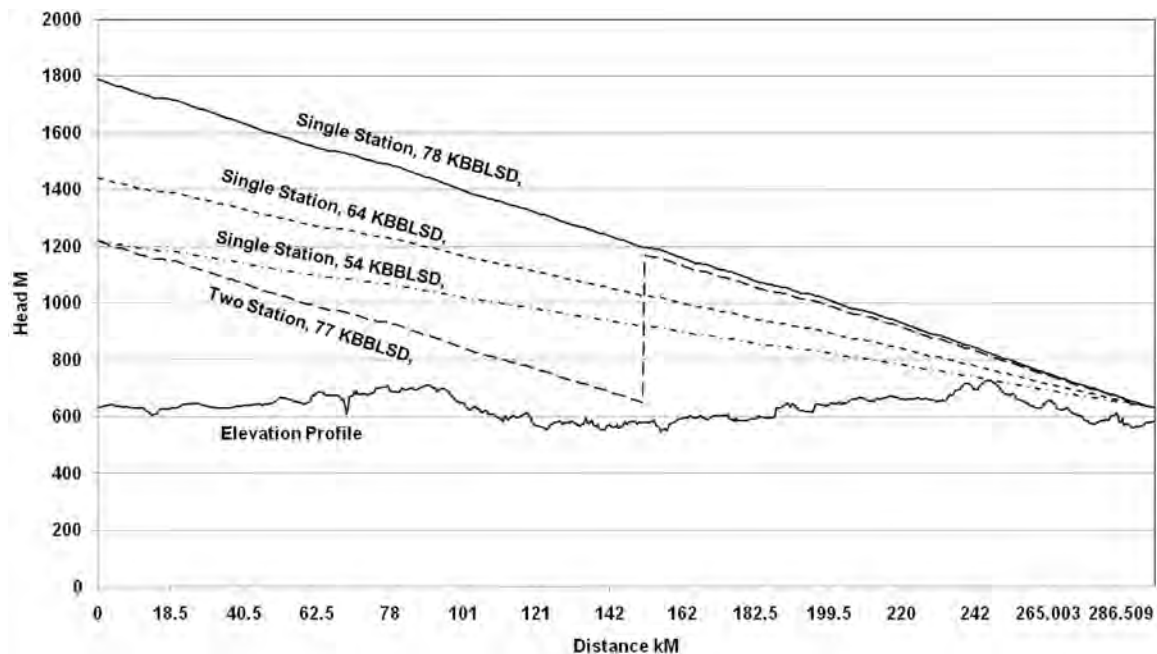


Figure 2-1. Typical pipeline hydraulics gradient and route profiles (NPS 16,295 km, fluid SG 0.7, summer conditions).

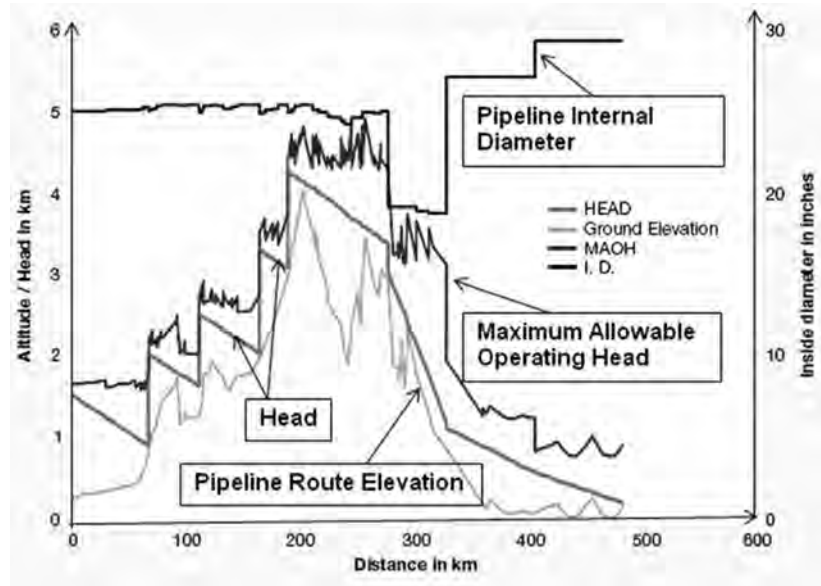


Figure 2-2. Typical hydraulic gradient for a pipeline over mountainous areas.

However, pipeline sizes are optimized with pump costs, which will depend on volume and facilities build up requirements. Since the friction loss varies with the square of the velocity, larger diameter piping will not only reduce the size and cost of the pump and driver but also reduce operating costs by reducing power costs in overcoming friction. The importance of pipeline system optimization, i.e., balancing the pipe size versus pumping facilities requirement, are detailed elsewhere [2,3].

Meeting pipeline pressure requirement is an extremely important consideration when selecting pipeline pumps, pump location intervals, and duty(ies). There are a number of reasons that must be considered to assure a cost-effective solution. Commercially available/standard fittings follow ANSI pressure limitations [4]. There are very significant cost increases as the pressure rating class is increased, especially in the higher classes (i.e., ANSI 600, 900, and 1500). Care must be exercised when designing systems to ensure the ANSI class limits (pressure and temperature limitations) are not exceeded.

Of importance are the fluid characteristics when selecting a pump. The type of fluid to be transported affects pipeline design and facility requirements and configuration, including pumping systems. The properties of fluid to be transported have significant impact on pipeline system design. For liquid lines, the liquid properties which affect pipeline design are:

- viscosity
- density
- specific heat

These properties are influenced by the pressure and temperature. Temperature considerably affects the above properties in liquid pipelines and, specifically, crude oil or heavy crude oil pipelines. Viscosity is also affected by the liquids' shear rate. Liquids that have a constant shear rate with respect to shear stress at any given temperature are termed Newtonian fluids, and the viscosity is a function of temperature only. It increases with decreasing temperature. Non-Newtonian fluids have viscosities which are not only a function of temperature but also of shear rate (Fig. 2-3) [5]. Non-Newtonian fluids which are time-dependent are classified as thixotropic (fluids that require a decreasing stress to maintain a constant strain rate) and rheopectic fluids (ones that need an increasing shear stress to maintain a constant strain rate).

Other time-independent ones are pseudo-plastic, yield pseudoplastic, dilatants, and Bingham fluids shown in Fig. 2-4. As can be seen from Fig. 2-4, when transporting non-Newtonian products through the pipeline, a definite minimum stress must be applied to the product (to reach its yield point) before any flow of the product takes place.

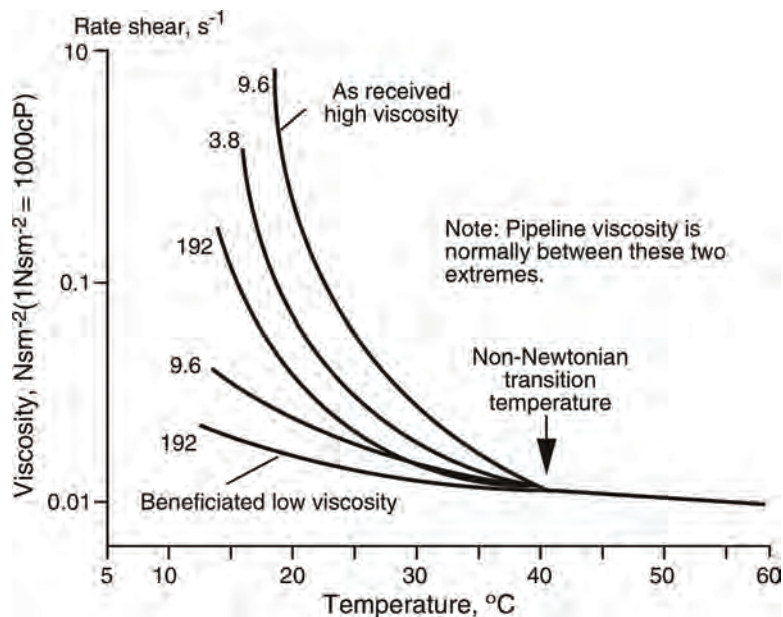


Figure 2-3. Viscosity characteristics for a typical non-Newtonian heavy crude oil [5].

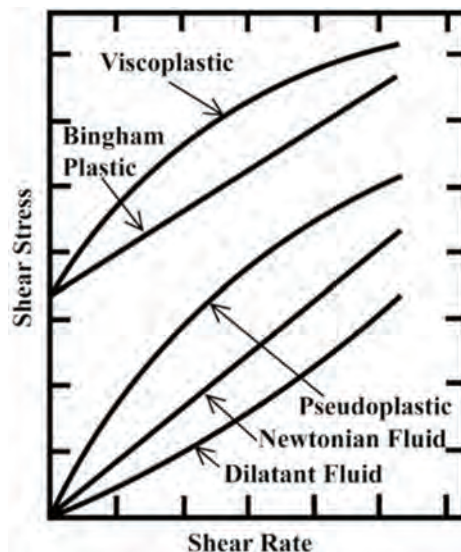


Figure 2-4. Curves illustrating shear characteristics for various products.

Pumping capacity and power requirement must therefore consider the fluid condition over time because pumping operation will be influenced by any changes in liquid viscosity and density that may occur. Such change can affect:

- net-positive suction head
- priming flexibility
- fluid condition and corrosion, and useful life
- maintenance
- quantity pumped
- pumping head
- power source
- transportation economics

When the product being transported is always a low viscosity liquid such as water, gasoline, diesel oil, or very light crude oil, centrifugal pumps are cost-effective, reliable, and efficient. However, as the liquid viscosity increases, the frictional losses within a centrifugal pump quickly reduce pumping efficiency dramatically (Fig. 2-5). For this reason, rotary, positive displacement pumps are often used when products such as heavy crude oil, bunker fuels (no. 6 fuel oil), low sulfur fuels, asphalt, and similar products are to be transported.

Pipeline pump station costs are dependent on the type of pump envisioned for the service, piping design, and operational aspects. Because steps in cost occur, design pressures are maximized of a certain piping class to take advantage of system design to offset any cost increase. This can prove a dilemma in the system design. For positive displacement (reciprocating) pump systems, pressure relief valves are generally required, whereas for centrifugal systems the additional cost of the relief valve is usually avoided. In all cases, variations in SG, percent rise to shut-off, and test tolerances must be also considered.

- *Specific gravity.* If the system requires that the pumps handle a wide variety of fluids with varying SG (such is the case for batched product transportation), the pumps must be sized for the lowest SG to assure minimum discharge pressure is possible.

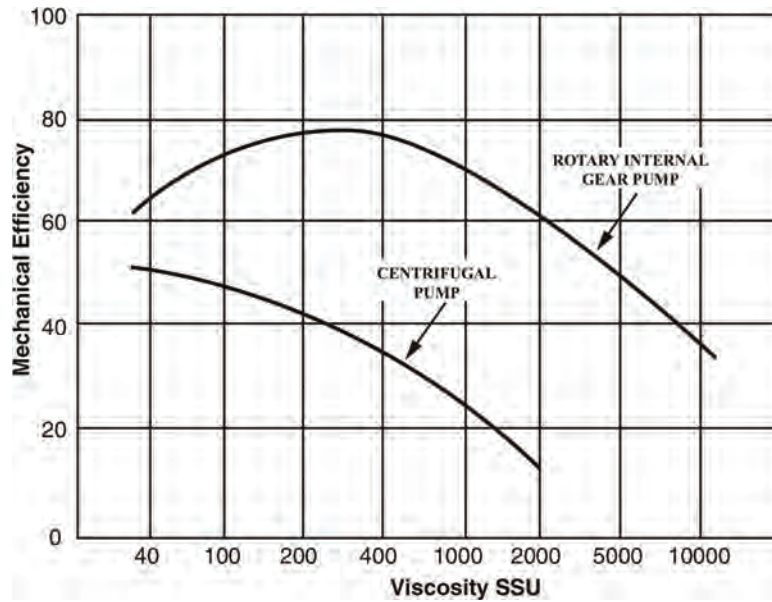


Figure 2-5. Example of rotary versus centrifugal efficiency.

However, because centrifugal pumps produce head and not pressure, the highest discharge pressure will occur with the highest SG.

- *Rise to shutoff.* As discussed in Chapter 5, centrifugal pumps generate a performance curve that rises as the flow decreases. Therefore, it is not sufficient to calculate the discharge pressure at the rated point. It must be calculated at shutoff, which can be 10% to 20% higher than rated flow.
- *Test tolerances.* Pump manufacturers only guarantee the rated point. The shape of the curve and the shut-off pressure can vary dramatically from bid to test. This variation must be specified or test tolerances at shut-off must be accounted for.

The properties of the fluids being pumped can significantly affect the choice of pump. Key considerations include:

- *Acidity/alkalinity (pH) and chemical composition.* Corrosive and acidic fluids can degrade pumps and should be considered when selecting pump materials. Operating temperature. Pump materials and components expansion, mechanical seal design, and packing materials need to be carefully considered when pumping high-temperature liquids.
- *Solids concentrations/particle sizes.* When pumping abrasive liquids such as industrial slurries, selecting a pump that will not clog or fail prematurely depends on particle size, hardness, and the volumetric percentage of solids.
- *Specific gravity.* The fluid SG affects the energy/head required to lift and move the fluid and must be considered when determining pump power requirements.
- *Vapor pressure.* A fluid's vapor pressure is the force per unit area that a fluid exerts in an effort to change phase from a liquid to a vapor and depends on the fluid's chemical and physical properties. Proper consideration of the fluid's vapor pressure will help to minimize the risk of cavitation.
- *Viscosity.* The viscosity of a fluid is a measure of its resistance to motion. Since kinematic viscosity varies directly with temperature, the pumping system designer must know the viscosity of the fluid at the lowest anticipated pumping temperature.

High-viscosity fluids result in reduced centrifugal pump performance and increased power requirements. It is particularly important to consider pump suction-side line losses when pumping viscous fluids.

2.1.3 Pipeline System Head Curve

A pipeline system head curve shows the relation between capacity and the resulting head occurring in the pumping system. The corresponding system curve for one station case is illustrated in Fig. 2-6. The total head of a system against which a pump is required to operate is a combination of the following heads/pressure:

- the static head of a system (which is the difference in elevation between the discharge liquid (elevation) level and the suction liquid (elevation) level)
- the pressure head of a system (which is the energy available to do work after the static head and the friction head in the pipe is overcome)
- friction head is the energy that is necessary to overcome the frictional losses caused by the flow of liquid through the pipeline piping, including valves and fittings. There are various means of calculating such a frictional loss. These include the following:
 - Simple Darcy equation (for laminar flow)
 - Coolbrook–White (fully turbulent flow)
 - Hazen–Williams (fully turbulent flow)
 - Hetzel (fully turbulent flow)
 - Aude (fully turbulent flow)

The equations that are extensively used in the liquid pipeline transmission industry are Coolbrook–White and Hazen–Williams for fully developed flows. However, Hetzel is an older equation which is still used for Reynolds numbers (Re) from 4000 to 57,600. Aude equation is quite accurate and is generally used in smaller transmission lines for Re range from 6000 to 130,000 (NPS6 to NPS12 for crude oil) and over 57,000 for NPS 6 and NPS 8 (for refined products pipelines) [6].

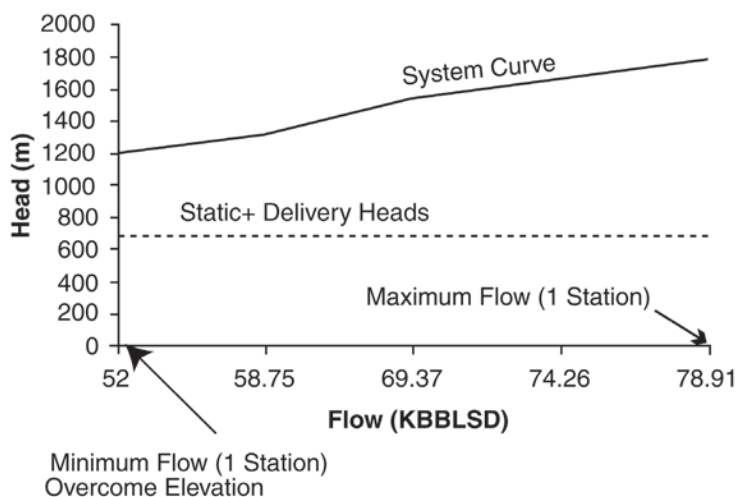


Figure 2-6. Pipeline system head curve (single station operation).

An example is the Darcy equation for friction loss, h , for incompressible fluid flow through a pipe:

$$h_f = f \frac{L}{d} \frac{v^2}{2g} \quad (2-1)$$

where

f = friction factor (from Re) and is a function of pipe roughness (Fig. 2-7); for laminar flow, $f = 64/\text{Re}$ and is independent of pipe roughness

L = pipe segment length (ft, m)

d = pipe inside diameter of pipe (ft, m)

v = fluid velocity (ft/s or m/s)

g = gravitational acceleration (ft/s² or m/s²)

Velocity in a pipe is generally achieved at the expense of static head. The higher the pressure/head the lower the velocity and vice versa.

The term $[v^2/(2g)]$ is defined as the velocity head:

$$h_f = \frac{v^2}{2g} \quad (2-2)$$

Flow through a pipe or a fitting also causes a reduction in static head, which can be expressed in terms of velocity head. The resistance coefficient K is defined as the number of

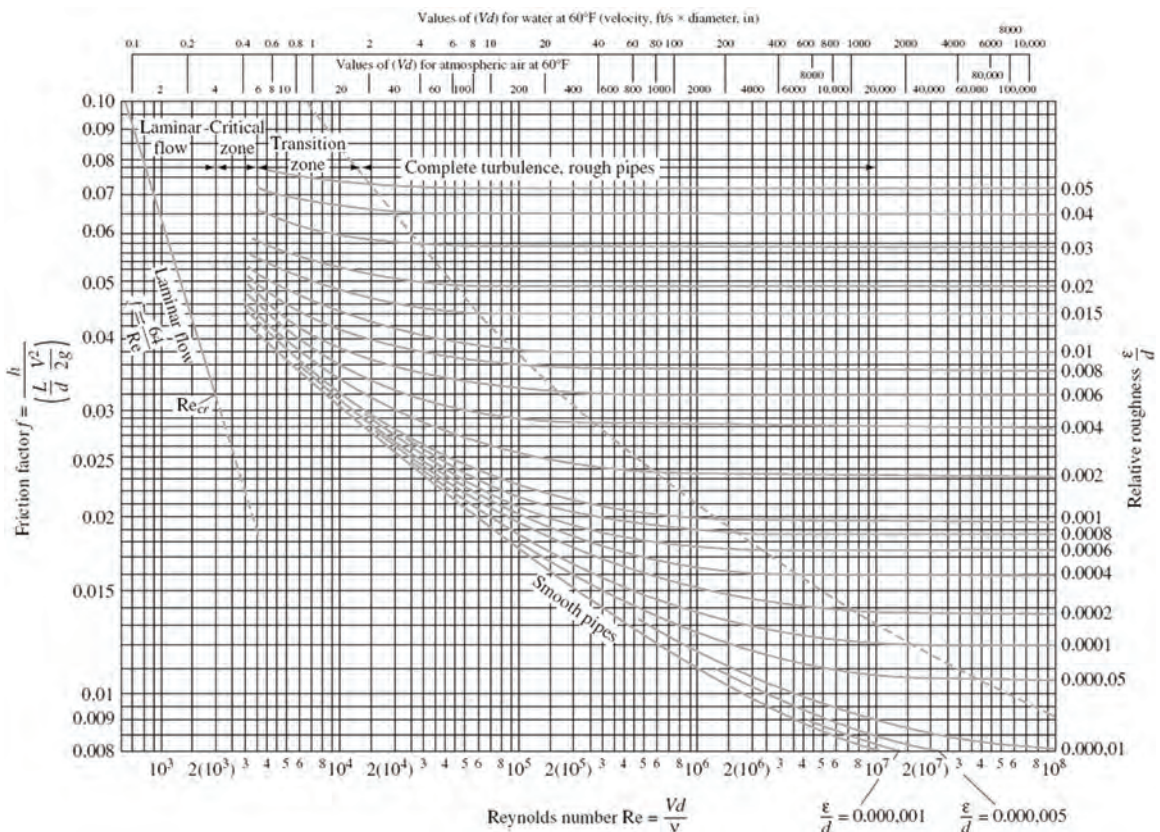


Figure 2-7. Moody's diagram depicting friction factor for flow of fluids through pipes [7].

velocity heads lost due to flow through a valve or fitting. The K factor may be considered as being independent of friction factor or Re (Reynolds no). It may be treated as a constant for any given obstruction in a piping system under all conditions, including laminar flow.

$$Re = \frac{\rho \cdot d \cdot v}{\mu} \quad (2-3)$$

where

- ρ = fluid density [lb_m/ft^3 (kg/m^3)]
- d = pipeline internal diameter [ft, (m)]
- v = fluid average velocity [ft/s (m/s)]
- μ = fluid viscosity [$\text{lb}_m/\text{ft}\cdot\text{s}$ (kg/m·s)]

Therefore, the head loss caused by a valve or fitting can be calculated with the following equation:

$$h_f = K \frac{v^2}{2g} \quad (2-4)$$

The head loss in straight pipe can also be expressed by inserting the above equation into the Darcy formula, resulting in the following equation:

$$K = f[L/d] \quad (2-5)$$

The ratio L/d is the term equivalent length. It is defined as the length of straight pipe that will produce the same pressure drop as the obstruction.

The following example illustrates how the system head curves are developed.

2.1.4 Pipeline System Curve Development Example

It is required to transport water through an NPS 6 (diameter 6.625-in., wall thickness 0.312 in.) from a source of supply to a tankage 60 m away.

Elevation differential between the supply (i.e., location of pump station) and the tank will be about 30 m (Fig. 2-8).

The piping arrangement that will make up the system includes:

- 60 m, NPS 6 pipe (inside diameter 6 in.)
- 10 elbows, $K = 2.8$ each

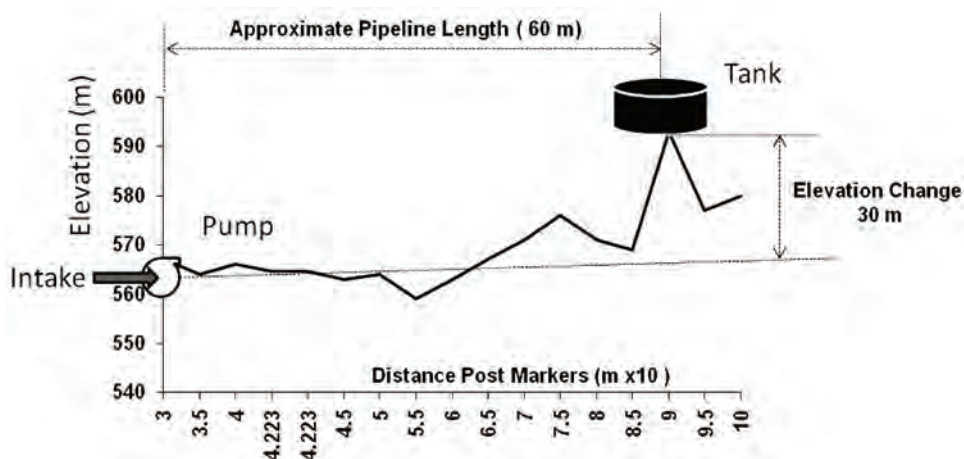
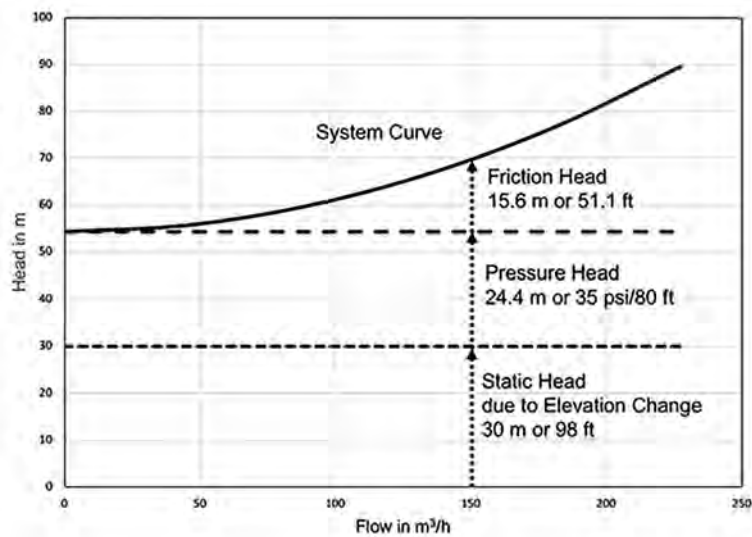


Figure 2-8. Physical system layout.

Table 2-1. Pump head (h_p) overcoming pipe friction

Flow (gpm)	Flow (m ³ /h)	Flow (m ³ /s)	Velocity (v) (m ³ /s)	Velocity Head ($v^2/2g$)	Pipe friction head (h_f)(m)	Fittings friction head (h_f)(m)	Total friction head (h_f)(m)
0	0	0	0	0	0	0	0
200	45.6	0.0127	0.69	0.02	0.19	1.21	1.40
400	90.6	0.0252	1.38	0.10	0.77	4.84	5.61
600	136.2	0.0378	2.08	0.22	1.73	10.89	12.62
800	181.8	0.0505	2.77	0.39	3.07	19.36	22.43
1000	227.4	0.0632	3.46	0.61	4.80	30.25	35.05

**Figure 2-9.** Pipeline system curves.

- 4 gate valves, $K = 0.9$ each
- 1 check valve, $K = 2.0$, total $K = 49.6$
- 1 globe valve, $K = 6.0$
- 1 exchanger, $K = 10$
- assume pipe friction factor $f = 0.02$
- water SG, $SG = 1$
- elevation difference = 30 m
- tank inlet pressure = 240 kPa (35 psi)
- flow variables 0 to 1000 gal/min (0–273 m³/hr)

Table 2-1 provides the sample calculations in metric units for values of friction head through the pipe, while Fig. 2-9 provides the system curves in SI and US Customary units.

2.1.5 Considerations for System Curves

Pipeline pump applications generally experience constant changes in capacity and product being transported. This is particularly true in the transportation of crude oil and hydrocarbons. The variation of liquid characteristics, flow rates, pressure, and environmental conditions can result in a wide range of system head curves, requiring extreme flexibility in pump operation. Operating points thus vary even for controlled flow conditions due to

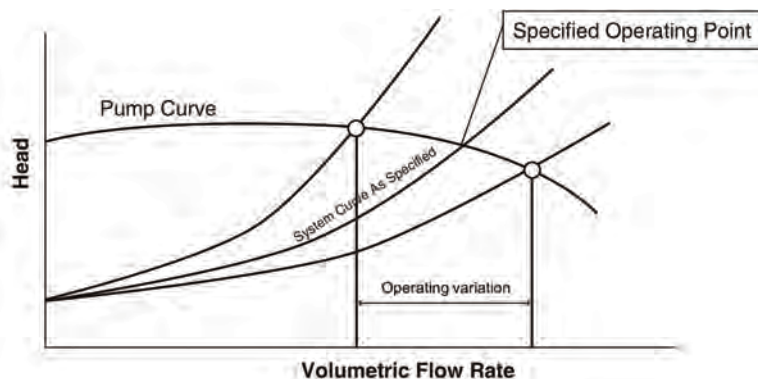


Figure 2-10. Pump curve meeting variable system operating points.

changes that may occur in usage, environmental, and other conditions. An example of this is shown in Fig. 2-10.

It is the operators who select pumps to meet the varying operating scenarios. Pump selection can thus be very complex, usually requiring multiple series pumps installations at various stations. Selection may also require parallel operation, variable speed, and/or pump modifications to meet future requirements.

Many pipeline conditions require low capacity (low flow rate)/low pressure startup with ultimate change-over to high capacity/high pressure. By considering future requirements in the design stage, specific pipeline pumps can be engineered to allow for future condition changes. Impeller modifications, volute chipping, under-filing, volute inserts, and destaging techniques are typical examples and are described in Chapter 5.

2.2 PUMP STATION CONFIGURATION

2.2.1 General

The number of pumps and their configuration involve an optimization process for all predicted modes of operation. It may be noted that pumps have a limited range of operation. Operation outside of those ranges result in low-efficiency operation and high-power consumption costs.

However, depending on the pressure/head requirements, they may be configured as follows:

- single unit
- multiple units in series
- multiple units in parallel
- a parallel-series system

For a single unit system (i.e., where only one pump meets delivery requirements), the only consideration must be of flow and head requirements. Although in theory, a pump can operate from shut-off point to around 120% of flow, for reliability reasons, the practical flow range is only 80%–120%.

Pumps can be arranged in series or parallel to provide additional head or flow rate capacity. However, to overcome a larger system head/pressure, pumps are configured in series or series/parallel combinations to overcome a larger system head loss than one pump can compensate

for individually. This also provides a better system control and reliability. Multiple pumps often include an extra pump for backup in case of failure or for maintenance purposes.

2.2.2 Pumps in Series

When two (or more) pumps are arranged in series, their resulting pump performance curve is obtained by adding heads at the same flow rate. However, as Fig. 2-11 illustrates for two equal pumps, the new operating point is dependent on the system curve and the resultant head is less than twice the head of each pump. When pumps with different curves are placed in series (Fig. 2-12), the resultant head is again a function of the system curve. Moreover, if the flow is higher than that of the lower flow pump, there is a region to the right of the maximum flow of the smaller pump where it does not contribute any more to the increase in head and the total head is only that of the other pump.

2.2.3 Pumps in Parallel

When the system characteristic curve is considered with the curve for pumps in parallel (Fig. 2-13), the operating point at the intersection of the two curves represents a higher volumetric flow rate than for a single pump and a greater system head loss.

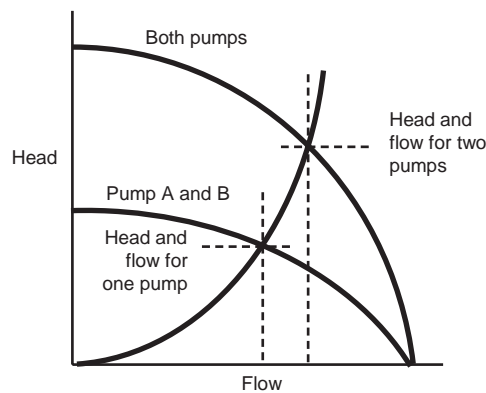


Figure 2-11. Pumps in series where the curves are the same.

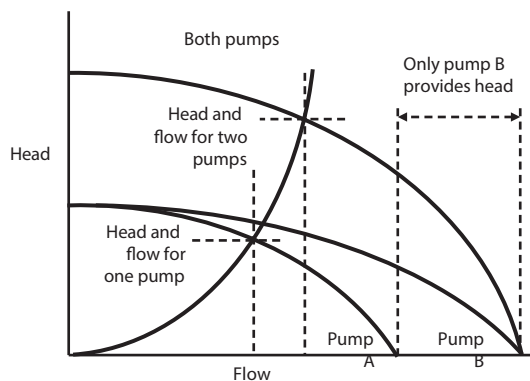


Figure 2-12. Pumps in series with different curves.

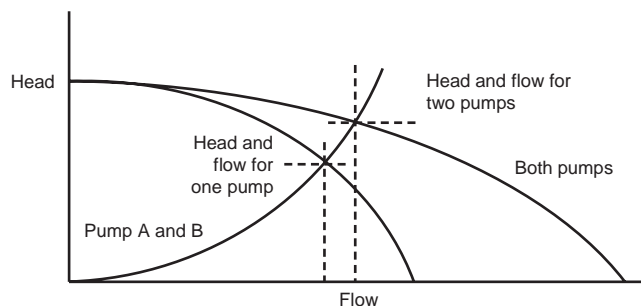


Figure 2-13. Pumps in parallel with system curve.

However, as can be inferred from Fig. 2-13, a greater system head loss occurs with the increased fluid velocity resulting from the increased volumetric flow rate. Because of the greater system head, the volumetric flow rate is actually less than twice the flow rate achieved by using a single pump. The actual increase in flow is dependent on the shape of the system curve.

A consideration that also affects the number of pumps is the available power limitations. For example, electric motor size is quite often limited by the availability and location of suitable power grid. When large motors are started, the resulting in-rush causes voltage drops that may upset the power grid system. A check with the utility company is always required, especially in remote areas. The capital cost of gas engines also increases in steps and may prove to be the limiting factor in determining the size of the pump.

2.2.4 Number of Units

Along with station configuration, considerations are generally given for the number of units required when evaluating the installation of pumping/compression. A larger single unit may be considered from the consideration of minimizing maintenance, station operations, and control; however, the reliability of the pipeline system in general and station in particular decides the type and number of units that will be required.

Systems hydraulics generally decide on station requirements including power as well as location. Based on the overall station power requirement, the number of units (including spares) are decided on based on economics, types of pumps, pipeline operations/controls, as well as required system capability/reliability and capacity.

Pipeline system flow requirements are usually contractually determined or assessed based on demand requirements over the life of a pipeline project. The detailed hydraulic simulations would demonstrate the system's ability to meet these required flows with all units operational. However, a historical assessment of the reliability of various units can also be made, and the capability of the system can be calculated for the outage of a single unit at a particular station, a station outage, or a combination of outages at more than one station.

Probability theory can help to assess the likelihood of each event, and the effective capability over a period, C , is given by the following [8]:

$$C = \frac{n!}{r!(n-r)!} p^r q^{(n-r)} (\text{capability with } r \text{ units down}), \quad (2-6)$$

where:

- n = total number of units on the pipeline
- r = number of units down
= 0 to n
- q = typical unit availability
= (total hours available per month)/744 hours per month
- $p = 1.0 - q$

As an example in compression system, if the effective capability, C , is below the average day flow, standby units at stations are necessary to meet the required annual flow. If C is greater than the average day flow but less than the design day maximum flow, an acceptable level of occurrence of shortfalls should be defined, and standby units are added only as required.

Probability theory would involve the considerations for:

Pipeline system (number of units): the physical pipeline system: size, length, station location and number of compressor/pump stations and units assumed/available

Flow rates: flow rates for various configurations of the pipeline system

Typical unit availability: the typical unit availability is the weighted average of all individual unit availabilities on the pipeline system. For example, if two units were available for operation 729 and 714 hours, respectively, of a total possible 744 hours a month, their unit availabilities would be $(729/744) 100\% = 98\%$ and $(714/744) 100\% = 96\%$. The "typical unit availability" would be $(98 + 96)/2 = 97\%$.

Probability theory application: Application of probability theory is to calculate a "probable average" flow rate or system capability for the pipeline. This consists of multiplying and summing the products of:

1. the representative average flow rate for each operating condition of units offline,
2. the probability for each number of units offline, and
3. the possible independent combinations for each number of units offline.

Determining the representative average flow rate consists of calculating the flow capability for all possible unit offline operating conditions.

Example. A pipeline has three stations, A, B, and C, each with 97% availability. There are eight combinations upon which the pipeline system can operate. These are:

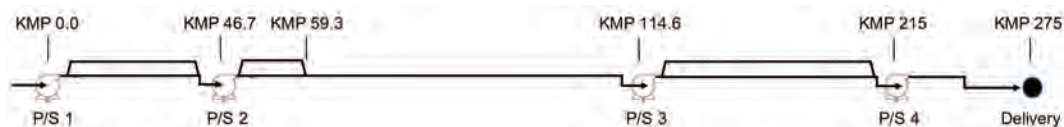
Operating Condition	Units Running	Units Offline	Number of Independent Combinations
All units running	ABC	0	1
One offline	BC	A	3
	AC	B	
	AB	C	
Two offline	A	BC	3
	B	AC	
	C	AB	
Three offline	0	ABC	1

With the use of the probability equation given above, it is then possible to calculate a percentage of time for operating conditions as given below. It may be noted that the number of combinations arrived at by deduction as given above equals the mathematical determination of the number of independent combinations.

Operating Condition	Number of Independent Combinations	Probability of Occurrence	Percentage of Time
All units running	$\frac{3!}{0!(3-0)!}$	$(0.03)^0(0.97)^{3-0} = (1)$ $(0.912673) =$	91.2673%
One offline	$\frac{3!}{1!(3-1)!}$	$(0.03)^1(0.97)^{3-1} = (3)$ $(0.028227) =$	8.4681%
Two offline	$\frac{3!}{2!(3-2)!}$	$(0.03)^2(0.97)^{3-2} = (3)$ $(0.000873) =$	0.2619%
Three offline	$\frac{3!}{3!(3-3)!}$	$(0.03)^3(0.97)^{3-3} = (1)$ $(0.000027) =$	0.0027%
TOTAL			100.0000%

This “percentage of time” can then be multiplied by representative flow rates for the operating conditions and a total average flow rate (or capability) obtained.

2.2.4.1 Exercise



For the above pipeline system with design/operating characteristics, establish:

1. Availability of each station in percent,
2. Number of combinations of pump station operating conditions, and
3. Percentage of probability of operating conditions using:

Percentage of time:

$$C = \frac{n!}{r!(n-r)!} p^r q^{(n-r)} \text{ (capability with } r \text{ units down),} \quad (2-7)$$

where

$$\begin{aligned} n &= 3 \\ r &= 0, 1, 2, 3 \\ q &= 97\% \end{aligned}$$

4. System capability

Design and operating characteristics

Pipeline diameter and wall thickness	28 in., 0.281 in.
Corrosion allowance	None
Design pressure	52.8 kg/cm ² (g) [750 psig, 5188 kPa (g)]
Maximum operating pressure	52.0 kg/cm ² (g) [740 psig, 5100 kPa (g)]
Pipe material	API 5L Grade X52 (with wall thickness rounded)
Up to nearest API table	
Pipe roughness	25.4 microns (0.001 in.), assumed
Depth of cover	1 meter (assumed) design factor 0.72
Ambient/air temperature	10°C (min.), 48°C (max.)
Ground temperature	25–35°C

Inlet temperature	10–48°C (winter-summer conditions)
Minimum delivery to and suction pressures to pump stations	
1.5 kg/cm ² (g) [150 psi (g), 1030 kPa (g)]	
Base pressure and temperature	101.326 kPa and 15°C
Design flow rate (4 pump stations)	3150 kL/hr (75.6 10 ³ m ³ /d, 457,510 BBLD)

Pump station information (all units operate in parallel)

Station	No. of Units/Brake Horse Power (BHP)	Station Availability/Month (hr)			
		Unit 1	Unit 2	Unit 3	Unit 4
1	3 (2388 BHP each) + 1 (2352 BHP)	744	736	740	Standby
2	3 (3136 BHP each)	716	729	736	None
3	2 (2400 BHP each) + 2 (2352 BHP each)	740	744	Standby	Standby
4	3 (2352 BHP each)	729	713	732	None

Crude viscosity data

Viscosity (cst)	Temperature (°C)
9.2	20
3.75	37.8
3.28	40
2.24	50

Pipeline right of way elevation profile

Kilometer Post	Elevation (m)	Kilometer Post	Elevation (m)	Kilometer Post	Elevation (m)
0.0	4.5	72.8	47.3	194.7	108.4
1.4	13.4	75.5	55.0	199.8	96.5
3.5	3.1	78.8	56.0	200.7	100.5
5.6	17.1	79.9	63.2	214.5	73.2
7.1	3.1	84.1	74.8	243.6	30.5
9.2	4.7	87.8	88.0	256.3	14.7
11.3	17.7	93.8	57.8	263.4	23.4
13.3	19.7	114.8	116.6	274.5	25.3
15.6	31.6	118.7	124.9		
17.9	9.2	126.8	154.4		
24.9	2.6	132.8	121.8		
29.4	18.6	136.9	170.7		
31.5	12.7	137.7	140.7		
38.0	25.0	138.9	185.7		
39.1	11.7	143.4	209.0		
40.9	29.5	146.4	170.6		
41.8	11.7	154.8	232.2		
46.6	22.6	165.0	176.8		
59.3	35.9	181.6	124.2		
63.0	52.7	189.0	116.4		
70.7	2.0	193.2	101.9		

2.3 PUMP STATION PIPING DESIGN

2.3.1 General Station Design

The design of a piping system can have an important effect on the successful operation of a centrifugal pump. Such items as sump design, suction piping design, suction and discharge pipe size, and pipe supports must all be carefully considered.

The following lists other physical requirements for centrifugal pump station piping design:

- Piping configuration: acceptable piping configurations should not cause excessive misalignment between the pump and driver.
- Fitting Limitations: commercially available/standard fittings follow ANSI pressure limitations [4]. There are very significant cost increases as the pressure rating class is increased, especially in the higher classes (i.e., ANSI 600, 900, and 1500). Care must be exercised when designing systems to ensure the ANSI class limits (pressure and temperature limitations) are not exceeded.
- Pressure relief: a centrifugal pump is limited to pressure and power for a given design and speed. A pressure relief valve is usually not required for the pumping system.
- Suction piping size and design: these need to be given careful consideration as many centrifugal pump troubles are caused by poor suction conditions. The suction pipe must not be smaller than the suction connection of the pump, and in general, at least one size larger is usually selected. Suction pipes are designed to be as short and as straight as possible.
- Piping velocity limitations: the general experience to limit suction pipe velocities between 1.5 and 2.5 m/s (5–8 ft/s) range depending on pipe size unless suction conditions are unusually good. Higher velocities increase the friction loss and can result in troublesome air or vapor separation. This is further complicated when elbows or tees are located adjacent to the pump suction nozzle and can result in uneven flow patterns or vapor separation keeping the liquid from evenly filling the impeller. Such a situation upsets pump hydraulic balance leading to vibration, possible cavitation, and excessive pump shaft deflection. Shaft breakage or premature bearing failure may also result.
- Suction lift: on pump installations involving suction lift, air pockets in the suction line can be a source of trouble. The suction pipes are generally designed to be perfectly horizontal, or with a uniform slope upward from the sump to the next pump. The piping is designed such that there will not be high points where air can collect and cause the pump to lose its prime. Eccentric rather than concentric reducers are also used with flat side up at the pump suction.

The piping layout for a pump station generally consists of station bypass valve, suction, and discharge headers and a pressure control valve (PCV) to control the discharge pressure. A sump system is also needed to enable pressure relief for maintenance and emergency purposes. It may include station filter/scrubber, a pig launcher and a pig receiver, and locations for corrosion coupons (if incorporated). The units will have typical pressure and temperature monitoring systems.

Figure 2-14 provides the general piping layout for a series pump arrangement when the pump station is operational and is receiving products from upstream locations.

When maintenance has to be done on high pressure piping or components or when hazardous conditions are detected, the station bypass valve opens, and the station suction and discharge valves close (Fig. 2-15). When the station suction and station discharge valves are

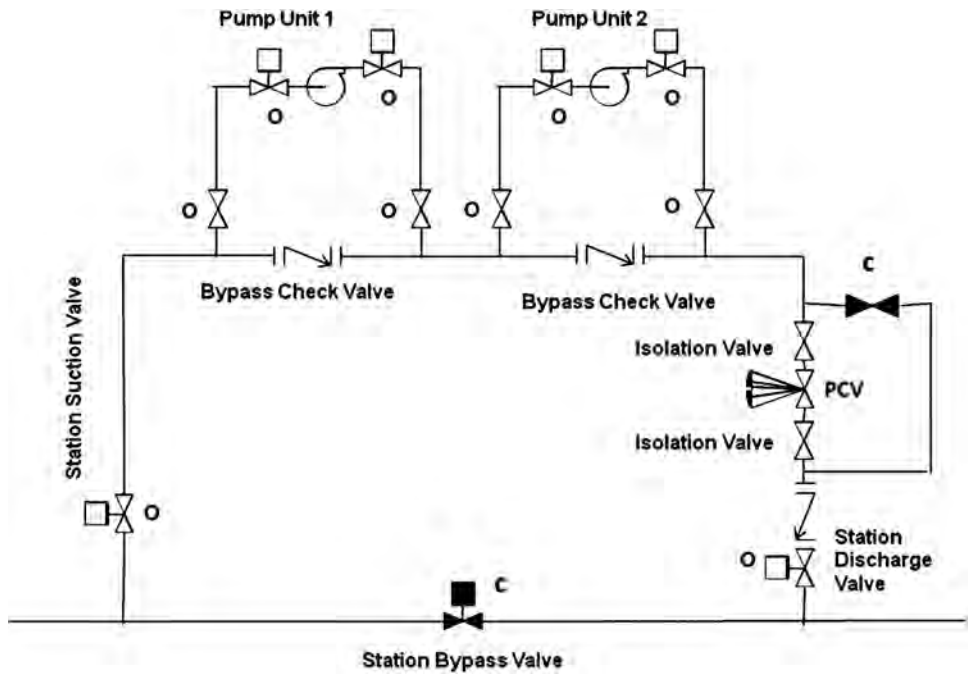


Figure 2-14. Basic pump station piping configuration (O = open, C = closed).

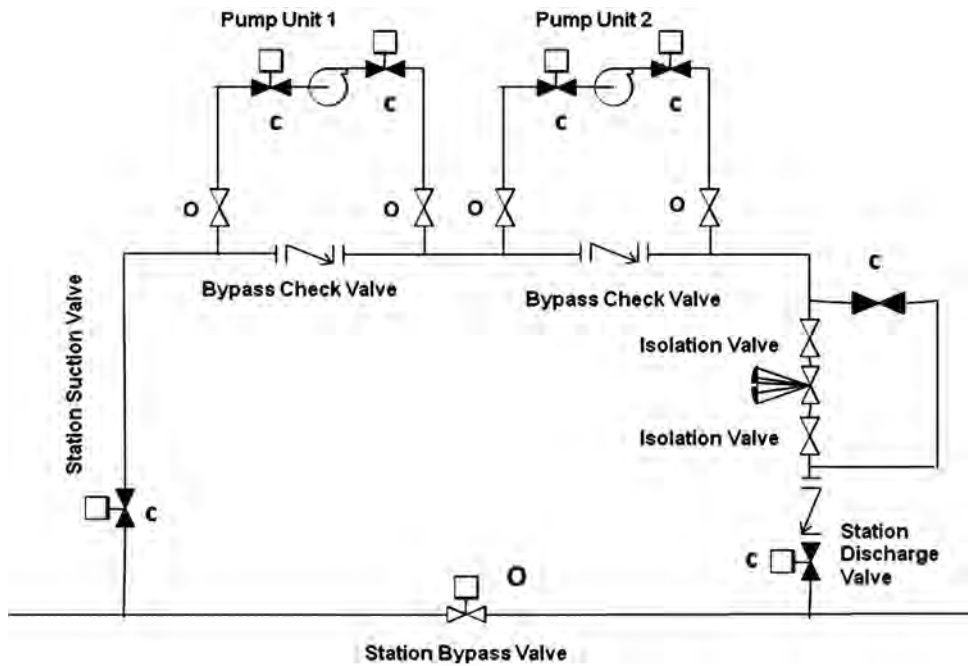


Figure 2-15. Pump station configuration under maintenance.

closed and the bypass valve is open, liquid is unable to enter the pump station and continues down the pipeline. This is the normal configuration for pump stations. Even when no pumps are turned on, the station isolation valves are left in the open position.

The piping system includes a station check valve downstream of the PCV to prevent back-flow into the station. There is also a bypass line around the PCV to enable maintenance of the PCV and permit operation to continue by manually throttling the bypass valve.

Under normal operating conditions, the station bypass valve is closed, and the station suction and station discharge valves are open. Even when the pumps are not turned on, liquids flow into the station. In some cases, the “bypass” valve is a check valve that is kept shut by the higher pressure on the discharge side of the station, so all the liquid flows into the station if one or more pumps are running.

Series operation is most common where the major purpose of the pumps are to overcome pipeline friction. Normally, up to three or more pumps are used in series with at least as a backup spare, which provides flexibility, particularly for pumps with constant speed motors (Fig. 2-16). There is also less difficulty from a starting and stopping point of view than a parallel configuration.

If there is a substantial increase in downstream elevation, parallel units are more appropriate since the head of the pump is already predetermined. Each unit then requires a separate discharge control valve (Fig. 2-17). In parallel pump configuration, the liquid splits into two (or more) streams. Each stream flows through one pump only. After being discharged from their respective pumps, the two streams flow into a header where they are recombined.

If more flexibility is needed, the design may call for a combined series/parallel configuration (Fig. 2-18). However, it may be noted that this arrangement is an effective but inefficient method of minimum flow protection.

Often, there is a set of series-configured pumps already in place, and a single pump is installed parallel to the whole series (Fig. 2-18). Since the parallel pump must produce the same pressure as the series pumps' combined discharge, parallel pumps are usually multi-stage.

Generally, for fixed speed units, it is normal practice for both suction and discharge valves to be closed on shutdown. The suction valve is then opened fully, and the discharge valve is

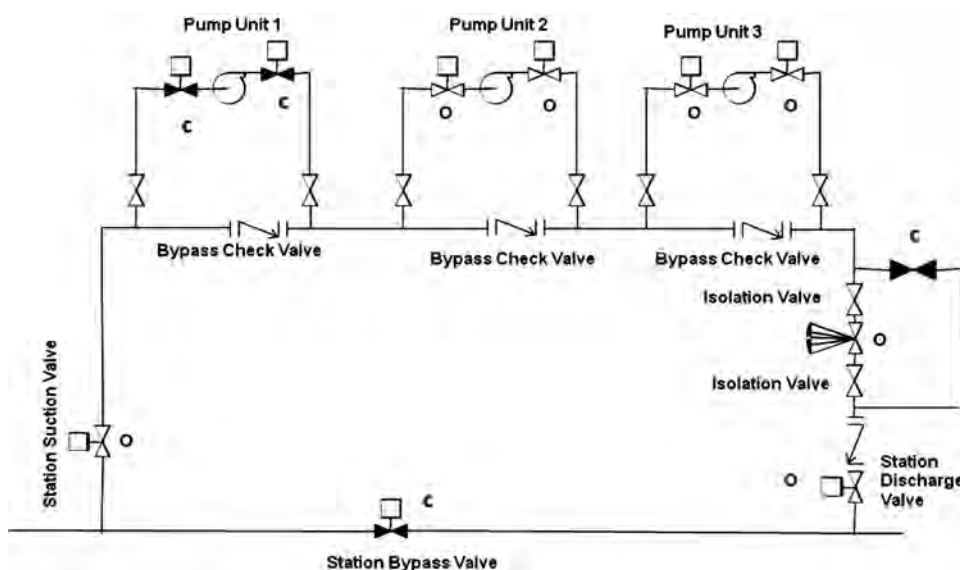


Figure 2-16. Series pumping piping arrangement.

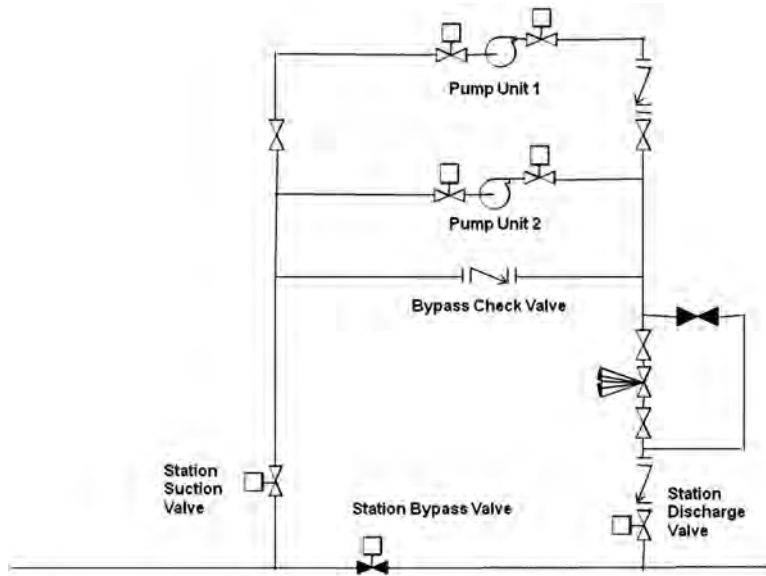


Figure 2-17. Parallel pumping piping arrangement.

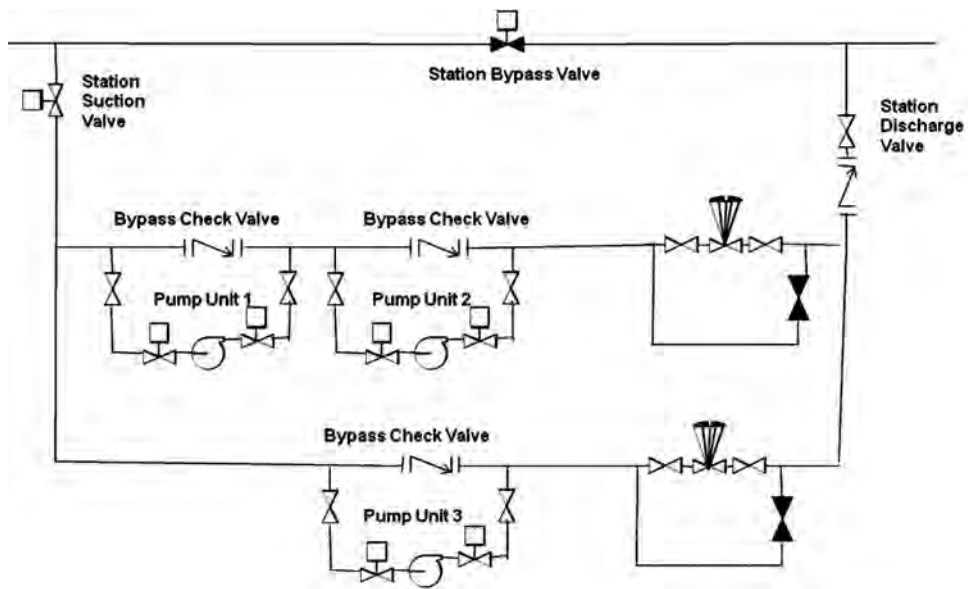


Figure 2-18. Combined series/parallel station piping configuration.

opened partially to provide some head as the motor starts until the final speed has been reached, after which the discharge valve is fully opened. A faster start sequence is to keep pumps at fully primed condition on shutdown with the suction valve open and the discharge valve closed as shown in Fig. 2-19(a). This configuration will utilize minimal power, letting the driver run up to speed quickly, also against a partially open discharge valve. The discharge valve is then fully opened slowly to avoid pressure surges. Starting a pump with the discharge valve wide open takes the maximum amount of power and may overload an electric motor driver if used. Delayed opening of the discharge valve can heat the liquid, potentially to high temperatures.

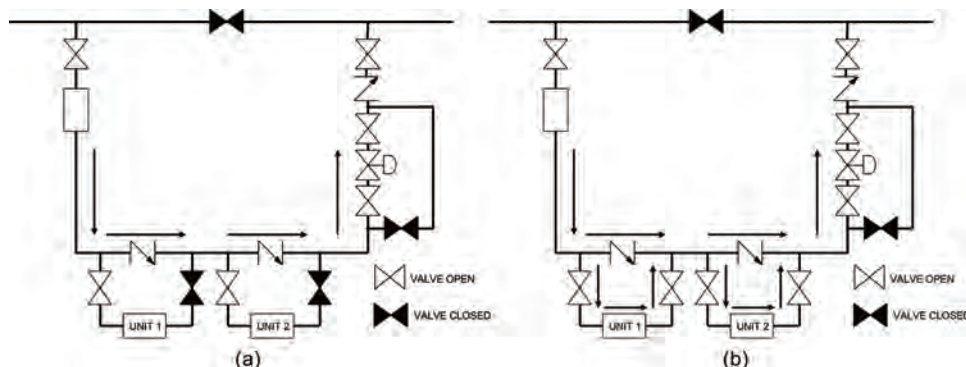


Figure 2-19. Pump unit fast start-up valve positions for (a) a single product (b) batched products.

The fast start sequence is then:

- start the motor cooling fan
- start bearing oil pumps
- partially open the discharge valve
- start the motor with vibration switches inhibited
- fully open the discharge valve

For refined products that are batched, the shutdown position has both suction and discharge valves open to minimize batch contamination (Fig. 2-19(b)). The start sequence is then:

- start the motor cooling fan
- start bearing oil pumps
- partially close the discharge valve
- start the motor with vibration switches inhibited
- fully open the discharge valve

Where a VFD is available, both suction and discharge valves can be fully open when the motor is started since this provides a smooth ramp-up of speed and pressure.

No pump should ever be throttled by the suction valve, as this is likely to create cavitation and damage the pump. Severe cases result in loss of performance due to internal pump damage. While it is possible to throttle on discharge valve, on a large or high head pump, this is likely to damage the valve over time, and tight closure of the valve will then not be possible.

2.3.2 Station Piping Design

2.3.2.1 General

Design of pump stations has evolved over time with objectives of a design study by a major pipeline company [9] that included:

- improvement of operational integrity
- reduction in station construction costs
- improvement in station constructability
- improvement in environmental protection

Improving operational integrity includes elimination of buried piping that cannot be internally inspected. This objective also means that equipment is to be readily accessible for

maintenance and “dead ended” piping should be minimized to reduce contamination between batches. These maintenance requirements do not permit burying of piping components like instrumentation, flow meters and pressure control valves.

Reductions in station construction costs are obtained by minimizing pipe, fitting and equipment sizes. A typical 4-unit, NPS 24 station has been consolidated such that total extend of the station piping is less than 100 m. Culverts are not acceptable for access to larger equipment, so keeping piping systems aboveground also helps to minimize the length of piping, number of fittings and welded joints needed to “porpoise” buried piping aboveground to allow access to these components. Due to this advantage and others, it became an early design philosophy to keep station piping above grade.

Keeping station piping aboveground also improves constructability as it increases the potential for prefabrication. Aboveground piping also minimizes the costs associated with excavation, shoring, treatment of groundwater collecting in excavations and the complexities attendant with confined spaces.

Finally, improvements in environmental protection are achieved by upgrading containment for minor leaks and improving detection of major leaks. These improvements would also include the potential to minimize cleanup costs associated with a leak resulting from an operational error and minimize site disturbance during construction.

These design objectives are not mutually exclusive. Concepts that emerged included: keeping the piping aboveground; creation of better containment and detection systems; and minimization of pipe, fitting and equipment sizes. To further eliminate buried piping, an aboveground sump tank was incorporated into the design so that all drain lines would be aboveground. Putting the sump tank aboveground also minimizes drain line runs as it can be placed in closer proximity to the drain source. This is an incidental use tank, not a storage tank, and is empty most of the time. Aside from compliance with accepted tank construction and venting standards, it does not pose a safety risk.

2.3.2.2 Station Piping Layout

In terms of piping geometry (isometrics), there are two commonly used designs shown in Figs. 2-20 and 2-21. The first design (Fig. 2-20) offers more piping flexibility and is less prone to high thermal stresses. The unit by-pass check valves are installed on a relatively short pipe connection suction to discharge, hence is less susceptible to contamination between batches due to the relatively short dead legs. The main disadvantage of this design is the large number of fittings, in particular elbows, resulting in higher cost. The second design (Fig. 2-21) involves lower number of fittings (elbows), hence would be lower in cost relative to the first design. However, this design, is stiff in terms of piping flexibility and might lead to higher loads on pump nozzles and increased pipe stresses. In addition, the longer dead-legs of the pump by-pass may lead to significant contamination between product batches, as these dead-legs will be filled with stagnant product from a previous batch that would slowly trickle out when the following batch arrives. This has been discussed in more detail in [10,11].

2.3.2.3 Pipe Sizing

At the outset of design efforts [9], pipe sizing was based on limiting the velocity in station piping to 3.65 m/s (12 ft/s). It was felt that this limit was too conservative. Pipe sizes determined by this method yielded lower pressure drops, but it also resulted in significantly higher station construction costs and greater pipe stresses owing to the larger and more rigid piping. This limiting velocity was based on recommendations in API RP 14E [12].

Many publications have shown API RP 14E to be too conservative. It was subsequently decided to increase the limiting velocity based on the work of Salama [13] on piping erosion with fluids containing sediment. The accuracy of his work was verified by four independent laboratories by measuring erosion rates in pipe bends. Testing of various crude streams

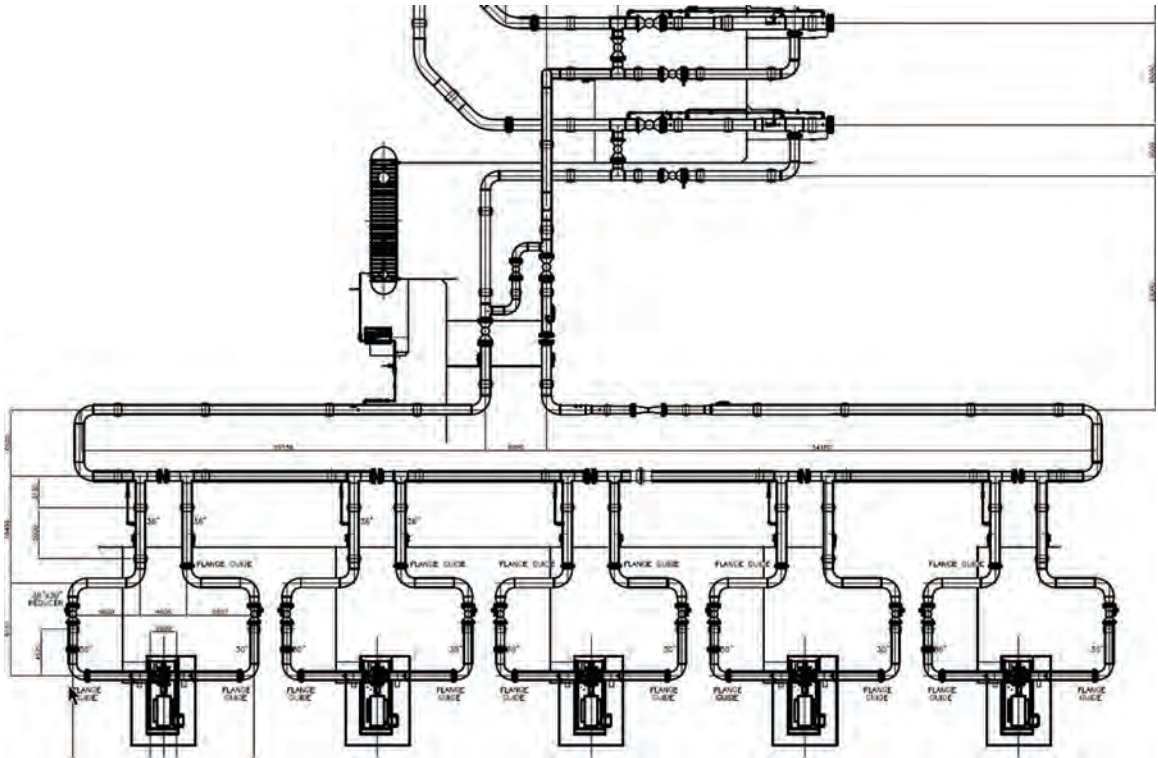


Figure 2-20. Typical piping design (1) of a multi-unit pump station series-configuration.

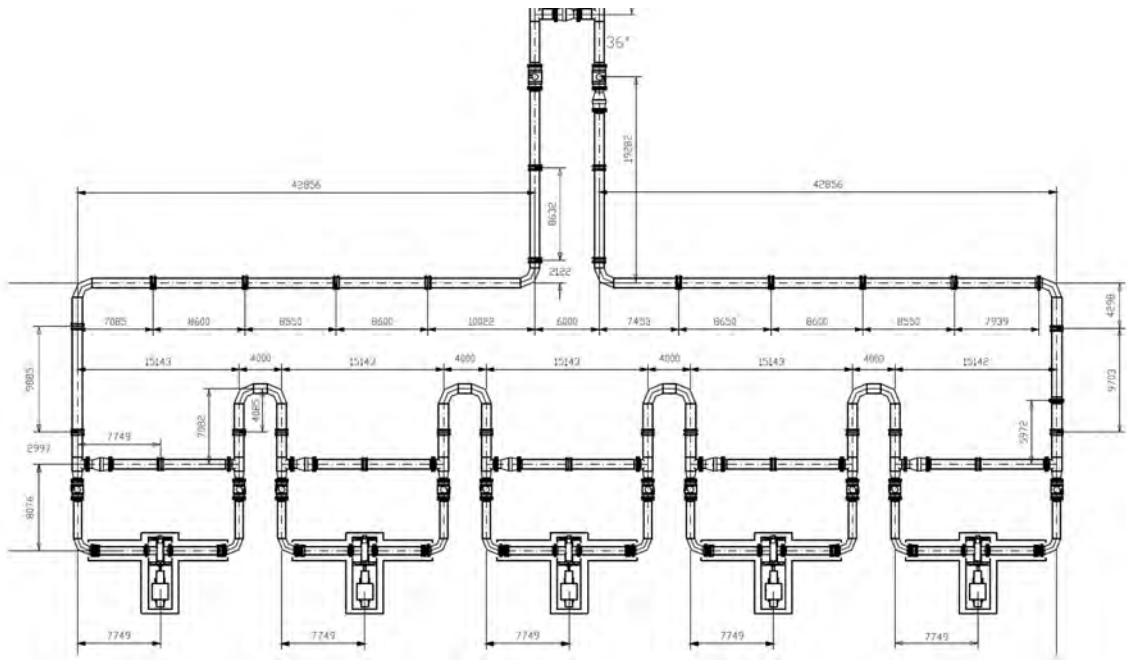


Figure 2-21. Typical piping design (2) of a multi-unit pump station series-configuration.

helped to determine a basis for particulate size and concentration. This work indicated that a maximum velocity of 11.74 m/s (38.5 ft/s) in crude oil would result in an acceptable erosion rate. Therefore, the limiting velocity was increased to 6.1 m/s (20 ft/s). This decreased the station piping size from NPS 30 to NPS 24, saving over \$2.5 million per station (see also Sections 2.4.2 and 2.4.3).

2.3.2.4 Pump Piping Design

One of the major determinants of pump station piping design is the hydraulic considerations associated with the pumps [9]. Elbows generate turbulence that can affect the flow distribution entering a pump nozzle as shown in Fig. 2-22. This is particularly problematic on the single-stage double suction pumps most commonly used in pipeline applications. Company required keeping suction elbows out of plane with the pump axis or adding 5D to 7D of straight pipe between the elbow and the pump suction.

Adding straight pipe to the pump suction to keep the piping flat increases the spacing between the pumps and ultimately increases the footprint of the station. This configuration also inhibits access to the pump for maintenance and usually requires more pipe and fittings to achieve the necessary piping flexibility. Therefore, the most common piping schemes keep the elbows vertical with 2D of straight pipe between the elbow and the pump suction. This ensures the turbulence induced by the elbow in the vertical plane does not affect the axial or horizontal flow split in the pump case as the fluid is distributed between the two suction eyes of the pump impeller.

Past practice turned the elbows down to allow good access to the pump, but the pump suction and discharge lines had to be routed under the pump house floor which made inspection problematic and also increased construction challenges. As pumps became larger, it became common to elevate the pumps such that a horizontal flange pair could be installed near floor level at the base of the elbow to facilitate removal of the piping and to add a degree of flexibility in the fit-up of the piping. Alternately trenches or basements have been employed to allow access to the piping, but this introduces structural complexity and, added cost, and also creates a confined space.

Some station designs have been executed with the pump elbows turned up. The advantage of this type of arrangement is that the pump and motor can be placed at ground level providing good access to the equipment while eliminating the need for platforms. The

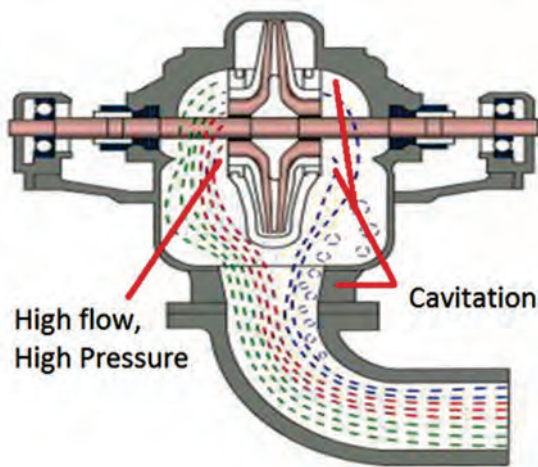


Figure 2-22. Flow distortion due to an elbow upstream of a double-suction pump [9].

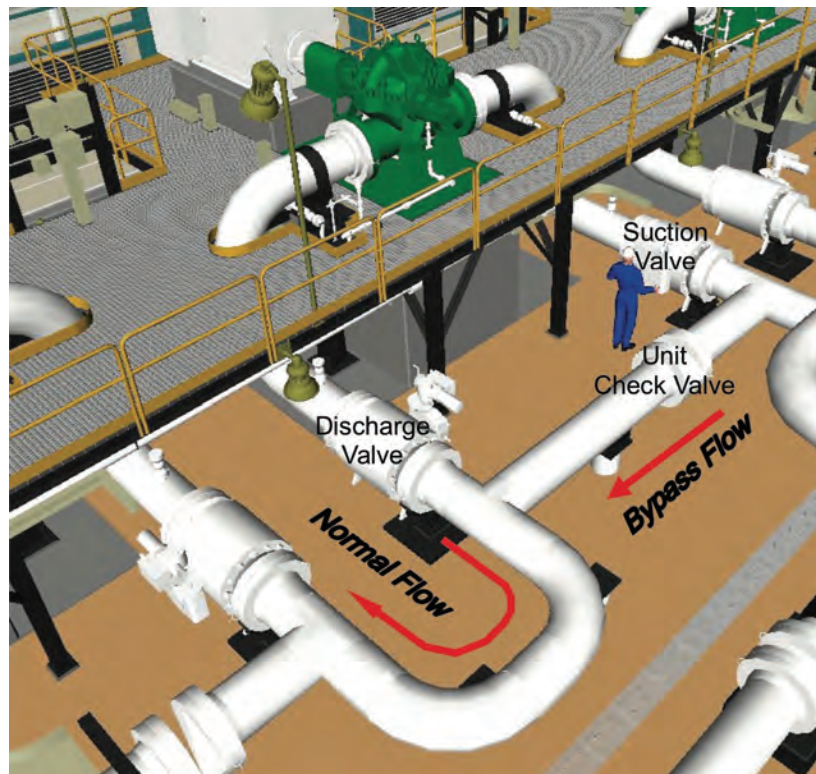


Figure 2-23. Pump unit piping [9].

drawback with this design is that what goes up must come down. There is a significant volume of additional fluid in these vertical loops that has to be drained to allow equipment maintenance. Proper venting of the loops can be problematic, and this approach requires extra fittings, pipe and welded joints. While these vertical loops can provide excellent flexibility, this can also be a drawback as they need to be stabilized to prevent excessive vibration. Due to adverse experiences, this type of design is discouraged.

The approach adopted was to elevate the pumps on raised foundations to allow the elbows to be placed in a vertical down orientation (Fig. 2-23). The pumps were elevated so that all station piping was kept aboveground for ease of access and leak monitoring. This configuration requires the addition of an access platform around the pumps and motors, but it allows a critical ancillary benefit. The sump tank and associated drain piping can be brought aboveground. The pumps can drain by gravity to the sump tank and the sump can be placed on the pump shelter containment slab which in turn provides secondary containment and leak monitoring.

2.3.2.5 Header Piping Design

The other major hydraulic consideration is in the manifolding or interconnection of the mainline pumps. Pumps can be connected in either series or parallel to provide the specific combination of flow and pressure required. Most systems are currently being designed to accommodate higher viscosity crudes. Due to the steep “system curve” or higher pressure gradient associated with viscous crudes, series pumping configurations tend to provide the greatest utility.

The general configuration (Fig. 2-24) starts with the station suction entering one end of the pump shelter with connection to a Tee at the suction of the first pump. The Tee

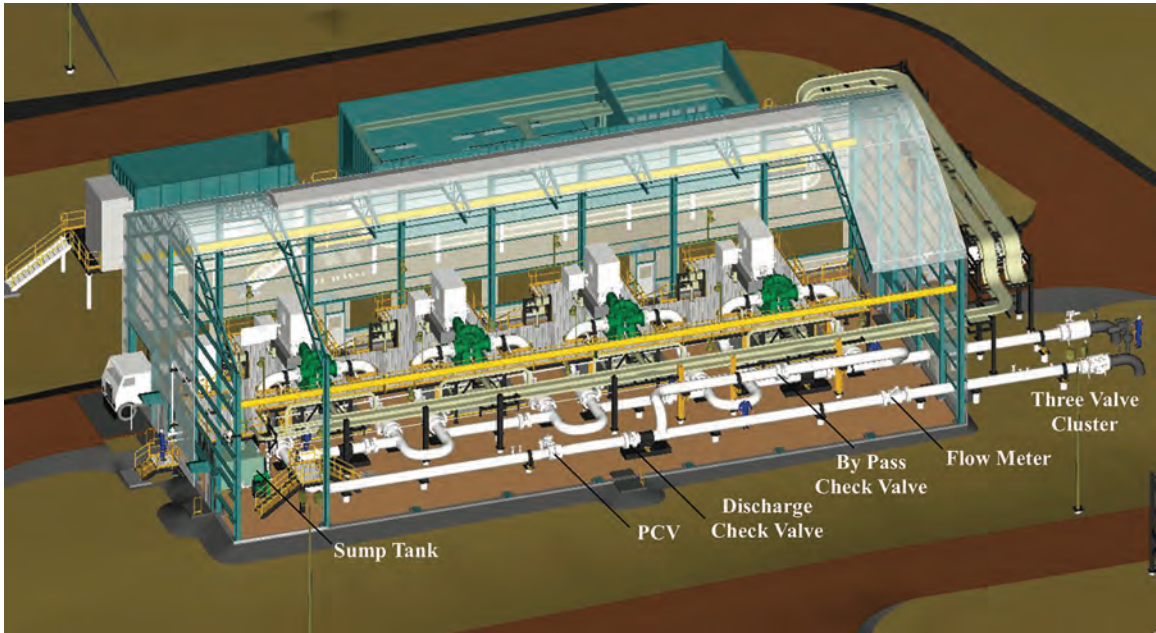


Figure 2-24. Station piping layout [9].

directs the flow into the suction of the first unit or allows the flow to bypass the pump if it is out of service. The bypass outlet from the Tee is the beginning of the “station header”. This common length of piping provides the manifold that connects to the suction and discharge of each pump. Each pump has a valve on the suction and discharge piping to allow isolation for maintenance.

The length of station header between the pump isolation valves includes a check valve. This check valve closes to prevent recirculation from the pump discharge to its suction during normal operation. When the pump is isolated, this check valve opens to allow flow to bypass the pump as shown in Fig. 2-23. There can be significant turbulence at the discharge Tee as the flow turns into the header. This turbulence can cause the check valve to remain open temporarily during pump start-up. If the check valve remains open as the pump continues operation, it will eventually close under full differential pressure developed by the pump. Closure of the check valve under these conditions will cause water hammer and premature wear to the check valve seats. For this reason, the check valve is usually positioned closer to the suction Tee to minimize the influence of the turbulence at the discharge Tee.

After the last pump, the header is normally turned back 180° towards the 3-valve cluster. This “return” header provides the necessary straight pipe for the pressure control valve (PCV) if required and the station flow meter. The flow meter was not always a common component of pump station design, but it is now considered essential to augment the accuracy of leak detection systems. To obtain the desired accuracy, company standards require 20D of straight pipe immediately upstream of the meter and 10 D downstream.

The bypass check valve is only required on pump stations that employ PCVs. This safeguards against inadvertent closure of the PCV. If such an event occurs, it can cause a significant transient and lead to a cascading shutdown of the pipeline. To prevent damage and this loss of control, a bypass line complete with check valve is installed connecting the station suction to the return header downstream of the PCV, but upstream of the station flow meter. This provides an alternate “relief” flow path should the PCV close while continuing to provide flow measurement. The 20D of straight pipe required upstream of the flow

meter means this line is significantly longer than it would be prior to the inclusion of the flow meter.

The station discharge check valve is usually positioned between the PCV and the bypass connection to the return header. The function of the discharge check valve is to prevent a major back flow through the station that might cause the loss of line pack or an idle pump to “windmill” in reverse rotation. Starting a pump under this condition could cause shaft or coupling damage. The one unintended outcome of adding this check valve is that it can separate the header into two sections complicating thermal relief.

2.3.2.6 Valve Selection

Historically station designs used through conduit, slab gate valves for all large bore piping [9]. This type of valve has been favored for pipeline applications because it is simple, relatively low in cost, includes a double block and bleed capacity (DBB) and can be maintained in place as it is normally a top entry design. The problem with this type of valve is that they are a rising stem design, so the actuator is located on top. Due to the tall body, a platform is required to access the actuator. Another feature of the design is that the valve body is isolated from the flowing fluid when it is fully open or closed. This minimizes contamination between the flowing fluid and the fluid trapped in the valve body cavity. The problem with this feature is there isn't a lot of mixing as the valve transitions and emulsified water can precipitate out of the crude and become trapped in the valve body where it can freeze.

Ball valves are being used more extensively in the pipeline industry as they are more compact, and competitively priced. They can also eliminate the need for platforms to access the actuator. They also have the added benefit of providing greater flushing of the body cavity as the ball transitions between the closed and open position.

There have been some adverse experiences with the use of ball valves in liquid pipelines. The one assumed weakness of the ball valve with the stem in the vertical position was the lower trunion bearing. The result is that water could precipitate into this region like the slab gate and cause corrosion of the trunion bearing or inhibit valve operation if it became frozen. The option to install the valve with the stem in the horizontal orientation. This alignment had two other benefits; it positioned the actuator on the side of the valve where it can be accessed without a platform and changed the rotation of the ball such that it mimicked the movement of the gate in a slab gate valve.

2.4 CONTAMINATION IN LIQUID PIPELINES

2.4.1 Contamination Between Products

Batch transportation of different crude grades and petroleum products through the same pipeline is a current practice globally. Examples are transporting heavy and light crudes from production facilities to refineries or export terminals. Unless mechanical separators such as scrapers or pigs are employed, there will be a certain amount of mixing between products which is often called interfacial contamination between batches. From an operational perspective, the occurrence of contamination implies additional costs related to handling the contaminated volumes between the batches at the delivery terminal and, of course, the associated commercial aspects of these mixed volumes. Thus, minimization of interfacial contamination between batches should always be pursued.

The literature contains several key papers and theories dealing with turbulent diffusion between batches in a pipeline. Austin and Palfrey [14] examined turbulent flow in pipelines with the intent of deriving empirical relationships between the length of the mixed region between the leading and trailing interface in a pipeline, and select dimensionless

flow characteristics, primarily Reynolds number. Primary factors affecting the length of the mixed region were considered as distance traveled along the pipeline, viscosity and density of the two products, relative roughness of the pipe, mean flow velocity, inside diameter of the pipeline and the intensity of turbulence. They listed the factors that have been found by experience to increase the level of mixing between two batches in a pipeline. These are:

- laminar flow at start-up of a pumping operation
- slow valve switching from the leading product to the trailing product
- sharp bends and other complicated piping features
- passage through filters, which can lead to a brief section of laminar flow

Levenspiel [15] affirmed the notion that in turbulent pipe flow molecular diffusion does not affect the extent of mixing to any appreciable amount. Songsheng and Jianing [16] developed equations that are used in a 2-D finite difference method, which predicted the “tail effect” observed earlier by Austin and Palfrey. Variations of the mixing length between different fluids in a pipeline then emerged [17–23] and generally take the form:

$$x = \lambda d^\alpha L^\beta \text{Re}^\gamma \quad (2-8)$$

where λ , d , L , and Re are correlation constants depending on the whether the flow is laminar or turbulent.

Fundamentally, axial diffusion of two different fluids (e.g. heavy and light crudes) is governed by the general one-dimensional diffusion equation in the form [24]:

$$\frac{\partial c}{\partial t} = D \frac{\partial^2 c}{\partial x^2} \quad (2-9)$$

where D is the diffusion coefficient (diffusivity) between the two fluids. Solution of this equation delineates the spread (x in Fig. 2-25) of the interface contamination of one batch into the other (primarily by turbulent diffusion) after an elapsed time $t = L/U$. Sherwood

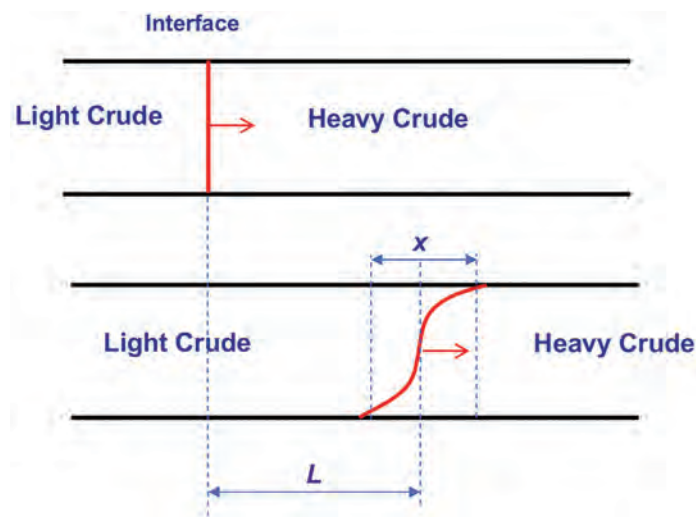


Figure 2-25. Schematic of interface development due to axial turbulent mixing between heavy and light crude batches (L is the distance along the pipeline from the start to the location of the mid concentration point within the mixed zone).

et al. [24] examined key theories developed in the topic area of axial dispersion in pipelines. The authors reaffirmed that dispersion is greater if flow is laminar by stating that an increased velocity gradient increases axial dispersion. They also discussed a paper by Taylor [25], where it was determined that given a specific velocity profile, the effective axial dispersion coefficient can be found. Using a “universal velocity profile,” Taylor [26] arrives at the following relationship:

$$\frac{D}{Ud} = 3.575\sqrt{f} \quad (2-10)$$

which is valid for $Re_d > 10,000$. The Fanning friction factor ($f = \lambda_d/4$) is a function of Reynolds number and the relative roughness of the pipe which can be determined from the Colebrook-White equation in implicit form [27]:

$$\frac{1}{\sqrt{\lambda_d}} = 2 \log \left(\frac{k_s}{3.71d} + \frac{2.51}{Re_d \sqrt{\lambda_d}} \right) \quad (2-11)$$

The correlation given by Eq. 2-10 matches very well with those published in the literature [24] and summarized in Fig. 2-26. The concentration profile across an interface between different fluids in a pipeline has been derived [28] and takes the form:

$$c(x, t) = \frac{1}{2} \left(1 \pm \operatorname{erf} \left(\frac{x}{2\sqrt{Dt}} \right) \right) \quad (2-12)$$

where, c is the concentration, x is the spatial distance along the interface with the origin taken from the 50% concentration point and t is the time elapsed since the two fluids came in contact with each other. To make this diffusion equation specific to pipeline problems

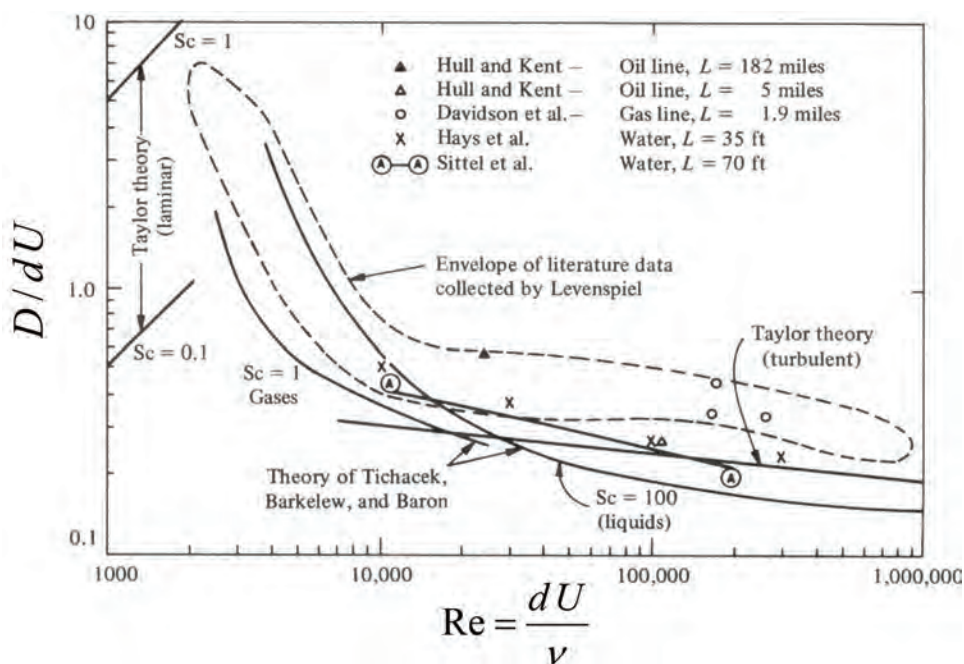


Figure 2-26. General correlations for axial diffusion coefficient [28].

where the mean flow velocity is known, the time (t) can be replaced with the length of pipeline traveled (L) divided by the mean velocity of flow in the pipeline (U).

This equation does not allow for the diffusivity coefficient (D) to vary with time, which is assumed in the present work since the properties of the two crudes do not vary significantly as they travel down the pipeline. However, different D could be assigned to different sections of the pipeline if deemed necessary.

An example of determining the interfacial contamination is taken from Keystone pipeline from Hardisty (Canada) to Patoka (US). There are 39 pump stations along this line with multiple pump units incorporated in each station along a 2982 km, NPS30/36 pipeline. Comparison of this concentration profile with that based on axial diffusion along this 2982 km pipeline (and use of Eq. 2-12) is shown in Fig. 2-27. Properties of the crude, and flow characteristics and resulting diffusion coefficient are given in Table 2-2 [29]. It is shown that first, the leading part of the spread is in very good agreement with the predicted axial

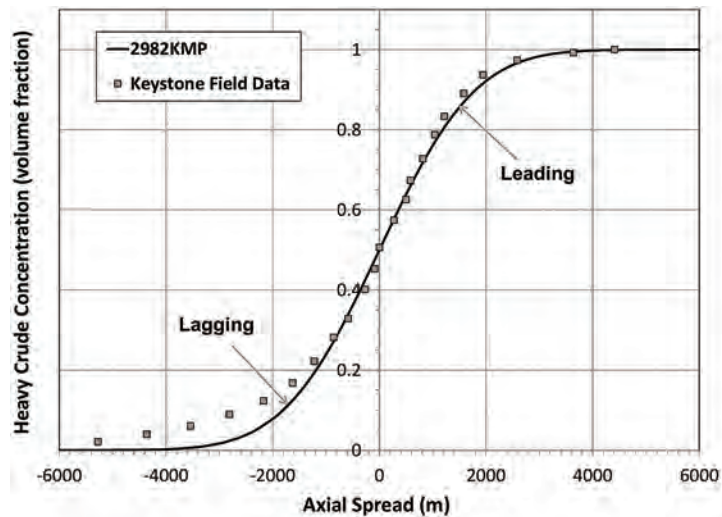


Figure 2-27. Comparison between field data from Keystone Pipeline and strictly axial diffusion along the pipeline based on the condition in Table 2-2.

Table 2-2. Keystone pipeline flow and crude characteristics [29]

	Heavy Crude	Light Crude
Density (kg/m^3)	920	864
Viscosity (Pa.s)	0.245	0.0063
Internal Diameter (mm)	742	
Velocity (m/s)	1.349	
Re	7106	
Fanning Friction Factor	0.00854	
Diffusion Coeff (m^2/s)	0.450	

diffusion along a length of 2982 km of the pipeline at a flow velocity of 1.349 m/s. Secondly, there is an increase in the spread at the trailing part from −3232 m (due to axial mixing only, solid line) to −5600 m (both taken at 1% concentration). This is an increase of 2368 m over a total spread of 6464 m (between concentration levels of 99% to 1%). This amounts to a 36.6% increase. This is likely due to additional contamination from minor dead-legs in the 39 pump stations and other side dead-legs along the length of the pipeline.

2.4.2 Erosion Due to Solid Contamination

A common problem in petroleum pipeline, particularly in heavy crude transportation is erosion due to solid (sand) particles and bottom sediments and water (BSW). There are numerous erosion models in the literature for both solids and liquid loadings in liquid flow. Parsi et al. [30] provided a comprehensive review of solid particle erosion modeling for oil and gas wells and pipelines applications. The most notable and widely used models for solid loading are those by Det Norske Veritas DNV [31] and Zhang et al. [32]. These two models are described below in Sections 2.4.2.1 and 2.4.2.2, respectively.

2.4.2.1 DNV Erosion Model

The DNV model [31] was formulated based on an extensive review of experimental investigations from the literature, experimental results obtained over time by DNV and experience. The majority of empirical data used for model development was obtained at low pressure with small line size pipe. Extrapolation to field conditions was performed based on model simulations and engineering justifications. The functional form of the erosion equation is the same as that of the Finnie model [33], but uses a high-order polynomial fit for the impact angle function for ductile materials and a simple linear equation, for brittle materials:

$$SE = Kv^n f(\alpha) \quad (2-13)$$

where SE is the specific erosion defined as the ratio of the amount (by mass) of material removed to the amount (by mass) of impacting solid material, v is the impact velocity and α is the impact angle in radians (90° is perpendicular). The impact angle function is given as:

$$f(\alpha) = 9.37\alpha - 42.295\alpha^2 + 110.864\alpha^3 - 175.804\alpha^4 + 170.137\alpha^5 - 98.398\alpha^6 + 31.211\alpha^7 - 4.17\alpha^8 \quad (2-14)$$

for ductile materials. This function is shown in Fig. 2-28. Note that the maximum erosion rate is at $\alpha = 30$ – 40 degrees.

For brittle materials, the angle function is given as:

$$f(\alpha) = 2\alpha/\pi \quad (2-15)$$

The default constants are: $K = 2 \times 10^{-9}$ for steel and the velocity exponent $n = 2.6$.

An example calculation for oil velocity of 2.7 m/s in a pipe fitting of internal diameter = 0.736 m is given in Table 2.3. In this example, the erosion rate in terms of material wall thickness loss over 10 years of continuous service of a solid loading of 0.1% or 1000 ppmW (by weight) is approximately 1.38 mm.

2.4.2.2 Zhang et al. Erosion Model

The form for specific erosion proposed by Zhang et al. [32] utilizes a lower-order polynomial equation for the impact angle function as compared to the DNV model. A sharpness

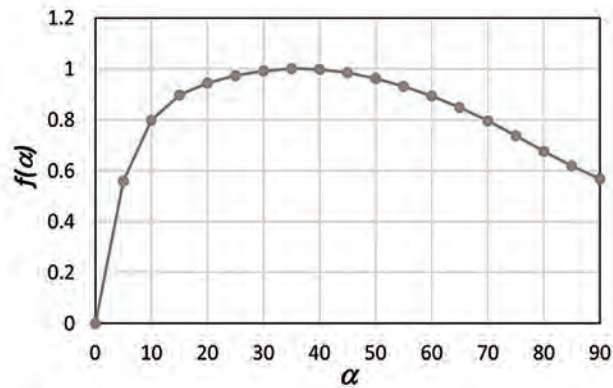


Figure 2-28. Impact angle function in the erosion model of DNV [31].

Table 2-3. Example of erosion rate calculation based on the DNV model

Velocity	2.7	m/s
Impact angle	35	degrees
	0.61	Radians
$f(\alpha)$	1.0	for ductile
	0.39	for brittle
n	2.6	
K	2.00E-09	
Specific erosion (SE) - by mass	2.65E-08	for ductile
Liquid density	833	kg/m ³
Stream diameter	0.736	m
Stream X-area	0.425447044	m ²
Mass flow	956.8729456	kg/s
Solid loading (by mass)	1000	ppmW
Solid density	2400	kg/m ³
Impacting material	0.956872946	kg/s
Material removed	2.54E-08	kg/s
Material loss in 10 years	1.38	mm

factor F_s for the solid particles is also included in the equation. The Zhang et al. [32] equation is expressed as:

$$SE = K F_s B_h^{0.59} v^n f(\alpha) \quad (2-16)$$

where again, SE is the specific erosion defined as the ratio of the amount (by mass) of material removed to the amount (by mass) of impacting solid material, v is the impact velocity and α is the impact angle in radians (90° is perpendicular). The impact angle function is given as:

$$f(\alpha) = 5.4\alpha - 10.11\alpha^2 + 10.93\alpha^3 - 6.33\alpha^4 + 1.42\alpha^5 \quad (2-17)$$

This function is shown in Fig. 2-29. Note that the maximum erosion rate is at $\alpha = 50$ degrees.

The default constants for this model are: $K = 2.2 \times 10^{-7}$, the velocity exponent $n = 2.41$, $F_s = 0.2$ for fully rounded particles, $=0.53$ for semi rounded particles, and 1.0 for sharp particles. The default Brinnell hardness parameter $B_h = 485.5$.

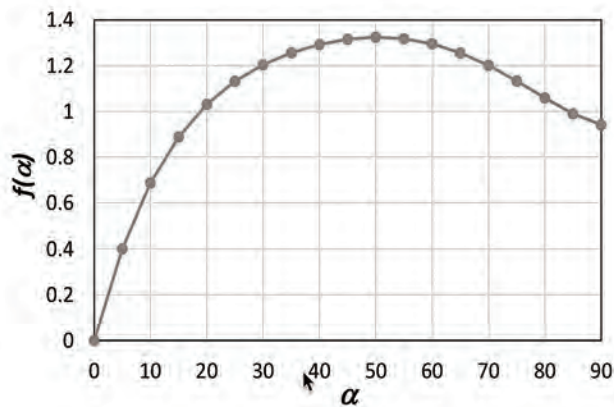


Figure 2-29. Impact angle function in the erosion model of Zhang et al. [32].

Table 2-4. Example of erosion rate calculation based on Zhang et al. Model [32]

Velocity	2.7	m/s
Impact angle	50	degrees
	0.873	Radians
$f(\alpha)$	1.325	for ductile
	0.56	for brittle
n	2.41	
K	2.20E-07	
F_s	0.53	
B_h	485.5	
Specific erosion (SE) - by mass	4.40E-08	for ductile
Liquid density	833	kg/m ³
Stream diameter	0.736	m
Stream X-area	0.425447	m ²
Mass flow	956.8729	kg/s
Solid loading (by mass)	1000	ppmW
Solid density	2400	kg/m ³
Impacting material	0.956873	kg/s
Material removed	4.21E-08	kg/s
Material loss in 10 years	3.07	mm

Calculation for the example parameters above and using Zhang erosion model gives an erosion rate in terms of material wall thickness loss over 10 years of continuous service of a solid loading of 0.1% (by weight) = 3.07 mm as shown in Table 2-4.

2.4.3 DNV RP O501 Erosion Model for a 90 deg Elbow

The DNV Recommended Practice RP-O501 [31] also contains a model for the calculation of the erosion rate on an elbow. This model is comprehensive in the way that it takes most parameters that are thought to impact erosion rates into account, such as the fluid properties, pipe properties, solid content and impact angle. It is current relative to other models that are used to calculate the erosion rates on an elbow. The calculation procedure to determine the erosion rate on an elbow based on the DNV erosion model (in mm/year) is given in the following steps:

1. Calculate the impact angle based on the elbow's radius of curvature (R_c):

$$= \arctan \frac{1}{\sqrt{2R_c}} \quad (2-18)$$

2. Calculate the impact angle function:

$$F(\alpha) = \sum_{i=1}^8 (1)^{i+1} A_i \alpha^i, \quad (2-19)$$

where, the values of A_i are listed in Table 2-5.

3. Calculate the normalized particle diameter (d) w.r.t. elbow inner diameter (D):

$$\gamma = d/D \quad (2-20)$$

4. Calculate the flow Reynolds number based on elbow inner diameter:

$$\text{Re}_D = \frac{\rho u D}{\mu} \quad (2-21)$$

where, Re_D is the Reynolds number based on the elbow inner diameter (D), fluid density (ρ), flow velocity (u) and fluid viscosity (μ).

5. Calculate the density ratio between solid (ρ_s) and fluid (ρ):

$$\beta = \rho_s / \rho \quad (2-22)$$

6. Calculate the dimensionless parameter group κ :

$$\kappa = \frac{\text{Re}_D \tan \alpha}{\beta} \quad (2-23)$$

7. Calculate the critical normalized particle diameter:

$$\gamma_c = \begin{cases} \beta^{-1} [1.881 \ln(\kappa) - 6.04]^{-1}, & \gamma_c < 0.1 \\ 0.1, & \gamma_c \geq 0.1 \end{cases} \quad (2-24)$$

8. Calculate the viscosity correction factor:

$$G = \begin{cases} \gamma / \gamma_c, & \gamma < \gamma_c \\ 1, & \gamma \geq \gamma_c \end{cases} \quad (2-25)$$

9. Calculate the erosion rate:

$$\text{Erosion Rate (mm/year)} = \frac{7.875 \times 10^4 \rho_y G K F(\gamma) \sin(\gamma) u^{n+1}}{\rho_m} \quad (2-26)$$

where n is the velocity exponent ($=2.6$) and K is the material constant ($=2 \times 10^{-9}$ for ductile steel), y is the solid loading (in ppmW) and ρ_m is the elbow wall material density.

Table 2-5. Coefficients used in Equation (2-19)

A_1	A_2	A_3	A_4	A_5	A_6	A_7	A_8
9.370	42.295	110.864	175.804	170.137	98.398	31.211	4.170

Table 2-6. Example of Erosion Rate Calculation on a 90 deg Elbow Based on DNV-O501 [31]

Input Parameters		
Fluid Properties:		
Density	833	kg/m ³
Viscosity	6.30E-03	Pa-s
Velocity	2.7	m/s
Pipe Properties:		
Elbow inner diameter	0.7366	m
Elbow radius of curvature	1.5	
Steel density	7800	kg/m ³
Material constant K	2.00E-09	
Velocity Exponent	2.6	
Solid Properties:		
Solid Loading (y)	1000	ppmW
Particle size	500	μm
Particle density	2400	kg/m ³
Calculated Parameters		
	0.5236	radians
Re	2.63E+05	
	2.881	
A	5.27E+04	
	0.000679	
c_c (calc)	0.0241	
c_c	0.0241	
G	0.02816	
F	0.9925	
Erosion Rate	0.0084	mm/year

Table 2-6 shows an example calculation for oil flow containing 1000 ppmW of solids through a 0.736 m I.D. 90 degree elbow at velocity = 2.7 m/s. Note that the erosion rate in this case is much lower than that in Tables 2-3 and 2-4 primarily due to the viscosity effects and turning of the flow through the elbow.

2.5 TERMINAL DESIGN

2.5.1 Terminal Piping Design

Due to the incompressibility of liquids, these pipelines require terminals at each end of the pipeline and often at intermediate locations to control the delivery of product into the pipeline and to manage batching of different products where required. An example of an oil terminal can be seen in Fig. 2-30 with the triangular section containing a piping manifold, booster pumps, mainline pumps, high voltage electrical buildings and other support facilities. Figure 2-31 provides a more detailed view of the piping manifold that routes liquid



Figure 2-30. Example of an oil pipeline terminal (courtesy of Enbridge Inc.).



Figure 2-31. Piping manifold and meter prover (courtesy of Enbridge Inc.).

between the storage tanks and the pipeline along with a meter prover on the left hand side to calibrate measurement devices.

Terminals consist of large liquid holding tanks, each of which may contain a separate grade of product. By switching valves between tanks, product batches can be created and transported to the delivery point where each batch is again flowed into a specific tank.

The major components of a terminal are:

- connection to injection points from upstream or other pipelines
- product tanks
- piping and valves
- booster pumps
- mainline pumps
- custody transfer measurement and sampling
- fire ring and fire-fighting facilities
- maintenance and utility buildings
- containment berms/bund walls
- transfer to/from rail, truck or ocean tanker (where applicable)

The general layout of a terminal is shown in Fig. 2-32. A series of valves allow individual tanks to be filled (such as tank 2 in Fig. 2-32) while product from another tank is injected into the pipeline (such as tank 1).

Booster pumps are located close to the tanks to provide sufficient suction pressure for the first main pump station. Because the suction pressure of the booster pumps is limited to the elevation of fluid in the tanks, they are normally vertical pumps. They are configured in parallel to provide a wide range of available flows while providing a consistent head to the mainline pumps.

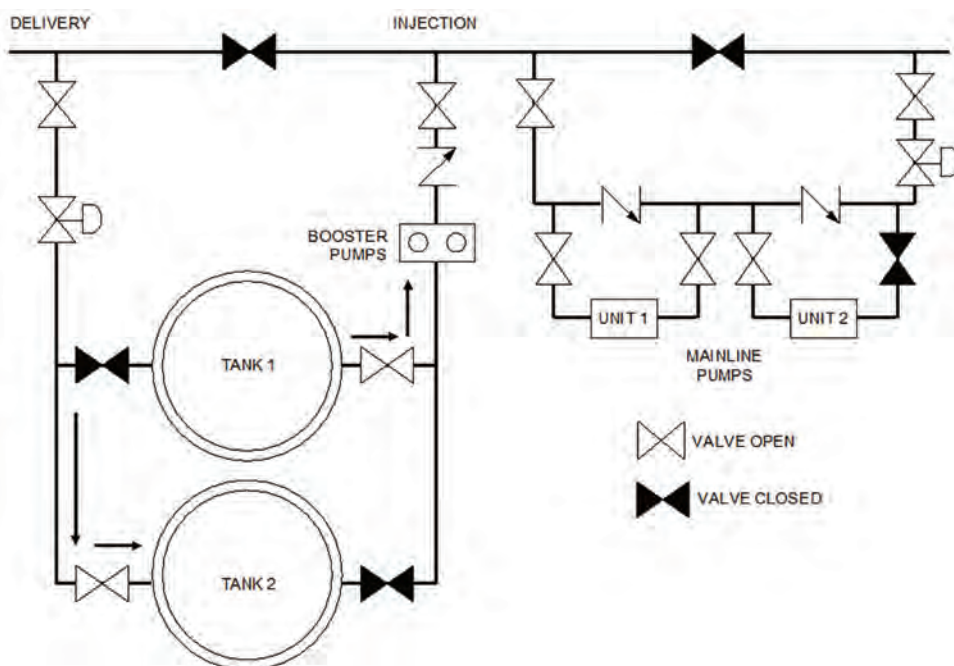


Figure 2-32. General layout of a terminal.

2.5.2 Overpressure Protection and Surge Relief

2.5.2.1 Pressure Surges in Pipelines

Pressure waves in pipelines develop any time there is a change in fluid velocity. If the change in velocity is large enough, the magnitude of a travelling pressure wave can exceed the Maximum Operating Pressure (MOP) of the piping. It is a violation of the Canadian and US regulations for petroleum pipelines (Canada – CSA Z662 4.18 [34] and United States – ASME B31.4 [35]) to operate a pipeline at pressures in excess of 110% MOP even for short periods of time. In order to meet standards and regulations, transient analyses are undertaken to verify whether the pipeline MOP profile is susceptible to over-pressures and to recommend solutions for such cases [36].

Pressure surge results from a sudden change in fluid flow velocity in a pipeline [37]. A sudden velocity change can be initiated by normal pump operations, valve manipulations or emergency operations. These events arise in normal operation, which are naturally occurring and inevitable. The disturbance is in a form of pressure wave that propagates energy and momentum from one point to another throughout the hydraulic system without significant displacement of the fluid in the system. A sudden velocity drop can cause a high pressure surge resulting in a positive pressure wave that travels upstream, expands the pipe and stores energy. The pressure wave can be large and put the integrity of pipe and piping components at risk. On the other hand, a negative pressure wave can also develop travelling downstream resulting in column separation. This negative pressure wave can return as a high pressure surge after reflecting back from downstream.

The earliest recorded transient flow observation is from the mid-nineteenth century when Weber measured the effects of pipe wall elasticity on wave propagation speed and developed fluid dynamic equations. However, the most famous equation that is widely used today is the Joukowsky equation. It demonstrates that a pressure rise in a pipe is directly related to the change in fluid flow velocity, the wave propagation speed, and the fluid density [38].

$$\Delta P = \rho \cdot \alpha \cdot \Delta v \quad (2-27)$$

where ρ is the fluid density; α is the wave propagation velocity through the fluid in pipe-line; and Δv is the fluid flow velocity change. This equation can be used for estimating instant surge pressure in a pipeline. From the equation, it becomes immediately apparent that a heavier fluid will achieve a higher value of pressure surge, which is also direct proportional to larger velocity change. This instantaneous transient pressure surge is superimposed on the steady state conditions in the pipeline at the time the disturbance occurs.

Another cause of pipeline pressure surge is due to packing pressure when fluid continues to be injected into a closed system by pumping equipment. The maximum surge pressure in any pipeline is a combination of two components: the instantaneous pressure increase in an event of total flow blockage, and the subsequent gradual pressure rise due to the line-packing effect, during the transient period. The overall surge pressure may be severe and significantly above the maximum allowable pressure limit of the system that it may lead to considerable damage to valuable assets.

There are a number of pressure transient events that can cause pressure surges in a pipeline system [37], usually initiated at a terminal by valve opening or closure, or at pump stations during startup or shutdown.

Pump startup: A pump is used to move liquids from a lower pressure region to a higher pressure region. As a pump starts up and comes on-line, the driver energy is added to the fluid resulting in a pressure temporary overshoot. A positive pressure surge is created in the downstream pipeline. The magnitude of pressure rise depends on the sudden increase in velocity which occurs when the check valve is forced open and the liquid in the pipeline begins to move. When the fluid in the pipeline is continuous, the pressure increase is

generally mild as the pump ramps up its speed. If the pump has an excessively high shutoff head, it will ride up its performance curve to the maximum pressure in case of blocked flow. If there is void space in the discharge column or in the downstream pipeline, it can cause a rapid collapse of the void space downstream from a starting pump. This can develop into a substantial transient pressure in the pipeline system.

Pump shutdown: A pump shutdown due to a loss of power is one of the most common surge events in pipeline operation. A pump can trip as a result of power supply being switched off, power failure, control device failure, pressure reaching a trip set point, or tripping signals from an external link in the pipeline system. As the pump spins down, the flow through the pump reduces rapidly. The high discharge pressure starts to decrease, while the flow reduces, and the suction pressure increases. When the flow and pressure differential drop to zero, the check valve closes. A small amount of fluid backflows because the discharge pressure is significantly larger than the suction pressure, which results in a pressure increase in the suction side. The flow upstream of the pump is not zero and the fluid flow momentum continues pushing towards the closed check valve causing the pressure to increase at the suction side.

Valve closure: A pipeline usually contains a number of remotely actuated valves for isolation purposes in case of pipeline rupture or maintenance activities. Valve closure is a common event that can cause pressure surge in the pipeline. As a valve closes and starts restricting fluid flow, the upstream pressure rises and the downstream pressure drops. A valve closure is considered as sudden valve closure and the Joukowsky equation applies if the closing time is less than the time for the pressure wave traveling upstream and reflecting back from an obstruction. This can be misleading. For linear valve closing characteristics, only the last few seconds of closure are effective valve closure that has a closing behavior like sudden valve closure. The decreasing pressure at the valve downstream can reach the vapor pressure of the liquid, resulting in column separation. If the pipeline elevation profile rises rapidly immediately downstream of the closed valve, the fluid momentum is eventually overcome by the opposing force of downstream static head. This can cause the liquid column accelerating back towards the closed valve and leading to subsequent cavity collapse with a large magnitude of pressure surge. The pipeline can potentially be subjected to severe pressure transients. In addition to the surge pressure created by rapid valve closure, the pipeline is also subjected to gradual pressure rise due to line packing when the pump continues to pack the fluid into pipeline after valve closure. The pressure waves oscillate in the pipeline between the check valve at pump discharge and the closed valve. The final pressure locked in pipeline may exceed the maximum allowable pressure during this packing period.

2.5.2.2 Transient Analysis

Analyzing pipeline transient behavior involves detailed computer modeling to simulate the complex interactions among equipment, pipelines, fluid, operating modes, control logics, emergency events and mitigation methodology, etc. A modern sophisticated pipeline transient hydraulic simulator is the best tool for analyzing operation safety and performing consequence analysis in the pipeline design. If the configuration of facilities can produce harmful pressure surges, a mitigation strategy must be developed to manage or prevent overpressure from occurring. Transient hydraulic analysis provides the techniques for identifying potential operation issues, addressing overpressure scenarios, recommending effective and economical ways of mitigating pressure surges through adequate controls and protective devices for the pipeline system. The objectives of transient hydraulic simulation of pipeline system are [37]:

- identify operational and control problems, and potential causes and events of pipeline overpressure
- evaluate and examine the system vulnerability and the need for additional mitigation supports

- investigate different mitigation options for preventing excessive pressure surges
- verify the proposed pressure control and overpressure protection systems are sufficient to prevent overpressure from occurring in the pipeline system
- finalize the engineering design and recommendations based on the modeling results and ensure the compliance with applicable codes

In recent years, pipeline regulating bodies have highlighted the importance of performing transient studies as a means for preventing overpressure situations along any piping system. As a response to this emphasis on regulations for protection from surge pressures that exceed MOP limits, there has been an increase in the amount of transient studies performed on terminal piping at injection and delivery terminals, generally called low rated piping, connected to the pipeline [39].

The methodology for performing these transient studies on terminal piping had not been addressed rigorously since the focus of surge pressure analysis was normally pipeline sections between pump stations. Whereas the majority of liquid pipelines have high MOP values and control logic that monitors pressures and provides automated protection [36], injection terminals are normally built with low rated piping and have limited control logic which applies mostly to mainline pump discharge. To comply with regulations and to improve the quality of transient analyses are required to assess the methodology used for analyzing injection terminals.

It was discovered that several drawbacks in analysis methodology needed to be corrected and improved [40]. Amongst the most important ones were:

- *PCV Closure Scenario:* In the original standard, the only simulation scenario required was the simultaneous trip of all mainline pumps, since that was identified at the time as being the worst case. However, it was discovered that the closure of the injection PCV could generate surge pressures greater than that of the pump trip scenario. This important scenario was included in the new methodology as part of the requirements thus allowing the studies to be more conservative and to address mitigating measures.
- *Flow path:* Another pitfall of the previous methodology was that the studies did not include a detailed flow path analysis of all the injecting tanks into the booster pumps. The general rule was to analyze the tank that provided the highest suction pressure to the booster pump (generally the closest tank to the booster pumps that also presented the highest fluid elevation), but several sensitivity studies performed in-house determined that the closest or highest tank may not always generate the worst surge pressures. The momentum of the fluid increases with the length of the pipe and this affects the behavior of the pressure profile inside the terminal. The new methodology now includes a detailed flow path analysis of all the injection tanks to determine which one will be used as the worst case.
- *Initial States:* The initial states that are used for a transient study normally include the highest flow rate allowed on the line (normally called Q_{max}). Injection terminals also need to include the flow rates that generate the highest pressure profile along the low rated piping (generally given by the minimum flow rate Q_{min}). If the minimum flow rate cases are not included, there could be a risk of not considering the worst initial state for a given terminal and this was also addressed by the new methodology.

Several examples were validated with operational data compared to simulation results [40]. Figure 2-33 provides an example of operational data where the percentage open of an injection PCV decreases from 60 to 20% in 5 seconds, reaching its lowest (15%) open in 10 seconds. During this same period of time, the suction pressure of this terminal increases

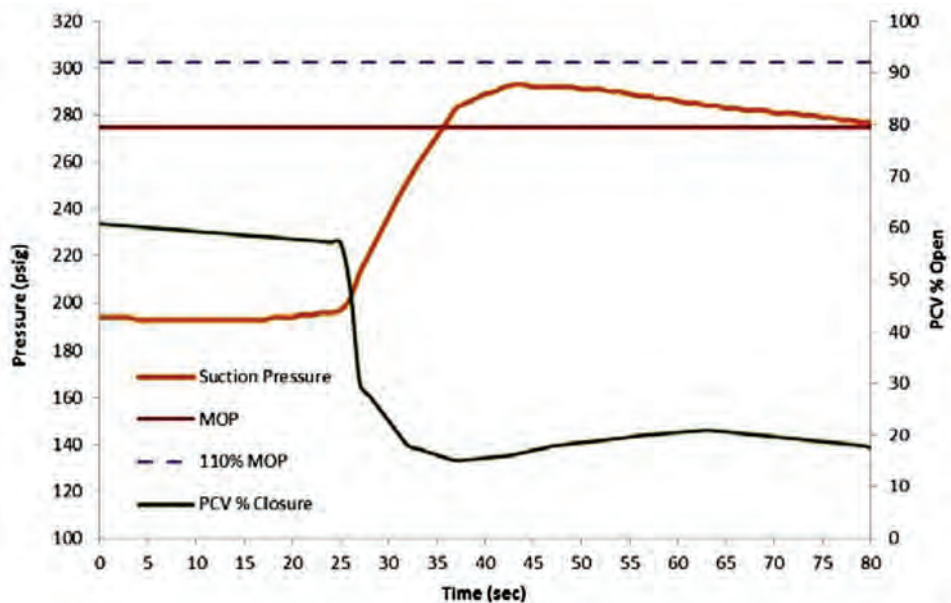


Figure 2-33. Example of the sudden closure of a PCV [40].

from 193 to 271 psig (13.13 to 18.44 atm) and keeps increasing due to the sudden stopping of almost all the flow. It can be seen that the sudden closure of a control valve causes a surge pressure that could reach extreme values if the operational conditions (such as flow rate or % closure) were worse than in this case. The reaction of the pressure to this event (as seen in Fig. 2-33) shows the importance of simulating the sudden closure of an injection PCV as a probable and significant scenario.

A comparison was also performed between two tanks that feed into the same injection system where the only variable changed was the distance from the tanks to the booster pumps [40]. The transient scenario simulated was the simultaneous shut down of all mainline pumps. It showed that the surge pressure was higher for the longer flow path. The surge pressure caused after the upset on the suction side of the booster pumps is also higher for the longer flow path. The results from these two simulations of flow path lengths serves to validate the need to consider all flow paths that inject into the mainline pumps and not assume that the shortest distance will generate the highest surge pressure.

Hydraulic simulations were also performed to study the effect of three valve characteristics on transient responses when delivering from pipelines into tanks [41]. Simulation results show that a faster stroke time leads to higher pressure surges, as well as a valve with a quick closing or linear curve. However, the flow coefficient of the valves will have varying effects on transients depending on the piping system being analyzed.

2.5.2.3 Overpressure Protection and Surge Relief

There are many mitigation options available for suppressing pressure surges in a terminal system. Each measure has its own advantages and disadvantages. The best surge suppression method is to eliminate the pressure surge initiators in the design. However, this is not always possible when designing a complex transport system. In most cases, pressure relief devices must be used to mitigate the potential pressure surge problems in the system. The primary factors that affect the performance of a pressure relief device include the type of relief device, the location of the device, the size of the device, and the pressure set point of the device. In general, all pressure relief facilities should be located near the point where the high pressure wave will reach first after the surge event is initiated.

Mitigation options are:

- using a soft starter or variable frequency drive to start the pump motor to allow the fluid flow to increase gradually, eliminating any pressure overshoot in the piping system
- increasing pipe diameter to reduce the average flow velocity in the pipe that directly contributes to the instant surge pressure
- selecting higher pressure rated piping to withstand the maximum pressure surges
- installing a rupture disc to provide fast pressure relief and high relief flow capacity
- installing a relief valve to release some of the excess fluid during a pressure surge event, thus limiting the effect of the dynamic pressure surge
- adding a surge vessel
- managing valve closure characteristics including the closing characteristic curve and the closure time interval
- interlocks to trigger some device to act when some conditions satisfy the criteria set out in the design such as tripping pumps when the hydraulic flow path is misaligned, and closing a valve that causes less severe pressure surge when a critical valve closes

A surge vessel is a very effective method for mitigating a pressure surge in a pipeline terminal. When designed properly, a surge vessel provides fast pressure relief without releasing fluid outside the piping system. Because surge vessels tend to be small in volume, they are more suitable for systems with a small packing volume, which works well for pressure relief in terminal designs. In addition, vessel connecting piping length, size and flow velocity can all affect the pressure surge mitigation performances. Surge vessels are best installed upstream of mainline pumps to absorb excessive energy when the mainline pumps are tripped. The bladder type surge vessel contains a bag-like enclosure that separates the process fluid from the damping gas, normally nitrogen, in the bladder. The enclosure is flexible and could be ruptured during operation due to manufacturer defects, improper installation, aging or some other reasons. Thus, it is important to adequately monitor the health of the vessel during operation. Attention needs to be paid to monitoring the liquid level in the vessel and the gas pressure and for leaks from the enclosure [42].

Nitrogen loaded surge relief valves come in a variety of designs (Fig. 2-34). All of them are known for their quick speed of response and excellent flow characteristics. Some use pistons with external plenums while others use elastomeric tubes and internal chambers. In spite of their design differences the one thing they have in common is that they rely on a charge of nitrogen to establish their set point.

When using nitrogen loaded surge relief valves, it is believed that the relief valve is in control of the upper pressure limit of the pipeline. In reality, it is the nitrogen system together with the valve in a master and slave relationship that sets the upper threshold. The negative effects of changing temperature on the stability of a nitrogen loaded relief valve's set point is well known but poorly understood. There have been many attempts to minimize this effect. Burying the plenum and using the soil as an insulator has proven to be ineffective. Manual adjustments are not cost effective. Regulators offer inconsistent performance and are often misapplied.

The way operators have dealt with this in the past is by monitoring the set point and responding to high/low pressure alarms. This method requires a technician to visit the site to add or vent nitrogen from the system. That can translate to numerous visits over the course of a year depending on the number of valves in the system, the set point of the valves, ambient weather conditions, and the valve set point tolerance.

Evolving technology now allows for this process to be automated. Set points can be held with remarkable accuracy and plenums no longer need to be buried. With the evolution of automation, the negative issues associated with operating surge relief valves can

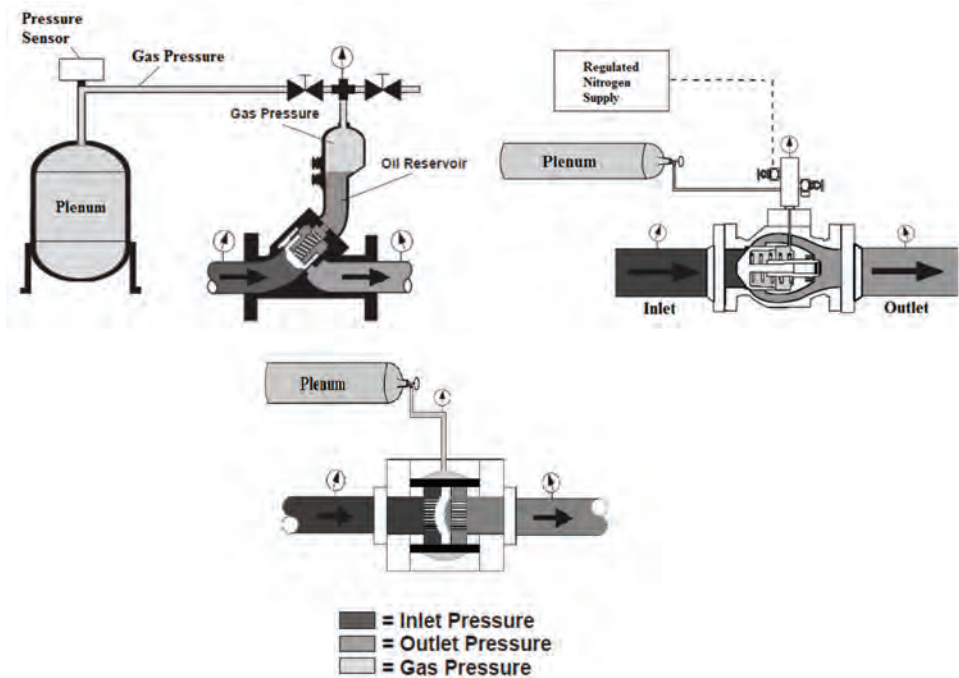


Figure 2-34. Different designs for nitrogen loaded surge relief valves [43].

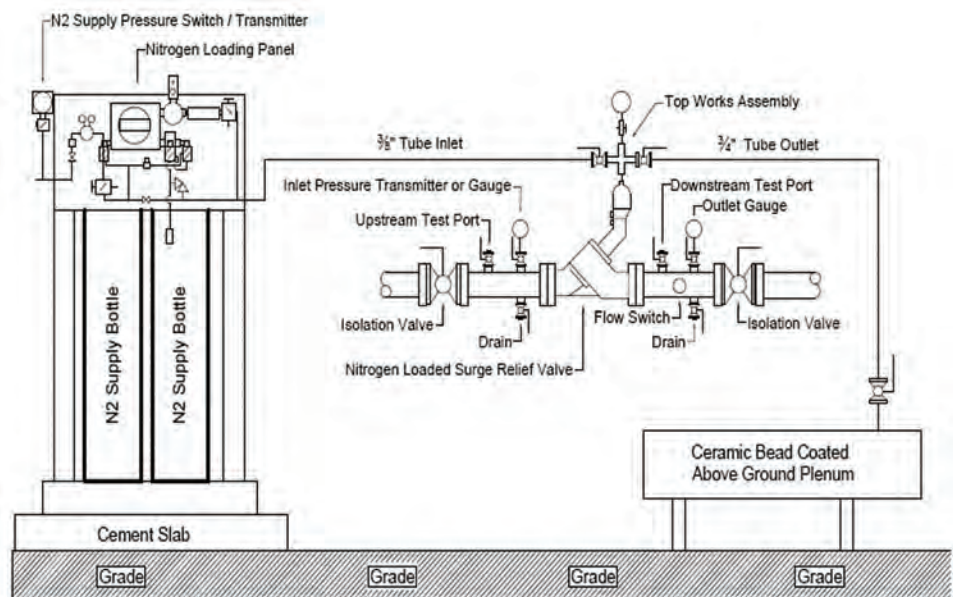


Figure 2-35. An automated surge relief installation [43].

be overcome. Automated nitrogen loading systems can precisely maintain a set point due to their ability to add and vent nitrogen from the plenum when necessary. When the temperature rises nitrogen from the plenum is vented to atmosphere. This part of the process does not consume nitrogen from the supply but, when the temperature starts to drop and the plenum pressure decreases, the nitrogen that was previously vented from the system

will need to be replaced. In a traditional mechanical system, the reason for insulating the plenum was to minimize the impact temperature had on the pressure in the closed system. In an automated system, plenum insulation is relegated to the secondary role of reducing nitrogen consumption.

Mechanically the surge relief run remains the same. It still consists of the relief valve, test ports, gauges and isolation valves. In terms of the nitrogen supply very little remains the same. Figure 2-35 shows a typical installation with an automated nitrogen loading system and above ground plenum. The nitrogen system is mounted on a concrete slab. The plenum is attitude insensitive making it easy to mount near the relief valve.

REFERENCES

- [1] Greaves, T.H., 2016. "Pump Replacement at a Critical 63 Year Old Pump Station," Proceedings of the 2016 11th International Pipeline Conference. IPC2016-64003, September 26–30, 2016, Calgary, Alberta, Canada, 16 pages.
- [2] Mohitpour, M., Golshan, H., and Murray, A., 2007. *Pipeline Design & Construction A Practical Approach*, 3rd ed., ASME Press, New York.
- [3] Mohitpour, M., Thompson, W., and Asante, B., 1996. "The Importance of Dynamic Simulation on the Design and Optimization of Pipeline Transmission Systems," Proc. ASME-OMAE International Pipeline Conference (IPC), Palliser Hotel, Calgary AB, Canada, June 9–13.
- [4] ASME/ANSI, 2017. "Standard B16.5—Pipe Flanges and Flanged Fittings."
- [5] Kung, P. and Mohitpour, M., 1986. "Non-Newtonian Liquid Pipeline Hydraulics Design and Simulation Using Microcomputer," Proceedings, Pipeline Engineering Symposium, 9th ETCE Conference, 3, 73–78.
- [6] ASCE, 1975. "Pipeline Design for Hydrocarbon Gases and Liquids: Committee on Pipeline Planning, Report of the Task Committee on Engineering Practice in the Design of Pipelines," New York, NY.
- [7] Moody, L.F., 1944. "Friction Factor for Pipe Flow," ASME Transaction, 66, p. 671.
- [8] Mohitpour, M., Szabo, J., and Van Hardeveld, T., 2004. *Pipeline Operation and Maintenance—A Practical Approach*, ASME Press, New York, pp. 565–606.
- [9] Horner, J.W. and DeBusman, M.R., 2014. "Pump Station Design," Proceedings of the 10th International Pipeline Conference, IPC2014-33740, September 29–October 3, 2014, Calgary, Alberta, Canada, 12 pages.
- [10] Botros, K.K., Clavelle, E. and Vogt, G.M., 2016. "Interfacial Contamination between Batches of Crude Oil Due to Dead-legs in Pump Station Piping", ASME Journal of Energy Resources, vol. 138, pp.052908-1-052908-8, DOI:10.1115/1.4033401, 2016.
- [11] Botros, K.K., Clavelle, E. and Vogt, G.M., 2016. "Innovations into Minimizing Interfacial Contamination between Crude Batches Due to Dead-legs in Pump Station Piping Layouts", ASME International Pipeline Conference, Calgary, Alberta, Canada, September 26–30, 2016.
- [12] API Recommended Practice 14E, "Recommended Practice for Design and Installation of Offshore Production Platform Piping", 1991. American Petroleum Institute.
- [13] Salama, M.M., 1998. "Alternative to API 14E Erosional Velocity Limits for Sand Laden Fluids", Proceedings of the Annual Offshore Technology Conference OTC Paper 8898 Tulsa, OK.
- [14] Austin, J.E. and Palfrey J.R., 1964. "Mixing of Miscible but Dissimilar Liquids in Serial Flow in a Pipeline," Proceedings of the Institution of Mechanical Engineers, Vol. 178, p. 377.
- [15] Levenspiel, O., 1958. "Longitudinal Mixing of Fluids Flowing in Circular Pipes," Industrial and Chemical Engineering, Vol. 50, p. 343.
- [16] Songsheng, D. and Jianing, P., 1998. "Application of Convection-Diffusion Equation to the Analyses of Contamination between Batches in Multi-Product Pipeline Transport," Applied Mathematics and Mechanics (English Edition), Vol. 19, p. 757.
- [17] Aunicky, Z., 1970. "The longitudinal mixing of liquids flowing successively pipelines". The Canadian Journal of Chemical Engineering, 48, pp. 12–16.

- [18] Krantz, W.B. and Wasan, D.T., 1974. "Axial dispersion in the turbulent flow of power-law fluids in straight tubes". *Ind. Eng. Chem. Fundam.*, 13(1), 56–61.
- [19] Botros, K.K., 1984. "Estimating Contamination between Batches in Product Lines," *Oil and Gas Journal*, p. 112.
- [20] Deng, S., and Pu, J., 1997. "The comparison between 1-d model and two-dimensional model of the multi-product pipeline," *Oil & Gas Storage and Transportation*, Vol. 16, No. 1, pp. 16–18.
- [21] Dai, F., and Hu, X., 2009. "The Contamination calculation Formula for the Southwest Multi-product Pipeline," *Oil & Gas Storage and Transportation*, Vol. 28, No. 2, pp. 40–42.
- [22] Chen, Q., 1999. "Calculations on the Mixing Volume of Products Pipeline with Variable Diameter Pipes," *Oil & Gas Storage and Transportation*, Vol. 18, No. 1, pp. 7–8.
- [23] Freitas Rachid, F.B., Araújo, J. H.C., Baptista, R.M., 2002. *Mixing Volumes in Serial Transport in Pipelines*, *J. Fluids Eng.* 124(2), 528–534.
- [24] Sherwood, T.K., Pigford, R.L. and Wilke, C.R., 1975. *Mass Transfer*, Chapter 4, McGraw Hill Inc., New York.
- [25] Taylor, G.I., 1953. "Dispersion of Soluble Matter in Solvent Flowing Slowly Through a Tube," *Proc. Royal Soc. London*, Vol. A219, pp. 186–203.
- [26] Taylor, G.I., 1954. "The dispersion of matter in turbulent flow through a pipe," *Proceedings of Royal Society, Series A*, Vol. 223, pp. 446–468.
- [27] Colebrook, C.F. and White, C.M., 1937. "Experiments with fluid friction in roughened pipes", *Proc. Royal Soc. (A)* 161, 367–378.
- [28] Tichacek, L.J., Barkelew, C.H. and Baron, T., 1957. "Axial Mixing in Pipes," *AIChE Journal*, Vol. 3, No. 4, 1957, pp. 439–442, doi:10.1002/aic.690030404
- [29] Konecnik, C., 2012. "Keystone Pipeline – Optimizing Delivered Quality", June 19, 2012; http://www.coqa-inc.org/docs/default-source/meeting-presentations/20120619-20_Konecnik_Pipeline_Quality.pdf, accessed on March 31, 2016.
- [30] Parsi, M., Kamyar, N., Najjaffard, F., Hassani, S., McLaury B., and Shirazi, S., 2014. "A comprehensive review of solid particle erosion modeling for oil and gas wells and pipelines applications," *Journal of Natural Gas Science and Engineering*, vol. 21, pp. 850–873.
- [31] Det Norske Veritas, 2007. "Recommended Practice RP0501: Erosive Wear in Piping Systems," Det Norske Veritas, Revision 4.2.
- [32] Zhang, Y., Reuterfors, E., McLaury, B., Shirazi, S. and Rybicki, E., 2007. "Comparison of computer and measured particle velocities and erosion in water and air flows," *Wear*, vol. 263, pp. 330–338.
- [33] Finnie, I., 1960. "Erosion of Surfaces by Solid Particles", *Wear*, Vol. 3, pp. 87–103.
- [34] CSA Z662-15, 2015. "Oil and Gas Pipeline Systems," Canadian Standards Association, 868 pages.
- [35] ASME (American Society of Mechanical Engineers), 2016. "Pipeline Transportation Systems for Liquid Hydrocarbons and Slurries," ASME Code for Pressure Piping, B31.4, An American National Standard.
- [36] Rodriguez, G. and Pavel, B., 2012. "A Rational Methodology for Detailed Pipeline Transient Hydraulic Analysis," *Proceedings of the 2012 9th International Pipeline Conference, IPC2012-90684*, September 24–28, 2012, Calgary, Alberta, Canada, 8 pages.
- [37] Zhou, A.X.L., Yu, D. and Cabrejo, V., 2016. "Overpressure Protections in Liquid Pipeline Hydraulic Design," *Proceedings of the 2016 11th International Pipeline Conference, IPC2016-64687*, September 26–30, 2016, Calgary, Alberta, Canada, 9 pages.
- [38] Watters, G.Z., 1984. "Analysis and Control of Unsteady Flow in Pipelines," Butterworths Publishers, Boston, MA (USA), ISBN 0-250-40492-3, 349 pages.
- [39] Modisette, J. and Bachman, S., 2007. "Surge Analysis – Coping with Fuzzy Regulations", *PSIG Annual Meeting*, Calgary, AB.
- [40] Perez, E. and Thomson, L., 2014. "Transient Modeling of Surge Pressures within Injection Terminal Facilities," *Proceedings of the 2014 10th International Pipeline Conference, IPC2014-33607*, September 29–October 3, 2014, Calgary, Alberta, Canada, 6 pages.

- [41] Perez, E. and El-Bayoumi, A., 2016. "Valve Characteristics and Their Effect on Transient Surge Pressures in Delivery Terminals," Proceedings of the 2016 11th International Pipeline Conference, IPC2016-64081, September 26–30, 2016, Calgary, Alberta, Canada, 6 pages.
- [42] Zhou, X.L., Cabrejo, V. and Yu, D., "Pressure Surge Relief Options in Terminal Design," IPC2014-33488, Proceedings of IPC2014, Sept 29–Oct 3, 2014, Calgary, Alberta, Canada, 9 pages.
- [43] Konopa, J.W. and Konopa, K.A., 2014. "Benefits and Methods of Automating Surge Relief Valves," Proceedings of the 2014 10th International Pipeline Conference, IPC2014-33085, September 29–October 3, 2014, Calgary, Alberta, Canada, 8 pages.

GAS PIPELINE COMPRESSION SYSTEM DESIGN

3.1 GAS PIPELINE DESIGN

3.1.1 Gas Pipeline Hydraulics

Gas pipelines have the distinct advantage that gas is compressible and the higher the pressure, the more gas can be transported. In other words, the mass flow (or number of molecules) is what is important. Depending on the source of supply, compression may first have to be compressed up to a favorable main pipeline pressure.

Compression is subsequently required in the main pipeline systems to overcome friction losses, which increase as the rate of gas flow increases. Gas is received from receipt points along the pipeline and delivered to delivery/sales stations at specified flows and pressures. In between these points, pressure drop occurs because of expansion, friction loss, change in elevation, or change in temperature. Three methods can be used to maintain the required pressure at an existing delivery point when there is an increase in flowrate beyond the design point (Fig. 3-1):

- looping the pipeline (i.e., add a parallel pipeline, connected to the existing pipeline); this reduces the flow in each line, thereby decreasing velocity and, hence, pressure loss due to friction
- adding a compressor station to boost the pressure sufficiently to maintain the required pressure at the delivery point
- a combination of loop and compression
- line pack usage based on diurnal gas delivery fluctuations

The evaluation of which method will be economically more feasible depends on many factors such as:

- capital expenditures
- fuel cost
- emissions
- maintenance
- future expansions

3.1.2 Pipeline Optimization with Respect to Compression

The objective of hydraulic design and economic simulation is to define a technically and economically optimum pipeline facilities system. The optimization process is thus an attempt to determine the best and most favorable option for all stakeholders. Considerations are:

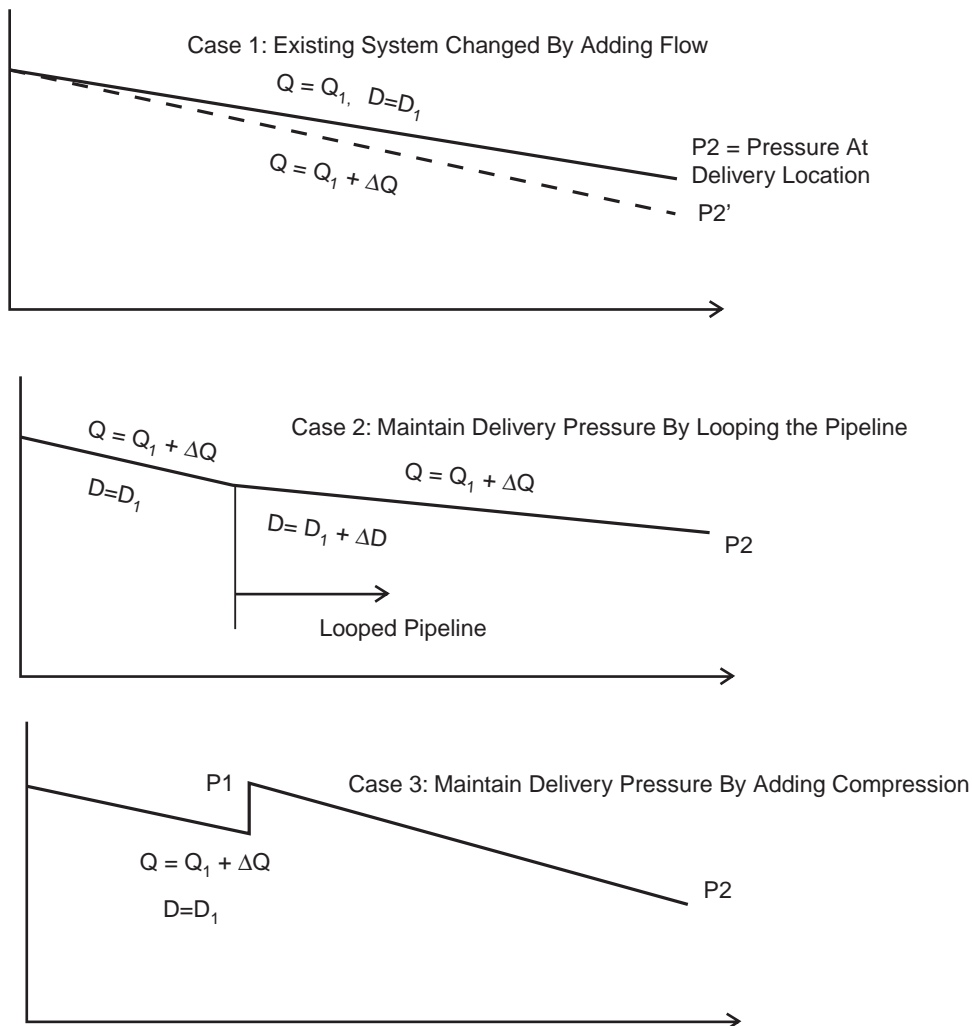


Figure 3-1. Pipeline looping versus compression.

- engineering [including balancing technical alternatives, e.g., route 1 versus route 2, pipe (diameter/loop/material/addition) versus compression]
- design
- construction
- timing facilities put in operation
- operational flexibility

The optimization process is diagrammatically depicted in Fig. 3-2 and is described in detail by Mohitpour et al. [1].

Optimization is undertaken to determine the following:

- optimum pipe size and compression requirements
- optimum operating pressure
- appropriate compression ratio
- optimum pipeline route
- optimum system load factor
- necessary storage facilities

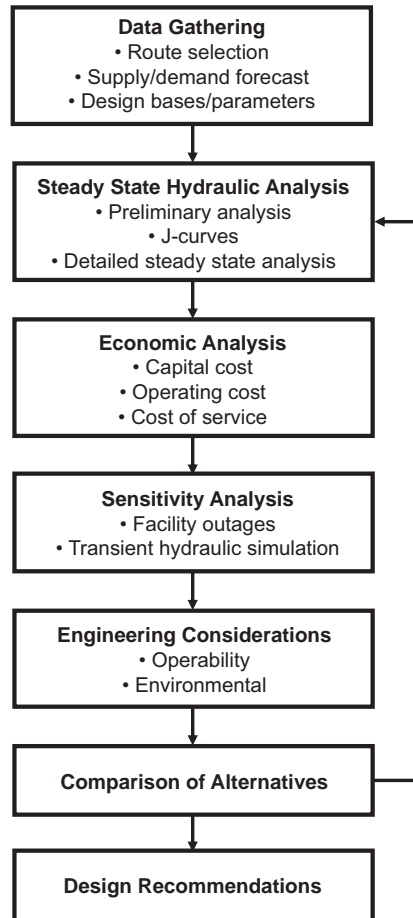


Figure 3-2. Optimization process chart for pipeline design.

The above involves the following:

- pipeline routing
- supply and demand locations
- volume and volume build up, design year(s)
- load factor
- maximum and minimum operating pressures and temperatures
- pipe size and material
- compressor units and compressor station spacing/location intervals
- compression unit drivers (gas diesel, electric)
- cooling requirement (types and size)
- protection
- others

All reasonable optimization parameters must be considered in technical and economic assessment of alternatives.

When all reasonable combinations of the optimization parameters are considered, and if the system is such that there are several pipeline segments each with significantly different flow requirements (and, hence, requiring separate optimization), then it is possible to assess alternatives for the most economically optimum and technical feasible solution.

Alternatives are generally assessed through a screening process to reduce the number of options.

The results of preliminary simulations and economic evaluation are often presented in the form of J-curves. J-curves graph the cost of service against design flows for different sizes of pipe and compressor combinations in order to determine the most cost-effective solution.

Of importance are the flow, design year, and load factor.

Firstly, for each flow (/design) year, usually, a separate analysis of alternatives is undertaken prior to comparing alternative flow/design years. For each alternative, flow simulations is performed for the maximum flow condition in the selected/given design year. This can be used to locate all compressor stations and to determine the size of the stations and number/type of units required. Further flow simulations can then be performed for the buildup years to determine when each station need be installed and to establish the power buildup for each station.

Knowing the availability of stations in each year, seasonal average flow simulations can be undertaken for each year up to the design year to determine if the available stations are required under seasonal average flow conditions and, if so, to establish fuel requirements for these stations.

For each alternative, it is then possible to estimate the capital costs to acquire and construct/install the facilities. These estimates are usually costed to the year of installation, i.e., in as-spent costs. Fuel costs in as-spent terms along with other operating and maintenance costs are also estimated.

In reviewing the capital, fuel, and operating and maintenance costs, it is possible that some of the alternatives will have higher costs in all categories than other alternatives. These higher cost alternatives are eliminated, thus giving preference to most economically viable solutions.

In reviewing the capital, fuel and operating and maintenance costs, it is also possible that some of the alternatives will have higher costs in all categories than other alternatives. These higher cost alternatives are the eliminated as applicable.

For the remaining alternatives, it is necessary to estimate project all annual costs (i.e., to the limit of the facilities life), present-value these, and cumulate the present-valued costs in order to establish the lowest cost alternative. Thus, in addition to the capital, fuel, and operation and maintenance costs, other cost factors that will need to be allowed include depreciation expenses, financing costs, return on equity, and any taxes, if applicable. The discount rate applied in the present-valuing of the annual costs is usually the owners/proponents cost of money (i.e., a mix of debt financing at the rates available based on credit rating plus equity financing at the minimum acceptable rate of return).

In comparing design flow years, the best of the alternatives for each design/flow year are selected, but a direct comparison is not immediately possible since each of these cases has a different throughput capacity. Therefore, the alternatives with a lower capacity need to be expanded (e.g., adding compression to the pipeline) to the highest capacity. This again requires some effort to ensure the expansion is done in a close-to-optimum manner. The additional capital, fuel, and operation and maintenance costs are estimated, and then the total annual costs are extended to the highest design year. The alternatives can then be compared on the basis of cumulative present-valued costs.

With the best two or three alternatives, we can go back and test the sensitivity when some of the other parameters are varied.

As referred to above, optimum design would normally be selected on the basis of the lowest cumulative present value of total annual costs. However, as is often the case, a number of the alternatives will be very close on this cumulative present-valued costs basis (say within 5%). Thus, for practical purposes, these alternatives are equal. The selection then switches to other considerations.

Perhaps, the first of these other considerations would be:

- lowest initial capital investment
- probability of increased flow beyond the estimate/design flow
- ease and reliability of operation

In the assessment of how the last few alternatives compare, the following sensitivities need to be addressed:

- What if the so-called fixed parameters are varied?
- What if the throughput requirements built up faster or slower?
- What if the capital costs were higher or lower?
- What if the fuel or operation and maintenance costs were higher or lower?
- What if inflation factors changed?
- What if the taxes, discount and other cost factor changed?

3.1.3 Pipeline Looping and Compression (Location and Spacing)

Looping Versus Compression. For long pipe systems, options are either loops or compression or a combination of pipe and compressor facilities. The possible combinations are almost unlimited and, thus the industry has developed some rules of thumb to guide pipeline sizing and decide loop versus compression.

Industry experience has shown that the pressure drop along a gas pipeline should be within a range of 1 to 8 psi/mi or about 4 to 35 Pa/m for an efficient pipeline system. Below this range, the capital expenditure can be excessive because the pipe is generally underused. Above this range, the fuel consumption is excessive because of extremely high frictional losses due to higher velocities and, hence, pressure drops. However, it may be noted that the range may vary depending on costs in specific pipeline systems. Nonetheless, this will provide a guide looping versus compression.

When looping an existing system, the pressure drop can also be considered as a guide to selecting the size and length. However, industry experience indicates that the loop size should be at least as large as the largest existing line being looped. This is especially true if the throughput is growing.

One other factor to consider in looping is whether to add just enough loop to meet the requirement (neat loop) or to add loop between existing valve sites (practical loop).

Compressor Station Spacing. For gas pipeline systems where intermediate compression is required, there is considerable flexibility in the location of these compressor stations. Shifting the location changes the pressure at the inlet to the station and, hence, the compression ratio. Thus, if the stations are located using the compression ratio, then the compression ratio is one of the optimization parameters.

If the throughput requirements are relatively low, one may consider either centrifugal or reciprocating compressors; but for higher flows typically found in mainline pipeline systems, centrifugal compressors are generally used. For centrifugal compressors, compression ratios are generally below about 1.4 to 1.5. Although up to 2 to 2.2 are also considered in the industry, staging above 1.5 compression ratio is required. Reciprocating compressors can go well above this, but they tend to be flow-limited.

Industry's experience shows that the most efficient compression ratios tend to be in the 1.25 to 1.35 ratio range. Capital costs and fuel costs will be the key factors in looking at the optimum spacing.

Gas Versus Electric Compressor Drivers. Depending on the availability, the current prices and projected future prices of alternative energy sources, and depending upon capital costs, there may be an advantage to choosing one driver type over another.

Cooling Requirements. For gas pipeline systems, high gas temperatures result in high pressure losses and thus there may be significant savings achievable by installing cooling facilities on the discharge side of the compressors, whereas coolers cost money to install and they also incur additional operating expenses. However, cooling may reduce the downstream pipe size or reduce the total system compression requirements; the additional costs of cooling can be worthwhile.

If cooling is not used, it is also possible to get an effect called “cascading.” What happens in this case is the inlet temperature progressively rises for each successive compressor station on the system, and the discharge temperature also rises.

Generally air cooled heat exchanges (“air coolers” or “fin-fan” coolers) are used to cool the compressed gas by moving ambient air over the exterior of “finned” tubes through the use of a fan or blower. The performance of such coolers is therefore ambient temperature-dependent.

The applications of cooling in a typical gas compressor station include:

- engine jacket water cooling (if applicable)
- combustion air/lube oil-water cooling
- water cooling
- lube oil cooling
- high pressure gas cooling

3.1.4 Hydraulic Simulation

Hydraulic simulation is an integral part of pipeline system assessment and assessment of needs for compression and appertaining facilities.

Pipeline system planning is traditionally based on steady-state hydraulics for facility selection process. This process involves reviewing flows and pressure drops and determining capacity, pipeline diameters, pipeline loop lengths, and overall pump or compressor station power requirements. The facility selection process begins with the creation of a demand and supply forecast. These forecasts usually involve examining all existing and potential customers along the pipeline route and creating a projection of their demand requirements over a predetermined time frame.

The next step is the creation of a hydraulic computer model of the pipeline system to which the forecast for supply and demand is added. Nowadays, many hydraulic simulation software is available. For example, PipelineStudio [2] nSteady state simulations are run to determine where the flow is restricted. Additional facilities, which may mean either loops, pumps, or compression facilities, are added to the model to eliminate the restrictions. Usually, several alternate facility buildups are created over the forecast period. Ultimately, and as indicated previously, these alternate facility buildups are compared on an economic and technical basis to choose the best alternative. Steady-state analysis is also used to determine system design flow capacity and to provide a “best guess” of future pipeline operation so that detailed design can be performed on new facilities. To a lesser extent, it is also used in determining operational problems.

A typical steady-state model of the system is shown in Fig. 3-3. The pipeline includes one centrifugal compression facility (Solar C505 compressor with a MARS T12000 gas turbine driver), one supply, and 12 delivery locations.

The pipeline consisted of 115.5 km of NPS 22 (0.406-in. wall thickness) and 35 km of NPS 2, 2.5, and 3 laterals feeding many industrial areas as shown in Fig. 3-3.

The NPS 22 mainline pressure and flow profiles are shown in Fig. 3-4, and corresponding elevation and temperature profiles are shown in Fig. 3-5.

When pipeline gas is typically supplied by a gas processing plant (Fig. 1-5), it is usually at the required pipeline pressure. However, this not always the case and the gas supply into the pipeline must be compressed to the required line pressure.

The above system incorporates a gas turbine/centrifugal compressor unit installed at the initiation of the pipeline (right after the supply location). Assuming a low supply

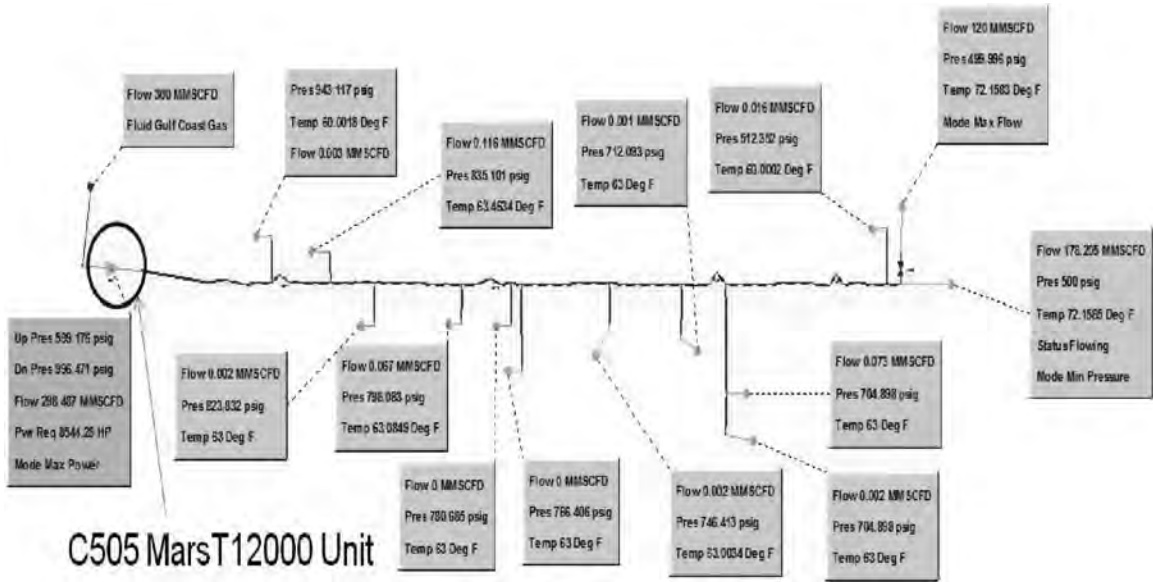


Figure 3-3. Example of a typical gas pipeline network.

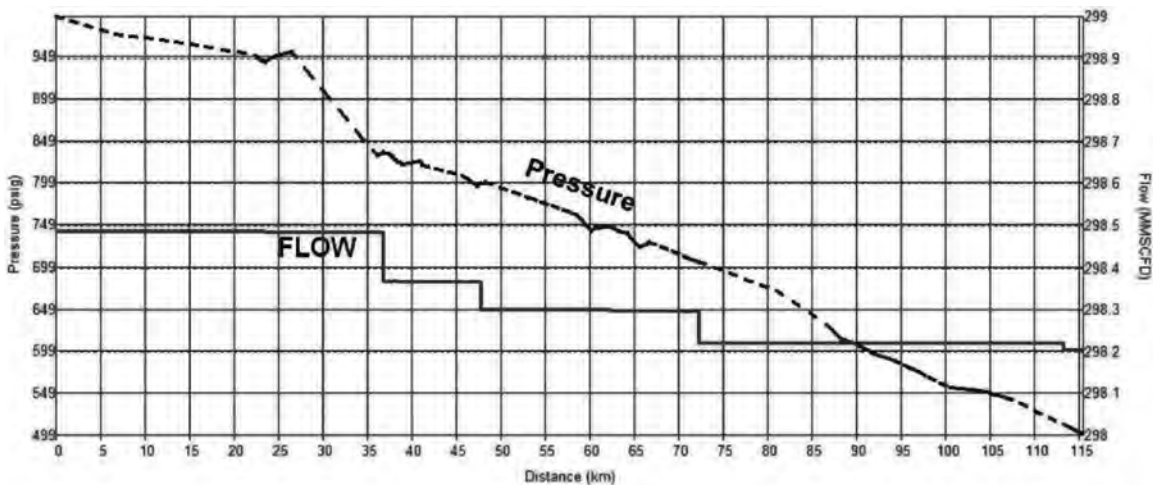


Figure 3-4. Hydraulics profile (NPS 22, 115.k mainline, roughness 0.001', efficiency and drag factor = 0.97).

pressure (500 psi) and the required pipeline pressure (of 900 psi), the system was also simulated to ascertain the compressor compression operating point and power requirement. The appropriate compressor curve, with the operating point superimposed on it, is shown in Fig. 3-6.

System design with transient consideration can provide:

- increased economic viability
- prediction on effects of system outages or deliveries
- information on safety and operational performance
- operational conditions
- others

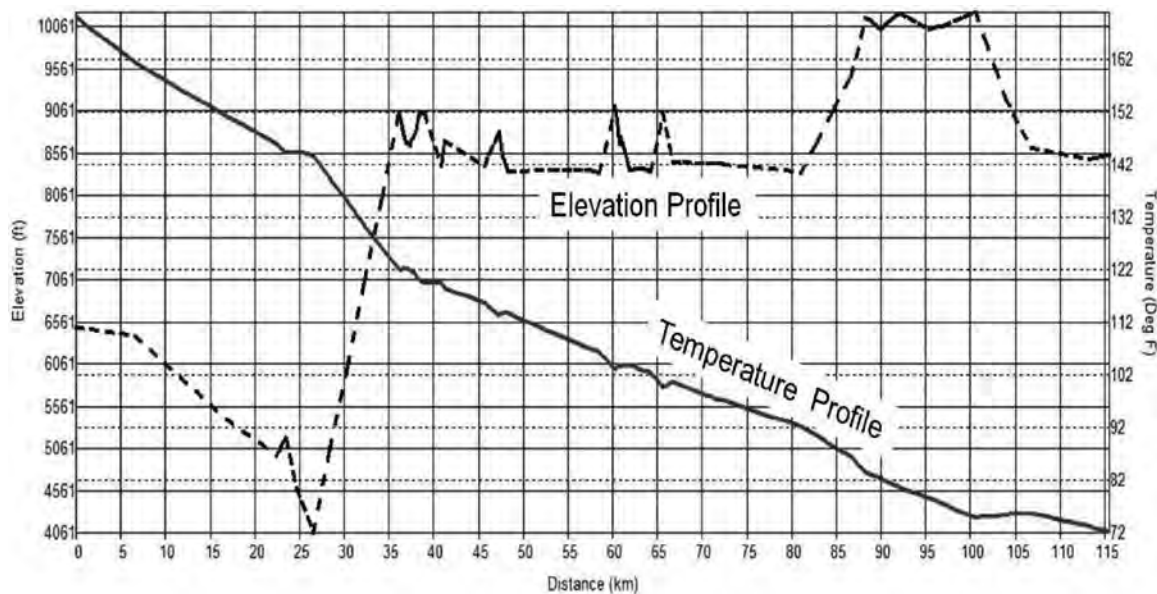


Figure 3-5. Route elevation and temperature profiles (pipeline inlet and ambient temperatures 90°F and 60°F, overall heat transfer coefficient 1.42036 W/m²K).

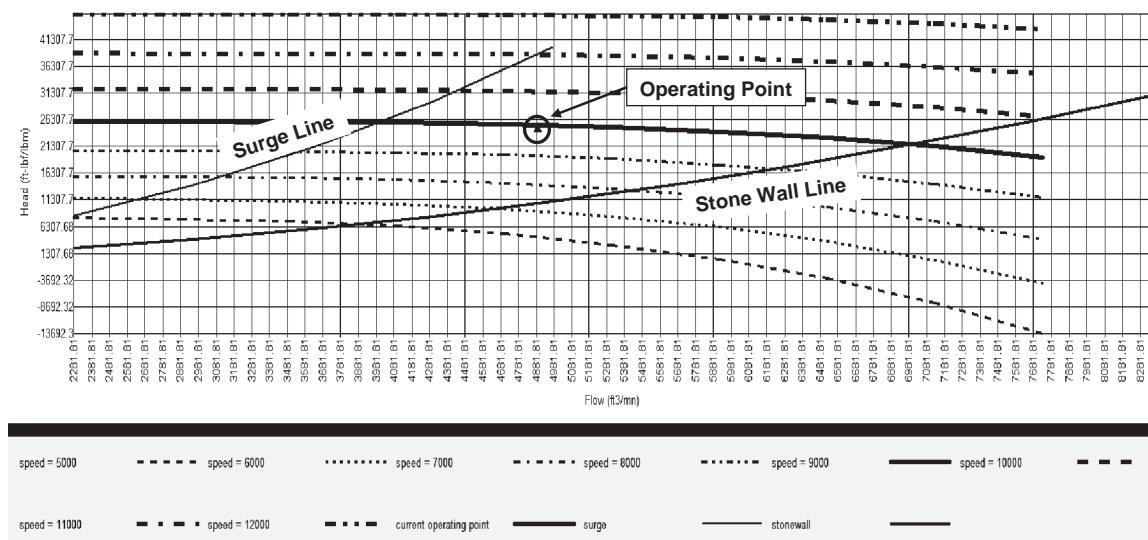


Figure 3-6. Compression performance curve and pipeline operating point (C505 compressor with MARS T12000 driver), graphs generated using Energy Solutions International (ESI) pipeline studio TGNET.

The fundamental application of transient simulations for gas pipeline systems will provide options for the assessment of:

- blow downs
- leak and rupture
- system capability determination under varying supply and demand conditions
- quantified impact of facilities outages on deliveries
- pipeline system responses due to compression change and interruption in services

- effect of valve closure and equipment downturn
- linepack determination
- pipeline commissioning
- pigging operation
- gas management and gas switching
- critical assessment of facilities requirement

The subject of transient simulation in gas pipeline systems is fully covered with examples given elsewhere [6].

3.1.5 Cost of Compressor Operation

In general, centrifugal compressors on pipelines are powered by gas turbines and reciprocating compressors by gas engines. These drivers provide variable speed control and use pipeline gas as fuel. They also tend to match the compressor in terms of operating speed, eliminating complications such as speed changing gears.

When selecting or operating drivers—particularly gas turbines—care must be taken to ensure that the power output is corrected for site conditions of elevation, ambient temperature, and intake and exhaust losses. Power variation with ambient temperature is usually obtained from the manufacturer (since performance limits may be encountered).

The power output of a compressor is measured at the coupling between the driver and compressor as brake power (bhp or kW) and defines the ability of a compressor to add pressure for a specific flow to the pipeline system.

The cost of a compression system is the operating and maintenance cost of a compressor under normal conditions and is a major cost of operation.

The following describes a method for calculating compression operating costs [3].

$$OP_{ij} = \frac{E_{ij} \times R_{\text{elec/gas}}}{\text{bhp}_{ij}} \quad (3-1)$$

where OP_{ij} is the operating cost of compressor j at location i , E_{ij} is the energy required to run compressor j within one day at location i , $R_{\text{elec/gas}}$ is the rate of electricity or gas and bhp_{ij} is the bhp_{ij} output of compressor j at location i .

When a compressor is shut down or restarted, generally, more energy is spent. The cost to start or stop a compressor is denoted as penalty costs. The equations for the penalty costs are:

$$e_{ij}^{\text{start}} = \frac{E_{ij}^{\text{start}}}{\text{bhp}_{ij\text{ave}}^{\text{start}}} \times T_{ij}^{\text{start}} \quad (3-2)$$

$$P_{ij}^{\text{start}} = e_{ij}^{\text{start}} \times R_{\text{elec/gas}} \quad (3-3)$$

Where e_{ij}^{start} and e_{ij}^{stop} are the coefficients of energy used by compressor j at location i to start and stop, P_{ij}^{start} and P_{ij}^{stop} are the penalty costs to start and stop a compressor j at location i , E_{ij}^{start} and E_{ij}^{stop} are the excessive energy used to start/stop the compressor, $\text{bhp}_{ij\text{ave}}^{\text{start}}$ and $\text{bhp}_{ij\text{ave}}^{\text{stop}}$ = the average bhp generated within the time interval T_{ij}^{start} and T_{ij}^{stop} = the time to start and stop the compressors.

The following may be noted in connection with calculating compression operational costs:

1. To calculate the penalty costs, it is necessary to obtain the average power output. However, the value is usually unknown in practice because the operator generally operates the compressors in full capacity. bhp can be averaged by dividing each compressor by two

2. Only three costs may be considered: operating cost, start penalty, and stop penalty. The maintenance cost can be ignored since this kind of data is uncertain.
3. If two compressors are of the same types with identical properties, priority may be set between them. The priority should be based on preference of the operator.
4. The location of compressors does not affect the transmission efficiency of gas transmission.

3.2 COMPRESSOR STATION CONFIGURATION

3.2.1 Operating Considerations

When planning a compressor station or, for a new pipeline, a number of stations, certain considerations have to be taken into account. These include:

- steady-state and transient capabilities and requirements of the system
- growth requirements and capability
- total cost of ownership and delivered cost to shippers and customers

The first consideration involves the capability to cope with changes in flow capacity on all time scales (i.e., hourly, daily, seasonally). The pipeline hydraulics relate pressure losses to the flow through the pipeline, determine the compressor operating conditions in terms of head and actual flow, and, subsequently, determine the required power from the driver. Contractual requirements and obligations, such as pressures and volumes at transfer points, have to be considered. The second consideration deals with the fact that the nominal capacity of a pipeline may grow when additional customers demand a higher supply of natural gas. In fact, many new pipelines start out with 50% and less capacity and grow to full capacity over several years or are sized for easy expansion. Often, the prediction of the rate of growth shows a significant degree of uncertainty. The growth scenarios, if foreseeable, drive a station layout to possibly allow additional power to be installed at the station level later or additional stations along the pipeline. The alternative scenario, where the pipeline usage declines over the years (e.g., because the gas supply from the field declines), is also a possibility.

It is important to distinguish between growth scenarios that increase pipeline capacity by adding power along the pipeline and scenarios that add power and loop the pipeline. The former scenario will always require an increase in pressure ratio in the station. It is often necessary to replace single-stage compressors with two-stage compressors or install compressors in series to meet the higher pressure ratio. The latter scenario will usually increase the flow through the station and will be covered by installing additional units parallel to the existing ones.

Total cost of ownership reflects the cost to install, operate, and decommission the stations. Although the first two considerations reflect the capability to generate revenue, the latter focuses on the necessary costs. These costs may appear at any point in time during installation, operation, and decommissioning of the station. An easy way to compare cost of ownership is to use a net present value (NPV) calculation, assuming a fixed discount rate r for n time periods.

Revenue reduction resulting from equipment downtime is an important element of the total cost of ownership. To determine the lost revenue, total annual downtime is multiplied by the estimated lost revenue per hour [4]. Another problem lies in the modeling of risk through the useful life of the project, as well as the economic value associated with this risk [5]. The risk can range from hardware selection to maintenance practice and control system set points. The net effect of these risks translates into downtime or added fuel costs and, hence, added cost or lowered production output. In many cases, lost production for a day creates a loss in the same order of magnitude as the fuel cost for one driver for a whole year. A few days of otherwise lost production can “pay” for the cost of a spare gas turbine.

The requirement derived from this is to plan the stations such that they are tolerant to planned and unplanned outages. This could mean installing a spare unit or to optimize the installation such that the failure or downtime of one unit has the smallest possible impact on the capacity of the overall pipeline. It also means that the downtime in case of failure or planned outage has to be minimized. Possible concepts include engine exchange programs, available spare engines, and preventive maintenance, to name a few.

3.2.2 Types of Compression Equipment

In designing a pipeline, it is important to evaluate the most appropriate type of compression equipment. In general, four different combinations can be considered:

- GT-CC: centrifugal compressors driven by gas turbines
- EM-CC: centrifugal compressors driven by variable speed electric motors
- GM-RECIP: reciprocating compressors driven by gas engines
- EM-RECIP: reciprocating compressors driven by variable speed electric motors

The decision criteria are often based on life cycle cost, flexibility considerations (that usually consider cost as well as the capacity to generate profit), or (in rare cases) acquisition cost. Table 3-1 outlines some general tendencies.

The difference between GT-CC and EM-CC is the type of driver used. While the gas turbine uses small portions of the pipeline gas as fuel, the electric motor requires a reliable source of electric power. The cost of electricity is thus a key factor in the life cycle cost assessment. According to one source (remembering that these costs fluctuate constantly), unless the true cost of electricity is below about US \$0.02/kWh, electric motor-driven concepts are at a disadvantage compared to gas turbine drivers [6]. It also should be noted that, while the local environmental impact of an EMD is low, transmission losses and the source of electricity (which could be a pollution-generating power plant) can increase the overall environmental impact. If the necessary electricity infrastructure is not yet built, the disadvantages become even greater. In particular, the lost opportunity cost during downtime due to an unreliable electricity supply can be significant. It should be noted that an electric motor drive as a system can be very reliable, as long as the electrical power supply is assured. Because the key factor that determines the availability of an EMD station may be the reliability of the power supply, multiple units per station will not increase the reliability significantly.

While many of the older pipeline systems in the United States still use a significant number of gas engine-driven reciprocating compressors, virtually all new installations for mainline pipelines use centrifugal compressor concepts. The reasons typically include the very high maintenance cost of reciprocating machines, as well as the lower availability and reliability and environmental concerns (emissions, lube oil, cooling fluids, etc.).

Table 3-1. General comparison between compressor types [7] (with last column added by author)

Concept	GT-CC	EM-CC*	GM-RECIP	EM-RECIP*
Compressor efficiency	High	High	Medium	Medium
Fuel cost	Low	High**	Low to medium	High**
Installation cost	Medium	Low to medium	Medium to high	Medium
Reliability/availability	High	Medium to high***	Medium	Medium***
Maintenance	Medium	Low	High	Medium
Environmental impact	Low to medium	Low	Medium to high	Low

*Variable frequency drive.

**Dependent on cost of electricity.

***Dependent on the reliability of the electricity supply.

Reciprocating compressors also are at an efficiency disadvantage compared to centrifugal compressors, especially under the typical conditions of a pipeline operation with large flow and relatively low head requirements. However, for smaller pipelines in gathering systems, reciprocating compressors are still quite viable, particularly because small gas turbines are less efficient.

3.2.3 Parallel and Series Configuration

The pressure and flow characteristics of pipelines and other factors may influence the arrangement of compressors in a station as well as the type of equipment used. Besides the question about series or parallel arrangements in a station, the more general question arises about the number of units, standby requirements, type of driver, and type of compressor.

Whether centrifugal or reciprocating, compression can be installed in a number of arrangement/combinations. The following briefly describe the most commonly used configurations, depending on the flow requirements.

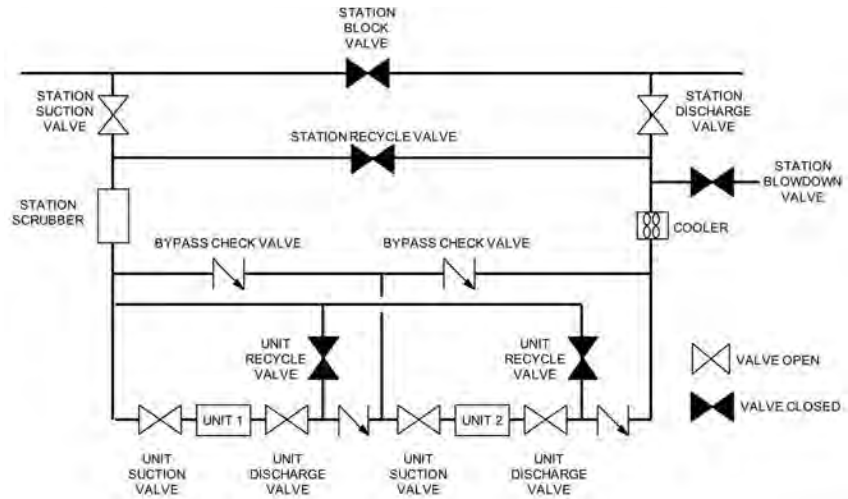
- **Series arrangement.** In a series arrangement (Fig. 3-7(a)), the discharge of one unit becomes the suction of the other. This arrangement is used when a high compression ratio is required across a station. If it is a new station, a two-stage compressor may often meet this same demand.
- **Parallel arrangement.** A parallel arrangement (Fig. 3-7(b)) is used when flows through a station vary to a point where one unit is not capable of accommodating the complete range of flows. In this case, flow is split between the two units. Both units have common suction and common discharge.
- **Series-parallel arrangement.** A series-parallel arrangement may be used when compression is added to an existing station. If a site already has two units in series, an additional larger unit may be added in parallel. This unit will have similar flow and compression ratio capabilities as the other two units combined.

3.2.4 Number of Units

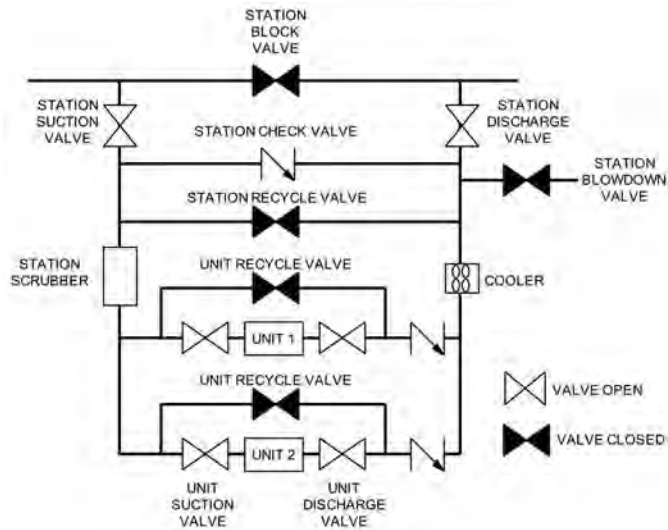
Operational flexibility under a larger number of different operating scenarios has to be studied. Figure 3-8 [7] shows operating points of a compressor station gathered during 6 months of operation. Because of hourly, daily, and monthly variations in demand, the only way to cover the large range of flow and head requirements efficiently was to install three gas turbine-driven centrifugal compressors. Depending on the demand, the station either operates one, two, or all three of the compressors. The map shows the operating envelopes of the compressors. Also indicated are the driver power limitations, based on 75°F (23.9°C) ambient temperature and site conditions. The gas turbines allow for immediate starting capability if the need arises.

Similarly, transient studies on pipeline systems can reveal the often large range of operating conditions that needs to be covered by a compressor station. Lastly, scenarios that arise from failures of one or more systems have to be considered [7]. The quest for operational flexibility can be satisfied on various levels: the compressor and the driver should have a wide operating range. Using multiple smaller units per station rather than one large unit can be another way. Here, the arrangement in series or in parallel will impact the flexibility.

Pipeline systems usually are not operated at full capacity from the very beginning of the project but rather increase the demand when new customers for the gas are found. Smaller units tend to be advantageous in cases where the pipeline system is built up to full capacity over a number of years. The project can then be started with fewer small units. Additional units are installed later to meet the increasing demand on compression. The expenses for



(a) Series compressor configuration



(b) Parallel compressor configuration

Figure 3-7. Most common compressor configurations for gas compression.

portions of the equipment can therefore be delayed. On the other hand, if larger units are used, all of them have to be purchased at the beginning of the project.

3.2.5 Case Study: NPV Comparison Between Immediate and Deferred Unit Installation

An NPV analysis reveals the advantages of the deferring the installation of units if flow increases over a number of years for a new pipeline. It shows in particular that even a higher total cost can translate into a lower NPV if parts of the cost can be deferred (Table 3-2).

Table 3-2(a) defines the number of units required by year and unit size. Table 3-2(b) assumes one standby unit per station, while Table 3-2(c) assumes no station standby unit. For example, in the case of no standby units, installing 5000 hp units in increments (as per

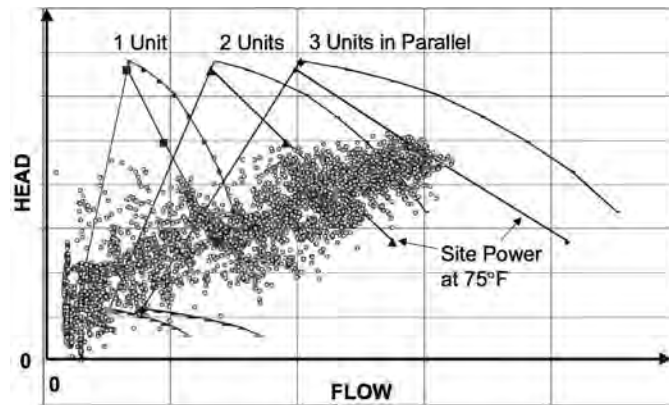


Figure 3-8. Operating points for a six-month period at a compressor station, case A [7].

Table 3-2. NPV evaluation [7]

(a) Number of units necessary

Year/Unit Size	5000 hp	10,000 hp	20,000 hp
1	1 + 1	1 + 1	1 + 1
2	2 + 1	1 + 1	1 + 1
3	3 + 1	2 + 1	1 + 1
4	3 + 1	2 + 1	1 + 1
5	4 + 1	2 + 1	1 + 1

(b) NPV evaluation with standby unit

Unit Size	5000 hp	10,000 hp	20,000 hp
Total first cost	5 × \$4 MM = \$20 MM	3 × \$7.5 MM = \$22.5 MM	2 × \$14 MM = \$28 MM
Net present value (10% discount)	\$17.67 MM	\$21.2 MM	\$28 MM

(c) NPV evaluation with no standby unit

Unit Size	5000 hp	10,000 hp	20,000 hp
Total first cost	4 × \$4 MM = \$16 MM	2 × \$7.5 MM = \$15 MM	1 × \$14 MM = \$14 MM
Net present value (10% discount)	\$13.67 MM	\$13.7 MM	\$14 MM

the 5000 hp column in Fig. 3-2(a) but without the standby unit), the NPV cost will be \$13.67 MM instead of the \$14 MM cost of installing one 20,000 hp unit. The difference for standby units is much larger since the size of the standby unit is much larger for the 20,000 hp scenario.

There are also several potential advantages for using smaller units. During the buildup phase, the smaller units should be operating at peak or near efficiency while the large unit will be running at part load and lower efficiency. However, this will be offset in later years since the efficiency of the larger unit will be higher than that of the smaller units. The other advantage for the smaller unit scenario without a standby unit is that preventive or corrective downtime of one or two units still provides some compression capability.

3.2.6 Standby Units

Because the failure or unavailability of compression units can cause significant loss in revenue, the installation of standby units must be considered. These standby units can be arranged such that each compression station has one standby unit, that some stations have a standby unit, or that the standby function is covered by oversizing the drivers for all stations.

It must be noted that the failure of a compression unit does not mean that the entire pipeline ceases to operate but, rather, that the flow capacity of the pipeline is reduced. Since pipelines have a significant inherent storage capability ("line pack"), a failure of one or more units does not have an immediate impact on the total throughput. In addition, planned shutdowns due to maintenance can be planned during times when lower capacities are required.

Standby units are not always mandatory because modern gas turbine-driven compressor sets can achieve an availability of 97% and higher. A station with two operating units and one standby unit thus has a station availability of $100(1 - 0.032) = 99.91\%$ (because two units have to fail at the same time in order to reduce the station throughput to 50%). A station with one standby unit and one operating unit also yields a 99.91% station availability. However, while failure of two units in the first case still leaves the station with 50% capacity, the entire station is lost if both units fail in the second case. Arguably, installing two smaller 50% units rather than one larger 100% unit could avoid the need for installing a standby unit. A concept that has been discussed from time to time is the approach to have "power" backup rather than "unit" standby on a station. The idea is to have an oversized driver, operating at part load during normal operation rather than an additional standby unit. In this case, the driver has to be sized such that it, together with other (equally oversized) units located further downstream along the pipeline, can pick up the duty of an unavailable station upstream. The advantage of this concept lies in the reduction in the number of units. The disadvantage is that the gas turbine operates at part load and, thus, at lower efficiency for most of the time. Even if the larger gas turbine has an efficiency advantage over a smaller gas turbine at full load (which is, however, not necessarily the case), operating it at part load makes that advantage disappear. Oversized units also limit the turndown capability of a station significantly.

It has often been assumed that for two-unit stations without a standby unit, a parallel installation of the two units would yield the best behavior if one unit fails. However, Ohanian and Kurz [8] have shown that, usually, a series arrangement of identical compressor sets yields a lower deficiency in flow than a parallel installation. This is due to the fact that pipeline hydraulics dictate a relationship between the flow through the pipeline and the necessary pressure ratio at the compressor station. This follows from the fundamental flow equation for a pipeline.

For parallel units, the failure of one unit forces the remaining unit to operate at or near choke, with a very low efficiency. Identical units in series, upon the failure of one unit, would initially require the surge valve to open, but the remaining unit would soon be able to operate at a good efficiency, thus maintaining a higher flow than in the parallel scenario. Figure 3-9 shows the operating point of the respective compressor after the other unit is shut down at $T = 1.0$. While the remaining unit in the series arrangement requires to recycle initially, it moves, starting at about $T = 2.0$, slowly to efficient operating points.

The remaining parallel unit, on the other hand, moves further and further into choke. At time $T = 10.1$ and 7.26 , respectively, either scenario would lead the pressure at the pipeline outlet to drop below the minimum level [8]. Therefore, the compressor in series arrangement gives the operator more time for corrective action. Given the fact that the gas stored in the pipeline will help to maintain the flow to the users, a series installation would often allow for sufficient time to resolve the problem. Therefore, a standby unit could be avoided.

Arranging compressor units in series rather than in parallel can offer a number of advantages in many applications. However, especially if the compression ratio is rather high, it is desirable to use different impellers for the low- and the high-pressure compressor. Otherwise, one or both operate off their best efficiency points. This allows the use of smaller drivers than the drivers needed for installing the compressors in parallel.

This leaves, however, the problem of the staging of a spare unit. A potential solution is described by reference [9]. Providing a spare for every one of the two units in series would have obliterated the advantages of having to install less power. To alleviate this superior series

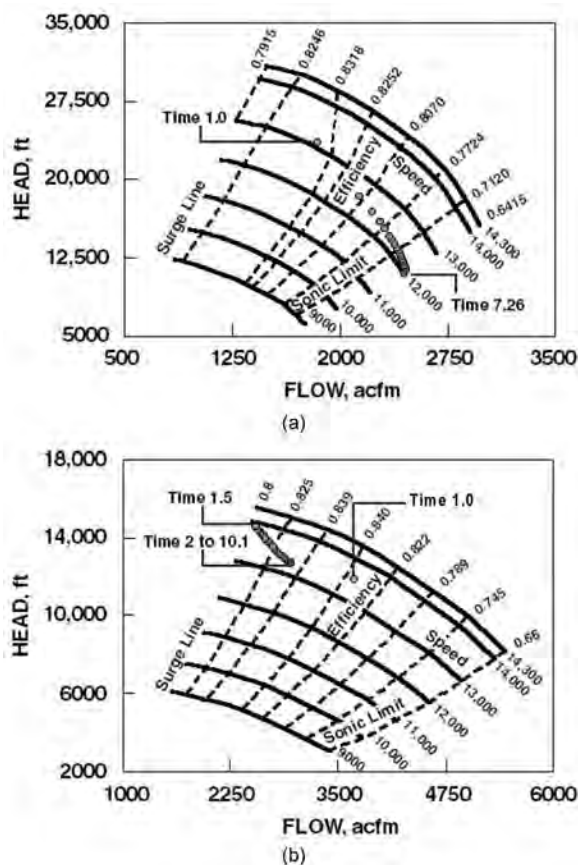


Figure 3-9. Operating points after one unit out of two fails [7]. (a) Parallel compressor arrangement. (b) Series compressor arrangement.

configuration's disadvantage, the station asymmetrical approach was devised. The uniqueness of this approach assumes two identical turbine compressor units in series arrangement (i.e., one LP and one HP unit), with the standby unit identical to LP and HP units (Fig. 3-10). Because of the high-pressure ratio (this was explained earlier in chapter), the staging for all three units are different from each other. However, an aerodynamic design was found for the "spare" such that it can cover either LP or HP duties without exceeding any aerodynamic or mechanical limits. In this design, the compressor characteristic curve of the spare unit is in between those of the LP and HP compressors.

3.2.7 Environmental Considerations

Any activity has to be judged by its impact on the environment. This includes the requirement to keep NO_x, CO, and UHC emissions at an acceptable level. For many operations, meeting certain maximum emission levels is a requirement for continuous operation. Further, the amount of CO₂ produced as a result of the combustion process has to be considered. For a given fuel, the only way to reduce the amount of emissions is to improve the gas turbine or engine efficiency.

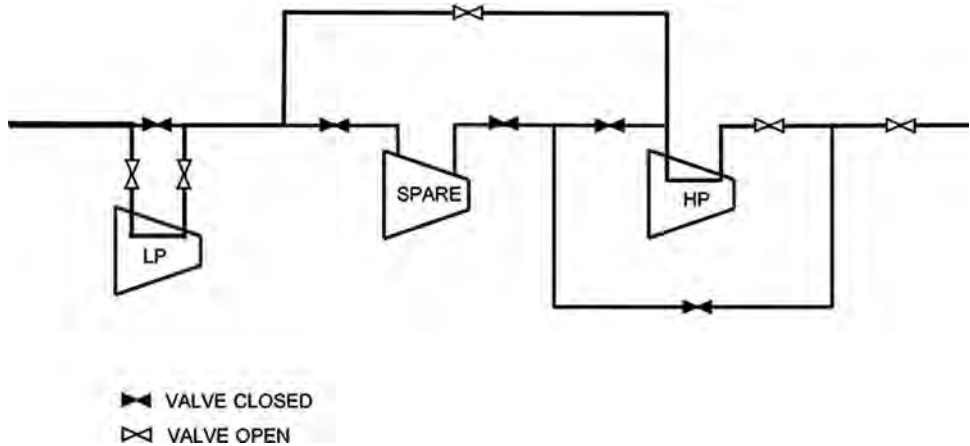


Figure 3-10. Arrangement of asymmetric series compressors with spare unit [9].

3.2.8 Case Study: Comparison of Different Usage Scenarios for Pipeline Stations

A typical operating scenario for pipeline stations, showing a wide variety of operating points, can be seen in Fig. 3-8 (case A). Figure 3-11 shows another scenario for a typical mainline pipeline (case B). Here data for four stations along the pipeline under summer and winter conditions were averaged.

For the purpose of this evaluation, the load (i.e., the power requirement relative to the available power at each station and respective ambient conditions) for each of the two scenarios was mapped into different load classes, shown in Figs. 3-12 and 3-13, respectively. The data lend themselves to a study to assess the effect of different station designs, in particular, the number of units used.

We can calculate the fuel usage, as well as the amount of emissions for cases A and B, assuming the following scenarios:

- I. One 100% unit with driver efficiency of 35% at full load and a compressor efficiency of 87%
- II. Two 50% units with driver efficiency of 34% at full load and a compressor efficiency of 86%
- III. Two 50% units with driver efficiency of 35% at full load and a compressor efficiency of 87%
- IV. Three 33% units with driver efficiency of 32% at full load and a compressor efficiency of 85%
- V. Three 33% units with driver efficiency of 35% at full load and a compressor efficiency of 87%

Gas turbines exhibit different behavior regarding part-load efficiency, as seen in Fig. 3-14, with the steeper drop in thermal efficiency at part load associated with dry low-emission engines. The following series of calculations is performed using a curve that reflects the steepest drop in part-load efficiency (series 2) and one that reflects the least steep drop in part-load efficiency (series 1). There is a minimum in fuel usage for the curve that reflects the steepest drop in part-load efficiency and one that reflects the least steep drop in part-load efficiency in three units (which incidentally is the station layout).

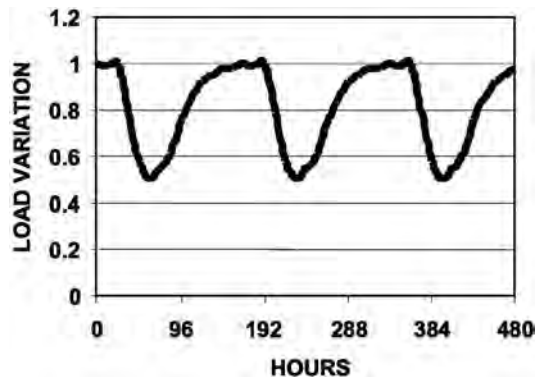


Figure 3-11. Averaged load variations for four stations of a mainline pipeline during winter and summer scenarios, case B [7].

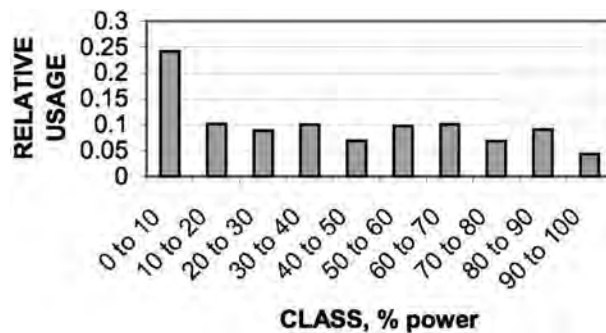


Figure 3-12. Power usage distribution for case A [7].

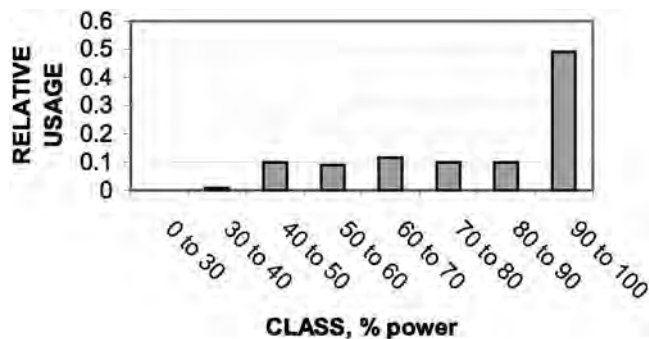


Figure 3-13. Power usage distribution for case B prior to averaging [7].

Figure 3-15 shows the relative fuel usage (and thus also CO emissions) for the different scenarios, based on a part-load efficiency penalty. The more stations used, the less important the slope for part-load efficiency becomes. The minimum in fuel usage also implies a minimum in CO production. Case A exhibits the clear advantage of multi-unit stations. Because the smaller units are operated closer to full load for most of the time, the resulting fuel usage is lower than for single-unit stations. This holds true for both slopes in part-load efficiency and even if the smaller units achieve a lower base efficiency than the larger units. For virtually all cases, a station with three or four units minimizes the fuel usage. Additional units yield no additional benefits.

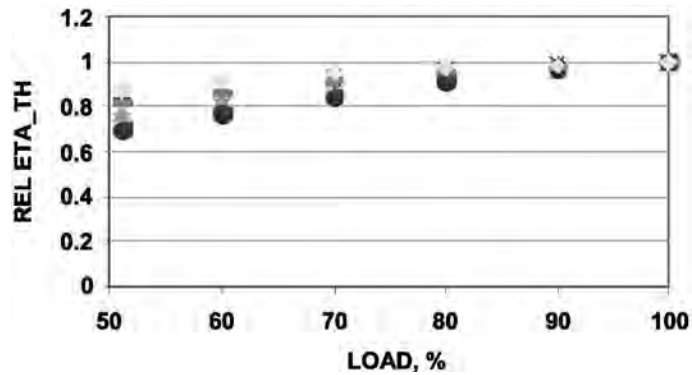
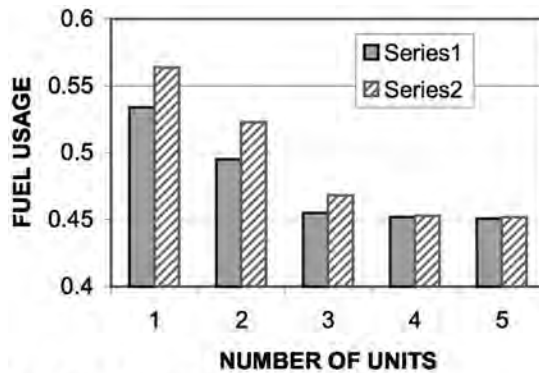
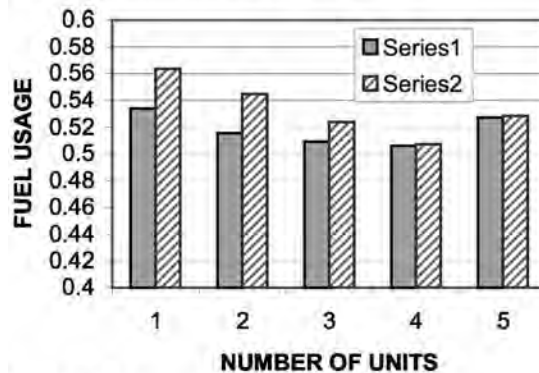


Figure 3-14. Relative thermal efficiencies for typical two-shaft gas turbines [7].



a. Case A Scenarios I, III, and V



b. Case A Scenarios I, II, and IV

Figure 3-15. Fuel usage scenarios for case A [7].

Case B gives a somewhat different picture. Comparing Fig. 3-16a and b shows that the conclusion regarding the optimum number of stations depends highly on the baseline efficiency of the packages involved. If the smaller units have the same design efficiency as the larger units, then a three-unit station is advantageous. If we assume lower efficiencies for the smaller units than for the larger units, a one- or two-unit station uses less fuel.

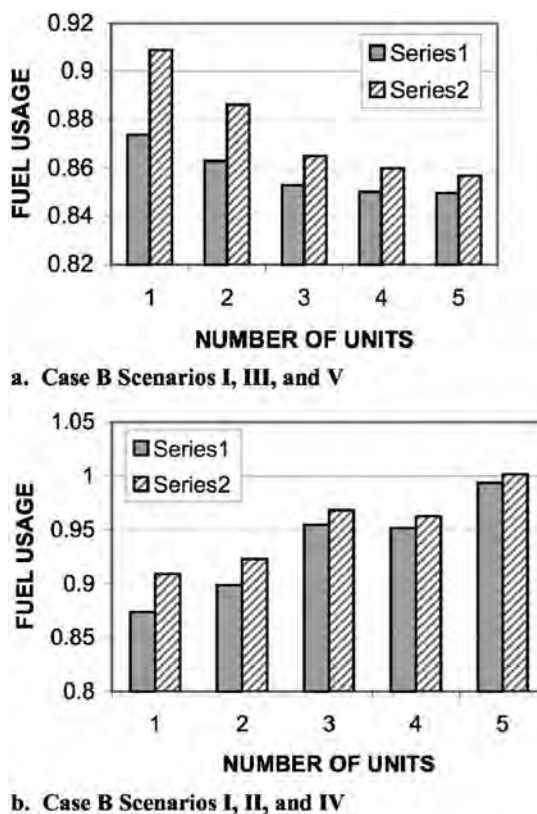


Figure 3-16. Fuel usage scenarios for case B [7].

Having said that, it again needs to be emphasized that a station outage may cause significantly higher cost due to lost revenue than the fuel cost for an entire year. Obviously, a standby unit reduces the exposure significantly. In addition, if the station uses multiple units, then the unavailability of one of these units has a smaller impact on the amount of gas that can be produced (admittedly, the chances that one out of four units fails are higher than the chances that one out of two units fail).

One result seems to be that for EMDs, with a relatively smaller penalty for part-load operation, the differences in power usage become very small. This means that the decision will depend more on the installation and first cost, thus probably favoring the larger units. This is particularly true if a significant impact on availability is driven by the reliability of the power supply, where obviously the number of units has little impact on the overall availability.

The emission calculations are based on the assumption that most DLN engines achieve a constant level of NO_x emissions, on a PPMV or mg/nm³ basis, for a load range from 50% to 100%. Standard combustion systems achieve reduced NO_x levels on a PPMV or mg/nm³ basis at part load because the fuel-to-air ratio is reduced at part load. CO emissions, on the other hand, are entirely dependent on engine efficiency (assuming the fuel composition, especially the carbon-to-hydrogen ratio, remains unchanged).

Interestingly, multiple units also provide for advantages in the absolute amount of emissions. As outlined in Fig. 3-17, the lowest absolute NO_x emissions for engines with dry low-NO_x systems occur for a four-unit station. This is due to the usually lower part-load efficiency of dry low-NO_x engines. Standard combustion engines are less sensitive, but even here, there is a slight advantage for a three-unit station. It should be noted that the emissions displayed in Fig. 3-17 are normalized, with the numbers from the respective

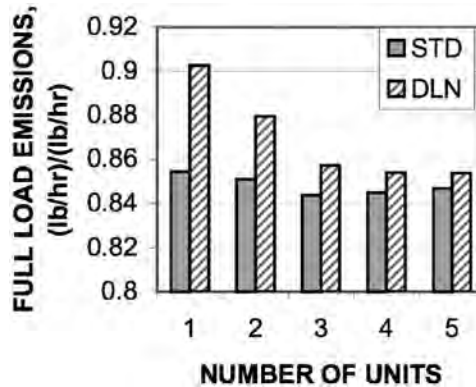


Figure 3-17. Comparison of NOx emissions for standard and DLN combustion systems for case B [7].

combustion systems at full load. Thus, the absolute amount of NOx emissions in lb/hr for a dry low-NOx system is significantly lower than for a standard combustion system. The other cases follow a similar trend as the calculations for fuel usage.

3.2.9 Compressor Requirements

The study of operating scenarios suggests certain requirements for the compression system. Beyond the quest for higher compressor peak efficiencies, operating requirements [8] require a compressor capable of operating over a wide operating range at high efficiency. Wide operating range in a centrifugal compressor can be achieved by a combination of means. Aerodynamic theory suggests a strong relationship between operating range, efficiency, and impeller backswamp [10]. However, there is a practical limit to the amount of backswamp. In particular, increasing backswamp reduces the capability of an impeller of given tip speed to make head. With the capability to use two impellers in a casing, this perceived disadvantage can be eliminated. The operating range is further increased by the use of a vaneless diffuser. The question whether a station should be equipped with compression units in series or in parallel cannot be answered universally. While the series approach can have advantages in case one of the units fails [11], the decision process has to take into account issues such as further expansion, backup strategies, operational strategy and aerodynamic performance.

The aerodynamic aspects can be considered with the following equation for specific speed:

$$N_s = N \frac{q^{1/2}}{H^{3/4}} \quad (3-4)$$

Equation 3.4 and the subsequent discussion use N in rpm, H in J/kg, and q in m³/s.

Centrifugal impellers can be described by their specific speed, where a high specific speed depicts a low-head, high-flow impeller. There is a range of specific speeds where centrifugal impellers tend to exhibit good aerodynamic performance, while both very low and very high specific speeds penalize the performance. From data presented in Fig. 3-18, one can conclude that specific speeds between 0.09 and 0.14 tend to yield good efficiency. Mixed-flow impellers can extend this range to higher specific speeds. It must be noted that the actual running speed (N) is determined by the power turbine speed of the gas turbine, unless a gearbox is used. For aerodynamic and mechanical

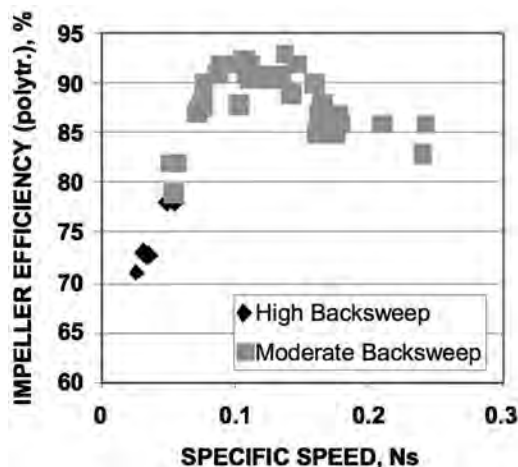


Figure 3-18. Impeller efficiency vs. specific speed for various well-designed impellers [12].

reasons, power turbine speeds are lower for larger gas turbines than for smaller ones. For example, a typical 15 MW (20,000 hp) class gas turbine may have a power turbine speed of about 8500 rpm, while a typical 3.5-MW (5000-hp) class gas turbine may run at about 16,000 rpm.

For any given pipeline compressor station, two units in series will yield a higher specific speed than two units in parallel. Thus, once the driver size (and, thus, the power turbine speed) and the desired head and flow through the station are known, one can conceptually decide whether the series or the parallel approach would lead to better aerodynamic performance.

Consider a pipeline application with two units in a station. The total station flow is 7 m³/s. The total station head is 50,000 J/kg. The driver required has an optimum power turbine speed of 11,000 rpm.

The specific speed for the first unit if the units are in series (the second unit would have to use the same impeller, but at a different operating point closer to surge), is:

$$N_s = 11,000 \frac{7^{1/2}}{60 \times 25,000^{3/4}} = 0.244 \quad (3-5)$$

The specific speed for the first unit if the units are in parallel is:

$$N_s = 11,000 \frac{3.5^{1/2}}{60 \times 50,000^{3/4}} = 0.103 \quad (3-6)$$

In this case, parallel operation would yield an impeller that potentially has a better efficiency.

3.2.10 Driver Requirements

Certain driver operating characteristics need to be considered:

- Power and heat rate depend on ambient temperature and barometric pressure for gas turbines and naturally aspirated engines but not for electric motors and turbo-charged engines except at high altitudes.

- For gas turbines, driven equipment speed has an impact on power turbine efficiency. The impact of different speeds can be described by the difference between the operating speed and the optimum power turbine speed. This optimum power turbine speed is a function of engine load and ambient temperature.
- Efficiency is significantly reduced at part load for gas turbines, depending on their type, and only moderately for engines and electric motors.

3.3 STATION LAYOUT AND FACILITIES

3.3.1 Station Layout

Compressors for gas transmission service are installed in various configurations, depending on the range of head-flow characteristics expected at the compressor station site. However, station layout is standardized to the maximum extent possible, incorporating all requirements of pipeline, compression and other applicable codes.

A pipeline compressor station normally consists of the following systems and components:

- high-pressure piping and valves
- scrubbers or filters and liquid removal
- gas coolers
- compressor(s) and driver(s)
- station and unit auxiliary systems
- station and unit control systems
- buildings and weather protection
- environmental controls and safety systems
- security systems

Compressor stations generally include the above facilities laid out systematically in an enclosed area that considers safety and security. An example of such a station layout is shown in Fig. 3-19.

The compressor station may include the following, as detailed in Fig. 3-20:

1. Gas compressor building
2. Station control building
3. Utility gas building
4. Fire hut
5. Gas compressor building (future)
6. Covered drum rack
7. Aerial coolers
8. Recycle valve building
9. Cold storage building

Although more southern stations feature normal air cooling, those in the north where permafrost is encountered require facilities such as gas-to-gas exchangers or refrigeration. This is done to lower discharge temperatures to manage thawing of the permafrost and ensure integrity of the downstream pipeline.

3.3.2 Station Piping Layout

Station piping and associated components common to centrifugal stations can be described from the suction side valve to the discharge side valve, with reference to Fig. 3-21.



Figure 3-19. Typical compressor station layout (courtesy of TransCanada).

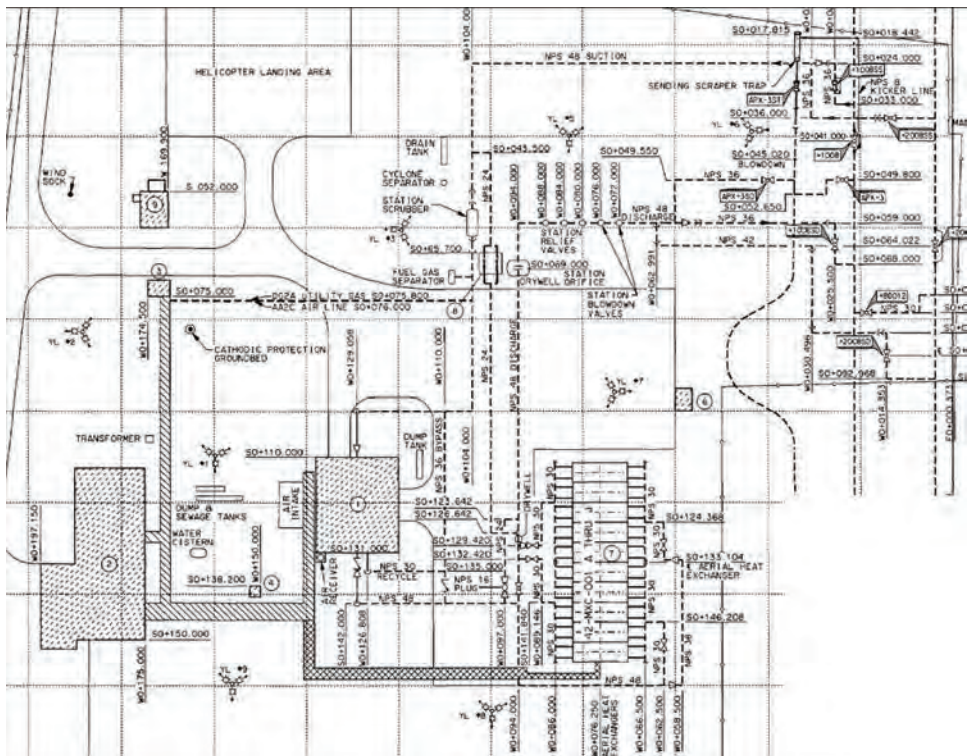


Figure 3-20. Typical station layout (courtesy of TransCanada).

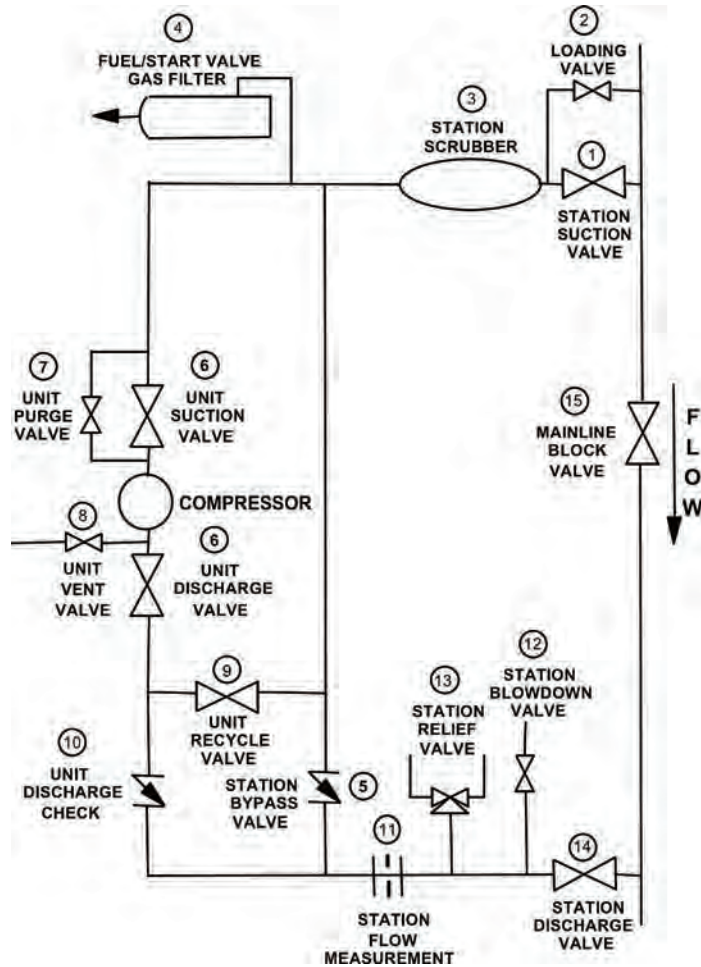


Figure 3-21. Typical centrifugal compressor station piping arrangement.

1. A station suction side valve is installed to isolate the station from the pipeline.
2. A station loading valve is used to purge and pressurize the compressor station piping.
3. A station scrubber is installed to clean the gas, knocking out liquids and solid contaminants to protect the compressors.
4. A fuel/start gas filter further cleans the gas to the quality required for the compressor driver fuel/start gas systems.
5. A bypass line with check valve is installed between the suction and discharge header to allow bypassing of compressors when they are not operating and to allow gas on the suction side to be vented in the event of a blow-down.
6. Unit suction and discharge valves are used for isolating the compressor units while the yard piping remains pressurized.
7. A unit purge valve is used to purge and pressurize the compressor in preparation for operation.
8. A unit vent valve is used during purging the compressor and to depressurize the compressor after shutdown.
9. A unit recycle valve is used to unload the compressor while it is starting or stopping, and occasionally during operation, to keep the dynamic compressor from surging.
10. A unit discharge check valve is installed to prevent backflow through the compressor while it is starting or stopping.

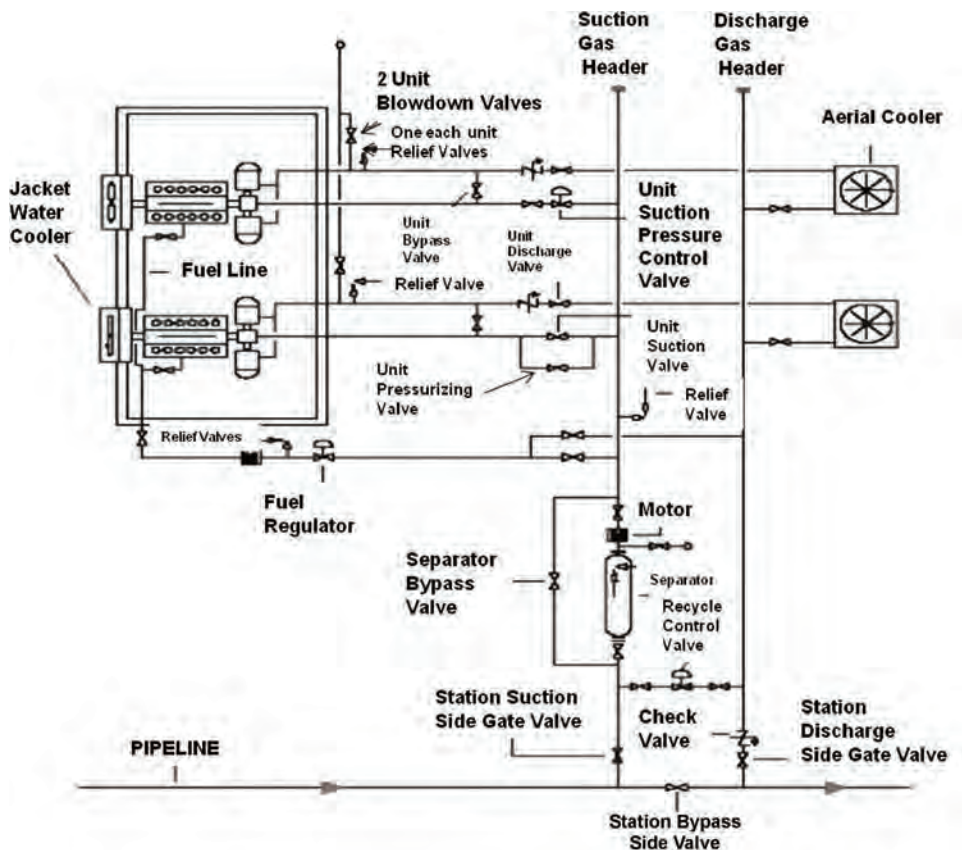


Figure 3-22. Typical reciprocating compressor station piping arrangement.

11. A flow measurement device, typically an orifice meter, is installed to measure the flow of gas going through the compressor.
12. A blow-down valve is installed to vent all high pressure piping in the yard. Valves 1, 2, 6, 7, 8, 12, 14, and 15 are connected to the station emergency shutdown system and are sequenced on gas or fire detection, power failure, or manual operation of the ESD system.
13. A station relief valve is installed to protect the station piping/equipment from over-pressure in the event of failure of the protective and pressure control systems.
14. A station discharge side valve is installed to isolate the station from the pipeline.
15. A mainline block valve is installed in the pipeline and is closed to divert gas through the station when compression or free flowing through the station is desired and opened when the flow is to bypass the station.

Station layout, equipment, and piping for a reciprocating station is indicated in Fig. 3-22. This layout shows internal combustion engines driving reciprocating compressors. The primary difference is that it has a bypass valve for use on startup and shutdown instead of the surge control/recycle valve needed to prevent surge with a centrifugal compressor.

3.3.3 Scrubbers and Filters

Although pipeline gas is usually quite clean, there is still the possibility of entrained liquids and particulates that must be removed prior to compressions. Liquid removal occurs on the



(a)



(b)

Figure 3-23. Inlet liquid removal. (a) Cyclone scrubber. (b) Filter.

suction side of the compressor station. Scrubbers such as the one shown in Fig. 3-23(a) are constructed with a plate to catch liquid slugs followed by plates that swirl the flow and inertially separate the liquids. Filter-type separators [Fig. 3-23(b)] incorporate demister pads in addition to inertial separation. Liquids are collected in a tank below the scrubber or filter and disposed of according to local environmental practices and regulations.

3.3.4 Gas Coolers

Gas coolers are often used on the discharge side of the compressors to protect downstream pipe coatings and improve pipeline efficiency, particularly at stations with a high-pressure ratio and resultant high discharge temperature. They may also be placed between stages to increase the compression efficiency of the downstream compressor and increase reliability. However, they contribute to pressure losses and a total economic analysis must be done in order to weigh the costs of increased capital against the operating benefits.

Figure 3-24 illustrates a standard gas cooling arrangement with forced-draft air cooling over a piping manifold and another example can also be seen in Fig. 3-19.



Figure 3-24. Typical aftercooler for gas cooling.

3.3.5 Station and Unit Auxiliary Systems

The specific auxiliary systems found at a compressor station will depend largely on the driver, driven equipment and design philosophy. If gas turbines or gas engines are utilized, a fuel gas system will be needed to remove liquids, reduce pressure, and apply heating if necessary. For electric motors, a high-voltage electrical system will be needed. Instrument air is commonly used for instrumentation and this requires air compressors, vessels, and distribution. For some components such as large valves, high-pressure gas may be used for actuation and may serve a similar purpose as air for instrumentation. Low-voltage electrical supply is an obvious necessity.

3.3.6 Station and Unit Control Systems

Control systems have gone through major changes over the past few decades and advances in computerization and information technology will continue to impact them. Station control systems are not only integrated with pipeline supervisory systems in support of remote operation, but they are being tied into corporate information networks to make general monitoring information available to operations, maintenance and engineering departments.

Control systems for compressor stations exist at four levels:

- Supervisory control—remote operation of the station from centralized pipeline control
- Station level control—overall control of valves, drivers and driven equipment at the station level
- Driver and driven equipment unit control—specific control of the driver and its driven equipment, including fuel control, start-up and shutdown sequencing, protection and monitoring
- Auxiliary system level control—lower level independent control of specific system functions such as the lube oil system

Modern station and unit control systems use digital control, although some older ones may still have systems based on solid-state electronics, relays, or possibly, even pneumatic control. They are fully integrated into the pipeline automation network and are accessible not only to the SCADA system but also company and customer networks.

The overall control and monitoring of a pipeline system occurs at a central control location. The major ability to control and change pipeline flow and pressures is obtained by pump and compressor units. In modern pipeline systems, these units are started and stopped remotely by the supervisory control and data acquisition (SCADA) system. Set-points of flow or pressure for the station are provided to the station control system. The supervisory system will have access to basic operating data, including process flows, temperatures and pressures, unit running status and engine speed. More detailed monitoring information may be passed to engineering and maintenance groups.

Overall control of the station can be based on flow, suction, or discharge pressure bounded by various applicable limits. For mainline transmission, discharge pressure is the most widely used since operation at MAOP (maximum allowable operating pressure for the pipeline) yields the most efficient operation for the pipeline. The pressure rise across the compressor is directly linked to flow since a higher pressure ratio leads to higher flow.

Suction throttling or recycling can also be used to control flow for both reciprocating and centrifugal compressors but are only temporary measures because they waste large amounts of energy. Reciprocating compressors can use clearance volume or speed control to vary capacity.

Compressor control is accomplished by adjusting the fuel source and thus the driver speed. Minimum and maximum limits depend on the type of driver. Gas turbines are limited by speed and turbine inlet temperature as a function of inlet air temperature. Electric motors are speed-limited as are gas engines.

The centrifugal compressor has its own limits of minimum and maximum speed, minimum flow, and choke or high flow. The antisurge system protects the compressor against the damaging effects of surge by opening a recycle valve and thus increasing flow through the compressor. Reciprocating compressors are speed-limited to prevent mechanical damage at high piston and component speeds.

Operating conditions are extensively monitored with the use of computer-based HMI (human-machine interface) with the ability to store large amounts information in data historians. This data is invaluable for condition monitoring systems both on site and remotely.

A variety of auxiliary systems are not controlled by the main unit control system. Examples are lube oil cooling temperature control carried out by a thermostatic valve, pulsing of air intake filters based on pressure drop, and control of gas turbine inlet guide vanes.

3.3.6.1 Shutdown Control

An important part of station control is managing the shutdown of units and control of station valves in response to different situations.

1. Station shutdown restartable (SSDR) mode

This shutdown mode is triggered by one of the following transient process conditions:

- High discharge pressure
- Low suction pressure
- High discharge temperature

On detection of one of these conditions, a normal stop is sent to the units. As seen in Fig. 3-25, valves return to a normal shutdown position with no change in station main valve position. Units can be restarted remotely when desired. The unit valves stay open and the compressor is pressurized for a certain time period.

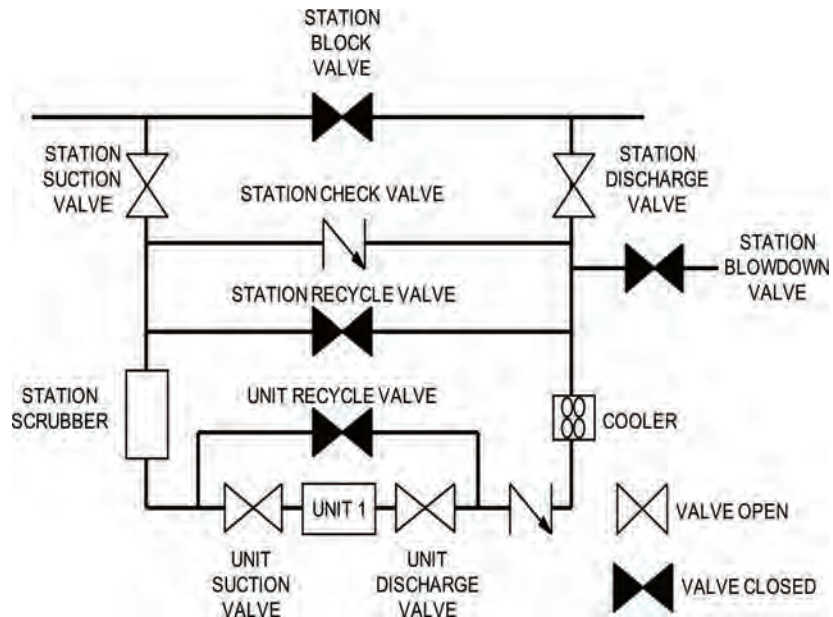


Figure 3-25. Station Shutdown Restartable (SSDR) Mode.

2. Station shutdown lockout (SSDL)

This shutdown condition is triggered by any of the following non-transient conditions:

- Valve fault
- Station scrubber high liquid level shutdown
- Station scrubber high differential pressure shutdown

On detection of any of these conditions, a hard-wired emergency stop is issued to the units and the station suction and discharge valves signaled to close. As soon as the differential pressure across the station block valve is at a low enough value to permit safe opening of the block valve, it is signaled to open (see Fig. 3-26). The condition has to be cleared before the station can be brought back into service.

3. Emergency shutdown (ESD)

This shutdown condition is triggered by a non-transient condition during which it is unsafe to have piping pressurized. Any of the following can trigger an ESD:

- fire
- high gas level (gas leak)
- unit seal failure and unit valves fail to close
- low control voltage
- manual ESD via push button

On detection of any one of these conditions, the following occurs (see Fig. 3-27):

- A station shutdown lockout is issued, causing the units to stop, the suction and discharge valves to close, and the block valve to open.
- When the station suction and discharge valves are both fully closed, the station blowdown valve opens, venting all gas within the station to the atmosphere.

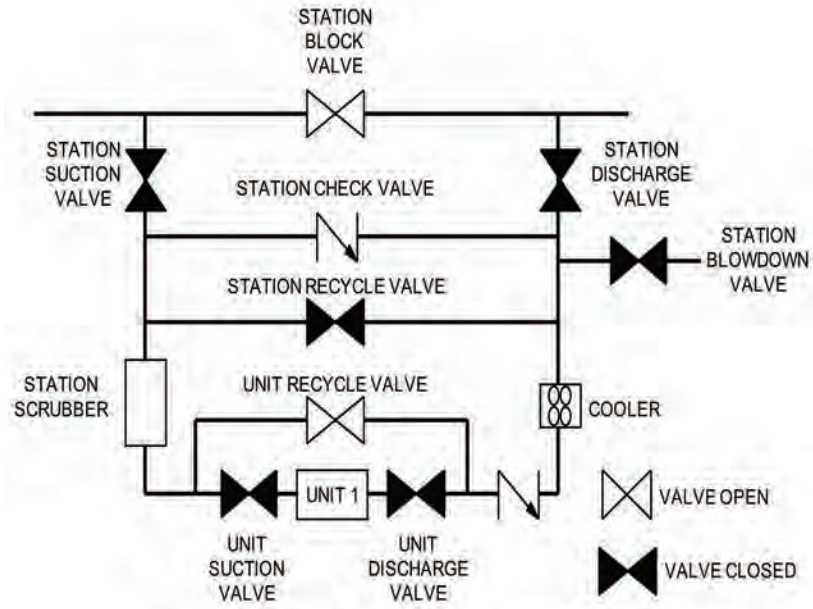


Figure 3-26. Station Shutdown Lockout (SSDL).

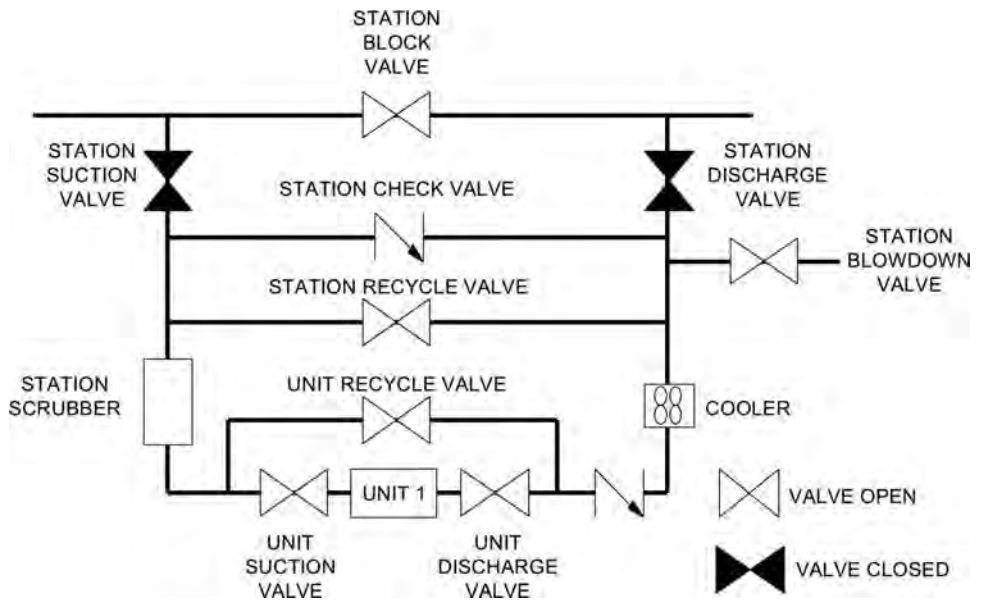


Figure 3-27. Emergency Shutdown (ESD).

3.3.7 Buildings and Weather Protection

Requirements for buildings and weather protection are specific to local climatic conditions as well as environmental regulations. Noise especially is becoming a more critical issue where compressor stations are close to human habitation. Gas turbines normally are placed in an enclosure for safety and operator protection purposes. These enclosures are vented for cooling and elimination of minor gas leakage. In cold climates, heating has to be provided in buildings.

3.3.8 Safety Systems and Environmental Controls

Various safety systems are standard at all compressor stations. An ESD system reacts automatically to emergency conditions such as fire and gas detection and excessive pressure. Manual activation can be done not only from the control room but also from at least two points outside of the gas area, preferably near exit gates. This shuts down all compression equipment, de-energizes electrical equipment close to gas facilities, closes station block valves, and blows down station piping. Automatic pressure relief valves activate if the pressure rises more than 10% above MAOP.

Venting of gas on unit or station shutdown must be done safely and many compressor stations vent gas to a flare system where it is discharged without hazard or combusted to reduce emissions.

3.3.9 Codes and Standards

Many codes and standards are used by compressor manufacturers and users to specify, select, and characterize their equipment. Codes are generally used to provide design guidelines and definitions, describe procedures for manufacturing, procurement, and testing and indicate where modifications or exceptions may apply. They do not specify the actual design. User requirements may override or enhance the codes.

For compression applications in the pipeline sector, the most commonly used standards are:

- API 541: Form-Wound Squirrel-Cage Induction Motors 500 Horsepower and Larger
- API 546: Brushless Synchronous Machines 500 kVA and Larger
- API 612/ISO 10437: Petroleum Petrochemical and Natural Gas Industries—Steam Turbines—Special-Purpose Applications
- API 613: Special Purpose Gear Units for Petroleum, Chemical and Gas Industry Services
- API 614/ISO 10483-1: Lubrication, Shaft-Sealing, and Control-Oil Systems and Auxiliaries for Petroleum, Chemical and Gas Industry Services
- API 616: Gas Turbines for the Petroleum, Chemical and Gas Industry Services
- API 617: Axial and Centrifugal Compressors and Expander-Compressors for Petroleum, Chemical and Gas Industry Services
- API 618: Reciprocating Compressors for Petroleum, Chemical and Gas Industry Services
- API 619/ISO 10440-1: Rotary-Type Positive Displacement Compressors for Petroleum, Petrochemical and Natural Gas Industries
- API 670: Machinery Protection Systems
- API 671/ISO 10441: Special Purpose Couplings for Petroleum, Chemical and Gas Industry Services
- API 672: Packaged, Integrally Geared Centrifugal Air Compressors for Petroleum, Chemical, and Gas Industry Services
- API 677: General-Purpose Gear Units for Petroleum, Chemical and Gas Industry Services
- API RP 684: API Standard Paragraphs Rotordynamic Tutorial: Lateral Critical Speeds, Unbalance Response, Stability, Train Torsionals, and Rotor Balancing
- API RP 686: Machinery Installation and Installation Design
- API RP 688: Pulsation and Vibration Control in Positive Displacement Machinery Systems for Petroleum, Petrochemical, and Natural Gas Industry Services
- ASME B133: A Series of Standards for Gas Turbines

- ASME PTC-22: Performance Test Code On Gas Turbines
- ASME PTC-10: Performance Test Code on Compressors and Exhausters
- ISO 3977: Gas Turbines—Procurement
- ISO 5389: Turbocompressors—Performance Test Code
- NFPA 70: National Electrical Code

The American Petroleum Institute (API) is the primary trade organization for the US petroleum industry. API has over 400 member companies that cover all aspects of the oil and gas production. API is an accredited American National Standards Organization and started developing industry specific codes in 1924. Currently, API publishes about 500 standards, which are widely referenced by the Environmental Protection Agency, Occupational Safety and Health Administration (OSHA), Bureau of Land Management, American Society of Mechanical Engineers, and other codes and regulations. API's philosophy for developing codes is based on the following principles:

- improve safety
- improve environmental performance
- reduce engineering costs
- improve equipment interchangeability
- improve product quality
- lower equipment cost
- allow for exceptions within reason

However, as with most other codes, API specifications often lag technology developments, especially in the rapidly changing gas turbine and compressor markets. There is a trend to adoption and development of international standards, namely, ISO (International Standards Organization) and IEC (International Electrotechnical Commission), and many API standards are in the process of being converted.

REFERENCES

- [1] Mohitpour, M., Golshan, H., and Murray, A., 2007. "Pipeline Design & Construction, A Practical Approach," 3rd ed., ASME Press, ISBN 0-7918-0156-X.
- [2] Emerson ESI (Energy Solutions International), 2008. "PipelineStudio®," <http://www.emerson.com/en-us/catalog/emerson-pipelinestudio>.
- [3] Uraikul, V., Chan, C. W., and Tontiwachwuthikul, P., 2003. "MILP Model for Compressor Selection in Natural Gas Pipeline Operations," Environmental Informatics Archives, Volume 1, 138-145, ISEIS Publication #002.
- [4] Hsu, L. L., and Hasselfeld, D. E., 1998. Total Cost of Ownership as a Business Tool in Turbomachinery Decisions, Turbomachinery Technology Seminar, San Diego.
- [5] Smalley, A. J., and Mauney, D. A., 1997. "Risk-Based Maintenance of Turbomachinery," Proceedings 26th Turbomachinery Symposium, Houston, Texas, pp. 177-187.
- [6] McKee, R. J., Durke, R. D., Kuhl, C. A., 1999. "Factors that Influence the Selection of Electric Motor Drives for Natural Gas Compressors," The INGAA Foundation, pp. 1-58.
- [7] Kurz, Ohanian, and Lubomirsky, 2003. "On Compressor Layout," Proceedings of ASME Turbo Expo 2003, Power for Land, Sea and Air, June 16-19, 2003. Atlanta, Georgia, USA, pp. 1-10.
- [8] Ohanian, S., and Kurz, R., 2002. "Series or Parallel Arrangement in a Two-Unit Compressor Station," Transactions of the ASME, 124, pp. 936-941, October 2002.
- [9] Kurz, R., and Lubomirsky, M., 2003. "Asymmetric Solution for Compressor Station Spare Capacity," Proceedings of ASME Turbo Expo 2006: Power for Land, Sea and Air, May 8-11, 2006, Barcelona, Spain, GT2006-90069, pp. 1-10.

- [10] Cumpsty, N. A., 1989. *Compressor Aerodynamics*, Longman, Essex, UK.
- [11] Ohanian, S., Kurz, R., and Lubomirsky, M., 2001. "Compressor Station Layout and Operation Considerations," *Proceedings of the Beijing International Pipeline Conference*, PRC.
- [12] Rogers, C., 1980. "Efficiency of Centrifugal Compressor Impellers," *Centrifugal Compressors Flow Phenomena and Performance*, AGARD CP 282.

DESIGN AND OPERATION OF PUMPS

4.1 PUMPS FOR LIQUID PIPELINE STATIONS

Pumps convert externally supplied mechanical energy into potential energy within the fluid. This energy is used to:

- raise the liquid elevation
- force the fluid into a pressurized system
- overcome flow generated friction caused by pipe roughness

The type of pump selected depends on both technical, operating, and economic considerations including:

- process parameters for capacity, pressure and temperature
- system discharge head required
- suction head available
- sizes of pumps
- efficiency of pumps
- suitability of pump for fluid handled
- reliability, availability, and capability of pump
- flexibility and ease of pump operation
- maintainability of pump
- capital cost for pumping system
- operating and maintenance costs

Type of pumps that are meet various industrial and specific needs are [1]:

- kinetic pump types (ANSI/HI 1.1–1.2)
- vertical pump types (ANSI/HI 2.1–2.2)
- rotary pump types (ANSI/HI 3.1–3.5)
- seal-less centrifugal pump type (ANSI/HI 5.1–5.6)
- reciprocating power pump type (ANSI/HI 6.1–6.5)
- direct-acting (steam) pump type (ANSI/HI 8.1–8.5)

Figure 4-1 illustrates pump families and indicates that types of pumps to choose from are very diverse. To select the optimum pump for the application, technical and economic aspects must be carefully determined and evaluated. Two categories of pumps are generally used by the pipeline transmission industry: kinetic and positive displacement as shown in

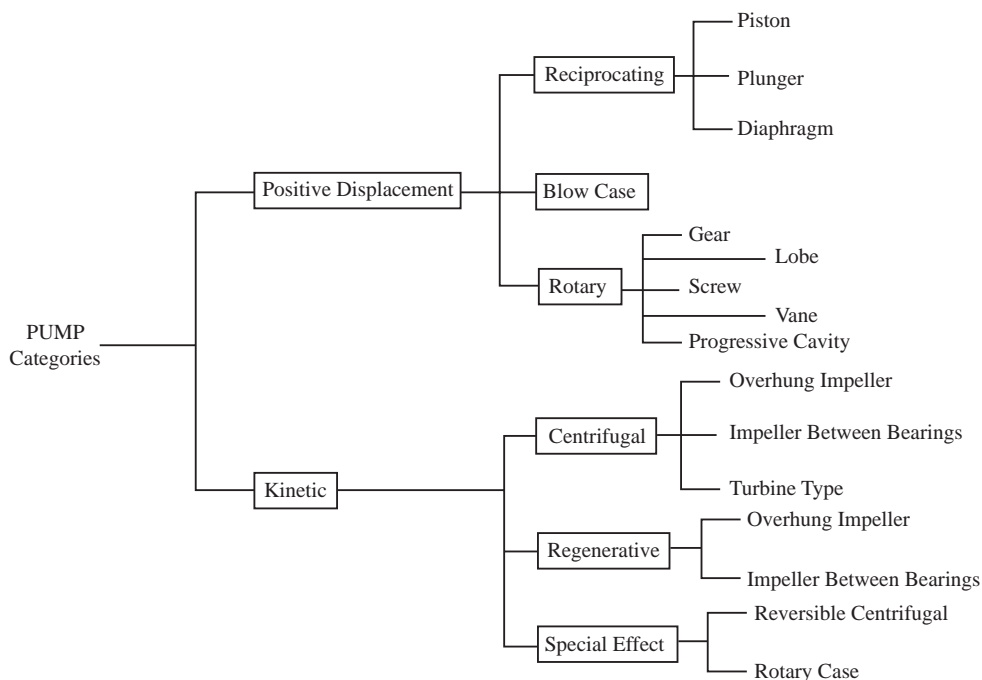


Figure 4-1. A generalized pump family group.

Fig. 4-1. Generally, pipeline transmission applications use centrifugal pumps which fall under the category of kinetic pumps (Fig. 4-2) while upstream and lower flow pipelines may use a variety of centrifugal, reciprocating, and rotary pumps.

Centrifugal pumps are generally high-speed, high-volume units connected through speed increasers to internal combustion engines or directly to electric motors. In large stations, such pumps are generally connected in series, allowing each pump to handle total flow, and each adds an increase in pressure (head) to the liquid being moved.

Centrifugal pumps offer certain distinct advantages; principal among these is that the flow of liquid from them is relatively even and smooth with very few pulsations. Properly installed and operated, little or no vibration results from their use. These pumps can be used outside or in small buildings, need only light foundations, and can be easily kept clean. In addition, they are comparatively low-cost, simple to construct and flexible to operate, and require a comparatively small space.

For upstream and lower flow applications, positive displacement pumps are more common. Positive displacement pumps of the reciprocating type can be categorized as in Fig. 4-3 and rotary pumps are shown in Fig. 4-4.

One significant difference between the various pump types is the relationship between the head produced for a certain flow. As shown in Fig. 4-5, the reciprocating pump can develop a constant head regardless of flow while the head decreases with flow for rotary pumps and even more so for centrifugal pumps.

4.2 PUMP HISTORY

Pump history dates back as far back as when the fire piston was invented in Southeast Asia for starting fires (and subsequently in Europe in the early 1800s). It consists of a piston which, when quickly rammed into a cylinder, causes adiabatic compression and

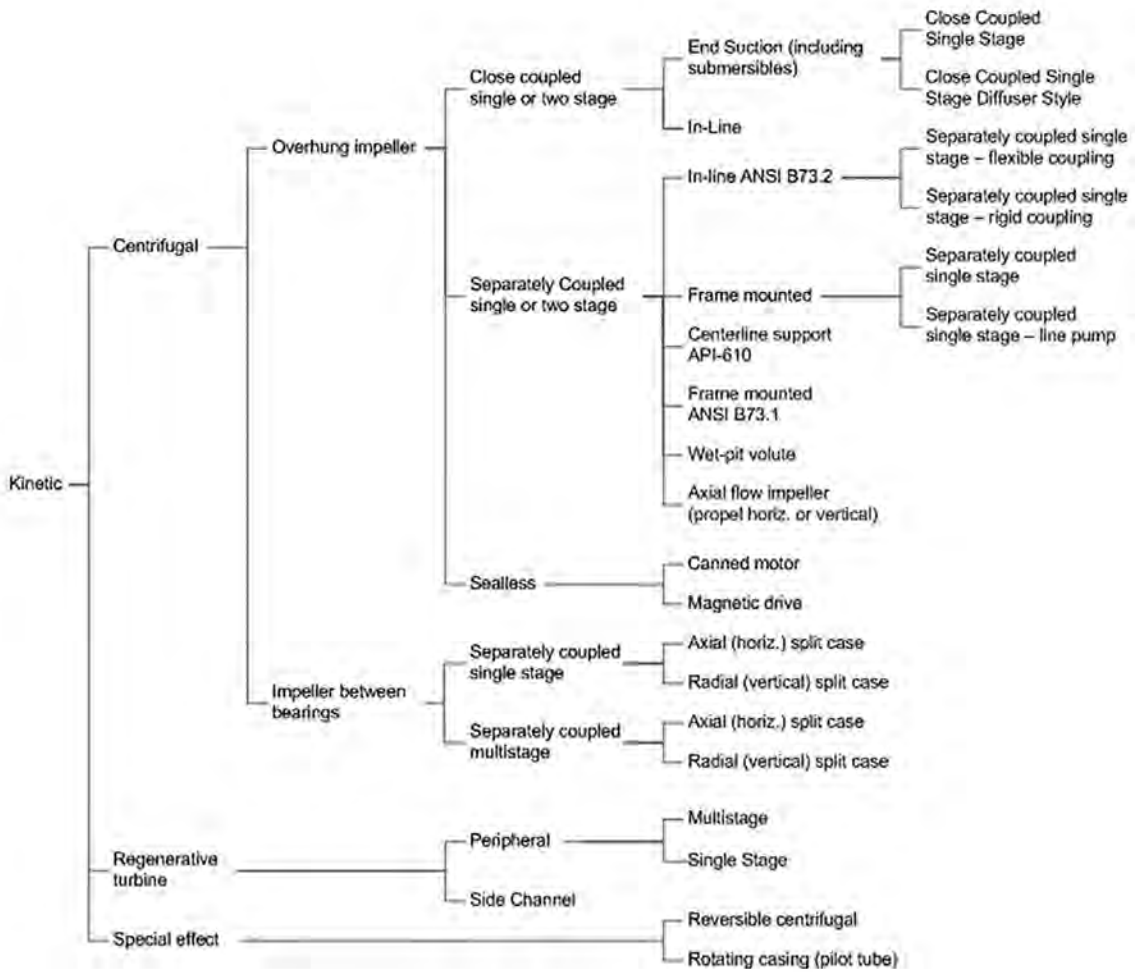


Figure 4-2. Family of kinetic pumps (courtesy: Hydraulic Institute, Parsippany, NJ, www.Pumps.org).

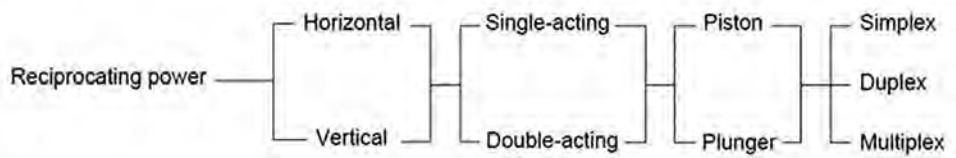


Figure 4-3. Family of reciprocating pumps (courtesy: Hydraulic Institute, Parsippany, NJ, www.Pumps.org).

a rapid increase in temperature that then ignites kindling. The fire piston preceded the match which has its origin from southeast Asia.

Romans in Britain (ca. 409) produced a two-barreled reciprocating pump cut from a block of wood, lined with sheet lead. However, rotary pumps were too difficult to make until after 16th century (as described by Ramelli in 1588). Bellow pumps were first demonstrated in 1511, and bucket pumps for water, driven by waterwheels or animal gears, were introduced in Saxon mines ca. 1540.

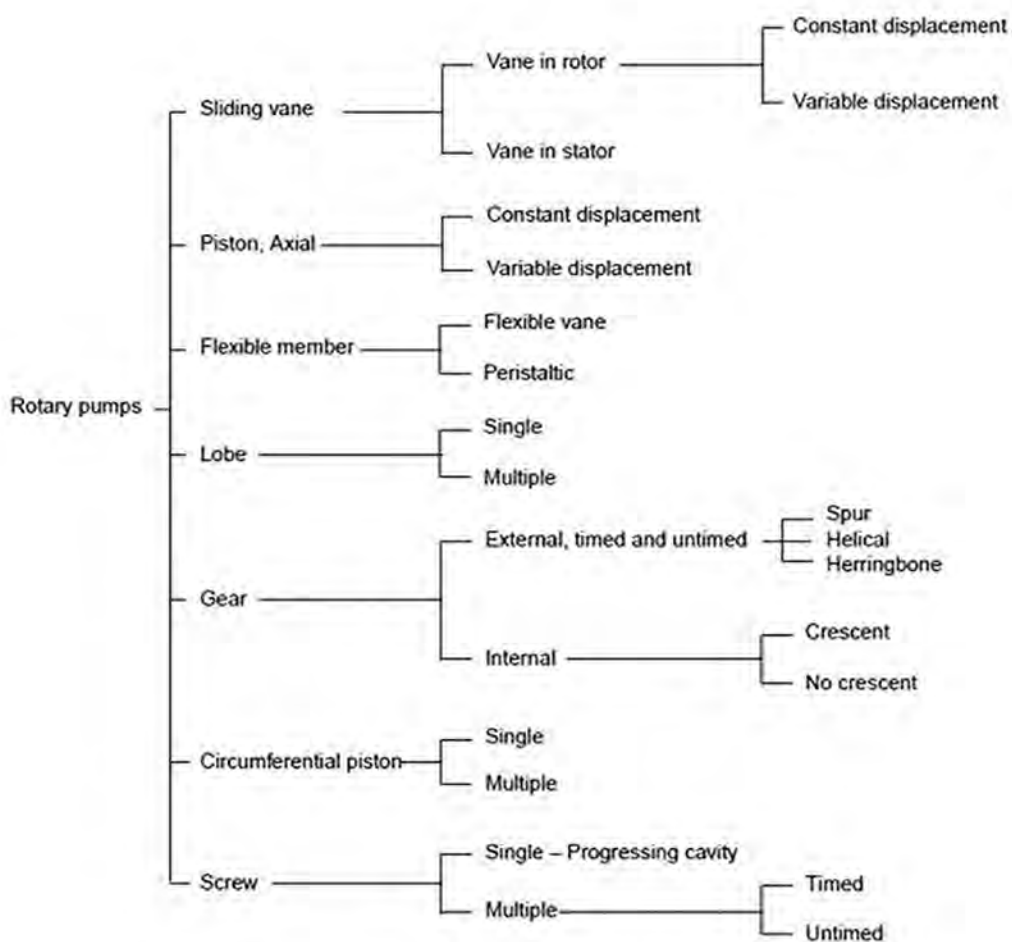


Figure 4-4. Family of rotary pumps (courtesy: Hydraulic Institute, Parsippany, NJ, www.Pumps.org).

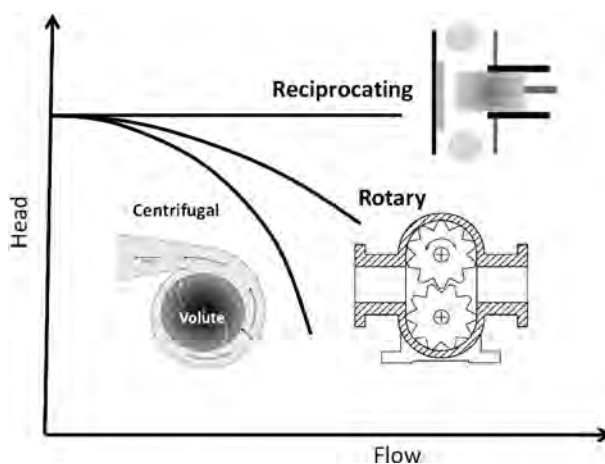


Figure 4-5. Typical pump types for pipeline application and head-flow curves [2].

London Bridge Waterworks was established in 1582 using undershot tide-mill pumps. Other important events in pump development and usage since 1600 are chronologically listed below [3]:

1600	Gear pump invented by Kepler
1600–1699	Various rag-and-chain pump used to drain Cornish mines in Britain
1600–1699	Appearance and basic development of centrifugal water pumps
1629	Giovanni Branca described water-operated pumps (impulse steam turbine)
1635	Gearwheel pump was illustrated by Schwenter
1650 ca.	Use of machine-bored pump barrels and use of flanged and bolted pipes
1652	First air (vacuum) pump devised
1658	Air pump experiments conducted by Boyle and Hooke
1674–1675	Patent of plunger-type pumps, by Isaack Thomson (1675)
1680	Invention of simple centrifugal pump
1689	Centrifugal (Hessian) relates to internal combustion engine
1721	Evolution of modern manual fire engine
1732	First description of simple centrifugal pump
1732 ca.	Diaphragm pump invention, Gosset and Deville in UK
1739	First design of semi-balanced valve and brass pump bucket
1746	Lifting pump devised using Archimedian screw
1755	Direct air-pressure mine pump used at Chemnitz
1768	Introduction of chain pump into ships
1772	Statical mercury vacuum pump
1781	Introduction of rope pump
1818	Introduction of centrifugal pump in the United States (Massachusetts)
1830 ca.	Pelton wheel, first use of bucket vanes curved to Archimedean spirals
1830 ca.	Bucket-pump system introduced at British colliery to sink shaft
1834	Patent of hydraulic belt pump
1849	Steam direct-acting steam pump invented: for Simplex pumps
1857	Patent of Feathering chain pump
1857–1859	Invention of duplex steam pump invented
1860	Duplex water-works engine built
1865	Invention of mercury vacuum pump (to solve a problem with the carbon filament lamp)
1868	Patent of vertical direct-acting flywheel pump
1870 ca.	Introduction of jet pump
1871	Patent of differential valve motion for direct-acting pump
1872	Invention of pulsometer steam pump in UK
1875	Patent of multistage centrifugal pump
1877	Direct air-pressure pump for sewage system in Britain
1880	Introduction of vertical direct-acting compound pumping engine
1880	Air-lift pump
1886	Introduction of vertical triple-expansion pumping engine in US
1891	First British vertical triple-expansion pumping engine (Britain)
1900 ca.	Direct air pressure pump
1910	Water elevator
1916	Establishment of the Baumé scale by The US National Bureau of Standards
1919	Caruelle water elevator
1921	Creation of API Gravity Scale for measuring hydrocarbon densities
1945 ca.	Joint development for high pressure vessels

4.3 CENTRIFUGAL PUMPS

4.3.1 Types of Centrifugal Pumps

Centrifugal pumps are fluid-kinetic machines designed for energy increase within a rotating impeller. Therefore, it is also called the hydrodynamic pumping principle. According to this principle, the fluid is accelerated through the impeller. In the outlet connection of the centrifugal pump, the resulting increase in speed is converted into delivery head.

Centrifugal pumps have prevalent application in liquid pipeline transmission systems because they are capable of handling variable heads and flow rates. There are two types of centrifugal pumps typically used on a liquid pipeline: booster pumps and mainline pumps. Booster pumps are used to pressurize oil at a terminal in order to provide sufficient suction head for the subsequent mainline pumps. These are often vertical pumps as shown in Fig. 4-6 since these have a built-in positive suction due to their design but may also be standard horizontal pumps such the ones shown in Fig. 4-7. The use of multiple lower flow pumps provides flexibility in managing flows from terminal tanks. Larger mainline pumps, such as the one in Fig. 4-8, are applied on transmission lines both after terminal booster pumps and along the pipeline. These pumps can handle multi-products and other liquids over a wide range of viscosities and other properties.

Centrifugal pumps are traditionally divided into three types: radial flow, mixed flow, and axial flow (Fig. 4-9). There is a continuous change from the radial flow impeller, which develops pressure principally from the action of centrifugal force, to the axial flow impeller, which develops most of its head by the propelling or lifting action of the vanes on the liquid.



Figure 4-6. Vertical booster pump (courtesy of Flowserve).



Figure 4-7. Centrifugal booster pumps.

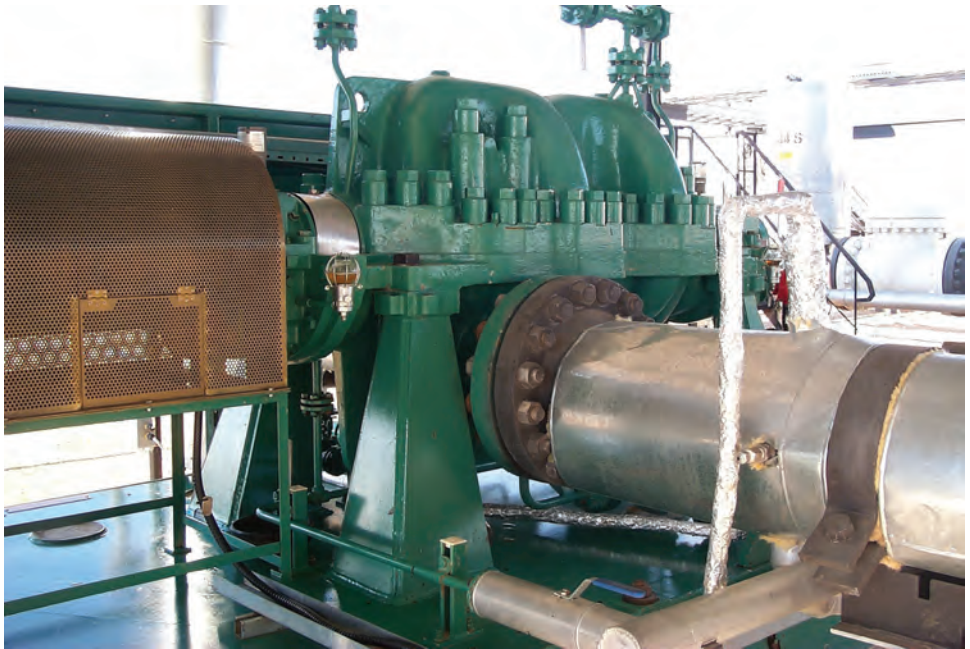


Figure 4-8. Centrifugal pump for mainline transmission.

Radial Flow. Pumps in which pressure is developed principally by the action of a centrifugal force are classified as radial flow pumps. Generally, such pumps with a single inlet impeller have a specific speed below 4200, and pumps with double suction impellers have a specific speed below 600. Liquid enters the impeller at the hub and flows radially to the periphery.

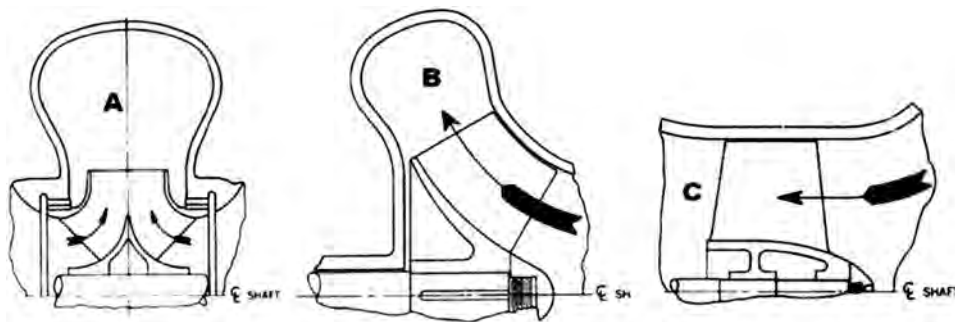


Figure 4-9. Centrifugal pump cross sections, A: radial flow, B: mixed flow and C: axial flow (courtesy: Hydraulics Institute, Parsippany, NJ, <http://www.pumps.org/www.Pumps.org>), ANSI/HI 2007.

Mixed Flow. Pumps in which head is developed partly by centrifugal force and partly by the lift of the vanes on the liquid are classified as mixed-flow pumps. This type of pump has a single inlet impeller with the flow entering axially and discharging in an axial and radial direction. Specific speeds generally range from 4200 to 9000.

Axial Flow. Axial-flow pumps are sometimes called propeller pumps and develop most of their head by the propelling or lifting action of vanes on the liquid. These pumps have single inlet impellers with flow entering axially and discharging nearly axially. Specific speed of this type of pump is usually above 9000.

Other ways of classifying centrifugal pumps are:

- Single-stage pump: pumps in which total head is developed by one impeller.
- Multi-stage pump: pumps having two or more impellers acting in series in one casing.
- Volute pump: pumps having a casing made in the form of a spiral or volute.
- Circular casing pump: pumps having a casing of constant cross-section concentric with the impeller.
- Diffuser pump: pumps with diffusion vanes.
- Horizontal pump: pumps with the shaft normally in a horizontal position.
- Vertical pump (dry pit-type): vertical shaft-type pumps located in dry wells.
- Single-suction pump: pumps equipped with one or more single suction impellers.
- Double-suction pump: pumps equipped with one or more double suction impeller.

Centrifugal pumps are designated as rotating either clockwise or counterclockwise. To determine the type of rotation for horizontal pumps, stand at the driving end facing the pump and note the type of rotation. For vertical pumps, determine the rotation by looking at the top of the pump.

4.3.2 Centrifugal Pump Design

Centrifugal pumps function by spinning an impeller submerged in a fluid (Fig. 4-10). Impeller vanes impart rotary motion to the liquid; centrifugal effects push the liquid towards the outer edge of the impeller. This displaced liquid leaves the impeller and is collected by the shaped volute, which decelerates the fluid, converting kinetic energy to potential energy. This potential energy is expressed as increased pressure and decreased velocity. The liquid being displaced from the impeller creates a partial vacuum at the centre of the

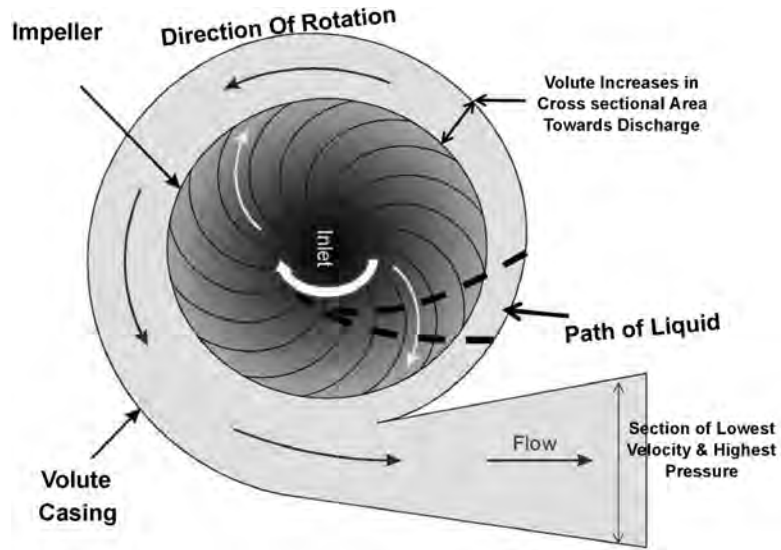


Figure 4-10. Functioning of a centrifugal pump.

impeller, permitting more liquid to enter from the pump suction. The impeller is a close fit in the volute casing to reduce the amount of back-flow bypass in the impeller. Centrifugal pumps may include several stages in series, each comprising one impeller, stage casing, and volute.

The impeller provides velocity energy to the liquid. The high velocity at low pressure is converted into low velocity at high pressure in the volute or diffuser by gradually increasing the flow area. Generally, the impeller provides 40% of the energy and volute casing the remainder. There are different impeller design which are use depending on application. These are:

- straight vane, single suction closed
- francis vane, double suction close
- open mixed flow
- axial flow
- open impeller with partial shroud
- radial vane, non-clogging impeller
- paper pulp impeller

Centrifugal pump configuration includes the following:

- horizontal single stage, end suction pump
- vertical in-line single stage pump
- high speed vertical in-line pump
- horizontal two stage end suction pump
- vertical in-line multi-stage pump
- single-stage radial split casing pump
- horizontal multi-stage split casing pump
- multi-stage barrel casing pump
- horizontal multi-stage ring section pump
- high-pressure multi-stage barrel casing pump

Most process pumps are of end-suction design; these pumps have an axial suction flange and a radial delivery flange generally cast or fabricated into a single casing (Fig. 4-11). Pipeline pumps are mostly side suction and discharge. The centrifugal action within the pump takes place as follows:

- The pump shaft is rotated by an external source (e.g., an electrical motor). The impeller rotates inside the stationary casing.
- Liquid flows into the impeller from the suction piping. The impeller imparts velocity energy to the fluid.
- The liquid velocity energy is converted into pressure energy as it passes through the volute or diffuser.

Pump components include the rear housing/cover, containing the mechanical shaft seal that is clamped to the rear of the casing, with a static seal formed by a gasket or O-ring. The pump shaft passes through the rear cover and carries the impeller. The pump shaft is supported by a bearing housing fitted with two rolling element bearings. There is a large air gap between the rear of the mechanical seal and the bearing housing to prevent process liquid leakage past the seals and hence compromising the bearing system. The rear end of the shaft is normally fitted with a flexible coupling, linking the pump to the driver.

Modern end suction pumps are designed such that the working parts of the pump may be withdrawn in a single unit for maintenance. This “back pull out” unit is the complete pump, including the seal, less the front casing. Back pull out units can be exchanged quickly but it is still necessary to inspect the front casing for damage and carry out an alignment check as part of the job.

Centrifugal impeller pump arrangements depend on fluid entry and discharge type, casing arrangement, and staging. Such impeller arrangements are indicated in Fig. 4-12.

Centrifugal pumps are generally the most common and preferred for pipeline applications and are characterized by:

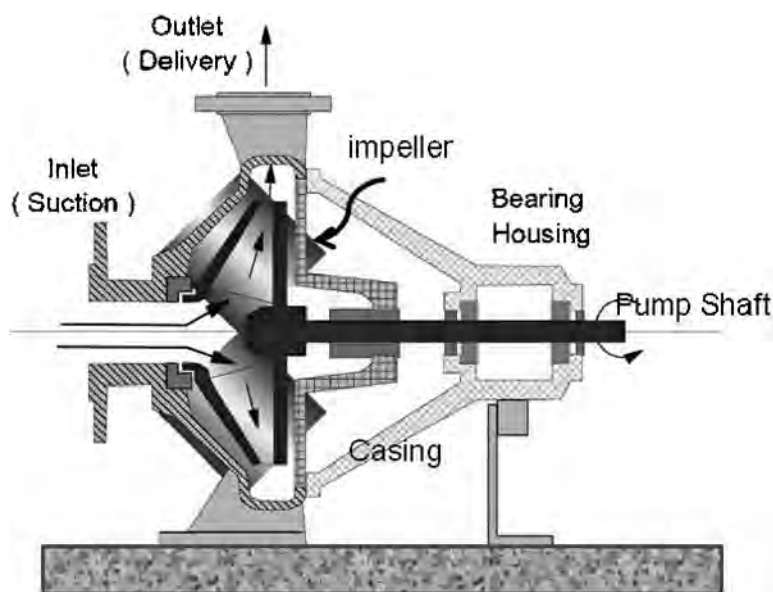


Figure 4-11. Typical suction end overhung impeller pump.

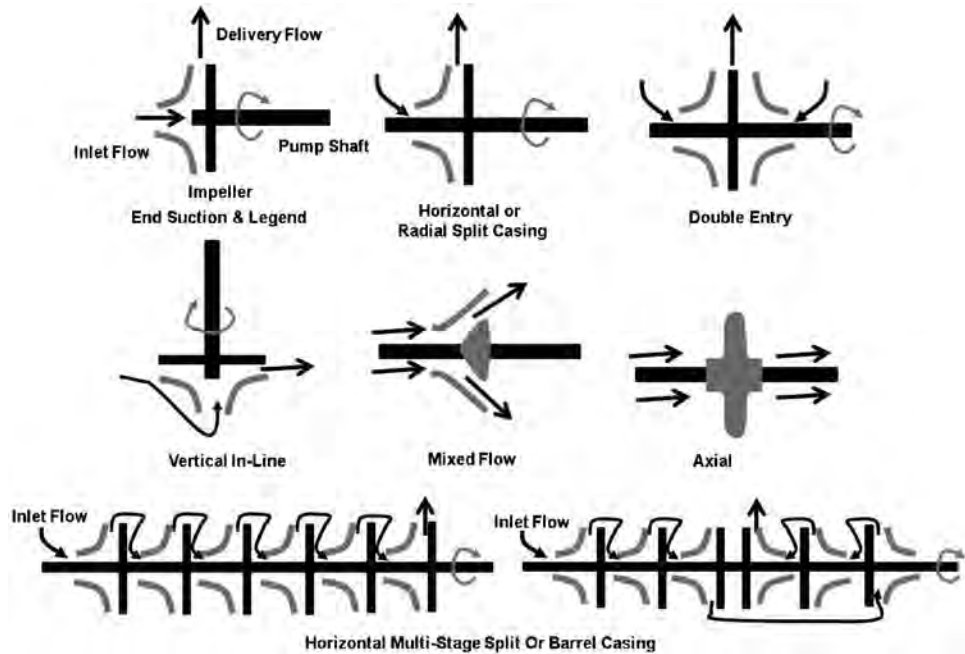


Figure 4-12. Centrifugal pump impeller design/arrangements.

- minimal discharge pulsation;
- capability of efficient performance over a wide range of pressure and capacities (a requirement for most pipeline applications);
- capability of high and variable throughputs;
- discharge pressure and hence head mostly a function of fluid density;
- relatively small devices so they are less costly than other types of pumps;
- high reliability;
- able to be used with viscosities up to 300 centipoise (cP), depending on pump size and speed before efficiency losses begin to be economically significant;
- ability to be multi-staged for higher heads.

Some typical mainline pipeline centrifugal pumps are shown in Figs. 4-13 and 4-14. The double-suction design in Fig. 4-13 is the most common one since the axial thrust is balanced and it can handle higher flows. The multi-stage version in Fig. 4-14 is more appropriate for upstream and high head applications.

Various configurations exist for vertical pumps with the most appropriate one for pipeline boosting featuring suction and discharge at the top of the pump to facilitate piping connections (Fig. 4-15). With the suction at the bottom, this ensures sufficient suction head, even as the tank levels in the terminal decline.

4.3.3 Centrifugal Pump Mechanical Seals

The most sensitive and critical component of a pump is the mechanical seal. It is required to operate at a wide range of pressures and temperatures. On multi-product pipelines, it must handle a variety of fluids of varying specific gravities from light hydrocarbons to heavy viscous sulfurous crude oils and contaminants. Sealing must be reliable with low leakage and perform well under intermittent service with many stops and high-pressure startups.

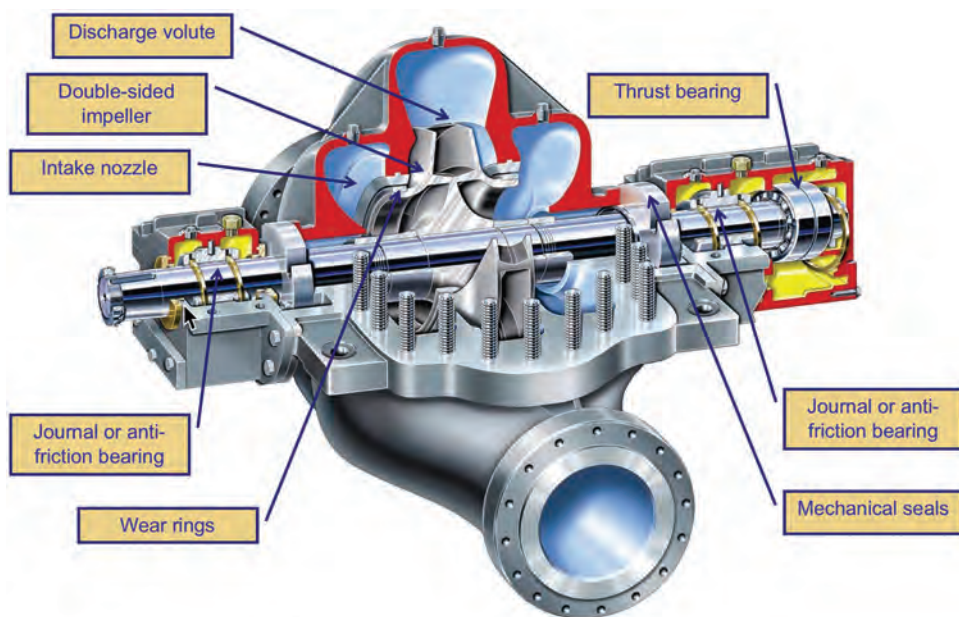


Figure 4-13. Typical pipeline double-suction centrifugal pump (courtesy of Flowserve).

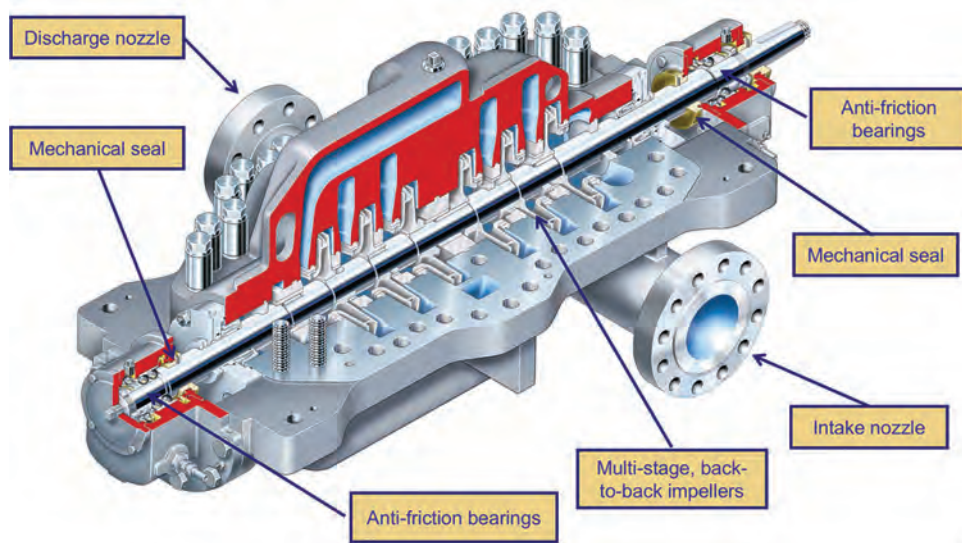


Figure 4-14. Typical pipeline multi-stage centrifugal pump (courtesy of Flowserve).

Two distinct maximum pressures apply to a mechanical seal. The maximum static sealing pressure is the maximum pressure encountered by the seal when the pump is shut down. The maximum dynamic sealing pressure is the maximum pressure while the pump is running or during startup and shutdown conditions. These pressure may vary widely, particularly where there are several pumps in series. The static pressure may be 2–10 times higher than the dynamic pressure depending on the configuration of the pump with respect to its position in the series of pumps.

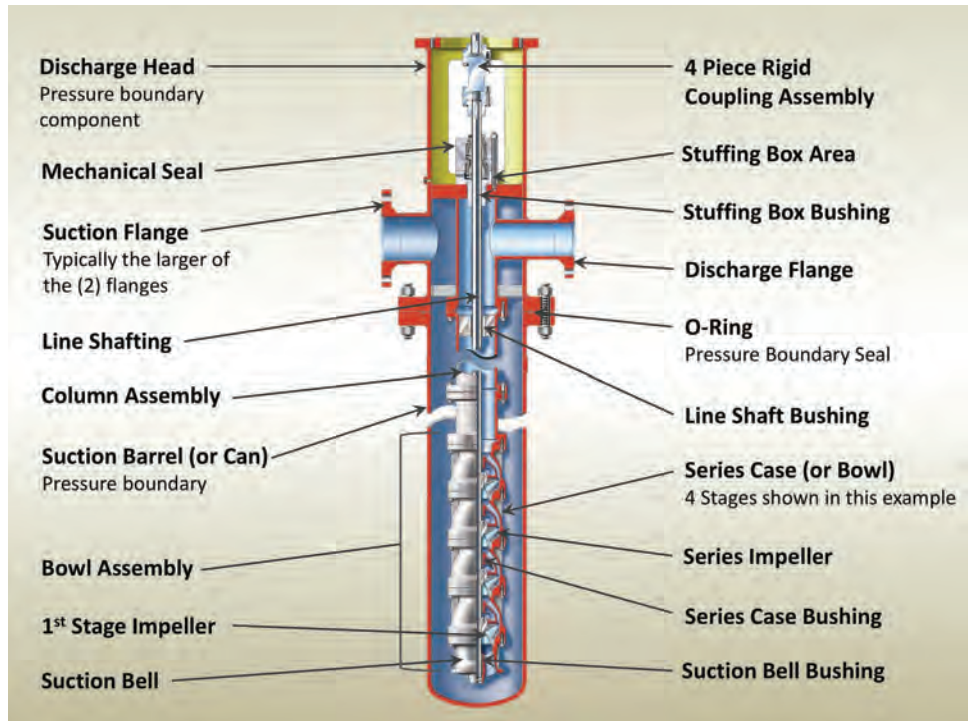


Figure 4-15. Typical pipeline multi-stage booster pump (courtesy of Flowserve).

A typical pusher type of mechanical seal (Fig. 4-16) consists of a rotating face, a stationary face and secondary sealing elements with adaptive metal parts such as a flange and a sleeve. The stationary face is seated in a flange which is bolted onto the pump cover. For most seals the rotating face can move in an axial direction and is kept in place by a spring holder and springs or a bellow. The gasket that can move axially with the rotating face is called the dynamic gasket. A bellow type mechanical seal uses a welded metal bellows and avoids the use of a dynamic gasket for higher temperature applications.

The key to reliable operation and low leakage is maintaining a minimal but sufficiently thick fluid film between the faces, with the gap normally below $40\text{ }\mu\text{m}/1\text{ }\mu\text{m}$. This thickness is typically in the order of the surface roughness which allows for a low friction coefficient and thus low heat generation. This mode of lubrication is referred to as mixed lubrication (Fig. 4-17).

Designers of mechanical seals tune their mechanical seals so that the forces are balanced between hydrostatic pressures (closing and opening forces), mechanical contact (minimal during normal operation), hydrodynamic pressure (low for a liquid seal), spring force and gasket friction (O-ring drag).

Hydraulic pressure on the faces causes a concave deformation (Fig. 4-18) that closes off the liquid film in the gap and changes the hydrostatic pressure distribution between the faces. Fortunately, this is compensated for by the frictional heat generation in the gap which by nature of the temperature distribution results in an opposite convex thermal deformation (Fig. 4-19).

Materials used for the seal faces are critical for reliable operation of the mechanical seal and have evolved from simple carbon mixes to advanced antimony impregnated faces and silicon carbides. They have proven to be suitable for marginal lubrication conditions such as those found with light hydrocarbons. As illustrated in Fig. 4-20, hardness, strength and heat conduction are important factors.

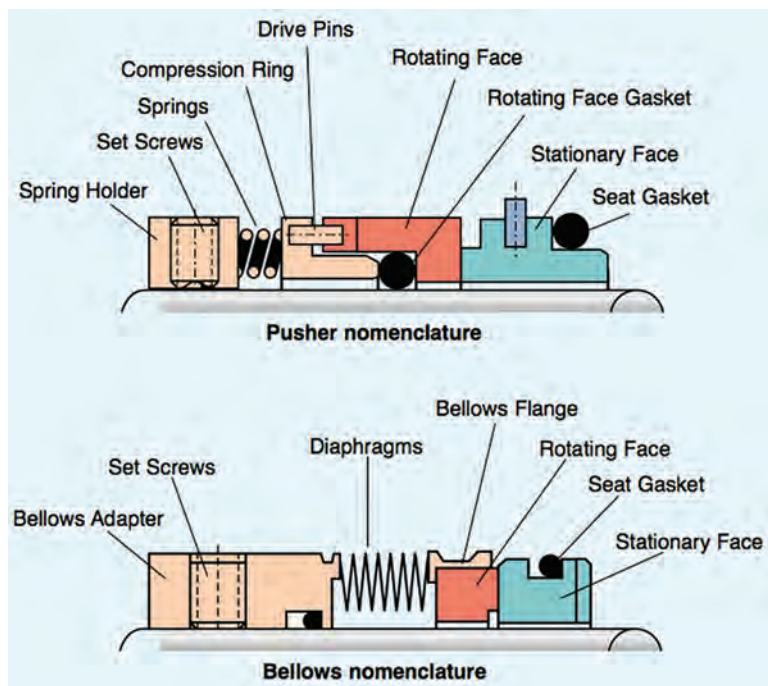


Figure 4-16. Components of a pusher seal (courtesy of Flowserve).

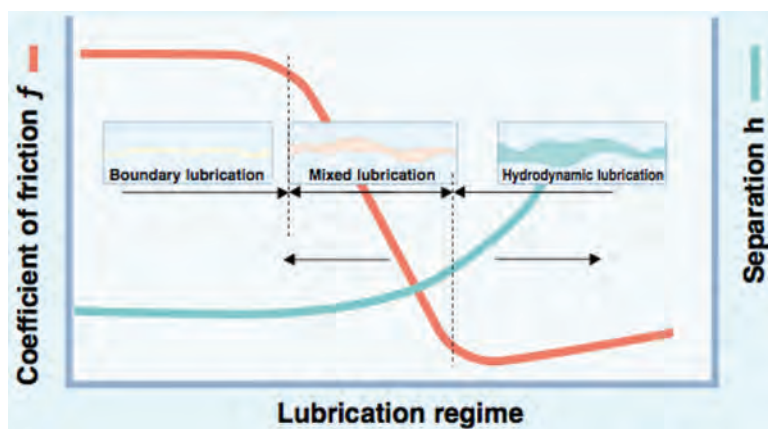


Figure 4-17. Lubrication regimes (courtesy of Flowserve).

For corrosive liquids, components are made from stainless steel or a higher alloy. Resin impregnated carbons and sintered silicon carbides provide the highest resistance to corrosion for the seals. A wide range of gasket materials is used from fluoroelastomers to virtually chemically inert PTFE to high temperature grafoil.

A standard pusher seal suitable for general pipeline service is shown in Fig. 4-21 and features a single, balanced spring. It complies with the requirements of API 682 type A.

With liquid pipelines carrying such a variety of products, selection of mechanical seals cannot be easily generalized and close cooperation with seal vendors is necessary to take advantage of their experience. A typical chart of seal types with respect to pressure is given

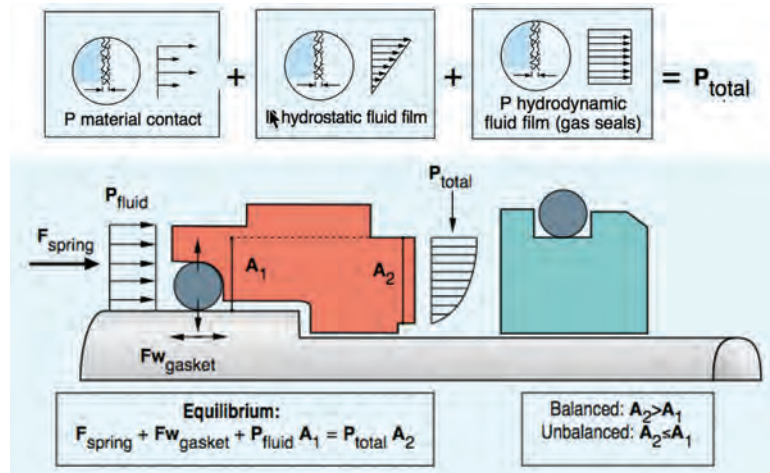


Figure 4-18. Equilibrium between forces for a balanced mechanical seal (courtesy of Flowserve).

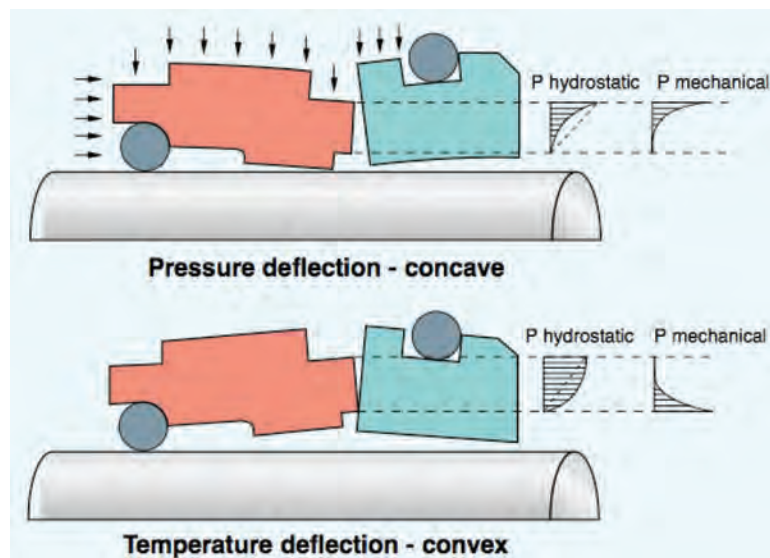


Figure 4-19. Effect of pressure and temperature on the seal faces (courtesy of Flowserve).

in Fig. 4-22 and illustrates that many options exist and must be considered for successful seal operation.

An integral part of the mechanical seal is the piping plan used to flush the seal. Piping plans help to keep the mechanical seal cool and clean and promote the safe handling of dangerous fluids. They are numbered and referenced in API 682 [4]. A basic flush plan applicable to clean fluids recirculates from the discharge with an orifice to control flow (Plan 11 in Fig. 4-23). For dirty or contaminated fluids, a cyclone separator centrifuges the solids away from the seal (Plan 31 in Fig. 4-23). For hot oil applications, a cooler can be added (Plan 41 in Fig. 4-23).

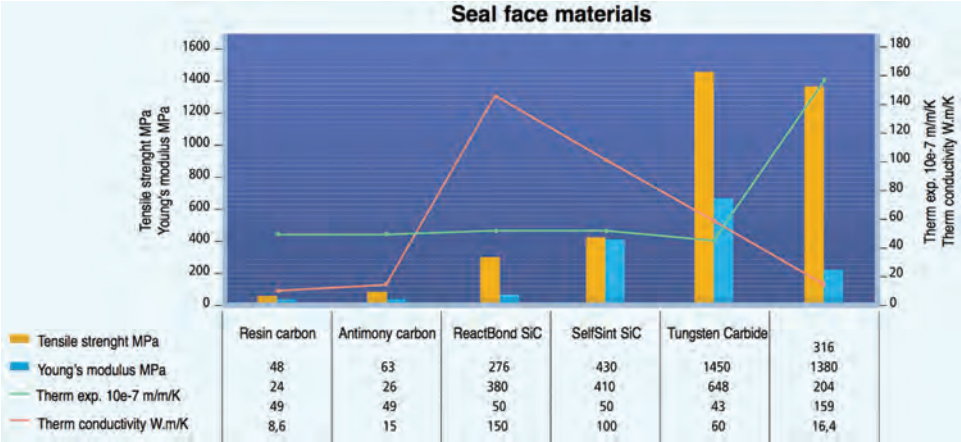


Figure 4-20. Comparison of properties for materials seal faces (courtesy of Flowserve).

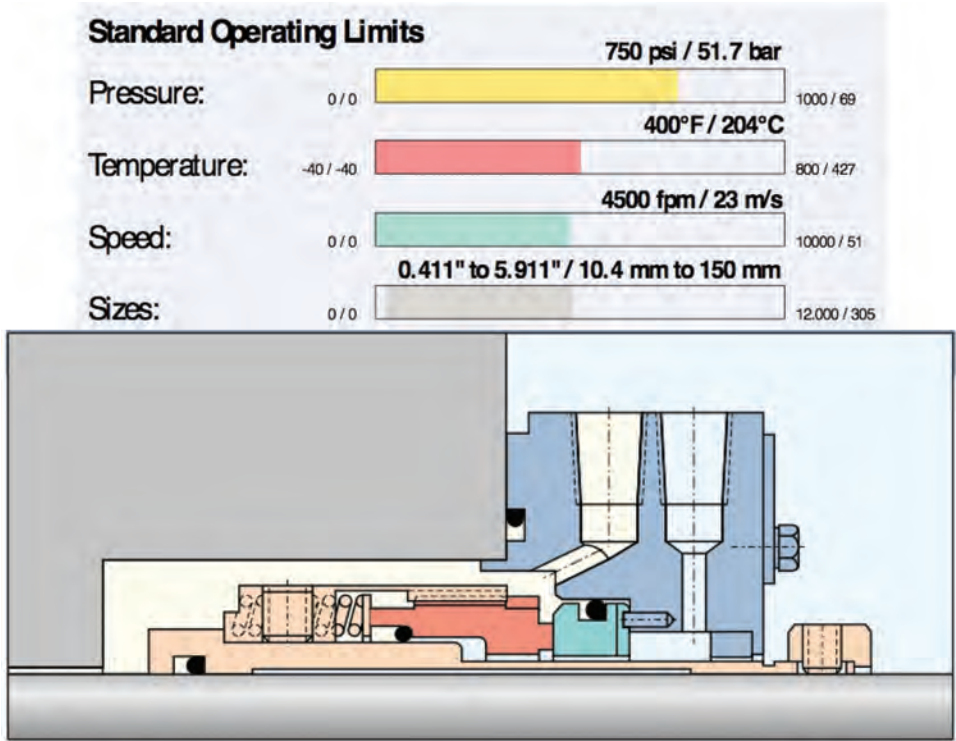


Figure 4-21. A typical pusher seal (courtesy of Flowserve).

4.3.4 Centrifugal Pump Nozzle Loading

To ensure carefree pump operation with minimal maintenance, it is essential to remove all external forces that act on the pump casing and that could distort internal clearances or cause pump driver misalignment.

Removal of all forces is not possible or practical due to presence of piping dead weights and piping misalignment as well as and thermal expansion introduced forces and movements on the pump nozzles, but best design usually eliminates most undesirable effects.

application	pressure	category
light hydrocarbons (LHC)	medium	pusher LHC
hydrocarbons, crude oil		pusher bellows
	high	pusher single spring
	very high	pusher
dry contacting gas back-up	medium	gas back-up seal
dry lift-off gas back-up	medium	gas back-up seal
produced water		pusher

Figure 4-22. General application chart for mechanical seals (courtesy of Flowserve).

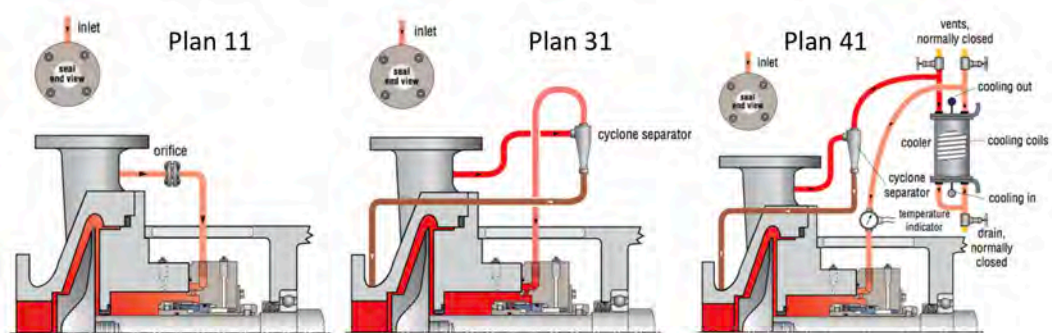


Figure 4-23. Basic flush plans for mechanical seals (courtesy of Flowserve).

Maximum allowable nozzle loads that must be allowed in the piping design are defined in API 610 Standard [5]. For horizontal and vertically configured centrifugal pumps, the forces and moments given in Table 4-1 and Fig. 4-24 as adopted from API 610 are applicable. Fig. 4-24 indicates the appropriate loading orientations.

Generally, API recommended force and moments on pump nozzles are conservative. Piping configurations that produce component nozzle loads lying within the ranges specified in Table 4-1 limit casing distortion to one half the pump vendor's design criterion and ensure pump shaft displacement of less than 0.250 mm (0.010 in.).

However, piping configurations that produce loads outside the ranges specified in Table 4-1 are also acceptable providing conditions specified in a through c below are satisfied.

Horizontal Pumps

- The individual component forces and moments acting on each pump nozzle flange must not exceed the range specified in Table 4-1 by a factor of more than 2.
- The resultant applied force (FRS_A , FRD_A) and the resultant applied moment (MRS_A , MRD_A) acting on each pump nozzle flange needs to satisfy the appropriate interaction equations below.

$$[FRS_A/(1.5 \times FRS_{T4})] + [MRS_A/(1.5 \times MRS_{T4})] < 2 \quad (4-1)$$

$$[FRD_A/(1.5 \times FRD_{T4})] + [MRD_A/(1.5 \times MRD_{T4})] < 2 \quad (4-2)$$

- The applied component forces and moments acting on each pump nozzle flange must be translated to the centre of the pump. The magnitude of the resultant applied force (FRC_A),

Table 4-1. Centrifugal allowable nozzle loads [5]

	Nominal Size of Flange (DN)									Nominal Size of Flange (NPs)								
	50	80	100	150	200	250	300	350	400	2	3	4	6	8	10	12	14	16
	Forces (N) and Moments (Nm)									Forces (lbf) and Moments (ft-lbf)								
Each top nozzle																		
FX	710	1070	1420	2490	3780	5340	6670	7120	8450	160	240	320	560	850	1200	1500	1600	1900
FY	580	890	1160	2050	3110	4450	5340	5780	6670	130	200	260	460	700	1000	1200	1300	1500
FZ	890	1330	1780	3110	4890	6670	8000	8900	10,230	200	300	400	700	1100	1500	1800	2000	2300
FR	1280	1930	2560	4480	6920	9630	11,700	12,780	14,850	290	430	570	1010	1560	2200	2600	2900	3300
Each side nozzle																		
FX	710	1070	1420	2490	3780	5340	6670	7120	8450	160	240	320	560	850	1200	1500	1600	1900
FY	890	1330	1780	3110	4890	6670	8000	8900	10,230	200	300	400	700	1100	1500	1800	2000	2300
FZ	580	890	1160	2050	3110	4450	5340	5780	6670	130	200	260	460	700	1000	1200	1300	1500
FR	1280	1930	2560	4480	6920	9630	11,700	12,780	14,850	290	430	570	1010	1560	2200	2600	2900	3300
Each end nozzle																		
FX	890	1330	1780	3110	4890	6670	8000	8900	10,230	200	300	400	700	1100	1500	1800	2000	2300
FY	710	1070	1420	2490	3780	5340	6670	7120	8450	160	240	320	560	850	1200	1500	1600	1900
FZ	580	890	1160	2050	3110	4450	5340	5780	6670	130	200	260	460	700	1000	1200	1300	1500
FR	1280	1930	2560	4480	6920	9630	11,700	12,780	14,850	290	430	570	1010	1560	2200	2600	2900	3300
Each nozzle																		
MX	460	950	1330	2300	3530	5020	6100	6370	7320	340	700	980	1700	2600	3700	4500	4700	5400
MY	230	470	680	1180	1760	2440	2980	3120	3660	170	350	500	870	1300	1800	2200	2300	2700
MZ	350	720	1000	1760	2580	3800	4610	4750	5420	260	530	740	1300	1900	2800	3400	3500	4000
MR	620	1280	1800	3130	4710	6750	8210	8540	9820	460	950	1330	2310	3500	5000	6100	6300	7200

Each value indicates ranges from minus that value to plus that value (refer to Fig. 4-22, reproduced courtesy of the American Petroleum Institute).

Note:

FR is the resultant force;
FX is the applied force on the *X* axis;
FY is the applied force on the *Y* axis;
FZ is the applied force on the *Z* axis;
MR is the resultant moment;
MX is the applied moment on the *X* axis;
MY is the applied moment on the *Y* axis;
MZ is the applied moment on the *Z* axis.

the resultant applied moment (MRC_A), and the applied moment must be limited by the following equations, respectively. Sign convention shown in Fig. 4-21 and the right-hand rule should be used in evaluating these equations.

$$FRC_A < 1.5 (FRS_{T4} + FRD_{T4}) \quad (4-3)$$

$$|MYC_A| < 2.0 (MYS_{T4} + MYD_{T4}) \quad (4-4)$$

$$MRC_A < 1.5 (MRS_{T4} + MRD_{T4}) \quad (4-5)$$

where:

$$FRC_A = [(FXC_A)^2 + (FYC_A)^2 + (FZC_A)^2]^{0.5} \quad (4-6)$$

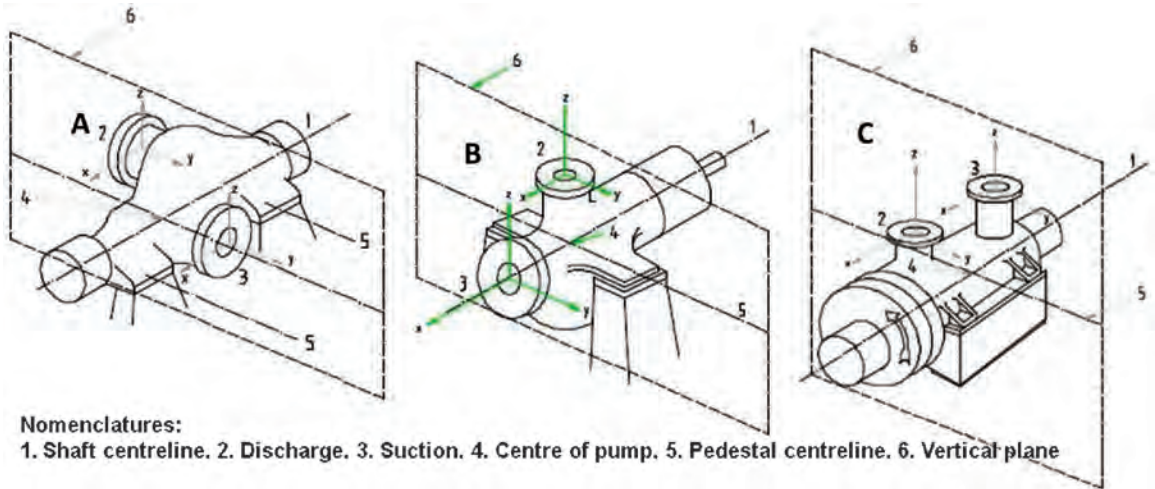


Figure 4-24. Co-ordinate system for the forces and moments on pump nozzles (refer to Table 4-1). A: Horizontal pumps with side suction and side discharge nozzles, B: Horizontal pumps with end suction and top discharge nozzles, C: Horizontal pumps with top nozzles (reproduced courtesy of the American Petroleum Institute, API Standard 610).

where:

$$FXC_A = FXS_A + FXD_A \quad (4-7)$$

$$FYC_A = FYS_A + FYD_A \quad (4-8)$$

$$FZC_A = FZS_A + FZD_A \quad (4-9)$$

$$MRC_A = [(MXC_A)^2 + (MYC_A)^2 + (MZC_A)^2]^{0.5} \quad (4-10)$$

where:

$$MXC_A = MXS_A + MXD_A - [(FYS_A)(zS) + (FYD_A)(zD) - (FZS_A)(yS) - (FZD_A)(yD)]/1000 \quad (4-11)$$

$$MYC_A = MYS_A + MYD_A + [(FXS_A)(zS) + (FXD_A)(zD) - (FZS_A)(xS) - (FZD_A)(xD)]/1000 \quad (4-12)$$

$$MZC_A = MZS_A + MZD_A - [(FXS_A)(yS) + (FXD_A)(yD) - (FYS_A)(xS) - (FYD_A)(xD)]/1000 \quad (4-13)$$

In US customary units, the constant 1000 should be changed to 12. This constant is the conversion factor to change millimeters to meters or inches to feet.

Vertical Inline Pumps

Vertical inline pumps that are supported only by the attached piping may be subjected to component piping loads that are more than double the values shown in Table 4-1 if these loads do not cause a principal stress greater than 41 N/mm² (5 950 psi) in either nozzle. For calculation purposes, the section properties of the pump nozzles shall be based on Schedule 40 pipe, the nominal size of which is equal to that of the appropriate pump nozzle.

The following equations can be used to evaluate principal stress, longitudinal stress, and shear stress, respectively, in the nozzles.

$$P = (s/2) + (s^2/4 + t^2)0.5 < 41 \quad (4-14)$$

$$\sigma_s = [1.27 \times FY / (D_o^2 - D_i^2)] + [10200 D_o (MX^2 + MZ^2)^{0.5}] / (D_o^4 - D_i^4) \quad (4-15)$$

$$\tau = 1.7 (FX^2 + FZ^2)^{0.5} / (D_o^2 - D_i^2) + [5100 \times D_o (|MY|)] / (D_o^4 - D_i^4) \quad (4-16)$$

For US units, the following equations apply:

$$P = (s/2) + (s^2/4 + t^2)0.5 < 5950 \quad (4-17)$$

$$\sigma_s = [1.27 \times FY / (D_o^2 - D_i^2)] + [122 \times D_o (MX^2 + MZ^2)^{0.5}] / (D_o^4 - D_i^4) \quad (4-18)$$

$$\tau = [1.27 \times (FX^2 + FZ^2)^{0.5}] / (D_o^2 - D_i^2) + [61 \times D_o (|MY|)] / (D_o^4 - D_i^4) \quad (4-19)$$

where:

- C = pump centerline defined by the intersection of the pump shaft centerline and a vertical plane passing through the two pedestals, refer to Fig. 4-24
- D = discharge nozzle
- D_i = inside diameter of Schedule 40 pipe, the nominal size of which is equal to that of the pump nozzle in question, expressed in millimeters (in.)
- D_o = outside diameter of Schedule 40 pipe whose nominal size is equal to that of the pump nozzle in question, expressed in millimeters (in.)
- F = force, N (pounds force)
- FR = resultant force (FRS and FRD are calculated by the square root of the sum of the squares method using the applied component forces acting on the nozzle flange FRS_{T4} and FRD_{T4} = see Table 4-1 using the appropriate nozzle size)
- M = moment, Newton meters (foot-pounds force)
- MR = resultant moment (MRS and MRD are calculated by the square root of the squares method using the applied component moments acting on the nozzle flange MRS_{T4} and MRD_{T4} = see Table 4-1 using the appropriate nozzle size)
- PI = principal stress, megaPascals (pounds force per square inch)
- S = suction nozzle
- x, y, z = location coordinates of the nozzle flanges with respect to the centre of the pump, millimeters (inches)
- X, Y, Z = loads direction (see Fig. 4-24)
- σ_s = longitudinal stress, Newtons per square millimeter (pounds per square inch)
- τ = shear stress, Newtons per square millimeter (pounds per square inch)

Subscript A is an applied load. Subscript T4 is a load extracted from Table 4-1.

4.4 POSITIVE DISPLACEMENT PUMPS

4.4.1 Rotary Pumps

There are many types of rotary pumps (Fig. 4-25); the most common on pipeline services are two- and three-screw pumps, gear pumps (internal and external), and vane pumps for low-pressure services. Two- and three-screw pumps are used for higher pressure services, especially at medium to high flow rates. Approximate capability for each type is illustrated in Table 4-2. It may be noted that vane-type pumps are not used for pipeline applications but is commonly used in oil batteries.

Rotary pumps such as gear and vane pumps (Fig. 4-25A, B) normally operate at relatively low speeds, generally requiring speed reducers on all but the very smallest sizes. Screw pumps (Fig. 4-25C) move liquid axially rather than in a radial direction, so fluid

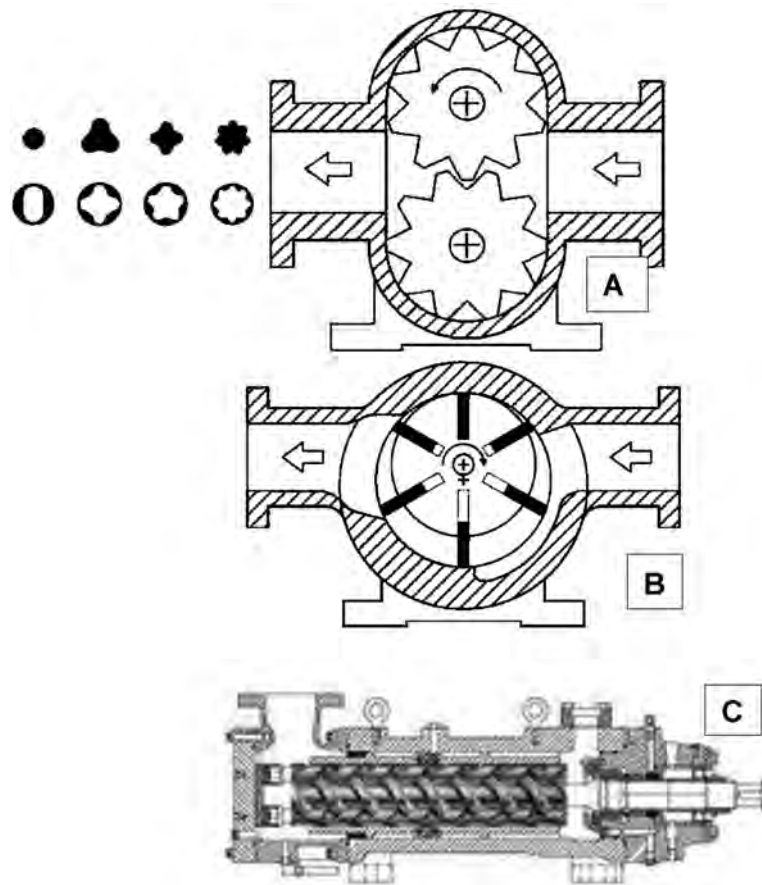


Figure 4-25. Positive displacement pumps (a: rotary gear with various rotor (solid) and stator lobe configurations, b: rotary vane and c: screw type) [6].

Table 4-2. Rotary capability range

Rotary Pump Type	Maximum Volumetric Flow		BBLSD	Maximum Discharge Pressure	
	GPM	m ³ /D		PSI	kPa
Gear	1500	9840	61,892	250	1724
Vane	1000	6560	41,261	250	1724
2-Screw	5500	36,080	226,937	1500	10,343
3-Screw	3400	22,304	140,288	2000	13,790

velocities are generally relatively low. Efficiencies are high over a much broader range of differential pressure than centrifugal pumps.

Rotary pumps commonly used in liquid/oil pipeline service for viscous product include:

- oil batteries: booster—internal gear
- sipper—double and triple screw
- mainline pumps: booster—triple screw
- mainline—double and triple screw

As with other pumps, in selecting the rotary pumps, the following is defined:

- location of pump stations and number of pumps per station
- product heating requirement
- possible range of
 - pump inlet pressures
 - pump discharge pressures
 - liquid temperature range
 - liquid viscosity range
 - per pump flow rate range
 - liquid particulate content
 - upset and static conditions
- driver requirements
- pump instrumentation
- pump leak detection

Of all points listed above, upset and static conditions are the most important considerations that need to be assessed during pipeline design. Most rotary, high-pressure pumps cannot tolerate anything close to discharge pressure at their inlet (suction) port. In a tight system, if an upstream pumping station is started and the downstream station is not started in very close synchronization, the downstream station may see excessive pressure on its inlet side. A low-pressure set inlet side relief valve may be necessary, together with an overspill tank and appropriate instrumentation.

Also important is the particulate contained in the liquid that is pumped. This is mostly true for oil battery booster pumps when large sand particulate may be present. In this case, design usually calls for pump inlet filtration; otherwise, rotor damage can occur (Fig. 4-26).

Rotary pumps, unlike reciprocating pumps, are not subject to flow induced vibration/pulsation. This is due to the absence of reciprocating plunger/piston and valves as well as having constant discharge area (Fig. 4-27).

A positive displacement pump will continue to pump as the pressure rises (e.g., if discharge valve is closed). A relief valve is required to prevent overloading the driver and to protect the pump casing and downstream components from damage or failure from high pressure. The relief valve must be able to handle the pump rated capacity when fully open, at a pressure not more than 10% above the maximum allowable working pressure of the pump. Some rotary pumps are equipped with built-in relief valves that are designed



Figure 4-26. Pump rotor damage caused by hard contaminant.

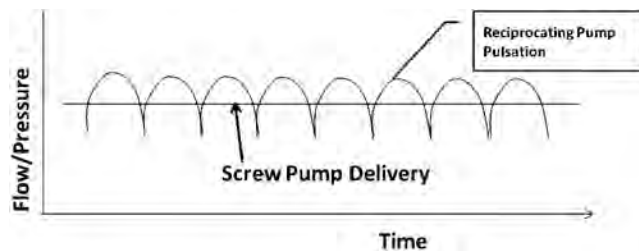


Figure 4-27. Comparison of rotary screw and reciprocating pumps flow induced pulsation/vibration.

primarily to protect the pump casing. The preferred system is an external relief valve on the discharge piping designed to return the flow to the source of suction upstream of the pump to prevent overheating. For lower-pressure applications, the pressure valve discharge is sometimes directed back to the pump suction line. The pump driver must be sized to handle the added pressure when the relief valve is fully open.

Flow/capacity control is achieved by using a bypass valve to direct liquid from the pump discharge to the source of suction when the system cannot accept the total pump capacity. The bypass liquid must be returned sufficiently upstream of the pump to prevent overheating of the pump fluid. Another method of flow control would be to vary the rotational speed of the pump.

Typical piping design configurations are as indicated in Chapter 2; similar arrangement generally apply for rotary pump piping. A well-designed pumping system for a rotary pump is shown in Fig. 4-28.

4.4.2 Reciprocating Pumps

Reciprocating pumps are more common on the upstream side of pipelines with a series of parallel pumps such as the ones shown in Fig. 4-29. There is a wide range of reciprocating pumps on the market. Reciprocating pumps are further divided into two types: plunger and piston.

Plunger pumps always have a plunger longer than their stroke, and only one end is available for pumping. Double-acting plunger pumps require at least two cylinders and plungers. Although not as adaptable as piston-type pumps, plunger pumps can be made to

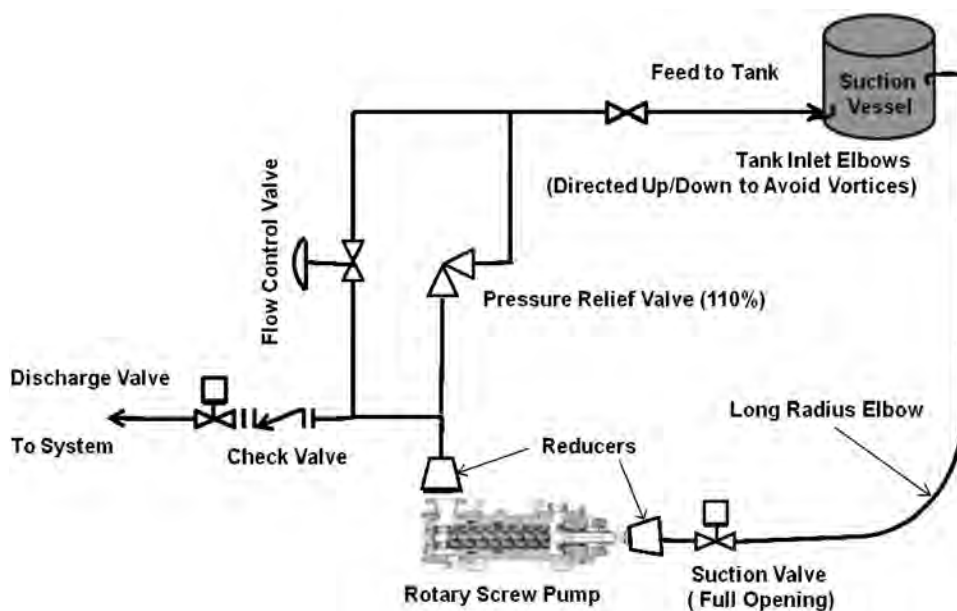


Figure 4-28. Typical rotary pump system configuration.



Figure 4-29. Duplex reciprocating pumps in oil field operation.

provide higher pressures and greater capacities. Nearly all large, high-pressure, reciprocating pumps used in pumping stations are plunger-type.

Piston pumps have pistons shorter than their stroke, and both ends are available for pumping with the same cylinder. Piston-type pumps are used extensively at gathering stations because of their flexibility in capacity, range in pressure and portability. They can

serve either as suction or discharge pumps. Most field pumps are piston pumps. Capacity and pressure rating are varied easily by changing the diameter of the piston and cylinder liners.

Reciprocating pumps are of single construction, have a long service life, and are highly efficient. Disadvantages include their large weight, greater space requirements than required by other types, higher initial cost, pulsations, and sometimes, the need for speed reducers in the case of very slow-speed reciprocating pumps. Vertical, multi-cylinder, high-speed plunger pumps used in recent installations have helped overcome the disadvantages of the horizontal types. Vertical arrangement of cylinder reduces the amount of floor space required; the higher speed range allows direct connection (without reduction gearing), and the increased number of cylinders reduces the effects of surges (pulsations).

The pipeline industry uses both horizontal and vertical pumps. A plunger pump is shown in Fig. 4-30. This pump consists of:

- a liquid end that includes the cylinders, the plungers, and the valves
- a power end that transmits energy from a rotating shaft to plungers by means of a crankshaft, crossheads and connecting rods
- a frame or distance piece that connects the liquid end and power end

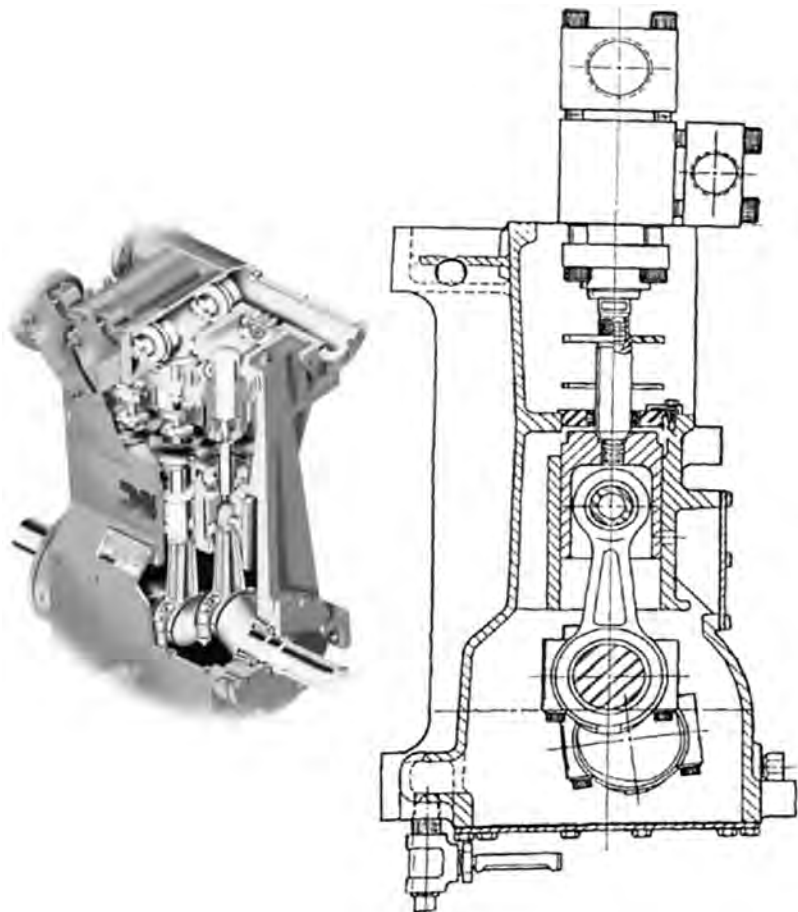


Figure 4-30. Typical reciprocating pump cross section.

The power pump is a positive displacement pump that:

- traps a fixed volume of fluid at suction conditions in the cylinder
- compresses the fluid in the cylinder by a plunger to discharge pressure
- pushes the fluid out the discharge nozzle

Reciprocating power plunger pumps are generally characterized by:

- constant flow, varying discharge pressures
- high efficiency normally ranging from 85% to 94%
- suitable for high-pressure and low-flow applications
- high pressures obtained by low velocities in the pump
- pump capacity is a function of speed and relatively independent of discharge pressure
- pulsating flow
- high maintenance
- high reliability
- compact size
- requirement for a relief valve

4.4.3 Pulsation Dampeners

The reciprocating action of the pump produces pressure pulsations in the piping. Whether or not the pulsation is severe enough to create problems depends upon many system variables. A few of these variables include:

- pump type
- pump size (power)
- number of plungers
- speed range
- pumped fluid properties
- system operational conditions
- piping layout

Because the discharge pressures are usually high, these pulsations can cause significant piping loads. Therefore, most installations would require to be provided with a discharge pulsation suppression device/dampener, particularly those multi-plunger pump service having a discharge pressure over 3500 kPag (500 PSIG), or on any service, regardless of pressure, whether pulsation problems are expected and a maintenance-free device is required.

The basic techniques used for control of detrimental pulsations and vibrations are the following:

- pulsation control devices such as dampeners, accumulators, dampers, preventors, hydraulic isolators, inhibitors, suppressors, stabilizers, acoustic filters, and selected piping configurations
- system design based on studies of the interactive effects of pulsations and the attenuation requirements for satisfactory piping vibration, pump performance, and valve life
- mechanical restraints including such things as type, location, and number of pipe hold-downs

For detailed pulsation/vibration design approach refer to Chapter 11.

The most common and least expensive device is a bladder type dampener, shown in Fig. 4-31. These types of dampeners utilize an elastomeric bladder that is charged with a

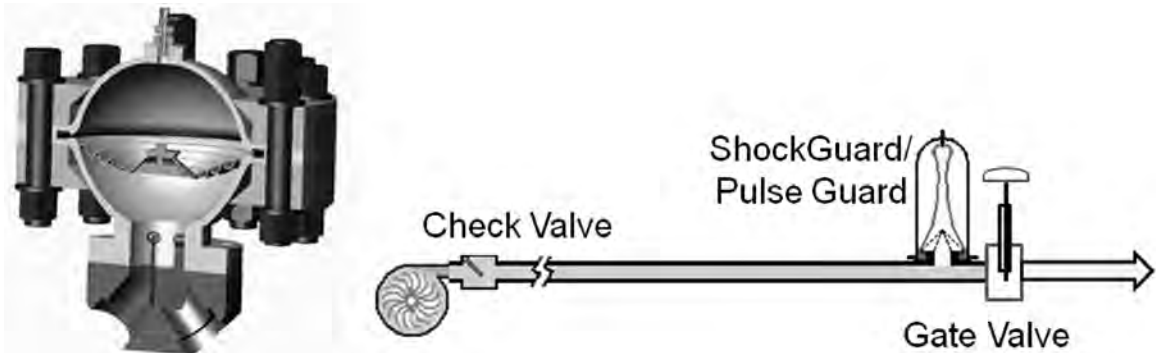


Figure 4-31. Pump pulsation & shock dampeners (bladder type), (courtesy of PulseGuard & Shock-Guard, UK).

compatible gas, usually nitrogen, charged to around 75% of the discharge pressure. These dampeners are quite effective and can reduce the discharge pressure pulsation up to 95% but require constant monitoring and maintenance is to maintain the gas charge.

A more sophisticated and maintenance-free device is a dynamic dampener (Fig. 4-32). This dampener eliminates discharge pulsations by hydraulically uncoupling the piping from the pump, introducing slight throttling, adding viscous drag, and causing a hydraulic flywheel effect and a hydraulic spring effect. Although not as efficient as a bladder dampener, the maintenance-free design is generally more desirable.

Dynamic pulsation dampeners are completely liquid filled, with no moving parts, and do away with maintenance and gas charging requirements.

The stationary internals guide the incoming flow into a rotating path within the spherical shell. The spinning liquid mass creates a system smoothing effect. Viscous drag on the sphere walls and the capacitance effect of the relatively large volume located next to the pump further aid to dampen pressure pulsation.

Suction pulsation dampeners are also sometimes provided on the suction side of a reciprocating pump to combat the acceleration head phenomenon. It can be eliminated by adding a large volume to the suction piping just before the pump, but it is generally easier to add a self-contained device to the piping. A suction dampener is identical to the discharge bladder dampener. A more sophisticated suction stabilizer is available that also eliminates trapped vapors (Fig. 4-33).



Figure 4-32. Typical dynamic pulsation dampener, courtesy of IMI Fluid Kinetics <http://www.imi-critical.com>.

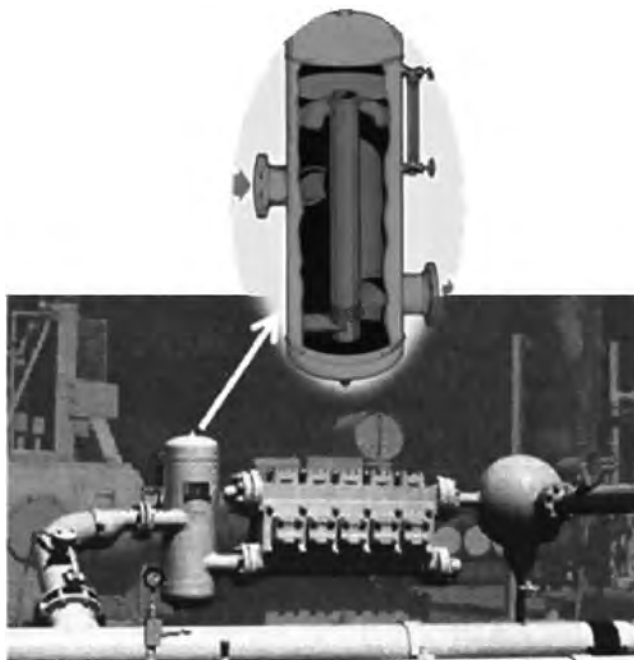


Figure 4-33. Suction side pulsation dampener/stabilizer/separator (courtesy of IMI Fluid Kinetics <http://www.imi-critical.com>).

In this design, liquid enters and leaves the stabilizer/separator tangentially, forming a low-velocity vortex. This vortex and the increased path length created by the elevation difference between inlet and outlet stimulates the release of any entrained gas. The freed gas moves through the perforated center tube to the gas or air pocket maintained at the top of the unit. The figure also shows a typical pump installation with a discharge dampener and a suction stabilizer.

4.4.4 Other Pump Design Considerations

Reciprocating Pump Torque Characteristics. The full-load breakaway torque for start up of a power pump against a full discharge pressure is usually at least 150% of the average full-load torque. As the speed increases, the proper lubrication in the packing end and power end is established. This reduces the torque to the full load/speed value.

When the pump discharge is piped back to the suction source during startup, the discharge pressure is approximately equal to the suction pressure. Breakaway torque is approximately 25% of the full load torque. As the speed is increased, the torque will reduce to about 10% of full-load torque. At higher speeds, the friction head in the bypass system increases, and the torque is increased as shown in the no-load curve in Fig. 4-34. If possible, power plunger pumps should be started at reduced load conditions to reduce pump wear and maintenance.

Reciprocating Pump Speed Rating. The recommended maximum allowable speed for reciprocating pumps in continuous service is stated in API Standard 674. Refer to Table 4-3 [7].

However it may be noted that factors such as viscosity, specific gravity, abrasiveness present (such as sand), vapor pressure, gas solubility or evolution in the pumped liquid, specified pressures and temperatures, or system acceleration head may require further speed limitations.

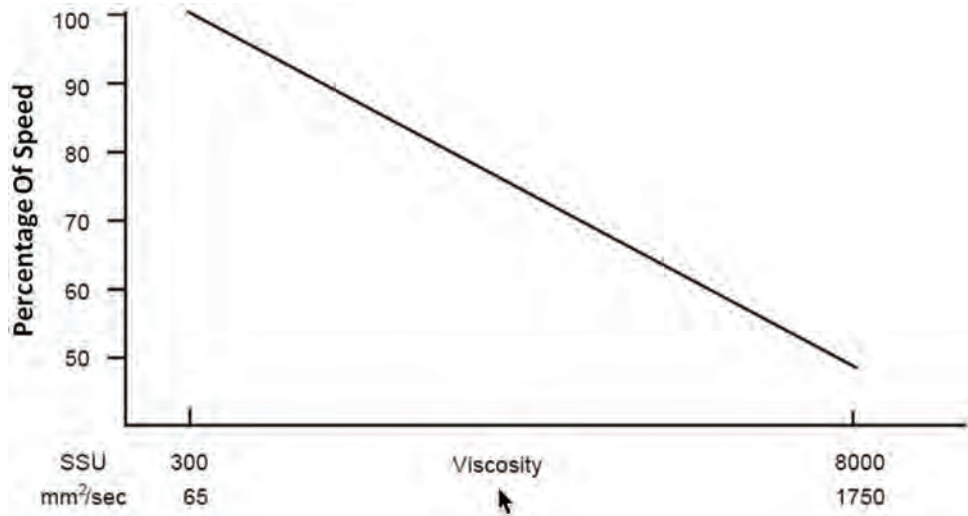


Figure 4-34. Viscosity correction to maximum allowable speed rating [7].

Table 4-3. Maximum allowable speed for power pumps in continuous service [7]

Stroke length (mm) (in)		Single-acting plunger-type pumps			Double-acting piston-type pumps		
		Revolution per Minute	Meters per Minute	Feet per Minute	Revolution per Minute	Meters per Minute	Feet per Minute
50	2	450	45	150	140	14	46.5
75	3	400	60	200	—	—	—
100	4	350	71	233	116	23	77
125	5	310	73	258	—	—	—
150	6	270	82	270	100	30	100
175	7	240	85	280	—	—	—
200	8	210	85	280	—	—	—
250	10	—	—	—	83	42	138
300	12	—	—	—	78	48	156
350	14	—	—	—	74	53	173
400	16	—	—	—	70	57	186

As a guide, for viscosities above 65 cS (mm²/s) or 300 SSU, pumping temperature should not exceed a percentage of the speeds given in API Standard 674 (as per Table 4-3) as indicated in Fig. 4-34.

The minimum speed of the pump is determined by the ability of the pump to provide sufficient lubrication to all bearing surfaces in the power end. This can range from under 20 rpm to over 100 rpm for different pumps.

Power pump speeds are normally below 450 rpm and require pump-driver speed reduction.

Station Piping Design For Reciprocating Pumps. Piping systems generally include piping, isolating, control and relief valves, as well as pressure reducers, orifices, temperature gauges and thermowells, pressure gauges, sight flow indicators, and all related vents and drains.

A pumping system for a reciprocating pump is shown in Fig. 4-35.

Suction Piping. The suction pipe should generally, and in most cases, be one or two sizes larger than the suction connection of the pump. It is best for suction piping be as short and as straight as possible with minimum elbows and tees. To avoid acoustic pulsation,

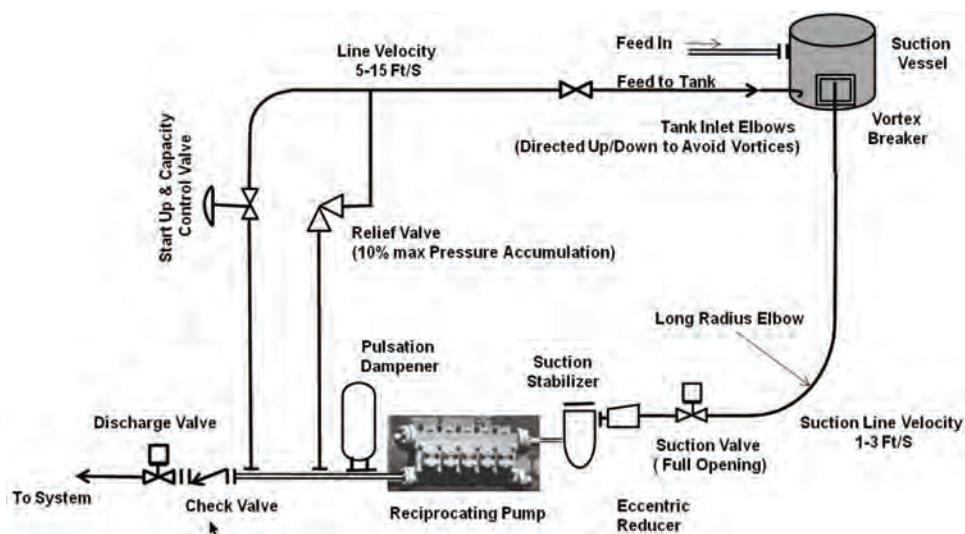


Figure 4-35. Reciprocating pump station — typical piping configuration.

suction piping is designed such that velocity values would not exceed those as shown in Fig. 4-36.

These recommended values are based on an acceleration head of 0.7 ft per foot of suction line length.

Unless venting is provided piping design should ensure that no high points are introduced in the piping where vapor may collect. Eccentric rather than concentric reducers should be used with flat side up. Sufficient absolute pressure must be available at the suction connection of the pump to account for acceleration head, vapor pressure of the liquid and the pump NPSHR.

Should the acceleration head be excessive, a suitable suction dampener would be required, to be installed in the suction line adjacent to the pump liquid end. Block valves in the suction piping should be in full opening so as not to restrict the flow. Regular maintenance is essential where strainers are used to ensure the pump is not damaged from a starved condition resulting from a plugged strainer.

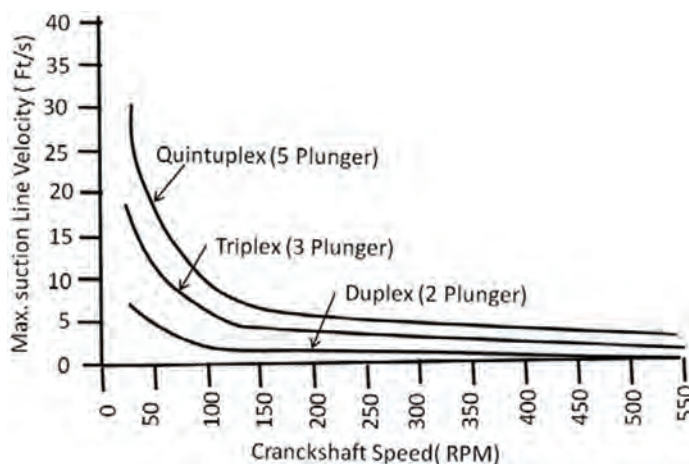


Figure 4-36. Reciprocating suction piping velocity (based on acceleration head of 0.7 ft per foot of suction line length, HI standard).

Discharge Piping. The discharge pipe is economically determined and is usually one or two sizes larger than the discharge connection of the pump. For conservative design, the average velocity should be less than three times the maximum suction line velocity. A pulsation dampener, or a connection for adding one, should be installed in the discharge pipe adjacent to the pump liquid end.

A relief valve, sized for the full pump capacity, should be piped back to the suction vessel. Any gases liberated by the relief valve, would then be transferred back to the suction vessel. A relief valve must be installed on the pump discharge piping before any block valves to protect the positive displacement pump and downstream components and prevent overloading the motor. The relief valve must be able to handle the pump rated capacity when fully open, at a pressure not more than 10% above the maximum allowable working pressure of the pump. A bypass line should be installed around the pump for starting the pump at the reduced discharge pressure and for flow control when required.

Suction Vessel. The suction vessel should be sized to provide sufficient retention time to allow entrained gas to rise to the surface of the liquid. The vessel feed and return lines should enter below the minimum liquid level. A vortex breaker may be required at the outlet to the pump suction line.

REFERENCES

- [1] Karassik, I. J., 2001. *Pump Handbook*, McGraw Hill, New York, USA.
- [2] Digby, S., 2007. "Pump theory—API Reciprocating Displacement Pumps," Presented at *Tekna Off-shore Pumps Conf.*
- [3] Hoffman, R. D., 2003. "AllAboutPumps, the Internet Glossary of Pumps," <http://www.animatedsoftware.com/pumpglos/pumpglos.htm>.
- [4] ANSI/API (American National Standard Institute/American Petroleum Institute), 2011. "API Standard 682—Pumps—Shaft Sealing Systems for Centrifugal and Rotary Pumps."
- [5] ANSI/API (American National Standard Institute/American Petroleum Institute), 2011. "API Standard 610—Centrifugal Pumps for Petroleum, Petrochemical and Natural Gas Industries."
- [6] Brennan, J. R., 2000. "Rotary Pumps On Pipeline Services," IMO Pump, Pump Users Expo 2000, Louisville, KY, September, <http://www.imo-pump.com/tech.htm>.
- [7] API (American Petroleum Institute), 1995. "Standard 674—Positive Displacement Pumps—Reciprocating."

PERFORMANCE OF PUMPS

5.1 INTRODUCTION TO PUMP PERFORMANCE

Liquid pipeline systems will generally require pumps to increase the pressure of the fluid to a level for overcoming pipe friction (due to pipe roughness), rise in elevation, and thermal losses that increase fluid viscosity and, hence, increase pressure loss. The performance of pumps at a pump station must meet the operating requirements of the pipeline.

Performance is therefore a critical aspect of the design of individual pump units and also of the station as a whole. Throughout the life of a pipeline system, units will be added, stations will be modified, and pipeline operating conditions will change. Performance thus remains a major component of pumping equipment for the entire life cycle. The major parameters that govern the performance of a pump are illustrated in Fig. 5-1.

Pump performance data such as developed head, efficiency, power and net positive suction head are subject to numerous standards (see section 5.11). However, with few exceptions, there is no standard that guides pipeline systems design with respect to hydraulics. Pipeline industry (engineers, owners, operators) are allowed to choose on how to calculate and determine system hydraulics. System hydraulics relate the pipeline system curve (head/pressure versus capacity) to that of pump capability and, hence, its operating point(s) (Fig. 5-1). The specified pump operating point is not subject to any standards and guidelines.

5.2 SYSTEM HEAD

The required pump energy is usually expressed in terms of head. The relationship of head and pressure can be seen from the simple equations given below:

$$H(\text{ft}) = \frac{[\text{pressure [psi]} \times 2.31]}{\text{SG}}$$

or

$$H(\text{m}) = \frac{(\text{pressure (kPa)})}{(9.7928 \times \text{SG})}$$
(5-1)

where:

- H = head (m) or (ft)
- P = pressure (psig) or [kPa (g)]
- SG = specific gravity

If a pump produces 30.48 m (100 ft) of total head, then the corresponding pressure (depending on the type of fluid the pump is pumping) will be as given in Table 5-1 and is illustrated in Fig. 5-2.

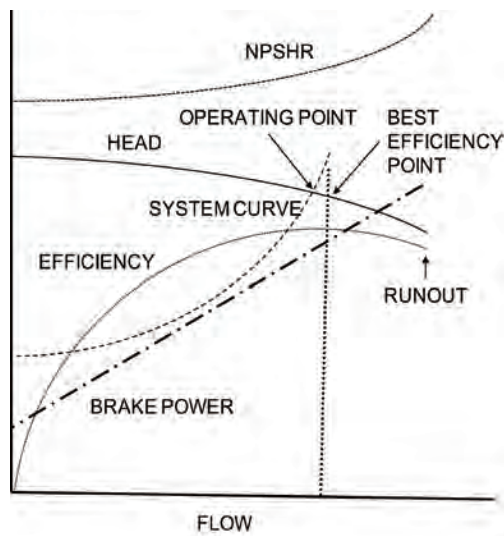


Figure 5-1. Pump versus pipeline system curves.

Table 5-1. Pump pressure for a 100 ft (30.48 m) head due to varying fluids

Fluid	SG	Pressure	
		(psi)	(kPa)
Salt water (brine)	1.2	51.95	358
Water	1	43.29	298
Medium crude	0.9	38.96	269
Gasoline	0.7	30.3	209
Butane	0.5	21.65	149

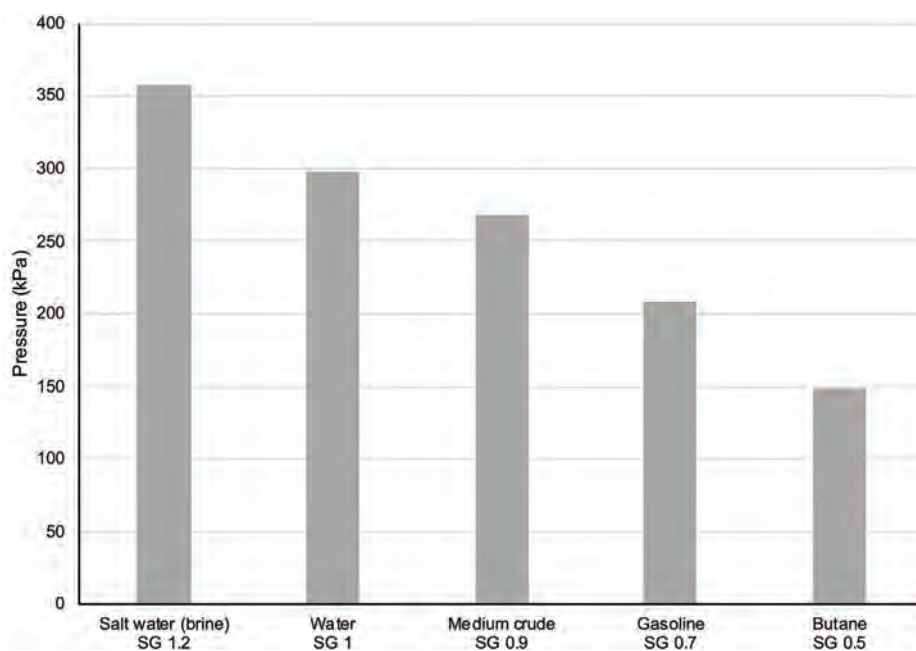


Figure 5-2. Pressure requirement for different fluids to produce a head of 100 ft (30.48 m).

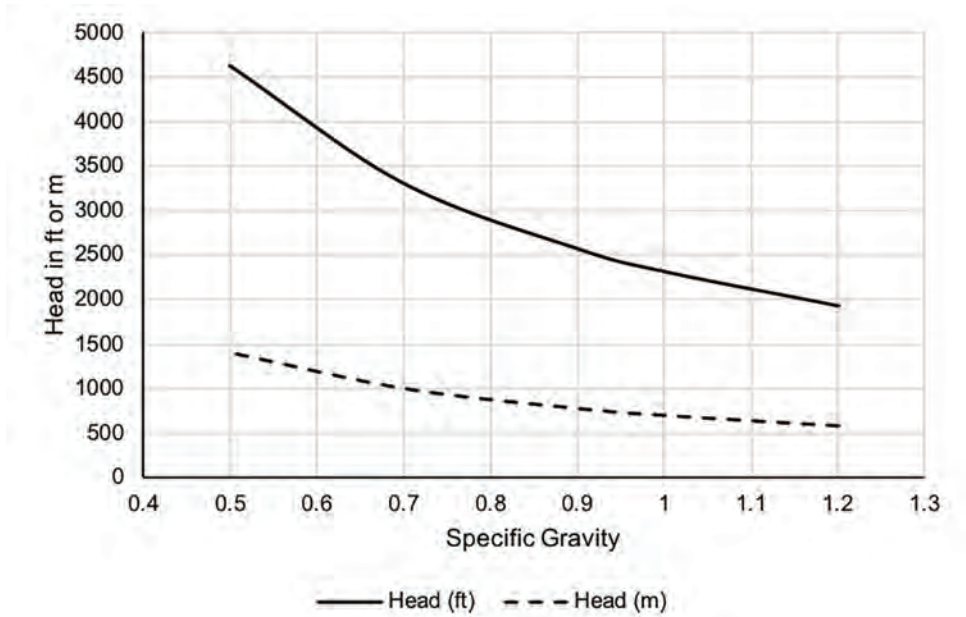


Figure 5-3. Head vs. specific gravity relationship for pumps handling different liquids to the same pressure (6895 kPa, 1000 psi).

Suppliers of dynamic machines (centrifugal pumps) generally provide all calculations in terms of head. Suppliers of positive displacement (reciprocating) pumps usually utilize pressure units.

The head specific gravity relationship of pumps delivering the same pressure (6895 kPa, 1000 psi), but handling different liquids is illustrated in Fig. 5-3. It is evident from Fig. 5-3 that head varies with SG at constant pressure, and that, to achieve the same pressure, different pump performance will be required.

For transporting different products through a pipeline through a batching operation, this means that pump performance may not be optimal for specific fluids.

5.3 AMERICAN PETROLEUM INSTITUTE GRAVITY AND SG RELATIONSHIP

Accurate determination of the density, relative density (SG), or API gravity of petroleum and its products is necessary for the conversion of measured volumes to volumes or masses, or both, at the standard reference temperatures during custody transfer and/or for facilities design.

The API gravity is a measure of how heavy or light petroleum liquid is compared to water. Fluids with API gravity greater than 10 are lighter and can float on water; API gravity is thus a measure of the relative density of a hydrocarbon liquids and the density of water, but it is used to compare the relative densities of petroleum liquids, and hence, it is important for assessment of pumps. For example, if one petroleum liquid floats on another and is therefore less dense, it has a greater API gravity.

There are several methods in use expressing SG of hydrocarbon liquids. One method is the ratio of the specific weight of the liquid at 60°F to the specific weight of water at 60°F. Another method is in °API.

The following provides the formulae used to define the API gravity of hydrocarbon liquids in relation to SG.

$$^{\circ}\text{API gravity} = (141.5/\text{SG at } 60^{\circ}\text{F}) - 131.5 \quad (5-2)$$

Conversely, the SG of hydrocarbon liquids can be derived from the API gravity value as

$$\text{SG at } 60^{\circ}\text{F} = 141.5/(\text{API Gravity at } 60^{\circ}\text{F} + 131.5) \quad (5-3)$$

There are methods that provide adjustments for temperature; ASTM [1] describes the methodology for temperature corrections. Alternatively, the following correction factors can be used to allow for temperature effects relative to 15°C (59°F) as divided into three ranges. All temperatures are expressed in °C.

- For temperatures less than 3.98°C:
correction = $-0.000032692^{\circ}\text{C} - 0.000740644$
- For temperatures less than 50.0°C and greater than or equal to 3.98°C:
correction = $-0.0008031922 - 0.0000473773^{\circ}\text{C} + 0.000007231263^{\circ}\text{C}^2 - 0.00000003078278^{\circ}\text{C}^3$
- For temperatures greater than or equal to 50.0°C:
correction = $-0.005431719 + 0.0001963596^{\circ}\text{C} + 0.000002661056^{\circ}\text{C}^2$

Therefore, SG corrected = SG + correction.

Thus, a heavy oil with a SG of 1.0 (i.e., with the same density as pure water at 60°F) would have an API gravity of:

$$\frac{141.5}{1.0} - 131.5 = 10.0^{\circ}\text{API} \quad (5-4)$$

Generally, 40 to 45 API gravity degree oils have the greatest commercial value. Above 45°API gravity, the molecular chains become shorter and less valuable to a refinery.

Crude oil is classified as light, medium, or heavy, according to its measured API gravity. Light crude oil is defined as having an API gravity higher than 31.1°API.

Medium oil is defined as having an API gravity between 22.3°API and 31.1°API.

Bitumen derived from the oil sand deposits in the northern Alberta, Canada, area has an API gravity of about 8°API. It is “upgraded” to an API gravity of 31°API to 33°API as synthetic crude.

A third method is °Baume. For liquids lighter than water:

$$^{\circ}\text{Baume} = \{ 140/\text{SG } 60^{\circ}\text{F}/60^{\circ}\text{F} \} - 130 \quad (5-5)$$

For liquids heavier than water:

$$^{\circ}\text{Baume} = \{ 145/\text{SG } 60^{\circ}\text{F}/60^{\circ}\text{F} \} \quad (5-6)$$

The relationship between API gravity, SG and density ID summarized in Fig. 5-4. SG of some hydrocarbon liquids is indicated in Table 5-2.

Dilutions. Often, dilution occurs in a pipeline system when one fluid stream is injected with another primarily for the purpose of making the final products transported lighter or less viscous. In the case of product batching, this is done through full or side stream injection or straight injection and delivery.

To calculate a new volume from current volume, current SG, and target SG

$$V_{\text{new}} = [(SG_c - 1.0)/(SG_t - 1.0)] * V_{\text{cur}} \quad (5-7)$$

where:

V_{cur} = current volume

SG_c = current SG

SG_t = target SG

For a new SG from current SG, current volume, and target volume

$$SG_{\text{new}} = [(SG_c - 1.0) * (V_{\text{cur}}/V_{\text{tar}})] + 1.0 \quad (5-8)$$

where:

SG_c = current SG

V_{cur} = current volume

V_{tar} = target volume

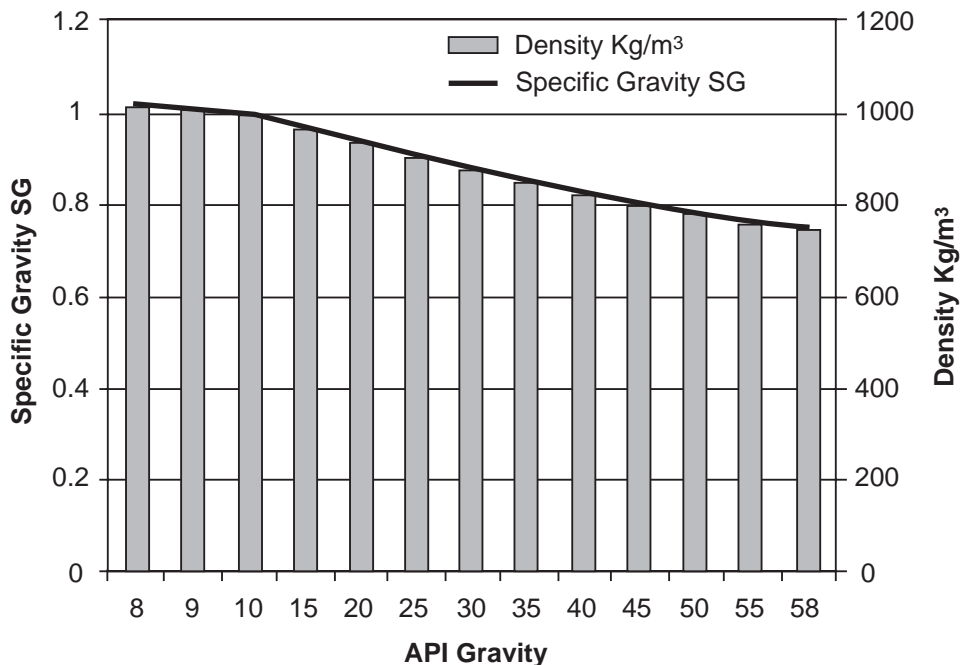


Figure 5-4. Relationships between API gravity, SG, and density.

Table 5-2. Specific gravity of some hydrocarbon liquids

Liquid Product	Temperature (°C)	SG
Alcohol-ethyl (grain) C_2H_5OH	20	0.789
	40	0.772
Alcohol-methyl (wood) CH_3OH	20	0.79
	20	0.804
Alcohol-propyl	0	0.817
	–17.8	0.662
Ammonia	–17.8	0.662
Automotive crankcase oils SAE-5W/10W/20W/30W/40W/50W	15.6	0.88–0.94
Automotive gear oils SAE-75W/80W/85W/90W/140W/150W	15.6	0.88–0.94
Butane	0.587	7.2
	0.58	15.6
Crude oil 48°API	15.6	0.79
	54.4	0.76
Crude oil 40°API	15.6	0.825
	54.4	0.805
Crude oil 35.6°API	15.6	0.847
	54.4	0.824
Crude oil 32.6°API	15.6	0.832
	54.4	0.84
Crude oil salt creek	15.6	0.843
	54.4	0.82
Diesel fuel oil 2D/3D/4D/5D	15.6	0.81–0.96
Furnace oil #1	7.2	0.815
	15.6	0.81
Furnace oil #2	7.2	0.845
	15.6	0.84
Gas oils	15.6	0.89
	7.2	0.764
Gasoline	15.6	0.757
	15.6	0.74
Gasoline A	15.6	0.72
Gasoline B	15.6	0.68
Gasoline C	15.6	0.67
Gasoline, natural	7.2	0.66
	15.6	0.688
Heptane-n	15.6	0.664
Hexane-n	15.6	0.815
Kerosene	7.2	0.81
	15.6	0.82
Jet fuel	15.6	13.6
Mercury	15.6	0.93
Methyl acetate	20	2.28
Methyl iodide	20	1.145
Naphthalene	20	0.91–0.92
Olive oil	15.6	0.924
Palm oil	15.6	0.92
Peanut oil	15.6	0.65
Pentane-n	0	0.631
	15.6	0.79
Power fuel	7.2	0.78
	15.6	0.527
Propane	7.2	0.51
	15.6	1
Water, fresh	4	1.02
Water, sea	20	

5.4 PERFORMANCE OF CENTRIFUGAL PUMPS

5.4.1 Pump Performance Curves

An individual set of pump performance curves is derived from a “family” set of pump curves, as illustrated in Fig. 5-5. The following information can usually be obtained:

- pump model and size
- rated speed
- curve identification number
- impeller type and eye area
- wear ring clearances
- range of impeller diameters available
- capacity versus head developed for the different impeller diameters (H-Q curves)
- power to drive pump (pressure head, flow P-Q) curves, based on water, specific gravity (SG = 1.0)
- pump efficiency (efficiency—Q curves)
- NPSHR
- pump specific speed, N_s
- pump suction specific speed, N_{ss} or S

In a double suction pump, the area of the impeller eye is the area of the impeller eyes in both of the impellers. Pump shutoff is the head developed at zero (0) capacity. Pump run-out is the pump capacity above which the pump should not be operated due to instability, excessive NPSHR, vibration, and a dramatic reduction in head. This point is usually 120% of best efficiency point.

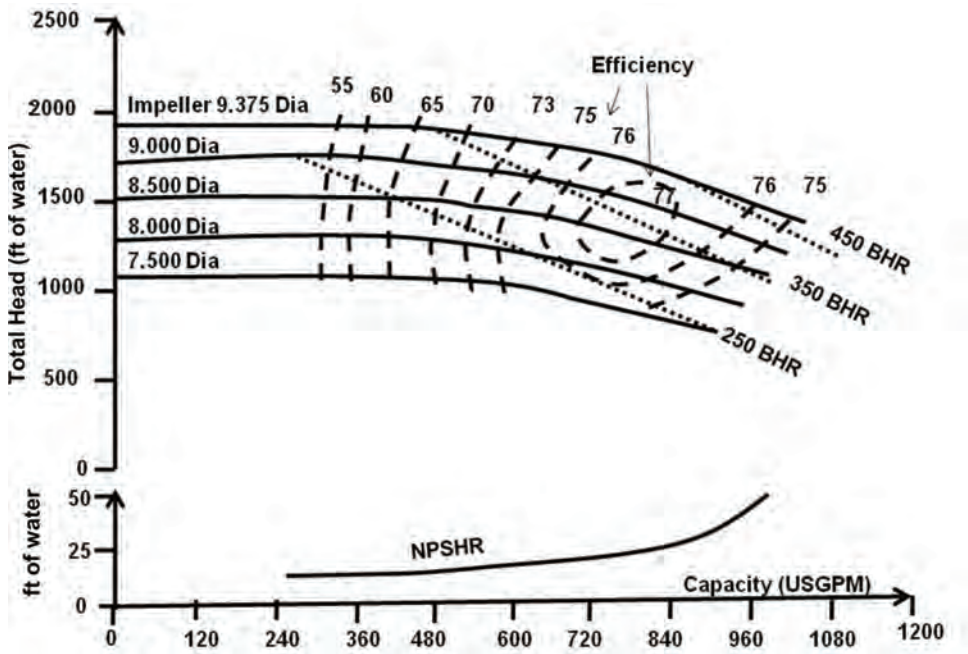


Figure 5-5. Typical centrifugal multistage pump performance curve, m-pump 3 × 6 MOF-S 5 Stage (after ref. [2]).

5.4.2 Centrifugal Pump Coverage Chart

A coverage chart makes it possible to do a preliminary pump assessment and, hence, selection by reviewing a wide range of pump casing/impeller sizes for a specific impeller speed. This chart helps narrow down the choice of pumps that will satisfy the pipeline system requirements. A typical pump selection chart is indicated in Fig. 5-6.

In selecting a pump to match the system curve, a pump with the appropriate impeller diameter must be selected to assure meeting the flow and head requirements. Determination of system total head for a given flow rate will determine pump selection based on pump performance curve for a given impeller diameter. As an example, Fig. 5-7 indicates the performance curve for a system operation with a pump that has an impeller diameter of 9 in.

A performance curve plot commences at zero flow. The head at this point corresponds to the shutoff head of the pump, point A in Fig. 5-7. Starting at this point, the head decreases until it reaches its minimum at point B. This point is sometimes called the run-out point and represents the maximum flow of the pump. Beyond this, the pump cannot operate. The pump's range of operation is from points A to B.

5.4.3 Impeller Selection

Quite often, the desired operating point is located between two curves on a given performance chart.

The required impeller size can be calculated by the linear interpolation of adjacent two curve that fall above and below the operating point, in this case, 9- and 9.375-in. impeller sizes (Fig. 5-8). The following equation will give the correct size:

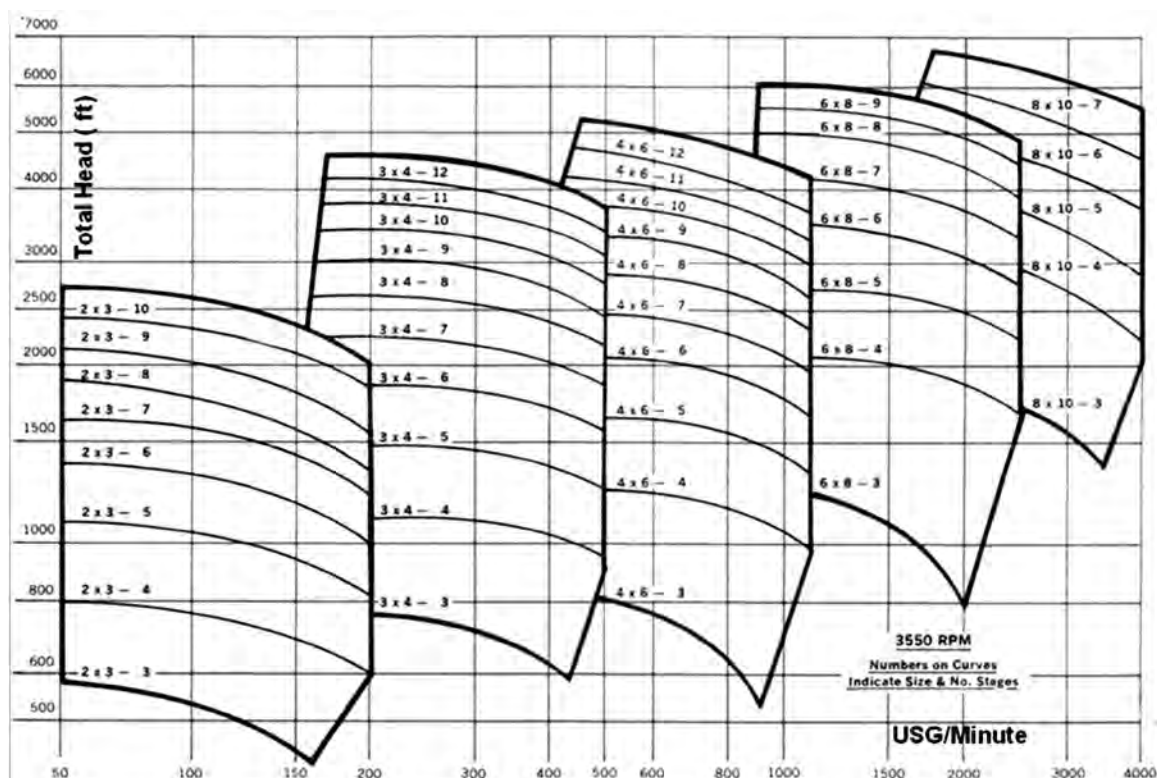


Figure 5-6. Typical range of multistage centrifugal pumps for pipeline booster applications.

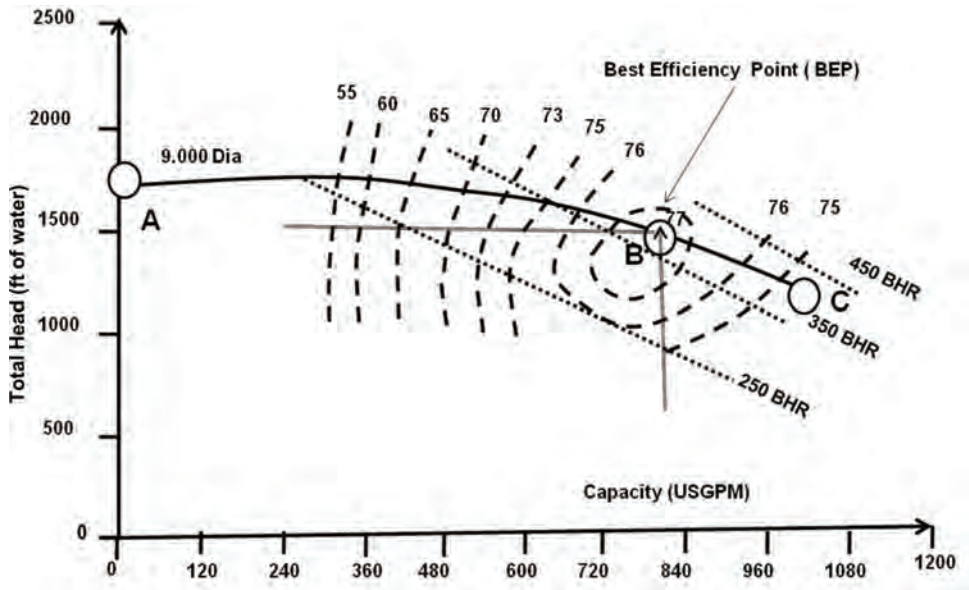


Figure 5-7. Typical performance curve for a specific 9 in. diameter impeller.

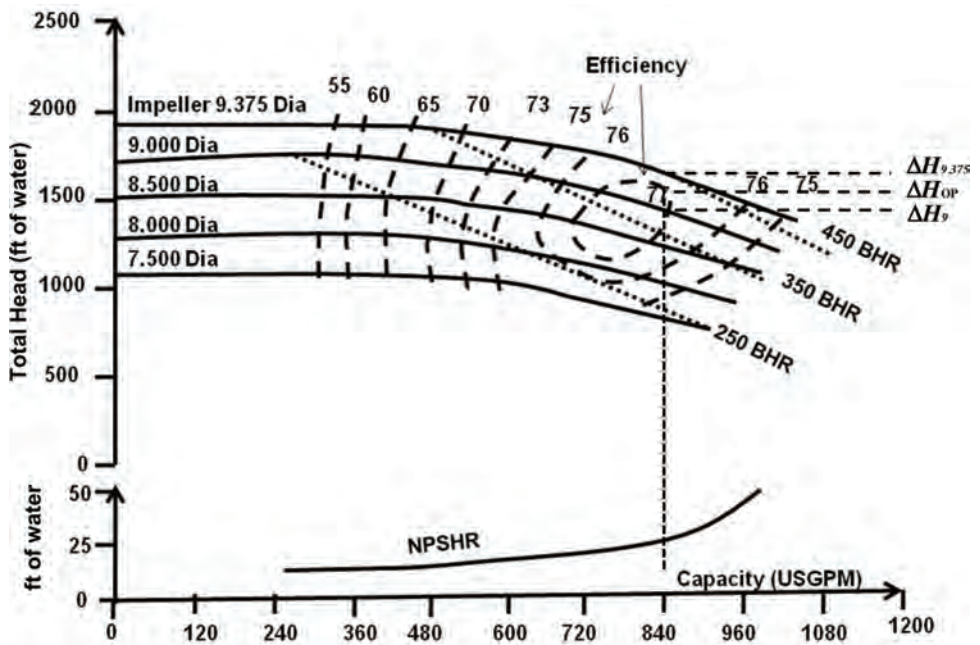


Figure 5-8. Impeller selection.

$$D_{OP} = 9 + \{(9.375 - 9) / (H_{9.375} - H_9)\} (H_{OP} - H_9) \quad (5-9)$$

where

- D_{OP} = impeller diameter required
- H_{OP} = pump total head at the operating point
- H_9 = pump total head at the intersection of the 9 in. impeller curve and flow rate

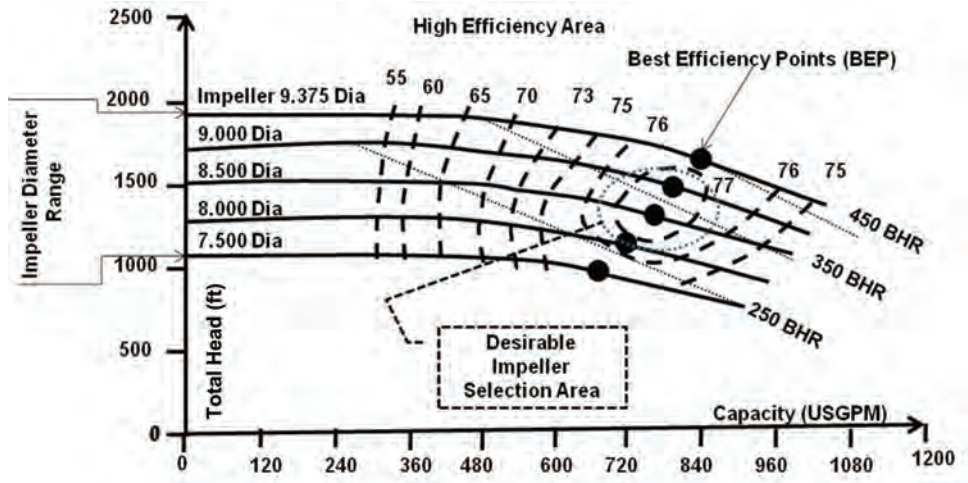


Figure 5-9. Desirable pump selection area.

$H_{9.375}$ = pump total head at the intersection of the 9.375 in. impeller curve and the flow rate

When possible, a pump is selected with an impeller that can be increased in size, permitting a future increase in head and capacity or, alternatively, an impeller which can be reduced in size. As a guide, select a pump with an impeller size no greater than between one third and two thirds of the impeller range for the pump casing with an operating point in the high-efficiency area (Fig. 5-9). It is also important not to go too far right or left from the Best Efficiency Point (BEP). A guideline is to locate the operating point between 110% and 80% ([3]).

5.4.4 Pump Head-Flow and System Head-Flow Curves

The system curve is a plot of the total head versus the flow for a given system. The higher the flow, the greater the head required (Fig. 5-10). The shape of the system curve depends on the type of system being considered. The system curve equation for a typical single outlet system such as in Fig. 2-9, Chapter 2 is:

$$\Delta H_P (q) = \Delta H_F (q) + \Delta H_{EQ} (q) + \Delta H_V (q) + \Delta H_{TS} \quad (5-10)$$

The system curve is superimposed on the pump performance chart. The total static head is constant and the friction head, equipment head, and velocity head are flow-dependent.

The calculation of total head at different flow rates produces a plot of total head versus flow, thus producing the system curve.

The operating point is the point on the system curve corresponding to the flow and head required. It is also the point where the system curve intersects the performance curve.

The design system curve is usually calculated with extra flow capacity in mind. As usually the demand changes towards higher deliveries, it is good practice to plot the system curve for higher flow rates than the design flow rate. Thus, unanticipated extra capacity can be accommodated if required.

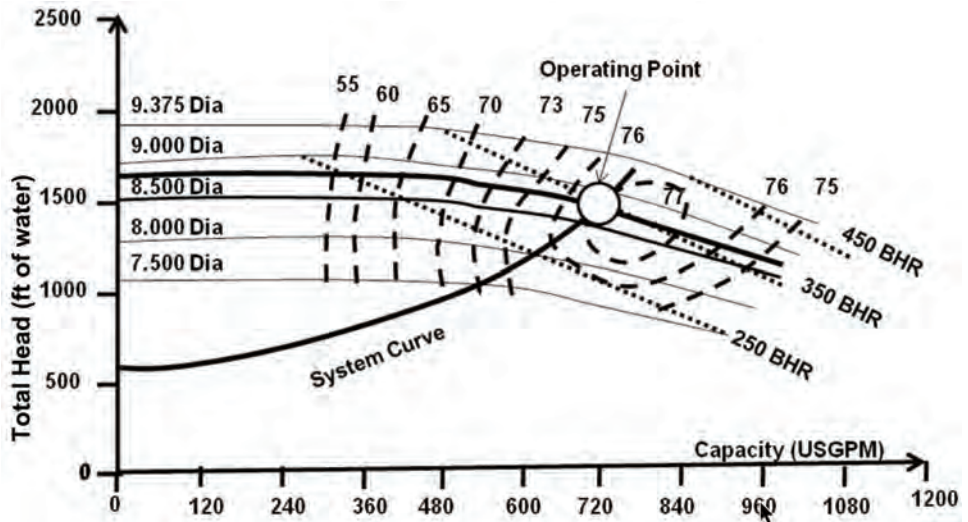


Figure 5-10. Pump performance–system curve superimposition.

5.4.5 Centrifugal Impeller Design Theory

The work of a centrifugal impeller (H) can be derived by applying the principle of angular momentum to the mass of fluid going through the impeller passages. This principle is applied to the inlet and exit conditions of a frictionless fluid in an impeller to drive the impeller head H_v .

Using the following nomenclature:

- U = peripheral velocity of impeller
- V_r = relative velocity of flow
- V = absolute velocity of flow
- V_m = radial velocity
- α, β = vane angle
- ω = angular velocity
- γ = density
- g = gravitational acceleration
- Q = flow
- W = weight flow
- 1 = inlet subscript
- 2 = discharge subscript

Figure 5-11 depicts a sketch of an impeller inlet and discharge velocity diagram.

The torque (T) is defined as the difference of the peripheral components of impulse forces:

$$T = (\text{outlet impulse} \cos \alpha_2) - (\text{inlet impulse} \cos \alpha_1) \quad (5-11)$$

$$T = \left[\left(\frac{\gamma}{g} \right) Q R_2 V_2 \cos \alpha_2 \right] - \left[\left(\frac{\gamma}{g} \right) Q R_1 V_1 \cos \alpha_1 \right] \quad (5-12)$$

$$T = \left(\frac{\gamma}{g} \right) Q (R_2 V_{2m} - R_1 V_{1m}) \quad (5-13)$$

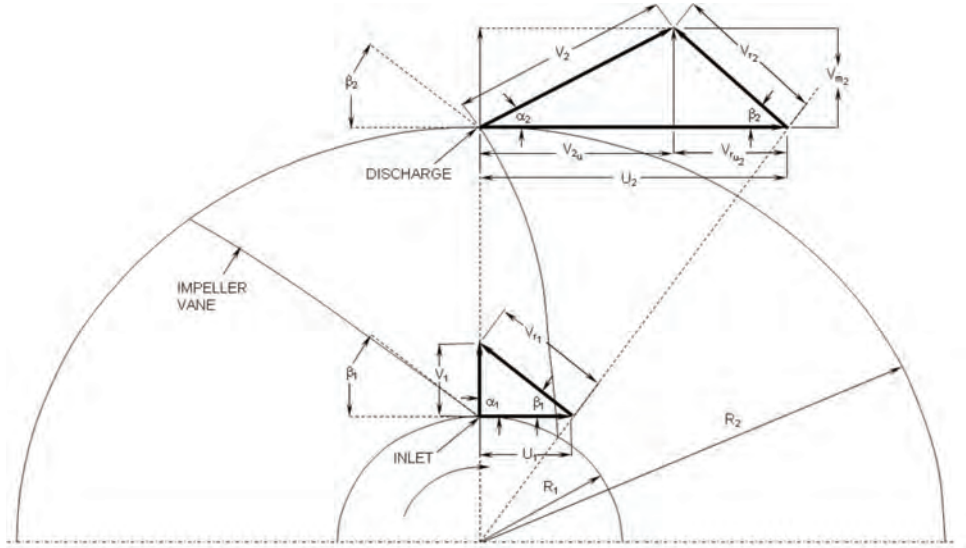


Figure 5-11. Impeller inlet and discharge velocity diagram.

Considering Euler's theory the following can be derived for the work done by the impeller (i.e., theoretical head H_t achieved):

$$H_t = \frac{\text{energy input}}{\text{weight (mass) flow}} \quad (5-14)$$

$$H_t = \text{torque} \left(\frac{\omega}{W} \right) \quad (5-15)$$

Substituting:

$$H_t = \frac{T\omega}{W} = \frac{T\omega}{\gamma Q} = \left(\frac{1}{g} \right) (R_2 \omega V_{2m} - R_1 \omega V_{1m}) \quad (5-16)$$

The Euler Equation for head H_t is thus:

$$H_t = \left(\frac{1}{g} \right) (V_{2m} U_2 - V_{1m} U_1) \quad (5-17)$$

Assuming the fluid enters the impeller without a tangential component (radial inlet), then $V_{1u} U_1 = 0$ and Euler's Eq. (5-17) can be reduced to:

$$H_t = \frac{V_{2u}}{g} \text{ where } V_{2m} = U_2 - \frac{V_{m2}}{\tan \beta_2} \quad (5-18)$$

$$H_t = \frac{U_2^2}{g} \left[1 - \frac{V_{m2}}{\tan \beta_2} \right] \quad (5-19)$$

For any given impeller size, V_{m2} will vary directly with flow, and if the rotative speed is held constant, U_2 will be constant and H_t will vary linearly with flow. For an angle β_2

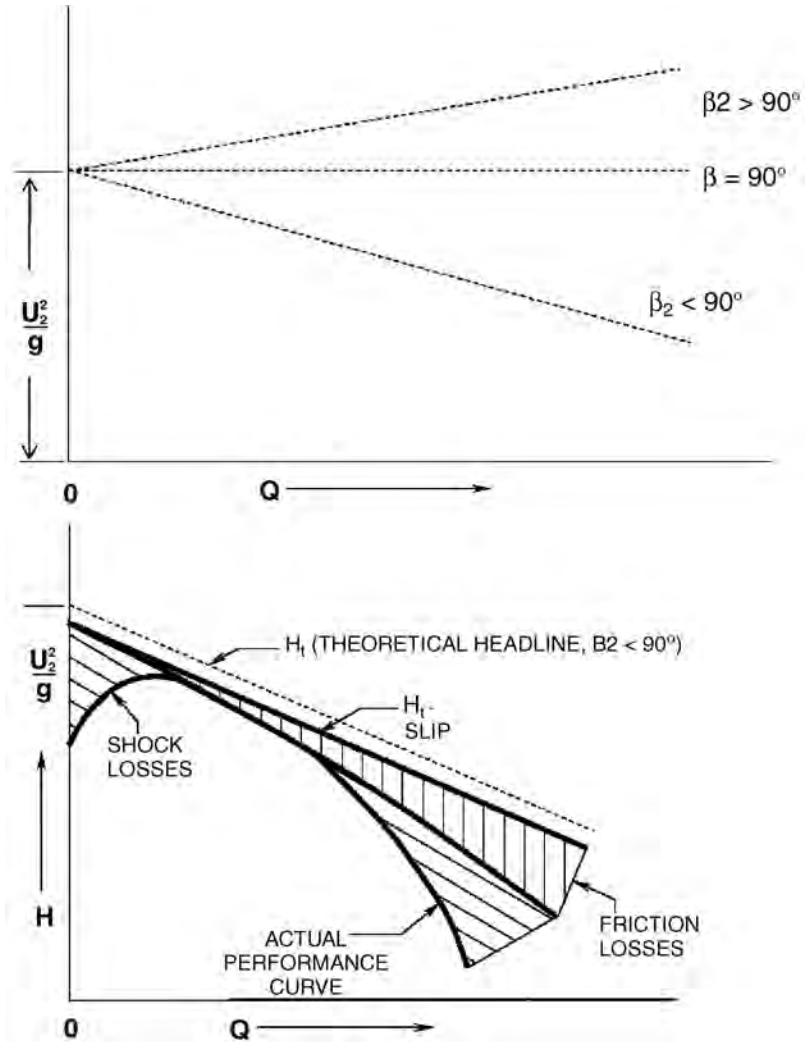


Figure 5-12. Development of the pump head capacity curve.

less than 90° (backward curved vanes), $V_m^2/\tan \beta_2$ will increase with flow and cause H_t to decrease with flow. This will result in a theoretical curve, as shown in Fig. 5-12. If shock losses, slip factors and friction losses are added to the theoretical curve, the typical pump characteristic curve (as shown in Fig. 5-12) is generated. It is these types of curves that pipeline engineers need to be familiar with in order to select pumps for a particular service application.

5.4.6 Specific Speed

Generally, there are a multitude of pipeline pump designs that are available for any given task including for pipeline applications. Pump users generally would like to know the pump performance for their applications and, hence, what efficiency can be expected from a particular pump design.

For pump performance comparison purposes, pumps are tested and compared using various criteria including and, importantly, the criterion of specific speed (N_s). The efficiency of pumps with the same specific speed can be compared providing the user or the

designer a starting point for comparison or as a benchmark for improving the design and increasing the efficiency.

Specific speed (N_s) is thus used to predict pump characteristics for the purpose of classifying pump impellers according to type, proportions and performance. It is expressed as:

$$N_s = \frac{N\sqrt{Q}}{H^{\frac{3}{4}}} \quad (5-20)$$

where

- N_s = pump specific speed (dimensionless)
- N = pump speed in RPM
- Q = capacity at best efficiency point (USGPM)
- H = total head per stage at the best efficiency point (ft)

The above equation is for single suction pumps. For double suction impellers, one half the flow needs to be used to calculate the specific speed. The specific speed (N_s) determines the general shape or class of the impeller. As the specific speed increases, the ratio of the impeller outlet diameter, D_2 , to the inlet or eye diameter, D_1 , decreases. This ratio becomes 1.0 for a true axial flow impeller.

Radial flow impellers develop head mainly through centrifugal force. Pumps of higher specific speeds develop head partially by centrifugal force and partially by axial force. A pump with a higher specific speed generates head more by axial forces and less by centrifugal forces. An axial flow or propeller pump with a specific speed of 10,000 or greater generates its head exclusively through axial forces.

The specific speed of an impeller can thus provide a wide variety of information about the performance:

- Impeller type: impellers with low-specific speed are long and thin and are used for low flow, high head applications. Impellers with high-specific speed are short and stubby and are used for high-flow, low-head applications.
- Efficiency: efficiency is arrived at by considering the losses through the pump impeller and driver system. Pump efficiency is affected by losses due to pump impeller friction, ring leakage, and mechanical losses as well as losses incurred by movement of the liquid within the pump, referred to as hydrodynamic losses. Specific speed affects pump efficiency (Fig. 5-13). The lower the specific speed, the lower

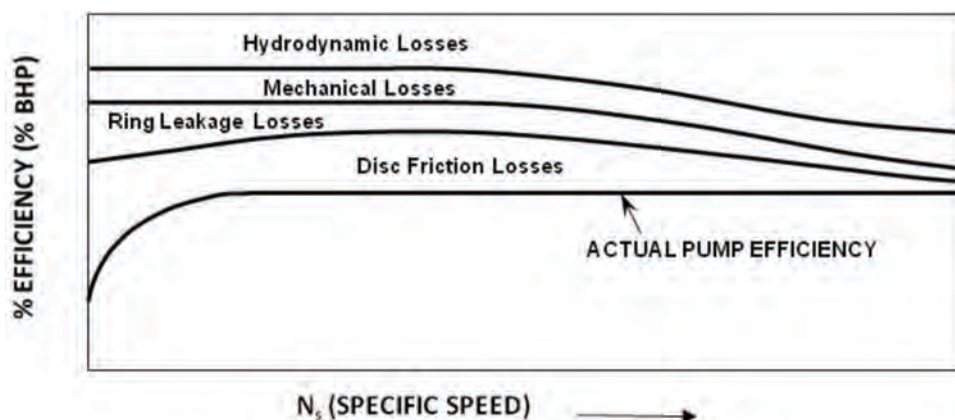


Figure 5-13. Specific speed and efficiency.

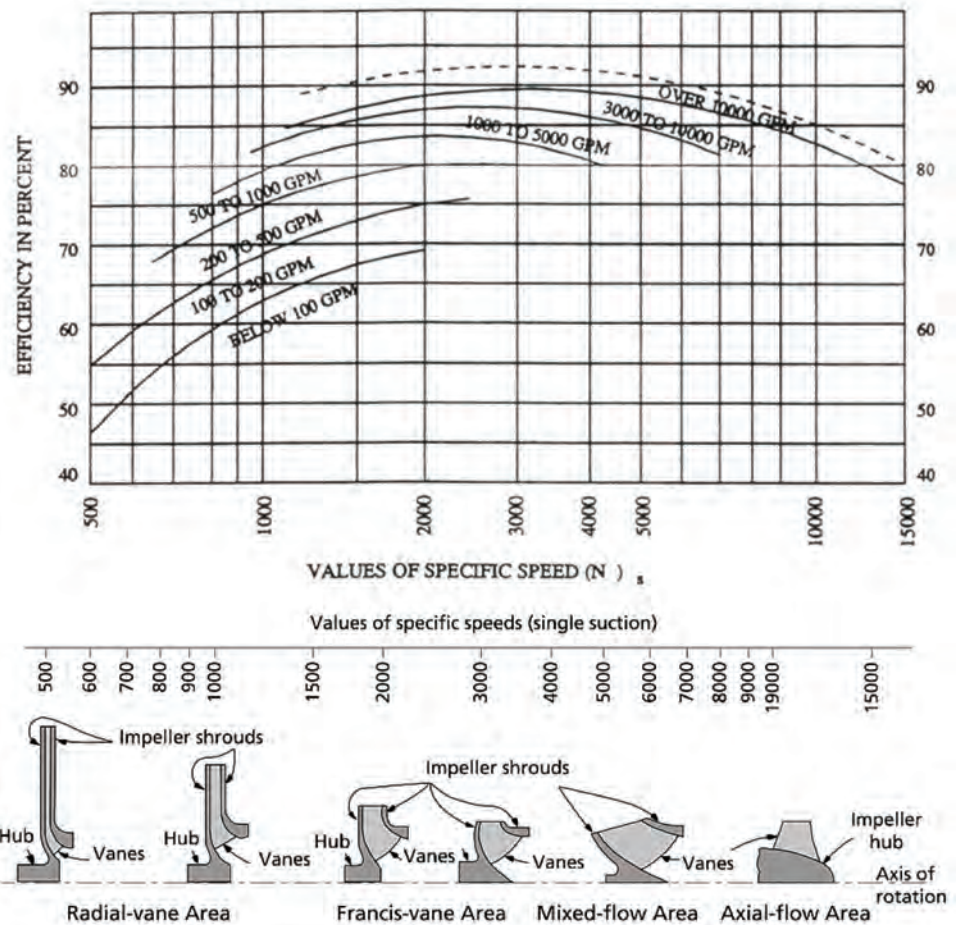


Figure 5-14. Specific speed and efficiency [4].

the efficiency. The reason is that a higher percentage of energy is lost to overcome the impeller disc friction that is necessary to generate the high heads (Fig. 5-14).

- Shape of curve: once an impeller is designed for a certain specific speed, it will produce a typical head capacity curve and efficiency curve shape. A low-specific speed impeller has a flat curve with a wide efficiency range. A high-specific speed impeller produces a steep curve with a narrow efficiency range (Fig. 5-15).

5.4.7 Impeller Curve Characteristics

There are a number of pump head capacity (H-Q) curve shapes that are shown in Fig. 5-16. These characteristic curves are listed below and described thereafter:

- rising
- drooping
- steep
- flat
- stable

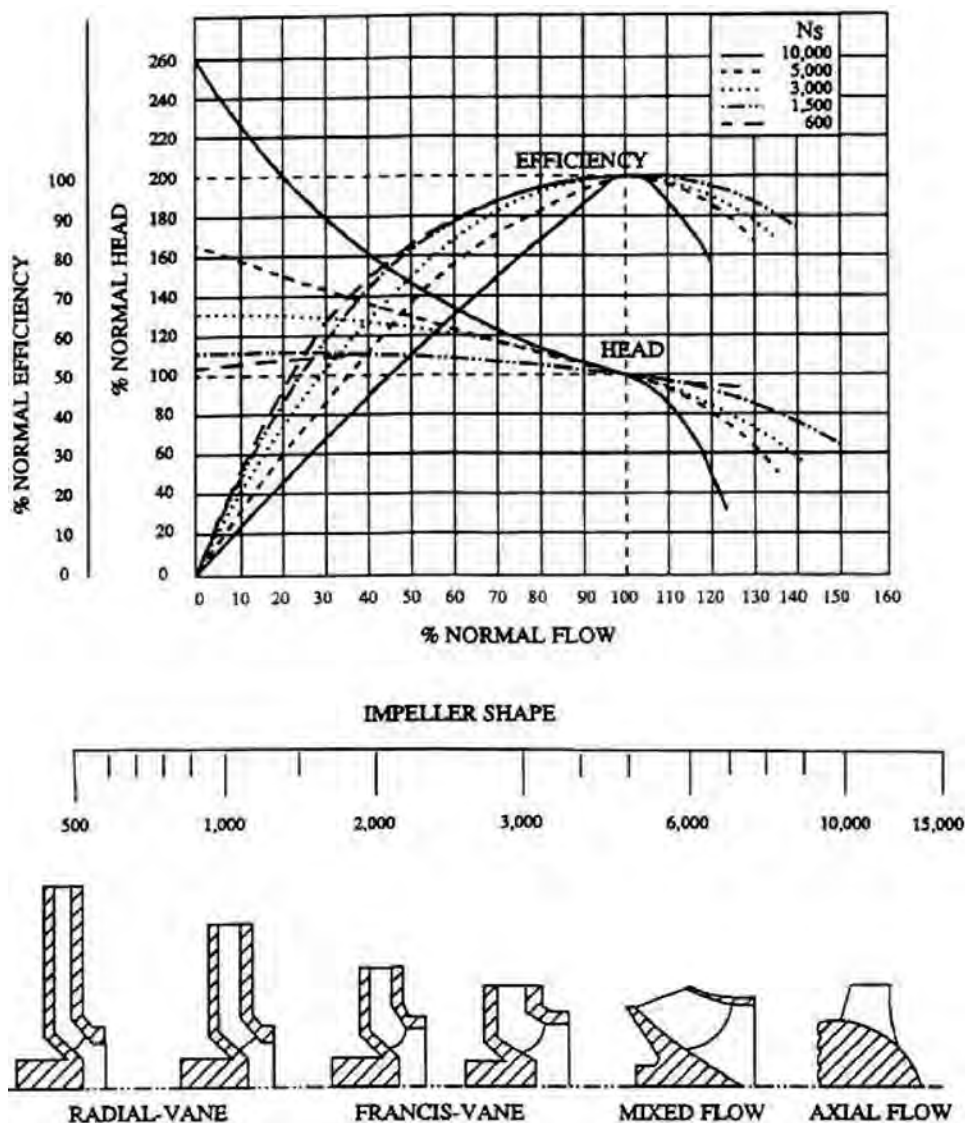


Figure 5-15. Specific speed and performance.

- unstable
- non-overloading
- overloading

Rising characteristic: the head rises continuously as the capacity is decreased to shut-off.

Drooping characteristic: the head developed at shut-off is less than at some of the other capacities.

Steep characteristic: the head developed at shutoff is significantly larger than that developed at the design capacity.

Flat characteristic: the head developed at shut-off is approximately that developed at the design capacity. The curve can be slightly rising or drooping.

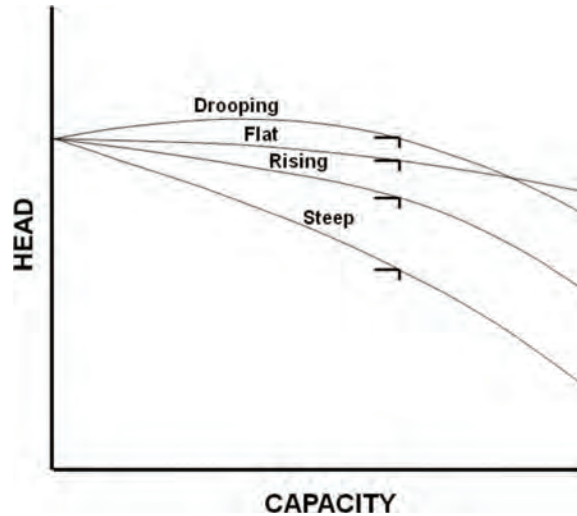


Figure 5-16. Various types of pump characteristic curves.

Stable curve: is a rising curve where only one capacity can be obtained at any one head. A curve with a rising characteristic would be an example of a stable curve.

Unstable curve: is a drooping curve where more than one capacity can be obtained at one head. A curve with a drooping characteristic would be an example of an unstable curve.

Non-overloading curve (Fig. 5-17): power curve continues to increase with an increase in capacity.

Overloading curve (Fig. 5-17): power curve continues to decrease with an increase in capacity.

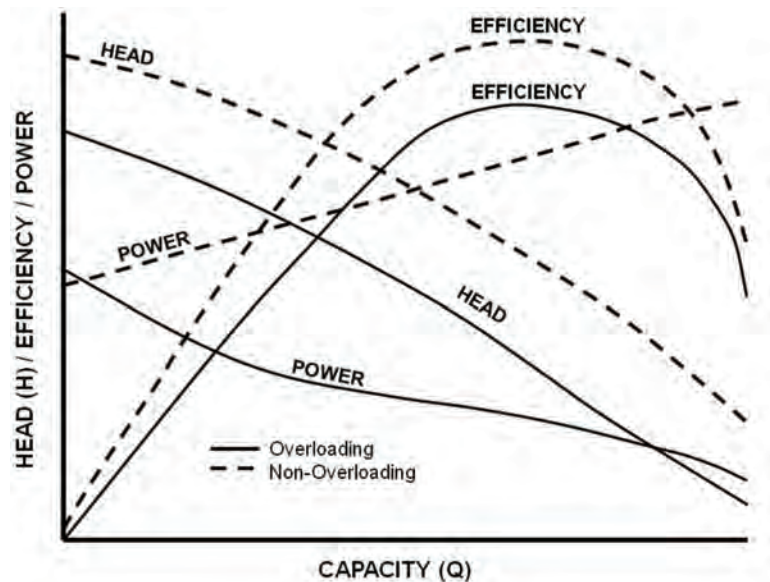


Figure 5-17. Typical characteristic curves for overloading and non-overloading.

5.4.8 Affinity Laws

The flow and head of a centrifugal pump may be changed by varying the pump speed or changing the impeller diameter. This results in a change to the impeller tip speed or velocity of the impeller vanes, which causes a change in the velocity at which the liquid leaves the impeller. Usually, the impellers can be cut down to 80% of the original diameter without lowering the efficiency significantly.

The affinity laws were developed using the laws of similitudes which provides three basic relationships:

- flow versus diameter
- total head versus diameter and speed
- power versus diameter and speed

For centrifugal pumps with radial impellers, the relationships are approximately as follows:

For diameter change only:

$$Q_2 = Q_1 \left(\frac{D_2}{D_1} \right), H_2 = H_1 \left(\frac{D_2}{D_1} \right)^2, \text{bhp}_2 = \text{bhp}_1 \left(\frac{D_2}{D_1} \right)^3 \quad (5-21)$$

For speed change only:

$$Q_2 = Q_1 \left(\frac{N_2}{N_1} \right), H_2 = H_1 \left(\frac{N_2}{N_1} \right)^2, \text{bhp}_2 = \text{bhp}_1 \left(\frac{N_2}{N_1} \right)^3 \quad (5-22)$$

For diameter and speed change:

$$Q_2 = Q_1 \left(\frac{D_2}{D_1} \times \frac{N_2}{N_1} \right), H_2 = H_1 \left(\frac{D_2}{D_1} \times \frac{N_2}{N_1} \right)^2, \text{bhp}_2 = \text{bhp}_1 \left(\frac{D_2}{D_1} \times \frac{N_2}{N_1} \right)^3 \quad (5-23)$$

where

- D = impeller diameter (typically in inches)
- H = head in (typically in feet or meter)
- Q = capacity (typically in USGPM)
- N = speed in RPM
- bhp = brake horsepower
- 1 = original conditions subscript
- 2 = new design conditions subscript

The process of arriving at the affinity laws assumes that the two operating points that are being compared are at the same efficiency. The relationship between two operating points, say 1 and 2, depends on the shape of the system curve (Fig. 5-18). The points that lie on system curve A will all be approximately at the same efficiency, whereas the points that lie on system curve B are not. The affinity laws do not apply to points that belong to system curve B. System curve B describes a system with a relatively high static head versus system curve A, which has a low static head [5].

5.4.9 Pipeline-Pump Operational Control

Pumps and pipelines can be controlled by several means including pressure/flow throttling through the appropriate suction/discharge valves, speed changes, etc. To illustrate these

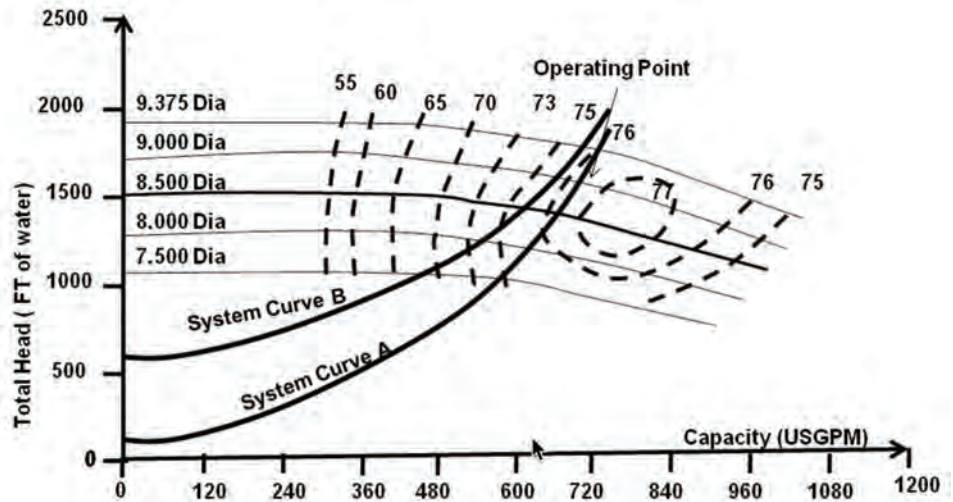


Figure 5-18. Limitation on the use of the affinity laws.

options, a pump H-Q curve overlaid on the pipeline system hydraulic system head curve is shown in Fig. 5-19.

In this example, the pump is designed to operate at point H_1 system curve is changed.

The pump includes a throttle valve on the discharge side. If such a throttle valve is partially closed, friction will be added to the system and the pump is forced to operate back on the curve at Point H_2 . When the system head curve is changed by throttling, it is called “throttle control.”

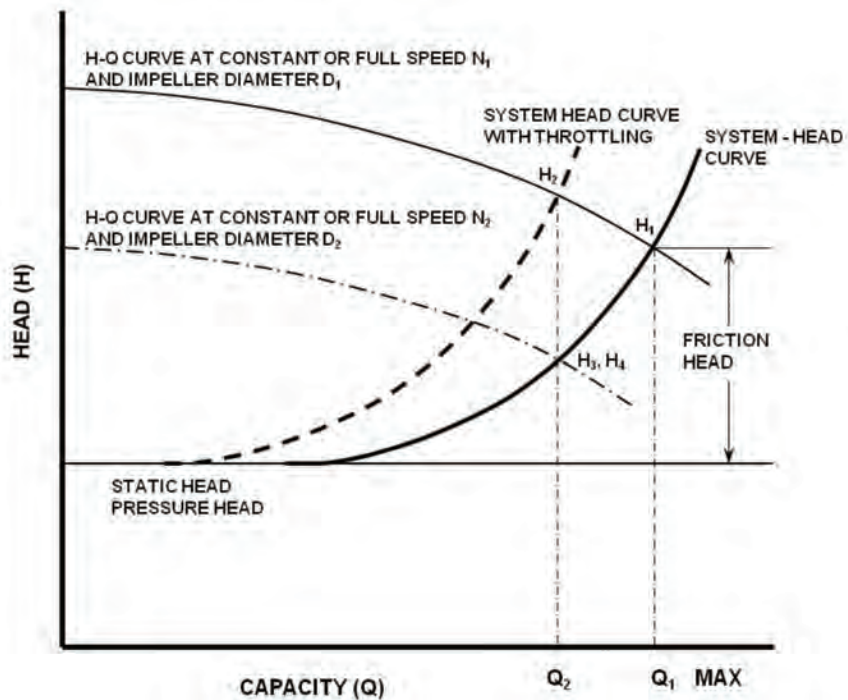


Figure 5-19. Capacity change with throttling.

If the speed of the pump is reduced from N_1 to N_2 or the impeller diameter is reduced from D_1 to D_2 , then the H-Q curve is changed, as shown in Fig. 5-19. The pump would now operate at point H_3 (for speed reduction) or H_4 (for diameter change).

5.4.10 Pump Power and Efficiency

Brake horsepower is the actual power delivered to the pump shaft. It is expressed as:

$$\text{bhp} = \frac{Q \ H \ G \ 100}{3960 \ \text{pump efficiency}} \quad (5-24)$$

Hydraulic horsepower is the liquid power developed by the pump. It is expressed as:

$$\text{hyd hp} = \frac{Q \ H \ G}{3960} \quad (5-25)$$

The pump efficiency is the ratio of hyd hp and bhp:

$$\text{Pump efficiency} = \frac{\text{hyd hp}}{\text{bhp}} \times 100 \quad (5-26)$$

where

Q = flow capacity (USGPM)

H = total developed head (ft)

G = specific gravity at the temperature of the liquid pumped

Pump efficiency = pump efficiency in percent (%)

5.4.11 Performance Modifications

The performance of pipeline pumps often needs to be altered to accommodate varying liquid transmission conditions. These generally require that the pump be physically modified to meet the new conditions. The following are considered for such modifications by the pipeline industry:

- *Impeller change.* In order to change the specific speed, impeller size may be changed to meet the new demand on performance. Pump manufacturers can usually offer several different impeller diameters and vanes that will fit the pump casing without any further internal modifications. The effect of changing the impeller characteristics are illustrated in Figs. 5-20 and 5-21.
- *Restaging.* Pumps with multistaging capabilities can be restaged (up or down) to meet the change in pressure, head, or flow requirements. For example, if an entire pressure range is not needed for a particular period of time, a number of impellers can be removed to meet the required conditions. Manufacturers provide destaging kits to block off the unused pump impeller areas to maintain efficiency (Fig. 5-22).
- *Impeller under-filing and over-filing.* This is undertaken to alter the performance of a pump. It involves modifying the flow area of the impeller by grinding metal off the impeller outlet vanes (Fig. 5-23).
- *Impeller volute chipping.* This is a technique that is used to alter the outlet flow area of the pump casing in order to modify performance (Fig. 5-24). Again, caution is needed to avoid making costly mistakes.
- *Impeller volute inserts.* This technique (Fig. 5-25) involves inserting special removable volutes into the pump to allow for a wider performance range. It also allows for more accurate and close control over the performance.

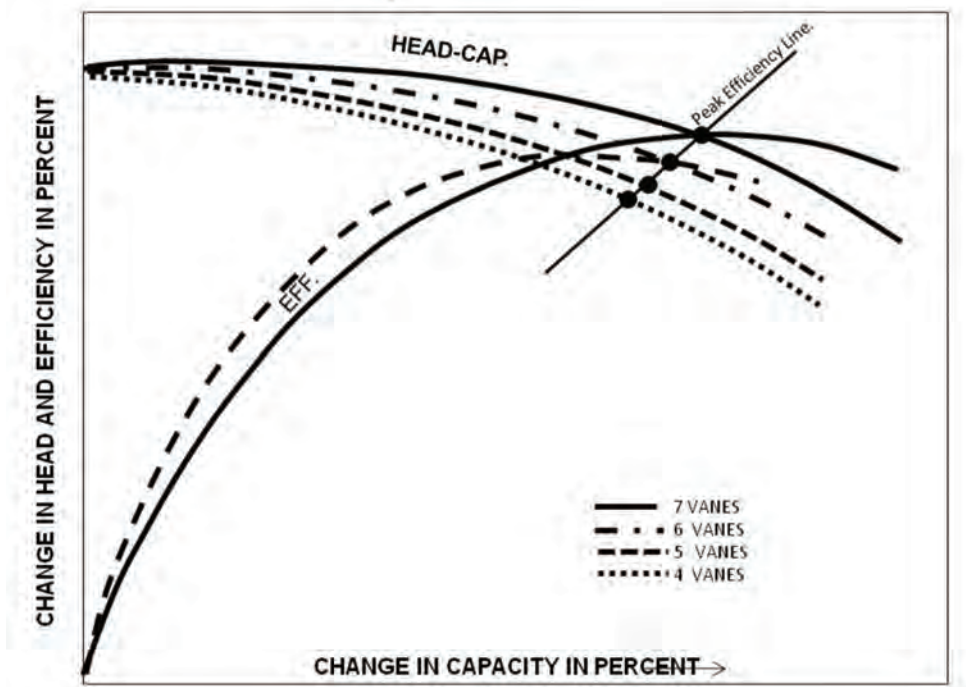


Figure 5-20. Changing performance by number of impeller vanes.

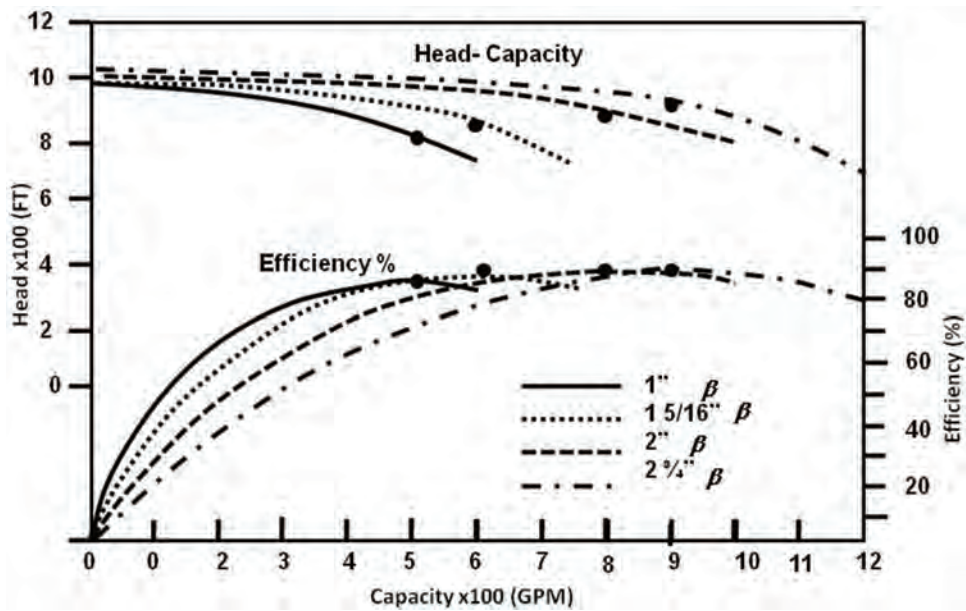


Figure 5-21. Changing pump performance by impeller vane angle β_2 .

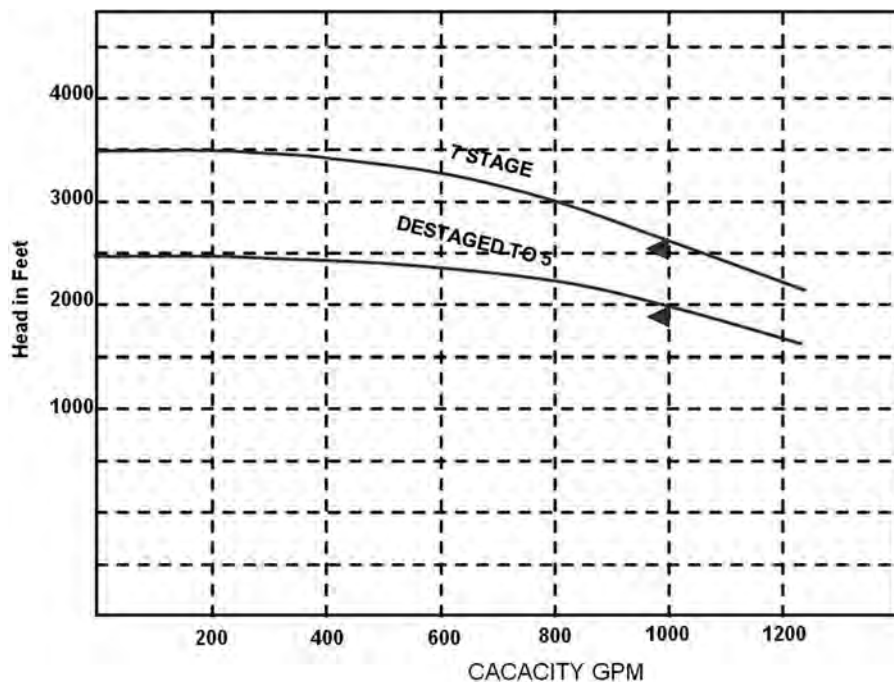


Figure 5-22. Changing performance by re-staging.

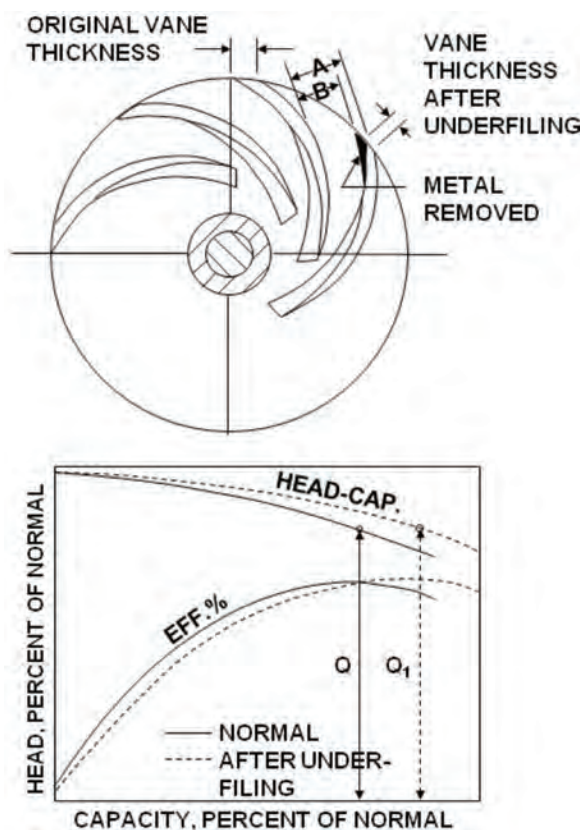


Figure 5-23. Changing performance with under-filing.

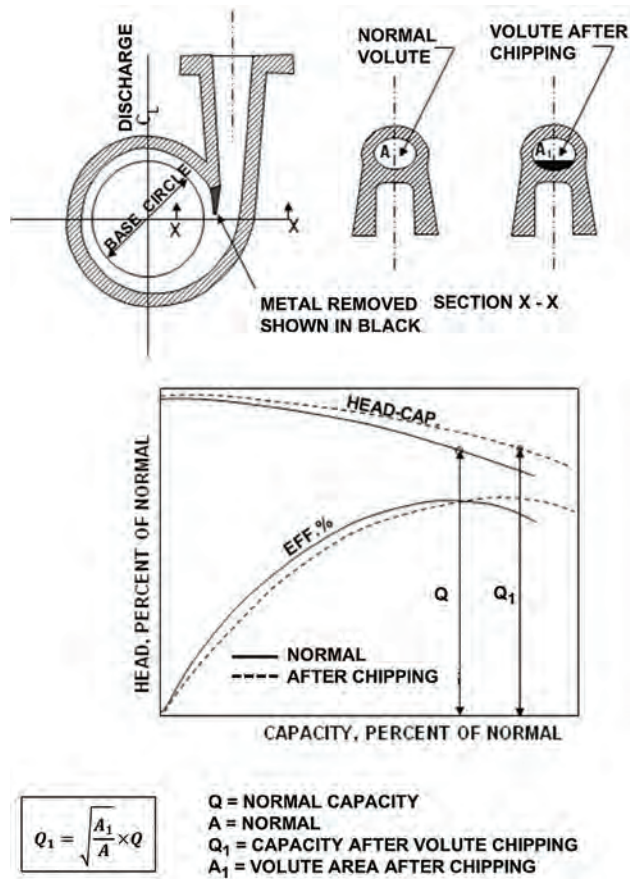


Figure 5-24. Changing performance with volute chipping.

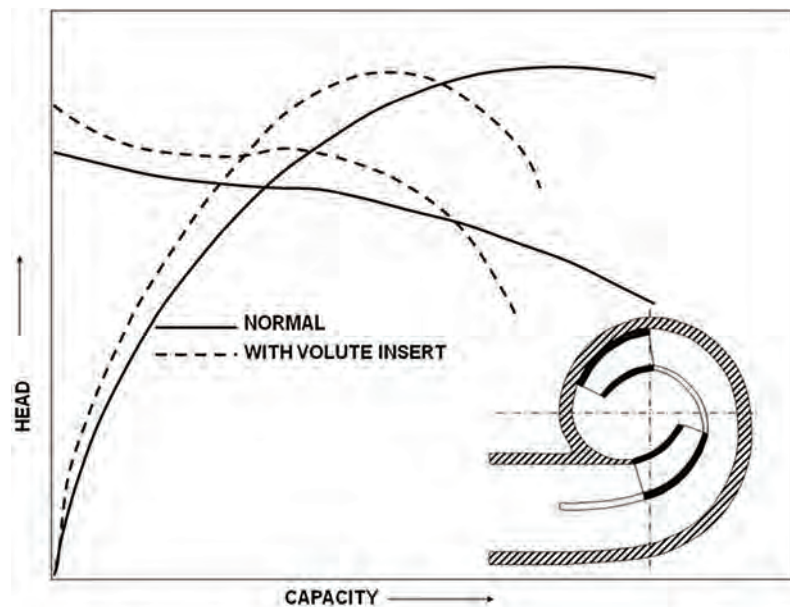


Figure 5-25. Changing performance with volute inserts.

5.5 CAVITATION IN CENTRIFUGAL PUMPS

5.5.1 Cavitation Phenomenon

Cavitation is the rapid formation and collapse of vapor bubbles formed in a pump inlet whenever the local absolute pressure of the liquid falls below its vapor pressure. These bubbles collapse rapidly and violently when the local absolute pressure increases due to kinetic forces being imparted by the impeller (Fig. 5-26) [6].

Implosion near a solid wall may be described as:

- deviation of the bubble shape from spherical symmetry
- development of a fluid micro-jet moving from the opposite of the solid wall through the bubble
- microjet strike at the wall (directly if the distance between bubble and wall is smaller-than-bubble radius) with velocity up to 1000 m/s
- bubble degeneration to a torus, microbubbles remain
- implosion of microbubbles, emitting a high-frequency, high-amplitude pressure wave

Therefore, collapsing cavitation bubbles cause noise (often sounds like gravel going through the pump), vibration, and erosion of material from the impeller (Fig. 5-27).

Damage due to cavitation may take the following forms:

- material fatigue
- microscopic plastic surface deformations (“pits”), statistically distributed



Figure 5-26. Cavitation bubble implosion onto a solid surface, arrows indicate fluid pressure (after ref. [6]).



Figure 5-27. Typical pump impeller destroyed by cavitation [6].

- pits overlapping
- material removal, cavitation erosion
- components functionality loss

The following, singularly or in combination can influence or can reduce cavitation aggressiveness [7,8]:

- NPSHA
- pump blade geometry
- fluid momentum on pump suction side
- contents of solids and dissolved gases
- air injection into the cavitation zone
- flow velocity, rotational speed

Cavitation control is a very important consideration in any liquid system, and thus, any cavitation-induced conditions must be avoided when operating centrifugal pumps. The formation of cavitation can be further understood by considering the following:

- A local pressure drop causes an increase in flow velocity and, hence, an acceleration.
- A liquid will boil when the local pressure falls below its vapor pressure.
- A vapor occupies many more times the volume of a liquid.

If a liquid is accelerated in such a manner that the local pressure falls below the liquid vapor pressure, the liquid will transform into the vapor phase, which results in the formation of bubbles. If the local pressure recovers, the vapor bubbles will transform themselves back into a liquid. There is a tremendous volume change during transformation, because collapsing bubbles release a large amount of energy. Because the bubbles are very small, the resulting impact loads on the surrounding metal can be significant. This can result in physical damage to the metal and thus the creation of high noise levels.

Some liquids (such as water) are more difficult to handle from a cavitation point of view. When the vapor pressure of a homogenous fluid such as water is reached, the entire fluid begins to change phase, resulting in the formation of a large number of damage-causing bubbles. For a nonhomogeneous fluid such as a hydrocarbon, only the light ends (such as condensates) with low-specific volume are affected.

Vapor pressures of some liquids commonly transported by pipelines are shown in Fig. 5-28. Figure 5-29 also provides similar temperature curves for lighter hydrocarbons.

In a centrifugal pump, the fluid is accelerated by the impeller. The area of lowest pressure in the pump suction system, as shown in Fig. 5-30, is the eye of the impeller at cross section A-A. If the pressure falls below the vapor pressure of the liquid, vapor bubbles form. As the mixture of liquid and bubbles continue through the pump, the pressure increases and the bubbles return to the liquid state. Damage to the impeller occurs where the bubbles collapse as shown at cross section B-B. This location varies for different impellers and different suction conditions:

As indicated previously, the effects of cavitation include:

- noise and vibration
- pump damage (e.g., pitting of the impeller)
- falloff of pump performance and efficiency

Cavitation in centrifugal pumps can be recognized by a characteristic noise, which sounds just like it is trying to pump gravel. A typical break-off in the performance curve of a pump due to cavitation is shown in Fig. 5-31.

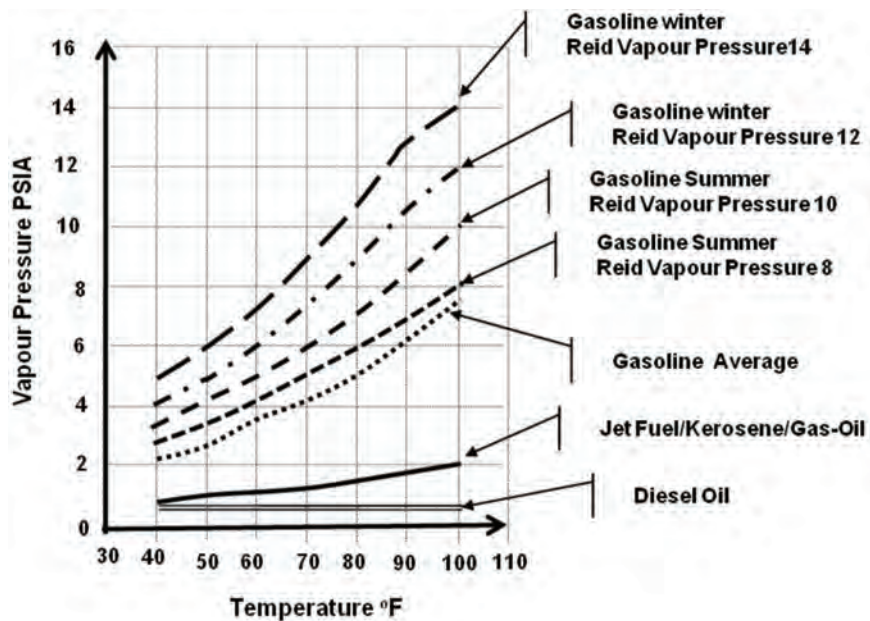


Figure 5-28. Vapor pressure of liquids commonly transported by pipelines [9].

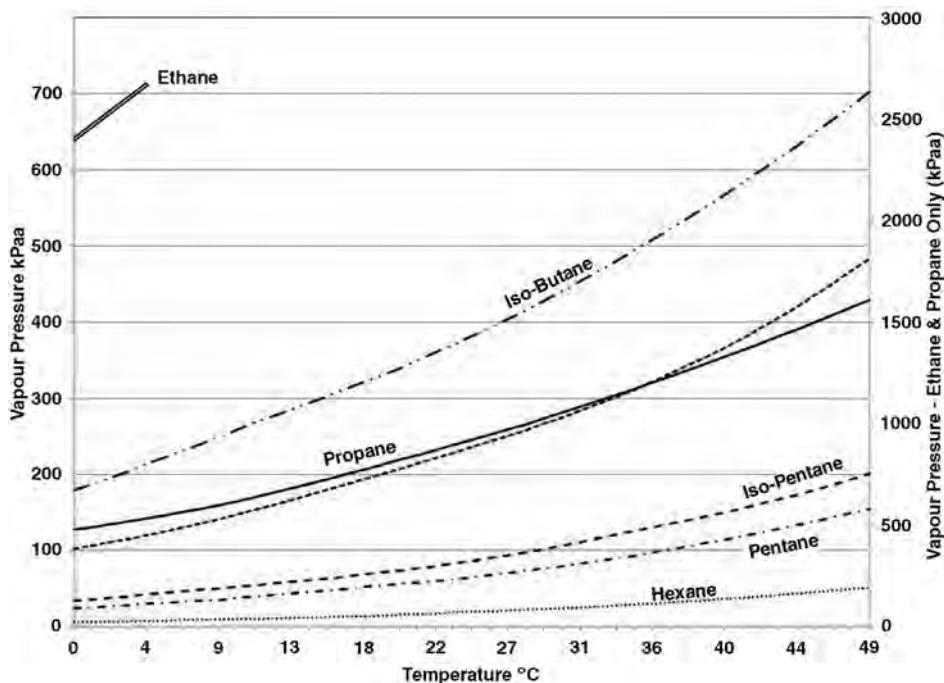


Figure 5-29. Vapor pressure of lighter hydrocarbons.

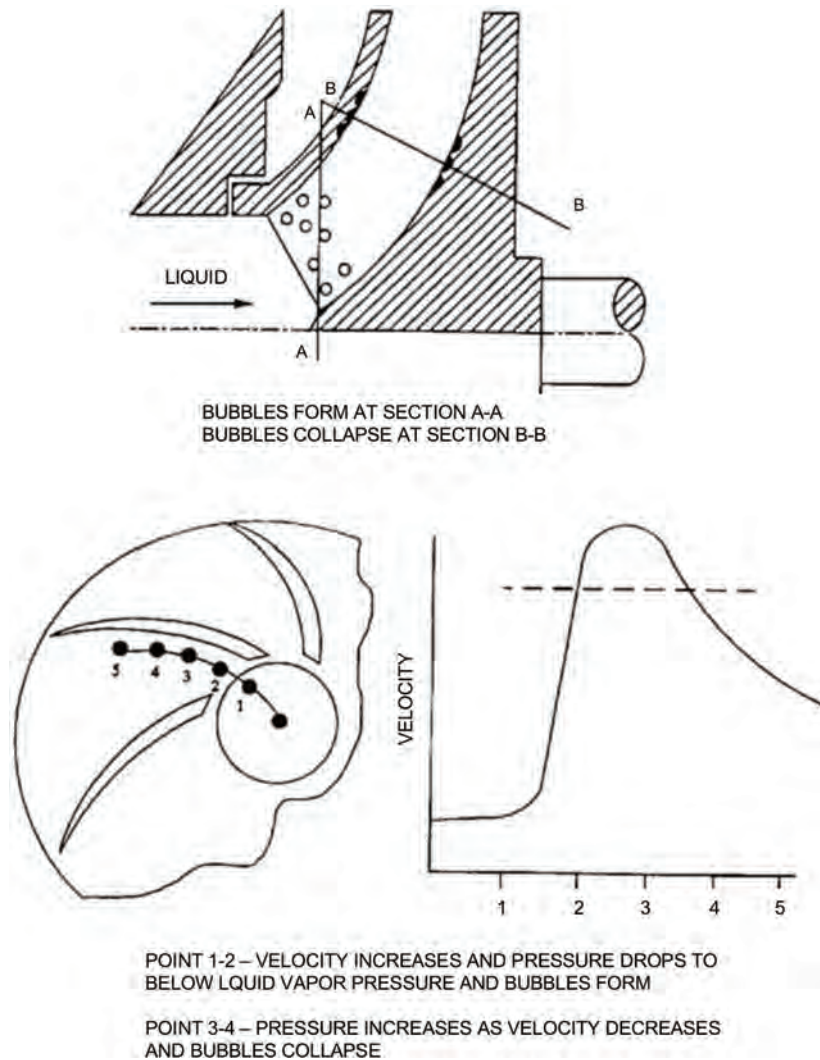


Figure 5-30. Cavitation formation.

5.5.2 Net Positive Suction Head

Net Positive Suction Head (NPSH) is a measure of how close the fluid being handled is to allowing the liquid to flash (or converting some of the liquid to vapor) in the pump suction and thus causing cavitation and/or affecting pump performance.

It is a calculated or measured value, expressing the difference between the vapor pressure of the fluid at pump suction conditions, and the actual pressure. It is expressed in meters or feet (of head of the relevant fluid) so that it can be displayed on the pump performance curve.

NPSH is the total absolute suction pressure at the impeller eye less the absolute vapor pressure of the liquid pumped and losses due to overcoming piping roughness. NPSH must be of a magnitude to avoid vapor formation in the liquid and hence cavitation. Another way to describe NPSH is that it represents the amount of head required to push the fluid into the pump to suppress cavitation.

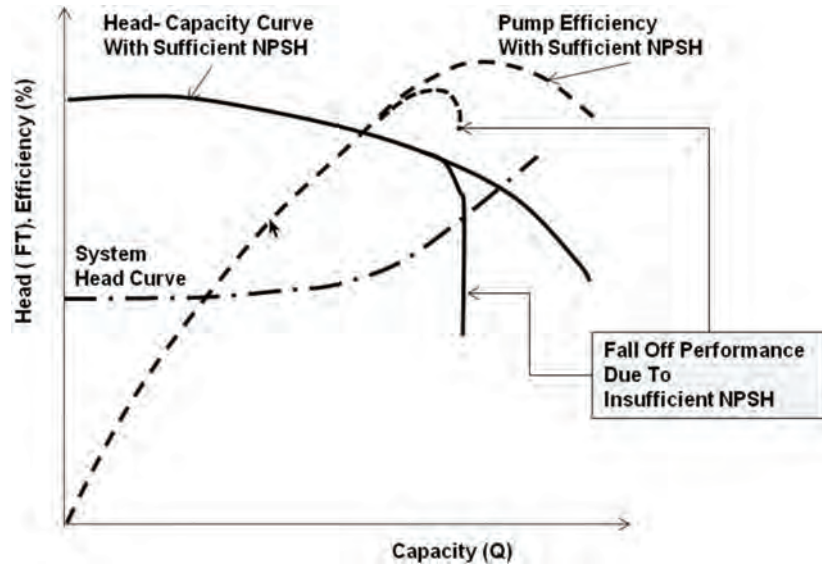


Figure 5-31. Result of cavitation on pump performance.

NPSH is characterized in two ways: Net Positive Suction Head Available (NPSHA) and Net Positive Suction Head Required (NPSHR). NPSHA must always be equal to or exceed NPSHR to prevent cavitation. Process/machine engineers calculate the NPSHA in the fluid system and pump designers determine the NPSHR.

5.5.3 Net Positive Suction Head Available

The determination of NPSHA is dependent on pumping system parameters as shown in Fig. 5-32 and can be calculated by the following expression:

$$\text{NPSHA} = h_a - h_{vp} + h_{st} - h_{fs} \quad (5-27)$$

where

P_a = absolute pressure at the surface of the liquid supply level (for suction from an open tank, this is the barometric pressure)

P_{vp} = vapor pressure of the liquid at the temperature it is being pumped

$h_a = P_a$ expressed in equivalent head

$h_{vp} = P_{vp}$ expressed in equivalent head

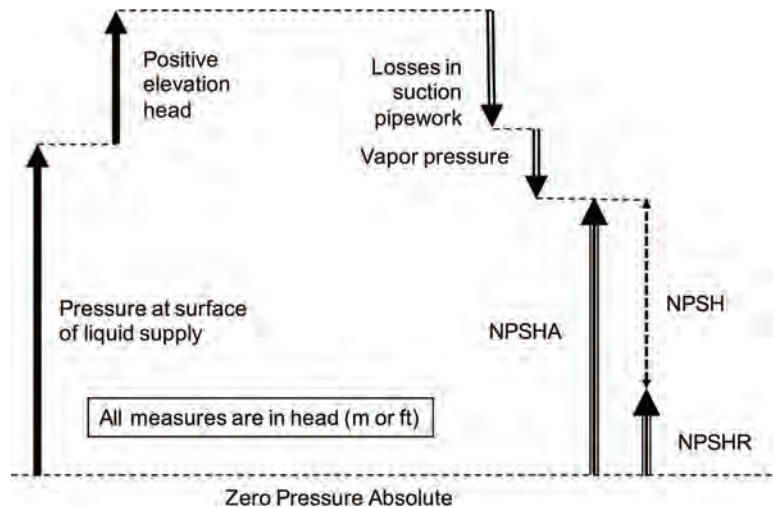
h_{st} = static elevation of the liquid supply above or below the pump inlet center line. This value is negative for suction lift.

h_{fs} = suction line losses, including entrance losses and friction of the piping

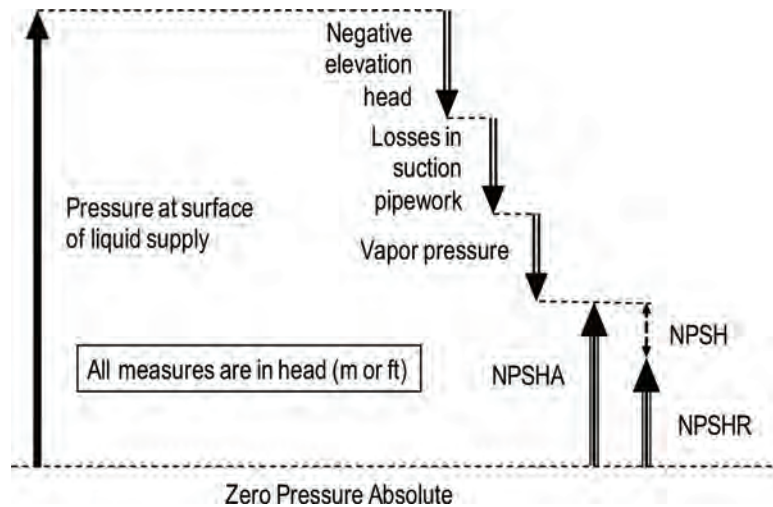
The NPSHA must always be equal to or exceed the NPSHR to prevent cavitation. Process/machine engineers calculate the NPSHA in the fluid system.

5.5.4 Net Positive Suction Head Required

All pumps accelerate fluid and possess a corresponding internal friction loss. Therefore, every pump requires a certain amount of positive suction pressure in order to avoid



(a) NPSHA with a positive elevation head



(b) NPSHA with a negative elevation head

Figure 5-32. Calculation of NPSHA.

cavitation. The pump NPSHR is determined by actual tests conducted by the pump manufacturer with procedures established by the Hydraulic Institute [10]. It must be understood that the NPSHR quoted by the pump manufacturer corresponds to the point at which the pump is fully cavitating. Therefore, it is important to allow a margin between NPSHA and NPSHR. At least 3 ft (1 m) of margin is generally considered to be adequate in the industry.

Manufacturers carry out tests on pumps to establish the required value (NPSHR). They perform a series of "breakdown" tests to determine the NPSHR. The pump is operated at a constant flow rate while the NPSHA is steadily decreased. A sudden drop in the total output head is evidence of cavitation. Industry standards establish that a 3% drop in total head as the point where the NPSHR reading is taken (Fig. 5-33).

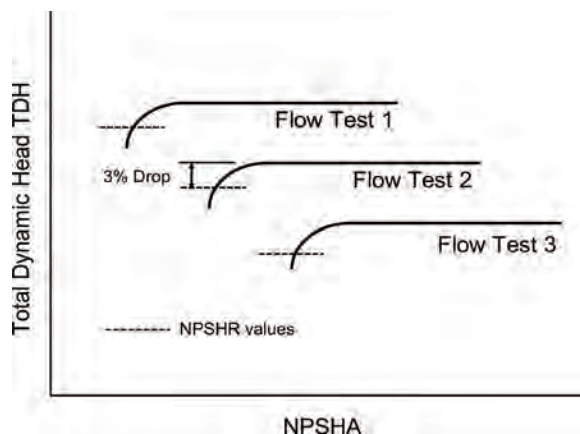


Figure 5-33. NPSH breakdown curves.

5.6 CENTRIFUGAL PUMPS AND VISCOUS LIQUIDS

The performance of centrifugal pumps is affected by fluids with higher viscosities, such as non-Newtonian fluids. A significant increase in brake power, a reduction in head and efficiency, and some reduction in capacity result when handling moderate and high viscosities. This is due to higher frictional losses particularly with low-flow (small passage), high-head (large diameter impeller) pumps (Fig. 5-34 [11]). The greatest impact that viscosity has on a centrifugal pump is increased power draw.

The increased power requirement is due to the increased frictional forces required to turn the impeller within the viscous fluid. Head and flow are also affected by the friction losses of fluid flow through the impeller and volute passages. The amount of viscosity

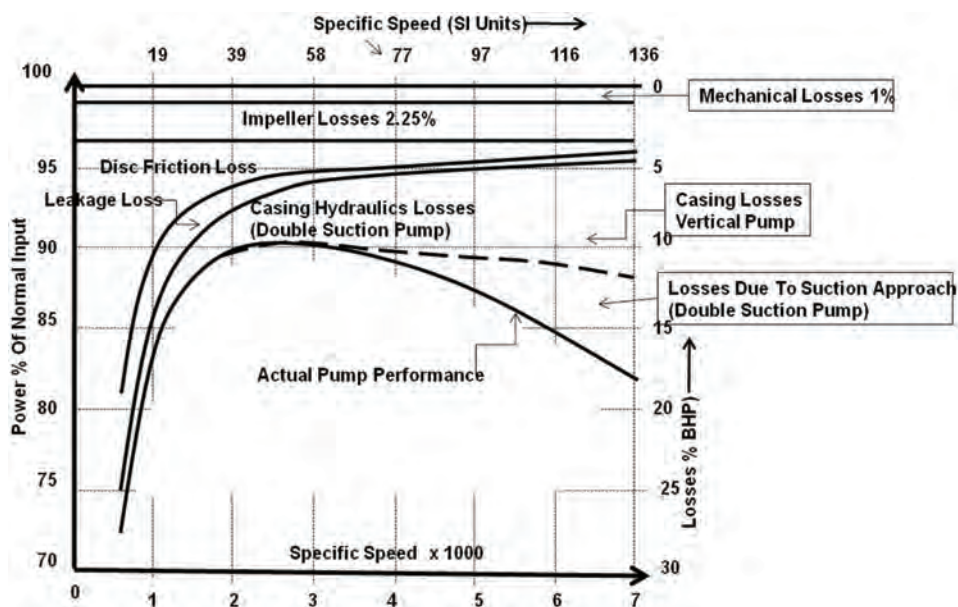


Figure 5-34. Centrifugal pump loss attributions (after ref. [13]).

that can be practically accommodated by a centrifugal pump is related to pump size and specific speed (Fig. 5-35). There is no specific limitation. Increased viscosity will result in decreased performance and increased power consumption. For any given style and size of pump, use of a centrifugal pump will, at some point, become limited for high-viscosity liquid applications.

A performance correction factor, as depicted in Fig. 5-36, can be utilized to determine the actual performance of a pump handling viscous flow [12]. For this purpose, the following are applicable for calculating the actual pump performance, i.e., the brake power when the water performance of the pump is known:

$$\text{bhp}_{\text{vis}} = \frac{Q_{\text{vis}}}{3960} \frac{H_{\text{vis}}}{N_{\text{vis}}} S \quad (5-28)$$

or

$$\text{bkW}_{\text{vis}} = \frac{\text{m}^3/\text{hr} \times \text{meters} \times \text{specific gravity}}{376.5 \times \text{efficiency}} \quad (5-29)$$

where:

$$\begin{aligned} Q_{\text{vis}} &= C_q + Q_w \\ H_{\text{vis}} &= C_h + H_w \\ N_{\text{vis}} &= C_n + N_w \end{aligned}$$

Q_{vis} = viscous capacity in gpm (m^3/hr)

H_{vis} = viscous head in ft (m)

N_{vis} = pump efficiency (%) for pumping viscous liquid

bhp_{vis} = pump bhp (HP or kilowatts) required by the pump for the viscous conditions

Q_w = pump capacity for pump water, gpm (m^3/hr)

H_w = pump water head in feet (meters)

N_w = pump water efficiency in percent

S = specific gravity of liquid pumped

C_q = pump capacity correction factor

C_h = pump head correction factor

C_n = pump efficiency correction factor

Q_{nw} = pump water capacity at which maximum efficiency is obtained

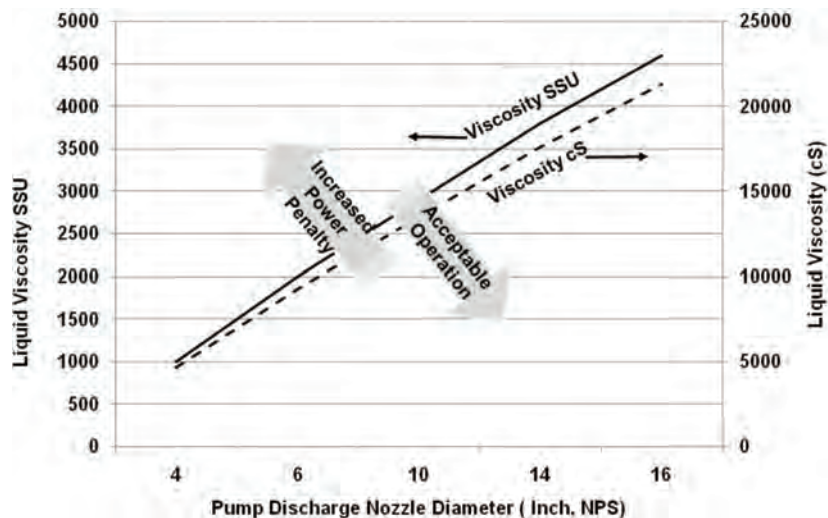


Figure 5-35. Limitation of centrifugal pumps for viscous liquid applications [12].

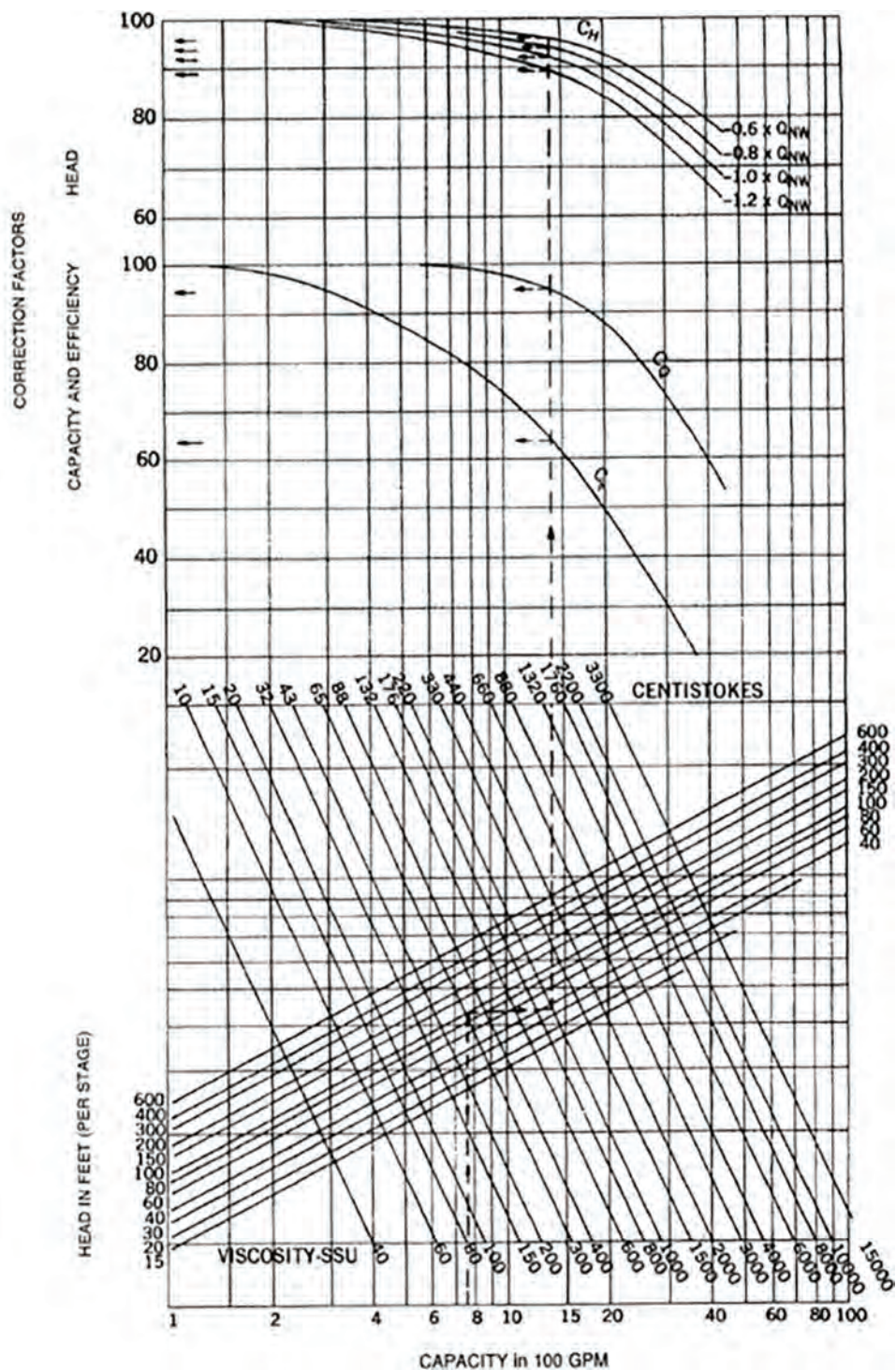


Figure 5-36. Performance correction chart for viscous liquids [12].

C_q , C_h , and C_n are determined from Fig. 5-36, which is based on water performance. On the chart, they are shown as C_q , C_h , and C_n .

The following equations are used for approximating the water performance when the desired viscous capacity and head are given and the values of C_q and C_h must be estimated from the chart using Q_{vis} and H_{vis} as:

$$Q_w(\text{approx}) = \frac{Q_{vis}}{C_q} \quad (5-30)$$

$$H_w(\text{approx}) = \frac{H_{vis}}{C_h} \quad (5-31)$$

Exercise [3]

Calculate the pump power required to pump 114 m³/hr of (660 cS) (3000 SSU) liquid against a head of 46 m (150 ft).

By referring to Fig. 5-36, $C_q = 0.80$ and $C_h = 0.81$.

Therefore:

$$Q_w = 114/0.80 = 142 \text{ m}^3/\text{hr}$$

$$Q_h = 46/0.81 = 57 \text{ m}$$

From Fig. 5-36 for flow rate (Q_w) of 142 m³/h, and water head (H_w) 57 meters, at viscosity of 660 cS, the graph shows $C_q = 0.83$.

Adjusting the water capacity: $Q_w(0.80/0.83) = 137 \text{ m}^3/\text{hr}$.

Adjusting the water head: $H_w(0.81/0.84) = 55 \text{ m}$,

Using Eq. (5-29)

$$\text{bkW}_{vis} = \frac{114}{376.5} \frac{46}{0.315} \frac{0.90}{0.315} = 40 \text{ kW}$$

Figure 5-36 is applicable only for conventional centrifugal pumps operating close to their best efficiency point (BEP), having sufficient NPSHA and transferring Newtonian fluids (such as crude oil). For description on non-Newtonian fluid, refer to Chapter 2.

5.7 CENTRIFUGAL PUMP LIMITS

5.7.1 Minimum Flow

Minimum flow limits for a pump are established to limit or accommodate the following:

- temperature rise
- radial thrust
- internal recirculation
- reduced bhp for pumps with high-specific speed and overloading curves

Operating a centrifugal pump more than 20% lower than the Best Efficiency Point will result progressively in increased maintenance due to bearing and seal wear, impeller erosion, cavitation and damage to the impeller wear ring and labyrinth seals.

5.7.2 Temperature Rise

The difference between bhp and hydraulic hp is the power loss within the pump. Most of the power loss is transferred to heating the liquid that is passing through the pump. The heat loss through the casing and other pump components is small. It is important that

such a temperature rise does not cause vapor formation, which would create abnormal operation.

The following equations can be utilized to determine the temperature rise across a pump impeller:

$$\text{Power loss} = \text{BHP} - \text{hyd hp} \quad (5-32)$$

$$T_{\text{Rise}} \text{ (}^{\circ}\text{F)} = \frac{(\text{bhp} - \text{hyd hp}) \times 2454 \frac{\text{Btu}}{\text{hr} \times \text{hp}}}{(Q) \text{lb/hr} \times C_p} \quad (5-33)$$

where

C_p = specific heat at constant pressure, Btu/lb $^{\circ}\text{F}$

Q = main flow rate, lb/hr

5.7.3 Re-Circulation in Centrifugal Pumps

A centrifugal pump is designed to operate at only one point and operation at any other point causes internal flow patterns to be modified, causing more internal friction with the characteristic reduction in efficiency. Should the flow be reduced dramatically, re-circulation at the impeller eye or the discharge tips will occur as shown in Figs. 5-37 and 5-38.

Excessive recirculation can cause vortices to form. Recirculation, coupled with pre-rotation, can upset the inlet flows so that separation can occur at the back of the impeller vanes. These phenomena can generate localized low-pressure areas that can cause cavitation,

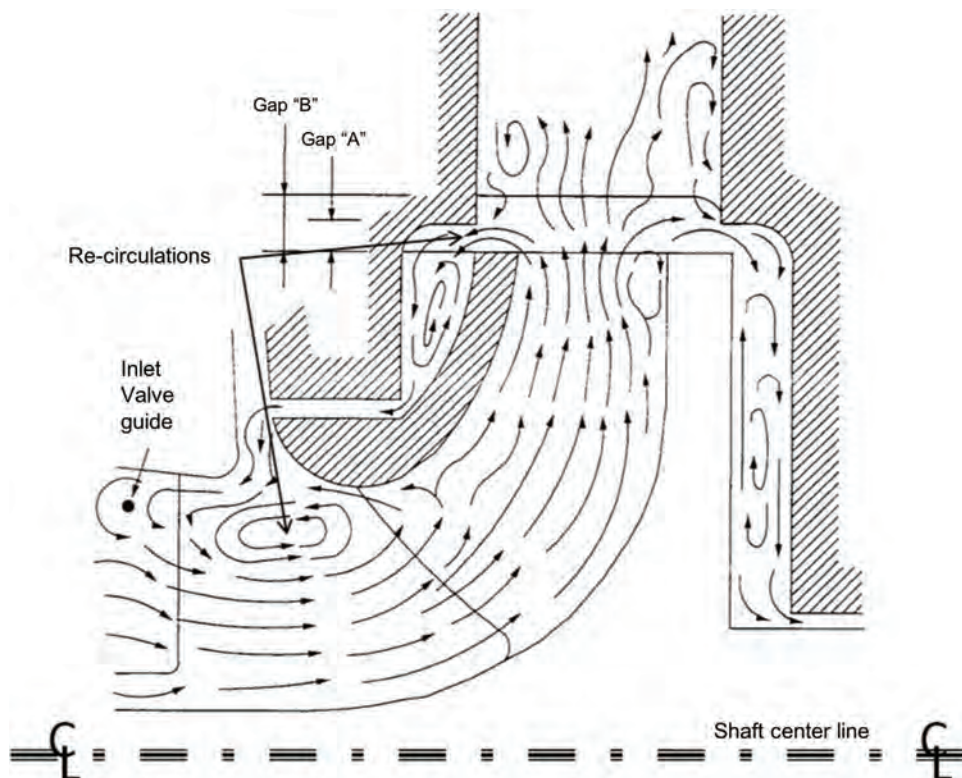


Figure 5-37. Off-design flow with re-circulation and secondary flow.

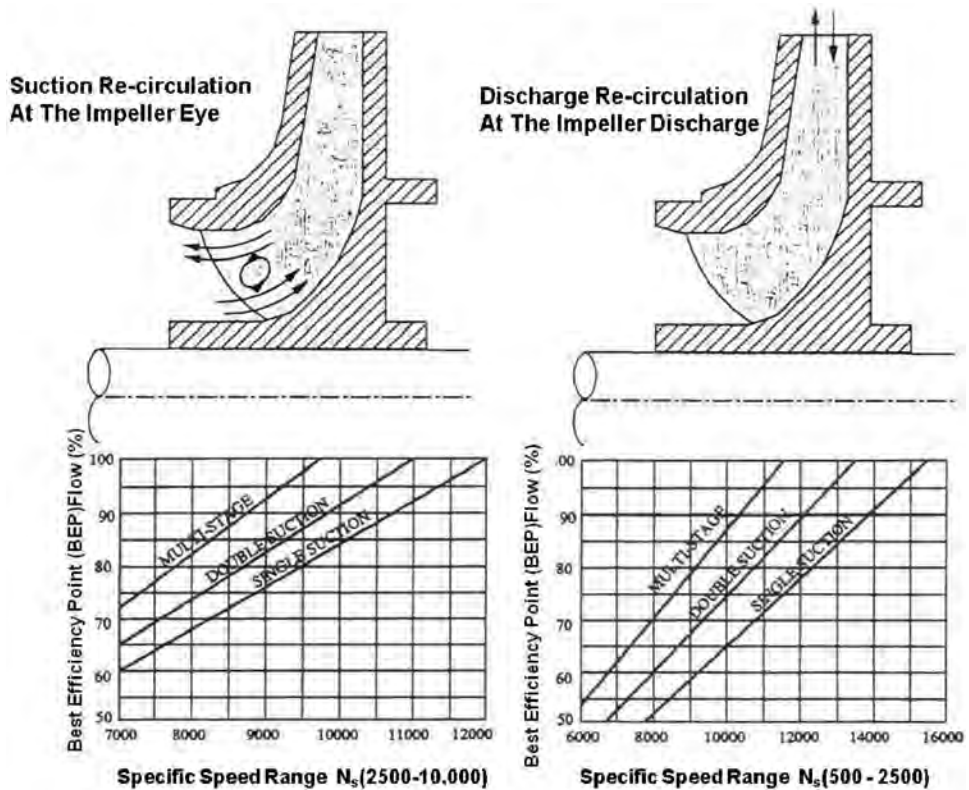


Figure 5-38. Re-circulation effects in pump suction and discharge (suction specific speed N measured at BEP flow, single suction or one side of double suction).

independent of available NPSH. In fact, an experienced trouble shooter can differentiate classic cavitation from recirculation cavitation by an analysis of where the cavitation damage takes place in an impeller. Classic cavitation from a lack of NPSH occurs on the front of the vane, downstream of the vane tips. Recirculation cavitation manifests itself at the vane roots, back of the impeller vane, or on the discharge tip or shroud.

Suction recirculation can cause cavitation damage to the impeller, random crackling noise in the suction, and surging of the suction. Discharge recirculation can cause cavitation damage to the impeller, cracking of impeller shrouds, shaft failures, axial movement of the shaft, and bearing damage [14,15].

Suction Specific Speed. Suction specific speed (N_{ss}) is a design index similar to specific speed used to describe the suction capabilities and characteristics of an impeller. It is expressed as:

$$N_{ss} = \frac{N\sqrt{Q}}{(\text{NPSHR})^{3/4}} \quad (5-34)$$

where:

- N_{ss} = suction specific speed (dimensionless)
- N = pump speed in RPM
- Q = capacity in USGPM
- NPSHR = net positive suction head required in ft

For double-suction impellers, the total flow should be divided by two to calculate the suction-specific speed.

It may be noted that specific speed and suction-specific speed are not related. For a given specific speed impeller, the suction-specific speed can vary widely. Increasing impeller eye area, decreasing inlet vane angles and reducing the number of vanes results in increase in suction specific speed. The higher the suction specific speed, the lower the NPSHR. However, this is not often desirable because the larger inlet area reduces the control of the inlet flow patterns and makes the impeller more prone to recirculation. This, in turn, will reduce the operating range of the pump.

While a range of between 6000 and 16,000 for suction speed can be expected for centrifugal pumps. It is the industry's practice to limit suction specific speeds in the range between 12,000 and 16,000 to avoid operating problems. Recirculation problems can cause the minimum flow to vary from 20% of BEP flow on small pumps with low suction-specific speeds up to 50% or even 60% of BEP flow on large pumps with high suction-specific speeds.

5.8 PUMP SURGE IN SYSTEM OPERATION

A pump system should not have surges, i.e., undesirable swings in head, capacity, and power. However, surge and transient operations can occur in a pumping system when three conditions are present.

1. The mass of liquid is free to oscillate.
2. Some part of the system is able to store and give back pressure energy.
3. Some part of the system provides impulses to start pressure/flow swing.

Oscillations can exist when the mass of liquid is suspended between two free surfaces, e.g., when the suction is taken from a vessel containing a free surface, and the discharge is sent to another such vessel.

If liquid is below its vapor pressure, there will be a likelihood of vapor formation and, hence, storing and giving back pressure energy.

The impulse can come from start up, shutdown, or discharge throttling.

The above can be illustrated by considering pumps in parallel operation (Fig. 5-39) [16]. Assuming that the pumps are identical, each having a drooping head-vs.-capacity curve, their combined curve (adding their capacities) is shown in Fig. 5-39.

In such pump operation, three problems can occur:

- a. If one pump is operating at a head (say, D) greater than the head at shutoff (A), then the other pump cannot be put on line, as its head at zero capacity will not be enough to open the check valve against backpressure.
- b. Now, should both pumps operate at point C, and flow demand is reduced by partly closing the throttle valve to point E, in this case, one pump or both may operate at E, but one or both may also operate at F, where the head is the same but the flow is lower. Under this situation, pumps will not be sharing the load equally, and flow and pressure may start fluctuating.
- c. Subsequently, should the throttle valve be opened, in response to a demand for greater flow, then a pump at point E will increase its flow, but one at point F will reduce its flow and may cease delivering entirely.

This can in return cause pressure fluctuations and the impulse necessary to start a surging situation. If surging begins, it will stop only if the pump or pumps at F are shut down. Surging in such a system can be prevented by taking the following actions:

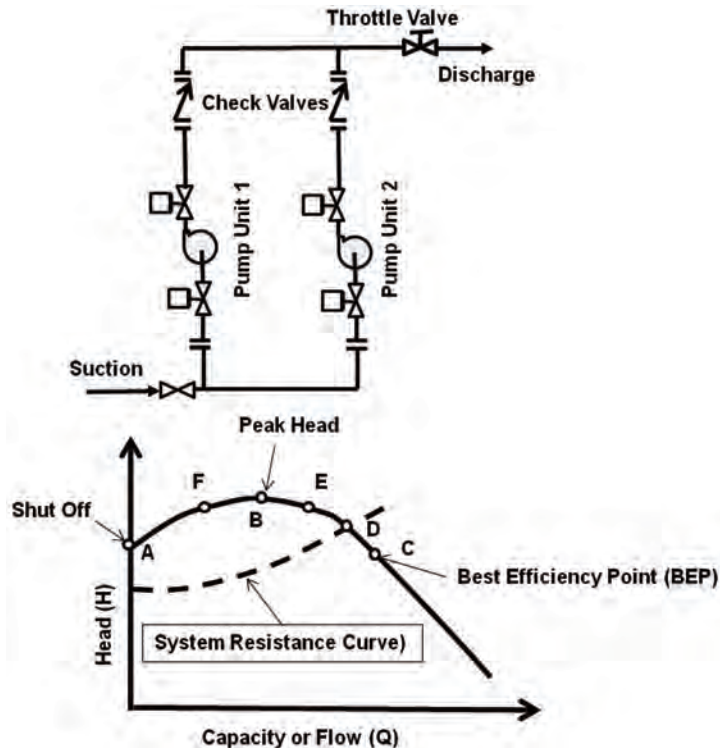


Figure 5-39. Operating two or more drooping pumps in parallel.

1. Installing in the discharge line a bypass that will pass all flow to the left of (i.e., less than) that at point B, as in Fig. 5-40. Such a bypass will allow the system to operate only to the right of point B (i.e., at greater flow and lower head), and so it will not start surging if head increases and flow decreases. The bypass will also protect the pump from overheating at low flow rates, when there might otherwise not be enough liquid to carry the heat away.
2. Installing a throttle valve or orifice on each of the pump discharge lines, either in place of or in addition to the single valve on the combined discharge. This changes the effective pumping curve to a constantly rising one, as shown in Fig. 5-40. However, this will take more power, due to the pressure drop added by the valves or orifices.

It is not advisable to operate drooping-curve pumps in parallel to the left of the peak head.

5.9 PERFORMANCE OF POSITIVE DISPLACEMENT PUMPS

5.9.1 Rotary Pump Performance Chart

Performance of a rotary pump depends on the type, design, applications, and the manufacturer. The performance charts for a rotary pump are generally presented differently for different pump manufacturers. A typical range for rotary pumps (three screw type) and associated performance charts is shown in Figs. 5-41 and 5-42.

Typical values plotted can include capacity, pressure, power, and efficiency. If the efficiency is not shown, it can be calculated knowing that mechanical efficiency is equal to the power input (hydraulic power) divided by the power output.

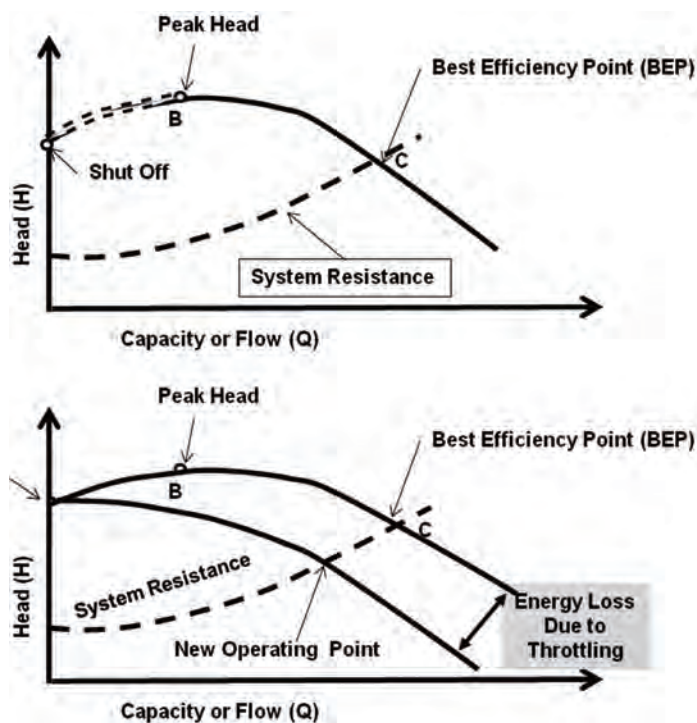


Figure 5-40. Controlling surge in parallel pump system [16].

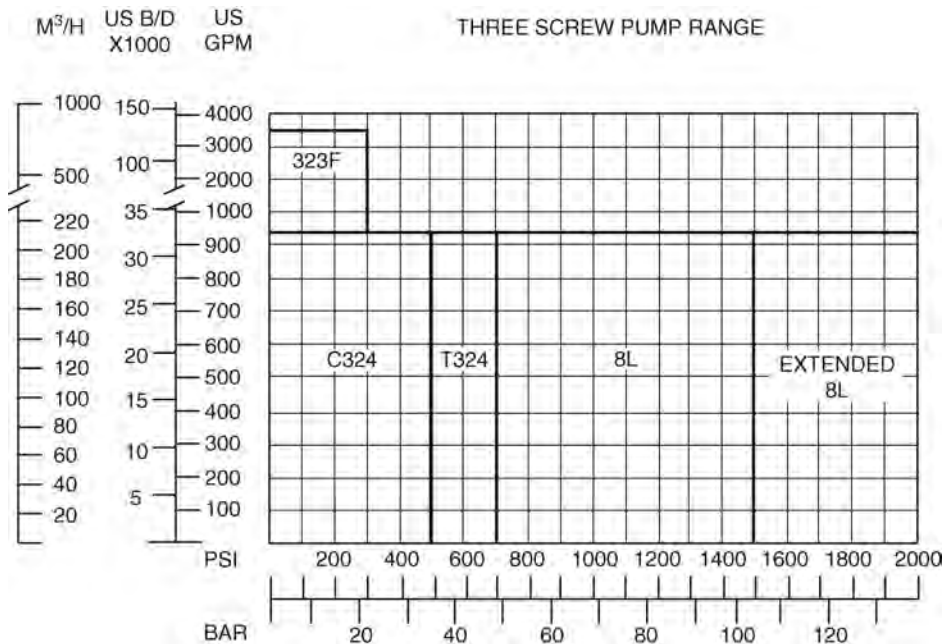


Figure 5-41. Range of a rotary screw pumps for pipeline application (IMO 3-screw pump line, courtesy of Colfax Corporation).

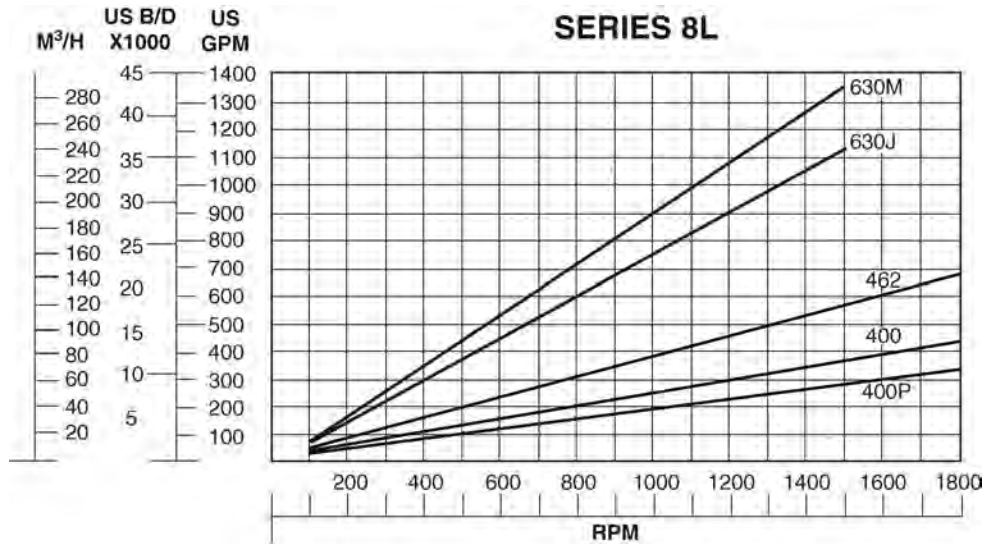


Figure 5-42. Performance characteristics for a typical screw type rotary pump for oil pipeline application (IMO 3-screw pump line, courtesy of Colfax Corporation).

5.9.2 Pump Power and Efficiency

Brake power (bhp or kW) is the actual power delivered to the pump shaft.

$$\text{bhp} = \frac{Q}{1714} \frac{P}{\text{pump efficiency}} \times 100 \quad (5-35)$$

$$\text{kW} = \frac{Q \times \Delta P \times 100}{\text{pump efficiency}} \quad (5-36)$$

where:

Q = capacity in USGPM, m³/h

P = differential pressure (discharge pressure minus suction pressure) in PSI, bar

Pump efficiency = pump efficiency in percent

Hydraulic power (hyd hp or hyd kW) is the liquid power developed by the pump.

$$\text{hyd hp} = \frac{Q}{1714} P \quad (5-37)$$

$$\text{hyd kW} = Q \times \Delta P \quad (5-38)$$

The pump efficiency is the ratio of power output and power input.

$$\text{Pump efficiency} = \frac{\text{hyd hp}}{\text{bhp}} \times 100 \quad (5-39)$$

The volumetric efficiency is the ratio of the pump capacity to displacement. It is expressed as:

$$\text{Volumetric efficiency} = Q/D \quad (5-40)$$

where:

Q = capacity

D = displacement (volume swept by the pumping element per unit time)

5.9.3 Rotary Pump Slip and Clearance

Slip is the rate of fluid that leaks through the internal clearances of a rotary pump. Slip is dependent on the internal clearances, differential pressure, characteristics of the fluid handled, and in some cases, the speed. Most rotary pumps have close clearances between moving parts and stationary parts to reduce slip.

Increased clearances in the pump result in increased slip. The mechanical efficiency and volumetric efficiency (capacity) is reduced, and NPIPR is increased.

5.9.4 System Head Curves and Rotary Pump Curve

The capacity of a rotary pump is relatively unaffected by a change in discharge pressure/head as illustrated in Fig. 5-43. An increase in the system head results in an increase in the pump discharge pressure and power required.

Most pipeline pumps are centrifugal units. When the product being transported is always a low-viscosity liquid like water, condensate gasoline, diesel, or light crude oil, centrifugal pumps are reliable and efficient and economically cost-effective.

However, as the liquid viscosity increases, the frictional losses within a centrifugal pump reduce pumping efficiency dramatically. For this reason, rotary, positive displacement pumps are often used when products such as heavy crude oil, fuels oil (no. 6 fuel oil), low-sulfur fuels, bitumen, and similar need to be transported.

Figure 5-44 compares the mechanical efficiency of an internal gear rotary pump to the efficiency of a typical centrifugal pump [17].

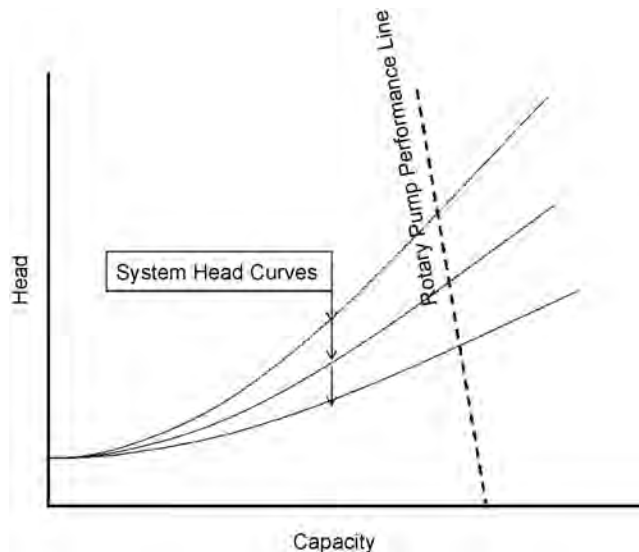


Figure 5-43. Liquid viscosity effect on rotary pump performance.

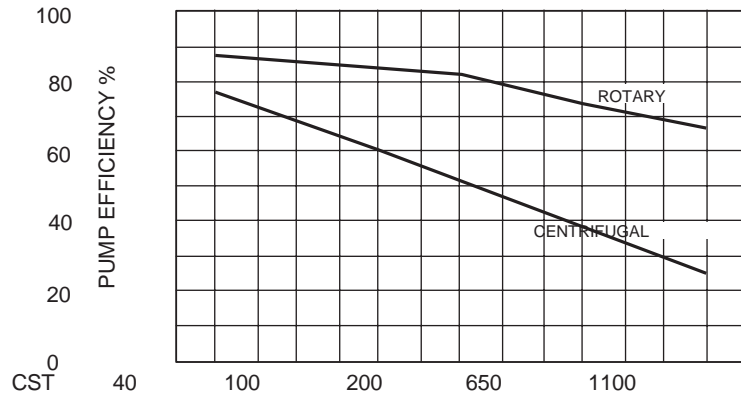


Figure 5-44. Rotary versus centrifugal efficiency.

As indicated the mechanical efficiency varies with viscosity for the rotary pump. To the left of best efficiency, internal slip at lower viscosities results in reduced efficiency. To the right of best efficiency, the drag of the liquid on the rotor and seals causes an increased power requirement resulting in reduced efficiency. At higher viscosities, rotary pumps are significantly more efficient than centrifugal pumps.

5.9.5 Reciprocating Pump Flow Characteristics

The reciprocating action of the liquid end results in varying flow at the pump inlet and discharge. The velocity of the liquid in the piping is proportional to the plunger velocity. The average liquid velocity for various reciprocating pumps at different crankshaft angles is shown in Fig. 5-45. This reciprocating arrangement causes discharge pressure pulsations that can be significant. The higher the number of plungers, the smoother the discharge flow.

Typical velocity variations of power pumps can be as follows:

Pump Type	No. of Single-Acting Pumping Elements	Variation in Velocity (%)
Duplex	2	160
Triplex	3	25
Quintuplex	5	7
Septuplex	7	4

5.9.6 Reciprocating Pump Acceleration Head

During each revolution of the pump crankshaft, the flow in the suction and discharge piping accelerates and decelerates a number of times. The head required to accelerate the fluid column is a function of the length of the suction line, average velocity in this line, speed of rotation, type of pump, and the relative elasticity of the fluid and the pipe. The acceleration head is calculated as follows:

$$h_{ac} = \frac{LVnC}{Kg} \quad (5-41)$$

where:

h_{ac} = acceleration head in feet, m

L = length of suction line in feet, m

V = velocity in suction line in ft/s, m/s

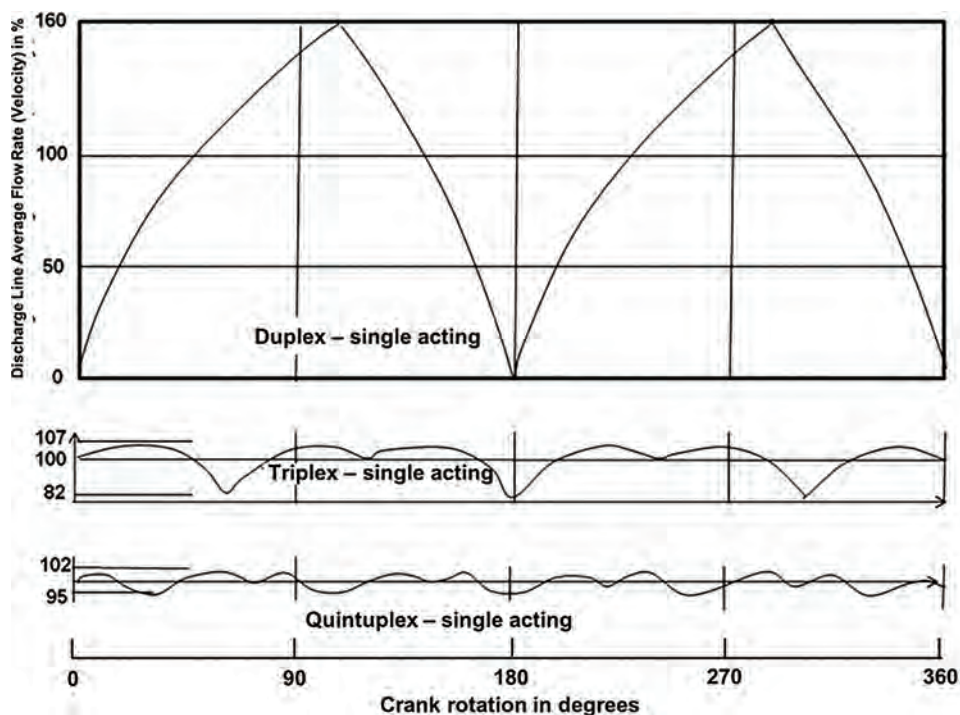


Figure 5-45. Reciprocating pump typical flow curves for various pump types (connecting rod length = 5 x crank throw).

n = Pump speed in rpm

C = 0.200 for simplex double-acting

= 0.200 for duplex single-acting

= 0.115 for duplex double-acting

= 0.066 for triplex single or double-acting

= 0.040 for quintuplex single or double-acting

= 0.028 for septuplex, single or double-acting

= 0.022 for nonuplex, single or double-acting

K = a factor representing the relative compressibility of the liquid ($K = 1.4$ for hot water, $K = 2.5$ for hot oil)

g = gravitational constant (32.2 ft/s², 9.82 m/s²)

Note: The constant C will vary from these values for unusual ratios of connecting rod length to crank radius.

The acceleration head equation is recommended for use in short lines (less than 15 m, 50 ft) and nonelastic suction lines. The velocity of pressure waves in the liquid and the system elasticity is not accounted for in the calculation.

The acceleration head should be minimized to allow for maximum net positive suction head available (NPSHA).

5.9.7 Net Positive Pressures

Net Positive Inlet Pressure. Net positive inlet pressure (NPIP) is the total absolute suction pressure available at the pump suction less the absolute vapor pressure of the liquid pumped expressed in pressure units.

Net Positive Inlet Pressure Available (NPIPA) is determined in the same way as NPSHA is for a centrifugal pump except that the head must be converted to pressure units. NPIPA is calculated by the following expression:

$$\text{NPIPA} = P_{\text{ab}} - P_{\text{vp}} + P_{\text{st}} - P_{\text{fs}} - P_{\text{ac}} \quad (5-42)$$

where:

- P_{ab} = absolute pressure on the surface of the liquid supply level; for suction from an open tank, this is the barometric pressure
- P_{vp} = vapor pressure of the liquid at the temperature being pumped
- P_{st} = static elevation converted to pressure that the liquid supply level is above or below the pump inlet center line; this value is negative for suction lift
- P_{fs} = suction line losses, converted to pressure, including entrance losses, and friction of the piping
- P_{ac} = acceleration head, converted to pressure for the suction line

Net Positive Inlet Pressure Required (NPIPR) is the net positive suction pressure required for a reciprocating pump to push the suction valve from the seat and to overcome the friction losses and acceleration head within the liquid end of the pump. The NPIPR expressed in pressure units is the same for fluids with different specific gravities and is determined by tests conducted by the manufacturer.

Correcting for Inadequate Suction Conditions can be done by increasing NPIPA or reducing NPIPR. Increased NPIPA can be achieved by:

- raising the liquid level, e.g., by increasing the tank elevation or increasing the liquid level
- reducing frictional losses in suction piping, e.g., increasing the suction pipe diameter or reducing the piping length
- using a booster pump (caution: the power pump should be installed with a pulsation dampener to protect the booster pump from pulsating flow)
- reducing the vapor pressure of the liquid, e.g., subcooling the liquid

NPIPR can be reduced by:

- operating at slower speeds, e.g., reducing the speed of the pump or selecting a larger pump to run at slower speeds (may be able to use lighter suction valves)
- installing a suction dampener on the suction line to the pump, e.g., reducing acceleration head

5.9.8 Reciprocating Pump Selection

5.9.8.1 Pump Selection Charts

Pump selection charts are used to provide performance information for reciprocating pumps (Fig. 5-46). Different charts are used by different pump manufacturers. Straight lines appear on the charts because displacement is directly proportional to speed.

The following guidelines are provided to aid in the selection of reciprocating pumps:

- The larger the physical size of the unit (i.e., the bore, the stroke, and number of cylinders), the higher the flow capacity.
- The higher the pump speed for a given pump, the higher the flow.
- The higher the speed, the higher the wear and maintenance. Use API-recommended speeds when selecting reciprocating pumps. The maximum values should never be exceeded.

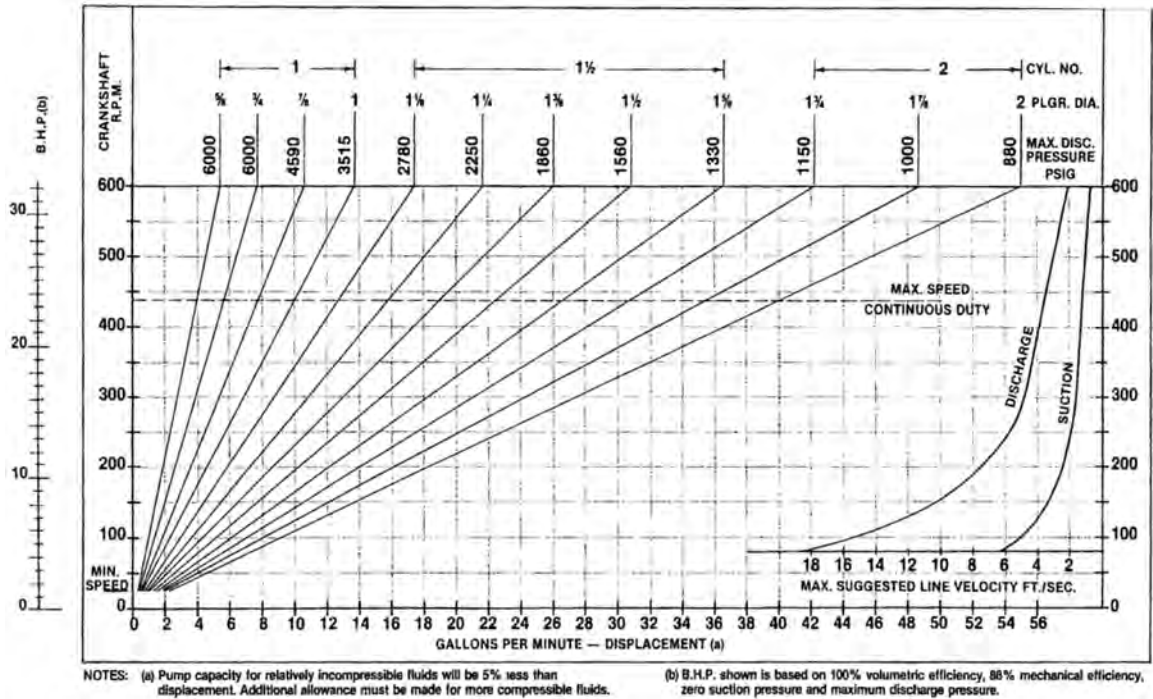


Figure 5-46. Typical reciprocating pump selection chart.

- The higher the speed, the higher the net positive suction head required (NPSHR) for equal valve configurations.
- As the plunger diameter is increased, the flow increases. Most pumps are offered with two or three sizes of fluid cylinder, each with several plunger diameters. The flow can be fine-tuned using this method.
- As the plunger diameter increases, the maximum allowable discharge pressure decreases. This limit is a result of the power end design restrictions, usually referred to as maximum allowable frame load.

Speed reduction is always required with reciprocating pumps. Pipeline industry generally considers motor speeds between 1800 and 1200 rpm. Any lower speeds require a special and therefore more expensive electric motor.

5.9.8.2 Theoretical Pump Volume Calculation

API 674 Metering Pump Equation $V = A \times h \times n$ can be used for calculation of volumetric flow (V) from the pump [18] (Fig. 5-47).

A = plunger square area

h = stroke length

n = stroking speed (stroke frequency, RPM)

5.9.8.3 Pump Power Calculations

The bhp is the actual power delivered to the pump shaft. It is expressed as:

$$\text{bhp} = \frac{(Q \times P_d) 100}{1714 \times \text{mechanical efficiency}} - \frac{Q \times P_s (\text{mechanical efficiency} - 5)}{(1714)(100)} \quad (5-43)$$

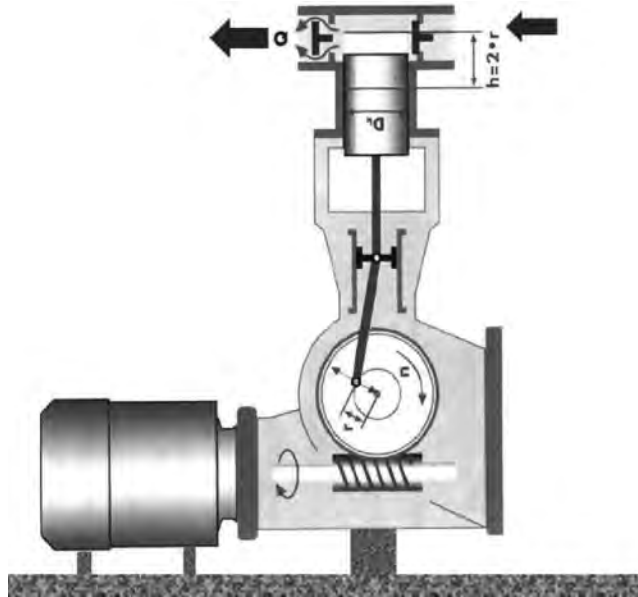


Figure 5-47. Nomenclature for reciprocating pump volume calculation [18].

The above equation is based on suction efficiency to be 95% of that of discharge efficiency. For equal suction and discharge efficiencies, shaft power can be expressed as:

$$hp = \frac{(Q \times \Delta P)}{1714} + \frac{(Q \times P_d)}{1714} \left[\left(\frac{1}{\text{Eff}} \right) - 1 \right] \left[\frac{1 + P_s}{P_d} \right] \quad (5-44)$$

$$kW = (Q \times \Delta P) + (Q \times P_d) \left[\left(\frac{1}{\text{Eff}} \right) - 1 \right] \left[\frac{1 + P_s}{P_d} \right] \quad (5-45)$$

It may be noted that for single-acting reciprocating pumps, the imposed loads in the power end are nearly equal to the sum of the discharge pressure and suction pressure. The power end is subjected to the full discharge pressure load from the plunger and the return plunger load. The return plunger load is nearly equal to that of the plunger discharging at suction pressure. The bearing loads and packing friction is increased causing the friction power to increase. The power input can be predicted by calculating the power that the pump would require at the rated discharge pressure and subtracting the power gained by the pump from the suction pressure. The suction efficiency is usually 3% to 5% lower than the discharge efficiency. Using 5% in Eq. (5-43) is thus conservative.

5.10 MEASUREMENT UNITS AND CONVERSION FACTORS FOR PUMPS

The pipeline and pump industries use both US Customary and SI (Système international (d'unités), also known as the metric system) units of measurement interchangeably. Therefore, although every attempt has been made to utilize SI units, some exceptions are evident through this chapter due to reference to source and availability of information. The use of following factors can assist in the conversion of units as appropriate:

Quantity (1)	US Customary Unit	Unit Symbol	SI Unit	Unit Symbol	US to SI	SI to US
Volume per unit time	Gallon per minute	gpm	Cubic meter per hour	m ³ /h	0.2271	4.403
	barrel per hour	BBLH	liters per second	L/s	0.044163	22.64
	barrel per day	BBLD	cubic meter per hour	m ³ /h	0.158987	6.2898
Velocity, linear	foot per minute	fpm	meter per second	m/s	0.00508 (9)	196.9
Volume	foot per second	fps	meter per second	m/s	0.3048 (9)	3.281
	cubic inch	in ³	milliliter [cm] ³ (2)	ml (3)	16.39	0.06102
	cubic foot	ft ³	cubic meter	m ³	0.02832	3.281
	gallon	gal	cubic meter	m ³	0.003785	264.2
	quart	qt	liter	l	0.9464	1.057
Length	foot (and inch)	ft. or ' , in. or ''	meter	m	0.3048 (9)	3.281
	inch	in. or ''	millimeter	mm	0.0254 (9)	1/0.0254 (9)
	mil		micrometer	μm	25.4 (9)	1/25.4 (9)
	microinch	μin.	micrometer	μm	0.0254 (9)	1/0.0254 (9)
	micron		micrometer	μm	1 (9)	1 (9)
Area	square foot	ft ²	square meter	m ²	0.0929	10.76
	square inch	in ²	square millimeter	mm ²	645.2	0.00155
Acceleration	foot per second-squared	ft/s ²	meter per second squared	m/s ²	0.3048 (9)	3.281
Fluid energy	foot	ft or m	meter	m	0.3048 (9)	3.281
Pressure	pound-force per sq. in. (psi)	lb/in. ²	kilopascal [kN/m ²]	kPa	6.895	0.145
	inch of mercury [60°F]	in. Hg	kilopascal	kPa	3.377	0.2961
	inch of water [60°F]	in. H ₂ O	kilopascal	kPa	0.2488	4.019
	microbar [0.0002 μbar]	μbar	microPascal [20 μPa]	μPa	100,000	0.00001
Specific speed	$N_{ss} = \frac{N\sqrt{Q}}{(NPSHR)^{3/4}}$	$\frac{\text{RPM GPM}^{5/4}}{\text{HEAD}^{7/4}}$		$\frac{r / \text{min} \times \sqrt{m^3 / h}}{m^{3/4}}$	1.162	0.8608
Specific speed				unitless (radians)	0.0003656	2735
Viscosity, dynamic	centipoise	cP	milliPascal-second	mPa•s	1 (9)	1 (9)
Viscosity, kinematic	centistokes (5)	cSt	square-millimeter per second	mm ² S	1 (9)	1 (9)
Viscosity, kinematic	SSU	SSU		cSt	4.4636	0.224
Power (see also heat)	horsepower [550ft•lb _f /s]	hp	kilowatt [kJ/s] (6)	kW	0.7457	1.341
Mass	pound (decimalized; do not use ounces with pounds)	lb or #	kilogram	kg	0.4536	2.205
Density (mass density)	pound per cubic foot	lb/ft ³	kilogram per cubic meter	kg/m ³	16.02	0.06243
Moment of inertia (dynamic)	pound foot-squared	lb•ft ²	kilogram meter-squared	kg•m ²	0.04214	23.73
Energy, work (see also heat)	foot pound-force	ft•lb _f	Joule [N•m] (6)	J	1.356	0.7376
Force	pound-force (decimalized; do not use ounces)	lb _f	Newton	N	4.448	0.2248

Quantity (1)	US Customary Unit	Unit Symbol	SI Unit	Unit Symbol	US to SI	SI to US
Moment of force, torque and bending moment	pound-force foot	lb _f •ft	newton-meter	N•m	1.356	0.7376
	pound-force inch	lb _f •in	newton-meter	N•m	0.113	8.851
Unbalance	ounce-inch	oz•in	gram-millimeter	g•mm	720.1	0.001389
Temperature	degree Fahrenheit	°F	degree Celsius (7)	°C	(tF – 32) 5/9 (9)	(tC 1.8) + 32 (9)
	degree Fahrenheit [t]	°F	Kelvin [t _K = t _C]	K	5/9 (9)	1.8 (9)
	British thermal unit	kilojoule				
Heat (energy)	British thermal unit	Btu (8)	kilowatt	kJ	1.055	0.9478
Heat (energy) rate	British thermal unit	Btu/s	watt	kW	1.055056	0.9478
	British thermal unit per minute	Btu/h	watt [J/s] (6)	W	0.293071	3.4121
Heat flow rate		Btu/min		W	17.58	0.05687

Notes:

1. As used in ISO-31 and ISO-1000, “quantity” means “measurable property”.
2. Symbols in brackets, [], are explanatory only.
3. As per US Department of Commerce, National Bureau of Standards, capital letter “L” is the unit symbol for liter for the U.S.
4. The unit for sound level will continue to be the decibel (db), and will continue to have the same value, 20 μPa = 0.0002 μbar.
5. Conversion from Saybolt Universal Seconds to centistokes can be done from a table.
6. By using J instead of N•m, the distinction from N•m for moment of force is made apparent.
7. Conversion requires a formula, wherein the Fahrenheit temperature is indicated by t_F , and the Celsius temperature by t_C .
8. All factors in this table are based on Btu (International Table).
9. Exact.

5.11 PUMP AND SYSTEM DESIGN STANDARDS

To design and select pumps for pipeline applications, a variety of standards may be referred to. Some of these are:

- Hydraulic Institute Standards
- American Society of Mechanical Engineers/American National Institute (ASME/ANSI) Standards for Pumps:
 - B73.1: Specification for Horizontal End Suction Centrifugal Pumps for Chemical Process
 - B73.2: Specification for Vertical In-Line Centrifugal Pumps for Chemical Process
 - B73.3: Specification for Seal-less Horizontal End Suction Centrifugal Pumps for Chemical Process
 - B73.5M (R2001): Thermoplastic and Thermoset Polymer Material Horizontal End Suction Centrifugal Pumps for Chemical Process
- American Petroleum Institute (API) 610: ISO 13709 Centrifugal Pumps for General Refinery Service
- API 614: General Purpose Lube Oil System components for Rotating Process Equipment
- ANSI/API 674: ISO 13710 Positive Displacement Pumps—Reciprocating
- API 675: Positive Displacement Pumps—Controlled Volume Pumps
- API 676: Positive Displacement Rotary Pumps
- API RP 1110: Pressure Testing of Steel Pipelines for the Transportation of Gas, Petroleum Gas, Hazardous Liquids, Highly Volatile Liquids or Carbon Dioxide. This RP applies to all parts of a pipeline or pipeline facility including line pipe, pump station piping, terminal piping, etc.

- BS 5257: Specification for horizontal end-suction centrifugal pumps (16 bar)
- BS5136: Acceptance Tests for Pumps for Centrifugal Mixed Flow and Axial Pumps
- ISO 13709: Centrifugal pumps for petroleum, petrochemical and natural gas industries, aimed at the medium duty single stage pumps (metric)
- ISO 13710: Petroleum, petrochemical and natural gas industries—reciprocating positive displacement pumps
- ISO/TR 17766: Centrifugal pumps handling viscous liquids—performance corrections
- ISO 21049: Pumps—shaft sealing systems for centrifugal and rotary pumps
- DIN. West German standard, DIN EN ISO 5199: Technical specifications for centrifugal pumps
- VDMA West German standard for pump seals.

REFERENCES

- [1] ASTM, 2005. “D 1298-99 Standard Test Method for Density, Relative Density (Specific Gravity), or API Gravity of Crude Petroleum and Liquid Petroleum Products by Hydrometer Method.”
- [2] Mohitpour, M., Golshan, H., and Murray, M., 2007. “Pipeline Design & Construction—A Practical Approach,” ASME Press, 3rd ed. p. 241.
- [3] McNally, W., 2007. “Viscosity Correction to the Pump Curves,” <http://www.mcnellyinstitute.com>.
- [4] Darby, R., 1996. Chemical Engineering Fluid Mechanics, Marcel Dekker.
- [5] Chaurette, J., 2004. “Centrifugal Pump Specific Speed Primer And the Affinity Laws,” http://www.pumpfundamentals.com/download-free/spec_speed_primer.pdf.
- [6] Lohrberg, H., & Stoffel, B., 2000. “Avoiding cavitation erosion,” Pump Users International Forum, Karlsruhe, Germany, 10–12 October.
- [7] Lohrberg, H., & Stoffel, B., 2000. “Intelligent maintenance management of pumps,” Training Seminar S2, Pump Users International Forum, Karlsruhe, Germany, 10–12 October.
- [8] Stoteman, D. P., Robertson, D. A., and Margolin, L., 2004. “Demonstration of Cavitation Life Extension for Suction Stage Impeller in High Energy Pumps,” Proc. 21st Int. Pump Users Symposium.
- [9] Big Inch Petroleum, 2007. “Hydrocarbon Vapour Pressure,” July, <http://www.eng-tips.com/viewthread.cfm?qid=191613&page=10>.
- [10] ANSI/HI (Hydraulic Institute), 2017. “Standard ANSI/HI 9.6.1—2017 Rotodynamic Pumps—Guideline for NPSH Margin.”
- [11] Andrews, D., 2007. “Viscosity and Pump Performance,” Run Times Vol. 4 Lawrence Pumps Inc. Feb, http://www.lawrencepumps.com/newsletter/news_v04_i2_feb07.html.
- [12] ANSI/HI (Hydraulic Institute), 2013. “Standard ANSI/HI 1.3—2013 Rotodynamic (Centrifugal) Pumps for Design.”
- [13] Lobanoff, V. S., and Ross, R. R., 1992. Centrifugal Pumps Design & Application, Gulf Publishing Company.
- [14] Frazer, W. H., 1981. “Recirculation in Centrifugal Pumps,” Presented at ASME Winter Annual Meeting, Washington, D. C., November 15–20.
- [15] Dyson, G., 2005. “Impeller Re-Rate to Reduce Hydraulically Generated Vibration,” Proc. 22nd Int. Pump Users Symposium. <http://turbolab.tamu.edu/pubs/Pump22/P22pg010.pdf>.
- [16] Paugh, J. J., 1984. “Head vs. Capacity Characteristics of Centrifugal Pumps,” Chemical Engineering, Oct 15, McGraw Hill Co, New York.
- [17] Brennan, J. R., 2000. “Rotary Pumps on Pipeline Services,” IMO Pump, Pump Users Expo 200, Louisville, KY, September, <http://www.imo-pump.com/tech.htm>.
- [18] Digby, S., 2007. “Pump theory—API Reciprocating Displacement Pumps,” Presented at Tekna Off-shore Pumps Conf.

DESIGN AND OPERATION OF COMPRESSORS

6.1 INTRODUCTION TO PIPELINE COMPRESSORS

Compressors and their drivers are the workhorses of the gas pipeline industry. They come in different combinations with the most common ones being reciprocating compressors driven by electric motors or engines and centrifugal compressors driven usually by gas turbines and increasingly by electric motors. Other types of compressors are not normally used on pipelines because they do not provide the most optimum match of pressure ratio and flow other than screw compressors in upstream gathering systems. In general, pipeline compressors occupy the middle ground in terms of pressure ratio and flow. Reciprocating compressors are the better choice for medium-pressure ratio applications, and moderate flows and centrifugal compressors are preferred for lower pressure ratios and higher flows.

Compressors may be classified into two main types, positive-displacement and dynamic, depending on the method used to achieve compression, and several subtypes (Fig. 6-1).

When these compressors are compared on an inlet volume flow versus overall pressure ratio basis, they each have areas where their compression performance is better than other compressor types. Figure 6-2 shows these in a general sense. The requirements of a specific application may change these areas, for example, for an offshore installation.

With positive displacement compressors, compression is achieved by trapping a volume of gas and applying a direct volume reduction. Flow is intermittent and subsequently, discharge pulsation results with reciprocating compressors producing higher levels of pulsation than with rotary or centrifugal compressors. Many reciprocating compressors are used on pipelines while rotary screw compressors are not very common due to their lower flow capability although their use is increasing.

In contrast, dynamic compressors achieve continuous compression by adding velocity energy and some pressure increase to the fluid utilizing rotating components and then converting the velocity energy into a further pressure increase. Centrifugal compressors are ubiquitous, particularly on larger pipelines where their high flow capability is a major advantage and their gas turbine drivers provide the higher power levels required.

6.2 RECIPROCATING COMPRESSORS

6.2.1 General Design

In a reciprocating compressor, a piston reduces volume within a cylinder. Valves are required in the cylinders to direct the flow of gas and to prevent back flow. Reciprocating compressors are found in all compression applications and in various configurations. Reciprocating compressors typically range in size from 75 to 7500 kW (100–10,000 hp) and operate at speeds from 300 to 1800 rpm. There are two major types of reciprocating compressors: integral and separable.

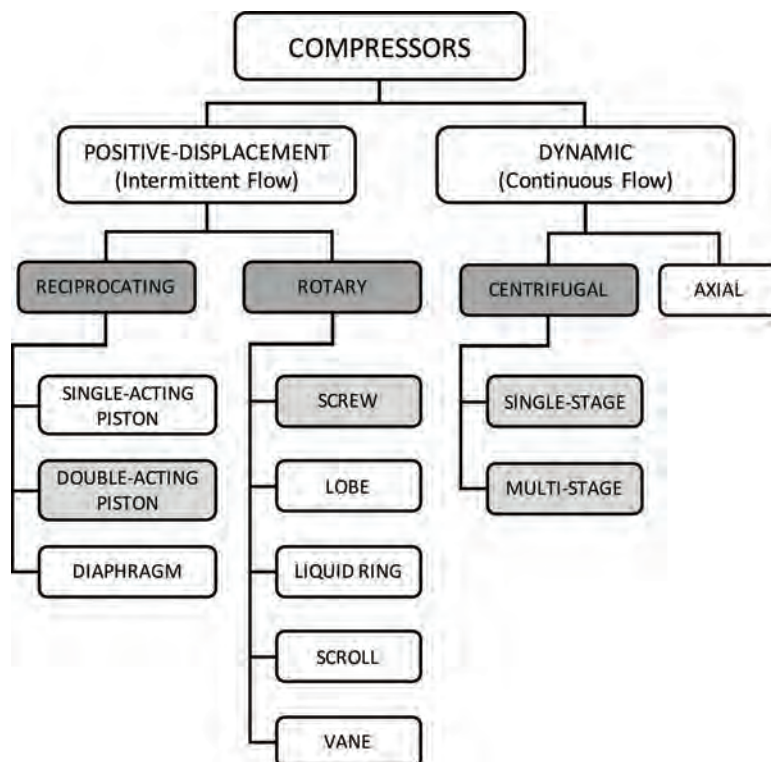


Figure 6-1. Compressor family tree highlighting types commonly used on pipelines.

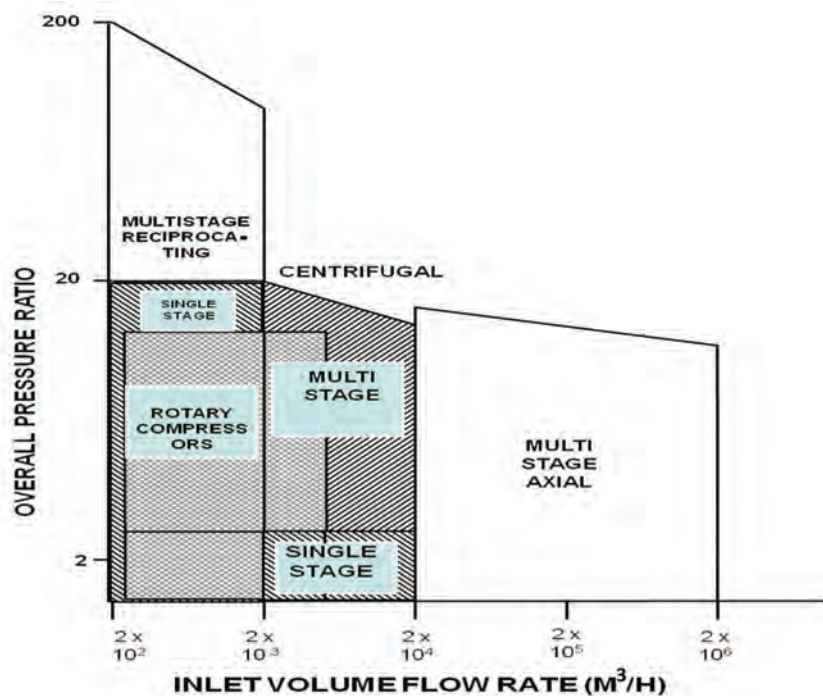


Figure 6-2. Optimal performance for various types of compressors.



Figure 6-3. Integral reciprocating compressor.

A reciprocating compressor can be connected to a driver in two ways. Integral compressors are designed so that the engine and compressor are on the same crankshaft, whereas a separable compressor has its own crankshaft that is coupled to the driver. From the crankshaft outwards, the main components are the same.

The integral compressor, as in Fig. 6-3, was very popular during the development of pipelines in the 1950s and 1960s, and many are still in operation, especially in the United States. With some minor exceptions, integral compressors have mostly been replaced by separable compressors.

Separable compressors consist of a compressor frame that is separate from the driver such as in Fig. 6-4 with the advantage that it can be driven by either an electric motor or an engine. This provides much more flexibility in configuring the compressor for different applications as well as the choice of driver.

The most common drivers used with reciprocating compressors are an electric motor or an internal combustion engine, either naturally aspirated or turbocharged. Generally, in pipeline applications, high-speed separables are used with higher operating speed (900–1200 rpm), lower initial cost, but higher maintenance costs than integrals. High-speed separable application is generally for the lower power range.

6.2.2 Running Gear

For both integral and separable compressors (see Fig. 6-5), the connecting rod transmits the energy of the driver (from the crankshaft) to the compressor pistons. The crosshead connects the connecting rod and the piston rod, and acts as a pivot point, allowing two-dimensional



Figure 6-4. Motor-driven separable reciprocating compressor.

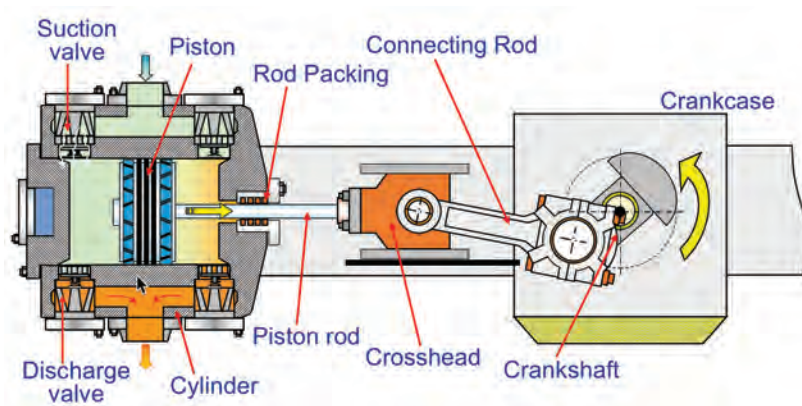


Figure 6-5. Cross-sectional view of a typical double-acting separable reciprocating compressor (courtesy of GE Oil and Gas).

motion on the crank side and only one dimensional (translational) motion in the compressor piston.

The crankshaft, the connecting rod, and the crosshead (in its crosshead guides) are housed in the bed section of the compressor frame (also known as the case).

For most applications, a distance piece is installed between the bed and cylinder sections of the compressor. This allows easy access to the compressor for maintenance. The distance piece is vented to atmosphere to release any gas leaking past the piston rod packing, and wiper rings are used to minimize the amount of oil seepage from the bed section.

The compressor cylinder(s) is attached to the distance piece and contains the cylinder liner, the piston and piston rod, the piston rod high pressure packing, any clearance pocket, and the suction and discharge valves.

A lubricator oil system feeds oil to the compressor cylinder. The system provides oil to the cylinder by means of crank-driven, plunger-type pumps and tubing to various lubrication points.

6.2.3 Frame and Cylinders

6.2.3.1 Compressor Foundations

A reciprocating compressor has to be mounted on a rigid foundation that can absorb the unbalanced forces naturally occurring in this type of compressor. An inadequate foundation may result in frame distortion that leads to misalignment and causes premature main journal bearing failure, eventually breaking the crankshaft. Foundation difficulties are probably the most difficult and expensive maintenance item for reciprocating compressors.

Separable compressors are usually mounted on a concrete pad supported by piles or other means depending on the local soil conditions. Anchor bolts are placed in the foundation, and the compressor is attached to these anchor bolts. Integral compressors are mounted on concrete pedestals that are connected to a common concrete mat onto which multiple engine pedestals and engines are mounted.

Dynamic forces produced by a reciprocating compressor and engine driver exist in multiple directions (see Fig. 6-6) and are caused by the rotating components, particularly the pistons, crosshead forces on inboard and outboard supports, gas pulsation forces, and the couple produced by offset between throws.

Because of a lack of industry standards on foundation design, there is often an inconsistent approach to foundation design that causes reliability problems during later operation. The best approach is to conduct a foundation analysis that takes into account soil conditions

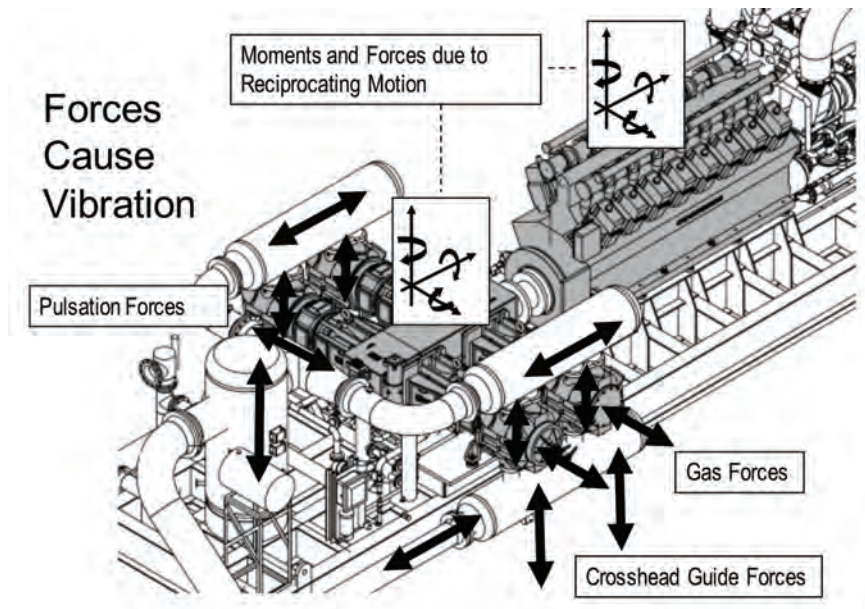


Figure 6-6. Dynamic forces generated by a reciprocating compressor (courtesy of Wood.).

to determine the dynamic response of the foundation system. This is then incorporated with the dynamic analysis of the reciprocating equipment and piping to produce a design that will not cause vibration problems [1].

Unbalanced vertical forces are restricted by the foundation and/or pilings and the anchor bolts. Because they are usually well able to handle these forces, they are less of a problem than horizontal forces that are carried by the friction between the chocks and the anchor bolts as well as attached piping. Contamination by lubricants or other fluids will reduce the coefficient of friction and must be avoided.

For the typical design of an integral compressor using a block foundation mounted on a mat, problems may occur because the interface between the mat, and block is often a cold joint with forces mainly being transmitted through the connecting rebar. The solution for a new installation is to construct the mat and foundation in one pour; for existing foundations, the solution may be to install post-tensioning bolts by drilling vertical holes through the pedestal into the mat. Additional factors that have to be considered are soil conditions, concrete quality, anchor bolts, and epoxy grouting [2].

Modern designs for separable compressors may utilize an engineered gravel pad or a pre-cast concrete pad mounted on metal or concrete pilings. Careful design has to be exercised to avoid future problems [1].

6.2.3.2 Separable Compressor Frame

The frame for a separable compressor as shown in Fig. 6-7 consists of a rigid central box which houses the crankshaft and to which the cylinders are attached by means of a distance piece. Cylinders are configured in opposing pairs to minimize unbalanced forces. Up to 8 cylinders can be accommodated by this type of design, with four cylinders being the most common. The offset between opposing cylinders produces an unbalanced force referred to as a couple but one manufacturer has a unique couple-free design for connecting the crankshaft to the cylinder [3].

The frame is normally made from ne grain cast iron reinforced through the use of heavily ribbed walls and bearing saddles to counteract the fluctuating forces imposed on it. Access plates are installed to facilitate maintenance of the running gear such as bearings and crossheads.

The crankshaft is forged from high-tensile-strength alloy steel that is fully stress-relieved. The journals are precision-ground to exacting tolerances. Connecting rods are die-cast, high-strength steel and drilled to deliver oil to the crossheads. Crossheads are attached to the connecting rod with a floating pin in order to properly lubricate its surfaces by means of rod reversal. Precision-manufactured rolled threads connect the piston rod to the crosshead and

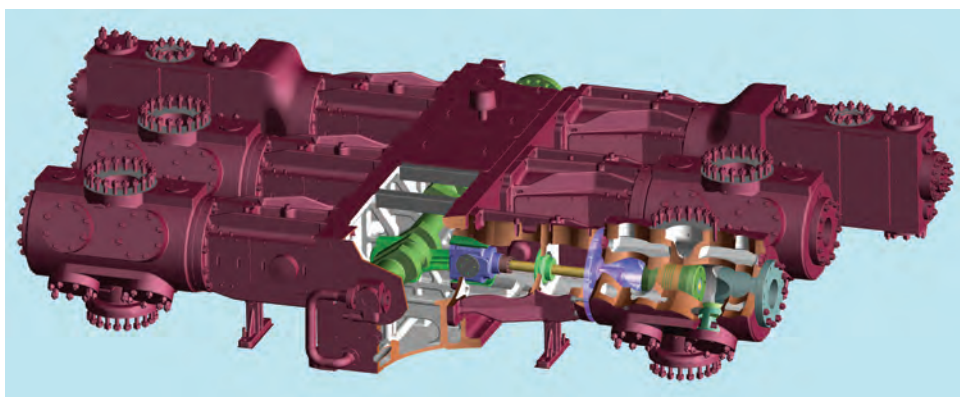


Figure 6-7. Frame of a separable reciprocating compressor (courtesy of Dresser-Rand).

provide the strength needed to transfer fluctuating loads. Some compressor manufacturers have switched to a bolted joint to attach the rod to the crosshead. Standard piston rod material is SAE-4140 carbon steel with the surface hardened to reduce wear caused by packings.

6.2.3.3 Integral Compressor Frame

An integral compressor has its compressor pistons driven directly from the engine crankshaft. Figure 6-8 shows the massive crankcase and upper engine block. The fact that many of this type of compressor are still in operation testifies to the rugged construction of this design. Its main drawback is that major maintenance is very time-consuming, usually 4 to 6 weeks, and its resultant availability is impacted. The engine efficiency is not high as for engines used in modern separable designs, although revamps have improved many of them. The compressor side of an integral, however, is more efficient due to large valves and lower velocities.

6.2.3.4 Compressor Cylinders

Cylinders suitable for pipeline service need to be engineered for long service life and high efficiency. They feature large streamlined suction and discharge flow areas for low pressure drop, flexible arrangements for capacity control, and easy access for maintenance. For low-pressure ratios below 2.0, cylinders can be air-cooled or, for higher ratios, gas- or water-cooled.

Materials appropriate for compressor cylinders are selected not only on required strength but also corrosion resistance and mechanical and thermal shock. Cylinders may be made from large castings for lower or medium pressures or forged steel for higher-pressure applications (see Fig. 6-9). Materials and their discharge pressure limits as generally used in the gas industry [4] are as follows:

- cast iron: up to 8300 kPa (1200 psig)
- nodular iron: about 10,300 kPa (1500 psig)



Figure 6-8. Assembly of a 12 cylinder integral compressor (courtesy of Dresser-Rand).

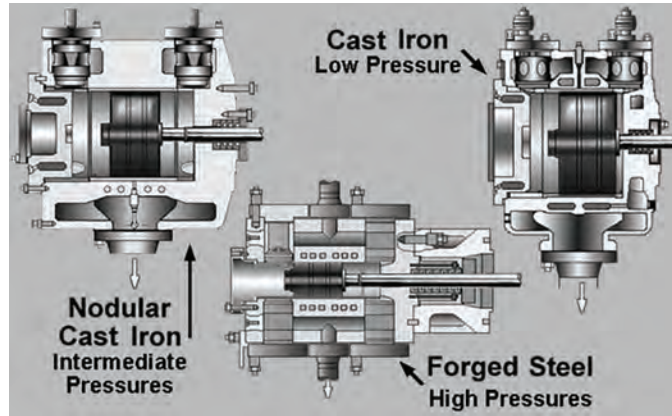


Figure 6-9. Different cylinder construction dependent on pressure (courtesy of GE Oil and Gas).

- cast steel: 8300 to 17,200 kPa (1200 to 2500 psig)
- forged steel above 17,200 kPa (2500 psig)

Most cylinders are double-acting, which has the advantage not only of being more compact for a certain design flow but also permits easier sealing around the piston rod instead of the piston, which results in a larger sealing area. Liners are usually installed to enable replacement when wear limits are exceeded. They can be of the dry liner-type, where they are not required to act as a pressure element or the wet liner type where the liner forms part of the pressure wall. The piston is either hollow or solid and is made from heat treated aluminum alloy or cast iron. In addition to piston rings to seal between the two compression compartments, there are often also rider rings (or wear bands) to reduce friction and wear.

A typical double acting compressor cylinder is shown in Fig. 6-10. It is attached to a distance piece with a packing assembly to prevent leakage around the piston rod. At the head end, there is a variable volume clearance pocket (VVCP) that as shown here is

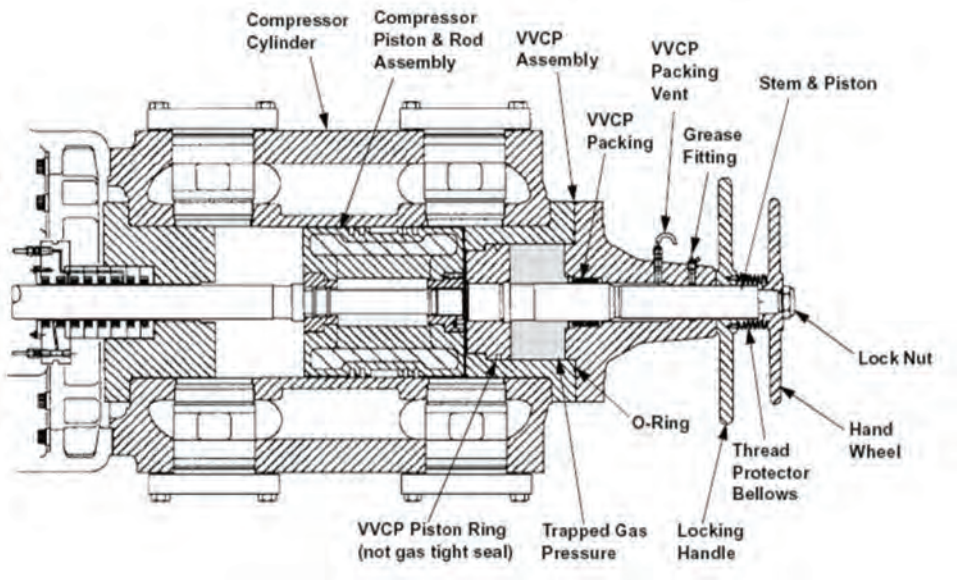


Figure 6-10. Double acting cylinder with variable pockets (courtesy of Ariel Corporation).

manually adjusted although automatic loading is an option. The cylinders are un-cooled since it has been shown that high speed cylinders do not require the cooling that previous designs used. This simplifies cylinder design and allows more room for intake suction and discharge passages and eliminates scaling and corrosion of cooling passages.

6.2.4 Capacity Control

Capacity (or flow) control can be achieved in one or more of the following ways:

- compressor speed (flows increases directly with speed)
- clearance volume (adding clearance volume decreases flow)
- deactivating one end (usually the head-end) of a double-acting cylinder by removing the suction valves
- recycle valve (opening the recycle valve increases the flow through the compressor while decreasing net process flow)
- suction valve (throttling the suction valve drops the pressure and thus the flow)

Clearance volume control can be done in different ways. A commonly used approach for pipeline compressors is fixed-volume pockets that are individually opened in a certain sequence to provide a series of steps in controlling volume. Also available are variable pocket unloaders that allow a more precise ability to trim the clearance volume for a required process condition. A comparison of the two is described by reference [5] and is illustrated in Fig. 6-11.

A very detailed review of capacity control options is provided by reference [6] along with extensive analysis of possible improved and more efficient methods for capacity control.

Since removing a suction valve necessitates a shutdown, some compressors have the option of installing a plug (or suction valve) unloader that can be activated during operation to hold a suction valve open (see Fig. 6-12). For the highest efficiency, the use of automatic volume control is quite desirable although, at the expense of complexity, possibly lower reliability and higher installed cost. However, for pipeline operation that sees less variation in required process conditions, it is more difficult to justify higher cost solutions for capacity control.

6.2.5 Valves

Suction and discharge valves are, without a doubt, the most critical components of a reciprocating compressor and ones that have the greatest impact on reliability. They are actuated by pressure differential and are required to actuate every rotation of the crankshaft. This increases linearly with speed, and therefore, valve dynamics become increasingly important with higher speed compressors.

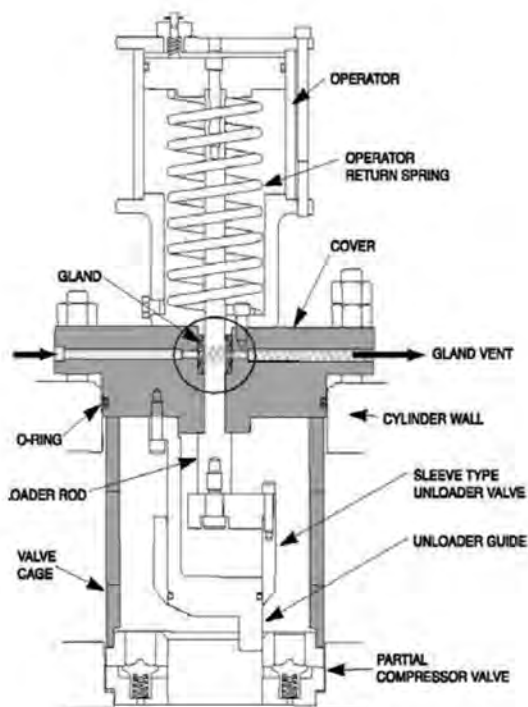
Valve failures are a major cause for downtime [7] and are a primary contributor to cylinder pressure losses and reduced overall efficiency.

Figure 6-13 illustrates the design and installation of cylinder suction and discharge valves which are critical to successful and efficient operation.

Compressor valves are designed in one of two ways:

- Poppet valves (Fig. 6-14(a)) which are suitable for high volume low compression ratios such as found on mainline compression
- Plate valves (Fig. 6-14(b)) which are used on high speed separable compressors with higher compression ratios

A



B

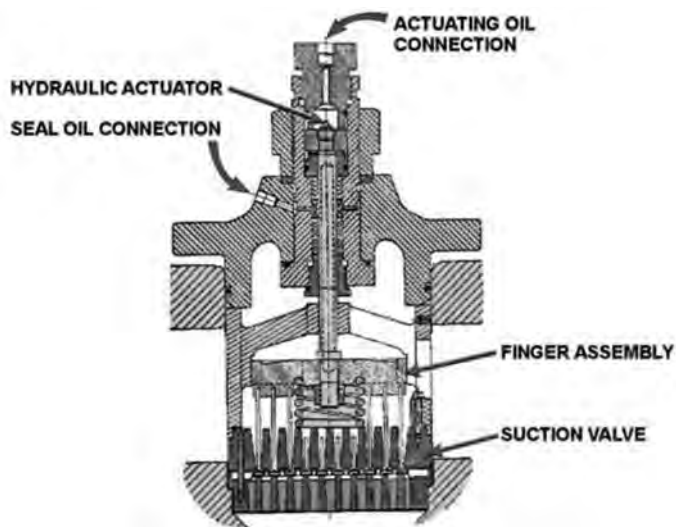


Figure 6-11. Types of unloaders: (A) pneumatic clearance valve and (B) infinite step control (courtesy of Dresser-Rand).



Figure 6-12. Typical plate valve with finger-type unloader (courtesy of GE Oil and Gas).

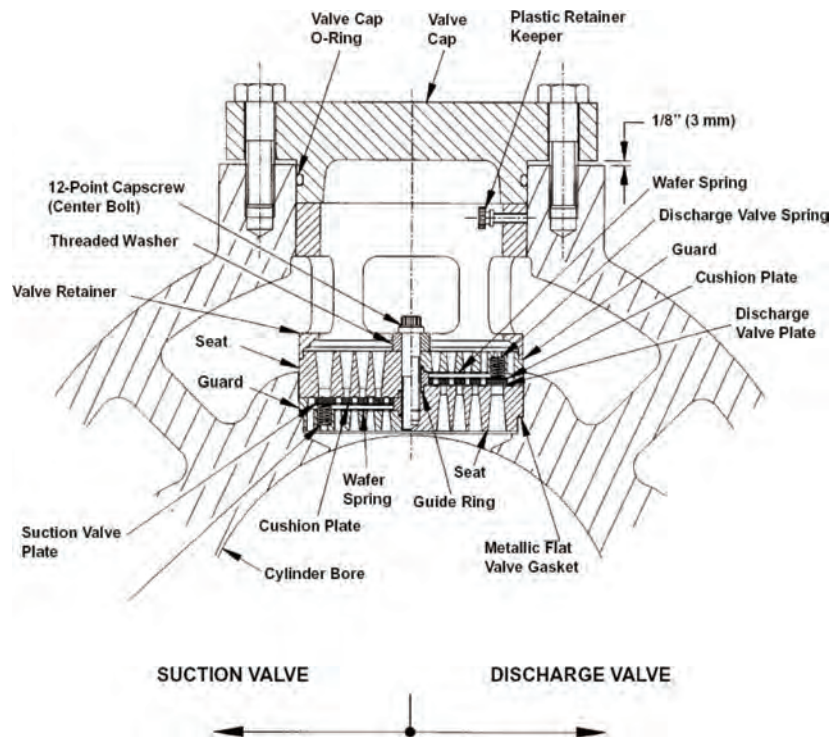


Figure 6-13. Cylinder suction and discharge valves (courtesy of Ariel Corporation).

General design considerations for compressor valves are as follows:

- Valve area must be sufficiently large to limit pressure drop through the valves.
- Design should be appropriate for both the working pressures and the pressure differential.
- Valve materials need to be compatible with process gas constituents, particularly those that result in corrosion.

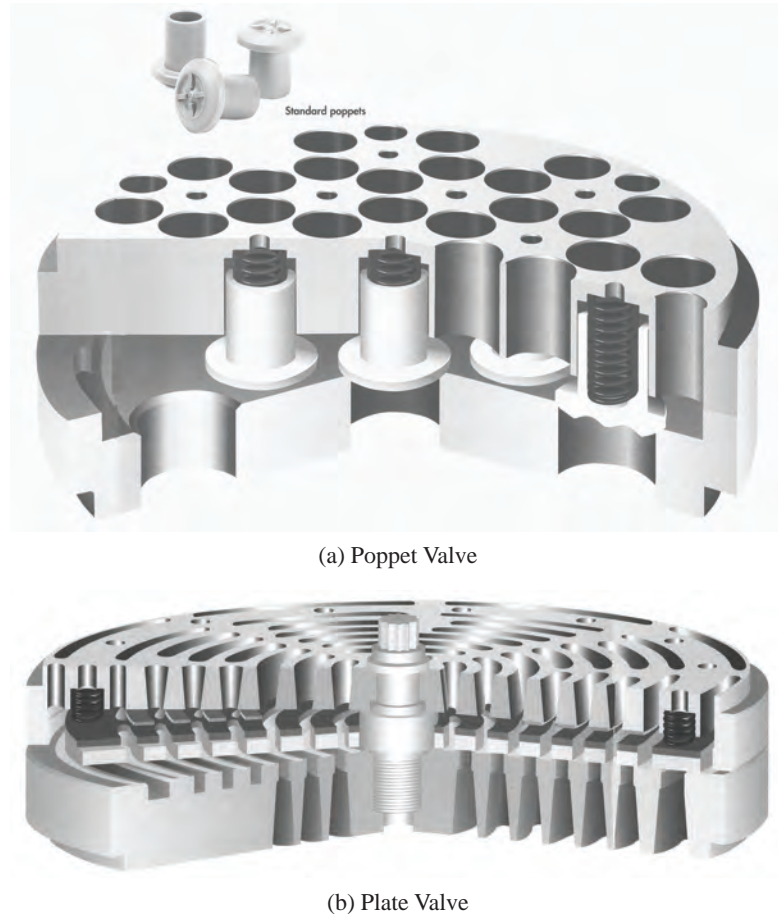


Figure 6-14. Types of compressor valves (courtesy of Hoerbiger).

- The design should be able to handle contaminants present in the gas.
- Acceptable reliability should be achieved.
- Maintainability (or ease of maintenance) is critical to minimizing downtime.

Poppet valves have been the valve of choice for pipelines because they offer large flow areas and streamlined gas flow for high efficiency at low-pressure ratios. The design of a poppet valve features spring loaded cartridges (poppets) held between two plates with ports to pass and guide the flow. Figure 6-15 illustrates two designs using poppet valves, one being the standard poppet design and the second the GT poppet valve designed specifically for gas transmission. The graph in Fig. 6-16 compares flow performance for different types of valves and confirms that poppet valves demonstrate a larger range of flow areas and valve lift. Since the 1980s, poppets have been made from a special plastic called PEEK (Poly-EtherEtherKetone), which is resistant to higher temperatures, stress and fatigue loading.

The schematic in Fig. 6-17 illustrates what occurs when a suction or discharge valve opens. The piston speed oscillates between zero at either end of the stroke and a maximum value in the middle. Pressures increase and decrease as shown in the pressure volume curve.

At the beginning of the suction stroke with the discharge valve closed, there is a small differential pressure created as the piston moves from top dead center. This opens the suction valve, first slowly since the pressure can act only on the exposed area of the plate and then more rapidly as the entire area is uncovered Fig. 6-18.

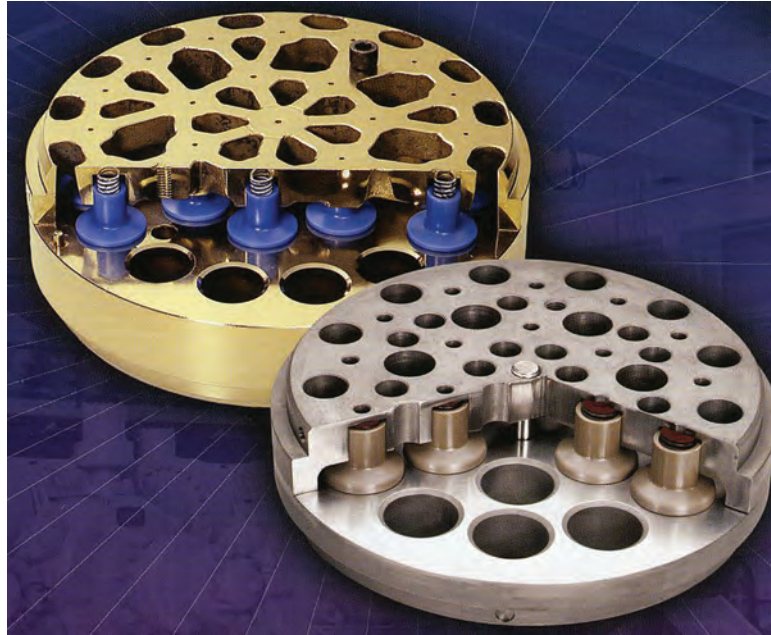


Figure 6-15. Typical poppet valves (courtesy of Dresser-Rand).

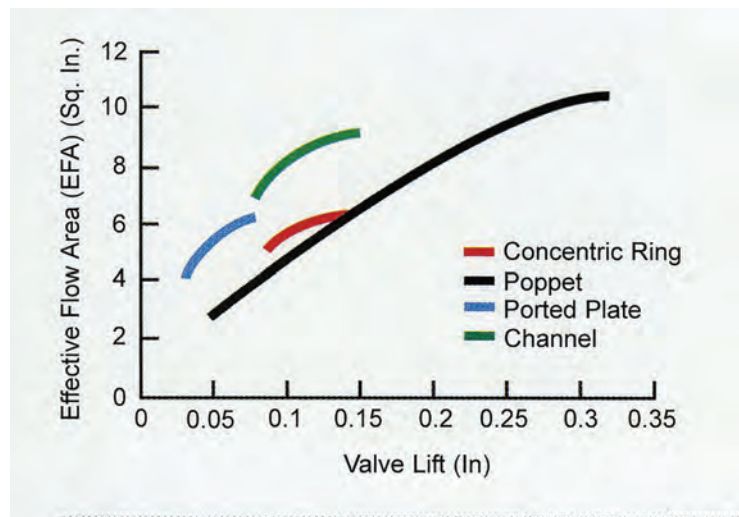


Figure 6-16. Comparison of valve lift and flow areas for various types of valves (courtesy of Dresser-Rand).

The resultant valve dynamics for both suction and discharge valves can be seen in Fig. 6-19. Ideally, valves should open early with a minimum pressure differential between cylinder and line pressure. It should open quickly but, at the end of the lift, the impact on the guard should be low. After opening, the valve should remain fully open without flutter.

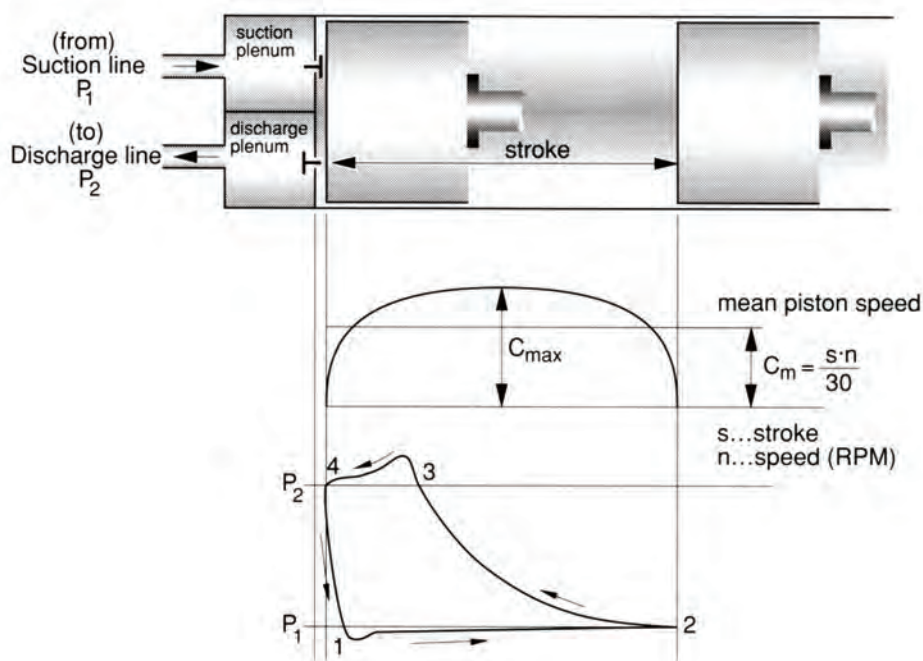


Figure 6-17. Piston dynamics (courtesy of Hoerbiger).

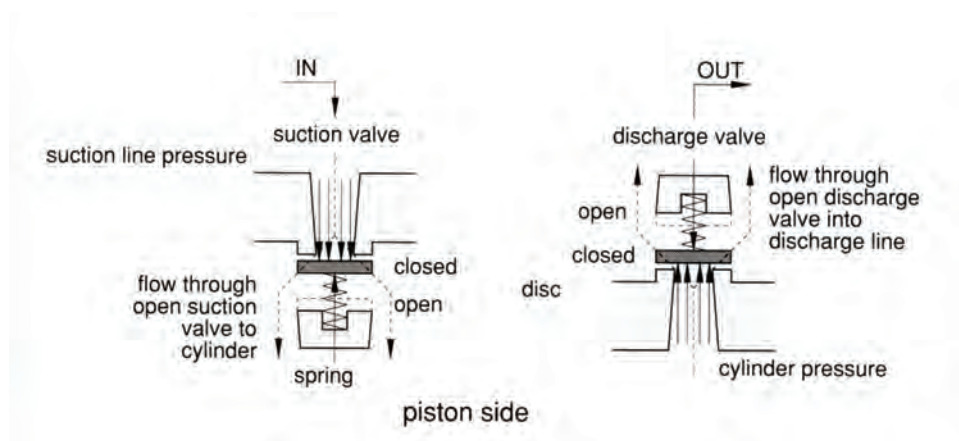


Figure 6-18. Schematic of compressor valves (courtesy of Hoerbiger).

In addition to the reliability and life of a compressor valve, its performance is measured by valve efficiency or the flow losses due to the compressor valves. Valve pressure losses are a function of the valve geometry, valve lift, free lift area and spring load. The final valve efficiency is the result of optimization in all of these areas. Valve lift is especially critical. High lift is desirable in order to reduce pressure losses but is detrimental to long valve life.

Considerable effort has been expended by manufacturers and research bodies to improve the performance of passive type valves [6]. This has led to investigations of active valves such as the semi-active compressor valve developed by Southwest Research [8].

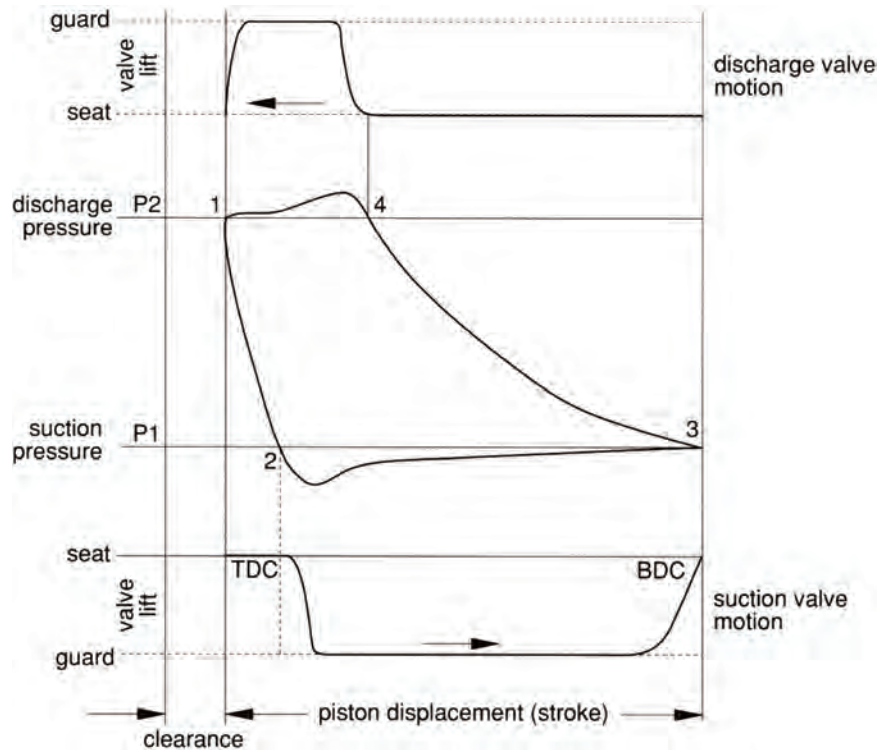


Figure 6-19. Valve dynamics (courtesy of Hoerbiger).

6.2.6 Packings

Packings are located where the cylinder is attached to the distance piece and seals the process gas in the cylinder by minimizing the leakage past the rod. Sealing elements for reciprocating compressors are (see Fig. 6-20):

- Piston rings to seal differential pressure across the piston and rider rings to support the weight of the piston and rod by acting as a bearing
- Main packing to seal against the high cyclic pressures inside the cylinder
- Intermediate packing which prevents any residual leakage from outboard to inboard distance piece
- Oil wiper packing to remove oil from the piston rod and return oil to the crankcase

A pressure packing consists of a series of three-segmented rings held in a packing cup. Internal cylinder pressure squeezes the ring segments around the piston rod to prevent leakage. Teflon-based material is the preferred choice for packings. Escaping gas is vented, and either pressure or temperature is monitored to detect excessive leakage and prevent impending packing failure. Sometimes, intermediate packings are used. Wiper rings on the frame side of the distance piece keep oil from the bearings from entering the distance piece.

6.2.7 Bearings and Lubrication Systems

Bearings used on reciprocating compressors are most often of the hydrodynamic or journal type. Tapered roller antifriction bearings are acceptable for frame sizes of less than 150 kW

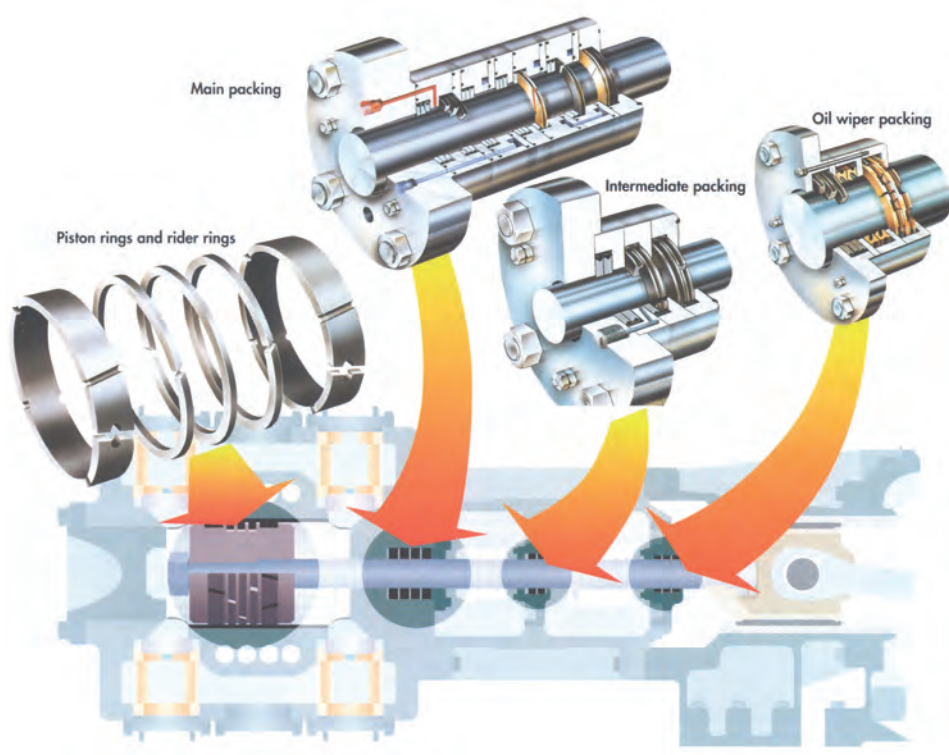


Figure 6-20. Rings and packings (courtesy of Hoerbiger).

(200 hp). Main crankshaft and connecting rod bearings as well as the crosshead pin and shoes are lubricated with a standard pressurized lubrication system fed from the crankcase and employing positive displacement pumps, filters, and cooling as prescribed in API Std 614. Crankcase temperature should not exceed 70°C (160°F), and supply temperature should no higher than 55°C (130°F). Full-flow filters shall be supplied with filtration of at least 10 μm .

Lubrication of the cylinder and packings [9] requires more precise control of flow rates and may be achieved either by plunger-to-point lubrication with individual positive displacement pumps or a divider block distribution system with a main pump forcing oil through a distribution block with individually sized plungers driven off the crankshaft. The latter is the more common solution.

For the block distribution system, the overall flow is adjustable, but not the individual blocks that are sized for each compressor and application. A cycle monitor protects against low flow and an indicator at each outlet warns when it becomes plugged.

Manufacturers have developed formulas for estimating required flow rates that take into account not only the amount of lubricant needed to effectively coat a specific bearing contact area but also operating and process conditions. Figure 6-21 is a rough guideline for normal feed rates. During equipment break-in period, feed rates should be increased to 1.5 to 3 times the normal rate.

Recently, there is growing consensus that over-lubrication is contributing to packing failures [10]. This causes the packing not to seal on startup or to fail after a short period of time. It also causes environmental problems by producing excess oil. If repetitive packings problems occur, it may be time to investigate whether over-lubrication is occurring. Carefully reducing the overall flow is one possible solution. If the distribution block is oversized, this is not expensive to rectify. In either case, the manufacturer should be consulted.

to each cylinder is roughly	1.5 to 5.5 U.S. pints (0.7 to 2.5 L) per day
to each suction port oiler is roughly	0.75 to 1.0 U.S. pints (0.3 to 0.5 L) per day
to each main packing is roughly	1 U.S. pint (0.5 L) per day
to each auxiliary packing is roughly	0.5 U.S. pints (0.25 L) per day

Figure 6-21. Typical oil feed rates [9].

The lubrication system for a reciprocating compressor is divided into two parts: the main lubrication of the internal frame running gear and force-feed lubrication of the cylinders. As shown in Fig. 6-22, oil is drawn from the sump through a strainer by a lube oil pump. Oil temperature is controlled by a thermostatically controlled oil cooler. At the cylinder, the oil is distributed through an oil gallery to the crankshaft main bearings and through drilled holes via the crankshaft to the connecting rod bearings. From the connecting rod, it passes through another set of drilled holes to the crosshead pins and bearings. The runoff collects back in the sump.

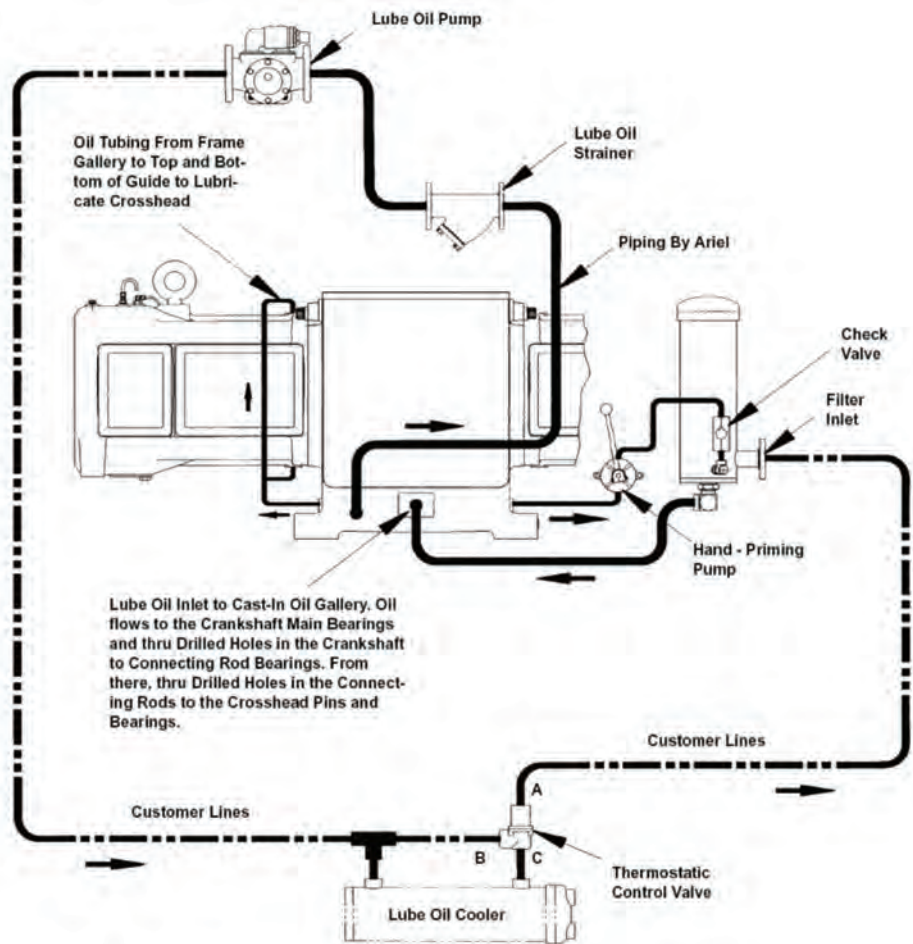


Figure 6-22. Main lubrication system (courtesy of Ariel Corporation).

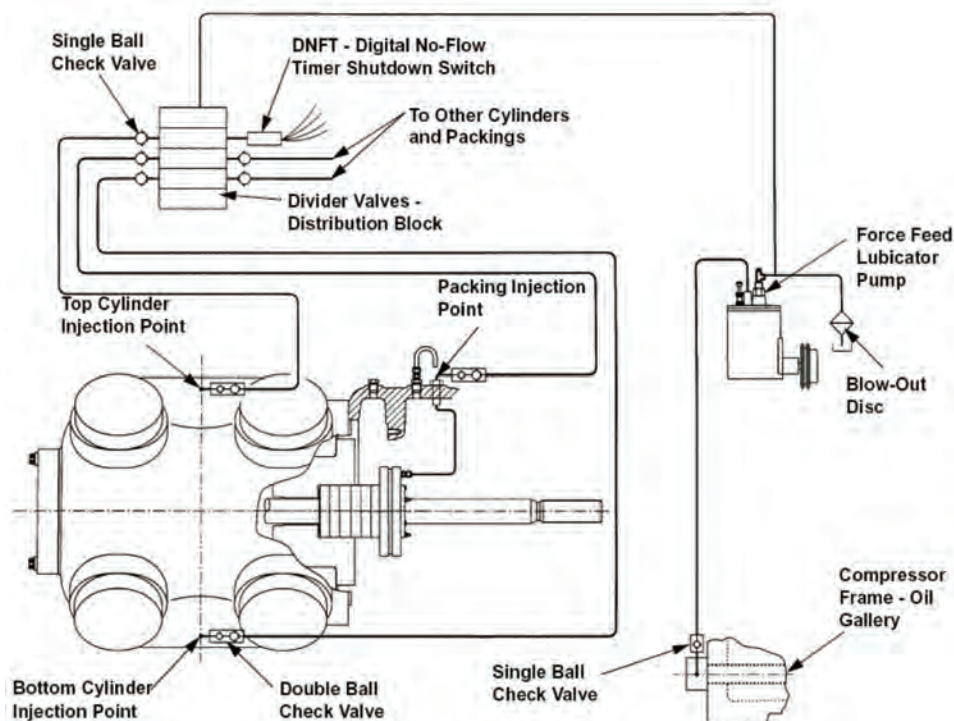


Figure 6-23. Force-feed lubrication system (courtesy of Ariel Corporation).

A force-feed system (Fig. 6-23) supplies oil to the compressor cylinders and crosshead packing. A force-feed pump supplies oil to a distribution block that apportions the correct amount of oil to prevent excessive amounts from being passed into the gas stream. A digital no-flow timer (DNFT) switch protects against loss of lubrication.

6.2.8 Controls and Monitoring

6.2.8.1 Control System

Controls and monitoring systems are becoming increasingly sophisticated and integrated. The control system for a reciprocating compressor is integrated with the driver and process control system and is usually implemented in a dedicated computerized control panel.

Major control-related functions consist of:

- capacity control: controlling flow
- limit control: limiting parameters, normally minimum and maximum speed for the compressor and limits due to the driver
- protective control: protecting the compressor by alarms and shutdown for critical parameters such as packing temperatures and vibration
- event sequencing: startup and shutdown sequencing

The primary means of control is a combination of speed and clearance control through the activation of volume pockets that increase capacity. Although reciprocating compressors have been automated for about the past 30–40 years, PLC-based systems are allowing more precise control and protection [11]. Protection of the compressor includes high discharge temperature (usually caused by leaking discharge valves), high rod loading, lubrication failure and high packing temperature.

6.2.8.2 Monitoring




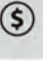
The nature of the reciprocating compressor lends itself to effective monitoring strategies. The main monitoring strategies are:

- valve temperatures
- packing temperatures
- vibration
- rod drop
- rod loading and reversal
- cylinder pressures

Various online monitoring systems are now available to carry some or all of these monitoring functions. For example, a system called ValveAlert™ has a special sensor that detects acoustic and temperature data (either handheld or online) with a software program to interpret the data and warn of impending failure. Other systems such as Platinum™ by Windrock provide online diagnosis of both reciprocating compressors and engine drivers including high-speed monitoring of cylinder pressures using p-V diagrams along with other parameters (see Fig. 6-24). However, something can still be said for off-site diagnosis with human intervention, which can address not only standard monitoring and trending but also optimization and fleet analysis [12].

6.2.8.3 Start-up and Shutdown

The start-up and shutdown of a reciprocating compressor is similar to that of a centrifugal compressor. Prelubrication and compressor purging and pressurization occurs prior to driver rotation. When the driver permits, the recycle or bypass valve is closed and the compressor is loaded by closing volume pockets and altering speed. Shutdown, likewise, follows the opposite procedure.

	PRESSURE	VIBRATION	ROD POSITION
Protection			
	Cross-Head	X	X
	Frame	X	
	Rod Load/Reversal	X	
	Over Pressure		
	Rod Looseness	X	X
Condition Monitoring			
	Valve, Ring, Packing Leakage	X	
	Rider Band Wear		X
	Bearing Wear	X	
	Liner and Piston Wear	X	
	Rod Wear		X
	Internal/External Looseness	X	
Performance Monitoring			
	Power Consumed	X	
	Gas Throughput	X	
	System Efficiency and Validation	X	
Economic Monitoring			
	Compressor & Driver Efficiency	X	
	Recirculation Losses	X	
	Unit to Unit Comparison	X	

Platinum systems comply with Hazardous Area, SIL, CE and API618/670 standards.
Windrock compressor monitoring technology is protected under US Patent #6292757.

Figure 6-24. Platinum™ Online Compressor Monitoring System (courtesy of Windrock).

6.2.9 Gas Cooling

Where higher compression ratios exist, generally more than 2.0, it becomes worthwhile to provide gas cooling. If the gas is cooled after the final discharge, it is referred to as an aftercooler, and if it occurs in between compression stages, it is known as an intercooler. The most common type of cooler is a series of cooling fans mounted either below or above a piping manifold.

There are several purposes for gas cooling:

- It reduces the volume flow prior to recompression and minimizes the power required for the next stage of compression due to the increase in efficiency.
- The discharge temperature is kept within safe operating limits for piping and coatings.
- Downstream pipeline efficiency is improved.

6.2.10 Operation and Optimization

6.2.10.1 Physical Operation

Figure 6-25 shows the steps in the compression cycle of a double-acting reciprocating compressor. For simplicity, the following outlines only the compression cycle at the head end (HE) of the cylinder. The crank end (CE) cycle is the same but 180° out of phase.

In point 1 on the graph in Fig. 6-20, the piston is at the end of its stroke toward the HE of the cylinder and is starting to move toward the CE of the cylinder. As the piston moves from point 1 to 2, the gas trapped in the HE clearance volume drops from discharge pressure to suction pressure (minus valve spring forces and valve/passage friction losses). The suction valve (always on the top of the cylinder) opens and a charge of new gas starts to enter the cylinder. Between points 2 and 3, the piston continues its movement toward the CE of the cylinder. At point 3, the piston is at the CE of its stroke, and the HE volume is at its maximum at suction pressure with the CE at minimum volume at discharge pressure.

As the piston now moves from points 3 to 4, the gas is compressed to discharge pressure (plus valve spring forces and valve/passage friction losses). Between points 4 and 1, the discharge valve opens and the gas is discharged to the receiver.

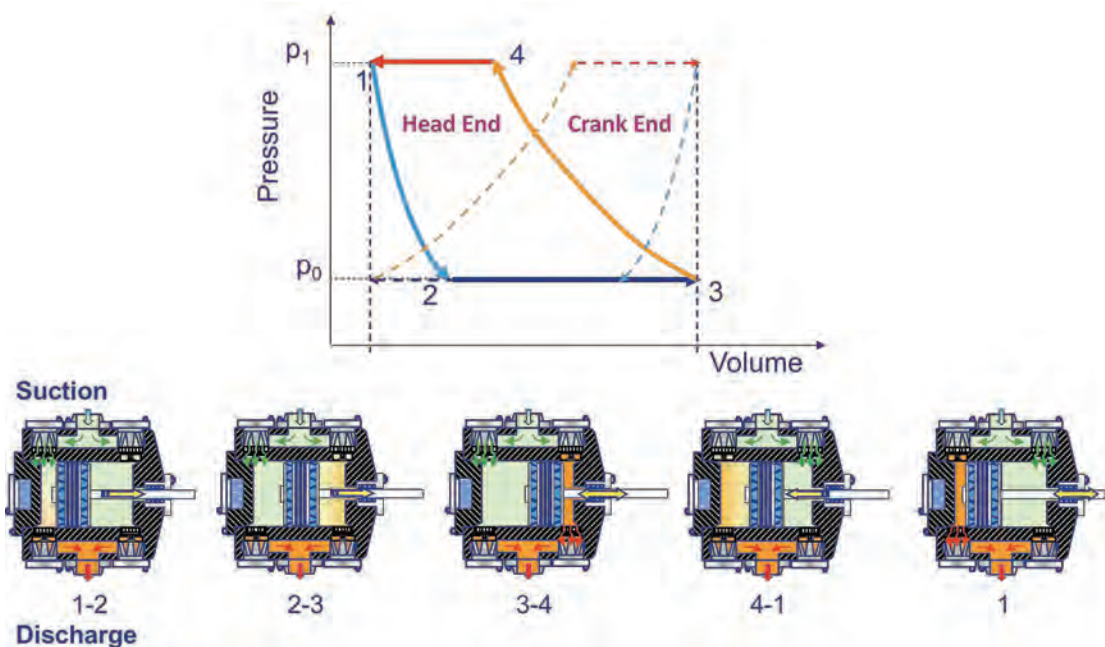


Figure 6-25. Compression cycle of a reciprocating compressor (courtesy of GE Oil and Gas).

Note that although the piston face sweeps a full stroke from points 1 to 3, the cylinder is only taking in gas as the piston face sweeps from 2 to 3. The ratio of suction sweep (points 2 to 3) over full sweep (points 1 to 3), or intake volume over piston displacement volume, is called “volumetric efficiency” (VE).

Figure 6-26 shows the effect that adding clearance volume has on the VE and, thus, the capacity of a reciprocating compressor. In most cases, only the HE of the cylinder can be equipped with a variable volume clearance pocket (VVCP).

In case 1, the variable VVCP is closed, and the clearance volume is equal to the residual clearance volume of 10% of piston displacement. Here, the head face of the piston must move 10% of its total displacement before starting to allow new gas into the cylinder.

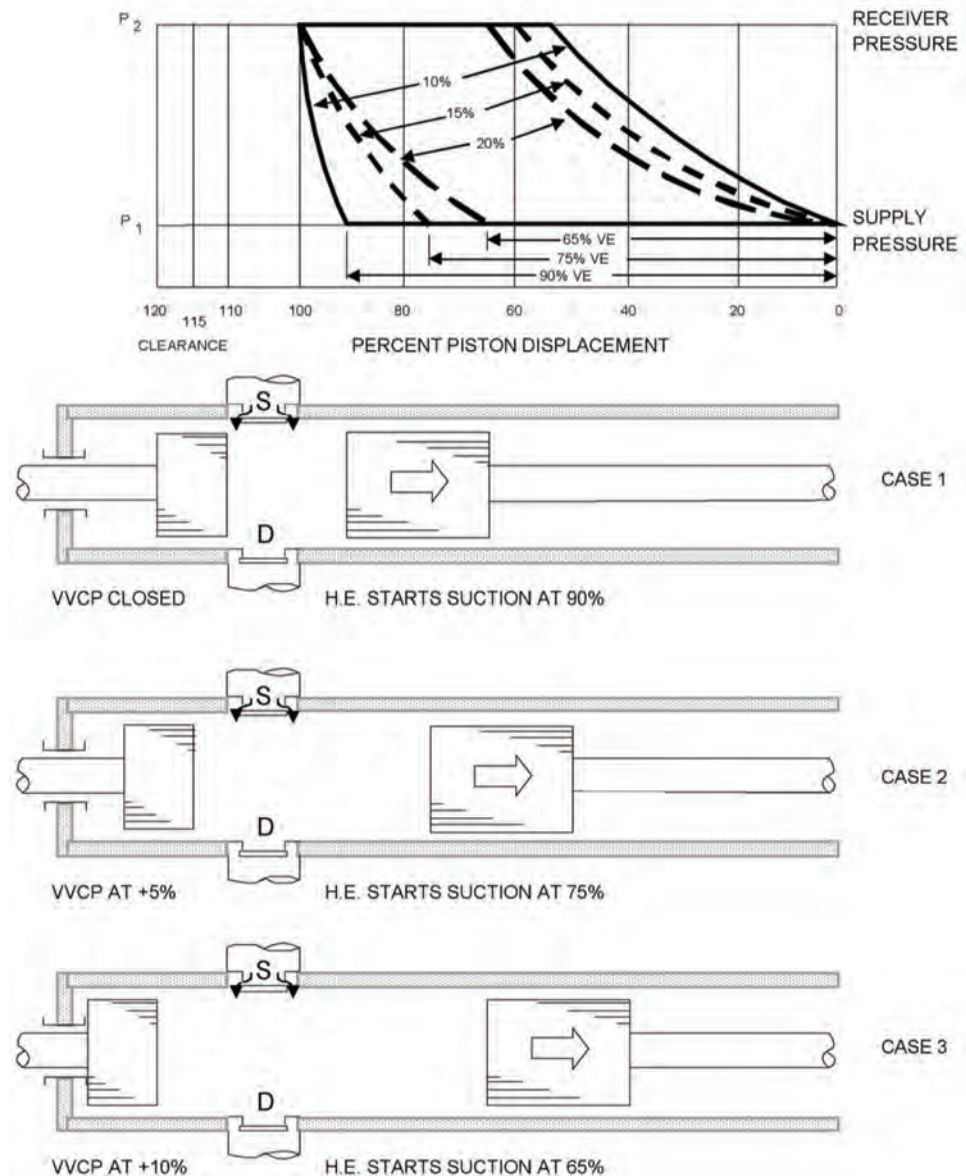


Figure 6-26. Effect of clearance volume on reciprocating compression cycle.

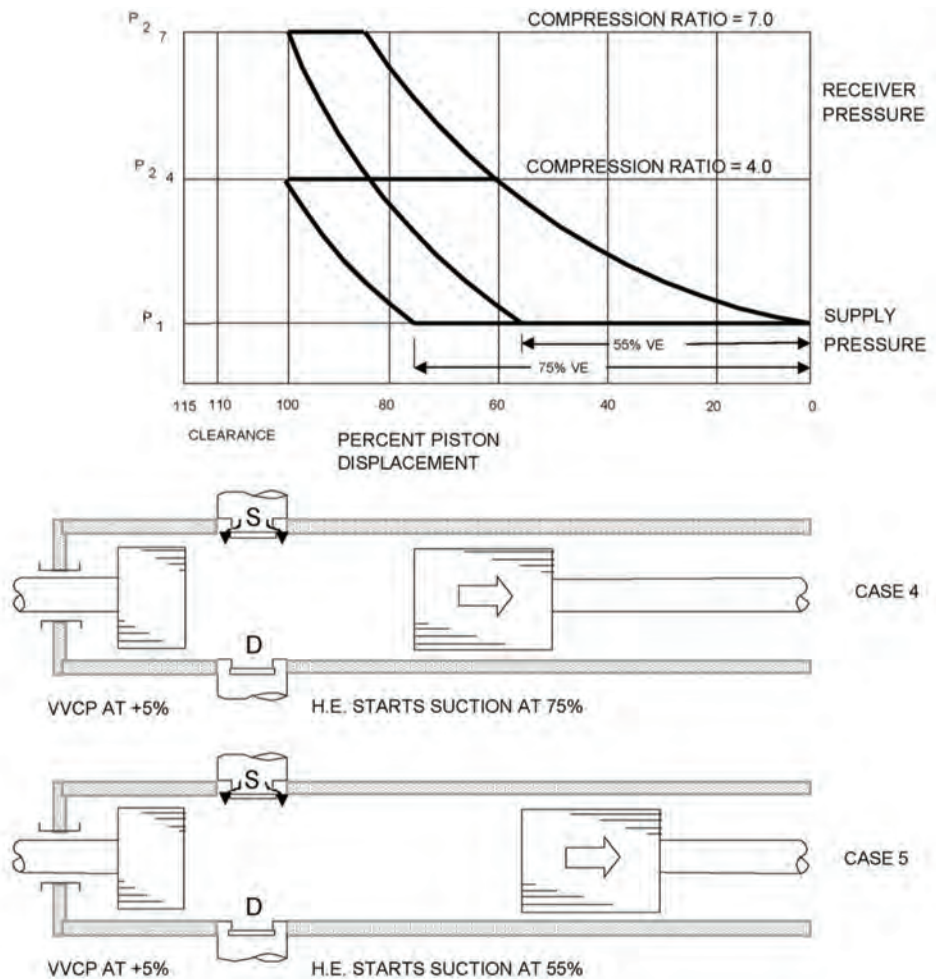


Figure 6-27. Effect of clearance volume on reciprocating compression cycle.

In case 2, the variable VVCP is open 5%, and the clearance volume totals 15%. In this case, the head face must move 25% before starting to introduce new gas.

In case 3, the clearance volume totals 20%, and the head face must move 35% before starting to introduce new gas.

Figure 6-27 illustrates the effect of increased pressure ratio on the VE and capacity of a reciprocating compressor. Again, for simplicity, only the HE is discussed, although both ends are affected in the same way.

In case 4, like case 2 above, at a pressure ratio of 4.0 the total clearance volume is 15%, and the head face of the piston must move 25% of its total displacement before starting to introduce new gas.

In case 5, the receiver pressure has risen until the pressure ratio is 7.0. Although the clearance volume is still 15%, the clearance gas has been compressed to a much higher pressure. Therefore, the piston's head face must move 45% of its total displacement before the clearance gas pressure reduces to supply pressure, and new gas starts to be introduced.

6.2.10.2 Optimization

Optimizing the efficiency of a reciprocating compression system is critical to successful and economic operation. A number of aspects have to be considered in order to achieve

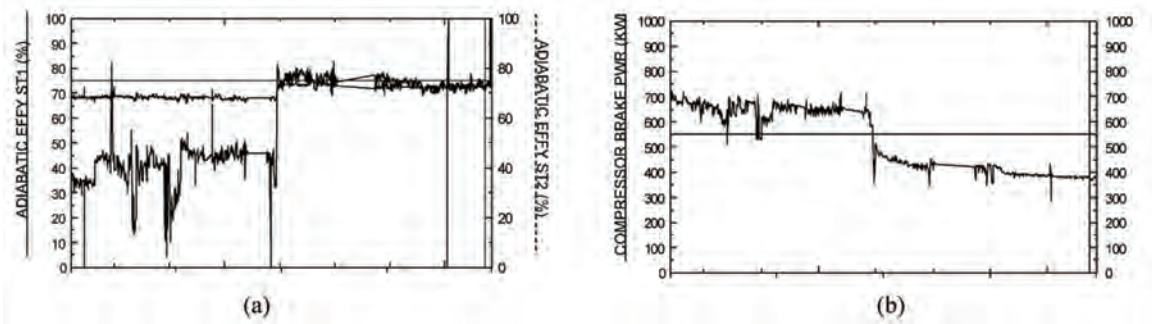


Figure 6-28. Example of optimization showing (a) increase in efficiency and (b) decrease in required power [12].

optimization although external constraints may limit the amount of optimization that can be implemented [12].

The first factor that affects optimum system operation is the position of suction and bypass (or recycle) valves. Suction throttling causes pressure drop and should be avoided. Opening the bypass valve is used to reduce net flow throughput but wastes energy and thus increases fuel consumption. Increasing clearance volume or reducing driver speed may enable the bypass valve to be closed although this may be constrained by a minimum speed or load on the engine.

Another factor is the VE of compressor. This decreases as clearance volumes increase and should be kept above 20% for efficient operation. Adjusting speed or deactivating the HE of one or more of the cylinders may be possible solutions.

As required pressure ratios change, a two-stage compressor may become inefficient and restaging to a single stage may be needed.

Where multiple units are installed in parallel, shutting down one or more units can improve individual unit and overall system efficiency. If a compressor and/or its driver are oversized for the application, it may be worthwhile to switch compressors.

An example of optimization [12] is illustrated in Fig. 6-28. Monitoring on a two-stage compressor showed poor efficiency in stage 2 and high hp losses. Adiabatic efficiency in stage 2 was running around 40%. Analysis of the configuration indicated that a single-stage configuration would be better. After the reconfiguration to single stage, efficiency improved to over 70%, as shown by the step improvement in Fig. 6-28(a). At the same time, power decreased by about 200 kW, as shown in Fig. 6-28(b). The resulting saving in fuel was about \$170,000 a year.

6.2.10.3 Rod Loading

Every reciprocating compressor has limitations on the power it can absorb and the loads it can sustain. The most critical component is most often the piston rod, not only because of its small cross-sectional area but also because the load imposed on it will vary with process conditions, speed and configuration such as clearance volume.

In addition to ensuring that the rod load limit is not exceeded, it is important to maintain what is referred to as rod reversal. As the load on the rod reverses in direction from tension to compression, it provides adequate lubrication of the pin that connects the crosshead to the connecting rod. The recommendation in API 618 [13] is that the reversal angle should not be less than 15° of rotation and that the peak load should not be less than 3% of the load in the opposite direction, depending on the bushing design.

For slow-speed reciprocating compressors, it has been traditional to calculate the rod load based on gas pressure only.

$$\text{Load in compression} = (P_d - P_s)A_p + P_s A_r \quad (6-1)$$

$$\text{Load in tension} = P_d(A_p - A_r) - P_s A_p \quad (6-2)$$

where: P_s = suction pressure, kPaa or psia

P_d = discharge pressure kPaa or psia

A_p = piston area, m^2 or in^2

A_r = rod area, m^2 or in^2

Load = kN or lb_f

It becomes important to include the inertial forces of the reciprocating weights for compressors operating at higher speeds (>300 rpm), lower compression ratios, and high mass piston and rod assemblies. The applicable reciprocating weights for the inertial calculation include the piston and rod weights. The inertial force is derived from the product of mass and acceleration at discrete intervals of crank rotation and generally follows the curve shown in Fig. 6-29. This figure also includes the gas force calculated for crank angle intervals and also shows the effect of head-end de-activation on the gas force.

It includes an estimate for valve losses at both the suction and discharge to allow for a more accurate estimate of reversal angle.

Inadequate rod reversal may occur under the following types of conditions:

- high clearance volumes or low VE, especially at lower speeds
- if the CE is unloaded (it is better to unload the head-end)
- high compression ratio in addition to high pressure

The rating of a reciprocating compressor with respect to rod load has evolved over time with the term interpreted differently by users, analysts and manufacturers [14]. In addition, most programs assume uniform pressure inside the cylinder, ideal valve motion, constant pressure at the cylinder flange and neglect gas inertia effects. The effects of real world compression including pressure pulsation at the outside of the valve, non-uniform piston-face pressure distributions and torsional pulsation effects on rod load are now better understood [14].

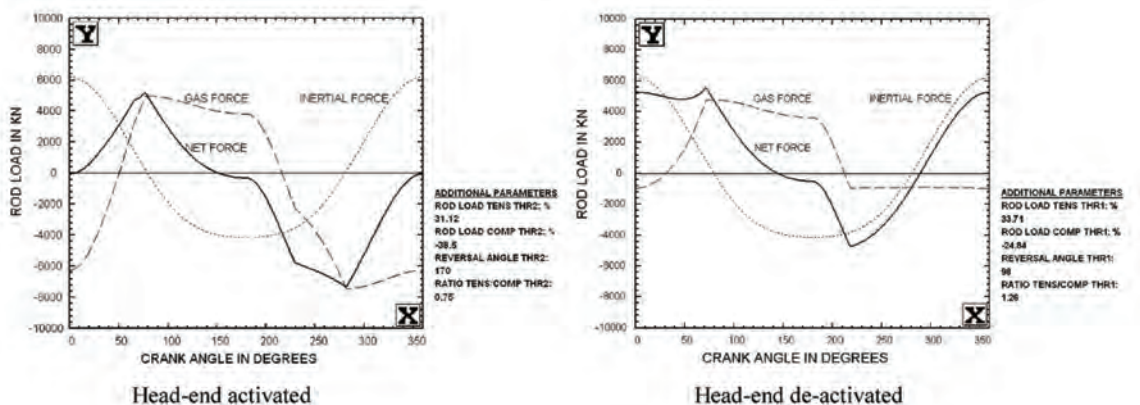


Figure 6-29. Gas and inertial rod loads as a function of crank angle (courtesy of Wood.).

6.2.11 Design Standards

Design considerations for reciprocating compressors are generally covered in API 618 [13] with additional information on lubrication systems covered in API 614 [15]. Most design aspects are quite straightforward except for pulsation and vibration control. These are covered further in chapters 11 and 12.

By its very nature, a reciprocating compressor produces regular pressure pulses on both the suction and discharge sides of the compressor. The shape of the pulse is affected by the piston velocity (almost sinusoidal depending on the ratio of the connecting rod length to the crank radius) and the effect of the valve action on the flow. The resulting frequency spectrum shows both odd and even harmonics of the rotating speed. In theory, for a double-acting cylinder, the odd frequencies should cancel out but cylinder differences usually result in all harmonics being present. Additional mechanical vibration occurs due to the reciprocating inertial forces of the compressor and cylinder stretch.

Pulsation produces significant dynamic forces on piping and vessels that leads to excessive vibration levels and failure due to fatigue. If the pulsation frequencies happen to coincide with a mechanical natural frequency, the forces are amplified dramatically. The optimum approach is to carry out acoustic, mechanical, and vibration studies that incorporate all aspects of a design including the foundation; compressor; and its associated piping, vessels, and supports. API 618 [13] provides guidance on what is appropriate for various situations. This guidance has changed significantly with successive editions, and the latest fifth edition incorporates more detailed guidelines [16].

A recent development is the recognition that pulsation attenuation devices can significantly affect overall performance [17]. An acoustic study in conjunction with a complete performance analysis can identify areas of operation that should be avoided based on such issues as excessive static and dynamic pressure drop, inadequate rod reversal, and rod loading. The resulting safe load steps and operating conditions can then be programmed into the unit control and compressor performance software.

6.3 CENTRIFUGAL COMPRESSORS

6.3.1 General Design

Centrifugal compressors are the most common compressor type used in gas transmission service. By using single or multi-stage compressors and series and/or parallel compressor configurations, a wide range of flow and head conditions can be achieved. A typical compressor installation is shown in Fig. 6-30 and features a barrel-type design that is preferred over the horizontally split approach found more commonly in process applications. The preference for the barrel compressor is based on its ability to handle higher pressures and the flexibility adapting the internal design for different applications.

Beam-type compressors have bearings on both sides of the impeller and are the most common design because the internals can easily be modified and changed out between single and double-stage impellers. An overhung compressor is supported by bearings on one side only as illustrated in Fig. 6-31 so that the inlet is unimpeded by a protruding shaft. This type of design can also have an axial inlet that improves the efficiency by approximately 2–3%.

A less common but promising design is that of the hermetic compressor, which is oil-free and does not require sealing (Fig. 6-32). This is accomplished by containing the electric motor driver along with the compressor in a sealed chamber with the shaft supported by magnetic bearings. Several manufacturers have designed and put into operation this type of compressor, but its acceptance has been gradual. It may not replace larger compressors and is limited to locations with available electric power but otherwise is a more acceptable



Figure 6-30. A typical barrel-type centrifugal compressor.



Figure 6-31. A typical overhung centrifugal compressor.

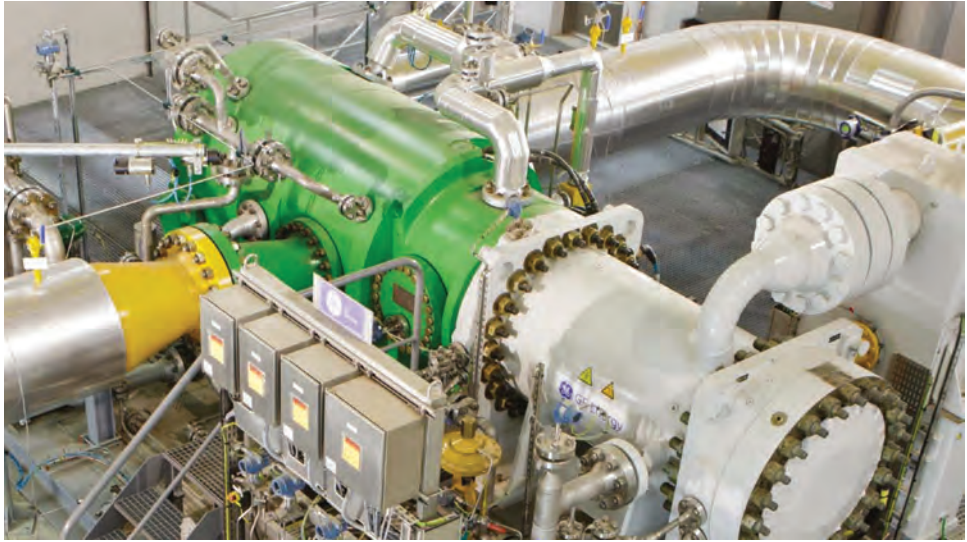


Figure 6-32. ICL – Integrated Compressor Line hermetically sealed pipeline compressor (courtesy of GE Oil & Gas).

environmental solution in inhabited areas. Maintenance is simpler because fewer auxiliary systems and components are involved, and downtime can be minimized because the whole module can be removed and replaced in a short time period [18].

The centrifugal compressor is basically a simple machine that consists of a rotating shaft on which is mounted one or more impellers. The flow is guided into the eye of the impeller by a suction volute. At the exit of the impeller, the gas enters a diffuser to further increase the pressure and is guided by a stator either into the next stage or into the discharge volute.

Figure 6-33 illustrates an example of new-generation compressors which have a more aerodynamic flow-oriented inlet housing and discharge volute, to assist in moving flow in and out of the compressor body with reduced losses. These plus improvements to the aerodynamic design of impellers and stationary inter-stage stationary vanes, help to improve both efficiency and the flow range (head/flow curve width). Also, these modern designs include mechanical improvements which address issues such as the use of full flanges allowing the use of studs with two nuts (rather than machined ports with threaded holes for stud insertion/single nut on the external side of pipe flange). Other features include fully removable assembled aero bundles, standard dry seal designs and increased pressure rating capabilities.

A specialized type of centrifugal compressor is the integrally geared compressor. It consists of a number of single-stage compressors in series with intercooling between the stages for efficiency and reduction of discharge temperature. It is used for very high pressure ratio applications such as the initial compression required for CO₂ pipelines where the suction pressure is close to atmospheric pressure (see Section 6.5).

Krain [19] has undertaken a full review of the development and application of centrifugal compressors. His review historically describes the application and development of the centrifugal compressor from the very beginning of its introduction until today. It focuses on selected practical and theoretical examples that have pushed the centrifugal standard from simple, low-efficiency designs to its current high-level status.

6.3.2 Compressor Internals and Sealing

The centrifugal compressor is made up of a stationary section, consisting primarily of the casing and gas passage components, and a rotating component (Fig. 6-34). The casing

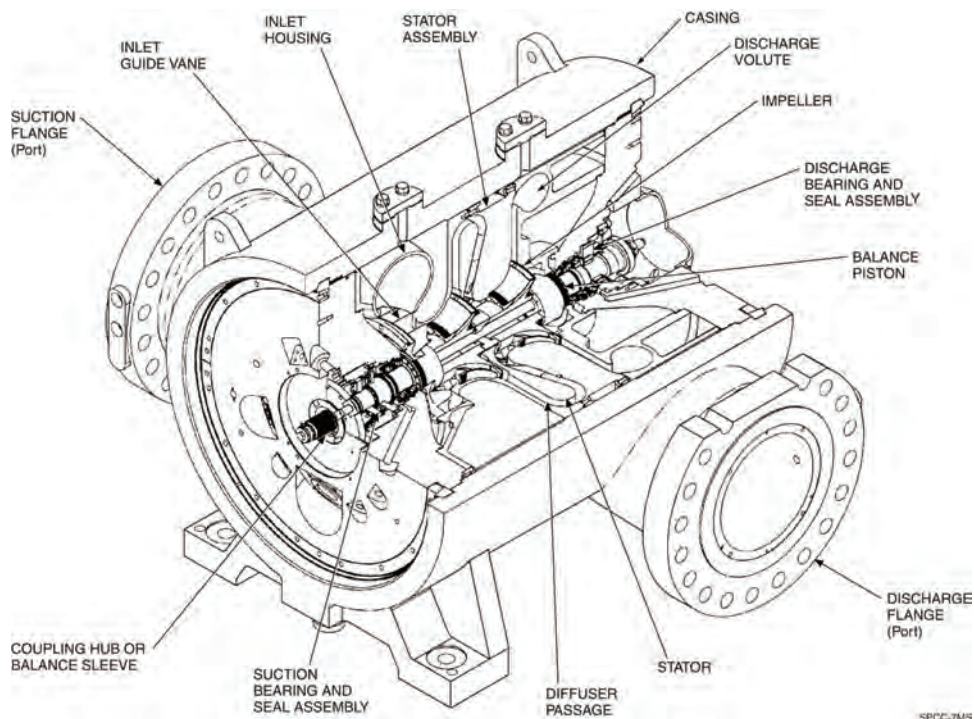


Figure 6-33. Typical centrifugal compressor design (courtesy of Solar Turbines Incorporated).

provides an enclosure for the high-pressure gas and gas passage components and consists of pieces of metal that have been precast or molded. Access is through an end cover (radial split) or by lifting the top half of the casing (axial split). The gas passage components direct the gas flow within the casing.

The rotating section or rotor consists of the shaft and impeller(s). One or more impellers are fitted onto the shaft and keyed to prevent rotation on the shaft. These impellers may be closed or semi-closed. The shaft extends through the casing, providing a means of transferring the power developed by the driver to the impeller(s). It is usually fitted with a flexible coupling on the driven end to connect it to the driver. This coupling prevents the transfer of torsional vibration and compensates to some degree for misalignment between the driver and the compressor.

Shaft seals are required where the rotor pierces the casing. These seals are either dry gas seals or oil-buffered seals. The rotor is supported at two points by oil-lubricated journal (radial) bearings (see Fig. 6-34) or active magnetic bearings (see Fig. 6-35). Thrust bearings constrain the rotor in the axial direction to counteract thrust forces and keep the rotor in a reasonably constant position to prevent rubbing of internal seals.

Labyrinth seals are located at the eye of the impeller and between stages to minimize leakage (shown in Fig. 6-36). Since the pressure rise across a stage is divided between the impeller and the diffuser (see Section 6.3.6.1), the pressure differential at the impeller eye labyrinth seal is the difference between the pressure at the exit of the impeller P_2 and that at the suction P_1 (see Fig. 6-37). Likewise, the pressure drop across the spacer labyrinth seal is the difference between the suction pressure of the next stage P_3 and the impeller exit pressure of the previous stage P_2 .

From Fig. 6-37, it can also be seen that a thrust force is generated by the pressure differential across the impeller. The net force is in the direction of the eye of the impeller and increases with the number of stages as long as they face in the same direction. For this reason, for multiple stages (usually more than 3), impellers are designed back to back, which mostly

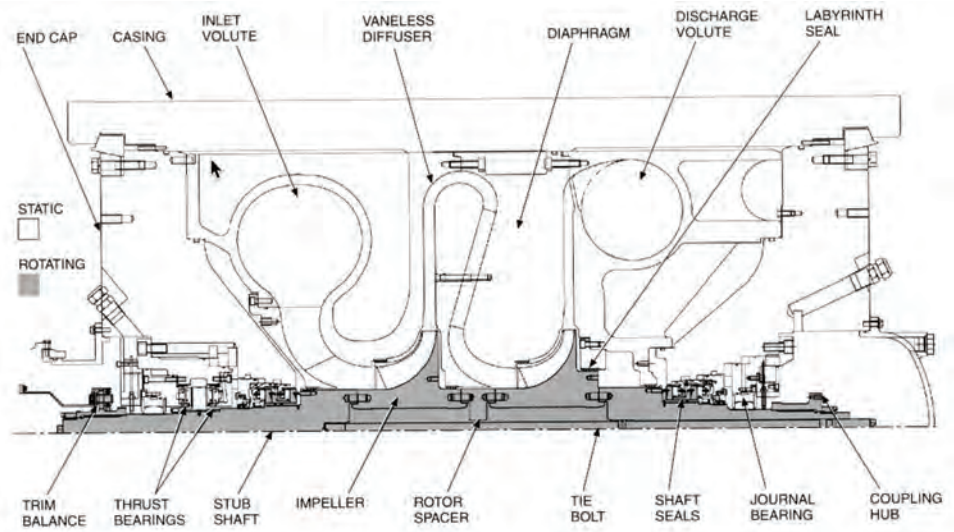


Figure 6-34. Typical centrifugal compressor cross section (courtesy of Solar Turbines Incorporated).

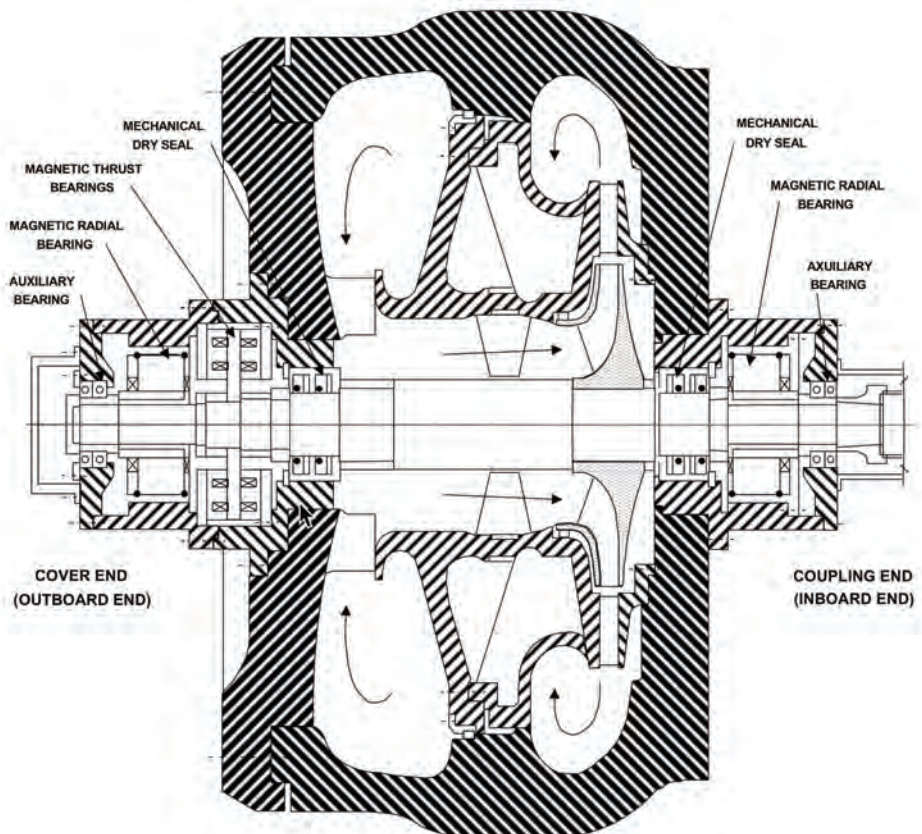


Figure 6-35. Internal design of a beam-type centrifugal compressor with magnetic bearings.

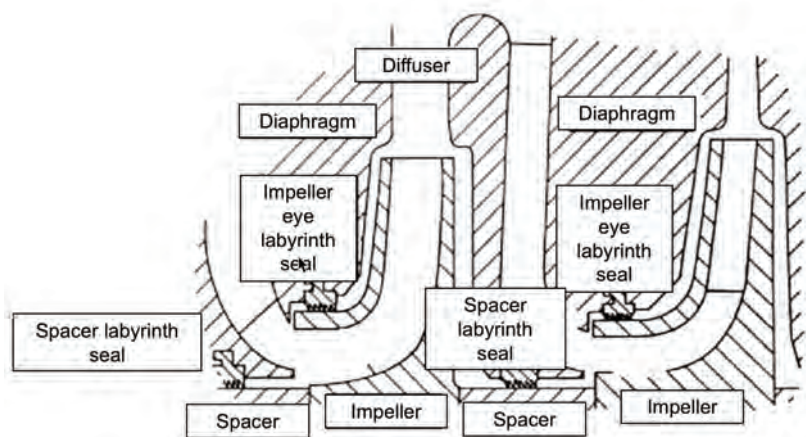


Figure 6-36. Internal seals in a centrifugal compressor (courtesy of Dresser-Rand).

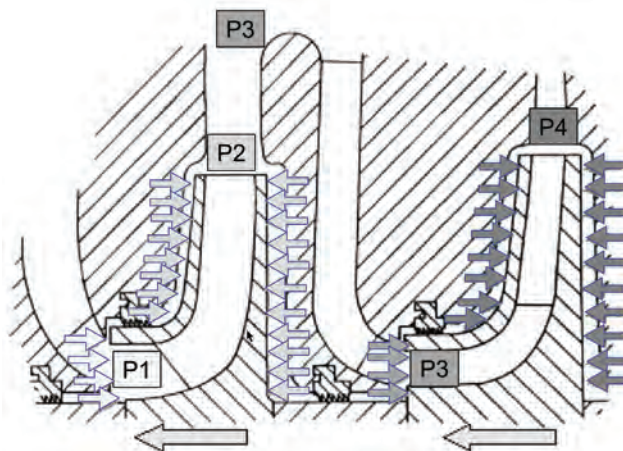


Figure 6-37. Thrust force due to pressure in a two-stage centrifugal compressor (courtesy of Dresser-Rand).

cancels the thrust force (note that there is still a net thrust force because the pressures in each stage are different). However, this type of design is not common for pipeline compressors.

It is normal to place a balance piston (also known as a balance drum) on the discharge of the last impeller to reduce the force thrust that has to be handled by the thrust bearing (see Fig. 6-38). It consists of a disk fitted to the shaft with impeller discharge pressure from the final stage on one side and suction pressure on the other side, separated by a labyrinth seal, so that the net force counteracts that of the impeller thrust force. Overhung compressors usually do not have a balance piston and compensate by having a larger thrust bearing.

There are two philosophies with respect to balance piston design. One approach is to design the balance piston so that the balance piston force is less than the impeller thrust. The thrust bearing takes the remainder of the load for all operating conditions and the axial position of the rotor is relatively fixed. The other method is to size the balance piston for a greater force than the impeller thrust so that the thrust bearing is unloaded as the labyrinth seals deteriorate.

Advances have been made in the accurate calculation of axial thrust, which is particularly important for medium and high pressure applications [20]. Failure to implement a proper design can result in high thrust bearing temperatures and ultimately in thrust bearing

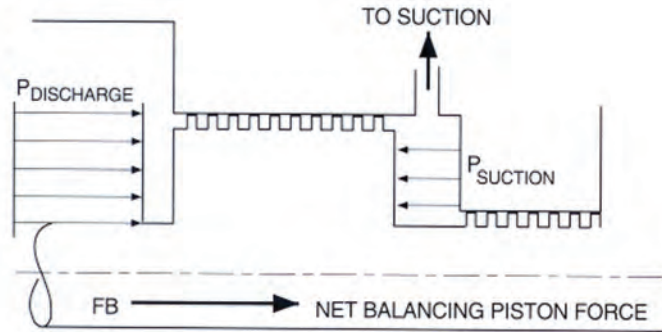
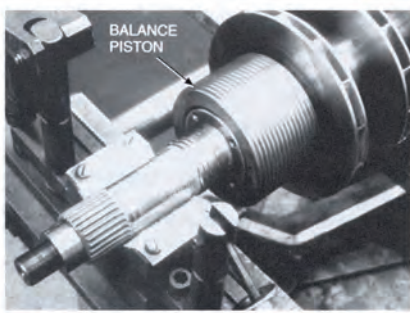


Figure 6-38. Balance piston forces (courtesy of Solar Turbines Incorporated).

failures. The main component of axial thrust design relates to the proper sizing of the balance piston. Since a major part of axial thrust is dependent on the pressures around the impeller, axial thrust varies across the performance map and is dependent on flow from surge to choke and pressure ratio from lowest to highest. Recent investigation of axial thrust during choke identified the need to consider this in balance piston design [21]. According to API 617 [22], calculations should be performed at twice the maximum clearances to accommodate the inevitable wear of the labyrinth seals of the balance piston and impellers. There are other factors that need to be considered for accurate calculation of axial thrust that are now beginning to be better understood [20].

6.3.3 Bearings and Lubrication Systems

6.3.3.1 Bearings

Most pipeline compressors use hydrodynamic bearings of the tilting pad type because they are better suited to carry the static and dynamic loads than antifriction bearings, which would be too massive for anything but the smallest compressors. Tilting pad bearings have successfully eliminated the oil whirl problems that were prevalent with the plain journal bearings used in early centrifugal compressors. Bearings for an overhung compressor are located as shown in Fig. 6-39 on the driven side of the compressor, while a typical arrangement for a beam compressor is provided in Fig. 6-35 (this figure shows magnetic bearings but the bearing location is the same regardless of the bearing type).

Although standard journal bearings have been used in the past, the most common type of bearing used for centrifugal compressors today is the tilting pad bearing. Figure 6-40 shows a Solar bearing that has five tilting pads on individual pivot pins. A tilting pad thrust bearing can be seen in Fig. 6-41. The tilting pads are self-equalizing where each pad rotates to generate a wedge-shaped load-carrying oil film. The theory behind tilting pad bearings is covered in [23] while the current practical application is extensively discussed in [24].

Conventional tilting pad are of a flooded design where the oil is supplied to the bearing through orifices between the pads with end seals to reduce axial leakage. This does not effectively provide cool oil to each pad with some of the oil coming from the upstream pad, leading to higher than desired oil temperatures at the pad inlet. This has led to the development of designs that direct the cool oil to the inlet of each pad with experimental investigations verifying their effectiveness [25].

The application of magnetic bearings to pipeline compressors was pioneered mainly in the NOVA Gas Transmission system in Alberta, Canada in the 1980s. With the resolution of some early control issues, these compressors have exceeded 25 years of reliable operation. The main advantage is that it eliminates the need for a lubrication system, reducing control

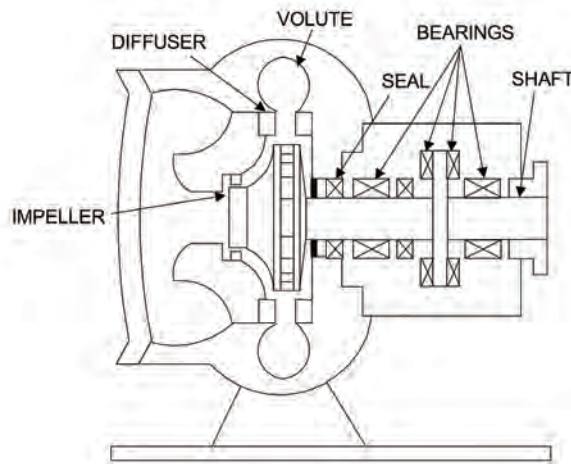


Figure 6-39. Internal design of an overhung centrifugal compressor.

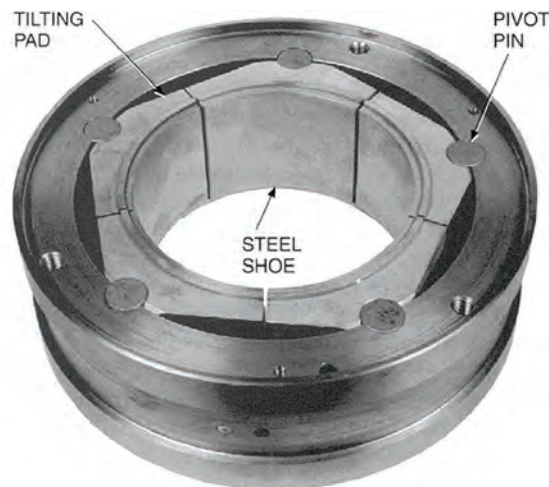


Figure 6-40. Typical radial tilting pad bearing (courtesy of Solar Turbines Incorporated).

system complexity, improving safety by the elimination of lubricant, and simplifying maintenance to a few minor tasks. It also improves overall efficiency by 2% to 3%, which reduces life cycle cost and enables active rotor shaft control that can be used to tune rotordynamics and reduce vibration. The primary reason for its lack of acceptance is the increased capital expenditure, although the total life cycle cost is less. A Net Present Value (NPV) analysis of a 25 MW motor-compressor indicates a potential savings of over \$500,000 at 95.7% certainty over tilt-pad bearings which can be used to justify the higher capital cost [26]. So far, it is mainly gaining acceptance in hermetically sealed compressors and specialized applications such as sub-sea compression, but ultimately, it is still a viable alternative for hydrodynamic bearings and oil systems.

A potential rival to both hydrodynamic and magnetic bearings, the air bearing, has emerged as an additional solution to certain turbomachinery applications [27]. Air bearing technology is not new but the development of a porous substrate to provide an even pressure distribution of air (or other gases) instead of the previous orifice method is key to

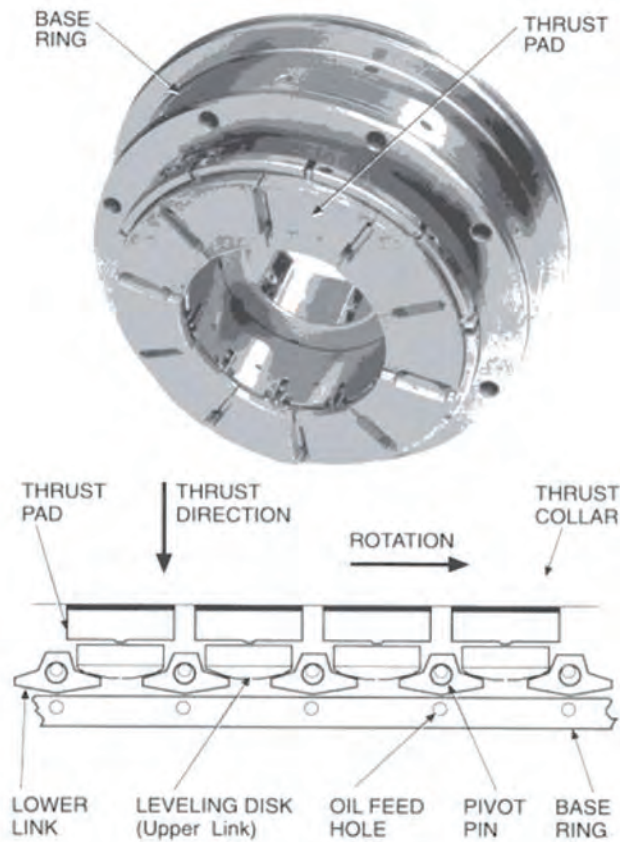


Figure 6-41. Typical tilting-pad thrust bearing (courtesy of Solar Turbines Incorporated).

its application (Fig-42). It offers external control over damping and stiffness as does the magnetic bearing, and as previously worked on by the Bently Pressurized (orifice) Bearing Company [28]. A comparison of gas bearing technology with those for magnetic and hydrodynamic bearings is shown in Fig. 6-43.

6.3.3.2 Lubrication System

The lube oil system supplies cooled and filtered oil at controlled pressure to lubricate and cool the journal and thrust bearings on a centrifugal compressor (and, sometimes, its driver). A typical lube oil system (Fig. 6-44) consists of a lube oil tank or reservoir, main lube oil pump, auxiliary lube oil pump, lube oil circulating pump, emergency DC lube oil pump, lube oil cooler, lube oil filters, and pressure control valves.

A lube oil tank maintains a reserve of oil for the system. The tank may be equipped with heaters (electric or glycol tubes) that keep the oil warm during shutdown periods. Level switches and sight glasses are mounted on the tank to ensure an adequate quantity of oil.

A main lube oil pump is usually driven off the gearbox on the compressor or power turbine shaft. This pump delivers oil at required volumes and pressures when the unit is running at various operating speeds. The auxiliary lube oil pump is usually electric motor driven. It supplies lubricating oil while the unit is starting or stopping until the main pump reaches operating speed, or while the unit is running and the oil pressure drops below a pre-set value. The lube oil circulating pump is also normally electric motor-driven and circulates a small amount of oil through the system when the unit is shut down to keep the bearings



Figure 6-42. Visual view of even pressure distribution from porous tilting pad (courtesy of New Way Air Bearings).

	Ext Pressurized Gas Bearing Technology	Mag Bearing Technology	Oil Bearings
Oil-free operation	Yes	Yes	No
Operable in process gas stream in bearing gap	Yes	Yes/No	No
Anticipate operability on steam in the bearing gap	Yes	No	No
Wear	None	None	Yes
Bearing contact at zero rpm	No	No	Yes
Control system needed	<i>None or minimal</i>	Yes	Yes
Back-up bearings needed	<i>No</i>	Yes	No
Overall turbo equipment system footprint, compared to when using hydrodynamic bearings	Less	Less	NA
Cost compared to hydrodynamic bearings	<i>Similar</i>	Higher	NA
Damping and stiffness, compared to hydrodynamic bearings	Similar—done by controlling gaps	Controlled electronically	NA
Complexity compared to oil bearings	<i>Simpler</i>	More complex	NA
Physical size of bearings, compared to oil brgs	<i>Similar</i>	Larger	NA
Compatibility for retrofitting into existing turbo equip	<i>Compatible</i>	Not always compat	NA
Load carrying capacity compared to oil bearings	400 psi*	70–80 psi	>200 psi
Can function as bearing and seal simultaneously	Yes	No	No

* Under certain circumstances

Figure 6-43. Comparison of bearing technologies (courtesy of New Way Air Bearings).

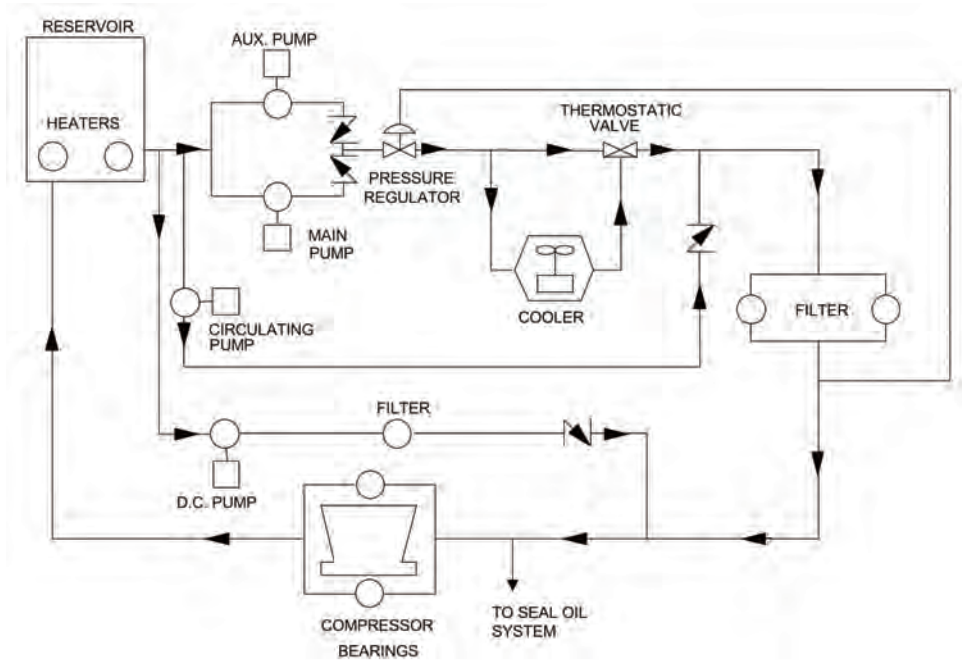


Figure 6-44. A typical lube oil system.

warm. The emergency DC lube oil pump is driven by backup power (DC) and is used only if there is a power failure to provide sufficient lubrication until the unit coasts to a stop.

A thermostatic control valve diverts some or all of the oil to a lube oil cooler in order to keep the temperature of the oil going to the bearings within set limits. There are two types of lube oil coolers. One is an aerial heat exchanger, with tubes for the oil to flow through and a fan that forces air over the tubes to cool the oil. The other is a shell and tube heat exchanger, which passes a glycol-water solution over the oil tubes. The glycol water solution is then cooled by an aerial heat exchanger.

A dual-filter system with full-flow transfer valve allows a clean filter to be put in operation while the other filter is being serviced. This avoids shutting the unit down to switch filters.

Pressure control valves regulate the oil pressure to the required value [normally 200–280 kPag (30–40 psig)]. Pressure relief valves (not shown) prevent the lube oil system from overpressurizing by returning excess oil to the tank.

Some compressors have resistance temperature detectors embedded in the bearings to indicate the temperature of the bearings.

6.3.4 Sealing System

6.3.4.1 General

The sealing system prevents escape of pipeline gas along the rotor shaft where it pierces the compressor casing. For beam compressors, two seals are required, while for an overhung compressor, only one seal is needed (see Figs. 6-35 and 6-39).

Pipeline compressors have traditionally used wet seal systems, but in the 1980s, dry gas seals were introduced and, since then, have almost entirely replaced wet seal systems for new compressors and also many existing ones through retrofits.

As many as 80% of all unsuccessful compressor starts can be attributed to seal oil system malfunctions. By using gas as the sealing medium, dry gas seals eliminate the need for conventional seal oil systems, reducing maintenance costs, downtime, and power losses.

Dry gas seals are simpler, safer (e.g., less risk of fire), less expensive, and more reliable. In addition, gas loss can be reduced as much as 97%, with the resultant gas saved providing a payback of 1 to 2 years on a retrofit [29]. Recent developments have been aimed at recovering remaining gas loss through the use of a supersonic injector [30] (see Section 13.5). In addition, there are new designs for gas seals under development that, in conjunction with aerostatic bearings, may revolutionize sealing systems again (see Section 6.3.4.4).

6.3.4.2 Wet Oil Seals

Despite the fact that wet seals are mainly being replaced by dry gas seals, many machines remain in operation and in limited applications; they are still being installed, although rarely for pipeline situations. It is therefore important to retain understanding of their design and operation [31].

Sealing is done in two stages with labyrinth seals and floating ring oil seals (Fig. 6-45). Labyrinth seals are mounted on the casing or are attached to the rotor and are designed to keep the seal oil from leaking into the compressor. They are single or two-piece sleeves that have multiple, sharp-edged ridges. The multiple ridges act as a series of restrictions that inhibit the passage of gas and/or oil.

Floating ring oil seals and high-pressure seal oil provide the actual seal between the rotating rotor shaft and the compressor casing. The seals are located where the shaft pierces the casing and are designed to fit very close to the shaft without touching it.

High-pressure seal oil is injected between the floating rings in each seal, and it seals, lubricates, and cools the floating ring faces. A seal oil differential pressure control valve is used to keep the injected seal oil at a certain differential pressure [70–345 kPa (10–50 psid)] above the pipeline gas pressure, thus preventing the escape of pipeline gas to the atmosphere.

The injected seal oil leaks between the floating rings and the rotor shaft. Most of the oil leaks outward towards the atmosphere, as the outer floating ring sees an oil differential

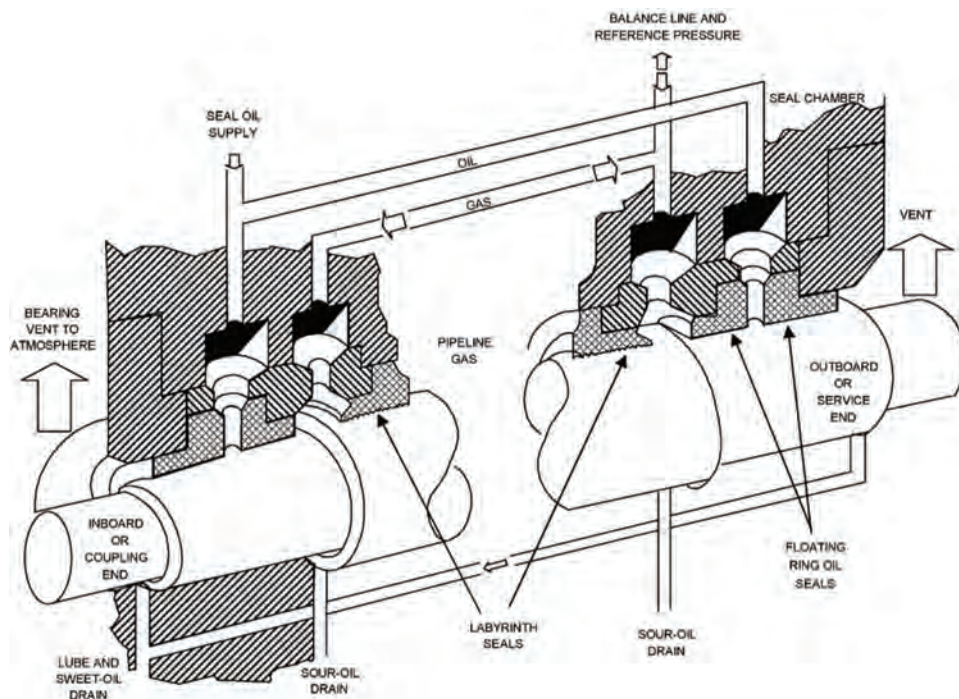


Figure 6-45. Wet seals for a beam-type compressor.

pressure of pipeline gas pressure plus the seal oil differential pressure. This outer seal leakage is considered “sweet” and normally drains back to the oil reservoir with the bearing oil.

A smaller flow of the injected seal oil leaks inward towards the pipeline gas, as the inner floating ring sees only the seal oil differential pressure across it. This inner seal leakage mixes with the pipeline gas at pipeline gas pressure, where the oil absorbs some of the gas.

Seal oil that has become contaminated with gas is called “sour oil.” The gas must be removed from the oil before it returns to the oil tank. This is accomplished by depressurizing it in seal oil drainers, and by allowing it time to effervesce the gas in a degassing tank.

The high-pressure seal oil is usually cooled and filtered lube oil, which has been pressurized to pipeline gas pressures (plus seal oil differential) by either the main or auxiliary seal oil pumps (Fig. 6-46). The main seal oil pump is usually driven off the gearbox on the compressor or power turbine shaft, and the auxiliary seal oil pump is usually electric motor driven.

When the unit is to be started, the auxiliary lube oil pump comes on first to lubricate the bearings and supply oil to the seal oil system. Then, the auxiliary seal oil pump comes on to fill the overhead seal oil tank and to establish the seal at the floating rings. After that, the compressor casing is purged and pressurized, the unit suction and discharge valves opened, the unit driver started, and the main seal oil pump takes over (with the auxiliary seal oil pump on stand-by).

If the main seal oil pump is unable to maintain the seal oil differential pressure and/or the oil level in the overhead tank, the auxiliary seal oil pump comes on to assist. If the seal oil differential pressure and/or the oil level continues to fall, the unit goes into emergency shutdown, and the compressor casing is isolated and vented to atmosphere. The overhead seal oil tank supplies high-pressure oil during this period, as it is mounted above the compressor and is pressurized by pipeline gas from the compressor. Gas is sometimes separated from the oil by a bladder so that the oil does not absorb gas.

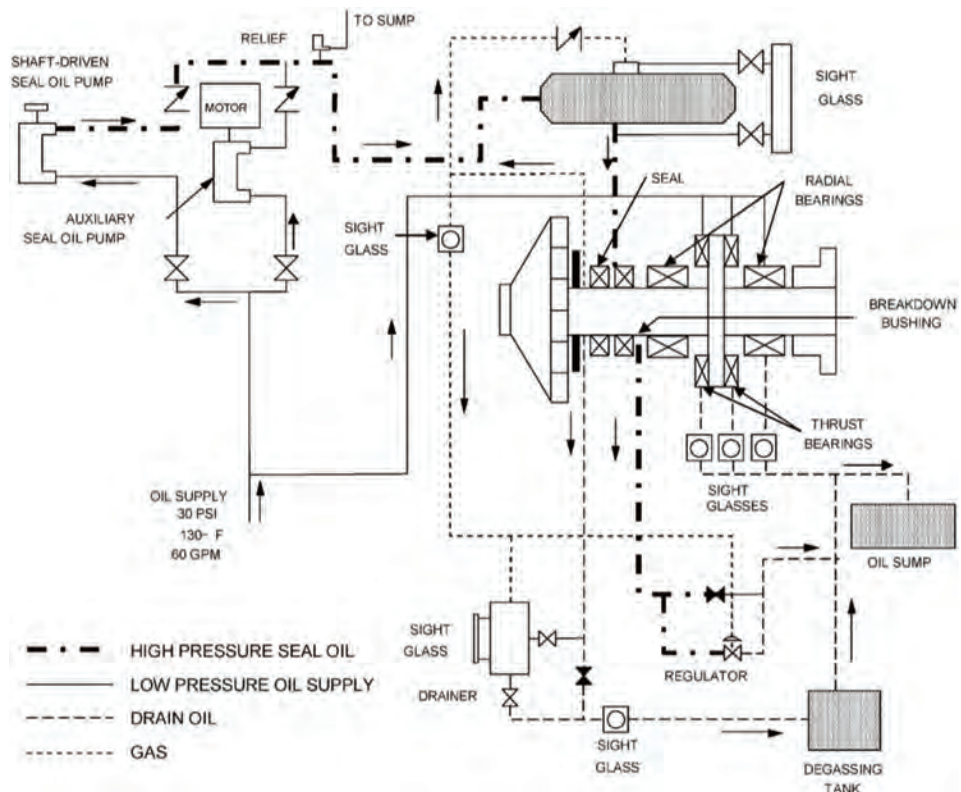


Figure 6-46. A typical wet seal system.

6.3.4.3 Dry Gas Seals

The mechanical dry seal consists of three components—a main seal, a backup seal, and a safety barrier (Fig. 6-47). The main and backup seals are usually identical. Both are designed to withstand full differential pressure at full speed. Under normal operating conditions, the compressor pressure is sealed by the main seal only, while the backup seal is completely unloaded and provides one hundred per cent backup. This is a feature that standard seal oil systems do not provide.

The safety barrier is usually a labyrinth seal split in two sections with an inert gas or air purge port in the middle to provide additional protection. The safety barrier restricts the amount of gas escaping from the seal cavity under emergency situations. It also prevents any mixing of oil and gas under normal operating conditions.

Each of the main and backup seals combine a rotating ring with grooves on its face and a stationary ring. During operation, there is no contact between the rings, as both components maintain an equilibrium position a few micrometers apart. Grooves in the upper diameter of the rotating seal produce hydrodynamic forces that maintain separation between the faces during operation. The inner diameter acts as a seal dam. Seals are either uni-directional (Fig. 6-48(a)) or bi-directional (Fig. 6-48(b)). The advantage of the bi-directional design is that the seal functions in either rotational direction and can be installed on either side of a beam-type compressor. The uni-directional design allows for lift-off at lower speeds, low-pressure hydrostatic lift, and better film stiffness performance.

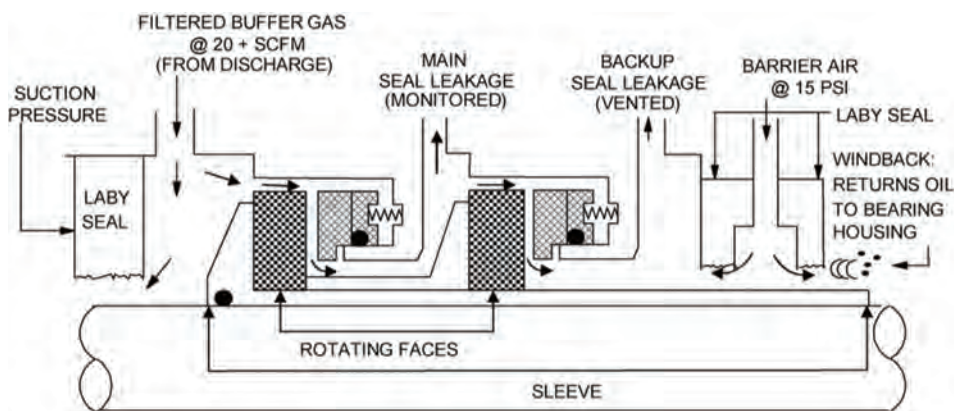
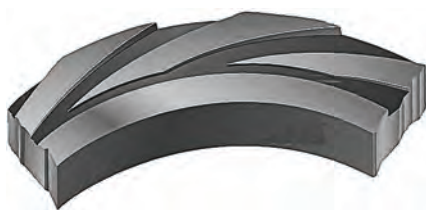


Figure 6-47. A tandem dry gas seal.



(a)



(b)

Figure 6-48. Types of seal face design: (a) Uni-directional; and (b) Bi-directional (courtesy of Flowserve).

The gap between the seal faces is established by balancing the hydrostatic and hydrodynamic forces. The hydrodynamic forces (which act to open the seal) are dependent on the compressor speed, the gas, and the gas viscosity. The hydrostatic forces (which act to close the seal) are determined by the gas pressure in the compressor casing.

A control panel for the mechanical dry seals (Fig. 6-49) ensures a clean gas supply is provided to prevent potentially dirty gas from entering the seals. It also monitors the gas leakage through the seals, providing alarms and shutdowns in the event of a problem.

Two methods are available to control the dry gas seal: differential pressure control and flow control [32]. Differential pressure systems [Fig. 6-50(a)] regulate the seal gas supply pressure by means of a control valve to a pressure usually set at 10 psi above a reference pressure. This essentially controls the flow of gas through the labyrinth seal that can sometimes result in higher flows across the inner labyrinth seal since normally very little supply gas flows through the primary seal. Especially for higher-pressure applications, this may lead to excessive recycling of seal gas which is inefficient. Flow control systems [Fig. 6-50(b)] ensure that the supply flow to the seal is maintained at a certain value regardless of the labyrinth seal clearances and thus are preferable.

Maintaining seal gas quality is the most important factor in ensuring dry gas seal reliability. Due to the very small gap between the seal faces, particulates should be less than 3 microns. A continuous supply of clean gas should be available for all modes of operation, including starts, stops and times of low head across the compressor (<30 psig). Since control panel filters are capable of removing only 0.05% of entrained liquids, a liquid knockout may need to be installed upstream of the seal panel. The temperature of the supply gas should be at least 20°C above its dewpoint.

The dry seal system that supplies gas to the seal and vents it is basically quite simple (Fig. 6-51). A dry seal panel is normally installed to handle seal gas supply and venting

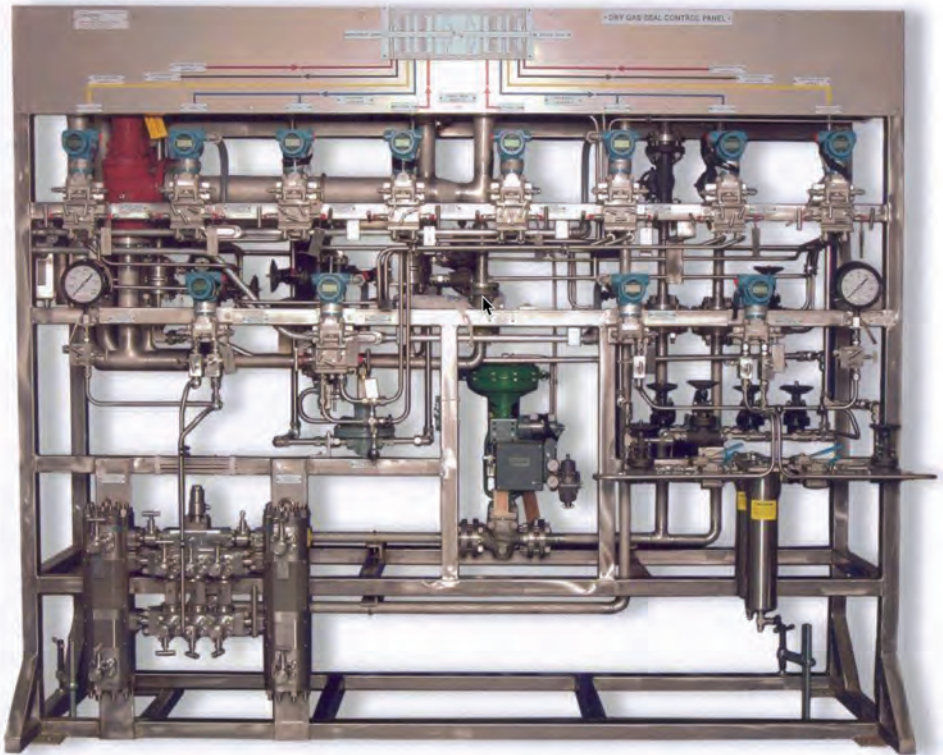


Figure 6-49. Dry gas seal control panel (courtesy of Flowserve).

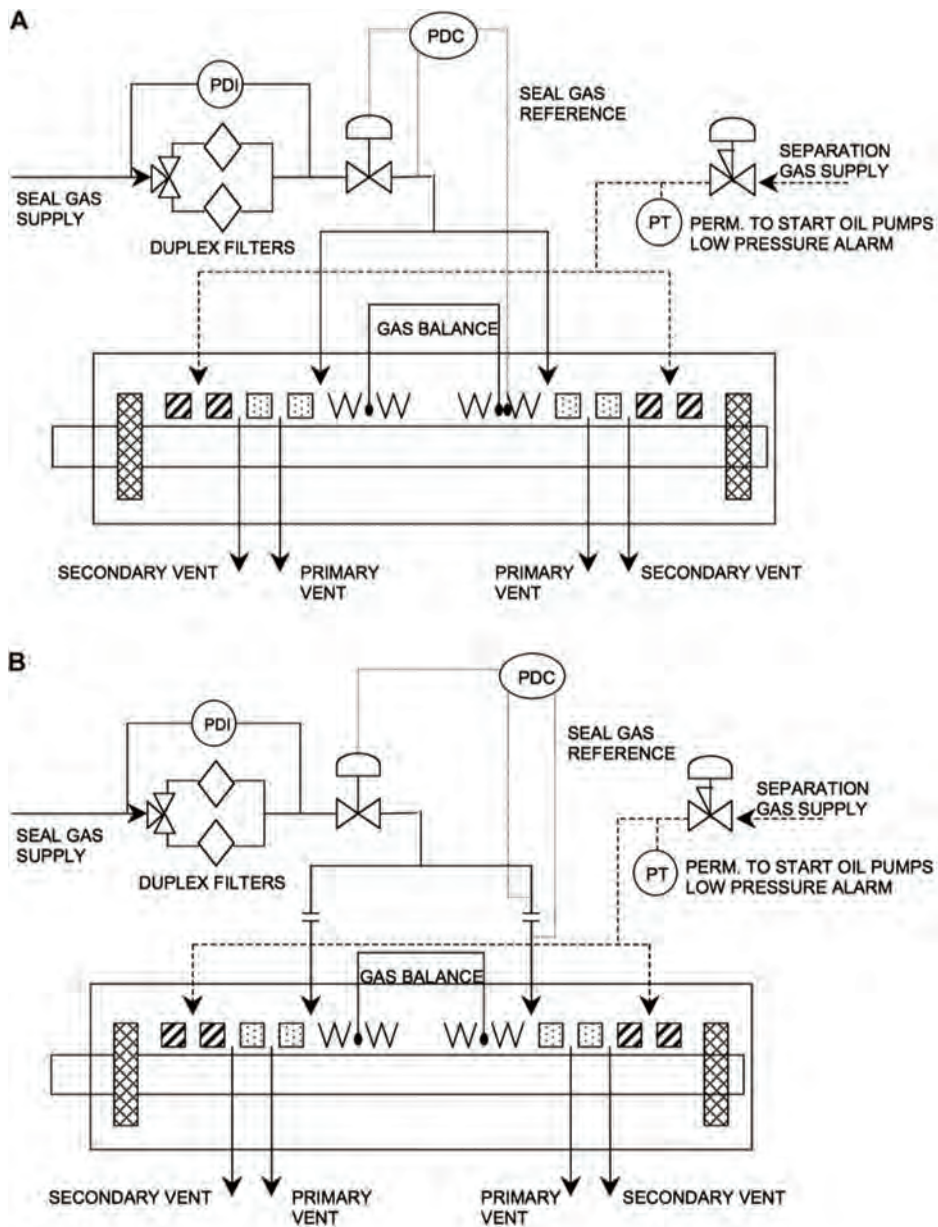


Figure 6-50. Dry gas seal control (a) based on differential pressure (b) based on flow (courtesy of Dresser-Rand).

control and monitoring. It first filters the supply gas from the discharge and regulates the pressure to the seal. The flow of the return gas is monitored since an increase in flow will indicate seal wear and failure. An alarm is placed on the filter differential pressure and an alarm and shutdown are placed on the leakage flow to protect against seal failure.

A typical design for ensuring an adequate supply of clean gas is shown in Fig. 6-52, known in this case as an Ampliflow™. It features a reciprocating air drive, boosting compressor (also called an intensifier) to increase the pressure of the available filtered gas if the supply drops to below the required pressure. A separator called the CleanPac™ may be installed to remove liquids and contaminants.

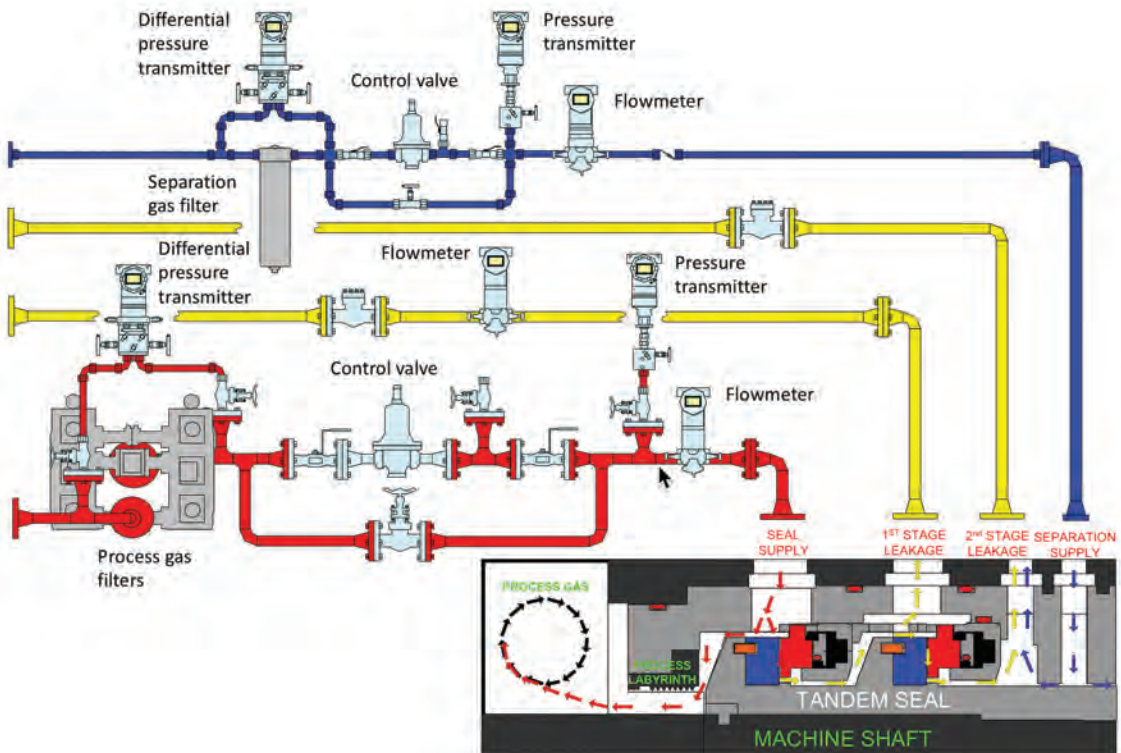


Figure 6-51. Dry gas seal system (courtesy of Flowserve).

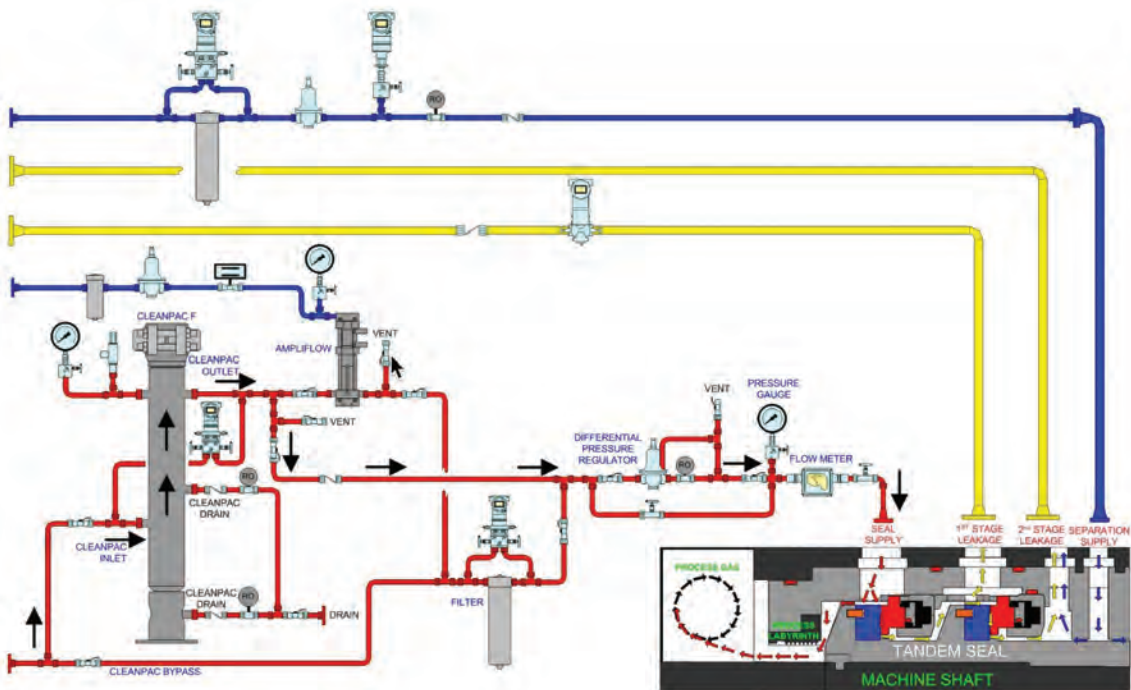


Figure 6-52. Dry gas seal protection system (courtesy of Flowserve).

6.3.4.4 Emerging Gas Seal Technology

In conventional dry gas seals, process gas is introduced into the seal cavity. A small amount flows across the seal while the majority of the gas returns to the compressor. The gas flowing across the seal goes from a high pressure to a low pressure, which results in the danger of liquids forming and damaging the seal (Fig. 6-53).

Emerging technology utilizes Externally Pressurized Porous (EPP) Gas Bearing Technology [33] with a porous seal face to create a pressure in the seal gap higher than the process pressure (Fig. 6-54(a)). No liquid can enter the seal face since the seal pressure is higher than the process pressure and the pressure drop across the porous seal face is very small so no liquids can drop out with a modest dew-point difference. The net flow back into the process is also much less than for a conventional seal.

With a small modification, the seal can be segregated with both a process gas and barrier gas supply (Fig. 6-54(b)), resulting in a “Zero Emissions Seal (ZES)”.

6.3.5 Controls and Monitoring

The control system for a centrifugal compressor is tightly integrated with the driver and process control system and is usually implemented in a PLC-based network.

Major control-related functions consist of:

- performance control: maintaining a process variable, usually discharge pressure set point but could also be suction pressure or flow
- surge control: preventing compressor surge by opening a recycle valve



Figure 6-53. Conventional dry gas seal (courtesy of New Way Air Bearings).

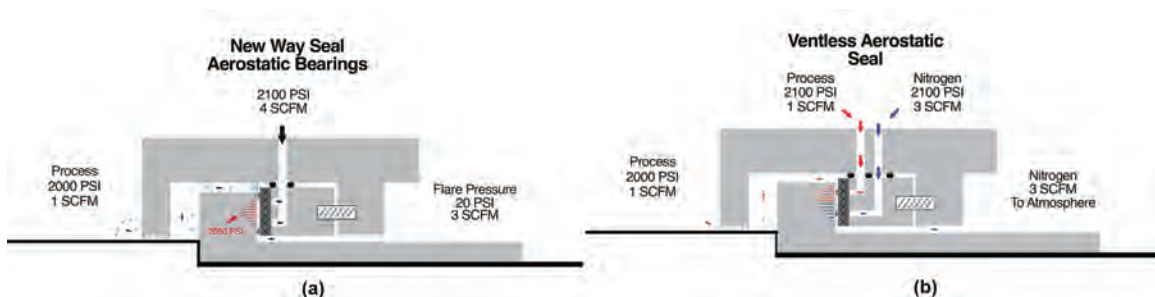


Figure 6-54. (a) A New Way seal (b) A zero-emissions seal (courtesy of New Way Air Bearings).

- limit control: limiting parameters, normally minimum and maximum speed and
- discharge temperature for the compressor and limits due to the driver
- load balancing and optimization: managing the control of several compressors to maximize efficiency
- protective control: protecting the compressor by alarms and shutdown for critical mechanical parameters such as bearing temperatures and vibration
- event sequencing: startup and shutdown sequencing

The most important and unique aspect of centrifugal compressor control is the surge system. One of the limits of a centrifugal compressor is that its flow cannot be allowed to be reduced past a minimum point that varies with the pressure rise across the compressor (see Fig. 6-55). As the operating point moves to the left due to changing process conditions, the pressure ratio across the compressor becomes too much and the flow reverses, first locally in a part of the impeller (known as stall) and then progressively across the entire compressor. The pressure ratio now decreases until positive flow is again established. The flow then increases rapidly until equilibrium is restored. The cycle time is often quite short, in the range of milliseconds. The frequency of surge is dependent on the downstream capacity with a small capacity increasing the frequency of oscillation. The violence of surge increases with pressure. For a single stage, surge normally occurs at approximately 60% of the design point where the slope of the speed line becomes positive. It is about 70% for multistage compressors.

At the beginning of surge, referred to as incipient surge, vibration increases, and pressure and flow start to fluctuate. These symptoms become much worse as surge deepens and without intervention usually leads to a massive failure with severe damage to bearings, dry gas seals, labyrinth seals, internals, and the impeller.

There is still considerable discussion and research around the whole phenomenon of stall and surge. Stall is the precursor to surge or complete reversal of flow. Stall can occur

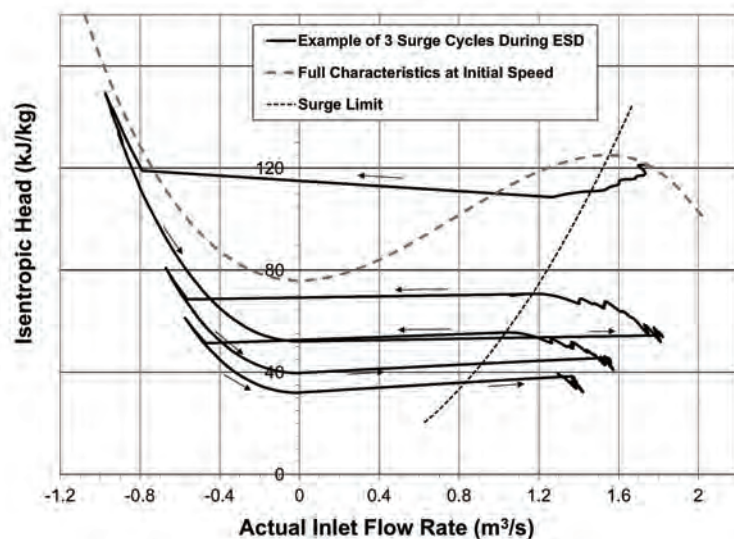


Figure 6-55. Effect of surge on a compressor.

in both the impeller and diffuser. In fact, where the surge line is normally defined, it is probably more correct to infer that a significant stall situation is occurring, and not flow reversal. This issue is more fully dealt with in [34].

A typical surge control system is shown in Fig. 6-56. Inputs to the surge control are flow, suction pressure, and discharge pressure. A control line is established usually at 10% to the right of the estimated or tested surge line (see Fig. 6-57). When the operating point reaches the surge control line, the recycle valve begins to open. Some of the discharge flow recycles

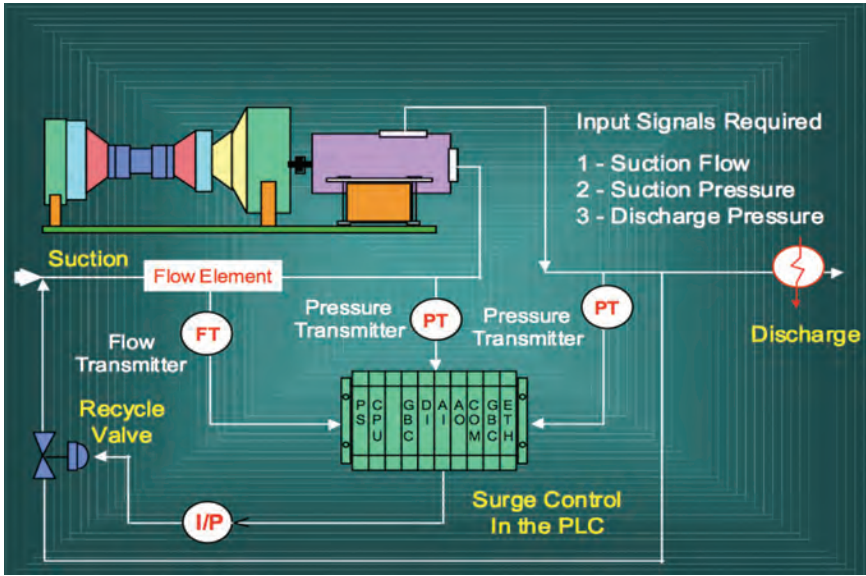


Figure 6-56. A typical surge control system (courtesy of Dresser-Rand).

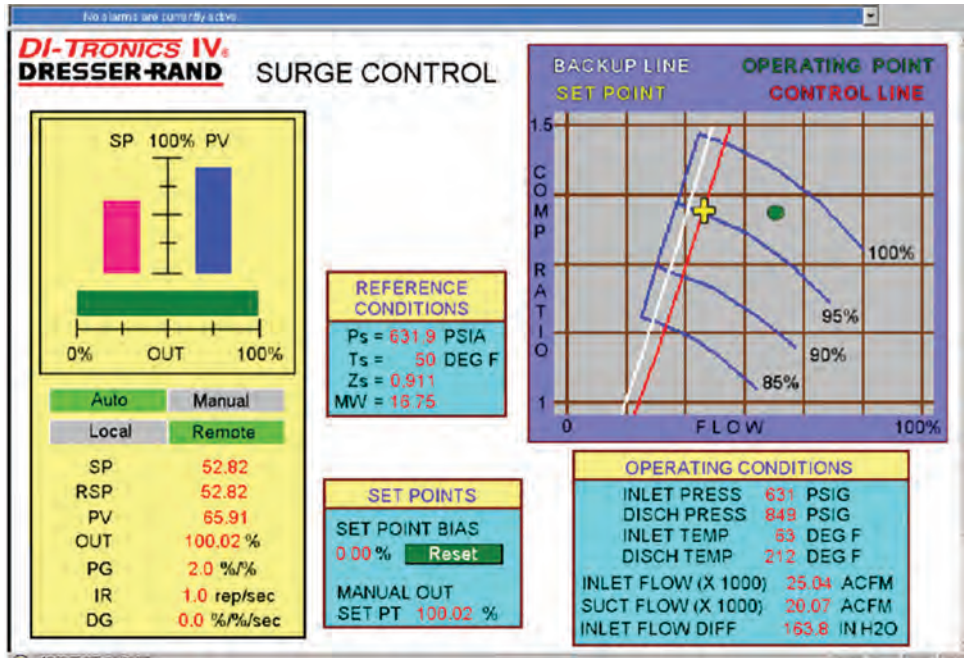


Figure 6-57. Example of a surge control system interface (courtesy of Dresser-Rand).

back to the suction, which reduces the discharge pressure, increases the suction pressure, and increases the flow through the compressor, thus moving the operating point back to the right of the surge line. Some surge control systems have a backup line at about 5% at which point the recycle valve should be 100% open. The operating point should never move beyond this line.

The recycle valve is sized to be able to handle 100% of the peak flow of the compressor. The flow characteristics of the control valve are quite important, particularly in situations where rapid response is required. It must provide accurate control, fast response (from 1 to 2 seconds for full opening) and wide flow rangeability. In some designs, a double-valve system is adopted with a quick acting valve is placed in parallel with a normal control valve. Adaptive control algorithms that sense the rate at which surge is being approached are also able to accommodate rapid changes in process conditions. For example, the surge system can be set up so that the recycle valve begins to open prior to reaching the control line if the operating point is more moving quickly.

Various control schemes exist to adapt the control line to changing process and operating conditions. Several proprietary algorithms exist to normalize the surge control line with respect to changes in molecular weight, suction temperature and suction pressure.

6.3.6 Physical Operation

6.3.6.1 Performance Characteristics

The performance characteristics of a centrifugal compressor are the result of the inlet configuration, the impeller, and the diffuser. The compressor designer has a number of options (as well as constraints) available to provide the required performance. At a specific speed, the performance as defined by head (or some equivalent measure of pressure rise) on the y axis versus flow (usually actual or volume flow but can also be mass flow) on the x axis. For most of the operational

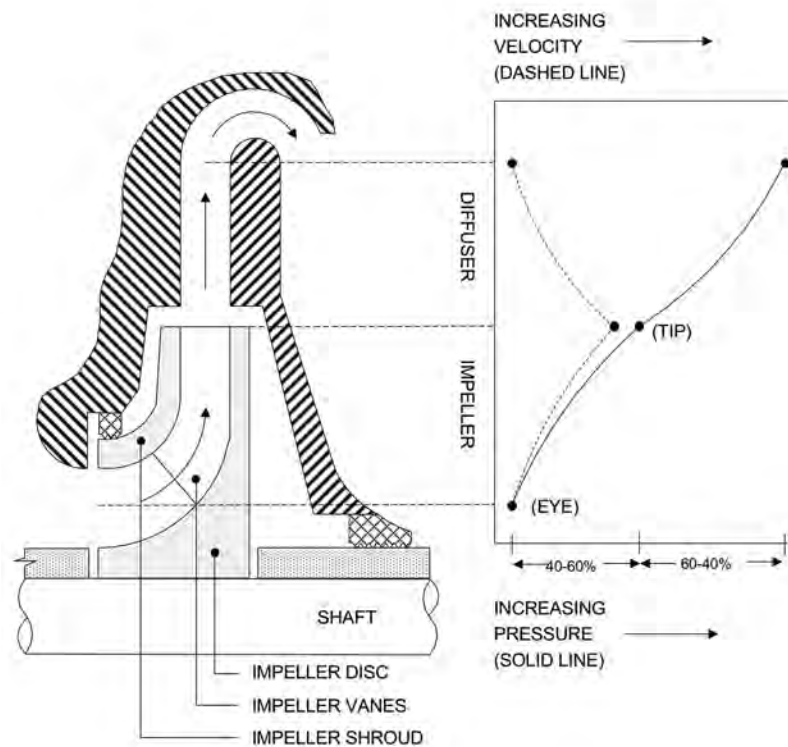


Figure 6-58. Pressure and velocity changes through a stage.

envelope, this produces a curve that is bounded by a surge limit on the left side and choke (or stonewall) on the right side of the curve. The shape and position of the curve, as is further discussed and illustrated below, is dependent on the design of the inlet, impeller and diffuser.

Gas enters the bladed impeller at the eye, moving in an axial direction (Fig. 6-58). The flow is then changed to a radial direction and accelerated as it moves through the impeller. It then exits into a diffuser. The diffuser converts the increased velocity of the gas into pressure—an example of the classical conversion of kinetic energy into potential energy.

Of the pressure rise, 40% to 60% occurs in the impeller itself, with the remaining increase occurring in the diffuser. The impeller is the only means of adding energy to the gas, and all the work on the gas is done by this element. Stationary components such as the diffuser or discharge volute can merely convert velocity energy into pressure energy.

In a single-stage compressor, the gas is collected in a volute and discharged, after passing through the impeller and diffuser (Fig. 6-35). In a multi-stage compressor (Fig. 6-34), the flow must return to the eye of the next impeller.

6.3.6.2 Impeller

Impellers have a distinctive shape dependent on the pressure ratio they produce and the flow they can handle. A high pressure ratio impeller has a higher radius but typically with lower flow capability and a lower specific speed, which achieves a somewhat lower maximum efficiency. Centrifugal compressors found on mainline pipelines normally require a more moderate pressure ratio of 1.3–1.7, which then results in a lower radius impeller and higher flow capability with a high efficiency. A typical pipeline impeller is shown in Fig. 6-59.

Some impellers suffer from cracking at the exit of the impeller due to resonance from vane passing frequencies which typically occur when operated away from design conditions. Other than a complete redesign of the impeller, one alternative approach is to scallop the shroud and backplate by removing some of the material [35]. This changes the natural frequencies of the impeller and provides a sufficient separation margin from resonance. This does not have a detrimental effect on performance and prevents major changes to the configuration of the compressor.

The basic slope of the performance characteristic curve is mostly dependent on what happens at the tip of the impeller. At the outside diameter or tip of the impeller and relative to the impeller, the gas exits the impeller at an angle parallel to the tip of the blade. This is represented by the “ V_{REL} ” vector on Fig. 6-60. As the volume flow increases through the impeller, the V_{REL} vector gets longer.



Figure 6-59. A typical pipeline impeller (courtesy of Dresser Rand).

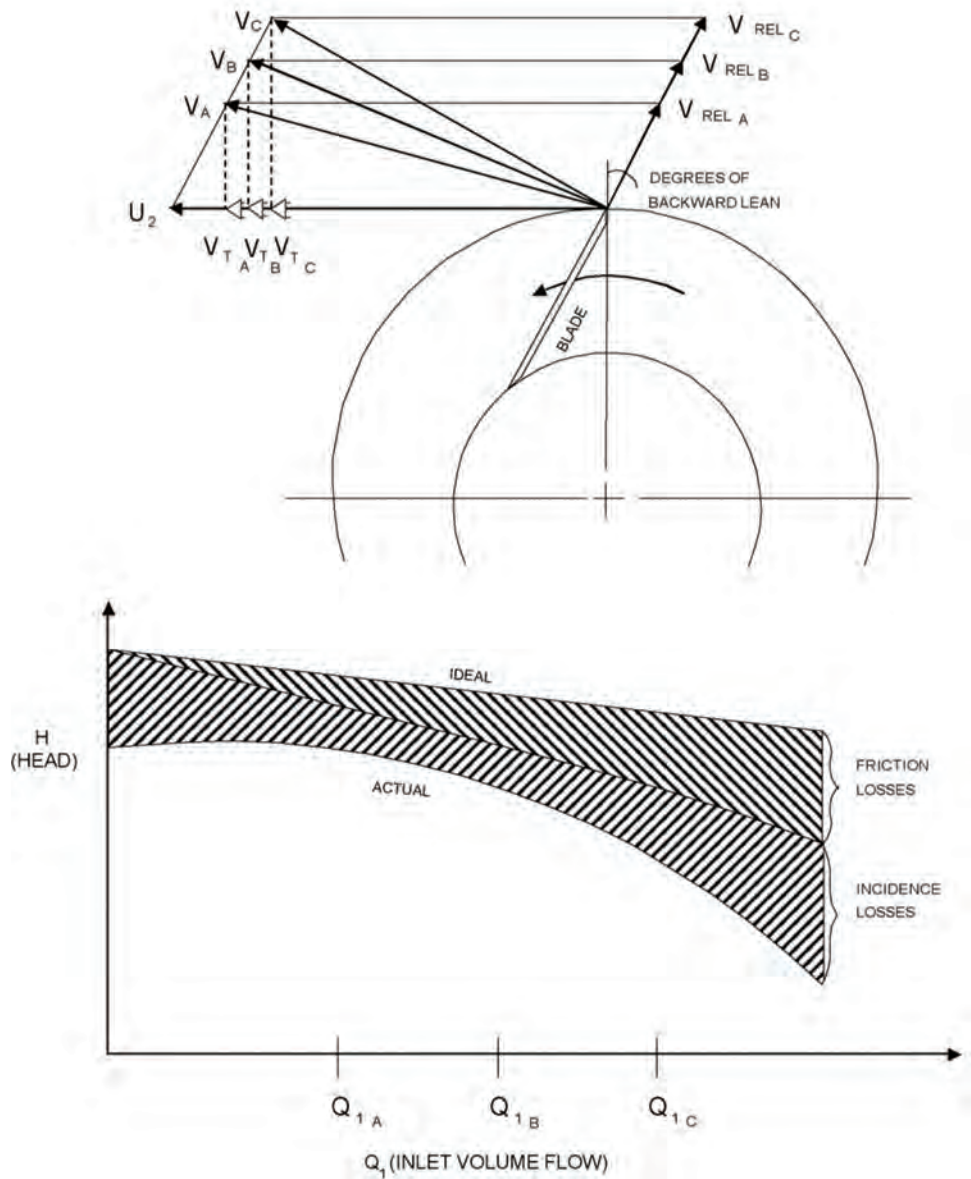


Figure 6-60. Velocity vectors at different flows at the tip of the impeller.

At the same time, the tip of the blade is moving tangentially as represented by the “ U_2 ” vector on Fig. 6-60, which is a function of impeller speed (rpm). The speed is assumed to be constant for this discussion.

Addition of the V_{REL} and U_2 vectors gives the “ V ” vector, which represents the velocity and direction of the gas exiting the impeller relative to the casing. Note that the tangential component of the V vector, or the “ V_T ” vector, is proportional to the head produced by the impeller under ideal conditions.

Thus the “ideal” performance curve of an impeller is a straight line, in that a lineal increase of ow from Q_{1A} to Q_{1B} to Q_{1C} produces a lineal decrease in head proportional to the vectors “ V_{TA} ” to “ V_{TB} ” to “ V_{TC} ”.

Friction losses, which increase with increased flow, add slope and some curvature to the ideal performance curve. Incidence losses, which increase as the flow varies from the

design condition, add curvature to the ideal performance curve. Therefore, the “actual” performance curve of an impeller is the ideal line, less friction and incidence losses.

The slope of the ideal performance line is determined by the degree of backward lean of the impeller blade at the tip of the impeller (Fig. 6-61). A radial blade (0° of backward lean) has a horizontal ideal performance line, which is sloped and curved by friction and incidence losses. As backward lean is increased, the slope of the ideal performance line is increased, and so is the actual performance curve.

It may be noted that the radial (or low backward lean) impeller’s performance curve is higher than the medium or high backward lean impellers. Since the tangential component vectors V_T are longer for the lower backward lean impellers, they produce more head for

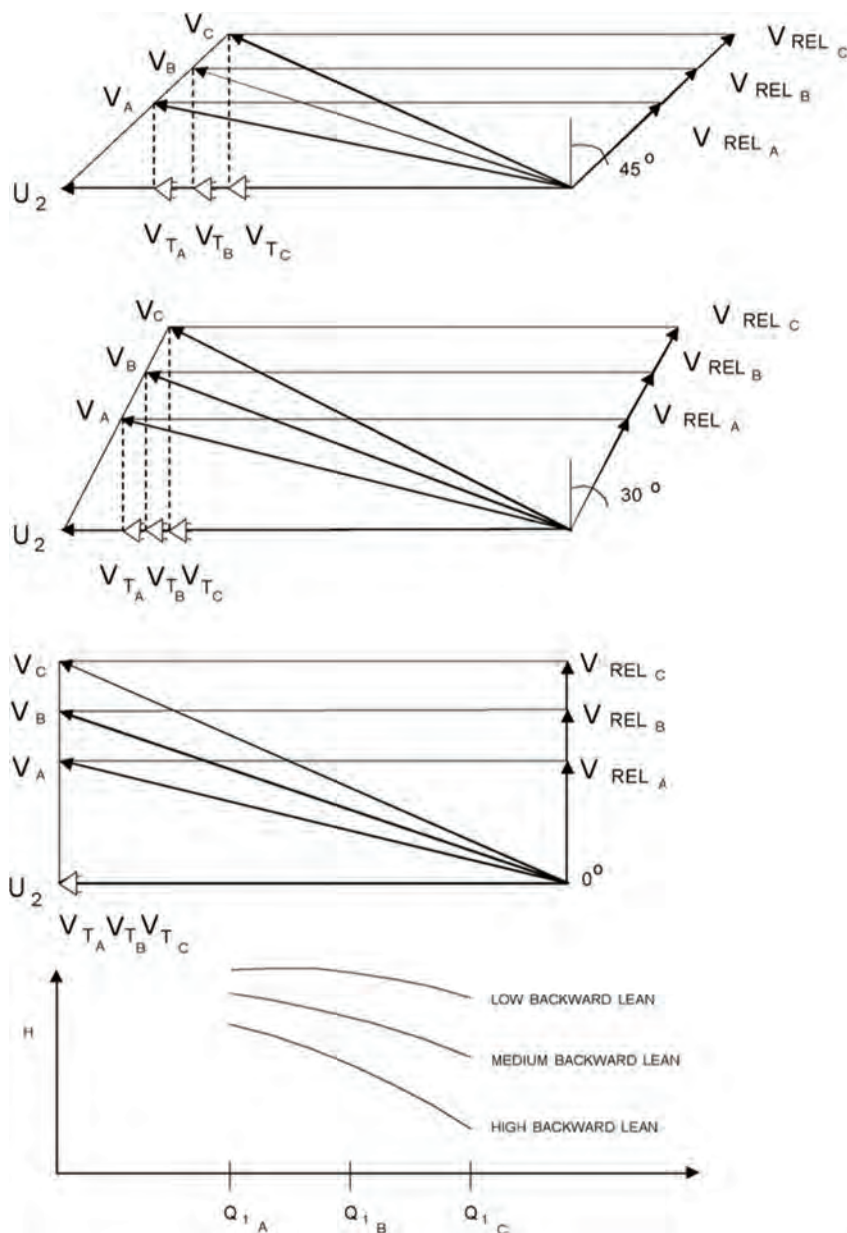


Figure 6-61. Velocity vectors at different blade angles at the tip of the impeller.

the same tip speed U_2 and gas exit velocities V_{REL} . Standard closed impellers vary between 25° and 35° of backward lean that is a middle point between obtaining higher head of a low backward lean and the better stability of a high backward lean impeller.

Similar velocity vectors exist at the intake or eye of the impeller (Fig. 6-62). Here, the incoming gas approaches the impeller eye in an axial direction, which changes to a straight radial direction, represented by the " V_c " vector, until the impeller blade is encountered.

The leading edge of the impeller blade is moving tangentially as represented by the " U_1 " vector on Fig. 6-62. Therefore, relative to the blade or impeller, the incoming gas seems to be approaching the leading blade edge along vectors " $V_{e REL}$."

At design conditions "B," the approach or incidence vector " $V_{e REL B}$ " is along the center line of the leading blade edge, and minimum incidence losses occur. As flow conditions change, the incidence vector swings away from the blade center line, and incidence losses increase. Flow reductions swing the incidence vector so that the incoming gas impinges on the leading or positive face of the moving blade, and "positive incidence" results. Flow increases result in the incoming gas impinging upon the trailing or negative blade face, giving "negative incidence."

Some impellers are manufactured with an inducer or an initial twist to the vane. This reduces the average Mach number of the flow and, thus, enables the impeller to be run somewhat faster and produce more head. The major problem is that this complicates the construction of the impeller. The other option is to install inlet guide vanes, most of which cannot be varied during operation but can be adjusted by opening the case.

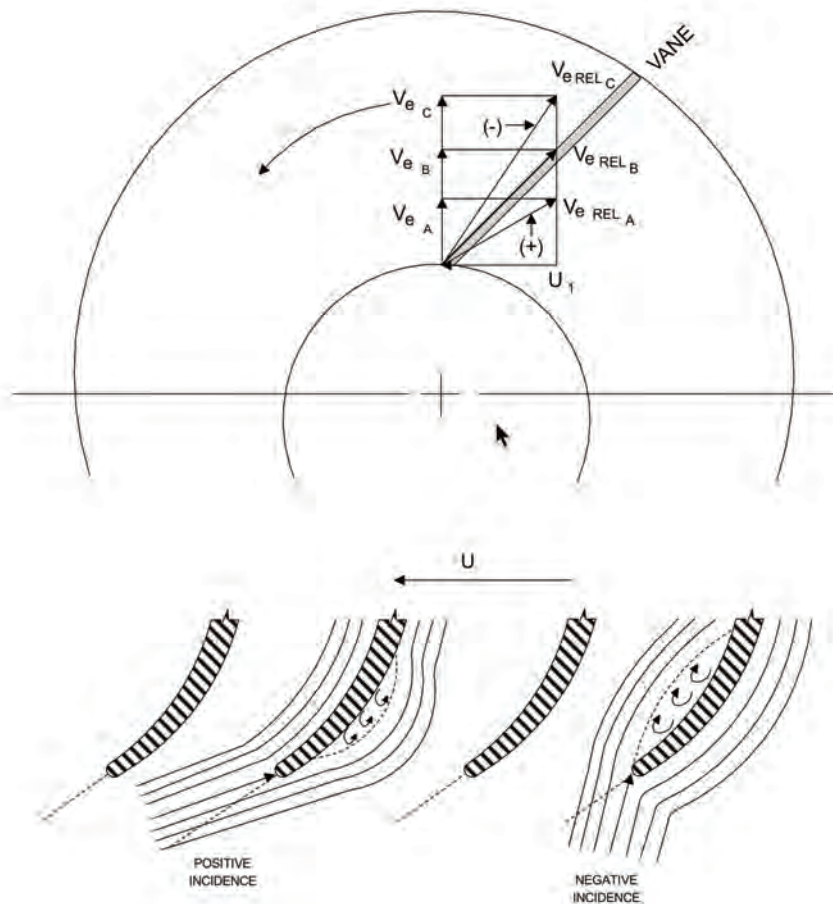


Figure 6-62. Incidence losses at leading edge of blade at the eye of the impeller.

6.3.6.3 Diffuser

The diffuser converts the kinetic energy provided by the impeller into pressure simply by an increase in area. For greatest efficiency (or lowest losses), there is an optimum angle for the diffuser. The surge point of the compressor is mainly controlled by the diffuser while the head is determined by the impeller.

The designer has the option of using a vaneless diffuser or installing vanes in the diffuser. The vaned diffuser provides higher efficiency and head but at the expense of a higher surge flow limit and a more rapid drop-off in the higher flow area which produces a smaller operating envelope [36] and more potential vibration and pulsation issues. For the lower-pressure ratios found in pipeline compressors, the vaneless diffuser provides a more reliable and larger operating range.

6.3.6.4 Effect of Fluid Properties

In addition to the physical configuration of the compressor, fluid properties affect the performance characteristics. In particular, for gases with a higher molecular weight, the characteristic curve is higher for a specific speed, but the surge point occurs at a higher flow and the stable range is lower. Conversely, lighter gases have a characteristic curve with a lower angle and larger stable range and overload capacity.

6.3.7 Design Standards

The primary design standard for centrifugal compressors is API 617 [22]. It provides valuable data sheets along with guidelines that have been widely accepted by users and vendors alike. Testing is described in ASME Power Test Code PTC 10 [37], and a full PTC 10 test is only feasible in the vendor's shop, although rarely with the same fluid as in the final installation.

Onsite testing is more difficult because instrumentation is less likely to be as accurate and the full range of operating conditions are not always available. A field test is, however, still highly desirable as a final verification. No official standard is available but the guideline prepared by [38] is very comprehensive and the closest thing to a standard.

The advent of accurate instrumentation and automated data acquisition already installed at a modern compressor station make field testing much easier than in the past. However, one must not be fooled into thinking that this ensures an accurate test. Some of the critical considerations are:

- Flow measurement needs to be accurate, and any shortcuts taken, such as insufficient piping length before the flow measurement device, will reduce the effectiveness of the test.
- Pressure and temperature measurements need to be close to the compressor, especially the discharge.
- Temperature should be measured at two points (still short of the four required for a PTC 10 test) to verify that flow distortions are not affecting the result. Again, this is most crucial for discharge temperatures.
- Process conditions should be as stable as possible, and temperatures have to stabilize for at least 5 to 10 minutes.
- Temperature measurement has probably the greatest impact on final accuracy, especially for efficiency measurement. Ideal accuracy is 0.1°C.
- A good gas sample is needed for the calculation of gas properties using the Benedict-Webb-Rubin (or other appropriate) equations of state.

A plan has to be prepared in conjunction with operations for achieving as wide a range of operating points as possible for both flow and head. This can, of course, be done first by

changing the speed of the compressor in steps from minimum to maximum. The existence of a parallel unit(s) makes this much easier, but arrangements may have to be made with pipeline operations (gas control) to vary the flow to the compressor station.

This may also be a good time to do a surge test that may reveal the opportunity to increase the operational envelope of the compressor. This naturally has to be approached with caution. The flow reduction needed to move the compressor towards surge can be achieved by increasing the speed of a parallel compressor and reducing speed for the tested compressor or throttling with a downstream valve. Staff should closely monitor the compressor using data from pressure and flow transmitters and vibration sensors, which will signal the advent of surge as well as observing close to the compressor to listen to noise signals. Instant communication between observers and staff in the control room is mandatory so that the recycle can be opened quickly when surge is being approached. It should be emphasized that it is not the purpose to put the compressor into surge but, instead, to determine the point of incipient surge, which is most likely where localized stall is occurring.

6.4 SCREW COMPRESSORS

6.4.1 Screw Compressor Design

Rotary compressors use rotors, equipped with either vanes or lobes, to trap gas in a fixed or variable volume between themselves and an outside casing, moving the gas from inlet to outlet as the rotors turn. Valves are not used as part of the compression process. They are found mainly in air compression for plant and instrument air systems, portable compressors for construction, and vacuum pumps. The main types of rotary compressors are:

- Straight lobe—employs two or three figure eight-shaped rotors
- Helical lobe—employs two spirally shaped rotors
- Sliding vane—uses a rotor equipped with movable vanes, positioned eccentrically in a cylindrical casing
- Liquid piston—employs a vaned rotor to drive a ring of liquid around an elliptical casing

The helical lobe or screw compressor is mostly utilized in upstream service such as the one shown in Fig. 6-63, but is starting to see more application in larger pipelines.

Although screw compressors are not common on larger pipelines, they have found useful application in gas gathering systems where lower flows and higher compression ratios are prominent. An example of this is illustrated in Fig. 6-64 for low pressure, sweet and sour gas applications with a suction pressure range of 0–100 psig and discharge pressure range of 50–350 psig. Screw compressors are able to operate in a compression ratio range of 2:1 to 20:1 in a single stage, thus providing a more cost-effective solution in comparison to multistage reciprocating packages in many applications.

There are two types of screw compressors: non-lubricated or dry and lubricated or flooded. The ones shown in Figs. 6-63 and 6-64 are of the lubricated type that is common in oil and gas applications. Oil is injected in the gas stream prior to the suction and this forms a film between lobes to prevent direct contact. The oil also absorbs heat which results in a lower discharge temperature, enabling a higher compression ratio. The oil is recovered down-stream of the discharge and recirculated to the suction. Screw compressors operate with minimal vibration and there is minimal wear as a result.

Screw compressors are most often driven by electric motors (Fig. 6-63) but engines as in Fig. 6-64 are also utilized.



Figure 6-63. Helical or screw compressor.



Figure 6-64. Engine-driven screw compressor used in a pipeline application (courtesy of Compass Compression).

6.4.2 Screw Compressor Operation

A screw compressor is a positive displacement compressor that consists of two lobes that mesh together and force the fluid into a smaller volume as it progresses from suction to discharge. On the suction side, the gas becomes trapped in between the helical cylinders formed by the screw threads and the housing. Due to the shape of the screws, the volume is reduced until it reaches the end of the screw and is discharged (Fig. 6-65).

The ratio of the volume at the suction V_s and volume at the discharge V_d is called the volume index V_i and is a fundamental characteristic of a screw compressor. This determines the internal compression ratio. However, the downstream conditions determine the final discharge pressure. If the V_i is too high for the operating conditions, the gas will be compressed

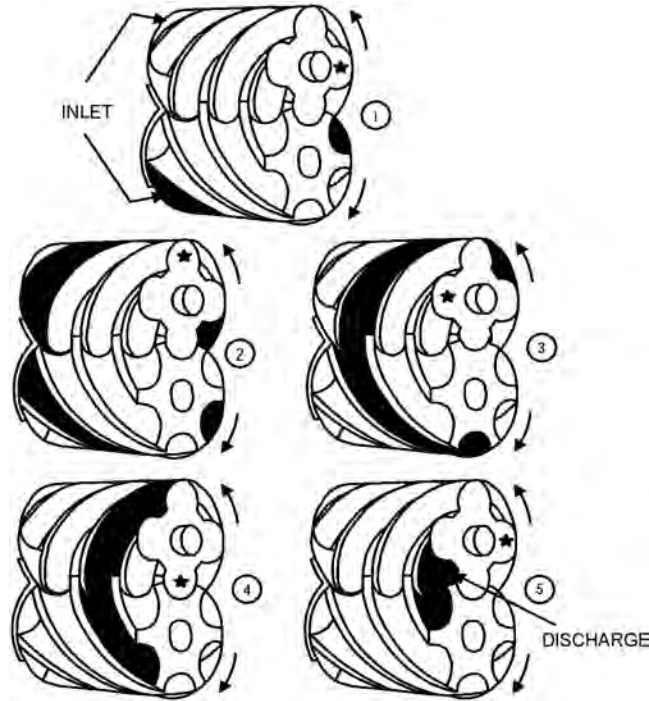


Figure 6-65. Helical lobe rotary compressor (compression steps).

to a higher pressure than the actual discharge pressure, and it will expand into the discharge until it is equalized. This is called over-compression and results in more work being done than necessary. The opposite, or under-compression, can also occur when the gas reaches the discharge, the discharged gas will flow back into the pocket and force the compressor to push against this higher pressure. Some compressors use a sliding valve to vary the volume ratio.

Most screw compressors driven by a constant speed motor will have capacity control to vary the flow with a common method being a slide valve controlling the discharge port, which permits some of the gas to be recirculated back to the suction while at the same time delaying the discharge so that the same volume index is maintained. This can control capacity for as much as 10% to 100%.

Screw compressors driven by engines or VFD motors can use speed control based on the driver to vary capacity.

6.5 INTEGRALLY-GEARED COMPRESSORS

6.5.1 Compressor Design

An integrally geared centrifugal compressor - IGCC (also called multi-shaft compressor) is a multi-stage compressor consisting of a multi-gear system with a central bull gear and different gear pinions, which drive many impeller stages (often up to 10 impellers; 5 pinions). The bull gear is generally driven by an electric motor, which can be a conventional 1,500–1,800 rpm unit or a high-speed 3,000–3,600 rpm induction motor. The compressor shafts (pinions) can run at high rotational speeds, up to 75,000 rpm, depending on the respective pinion/bull gear ratio. Figure 6-66 shows an example schematic of a 6 impeller - 3 pinion IGCC design, while Fig. 6-67 shows a cut-through view pointing to the salient auxiliary

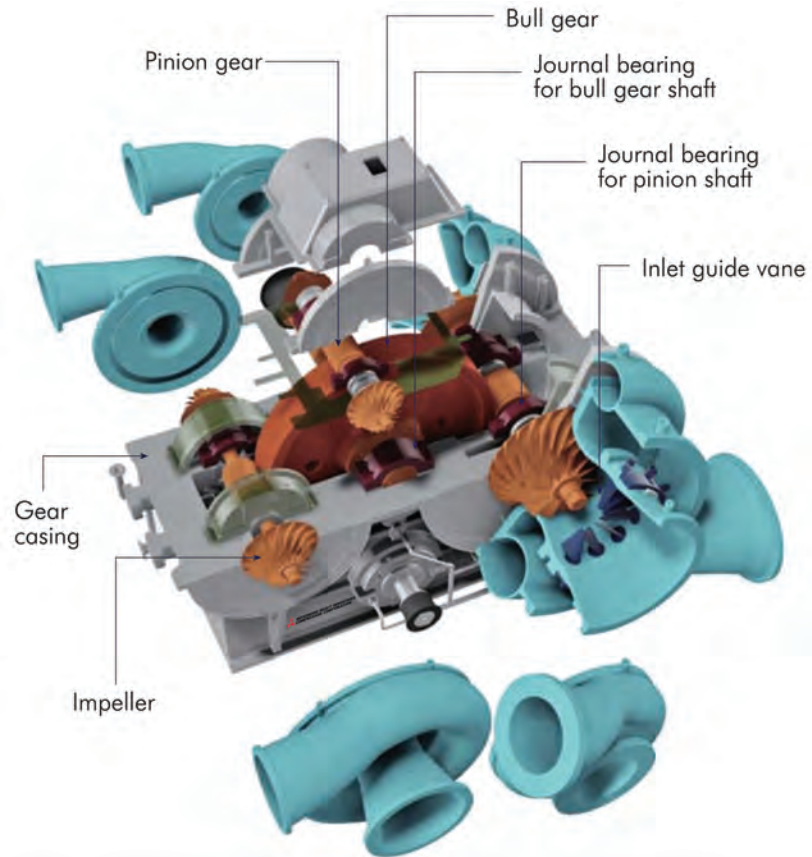


Figure 6-66. Example of 6-stage integrally geared compressor [39].

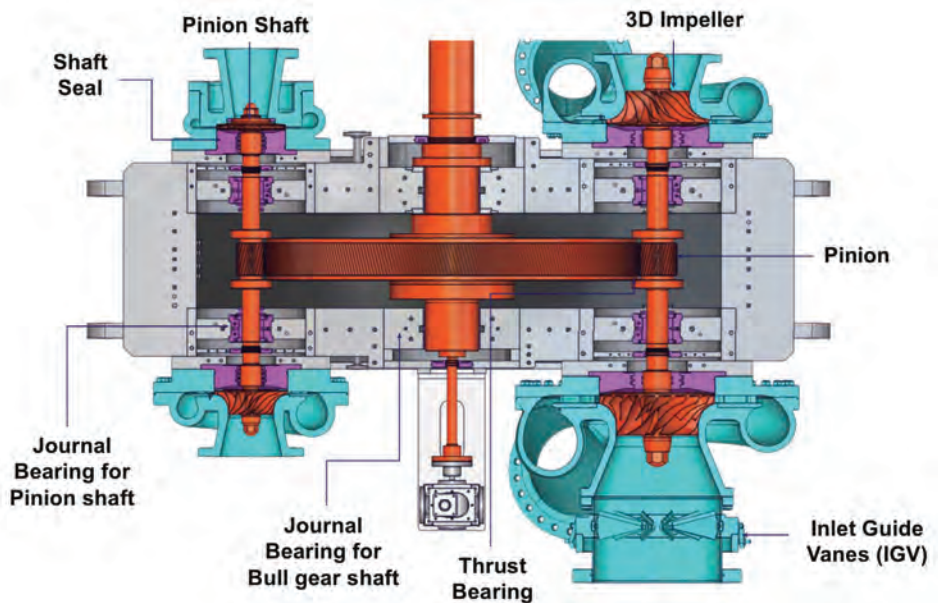


Figure 6-67. Cut-through details of the 6-stage integrally geared compressor shown in Fig. 6-66 [39].

components of this design [39]. In contrast to conventional centrifugal compressors, each pinion in an IGCC can run at a different speed. Thus, every impeller pair can operate at its optimum aerodynamic speed. This is an important advantage which results in higher overall efficiencies than conventional compressor designs. A multistage IGCC is usually designed so each stage shares the work equally, i.e., each impeller passes the same mass flow at almost the same compression ratio. For example, in the 6-impeller compressor example shown in Fig. 6-66 with a total pressure ratio of 10, the compression ratio per impeller would be around the sixth root of 20, i.e. approximately 1.65. For such high pressure ratio, the impellers need to run at relatively high speeds. To increase the capacity of the impeller, the height of each vane is about 35–50% greater than that of vanes on a conventional impeller. In addition, each impeller has more vanes, to reduce the load on each by about 30–40% compared to conventional impellers [40].

IGCCs provide many advantages such as advanced high-speed impellers, relatively low costs (compared to conventional compressors) and higher efficiencies. They also offer near-isothermal compression when intercoolers are employed after one or two impellers. The speed-increasing gear allows all stages to operate at a higher specific speed which is also optimized for maximum efficiency. Another advantage of integrally geared compressors is the reduced number of stages required while still provide higher efficiency. Many modern designs allow rotor removal without disconnecting process piping.

IGCCs are constant-speed machines because complex dynamic situations (rotordynamics, lateral, torsional, etc.) don't allow variable-speed operation. As such, many of the machines rely on an inlet guide vane (IGV) to control capacity. IGVs usually consist of a row of aerodynamically shaped blades placed at the inlet of impeller. The blades can rotate around their aerodynamic center to give the suction flow a pre-swirl that provides an optimum incidence angle with the impeller's leading edge even at reduced flows.

6.5.2 Bearings, Seals and Gears

IGCCs use multiple bearings, seals and gear meshes and operate at high speeds. In standard compressors, these usually cannot all be managed to achieve high reliability. Modern API integrally geared centrifugal compressors (i.e. designed and manufactured per API 617 and other applicable API standards, such as API 614 regarding lubrication oil systems), have provided increased reliability and availability over the past decade. However, IGCCs are often supplied with only one overall surge protection system and not individual impeller stage protection, hence are prone to surging. Therefore, dynamic surge analysis should always be performed to assess the adequacy and effectiveness of such one surge protection system for each specific application.

IGCCs often come with dry gas seals, but oil seals can also be used. Thrust loads from impellers and gears are absorbed by individual thrust bearings on pinions or transmitted to the bull-gear thrust bearing with thrust-rider rings fixed to the pinions and bull gear. Balance pistons are normally not used. Thrust balancing may be achieved by helix thrust force direction of the gearing and offsetting impeller aerodynamic thrust forces.

The bearing design and operation in an IGCC require special attention. Because of the very high operating speeds (particularly in the last stages), specially designed bearings are required, which should be tightly controlled during manufacturing, installation and operation. As a design criterion, bearing metal temperatures should not exceed 100°C at any specified operating condition. The oil inlet temperature range should be adjusted with great care. Often, the minimum oil inlet temperature could be 30–35°C. Most often, the maximum oil inlet temperature should be 50°C [40].

Lastly, the gear system is key in any IGCC as its complex configuration, high accuracy demands and high load operating conditions require stringent design and manufacturing criteria. The natural modes, vibration responses and generated noise levels should be properly

considered in the design. Two primary types of dynamic excitation in gear systems can cause excessive vibration and noise response. One is the gear meshing dynamic excitation that is an internal parametric type. This kind is unique to geared systems and arises from a combination of the periodic variation in the meshing tooth number, tooth impact forces and transmission error because of elastic tooth deformation, gear tooth profile manufacturing error and misalignments. The frequency of this dynamic force directly relates to the tooth-to-tooth period and, therefore, shows up mainly in the mesh harmonics in the response spectrum. The second type of dynamic excitation in gear systems is caused by an external set of dynamic shaft loads that typically occur at much lower in frequencies compared to the mesh harmonics. The sources of this dynamic excitation include shaft rotational imbalance, shaft geometrical eccentricity, and dynamic loads from other sources such as compressor stages, driver and rotational speed, and torque fluctuations under loaded conditions [40].

REFERENCES

- [1] Purslow, N., 2006. "Foundation Analysis and Design for Reciprocating and Rotating Equipment," *CompressorTechTwo*, pp. 28–36, April–May 2006.
- [2] Applegate, P., 1990. "Balanced forces and foundations keys to reciprocating-compressor life," *Oil & Gas Journal*, **88**(36), pp. 50–55, September 3, 1990.
- [3] Haight, B., 2006b. "The Birth of Evolution," *CompressorTechTwo*, pp. 72–76, October 2006b.
- [4] Unknown, 2006a. "Compressor and Expanders," *CompressorTechTwo*, CT2 Compression TechnologySourcing Supplement, p. 89.
- [5] Wirz, W. C., 2003. "Medium-Speed Separable Compressors, An Alternative to Slow-Speed Integral Engine/Compressors for Natural Gas Transmission and Gas Storage," *3rd European Forum for Reciprocating Compressors*, March 27th & 28th, Vienna, pp. 1–9.
- [6] Deffenbaugh, D. M., Smalley, A. J., Brun, K., Broerman, E. L., Harris, R. E., Hart, R. A., Harrell, J. P., Nored, M. G., McKee, R. J., Gernentz, R. S., Moore, J. J., Siebenaler, S. P., Svedeman, S. J., 2005. "Advanced Reciprocating Compression Technology (ARCT)," Southwest Research Institute, Final Report, SwRI® Project No. 18.11052, DOE Award No. DE-FC26-04NT42269, pp. 1–242, December 2005.
- [7] Foreman, S., 2002. "Compressor Valves and Unloaders for Reciprocating Compressors An OEM's Perspective," Dresser-Rand Literature, www.dresserrand.com.
- [8] Brun, K., Gernentz, R. S., Smolik, M. O., 2006. "Semi-Active Compressor Valve Development And Testing," *Pipeline & Gas Journal*, pp. 40–42, September 2006.
- [9] Scott, R., 2003. "Reciprocating Natural Gas Compressors," *Lubrication Machinery*, November 2003.
- [10] Miguez, J. P., 2007. "Problem of Compressor Over-Lubrication," *CompressorTechTwo*, pp. 56–64, August–September 2007.
- [11] Hickman, D. A. and Milum, R., 2003. "Reciprocating Compressor Performance Predictions: Control Methodologies from the PLC to the PC," GMRC Gas Machinery Conf., Salt Lake City, Utah.
- [12] Long, B., and Van Hardeveld, T., 2006. "Enhancing Compressor Productivity," *GPAC 18th Annual Operations/Maintenance Conference*, Friday, Calgary, Alberta, pp. 1–10, April 21, 2006.
- [13] API Standard 618, 2007. "Reciprocating Compressors for Petroleum, Chemical and Gas Industry Services," *American Petroleum Institute*, 5th ed., pp. 1–198, December 2007.
- [14] Hinchliff, M., Greenfield, S. and Bratek, W., 2014. "A Discussion of the Various Loads Used to Rate Reciprocating Compressors," Gas Machinery Conference 2014, Nashville TN.
- [15] API Standard 614, 1999. Lubrication, Shaft-sealing, and Control-oil Systems and Auxiliaries for Petroleum, Chemical and Gas Industry Services, American Petroleum Institute, 4th ed., pp. 1–200, April 1999.
- [16] Tyson, J. D., and Atkins, K. E., 2001. "The New Fifth Edition of API 618 for Reciprocating Compressors—Which Pulsation and Vibration Control Philosophy Should You Use?" *Proceedings of the 30th Turbomachinery Symposium, Turbomachinery Laboratory*, Texas A&M University, College Station, Texas, pp. 183–195.

- [17] Fernandez, J., Hickman, D., Buller, P., and Eberle, K., 2007. "Integrating Compressor Performance with the Effects of Pressure Pulsation across a Unit's Entire Operating Map," *Proceedings of GMC: 2007 Gas Machinery Conference*, Dallas, Texas, pp. 1–18, October 1–3, 2007.
- [18] Kleynhans, G., Pfrehm, G., Berger, H., and Baudelocque, L., 2005. "Hermetically Sealed Oil-free Turbocompressor Technology," *Proceedings of the 34th Turbomachinery Symposium, Turbomachinery Laboratory*, Texas A&M University, College Station, Texas, pp. 63–76.
- [19] Krain, H., 2005. "Review of Centrifugal Compressor's Application and Development," *J. Turbomach.* January 2005, Volume 127, Issue 1, 25 (10 pages).
- [20] Bidaut, Y. and Dessibourg, D., 2014. "The Challenge for the Accurate Determination of the Axial Rotor Thrust in Centrifugal Compressors," *Proceedings of the 43rd Turbomachinery Symposium, Turbomachinery Laboratory*, Texas A&M University, College Station, Texas, pp. 1–5.
- [21] Kurz, R., Marechale, R. K., Fowler, E. J., Ji, M., Cave, M. J., 2011. "Operation of Centrifugal Compressors in Choke Conditions," *Proceedings of the 40th Turbomachinery Symposium*, Turbomachinery Laboratory, Department of Mechanical Engineering, Texas A&M University, College Station, Texas, USA.
- [22] API Standard 617, 2002. "Axial and Centrifugal Compressors and Expander-compressors for Petroleum," *Chemical and Gas Industry Services*, American Petroleum Institute, 7th ed., pp. 1–193, July 2002.
- [23] Dimod, T., Younan, A. and Allaire, P., 2011. "A Review of Tilting Pad Bearing Theory," *International Journal of Rotating Machinery*, Volume 2011, Article ID 908469, 23 pages.
- [24] He, M., Byrne, J. M., Cloud, C. H. and Vazquez, J. A., 2016. "Fundamentals of Fluid Film Journal Bearing Operation and Modeling," *Asia Turbomachinery & Pump Symposium*, Singapore, February 22–25, 2016, pp. 1–30.
- [25] He, M., Byrne, J. M., Cloud, C. H. and Vazquez, J. A., 2012. "Steady State Performance Prediction of Directly Lubricated Fluid Film Journal Bearings," *Proceedings of the 41st Turbomachinery Symposium, Turbomachinery Laboratory*, Texas A&M University, College Station, Texas, pp. 1–16.
- [26] Swann, M., 2006. "Moving into larger machines," *Turbomachinery International*, Sept/Oct 2006, pp. 16–20.
- [27] Devitt, D., 2017. "Centrifugal Revolution," *CompressorTech2*, April 2017, pp. 44–47.
- [28] Devitt, D., 2017. "Damping and stiffness, a primer," *Turbomachinery International*, October 12, 2017.
- [29] Unknown, 2003. "Replacing Wet Seals with Dry Seals in Centrifugal Compressors," *Natural Gas Star Partners*, Environmental Protection Agency, 1EPA430-B-03-012, pp. 1–13, November 2003.
- [30] Botros, K. K., Geerlings, J., and Imran, H., 2007. "Implementation of a Supersonic Ejector for Capturing Dry-Gas Seal Vent Gases," *Presented at the 17th Symposium on Industrial Application of Gas Turbines (IAGT)*, Banff, Alberta, Canada, pp. 1–21, October 2007.
- [31] Wilcox, E., 2000. "API Centrifugal Compressor Oil Seals and Support Systems—Types, Selection and Field Troubleshooting," *Proceedings of the 29th Turbomachinery Symposium, Turbomachinery Laboratory*, Texas A&M University, College Station, Texas, pp. 225–237.
- [32] Stahley, J. S., 2001. "Design, Operation and Maintenance Considerations for Improved Dry Gas Seal Reliability in Centrifugal Compressors," *Proceedings of the 30th Turbomachinery Symposium, Turbomachinery Laboratory*, Texas A&M University, College Station, Texas, pp. 203–207.
- [33] Devitt, D., 2017. "Gas Bearing Principles Applied to Seals for Zero Emissions," *CompressorTech2*, November 2017, pp. 44–47.
- [34] Sorokes, J. M., 2003. "Rotating Stall—An Overview of Dresser-Rand Experience," Dresser-Rand paper, TP061, pp. 1–22.
- [35] Grebinnyk, K. and Widders, R., 2016. "Redesign of Centrifugal Compressor Impeller by means of Scallopings," *Proceedings of the 45th Turbomachinery Symposium, Turbomachinery Laboratory*, Texas A&M University, College Station, Texas.
- [36] Petela, G., and Motriuk, R. W., 2000. "Effect of Vaned Diffuser on Performance and Onset of Pressure Instabilities in Centrifugal Compressors," *Proceedings of Seventh FIV International Conference*, Lucerne, Switzerland, Flow-Induced Vibration, pp. 733–742.

- [37] ASME PTC 10, 1997. “Performance Test Code on Compressors and Exhausters,” *American Society of Mechanical Engineers*, pp. 1–200.
- [38] Brun, K., and Nored, M. G., 2006. “Guideline for Field Testing of Gas Turbine and Centrifugal Compressor Performance,” *Gas Machinery Research Council/Southwest Research Institute*, pp. 1–93, August 2006.
- [39] MITSUBISHI Integrally Geared Compressor, <https://www.mhicompressor.com/technology/catalog/pdf/geared.pdf>.
- [40] Almasi, A., 2017. “Integrally geared centrifugal compressors – Advantages include 3D impellers, lower costs and higher efficiency,” *Processing Magazine*, April 26, 2017.

PERFORMANCE OF COMPRESSORS

7.1 INTRODUCTION TO COMPRESSOR PERFORMANCE

The primary requirement of any compressor selection is that the compressor must meet the operating conditions required by the system in which it is installed. To achieve this, it is first necessary to understand the performance characteristics or “behavior” of the various compressors; secondly, to develop the actual system behavior; and thirdly, to match the compressor to the system such that all operating points are covered.

Performance is therefore a critical aspect of the design of individual units and also of the station as a whole. Throughout the life of a pipeline system, units will be added, stations will be modified, and pipeline operating conditions will change. Condition monitoring relies heavily on understanding performance deterioration, which factors into important maintenance decisions. Performance thus remains a major component of compression equipment for the entire life cycle.

7.2 BASIC ASPECTS OF PERFORMANCE

7.2.1 General

Many aspects of compression performance apply to any type of compressor, whereas others are specific to the nature of the compression process unique to that compressor. For pipeline applications, it is only necessary to deal with the performance of reciprocating and centrifugal compressors.

7.2.2 Nomenclature

The nomenclature in Table 7-1 applies to the equations in this chapter. All attempts have been made to use standard naming conventions, but differences do exist in practice. For consistency, temperatures and pressures are noted in absolute units, and it is left to the user to convert from measured conditions in the applicable equations.

7.2.3 Gas Properties

Determining relevant gas properties forms the basis for compression performance calculations. Different methods are often available, depending on various factors such as the accuracy of input data and the required result, calculation tools available, and industry standards.

7.2.3.1 Ideal Gas Laws

The logical starting point for describing the behavior of gases is the well-known laws of Boyle, Charles, and Amonton. Although the ideal or perfect gas does not exist, the laws

Table 7-1. Nomenclature for compression performance

Symbol	Name	US Customary	SI
c	clearance	%	%
c_p	specific heat at constant pressure	Btu/lb°R	kJ/kg K
c_v	specific heat at constant volume	Btu/lb°R	kJ/kg K
H	head (isentropic or polytropic)	ft·lb _f /lb _m	kJ/kg
k	ratio of specific heats		
m	mass flow	lb/min	kg/h
MW	molecular weight		
n	polytropic exponent		
N	speed	rpm	rpm
	efficiency	%	%
p	pressure (absolute)	psia	kPaa
PD	piston displacement	ft ³ /min	m ³ /sec
PS	piston speed	ft/min	m/sec
PWR	power	hp	kW
r	pressure ratio		
R	universal gas constant	ft·lb _f /lb _m °R	kJ/kMol K
Re	Reynolds number		
T	temperature (absolute)	°R	K
Q_a	actual volume flow	ft ³ /min	m ³ /s
Q_s	standard volume flow	mmscfd	10 ³ m ³ /d
v	specific volume	ft ³ /lb	m ³ /kg
V	volume	ft ³	m ³
VE	volumetric efficiency	%	%
Z	compressibility		

are useful in that they can be applied with experimental factors to closely approximate real conditions.

By combining Boyle's and Charles' laws, the pressure, volume, and temperature can be characterized by an equation called the perfect gas law, or

$$pv = RT \quad (7-1)$$

The value of R is 1545 if pressure is in lbs/ft² and is 10.729 if it is in psia (8.314 joule/mole K). Also, specific volume v in this case is in ft³/lb·mole.

Since real gases deviate from this relationship, a modified equation can be established with a compressibility factor Z (sometimes referred to as supercompressibility) to correct for actual gas behavior. The equation of state then becomes

$$pv = ZRT \quad (7-2)$$

7.2.3.2 Compressibility and Molecular Weight

Compressibility of gases has traditionally been read from charts such as the one shown for natural gas in Fig. 7-1. It has been found that experimental data can be expressed as functions of reduced pressure and temperature. This provides reasonable results as long as the gas is not close to the critical point or in two phases.

The ratio of the actual and reduced pressures and temperatures form curves as can be seen in Fig. 7-1. They are fitted by a third-order equation which can be solved. Some critical pressures and temperatures for natural gas components are shown in Fig. 7-2 with an example of the calculation of the mixture critical pressures and temperatures that can be used to determine the ratio of the actual to the reduced pressure to calculate Z as per Fig. 7-1.

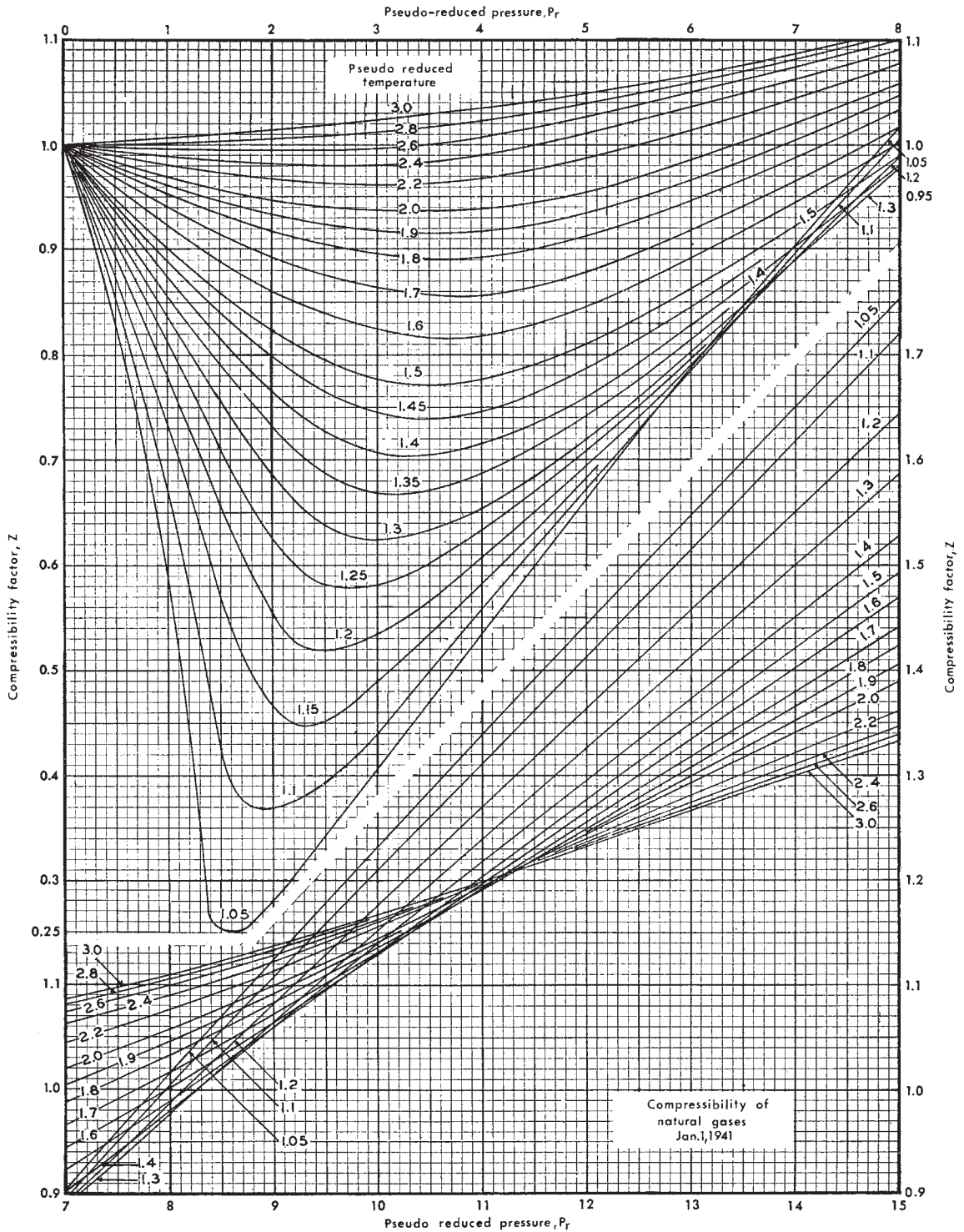


Figure 7-1. Generalized compressibility chart for natural gas mixtures.

Molar Heat Capacity MC_p (Ideal-Gas State), Btu/(lb mol · °R)

*Data source: Selected Values of Properties of Hydrocarbons, API Research Project 44; MW updated to agree with Fig. 23-2

Gas	Chemical formula	Mol wt	Temperature							
			0°F	50°F	60°F	100°F	150°F	200°F	250°F	300°F
Methane	CH ₄	16.043	8.23	8.42	8.46	8.65	8.95	9.28	9.64	10.01
Ethyne (Acetylene)	C ₂ H ₂	26.038	9.68	10.22	10.33	10.71	11.15	11.55	11.90	12.22
Ethene (Ethylene)	C ₂ H ₄	28.054	9.33	10.02	10.16	10.72	11.41	12.09	12.76	13.41
Ethane	C ₂ H ₆	30.070	11.44	12.17	12.32	12.95	13.78	14.63	15.49	16.34
Propene (Propylene)	C ₃ H ₆	42.081	13.63	14.69	14.90	15.75	16.80	17.85	18.88	19.89
Propane	C ₃ H ₈	44.097	15.65	16.88	17.13	18.17	19.52	20.89	22.25	23.56
1-Butene (Butylene)	C ₄ H ₈	56.108	17.96	19.59	19.91	21.18	22.74	24.26	25.73	27.16
cis-2-Butene	C ₄ H ₈	56.108	16.54	18.04	18.34	19.54	21.04	22.53	24.01	25.47
trans-2-Butene	C ₄ H ₈	56.108	18.84	20.23	20.50	21.61	23.00	24.37	25.73	27.07
iso-Butane	C ₄ H ₁₀	58.123	20.40	22.15	22.51	23.95	25.77	27.59	29.39	31.11
n-Butane	C ₄ H ₁₀	58.123	20.80	22.38	22.72	24.08	25.81	27.55	29.23	30.90
iso-Pentane	C ₅ H ₁₂	72.150	24.94	27.17	27.61	29.42	31.66	33.87	36.03	38.14
n-Pentane	C ₅ H ₁₂	72.150	25.64	27.61	28.02	29.71	31.86	33.99	36.08	38.13
Benzene	C ₆ H ₆	78.114	16.41	18.41	18.78	20.46	22.45	24.46	26.34	28.15
n-Hexane	C ₆ H ₁₄	86.177	30.17	32.78	33.30	35.37	37.93	40.45	42.94	45.36
n-Heptane	C ₇ H ₁₆	100.204	34.96	38.00	38.61	41.01	44.00	46.94	49.81	52.61
Ammonia	NH ₃	17.0305	8.52	8.52	8.52	8.52	8.52	8.53	8.53	8.53
Air		28.9625	6.94	6.95	6.95	6.96	6.97	6.99	7.01	7.03
Water	H ₂ O	18.0153	7.98	8.00	8.01	8.03	8.07	8.12	8.17	8.23
Oxygen	O ₂	31.9988	6.97	6.99	7.00	7.03	7.07	7.12	7.17	7.23
Nitrogen	N ₂	28.0134	6.95	6.95	6.95	6.96	6.96	6.97	6.98	7.00
Hydrogen	H ₂	2.0159	6.78	6.86	6.87	6.91	6.94	6.95	6.97	6.98
Hydrogen sulfide	H ₂ S	34.08	8.00	8.09	8.11	8.18	8.27	8.36	8.46	8.55
Carbon monoxide	CO	28.010	6.95	6.96	6.96	6.96	6.97	6.99	7.01	7.03
Carbon dioxide	CO ₂	44.010	8.38	8.70	8.76	9.00	9.29	9.56	9.81	10.05

* Exceptions: Air — Keenan and Keyes, Thermodynamic Properties of Air, Wiley, 3rd Printing 1947. Ammonia — Edw. R. Grubler, Thermodynamic Properties of Ammonia at High Temperatures and Pressures, Petr. Processing, April 1953. Hydrogen Sulfide — J. R. West, Chem. Eng. Progress, 44, 287, 1948.

Calculation of k

Example gas mixture		Determination of mixture mol weight		Determination of MC_p , Molar heat capacity		Determination of pseudo critical pressure, p_{pc} , and temperature, T_{pc}			
Component name	Mol fraction y	Individual Component Mol weight MW	$y \cdot MW$	Individual Component MC_p @ 150°F*	$y \cdot MC_p$ @ 150°F	Component critical pressure P_c psia	$y \cdot P_c$	Component critical temperature T_c °R	$y \cdot T_c$
methane	0.9216	16.04	14.782	8.95	8.248	666	615.6	343	316.1
ethane	0.0488	30.07	1.467	13.78	0.672	707	34.6	550	26.8
propane	0.0185	44.10	0.816	19.52	0.361	616	11.4	666	12.3
i-butane	0.0039	58.12	0.227	25.77	0.101	528	2.1	734	2.9
n-butane	0.0055	58.12	0.320	25.81	0.142	551	3.0	765	4.2
i-pentane	0.0017	72.15	0.123	31.66	0.054	490	0.8	829	1.4
Total	1.0000	MW =	17.735	$MC_p =$	9.578	$p_{pc} =$	667.5	$T_{pc} =$	363.7
		$MC_c = MC_p - 1.986 = 7.592$		$k = MC_p/MC_c = 9.578/7.592 = 1.26$					

*For values of MC_p other than @ 150°F, refer to Fig. 13-6

Figure 7-2. Chart to calculate molecular weight, pseudo-critical pressures and temperatures, and specific heat [1].

The application of more advanced methods using Equations of State (EOS) is shown below in Section 7.2.3.4.

The molecular weight (MW) of a natural gas mixture can also be determined by multiplying the individual component molecular weights by the mol fraction of each component with an example in Fig. 7-2.

7.2.3.3 Ratio of Specific Heats

All compressor calculations also involve the ratio of specific heats, or “k” value. Since the specific heat at constant pressure C_p and the specific heat at constant C_v are related by the equation

$$MC_p - MC_v = R = 1.986 \text{ Btu/(lbmol} \cdot ^\circ\text{F)} \quad (7-3)$$

the ratio of specific heats can be determined by

$$k = \frac{C_p}{C_v} = \frac{MC_p}{MC_v} = \frac{MC_p}{MC_p - 1.986} \quad (7-4)$$

where MC_p and MC_v are the molar heat capacities. For the SI version, the value of R becomes 8.314 kJ/kMole K with the units for MC_p and MC_v as per Table 7-1.

The k value of a natural gas mixture may be determined from the molar heat capacity data included as Fig. 7-2.

7.2.3.4 Equations of State

Simplified equations used to calculate gas properties are mostly based on the principle that the properties of a mixture can be derived by apportioning individual gas behavior based on mole fractions. While this works for simple gas mixtures at low pressures, it is not applicable for most gases and mixtures at elevated process conditions. Instead equations of state are commonly used in almost every calculation, and commercial numerous computer programs now exist that implement more sophisticated mixing rules that accurately predict the properties of almost all possible gas mixtures.

An equation of state (EOS) is a thermodynamic equation which provides a mathematical relationship between two or more properties of a substance, such as temperature, pressure, volume, or internal energy. There are two major groups of EOS: (1) cubic equations of state and (2) virial equations of state, in the following sections. Examples of the first group are: Peng-Robinson EOS [2], Redlich-Kwong EOS [3] and Soave-Redlich-Kwong EOS [4]. The form of Peng-Robinson EOS is described below as an example of this group of EOS [2].

$$P = \frac{RT}{v - b} - \frac{a(T)}{v(v+b) + b(v-b)} \quad (7-5)$$

where; P is pressure, T is temperature, v is specific volume and R is the gas constant for the gas mixture. The parameters a , b and α can be obtained from the critical properties of the fluid:

$$a = \frac{0.45724R^2T_c^{2.5}}{P_c} \quad (7-6)$$

$$b = \frac{0.0778RT_c}{P_c} \quad (7-7)$$

$$= 1 + \left(0.3746 + 1.54226\omega - 0.26992\omega^2 \right) \left(\frac{T}{T_c} \right)^{0.5} \quad (7-8)$$

where; T_c and P_c are the critical temperature and critical pressure, respectively, and ω is the acentric factor. This form of EOS only requires the critical properties and the acentric factor and can only be used for pure components. For gas mixture, mixing rules must be used. The most widely used mixing rule is the van der Waals mixing rule, namely:

$$a = \sum_i \sum_j x_i x_j a_{ij} \quad (7-9)$$

$$b = \sum_i \sum_j x_i x_j b_{ij} \quad (7-10)$$

where x_i and x_j are the molar fractions of components i and j , respectively, a_{ii} and b_{ii} are the constants of the equation for pure component i , and cross parameters a_{ij} and b_{ij} ($i \neq j$) are

determined by an appropriate combining rule with or without binary parameters. The most significant feature of the PR EOS is its ability to predict the existence of the critical point and to simultaneously consider the vapor and liquid phases, and phase equilibrium below the critical point.

The Benedict-Webb-Rubin-Starling (BWRS) equation [5] is an example of the virial class of EOS. It is a modification of original BWR EOS [6]. The density dependence of BWR is retained in BWRS, while the temperature dependence of the coefficient is changed. The form of the equation is

$$Z = 1 + \left(\frac{B_o RT - A_o \frac{C_o}{T^2} + \frac{D_o}{T^3} + \frac{E_o}{T^4}}{RTV} \right) + \left(\frac{bRT - a \frac{b}{T}}{RTV^2} \right) \quad (7-11)$$

$$+ \frac{\alpha \left(a + \frac{d}{T} \right)}{RTV^3} + \left(\frac{c}{RT^3 V^2} \right) \left(1 + \frac{\gamma}{V^2} \right) \exp \left(- \frac{\gamma}{V^2} \right)$$

where A_o , B_o , C_o , D_o , E_o , a , b , c , d , α , γ are eleven adjustable parameters. Values of the coefficient may be determined by fitting the experimental data. Starling conducted multi-property regression analysis to determine the 11 parameters for each of fifteen substances (light gases and hydrocarbons) [5]. The binary interaction parameters were determined from experimental data on liquid-vapor equilibrium. Lin and Hopke [7] and Hopke and Lin [8] conducted a simultaneous multi-property regression analysis on pure component, binary mixture and multi-component mixture data to develop an optimized set of pure component parameters and binary interaction parameters for the BWRS equation of state. The substances considered were methane, ethane, propane, iso-butane, n-butane, iso-pentane, n-pentane, nitrogen and carbon dioxide. A generalized correlation to determine the parameters for heavy hydrocarbon fractions (hexane and above) was also developed [8]. Once the coefficients are known for the fluid of interest, all state variables can be calculated from two known state variables. The BWRS EOS was developed for light gases and hydrocarbons. Probably because of its ability to cover both liquids and gases and the availability of coefficients and mixing rules for many hydrocarbons in one place, BWRS used to be (and still is to some extent) the most widely used EOS for simulation of pipeline processes.

Advances in the virial forms of the EOS are made by the development of GERG-2008 EOS [9] which was originally developed by the Groupe Européen de Recherches Gazières (GERG) in 2004 and called the GERG-2004 EOS [10]. GERG-2004 is valid for mixtures containing any of the following components: methane, nitrogen, carbon dioxide, ethane, propane, n-butane, iso-butane, n-pentane, iso-pentane, n-hexane, n-heptane, n-octane, hydrogen, oxygen, carbon monoxide, water, helium, and argon. GERG-2008, is an extended version of GERG-2004, in which three additional components were added, namely; n-nonane, n-decane, and hydrogen sulphide, resulting in a total of 21 components. GERG-2004 and GERG-2008 are based on pure substance EOS for each of the considered mixture components and correlation equations for binary mixtures consisting of these components. The GERG EOS are expressed in terms of the Helmholtz free energy as a function of temperature and density. The reduced Helmholtz free energy H is expressed in GERG equations of state by:

$$H(\delta, \tau, \bar{x}) = H^o(\rho, T, \bar{x}) + H^r(\delta, \tau, \bar{x}) \quad (7-12)$$

where the function H^o represents the properties of the ideal-gas mixture at a given mixture density ρ , temperature T , and molar composition \bar{x} , and H^r is the residual part (non-ideal) of

the reduced Helmholtz free energy of the mixture. The parameter δ is the mixture reduced density and τ is the mixture inverse reduced temperature defined as:

$$\delta = \frac{\rho}{\rho_r(\bar{x})} \quad ; \quad \tau = \frac{T_r(\bar{x})}{T} \quad (7-13)$$

The main feature of GERG-2008 is its incorporation of the most accurate experimental binary and multi-component data for gas phase and gas-like supercritical properties to within their respective low experimental uncertainties. GERG-2008 EOS is implemented in RefProp [11], a mixture property program made available by NIST, which is extensively used in the pipeline industry with great success and provides the most accurate prediction of most properties of a wide range of gas mixtures in a wide range of conditions.

7.2.4 Compression Behavior

The main purpose of compression is to transport gas from one location to another. This involves pressure losses, which then require the need to increase the pressure from a lower to a higher pressure. Compression also enables a higher mass flow for a certain pipeline size. This can be described in various ways, each with some advantages and drawbacks. The simplest ways of describing compression are as follows:

- pressure rise: the difference between suction and discharge pressures
- pressure ratio: the ratio of discharge to suction pressures (in absolute units)
- compression ratio: the ratio of volumes at suction and discharge conditions

Compression ratio is more useful for reciprocating compressors since the change in volume is easily determined by the physical movement of the piston. Pressure ratio is more relevant for centrifugal compressors.

Pressure ratio and compression ratio are often confused. For an ideal gas, according to Boyle's Law, they are the same, but for a non-perfect gas, the volume ratio is determined by the nature of the compression process.

The compression process is bounded by two limiting conditions. On the one hand, compression can be adiabatic, that is, no heat is added to or removed from the system. The entropy remains constant and the process is reversible. The compression process is defined by the equation

$$pv^k = \text{constant} \quad (7-14)$$

It should be noted that there are differences in the use of terminology in the compression industry. It has been common practice to call this case "adiabatic," but the more correct term is "isentropic" because the process is not only adiabatic but also at constant entropy and reversible.

If any of the heat produced by compression is being lost from the system, or if other losses occur, this equation has to be modified with a different exponent and written as

$$pv^n = \text{constant} \quad (7-15)$$

In this case, the process now takes into account changes in gas properties. It is still isentropic and reversible but is called polytropic. In practice, a real compression process also includes irreversible losses due to factors such as friction and leakage. The polytropic exponent can be calculated from Eq. (7-5) if the suction and discharge conditions are known.

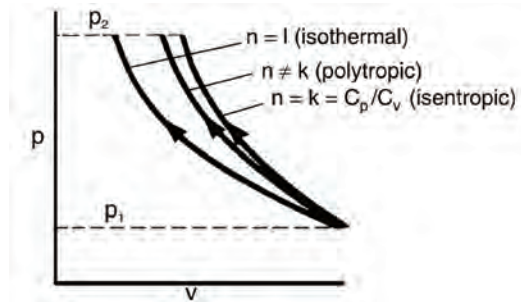


Figure 7-3. Compression process.

For pressure ratios greater than about 1.5, polytropic is more accurate and should be used, but many pipeline compressors can be adequately described using isentropic conditions.

At the other extreme, all of the heat of compression is removed as compression occurs and the process is isothermal. The exponent now has a value of 1. As can be seen from Fig. 7-3, the three compression processes follow different paths on a pressure-volume curve. The result is that isothermal compression requires the least amount of work to be performed. However, isothermal compressors are more difficult and expensive to construct and, thus, are mainly used in critical process applications and never in pipeline compression. Interstage cooling is applied for high-pressure ratio situations to reduce the amount of work needed for the next stage of compression, and aftercooling is common, although primarily to improve pipeline efficiency and reduce the impact of high discharge temperatures on pipeline coatings.

7.2.5 Head

These compression equations can be extended to produce a normalized pressure increase called “head.” For isentropic conditions, the equation for head is

$$H = \frac{Z_a R (T_s + 459.67)}{MW} \times \frac{k}{k-1} \left[\left(\frac{(P_d + P_{\text{bar}})}{(P_s + P_{\text{bar}})} \right)^{\frac{k-1}{k}} - 1 \right] \quad \text{US Customary} \quad (7-16)$$

$$H = \frac{Z_a R (T_s + 273.15)}{MW} \times \frac{k}{k-1} \left[\left(\frac{(P_d + P_{\text{bar}})}{(P_s + P_{\text{bar}})} \right)^{\frac{k-1}{k}} - 1 \right] \quad \text{SI}$$

If the exponent k is replaced by the polytropic one, it becomes the polytropic head.

7.2.6 Efficiency

The efficiency is a measure of the amount of energy that is usefully converted to pressure instead of to an increase in temperature. Again, for isentropic conditions (adiabatic, constant entropy, reversible), the efficiency is

$$\eta_{\text{isentropic}} = \frac{\left[\left(\frac{(P_d)}{(P_s)} \right)^{\frac{k-1}{k}} - 1 \right]}{\left(\frac{(T_d)}{(T_s)} - 1 \right)} \times 100 \quad (7-17)$$

The polytropic efficiency can be calculated from the ratio of specific heat and polytropic exponent

$$\eta_{\text{polytropic}} = \frac{\left(\frac{k-1}{k} \right)}{\left(\frac{n-1}{n} \right)} \times 100 \quad (7-18)$$

The efficiency can also be determined by using an equation of state such as the BWR equation.

7.2.7 Flow

The conventional method of stating a pipeline flow rate is to express it with respect to “standard” conditions of pressure and temperature in million standard cubic feet per day or 1000 m³/d. The “standard” or “base” pressure is normally 14.73 psi or 101.325 kPa but varies throughout the industry and may have values such as 14.16, 14.4, 14.65, 14.696, 14.7 psi, to name a few. The standard or base temperature is usually 60°F or 15°C. Note that this standard volume is the volume occupied by the gas if allowed to expand to the base pressure and temperature and should always be mentioned to avoid confusion.

For a reciprocating compressor, the flow (or capacity) can be calculated directly as is further described in Section 7.3.2. For centrifugal compressors (and also often for reciprocating compressors), the flow is independently measured using a flow meter. This can be an orifice, venturi, ultrasonic, or other type of flow meter with their output being a standard flow.

For centrifugal compressors, it is also useful to determine the “actual” flow, or the compressed flow, usually taken at suction conditions. The conversion from standard to actual flow is

$$Q_a = 694.444 Q_s \frac{P_{\text{base}}}{P_{\text{suct}}} \frac{T_{\text{suct}}}{T_{\text{base}}} \frac{Z_{\text{suct}}}{Z_{\text{base}}} \text{ US Customary} \quad (7-19)$$

$$Q_a = 0.011574 Q_s \frac{P_{\text{base}}}{P_{\text{suct}}} \frac{T_{\text{suct}}}{T_{\text{base}}} \frac{Z_{\text{suct}}}{Z_{\text{base}}} \text{ SI}$$

For multistage units, only the volume at the first stage inlet is usually considered (unless a significant amount of liquid drops out at the interstage), since this determines the capacity for the entire machine. If calculations are being done on a stage-by-stage basis, the inlet volume would be recalculated at the inlet to each stage. Multi-stage centrifugals on high pressures may have a minimum limitation for actual flow, particularly on the final stage. This should be checked with the manufacturer as recycle gas may be necessary around the last stage.

7.2.8 Power

The power required to compress the gas is a function of mass flow, head, and efficiency. Mass flow in US Customary units is determined by

$$m = \frac{Q_s * 144 * P * MW}{(R * Z * T * 60 * 24)} \quad (7-20)$$

where

m is lb/min

Q_s is mmscf/d (60*24 converts the per day in Q_s to per min)

P is psia (144 converts in² to ft²)

T is in °R,

R is 1545 ft-lb_f/lb_m °R

Mass flow in SI units is determined by

$$m = \frac{Q_s \cdot P \cdot MW \cdot 10^3}{(R \cdot Z \cdot T \cdot 24)} \quad (7-21)$$

where

m is in kg/h

Qs is in 10³m³/d

P is in kPa (10³ converts kPa to Pa)

T is in K

R is 8.314 kJ/kMole K

The standard power equation that you will find in most textbooks is

$$\text{Power} = \frac{\text{mass flow} \cdot \text{head}}{\text{efficiency}} \quad (7-22)$$

For US Customary units, this then becomes

$$\text{Power (hp)} = \frac{m \cdot H \cdot 100}{(E \cdot 33,000)} \quad (7-23)$$

where

E is in % (which is why it is multiplied by 100)

33,000 is the conversion of ft-lb/min to horsepower

For SI units, this then becomes

$$\text{Power (kW)} = \frac{m \cdot H \cdot 100}{(E \cdot 3600)} \quad (7-24)$$

where

E is in % (which is why it is multiplied by 100)

When combining the constants for these equations, the result is:

$$\begin{aligned} \text{PWR} &= 0.19614 \frac{MW \times P_{\text{base}}}{T_{\text{base}}} \times \frac{Q_s \times H}{\eta} \quad \text{US Customary} \\ \text{PWR} &= 0.13921 \frac{MW \times P_{\text{base}}}{T_{\text{base}}} \times \frac{Q_s \times H}{\eta} \quad \text{SI} \end{aligned} \quad (7-25)$$

Note that head and efficiency in these equations may be isentropic or polytropic. To determine the shaft power, other losses have to be included, and this can be done by adding a mechanical efficiency factor that will vary with the type of compressor. Estimated mechanical losses (not counting external losses such as pumps powered by other means or magnetic bearing power supply) are:

- 3% for integral reciprocating compressors
- 5% for separable reciprocating compressors
- 2% for centrifugal compressors with oil bearings and dry seals
- 0.2% for centrifugal compressors with magnetic bearings and dry seals

For centrifugal compressors with oil bearings and wet seals, approximate losses are dependent on power:

- 3% for gas power of 0–3350 hp
- 2.5% for gas power of 3350–6700 hp
- 2% for gas power of 6700–10,000 hp
- 1.5% for gas power of more than 10,000 hp

The brake power can be derived by one of the two options shown below or a combination of the two.

$$\begin{aligned} \text{PWR}_{\text{brake}} &= \frac{\text{PWR}_{\text{gas}}}{\eta_{\text{mech}}} \quad \text{or} \\ \text{PWR}_{\text{brake}} &= \text{PWR}_{\text{gas}} + \text{mechanical losses} \end{aligned} \quad (7-26)$$

7.3 PERFORMANCE OF RECIPROCATING COMPRESSORS

7.3.1 General

Reciprocating compressors are very efficient and provide reasonable flexibility for pipeline operation. They can accommodate a large range of single-stage compression ratios, from 1.1 to 3 being normal. A major drawback for pipeline service is their relatively low flow capability compared to what is normally needed for large mainlines. From a performance point of view, they differ substantially from that of a centrifugal compressor.

7.3.2 Flow

The capacity or flow of a reciprocating compressor can be calculated directly from its physical dimensions and configuration. A separate flow device is theoretically not needed, although it is useful as verification and in cases where flow is being bypassed.

Ideally, a compressor cylinder will handle a volume equal to the total volume swept by the piston. This volume, termed “piston displacement” (PD) is calculated as follows for a typical double acting cylinder, usually expressed in cubic feet per minute (cfm):

$$\left[\begin{array}{c} \text{piston area,} \\ \text{head end} \end{array} + \begin{array}{c} \text{piston area,} \\ \text{crank end} \end{array} \right] \times \text{stroke} \times \text{rpm} \quad (7-27)$$

Note that the crank-end piston area includes a deduction for the area of the rod, and the head end area may be reduced by a tail rod.

In practice, the capacity or volume handled by the cylinder is less than the PD due to several factors:

- **Clearance.** The volume inside the cylinder not swept by the piston, including space between the piston and cylinder head and space required for valves, gas passages, etc. Clearance volume is expressed as a percentage of PD, and its range varies with different cylinder designs. The amount of “built-in” clearance must be obtained from the manufacturer. On the compression stroke, gas at discharge pressure (or slightly above

it due to discharge valve pressure differential) is trapped in the clearance space and expands inside the cylinder before the suction valves open on the next intake stroke. This expanded gas occupies a portion of the cylinder volume, causing a reduction in actual capacity. Remember that this “actual” capacity is, by definition, measured immediately upstream of the cylinder. The expansion referred to takes place inside the cylinder, thereby preventing an equivalent volume from entering.

- Preheat. Gas entering a cylinder is partially heated by the warm cylinder head and walls that are heated by the previous compression stroke. This increases the incoming gas volume (due to temperature expansion), causing a further reduction in actual volume.
- Valves. Due to the pressure differential required to hold the suction valves open, the cylinder pressure during the suction stroke is slightly less than the actual suction pressure outside the cylinder, again causing a slight expansion of the incoming gas and reducing the actual volume.
- Flow losses. Friction losses in the valve and cylinder flow passages cause an additional pressure reduction, consequent expansion, and reduction in actual capacity.
- Leakage. Gas leaking past the piston rings and through closed valves also reduces the actual volume handled. There will always be some leakage present, but poor maintenance can cause a large increase and lead to an indeterminate amount of leakage.
- Compressibility. All real gases do not behave ideally, and the volume change during compression is not linear with pressure. This may increase or decrease the actual capacity depending on the pressures and temperatures involved.

It may be noted that, with the exception of clearance (and sometimes compressibility), all the other factors result in an increase in the power required to drive the compressor. Valve pressure differential and flow losses also occur during the discharge stroke, but these do not affect the inlet volume. They do, however, increase the required power.

All factors require the cylinder size to be somewhat different (usually larger) than would theoretically be the case, and manufacturers will provide cylinders accordingly. In practice, cylinders are manufactured in standard sizes, and fixed clearance volumes are added, if necessary, to tailor a basic cylinder to match the required capacity.

All these factors are included in the term “volumetric efficiency” (VE), which is the ratio (expressed as a percent) of the actual cylinder capacity to the PD, or:

$$VE = \frac{Q_a}{PD} \times 100 \quad (7-28)$$

Thus, a VE of 0.50 or 50% means the cylinder will deliver a gas volume equal to 50% of the total volume swept by the piston. Volumetric efficiency is not a constant value and is affected by clearance volumes, compression ratios, and k value, as shown by the following theoretical formula:

$$VE = 100 - c \left[r^{1/k} - 1 \right] \quad (7-29)$$

From this formula, the effect of changing clearance on the cylinder capacity is readily apparent. Clearance is added to a cylinder simply by adding “pockets” or dead volumes into which the gas is compressed on each stroke. Clearance pockets are normally supplied as fixed volumes, but variable volume pockets may also be used in some applications. The size and types of available clearance pockets for a particular compressor must be obtained from the manufacturer.

The k value in the above formula is for expansion of the gas and will often be different from the k value for compression. Since the true value is seldom known, the k value at an average of suction and discharge temperatures is normally used.

In practice, the VE formula is modified to include effects of the various factors mentioned previously and may be expressed as follows:

$$VE = (100 - L) - c \left[\frac{Z_{\text{suct}}}{Z_{\text{disch}}} r^{1/k} - 1 \right] \quad (7-30)$$

Z_{suct} and Z_{disch} are the compressibility factors at suction and discharge, respectively, and L is an experimental correction factor determined by a manufacturer from test data. L is a “blanket” term covering all other corrections. The value of $100 - L$ may range from around 88% to 98% and will vary with different cylinders and manufacturers. The actual value used by a manufacturer is often proprietary and difficult to obtain. For rough approximation, the following values can be used:

- large slow-speed cylinders with low ratios (<1.5): $100 - L$ may have values around 97
- slow-speed process cylinders with higher ratios (>1.5): $96 - r$ (pressure ratio)
- high-speed cylinders: $96 - 2r$

Because of the indeterminate nature of the previous factors, the actual VE of any cylinder is extremely difficult to pinpoint accurately. This is one of the major problems when applying analytical methods to reciprocating compressor performance and results in a discrepancy between measured and calculated capacities.

Assuming the correct VE is known, however, the actual cylinder capacity is found from:

$$Q_a = PD \times \frac{VE}{100} \quad (7-31)$$

It should be noted that a low VE, if a result of large built-in clearance within the cylinder, is not an indication of high power consumption. In this situation, large clearance volumes may indicate large valves and liberal gas passages, causing less pressure loss and, hence, a lower power consumption. If, however, clearance pockets are added, there may be an increase in power if the passages restrict the gas flow in and out of the pocket. If no restrictions exist, the power used to compress gas into the clearance volume is recovered when the gas re-expands.

Although the VE formula is used more by manufacturers than users, it can be helpful for capacity control of reciprocating compressors. For example, knowing the required actual flow and the compressor speed (PD), a required VE can be found. From this, the required clearance can be calculated and corresponding pockets opened or closed as required. Final adjustments to the flow can then be made by slight changes in speed. This is complicated by the often indeterminate values of the correction factor, L , but if a flow measuring device is available, this factor may be approximately determined from test measurements.

7.3.3 Power

For normal reciprocating machines, the compression process is taken to be isentropic (i.e., reversible adiabatic and at constant entropy). This assumes that no heat is added or removed from the gas during compression and that the temperature change results only from compression. Although this is not strictly correct (some heat is lost to the cylinders and some added by friction, etc.), it is reasonably close for reciprocating compressors.

The ideal isentropic power required for compression is:

$$\begin{aligned} \text{PWR}_{\text{ideal}} &= \frac{Q_a P_{\text{suct}}}{229} \frac{k}{k-1} \left[r^{(k-1)/k} - 1 \right] \text{ US Customary} \\ \text{PWR}_{\text{ideal}} &= \frac{Q_a P_{\text{suct}}}{3600} \frac{k}{k-1} \left[r^{(k-1)/k} - 1 \right] \text{ SI} \end{aligned} \quad (7-32)$$

The ideal power calculated above is the theoretical power added to the gas. This is not the required compressor power since the various losses mentioned previously as well as compressibility factors and mechanical losses have not yet been included. Taking these losses one at a time, we can correct for them as follows:

- Valve, thermodynamic and pressure losses. These are customarily grouped together under the term “compression efficiency” or “isentropic efficiency,” which ranges from around 72% to 88%. Process “standard” cylinders on high ratios (e.g., above $r = 2$) and large pipeline cylinders on low ratios would be near the upper end, with 83% being a reasonable assumption. Process cylinders with ratios around 1.4 would assume a value near the low end. Process cylinders below a 1.4 ratio can have very low efficiencies (e.g., 60%), and the manufacturer should be consulted for an accurate value. This “efficiency” is another blanket type of correction and accounts for a number of indeterminate losses.
- Mechanical losses. Power used to overcome friction in the bearings, packing, piston rings, etc. is accounted for under the term “mechanical efficiency,” with values ranging from around 88% to 95%. A value of 93% is a reasonable assumption for large compressors, and a lower value would be used for high-speed (i.e., 1000 rpm) machines.
- Compressibility factor correction. There are several methods of applying this correction that accounts for the deviation of the actual gas from the perfect gas laws. A rigorous calculation results in an awkward and cumbersome formula and will not be presented here. For most practical purposes, however, the following correction factor is sufficiently accurate:

$$\text{Compressibility correction} = \frac{Z_{\text{suct}} + Z_{\text{disch}}}{2Z_{\text{suct}}} \quad (7-33)$$

The result is the power added to the gas by the compressor:

$$\begin{aligned} \text{PWR}_{\text{gas}} &= \frac{Q_a P_{\text{suct}}}{229\eta} \frac{k}{k-1} \left[\frac{Z_{\text{suct}} + Z_{\text{disch}}}{2Z_{\text{suct}}} \left[r^{(k-1)/k} - 1 \right] \right] \text{ US Customary} \\ \text{PWR}_{\text{gas}} &= \frac{Q_a P_{\text{suct}}}{3600\eta} \frac{k}{k-1} \left[\frac{Z_{\text{suct}} + Z_{\text{disch}}}{2Z_{\text{suct}}} \left[r^{(k-1)/k} - 1 \right] \right] \text{ SI} \end{aligned} \quad (7-34)$$

Compressor brake horsepower is the power required to drive the compressor, equalling the gas horsepower plus mechanical losses:

$$\text{PWR}_{\text{brake}} = \frac{\text{PWR}_{\text{gas}}}{\eta_{\text{mech}}} \quad (7-35)$$

If the drive is through gears or belts, for example, the driver power must be increased by the amount of the drive losses. In addition, care should be taken to ensure that other auxiliary loads are accounted for, such as cooler fans, generators, and water and lube oil pumps.

Although the compression efficiency by itself may account for the power to overcome various losses, some manufacturers specifically isolate other corrections and include them separately. In this case, adjustments should be made to the efficiency to avoid correcting twice for the same item. Two of these corrections are preheat and valve losses.

Preheat correction involves raising the suction temperature to account for warming of the incoming gas by the cylinder. There is no commonly accepted correction and manufacturers have developed their own factors for use with their equipment, sometimes by actual testing (Prasad). Estimating the preheat, which can be significant, is dependent on different factors such as flow, pressure ratio, any cylinder cooling provided, and cylinder construction, so it is best to depend on manufacturer's estimates.

Since there is a pressure drop across the suction and discharge valves, various methods are used to estimate this since it affects the true pressure and its associated calculations. Some manufacturers determine an equivalent area which is the orifice area required to generate the same pressure drop as that through a compressor valve when flowing the same quantity of the same gas at the same conditions. Others calculate a resistance factor which relates a measured pressure drop to that which would be predicted by assuming a round hole with discharge coefficient of one and an area equal to the valve opening, all at the same process conditions.

7.3.4 Discharge Temperature

Using an isentropic (adiabatic) relationship, the theoretical discharge temperature can be found from:

$$T_{\text{disch}} = T_{\text{suct}} \left[r^{(k-1)/k} \right] \quad (7-36)$$

This is not strictly correct and a closer estimate has been found by the following equation which takes care of non-ideality as well as friction and performance losses:

$$T_{\text{disch}} = T_{\text{suct}} \left[1 + \frac{1}{\eta_{\text{isentropic}}} \left(r^{(k-1)/k} - 1 \right) \right] \quad (7-37)$$

In summary, it can be stated that due to several indeterminate factors, a completely accurate method of calculating reciprocating compressor performance is not available. For most purposes, however, the use of simplified theory and correction factors gives reasonable results.

Although the calculations presented deal with single-stage compression, multi-stage calculations are handled in the same way for each stage. On multi-stage units, however, the ratio per stage is usually close to a power of the overall ratio, that is, the square root for two-stage, cube root for three-stage, etc., with adjustment for inter-stage losses, rod loading and maximum discharge temperature limitations.

7.3.5 Performance Maps

The performance of a reciprocating compressor can be described on performance maps that show sets of curves.

The two example performance maps shown in Figs. 7-4 and 7-5 are really the same, the first being plotted with suction pressure versus a standard volume flow and the second with suction pressure and pressure ratio versus the compressor actual flow. These curves are plotted using a constant discharge pressure and constant speed. In practice, there would be

a series of maps covering the complete range of discharge pressure. As an alternate, maps could be plotted at constant suction pressure (discharge pressure versus flow), or constant flow (discharge versus suction pressure), depending on which type of map gives the best information for the particular situation.

Each map shows the effect of cylinder clearance (i.e., volume not swept by the piston) on performance with step 1 being minimum clearance and step 9 being maximum clearance. These steps are changed by progressively opening more clearance pockets on the cylinders, reducing the flow capability. Rather than a single line performance, the machine can now operate over a fairly wide area while maintaining a constant rpm. Note also that by increasing the clearance, the power required by the compressor decreases until, for example, at step 7, it becomes impossible to overload the engine.

If the performance map in Fig. 7-5 were extended upward, it could be shown that the power required would reach a peak with decreasing flow and then start to decrease even with increased ratios. This effect may be observed on the power curve (Fig. 7-6) corresponding to step 9, but it will also happen on all other steps.

These maps demonstrate how additional cylinder clearance can be used to alter the flow capability and prevent overloading the driver under variable conditions.

The flow and pressure corresponding to the maximum engine power output is plotted in Fig. 7-4 in the form of the “engine capacity” curve. Operation below this line results in overloading the engine. At startup, operation on a pipeline, for example, would commence on step 1. As pipeline flow became established, the suction pressure would fall, and operation would proceed down the step 1 curve until the engine capacity curve was reached. At this point, clearance would be added to prevent going below the engine capacity curve. The discharge would of course also rise, requiring progressive changes to higher discharge pressure curves, but the procedure is the same.

The effect of speed reduction on these curves is not shown, but it would simply shift any chosen cylinder (or clearance) curve horizontally to the left by the rpm ratio. The slope of the curve would remain constant as opposed to clearance changes that alter the slope. Note that with reduced speed, however, the engine maximum power capability will be less than shown, and this may or may not be a problem depending on how the power decreases as the driver speed is reduced. To analyze this latter problem, driver performance data in the form of power versus speed would be required.

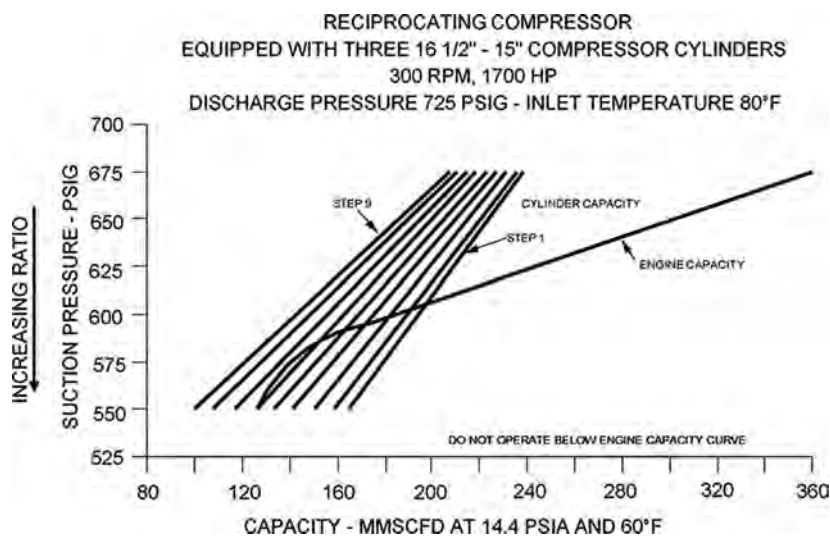


Figure 7-4. Example of a performance map for suction pressure versus standard flow.

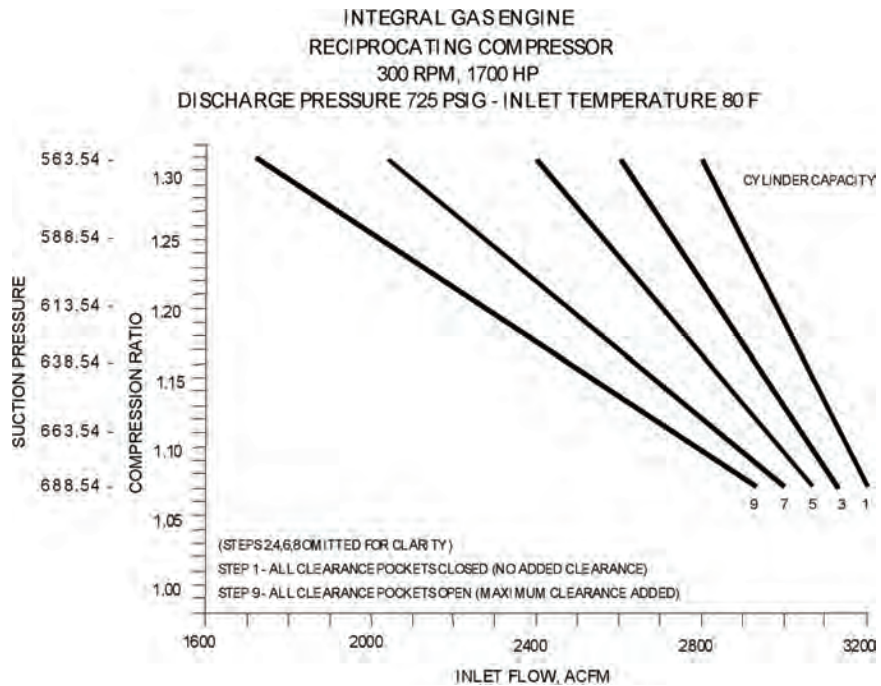


Figure 7-5. Example of a reciprocating compressor performance map for suction pressure and ratio versus actual flow.

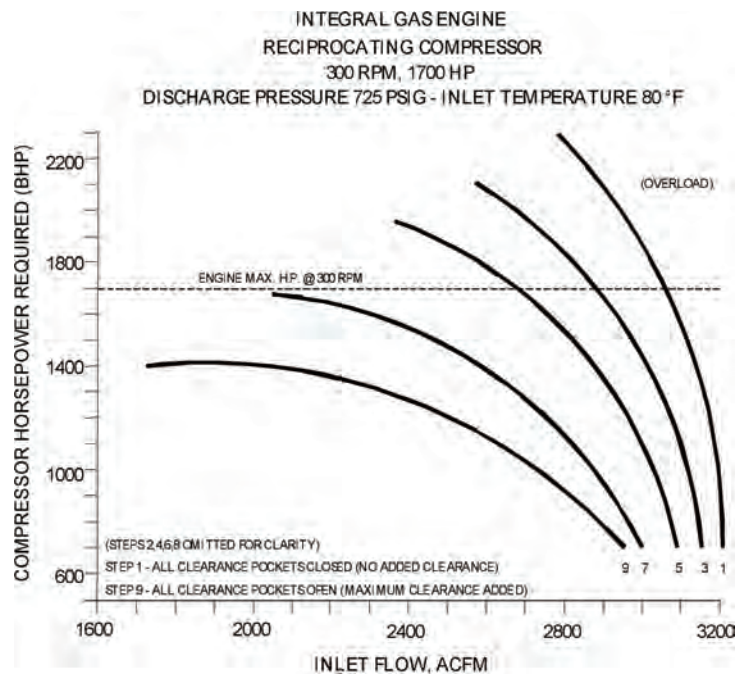


Figure 7-6. Example of a reciprocating compressor performance map for power versus actual flow.

For large, slow-speed engines (e.g., 300 rpm), power may be assumed to vary linearly with rpm.

Another previously mentioned method of capacity control—valve unloaders—is not very common on transmission machines as a control method. This effectively takes all or part of the cylinder out of operation (e.g., one end of a double-acting cylinder), having roughly the same effect as reduced speed. Unloaders can be valuable during startup and warmup periods to avoid overloading a driver until it has reached operating temperature.

Multi-stage reciprocating compressors are considered in the same manner as outlined above. In this case, a “stage” is a cylinder (or, possibly, one end of a double-acting cylinder) operating in series with another cylinder or end. These multistage units can sometimes be difficult to operate on pipeline systems since small changes in pressures—particularly the suction pressure—can have large effects on the compressor operation and power requirements. Fortunately, pipeline transmission ratios are usually low enough that reciprocating compressors are single stage, with several cylinders operating in parallel to achieve the required capacity.

7.3.6 Piston Speed

Another useful value to calculate is piston speed, since a number of practical aspects of the operation of reciprocating compressors are related to this value. Piston speed is usually calculated as the average speed, or

$$PS = 2 \times \text{stroke} \times N \quad (7-38)$$

The piston speed is important because it defines various tradeoffs. A manufacturer prefers as high a speed as possible because, for a certain required capacity, this results in a smaller cylinder and, thus, lower cost. The user would rather have a lower speed because it increases reliability and reduces maintenance expenses. Higher piston speeds affect the reliability not only of moving parts such as the piston rings and rod surface and packings but also suction and discharge valves since they activate at the same frequency as the speed. API 618 does not specify actual values, but general industry practice indicates a maximum piston speed of 700 ft/min or 4 m/s for horizontal lubricated cylinders.

7.4 PERFORMANCE OF CENTRIFUGAL COMPRESSORS

7.4.1 General

In this section, as in the previous section on reciprocating machines, performance is considered from a “required” viewpoint rather than compressor design. The basic head, flow, efficiency, and power calculations already defined apply to centrifugal compressors. Due to its dynamic nature, performance characteristics are different.

7.4.2 Dynamic Performance Characteristics

7.4.2.1 Basic Performance Curves

In a centrifugal machine, a stage of compression consists basically of the inlet guide vanes, an impeller or rotating component, and a stationary diffuser which surrounds the impeller, collecting the high velocity gas and slowing it down to recover pressure. In multistage units, the diffuser leads into a return channel, which directs the gas to the inlet of the next stage. Guide vanes, if used, are normally fixed, and direct the incoming gas into the impeller in the axial direction (no pre- or counter-swirl). However, movable guide vanes may be employed to add pre-swirl (sometimes counter-swirl) to the incoming gas, usually only on

the first-stage inlet. Once the geometry, speeds, and aerodynamic factors have been taken into account by the designer, each guide vane/impeller/diffuser combination will exhibit a definite performance characteristic. This must be obtained from the manufacturer.

In a reciprocating compressor, pressure is increased by mechanical volume reduction and is somewhat independent of the gas properties. In a centrifugal compressor, however, gas properties are a major factor in the pressure rise, causing the pressure–volume characteristic to be dependent on the particular gas being handled. To overcome this difficulty, centrifugal performance is described in terms of the “head” concept. Head is a measure of work done per unit mass of gas being compressed and is, for practical purposes, independent of the gas. Head is dependent on gas velocity changes through the impeller, which are, in turn, a function of geometry, speed, and volume flow rate. The head–volume characteristic for a given compressor stage can be considered constant, with the actual pressure ratio being a function of gas properties. This characteristic performance curve is always provided by the manufacturer and is fixed by the particular design (see Fig. 7-7). Due to its unique shape, it is also referred to as a wheel curve.

Centrifugal performance calculations are based on two compression relationships: isentropic or adiabatic ($PV^k = \text{constant}$) and polytropic ($PV^n = \text{constant}$). In general, the isentropic method is used for one- or two-stage compressors and polytropic for two or more stages. Some manufacturers, however, use either one or the other for all compressors, regardless of the number of stages. Basically, the isentropic relation allows for temperature changes due to the heat of compression only, while polytropic allows for additional heating, mainly from disc friction (spinning impellers) and internal leakage.

For initial sizing of centrifugal compressors on natural gas, the ratio of specific heats or k value used in performance calculations may be the value determined at the compressor (or stage) inlet temperature rather than at an average of suction and discharge temperatures. At this lower inlet temperature, k will be slightly larger, resulting in a slightly conservative result for head, power, and discharge temperature. For calculations on an existing machine, the k value at an average temperature is normally used.

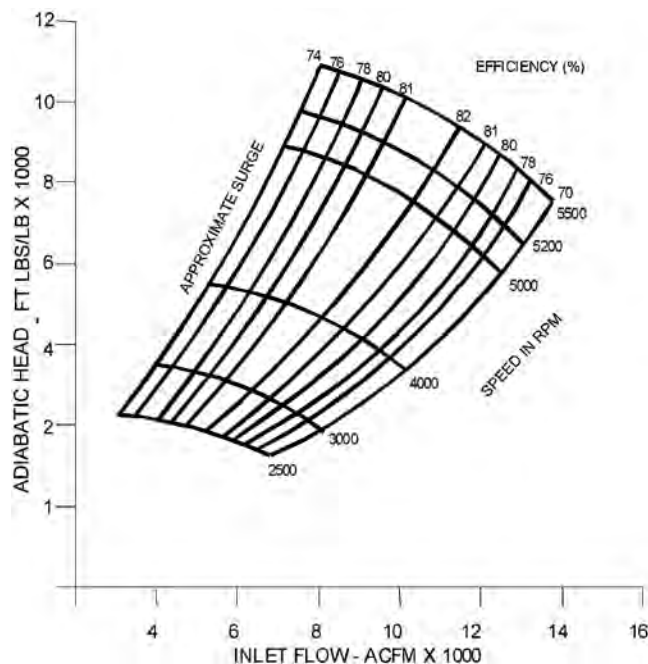


Figure 7-7. Example of a performance map for a centrifugal compressor.

For the same reason, compressibility factors should be averaged as shown. For most pipeline applications, this average will be slightly higher than the inlet value alone. Since compression efficiency affects discharge temperature, inefficient machines give a higher discharge temperature for the same ratio, raising the discharge compressibility and, therefore, the average.

Note that all thermodynamic and flow losses are again summarized in a single blanket correction, the isentropic or polytropic efficiency. Values of these efficiencies are determined by a manufacturer from test data and indicated on compressor performance curves.

Typical values of polytropic efficiencies for multistage centrifugals are from 72% to 78%, with the larger machines exhibiting the higher values. Very low flow, small-diameter impellers may have efficiencies down to around 60% and should be checked with the manufacturer. Large single- or two-stage pipeline machines typically show polytropic efficiencies from around 78% to 83%, with some newer machines reaching as high as 88%. Note that polytropic efficiencies are usually numerically larger than adiabatic efficiencies, depending on the k value and ratio. For low ratio pipeline compressors, however, these efficiencies are often the same. A chart for converting between isentropic and polytropic efficiency is included in Fig. 7-8.

To arrive at the total power required to drive the compressor, various mechanical losses must be added due to bearings, seals, and disc friction. Typical losses for centrifugal compressors may be estimated at 3% of gas power for larger single-stage machines, 5% of gas power for smaller and two-stage machines, and (3% + 1% per stage) for multi-stage centrifugals. These losses are added to the calculated gas power, resulting in the power required to drive the compressor. Drivers are sized to deliver this power (+ 4% for compressor guarantees), plus any drive gear loss or auxiliary equipment requirements.

As with reciprocating compressors, accurate performance calculations depend on accurate values of gas properties and various efficiencies. An examination of the equations will show the effect of changing gas properties, temperatures, and efficiencies on compressor performance.

Although a centrifugal compressor may be considered as a constant pressure, variable volume machine, this really applies only to one- or two-stage compressors. With higher ratio machines (centrifugals are made with up to eight stages) the characteristic curve shown previously becomes steeper and narrower as indicated in Fig. 7-9, being the sum

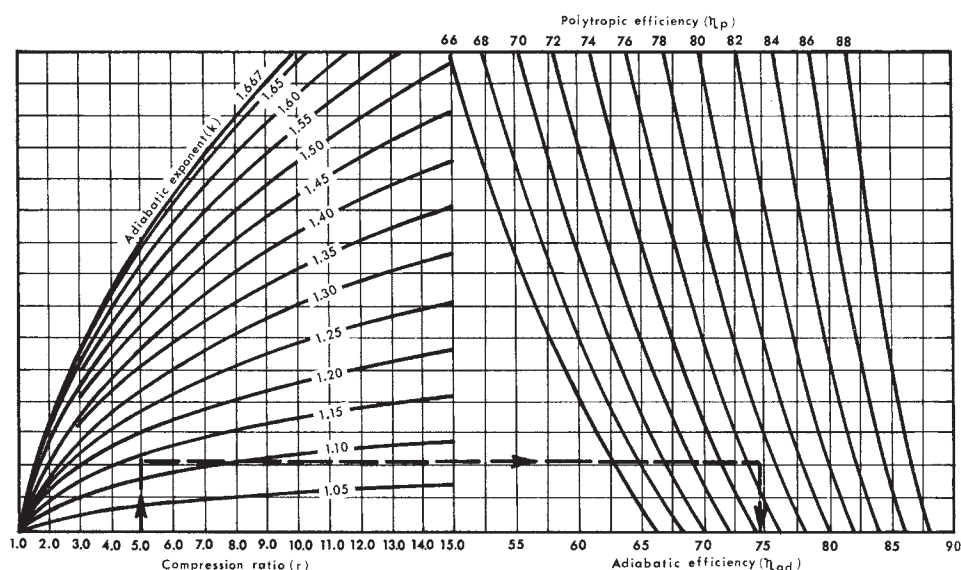


Figure 7-8. Conversion between adiabatic and polytropic efficiency [12].

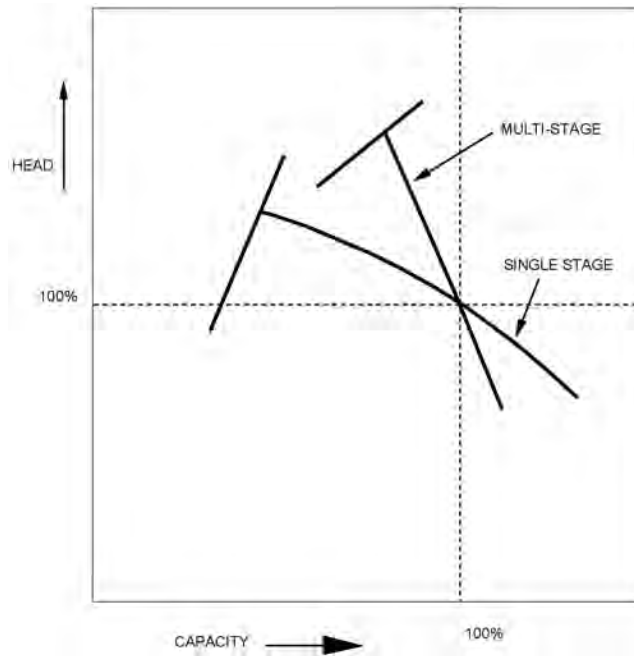


Figure 7-9. Performance map for single and multistage centrifugal compressors.

of the performance of each stage. For any particular compressor, the actual performance curve must be provided by the manufacturer and will be based on design, empirical factors, and test data.

Note that, for stable performance, compressors used in pipelines and industrial applications have impellers with backward leaning blades (rather than radial or forward leaning). This creates a negative slope to the curve, which is required for stability and control. Curves which exhibit a relatively flat shape should be avoided unless the process conditions are very steady, since a small increase in required head can force the compressor rapidly into surge. Most pipeline centrifugals have a surge point located at roughly 50% of rated flow. Reasonable stability can be expected if the curve shows a 5% head increase with each 20% reduction in flow or a 12% to 15% head rise from rated flow back to the surge point.

7.4.2.2 Fan Laws

Methods for calculating the effect of speed changes on the performance curve usually involve applying the affinity or “fan” laws which were first developed for pumps. These give close approximations for speed changes of up to 15% from an established point on the design curve of the compressor.

These relationships for an impeller of fixed diameter are stated as follows:

$$\begin{aligned}\frac{\text{Flow}_1}{\text{Flow}_2} &= \frac{\text{Speed}_1}{\text{Speed}_2} \\ \frac{\text{Head}_1}{\text{Head}_2} &= \left(\frac{\text{Speed}_1}{\text{Speed}_2} \right)^2 \\ \frac{\text{Power}_1}{\text{Power}_2} &= \left(\frac{\text{Speed}_1}{\text{Speed}_2} \right)^3\end{aligned}\tag{7-39}$$

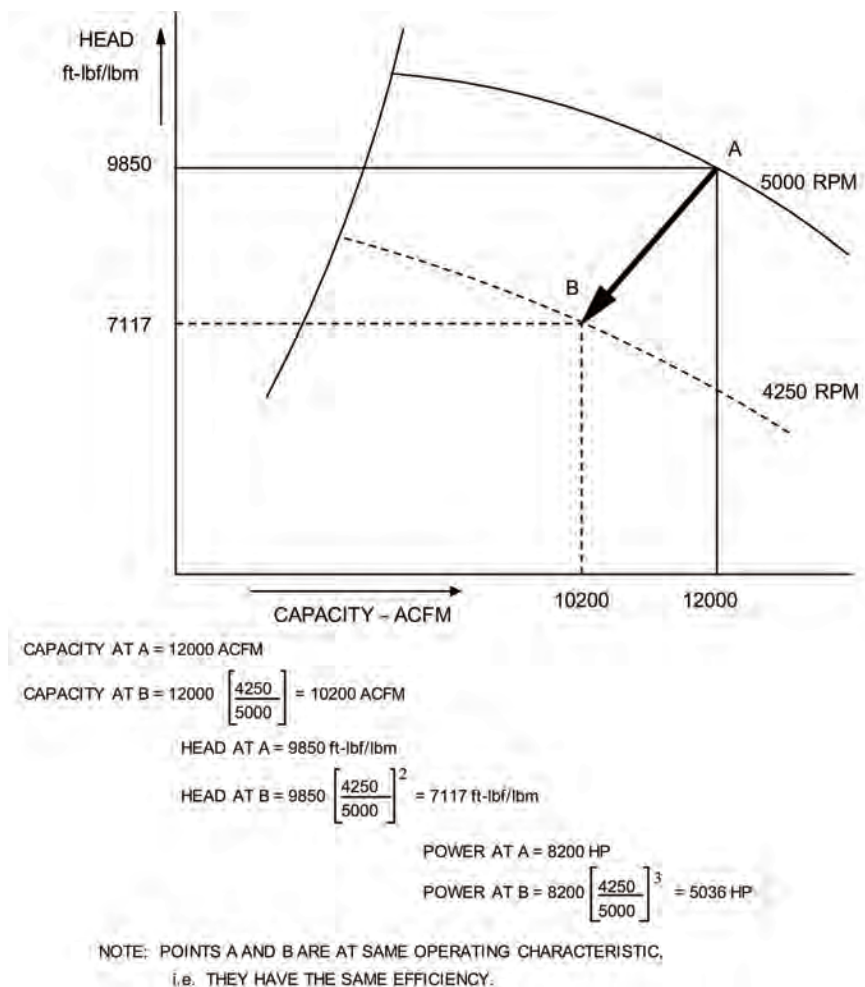


Figure 7-10. Effect of speed changes on compressor performance using the fan laws.

The fan laws can be used to derive two second order equations that describe the performance curve.

$$\begin{aligned} \text{Head} &= aN^2 + bQ_a N + cQ_a^2 \\ \text{Efficiency} &= d + e \frac{Q_a}{N} + f \left(\frac{Q_a}{N} \right)^2 \end{aligned} \quad (7-40)$$

As an example, the effect of changing the speed from 5000 to 4250 rpm is illustrated in Fig. 7-10. Small impeller diameter changes may be calculated in exactly the same way.

7.4.2.3 Performance Limits

A centrifugal compressor has a number of limits in its performance that are illustrated on the performance map in Fig. 7-11. These limits constrain the envelope in which it can operate but also have implications on its design and reliability.

The first set of constraints are speed-related. For a standard gas turbine-driven compressor, this will be the speed of the power turbine attached to the compressor. Since this will be a flexible shaft, the minimum speed needs to be above the first critical of the

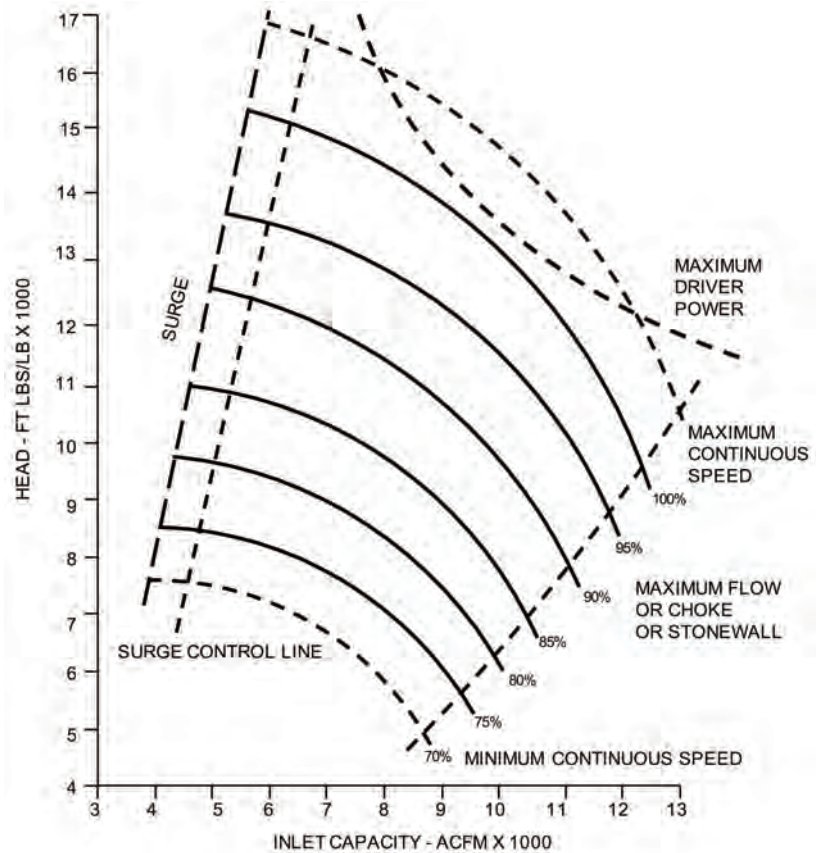


Figure 7-11. Performance limits for a centrifugal compressor.

shaft. A typical minimum power turbine/compressor speed is 70% of the design speed. Electric motors potentially have a much wider operating speed range but rotordynamic issues that may also be affected by electrical interferences from the VFD.

Maximum continuous speed is usually 105% of design speed with automatic overspeed shutdown at 110%. The maximum speed is a mechanical integrity limit well below the ultimate strength of the materials involved and a fatigue life appropriate for the expected life of the compressor and power turbine.

Competing with the maximum speed is the maximum power of the driver, which could limit the maximum speed. The maximum power for a gas turbine-driven compressor will vary with ambient temperature, reducing the top range of the compressor map at higher temperatures. This is not an issue with electric motors except at high altitudes and high ambient temperatures where motor cooling is affected.

On the left-hand side of the performance envelope is the low flow, surge limit with a surge control line at 10% that activates the recycle valve and prevents the compressor from entering surge. Since surge involves a transition zone, it is not always easy to decide exactly where the surge line, and by inference the surge control line, should be. It is safer to be conservative, but this will encroach on the operating region where the efficiency is the highest.

On the right-hand side of the performance map, the compressor reaches a high flow region that is also known as choke or stonewall. In this region, the speed lines drop dramatically as well as efficiency due to aerodynamic choking of the flow where the Mach

number approaches 1.0. This limit is reached sooner for high molecular weight gases than for low ones. This phenomenon, also known as overload, and the deleterious effects it has on both compressor degradation and mechanical integrity is further described in [13].

7.4.3 Selection and Sizing

Manufacturers estimate the off-design performance by utilizing various dimensional factors of importance. Dimensional analysis is a procedure where variables representing a physical situation are reduced into groups that are non-dimensional to:

- compare data from different machines
- select units for best efficiency and pressure rise
- predict a prototype's performance

The most important of these are the following:

$$\begin{aligned}\text{Specific speed } N_s &= \frac{N\sqrt{Q}}{H^{3/4}} \\ \text{Specific diameter } D_s &= \frac{DH^{1/4}}{\sqrt{Q}} \\ \text{Flow coefficient } \phi &= \frac{Q}{ND^3} \\ \text{Pressure coefficient } \varphi &= \frac{H}{N^2 D^2}\end{aligned}\tag{7-41}$$

This information remains proprietary, but is the basis for many of the manufacturer's design calculations.

Another aerodynamic parameter used in the design process is the Mach number, or the velocity of the gas inside the impeller and diffuser divided by the speed of sound. Mach numbers that approach unity or the speed of sound create excessive losses and reduce efficiency as well as setting up shock waves that can damage the compressor. A related parameter is the Reynolds number which is defined as:

$$\text{Re} = \frac{\rho \text{ (density of the gas) } V \text{ (velocity) } D \text{ (impeller diameter)}}{\mu \text{ (viscosity of the gas)}}\tag{7-42}$$

This denotes the type of flow, for example, if it is turbulent and is critical when comparing test results with the actual design.

The major tradeoff in compressor design is that between operating range and efficiency [14]. The methods by which increased efficiency are achieved often reduce the overall range of the compressor. When a user specifies the desired performance, this may consist of one point or a range of operating conditions. From this information, the manufacturer selects a design point where normally the efficiency will be the highest and the speed will be at 100% of rated.

The operating range is bounded by two general limits: surge and choke. As can be seen from Fig. 7-12, the design point is related to the surge line by a factor called stability. Stability is expressed as the ratio of the distance of the design point from the surge line with respect to the design flow and is a measure of a compressor's surge margin. Overload likewise measures the margin before choke or maximum flow is reached. The range ratio is the ratio of the overload flow and the flow at surge. The "rise to surge" estimates how much

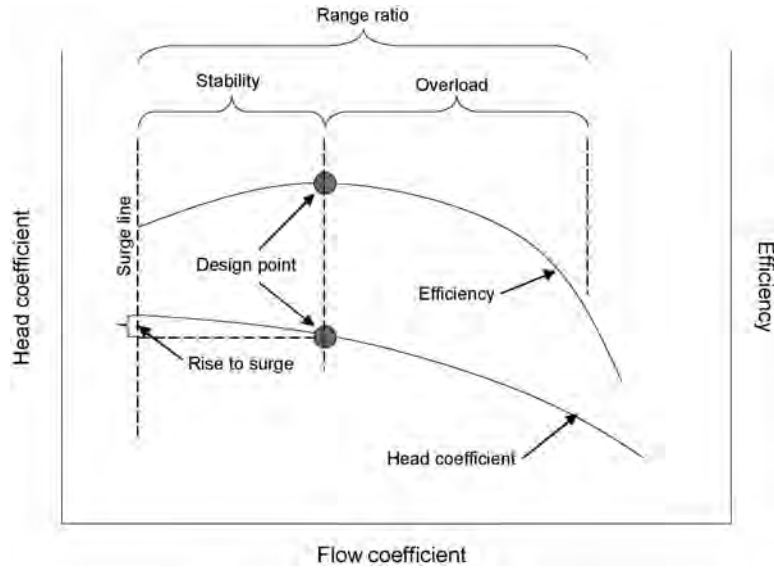


Figure 7-12. Compressor design terminology.

the head coefficient rises from the design point to the surge line. A greater rise to surge improves the controllability of the compressor.

For pipeline compressors, a wide range is typically desirable with a slower drop-off in efficiency, particularly at higher flows. This has the effect of decreasing maximum efficiency at the design point, but with the advantage that the average efficiency over time will be improved. It is also advantageous to have an impeller with a lower head coefficient since higher head coefficients produce a narrower range. Vaneless diffusers also have a higher flow range but again with a lower efficiency.

7.4.4 Performance Testing

Performance testing, both for acceptance purposes and later for operational verification, is important for centrifugal compressors. Because of its dynamic nature, centrifugal compressors may not perform as expected or may suffer from performance loss due to factors such as impeller erosion and fouling.

In contrast with mechanical tests such as the impeller overspeed test, API 617 [15] considers a performance test as optional and dependent on agreement between vendor and purchaser. Since it is, in fact, not feasible to define a test that will be acceptable and applicable in all situations, this is a logical situation.

Performance testing of centrifugal compressors is covered by ASME PTC 10 [16] and also ISO 5389 [17]. Their main purpose is for shop or factory testing. For site testing, the best source for guidance is the “Guideline for Field Testing of Gas Turbine and Centrifugal Compressor Performance” [18].

Full-scale factory testing is quite expensive, particularly for larger compressors, and rarely can all the conditions be simulated. For hydrocarbons, achieving the same gas composition and the same flows are the most difficult. For convenience and safety purposes, an inert gas or air can be substituted, and the results translated to the expected site conditions to predict expected performance. ASME PTC 10 establishes two possible tests, a type 1 test with the specified gas at pressures, temperatures and speeds close to the design with permissible deviations in process conditions. As an alternate, a type 2 may be done on a substitute gas and at different operating conditions which are corrected back to the actual ones. In this

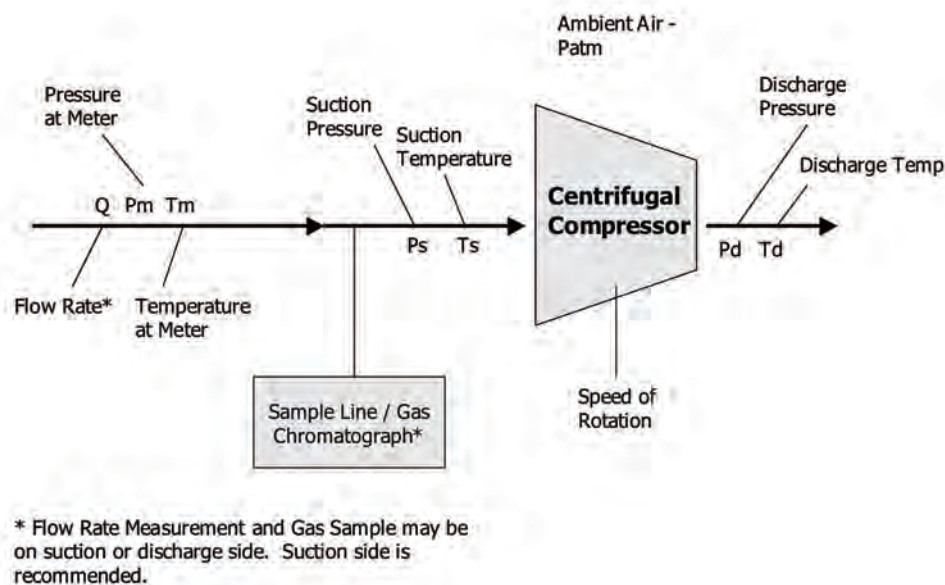


Figure 7-13. Typical location of instrumentation for a centrifugal compressor [18].

case, there are permissible deviations in dimensionless parameters such as flow ratio, flow coefficient, and Mach and Reynolds numbers.

Field testing is more feasible but has significant challenges to achieving a satisfactory result. Typical location of instrumentation for a centrifugal compressor is shown in Fig. 7-13. Some of the major issues are as follows:

- Instrumentation has to be very accurate and calibrated properly.
- Ideally, pressures and temperatures are measured at four points, spaced equally around the perimeter of the suction and discharge piping to average out any flow distortions that may exist. Usually, at best, only two are available and if only one exists; it is better to locate it a bit farther away from the compressor. Situating them close to the suction and discharge gives the most valid result but may introduce fluctuations from the compressor.
- Measurement of flow is critical and requires a flow meter properly installed to achieve maximum accuracy.
- It is important not only to test close to the design point but also across the range of flows (ideally five points from the surge line to choke) and head (ideally at three speeds, low, medium, and high).
- Sufficient time has to be allowed for stable operating conditions to be realized. Temperature especially is slower to stabilize.
- Uncertainty calculations have to be performed in order to properly understand the validity of the testing.
- If a direct comparison is to be made to a factory test, the same equations of state should be used.

7.4.5 Effects of Mixture Composition on Compressor Performance

When the centrifugal compressor performance characteristic maps are presented in terms of isentropic (adiabatic) or polytropic head vs. actual inlet flow rate, they are considered generalized in that they can be applied to a different mixture composition as long as the

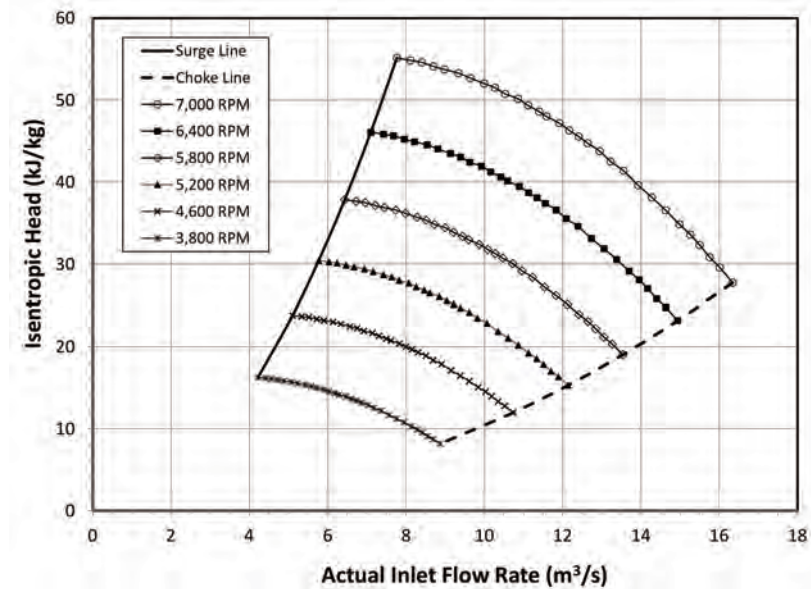


Figure 7-14. Generalized centrifugal performance characteristics in terms of isentropic head vs. actual inlet flow.

appropriate mixture properties are accounted for correctly. To illustrate this concept, consider the generalized centrifugal compressor performance map shown in Fig. 7-14 in terms of isentropic head (in kJ/kg) vs. actual inlet flow rate to the compressor first stage (in m³/s). The different curves are for different impeller speeds indicated.

Consider two different gas mixture compositions shown in Table 7-2, a lean mixture of MW = 16.89 and a rich mixture of MW = 18.40. If the same compressor is used to compress either mixture from a suction pressure = 5 MPa-a and suction temperature = 15°C, the corresponding discharge pressure will be different for any given actual inlet flow and compressor speed, yet the isentropic head for both mixture will be the same which is corresponding to the value on the y-axis of the compressor performance map. Applying Eqn. 7-6 the discharge pressure will be different since the gas constant R and isentropic exponent k will be different for the two mixture compositions.

Table 7-2. Example of lean and rich natural gas mixture composition for the example shown in Fig. 7-15

	Mole %	
	Lean	Rich
methane	95.50	88.02
ethane	3.10	7.60
propane	0.41	3.10
isobutane	0.12	0.31
N-butane	0.21	0.28
isopentane	0.03	0.03
N-pentane	0.09	0.12
Nitrogen	0.37	0.37
CO ₂	0.17	0.17
Sum	100.00	100.00
MW	16.89	18.40

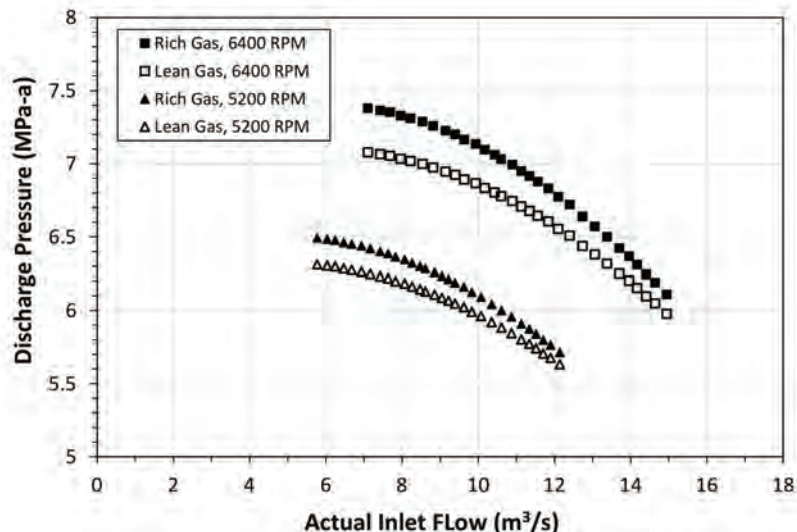


Figure 7-15. Effects of mixture composition on compressor discharge pressure at two different speeds of the compressor whose generalized performance map is shown in Fig. 7-14.

Alternatively, and more accurately, an appropriate equation of state (EOS) described earlier can be used instead. In this case, the discharge pressure can be determined from two intrinsic properties of the gas; entropy, which is the entropy of the gas at the inlet condition (since the head is expressed in terms of isentropic head), and the isentropic discharge enthalpy, which is equal to the inlet enthalpy plus the isentropic head from the generalized performance map at the given actual inlet flow and speed. This procedure was carried out for two different speeds (5200 RPM and 6400 RPM) and corresponding range of actual inlet flow rates shown in Fig. 7-14. GERG-2008 as implemented in RefProp was used in this example calculation. The results are shown in Fig. 7-15, indicating that for the same actual inlet flow and compressor speed, the gas discharge pressure will be higher for the rich gas (higher MW) than that for the lean gas (lower MW). Note that the ratios between the discharge pressures for the two different gas mixtures are not quite equal to the ratio of the respective MW. This is due to differences in the isentropic behavior of the respective mixtures, e.g. the isentropic exponent, k . Clearly, this exemplify that gas properties are not generally proportionate to its MW, but an appropriate EOS should always be considered as a common practice.

7.4.6 Compressor Performance Degradation Monitoring

Performance degradation monitoring of centrifugal compressor provides a means for the operators predict the behavior of their machines. Understanding the key principles in performance evaluation is essential for operators to benefit from this approach. The challenge is for operators to identify and quantify these degradations as the performance impact of an underperforming compressor is usually significant to the operation of the facility and ultimately to production capacity and even the profit of the operating company. Performance analysis on the other hand is able to provide an early indication of degradation and can potentially minimize downtime required for rectification efforts [19].

The major mechanisms for performance degradation are mechanical damage, fouling or blockage, erosion and corrosion and increased internal recirculation. Mechanical damage may be caused by external upstream devices such as filters or cracking of internal gas path components. Sudden increases in vibration levels will quickly be evident and likely cause

a shutdown so this type of degradation is not a good candidate for medium and longer term performance monitoring.

A common degradation mechanism is fouling or blockage. Operating a centrifugal compressor in hydrocarbon services is potentially damaging to compressor performance due to a multitude of gas component mixtures and the presence of contaminants such as wax, sand and free liquids in the natural gas, particularly close to the wellhead. An example of extreme fouling is shown in Fig. 7-16 where it affected both impeller internals and labyrinth seals.

The basis for monitoring compressor performance is recognizing that the compressor characteristic curve as shown by the speed lines shifts downward and to the left as degradation occurs. In other words, to achieve a certain head and flow, a higher speed is required. At the same time, there is probably also a decrease in the efficiency. The relative amounts of decrease in head and flow are dependent on the nature of the degradation so



(a)



(b)

Figure 7-16. Example of compressor degradation (a) impeller fouling (b) damaged labyrinth seals [19].

this cannot be easily predicted. However, if the speed lines are fairly flat, a reasonable approximation is to monitor the vertical drop in head and ignore the change in flow for trending. Since the purpose is to detect changes in performance, even if this approach overstates the situation somewhat, the ultimate objective is still served.

Although it is best to automate the calculation and trending of head deviation, there are instances where all one wants to do is to plot one point and check the deviation from the compressor curve. An example is shown in Fig. 7-17. First the calculated head and flow are plotted on the compressor curve. For this point, the speed according to the compressor curve is estimated by interpolation, in this case 19,700 rpm. The actual operating speed however is 20,200 rpm. This means that without degradation, the compressor should be able to achieve a head of 126 kJ/kg at the same flow. The deviation in head can then be calculated as -6.34% .

A somewhat more sophisticated method that applies similarity condition matching based on the fan laws can be found in [18]. The best approach is to automate this process and trend the results. Figure 7-18 illustrates this approach along with the improved result of applying an anti-fouling agent.

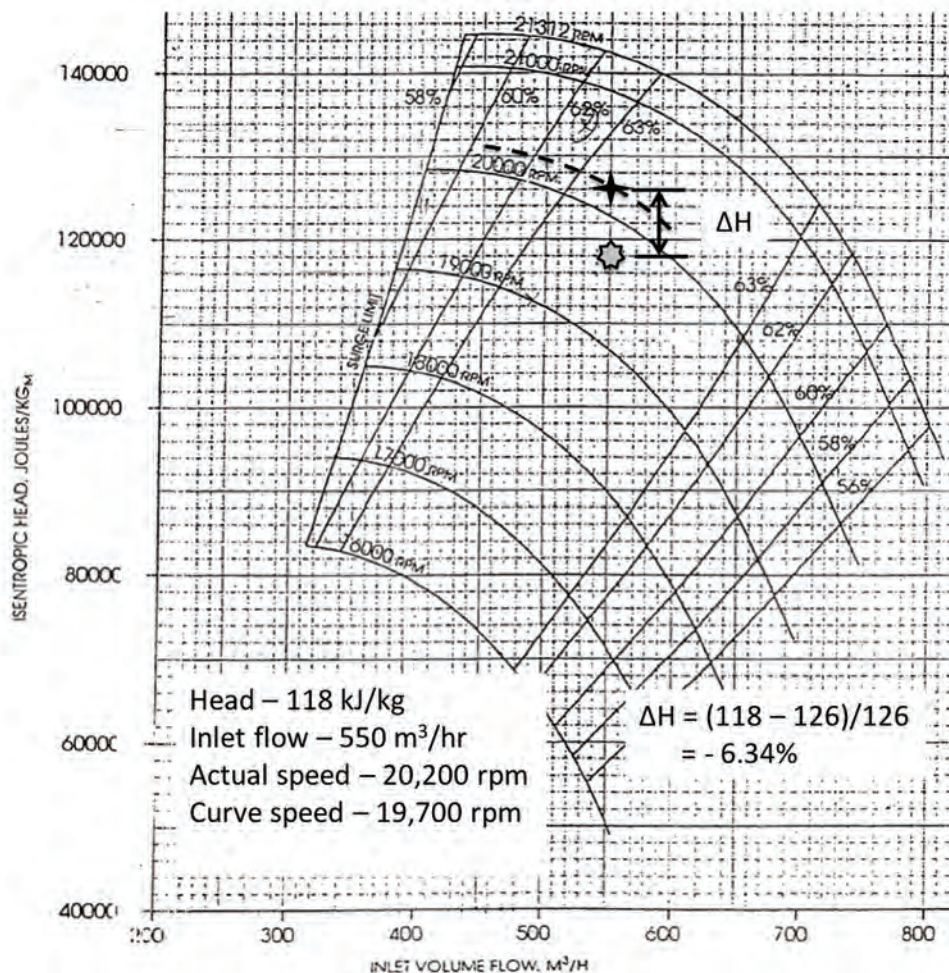


Figure 7-17. Example of a simplified method using manual plotting [19].

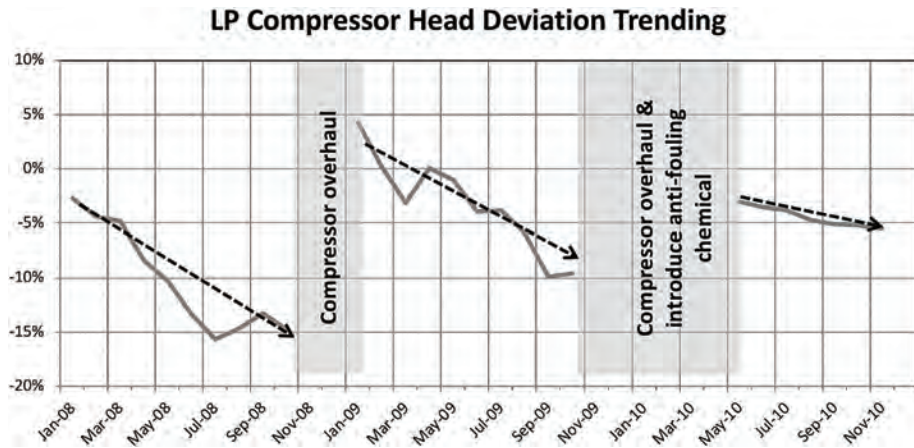


Figure 7-18. Trend of performance deviation [19].

7.5 SYSTEM CHARACTERISTICS

7.5.1 General

In order to select a compressor, it is necessary to compare the compressor performance characteristics with the operating conditions imposed by the system. This must be done at the design conditions and also at all “upset” or off-design points. This latter consideration is always very important and, if omitted, may result in the wrong compressor being selected.

7.5.2 System Curves

As far as compressors are concerned, systems will generally fall into three scenarios:

- variable volumes delivered under constant pressure
- fixed volumes delivered under variable pressures
- variable volumes delivered under variable pressures

System curves will consist of some combination of two components:

- frictional resistance
- constant (static) pressure

These are illustrated in Fig. 7-19 with the curve depicting pressure ratio versus flow change for a pipeline system at different capacity levels. Diameter and length of the pipeline are constant.

For each real system, curves may be drawn to indicate the total range of system demand, including effects of changing flows and other conditions or upsets. This is illustrated in Fig. 7-20 in the form of (a) a normal system friction curve of pressure versus flow (shown by the friction curve $x-x$), together with other curves indicating the range over which this curve may shift (e.g., due to non-flow-related changes in the opposite direction $y-y$); and (b) a chart of operating points for the system.

The actual range of system demand is indicated by both (a) and (b). In reality, chart (a) is irrelevant, since any upset will define a new system curve. Usually, the only system

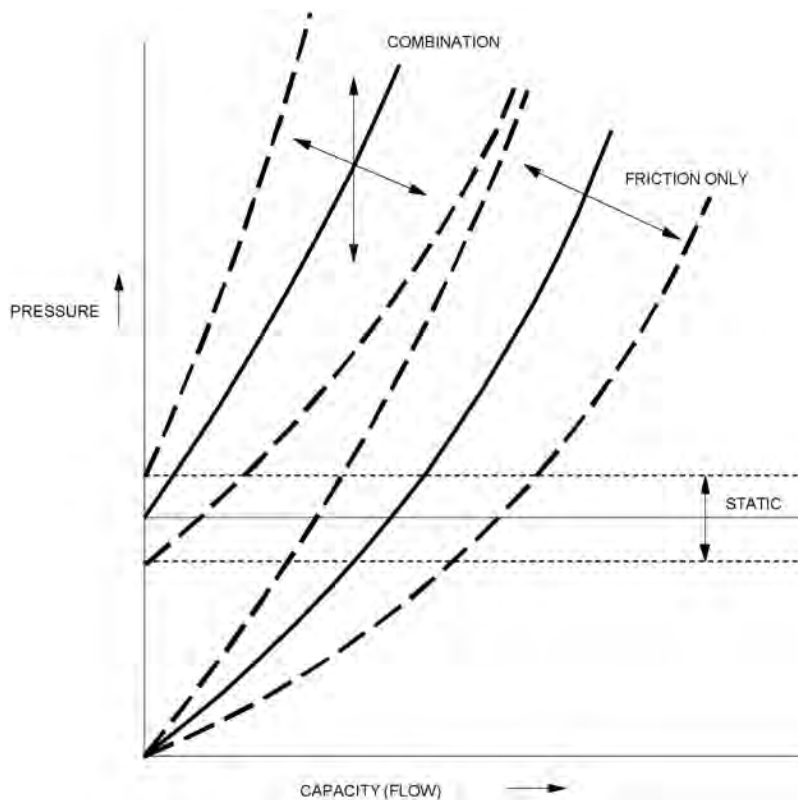


Figure 7-19. Pipeline system characteristic curves.

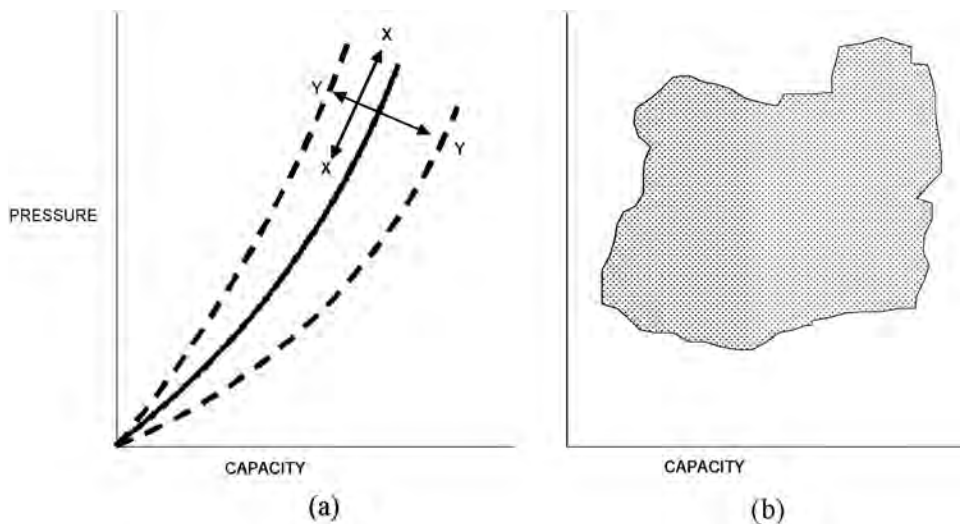


Figure 7-20. Pipeline system friction curves.

information available is in the form of seemingly “random” operating points, with no real reference to the actual curve the point is on.

Taking the centrifugal and reciprocating compressors as examples, it is possible to analyze the operation of these machines on the particular system by superimposing the system demand curve directly on a compressor performance curve, as shown in Fig. 7-21.

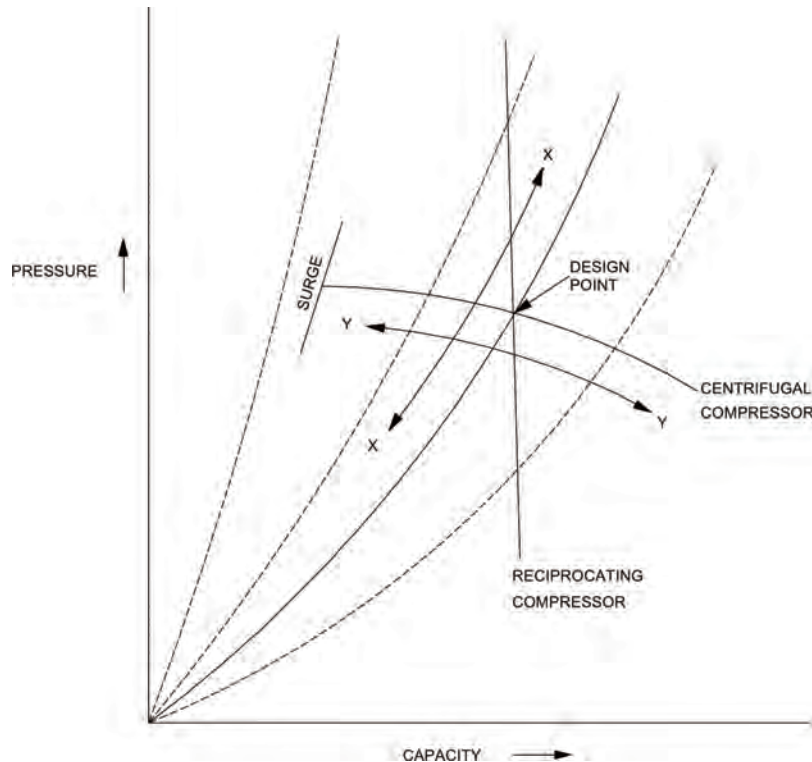


Figure 7-21. System demand curve superimposed on compressor performance curves.

This curve is typical of pipeline applications and many process situations, combining friction head changes (due to changing flows) and “upset” points (due to uncontrollable factors such as equipment breakdowns). By examining the compressor and system together in this manner, it becomes apparent whether or not the compressor is matched to the system. Since the compressor curve defines the only points where the compressor can operate and the system curve defines the operating points required by the system, it follows that the compressor/system combination will only operate where the curves intersect. By following this rule, various system operating points can be plotted directly on the compressor curve, showing immediately where problems may exist.

Some pipeline systems, for example, with growth occurring over a time period, may operate on different portions of the friction curve over their lifetime. Pipelines operating at or near their maximum capacity will show a steep curve, whereby small flow changes will require the pipeline compressor to undergo a large ratio change. Conversely, large pipelines operating below their capacity will exhibit large flow changes with small ratio changes. It is apparent that the required pipeline compressor performance characteristics may be entirely different for each situation. Both short-term (day to day) and long-term (future) changes in the pipeline operation are therefore important in making the initial compressor selection. For most pipelines, these changing conditions are usually not known at the outset, and it is therefore important to select a compressor with a reasonably wide operating range. In many cases, the compressor internals can be changed to alter the characteristic when required.

Due mainly to off-design conditions, the pipeline system operation will generally fall anywhere within an area, and it becomes apparent that a constant speed compressor curve, as discussed previously, does not adequately cover the range of system operating points. Something must be done to the compressor performance to allow it to cover an area rather than a single line.

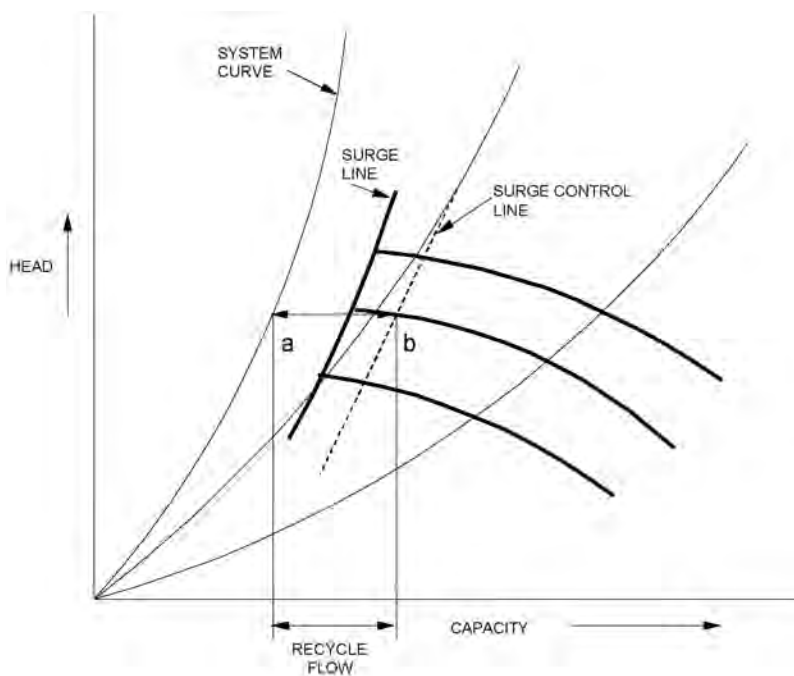


Figure 7-22. Surge protection and the system curve.

Basic surge protection for centrifugal compressors is illustrated in Fig. 7-22. When the surge control system detects operation on the surge control line (usually 10% to the right of the actual surge line), the recycle valve is opened such that the compressor operating point (b) remains on the performance curve. The difference in flow between this point and the new system operating points (a) is bypassed around the compressor via the recycle valve.

7.5.3 Compressor Performance Comparison

Figure 7-23 illustrates the pressure–volume characteristic of reciprocating and centrifugal compressors operating at constant speed, with the axial compressor included for comparison. Reciprocating compressors can meet widely varying pressure ratios at almost constant capacity (flow) and may be considered as constant flow, variable ratio machines (“vertical” characteristic). Centrifugal compressors, on the other hand, exhibit the opposite characteristic, handling wide variations in flow at an almost constant ratio (“horizontal” characteristic). The axial compressor shows a “steep” characteristic between the other two types, maintaining an almost constant volume under varying ratios—similar in many respects to the reciprocating compressor.

The general shape of each power curve should be also noted. The power required by both reciprocating and axial machines is greatly dependent on pressure ratio changes. An increase in ratio will result in a small reduction in flow, but with an increase in the power required to drive the compressor (reciprocating machines with a further increase in ratio, will experience a power “peak,” after which the power will decrease as the ratio increases). Conversely, a centrifugal machine will show a large decrease in flow with a small increase in ratio and will require less power. These curves also demonstrate the effect of a change in system operating conditions on a machine running at constant speed.

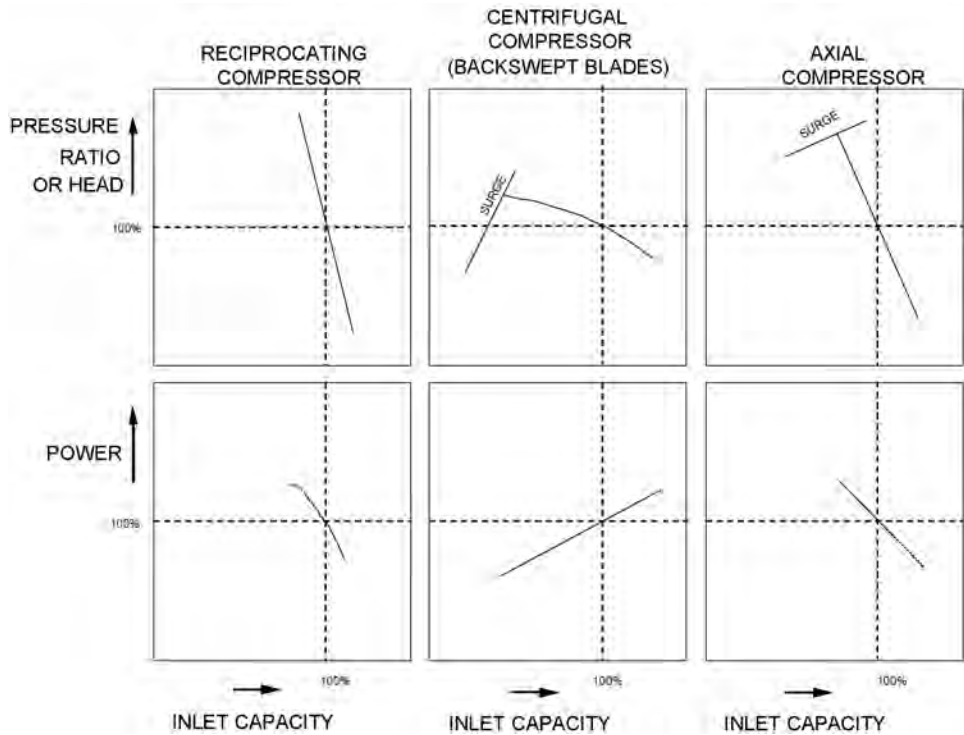


Figure 7-23. Pressure–volume characteristics of different compressor types.

7.5.4 Operating Limitations

In addition to the pressure–volume characteristics of a compressor, there are also certain limitations which should be noted:

- Discharge temperature (all compressors). Compressors themselves can be manufactured to withstand relatively high discharge temperatures, and can be multi-staged and intercooled (cooled between stages) to eliminate problems. Many temperature limitations, however, are imposed by the piping system from areas such as thermal expansion, chemical reactions or polymerization, lubricating oil temperature limits, and, on pipelines, from the protective wrapping applied to underground lines which can withstand only moderate temperatures (e.g., 45°C or 115°F). Care must be taken to establish these limits and design for them. Discharge temperature, if not in reasonable agreement with the value calculated from the operating conditions, is also a good indication of trouble within the compressor, especially for reciprocating compressors.
- Rod loading (reciprocating compressors). Each compressor has definite limits associated with power or torque-carrying ability (the ability of the supporting frame, crankshaft and bearings to withstand torque and dissipate heat) and also structural ability to withstand compression and inertia loads. These limits are generally grouped together and included under the term “rod loading” for which each manufacturer will set maximum values. Rod loading due to compression (gas pressure) loads, both in tension and compression, can be calculated knowing the compressor piston and rod diameters together with minimum suction and maximum discharge pressure, and then compared with the manufacturers allowable limits. For compressors on variable ratio applications (including pipelines), the control system must be designed to protect the compressor from damage if, under any conditions, these limits could be exceeded.

- **Surge and choke (centrifugal and axial compressors).** Dynamic compressors can operate only over a definite stable range, limited by an instability or “surge” point at the high head, low flow end of the curve, and “stonewall” or “choke” at the low head, high flow end of the curve. At this choke condition, the performance curve turns almost vertically downward, caused by sonic velocity being reached inside the machine (e.g., at the impeller inlet) which prevents any increase in capacity. The surge point at the opposite end of the performance curve is a complicated phenomenon, characterized by alternating flow reversals between the compressor and the discharge system. This can be quite violent, especially on axials and multistage centrifugals and can lead to damage in the compressor. One of the most important control aspects of dynamic compressors is to detect and prevent surge, usually by opening a recycle (bypass) valve to recirculate additional gas from discharge to suction. This moves the operating point further to the right, away from the surge line. On centrifugal or axial machines used on air compression (e.g., gas turbine compressors), surge may be prevented by blowing air to atmosphere, which will eliminate overheating problems that often plague a closed recycle system.
- **Critical speeds.** A compressor/driver rotating system has certain speeds at which either lateral (bending) or torsional vibrations may coincide with the natural (resonant) frequency. Manufacturers will analyze the equipment and set limits on operating speeds to avoid these criticals. In general, lateral critical speeds apply to dynamic machines and torsionals apply to reciprocating compressors; however, multistage centrifugal drive trains may also encounter torsional problems. Some machines (“stiff” shaft) operate below the first critical speed, whereas others (“flexible” shaft) operate between the first and second criticals. Operation above the second critical speed is usually avoided due to instability problems.

7.5.5 Compressor Performance Adjustments

To adjust compressor performance to match system requirements, various methods are available, depending on how the performance is to be adjusted. Compressors with a vertical characteristic can already meet pressure changes easily, so the required adjustment must shift the performance curve horizontally to create a flow change. Compressors with a horizontal characteristic can inherently accommodate flow changes, and the curve must be shifted vertically to create a pressure change.

Another concept, which will only be mentioned here, is to artificially adjust the system curve to match the compressor by placing a throttle valve on the compressor suction or discharge or adding a bypass valve to recirculate gas from discharge to suction. These three methods are wasteful of power and, in some situations, may not help. If, however, a dynamic compressor is operating in a steady-state process, throttling may sometimes be an easy and simple method of control for short-term or uncommon conditions. Normally, suction throttling is employed as it wastes less power than discharge throttling. Bypass control is also wasteful but is a simple method of allowing a compressor to remain operating under conditions where it would otherwise be unable to do so. Bypass control is, however, an important function when protecting a dynamic compressor from surge as mentioned earlier.

The most efficient method, then, of controlling compressor performance, is to adjust the compressor to match the system and not make the system match the compressor. To achieve this, the following methods are currently employed:

- For reciprocating compressors: speed variation, clearance adjustments and valve unloaders (lifters);

- For centrifugals: speed variation, adjustable inlet guide vanes, and adjustable diffuser vanes (uncommon);
- For axials: speed variation and adjustable stator blades.

For reciprocating and centrifugal compressors, the first two methods usually provide the required performance changes. The resulting effect on the characteristic curves is shown in Fig. 7-24, indicating how the performance may be adjusted to cover an area.

For all compressors, speed changes allow a wide range of operation without adding mechanical complications to the compressor. If a variable speed driver is not available, and if flexible operation is required, then the second method is normally used. These secondary methods may also be required in some cases for startup and placing a compressor into operation.

The capacity change indicated for reciprocating compressors varies linearly with speed, but is more involved when using clearance changes. Capacity on a centrifugal machine is also linear with speed, but the head capability changes as well, being a function of the square of the speed change. Guide vanes achieve their control by creating in the gas flow either a pre-swirl (rotation in the direction of impeller rotation) or a counter-swirl (opposite to impeller rotation). The pre-swirl or pre-rotation position is the most useful for control purposes, causing the characteristic curve to rotate downward around a point at zero flow and maximum head, thus steepening the curve (note that adjustable guide vanes are not available on all centrifugal compressors). All these effects will be discussed later in more detail.

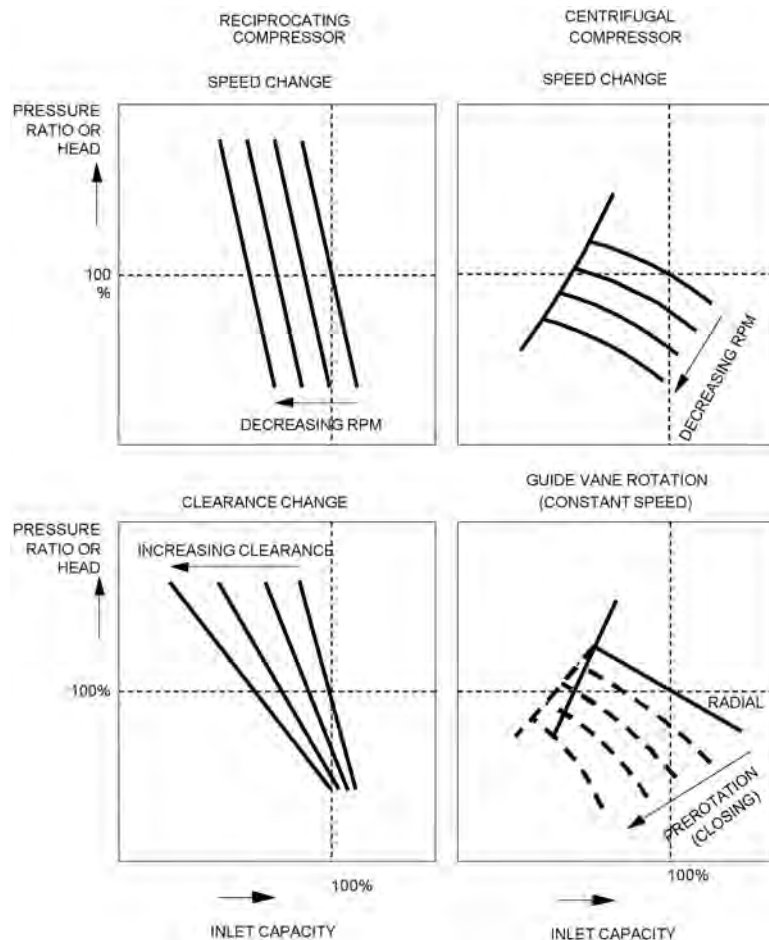


Figure 7-24. Compressor performance adjustments.

A further change in compressor performance involves using compressor combinations, including multi-stage compressors (several stages in series on one machine); separate compressors in series, parallel, or both; or combinations of different types of machines. The final selection will depend on an analysis of the compressor(s) and system together under all possible modes of operation. Some combinations can pose difficult operating and control problems which, if not considered, may result in an unstable and uncontrollable situation. By understanding both system and compressor behavior, this type of problem may be avoided.

7.5.6 Operating Considerations

7.5.6.1 Startup

Operation of a single compressor is not particularly difficult, as long as the compressor is properly matched to the system. In many applications, however, compressors will be operating in series or parallel with other units. In this situation, problems will occur on startup and under changing system conditions, requiring a properly designed control system for successful operation.

The solution to some operating problems can be extremely difficult. By combining a knowledge of system behavior and compressor characteristics together with performance equations and curves, most problems can be analyzed and solved. However, as modern compression systems become more complex, computer simulation is becoming a necessary tool.

Most drivers require a warm-up period before being loaded, requiring the compressor to be isolated from the system and unloaded for this time period. Centrifugal machines are isolated by a discharge check valve, and gas is circulated around the compressor through a bypass or recycle valve. This gas will heat up, and a large enough volume must be included in the loop or a recycle cooler provided. If no head exists across the discharge check valve, the recycle valve can be closed after warm-up, placing the unit on line. If a head exists, the compressor speed must be raised to develop sufficient head to prevent surge as the recycle valve is closed.

Figure 7-25 illustrates the interaction of the centrifugal compressor performance curves with the pipeline system curve and recycle loop system curves, as the compressor comes off warm-up and goes online. During driver's warm-up, the compressor is turning at a low speed (10–30%), the recycle valve is 100% open, and the compressor is operating with low head output. After warm-up, the compressor's speed is increased as the recycle valve is closed, but the control system prevents the recycle valve from closing too soon [e.g., in Fig. 7-14, if the recycle valve was allowed to close when the compressor had only reached 90% speed (N), the compressor would go into surge before going on line].

Referring to Fig. 7-25, we assume (for simplicity) that the compressor reaches 100% speed before the recycle valve starts to close. As the recycle valve closes from 100% to 80–60% open, the recycle loop system increases its head demands on the compressor (raises the system curves), and the flow through the compressor and recycle loop falls from Q_{100} to Q_{80} to Q_{60} in response to these rising head requirements. At Q_{60} , the compressor head output also matches the pipeline system curve requirement at zero flow, the check valve opens, and some of the compressor flow starts to go down the pipeline.

As the recycle valve continues to close to 20% open, the total flow through the compressor is Q_{20} , with part of this flow (Q_{20}) going down the pipeline and the rest of the flow ($Q_{20} - Q_{20}$) going through the recycle loop. Then when the recycle valve has fully closed, the total flow through the compressor (Q_0 or Q_A) goes down the pipeline.

Reciprocating compressors may be unloaded on startup by opening clearance pockets or using valve unloaders, which are then released to place the unit on line. If these methods are not available, a discharge check valve and bypass arrangement may be used if the driver's starting torque is suitable. However, the compressor may quickly go into a high power requirement situation when placed on line and head is established, as noted from the reciprocating compressor curves.

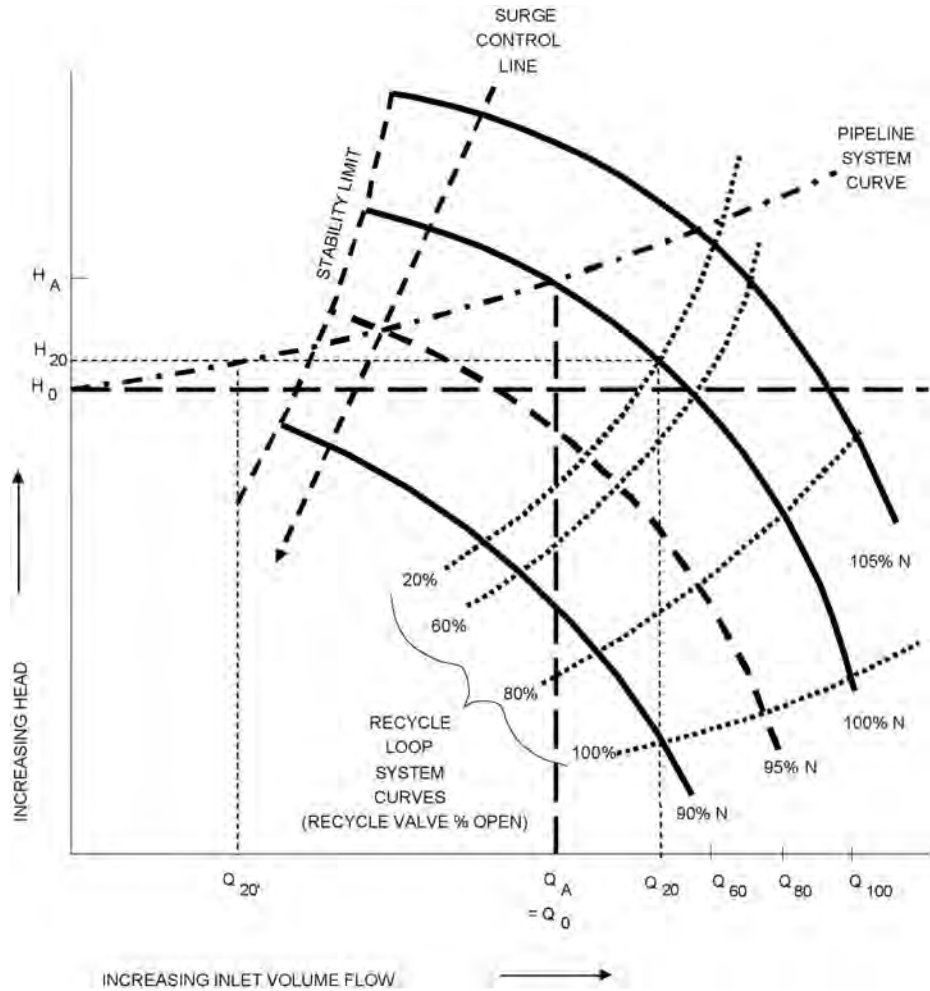


Figure 7-25. Interaction of centrifugal, pipeline system and recycle loop system curves during compressor startup.

7.5.6.2 Series Operation

Series operation may pose difficult problems as the compressors can interact in opposing ways. Since the flow and intermediate pressure are common to two adjacent units in series, the operation can be analyzed by plotting a series of constant flow curves for each compressor. By using these curves together, the correct intermediate pressure can be found. This pressure can be controlled by increasing the speed of one unit and decreasing the other unit to adjust for system changes. Series operation of centrifugals is essentially a “balancing” operation. If control changes are made incorrectly on one machine, the compressor system can become unstable.

Reciprocating compressors operating in series do not have the same dynamic problems, but changing system pressures can produce other effects. For example, an increased discharge pressure can result in excessive overheating or overloading of the last compressor (or stage). An increase in the initial suction pressure can substantially raise the power required and raise the intermediate pressure beyond safe limits.

Reciprocating machines operating in series with centrifugals can pose difficult problems. Since the performance characteristics of these machines are opposite to each other,

they operate together only at one point. Minor system changes can cause the performance to diverge in opposite directions, becoming uncontrollable. By providing speed and capacity control (e.g., clearance pockets), the common operating point can be expanded into a small area which helps to maintain stability.

The startup of compressors in series is similar to starting a single unit, except that changes must be gradual and kept under control at all times.

7.5.6.3 Parallel Operation

Successful parallel operation is a function of the “steepness” of the compressor performance curves. For this reason, reciprocating machines can be operated in parallel with no instability problems. Centrifugal compressors, however, will become unstable if the performance curves are relatively flat where, for example, small changes in pressure from one machine can force another compressor into surge.

7.5.6.4 Shutdown

Shutdown poses no major problems for an individual compressor but will cause problems with compressors operating in series. Again, the check valve/bypass valve combination is used to isolate the compressor from the system for a controlled shutdown. Check valves are mandatory for centrifugal compressors during shutdown to prevent high-pressure discharge gas from flowing backwards through the machine. If this happens, the compressor operates in reverse as an expander, often causing damage.

REFERENCES

- [1] Unknown, 2017. “Compressor and Expanders,” *CompressorTechTwo*, CT2 Compression Technology Sourcing Supplement, p. 76.
- [2] Peng, D. Y. and Robinson, D. B., 1976. “A New Two-Constant Equation of State,” *Ind. Eng. Chem. Fundam.*, 15, p. 59.
- [3] Redlich, O. and Kwong, J. N. S., 1949. “On the Thermodynamics of Solutions V: An Equation of State, Fugacities of Gaseous Solutions,” *Chem. Rev.*, 44, p. 233.
- [4] Soave, G., 1972. “Equilibrium Constants from a Modified Redlich-Kwong Equation of State,” *Chem. Eng. Sci.*, 27, p. 1197.
- [5] Starling, K. E., 1973. *Fluid Thermodynamic Properties for Light Petroleum Systems*, Gulf Publishing Company, Houston, Texas, USA, 1973.
- [6] Benedict, M., Webb, G. B., and Rubin, L. C., 1951. “An Empirical Equation for Thermodynamic Properties of Light Hydrocarbons and their Mixtures,” *Chemical Engineering Progress*, 47(8), pp. 419–422, August 1951.
- [7] Lin, C. J. and Hopke, S. W., 1973. Application of the BWRS equation to methane, ethane, propane and nitrogen systems, *75th National AIChE Meeting*, American Institute of Chemical Engineers, New Orleans, Louisiana, USA.
- [8] Hopke, S. W. and Lin, C. J., 1974. Application of BWRS equation to natural gas systems, *76th National AIChE Meeting*, American Institute of Chemical Engineers, Tulsa, Oklahoma, USA.
- [9] Kunz, O. and Wagner, W., 2012. *J. Chem. Eng. Data*, 57 (11), p. 3032.
- [10] Kunz, O., Klimeck, R., Wagner, W., and Jaeschke, M., 2016. “The GERG-2004 Wide-Range Equation of State for Natural Gases and Other Mixtures,” Groupe Européen de Recherches Gazières (GERG), Technical Monograph, 2007, GERG TM15, accessed on 25 May 2016, http://www.gerg.eu/public/uploads/files/publications/technical_monographs/tm15_04.pdf.
- [11] Lemmon, E. W., Huber, M. L. and McLinden, M. O., 2010. “NIST Standard Reference Database 23: Reference Fluid Thermodynamic and Transport Properties - REFPROP,” National Institute of Standards and Technology, Standard Reference Data Program, Gaithersburg, Maryland, USA.
- [12] Unknown, 2017. “Compressor and Expanders,” *CompressorTechTwo*, CT2 Compression Technology Sourcing Supplement, p. 97.

- [13] Sorokes, J. M., Miller, H. F. and Koch, J. M., 2006. "The Consequences of Compressor Operation in Overload," *Proceedings of the Thirty-Fifth Turbomachinery Symposium*, Turbomachinery Laboratory, Texas A&M University, College Station, Texas, 10 pages.
- [14] Sorokes, J. M., Kopko, J. A., Gilarranz, J. L. and Ranz, A. J., 2007. "Optimizing Peak Efficiency and Flow Range in Pipeline Centrifugal Stages," Dresser-Rand North American Operations, Olean, N.Y., USA, 28 pages.
- [15] API Standard 617, 2002. "Axial and Centrifugal Compressors and Expander-Compressors for Petroleum, Chemical and Gas Industry Services," American Petroleum Institute, 7th ed., pp. 1–193, July 2002.
- [16] ASME PTC 10, 1997. "Performance Test Code on Compressors and Exhausters," American Society of Mechanical Engineers, pp. 1–200.
- [17] ISO 5389, 2005. "Turbocompressors—Performance Test Code," International Standards Organization, 2nd ed., pp. 1–142.
- [18] Brun, K. and Nored, M. G., 2006. "Guideline for Field Testing of Gas Turbine and Centrifugal Compressor Performance," Gas Machinery Research Council/Southwest Research Institute, pp. 1–93, August 2006.
- [19] Jasmani, M. S., Van Hardeveld, T. and Mohamed, M. F. B., 2012. "Performance Degradation Monitoring of Centrifugal Compressors Using Deviation Analysis," *Proceedings of the 9th International Pipeline Conference*, IPC2012=90235, September 24–28, 2012, Calgary, Alberta, Canada, 9 pages.

PUMP AND COMPRESSOR DRIVERS

8.1 INTRODUCTION TO DRIVERS

Pump and compressor drivers form a critical part of pumping and compression systems. Decisions made on which ones to use have far-reaching and long-lasting implications for the entire life of the pipeline system. The selection of drivers entails many aspects such as the following:

- power size and range
- performance characteristics (e.g., ambient conditions, altitude)
- compatibility with driven equipment
- fuel source available
- starting requirements such as torque
- reliability and availability
- other drivers already installed at the same site or other sites
- maintenance support available
- auxiliary systems that need to be provided
- drivers available from driven equipment supplier
- physical dimensions and weight
- environmental requirements, especially for emissions
- need for sound control

When pumps or compressors are first installed on a pipeline system, there is often a plan for future expansion of which a major component is the desire to attain consistency in the type and even model of driver chosen. In spite of this desire for consistency, a pipeline system over time will end up with a variety of drivers and even the best laid plans can result in a less than optimum system over time. For example, even the same gas turbine model will change with time as technology advances and interchangeability between units and their spare parts may be lost. In contrast with driven equipment, drivers are much more likely to see changes and even entire replacement. In general, drivers may become obsolete and require replacement due to one or more of the following reasons:

- loss of maintenance support from the manufacturer for that model or even the vendor going out of business
- improvements in fuel efficiency
- changes in power requirements (driver may be over or undersized)
- environmental factors such as NO_x regulations
- major driver components reaching the end of their life with replacement being too expensive
- high-efficiency solutions such as waste heat recovery

The most common driver for pump stations is the electric motor with internal combustion engines and gas turbines less commonly used. The gas turbine is the driver of choice at most new mainline compressor stations while the internal combustion engine is more likely to be chosen for lower power applications (less than 5 MW). Electric motors are becoming more desirable because of their lower environmental footprint.

8.2 GAS TURBINES

8.2.1 Types of Gas Turbines

Gas turbines are the most common driver for centrifugal compressors. Although much less common than electric motors, they are also used for larger pumping applications. The most significant advantages of a gas turbine are high-power output for their size and higher potential availability due to the ability of rapid engine changeouts. Their one historical disadvantage—lower thermal efficiency—has largely been overcome by improvements in hot section metallurgy leading to higher turbine inlet temperatures (TITs).

Gas turbines used in the oil and gas industry can be first be divided into two major categories: aeroderivative and industrial with the industrial type divided into heavy-duty and light industrial. As the term implies, *aeroderivative gas turbines* were initially developed for airborne applications and then later applied for industrial use, often with significant modifications. *Industrial gas turbines* have been designed entirely for stationary use, although sometimes with technology transferred from aircraft engines.

The first gas turbines used on pipelines in the early 1950s were of the heavy-duty industrial type and were derived from steam turbine design, such as the General Electric Frame 3 and later the Frame 5 (see Fig. 8-1). Westinghouse and Orenda followed with similar designs. A few of these incorporated recuperators to improve efficiency.

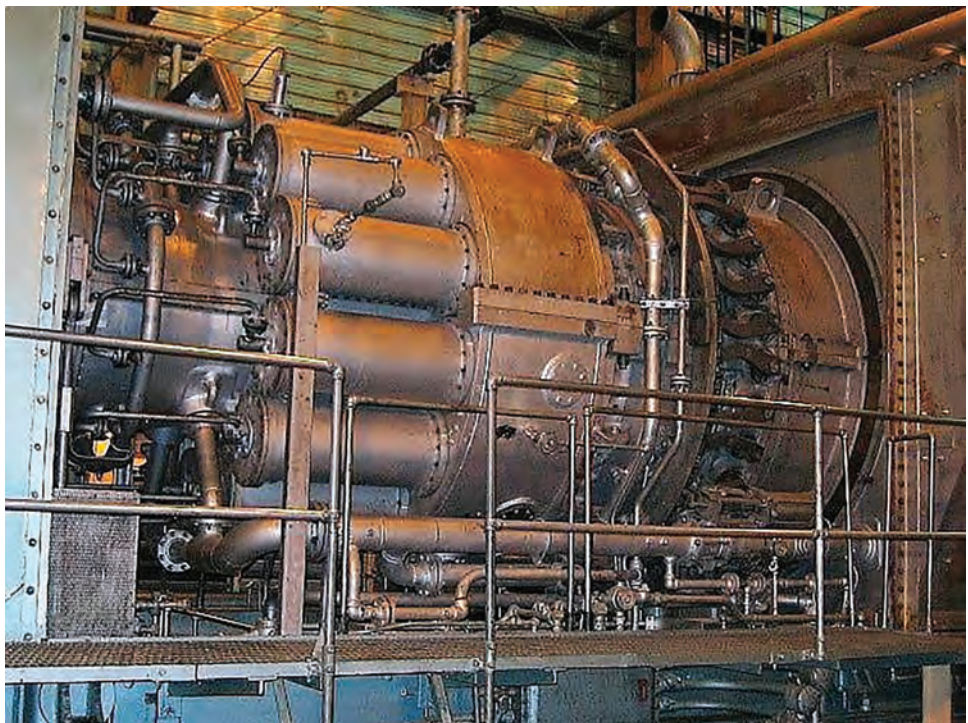


Figure 8-1. General Electric Frame 5—a heavy-duty gas turbine.

Some of these heavy-duty gas turbines are still installed on existing pipelines but are otherwise not any more considered to be a good solution for pipeline applications. They take longer to come online because of the thermal expansion of their heavier cases and, likewise, require a long cooldown period. Perhaps an even more important factor is that they need longer downtime for maintenance because casings have to be removed onsite and the whole unit cannot easily be shipped to an overhaul facility.

Aeroderivative gas turbines, in contrast, feature a much lighter construction which allows fast startup and shutdown with long cooldown periods. They are designed to be removed as a complete engine, and even large ones can be handled by normal lifting equipment. As a result, engine changeouts are relatively easy and can normally be accomplished in an 8-hour shift.

The first aeroderivative gas turbine used on a pipeline, the Rolls-Royce Avon, was installed at Caron, Saskatchewan, Canada, in 1963 for TransCanada Pipelines. It is estimated that about 900 out of more than 1200 sold are still in service, a remarkable accomplishment [1]. This was followed by the Rolls-Royce RB211, another popular gas turbine (Fig. 8-2) and the General Electric LM2500 (shown in Fig. 8-3). A number of other different aircraft engines have been converted to industrial use including the Allison 501, Pratt & Whitney FT4C, GE LM1600, and RR Spey.

A somewhat different class of gas turbine, the light industrial gas turbine, was pioneered by Solar Turbines starting in the 1950s with the 1000-hp (750 kW) Solar Saturn and followed by engines with increasing power output, the Centaur (Fig. 8-4), Taurus, Mars and more recently, the Titan. It is similar to the aeroderivative but with a heavier construction for the rotor and casing. The gas producer and power turbine are an integrated design along with the lubrication system. It is more rugged than the aeroderivative but with similar ease of operation and maintenance (see the GE10 internals in Fig. 8-5). Due to its many acquisitions, the other major manufacturer of this type of lighter industrial turbine is Siemens.

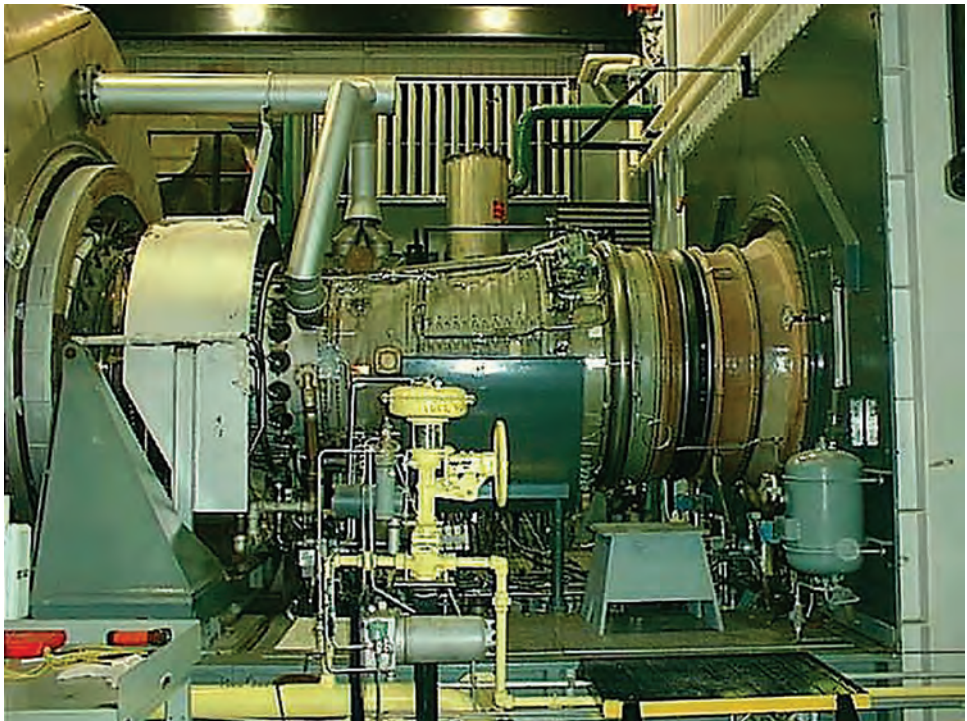


Figure 8-2. Rolls-Royce RB211—an aeroderivative gas generator.

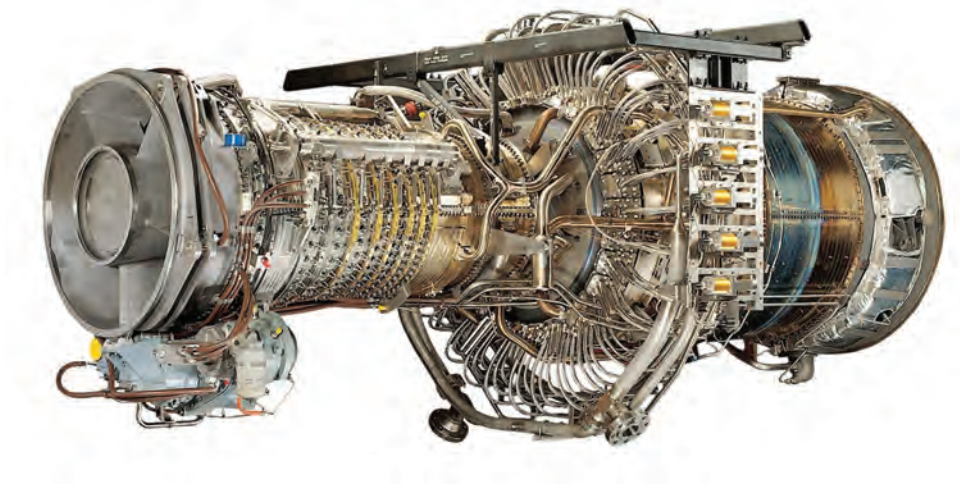


Figure 8-3. General Electric LM2500+G4 (courtesy of GE Oil & Gas).



Figure 8-4. Solar Centaur 40 light industrial gas turbine (courtesy of TransCanada).

Although the difference between aeroderivative and heavy-duty gas turbines is substantial, the same cannot be said for aeroderivatives and the light industrial gas turbine [2]. The major difference is still that aeroderivatives have rolling element bearings and a smaller lubrication system with high temperature fluid, while the industrial gas turbine uses hydrodynamic bearings and less expensive but higher volume mineral oil. However, starting times and maintenance requirements are very similar. The somewhat lighter weight of the aeroderivative, for at least the larger engines, may be a factor for offshore or inaccessible locations, but otherwise, the two types of engines are quite similar.

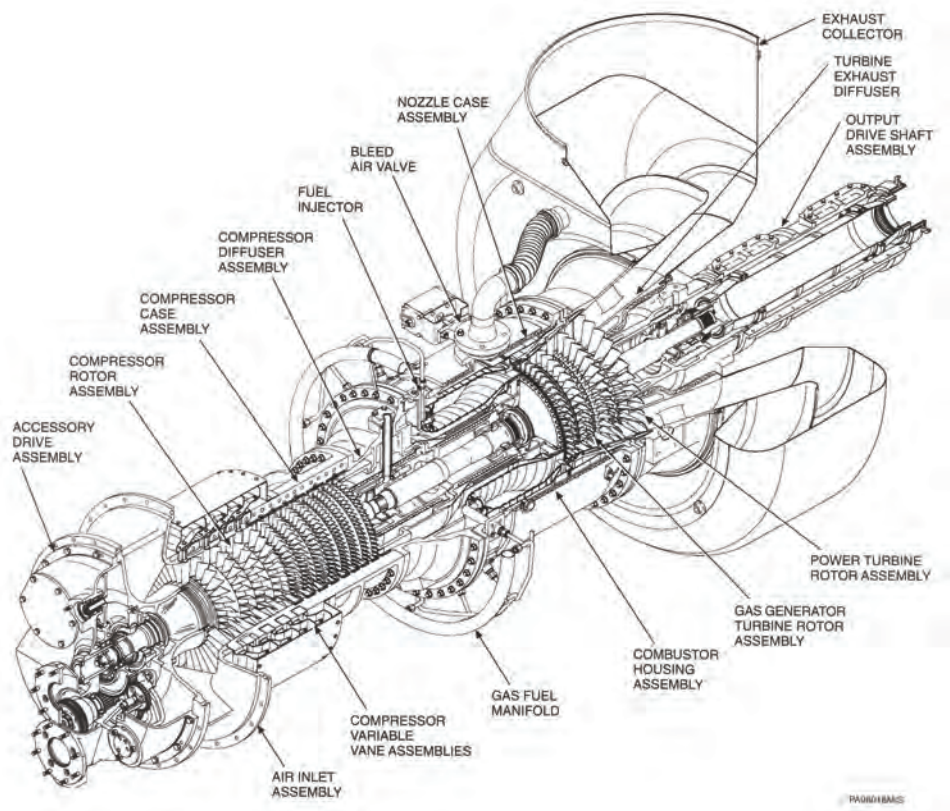


Figure 8-5. Basic layout of a gas turbine driving a compressor (courtesy of Solar Turbines Incorporated).

A note about terminology is worthwhile. The generic term commonly used for this type of driver is gas turbine, but due to its application in industry, several other terms are in use. The other common terms are gas generator, preferred for aeroderivatives, and gas producer, used mostly by Solar Turbines. These have come about primarily because, as opposed to the aircraft gas turbine whose main function is to produce thrust, the industrial version drives a power turbine that is attached to a mechanical load. This distinction between gas generator or gas producer and power turbine (also called a “free turbine” by some) is relevant especially for aeroderivatives because a separate power turbine has to be added that was not there for the aircraft version. In the following, the term gas turbine implies a combination of the gas generator or gas producer and the power turbine.

8.2.2 Basic Design of a Gas Turbine

A gas turbine consists of three major sections (see Fig. 8-5):

- compressor which increases the pressure of the air
- a combustion section where fuel is combusted to add energy
- a turbine that extracts energy, first of all to drive the compressor and secondly to provide mechanical energy to the driven equipment, a compressor or pump for pipeline applications

In general, the advantages of gas turbines for pipeline applications are:

- Low weight, which makes them suitable for remote locations where weight is important
- Easily maintained, removed and replaced, which maximizes availability
- Fast starting
- Highly efficient
- Able to use either natural gas or good quality liquid fuels and sometimes designed to allow switching between them

One of the unique aspects of a gas turbine driver is that design of these three basic components can be achieved by different shaft arrangements, as is shown in Fig. 8-6.

The most basic arrangement is a single shaft where the connections between the compressor, turbine and load are mechanically coupled [Fig. 8-6(a)]. The load can be attached on either the compressor or the turbine side, with the latter being more common. The single shaft arrangement is normally used for generator applications but is very rare in pipelines. This is due to the fact that a single shaft severely limits the speed range and, thus, its flexibility for pumping or compression.

The most common shaft configuration uses two shafts, one for the compressor and turbine needed for the compressor and the other for the power turbine and load [Fig. 8-6(b)]. Again, the load can be positioned on either side of the gas turbine, but hot end drives are, by far, the most prevalent. The shafts of the high-pressure gas generator and low-pressure power turbines are not mechanically connected but are “aerodynamically coupled.”

A variant of the two-shaft arrangement is shown in Fig. 8-6(c). The high-pressure compressor and turbine are connected on one shaft, and the low-pressure compressor and turbine are on a second shaft that runs inside the first shaft and can be connected on either side

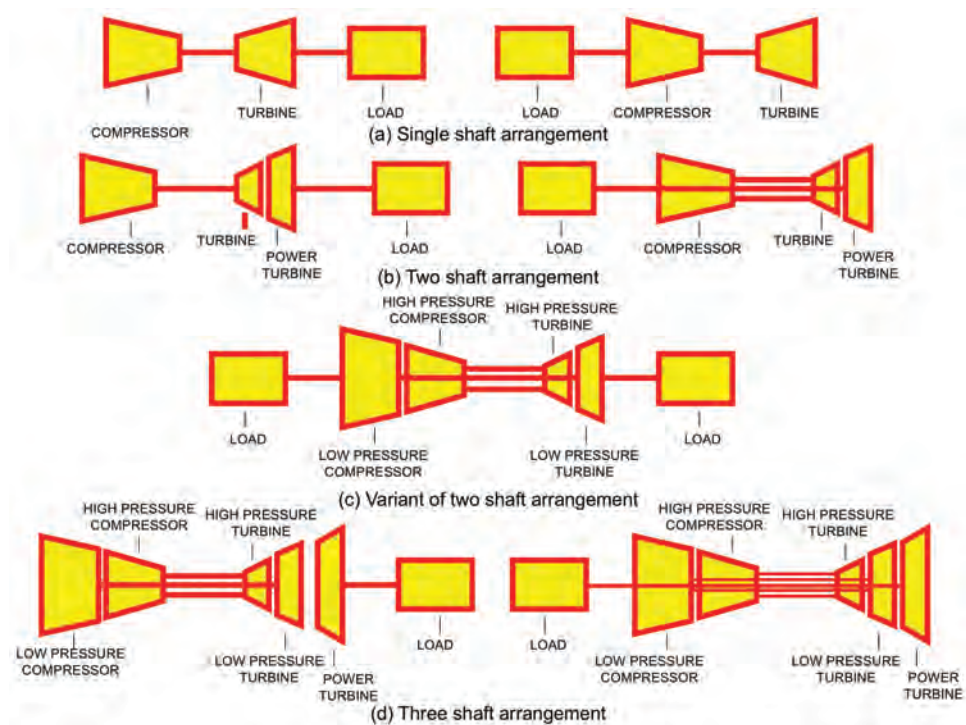


Figure 8-6. Different shaft arrangements for gas turbines.

to the load. This type of arrangement is specific to only one gas turbine, the GE LM6000, which was originally intended for power generation but is now being adapted for mechanical application.

The other relatively common type of shaft arrangement consists of three shafts [Fig. 8-6(d)]. The gas generator is a “twin-spool” design and is in series with an independent low pressure power turbine that drives the load. The front portion of the axial-flow compressor is mounted on the same shaft as the rear section of the high-pressure turbine, and the rear portion of the axial-flow compressor is mounted on the same shaft as the forward section of the high-pressure turbine. The rear axial-flow compressor drive shaft is hollow to allow the front axial-flow compressor drive shaft to pass through to the rear high pressure power turbine. The two axial-flow compressors of the “twin-spool” gas generator are not mechanically connected but are related aerodynamically.

Using the two-shaft arrangement shown in Fig. 8-5, the basic operation of a gas turbine driving a compressor can be described as follows.

Air drawn in through the intake is compressed by an axial-flow, multi-stage compressor and passed into the combustion chambers where fuel is injected and ignited. The hot expanding gases leave the combustion chamber at high velocity and pass through and rotate the high-pressure turbine, which is directly connected to and drives the axial-flow compressor. Remaining energy from these gases then drives the centrifugal compressor through a low-pressure power turbine assembly.

The axial-flow compressor consists of a series of metal discs attached to form a single shaft. The rim of each disc holds a set of airfoil-shaped blades mounted at an angle. As the shaft rotates, air is pushed along by the angled rotary blades. These rotors (set of bladed discs) act like a series of fans, pushing air along the axis of the compressor.

A set of vanes hangs between each successive rotor stage. These vanes are fixed to the inner wall of the compressor casing so they do not spin with the rotors. Since the vanes are stationary, they are called stators. The stators are angled to diffuse and redirect the air that passes between them. Compression is accomplished by slightly reducing the velocity of the air between each set of blades, building pressure.

Rotors impart both velocity and pressure to the air. As the air flows from the first-stage rotor into the first-stage stator, its velocity is reduced. The first-stage rotor, however, continues to push air into the first stage stator, building pressure. The slightly pressurized air then leaves the first stage stator at the correct approach angle for the second stage rotor's airfoil blades, and the velocity-pressurization cycle occurs again. An axial-flow compressor may contain up to twenty stages, each stage imparting greater air compression than the one before.

After the air is highly pressurized in the axial-flow compressor, it is ready for combustion. Heat is applied to the compressed air through combusted fuel at the inlet of the combustion chambers. Air that flows through the combustion section is divided into primary and secondary air. Primary air is mixed with fuel gas, ignited and burned at high temperatures to optimize combustion. Secondary air is then mixed in to lower the average temperature of the gases leaving the combustor. Tertiary air is also used in the combustion assembly to cool and protect metals.

The high-pressure turbine assembly receives the high-pressure hot gases - their energy having increased tremendously. These hot gases expand through the high-pressure turbine rotor blades to drive the axial-flow compressor.

About two-thirds of the total energy consumed by the gas turbine is used to run the axial flow compressor. The remaining power from the gases leaving the high-pressure turbine is used to drive the centrifugal compressor through the low pressure power turbine assembly.

As can be seen in Fig. 8-7, the gas turbine and compressor are normally mounted on a skid along with supporting systems that include air intake, exhaust, fuel gas system, lube oil system, and instrumentation and control devices.

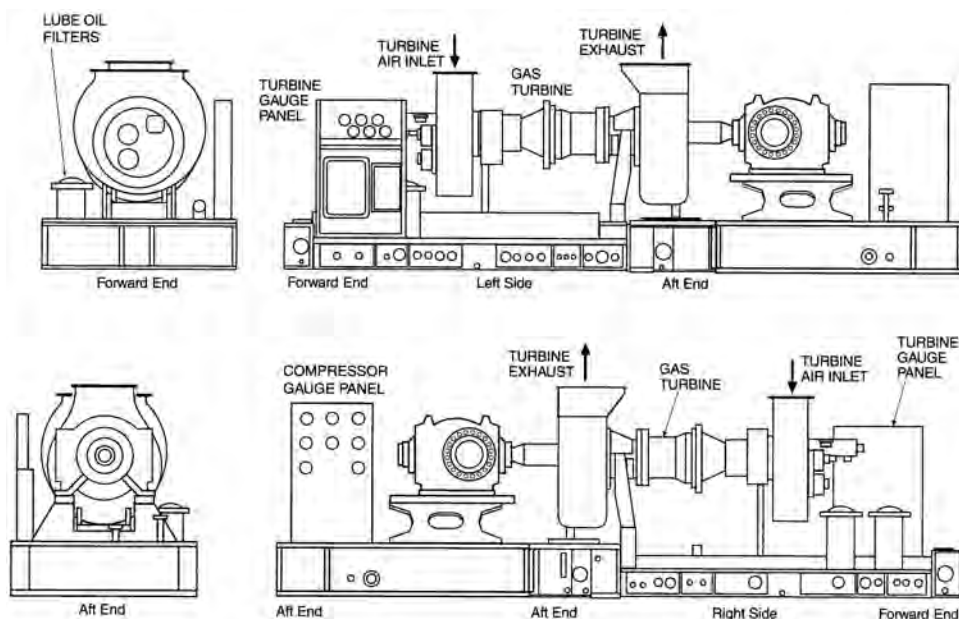


Figure 8-7. Typical inline gas turbine/pipeline compressor unit (1, centrifugal compressor discharge; 2, pneumatic start vent; 3, centrifugal compressor discharge; 4, degassing flue vent; 5, pneumatic seal motor exhaust; 6, turbine exhaust flange; 7, turbine air inlet flange; 8, AC electro-hydraulic start motor) (courtesy of Solar Turbines Incorporated).

8.2.3 Air Intake System

The air intake system ensures that clean air is provided to the gas turbine. To achieve this, air filters are installed in the intake to filter the air. The type of air intake system is dependent on the environmental conditions encountered at the location where the gas turbine is installed. Special challenges are posed when a gas turbine is installed on an offshore platform, close to the ocean, in a desert or dusty location or in an arctic environment.

The intake system becomes more complicated if intake cooling (to increase power at high ambient temperatures) is required or if icing conditions occur.

In the past many filter systems were based on inertial filtering, which consisted of a series of vanes that deflected the air to separate the contaminants using centrifugal force. The current approach is to use many small cylindrical filters. Compressed air is used to backflow individual filters and dislodge the dust that has collected on them. These self-cleaning pulse cleaning systems are commonly called “huff and puff” and operate automatically, based on pressure differential. They work well in both dusty and cold weather conditions. Depending on the environmental conditions of the installation, a combination of inertial separators, high efficiency filters and self-cleaning filters may be required [3].

8.2.4 Air Compressor Surge

At lower engine speeds, the angles of the compressor blades are not at the optimum design and flow separation may occur in a manner similar to that experienced when an aircraft wing stalls or loses lift. When starting the engine, the pressure ratio is very low and the compressor is trying to push the air into a much smaller area at the back of the compressor,

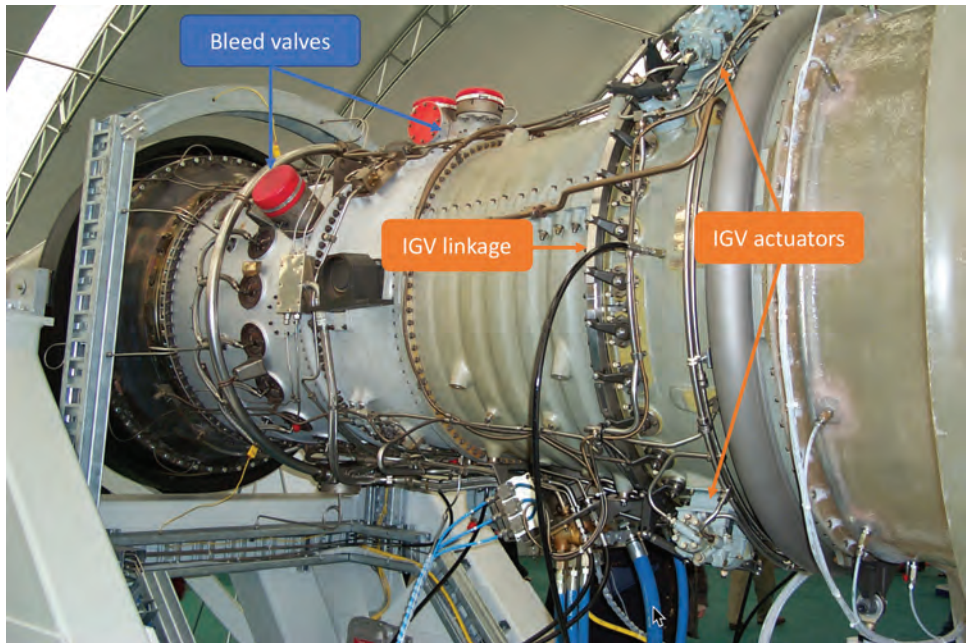


Figure 8-8. Bleed valve and IGV arrangement on a Rolls Royce RB211.

which has been designed for a larger compression ratio. This causes the air flow to choke. The result is called surge or rotating stall. It is a very complicated aerodynamic phenomenon that even today is not fully understood. However, the methods required to counteract it are well developed and the designer has a number of options.

The two basic options for countering compressor surge are bleed valves and variable geometry or a combination of the two. A bleed valve allows the compressor to avoid surge by dumping compressor air to increase compressor flow during start-up and then closing it at a predetermined speed. Sometimes multiple bleed valves are used. The Rolls Royce RB211 shown in Fig. 8-8 has a bleed valve at the exit of the first compressor rotor and another at the exit of the second compressor rotor, both of which activate at different speeds. The Solar Centaur in Fig. 8-5 has one bleed valve at the exit of the compressor, which is fed into the exhaust.

8.2.5 Variable Compressor Geometry

Variable compressor geometry consists of one or more stages of stator vanes that can be rotated to the appropriate angle for the operating conditions (speed and temperature). This is used on many gas turbines to improve efficiency at part load and reduce the likelihood of surge (surge can still occur if the blades become dirty or fouled). Most gas turbines have variable inlet guide vanes (IGVs), such as the ones shown in Fig. 8-9. They are positioned by a ring placed around the stage that is actuated by a hydraulic cylinder (Fig. 8-8). During starting, they rotate to a “closed” position where they restrict the flow of air by reducing the area between the blades. At a specified speed they begin to open until they reach a predetermined angle.

Some engines have multiple stages of variable stator vanes (VSVs) downstream of the IGV. The Solar Centaur in Fig. 8-5 has three VSVs in addition to the IGV. They actuate from a “closed” position to an “open” position between 80% and 92.5% speed (corrected for ambient temperature). The General Electric LM2500 shown in Fig. 8-10 has a very



Figure 8-9. IGVs on a Rolls Royce RB211.

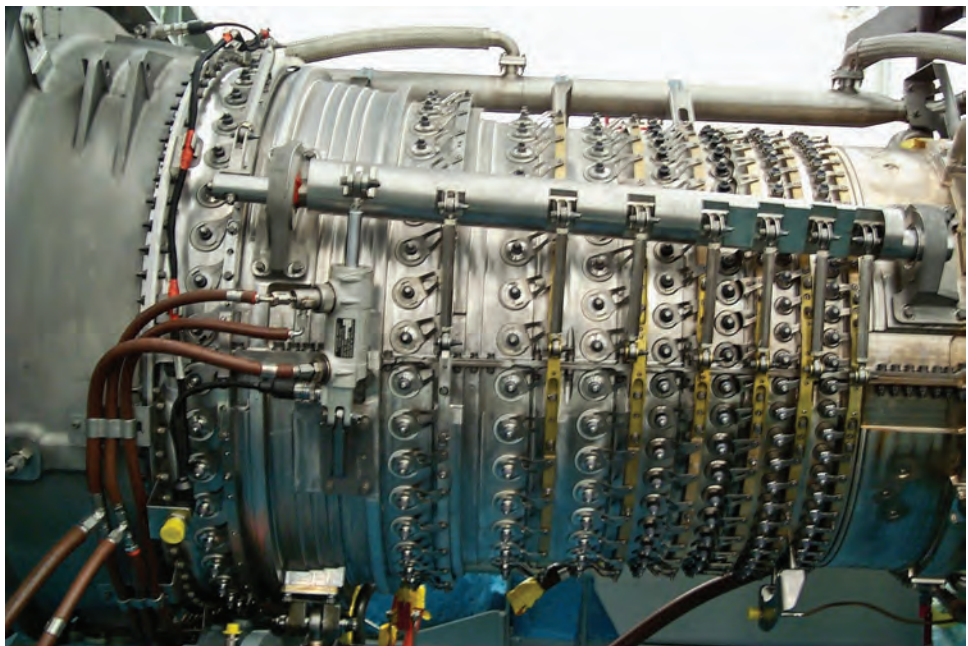


Figure 8-10. IGVs and VSVs on a GE LM2500.

extensive set of VSVs on seven stages plus the IGV. Because of this, it does not require bleed valves.

8.2.6 Anti-icing Systems

The formation of ice in the air intake or on the first few stages of the compressor can occur if a combination of temperature and humidity takes place. If chunks of ice are ingested into the compressor, major damage can result including catastrophic destruction of the compressor section blading.

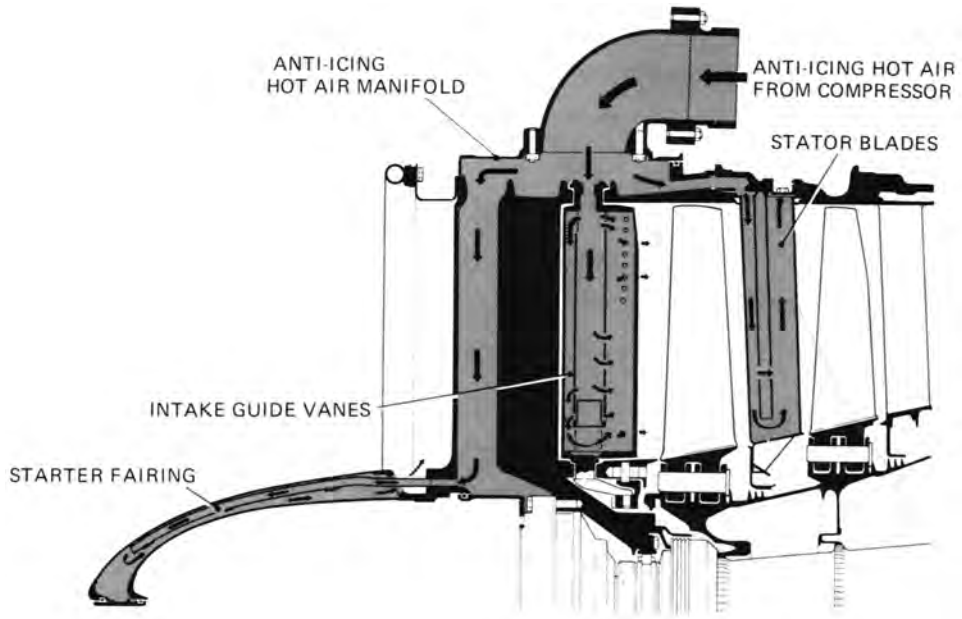


Figure 8-11. Anti-icing system for a Rolls Royce Avon (courtesy of Rolls Royce).

Anti-icing systems may be designed by:

- Bleeding air from the compressor and injecting it into the front of the compressor through the nose cone and the first few stator vanes (see Fig. 8-11)
- Installing heating coils in the air intake
- Feeding heated air from some other source (such as the exhaust) into the air intake

Since they reduce the efficiency and power output of the gas turbine, these systems are activated only when icing conditions are present.

8.2.7 Exhaust System

The exhaust system directs the hot turbine exhaust with as low a pressure loss as possible to a location that is safe for employees and other equipment. It has to be designed for the high temperature of the exhaust and be structurally sound. Noise attenuation and silencers are sometimes installed and are dependent on local requirements. Care has to be taken that the exhaust air does not recirculate into the air intake since this will result in a loss of maximum power.

8.2.8 Bearings and Lubrication System

8.2.8.1 Bearings

Lubrication systems used for gas turbines are always pressurized, but there are significant differences between aeroderivative and industrial gas turbine types. The fundamental reason for the difference is that aeroderivatives use antifriction bearings and industrial machines normally utilize hydrodynamic bearings. Since aeroderivative rotors are lighter, antifriction bearings are sufficient and, indeed, desirable since, at least for aircraft use, a much smaller lubrication system is needed. In particular, the lube oil reservoir is much smaller, which is fortuitous, considering that the cost of the synthetic oil needed for the higher oil

temperatures in an aeroderivative is much higher. Industrial gas turbines often have hydrodynamic bearings of the tilting pad type, which can easily tolerate mineral oils.

Figure 8-12 illustrates an antifriction (roller) bearing for a Rolls Royce RB211. It features a special squeeze film to dampen the bearing and increase its life. This engine also uses ball bearings for thrust. The bearing configuration for the Rolls Royce RB211 is shown in Fig. 8-13. The two rotors shown result in a more complicated bearing arrangement, with five bearings of which two are thrust (ball) bearings and the other three are for radial loads using rollers.

Industrial gas turbines require bearings that can take higher loads. Although standard journal bearings have been used in the past, the most common type of bearing used today is the tilting pad bearing as described in section 6.3.3.1. On a typical dual-shaft industrial gas turbine, bearings will be located on the front end of the compressor, at the end of the compressor, before the engine turbine and after the power turbine. Thrust bearings will be positioned at the front end of the compressor and next to the power turbine bearings (one for each shaft).

In addition to different bearings and oil types, aeroderivatives also employ scavenge pumps to assist with extracting oil from the bearings which permits the oil supply pressure

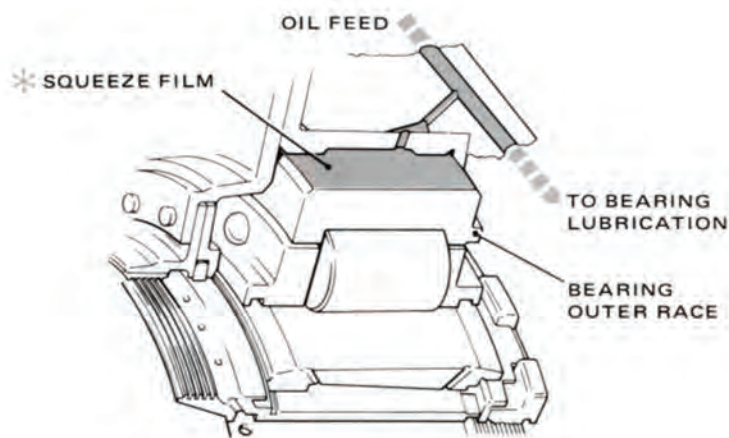


Figure 8-12. Antifriction bearing for a Rolls Royce RB211 (courtesy of Rolls Royce).

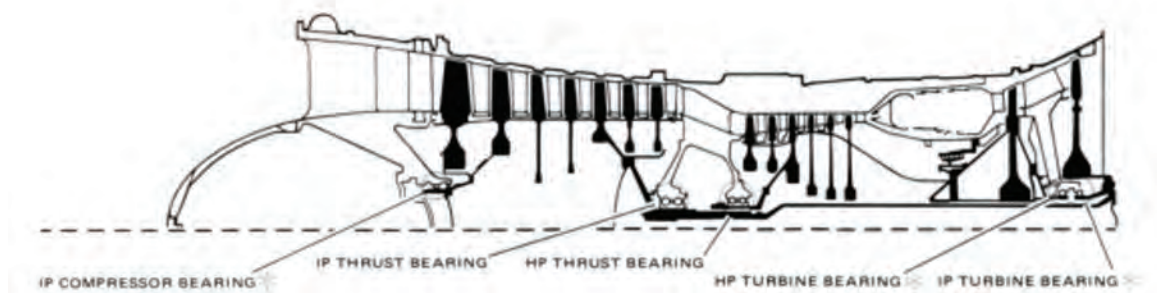


Figure 8-13. Bearing configuration for a Rolls Royce RB211 (courtesy of Rolls Royce).

to be lower and, thus, reduces the chance of internal leakage. Because of lower oil flow, cooling requirements are less than for industrials.

As with most situations, the advantage of a smaller lube oil system for aeroderivatives comes with a major downside, the need for two separate lube oil systems. Industrial gas turbines need only one oil system for gas turbine, power turbine, pump or compressor and, if necessary, a gearbox. Pumps or compressors driven by an aeroderivative gas turbine usually require separate lube oil systems which duplicates tanks, pumps, instrumentation, controls, and other devices. Increased complexity and more maintenance are the unfortunate result, although the reliability of these systems has been well proven.

Most of a lubrication system is standard from the manufacturer, but the end user does have to make a few decisions. One of them is what type of cooling is appropriate. Air cooling is more effective in cooler climates. In warmer climates, water cooling may be better if a sufficient supply of coolant is available. In any case, it is important to build in extra cooling capacity because cooling efficiency will deteriorate over time. As well, the problem will occur at higher ambient temperatures so this must be taken into consideration.

API 614 [4] is the standard that covers the design of all types of lubrication systems. Again, it is primarily the responsibility of the equipment vendor to follow its specifications, but the end user, as represented by the engineering company doing the overall design, has to take final responsibility for the end result.

8.2.8.2 Aeroderivative Gas Turbine Lube Oil System

Figure 8-14 describes a typical lube oil system for an aeroderivative gas turbine (Rolls Royce RB211). It lubricates the gas turbine with power turbine bearings and the driven equipment handled by a separate lubrication system.

This oil system is divided into two sections: a supply system and a scavenge system. All piping, fittings and reservoir are Type 304 Stainless Steel to prevent corrosion. The lube oil used is a synthetic oil suitable for high temperatures.

Protection devices are fitted against low oil level and low oil reservoir temperature. A thermostatically controlled heater is included and, for easy starting, ensures that a minimum temperature is maintained while the unit is not operating.

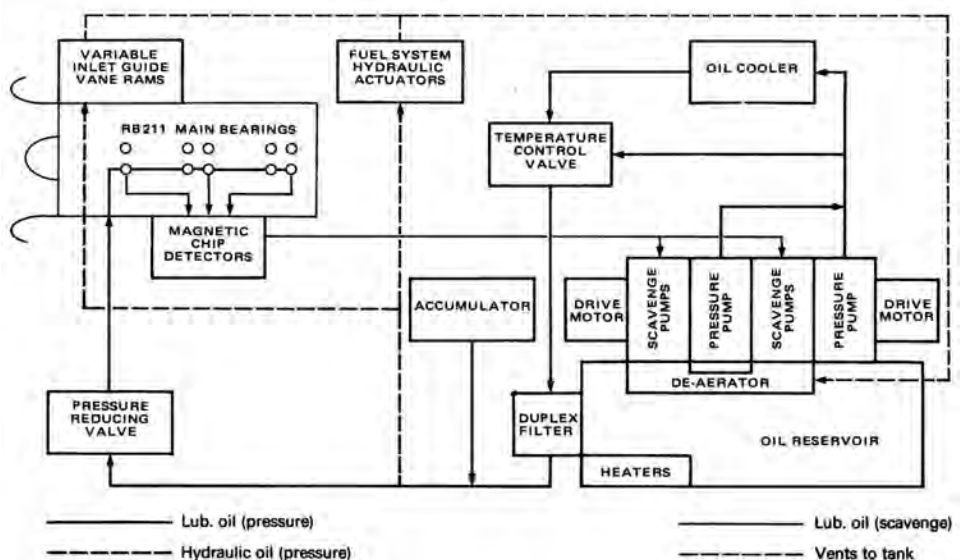


Figure 8-14. Lube oil system for a RB211 (courtesy of Rolls Royce Energy).

A positive displacement pump driven by an AC motor provides the required pressure to the bearings and is backed up by an AC, DC or hydraulic standby pump. After the pump, the oil flows through an oil cooler that is thermostatically controlled. The oil is then filtered by a duplex, full-flow filter that allows filter change-out while running. The oil supply is protected by high oil temperature, low oil pressure and high filter differential pressure switches.

The oil flows through a pressure-reducing valve to the bearings and accumulates in the bearing sumps. The oil temperature is measured at each scavenge line in case of bearing problems.

Chip detectors are often located in the sumps to detect metal particles from the bearings. If a bearing becomes damaged, metal particles will become entrained in the oil. The chip detector is basically a magnet that attracts these metallic particles and detects when they accumulate on the magnet. Upon alarm, the detector is removed and inspected to diagnose the type and extent of bearing damage.

Scavenge pumps, driven by the main and standby motors, extract oil from the bearings and provide the pressure to return the oil back to the reservoir.

8.2.8.3 Industrial Gas Turbine Lube Oil System

The lube oil system shown in Fig. 8-15 is typical for an industrial gas turbine with one integrated oil system for the gas turbine, gearbox and driven equipment.

The oil reservoir is much larger than for aeroderivative gas turbines. It normally contains mineral oil, which does not have as high a temperature capability as synthetic oil but is more economic. Generally, oil temperatures are not as high in heavy-duty gas turbines since the oil flow is greater. Oil heating may be supplied if required.

Oil pressure is supplied during normal operation by a main lube oil pump driven from the accessory drive mounted on the front of the compressor shaft. Prior to start-up and on shutdown, oil pressure is supplied by the AC-driven, pre-/post-lube oil pump. This pump runs for a period of time after shutdown to cool and lubricate the bearings and prevent damage. A third pump using another source of energy, for example, a DC pump driven from batteries, is available as backup in case of power loss or pre-/post-lube oil pump failure.

The oil is cleaned with duplex filters that allow filter replacement during operation. There is a differential pressure alarm and pressure gauge. The oil is then cooled prior to entering the bearings by either an air or water cooler. At the lube oil header, there is protection against high oil temperature and low oil pressure.

The oil drains back into the oil reservoir using gravity. The oil temperature is also normally measured in the drains to monitor bearing health.

A hydraulic pump is sometimes provided after the main lube oil pump to supply high-pressure oil to control variable inlet and stator vanes, as well as the fuel control and bleed valves.

8.2.9 Fuel System

8.2.9.1 Types of Fuel

The fuel system is a critical component of a gas turbine driver. Fuel availability is crucial when selecting pipeline drivers and will often be the deciding factor as to which driver is to be used.

For gas compressors, the fuel is almost always natural gas taken from the pipeline. For liquid pipelines, the product in the pipeline can sometimes be used if there is no batching and it is of sufficient quality. Some industrial gas turbines can tolerate heavier oils but aeroderivative gas turbines need higher quality liquid fuel such as kerosene. Where gas turbines are used on liquid pipelines, natural gas may be supplied separately if it is available in close proximity to the pipeline.

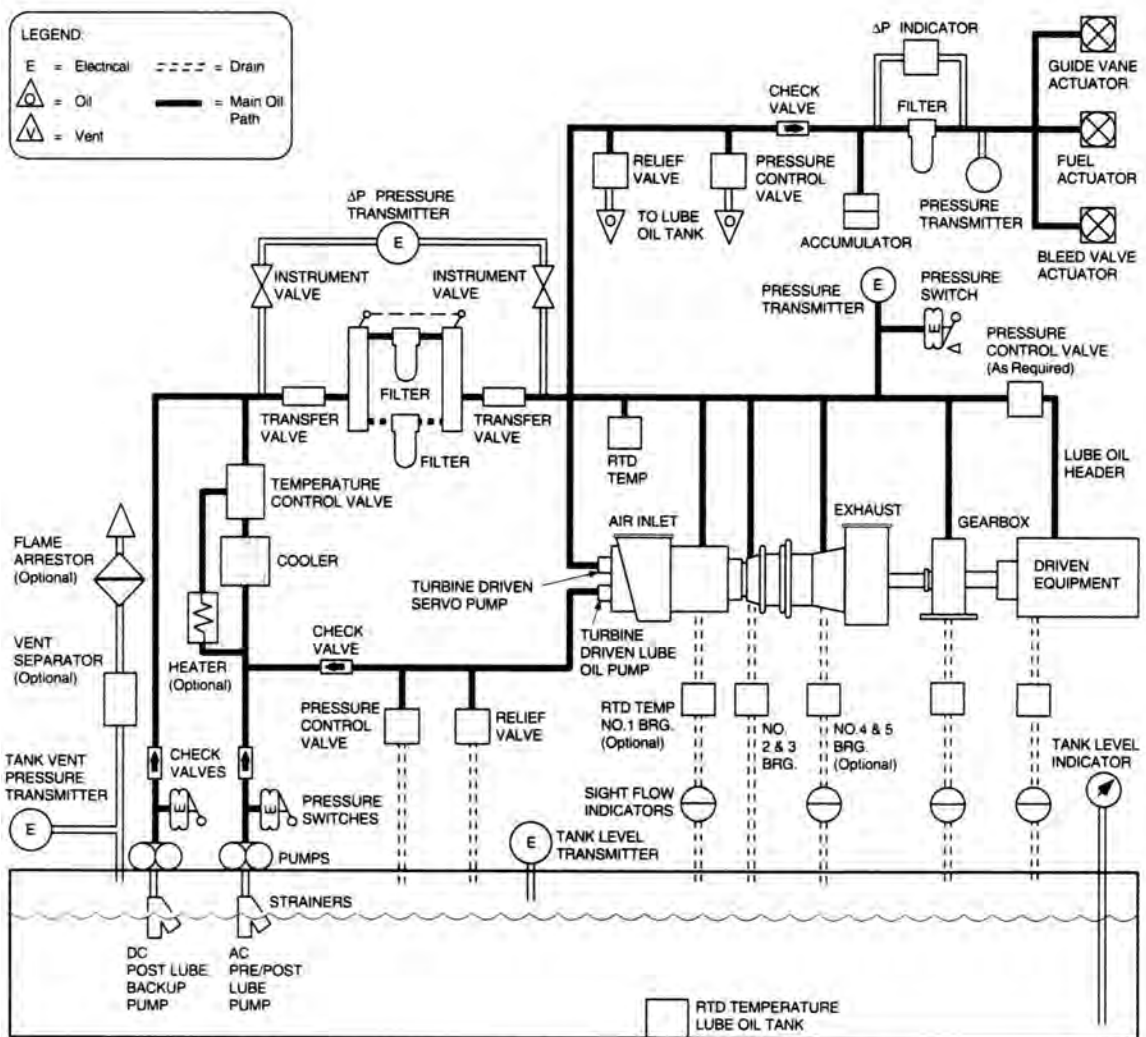


Figure 8-15. Lube oil system for a typical Solar gas turbine and driven equipment (courtesy of Solar Turbines Incorporated).

The issues with liquid fuels in gas turbines consist not only of their less desirable combustion characteristics but also the presence of trace contaminants that cause corrosion [5]. The main contaminants found in liquid fuels are sodium, vanadium, potassium, lead, and calcium. The first four form corrosive compounds, with vanadium and sodium being the most prevalent in liquid fuels. They impact the life and performance of downstream turbine blades and nozzles through both corrosion at elevated temperatures and deposition.

Contaminants can also be ingested from the intake air that may contain pollutants or salt from the ocean. If water or steam injection is used, these may also be a source of unwanted contaminants. Although most natural gas fuels are quite clean, even they may contain contaminants from upsets in gas processing. Gas turbine vendors will specify expected fuel quality, and the design of the fuel supply will need to handle any deficiencies.

For natural gas, the main issue is with potential liquids entrained in the gas, especially slugs of liquid. When a substantial amount of liquid enters the combustor, it upsets the combustion process and causes rapid changes in temperature, often over-temperaturing the

downstream nozzles and blades. In severe cases, the upper portion of first-stage blades may be destroyed.

Natural gas taken from the pipeline usually has to be reduced in pressure to match the discharge pressure from the gas turbine compressor. The resultant pressure drop may well cause the gas to fall below its dew point by the time it enters the combustion chamber since other components such as valves also cause a drop in pressure and temperature due to the Joule-Thompson effect. It is therefore common practice to add a separator or scrubber for the fuel gas and then heat the fuel gas to a temperature well above the dew point for that gas composition. It is accepted practice to achieve a superheat of 50°F or 28°C as per ASME B133.7 [6].

Gas turbines can operate on a wide range of natural gas heating values, normally between 800 and 1200 Btu/ft³ (30–45 MJ/m³). If lower heating values are used, combustor size has to be increased due to the higher volume of gas needed to produce the required heat input.

Fuel quality is characterized by a measure called the Wobbe index, which is defined as

$$WI = \frac{LHV}{\sqrt{SG}} \quad (8-1)$$

where LHV is the lower heating value in Btu/scf and SG is the specific gravity.

Some gas turbine manufacturers use a temperature-corrected version of the Wobbe index since the fuel supply temperature T_f has an impact on the volumetric volume flow. It uses a reference temperature T_{ref} , usually 15°C or 60°F with the Wobbe index defined as

$$WI = \frac{LHV}{\sqrt{SG}} \sqrt{\frac{T_{ref}}{T_f}} \text{ or } \frac{LHV}{\sqrt{SG} \sqrt{T_f}} \quad (8-2)$$

The Wobbe index for methane is 1360 Btu/scf (50.6 MJ/m³), and fuels with mostly heavier hydrocarbons will have a higher Wobbe index. If there are more inert components such as carbon dioxide or nitrogen, the Wobbe index will be reduced, and the power output will be somewhat increased. This is due to the fact that a larger fuel mass flow is needed for a certain amount of fuel energy. The mass flow through the turbine is thus increased, providing more power although this is partially reduced by an increase in pressure ratio through the compressor.

Since different fuel compositions with the same Wobbe index will have a similar pressure drop in a given fuel system, the energy flow will be the same [7]. Gas turbines are normally designed for a certain Wobbe index with a variation of, for example, +/- 5%. Any variations in Wobbe index greater than this will usually require special design considerations.

8.2.9.2 Emissions

Standard gas turbines produce relatively high levels of emissions. Typical emissions from a gas turbine are summarized in Table 8-1. They are divided into two groups: major species and minor species. Major species are measured in percentages while minor species are present in parts per million. The specific pollutants produced depend on the operating conditions of the gas turbine, especially the combustion characteristics and the type of fuel used.

The most important focus of emission control efforts has been on nitrogen oxides or what is also referred to as NO_x (NO_x = NO + NO₂). Nitrogen oxides are formed from the oxidation of free nitrogen already in the air by the high temperature of combustion. In general, the formation of NO_x can be managed by reducing the flame temperature.

Nitrogen oxides (NO_x), in particular, are formed due to high combustion temperatures and sufficient residence time for their formation. Thus, normal combustor design

Table 8-1. Typical gas turbine emissions [8]

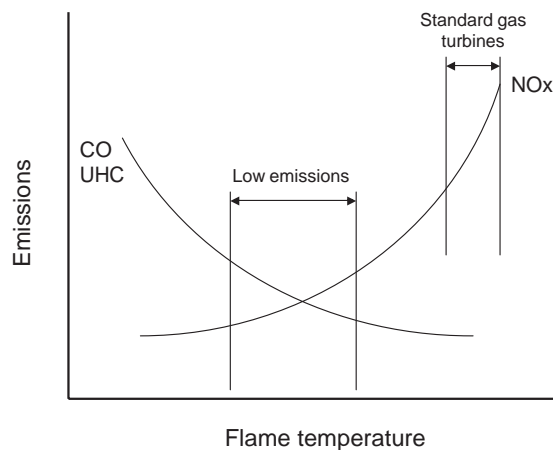
Major Species	Typical Concentration (% Volume)	Source
Nitrogen (N ₂)	66–72	Inlet Air
Oxygen (O ₂)	12–18	Inlet Air
Carbon Dioxide (CO ₂)	1–5	Oxidation of Fuel Carbon
Water Vapor (H ₂ O)	1–5	Oxidation of Fuel Hydrogen
Minor Species Pollutants	Typical Concentration (PPMV)	Source
Nitric Oxide (NO)	20–220	Oxidation of Atmosphere Nitrogen
Nitrogen Dioxide (NO ₂)	2–20	Oxidation of Fuel-Bound Organic Nitrogen
Carbon Monoxide (CO)	5–330	Incomplete Oxidation of Fuel Carbon
Sulfur Dioxide (SO ₂)	Trace - 100	Oxidation of Fuel-Bound Organic Sulfur
Sulfur Trioxide (SO ₃)	Trace - 4	Oxidation of Fuel-Bound Organic Sulfur
Unburned Hydrocarbons (UHC)	5–300	Incomplete Oxidation of Fuel or Intermediates
Particulate Matter Smoke	Trace - 25	Inlet Ingestion, Fuel Ash, Hot-Gas- Path Attrition, Incomplete Oxidation of Fuel or Intermediates

aimed at producing high efficiency inevitably results in levels of NO_x in the region of 100–200 ppmv. Environmental regulations are now commonly being set at 25 ppmv, and even lower levels are being set in some cases.

As Fig. 8-16 illustrates, the production of NO_x increases exponentially with flame temperature. Combustion temperature, therefore, has to be reduced. Excessive reduction in temperature decreases combustion efficiency and promotes the formation of carbon monoxide (CO) and unburned hydrocarbons (UHC), which must also be avoided.

Three primary methods are available for emission reduction:

- water or steam injection
- dry emission techniques (lean premixed)
- catalytic methods

**Figure 8-16.** Variation of emission levels with flame temperature.

Water or steam injection was the first method used in the past to reduce emissions. Injected directly into the combustion section, it depresses the combustion temperature by the amount of heat needed to raise the temperature of the water or steam. By increasing the mass flow through the turbine, it can significantly enhance the power output. However, it has some major deficiencies, which have restricted its use to peak power generation. It is limited to around 50 ppmv and is thus not sufficient for modern emissions regulations. Where water is used, it must be purified to minimize corrosion and erosion of gas path components. A large source of water is needed, and it cannot be economically recovered. Steam also has to be of very high quality and can likewise not be reused so it has to be replenished. Maintenance costs are increased, and intervals are reduced. One case study of an aeroderivative showed that the life of first stage nozzles can be reduced by 20% with a 3% injection of steam [9]. For pipelines especially, water or steam injection is not a viable option for emission reduction or performance enhancement.

As a result of the inadequacies of water injection, development commenced in the 1970s on combustor modifications to produce a dry emissions solution. It is based on a leaner mixture or lower fuel-to-air ratio to reduce NO_x emissions (Fig. 8-17). This is achieved by premixing air and fuel into a lean mixture prior to combustion to enable accurate control of the fuel-to-air ratio. Combustion has to be more closely controlled than on standard combustors, since it is now much closer to the lean limit and it is necessary to adjust the fuel-to-air ratio at part load conditions. There is a lean limit below which combustion cannot be sustained. An associated problem is a marked increase in combustion instabilities or oscillations at lean conditions, which has caused further development of “quiet” combustors.

Various schemes have been devised to achieve dry emissions in gas turbines. Various terms are in use including *DLN* (dry low NO_x), *DLE* (dry low emissions), and *SoLoNO_x* (Solar low NO_x). In all cases, the cross-sectional area of the combustion section has to be increased because of the lower fuel-to-air ratio. Staging of fuel nozzles over the speed range is one approach to optimize combustion at part load conditions [10]. In other cases, air is extracted from the combustion section and is then mixed in a controlled manner with fuel prior to combustion [11]. Sometimes at part load, some of the compressed air is dumped into the exhaust to optimize the fuel-to-air ratio. A result is that the fuel control system is considerably more complicated.

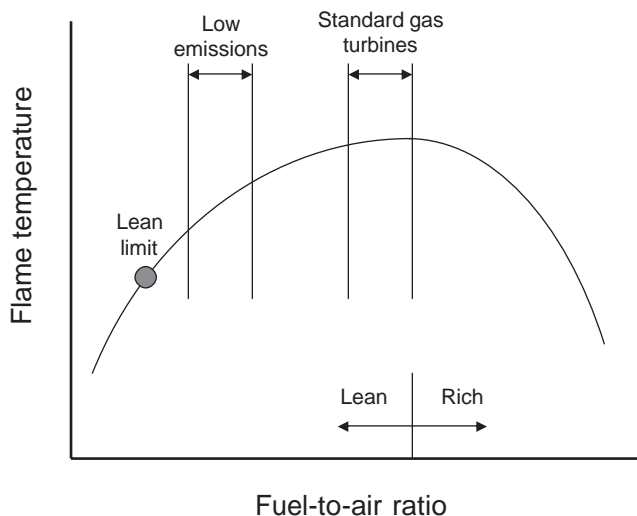


Figure 8-17. Variation of flame temperature with fuel-to-air ratio.

Some engines have been retrofitted with new combustors [12] with some compromises usually required to meet constraints such as installation parameters and impact on compressor and turbine design.

With DLN processes limited to about 15 ppmv, lower emission levels will have to depend on catalytic combustion. As is further described in Clapsaddle and Van Osdell [13], verification testing has already been carried out to show that emission levels below 5 ppmv are feasible. Catalytic combustion occurs in a flameless manner at much lower temperatures, where NO_x production is minimal, and limited to a preburner to provide the proper temperature for the catalytic reactor section.

8.2.9.3 Liquified Natural Gas

One significant change in gas turbine fuels is the impending use of natural gas fuel sourced from liquified natural gas (LNG) injected into pipelines. As discussed in length in Driscoll et al. [14], this introduces variability that may affect equipment that uses it as a fuel. This is particularly important for combustion systems that are designed to reduce emissions. The conclusion of the study was that conventional gas turbines can accommodate fairly wide swings in gas composition, up to 10%. For premix combustors, reasonable changes in fuel composition seem to have a minor effect on NO_x production and, so, should not be a major issue for most gas turbines. Specific designs of combustion systems are sufficiently diverse that some gas turbines may still have problems with fuel variability.

One vendor has implemented control system enhancements that can adjust for rapid changes in fuel quality that could result on LNG pipelines due to changes in supply source [15]. Conventional gas turbines can be tuned to adjust for different fuel compositions based on the Wobbe Index, but the results are then fixed into a schedule that then governs control system response. Further variations during operation cannot be accommodated by the control system. This is especially critical for units with lean combustion.

The system requires no additional instrumentation but does calculate surrogate readings such as airflow and firing temperature that cannot be easily measured by using an aerothermal model of the gas turbine. A model-based system is used to determine the operability boundaries such as emissions and combustion dynamics. The control system then adjusts control elements such as IGV position, fuel flow, and distribution between fuel nozzles. It is claimed that a variation of $\pm 20\%$ in Modified Wobbe Index can be accommodated while maintaining emission levels and performance. Testing indicates that a change of 18% per minute can be controlled by the system.

8.2.9.4 Natural Gas Fuel System

Natural gas is the best fuel for gas turbines since it promotes the most efficient combustion and produces the lowest environmental emissions. Its engine life is also the longest, with clean natural gas. It has to be within a specified range of heating values and free of liquid contaminants. Natural gas is often heated to ensure no liquids are present. If low BTU fuel is used, special fuel nozzles and combustors have to be installed and the fuel gas system has to be adapted because of the higher flow rates required to deliver the same fuel energy.

A natural gas fuel system (Fig. 8-18), which is for a Solar Centaur, is typical for most gas turbines.

The pressure of the fuel gas has to be higher than the compressed air delivered to the combustion section and, in some cases, a fuel gas compressor is required to boost a low-pressure fuel source. A pressure regulator and relief valve are installed upstream of the fuel gas system to ensure proper fuel gas supply. Low- and high-pressure switches protect against over- or under-pressure conditions.

A fuel filter is then installed to ensure contaminants do not enter the fuel system. Some systems also have a heat exchanger to remove liquids and increase fuel temperature to required levels.

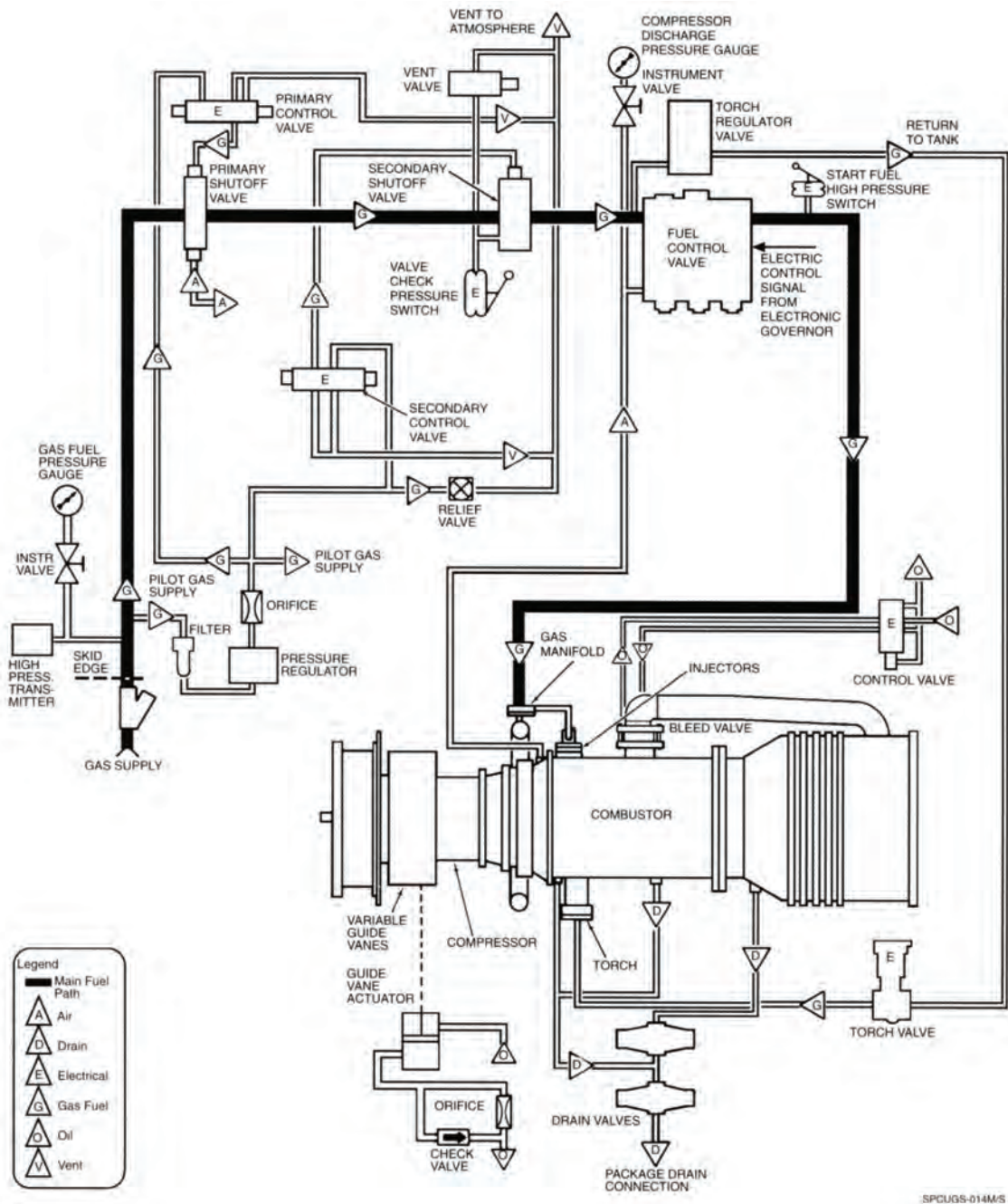


Figure 8-18. Typical natural gas fuel system (courtesy of Solar Turbines Incorporated).

A fuel gas flowmeter may be installed to enable the determination of fuel consumption but is otherwise not needed for fuel control.

Primary and secondary fuel shutoff valves are provided for isolation, start-up, shut-down and emergency purposes. The proper functioning of these valves is tested at every start-up by a valve check pressure switch.

The fuel is metered and controlled by an electric fuel metering valve, which is the most important component of the fuel gas system. It ensures that the right amount of fuel is provided

for the operating conditions. It is precisely controlled to ensure that the maximum turbine temperature is not exceeded and is an essential component of the start-up and shutdown sequence. The rate at which the fuel valve is opened or closed is also limited to prevent temperature increases that might damage the turbine. Fuel valves are normally electrically controlled with hydraulic actuation, but electrically actuated valves are starting to become common.

8.2.9.5 Liquid Fuel System

The gas turbine can operate on a wide range of liquid fuels, including:

- Distillates such as kerosene for which no fuel treatment is required
- Blended heavy distillates and low ash crude oils that require some treatment
- Residuals and heavy ash crude oils that require considerable cleaning and treatment

The life of the gas turbine (in terms of time between maintenance actions and overhauls) is reduced as the quality of the fuel decreases. Maintenance costs increase as well.

A typical liquid fuel system is shown in Fig. 8-19.

The system starts with a fuel storage tank and fuel treatment (not shown here). Treatment varies with the type of fuel and may include centrifuges, filters, dewatering and chemical treatment. Chemicals that are especially harmful to the turbine section are sodium, potassium and vanadium since they cause rapid corrosion.

The cleaned and treated oil is then filtered and pumped to the gas turbine. A boost pump may be required prior to the low-pressure filtration to 10 microns. A high-pressure fuel pump driven either by the turbine or an AC motor increases the pressure to a range of 600 to 800 psig (4,140 to 5,520 kPa). A 25-micron filter protects the fuel control valve. Similar to fuel gas systems, there is a main fuel control valve followed by a shutoff valve. At the fuel metering valve, there is an overflow for unused fuel back to the fuel tank. Drains are provided on the fuel manifolds.

Supplementary air supply is needed for up to three minutes during the start cycle to atomize the fuel. At operating speed, this is provided by compressor air. Protective instrumentation is installed for filter differential pressure and low pressure.

8.2.9.6 Dual Fuel Systems

Some gas turbine installations feature dual fuel capability so that the operator can switch to a less expensive fuel or as a backup. An example of a dual fuel system is shown in Fig. 8-20. A special fuel nozzle is required, and the control system is more complex to manage the two types of fuels and accommodate the switchover between them. With some systems, a mixture of gaseous and liquid fuels can be burned simultaneously.

8.2.10 Gas Turbine Performance

8.2.10.1 Performance Characteristics

The performance of a gas turbine is difficult to establish and monitor on a detailed basis. However, some basic aspects of gas turbine performance are quite important when considering its application for industrial use.

The main thing to understand about a gas turbine is that it is a mass flow machine, and all changes in mass flow will affect its performance. The power output is specified at ISO conditions that consist of:

- temperature of 15°C or 60°F
- altitude of sea level
- pressure of 101.3 kPa or 14.7 psi
- humidity of 60%

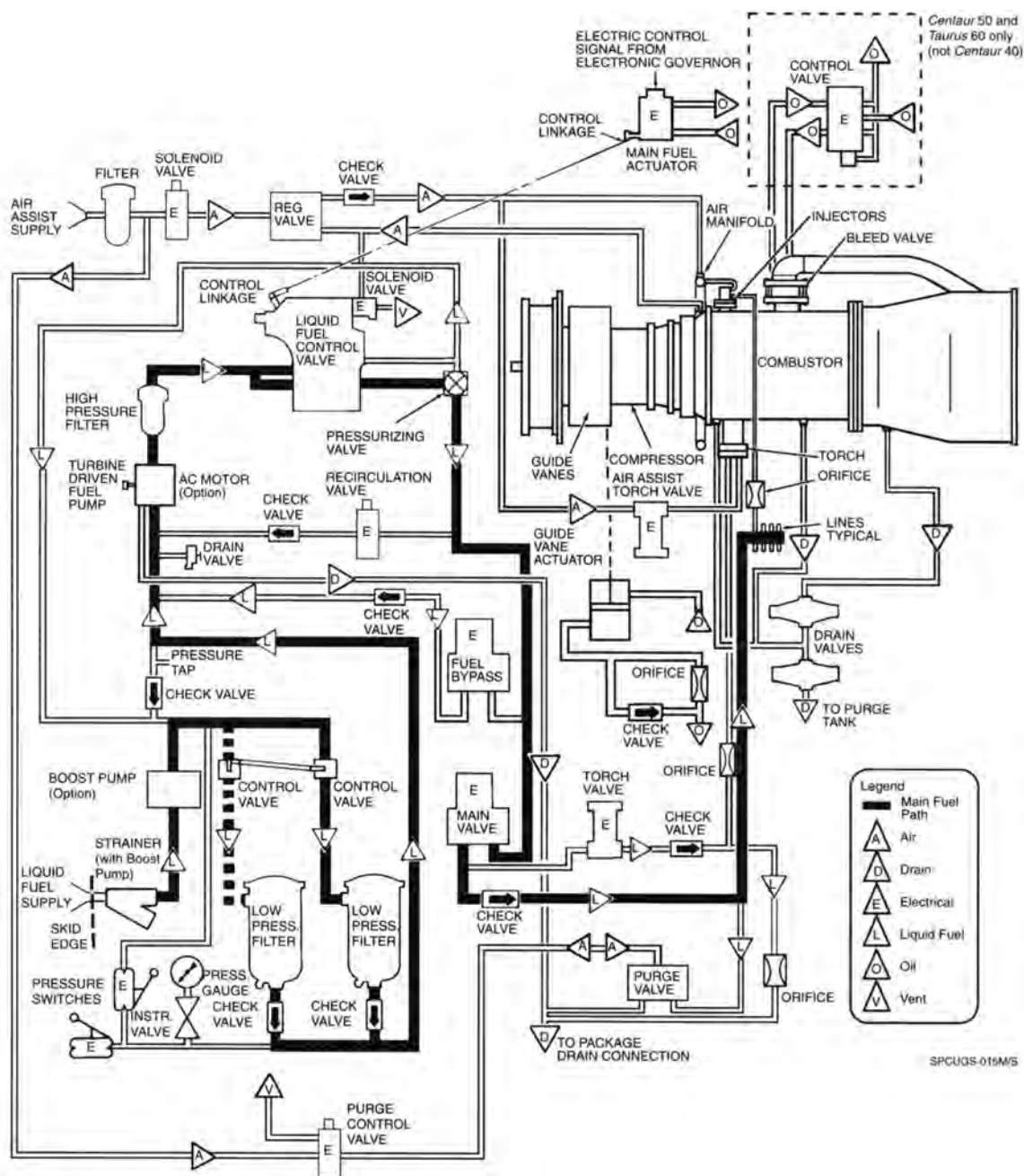


Figure 8-19. Typical liquid fuel system (courtesy of Solar Turbines Incorporated).

At lower temperatures, the density of the air increases and, thus, also the power. This increase is very significant and can easily be 30% to 40% higher at temperatures below 0°C. For some engines, the power is limited at some lower temperature to prevent overloading of the rotating components due to the higher mass flow. Conversely, at higher temperatures, the power output declines. The heat rate (fuel consumption) also varies with air intake temperature but in the opposite direction and less prominently. The correction factors that

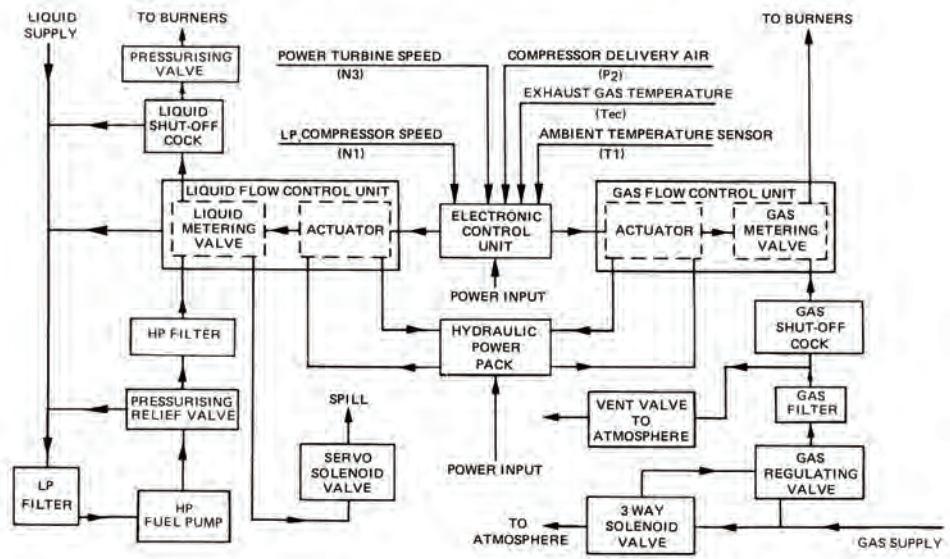


Figure 8-20. Dual fuel system (courtesy of Rolls Royce).

can be applied to power output and heat rate with respect to air inlet temperature for a two-shaft gas turbine can be seen in Fig. 8-21(a). The power output is not affected by relative humidity, and heat rate varies very little so can usually be ignored.

Similarly, a gas turbine will produce a lower power output at a higher altitude, again because of a decrease in inlet air density Fig. 8-21(b). The heat rate is not affected by altitude.

The next major correction that is not factored into most manufacturer performance specifications is inlet and exhaust losses. This affects both power output and heat rate as can be seen in Fig. 8-21(c) and (d). Of the two, inlet losses are more significant and will clearly depend on the type and design of the air inlet ducting and filters.

There may be a correction if the fuel composition differs from the standard fuel assumed by the manufacturer.

The final source of losses takes the form of power takeoff devices such as lube oil and hydraulic pumps and a gearbox (if needed).

A typical performance map from a manufacturer is shown in Fig. 8-22 [16]. In addition to the load, it also has curves for exhaust temperature, fuel flow, and exhaust flow. Unfortunately, exhaust flow is never measured, although intake flow is sometimes available if a calibrated bell mouth is installed.

The exhaust (or power turbine exit) temperature is not as useful as the power turbine inlet (or gas generator turbine exit) temperature T₅ (also referred to as TIT) that is normally measured by the control system. The ideal temperature to measure is the gas generator TIT T₃, but it is too high for thermocouples to survive for any reasonable length of time. Since the relationship between T₅ and T₃ varies, the control system compensates T₅ to maintain the maximum possible T₃. This is often done during final factory testing and may vary with each engine.

Maximum performance is attained either at maximum gas generator speed or TIT. They are equal at an air inlet temperature that is called the match point. Above this point, the gas turbine will limit on TIT, and the speed will be below what is allowed. Below this point, the engine will limit on gas generator speed, and TIT will be less than allowed.

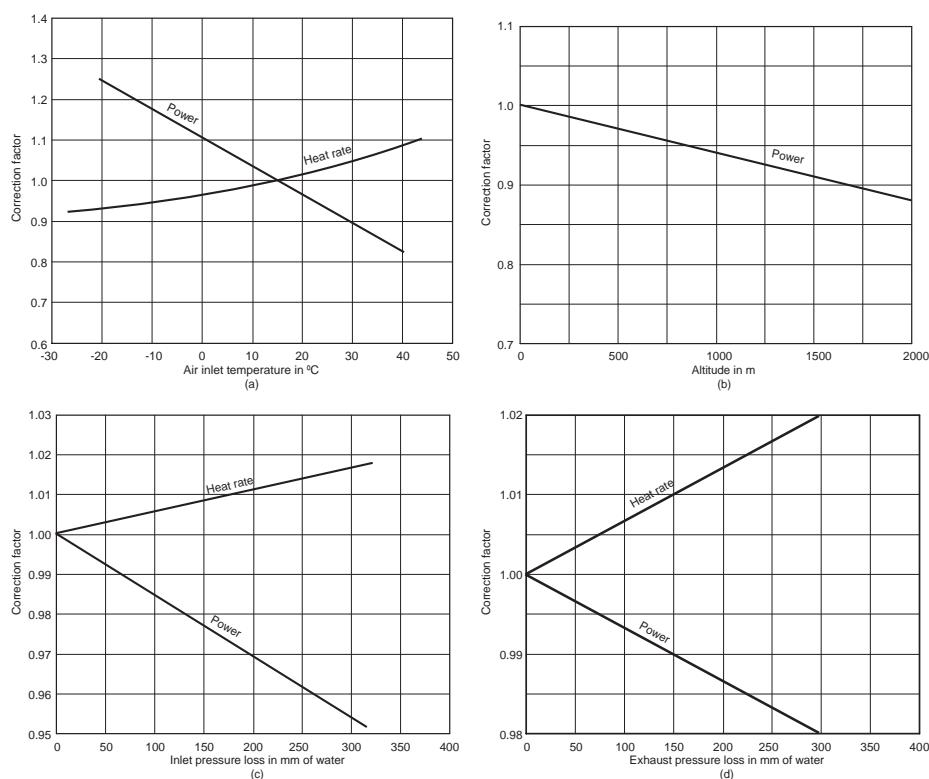


Figure 8-21. Correction factors for gas turbine performance (a) Air inlet temperature (b) Altitude (c) Inlet losses (d) Exhaust losses.

8.2.10.2 Performance Calculations

The performance of the gas turbine is a complicated dance between the aerodynamic properties of the compressor, the gas generator turbine and the power turbine. For a two-shaft unit, the first two are connected mechanically so will have the same speed but the power turbine is coupled aerodynamically. This is done by a process called component matching that takes into account matching of pressures, temperatures, and flows between each component. The situation becomes significantly more complicated for a three-shaft unit.

Gas turbine manufacturers have their own proprietary performance computer programs to aid in design optimization and predict final performance. There are software programs, such as GasTurbTM, that do provide quite sophisticated simulation of both design and off-design performance.

The basic thermodynamic performance of a gas turbine can be estimated, although without the sophistication of the inclusion of losses such as bleed flows from the compressor, mechanical efficiency, pressure drop across the combustor, fuel flow added to the turbine flow, heat energy lost through radiation and convection and other efficiency losses.

The enthalpy-entropy version of the Brayton cycle that is the standard thermodynamic cycle for a gas turbine is shown in Fig. 8-23. The first step is to describe and estimate the performance of the air compressor section of the gas turbine. From Fig. 8-23 (from point 1-2), it can be seen that the pressure increases from P_1 to P_2 , where P_1 is atmospheric pressure (minus an inlet pressure drop). Assuming adiabatic compression, there is also an increase in temperature and corresponding enthalpy and increase in entropy. In the combustor (from point 2-3), fuel is added and combusted with a large increase in temperature and enthalpy with a small pressure drop, but shown here at constant pressure. The air then expands in the

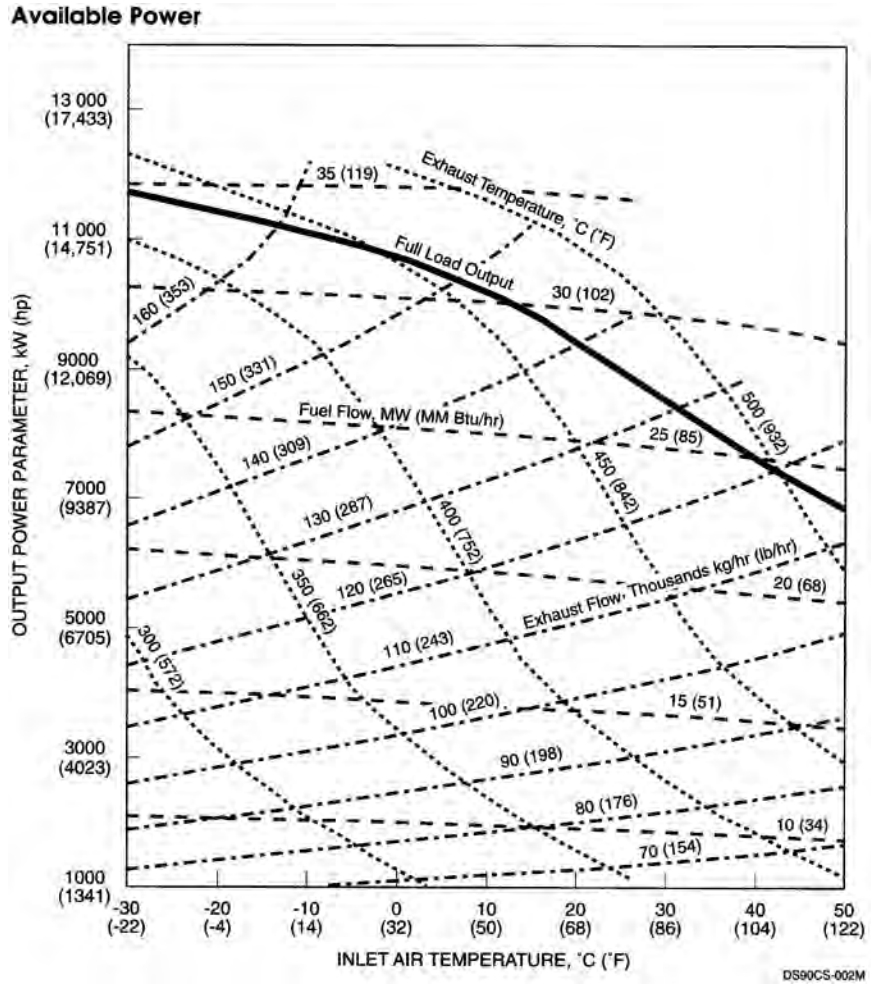


Figure 8-22. Typical gas turbine performance curves—Solar Mars 90 (courtesy of Solar Turbines Incorporated).

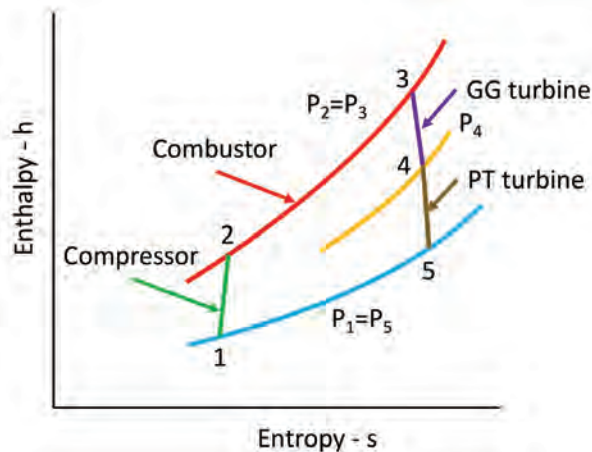


Figure 8-23. Enthalpy vs. entropy diagram for a Brayton cycle.

turbines (from point 3-4 for the gas generator turbine and point 4-5 in the power turbine) where the drop in pressure and temperature is converted into providing power to the compressor and the power turbine, which drives the output shaft.

The following example of basic thermodynamic calculations for the Brayton cycle illustrates the parameters involved and the resulting performance of a gas turbine. Air properties are assumed to be:

$$\begin{aligned}c_p &= 0.24 \text{ BTU/lb}^\circ\text{R} \\ k &= 1.4\end{aligned}$$

For the gas turbine parameters, it is assumed that:

$$\begin{aligned}p_1 &= 14.7 \text{ psia} \\ T_1 &= 80^\circ\text{F} \\ r &= 12 \\ \eta_{comp} &= 85\% \\ W &= 120 \text{ lb/s} \\ \eta_{turb} &= 95\% \\ T_3 &= 1700^\circ\text{F}\end{aligned}$$

The equations for the performance of the compressor are:

$$T_2 - T_1 = \frac{T_1}{\eta_{comp}} \left[\left(\frac{P_2}{P_1} \right)^{\left(\frac{k-1}{k} \right)} - 1 \right] = 656^\circ\text{F} \quad (8-3)$$

$$h_{comp} = c_p (T_2 - T_1) = 157.55 \text{ BTU/lb} \quad (8-4)$$

$$P = W h_{comp} * 1.415 \text{ hp/BTU/s} = 26,752 \text{ hp} \quad (8-5)$$

The equations for the performance of the turbine are:

$$T_3 - T_5 = T_3 \eta_{turb} \left[1 - \left(\frac{P_2}{P_1} \right)^{\left(\frac{k-1}{k} \right)} \right] = 1043^\circ\text{F} \quad (8-6)$$

$$h_{turb} = c_p (T_3 - T_5) = 250.3 \text{ BTU/lb} \quad (8-7)$$

$$P = W h_{turb} * 1.415 \text{ hp/BTU/s} = 42,503 \text{ hp} \quad (8-8)$$

The net output of the gas turbine that can drive the gas compressor is:

$$P_{net} = P_{turb} - P_{comp} = 15,751 \text{ hp} \quad (8-9)$$

The energy needed to raise the temperature from the gg compressor outlet to the turbine inlet is:

$$Q = W c_p (T_3 - T_2) = 27,750 \text{ BTU/s} = 99.9 \text{ mmBTU/hr} \quad (8-10)$$

The heat rate and overall efficiency are:

$$HR = \frac{Q}{P_{net}} = 6342 \text{ BTU/hp hr} \quad (8-11)$$

$$\eta_{overall} = \frac{2544.43 \text{ BTU/hp hr}}{HR} = 40.1\% \quad (8-12)$$

Since a number of losses have not been accounted for in these equations, this result is somewhat high when compared to actual performance, but this example is still representative of gas turbine performance. One interesting observation that can be made is the large amount of energy that is required to power the compressor, emphasizing the critical efficiency of the compressor.

8.2.10.3 Field Performance Testing

A very extensive document by Brun and Nored [17] describes field testing for gas turbines driving a centrifugal compressor and provides detailed guidance on instrumentation, calculations, and uncertainty analysis to obtain accurate results. One of the primary difficulties for gas turbine performance is determining the power output, usually taken at the power turbine shaft. At least in the field, this cannot be measured directly unless a torque meter is installed on the shaft, an expense most companies are not willing to absorb. Alternately, it can be derived from the compressor, but this introduces a much higher uncertainty because it requires the combined results of flow measurement, equations of state and compressor pressures and temperatures which can easily result in a total inaccuracy of $\pm 5\%$.

Over the life of the gas turbine, there will be losses mainly due to deterioration of gas path components as blades erode and blade tip and internal clearances increase. These will mostly be restored during overhauls but on average will account for an additional loss of performance and increase in fuel consumption.

8.2.11 Design Standards

The primary design standard for gas turbines used for pipelines as well as other industrial uses is API 616 [18]. Most of its requirements are handled by the manufacturer, but there are some exceptions. The major aspects of design that are the responsibility of the packager/end user are a function of local conditions such as ambient temperatures and elevation and how it is integrated into the overall compression system.

A partial list of items that have to be considered are:

- foundation for the gas turbine and driven equipment
- compatibility with driven equipment
- air intake filtration, cooling, and anti-icing
- exhaust system and silencing
- sound attenuation
- method of starting
- enclosure and possibly an external building
- unit and station control system
- fuel conditioning
- lube oil cooling

The standard contains detailed data sheets that can be used to specify requirements, but practical constraints usually limit available choices to a few gas turbine manufacturers and types.

8.2.12 Waste Heat Recovery

Most gas turbines are simple cycle so that 60–70% of the fuel energy is lost through the exhaust. Considering the large amount of installed gas turbine power used for pipelines, this is a huge loss of energy. Attempts have been made to recover some of this wasted heat, either for additional compression or power generation. One past effort consisted of using ammonia due to its advantage as a heat transfer medium but operational difficulties and environmental and safety concerns made it unsuccessful. Steam technology, although very successful for large power plants, is less economical for compressor stations due to their smaller size and the complications associated with operating a steam-licensed plant.

The latest attempt is to use an organic Rankine bottoming cycle based on experience gained in geothermal installations [19]. The process of design for a waste heat recovery power plant can be considered as one of matching and optimization. There is a source and a sink of heat of certain characteristics, and the problem is to match them with the working cycle, match the working cycle with the working fluid, and to match the working fluid with the expander. However, what matters most is the optimization of the whole system, involving the well-known process of trading-off a loss or gain.

The usual definition of thermal efficiency as the ratio between the net work done by the fluid and the total heat input to the cycle can be misleading in assessing the suitability of a given cycle in a heat engine. A concept of paramount importance in evaluating the suitability of a particular cycle for use in a heat engine is that of work ratio, which may be defined as the ratio of the net work output of the cycle to the total positive (expansion) work of the cycle. If there is very little negative work, as in a typical vapor cycle, where only liquid of small specific volume has to be pumped back into the boiler, the work ratio will be nearly unity. By contrast, this ratio is lower in a supercritical cycle where a larger portion of the positive work of the turbine is used to drive the feed pump. Taking into account all these practical implications of work ratio, it can be seen that, in many ways, the concept of work ratio can be regarded as almost more important than the concept of ideal cycle efficiency.

The organic motive fluid is selected to optimize power output for the specific gas turbine exhaust stream. A schematic of a bottoming plant based on an organic Rankine cycle is shown in Fig. 8-24 for heat recovery from a gas turbine. Thermal oil is heated in the heat

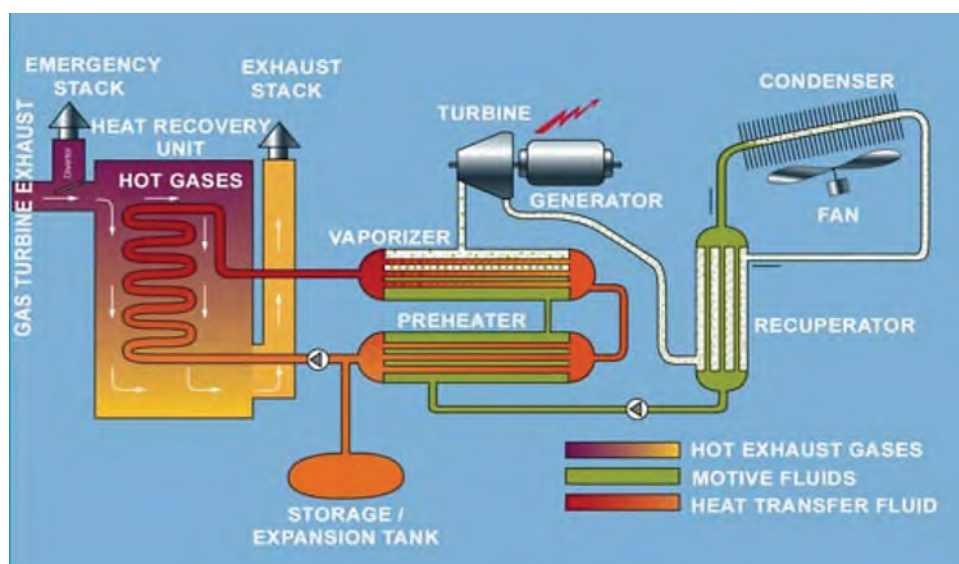


Figure 8-24. Schematic of an organic Rankine bottoming cycle [19].

recovery oil heater (HROH) to vaporize the pentane then returned to the HROH after being used for recuperation and preheat duty. After leaving the vaporizer, the pentane vapor is expanded through an axial turbine and then fully condensed in an air-cooled condenser. The liquid pentane condensate is pumped up to the pentane vaporizer's working pressure and then directed to a recuperator and preheater before entering the vaporizer.

For moderate enthalpy heat sources (e.g., 100–300°C), this technology offers many advantages over the conventional steam cycle, primarily due to higher efficiency in the recovery of sensible heat and also because of the simplicity of the turbine, the control system, and the balance of plant. As well, the turbine and piping sizes are smaller and, thus, less costly due to the fluid density differences. The condensing pressure in an organic cycle is generally above atmospheric thus eliminating the need for vacuum and gas-purging equipment that is utilized in condensing steam cycles. In locations where water is not available and air cooling is required, as is typical of compressor station sites, the plant's air-cooled condenser would be much smaller and less expensive than an air-cooled condenser for steam duty. This is a direct consequence of the order of magnitude difference in volumes between hydrocarbons (pentane) and steam. Experience has shown that remote and unattended operation is feasible and reliability is high.

8.3 ELECTRIC MOTORS

8.3.1 General

Electric motors offer efficient and simple operation for pipelines with high availability due to the fact that they are relatively maintenance-free. They are the mainstay for liquid pipelines where the product being moved is usually not appropriate as a fuel and gas or liquid fuels are not readily accessible. For smaller gathering systems, electric motors are often paired with reciprocating compressors. Mainline gas pipelines have traditionally preferred drivers that can tap into the pipeline for fuel and have avoided electric motors as a result. However, advances in variable frequency drives and the development of motors integrated with a centrifugal compressor have increased the number of electric motors being installed on gas pipelines. In environmentally sensitive areas, in terms of either emissions or noise, electric motors are preferable.

8.3.2 Types of Motors

All electric motor drives are of the AC type, either induction or synchronous. Induction motors have advantages below about 10 MW since their construction is simple and motor control requires no excitation equipment. It handles higher load inertias during acceleration and starts faster. Its main disadvantages are that it operates at a lagging power factor and a higher starting current is needed.

The AC induction motor uses the phase differences between the three phases of the poly-phase electrical supply to create a rotating electromagnetic field in the motor (see Fig. 8-25). Often, the rotor consists of a number of copper conductors embedded in steel. Through electromagnetic induction, the rotating magnetic field induces current to flow in these conductors, which, in turn, sets up a counterbalancing magnetic field, and this causes the motor to turn in the direction the field is rotating. In order for it to operate, it must always run slower than the frequency of the power supply feeding it, which causes the magnetic field in the motor to rotate; otherwise, no counterbalancing field is produced in the rotor.

An example of an induction motor used to power a liquid pipeline pump is shown in Fig. 8-26. Most legacy pipelines control flow in part by installing a number of pumps in series. This allows only the required number of pumps to operate with final flow control performed

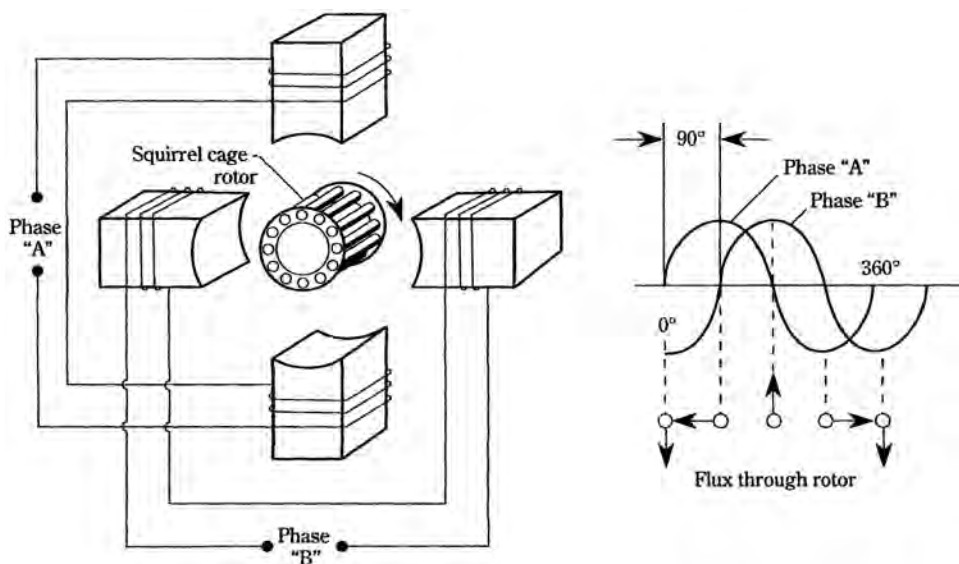


Figure 8-25. Principle of operation for an induction motor.



Figure 8-26. An example of a constant speed induction motor used for pumping.

by a pressure control valve. Most modern pump stations now use variable frequency drives to vary pump speed, sometimes with additional fine tuning of the flow with a control valve.

Synchronous motors, such as the one in Fig. 8-27, are more complicated and expensive but offer more exact load speed and an ability to match the motor to the power supply and the starting torque characteristics of the driven equipment during the design.

If the rotor coils are fed a separate field current to create a continuous magnetic field, one has a synchronous motor, because the motor will rotate in synchronism with the rotating magnetic field produced by the 3 phase AC power (see Fig. 8-28). A synchronous motor

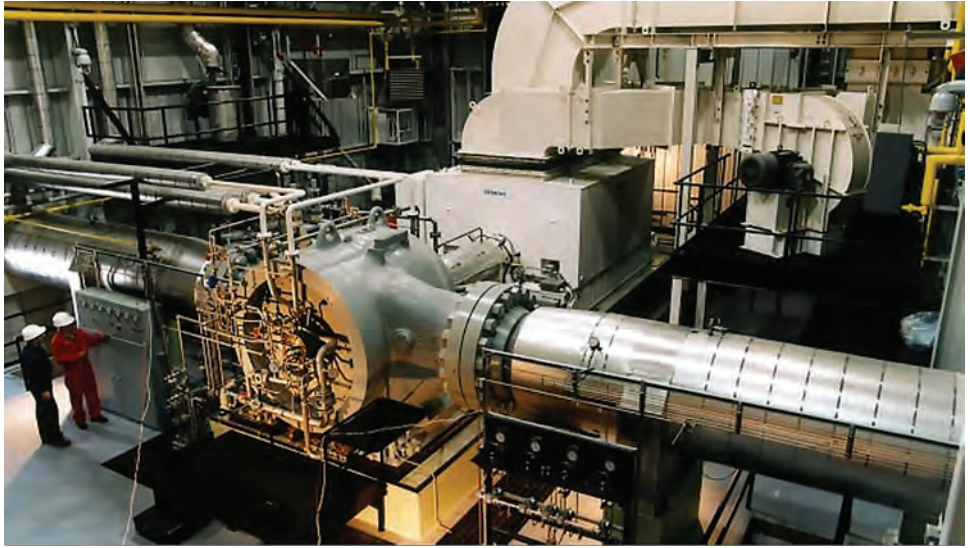


Figure 8-27. Large synchronous motor and centrifugal compressor (courtesy of Siemens).

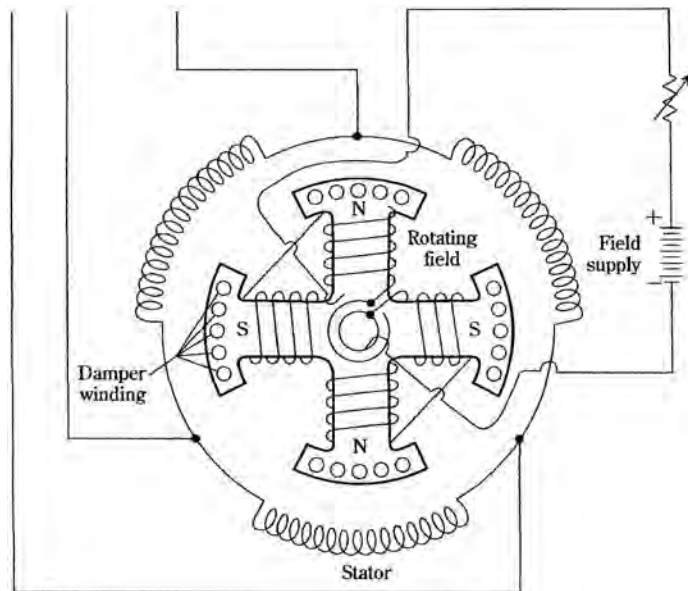


Figure 8-28. Principle of operation for an synchronous motor.

will run at speed regardless of load variations up to a point called the pullout torque. A load higher than this will pull the motor out of synchronism and cause it to stop. Such motors provide very little torque at zero speed and, thus, need some kind of separate starting apparatus. Synchronous motors can also be used as generators.

During operation, however, a different situation exists. Once started, induction motors are stable machines that can easily ride through dips in system voltage of 25% to 30%. Synchronous motors, on the other hand, start easier but will put out of synchronization if there is a sudden change in load. For large synchronous machines, it is important to do an electrical system study to understand whether it can support motor demands under transient conditions.

At higher speeds of 2500 to 3000 rpm, induction motors will be a more economical solution. For larger motors with slower speeds, a synchronous motor with a speed increaser is usually a better choice because their energy efficiency due to the higher power factor will compensate for its increased cost. Continuing developments in electric motor design are enabling higher speeds so that direct drive without a speed increaser is now feasible [20].

8.3.3 Motor Design Considerations

Once the type of motor has been established, a number of design issues have to be considered. The first one is the voltage for the motor. This will be determined not only by what is most efficient for the motor, usually a higher voltage, but also what is available from the electrical system. To obtain the desired voltage and load, particularly if large motors are added, additional substation capacity, new higher voltage lines, or other significant electrical system changes may have to be considered. For base load applications, this may be worthwhile, but for intermittent use, this may eliminate the electric motor as a viable alternative.

Motor enclosures will be dependent on the environmental conditions at the specific location. The design of the enclosure will affect the long-term reliability and maintenance cost to some degree. Isolation of the motor from hazardous gases, such as may be present in a compressor building, mandates a positive pressure, forced air system. Cooling of the motor itself add additional requirements to the enclosure.

Enclosures can be characterized as follows:

- Drip Proof: these are the simplest and are intended to be used indoors where the atmosphere is nonhazardous, and no chemical contaminants exist to cause deterioration of the motor internals.
- Weather-Protected Type I: this is the simplest and least expensive outdoor enclosure with some protection against the elements.
- Weather-Protected Type II: this is a more expensive outdoor enclosure with reasonable protection against the elements but still susceptible to external contaminants.
- Totally Enclosed Forced Ventilation: clean air is ventilated from an outside source which makes the type of enclosure applicable for contaminated or hazardous environment, either indoor or outdoor.
- Totally Enclosed Water-to-Air Cooled: this type of enclosure supplies water to the motor for cooling with the assistance of an air-to-water cooler. It is very quiet because there is no fan, but the cooling system is more costly (see Fig. 8-29).
- Totally Enclosed Fan Cooled: for very contaminated or hazardous environments, this is a good, although expensive, solution. The motor has an air-to-air heat exchanger in the motor with internal air circulated inside the motor and the external air cooling it by means of the heat exchanger (see Fig. 8-30).
- Explosion Proof: this type of enclosure is designed and constructed to be able to withstand an internal explosion and prevent the ignition of combustibles inside the enclosure.

The two most applicable standards for electric motors are API 541 [21] for induction motors and API 546 [22] for synchronous motors.

8.3.4 Variable Speed Drives

8.3.4.1 Variable Frequency Drive

Although constant speed motors have successfully been used for liquid pipelines, this is not an option for gas compressors where speed variability is essential. The development of variable speed drives has enabled the use of standard constant speed motors over the past 20

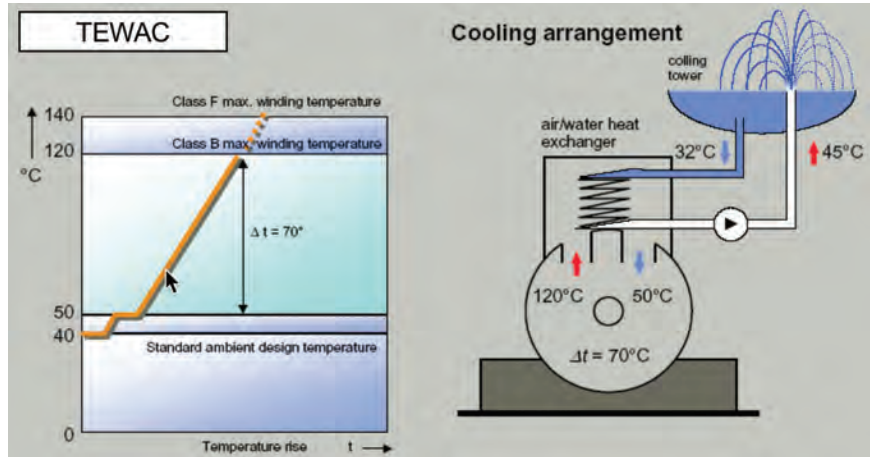


Figure 8-29. Totally enclosed water-to-air-cooled motor cooling.

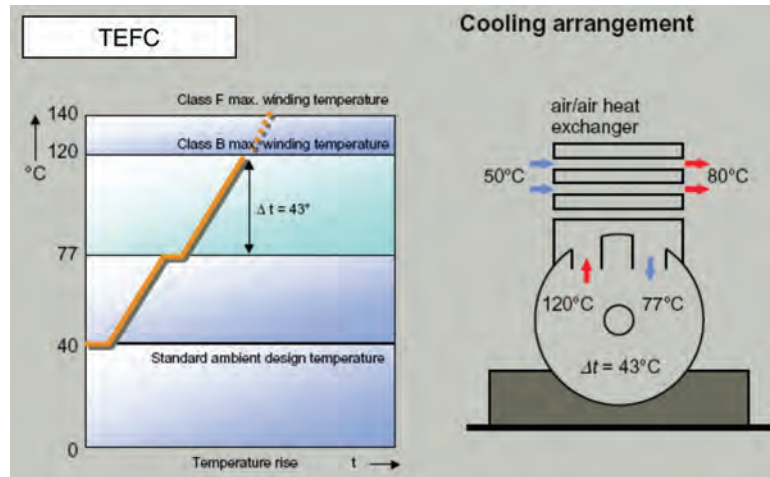


Figure 8-30. Totally enclosed fan-cooled motor cooling.

years has changed this situation and allowed application of electric motors for gas pipelines and enabled more efficient operation for liquid pipelines as well. Two approaches are possible: variable frequency drives and fluid couplings.

The most common method is the variable frequency drive (VFD) that functions by altering the frequency of the AC electrical supply by means of solid state electronics. Both induction and synchronous motors can be controlled in this manner.

The core of a VFD system (see Fig. 8-31) is first the conversion of AC to DC by means of a solid-state semiconductor converter or rectifier. The DC link smooths the DC current and limits the interaction between the converter and inverter. An inverter changes the DC signal back to a fluctuating one at the desired frequency and motor speed. Pulse width modulation is one method used to produce a sine wave at the required frequency for the motor. Harmonic filters are needed to reduce the voltage and current disturbances fed back from the converter. Subsequently, 6, 12, or 30 pulse transformers isolate the VFD from the supply and improve rectification.

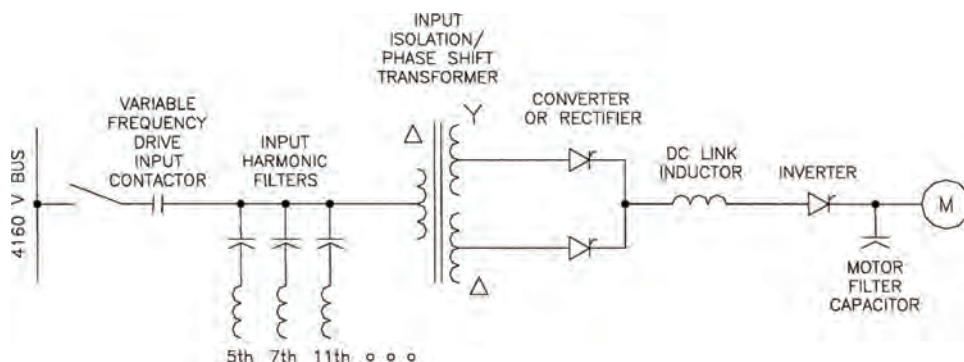


Figure 8-31. Basic design of a variable frequency drive.

Figure 8-31 shows a very simplified diagram and in reality, multiple legs are usually required. Weber et al. [23] provide a thorough discussion on various topologies that are in use as well as items that have to be considered for specific application. This is a rapidly changing field as devices become more efficient and higher component densities are achieved.

Where multiple motor-driven units are installed in parallel, it is possible to apply speed control to one unit and run the rest at constant speed. This approach reduces the cost, since only one VFD system is needed, and the first reaction is likely to be that this is the best solution in all cases. A recent study by Paulini and Pires [24] shows that a number of competing factors have to be considered before the optimum solution can be determined.

A full economic study has to be done to weigh capital against operating costs. In this study, there were two major operating scenarios with respect to the number of oil pumps normally running at the three pump stations on the pipeline. It also compared using one VFD for all units [Fig. 8-32(a)], one VFD for two units [Fig. 8-32(b)], and VFDs on all units.

The necessary equipment for the one pump driven solution is one inverter and $2n + 1$ contacts, where n = number of pumps. This is the cheapest solution as contacts are about ten times cheaper than a 3000 HP inverter. Although the inverter can be by passed at any time, assuring pump availability, it is necessary to maintain a backup control system to make pipeline control redundant.

To drive two of the four existing pumps, it would be necessary to have two sets of VFDs. The total equipment is two inverters and 10 contacts. It is possible to add one more contact to link both inverter buses to make them available for all the pumps, if necessary. Redundancy of drives eliminates the need for a backup control system.

In the last case, one inverter is used for each pump, giving a total of 4 inverters. There is no need for contacts, and the existing circuit breakers are enough to isolate the pump and inverter set. This is the most expensive redundant configuration, although it is not necessary to have a backup control system. The final capital costs of the three scenarios are given in Fig. 8-33(a), and the single station VFD is clearly the cheapest.

Hydraulic analyses were done so that the various operating points could be established. This is necessary because the pump efficiency point depends on its speed, and if VFDs are installed, the more likely it is that the best efficiency point can be reached. The resultant energy savings for the two operating scenarios (number of pumps operating at each of the three stations) is shown in Fig. 8-33(b), which favors the more complex solution.

Combined capital and operating efficiency results show that the two first configurations are economically viable because the net present values (NPVs) are positive, and the internal return rate (IRR) are higher than the supposed weighted average capital cost rate [see Fig. 8-33(c)]. Choosing one of them, the first presents a better profit index, which

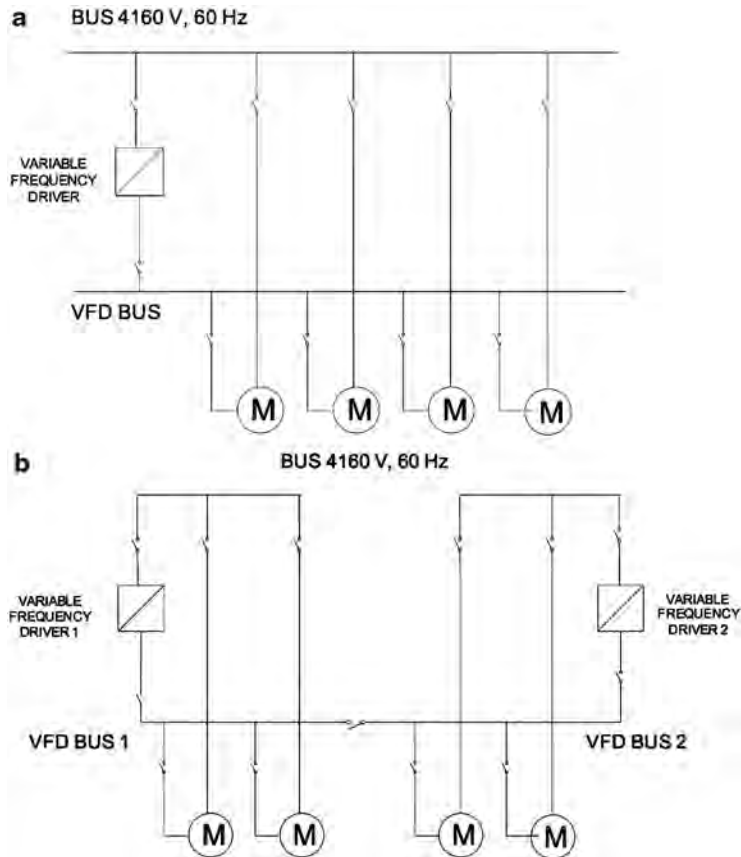


Figure 8-32. Different VFD scenarios. (a) One VFD for all pumps. (b) One VFD for every two pumps.

CONFIGURATION	INVERTER	CONTACT	TOTAL COST EQUIPMENT	TOTAL COST PROJECT
ONE PUMP DRIVEN	1	9	\$611,960	\$1,224,446
TWO PUMP DRIVEN	2	11	\$964,760	\$1,872,698
ALL PUMP DRIVEN	4	0	\$1,325,120	\$2,634,842

(a)

DRIVE CONFIGURATION	2 2 0	3 3 4
ONE PUMP	6.40%	2.59%
TWO PUMPS	7.76%	4.66%
ALL PUMPS	7.76%	5.74%

(b)

DRIVE CONFIGURATION	IRR	NPV	PI
ONE PUMP	15.68%	\$248,615	20.30%
TWO PUMPS	14.28%	\$232,653	12.42%
ALL PUMPS	10.90%	-\$153,365	5.82%

(c)

Figure 8-33. Example comparison of VFD scenarios. (a) Capital costs in US dollars. (b) Energy Savings. (c) Final investment results [24].

compares the amount of profit with the investment—in this case, the lowest investment overall. Therefore, the best choice for adding a new control and drive system for this pipeline is the one pump-driven scenario.

Extending the results, in the case of new plant with a similar architecture, the choice would be the two-pump-driven system due to the fact that redundancy of inverters would eliminate the necessity of implementing a redundant traditional control system. Since the cost of a traditional system is estimated at \$200,000, if considering it in the cash flow, the NPV would be \$374,000, and the IRR, 16%.

Speed control is also possible using a fluid coupling such as the one illustrated in Fig. 8-22. The fluid coupling consists of a pump connected to the driver shaft. The fluid discharges to a power recovery turbine on the driven end in the same casing. The amount of fluid circulated through the turbine modulates the speed with more fluid, increasing the speed of the turbine. The comparative efficiency with a VFD drive is basically equivalent at 95%. At minimum speed, however, the VFD drops to about 92%, while the fluid drive can range from 50% to 70% at 50% speed [21].

There is now sufficient historical operating data in order to quantify the benefits related to the operational reliability aspects of VFDs and equipment controlled by the VFD [25]. This includes failure probabilities and throughput performance over the life cycle of the system but excludes technical implications such as VFD selection, application, specification or design. From a pure maintenance perspective, VFDs contribute to a marked improvement in terms of failure reduction. For general pump failures including components such as mechanical seals, bearings, shaft, wear rings or couplings, it is demonstrated that the probability of failure is lower on pumps combined with VFDs compared to pumps without VFDs. In terms of mean time between repairs (MTBR), this equates to an increase of 65% relative to pumps with VFDs.

Comparisons were done between different options between dedicated VFDs on each pump and shared VFDs. The throughput performance between these options has been shown to differ substantially. On a specific pipeline built initially with shared VFDs then fitted with Dedicated VFDs, the number of pump failures decreased by 60% leading to a throughput loss reduction of 66%.

However, while the VFD helps preserve the asset it runs in conjunction with due to reduced impact of the soft start on the motor, the VFD itself introduces a high frequency of failures in the overall pumping system. For the systems studied, adding a VFD increases the frequency of downtime events by 118%. However, these failures are short in duration which in the long term add up to less downtime (276% less) on a pumping system with VFD.

VFD units do have a high capital cost which can double the cost of ownership of a pumping system over the life cycle of the asset. However, this cost can be offset by the increase in availability provide by the VFD but this needs to be vetted through a Life Cycle Cost analysis.

8.3.4.2 Fluid Coupling Drive

Speed control is also possible using a fluid coupling such as the one illustrated in Fig. 8-34 and is a self-contained unit that enables both speed control and an integral gearbox to facilitate the use of standard electric motors. As shown in Fig. 8-35, the fluid drive consists of a planetary gear along with torque converter that can provide a speed reduction typically to 60%. An additional hydrodynamic variable speed coupling can be added to enable speed reduction down to 20%. This also allows for load-free start-up of the motor.

The efficiencies of a VFD versus a fluid drive are similar at full load, typically around 95%. At minimum speed, however, the VFD drops to about 92%, while the efficiency of the fluid drive can range from 50% to 70% at 50% speed [26].

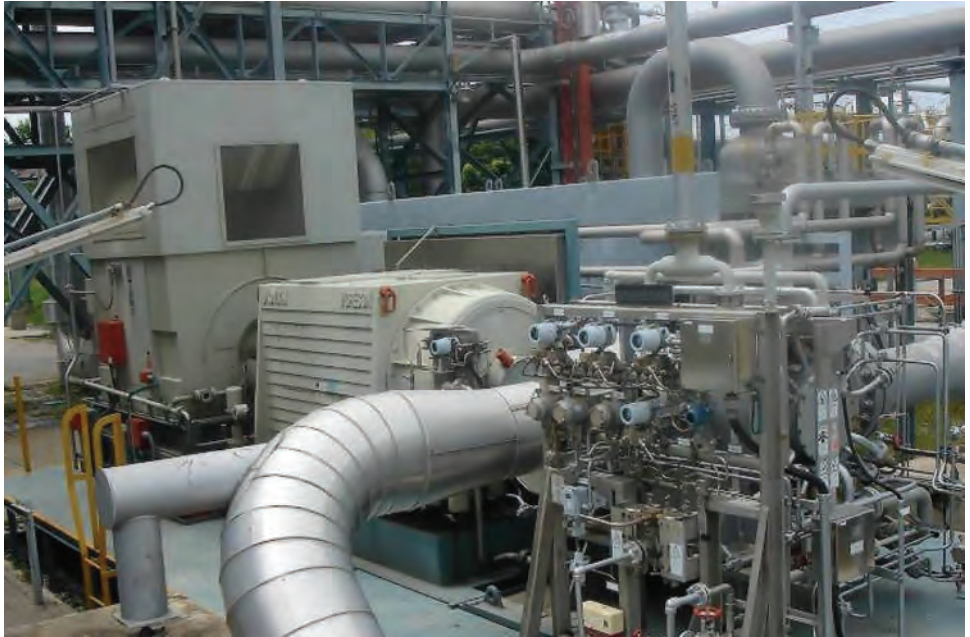


Figure 8-34. Motor driven compressor with a fluid coupling.

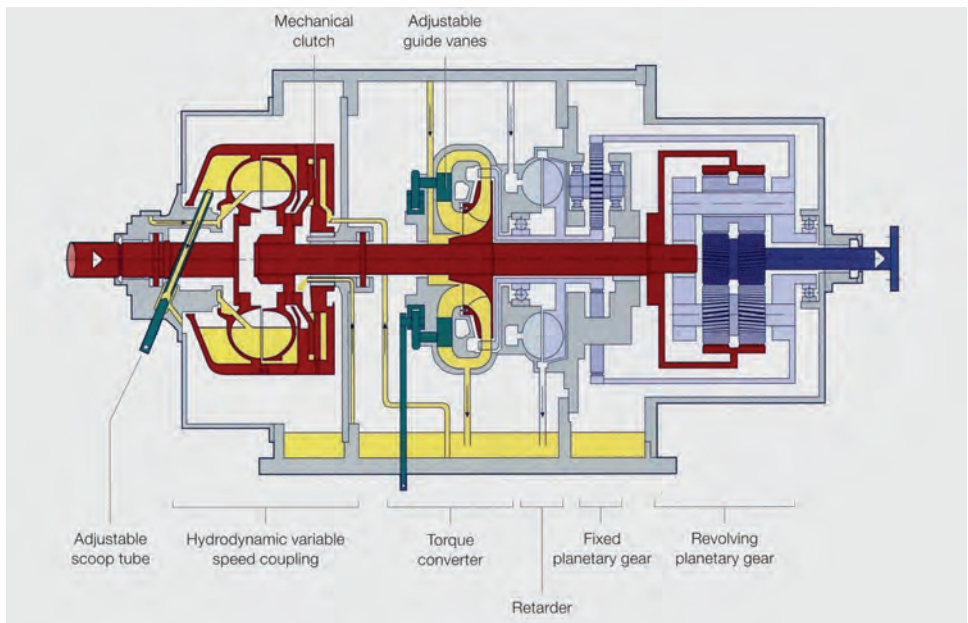


Figure 8-35. Design of a Vorecon fluid coupling (courtesy of Voith).

8.3.5 Hermetic Compressors

A unique application for a VFD-controlled electric motor is the hermetic electric motor compressor. Its development was pioneered in the 1990s as the MOPICO (motor pipeline compressor) compressor [27] as illustrated in Fig. 8-36. Further advancements called the HOFIM (high speed oil free intelligent motorcompressor) are being made and two basic

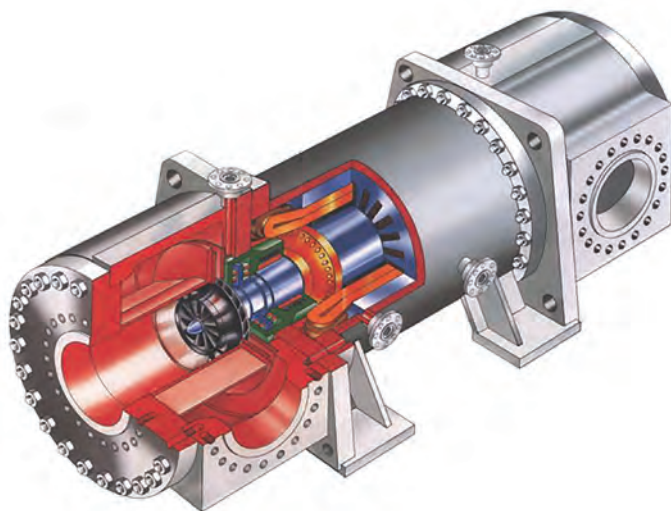


Figure 8-36. MOPICO hermetic compressor [26].

configurations are now available, one of them a flexible double compressor arrangement that can be operated in series or parallel and the other a multi-stage arrangement. With the use of magnetic bearings, their speed range can be extended typically to 30% to 105% due to their ability to dampen rotor response at critical speeds [28]. This makes these units ideal for gas storage and extraction service as well as peak pipeline compression.

A further development of the MOPICO design is the HOFIM (High Speed Oil Free Intelligent Motorcompressor) compressor, which retains the hermetically sealed compressor design with magnetic bearings but with the motor separated and the compressor sealed from the outside by dry gas seals.

Continuing development is taking place with hermetic compressors for both normal pipeline, process, and subsea applications. One example is the new Dresser-Rand Datum

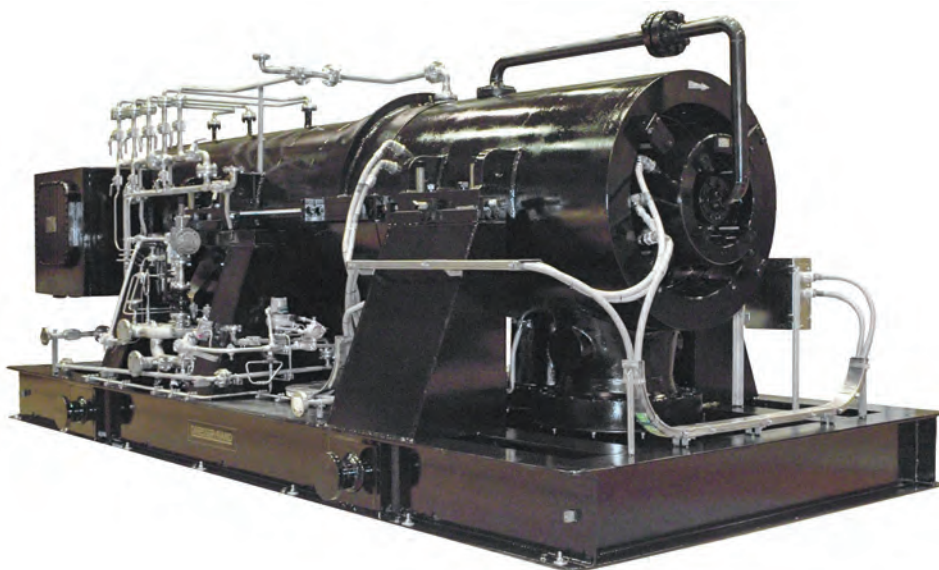


Figure 8-37. A hermetic compressor (courtesy of Dresser-Rand).

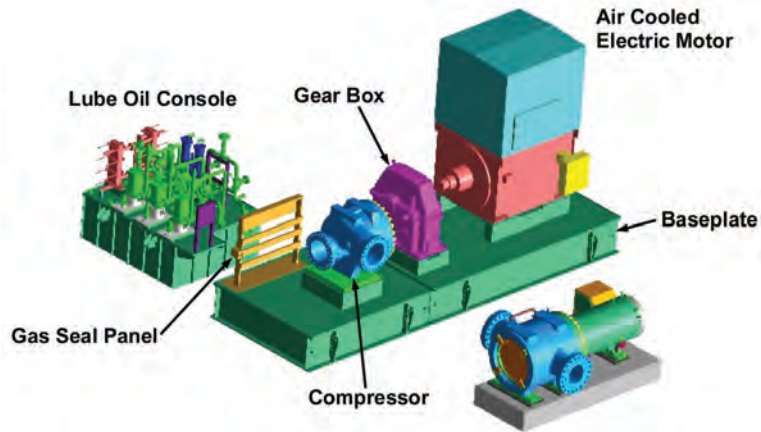


Figure 8-38. Comparison of standard motor-driven hermetic compressors (courtesy of Dresser-Rand).

C hermetic “compact” compressor [29] in Fig. 8-37. Figure 8-38 illustrates the significant saving in space (80% less) and weight (58% less) achieved by the elimination of the oil and sealing system through the use of magnetic bearings and its hermetic design. The magnetic bearings are the most important part of the design and feature digital controls with computer-based algorithms for tuning and adjusting the bearings. The driver is a close-coupled, variable-speed, high-speed induction motor cooled by either natural gas or hydrogen.

Hermetic electric motor compressors offer a relatively simple compression solution with a basic cooling arrangement for the motor using filtered discharge gas, which is then recycled to the suction side. No further auxiliary systems, other than the VFD, are needed for sealing or lubrication. Frequent starting can be tolerated. The reliability and availability can be very high as long as the electrical power supply is dependable.

8.3.6 Driver Economics

A recent comparison was performed between traditional gas turbine and electric motor solutions for pipeline service [30]. It highlights the difficulties in comparing these two solutions. When considering the basic characteristics of each design approach (see Fig. 8-39), the electric motor shows major advantages in environmental factors with respect to noise and emissions. Of course, it must be remembered that although the electric motor has no emissions, the power plant it depends on for electricity likely does although it may be easier to control. The efficiency comparison is likewise misleading since, once transmission costs are factored in, they probably will be very close. The gas turbine is assured of a dependable fuel supply while the electric motor is linked to the reliability of the electrical system. Any of these characteristics may be the sole decision-making factor for either case.

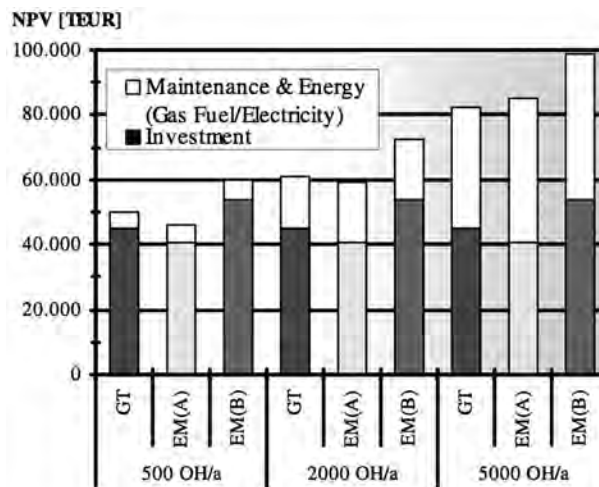
If the ultimate decision is based on economic reasons, an interesting picture emerges. The basic capital cost is generally 10% to 20% higher for gas turbines unless significant investment has to be made to extend the electrical grid to tie in the electric motor, in which case, it can be higher. Since the electric motor solution is more compact and no additional space is needed for noise attenuation, land costs may be considerably lower, although space needed for the VFD for larger motors may negate this advantage.

The following example summarized in Fig. 8-40 compares a compression station equipped with three trains, each having 10 MW, in a 2 + 1 (two operational and one stand-by

Driver	Gas Turbine	Electric Motor
Fuel	Natural gas	Electric power
Autonomous operation	Standard	Needs external power supply
Emissions	CO ₂ , CO, NO _x , UHC	No local emissions
Noise	85 dB(A) in 1 m for standard package	Low noise level
Efficiency level Note 1)	30% to 40% at full load, depending on engine size, decreases at part load	Approx. 95% less sensitive to load
Operating range	60% to 105% of nominal speed	10% to 105% of nominal speed
Performance	Depending on ambient conditions (T, P) "Cold Day Power"	No influence
Maintenance	Regular maintenance required	Almost maintenance free
Package size	100%	50 to 70%

Note 1)
Comparing the efficiency of the two alternative drivers it has to be taken into consideration that the content of convertible energy in electricity and fossil fuel is different. For the electric motor driver, the power plant efficiency as well as transmission line, transformer losses, etc. have to be considered.

Figure 8-39. Comparison of basic characteristics between gas turbine and electric motor drivers [30].



Data Basis (Example)

2+1 - Configuration, Individual Machine Size: 10MW

Total Investment Costs for Compressor Station:

Gas Turbine (GT): 45,000 TEUR,

Electric Motor EM (Case A): 40,500 TEUR

Electric Motor EM (Case B): 54,000 TEUR

GT-efficiency = 28%; EM-efficiency = 92%

Gas fuel cost 0.01 EUR/kWh, Electricity cost 0.045 EUR/kWh

Maintenance: GT: 50 EUR/OH + 50 TEUR/a, EM: 50 TEUR/a

Period: 20a, Interest Rate: 10%, Price escalation: 2%/a

Figure 8-40. Comparison of NPV between gas turbine and electric motor drivers [30].

train) configuration using either gas turbines or electric motors. Regarding investment costs for the electric motor-driven trains, two cases have been investigated, Case A (low high voltage-grid connection cost) and Case B (high HV-grid connection cost). To show the influence of the operating profile, three different cases in operating hours per annum (OH/a) have been calculated: 500, 2000, and 5000 OH/a.

The operating costs become a very important cost factor in the total LCC analysis with increasing OH/a. Another result of this evaluation is that the electric motor drive with high HV-grid connection cost (Case B) is not attractive, whereas the gas turbine and electric motor (Case A) are in a close competition. The gas turbine driver is advantageous at higher operating hours per year due to the dominating role of fuel costs. The electric motor drive with low HV-grid connection cost (Case A) is, in this example, the best economical solution for peaking units and operation of up to approximately 3000 OH/a, depending of course on the relation of electricity cost versus fuel cost. Figure 8-41 shows this influence by varying the electricity cost and keeping all other variables unchanged.

The decision for the gas turbine or electric motor solution is dominated by the initial cost (investment) at low OH/a. With increasing OH/a, the influence of operational costs becomes decisive. In the chosen example, the electric motor solution with 0.03 euros/kWh electricity costs, representing an extremely low level, beats the gas turbine (GT) solution independent from the OH/a. At higher electricity costs the gas turbine beats the electric motor solution, the transition point for the GT advantage is at approximately 3000 OH/a (0.045 euros/kWh) and approximately 1000 OH/a (0.06 euros/kWh), respectively.

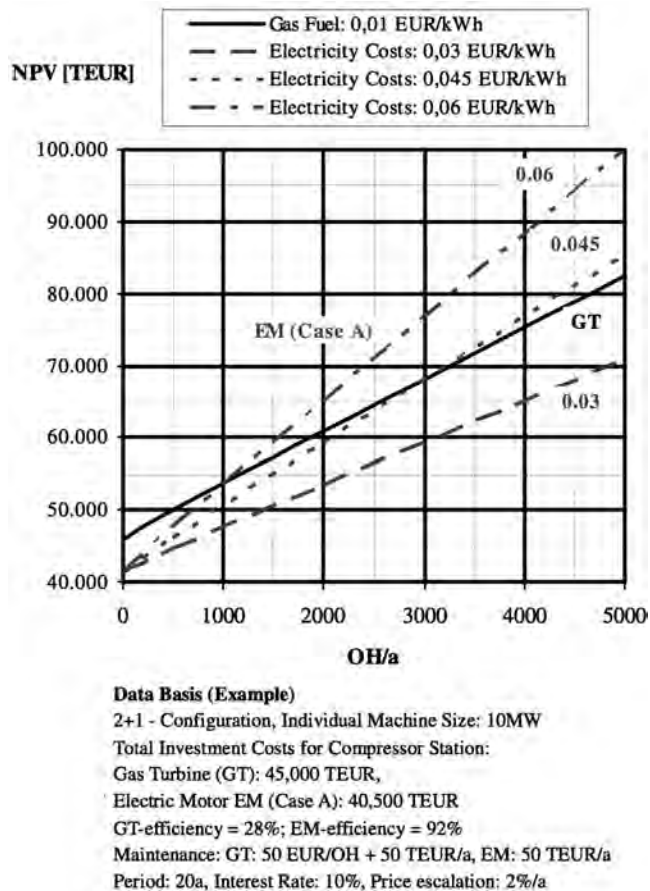


Figure 8-41. Impact of electricity cost on NPV calculation for electric motors [30].

8.4 INTERNAL COMBUSTION ENGINES

8.4.1 General

Internal combustion engines have played a major role in powering pipelines. This is particularly true for legacy gas compression since the majority of drivers installed in the 1950s and 1960s were integral compressors. Recently, separable compressors driven by internal combustion engines (and also electric motors) are returning to pipelines.

A reciprocating compressor can be connected to a driver in two ways. An integral compressor has its pistons driven directly from the engine crankshaft, while a separable compressor has its own crankshaft that is coupled to the driver. From the crankshaft outwards, the main components are the same. Generally, in pipeline applications, high speed separables are used with higher operating speed (900–1200 rpm) with lower initial cost but higher maintenance costs than integrals. High-speed separable application is generally for the lower power range.

8.4.2 Internal Combustion Engine Design

Internal combustion engines can be classified in various ways depending on the type of fuel, mode of ignition, type of cycle, and air intake configuration. Spark and compression are the two methods of ignition. Spark-ignited engines use natural gas or gasoline for fuel. High-voltage electrical spark plugs initiate combustion of the fuel and air mixture. Compression ignition engines produce combustion by the heat of compression. Because they use heavier fuel, they are often called diesel engines, and their compression ratio is higher than spark-ignited engines.

Engines can operate on either two or four strokes for a complete cycle of intake, compression, combustion, and exhaust. Two-stroke engines produce more power for a given size but are noisier and less efficient. The normal four-stroke engine completes the complete cycle in two revolutions of the crankshaft, while the two-stroke engine performs all four parts of the cycle in one revolution. Both spark-ignited and compression-ignited engines can operate with either two or four strokes.

One way to increase the power output of an engine is to pre-compress the air prior to entry into the cylinder. If this is done by a compressor run off the crankshaft, this is called supercharging. The more common method is to power the compressor with a turbine from the exhaust in which case it is referred to as turbocharging. Another advantage of turbocharging is that power output does not decrease with altitude as it does with a naturally aspirated engine.

The type of engine used on a pipeline is very much dependent on the type of fuel available for the location. Spark-ignited, four-stroke engines are the normal solution for gas pipelines since natural gas is the logical fuel (Fig. 8-42). Lean-burn technology has been added to control emissions. Many engines of this type driving separable reciprocating compressors such as the one shown in Fig. 8-43 are being used for lower power applications (500–1500 kW) on gathering systems and smaller pipelines. Their efficiency, both at full power and part load, is superior to that for gas turbines of the same size.

An interesting development has been a return to the use of larger engines for compression [31]. With the extension of separable compressors to larger frames, there is now a market for engines of 6000 kW (8000 hp) or even larger size that can replace older integral engines. These engines are derived from mature power generation and marine markets.

Some pipelines are even using these engines to drive centrifugal compressors through a fluid coupling. The coupling contains an integrated planetary gear that increases the engine speed of 750 rpm to typical compressor speeds of 7000 to 10,000 rpm (see Fig. 8-35). The



Figure 8-42. High-speed internal combustion engine used for gas compression.

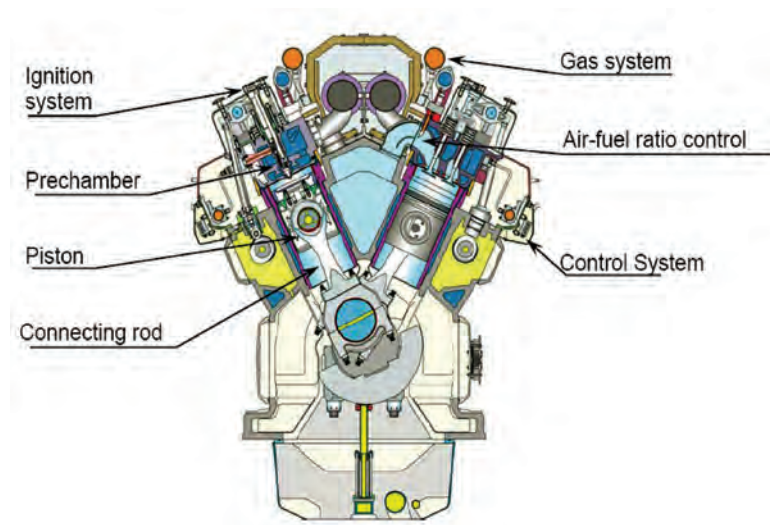


Figure 8-43. Cutaway of a typical four-stroke lean-burn engine [31].

engine is turbocharged with fuel-to-air control and, due to its operation at constant speed, can achieve high power and low fuel consumption at basically all operating conditions with little variation. The use of lean-burn, as shown in Fig. 8-44, improves efficiency and reduces emissions. Capital costs are somewhat higher than gas turbines, but for base load operation, its higher efficiency makes the life cycle cost lower.

The current design for internal combustion engines used for pipelines has probably reached close to its highest efficiency at 40% to 45%. Further increases will require a more radical change in design.

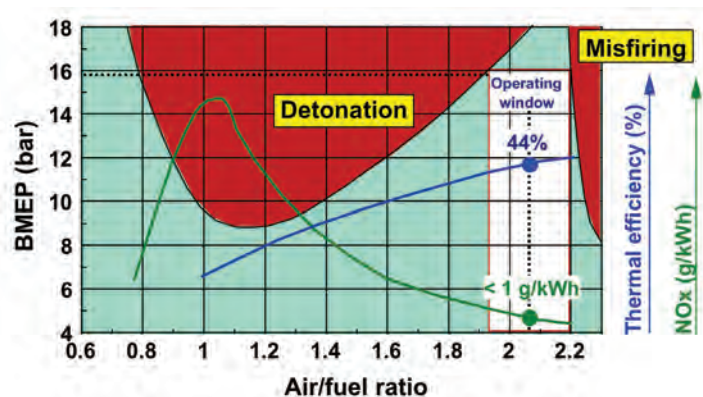


Figure 8-44. Operational envelope for a lean-burn engine [32].

8.4.3 Integral Engine/Compressors

With many legacy engine/compressors now in operation for around 50 or more years, increased pressures for improving efficiency and reducing emissions are spurring efforts either to revitalize facilities, decommission, or replace them [33]. This is particularly true in the United States where a significant proportion of compression equipment is essentially obsolete. A major reason for revitalization is the reduction of emissions for existing engines [34] by means of combined industry research efforts. This will require a multiple-pronged approach since no single technology is capable of meeting future requirements.

In the past few years, real improvements have been made, mostly targeted at the Cooper Bessemer GMW family of engines (see Fig. 8-45), of which an estimated 600 are still in



Figure 8-45. Example of a Cooper Bessemer integral engine/compressor (courtesy of Wood.).

operation [35]. A number of reliability issues were evaluated and highlighted major problems such as high parasitic load from the engine-driven intake blower, low scavenging efficiency, detonation and high maintenance costs. Replacement of the blower with a modern turbocharger resulted in a 7% improvement in fuel consumption. Subsequent retrofitting with high-pressure fuel injection, the fuel delivery, and filtration system, new control panels and electrical system further improved efficiency and emissions [36].

8.5 COUPLINGS

8.5.1 Functions of Couplings

A coupling is used to connect the driver to the driven part of a system. In some cases, multiple couplings are needed on a more complex system such as those that have a gearbox. The basic functions of any coupling are to:

- Accommodate angular and parallel misalignment between the shafts
- Adapt to axial movement
- Transmit power
- Manage torsional vibration

Alignment between shafts may be angular or parallel with the usual situation being both angular and parallel (Fig. 8-46). In addition, there may be axial displacement between the ends of the shaft that often varies as thermal expansion occurs.

Each type of coupling has its strengths and weaknesses which have to be considered but proper initial alignment of machinery is most important in ensuring coupling performance and reliability. Initial alignment values are typically one-third of the total misalignment capability of the coupling to allow for operational changes such as bearing wear, foundation settling, thermal growth and piping strain. However, the more reserve, the better the reliability of the coupling.

The transmission of power from one shaft to another consists of managing torque for a specific speed range which includes both a mean and fluctuating torques. Depending on the nature of the torque produced by the driver or driven equipment, the coupling may have to accommodate fluctuating torques or torsional vibration as defined later in Section 12.3.4.4.

8.5.2 Coupling Selection

Couplings are divided into general purpose and special purpose types. General purpose couplings are usually standardized and with less sophisticated design. Once a coupling is

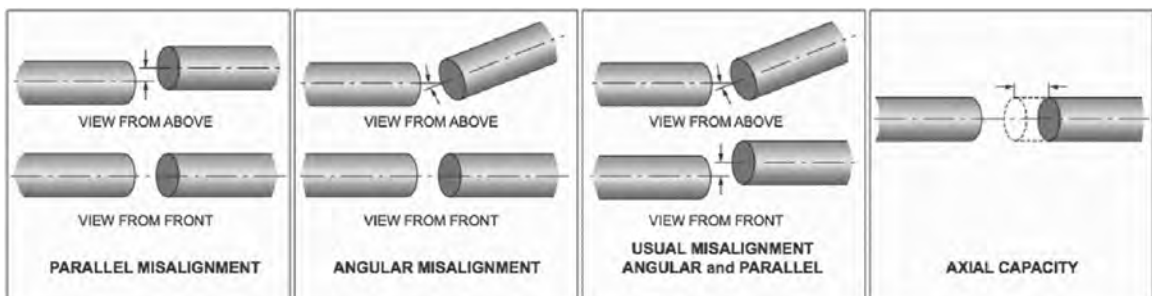


Figure 8-46. Types of misalignment.

used on critical equipment and is used for major turbomachinery, it is designated as a special purpose coupling [37].

Because different drivers and driven equipment produce unique load requirements, a general means of classifying them is by using a Service Factor, as shown in Fig. 8-47. This factor is then used in a calculation that includes power and speed to determine an HP/RPM number that can be used to pre-select a specific coupling from a manufacturer chart. It should be emphasized that this is only intended for initial pre-selection and, for critical applications with significant torque variations, a detailed torsional analysis is required before the appropriate coupling can be determined. The mass elastic data of the coupling, which includes its weight, inertia, stiffness, and damping, is crucial information for a torsional analysis. If the torsional analysis indicates that a flywheel is needed, this will also dictate the type of coupling connection.

There are many different designs of couplings, but they can generally be classified as:

- mechanical element or gear
- metallic element or flexible
- elastomeric/spring element or soft

Couplings can also be categorized into three types of connection:

- hub–hub: The most common type of coupling connection for reciprocating compressor is hub–hub connection.
- flange–hub: A compressor with a flanged stub/flywheel or engine with a flywheel requires a flange–hub connection. Normally, the coupling manufacturers have off-the-shelf standard couplings for the flywheel flange–hub connection. Due to the small number of flange stub couplings, a special coupling is typically designed for flanged stub compressor.
- flange–flange: For engines with a flywheel coupled to a flanged compressor stub/flywheel, a special coupling is needed as most of the coupling manufacturers do not have an off the shelf coupling for a flange–flange connection.

It is necessary to confirm the associated coupling maximum speed and compatibility of hub–shaft length dimensions such as hub inner diameter with shaft diameter.

For initial coupling selection, usually a service factor criterion calculation is used to determine the application torque of the system. The application torque can be calculated by the following equation:

$$\text{Application Torque (lb}_f\text{ - in)} = \frac{\text{BHP} \times 63,000 \times \text{Service Factor}}{\text{Operating Speed}} \quad (8-13)$$

The service factor of 3.0 is the approximated dynamic torque and not the actual dynamic torque. A thorough model of a system has to be considered in order to assess the

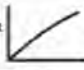


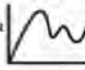
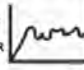
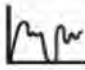
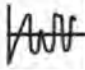
CLASS	SMOOTH	STEADY	MODERATE	MEDIUM	HEAVY	EXTRA HEAVY	EXTREMELY HEAVY
DRIVER TYPE	MOTOR OR TURBINE 	MOTOR OR TURBINE 	MOTOR OR TURBINE 	MOTOR OR TURBINE 	HIGH STARTING TORQUE MOTOR OR ENGINE 	ENGINE 	ENGINE 
LOAD TYPE	- SOFT START WITH STEADY LOAD - CENTRIFUGAL EQUIPMENT	- NORMAL STARTING LOADS - SLIGHT TORQUE VARIATIONS	- ABOVE AVERAGE STARTING LOADS - MODERATE LOAD VARIATIONS	- HIGH STARTING TORQUE - MEDIUM TO HEAVY LOAD VARIATIONS	- MILD SHOCK LOADING - ENGINES WITH SMOOTH LOADING - EXTREME RELIABILITY	- HEAVY SHOCK LOADING - LIGHT TO MODERATE REVERSING	- EXTREME SHOCK LOADING - HEAVY REVERSING WIDE TORQUE VARIATION
SERVICE FACTOR	1.0	1.5	2.0	2.5	3.0	3.25	4.0

Figure 8-47. General service factors for couplings (courtesy of Rexnord Industries Ltd.).

actual dynamic and mean torque levels. A service factor of 3.0 is used for Rexnord and TB Woods flexible disk couplings.

This selection method does not guarantee that the selected coupling will work and should only be considered as an approach for initial coupling selection which is then followed by a proper torsional analysis.

8.5.3 Gear Couplings

Lubricated gear couplings (Fig. 8-48) have in the past been extensively used for turbomachinery, but they are now largely being replaced by dry (flexible or soft) couplings. Great care must be taken if an existing gear coupling is replaced by a dry coupling to ensure all relevant factors are considered.

Gears can be incorporated into the hub or the spool. Lubrication of the gears can be accomplished by grease or oil from the lube oil system. If grease is used, it has to be restored on a regular basis. Continuous lubrication can result in sludging or contamination of the coupling.

8.5.4 Flexible Couplings

Metallic element couplings are commonly referred to as flexible couplings and can be divided into disc and diaphragm types. Flexible couplings are now very common for compressors because lubrication and the need for maintenance are eliminated.

The diaphragm coupling (Fig. 8-49) consists of discs clamped together by bolts. The torque capacity is limited by the clamping force of the bolts, and all torque is transmitted via friction as a result of the clamping force of the bolts.

Disc couplings such as in Fig. 8-50 transmit torque through a series of tangential links. Since steel is twice as strong in tension as in shear, the disc coupling normally has a smaller diameter and is best for low moment applications. It has high torsional and radial stiffness and low axial and angular stiffness which is a favorable combination of stiffness characteristics. Disc couplings accommodate shaft misalignment by angular deflection of the disc packs, and two disc packs are required to handle parallel offset. Axial displacement is taken care of by axial displacement of the disk pack.

Fixed speed motors driving a reciprocating compressor normally use a flexible disc coupling. The flexible disc coupling is relatively cheap and is almost maintenance free. A standard design can be seen in Fig. 8-51 with two disc packs that provide a mostly constant stiffness.

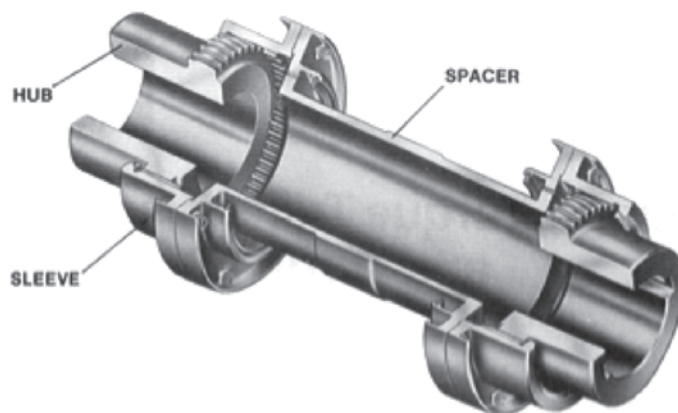


Figure 8-48. A typical gear coupling used for turbomachinery.

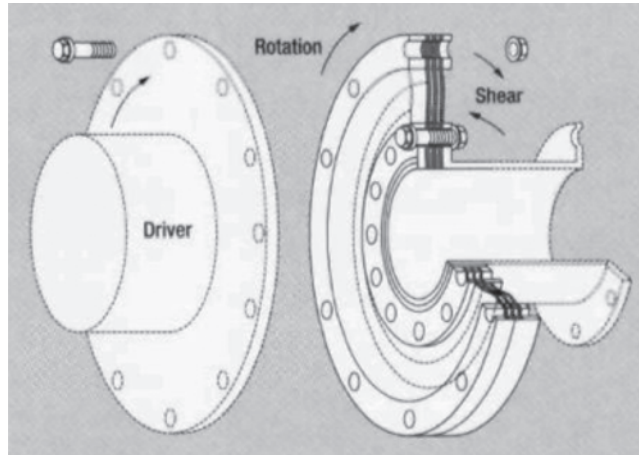


Figure 8-49. A diaphragm coupling [38].

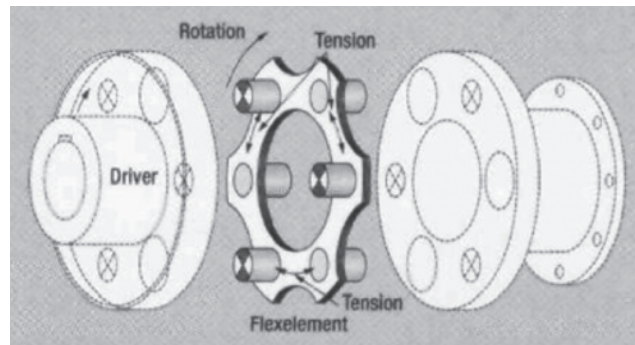


Figure 8-50. A disc coupling [38].

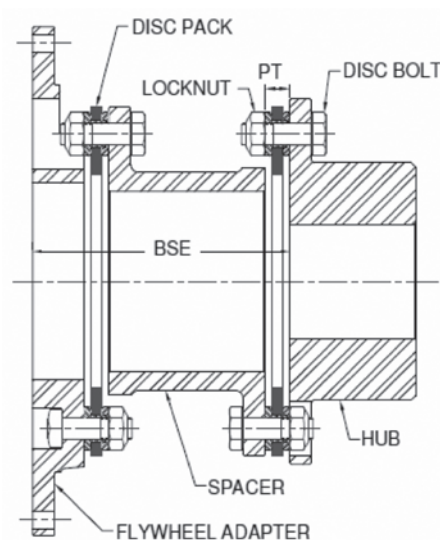


Figure 8-51. A flexible disc coupling.

8.5.5 Elastomeric Soft Couplings

Soft couplings, which may be elastomeric or mechanical, are normally considered when flexible coupling options are exhausted mainly because they are more expensive and require more maintenance. They incorporate elements that drastically reduce the stiffness of the coupling so that the first TNF ends up being below the primary rotational frequency and thereby avoids resonance conditions. These elements are usually elastomeric components arranged circumferentially with an example of a typical design with rubber disks that flex as torque is applied. Soft couplings require regular maintenance to replace the elastomeric elements that deteriorate over time with heating which makes them less desirable from an operating perspective.

One thing that has to be taken into consideration during torsional analysis is that the stiffness of an elastomeric coupling is not constant and varies with applied torque. Significant deflection of the elements can result in large energy loss due to hysteresis effects. The couplings tend to lose their stiffness ratings with time, temperature, and applied torque.

8.5.6 Steel-Spring Soft Couplings

A soft coupling that avoids the disadvantages of the elastomeric coupling is the steel-spring flexible coupling developed in the mid 1950s [38]. The springs can be in either cantilever (leaf) or helical coil arrangements. Metal springs have the advantage of maintaining precise torsional characteristics, so that system operation will not change as is the case with rubber. Although initially more expensive, metallic couplings have far greater life so that life-cycle costs are lower than with rubber couplings.

An example of a steel-spring coupling can be seen in Fig. 8-52 with (a) helical coil springs arranged circumferentially between lugs on the driver and driven halves of the coupling and (b) a sketch showing inner arrangements to prevent springs from clashing and also provision for optional friction dampers.

Case Study: Tuning Out a Difficult Torsional Vibration Problem in a Reciprocating Compressor Installation [39]

A midstream oil and gas company encountered a continuing series of failures at one of their compressor stations, which has two identical units with 1250 HP, 1190 RPM electric motors driving 4-throw reciprocating compressors coupled by a “flexible” disc coupling as shown

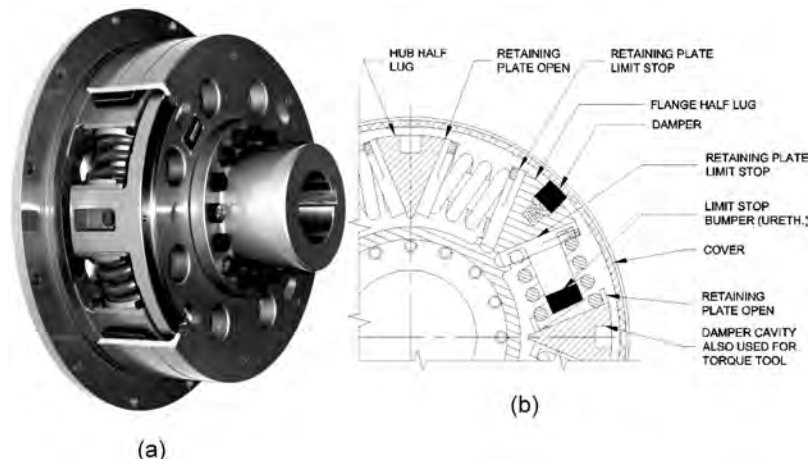


Figure 8-52. General features of a steel-spring coupling (courtesy of Lo-Rez Vibration Control Ltd.).

in Fig. 8-51. Over a period of just 1 year, there were five instances of either a cracked motor shaft, a cracked rotor, or both cracked rotor and motor shaft!

Rather than proceeding to elaborate modeling studies, it was decided to consider a completely different approach: the use of a much lower (1/135) torsional stiffness coupling to torsionally isolate the motor from the compressor, so that rotor and rotor shaft failures might be avoided.

The overall effect of a very torsionally soft coupling is shown in Fig. 8-53. The main features to be noted in Fig. 8-53 are that the first TNF is now below the normal operating RPM, with very little relative twist in either the motor shaft or compressor crankshaft; the “swing” is across the soft coupling. In this manner, the system is “tuned” so that torsional vibrations in either the motor or compressor are isolated from each other, without the need for energy loss associated with damping.

Figure 8-54 shows how the vibratory torque on the coupling varies during a startup: as the system passes through successive orders of the first TNF, the vibratory torque peaks, then subsides to a low level during steady operation.

The results of the TVA with a soft coupling revealed that the maximum predicted vibratory stress in the motor shaft is reduced from 45.9 MPa with the stiffer coupling 4.8 MPa with a “soft” coupling.

Several important points have been brought out as a result of this study:

1. Field measurements, regardless of how carefully carried out, may not fully point to a root cause of failure in a drive line. Increasingly complex measurement and analysis procedures may be required.
2. Torsional vibration analysis may not directly indicate ways to remedy operating difficulties. Assessment of model results and the need for more complex modeling have to be balanced against the need to solve problems in a timely way.
3. Isolating torsional vibrations between driver and driven parts of a drive train can be effectively achieved by soft “tuning” the system so that the first torsional natural frequency is well below the lowest operating speed (coupling mode). As a precaution, second, third, and perhaps higher natural frequencies should be evaluated with a standard Campbell diagram to be sure there are no further significant resonances.

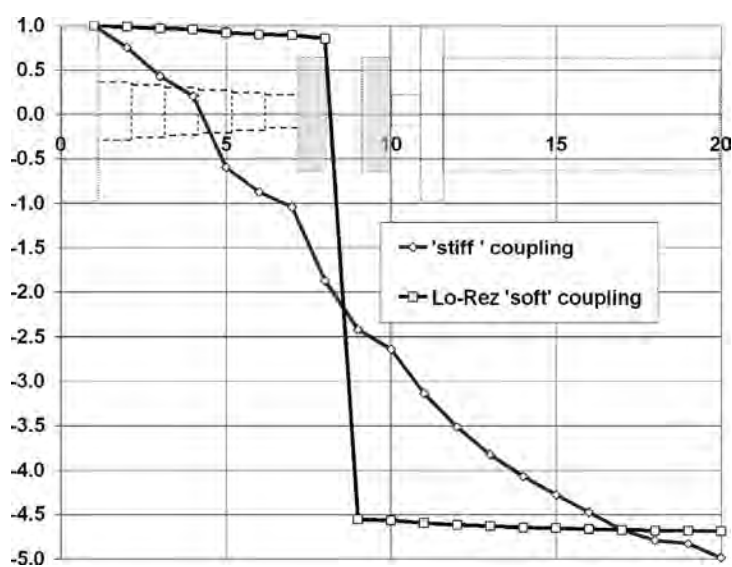


Figure 8-53. A comparison of system behavior with a “stiff” versus a “soft” coupling (courtesy of Lo-Rez Vibration Control Ltd.).

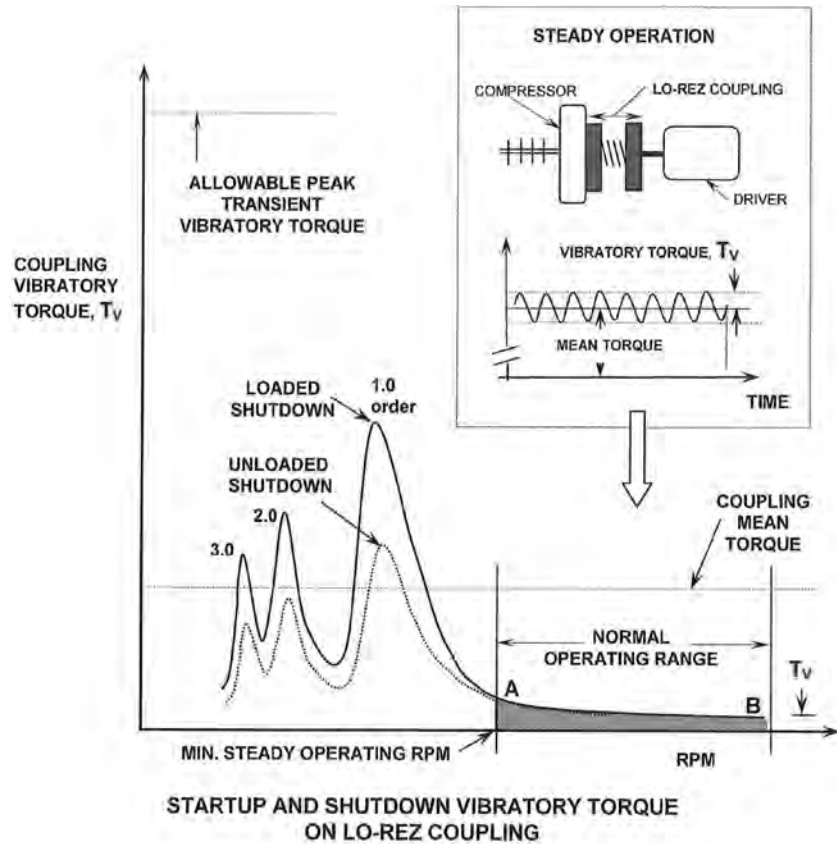


Figure 8-54. Schematic representation of steady and vibratory torque characteristics of a soft coupling, with a “tuned” first TNF below the normal running speed (courtesy of Lo-Rez Vibration Control Ltd.).

8.5.7 Coupling Standards

The American Petroleum Institute (API) has set a minimum requirement for special purpose couplings in the petroleum, chemical, and gas industries in API 671 [40]. It states, a special purpose coupling is to be designed and constructed for a minimum service life of 5 years for flexible element couplings and 3 years for gear and torsionally damped and resilient couplings. The coupling is to operate continuously without interruption for this time period in an equipment train that is normally without spares and is critical to the continued operation of the installation.

The standard states that couplings are designed to accommodate misalignment and axial displacement of the shafts without imposing excessive mechanical loading on the coupled equipment.

Couplings covered in this standard include gear, flexible element, quill shaft, and selected types for torsional damping and torsional tuning in horizontal applications. All other couplings, including clutch, hydraulic, and general purpose couplings are excluded from the scope of this standard.

API 671 standard covers design, materials of construction, manufacturing quality, inspection, and testing of special purpose couplings. The API 671 standard does not define criteria for the selection of coupling types for specific applications. It is supplemented by a number of standards produced by the American Gear Manufacturers Association (AGMA)

which cover aspects such as bores and keyways, keyless fits, load classification, and service factors and mass elastic data.

8.6 COMPARISON BETWEEN DRIVERS AND DRIVEN EQUIPMENT

8.6.1 General Factors

The pipeline industry has seen many changes in the configuration of drivers and driven equipment and these are expected to continue. These changes have largely affected the choice of drivers for compressor units with increasing emphasis on the use of electric motors due to their advantages of low noise, no emissions and elimination of hydrocarbon fuels (at least the compressor station). Pump units, on the other hand, have always depended mainly on electric motors and the most significant change has been to the use of variable frequency drives for speed control instead of control valves to control the flow.

For higher flow, low compression ratio compression, the main choice is between a gas turbine-centrifugal compressor and an electric motor-centrifugal compressor combination. For the electric motor-centrifugal compressor combination, there is a choice between a separate electric motor driving a centrifugal compressor, usually with a gearbox and a hermetic, totally sealed motor-compressor.

At lower flows and higher compression ratios, the reciprocating compressor driven by either an electric motor or internal combustion engine is usually a more appropriate choice.

Pump units on pipelines have traditionally used centrifugal pumps driven by an induction electric motor, except for high viscosity fluids where a positive displacement pump becomes more efficient. As a result, there is normally little need to compare different options since the use of vertical pumps for boosting at a terminal and the subsequent centrifugal, double-suction pumps for mainline pumping.

The basic factors that influence the selection of a specific driver-driven equipment combination can be summarized as:

- flow requirements (both at design point and range)
- required power (both at design point and range)
- thermal efficiency (both at design and part load)
- effect of altitude and temperature on power and efficiency
- type of energy source available
- compatibility between driver and driven equipment
- availability (combination of reliability, maintainability and supportability)
- life cycle (capital, operating and maintenance) costs
- noise emissions
- exhaust emissions
- maintenance support resources available
- compatibility with existing equipment

8.6.2 Advantages and Disadvantages of Gas Turbines

Since the 1960s, gas turbines have become the driver of choice as pipeline flows increased dramatically and power requirements increased. As the efficiency of gas turbines improved, it surpassed the previous integral compressor as the preferred driver along with the centrifugal compressor.

Advantages of the gas turbine are:

- power range. Gas turbines used on pipelines range approximately from 3–40 MW with many choices available in this range. The operating range is typically 70%–105% of design speed and is a good match for a centrifugal compressor.
- thermal efficiency. The efficiency of a large gas turbine at the design point (approximately 30 MW or more) is now close to 40% but this drops to close to 30% for smaller (approximately 4 MW) gas turbines. The efficiency of aeroderivative gas turbines has always been superior to that of industrial gas turbines but the difference is no nearly so significant any more.
- effect of temperature on power and efficiency. Since the gas turbine is a mass flow machine, it is affected by inlet air temperature, in a positive way at lower temperatures yielding higher power.
- type of energy source available. The gas turbine has the advantage of being able to use the clean natural gas available from the gas pipeline at normal gas compositions available in the pipeline.
- compatibility between driver and driven equipment. The gas turbine is most compatible from a power and flow perspective with a centrifugal compressor since speeds can be matched, eliminating the need for a gearbox. It is inappropriate for other types of driven equipment although there is limited use to drive large centrifugal pumps.
- availability (combination of reliability, maintainability and supportability). Even a major failure of the gas turbine can be rectified within a short period of time, as low as 8 hours assuming a spare gas generator is readily available (note that this does not apply to heavy-duty gas turbines where maintenance has to be done in-situ). For most gas pipelines, this outage will not cause a significant impact on pipeline availability. For planned preventive maintenance, the impact of a major overhaul can be limited to a day by swapping the gas generator with a spare. Reliability can be as high as 98%–99% and unit availability 97%–98%.
- life cycle (capital, operating and maintenance) costs. With the many factors involved, there is no clear advantage or disadvantage. Capital costs are competitive with other options. Operating costs will depend on gas turbine efficiency and the cost of energy, but maintenance costs will be higher.
- compatibility with existing equipment. There is a distinct advantage in choosing a gas turbine that is already being used on the pipeline since operating experience and maintenance support resources will already be available.

Disadvantages of the gas turbine are:

- thermal efficiency. The efficiency of a gas turbine degrades at part load and also at lower power outputs.
- effect of altitude and temperature on power and efficiency. Since the gas turbine is a mass flow machine, it is affected by inlet air temperature, negatively at higher ambient temperatures where maximum power can be reduced by as much as 30–40%. Maximum power output will also be decreased at higher elevations. Thermal efficiency is also affected but not nearly so dramatically.
- noise emissions. The gas turbine does produce significant exhaust noise, not a problem in uninhabited areas, but one which could be an issue in inhabited areas, requiring noise mitigation measures.
- exhaust emissions. The major pollutant from a gas turbine is NO_x but much progress has been made to reduce levels. It also produces large amounts of CO₂ and CO that contribute to global warming.

- maintenance support resources available. Gas turbines are a very sophisticated and high technology machine that requires equally high levels of expertise for maintenance support. This is generally widely available in developed areas of the world but could be a factor elsewhere. Manufacturers vary with respect to their coverage for maintenance support centers for spare parts and repair/overhaul; facilities and this should be consideration for choice of a gas turbine.

8.6.3 Advantages and Disadvantages of Electric Motors

A combination of technology advances and environmental and social concerns have brought the electric motor to the forefront as a more desirable driver for centrifugal compressors. Its use to drive reciprocating compressors and centrifugal pumps, in contrast, has been long standing. The one major development has been that of hermetic compressors using magnetic bearings and eliminating the need for compressor seals. Since they are significantly different in their advantages and disadvantages, they will be treated separately.

Advantages of a separate electric motor and driven equipment are:

- power range. Electric motors used on pipelines range approximately from 1–40 MW with many choices available in this range. The operating range is as much as 30%–100% of design speed with a variable frequency drive. If a modern high speed motor is used, it is a good match for a centrifugal compressor or centrifugal pump but, with a standard (usually induction) electric motor, a gearbox is needed. No gearbox is needed when driving a reciprocating compressor where other options than speed control are available for flow control.
- thermal efficiency. The efficiency of an electric motor is typically 95% at full load with some decrease due to the efficiency of the VFD or fluid drive. There is only a small decrease at part load.
- effect of temperature on power and efficiency. The electric motor is not affected by inlet air temperature or elevation up to the point where cooling to the motor is decreased.
- type of energy source available. Since electrical power is supplied externally, there is no shrinkage of flow that occurs when gas is extracted from the pipeline.
- compatibility between driver and driven equipment. The electric motor is compatible with centrifugal compressors, reciprocating compressors and centrifugal pumps although a VFD and gearbox or fluid drive will be needed for centrifugal compressors and considered for centrifugal pumps.
- availability (combination of reliability, maintainability and supportability). Electric motors require very little maintenance and resultant availability is very high. Reliability can be as high as 99.5% and unit availability 99%. However, recent experience, as described below in the disadvantages, indicates this may not be accurate.
- life cycle (capital, operating and maintenance) costs. With the many factors involved, there is no clear advantage or disadvantage. Capital costs are competitive with other options. Capital cost will be affected by the potential additional cost of transmission lines to the station, particularly an issue in remote areas. Operating costs will depend mainly on the cost of electrical energy, and maintenance costs should be moderate but with exceptions as noted below in the disadvantages.
- noise emissions. the electric motor produces low levels of noise that are easily mitigated.
- exhaust emissions. There are no exhaust emissions from an electric motor.
- compatibility with existing equipment. There is a distinct advantage in choosing an electric motor that is already being used on the pipeline since operating experience and maintenance support resources will already be available.

Disadvantages of a separate electric motor and driven equipment are:

- availability and reliability of electrical power. In uninhabited and remote areas, the electric motor is dependent on both the availability and reliability of power. Wide spread damage due to weather events such as ice storms can severely impact motor and pipeline availability.
- compatibility between driver and driven equipment. A VFD and gearbox or fluid drive will be needed for centrifugal compressors and considered for centrifugal pumps. For a VFD drive, this will add high voltage equipment with restricted electrical areas, especially for large electric motors.
- availability (combination of reliability, maintainability and supportability). Electric motors are purported to require very little maintenance, but actual experience indicates this may not be accurate. A review of frequently quoted studies [41] identifies reliability issues and recommended improvement strategies. Although electric motors are generally very reliable, some failure modes, such as one experienced by one of the authors of a manufacturing defect that resulted in a major rotor failure and extended downtime of more than six months, can result in major costs and downtime. When the end of life is reached, motor rewinding can also cause a spike in costs and availability.
- maintenance support resources available. Large electric motors, especially synchronous ones, are a sophisticated and high technology machine that requires equally high levels of expertise for maintenance support, particularly for medium to high voltage electrical equipment. This is generally widely available in developed areas of the world but could be a factor elsewhere. Manufacturers vary with respect to their coverage for maintenance support centers for spare parts and repair/overhaul; facilities and this should be consideration for choice of gas turbine.

In addition to the above, advantages of a hermetic electric motor compressor are:

- power range. Hermetic compressors range approximately from 3–18 MW which does cover a major part of required power for pipelines.
- emissions. Since the unit is fully sealed, there are no exhaust or gas emissions, a major advantage in inhabited areas.

Disadvantages of a hermetic electric motor compressor are:

- power range. Hermetic compressors have a more limited power range, although not usually a problem for typical pipeline compression but also with more limited choices available in this range.
- operating experience. There is less experience available and fewer manufacturers although this has not necessarily been a problem.
- motor cooling. Since process gas is used for cooling the motor, it is vulnerable over the long term even to minor concentrations of process contaminants such as sulfur.

8.6.4 Advantages and Disadvantages of Internal Combustion Engines

Advantages of the internal combustion engine are:

- power range. Engines are an excellent choice at the low to medium power range and ones used on pipelines range roughly from 500 kW–8 MW with many choices available in this range. The operating range is typically 80%–100% of design speed and is a good match for a reciprocating compressor.

- thermal efficiency. The efficiency of an engine varies between 35%–40% and varies little with maximum power or at part load.
- effect of temperature on power and efficiency. Naturally aspirated engines are affected by ambient air temperature but the more common turbocharged engines are only affected above certain elevations and ambient temperatures.
- type of energy source available. The internal combustion engine has the advantage of being able to use the clean natural gas available from the gas pipeline at normal gas compositions available in the pipeline.
- compatibility between driver and driven equipment. The engine is most compatible from a power and flow perspective with a reciprocating compressor since speeds can be matched, eliminating the need for a gearbox. There is limited use of engines to drive centrifugal pumps.
- availability (combination of reliability, maintainability and supportability). Engines are more complicated, although the technology is well established, and require more maintenance which will affect its availability. Reliability can be as high as 98%–99% and unit availability 96%–97% with a proper maintenance program and maintenance support.
- life cycle (capital, operating and maintenance) costs. With the many factors involved, there is no clear advantage or disadvantage. Capital costs are competitive with other options. Operating costs will depend on the cost of energy, but maintenance costs will be higher.
- compatibility with existing equipment. There is a distinct advantage in choosing an engine that is already being used on the pipeline since operating experience and maintenance support resources will already be available.

Disadvantages of the internal combustion engine are:

- noise emissions. The engine does produce significant exhaust noise, not a problem in uninhabited areas, but one which could be an issue in inhabited areas, requiring noise mitigation measures.
- exhaust emissions. A major pollutant from an engine is NO_x but progress has been made to reduce levels using lean combustion. It also produces large amounts of CO₂, CO and UHC (unburnt hydrocarbons) that contribute to global warming.
- maintenance support resources available. Modern engines are a sophisticated and high technology machine that requires equally high levels of expertise for maintenance support. This is generally widely available in developed areas of the world but could be a factor elsewhere. Manufacturers vary with respect to their coverage for maintenance support centers for spare parts and repair/overhaul; facilities and this should be consideration for choice of an engine.

8.6.5 Advantages and Disadvantages of Centrifugal Compressors

Centrifugal compressors are the compressor of choice for high flow, relatively low pressure ratio applications since they provide efficient operation over a reasonable flow range. There are limits, however, at lower flows due to surge, at higher flows where the flow chokes and efficiency decreases dramatically, at a lower speed needed to avoid the first critical speed and at maximum speed where the maximum power level is reached. The available operating range is widest at low pressure ratios favored for mainline pipelines but is decreased at higher heads, also with a decrease in maximum efficiency. They require little maintenance with clean natural gas and can reach up to 50,000 hours before overhaul.

8.6.6 Advantages and Disadvantages of Reciprocating Compressors

Reciprocating compressors are best for lower flow applications and feature excellent flexibility in providing different pressure ratios at high efficiency. Care has to be taken not exceed mechanical integrity limits such as rod loading. They are relatively easy to maintain but are more maintenance intensive with discharge valves especially being a higher maintenance item.

REFERENCES

- [1] Cameron, I., 2007. "Upgrade Unveiled for Rolls-Royce Gas Turbine," *CompressorTechTwo*, October 2007, pp. 59–60.
- [2] Robb, D., 2008. "Aero vs Industrial," *Turbomachinery International*, January/February 2008, pp. 34–36.
- [3] Wilcox, M., Baldwin, R., Garcia-Hernandez, A. and Brun K., 2010. "Guideline for Gas Turbine Inlet Air Filtration Systems," *Gas Machinery Research Council and Southwest Research Institute*, April 2010, 122 pages.
- [4] API Standard 614, 1999. "Lubrication, Shaft-Sealing, and Control-Oil Systems and Auxiliaries for Petroleum, Chemical and Gas Industry Services," *American Petroleum Institute*, Fourth Edition, Washington, DC, pp. 1–240.
- [5] Foster, A. D., von Doering, H. E. and Hilt, M. B., 2000. "Fuel Flexibility in Heavy Duty Gas Turbines," *GE Reference Document*, GER3428a, Sept. 2000, pp. 1–33.
- [6] ASME B133.7, 1992. "Gas Turbine Fuels," *American Society of Mechanical Engineers*, New York, NY.
- [7] Kurz, R., Etheridge, C. and Kaiser, R., 2004. "On Fuel Suitability for Gas Turbines," *Proceedings of the 33rd Turbomachinery Symposium*, Turbomachinery Laboratory, Texas A&M University, College Station, Texas, pp. 67–75.
- [8] Pavri, R. and Moore, G. D., 2001. "Gas Turbine Emissions and Control," *General Electric Reference GER-4211*, 36 pages.
- [9] Jin, H., 2007. "Affecting component lives," *Turbomachinery International*, July/August 2007, pp. 29–31.
- [10] Davis, L. B. and Black, S. H., 2000. "Dry Low NO_x Combustion Systems for GE Heavy-Duty Gas Turbines," *GE Reference Document*, GER-3569G, 10/00, pp. 1–26.
- [11] Smith, K. O., 1998. "Advanced Combustion Systems," *Solar Turbomachinery Technology Seminar*, TTS120, pp. 1–15.
- [12] Todman, M. T., 2000. "The Industrial Avon DLE—Concept to Reality," *Rolls Royce Technical Paper*, pp. 1–15.
- [13] Clapsaddle, C. and Van Osdell, D., 2000. "NO_x Control Technologies—Catalytica Combustion Systems, Inc. Xonon™ Flameless Combustion System," *Environmental Technology Verification Report*, Midwest Research Institute (MRI) with funding from US EPA, pp. 1–42.
- [14] Driscoll, D., Richards, G. et al., 2007. "LNG Interchangeability/Gas Quality: Results of the National Energy Technology Laboratory's Research for the FERC on Natural Gas Quality and Interchangeability," *Prepared by U.S. Department of Energy National Energy Technology Laboratory*, DOE/NETL-2007/1290, June 2007, pp. 1–257.
- [15] Healy, T. and Frederick, G., 2007. "Tuning for LNG, on the Fly," *Turbomachinery International*, Sept/Oct 2007, pp. 24–26.
- [16] Kurz, R. and Brun, K., 2000. "What Makes the Map?," *Proceedings of the 29th Turbomachinery Symposium*, Turbomachinery Laboratory, Texas A&M University, College Station, Texas, pp. 247–262.
- [17] Brun, K. and Nored, M. G., 2006. "Guideline for Field Testing of Gas Turbine and Centrifugal Compressor Performance," *Gas Machinery Research Council/Southwest Research Institute*, August 2006, pp. 1–93.
- [18] API Standard 616, 1998. "Gas Turbines for the Petroleum, Chemical and Gas Industry," *American Petroleum Institute*, Fourth Edition, Washington, DC, pp. 1–100.

- [19] Bronicki, L. Y. and Schochet, D. N., 2005. "Bottoming Organic Cycle for Gas Turbines," *ASME Turbo Expo 2005: power for Land, Sea and Air*, June 6–9, 2005, Reno-Tahoe, NV, pp. 1–8.
- [20] Beer, P., Tessaro, J. E., Eckels, B. and Gaberson, P., 2006. "High-Speed Motor Design for Gas Compressor Applications," *Proceedings of the 35th Turbomachinery Symposium*, Turbomachinery Laboratory, Texas A&M University, College Station, TX, pp. 103–112.
- [21] API Standard 541, 2004. "Form-wound Squirrel-cage Induction Motors 500 Horsepower and Larger," 4th Edition, June 2004 *American Petroleum Institute*, Fourth Edition, Washington, DC, pp. 1–84.
- [22] API Standard 546, 1997. "Brushless Synchronous Machines—500 kVA and Larger," 2nd Edition, June 1997, *American Petroleum Institute*, Fourth Edition, Washington, DC, pp. 1–108.
- [23] Weber, W. J., Cozner, R. M., Ruckstadter, E. and Smith, J., 2002. "Engineering Fundamentals of Multi-MW Variable Frequency Drives—How They Work, Basic Types and Application Considerations," *Proceedings of the 31st Turbomachinery Symposium*, Turbomachinery Laboratory, Texas A&M University, College Station, TX, pp. 177–194.
- [24] Paulini, R. M. P. and Pires, L. F. G., 2006. "Optimizing Energy in Orbel II Pipeline," *Proceedings of IPC 2006, 6th International Pipeline Conference*, Sept 25–29, 2006, Calgary, Alberta, Canada, pp. 1–12.
- [25] Ferrari, A.-M., 2016. "Benefits of Variable Frequency Drives on Pumping Systems in Enbridge Liquids Pipelines," *Proceedings of IPC 2016, 11th International Pipeline Conference*, Sept 26–30, 2016, Calgary, Alberta, Canada, pp. 1–9.
- [26] Unknown, 2017. "Mechanical Drives," *CompressorTechTwo*, CT2 Compression Technology Sourcing Supplement, 2017, p. 182.
- [27] Ryrie, J. and McLean, G. S., 2000. "MOPICO—Operating Experience with a Unique Pipeline Compressor System," *Proceedings of IPC 2000, 3rd International Pipeline Conference*, Calgary, Alberta, Canada, pp. 1263–1270.
- [28] Kleynhans, G., Pfrehm, G., Berger, H. and Baudelocque, L., 2005. "Hermetically Sealed Oil-free Turbocompressor Technology," *Proceedings of the 34th Turbomachinery Symposium*, Turbomachinery Laboratory, Texas A&M University, College Station, Texas, pp. 63–76.
- [29] Anonymous, 2010. "DATUM Centrifugal Compressor Line Sees Continuing Improvement," *Pipeline & Gas Journal*, 237, pp. 75–76.
- [30] Jordan, K., Walter, P., Emde, A. and Comberg, C., 2004. "The Respective Merit of Gas Turbine vs Electric Drive for Pipeline Turbocompressors," *Proceedings of IPC 2004, 5th International Pipeline Conference*, Calgary, Alberta, Canada, pp. 1–9.
- [31] Miller, R., 2004. "The Horsepower Revolution—Considerations for Adding Larger Horsepower Reciprocating Engines," *CompressorTechTwo*, May 2004, pp. 10–12.
- [32] Amundsen, B., Sautter, W. and Goodenough, R., 2003. "High Power Four Stroke Lean Burn Gas Engines with Centrifugal Compressors in Main Transmission Applications," *2003 Gas Machinery Conference*, October 2003, Salt Lake City, UT, pp. 1–24.
- [33] Potter, R., Holden, J. and Flores, V., 2002. "Integrated Station Revitalization Design Considerations for The Reciprocating Engine Natural Gas Compressor Station," *2002 Gas Machinery Conference*, October 2002, Nashville, TN, pp. 1–11.
- [34] Whelan, M. and Bestor, T., 2007. "PRCI's Emissions Reduction for Legacy Engines Program—An Update," *2003 Gas Machinery Conference*, Dallas, Texas, pp. 1–12.
- [35] Fletcher, Potter and Hutcherson, 2000. "Revitalization of the GMW Engine Family," *2000 Gas Machinery Conference*, October 2000, Colorado Springs, Colorado, pp. 1–15.
- [36] Holden, J. and Schmidt, J., 2001. "Revitalization of the GMW Engine Family Part 2—Complete Station Upgrade," *2001 Gas Machinery Conference*, October 2001, Austin, Texas, pp. 1–12.
- [37] Mancuso, J. and Corcoran, J., 2003. "What are the differences in high performance flexible couplings for turbomachinery?," *Processing of the Thirty-Second Turbomachinery Symposium*, pp. 189–207.
- [38] Saunders, M. F., 2006. "Coupling retrofits and upgrades," *Hydrocarbon Processing*, August 2006, pp. 61–62.

- [39] Jani, W. and Hauptmann, E. G., 2011. "CASE STUDY: Tuning out a difficult torsional vibration problem in a reciprocating compressor installation," *2011 GMRC Conference*, Nashville, Tennessee.
- [40] ANSI/API Std 671. "Special-Purpose Couplings for Petroleum, Chemical, and Gas Industry Services," *American Petroleum Institute*, 01 Aug 2007, 56 pages.
- [41] Penrose, H., 2012. "Large Electric Motor Reliability: What Did the Studies Really Say?" *Efficient Plant*, February 2012.

DYNAMIC BEHAVIOR OF PUMPING SYSTEMS

9.1 INTRODUCTION

Many of the dynamic analyses conducted during the design phase of a pump station or for trouble shooting problems are invariably involved in the startup and shutdown of centrifugal pumps, flow controls, and in the opening and closing of valves during operation scenarios. Interaction between system hydraulic dynamics and associated control protocols could also trigger severe dynamics and catastrophic failure or system overall reliability issues. Expansion of pump stations to cope with either capacity increases or changes in conditions or products can be a challenge. The addition of various units in series or parallel with different pump head-flow characteristics, and drivers' type and inertias, require attention and thorough analysis.

In order to understand the dynamic behavior of a pumping system, the governing equation describing the unsteady incompressible flow through various piping elements needs to be solved in both temporal and spatial domains. A constant area pipe is described by the continuity and momentum equations. Therefore, the fundamental governing one-dimensional equation is described first and are solved using the method of characteristics. Since the pump driver exerts a torque on the rotating shaft, which in turn, conveys energy to the impeller to develop a total dynamic head across the pump, the dynamic behavior of this system is also described and combined with the unsteady flow of the connecting piping system. The transient-state pressures at some locations in the system may be reduced to or below the vapor pressure of the liquid. This may produce vapor cavities in the flow or may cause the liquid column to separate. Rejoining of the separated columns or collapse of the cavities results in a large pressure rise, which may damage the piping system. This chapter deals with these dynamic phenomena frequently observed in pumping systems.

9.2 UNSTEADY GOVERNING EQUATIONS AND SOLUTION TECHNIQUES

9.2.1 Governing Equation for Constant Area Pipes

The unsteady flow through a constant area pipe is described by the continuity and momentum equations. The following assumptions are made in the derivation of these equations.

1. The flow in the pipe is one-dimensional and that the velocity distribution over the cross section of the pipe is uniform.
2. The pipe wall and the fluid are considered linearly elastic, i.e., the respective stress is proportional to the strain.
3. The unsteady frictional losses are assumed to be the same as that pertaining to steady flow frictional losses having the same instantaneous flow and fluid properties.

The one-dimensional continuity equation can be written in the form:

$$\frac{\partial \rho}{\partial t} + U \frac{\partial \rho}{\partial x} + \rho \frac{U \partial}{\partial x} = 0 \quad (9-1)$$

where:

- ρ = density of the fluid
- U = mean flow velocity $U(x, t)$
- x = axial distance along the pipe
- t = time

From the definition of the speed of sound in the fluid;

$$c_0 = \sqrt{\frac{\partial P}{\partial \rho}} \quad (9-2)$$

equation (9-1) can be written in terms of the static pressure (P) as follows:

$$\frac{\partial P}{\partial t} + U \frac{\partial P}{\partial x} + \rho c_0^2 \frac{\partial U}{\partial x} = 0 \quad (9-3)$$

In a circular pipe, the speed of sound (c_0) is a function of the bulk modulus of the liquid (K) and its density (ρ), as well as the bulk modulus of elasticity of the pipe material (E) and its diameter to thickness ratio (D/t), by the following relation [1]:

$$c_0 = \sqrt{\frac{1/\rho}{\frac{1}{K} + \frac{1}{E}(D/t)}} \quad (9-4)$$

Table 9-1 gives approximate bulk modulus and density for common liquids, while Table 9-2 gives typical values of the modulus of elasticity of common pipe materials.

The one-dimensional momentum equation of the flow in a constant area pipe can be written as:

$$\frac{\partial U}{\partial t} + U \frac{\partial U}{\partial x} = -\frac{1}{\rho} \frac{\partial P}{\partial x} - g \sin(\alpha) - \frac{fU|U|}{2D} \quad (9-5)$$

where:

- f = Darcy-Weisbach friction coefficient which is function of the local Reynolds number and internal wall surface roughness; it can be determined from a derivative of Colebrook-White equation in explicit form [3]
- D = pipe internal diameter
- α = pipe inclination (positive in the positive direction of (x))

Table 9-1. Example of bulk modulus and density for typical liquids

	Modulus of Elasticity K (GPa)	Density (kg/m)	Sound Speed (m/s)
Water at 0°C	1.89	1000	1375
Water at 40°C	2.18	992	1482
Sea water at 0°C	2.04	1028	1408
Petroleum	1.50	835	1340
Oil	1.1–1.6	855–963	855–963

Table 9-2. Modulus of elasticity for typical pipe materials

Pipe Material	Modulus of Elasticity E (GPa)
Steel	200–220
Cast iron	44–120
Copper	120
Glass	5–8
Aluminum	73
Asbestos cement	25
Concrete	20–30
Lead	5–17
Rubber	0.0002–0.0006

The static pressure can be replaced by the piezometric head (H), which is the elevation of the hydraulic gradient above an arbitrary datum, as follows:

$$P = \rho g(H - z) \quad (9-6)$$

where:

g = is the gravitational acceleration.

z = elevation of the pipe center-line above the arbitrary datum.

and:

$$\frac{\partial P}{\partial x} = \rho g \left[\frac{\partial H}{\partial x} - \sin(\alpha) \right] \quad (9-7)$$

The continuity equation (9-3) and the momentum equation (9-5) can then be written in terms of the piezometric head (H), in the form:

$$\frac{\partial H}{\partial t} + U \frac{\partial H}{\partial x} + \frac{c_0^2}{g} \frac{\partial U}{\partial x} = 0 \quad (9-8)$$

$$\frac{\partial U}{\partial t} + U \frac{\partial U}{\partial x} + g \frac{\partial H}{\partial x} + \frac{fU|U|}{2D} = 0 \quad (9-9)$$

9.2.2 Solution Techniques

The above two equations (9-8) and (9-9) form a pair of partial differential equations in terms of the two dependent variable (U) and (H) and the two dependent variables (x) and (t). These two equations can be transformed into two ordinary differential equations along two characteristics paths defined by two slopes C^+ and C^- [4] in the form:

$$\frac{g}{c_0} \frac{dH}{dt} + \frac{dU}{dt} + \frac{fU|U|}{2D} = 0 \quad \text{along the path } C^+ : \frac{dx}{dt} = +c_0 \quad (9-10)$$

and

$$-\frac{g}{c_0} \frac{dH}{dt} + \frac{dU}{dt} + \frac{fU|U|}{2D} = 0 \quad \text{along the path } C^- : \frac{dx}{dt} = -c_0 \quad (9-11)$$

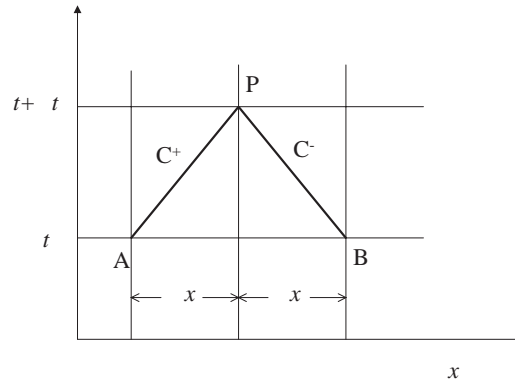


Figure 9-1. Characteristics lines in the x - t plane.

The above two paths, C^+ and C^- , are represented by two straight lines on the x - t plane, having slopes of $\pm 1/c_0$ as shown in Fig. 9-1. These are called the “characteristic lines.” If a pipe is divided into equal increments (Δx), and a time step is defined by

$$\Delta t = \frac{\Delta x}{c_0} \quad (9-12)$$

then the slope, C^+ , will be satisfied by a positively sloped diagonal, AP as shown in Fig. 9-1. If the dependent variable U and H are known at location A at time t , then Equation (9-10), which is valid along C^+ , can be integrated between A and P to reveal:

$$H_P - H_A + \frac{c_0}{gA}(Q_P - Q_A) + \frac{f\Delta x}{2gDA^2} Q_A |Q_A| = 0 \quad (9-13)$$

Likewise, the slope, C^- , will be satisfied by a negatively sloped diagonal, BP as shown in Fig. 9-1. If the dependent variable U and H are known at location B at time t , then Equation (9-11), which is valid along C^- , can be integrated between B and P to reveal:

$$H_P - H_B - \frac{c_0}{gA}(Q_P - Q_B) - \frac{f\Delta x}{2gDA^2} Q_B |Q_B| = 0 \quad (9-14)$$

Equations (9-13) and (9-14) are two algebraic equations that describe the temporal variation of the two independent variables H_P and Q_P based on these variables at time t upstream and downstream of the point P. These two equations can thus be solved algebraically and simultaneously to reveal the values of H_P and Q_P at time $t + \Delta t$. If this calculation is repeated for all points (nodes) along the discretized pipe section, and progressed in time, the transient behavior of the flow in terms of the variables (Q and H) can be determined.

9.3 BOUNDARY CONDITIONS

At the extreme end of piping elements, only one of the above two characteristics lines and the corresponding algebraic relations is available. For the upstream end, Equation (9-14) holds along the C^- characteristic. Likewise, for the downstream end, Equation (9-13) holds along the C^+ characteristic. Each of these two equations is a relationship between the two variables H_P and Q_P at the boundary. Additional information (i.e., relationship) between

these two variables is needed at either end to close the system of equations. These are given by known information at the boundary, called the “boundary conditions.” Examples of boundary conditions are:

1. The piezometric head is a known function of time, i.e., $H_p = H_p(t)$.
2. The flow is a known function of time, i.e. $Q_p = Q_p(t)$.
3. Closed end, i.e. $Q_p = 0$.

9.3.1 Flow Transients Across Other Elements

The characteristic equations (9-13) and (9-14) are also used to resolve the flow transients across a pressure loss (resistive) element, such as a valve, orifice, fittings, etc. We assume that the flow transients across such an element behaves in a quasi-steady state manner, in that the instantaneous head loss across the element is related to the instantaneous flow according to the following relations with reference to Fig. 9-2:

$$H_{P1} - H_{P2} = C_v Q_{P1} |Q_{P1}| \quad (9-15)$$

$$Q_{P1} = Q_{P2} \quad (9-16)$$

where C_v is the element flow resistance coefficient. In case of a valve this coefficient is function of the valve type and opening at time $t + t$. Equations (9-15) and (9-16) are solved simultaneously with the characteristics equations (9-13) and (9-14) to reveal the parameters H_{P1} , H_{P2} , Q_{P1} , and Q_{P2} at time $t + t$.

In the case of a capacitance element, like a large closed volume (e.g. pressure vessel with no head space), similar treatment is applied to resolve the flow transients across the element. We assume that the effective bulk modulus of the fluid and the vessel (K) is defined by:

$$K = -V_0 \frac{\partial P}{\partial V} \quad (9-17)$$

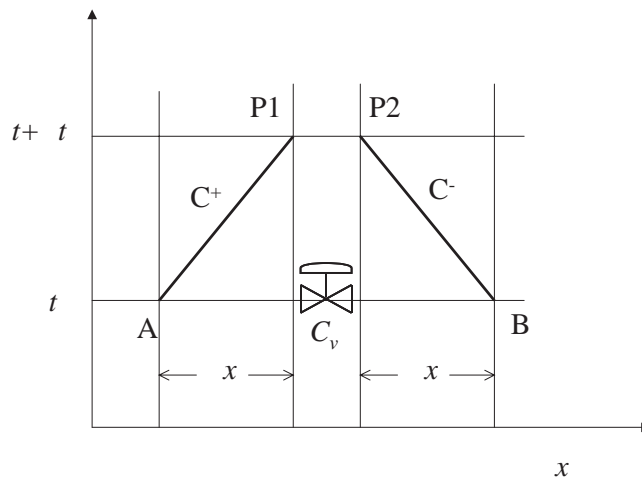


Figure 9-2. Characteristics lines across a flow-resistive element.

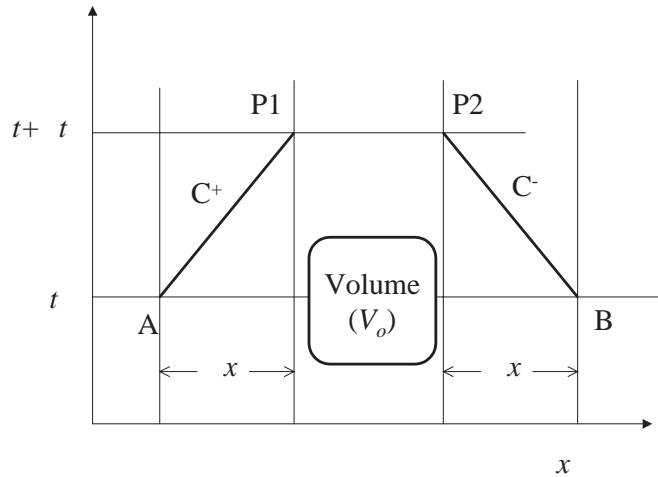


Figure 9-3. Characteristics lines across a flow capacitance element.

where V_0 is the volume of the capacitance element. At time $t + t$, we can write the following two relationships between the flows and the pressure heads across the capacitance element (see Fig. 9-3):

$$Q_{P1} - Q_{P2} = \frac{V_0}{K} \frac{\partial P}{\partial t} = \frac{\rho g V_0}{K} \frac{\partial H_{P1}}{\partial t} = \frac{g V_0}{c_0^2} \frac{\partial H_{P1}}{\partial t} \quad (9-18)$$

$$H_{P1} = H_{P2} \quad (9-19)$$

Equations (9-18) and (9-19) are solved simultaneously with the characteristics equations (9-13) and (9-14) to reveal the parameters H_{P1} , H_{P2} , Q_{P1} and Q_{P2} at time $t + t$.

9.3.2 Flow Transients of an Accumulator

A hydraulic accumulator is an energy storage device. It is a pressure storage reservoir in which a non-compressible hydraulic fluid is held under pressure by a compressed gas. The main reasons that an accumulator is used in a hydraulic system are so that the pump does not need to be so large to cope with extremes of demand, so that the supply circuit can respond more quickly to any temporary demand and to smooth pulsations. A compressed gas accumulator consists of a cylinder with two chambers that are separated by an elastic diaphragm or by a floating piston. One chamber contains hydraulic fluid and is connected to the hydraulic line. The other side contains an inert gas under pressure that provides the compressive force on the hydraulic fluid. Inert gas is used because oxygen and oil can form an explosive mixture when combined under high pressure. As the volume of the compressed gas changes the pressure of the gas, and the pressure on the fluid changes inversely. Usually, an accumulator is placed close to the pump with a non-return valve preventing flow back to it. In the case of positive displacement pumps, this accumulator is placed in the best place to absorb pulsations of energy from the pump. It also helps protect the system from water hammer. This protects system components, particularly pipework, from both potentially destructive forces.

An additional benefit is the additional energy that can be stored while the pump is subjected to low demand. The designer can use a smaller-capacity pump. The large excursions

of system components, such as landing gear on a large aircraft, that require a considerable volume of fluid can also benefit from one or more accumulators. These are often placed close to the demand to help overcome restrictions and drag from long pipework runs. The outflow of energy from a discharging accumulator is much greater, for a short time, than even large pumps could generate.

An accumulator can maintain the pressure in a system for periods when there are slight leaks without the pump being cycled on and off constantly. When temperature changes cause pressure excursions the accumulator helps absorb them. Its size helps absorb fluid that might otherwise be locked in a small fixed system with no room for expansion due to valve arrangement.

The gas precharge in an accumulator is set so that the separating bladder, diaphragm, or piston does not reach or strike either end of the operating cylinder. The design precharge normally ensures that the moving parts do not foul the ends or block fluid passages. Poor maintenance of precharge can destroy an operating accumulator. A properly designed and maintained accumulator should operate trouble-free for years.

Consider a simple accumulator shown in Fig. 9-4 placed in a line containing fluid. The fluid level in the accumulator is at elevation (z) from the arbitrary datum used in defining the piezometric head. The pressure at any instant in time in the gas space is assumed uniform. The compressibility of the fluid inside the accumulator is considered negligible compared to the compressibility of the gas. Additionally, inertia and friction of the fluid motion inside the accumulator are neglected. The gas is assumed to follow a polytropic relation, i.e.,

$$\left(H_{P1} - z + \frac{P_{amb}}{\rho_f g} \right) (V_0)^n = C \quad (9-20)$$

where:

V_0 = gas volume inside the accumulator

P_{amb} = ambient pressure

ρ_f = fluid density (subscripted here to emphasize that it is the fluid density and not the gas density)

C = constant

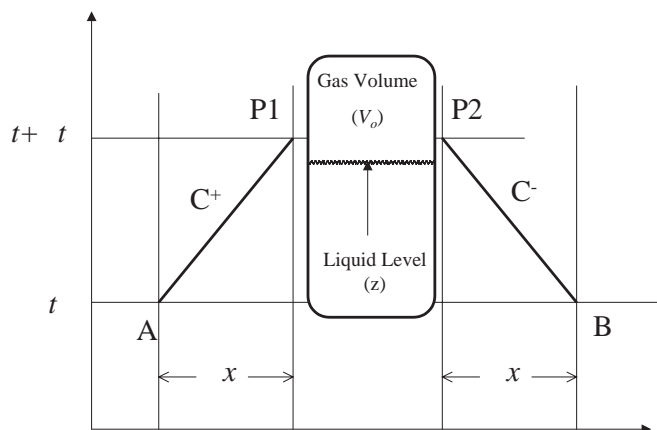


Figure 9-4. Characteristics lines across an accumulator.

The exponent (n), is the polytropic exponent which depends on the process followed by the gas in the accumulator. For perfect gas, one extreme would be an isothermal process where $n = 1$, while the other extreme is an isentropic process where $n =$ isentropic exponent for the gas (e.g., 1.4 for nitrogen). For small accumulators with fast response time, the process would be close to isentropic, whereas for large accumulators with small gas volume, it would be close to isothermal. Rewriting Equation (9-20) in terms of the line flows, Q_{P1} and Q_{P2} , we get:

$$\left(H_{P1} - z + \frac{P_{amb}}{\rho_f g} \right) [V_0 - t(Q_{P1} - Q_{P2})]^n = C \quad (9-21)$$

and

$$H_{P1} = H_{P2} \quad (9-22)$$

Equations (9-21) and (9-22) are solved simultaneously with the characteristics equations (9-13) and (9-14) to reveal the parameters H_{P1} , H_{P2} , Q_{P1} and Q_{P2} at time $t + \Delta t$.

9.4 DYNAMICS BEHAVIOUR OF CENTRIFUGAL PUMPS

Many of the dynamic analyses conducted during the design phase of a pump station or for trouble shooting problems are invariably involved in the startup and shutdown of centrifugal pumps, flow controls, and in the opening and closing of valves during operation scenarios. Interaction between system hydraulic dynamics and associated control protocols could also trigger severe dynamics and catastrophic failure or system overall reliability issues. Expansion of pump stations to cope with either capacity increases or changes in conditions or products. The addition of various units in series or parallel with different pump head-flow characteristics and drivers' type and inertias require attention and thorough analysis.

As mentioned in earlier chapters, the pump driver exerts a torque on the rotating shaft, which, in turn, conveys energy to the impeller to cause flow through the pump and to develop a total dynamic head across the pump. In the case of a sudden shutdown, like in the case of emergency shutdown (ESD) or a power failure, the reactive torque of the liquid on the impeller causes it to decelerate. During this phase, a series of expansion waves propagate downstream, and pressure waves propagate upstream through the connected piping. If the system primarily develops its head by lifting the liquid to a higher elevation, the flow at the pump reverses in a few seconds, and then a short time later the rotation of the pump could reverse and it starts to turn backwards. As it spins up to a high reverse speed, it causes a high resistance to the flow, which develops a high head at the pump that must be provided for in the design. There is also the possibility that the discharge pipeline, due to its profile, may suffer low pressures, causing vapor to come out of solution and vapor cavities to form. The collapse of the vapor cavities and compression of the vapor pockets may cause dangerously high pressures to develop.

If the pumping system acts against a friction head, as in the case of long lines, then there are no adverse forces to cause reversal of the flow. The flow at the pump does decrease rapidly when power is cut off, however, which may overpressure the suction line unless it is designed to withstand it. On the discharge side of the system, the slowing of flow at the pump causes a succession of rarefaction waves to move downstream causing vapor and other gases to come out of solution and vapor column separation. Depending upon the profile of the line, these pockets of gas and vapor may cause high pressure upon closure. In addition, the initial low pressure waves may collapse the pipe unless designed to withstand vapor pressure.

9.4.1 Homologous Relations

The four parameters that characterize the performance of a centrifugal pump are the total hydraulic head H developed by the pump, the discharge flow Q , the shaft torque T , and the rotational speed N . Two of these parameters may be considered independent, and normally, they are the flow Q and the speed N . In this case, for a given Q and N , the head H and the torque T are determined from the pump characteristics. Two basic assumptions are made in the dynamic analysis. The pump behaves in a quasi-steady-state manner, which means that the pump steady-state characteristics hold for unsteady-state situations. Although Q and N are changing with time, their values at an instant determine H and T . Secondly, homologous relationships hold during any unsteady-state behavior. These relationships are written as follows for geometrically scaled pumps:

$$\left(\frac{Q}{N D^3}\right)_1 = \left(\frac{Q}{N D^3}\right)_2 \quad \text{and} \quad \left(\frac{H}{N^2 D^2}\right)_1 = \left(\frac{H}{N^2 D^2}\right)_2 \quad (9-23)$$

where D is a characteristic length of the pump (e.g., impeller diameter) and subscripts 1 and 2 are referred to two different-sized pumps at homologous operating conditions. For a given pump unit, the homologous equation becomes:

$$\left(\frac{Q}{N}\right)_1 = \left(\frac{Q}{N}\right)_2 \quad \text{and} \quad \left(\frac{H}{N^2}\right)_1 = \left(\frac{H}{N^2}\right)_2 \quad (9-24)$$

and, introducing the torque, we get:

$$\frac{T}{N^2} = \frac{T}{N^2}; \quad \frac{T}{Q^2} = \frac{T}{Q^2}; \quad \frac{H}{Q^2} = \frac{H}{Q^2} \quad (9-25)$$

9.4.2 Full Pump Characteristics

Let us define the characteristics of a centrifugal pump by the following dimensionless variables:

Dependent dimensionless variables:

$$h = \frac{H}{H_R}; \quad \beta = \frac{T}{T_R} \quad (9-26)$$

Independent dimensionless variables:

$$v = \frac{Q}{Q_R}; \quad \alpha = \frac{N}{N_R} \quad (9-27)$$

where the subscript R refers to the respective parameter at the rated (design) condition of the pump, which is typically at the pump maximum efficiency. The dimensionless homologous relations relating the dependent dimensionless variables h and β to the independent dimensionless variables v and α , as follows:

$$\frac{h}{v^2} = F_h\left(\frac{\alpha}{v}\right); \quad \frac{\beta}{v^2} = F_B\left(\frac{\alpha}{v}\right) \quad (9-28)$$

or:

$$\frac{h}{\alpha^2} = F_h \left(\frac{v}{\alpha} \right); \quad \frac{\beta}{\alpha^2} = F_B \left(\frac{v}{\alpha} \right) \quad (9-29)$$

During transients, there is a possibility that the speed may become zero, which would make α also zero, and the dependent variables in equation (9-28) becomes infinite. To avoid this problem, Marchal et al. [5] suggested a modification the form of the relationships in (9-28) to the following form:

$$\frac{h}{\alpha^2 + v^2} = F_h(\theta); \quad \frac{\beta}{\alpha^2 + v^2} = F_B(\theta) \quad (9-30)$$

where:

$$\theta = \tan^{-1} \left(\frac{v}{\alpha} \right) \quad (9-31)$$

Four operating zones can then be identified following the above formulation:

1. normal operating zone: $0 \quad 90^\circ$
2. reversed speed and forward flow dissipation zone: $90^\circ \quad 180^\circ$
3. reversed flow and positive speed dissipation zone: $90^\circ \quad 0$
4. reversed speed and reversed flow (turbine): $180^\circ \quad 90^\circ$

Figures 9-5 and 9-6 show examples of complete pump characteristics in terms of the head coefficient (F_h) and torque coefficient (F_B) as a function of the dimensionless parameter (θ), respectively. Numerical values are given in Table 9-3. Three characteristics are given for three different pump specific speeds. Pump specific speed is defined as:

$$N_s = \frac{N_R \sqrt{Q_R}}{(H_R)^{3/4}} \quad (9-32)$$

which is a dimensional number. If N is given in (rpm), Q in gpm, and H in ft, the N_s is said to be given in (gpm units), for short. If N is given in (rpm), Q in m^3/s , and H in m, the N_s is said to be given in (SI units).

In addition to having the proper data for pump characteristics, information is needed on the moment of inertia of pump impeller and entrained liquid, plus that of motor rotor, shaft, and couplings. This information should be obtained from the manufacturers.

9.4.3 Dynamic Equation

The centrifugal pump is assumed to respond to any perturbation in a quasi-steady manner following its full head and torque characteristics, including all of the four zones described above. Pump/driver dynamics are governed by the following equation; relating the driver power to the hydraulic and the inertias of both units:

$$\eta_m \dot{W}_d = I_d \cdot N_d \cdot \frac{dN_d}{dt} + I_P \cdot N_P \cdot \frac{dN_P}{dt} + \frac{g \rho Q H}{\eta_p} + \text{losses} \quad (9-33)$$

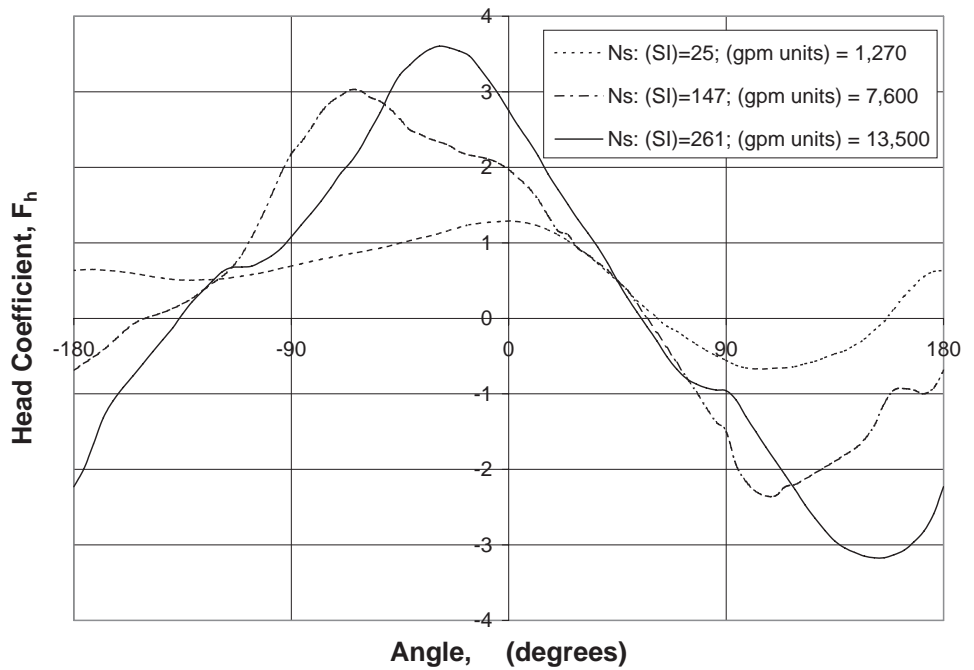


Figure 9-5. Complete head coefficient for three pump specific speeds.

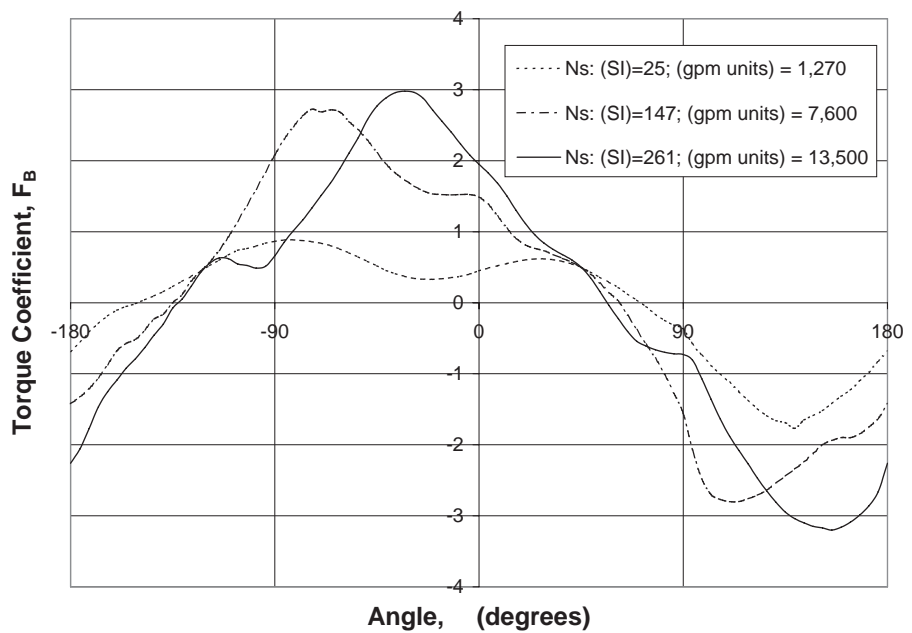


Figure 9-6. Complete torque coefficient for three pump specific speeds.

Table 9-3. Full pump head and torque coefficients for three pump specific speeds

θ (degrees)	N_s : (SI) = 25; (gpm Units) = 1270		N_s : (SI) = 147; (gpm Units) = 7600		N_s : (SI) = 261; (gpm Units) = 13,500	
	F_h	F_B	F_h	F_B	F_h	F_B
180.000	0.634	0.684	0.690	1.420	2.230	2.260
175.909	0.643	0.547	0.599	1.328	2.000	2.061
171.818	0.646	0.414	0.512	1.211	1.662	1.772
167.727	0.640	0.292	0.418	1.056	1.314	1.465
163.636	0.629	0.187	0.304	0.870	1.089	1.253
159.545	0.613	0.105	0.181	0.677	0.914	1.088
155.455	0.595	0.053	0.078	0.573	0.760	0.921
151.364	0.575	0.012	0.011	0.518	0.601	0.789
147.273	0.552	0.042	0.032	0.380	0.440	0.632
143.182	0.533	0.097	0.074	0.232	0.284	0.457
139.091	0.516	0.156	0.130	0.160	0.130	0.300
135.000	0.505	0.227	0.190	0.000	0.055	0.075
130.909	0.504	0.300	0.265	0.118	0.222	0.052
126.818	0.510	0.371	0.363	0.308	0.357	0.234
122.727	0.512	0.444	0.461	0.442	0.493	0.425
118.636	0.522	0.522	0.553	0.574	0.616	0.558
114.545	0.539	0.596	0.674	0.739	0.675	0.630
110.455	0.559	0.672	0.848	0.929	0.680	0.621
106.364	0.580	0.738	1.075	1.147	0.691	0.546
102.273	0.601	0.763	1.337	1.370	0.752	0.525
98.182	0.630	0.797	1.629	1.599	0.825	0.488
94.091	0.662	0.837	1.929	1.839	0.930	0.512
90.000	0.692	0.865	2.180	2.080	1.080	0.660
85.909	0.722	0.883	2.334	2.300	1.236	0.850
81.818	0.753	0.886	2.518	2.480	1.389	1.014
77.727	0.782	0.877	2.726	2.630	1.548	1.162
73.636	0.808	0.859	2.863	2.724	1.727	1.334
69.545	0.832	0.838	2.948	2.687	1.919	1.512
65.455	0.857	0.804	3.026	2.715	2.066	1.683
61.364	0.879	0.758	3.015	2.688	2.252	1.886
57.273	0.904	0.703	2.927	2.555	2.490	2.105
53.182	0.930	0.645	2.873	2.434	2.727	2.325
49.091	0.959	0.583	2.771	2.288	3.002	2.580
45.000	0.996	0.520	2.640	2.110	3.225	2.770
40.909	1.027	0.454	2.497	1.948	3.355	2.886
36.818	1.060	0.408	2.441	1.825	3.475	2.959
32.727	1.090	0.370	2.378	1.732	3.562	2.979
28.636	1.124	0.343	2.336	1.644	3.604	2.962
24.545	1.165	0.331	2.288	1.576	3.582	2.877
20.455	1.204	0.329	2.209	1.533	3.540	2.713
16.364	1.238	0.338	2.162	1.522	3.477	2.556
12.273	1.258	0.354	2.140	1.519	3.321	2.403
8.182	1.271	0.372	2.109	1.523	3.148	2.237
4.091	1.282	0.405	2.054	1.523	2.962	2.080
0.000	1.288	0.450	1.970	1.490	2.750	1.950
4.091	1.281	0.486	1.860	1.386	2.542	1.826
8.182	1.260	0.520	1.735	1.223	2.354	1.681
12.273	1.225	0.552	1.571	1.048	2.149	1.503
16.364	1.172	0.579	1.357	0.909	1.909	1.301
20.455	1.107	0.603	1.157	0.814	1.702	1.115
24.545	1.031	0.616	1.106	0.766	1.506	0.960
28.636	0.942	0.617	0.927	0.734	1.310	0.840
32.727	0.842	0.606	0.846	0.678	1.131	0.750
36.818	0.733	0.582	0.744	0.624	0.947	0.677
40.909	0.617	0.546	0.640	0.570	0.737	0.604

Table 9-3. (continued)

θ (degrees)	Ns: (SI) = 25; (gpm Units) = 1270		Ns: (SI) = 147; (gpm Units) = 7600		Ns: (SI) = 261; (gpm Units) = 13,500	
	F_h	F_B	F_h	F_B	F_h	F_B
45.000	0.500	0.500	0.500	0.500	0.500	0.500
49.091	0.368	0.432	0.374	0.407	0.279	0.352
53.182	0.240	0.360	0.191	0.278	0.082	0.161
57.273	0.125	0.288	0.001	0.146	0.112	0.040
61.364	0.011	0.214	0.190	0.023	0.300	0.225
65.455	0.102	0.123	0.384	0.175	0.505	0.403
69.545	0.168	0.037	0.585	0.379	0.672	0.545
73.636	0.255	0.053	0.786	0.585	0.797	0.610
77.727	0.342	0.161	0.972	0.778	0.872	0.662
81.818	0.423	0.248	1.185	1.008	0.920	0.699
85.909	0.494	0.314	1.372	1.277	0.949	0.719
90.000	0.556	0.372	1.500	1.560	0.960	0.730
94.091	0.620	0.580	1.940	2.070	1.080	0.810
98.182	0.655	0.740	2.160	2.480	1.300	1.070
102.273	0.670	0.880	2.290	2.700	1.500	1.360
106.364	0.670	1.000	2.350	2.770	1.700	1.640
110.455	0.660	1.120	2.350	2.800	1.890	1.880
114.545	0.655	1.250	2.230	2.800	2.080	2.080
118.636	0.640	1.370	2.200	2.760	2.270	2.270
122.727	0.600	1.490	2.130	2.710	2.470	2.470
126.818	0.570	1.590	2.050	2.640	2.650	2.650
130.909	0.520	1.660	1.970	2.540	2.810	2.810
135.000	0.470	1.690	1.895	2.440	2.950	2.950
139.091	0.430	1.770	1.810	2.340	3.040	3.040
143.182	0.360	1.650	1.730	2.240	3.100	3.100
147.273	0.275	1.590	1.600	2.120	3.150	3.150
151.364	0.160	1.520	1.420	2.000	3.170	3.170
155.455	0.040	1.420	1.130	1.940	3.170	3.200
159.545	0.130	1.320	0.950	1.900	3.130	3.160
163.636	0.295	1.230	0.930	1.900	3.070	3.090
167.727	0.430	1.100	0.950	1.850	2.960	2.990
171.818	0.550	0.980	1.000	1.750	2.820	2.860
175.909	0.620	0.820	0.920	1.630	2.590	2.660
180.000	0.634	0.684	0.690	1.420	2.230	2.260

Equation (23) can also be expressed in terms of driver's torque as follows:

$$\eta_m T_d = I_d \cdot \frac{dN_d}{dt} + I_P \cdot \frac{N_P}{N_d} \cdot \frac{dN_P}{dt} + \frac{g \rho Q H}{\eta_P N_d} + \text{losses} \quad (9-34)$$

where:

H = head across the pump

I_d = driver rotor inertia

I_P = pump rotor inertia

N_P = pump speed

N_d = driver speed

T_d = driver torque

T_P = pump torque

\dot{W}_d = driver power

η_P = pump efficiency

η_m = mechanical efficiency

g = acceleration of gravity

The driver torque T_d is related to the pump torque T_p by the following relation:

$$\eta_m T_d N_d = T_p N_p \quad (9-35)$$

As in the case of other piping elements, the system dynamics and interaction with centrifugal pumps are handled with the method of characteristics, the C^+ and C^- equations from the adjoining pipe sections convey all system response to the suction and discharge sides of the pump. The above equation (9-33) and (9-34) are solved simultaneously with the characteristics equations (9-13) and (9-14) along with the pump head and torque characteristics (Eq. 9-30) to reveal the parameters H_{p1} , H_{p2} , $Q_{p1} = Q_{p2}$ across the pump at time $t + \Delta t$.

9.4.4 Pump and Motor Inertias

The combined inertia of pumps and electric motor drivers is required for the dynamic analysis of pumping systems. This information is typically not available during the design phase or when the dynamic analysis commences. Faithfull [16] developed the following correlations based on a large collection of pumps and motors from different manufacturers.

Data from several manufacturers of pumps used in water supply, sewage, process and petrochemical plants are shown in Fig. 9-7. They include horizontal spindle, single and double entry, split-case pumps as well as vertical spindle borehole and wet-well pumps. The general style of impeller is radial and mixed flow. The group of data points that clearly separate out from the others applies to a small, quite slim type of pumps, which are typically of a radial flow design.

Over 300 data points are plotted in Fig. 9-7 in the form of pump inertia, including entrained fluid, against a power coefficient. The power coefficient is defined as (P/N^3) , where P is the shaft power in kW supplied to the pump at its rated conditions and maximum efficiency, and N is the rotational speed in thousands of rpm. The rationale for this correlation follows a from the homologous relation:

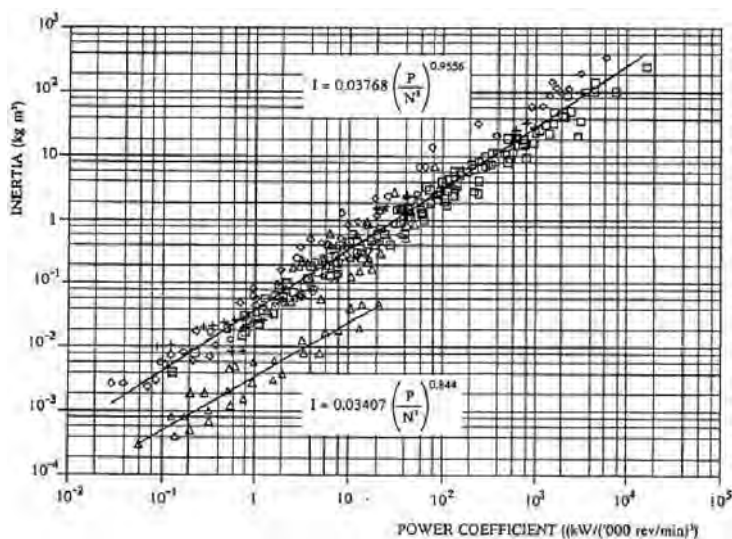


Figure 9-7. Pump moment of inertia including entrained fluid (water), for radial and mixed flow design [16].

$$\left(\frac{P}{\rho_f N^3 D^5} \right) = \text{Constant} \quad (9-36)$$

where ρ_f is the fluid density. From linear regression analyses of the data points shown on Fig. 9-7, the following relations were developed for predicting the inertia I (in kg-m²) of pump impellers, including the entrained fluid and the shaft on which the impeller is mounted. The main bulk of the data, comprising some 284 data points provided by five pump manufacturers, and covering the variety of pump types described above, yielded [15,16]:

$$I_{\text{pump}} = 0.03768 \frac{P^{0.9556}}{N^3} \quad (9-37)$$

The set of 28 data points for one particular type of pump from one manufacturer did not fall in line with the general mass of data, and these have been characterized by a separate correlation, as shown in Fig. 9-7. Despite these apparently good correlations, it should be pointed out that the actual range of inertias above and below the predictions is of the order of +50% and -50% [15].

Motor inertia data are plotted in a similar manner except that the speed is not cubed, i.e., the inertia I (kg-m²) is correlated with (P/N) , as shown in Fig. 9-8. The linear regression of 272 data points yields the following equation [16]:

$$I_{\text{motor}} = 0.0043 \frac{P^{1.48}}{N} \quad (9-38)$$

where, as above, P denotes the shaft power in kW and N is the speed in thousands of rpm. An interesting point about this set of data is that, in addition to the data collected originally by Linton [17], about 60% of the data points are for modern motors. This not only extends the range of data but also indicates that, contrary to popular belief, there is not a significant difference in the inertias of motors of old and new designs [15].

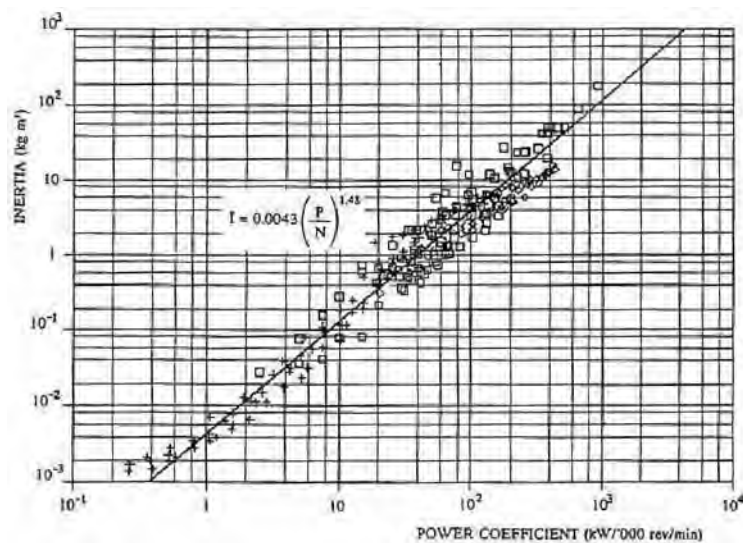


Figure 9-8. Moment of inertia of a variety of electric motors used from driving rotary pump [16].

9.5 OTHER USEFUL REPRESENTATIONS OF PUMP FOUR QUADRANTS

In Section 9.4.2 four operating zones were identified based on two independent parameters related to pump flow (positive if it is from suction to discharge) and speed (positive in the forward direction). These two parameters were normalized w.r.t. their respective rated values for the pump. The other two parameters, namely head (H) and torque (T) are the dependent parameters and hence head and torque coefficients were developed to represent the full performance of the pump in the four operating zones (called four quadrants) as shown in Figs. 9-5 and 9-6. A closer examination of these Figures reveals that three of these four quadrants can be further divided in sub-zones depending whether H and or T are positive or negative. For example, in the first quadrant where 0° to 90° , three sub-zones can be identified; normal pump operation for $+H$ and $+T$, energy dissipation for $-H$ and $+T$, and reverse flow turbine for $-H$ and $-T$. Likewise in the second quadrant where 90° to 180° , two sub-zones can be identified; a reverse rotation pump for $+H$ and $-T$, and energy dissipation for $-H$ and $-T$. In the third quadrant where 180° to 270° , there are no sub-zones as all of this zone is considered energy dissipation. Finally, in the fourth quadrant where 270° to 360° , two sub-zones can be identified; a normal turbine operation is noted for $+H$ and $+T$, and energy dissipation for $+H$ and $-T$. Therefore, a more generalized useful representation of the pump full characteristics would be able to identify these sub-zones, which when summed, it would be composed of a total of eight sub-zones. Two formats of such representation are typical, first involves Q vs. N as the two independent axes, and H and T as the variable parameters plotted as constant lines as in the example of a double suction pump of Ns-SI = 35 (Ns-gpm = 1800) shown in Fig. 9-9. Note the insert in the Figure identifying the eight different sub-zones described above.

Another representation of a pump full characteristics is by plotting constant speed lines with x-axis represents flow through the pump (positive in the forward direction and negative in the reversed direction), while the y-axis represents the head (positive for higher head at the discharge side, and negative for higher head at the suction side). The y-axis can also represent the pump torque (defined in the insert of Fig. 9-9). An example of such presentation is shown in Figs. 9-10 for the same pump. Note that the percentage of the parameters in both Figs. 9-9 and 9-10 are with respect to the respective rated parameter taken at the best efficiency point (BEP) of the pump.

9.5.1 Application Examples of the Use of Pump Four Quadrant Charts

Pipeline operators typically design their pumping stations with variable capacity such that a range of flow rates can be accommodated while maintaining safe and efficient pump operation. One method of accomplishing variable capacity pipeline operation is to have standby pumps at each pump station such that the number of operating pumps can be varied to meet a range of demand. In order to bring a non-operating (standby) pump into operation the pump must first be filled with liquid and the difference between the pump temperature and the fluid temperature must be within pump OEM limits. Due to the operating environment (remote unmanned pump stations) and physical characteristics of the fluid (e.g. viscous crude oil), the preferred method of ensuring immediate availability of non-operating pumps is to continuously circulate a small volume of fluid through the stand-by pumps. Thus, ensuring that the stand-by pump(s) is (are) filled with fluid and also that the pump temperature is close to the fluid temperature. The issue of stand-by pump temperature can become important during the cold winter months. The viscosity of the fluid will quickly increase, to the point where the fluid will not flow if it is permitted to stagnate in a low temperature environment. Additionally, the viscosity of the pump bearing lubricating oil will

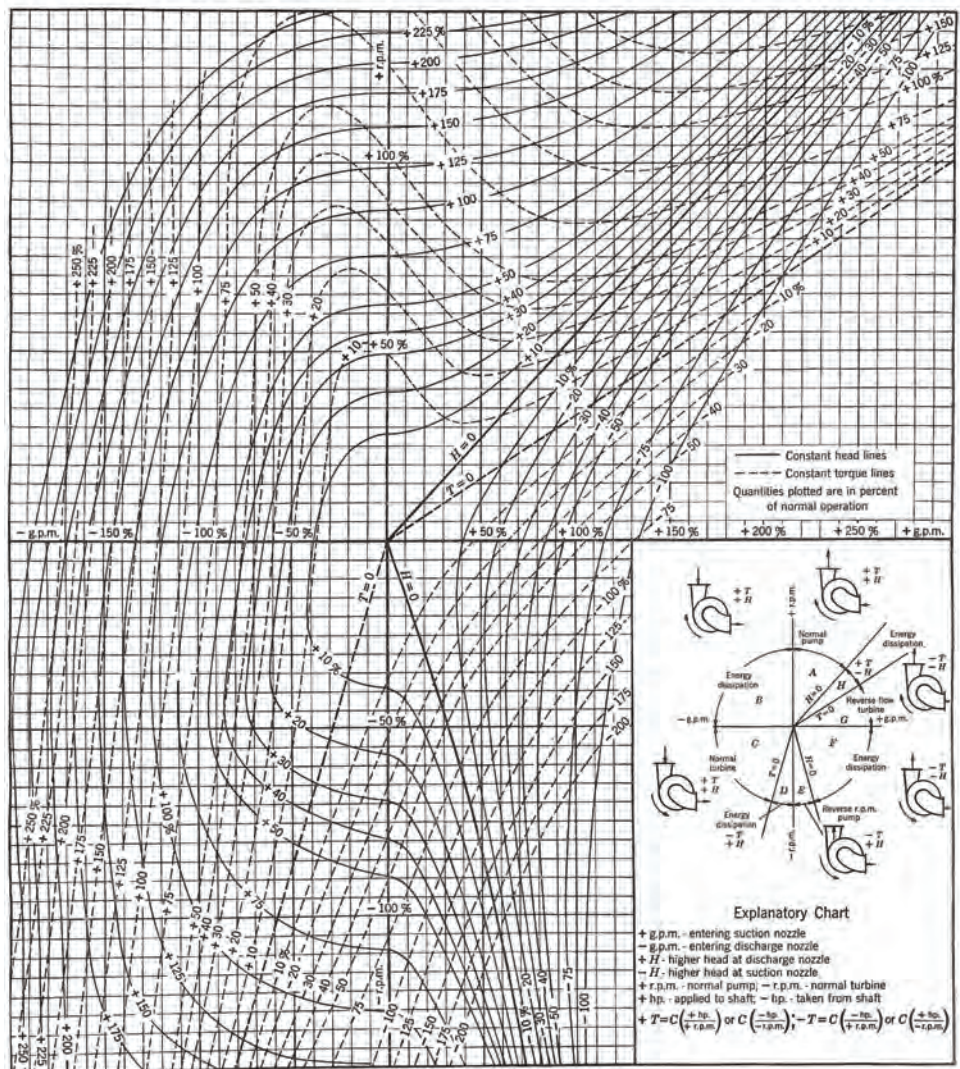


Figure 9-9. Complete four quadrant characteristics in the form of constant head/torque lines for a $N_s = 35$ (N_s ; gpm = 1800) double suction pump [23].

increase resulting in insufficient bearing lubrication if the bearing oil temperature becomes too low.

When a small volume of flow is circulated through a non-operating (standby) pump attention must be given to the possibility of pump rotation. Whether the circulating flow is forward (suction-to-discharge) or reverse (discharge-to-suction) the possibility of flow induced pump rotation exists if the flow is sufficient to produce a torque on the pump rotor system greater than the “break-away” torque. The break-away torque is the term given to the static torque required to overcome all the static friction (pump bearings and seals and motor bearings) in the rotor system such that rotation is initiated. Typical values of break-away torque for pumps fitted with fluid film bearings is 15% and 10% for pumps fitted with rolling element bearings [25]. The bearing design and bearing load, lubrication method, and the lubricant viscosity will all effect the resulting static friction and breakaway torque. The pump breakaway torque will also be dependent on the shaft sealing; mechanical seal versus packed stuffing box. In the case of mechanical seals the pump suction pressure and resulting

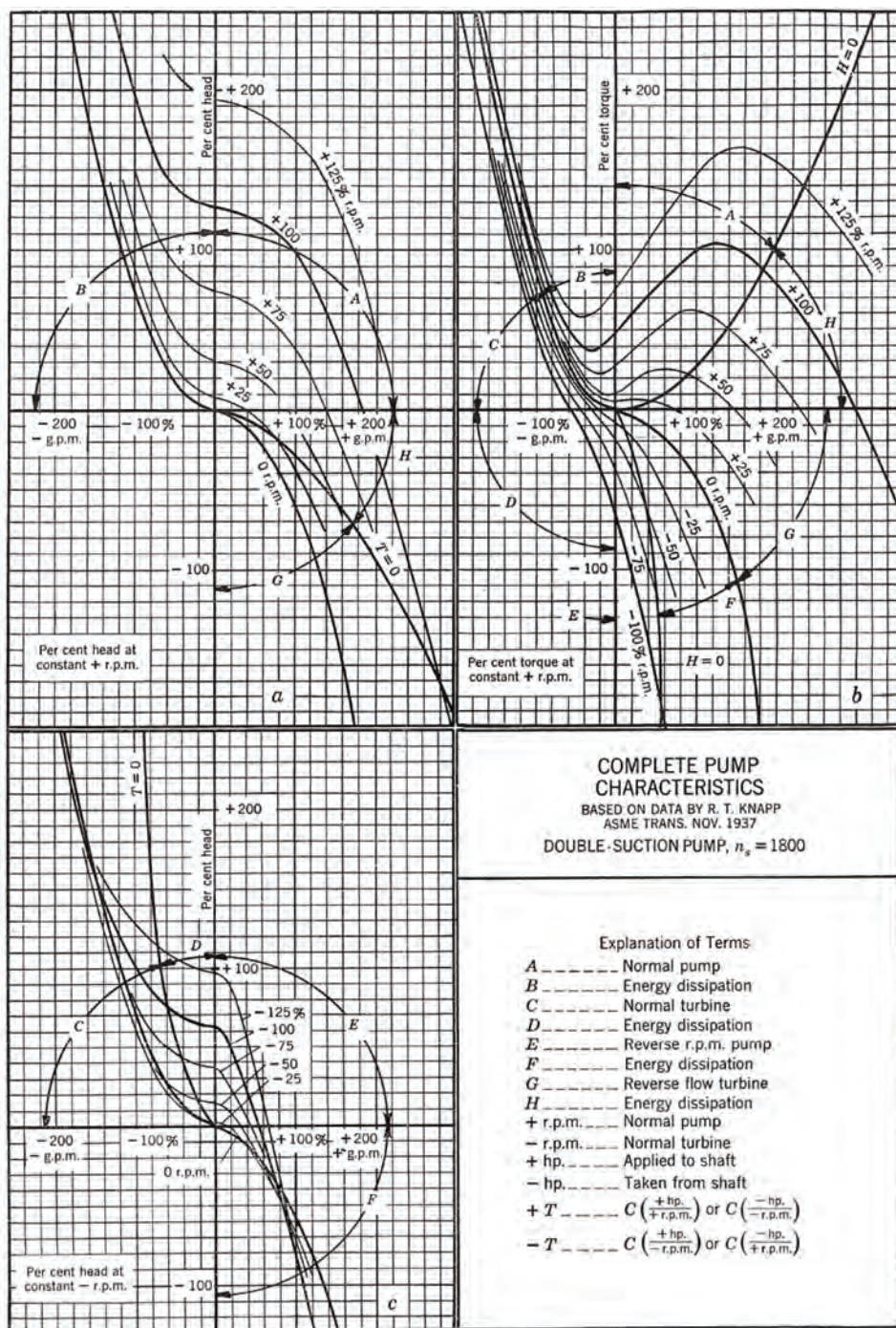


Figure 9-10. Complete four quadrant characteristics in the form of constant speed lines for a $N_s = 35$ (N_s ; gpm = 1800) double suction pump [23,24].

load on the mechanical seal faces will influence breakaway torque while the gland tightness will effect breakaway torque in the case of a packed stuffing box. Clearly, it is impossible to know a priori the exact value of a given pumps breakaway torque when installed in a varying environment such as on a pipeline service. Unless a pump is specifically designed to tolerate continuous slow roll operation the flow through a non-running (standby) pump must be less than the flow required to overcome the breakaway torque if damage to the pump and/or rotor is to be avoided.

The four quadrant charts described above comes very handy to estimate the minimum forward flow to overcome a pump breakaway torque. If the breakaway torque is assumed to be 10% of the pump BEP torque, for example, the intersection of -10% torque line with the x-axis of Fig. 9-9 will give the minimum flow to break-away, or to begin turning the pump impeller forward. For this particular pump, this minimum flow is shown to be 46% of the flow at the BEP. Conversely, the minimum flow to turn the pump backward can be estimated from the intersect of the $+10\%$ torque line with the x-axis of Fig. 9-9, which gives -38% of the flow at the BEP in this case.

The same procedure can be applied using the full characteristics of Fig. 9-10. Again, if the breakaway torque is assumed to be 10% of the pump BEP torque, the -10% torque, hence from Fig. 9-10, the corresponding forward flow at this torque and zero speed is again approximately $= 40\%$. Conversely, the minimum flow to turn the pump backward can be estimated from the same Figure, where the flow corresponding to $+10\%$ torque and zero speed is again approximately $= -38\%$.

Another example to illustrate the use of the full characteristics of a pump is in the case of deep-well pumps which have presented a number of problems related to reverse rotation when they stop. In a great majority of cases, the deep-well pumps used for irrigation lift water to the surface, and thus work predominantly against all static head. Every time the power is shut off, the pump is subjected to a full pump head and works as a turbine in a reverse direction at runaway speed and zero torque (if there is no check valve). By following the 100% head line of Fig. 9-9 from the first quadrant through the second and to the intersection with the zero torque line in the third quadrant, it is found that this particular pump will develop 117% reverse speed and 68% back flow through the pump.

9.6 WATER HAMMER, CAVITATION, AND COLUMN SEPARATION

9.6.1 Water Hammer

Water hammer (or, more generally, fluid hammer) is a pressure surge or wave caused by a sudden drop, a stop or a change in direction of the fluid velocity. It depends on the fluid compressibility, its density, and the magnitude of the change in the flow velocity. The magnitude of a pressure surge under a water hammer transient condition is expressed by Joukowsky's law:

$$H_{\text{water hammer}} = \frac{c_0 \Delta U}{g} \quad (9-39)$$

where U is the change in the mean flow velocity.

For this reason, pipe-sizing charts for some applications recommend flow velocity at or below 1 to 2 m/s. If the pipe is suddenly closed at the outlet (downstream), the mass of water before the closure is still moving forward with some velocity, building up a high pressure (water hammer). In domestic plumbing, this is experienced as a loud bang resembling

a hammering noise. Water hammer can cause pipelines to break if the pressure is high enough. Air traps, stand pipes (open at the top), surge vessels, or accumulators are sometimes added as dampers to liquid systems to provide a cushion to absorb the force of moving fluid in order to prevent damage to the system. Other means to protect the system from water hammer are:

1. One-way surge tower: An open-ended device, which is connected to the pipeline by a check valve. It allows liquid to enter the pipeline when the pipeline is subjected to vacuum pressures.
2. Non-return valves: These are often used on steeply rising pumping mains. They help to prevent the pipeline length of liquid falling back on the pump's check valve following pump stoppage.
3. Control valves: They are often fitted on pump discharges. They are opened and closed slowly to minimize fluid during pump stoppage and startup. They are not effective during a sudden pump stoppage.
4. Surge anticipator valves: They are fitted to a pump delivery. They are hydraulically activated control valves, which open when a pump stops and start to close as the pressure starts to build up when downsurge reaches the pump. The slow closure of the valve minimizes water hammer pressures.
5. Flywheel: An effective device attached to pumps for generally shorter pipeline lengths. They help to dampen surges by slowly decelerating the pump speed on pump stoppage.

On the other hand, when a valve in a pipe is closed, the fluid downstream of the valve will attempt to continue flowing, creating a vacuum that may cause the pipe to collapse or implode. This problem can be particularly acute if the pipe is on a downhill slope. To prevent this, air and vacuum relief valves, or air vents, are installed just downstream of the valve to allow air to enter the line and prevent this vacuum from occurring.

9.6.2 Cavitation and Column Separation

In the previous analysis, we assumed that the transient-state pressures throughout the system remained above the vapor pressure of the liquid. However, this is not always the case. In many low-head systems or systems in which transients are produced rapidly, the pressure may be reduced to or below the vapor pressure of the liquid. This may produce vapor cavities in the flow or may cause the liquid column to separate. Rejoining of the separated columns or collapse of the cavities results in a large pressure rise, which may damage the piping system.

The term “transient cavitation” is used herein to refer to the phenomenon of the formation and growth of cavities within a liquid due to reduction of transient-state pressures to the vapor pressure of the liquid. Depending upon the pipeline geometry and the velocity gradient, the cavity may become so large as to fill the entire cross section of the pipe. This is called column separation. The liquid is divided into two columns at the location of column separation (see Fig. 9-11).

Almost all industrial liquids and especially natural water contain a small gaseous phase either in the form of free bubbles or as nuclei adhering to or hidden in the fissures of solids. The solids may form a boundary containing the liquid, or they may be present as contaminants in the liquid. The nuclei grow in size when the liquid pressure is reduced to the vapor pressure and may become bubbles of sufficient size to act as nuclei for cavitation. The growth of a bubble depends upon the force acting on the bubble due to surface tension, the ambient liquid pressure, the vapor pressure of the liquid, the gas pressure inside the bubble,

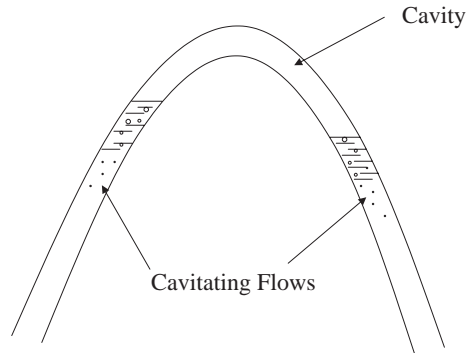


Figure 9-11. Column separation.

and the time-pressure history to which the bubble has been exposed. Furthermore, the molecules of free gases may enter the bubble, and two or more bubbles may coalesce to form a large cavity. The size of this cavity increases until the difference between its internal pressure and the decreasing external pressure is sufficient to offset the surface tension. Once this critical size is reached, the vapor-filled cavity becomes unstable and expands explosively. This hypothesized sequence of events, i.e., from the pressure reduction to the onset of explosive cavitation, occurs in a very short time period, probably in a few milliseconds.

Depending upon the system geometry and the velocity gradient, the cavity may become so large as to fill the entire cross section of the pipe and thus divide the liquid into two columns. This usually occurs in vertical pipes, pipes having steep slopes, or pipes having “knees” in their profile. Experimental investigations (citations 2-6 in ref. [2]) have shown that bubbles are dispersed in the pipeline over a considerable distance on either side of the location of the column separation.

In horizontal pipes or pipes having mild slopes, a thin cavity confining to the top of the pipe and extending over a long distance may be formed. In addition, in this case, cavitation bubbles are produced over a considerable length of the pipe. Such a flow is referred to as cavitating flow. The low pressures that may lead to column separation or cavitating flows are produced by negative or rarefaction waves. These waves are reflected as positive waves from various boundaries (e.g., a reservoir) in the system, and compress the bubbles in the cavitation-flow region and progressively reduce the size of the cavity where column separation had occurred. When the cavities collapse or when the separated columns rejoin, very high pressures are produced. These pressures may burst the pipe if they are not allowed for in the design.

The pressure inside a cavity is equal to the sum of the partial pressures of the liquid vapors and the released gases. If the temperature of the liquid is assumed constant, the partial pressure of the liquid vapors is constant. The partial pressure of the gases can, however, increase or decrease if their mole fraction in the cavity increases or decreases. A good review paper on column separation is by Bergant et al. [22].

9.6.3 Steam Condensation-Induced Water Hammer

A condensation induced water hammer is a rapid condensation event. It could also be aptly termed a “rapid steam bubble collapse.” It occurs when a steam pocket becomes totally entrapped in subcooled condensate. As the steam gives up its heat to the surrounding condensate and pipe walls, steam changes from a vapor to a liquid state. As a liquid, the volume formerly occupied by the steam shrinks by a factor of from several hundred to over

a thousand, depending on the saturated steam pressure. Likewise, the pressure in the void drops to the saturated vapor pressure of the surrounding condensate (e.g., the saturated vapor pressure of condensate at ambient temperature is less than 1 psia). This leaves a low pressure void in the space formerly occupied by the steam that the surrounding condensate, under steam pressure itself, will rush in to fill. The resulting collision of condensate generates an overpressurization, which reverberates throughout the condensate filled portion of the pipe (Fig. 9-12).

The specific factors which influence the severity of a condensation-induced waterhammer are: (1) the steam pressure, (2) the degree of condensate subcooling, (3) the presence of non-condensables left over in the void, and (4) the size of the void. If the steam pressure is high, the condensate is subcooled, non-condensables are absent, and the void is large enough for a slug to pick up some velocity, the overpressure resulting from an event can easily exceed 1000 psi. This is enough pressure to fracture a cast iron valve, blow out a steam gasket, or burst an accordion type expansion joint, and, in fact, failure of each of these components in separate condensation induced waterhammer accidents has resulted in operator fatalities.

Good design and operating practice aim to avoid mixing high pressure steam and excess condensate by making sure steam mains are properly trapped and live steam is kept out of condensate return systems. Nevertheless, it does happen. Condensate lines, for instance, are often heard to pop and bang when steam squirts into them through traps. Why don't the collapsing steam bubbles destroy condensate pipes? They can, over time. But the shock waves generated are not catastrophic because the pressure in a condensate system is generally low—on the order of just a few psi, subcooling is not great, and the steam bubbles are small. Of course, high pressure steam can contact subcooled

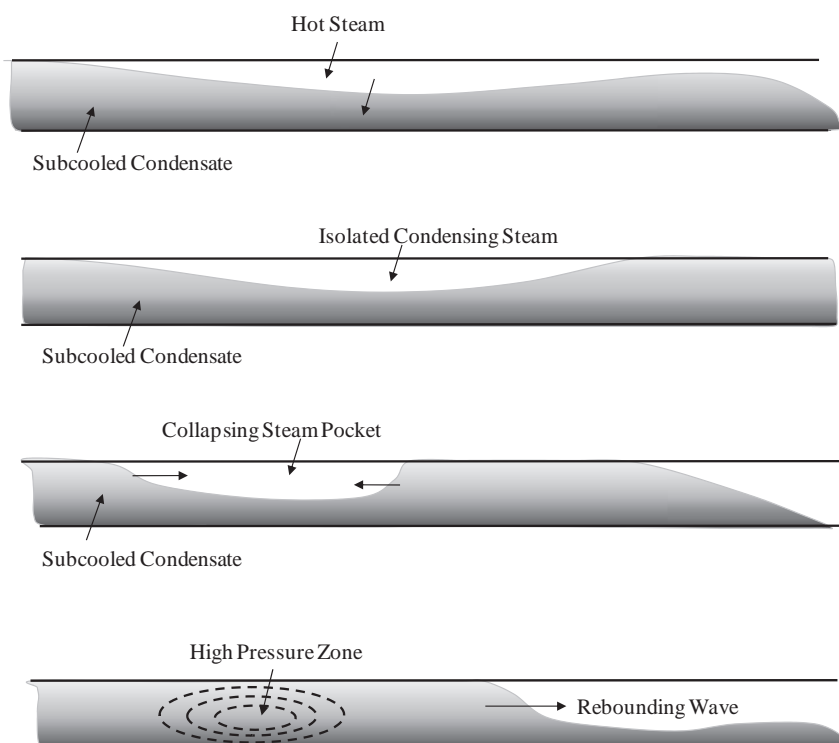


Figure 9-12. Steam entrapment and slug formation in a horizontal pipe [6].

condensate in steam lines when something goes wrong—for example, when a trap assembly becomes plugged with scale causing a drip leg to fill with condensate. A steam bubble must become entrapped for there to be a collapse. In a vertical pipe such as a drip leg where steam is above the condensate, it is difficult to entrap the steam because natural buoyancy tends to keep the two fluids separate. In fact, research experiments show that it is difficult to entrap a steam void in any pipe sloped downward in the direction of steam flow more than 1/2 in. in 1.0 ft. At slopes less than this, however, and in upwardly sloped pipes, it is a different story.

9.7 EXAMPLES AND CASE STUDIES

9.7.1 Styrene Transfer System

A styrene monomer transfer system consists of approximately 160 meters of mostly 8-in. pipe from two tanks (T810/T811) upstream, through two centrifugal pumps (P802A/B), a spill-back loop (3 in.) and a discharge line of approximately 565 m of mostly 4-in. line, to tank (V105) downstream. There are small sections of 6 and 4 in. along the way. Detailed isometric schematic of the system showing elevation changes and axial length is given in Figs. 9-13 and 9-14. Steady-state hydraulic analysis determined the size of an R.O. (diameter ratio, $\phi = 0.479$) on the pump discharge and another R.O. ($\phi = 0.3$) on the spill-back line. In addition, a level control valve (LCV) would have to be throttled to approximately 62.2%, while a shutdown valve (SDV) is fully open, or SDV throttled to 32.6% while LCV is fully open. Dynamic analysis was performed on this system to determine the level of surge pressures at key points along the system following closure of the LCV from initial position of 62.2% open to fully closed position and to evaluate the system transient response following a sudden pump shutdown.

Relevant properties of styrene, and pipe internal diameters, wall thicknesses, and corresponding speed of sound taken into account pipe material bulk modulus of elasticity of 207 GPA is given in Table 9-4. Pump forward flow characteristics is given in Fig. 9-15. Based on the rated value of $H = 37.5$ m, $Q = 0.015998$ m³/s, and speed = 2920 rpm, this pump has a specific speed $N_s = 24.37$ (SI units; see Equation 9-32). The full characteristic of the pump in the four quadrants was taken from Table 9-3 corresponding to $N_s = 25$ being close to the calculated value. LCV valve characteristics are given in Fig. 9-16.

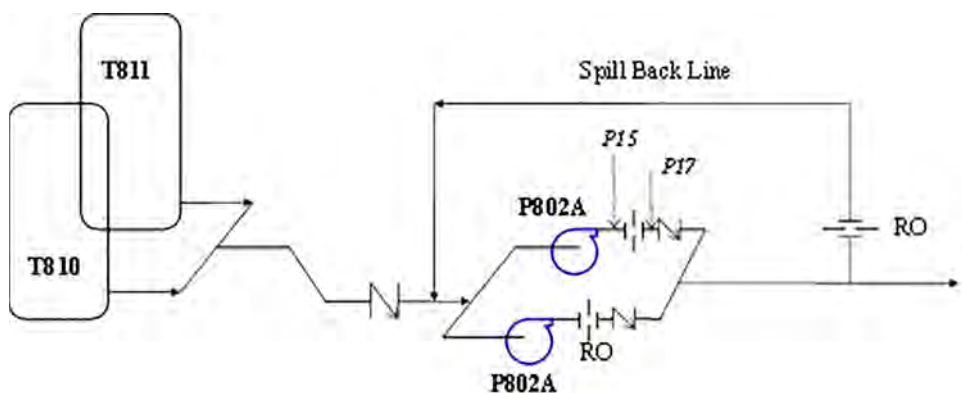


Figure 9-13. Isometric schematic of the piping system from T810/811 to pumps P802A/B.

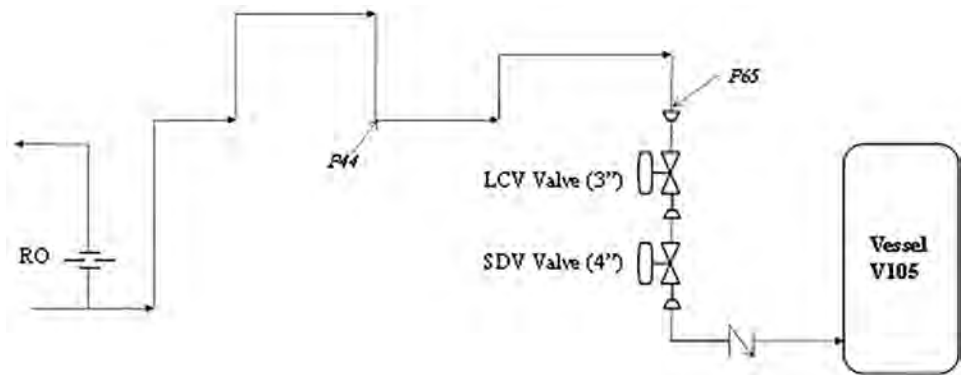


Figure 9-14. Isometric schematic of the piping system from pumps P802A/B to V105.

Table 9-4. Styrene and piping properties

Density	905	kg/m ³
Speed of sound	1318	m/s
Viscosity	8.00E-04	Pa·s
Bulk modulus	1.57E+09	Pa
Pipe roughness	4.50E-05	m

ID (mm)	WT (mm)	c (m/s)
202.7	8.18	1209.132
154.1	7.11	1221.316
102.3	6.02	1240.391
77.9	5.49	1252.256

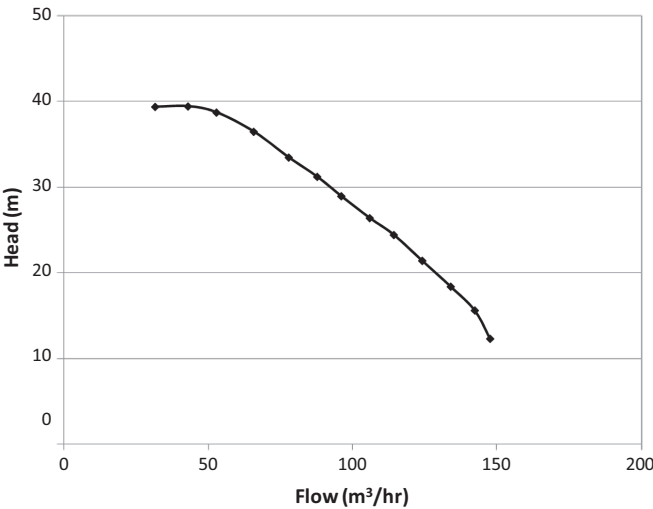


Figure 9-15. P802A/B pump characteristics.

A transient hydraulic model was composed on the ping elements, elevation changes, and interconnections with fittings, R.O.'s, spill-back loop, and valves. A steady-state simulation was first established prior to initiation of any upsets (e.g., valve closure or pump shutdown). The resulting total piezometric head (static pressure head + elevation) of the system is shown in Fig. 9-17. Notice that most of the pump-developed head is taken by the

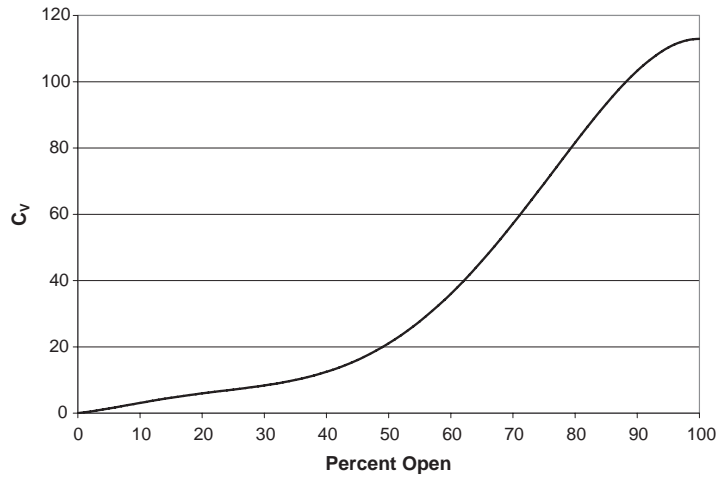


Figure 9-16. LCV valve characteristics.

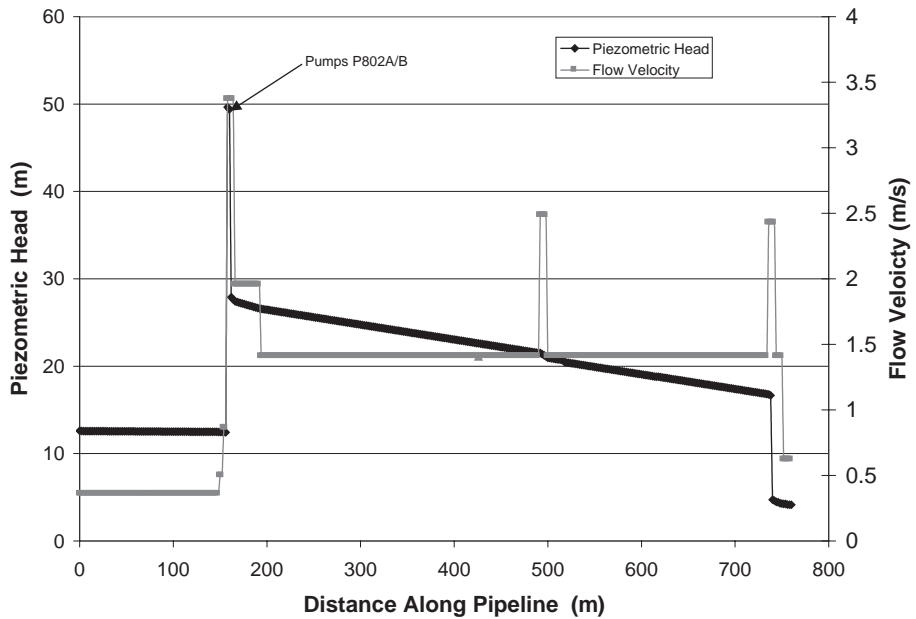


Figure 9-17. Piezometric head and flow velocities along the transfer line system from t810/811 tanks to V105 tank.

pump R.O. and, the valves, upstream of tank V105. The suction head loss is minimal (due to the large pipe) and that on the discharge side is approximately 10 m of head loss.

The steady-state flows are as follows:

- forward flow = 41.3 m³/hr
- spill-back flow = 16.2 m³/hr
- total pump flow = 57.5 m³/hr
- pump differential head = 37.5 m.

The corresponding steady state mean flow velocity along the transfer system is also shown in Fig. 9-17.

Transient hydraulic simulations were performed corresponding different LCV valve closure times. Results of each simulation are shown in terms of the absolute pressure at key points identified on the isometrics of Figs. 9-13 and 9-14. Also reported are pump flow, forward flow, spill-back flow, and pump break torque. The criterion for evaluating a safe valve-closing scenario is based on maximum static pressure at any point in the system not exceeding the rated pressure of the pipe, which is 1900 kPa-g.

Figure 9-18 shows the results of the first simulation of LCV valve closing in short time (0.1 seconds) from a steady state condition where this valve was 62% open to fully closed, while SDV was kept open at 100% open position. Clearly, the results indicate that maximum pressure reached at locations upstream the valve exhibits values higher than 1900 kPa-g. Figure 9-19 shows the pump flow, head and torque conditions during this valve closure event.

In order to alleviate this problem of the surge pressure exceeding the pipe rated pressure, LCV valve must be closed in a slower rate. Figure 9-20 shows similar results when LCV closes in 1.0 second instead of 0.1 seconds. Again, high surge pressures were reached indicating that further slower valve closure is required. Figure 9-21 shows the results of closing LCV valve in 2 seconds. Here, it is shown that surge pressure at the critical locations identified are below the pipe rating pressure, and hence, the 2.0 seconds closing time is selected to be minimum closing time for the LCV to close from its 62% open position to fully closed position.

With regard to the same steady-state scenario, further series of surge simulations were conducted to determine the safe closing time for the SDV valve from the 100% open to fully close, while LCV remains at 62% open position. Results indicates that, for this scenario, the minimum closing time for the SDV valve to close from 100% open to fully closed position is 5.0 seconds.

Simulation of a pump shutdown scenario was also performed. Here, it was assumed that the shaft motor torque winds down from steady-state value of 35.0 N·m to zero in 1.0 second. Motor/coupling/pump impeller combined inertia was estimated (from Equations 36 and 37) to be approximately 0.0493 kg·m² based on rated pump power of 11.25 kW and rated speed of 2920 rpm (more accurate information were not available as these pumps were purchased in the 70s). Results of the shutdown are shown in Figs. 9-22 and 9-23. The level of surge pressure reached is very low due to lower initial velocity in the upstream (suction) side of the pump. Therefore, it was concluded that there is no issue associated with pump shutdown in this system.

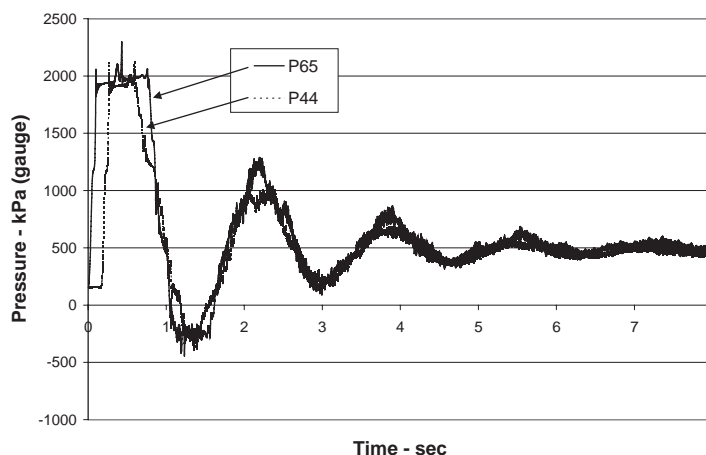


Figure 9-18. Pressure surges following valve LCV closure in 0.1 seconds.

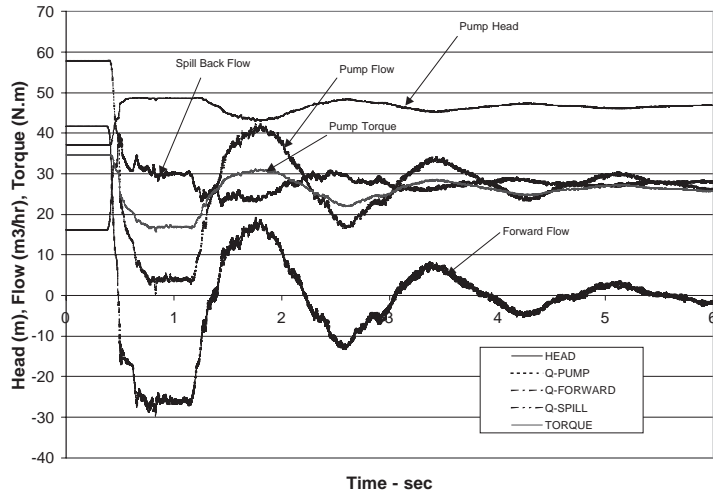


Figure 9-19. Corresponding pump head, flow and torque condition following valve LCV closure in 0.1 seconds.

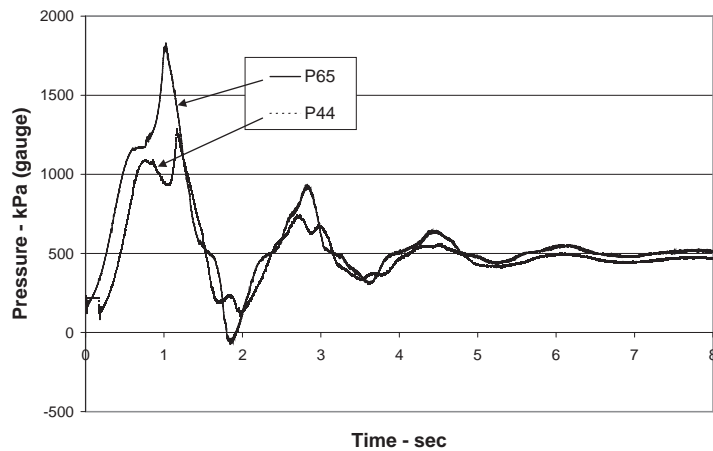


Figure 9-20. Pressure surges following valve LCV closure in 1.0 second.

9.7.2 Ethylene Pump

A 12-stage ethylene pump is employed in an ethylene manufacturing plant to increase the pressure from the produced ethylene from 1350 kPag in the storage drums to a pipeline pressure of 9000 kPag. Once pressurized, the ethylene will undergo cooling through two heat exchangers in series as shown schematically in Fig. 9-24. The pump rated parameters are $H_r = 138.3$ m, $N_r = 4000$ rpm, $Q_r = 0.0305$ m³/s and $T_r = 751.92$ N.m. The specific speed for this pump N_s (SI) = 17.33, and hence the full four quadrant characteristics of $N_s = 25$ in Figs. 9-5 and 9-6 can be used as an approximation. The pump is driven by a steam turbine.

In order to minimize the amount of ethylene spills in the event of pipe ruptures, three emergency block valves (EBV) were employed at respective locations shown in Fig. 9-24. In the event of pipe rupture, the steam turbine is turned off with a known torque decrease from full to zero torque in 1 s. All three EBV are equipped with a motor operator which

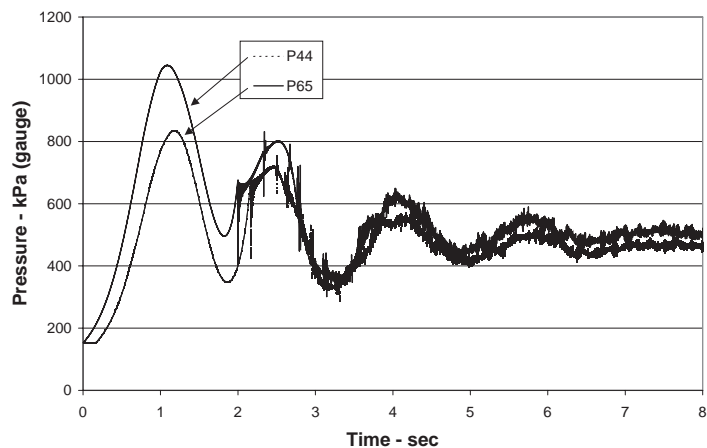


Figure 9-21. Pressure surges following valve LCV closure in 2.0 seconds.

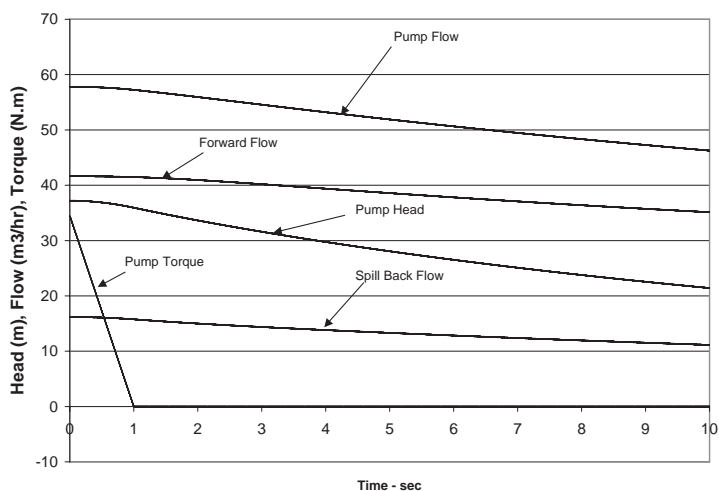


Figure 9-22. Pump head, flow and torque condition following pump shutdown.

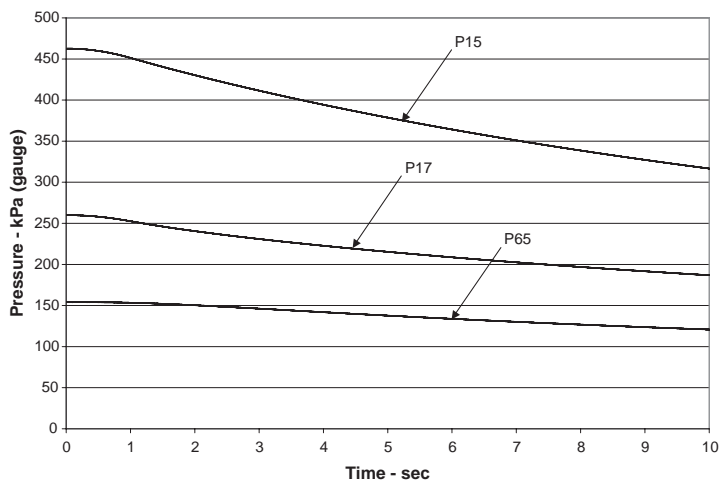


Figure 9-23. Example of static pressures at three identified locations following pump shutdown.

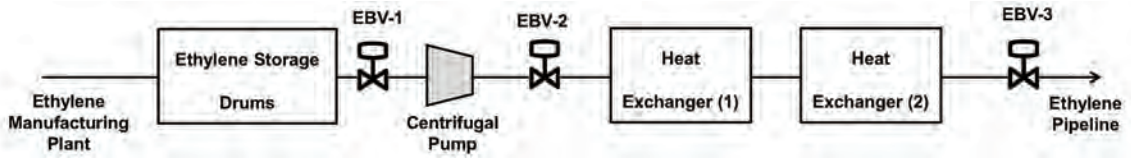


Figure 9-24. Schematic of the ethylene pumping system.

control the closing time from full open to full close in 12 s so as not to create a potential pressure spike if they are closed quickly. The steady state flow of ethylene through pump is $90 \text{ m}^3/\text{hr}$ at pump speed = 4000 rpm. Ethylene density is approximately $= 440 \text{ kg/m}^3$, and speed of sound in the piping system $= 520 \text{ m/s}$. The combined total inertia of the pump, coupling and steam turbine driver is $1.71 \text{ kg}\cdot\text{m}^2$.

A dynamic simulation was conducted based on the methodology described in this chapter, pump full characteristics corresponding to $N_s = 25$ and flow conditions provided above. The main concern is to determine if the pump will be subjected to reverse flow and reverse rotation in the event of an emergency shutdown of the system and if a check valve is not employed on the pump discharge side. The results are shown in indicative plots in Fig. 9-25. It is shown that the pressures across the pump equalize (i.e. head decreases to zero) in approximately 15 s, during which pump undergoes reverse flow and reverse rotation at the 1 s mark, until all three EBV valves are completely closed. The H - Q trajectory during this period is shown in Fig. 9-26. The period from 1 s onwards is characterized with $+H$, $-Q$ and $-N$ which follows $T = 0$ line in the third quadrant of Fig. 9-9 with the torque changes from positive to negative (crossing $T = 0$ in Fig. 9-9) due to the inertial of the pump/driver. This demonstrates the importance of having a check valve installed on the discharge side of the

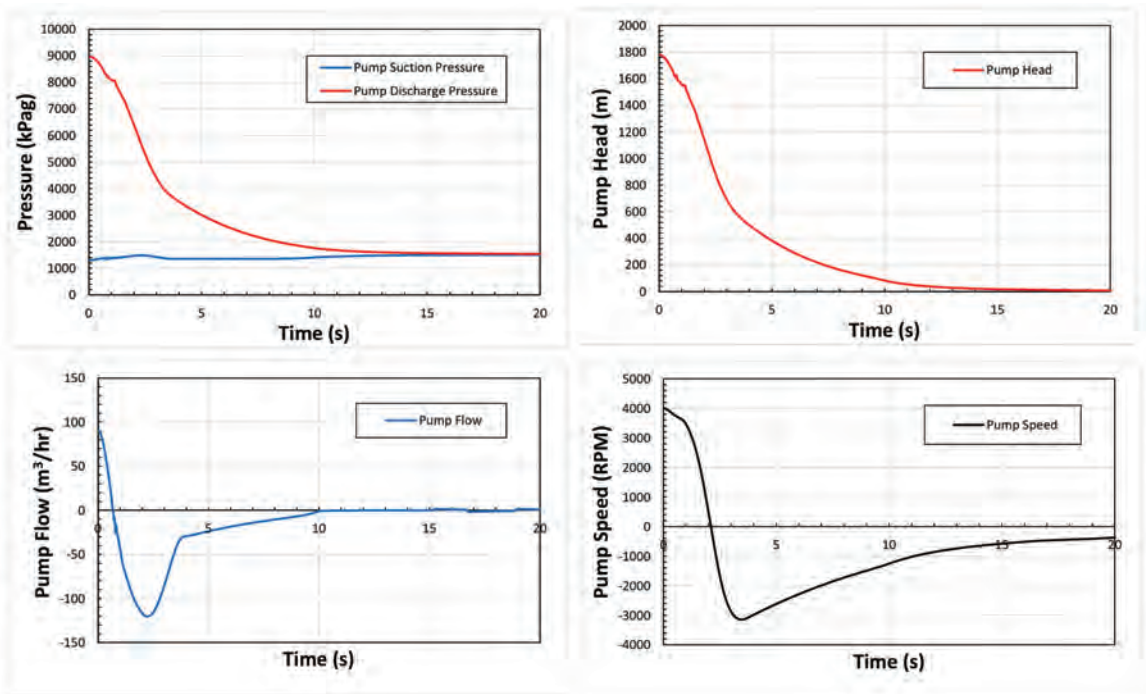


Figure 9-25. Results of a dynamic simulation of a pump shutdown and EBV valve closure of the system in Fig. 9-24.

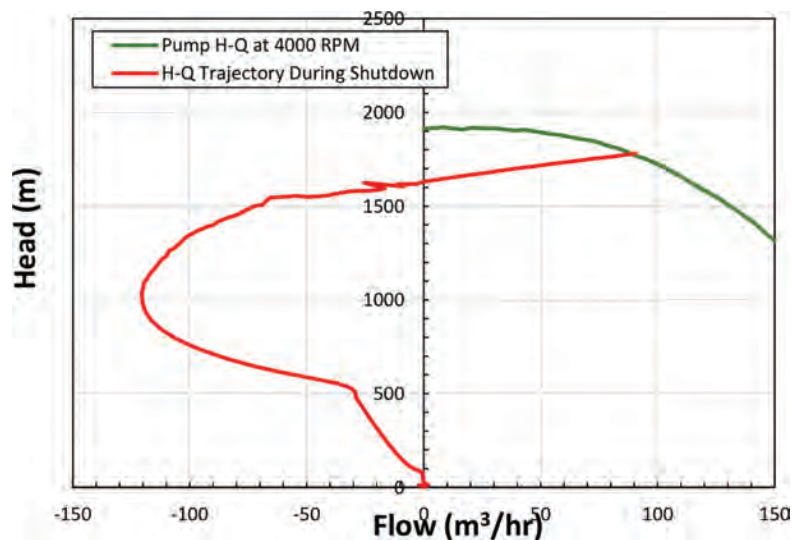


Figure 9-26. Head-flow trajectory of a pump shutdown and EBV valve closure of the system in Fig. 9-24.

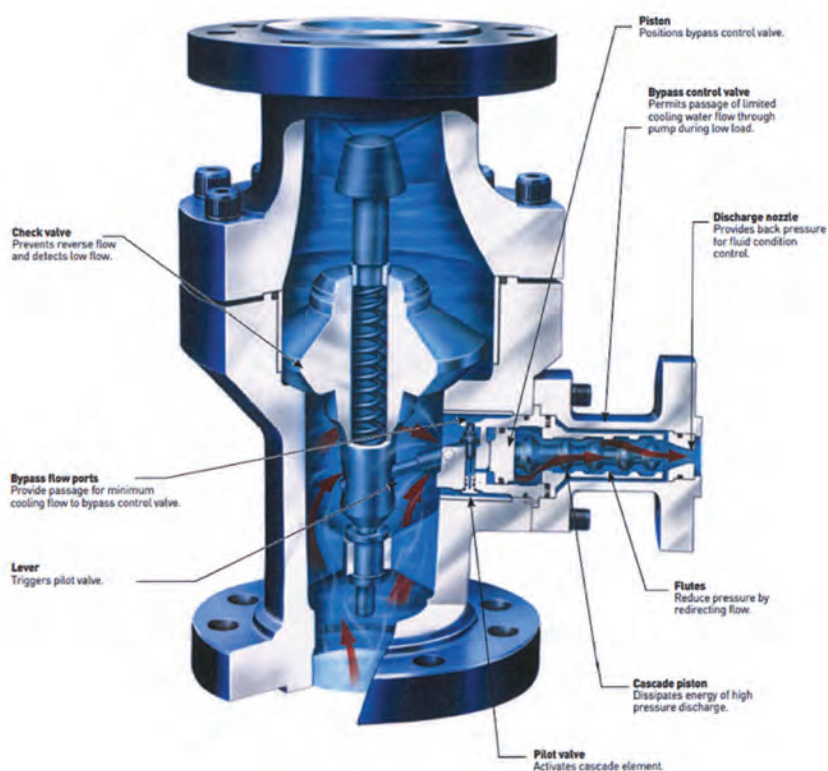


Figure 9-27. An example design of minimum-flow check valves.

pump, which is a common practice in most installation. In some cases, these check valves are equipped with a side port to allow for a spill-back flow from the discharge side to the suction side around the pump, as shown in the example design of Fig. 9-27. In this design as the check valve closes, a link is devised to open the side port to allow for the spill-back flow around the pump. When the check valve is fully open, the mechanism closes this port and stops the back-spill flow. Therefore, this check valve also serves as a minimum flow valve, hence it is often called min-flow check valve. Also, note that the remaining reverse rotational speed after 20 s will eventually wind-down to zero speed due to friction and hydrodynamic losses.

REFERENCES

- [1] Wylie, E. B., and Streeter, V. L., 1982. *Fluid Transients*, FEB Press, Ann Arbor, Michigan.
- [2] Chaudry, M. H., 1979. *Applied Hydraulic Transients*, Van Nostrand Reinhold Company, New York.
- [3] Miller, D. S., 1990. *Internal Flow Systems*, 2nd ed., Chapter 8, Gulf Publishing Company.
- [4] Method of characteristics.
- [5] Marchal, M., Flesh, G. and Suter, P., Nov. 1965. "The Calculation of Waterhammer Problems by Means of the Digital Computer", *Proc. Int. Symp. Waterhammer Pump Storage Projects*, ASME, Chicago.
- [6] Kirsner, W., January 1998. "Steam Condensation Induced Waterhammer," *HPAC*.
- [7] Bergant, A., Simpson, A. R., 1999. "Pipeline Column Separation Flow Regimes," *Journal of Hydraulic Engineering*, **125**(8), pp. 835–848.
- [8] Fan, D., Tijsseling, A., 1992. "Fluid Structure Interaction With Cavitation in Transient Pipe Flows," *ASME. Journal of Fluids Engineering*, **114**(6), pp. 268–274.
- [9] Kot, C. D., Youndahl, C. K., 1978. "Transient Cavitating Effects in Fluid Piping Systems," *Nuclear Engrg. and Des.*, **45**(1), pp. 93–100.
- [10] Kronenburg, C., 1974. "Gas Release During Transient Cavitation in Pipes," *Journal of Fluids Div. ASCE.*, **100**(10), pp. 1383–1398.
- [11] Mitosek, M., 1997. "Study Of Cavitation Due to Water Hammer in Plastics Pipes," *Plastics, Rubber and Composites Processing and Applications*, **26**(7), pp. 324–329.
- [12] Mitosek, M., 2000. "Study of Transient Vapor Cavitation in Series Pipe Systems," *Journal of Hydraulic Engineering. ASCE.*, **126**(12), pp. 904–911.
- [13] Mitosek, M., 2001. *Mechanika plynów w inżynierii i ochronie środowiska*, PWN, Warszawa.
- [14] Rybak-Wilusz, E., 2001. "Zjawisko kawitacji w przewodach warunkach nieustalonego przepływu wody," Ph.D. thesis, Warsaw University of Technology.
- [15] Thorley, A. R. D., 1991. *FLUID TRANSIENTS PIPELINE SYSTEMS - A Guide to the Control and Suppression of Fluid Transients in Liquids in Closed Conduits*, D. & L. George Ltd.
- [16] Faithfull, E. M., 1989. "Surge Analysis," *M.Sc. thesis*, The University of Newcastle upon Tyne.
- [17] Linton, P., 1972. "Note on Pressure Surge Calculations by The Graphical Method—Pump Stoppage After Power Failure," 3rd ed., BHRA Technical Note TN447.
- [18] Simpson, A. R., Wylie, E. B., 1991. "Large water hammer pressures for column separation in pipelines," *Journal of Hydraulic Engineering. ASCE.*, **117**(10), pp. 1310–1316.
- [19] Simpson, A. R., Bergant, A., 1994. "Numerical comparison of pipe column separation models," *Journal of Hydraulic Engineering. ASCE.*, **120**(3), pp. 361–377.
- [20] Shima, A., 1997. "Studies on bubble dynamics. Shock Waves," Springer Verlag, **7**, pp. 33–42.
- [21] Wylie, E. B., Streeter, V. L., Suo, L., 1993. *Fluid Transients in Systems*, Prentice-Hall, Inc., Upper Saddle River, New York.
- [22] Bergant, A., Simpson, A. R., Tijsseling, A. S., 2004. "Water hammer with column separation: a review of research in the twentieth century," *RANA Report No. 04-34*, Technische Universiteit Eindhoven, Eindhoven, pp. 88.
- [23] Stepanoff, A. J., 1957. *Centrifugal and Axial Flow Pumps, Theory, Design, and Application*. John Wiley & Sons, New York.

- [24] Knapp, R. T., 1937. "Complete Characteristics of Centrifugal Pumps and Their Use in the Prediction of Transient Behaviour", *Trans. ASME* pp. 683–689, November 1937.
- [25] Gülich, J. F., 2010. *Centrifugal Pumps*. Second Edition, Springer, New York.

OTHER BIBLIOGRAPHY

- [26] Bergeron, L., 1961. *Waterhammer in Hydraulics and Wave Surges in Electricity*, John Wilye & Sons, Inc., New York.
- [27] Siemons, J., 1967. "The phenomenon of cavitation in a horizontal pipeline due to a sudden pump failure," *Journal of Hydraulic Research*, **5**(2), pp. 135–152.
- [28] Kalkwijk, J. P. Th., & Kranenburg, C., 1973. "Cavitation in horizontal pipelines due to water hammer," *ASCE Journal of the Hydraulics Division*, **99**(HY3), pp. 529–530.
- [29] Wylie, E. B., 1984. "Simulation of vaporous and gaseous cavitation," *Journal of Fluids Engineering*, **106**, pp. 307–311.
- [30] Bergant, A., & Tijsseling, A., 2001. "Parameters affecting water hammer wave attenuation, shape and timing," *10th Int. Meeting of the Work Group on the Behaviour of Hydraulic Machinery Under Steady Oscillatory Conditions*, Trondheim, Norway.
- [31] Shu, J. J., 2003. "Modelling vaporous cavitation on fluid transients," *International Journal of Pressure Vessels and Piping*, **80**(3), pp. 187–195.
- [32] Kranenburg, C., 1974. "Gas release during transient cavitation in pipes," *Journal of the Hydraulics Division, ASCE*, **100**(HY10), pp. 1383–1398.
- [33] Anderson, A., Sandoval-Pena, R., & Arfaie, M., 1991. "Column separation behaviour modes in a simple test rig," *9th Round Table of the IAHR Group, Int. Meeting on Hydraulic Transients with Water Column Separation*, Valencia, pp. 33–50.
- [34] Tijsseling, A. S., & Lavooij, C. S. W., 1990. "Water hammer with fluid–structure interaction," *Applied Scientific Research*, Kluwer Academic Publishers, **47**, pp. 273–285.
- [35] Courant, R., & Friederichs, K. O., 1948. *Supersonic Flow and Shockwaves*, Interscience Publishers Inc., New York.
- [36] Hadj-Taïeb, E., & Thirriot, C., 1988. "Cavitation à bulles de vapeur," *1st Int. Conf. on Computer Methods and Water Resources*, Computational Hydraulics, Rabat, Morocco, **2**, pp. 73–180.
- [37] Hadj-Taïeb, E., & Khabou, M. T., 1993. "Mathematical modelling of bubbly cavitating flow in water supply pipelines," in B. Coullbeck, ed., *Integrated Computer Applications in Water Supply*, 1 (Taunton (Somerset), UK: Research Studies Press Ltd.), pp. 123–138.
- [38] Hadj-Taïeb, E., and Lili, T., 2001. "Les écoulements transitoires dans les conduites déformables avec dégazage de l'air dissous," *La Houille Blanche*, **5**, pp. 99–107.
- [39] Hadj-Taïeb, E., & Lili, T., 1996. "Transients in Flexible Pipes With Gas Release," *7th Int. Conf. on Pressure Surges and Fluid Transients in Pipelines and Open Channels*, Harrogate.
- [40] Stuckenbruck, S., Wiggert, D. C., & Otwell, R. S., 1985. "The Influence of Pipe Motion on Acoustic Wave Propagation," *Transactions of the ASME*, **107**, pp. 518–522.
- [41] Lax, P. D., & B. Wendro, A., 1966. "Difference Schemes For Hyperbolic Equations With High Order of Accuracy," *Communications on Pure Applied Mathematics*, **17**, pp. 381–398.
- [42] Peyret, R., & Taylor, T. D., 1982. *Computational Methods for Fluid Flow*, Springer-Verlag, New York Heidelberg Berlin.
- [43] Hadj-Tareb, E., & Lili, T., 1999. "The Numerical Solution of The Transient Two-Phase Flow In Rigid Pipelines," *International Journal for Numerical Methods in Fluids*, **29**, pp. 501–514.
- [44] Hadj-Tareb, E., & Lili, T., 1998. "Transients Flow of Homogeneous Gas–Liquid Mixtures In Pipeline," *International Journal of Numerical Methods for Heat and Fluid Flow*, **8**(3), pp. 350–368.
- [45] Martin, C. S., 1983. "Experimental Investigation of Column Separation With Rapid Closure of Downstream Valve," *Proc. 4th Int. Conference on Pressure Surges, Bath*, **B3**, pp. 77–88.
- [46] Sanada, K., Kitagawa, A., & Takenaka, T., 1990. "A Study on Analytical Methods by Classification Of Column Separations in Water Pipeline," *Transactions of the Japan. Society of Mechanical Engineers, Series B*, **56**(523), pp. 585–593 (in Japanese).

DYNAMICS OF CENTRIFUGAL COMPRESSION SYSTEMS

10.1 INTRODUCTION

Compression systems employed in gas processing plants and in gas pipeline transmission systems provide vital function to the overall operation of both systems, and therefore, must be vigilantly attended to in order to ensure a high level of operational reliability. The majority of these compression systems employ centrifugal compressors, either single- or multi-staged, driven by either gas turbines or electric motors with/without gearboxes. These compression systems are required to not only withstand uninterrupted operation for extended periods of time but also be able to cope with flow and pressure transients associated with surge control, startup and emergency shutdown (ESD) [1–8]. During these transients, the centrifugal compressors interact dynamically with system components around them, i.e. piping, fittings and equipment, drivers, as well as the associated control protocols. Fluid inertias and compressor/driver rotor inertias play an important role in either stabilizing or destabilizing the system dynamics [9]. The compressors' performance characteristics have also an important role in the system dynamics behaviour [10]. Ensuring reliable and safe operation of the various aspects of these compression systems requires a good understanding of their dynamic behavior, which enables sound system design, operation and control.

Several experimental and numerical investigations aimed at analyzing the dynamic interactions that take place between compression system components, particularly during ESD, have been reported, e.g. [11–13]. In these investigations, the surge model proposed by Greitzer and Moore [14,15] has been extended to centrifugal compressors. The method of characteristics for the solution of the governing one-dimensional equations of gas flow [16] has been proven to be adequate and correlates well with field measurements [10].

Furthermore, the recycle system around the compressor unit in any compression system is an essential component in the operation of the centrifugal compressor. It is necessary for startup, shutdown, surge protection and flow control (turndown capability). As these operations are transient in nature, all dynamic parameters of gas flow, equipment and control, play an important role and those impact on the system instabilities, performance and safety. For example, parameters that affect the potential for the compressor to undergo surge during ESD are the recycle valve characteristics such as maximum capacity, flow vs. opening characteristics, opening delay (i.e. the time between valve open solenoid drop out and the start of the stem movement on the valve – often called 'pre-stroke' delay), and valve travel time (i.e. the time taken for the valve to travel from closed to open positions – often called 'stroke' time) [11,12]. Additionally, timing of the compressor ESD signal, the fuel gas shutoff signal, fuel gas manifold size (in case of gas turbine drivers), power train inertias, and compressor aerodynamic characteristics close to surge point, all contribute to the complexity of the problem [9,10].

This chapter addresses these issues and attempts to quantify the effects of the aforementioned parameters on the potential for the compressor to undergo surge, specifically upon ESD, which is considered the fastest expected transient to occur in any compression

system involving centrifugal compressors. The chapter first presents the general dynamics of a simple system to demonstrate that it is akin to a second order dynamical system and, hence, is prone to both static and dynamic instabilities. Treatment of a more complex geometry compression system is then described along with the pertinent governing equations describing the dynamic response of each sub element in the system. Solution techniques, based on the method of characteristics to solve the resulting one-dimensional set of equations describing the gas dynamics, are briefly outlined followed by assessment of how the various parameters affect the system instabilities. A new dimensionless parameter called “Inertia number” is introduced, which gives a quick assessment criterion to indicate the stability/instability threshold of any given compression system under consideration. Data are drawn from a number of compressor stations of various systems, compressors and driver types. An example is presented to illustrate the concept of instabilities.

Gas and equipment dynamic interactions of other elements employed in compression systems, such as check valves, relief valves, blowdown systems, will also be analyzed and discussed. This leads to the last three Sections, which discuss the basis for mechanical stress analysis, thermal analysis and suction and by-pass valve design and selection criteria.

10.2 FUNDAMENTALS OF DYNAMIC INSTABILITIES OF COMPRESSION SYSTEMS

10.2.1 Simple Compression Systems

Consider the simple compression system shown in Fig. 10-1, which is composed of a centrifugal compressor (between nodes 1 and 2), followed by a pipe element of length (L) and cross sectional area (A), a vessel of a volume (V) (between nodes 3 and 4), and a flow resistance element represented by a throttling valve (between nodes 4 and 5). For simplicity we will assume that the compressor suction (node 1) and the downstream discharge (node 5) are both maintained at the same and constant pressure.

The pressure (or enthalpy) rise across the compressor is given by the characteristic performance curve (Fig. 10-2a), while the pressure drop across the resistance element is given by the characteristics shown in Fig. 10-2b, both in terms of the respective mass flow rate, \dot{m} . The slope of the compressor characteristics at any given \dot{m} is noted as C , while the slope of the resistance element at any given \dot{m} is noted as S .

Cumpsty [17] derived the perturbation equations for each of the four elements of this simple compression system, namely the compressor, the duct (or pipe), the plenum (capacitance element or a vessel), and the end-throttling device (valve). He arrived at a single second-order ordinary differential equation (ODE), written here in terms of z , which could be any one of the pressure perturbations (p_i) or the mass flow perturbation (\dot{m}_i).

$$\frac{LV}{A^2 a} \frac{d^2 z}{dt^2} + \left(\frac{L}{A} - \frac{CSV}{a^2} \right) \frac{dz}{dt} + (S - C)z = 0 \quad (10-1)$$

where, a is the speed of sound in the medium fluid. The stability of this system may be analyzed by examining the coefficients of z and the first derivative dz/dt , in the third and

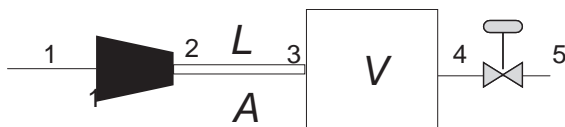


Figure 10-1. Simple compression system.

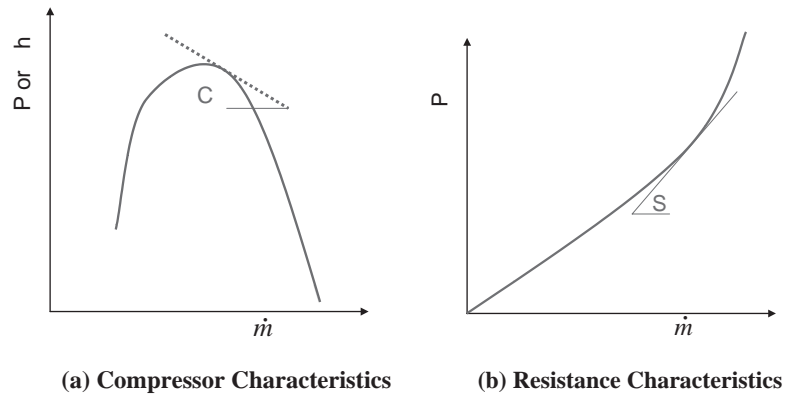


Figure 10-2. Compressor and resistance characteristics.

second terms in the above equation, respectively. If the coefficient of z becomes negative, that is:

$$(S - C) < 0 \text{ or } C > S \quad (10-2)$$

the system is said to be *statically unstable*, analogous to a spring-mass system in which the spring has a negative rate. Equation (10-2) suggests that the above compression system will be statically stable if the slope of the system resistance characteristic (S) is higher than the slope of the compressor characteristic (C). If, however, the slope of S is lower than that of C , the system will be statically unstable and will attempt to move to the nearest operating point which satisfies the statically stable condition. Figure 10-3 illustrates the various statically stable/unstable scenarios of such a system. Points 1, 2, 3 and 4, which are at the intersection between the compressor characteristic and resistance curves are said to be statically stable. Point 4 defines the limit of a statically stable system. Point 5, though it is a solution of the system of equations describing the system, is characterized by being statically unstable. The system cannot stay operating at this point, and will immediately jump to point 3 which is statically stable where the condition $S > C$ is satisfied.

If the coefficient of the first derivative dz/dt in Eq. (10-1) is negative, (equivalent to negative damping in a mechanical system), the system will be *dynamically unstable*. This condition occurs if:

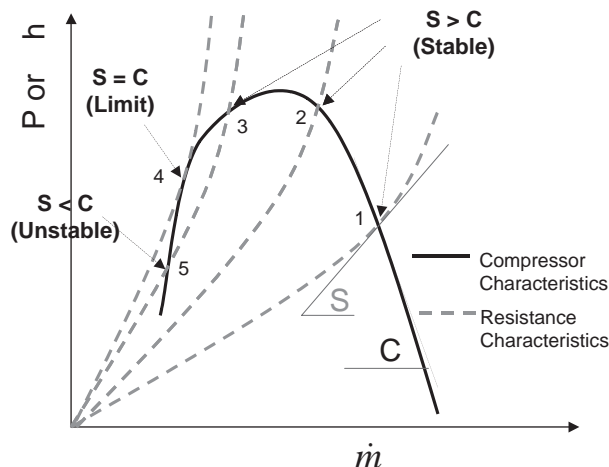


Figure 10-3. Static stability limit of the compression system of Fig. 10-1.

$$\frac{L}{A} \frac{CSV}{a^2} < 0 \text{ or } C > \frac{La^2}{ASV} \quad (10-3)$$

Let us examine the above conditions with the aid of the schematics of Figs. 10-4 and 10-5. If the system does not include the inertia element represented by the duct (L) in Fig. 10-1, the condition for dynamic instability is simply:

$$C > 0 \quad (10-4)$$

that is, when the slope of the compressor characteristic curve is positive. Hence, the limit of the dynamically stable system in this case is the maximum point on the compressor characteristic curve as shown in Fig. 10-4.

If the system includes the inertial element represented by the duct (L) in Fig. 10-1, the condition for dynamic instability is simply that represented by Eq. (10-3), where C could assume a positive value and, hence, moves the dynamic stability limit to the left of the maximum point on the compressor characteristics curve as is shown in the schematic of Fig. 10-5. It should be pointed out that, as the system depicted in Fig. 10-1 is gradually throttled, (and assuming that both the compressor and the throttle element respond in a quasi-steady manner), the dynamic stability limit is often (if not always) reached before the static stability limit. Hence, system static instability is often not analyzed, while dynamic instability is clearly a concern.

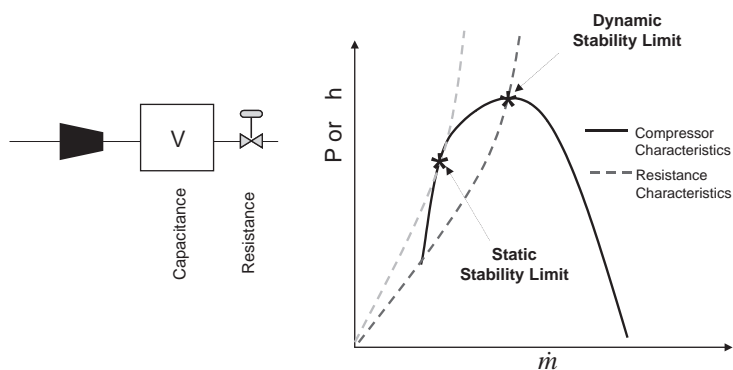


Figure 10-4. Dynamic stability limit of the compression system of Fig. 10-1, without the pipe element (no inertia).

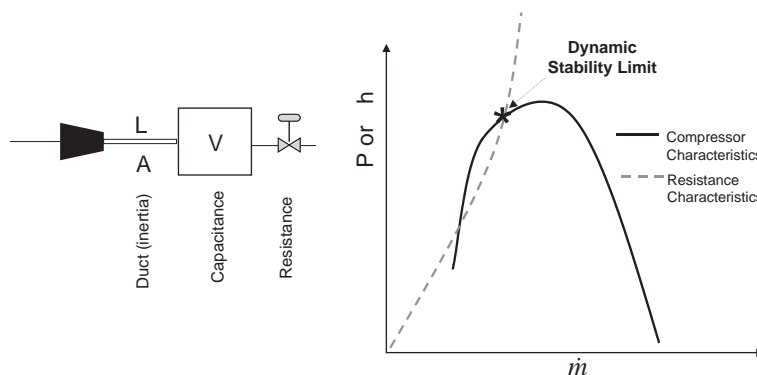


Figure 10-5. Dynamic stability limit of the compression system of Fig. 10-1.

10.2.2 Complex Compression Systems

Compression systems in process plants and in pipeline transmission systems are not as simple as that depicted in Fig. 10-1. By and large, in addition to the compressor units, compression systems are composed of suction equipment such as scrubbers or separators, control valves, upstream process equipment that could either be close (like in gas plants) or separated by a long section of pipe (like in a pipeline system), a number of bays of coolers on the discharge side, check valves, recycle system with recycle valves, blow-down or vent lines and valves leading to a flare header system, etc. Although, in principle, the dynamic equation that describes such a system can still be reduced to a second-order ordinary differential equation in nature, it simply cannot be derived analytically due to the complexity of the system and the sheer number of elements comprising it. The problem could be doubly or triply accentuated if there are two or three compressor units operating in a parallel/series configuration (Fig. 10-6). For this reason, numerical simulations are resorted to, where the fundamental governing equations describing the gas and equipment interaction dynamics between all of the piping and control systems still need be employed.

In any dynamic numerical simulation of such compression systems, it is important to include the temporal-spatial dependence terms in all three governing equations for the gas flow in each pipe elements. In many of the commercial codes, only the time gradients are considered in dynamic simulations, which amounts to describing the dynamics of the system using Ordinary Differential Equations (ODEs) that are much less rigorous than the Partial Differential Equations (PDEs). This is referred to as the “lumped parameter” method, which gives a solution that is a reasonable approximation of the distributed model solution. This approach is not adequate for dealing with compression dynamics involving recycle systems and surge phenomenon of compressors going into, and out of, surge. The spatial gradients along the length of the pipe segments are crucial, as they describe the time taken for perturbations in pressure, flow and temperature to propagate from one point in the system to another. A good simulation model would retain all terms in the following one-dimensional governing PDEs [16]:

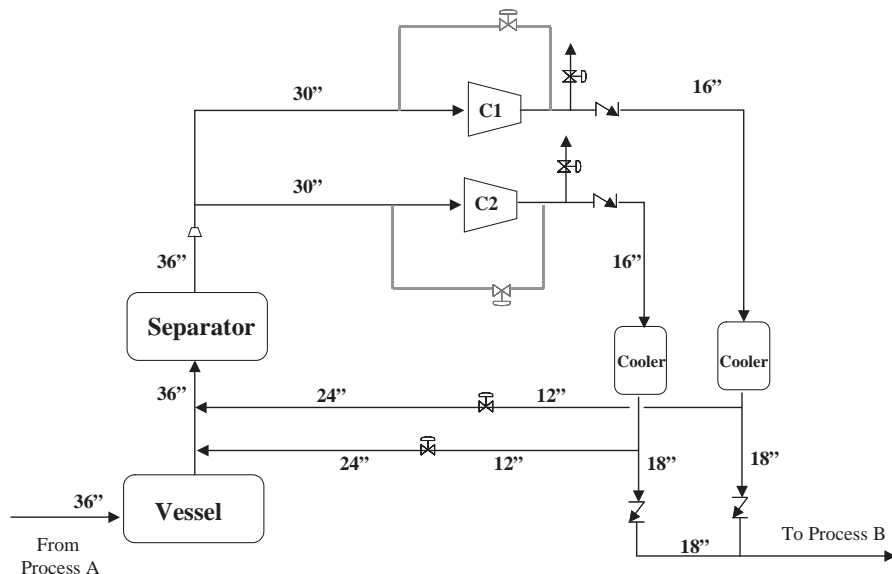


Figure 10-6. Schematic of an example of an industrial compression system involving two centrifugal compressors in parallel.

Continuity

$$\frac{\partial \rho}{\partial t} + \rho \frac{\partial v}{\partial x} + v \frac{\partial \rho}{\partial x} = 0 \quad (10-5)$$

Momentum

$$\frac{\partial v}{\partial t} + v \frac{\partial v}{\partial x} + \frac{1}{\rho} \frac{\partial p}{\partial x} + \frac{f_{DW}}{2D} v |v| = 0 \quad (10-6)$$

Energy

$$\frac{\partial p}{\partial t} + v \frac{\partial p}{\partial x} - a^2 \left(\frac{\partial \rho}{\partial t} + v \frac{\partial \rho}{\partial x} \right) - E = 0 \quad (10-7)$$

where

$$E = \frac{f_{DW}}{2DC_v} \left(\frac{\partial p}{\partial T} \right)_v v^2 |v| + \frac{4k}{DC_v \rho} \left(\frac{\partial p}{\partial T} \right)_v (T_a - T) \quad (10-8)$$

where:

- a = speed of sound
- C_v = gas specific heat at constant volume
- D = pipe internal diameter
- E = friction and heat transfer term defined in Eq. 10-8
- f_{DW} = Darcy Weisbach friction factor
- k = overall heat transfer coefficient between fluid in pipe and surrounding temperature
- p = pressure
- v = gas mean flow velocity
- x = spatial length along a pipe
- t = time
- T = gas temperature
- T_a = surrounding (ambient) temperature
- ρ = gas density
- $()_v$ = derivative at constant specific volume

Note that both pipe wall friction and heat transfer with the surroundings are taken into account based on Eq. (10-8). Using the method of characteristics, the above hyperbolic partial differential equations are transformed into total differential equations, which lead to a set of algebraic compatibility equations along two characteristic lines and a particle path line [18–22]. These compatibility equations, together with the respective characteristic lines are integrated in the time-space domain. In the derivation of the finite-difference compatibility equations, the real gas assumption is introduced and either AGA-8 (American Gas Association) [23] or Peng-Robinson [24] equations of state were employed, depending on the nature of the gas mixtures, to specify the relation between the gas density, temperature and pressure, as well as to determine the physical and thermodynamic properties at each node in the system.

Similar governing equations describing the transient flows through physical components in the system are also formulated and combined with Eqs. (10-5)–(10-8). These elements are throttle or pressure loss elements, combining and dividing tees, reducers or expanders, capacitance (plenum, volume, vessels), choked and un-choked valves, heat exchangers with a set duty or a set outlet temperature, adiabatic or isothermal flash separators, etc. A full account of the governing equations for these elements is given in [16]. Throttle elements and capacitance elements are modeled based on quasi-steady state equations describing pressure changes as well as energy and mass balances across the element. These

equations, when combined with the three compatibility equations for the pipes connected upstream and downstream of the element, are solved simultaneously to give the unknown variables on both sides of the element at each time step. Different formulations of the equations are used to account for reversed flow situations.

The governing equations for combining and dividing tee junctions represent conservation of pressure, mass and energy. In these cases, the conservation equations require the equality of all three pressures at a common node (pressure losses due to mixing are neglected) and the total flux of mass and energy which enters the junction has to be equal to the corresponding mass and energy flux leaving the junction (accumulation of mass or energy is not possible at a node). Again, quasi-steady state equations, together with the compatibility equations written for each of the three pipe elements, constitute the general model for these types of elements. Tracing the reversed flow scenarios in the tee junction becomes more complicated since the flows can be reversed in one, two or three pipe elements. Additionally, each of these scenarios can occur with a different pipe element. The simulation code should consider all possible combinations of reversed flow and different treatments have been applied. Equations governing flow through choked and un-choked valves are based on flow through a converging-diverging passage, which are described fully in [25].

The compressor itself is assumed to respond to any perturbation in a quasi-steady manner following its full characteristic curve, including that to the left of the surge limit [2,3,14,15]. Compressor/driver dynamics are governed by the following equation; relating the driver power to the gas power and the inertias of both units:

$$\dot{W}_{\text{driver}} = I_{\text{driver}} \times N_{\text{driver}} \times \frac{dN_{\text{driver}}}{dt} + I_c \times N_c \times \frac{dN_c}{dt} + \frac{\dot{m} H_a}{\eta_m} + \text{Windage \& Losses} \quad (10-9)$$

where:

H_a	=	adiabatic head across the compressor
I_{driver}	=	driver rotor inertia
I_c	=	compressor rotor inertia
\dot{m}	=	gas mass flow rate through the compressor
N_c	=	compressor speed
N_{driver}	=	driver speed
t	=	time
\dot{W}_{driver}	=	driver power
η_a	=	Compressor adiabatic efficiency
η_m	=	mechanical efficiency

It should be noted that the driver and compressor inertias should also include the inertia of the elements of the gearbox and couplings connected to either side, respectively. Additionally, in the case of a two-shaft gas turbine driver, the applicable driver inertia in Eq. (10-9) above is only the power turbine (i.e. the driver rotor), and coupling inertias and not inclusive the gas generator inertia.

The compressors' performance characteristics are often provided in terms of polytropic head and polytropic efficiency vs. actual inlet flow. These can be converted to adiabatic head and adiabatic efficiency via the following relationships [26]:

Adiabatic head:

$$H_a = \frac{Z_{av} R T_1}{\left(\frac{k-1}{k}\right)} \left[\left(P_r\right)^{\frac{k-1}{k}} - 1 \right] \quad (10-10)$$

Polytropic head:

$$H_p = \frac{Z_{av}RT_1}{\left(\frac{n-1}{n}\right)} \left[\left(P_r\right)^{\frac{n-1}{n}} - 1 \right] \quad (10-11)$$

Polytropic efficiency:

$$\frac{n}{n-1} = \frac{k}{k-1} \eta_p \quad (10-12)$$

Adiabatic efficiency:

$$\frac{H_a}{\eta_a} = \frac{H_p}{\eta_p} \quad (10-13)$$

where:

- H_a = adiabatic head across the compressor
- H_p = polytropic head across the compressor
- k = average isentropic exponent of the compressed gas
- n = polytropic exponent of compression
- P_r = pressure ratio
- R = gas constant
- T_1 = upstream gas temperature
- Z_{av} = average compressibility factor across the compressor
- η_a = Compressor adiabatic efficiency
- η_p = Compressor polytropic efficiency

In order to simulate the dynamic behavior of the compressor, including possibility of surging, the complete steady characteristics of the unit beyond the surge point (i.e. left of the surge point) and into the negative flow is required. At a given flow to the left of the surge limit, however, the actual head may differ from the steady state characteristics, which is the consequence of the compressor going into surge. A physically realistic and commonly used representation of this characteristic is that of a simple cubic given by the following equation [14,15]:

$$H_a = H_0 + \beta \left[1 + 1.5 \left(\frac{2Q_a}{Q_s} - 1 \right) - 0.5 \left(\frac{2Q_a}{Q_s} - 1 \right)^3 \right] \quad (10-14)$$

where:

- Q_a = compressor actual inlet flow
- H_a = compressor adiabatic head at any given inlet flow (Q_a)
- H_0 = compressor adiabatic head at zero flow = $0.5(\pi N)^2(D_0^2 - D_i^2)$
- β = parameter = $0.5(H_s - H_0)$
- H_s = compressor head at surge point at the current running speed
- Q_s = compressor actual inlet flow at surge point at the same speed
- D_0 = impeller outer (tip) diameter
- D_i = impeller average inlet diameter

An example for the full compressor characteristics for a single impeller compressor is shown in Fig. 10-7. Here, the compressor characteristics for a given speed up to the surge point are shown in discrete points at $N = 6825$ rpm. The full characteristics at any other speed can be determined from Eq. (10-15) with the aid of the affinity (fan) laws for centrifugal compressors [27], namely:

$$\frac{Q_a}{N} = K_1; \quad \frac{H_{ad}}{N^2} = K_2 \quad (10-15)$$

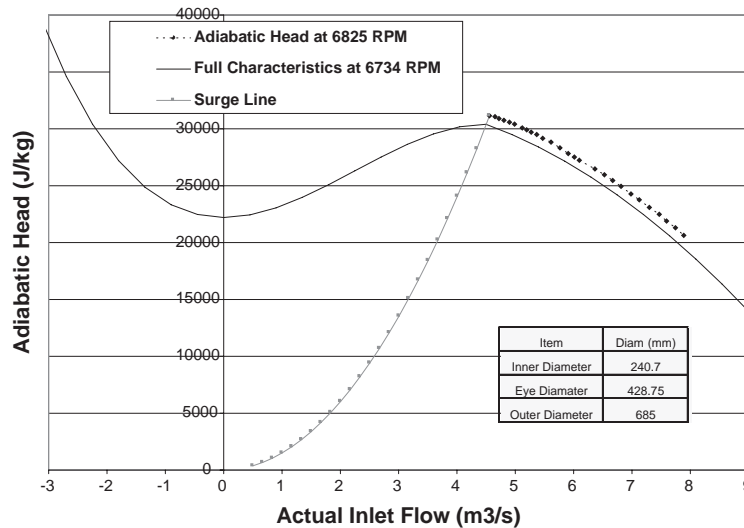


Figure 10-7. Example of full compressor characteristics beyond the surge line at $N = 6734$ rpm, for a single impeller compressor.

where, K_1 and K_2 are similarity constants and N is the compressor rotational speed.

Generally, a compression system consists of most of the elements described above, whether it is a pipe element, a connecting element or boundary condition. These constitute sets of highly non-linear equations, which must be solved to determine the unknowns (pressure, mass flow rate and temperature). Each set of equations requires solution at each x location along each pipe element for each t time step. To achieve numerical stability, the Courant stability condition [23] is applied which stipulates that:

$$t \leq \frac{x}{a+v} \quad (10-16)$$

where:

- a = local speed of sound of the flow medium
- v = instantaneous mean gas flow velocity

The Newton-Raphson method for the solution of non-linear equations was used because of its convergence speed and efficiency. The method is iterative in nature and solves all equations simultaneously. The starting point for a variable at a given time step is the value obtained as a solution from the previous time step. With small time steps (required by the stability condition), parameter changes longer than this time step will be captured and therefore transients occurring over several time steps will certainly be accounted for. Variables calculated at a given time step represent a good starting point for the next time step calculation. The iteration process within each time step is continued until the desired solution tolerance is achieved. Generally, the required calculation accuracy is obtained in under ten iterations at each time step.

10.2.3 Control Dynamics

In order to analyze the dynamics of any compressor station, the response of the control system and its control elements must be included. In the last section, the mathematical descriptions of the dynamic behavior of gas through various gas handling elements and

devices were presented. Typically, these elements are connected with some sort of autonomous control system whose behavior is very important for any simulation of the flow transients.

The purpose of the station control system is to provide a collection of automatic functions so that the station operator may make major decisions, but not to have to continually adjust the setting of a valve or the speed of each compressor unit, etc. The control system also has built in safety protocols so as to response to any un-expected upsets in operational conditions that could lead to equipment damage or destruction. Additionally, the control system permits remote operation from a central gas control location so as to provide overall operational integrity of the gas transmission network in an efficient and safe manner.

In the field, these functions are accomplished using a number of standard control elements, such as sensors, controllers, actuators, relays, ramp generators, filters, etc. All control circuits, whether pneumatic or electronic, can be described by a set of ordinary differential equations (O.D.E.) in the form:

$$\frac{dy}{dt} = f(y) \quad (10-17)$$

together with a set of subsidiary nonlinear algebraic equations in the form:

$$F(y) = 0 \quad (10-18)$$

where (y) is a vector representing the state variable of measurements, control equipment, and controllers' outputs, and F is the transposition of $[F_1, F_2, \dots]$. The following is a brief description of the basic control elements and the respective governing control equations.

PID Controller. The output signal $y_3(t)$ from a PID controller is related to the control signal $y_1(t)$ and the set point signal $y_2(t)$ (see Fig. 10-8a) via the known equation:

$$y_3 = K \left[E + T_d \frac{dE}{dt} + \frac{1}{T_i} \int_0^t E dt \right] + V_s \quad (10-19)$$

where

$$E = \text{error} = (y_1 - y_2)/N_c.$$

The derivative term in the above equation is approximated by a backward two-point difference form, while the integral term is approximated by the trapezoidal summation. This yields equation (10-19) above, a linear algebraic equation in y_1 , y_2 , and y_3 . Anti-reset windup is often incorporated in the PID controller to help avoid problems related to saturation at the full limits of the controller output.

Dynamic Actuator/Positioner. The actuator is the part of a control loop that is attached directly to the station piping elements and adjusts the connected element setting in response to time-varying input signals from a controller, sensor, or relay. Second-order actuators are modeled by describing the varying relation between the actuator position, X , input signal (y_1) , and the actual position (y_2) , (see Fig. 10-8b).

$$\frac{d^2 y_2}{dt^2} + 2\xi\omega_n \frac{dy_2}{dt} + \omega_n^2 [y_2 - X(y_1)] = 0 \quad (10-20)$$

where ξ and ω_n are the actuator constants (damping coefficient and natural frequency, respectively), that determine its response. The above second-order ordinary differential equation can be converted into two first-order ordinary differential equations in accordance with the system equation (10-17).

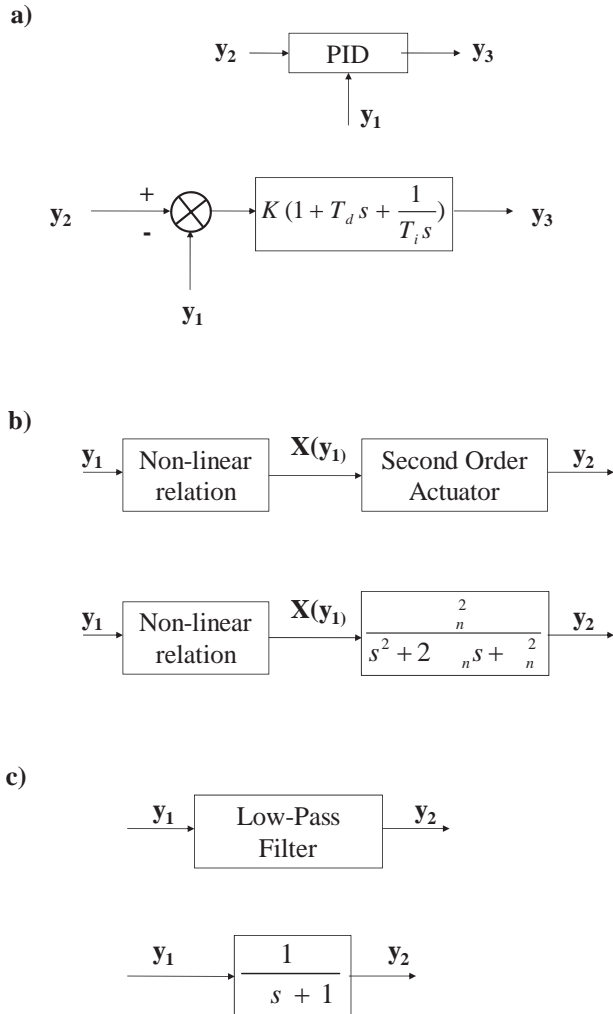


Figure 10-8. Schematic of basic control elements and the corresponding laplace transform.

Low-Pass Filter. A low-pass filter provides a slowly varying output signal, which tends asymptotically to the input signal. Examples of such control devices in the field are ramp generators and first-order actuators. The rate of change of the output signal depends on the time constant (τ) of the filter. The equation governing the relation of the output signal (y_2) to the input signal (y_1), (see Fig. 10-8c) is given by:

$$\tau \frac{dy_2}{dt} = [y_1 - y_2] \quad (10-21)$$

which is a first-order ordinary differential equation.

The above three control elements constitute the basic building blocks for a variety of other control elements, filters, and compensators that can be found in the field. For example, a lead-lag filter or a lag-lead filter can be represented by a PD controller and a ramp generator in series; a washout filter can be represented as a differentiator (i.e., only the derivative component in a PID controller) and a ramp generator also in series. Once the Laplace transform of a control element is known, it is possible to construct from the building blocks of the above three basic elements the required model and proceed with the analysis. Other control elements such as comparators, multipliers, etc., can be mathematically described by Eq. (10-18).

10.2.4 Solution Techniques

The mathematical description presented in the above sections indicates that two levels of interconnected computations exist, which must be solved either simultaneously in a parallel mode, or sequentially. The first level is the gas dynamics part of the flow-handling piping system in the compressor station. This level of computation involves a solution of a set of mixed nonlinear P.D.E. and algebraic equations with appropriate boundary conditions and elements setting dictated by the control system. The other level of computation solves the dynamic behavior of the station control system, which involves a set of mixed nonlinear algebraic and O.D.E. together with boundary conditions represented by set points and measured quantities. Figure 10-9 illustrates schematically the two levels of computations, where in most applications are performed sequentially, although a parallel computer technique can lend itself quite well in this application.

The basic framework for the simulation model adopted for the piping system is the nodal approach, in which the system is said to be comprised of nodes and elements connecting these nodes. The relationship between the state-space vector on each side of each element is formulated in a delta form using the concept of the transfer matrix and properly pooled in the system overall transfer matrix relating all space vectors at all system nodes. An effective solution technique, which takes advantage of the sparse characteristics of the system matrix can be implemented.

As for the control system, solution of the mixed algebraic and ordinary differential equations [Eqs. (10-17) and (10-18)] is required. In the literature one finds very few algorithms for solving numerically such systems. One method [28] is to transform the algebraic equations into O.D.E., which, combined with the original O.D.E., can be solved relatively easily by standard numerical techniques. Another method stems from the multivalued method proposed by Gear [29], which replaces the system 'of the mixed equations by a system of purely algebraic equations obtained by substituting the finite difference approximations for all of the derivative terms.

The following is an example of a dynamic simulation of a compressor station involving transients during compressor surge protection. The example is taken from a compressor station on TransCanada's gas transmission system in Alberta, Canada. The station layout is shown schematically in Fig. 10-10. The objective was to assess the effectiveness of the surge protection control system as the field personnel indicated that the recycle valve tends to oscillate violently (from 0 to 50 percent open) when the compressor operates close to the surge control line. A field test was conducted and measurements were taken while the compressor was running at approximately constant speed of 18,000 rpm. The station suction and discharge valves were used to throttle the flow and thereby bring the compressor operating point toward the surge region. Measurements of the suction and discharge static

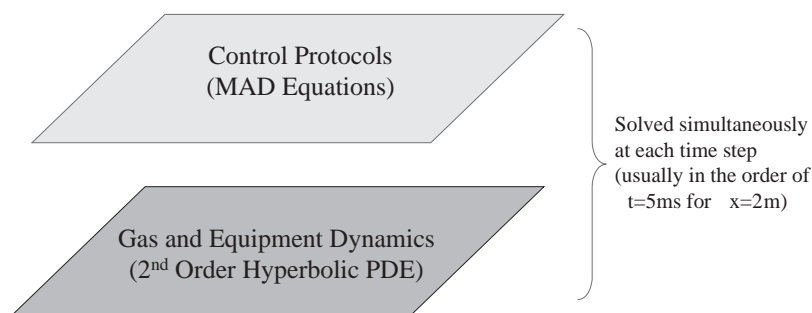


Figure 10-9. The two distinct computational platforms of the compression dynamic simulation.

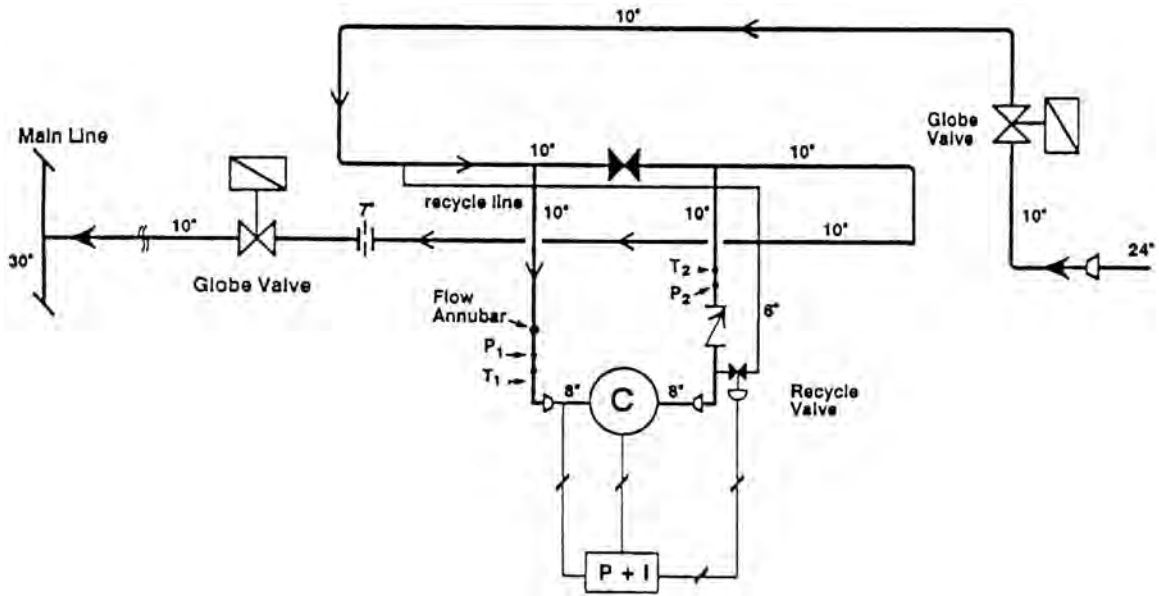


Figure 10-10. Schematic of a single unit compressor station.

pressures and temperatures, and differential pressures across the suction side annubar and the discharge side orifice meter, were recorded. Recycle valve position was also observed during the test.

The measured data are plotted in indicative Fig. 10-11 for a period of 100 seconds taken during operation near the surge control line while the surge protection control system was activated. Obviously, this surge control system is shown to be unstable as manifested by the pressure and flow oscillations (Fig. 10-11a and 10-11c, respectively) and the resulting cyclic behavior on the compressor performance map (Fig. 10-11d).

The surge controller was a PI controller whose settings at the time of the test were $K = 5.0$ and $T_i = 1/9.5$ seconds. With these settings and system boundary conditions, the simulation resulted in a remarkably good agreement with the field measurements as is demonstrated by corresponding data in Fig. 10-12. The recycle valve position (Fig. 10-12e) shows oscillations between 0–50% open as has been observed during the test but was not measured and recorded due to lack of valve position indicator on the valve. Although pressure and flow oscillations both through the compressor and the recycle line agree very well with those measured in the field, the temperature oscillations predicted by the simulation do not agree with those measured (compare Fig. 10-11b, and Fig. 10-11b). This is due to the slow dynamic response of the temperature gages placed in relatively high thermal capacitance jackets. However, the mean temperatures agree very well in both cases.

The constants representing the damping coefficient (ξ) and natural frequency of the actuator (ω_n) of the recycle valve had to be estimated from the simplified control feedback loop shown in Fig. 10-13. In this feedback loop, the transfer function of the process representing the piping dynamics is assumed unity with respect to flow and pressure only and not to temperature. The open loop transfer function of the feedback loop represented in Fig. 10-13 is

$$K \left(1 + \frac{1}{T_i s} \right) \left(\frac{\omega_n^2}{s^2 + 2\xi\omega_n s + \omega_n^2} \right) \quad (10-22)$$

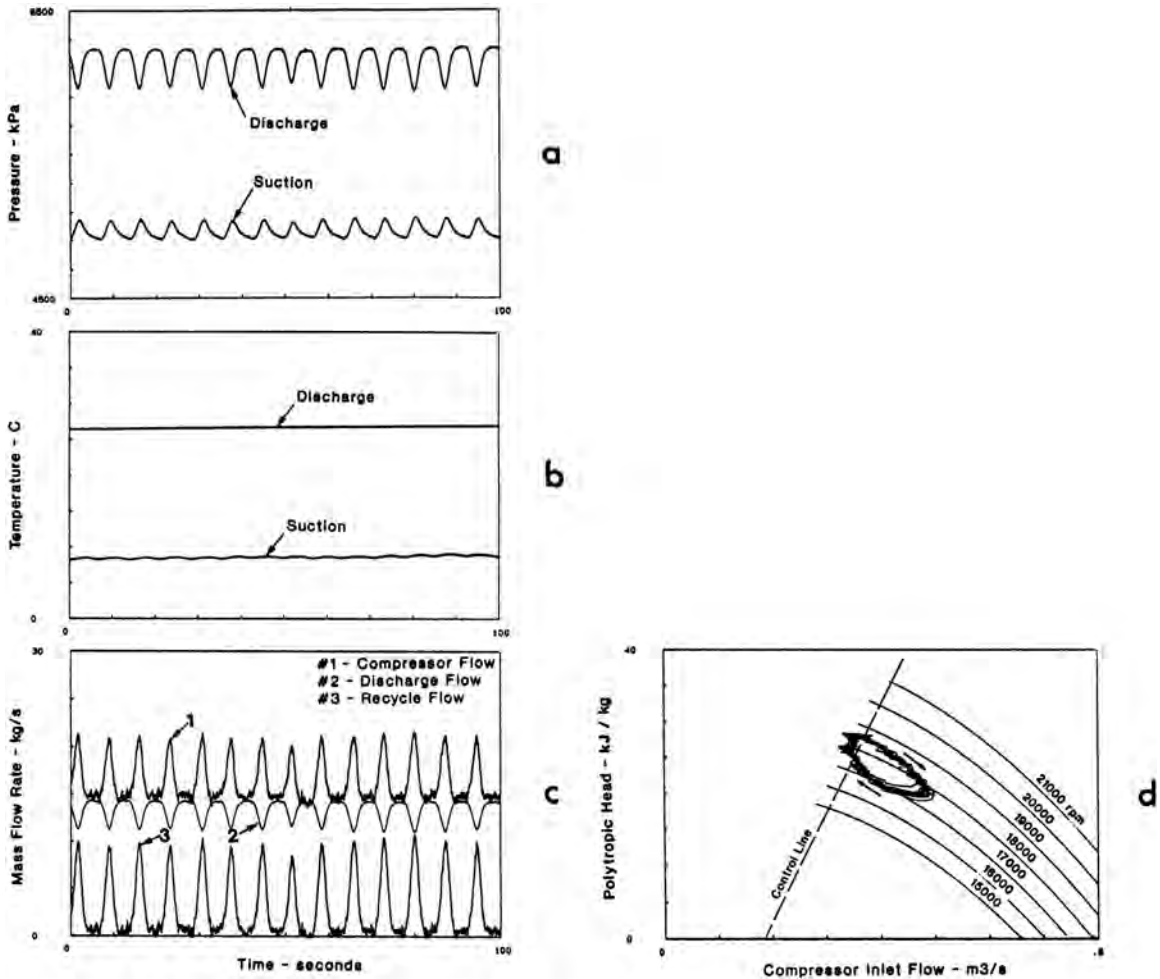


Figure 10-11. Field measurement during the process of compressor surge protection of the system shown in Fig. 10-10.

while the root locus of the closed-loop system is determined from solving the characteristic equation

$$T_i s^3 + 2T_i \xi \omega_n s^2 + (K + 1)T_i \omega_n^2 s + K\omega_n^2 = 0 \quad (10-23)$$

Since measurements were showing steady oscillation at a period of 7.2 seconds (see Fig. 10-11c), i.e., at frequency where $\omega_n = 0.873$ rad/s, then two roots of the characteristic equation must be $\pm i\omega$. Equating both real and imaginary parts of the left-hand side of the equation to zero yields $\omega_n = 0.356$ and $\xi = 11.12$ for $K = 5.0$ and $T_i = 1/9.5$ seconds.

The root locus of the feedback control loop shown in Fig. 10-13 is plotted in Fig. 10-14, where the three *poles* of the open-loop transfer function are located at 0.0, -0.0161 , and -7.9005 . Only the first two *poles* are shown in Fig. 10-14 since the third one goes to the *zero* at $-1/T_i$, i.e., to -9.5 and hence has no influence on the control loop stability. The root locus plot of Fig. 10-14 indicates that stability will improve for a value of gain less than 5.0, and the lower this value; the higher damping that will be achieved. A value of $K = 0.5$ was therefore chosen and introduced in the dynamic simulation of the system. The results obtained confirmed the above analysis and are shown in corresponding Fig. 10-15.

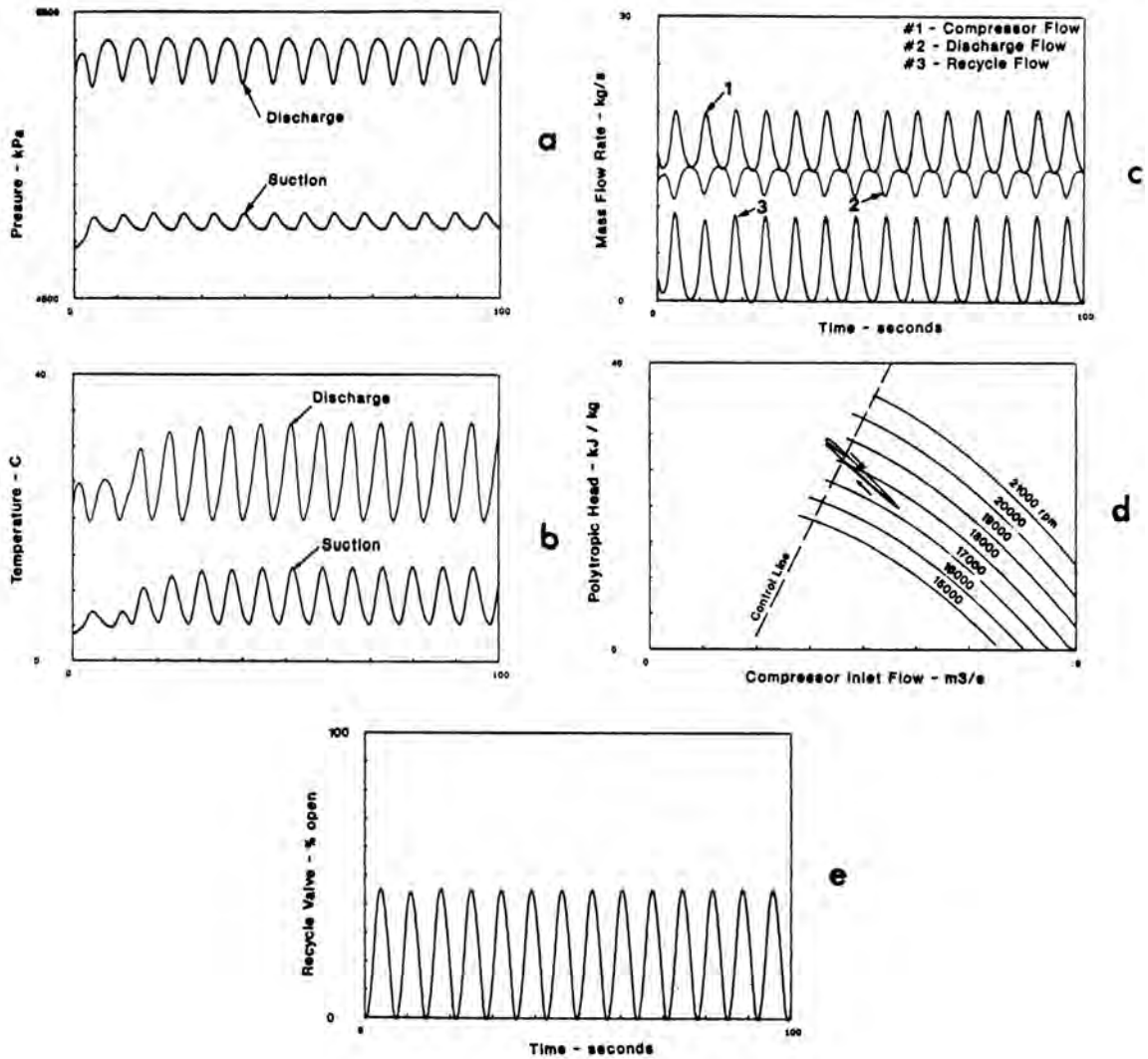


Figure 10-12. Simulation results during the process of compressor surge protection of the system shown in Fig. 10-10 ($k = 50$).

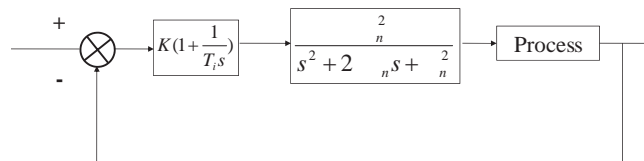


Figure 10-13. Closed-loop representation of the surge control system of Fig. 10-10.

Remarkable damping and suppression of oscillations were also achieved in the field with this lower value of K . The results of a subsequent field test (with $K = 0.5$) are shown in Fig. 10-16. This example demonstrates that small adjustment of the PI controller can lead to a remarkable improvement in the control process. Full dynamic simulation is useful in selecting the appropriate parameter(s) to adjust in order to achieve best results, before final implementation is executed in the field.

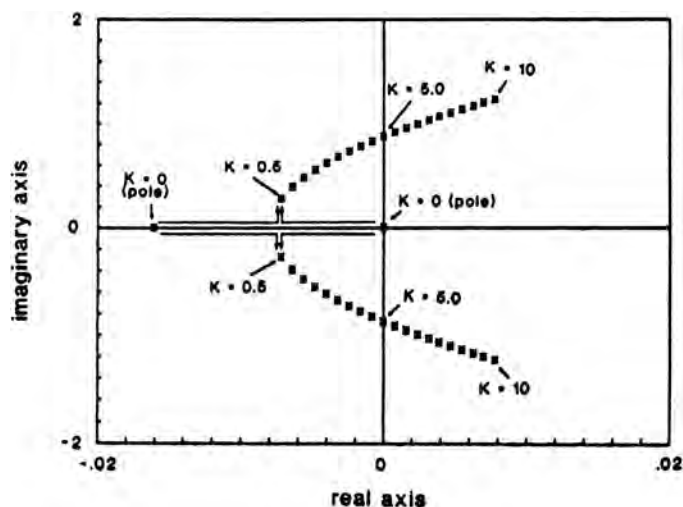


Figure 10-14. Root-locus of the closed loop system shown in Fig. 10-13.

10.3 EMERGENCY SHUT DOWN

The process of compressor station ESD is schematically depicted on a head-flow diagram in Fig. 10-17, following a trend observed both experimentally and numerically [9–11]. Six phases are identified as the compressor decelerates from a steady state point (S.S.) to zero flow and zero head across the compressor. Following an ESD, the operating point of the compressor follows approximately a straight line characterized by the slope (S_d) for a period of time corresponding to recycle valve pre-opening (pre-stroke) delay (phase I). This time delay is a combined effect of a process signal delay and inherent mechanical delay in opening of the recycle valve once an ESD signal is issued. During this phase, although the driver power is assumed to be completely shutoff, the compressor continues to rotate due to the combined inertia of its shaft, impeller and driver. Following Eq. (10-9), the compressor decelerates due to the head across it, windage, friction, etc., according to the balance of the following equation:

$$-I_{\text{driver}} \cdot N_{\text{driver}} \cdot \frac{dN_{\text{driver}}}{dt} - I_c \cdot N_c \cdot \frac{dN_c}{dt} = \frac{\dot{m} H_a}{\eta_a \eta_m} + \text{Windage and Losses} \quad (10-24)$$

In the above equation, it is assumed that the driver power was set to zero instantaneously at the instant of ESD. While this is correct for cases where electric motor the drivers, it is not absolutely correct for cases with gas turbine drivers. White and Kurz [30] have shown that one of the key problems is that there is residual power from the gas turbine even after the fuel is shut off. This is due to two effects; one is that there is always some fuel gas remaining in the fuel gas manifold system which will continue to feed the gas turbine combustor and hence sustain power for a few hundred milliseconds; and secondly, the rotor inertia of the gas generator itself will continue to provide hot gas to the power turbine even at a decreasing temperature. These effects can be mathematically represented by describing the power term on the right hand side of Eq. (10-9), \dot{W}_{driver} , as a declining function of time instead of setting it to zero at the instant of ESD. Similar treatment can be adopted to steam turbine drivers.

Once the recycle valve opens, a pressure wave travels downstream of the valve along the lower pressure part of the recycle line and along the main suction line, while an expansion wave travels upstream of the valve along the higher pressure part of the recycle line and along the main discharge line. The first wave to arrive at the compressor suction or

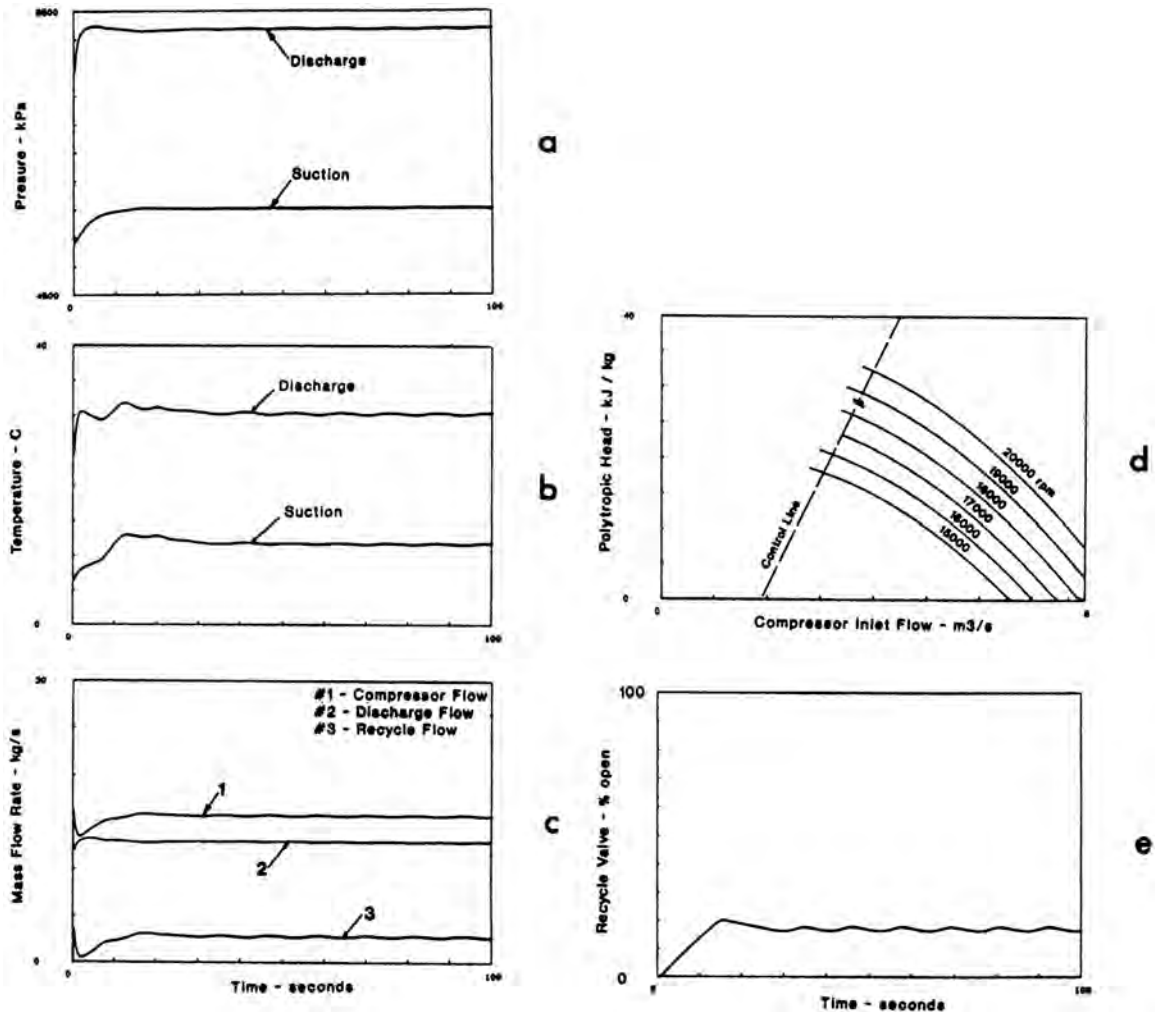


Figure 10-15. Simulation results during the process of compressor surge protection ($K = 0.5$).

discharge sides depends on the distance, which either wave needs to travel, and the local speed of sound along the corresponding path. The time taken for either wave to arrive first to the compressor determines the duration of phase II shown in Fig. 10-17. Once this wave arrives at the compressor, flow starts to increase through the compressor and head decreases, beginning phase III. It can be shown that the slope of the line identified in Fig. 10-17 for phases I and II can be expressed as [11]:

$$S_d = \frac{\partial H}{\partial Q} = \left(\frac{k-1}{k} \right) (H_{ss} + \xi) \frac{\rho_1 a_1}{P_1 A} \left[1 + \frac{a_2 P_1}{a_1 P_2} \right] \quad (10-25)$$

where:

- A = pipe cross-section area
- a_1 = sound speed of the gas at suction condition
- a_2 = sound speed of the gas at discharge condition
- H_{ss} = compressor head at steady state point
- k = isentropic expansion of the gas
- P_1 = suction static pressure
- P_2 = discharge static pressure

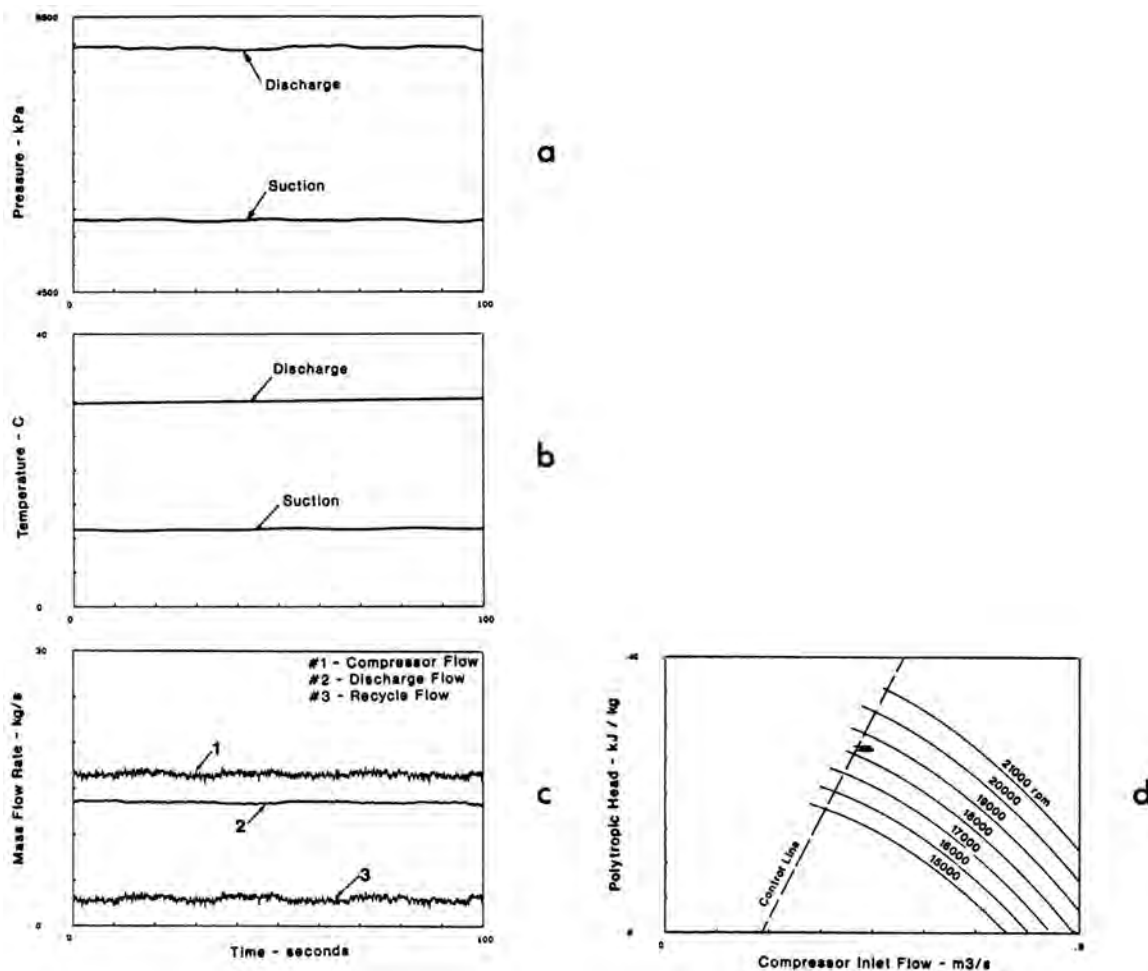


Figure 10-16. Field measurement during the process of compressor surge protection ($K = 0.5$).

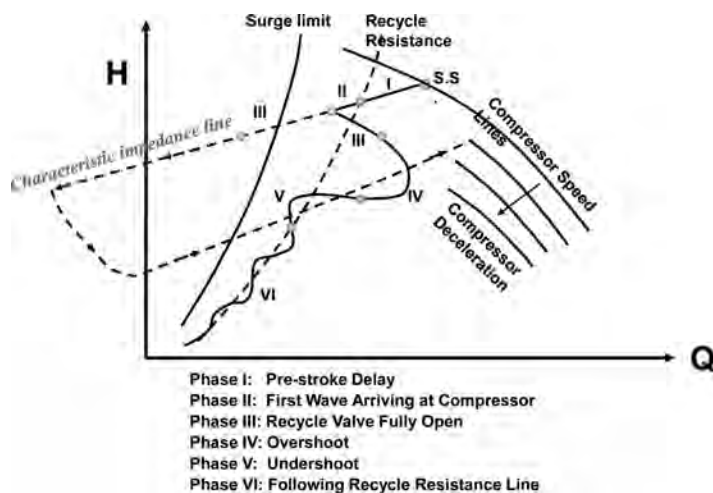


Figure 10-17. A schematic of the different phases of head-flow through the compressor during an ESD process [11].

of the recycle valve), the compressor will undergo reverse flow (surge). This is because the compressor impeller at this speed cannot sustain a positive flow against the prevailing high differential pressure (head) across it. In this case, the high differential pressure will drive reverse flow through the impeller while it is spinning forward, which is defined by the intersection of the characteristic line with the full compressor characteristic at the prevailing speed at this instant (point B in Fig. 10-18), hence the first surge cycle. In summary:

$$\text{if } \delta N > \delta N_{\max} \text{ surge will occur} \quad (10-26a)$$

$$\text{if } \delta N < \delta N_{\max} \text{ surge will not occur} \quad (10-26b)$$

Here δN is determined from ESD Eq. (10-9), which can be simplified for the case of gas turbine driven compressors as follows:

$$-I N_0 \cdot \frac{dN}{dt} = \frac{\dot{m}_0 H_0}{\eta_a \eta_m} \quad (a)$$

Figure 10-19 shows a surge-free schematic illustrating the case when δN resulting from the integration of Eq. (10-17) is less than δN_{\max} .

Theoretically, if the characteristic slope ' S ' is known, and the initial condition of the compressor (point 'o') is known, the maximum speed drop can be determined from geometrical algebra established by Fig. 10-18 and the fan laws of the compressor characteristics, including the cubic representation of the full compressor characteristics to the left of the surge point. One approximation is to assume that $(N_0 - \delta N_{\max})$ corresponds to the main-line characteristics line meeting the compressor speed line at the surge point (s) at speed = $N_0 - \delta N_{\max}$ instead of being tangent to it at point (t) as shown in Fig. 10-18. This approximation is, in fact, more realistic as the surge point (s) defines the surge limit. Following the fan laws [Eq. (10-15)], the relation between adiabatic heads, actual inlet flows and compressor speeds at surge points can be correlated as follows:

$$\frac{Q_s}{N} = \frac{Q_{so}}{N_0} = K_1; \quad \frac{H_s}{N^2} = \frac{H_{so}}{N_0^2} = K_2 \quad (b)$$

According to the above discussion and referring to Fig. 10-18, the following relation can be written:

$$S_d = \frac{H_0 - H_s}{Q_0 - Q_s} \quad (c)$$

where ' S ' is the slope of the characteristic line defined by Eq. ().

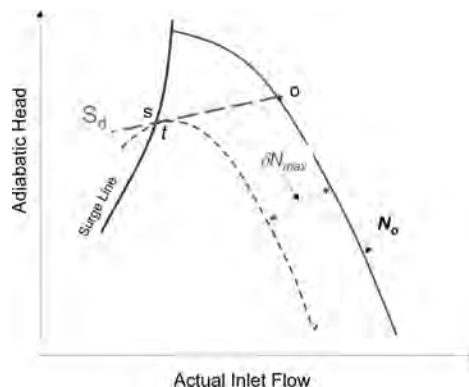


Figure 10-19. Maximum speed deceleration increment for surge-free ESD operation.

Introducing Eq. (b) into Eq. (c), the following equations can be developed:

$$H_0 - H_s = S_d (Q_0 - Q_s)$$

$$H_0 - K_2(N_0 - \delta N)^2 = S_d [Q_0 - K_1(N - \delta N)]$$

$$H_0 - K_2 N_0^2 + 2K_2 N_0 \delta N = S_d [Q_0 - K_1 N_0 + K_1 \delta N]$$

$$H_0 - H_{so} + 2H_{so} \frac{\delta N}{N_0} = S_d \left[Q_0 - Q_{so} + Q_{so} \frac{\delta N}{N_0} \right]$$

and finally,

$$\frac{\delta N_{\max}}{N_0} = \frac{S_d (Q_0 - Q_{so}) + (H_{so} - H_0)}{2H_{so} - S_d Q_{so}} \quad (d)$$

Now combining Eq. (d) and Eq. (a) and integrating, we arrive at the simple equation that determines the maximum (longest) time that the compressor can withstand before going into surge, i.e., before the arrival of the relief expansion or pressure waves resulting from opening the recycle valve, as follows:

$$\delta t_{\max} = I N_0^2 \left[\frac{S_d (Q_0 - Q_{so}) + (H_{so} - H_0)}{2H_{so} - S_d Q_{so}} \right] / \left[\frac{\dot{m}_0 H_0}{\eta_a \eta_m} \right] \quad (10-27)$$

The above equation, though simple and easy to evaluate, is significant. The δt_{\max} calculated by this equation can be compared to the time it will take for the first relief expansion or pressure wave to arrive at the compressor discharge or suction side, respectively. This time of arrival can be estimated from the sum of the recycle valve pre-stroke delay and the travel time of either the expansion or the pressure wave to arrive at the compressor. The latter is calculated from the distance along the corresponding piping between the recycle valve and the compressor and the local speed of sound in the gas, either on the discharge or the suction side, respectively.

Following the above formulation, it would be possible to examine the effects of the compressor performance characteristics on the potential for the compressor to surge during an ESD operation. Two different compressor performance characteristics are shown in Fig. 10-20; one is characterized with a flatter (less steep) slope near the surge line than the other. If the combined compressor/driver inertia is the same, both compressors are employed in identical compression systems with the same geometries (i.e., piping configuration), the deceleration slope (S_d) and the deceleration speed (δN_{\max}) will be the same. However, in the case of the flatter compressor performance characteristics, the compressor will be more prone to surge during ESD than the compressor with steeper characteristics, as demonstrated by the schematic of Fig. 10-21.

Since centrifugal compressor units can vary in the number of stages, flow capacity, and overall design, the best way to compare their performance characteristics is by normalizing the actual inlet flow at a given speed by the actual inlet flow at the surge point, and normalizing the adiabatic (or polytropic) head by the head at the surge point. Figure 10-22 gives examples of several compressor units from different manufacturers, which demonstrates the relative steepness or flatness of their characteristics one to another. Figure 10-23 shows the percent in compressor normalized head over the first 10% increase in the actual inlet

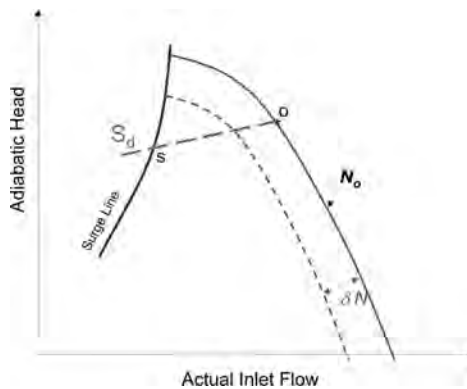


Figure 10-20. Surge-free deceleration during ESD operation for the case when $\delta N < \delta N_{\max}$.

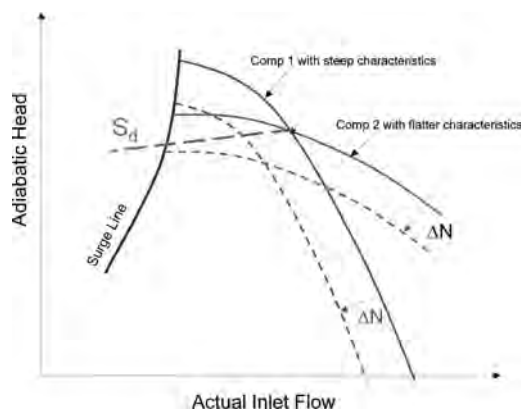


Figure 10-21. Schematic to illustrate compressor performance characteristics that can lead to surge during ESD operation.

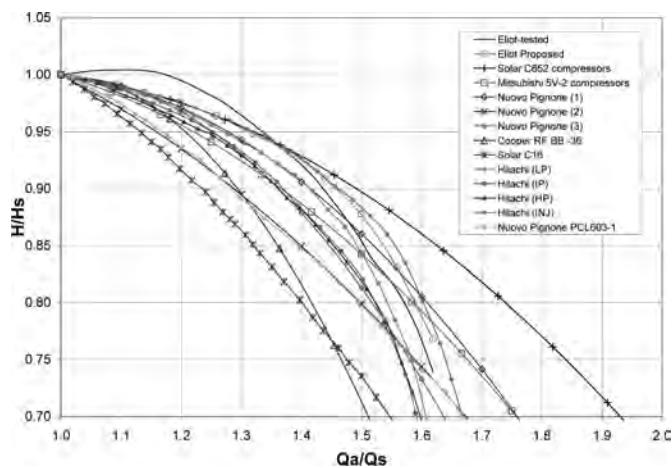


Figure 10-22. Comparison of normalized performance characteristics of various centrifugal compressor models.

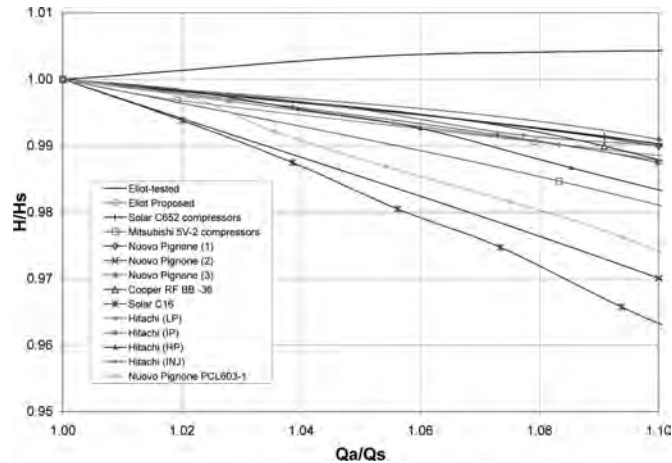


Figure 10-23. Drop in compressor adiabatic head due to increase in the actual inlet flow near the surge point.

flow through the compressor from the surge point. Clearly, there are significant variations between these compressor units, in the order of 1–4% drop in the head for 10% increase in the actual inlet flow. These variations will definitely affect the respective response of these units to an ESD operation, in that the compressors with flatter characteristics would be more prone to undergo surge during an ESD operation. There is one compressor characteristic in Fig. 10-23, showing even a positive slope close to surge point, which should not happen in a good design. That is why API 617 recommends that the head-flow characteristic curve shall be continuously rising from the rated point to the surge point (at the same speed) [31], thus establishing the requirement for a negative slope in the characteristic curve. Some engineering companies have instituted in their design standards the following metric in their compressor specifications:

1. The Surge point pressure at maximum speed is higher by at least 1% than the pressure at the surge control line (typically set at 10% flow higher than the surge flow) at the same speed, and
2. The Surge point pressure at the design speed is higher by at least 5% than the pressure at the design flow at the same speed.

10.3.2 Effects of Rotor Inertia

Turning back to Eq. (10-26), the degree of speed deceleration (δN) determines the potential for the compressor to surge during an ESD operation. It was also mentioned that the magnitude of (δN) is determined from integrating Eq. (10-24) over the period of phases I and II, which is dependent on the compressor rotor inertia (I_c) and driver rotor inertia (I_{driver}) among other parameters involved in the two terms on the right hand side of Eq. (10-24). If the combined compressor/driver inertia is relatively low, the magnitude of (δN) will be higher, and the possibility of the compressor to undergo surge is increased. This can be explained by the schematic of Fig. 10-24, where the perturbation characteristic slope (S_d) does not intersect the compressor performance characteristics at speed ($N_0 - \delta N$) regardless of the slope of the compressor performance characteristics.

The effects of the above two parameters, namely, compressor performance characteristics and combined driver/compressor rotor inertia can be illustrated by simulation examples conducted on an industrial compression system with a complex geometry as shown in the respective Figs. 10-25 through 10-27.

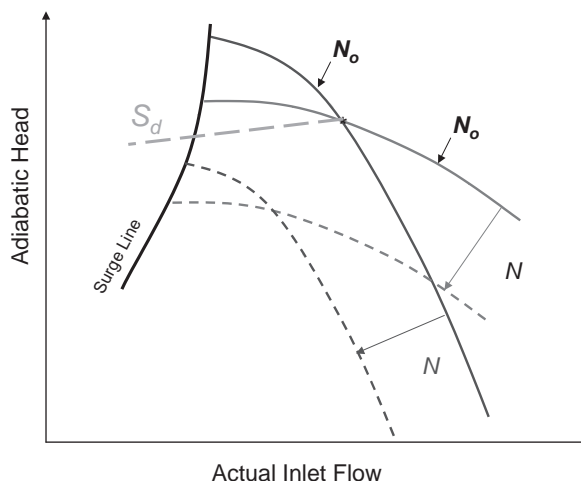


Figure 10-24. Schematic to illustrate the effects of low combined compressor-driver rotor inertia on potential for compressor surging during ESD operation.

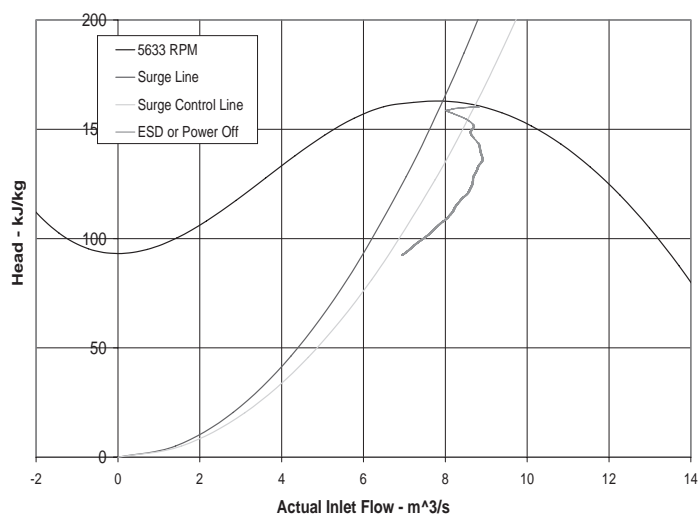


Figure 10-25. Example of dynamic simulation results of a surge-free deceleration of a compressor during ESD operation (high inertia rotor and steep performance characteristics of the compressor).

10.3.3 Example of Dynamic Instabilities in an Industrial Compression System

Several industrial compression systems were analyzed, which ranged from single unit (single or multi-impellers) up to four units operating either in series (typically in gas injection stations) or in parallel (typically in gas transmission stations). An example of a typical dynamic analysis conducted on an industrial compression system is briefly described in this section.

A wet gas, hydrogen sulfide (H_2S) rich (see composition in Table 10-1), relatively hot, gas from the top of a Fractionator in a Coker Unit is compressed with an electric motor driven six-stage centrifugal compressor as depicted in Fig. 10-28. Following a plant expansion redesign, this centrifugal compressor had to be replaced with a higher capacity compressor to handle the extra gas flow from the top of the Fractionator.

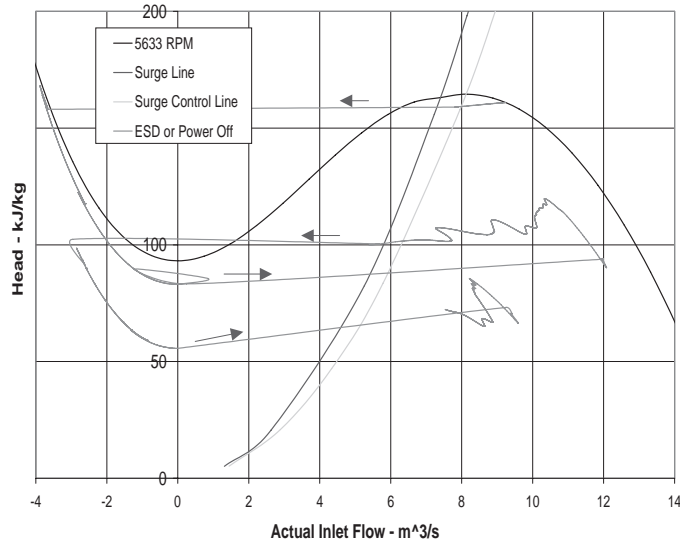


Figure 10-26. Example of dynamic simulation results of a compressor surging during esd operation (high inertia rotor but flatter performance characteristics of the compressor).

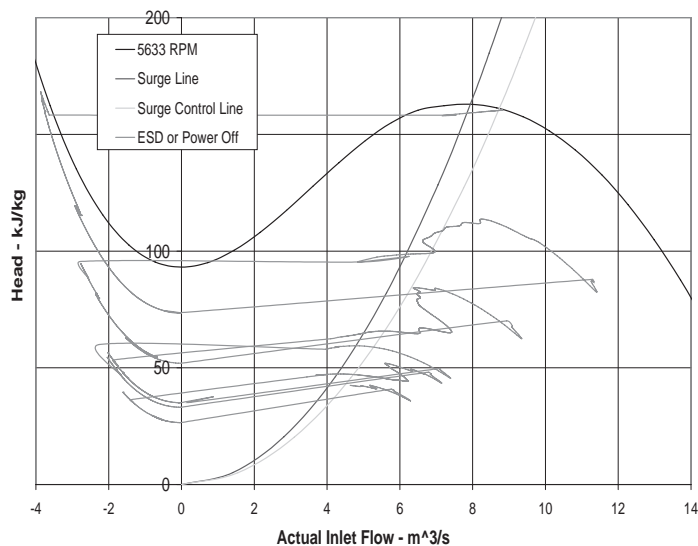
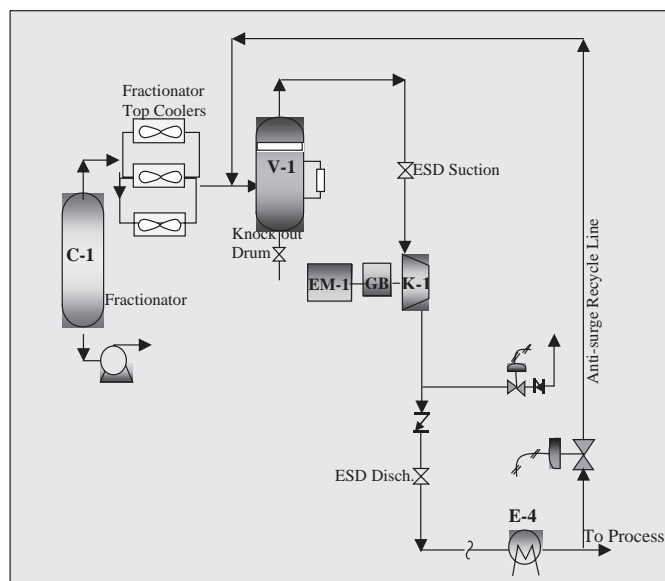


Figure 10-27. Example of dynamic simulation results of a compressor surging during ESD operation (steep performance characteristics of the compressor but low rotor inertia).

A water cooler heat exchanger (E-4) was required to cool the high-pressure gas downstream of the compressor before proceeding onto the next process train. For compressor startup, normal shutdown and capacity control, a recycle system connects downstream of the cooler to upstream of the knock-out drum as shown in Fig. 10-28. Actually, the cooler (E-4) existed before the unit was redesigned for expansion, and it had to be re-used. The physical separation of the cooler (E-4) from the compressor discharge flange (in terms of piping length) is rather significant. During the initial design phase the resulting substantial volume capacitance of the recycle system raised a concern as to the effectiveness of the recycle system when used as anti-surge protection. The emergency blow-off system between

Table 10-1. Gas mixture composition of the top of the fractionator

Component	Mole %
O ₂	0.253
N ₂	2.387
H ₂ O	2.103
CO	0.163
CO ₂	1.009
H ₂ S	13.021
H ₂	17.386
C ₁	28.597
C ₂	11.063
C ₃	10.462
Butene	1.858
iC ₄	0.845
nC ₄	3.145
iC ₅	1.879
nC ₅	2.439
C ₆ +	3.412
	100

**Figure 10-28.** Compression system for the wet gas stream from the top of a fractionator in a coker unit.

the compressor discharge flange and check valve comprised of a quick opening valve and a check valve leading to the Flare header of the facility.

It was duly recognized, given the design considerations above, that a detailed dynamic stability study for the entire system was in order to ascertain the effectiveness of the recycle system to provide adequate anti-surge protection to the compressor unit, particularly during ESD scenarios. The compressor head flow characteristics proposed by the compressor manufacturer during the design phase is shown in Table 10-2. The rotor inertia of the six impellers, shaft, gearbox and driver motor are given in Table 10-3. The total effective inertia (relative to compressor speed) was found to be approximately 242 kg.m².

The main outcome from the dynamic simulation at this initial stage of design was that, the compressor deceleration rate was rather slow due to the relatively high inertia of the

Table 10-2. Proposed compressor performance characteristics

Compressor Characteristics		
Q_a -m ³ /s	H = (J/kg)	Efficiency
7.787133	190767.6	0.785
8.023107	190169.6	0.79
8.495054	188973.6	0.8
8.967001	187777.5	0.81
9.438949	185983.5	0.818
9.910896	183890.4	0.825
10.38284	180900.3	0.83
10.85479	177910.2	0.834
11.32674	173425.1	0.835
11.79869	167444.9	0.83
12.27063	158474.7	0.82
12.74258	146514.3	0.8

Table 10-3. Compressor train inertia data

Impeller #	OD (in.)	Eye (in.)	Inertia (lb·in. ²)
1	28.49	20.015	14,360
2	28.49	18.665	13,787
3	29.67	17.736	16,573
4	29.67	16.86	15,906
5	29.67	16.18	15,413
6	29.67	15.14	14,795
Rotor			30,680.4
Gear box			1,344,672
HS coupling			14,500
LS coupling			1,300
Motor			2,355,408

compressor-driver train (242 kg.m²). In this case, the compressor unit does not undergo any surge cycle following an ESD operation. The results of this simulation were depicted in a previous figure (Fig. 10-25). One important remark should be noted on the system design as depicted in Fig. 10-28, and that is the location of the suction and discharge block (or ESD) valves. These two valves would isolate the compressor from the recycle system on closing. Recognizing this, a time delay of 30 seconds to these valves when an ESD signal is initiated to shut down the unit, as well as to open the blow-off valve to the flare system, was recommended.

Post-Installation. Detailed design, fabrication, testing, installation and commissioning activities were continued for this compression system. One of the commissioning activities was to test an ESD operation. A test was then setup whereby the anti-surge recycle valve was set at approximately 50% open position, and the compressor was running at maximum speed with only gas recycling around the recycle system. As a reminder, the recycle loop contains the aerial cooler as well as the suction knock-out drum. When a steady state operation was reached, an ESD command was activated and data were collected with a sampling frequency of 1 Hz (i.e. 1 second intervals). These data (Fig. 10-29) show that the compressor has actually gone one surge cycle during the speed coast down following ESD. In this installation, compressor flow is measured by an orifice plate located at the discharge side of the compressor unit. Therefore, the reversed flow through the compressor during this surge cycle was registered as zero flow because the differential pressure across the orifice plate was not set up to measure negative differential pressure (DP). This test was repeated but with the VFD of the motor initiated the ESD. Again the same trend

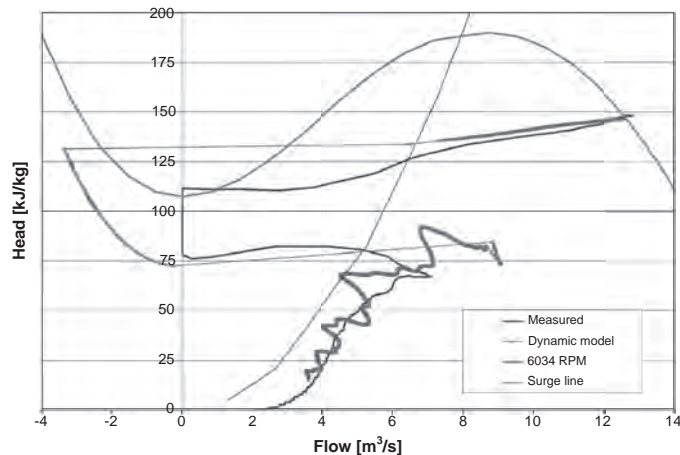


Figure 10-29. Field measurement showing compressor surging following an ESD.

occurred and the event confirmed the occurrence of one surge cycle during the coast down following ESD.

Re-Evaluation of “As-Built” Condition. The above problem triggered another re-evaluation of the compression system dynamics study. In this case, all of the pertinent parameters that were used in the initial dynamic simulation were reconfirmed. During this process, three major differences in the data used were discovered. Those were:

- The as built compressor train inertia data were provided by the manufacturer, which revealed that the actual with total effective inertia (w.r.t. to the compressor side) was 102.5 kg.m², instead of the 242 kg.m² previously used during the design phase.
- Secondly, the shop-tested compressor performance characteristics showed a much flatter characteristic, especially at flows close to the surge limit. Figure 10-30 shows comparison between the shop-tested compressor characteristic vs. the initially

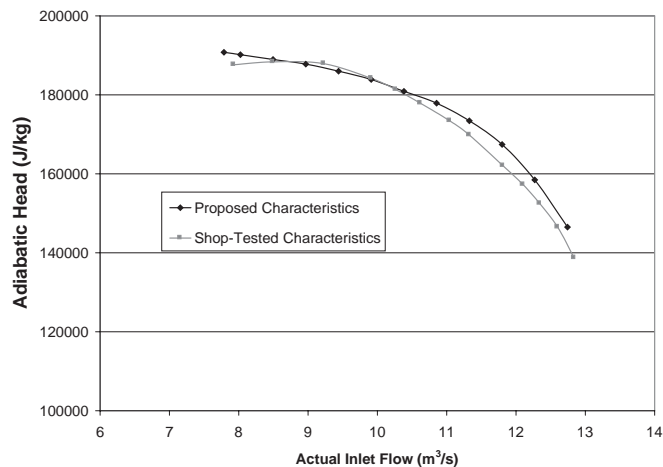


Figure 10-30. Shop-tested versus. proposed compressor characteristics at the same speed (6034 RPM).

proposed characteristic. In fact, the shop-tested performance curve exhibits a positive slope close to the surge point as shown in the Fig. 10-31.

- Thirdly, the pre-stroke delay as well as the actual travel time to full stroke of the blow-off valve to the flare system were found to be approximately 330 milliseconds and 1.667 seconds, respectively. These values were recognized to be much too slow, and that the pressure relief that should be provided by the blow-off valve to protect the unit from surge would come after the compressor would have gone through the first surge cycle. Figure 10-32 shows the process parameters (suction, discharge pressures and compressor flow, starting from the time when the ESD signal was initiated. Clearly, a combined 2-second delay until the blow-off valve is fully open comes too late, during which the compressor has already undergone one complete surge cycle.

Dynamic simulations of several ESD scenarios were then conducted using these new data, particularly since the compressor shop-tested performance characteristics showed much flatter characteristics, which raised considerable concerns. The first suggested solution scenario was to increase the size of the blow-off valve from 8" to a 12" valve with a

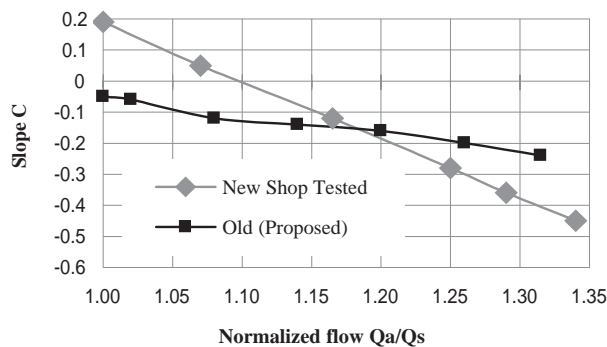


Figure 10-31. Normalized flow versus compressor curve slope for both proposed and tested curves.

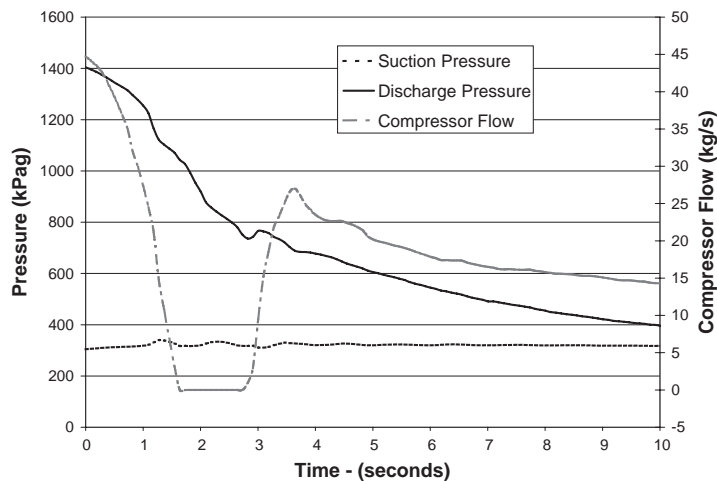


Figure 10-32. Process parameters during compressor surge following ESD.

quick-open trim with $C_v = 1210$, pre-stroke time of 100 milliseconds and stroke time of 1.0 second. Dynamic simulation showed that with this scenario, the compressor would be protected from surging during ESD. However, this option required considerable shutdown time and significantly longer lead-time to procure the specified 12" valve. (Note: opening the existing blow-off valve to flare 1 or 2 seconds before initiating the ESD signal was also considered and discarded since in the event of power failure or VFD failure, it is impossible to impose this delay on the power to electric motor). In the end, all changes and modifications to the blow-off to flare valve to protect the unit from surging were not possible. The only viable option was to install a short (hot) recycle system around the compressor unit, utilizing the existing check valve at the blow-off point.

A short recycle system was then sized, and dynamic simulations of the ESD indicated that a 12" globe valve with a quick-open trim and $C_v = 1600$ would be adequate. However, due to the flat compressor performance characteristics, operation of the compressor had to be limited to flow rates higher than those specified by the commonly used approach of specifying minimum operating flows to be 10% greater than the surge line. This margin was determined from several dynamic simulations and was found to depend on the hot recycle valve pre-stroke time. Figure 10-33 shows these margins for different pre-stroke times of 100, 215 and 280 ms.

After several iterations of the dynamics study, it was concluded that either one 12" valve with a quick open trim with a surge control line set at 37% off the surge limit would guarantee a safe ESD operation of the compressor. Figure 10-34 shows the results of the dynamic simulation of the final design modification scenario recommended for implementation. Table 10-4 summarizes the simulation data.

Performance After Implementing the Solution: A 12" Hot recycle system starting upstream of the check valve and the blow off to flare valve stream was installed with associated control systems to quickly open the valve in case of ESD. The pre-stroke time and the full valve opening time were 215 ms and 650 ms, respectively both of which included

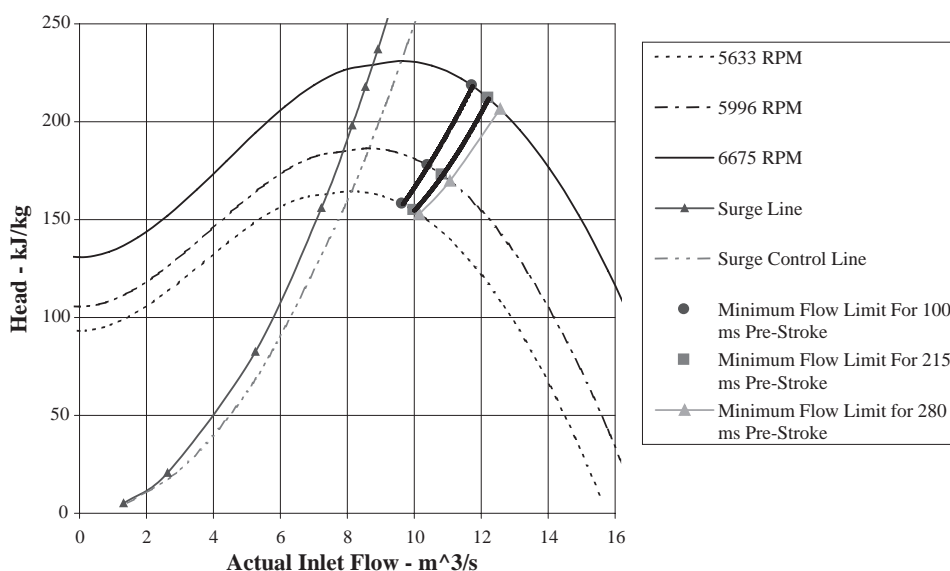


Figure 10-33. Surge control line margin increased due to the flatness of the compressor performance characteristics.

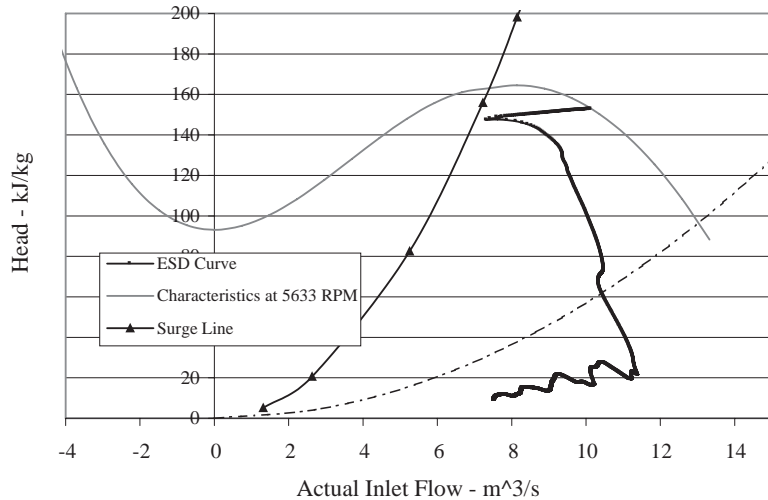


Figure 10-34. Simulation results of compressor coast-down during esd from a steady operating point at 37% of the surge limit - using 12" valve in the hot recycle system.

Table 10-4. Simulation data for new hot recycle system

Parameter	Value	Units
Steady State Speed	5633, 5996, 6675	RPM
Flow delivered to downstream	2.6	million SCFH
Suction pressure	333	kPaa
Suction temperature	32	Celsius
Discharge pressure	1500, 1910, 2720	kPaa
Cold ASV SS open	32.5, 34, 33	%
Unit check valve operational	Yes	
Effective inertia at compressor	102.5	kg.m ²
Cold ASV size	12	inches
Cold ASV trim	Modified linear	
Cold ASV C _v	1210	
Cold ASV prestroke time	100	ms
Cold ASV open time	750	ms
Flare valve size	8	inches
Flare valve trim	Equal percent	
Flare valve C _v	9800	
Flare valve prestroke time	333	ms
Flare valve open time	1667	ms
Hot ASV size	12	inches
Hot ASV trim	Quick open	
Hot ASV C _v	1600	
Hot ASV prestroke time	215	ms
Hot ASV open time	650	ms

the signal processing time. A schematic or the recommended modification is depicted in the Fig. 10-35.

A field test of an ESD operation was then carried out following installation of the new hot recycle system, and data were recorded (at 1 s time interval). The result of this test is shown in Fig. 10-36 indicating that the compressor did not undergo surge during this ESD.

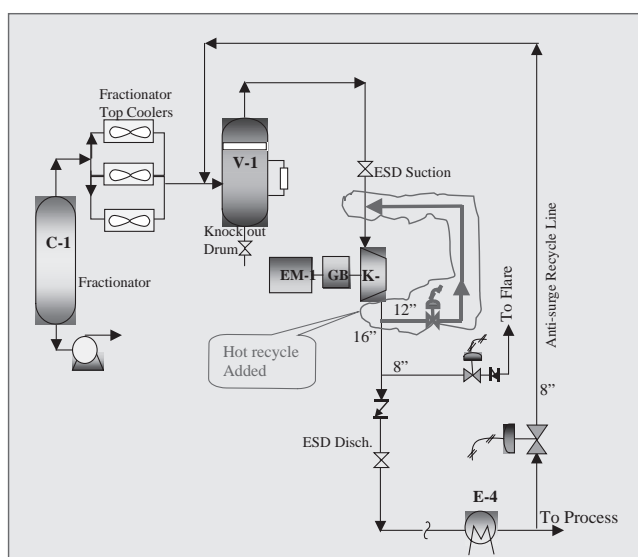


Figure 10-35. Recommended hot recycle system for the wet gas stream off the fractionator at a coker unit.

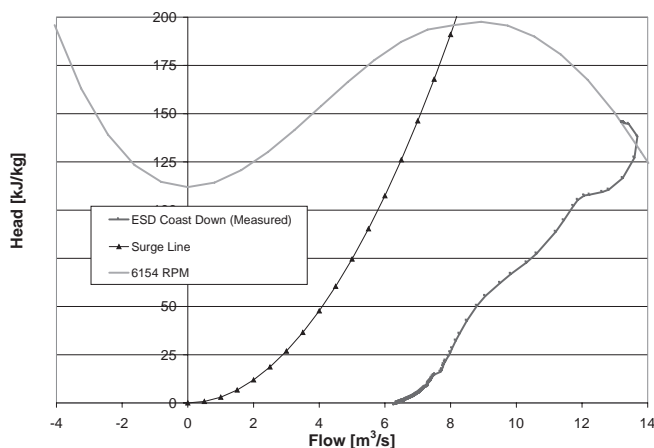


Figure 10-36. Field test results of an ESD operation after the implementation of the hot recycle system.

10.3.4 Integrally-Geared Compression Systems

For high pressure ratio compression, often it is cost effective to employ an integrally geared compression system where the driver (often induction motor) is driving the main wheel shaft and the main bull gear as shown in Fig. 10-37. The bull gear in turn, drives multiple pinions at much higher speed ratios. The example in Fig. 10-37 shows the bull gear drives two pinions and two shafts. The shaft on the right drives stages 1 and 2, while that on the left drives stages 3 and 4. Thus, there are four stages of compressions all driven by the same motor. In order to perform dynamic simulation of this system, the compressor dynamic equation, (Eq. 10-24) can be re-written in the form:

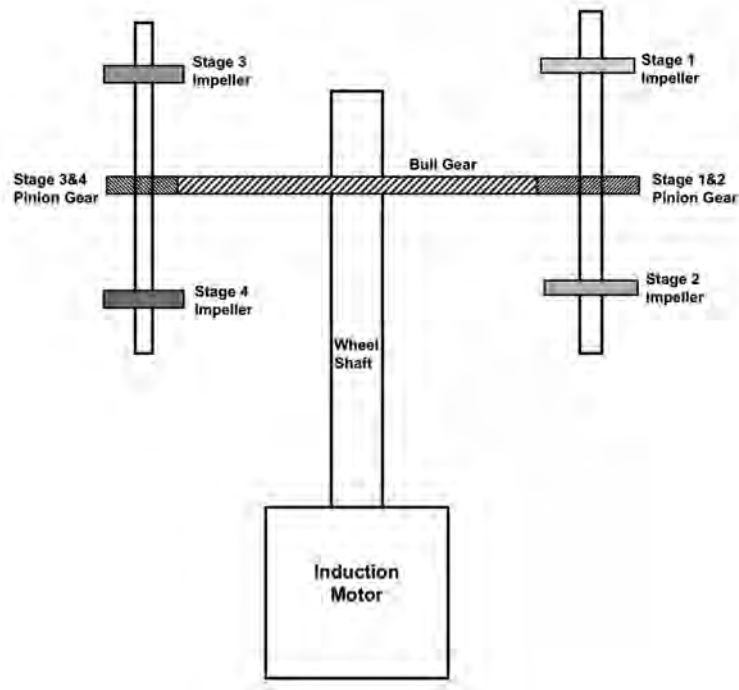


Figure 10-37. Schematic of an integrally-gear four stage compression system.

$$-\left[\sum I_c \cdot N_c \cdot \frac{dN_c}{dt} \right]_{\text{referencetobullgear}} = \sum \left(\frac{\dot{m} H_a}{\eta_a \eta_m} \right)_{\text{allstages}} + \text{Windage \& Losses} \quad (10-28)$$

where, the term on the L.H.S. represents the combined inertia of the driver, the wheel shaft, the bull gear, and all driven pinions and shaft, and compressor impellers, all referenced to one speed, typically taken as the driver speed. An example of such combined inertia of the system shown in Fig. 10-37 is given in Table 10-5.

The above integrally-gear compressor is employed in a urea fertilizer plant to compress carbon dioxide and nitrogen mixture to a pressure ratio of the order of 16. Low pressure gas goes through stages 1 and 2 of compression, where the outlet undergoes cooling through a heat exchanger, and a knock-out drum. The dry gas then goes to the next two stages (3

Table 10-5. Combined rotor polar inertia of the integrally-gear compression system shown in Fig. 10-37

Component	Inertia (kg.m ²)	N (RPM)	I.N ²	Inertia referenced to motor speed (kg.m ²)
Induction Motor	35	2980	3.108E+08	35.000
Bull gear & wheel shaft	41.078	2980	3.648E+08	41.078
Pinion shaft (stage 1 & 2)	0.0518	25202	3.290E+07	3.705
Stage 1 Impeller	0.0544	25202	3.455E+07	3.891
Stage 2 Impeller	0.028	25202	1.778E+07	2.003
Pinion shaft (stage 3 & 4)	0.0207	35283	2.577E+07	2.902
Stage 3 Impeller	0.0064	35283	7.967E+06	0.897
Stage 4 Impeller	0.0043	35283	5.353E+06	0.603
Combined Inertia				90.078

and 4) of compression, and again followed by another set of cooler/knock out drum before it passes onto the rest of the plant. A schematic of this system is shown in Fig. 10-38 showing an anti-surge valve at the downstream of the second knock-out drum (V-0102). A full dynamic simulation of an ESD operation was conducted on this system to determine if the compressor is protected from surging with the anti-surge valve whose $C_v = 67$ and of a linear trim characteristic. The results of this simulation is shown in Fig. 10-39 in terms of the flow through sections 1 and 2. Clearly, section 1 is shown to have gone into deep surge characterized by reverse flow through this section for extended period of time which is not acceptable. If two short (hot) recycle systems are employed in the design as shown in Fig. 10-40, the two sections would be winding down following an ESD operation in a more desirable way without undergoing any surge cycles – see Fig. 10-41. This is a vivid demonstration of the importance of employing hot recycle systems to protect the compressor from surging in particular when there are large volume capacitance involved upstream of the anti-surge valve as is the case in Fig. 10-38.

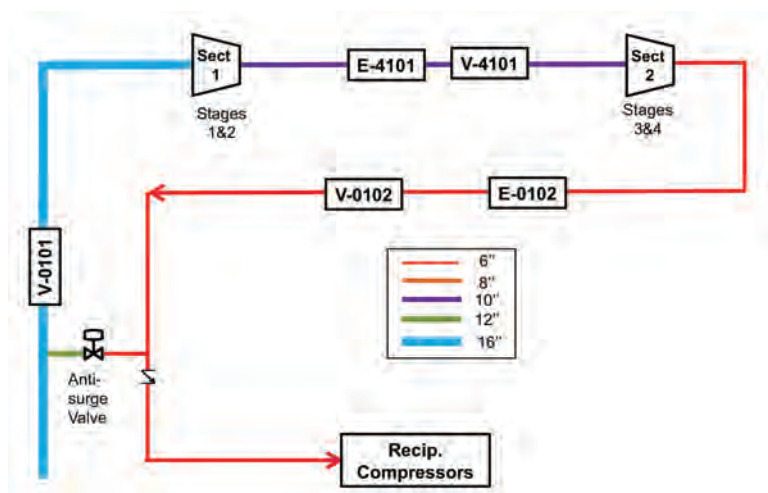


Figure 10-38. Schematic of the integrally-gear four stage compression system employed at the front end of a urea fertilizer plant.

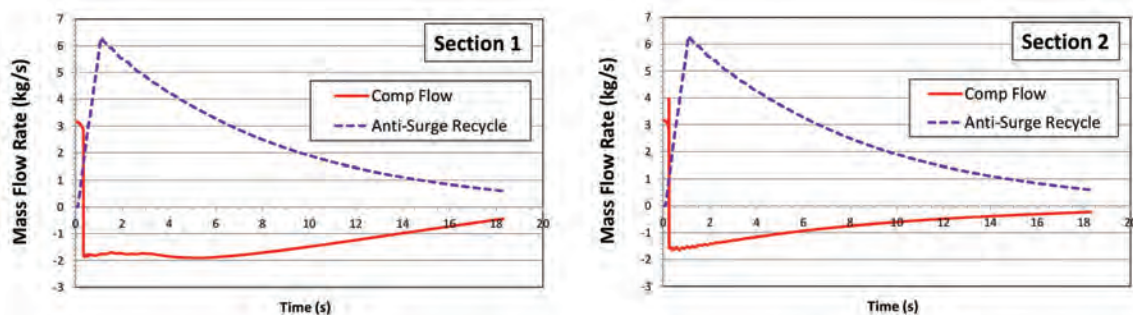


Figure 10-39. Results of Dynamic simulation on an ESD operation on the integrally-gear four stage compression system shown in Fig. 10-38.

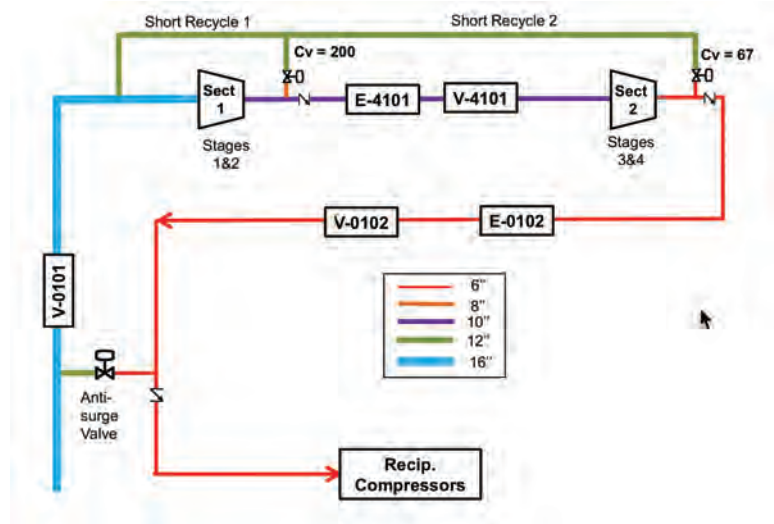


Figure 10-40. Schematic of the integrally-gear four stage compression system with two hot recycle systems around sections 1 and 2.

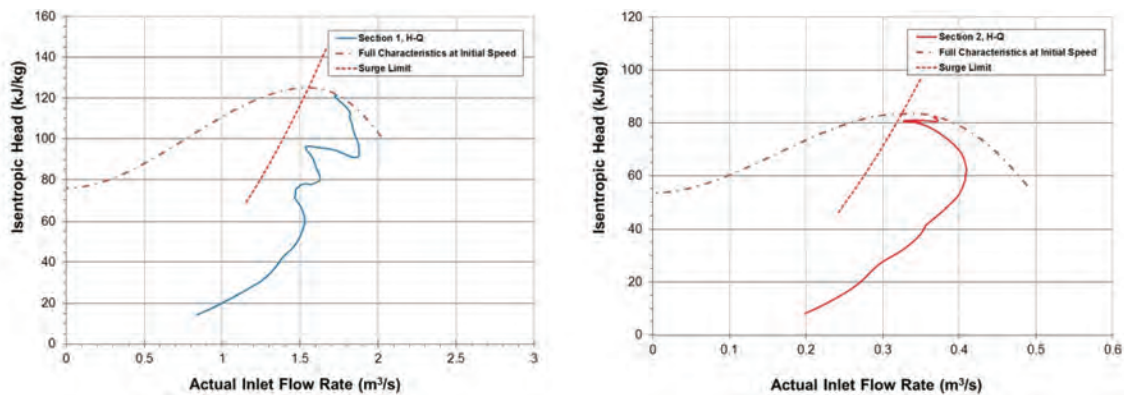


Figure 10-41. Results of Dynamic simulation on an ESD operation on the integrally-gear four stage compression system shown in Fig. 10-40.

10.3.5 Concept of Inertia Number

Following the numerous analyses conducted on different design philosophies of compression systems, and incorporating different types of centrifugal compressors, the decision to employ a short recycle system around the compressor unit to overcome the possibility of surging the unit during ESD operation lies in the balance between the following parameters:

1. Effective compressor/driver rotor inertia defined at the compressor end, (I).
2. The delay time before the recycle valve starts its opening stroke (that is the time associated with phases I and II in the ESD process described above), (τ).
3. The maximum fluid energy extracted from the compressor/driver power train; and the compressor speed – which can be approximated by the product $\dot{m}_s H_s$, where subscript (s) refers to conditions at the surge point at maximum compressor speed.

With the aid of Eq. (10-24), a non-dimensional number can be derived that includes all of the above independent parameters. This dimensionless number, we call *Inertia number* (N_I), is defined as:

$$N_I = \frac{IN^2}{\dot{m}_s H_s \tau} \quad (10-29)$$

A threshold value of the Inertia number was found from analyses conducted on 17 industrial compression systems employing different compressor models and station design. This threshold value was found to be ~30, below which a shorter recycle system would definitely be needed to prevent the compressor unit from undergoing surge during ESD operation. When the Inertia number is greater than 100, the proposed recycle line geometry and location of the recycle valve would be acceptable or satisfactory. For an Inertia number (N_I) in the range of 30–100, detailed dynamic simulation on the station should be conducted in a manner similar to the examples presented in the previous section. Table 10-6 gives the various operating and design parameters for those 17 industrial compression systems analyzed, the respective Inertia number based on a value of τ corresponding to the cold recycle system. The comment column in Table 10-6 indicates whether the final design incorporated a shorter (hot) recycle or not. Figure 10-42 gives the upper and lower bounds of power train inertias of several centrifugal compressors (single and multi-stages) driven primarily by gas turbines. The train inertia included the power turbine, coupling, shafts, impellers and connected bearings and seals.

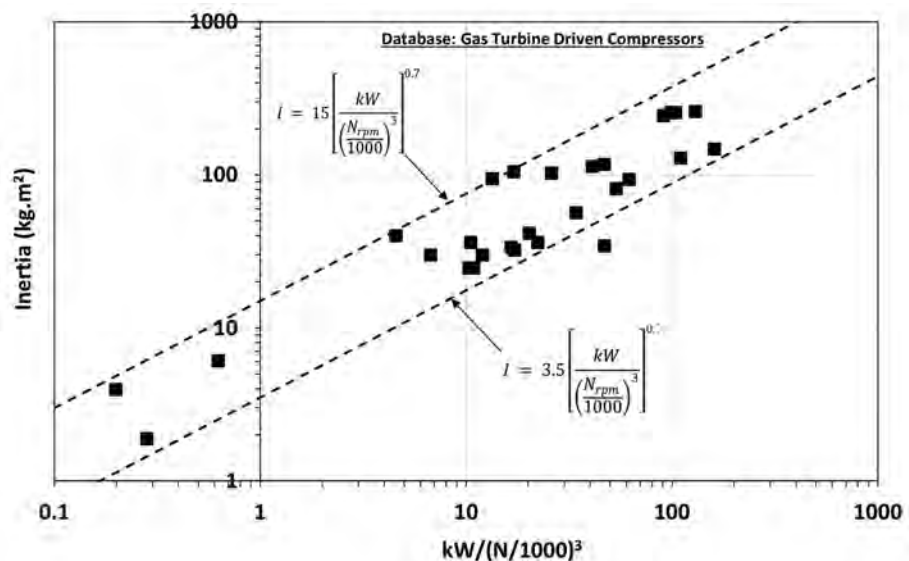
The above threshold value of the Inertia number is useful for station design engineers, which allows a quick check to determine whether a short (hot) recycle system would be required for type and model of the compressor unit and the neighbouring equipment, particularly cooler and suction separators being in the recycle loop. If the calculation of the Inertia number reveals a value less than or equal to 30, a shorter recycle system would be needed, and a detailed dynamic simulation should be conducted. If on the other hand, the Inertia number was approximately 100 or greater, the current recycle system is acceptable, and a detailed dynamic simulation may not be required.

However, when short (hot) recycle system is employed, often the compressor suction and discharge temperatures gradually climb during ESD, as warmer gas is recycled back to the suction of the compressor, which in turn, increases the discharge temperature. Although throttling of the gas through the recycle valve will reduce the temperature to some extent, and the continually decreasing head will moderate the temperature rise across the compressor, it is important to ascertain that the compressor discharge temperature does not increase to a level that could affect the integrity of the compressor internals, e.g. o-rings and seals. Higher pressure-ratio compressors would be more prone to such a problem, and therefore a dynamic analysis should be conducted to determine the temporal temperature distribution during this process. In order to mitigate higher temperature rise in such scenarios, the cold recycle system is also opened simultaneously with the short recycle, such that gas from the cold recycle (having gone through the unit after coolers) would mix with the warmer gas from the short recycle and result in a moderated gas temperature at the compressor suction. Figure 10-43 shows a comparison of hot recycle vs. combined hot and cold recycle temperature profiles for a high-head compressor (pressure ratio ~3.2). The maximum temperature reached using only the hot recycle system during ESD reaches 218°C, while if both the hot and cold recycles are opened, the maximum temperature reaches 178°C. Note also the decline in the temperature beyond the peak point in the case of using both the hot and cold recycle systems.

There are different practices regarding what constitute an adequate size of recycle system [85,86]. The flow resistance characteristics of a recycle system includes the pres-

Table 10-6. Operating and design parameters of several industrial compression systems showing the respective inertia numbers

Station	I (kg.m ²)	N (RPM)	Flow (kg/s)	Hso (J/kg)	τ (ms)	No of Stages	Cooler	Inertia Number	Comment
1	36.1	6800	250	28000	200	1	No	13.1	Delay in Fuel Gas by 100 ms
2	33.7	8856	143	80600	200	2	Yes	12.6	Hot & Cold Recycle Installed
3	32.2	7780	125	64500	200	2	Yes	13.3	Hot & Cold Recycle Installed
4	56.5	6500	180	52000	200	2	Yes	14.0	Hot & Cold Recycle Installed
5	41.5	6671	150	40000	200	2	Yes	16.9	Hot & Cold Recycle Installed
6	243.6	6100	299	68772	200	2	Yes	24.2	Hot & Cold Recycle Installed
7	259.6	4250	380	26220	200	1	Yes	25.8	Hot & Cold Recycle Installed
8	117.0	6500	244	52625	288	2	Yes	14.7	Hot & Cold Recycle Installed
9	102.5	6000	35	160000	215	6	Yes	33.6	Hot & Cold Recycle Installed
10	113.5	6825	420	31000	588	1	Yes	7.6	Hot & Cold Recycle Installed
11	3.9	11967	3	117000	337	4	Yes	54.0	Hot & Cold Recycle Installed
12	6.1	11970	9	124386	324	4	Yes	27.6	Hot & Cold Recycle Installed
13	104.8	7850	51	160612	368	5	Yes	23.4	Hot & Cold Recycle Installed
14	94.3	8311	50	152825	368	6	Yes	25.3	Hot & Cold Recycle Installed
15	0.2	20000	20	32000	185	1	No	6.5	Hot Recycle
16	128.6	5194	480	32000	200	1	No	12.4	Hot Recycle
17	870.0	5775	350	39000	200	2	Yes	116.6	Only Cold Recycle
18	1.885	14000	5.00	154000	260.29	6	Yes	20.2	Hot & Cold Recycle Installed
19	29.86	8000	104.9	58400	200	2	Yes	17.1	Hot & Cold Recycle Installed
20	29.86	8000	58	59200	200	2	Yes	30.5	Hot & Cold Recycle Installed
21	24.6	9053	154	52130	190	2	Yes	14.5	Hot & Cold Recycle Installed
22	24.6	9500	155	56947.7	200	2	Yes	13.8	Hot & Cold Recycle Installed
23	147.3	5000	550	36400	200	2	Yes	10.1	Hot & Cold Recycle Installed
24	80.9	6400	550	25471	200	1	Yes	13.0	Hot & Cold Recycle Installed
25	255.3	6100	367	60740	344	2	Yes	13.6	Hot & Cold Recycle Installed
26	24.6	9053	154	52130	190	2	Yes	14.5	Hot & Cold Recycle Installed
27	255.3	6100	388.3	60740	321.7	2	Yes	13.7	Hot & Cold Recycle Installed
28	93.2	6500	353	48000	300	2	Yes	8.5	Hot & Cold Recycle Installed
29	106.119	1800	20	200000	300	2	Yes	3.1	Hot & Cold Recycle Installed
30	34.3	8000	200	120000	300	2	Yes	3.3	Hot & Cold Recycle Installed
31	36.17	9000	105	73000	300	2	Yes	14.0	Hot & Cold Recycle Installed
32	40	13000	50	200000	300	2	Yes	24.7	Hot & Cold Recycle Installed

**Figure 10-42.** Upper and lower bounds of power train inertia of gas turbine driven centrifugal compressors.

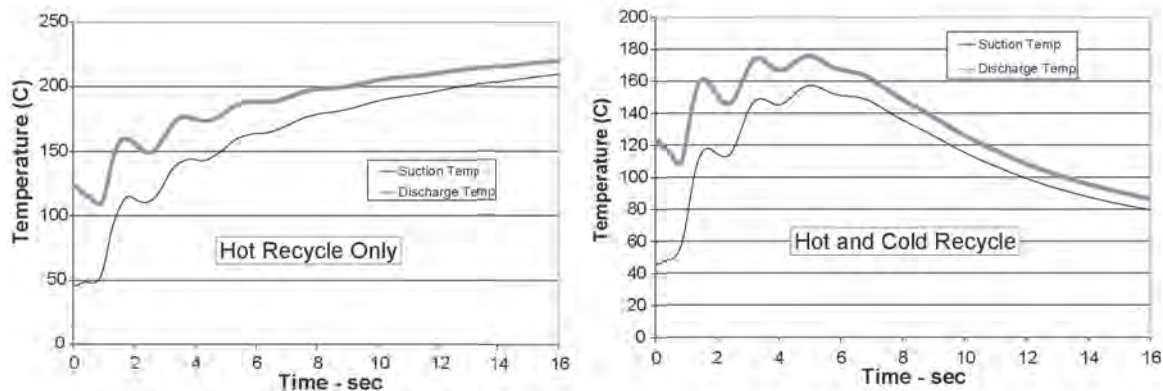


Figure 10-43. Example of increases in suction and discharge temperatures during ESD.

sure drop across the recycle valve of a given capacity (C_v) when full open, along with the flow resistance imposed by the piping and fitting elements comprising the recycle path from the compressor discharge flange to compressor suction flange. The flow resistance characteristics can be presented in terms of equivalent adiabatic head, by means of Eq. (10-10), and the actual flow at compressor suction. The valve (C_v)_{surge} combined with piping/fitting resistance curve that corresponds to the compressor surge line can be used as reference characteristics. One sizing practice requires that the minimum recycle valve capacity should have a (C_v) equal to twice that of (C_v)_{surge}. Another more stringent practice requires that the minimum recycle valve capacity should have a (C_v) equal to twice that of a valve that has resistance characteristics passing through the normal operating point of the compressor, i.e. $2 (C_v)_{\text{operating point}}$. As an example, Fig. 10-44 shows the difference between those two practices on a high-head compressor unit. Clearly, while the second practice is more conservative, it is important to select a recycle valve with a (C_v) such that it would not drive the overall recycle flow characteristics beyond the choke limit of the compressor performance characteristics. Figure 10-44, shows that the second practice of $2 (C_v)_{\text{operating point}}$ is very close to the choke limit of this compressor in this case.

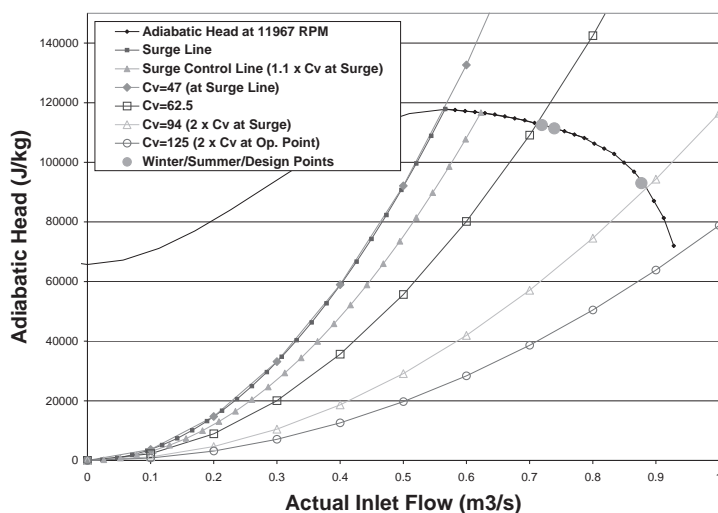


Figure 10-44. Flow resistance characteristics of different recycle valve capacities plotted on compressor head-flow chart.

10.3.6 Recycle System around Compressors Arranged in Series

It is noted that the two compressor sections of Fig. 10-40 are connected in series, and that the respective hot (short) recycle lines are joined and form a common connection point at the suction of Section 1. While this is a typical configuration in general based on the argument that in such arrangement the recycle valve of the downstream unit would be subjected to a higher pressure ratio and hence admit higher relief flow to that unit. This is generally true in cases where there is little gas capacitance between the upstream and downstream units, which is not the case in this example. If an independent short recycle lines are employed for this station as shown in Fig. 10-45, the required downstream recycle valve capacity C_v would have been smaller at 53 instead of $C_v = 67$. The results of a dynamic simulation for the configuration of Fig. 10-45 and the noted recycle valve C_v 's are shown in Fig. 10-46, which shows that both compressor units wind-down during an ESD operation in a desired manner without undergoing any surge cycles. The fact that a large valve capacity is required for the configuration of Fig. 10-40 is due to the existence of large gas capacitance between sections 1 and 2 (namely; E-41 and V-4101).

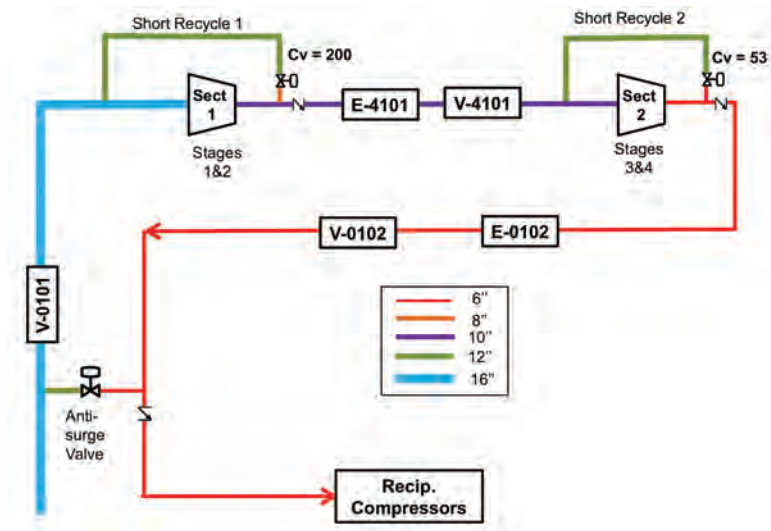


Figure 10-45. Schematic of the integrally-g geared four stage compression system with two independent hot recycle systems around sections 1 and 2.

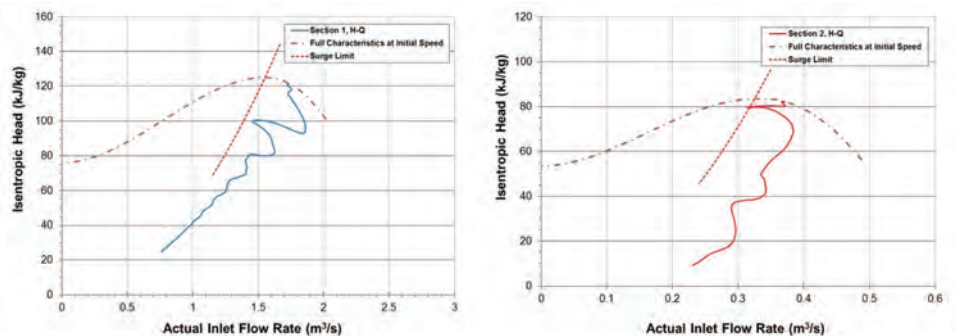


Figure 10-46. Results of dynamic simulation on an ESD operation on the integrally-g geared four stage compression system shown in Fig. 10-45.

To further understand the effects of the gas capacitance between two compressor units in series on the optimum arrangement of their respective hot recycle systems, another compressor station is considered which does not exhibit large gas capacitances between the upstream and downstream units apart from the connecting piping only. This is shown schematically in Fig. 10-47 [84]. The two hot recycle lines are connected to one common point at the suction of Unit A1 as shown. Dynamic simulation of an ESD operation was conducted on this system to size the respective recycle valve capacity. The results of compressor wind down following an ESD trigger are shown in Fig. 10-48. The optimum recycle valve sizes in this case are noted on Fig. 10-47 as $C_v = 3750$ for Unit A1 and $C_v = 1750$ for Unit A3.

If the respective hot recycle systems for Units A1 and A3 are separated such that each recycle line is connected back to the respective unit suction side as shown in Fig. 10-49, the required recycle valve capacity for Unit A3 would be higher at $C_v = 3750$, similar to that for Unit A1 whose recycle valve capacity remains unchanged at $C_v = 3750$. The result of the dynamic simulation of an ESD operation are shown in Fig. 10-50 showing that both units wind down surge-free, but Unit A3 required larger recycle valve capacity to attain these results.

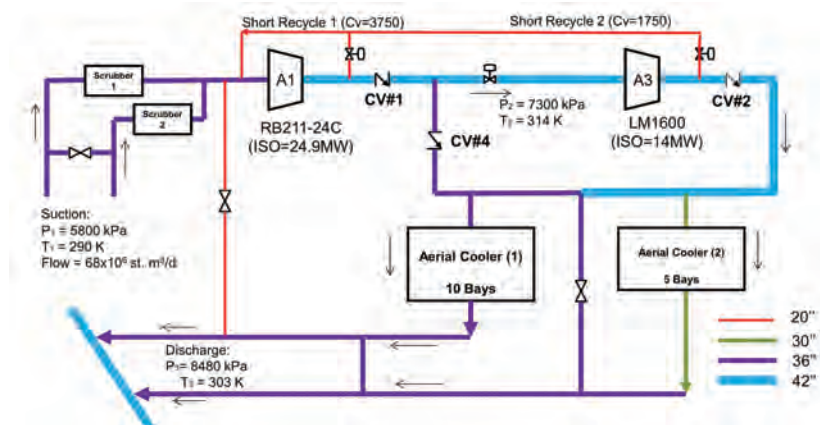


Figure 10-47. Schematic of the two compressor units arranged in series and *connected* hot recycle lines.

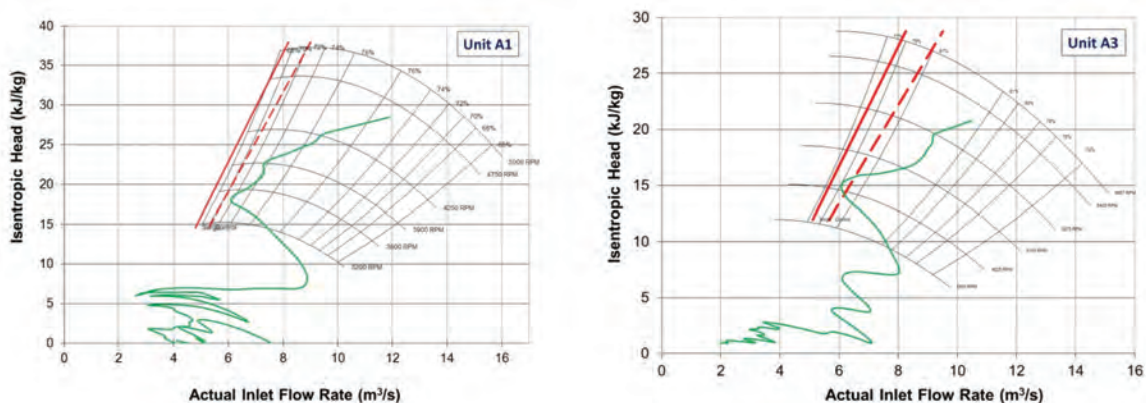


Figure 10-48. Results of dynamic simulation on an ESD operation on the series compressor units of Fig. 10-47.

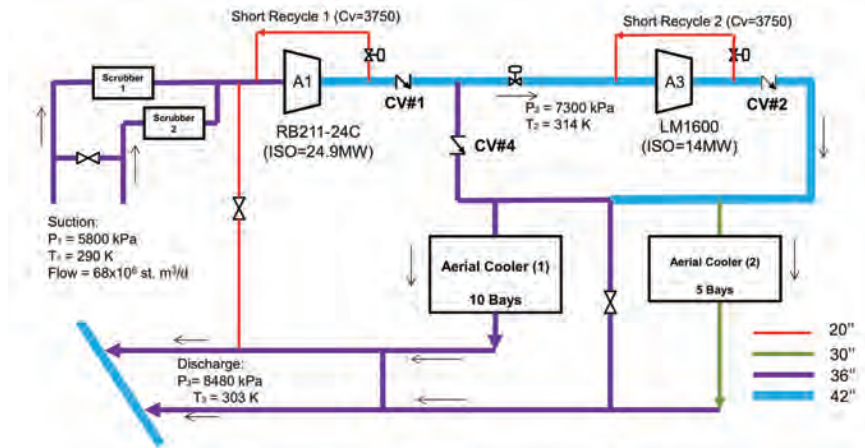


Figure 10-49. Schematic of the two compressor units arranged in series and *independent* hot recycle lines.

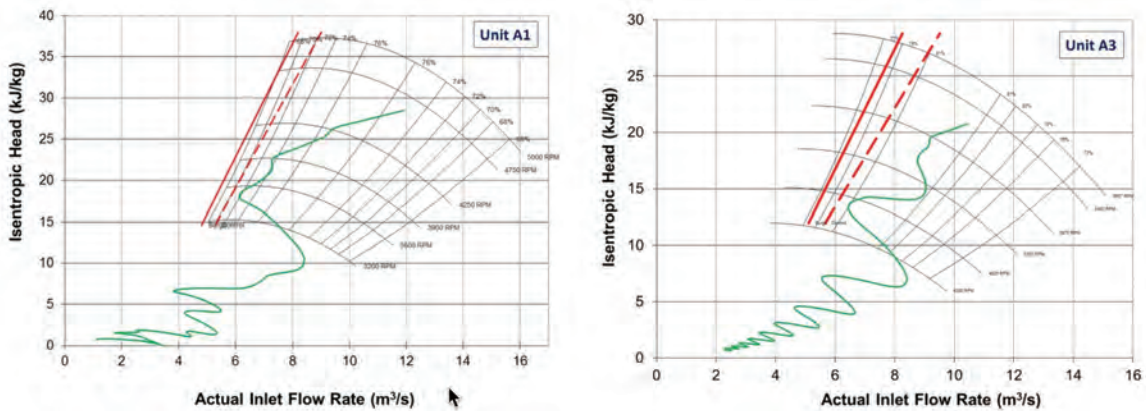


Figure 10-50. Results of dynamic simulation on an ESD operation on the series compressor units of Fig. 10-49.

10.4 CHECK VALVE DYNAMICS

In the design of natural gas compressor stations, a check valve is a critical element, which is commonly placed on the discharge side of the compressor to prevent reverse flow that can cause serious damage to the compressor itself and other components such as seals and bearings. One of the selection criteria of the check valve for this particular application is the valve flow characteristics in steady flow, and its dynamic characteristics in unsteady flow operation. With regards to steady flow valve characteristics, current models for the determination of the check valve open angle vs. mean flow velocity are based on semi-empirical data obtained from water tests and are extended to gaseous flow applications.

To explain this further, a swing-type check valve is characterized by a circular disc that pivots or swings about a hinge that is located outside the flow path (Fig. 10-51). As such, the disc can open a certain degree depending on the upstream flow velocity. Traditionally or conventionally, swing check valves have the ability to open to disc angles of 75° to 85° from a plane perpendicular to main valve centerline. The large openings are preferable to

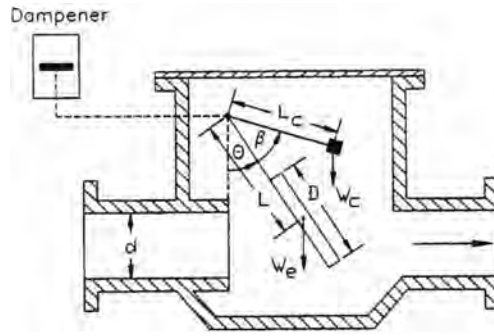


Figure 10-51. Schematic of a typical swing-type check valve.

reduce pressure loss due to flow obstruction. However, large disc openings require higher flow velocities to fully open the valve and to keep the disc stable and to minimize chattering. The mean flow velocity required to open the valve to maximum disc opening is known as the critical flow velocity (v_0) and is a function of the valve/disc geometry, fluid properties (such as density and viscosity) and upstream flow conditions. Different models have been proposed to predict (v_0) based on the equilibrium of moments about the hinge of the disc assembly at steady state. Chiu and Kalsi [32] proposed a simplified equation for valves without a counter balance (which is also known as the EPRI model [33]), in the form:

$$v_0 = \sqrt{\frac{c \cdot W_e \cdot \sin(\theta)}{K \cdot \rho_f \cdot A_d \cdot \cos^2(\theta)}} \quad (10-30)$$

where

c = 0.9 for water, and

W_e = effective weight of the disc/arm assembly in the fluid (usually taken as the disc weight + 1/2 of arm weight in the fluid)

θ = disc angle from a plane perpendicular to valve centerline

K = an empirical body shape factor (= 2.0)

ρ_f = fluid density

A_d = disc area

This model greatly underestimates the flow velocity requirements by as much as 50% for clearway valves [33].

Rahmeyer [34] developed a more fundamental model taking into account the hydrodynamic torque resulting from two contributions: i) the impingement of the flow jet on the valve disc and, ii) lower back pressure distribution on the disc than the main stream static pressure. Two different torque coefficients (K_v and K_p) were developed by Rahmeyer [34] from which the hydrodynamic torque T_H can be determined from:

$$T_H = K_H D^3 \rho_f v^2 = (K_v + K_p) \rho_f v^2 \quad (10-31)$$

The hydrodynamic coefficient K_H is then used in determining the valve opening characteristics vs. mean flow velocity in steady state, and accounting for the counter balance weight as follows:

$$v^2 = \frac{1}{\rho_f D^3 K_H} [W_e \cdot L \cdot \sin \theta' + W_c L_c \cdot \sin(\theta + \beta)] \quad (10-32)$$

where:

D = valve dimensional characteristics (I.D.)

K_H = hydrodynamic coefficient, $K_H(\theta)$

- L = distance between c.g. of the disc/arm assembly and hinge (see Fig. 10-51)
 L_c = distance between c.g. of the counter balance assembly and hinge (see Fig. 10-51)
 W_c = counterbalance weight in air
 W_e = effective weight of the disc/arm assembly in the fluid (usually taken as the disc weight + 1/2 of arm weight in the fluid)
 β = angle between plane of the disc and counterbalance weight (see Fig. 10-51)
 θ = disc angle from a plane perpendicular to valve centerline
 θ' = angle of the cord to disc centre of gravity from a plane perpendicular to valve centerline
 ρ_f = fluid density

The expressions for both K_v and K_p according to Rahmeyer [34] are as follows:

$$K_v = A_0 \cdot \cos(\theta) \left[h + \frac{z}{2} \right] \quad (10-33)$$

in which h is the height of the disc hinge above the flow area of the valve inlet, z is the length of the disc protruding into the flow, and A_0 is the area of the disc in the flow. Disc and valve inlet diameters are D and d , respectively.

$$h = \left[L - \frac{d}{2} \right] / \cos(\theta) \quad (10-34)$$

$$z = L + \frac{D}{2} - h \quad (10-35)$$

$$A_0 = \sqrt{2Dz^3 \cos^3(\theta) - z^4 \cos^4(\theta)} \quad (10-36)$$

$$K_p = \frac{\pi D^2}{4} \cdot C_d \cdot L \quad (10-37)$$

$$C_d = (K_b \cdot \theta)^{-3} \quad (10-38)$$

According to over 30 swing valves tested in water, the value of K_b was found to be 0.025 for predicting the velocities necessary to just open the valve. Limited tests with one valve in air by Rahmeyer [34] verified that the amount of turbulence is reduced and, hence, a value of $K_b = 0.02$ was suggested for the prediction of disc positions up to the critical velocity. Botros et al. [35] extended the above model and refined it for applications with gaseous fluid flows.

10.4.1 Dynamics of Swing Type Check Valves

There are two aspects of the dynamic behavior of swing type check valves, namely: slamming of the disc and the maximum attainable reverse flow as the valve closes due to flow deceleration. Dampeners (slam retarders) are often recommended to improve the mechanical integrity of the valve and reduce any potential risk of disc damaged if slammed. As dampeners have the adverse effects of increasing the reverse flow through the valve as it closes, counterbalance weights are introduced to assist in closing the valve and also to overcome seal friction. Hence comes the complexity of the problem and the intricacy of the two dynamic aspects (slamming and reverse flow) as being affected by these external devices (dampeners and counterbalance) in addition of course to the local mean flow deceleration.

The dynamic behavior of check valves in incompressible flows were studied experimentally and numerically by several authors [36–47]. A good review paper on this topic is by Thorley [36]. Two lines of research can be identified: the first is an attempt to deduce the dynamic behavior of the check valve from combining the valve geometrical and physical properties and fluid flow characteristics in developing and solving the equation of motion for the valve. This technique has been successful for swing type check valves [e.g. 39–41]. The second technique, which was first developed by Provoost [40], is based on direct measurements of the maximum reverse flow velocity (v_r) as a function of the local mean flow deceleration (dv/dt)—see Fig. 10-52. In this technique, direct manifestation of valve components and flow characteristics is revealed by these two parameters rather than a detailed account of all parameters (i.e. focus on end behavior than on causes or contributing parameters). This latter technique was first applied to swing- and ball-type valves [33] and later was introduced formerly by Delft Laboratory [41] and is known as the ‘Dynamic Characteristic Curve (DCC)’ of the valve. The above two parameters (v_r , dv/dt) can be described in a dimensionless manner in the form [42]:

$$v_r/v_0 \quad \text{and} \quad \frac{D}{v_0^2}(dv/dt) \quad (10-39)$$

Because of the simplicity of this latter technique, many investigators have adopted it in the dynamic analysis of systems involving undamped valves [42–46], and extended to damped valve [47].

A general equation of motion for a swing type check valve with a counterbalance weight and damping produced by an external dampener and seal friction can be written as follows (Fig. 10-51):

$$I\ddot{\theta} = -W_c L \sin\theta - W_c L_c \sin(\theta + \beta) + K_H D^3 \rho_f v^2 - C_d D^5 \rho_d \dot{\theta} |\dot{\theta}| - T_f \quad (10-40)$$

where:

C_d = damping coefficient

I = effective inertia of the moving parts (including the disc, arm, counterbalance, moving fluid)

L = distance between c.g. of the disc/arm assembly and hinge

L_c = distance between c.g. of the counter balance assembly and hinge

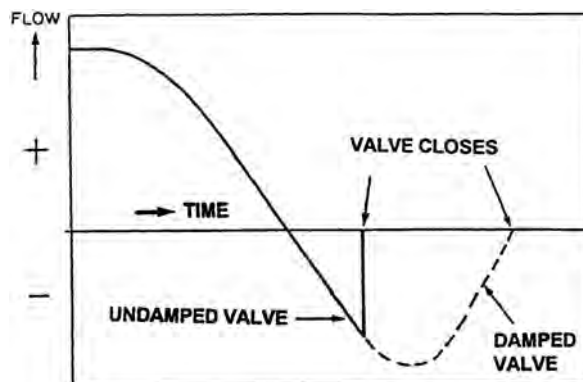


Figure 10-52. Schematic of a typical swing-type check valve [41,45].

T_f = frictional torque
 ρ_d = damping fluid density

The left hand side of Eq. (10-40) represents the inertia of the moving elements including the effect of the adjacent fluid. The terms on the right hand side represent, respectively, the external torques due to effective gravitation (including buoyancy), counterbalance weight, hydrodynamic, effective damping and seal friction. All of these terms are scaleable except for the frictional term (T_f). The hydraulic coefficient K_H is a function of the valve geometry and the disc angle, as discussed earlier. If the following dimensionless variables are introduced [47];

$$a = \theta, \quad \dot{a} = \frac{\dot{\theta}D}{v_0}, \quad \ddot{a} = \frac{\ddot{\theta}D^2}{v_0^2}, \quad \tau = \frac{tv_0}{D} \quad (10-41)$$

where:

t = time
 v_0 = minimum mean flow velocity upstream of the valve to just open the valve to a fullyopen position
 α = same as θ
 τ = dimensionless time

and assuming that the flow velocity is decelerating linearly from an initial condition (v_0), then [47]:

$$v = v_0 + \left(\frac{dv}{dt} \right)_- (t - t_0) \quad (10-42)$$

The equation of motion Eq. (10-40) can be written in the following dimensionless form:

$$\begin{aligned} \left[\frac{I}{\rho_f D^5} \right] \ddot{a} = & - \left[\frac{W_e L}{\rho_f v_0^2 D^3} \right] \sin a' - \left[\frac{W_c L_c}{\rho_f v_0^2 D^3} \right] \sin(a + \beta) \\ & + K_H \left[1 + \frac{D}{v_0^2} \left(\frac{dv}{dt} \right) (\tau - \tau_0) \right]^2 - \left[\frac{C_d \rho_d}{\rho_f} \right] \dot{a} |\dot{a}| - \left[\frac{T_f}{D^3 \rho_f v_0^2} \right] \end{aligned} \quad (10-43)$$

which leads to the following dimensionless numbers:

$$\text{Inertia number } [N_1] = \left[\frac{I}{\rho_f D^5} \right]$$

$$\text{Disc Weight number } [N_2] = \left[\frac{W_e L}{\rho_f v_0^2 D^3} \right]$$

$$\text{Counterbalance number } [N_3] = \left[\frac{W_c L_c}{\rho_f v_0^2 D^3} \right]$$

$$\text{Hydrodynamic number } [N_4] = [K_H]$$

$$\text{Deceleration number } [N_5] = \left[\frac{D}{v_0^2} \left(\frac{dv}{dt} \right) \right]$$

$$\text{Damping number } [N_6] = \left[\frac{C_d \rho_d}{\rho_f} \right]$$

Neglecting the frictional torque (T_f), solution of the above equation in a dimensionless form will be self-similar if the above six dimensionless groups are maintained for valves of similar geometry. In a steady state case, when the valve is fully open, $\theta = \theta_0$, $\dot{\theta} = \ddot{\theta} = 0.0$ and $v = v_0$, the equation of motion is reduced to Eq. (10-32) at fully open position, which determines the critical flow velocity:

$$v_0^2 = \frac{1}{\rho_f D^3 K_H} [W_e \cdot L \cdot \sin \theta_0 + W_c L_c \cdot \sin(\theta_0 + \beta)] \quad (10-44)$$

For geometrically similar valves and for $W_e \cdot L / W_c \cdot L_c = \text{constant}$, three of the above similarity numbers (N_2 , N_3 and N_4) become the same, and the solution of Eq. (10-43) above depends only on the relative magnitude of the inertia parameter N_1 , the deceleration parameter N_5 and the damping parameter N_6 . Finally, it is assumed here that the coefficients K_H and C_d determined from steady state test data can be applicable in a quasi-steady (dynamic) behavior of the valve.

The above equation of motion is a non-linear second order O.D.E. that can be solved in a marching-in-time numerical scheme from an initial value. A standard 4th order Runge-Kutta method can be used to advance the solution an incremental time step. The time step for the solution of these equations should be selected to be at least 1/50th of that required by the method of characteristics applied to the solution of the full one-dimensional conservation equations (mass, momentum and energy) of the flow in the attached piping system [48]. This is necessitated for a stable solution of the O.D.E. system of equation and also to minimize the resulting higher order truncation errors.

Figure 10-53 shows an example of experimental data for various types of check valves [36]. It shows that the swing type valve displays steeper DCC characteristics than other types of check valves. Figure 10-54 shows numerical results [46] for a 100 mm swing type check valve with and without damping [48]. The reason for a higher reversed flow for the case of damped valve can be easily explained by the schematic plot of Fig. 10-52, where the dotted line representing the reversed flow through the valve continues further in time

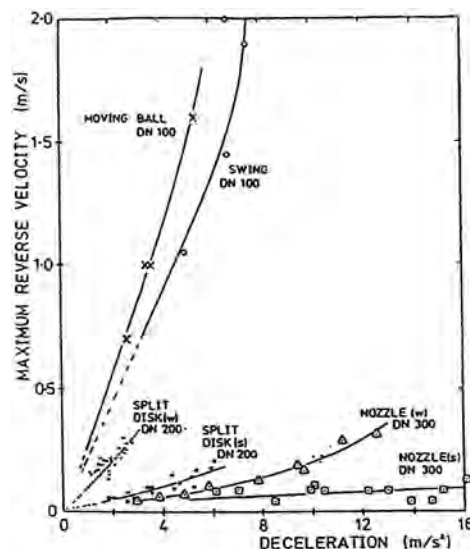


Figure 10-53. Dynamic characteristic curves for different types of check valves [36].

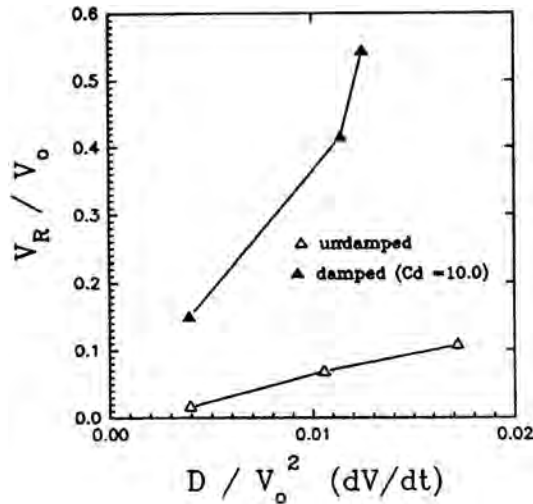


Figure 10-54. Effects of damping on the dcc of 100 mm swing type check valve [48].

to a maximum reversed flow. In the undamped case, the reversed flow tends to abruptly get truncated earlier before maximum reversed flow is attained [36,40].

10.4.2 Slamming Characteristics of Swing Check Valves

Dampeners (slam retarders) are used with swing type check valves to either: (a) dampen disc flutter when flow velocity is at, or below, the critical velocity (v_0); or (b) prevent slamming the disc against the valve seat when it closes. Severe slamming can cause mechanical failure of the disc and the seat.

Experimental and numerical investigation by Botros and Roorda [35,48] was carried out on a 100 mm swing type check valve to assess the terminal velocity of the disc just prior to touching the valve seat during its closure. The investigation was conducted for both air and water applications, hence, different fluid density, disc weights, inertias and v_0 's. Several tests were also conducted in air and water to verify the numerical results obtained. For the water application, the disc/counterbalance assembly was made 10 times heavier and since the water density is approximately 1000 times greater than air, the resulting critical velocity (v_0) was approximately ten times higher for air (50 m/s) than for water (4.5 m/s). Inertias in water were also scaled up 10 times from those in air as a result of heavier disc weights. The geometry of the disc assembly was maintained the same in the lighter and heavier discs, and the same valve body was used in all tests. The following are pertinent data of the swing valve used in water tests:

Pipe I.D.	= 0.102 m
Disc Diameter	= 0.129 m
Maximum Disc Opening	= 70 degrees
Disc Mass	= 1.99219 kg
Arm Mass	= 0.56157 kg
Length (L)	= 0.08172 m
Counterbalance Mass	= 1.04787 kg
Length (L_c)	= 0.08732 m
Fluid Density	= 1000.0 kg/m ³

The scenario posed is one which corresponds to an infinite deceleration of the flow, i.e. a case when the valve was fully open due to mean flow velocity equal to or greater than (v_0) and then flow was stopped momentarily at the check valve location to zero velocity. An experiment was devised to simulate this case, in which the disc was pulled by a string to the fully open position and was then released to allow the disc to free fall in the stagnant fluid medium. Disc position-time profile was measured by a position transmitter mounted on the valve shaft and disc velocity is determined from the derivative of the $(\theta-t)$ profile. Results of these free fall tests in air and in water are shown in Fig. 10-55, without counter balance weights attached. Two phases can be identified; the initial phase is governed by the balance between the inertia term $[N_1]$, the disc/arm weight and the fluid hydrodynamic resistance offered by the relative velocity between the disc and the fluid. From this initial phase, it was possible to determine the inertias of the moving elements about the hinge. It was determined from the measured profile that $I = 4.06 \times 10^{-3} \text{ kg.m}^2$ for the air system and $5.8 \times 10^{-2} \text{ kg.m}^2$ for the water system.

The final phase of valve closure exhibits a distinct difference between air and water tests. It is evident from Fig. 10-55 that the disc takes a sharp dive with a much higher terminal (impact) velocity at the valve seat in the air case than that in the water case. Numerical results also confirmed the same trend and are shown in Fig. 10-55 for comparison with measurements (time scales were intentionally shifted to separate the two results). Good agreements between the two results are demonstrated and, more importantly, the final phase of valve closure exhibits the same trend as those observed experimentally. As a result, it is concluded that disc impact velocity during swing check valve closure is higher in air (gaseous fluid) than in water (incompressible fluid). It seems

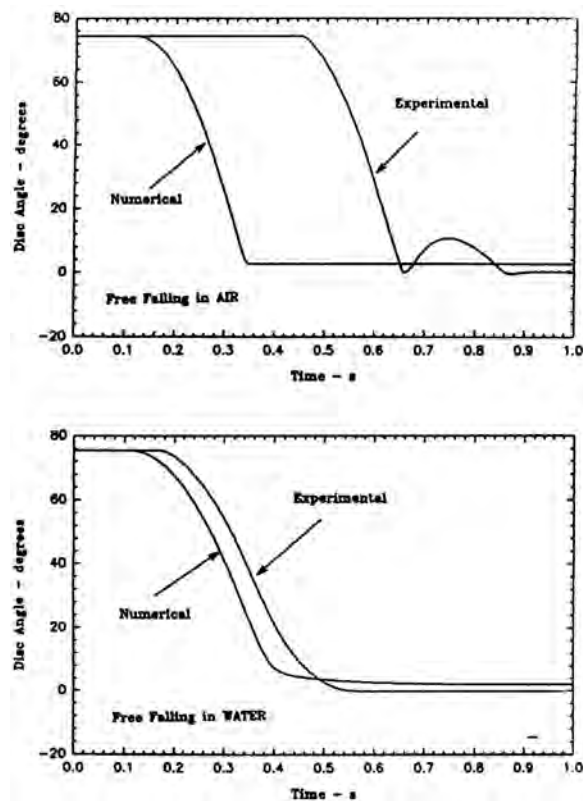


Figure 10-55. Experimental and numerical results of free-falling disc of a swing check valve in air and water [48].

that the compressibility of the fluid in this final phase is responsible in shaping the $(\theta-t)$ profile, yielding soft impacting on the valve seat in case of incompressible fluid than in a compressible fluid. It is also worth mentioning at this point that the good agreement between measurements and simulation results demonstrated in Fig. 10-55 confirms the validity of using steady state values of K_H in describing the dynamic behavior of the valve.

Botros and Roorda [48] conducted further investigations to assess the effects of the deceleration rate (dv/dt) . Simulations were conducted again on air, water and natural gas. The natural gas application was selected as the check valve is an essential component in the design of compressor stations on gas transmission systems. Here for the applicable pressure range, the gas density can vary from 40 to 60 kg/m³, which constitute a range of density between air (~ 1.0 kg/m³) and water (~ 1000 kg/m³). The results are shown in Fig. 10-56, for these different fluids and for various dv/dt . The corresponding inertia numbers are also shown in the Fig. 10-56 (note that the heavier valve disc used in the water system is assumed for the natural gas application resulting in a $v_0 = 20$ m/s). Again, it is clear that the impact velocity of the disc on the valve seat is higher in compressible fluid than in incompressible fluid. Also notice the asymptotic trend of the impact velocity as the deceleration rate increases. Clearly, the asymptotic value of the impact velocity corresponds to free falling of the disc or infinite dv/dt . The natural gas case falls between air and water cases but closer to air.

Another set of numerical investigations was carried out [46] to study the effects of reversed velocities on disc impact velocity. Here the flow velocity is assumed to suddenly drop from a positive value equal to v_0 to a negative value equal to v_r and remained at this negative value to the end of the simulation. This was conducted to accentuate the severity of the terminal velocity of the disc when slamming against the seat. The results are shown in Fig. 10-57 for the three fluids; air, natural gas and water. Again, for the same v_r/v_0 ratios, the impact velocity of the disc during closure is higher in compressible fluids than in incompressible. Note that the asymptotic values in Fig. 10-56 correspond to $v_r/v_0 = 0.0$ in Fig. 10-57. The main conclusion from this investigation is the obvious and consistent trend of the disc impact velocity during valve closure being higher in compressible fluids (air and natural gas) than in incompressible fluids (e.g. water).

The maximum (asymptotic) impact angular velocity in the case of zero damping can also be determined analytically from balancing the potential and kinetic energy of the check valve disc/counterbalance assembly. At high deceleration rate (dv/dt) , the flow can be assumed to have come to zero velocity from the critical velocity v_0 in zero time. The balance

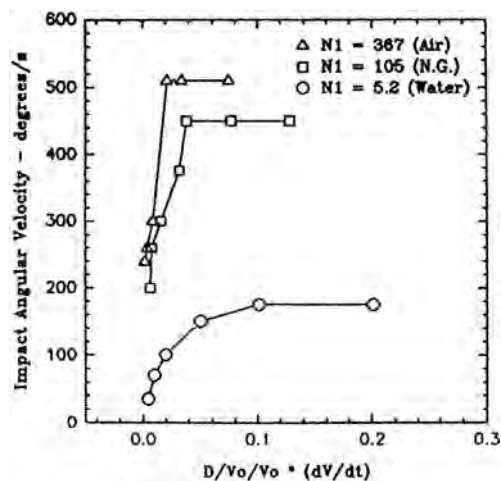


Figure 10-56. Impact angular velocity of swing disc during valve closure due to fast flow deceleration [48].

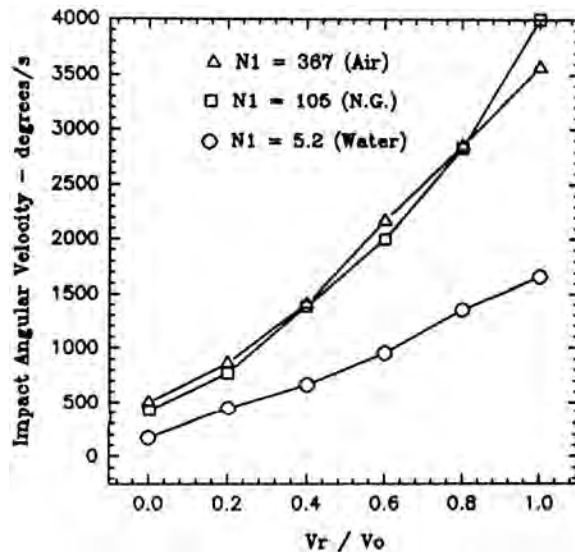


Figure 10-57. Dependence of the impact angular velocity of swing disc during valve closure on reversed flow velocity [46].

between potential energy when the disc at maximum open position, to the kinetic energy when it is at the closing position, can be written as follows:

$$\frac{1}{2} I \dot{\theta}_i^2 = W_e L (1 - \cos \theta_0) + W_c L_c [\cos \beta - \cos(\theta_0 + \beta)] \quad (10-45)$$

Hence, the maximum impact angular velocity ($\dot{\theta}_i$) at the closed position is expressed as:

$$\dot{\theta}_i = C_i \sqrt{\frac{2}{I} [W_e L (1 - \cos \theta_0) + W_c L_c (\cos \beta - \cos(\theta_0 + \beta))]} \quad (10-46)$$

The above equation suggests that in the case of no damping and no counterbalance, the ratio W_e/I is almost the same for air and water except that it might be slightly smaller in water than in air due to the effect of buoyancy on W_e . Hence, it suggests that the

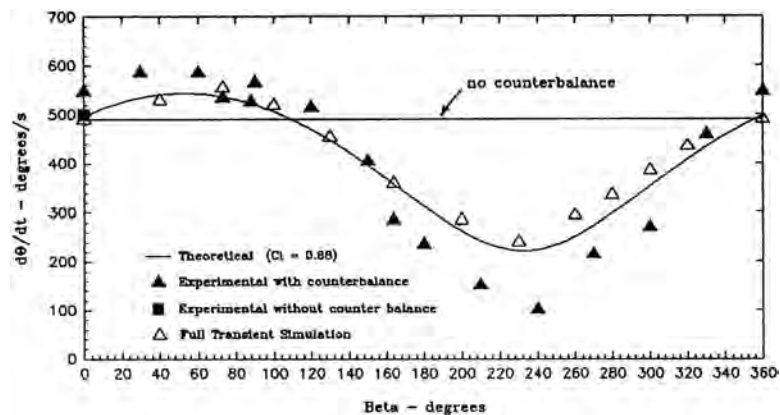


Figure 10-58. Effects of counter balance weight on the impact angular velocity of swing disc free falling in air [48].

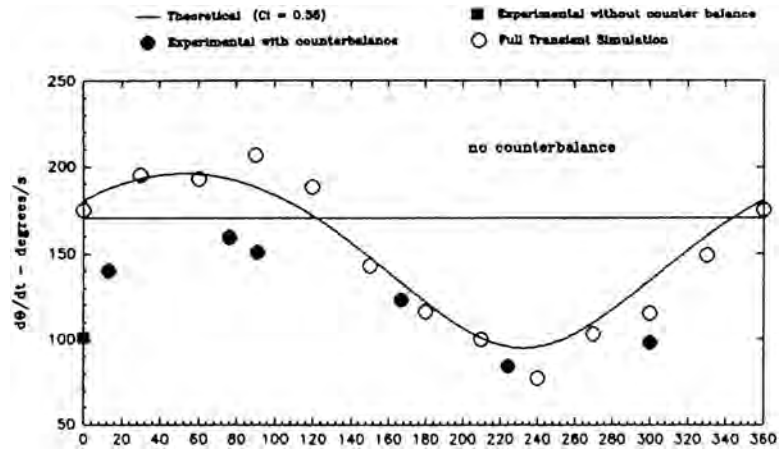


Figure 10-59. Effects of counter balance weight on the impact angular velocity of swing disc free falling in water [48].

maximum impact velocity of the disc, at the closed position, is the same for air and water. This argument is, however, negated from both measurements and numerical results, due to fluid compressibility and fluid resistance. Therefore, an impact velocity coefficient (C_i) is needed to correct for these effects. From measurements without counter balance, this C_i coefficient was found to be 0.88 for air and 0.38 for water [48].

Several free fall tests were then conducted with counterbalance weights and the disc impact velocity were determined and compared to that calculated using Eq. (10-46) above, and also using the full transient simulation analysis. The results are shown in Fig. 10-58 for air and Fig. 10-59 for water. It can be seen that a counterbalance weight can be used to reduce the disc impact velocity (slamming) if it is set an angle $\beta > 180 - \theta_0$ in this range, the second term in Eq. (10-45) becomes negative, resulting in reducing the disc impact velocity. Also, the addition of w_c increases the total system inertia (i), resulting again in further reduction in the disc impact velocity.

10.4.3 Effects of Counterbalance on Maximum Reverse Velocity

Another series of experiments were conducted by Botros and Roorda [48] to determine the effects of the counterbalance angle on the maximum reverse flow through the swing check valve for different flow deceleration. The results are shown in Fig. 10-60 for three deceleration rates and β angle varied between 0.0 and 330° in steps of 30° . Results of the no counterbalance case is also presented for comparison. It is clear that the counterbalance set angle (β) has a dramatic effect on the maximum reverse flow velocity through the check valve for a given deceleration rate. For $0.0 < \beta < 180 - \theta_0$, the counterbalance weight reduces dramatically the reverse flow through the check valve. Maximum reverse flow occurs for $\beta > 180 - \theta_0$. It should be noted that the results presented here was obtained for a specific case of $W_c = 0.5 W$, to illustrate the effects of the counterbalance setting angle β .

Comparing the results of Fig. 10-58 to that of Fig. 10-60 indicates that there are three competing effects that dictate the setting the angle of the counterbalance weight w.r.t. the check valve disc. Figure 10-58 suggests that for a lower disc impact velocity the range of $\beta > 180 - \theta_0$ is recommended. A similar range is recommended for lower values of the critical velocity (v_0) [35]. An opposite range is recommended, however, to reduce the reverse flow through the valve due to flow deceleration (see Fig. 10-60). These opposite trends point out to the importance of optimizing the counterbalance angle β to achieve optimum values

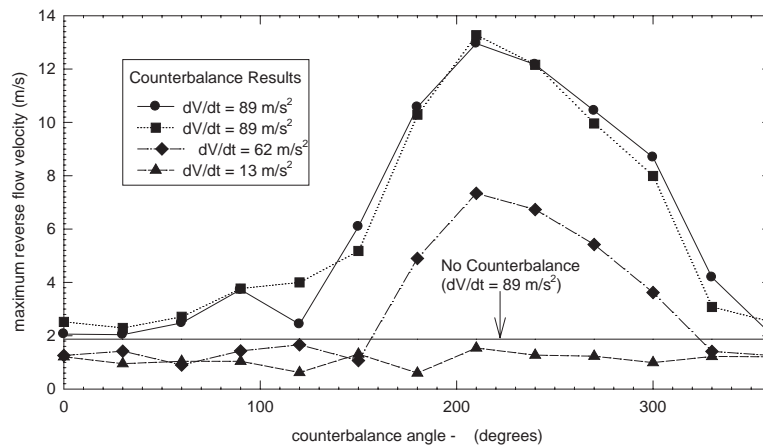


Figure 10-60. Experimental data of the effects of counter balance angle on the maximum reverse velocity through 100 mm swing type check valve [48].

for these three parameters (v_0 , impact velocity and maximum reverse flow), for a given application where one or more of these three parameters may be more important than the others.

10.4.4 Dynamics of Piston Type Check Valves

A similar equation of motion for the piston type check valves can be derived with reference to Fig. 10-61 as follows:

$$M\ddot{X} = -F_0 - KX + K_H(X)D^2\rho_f v^2 - C_D\rho_d D^2\dot{X}|\dot{X}| \quad (10-47)$$

The left hand side of this equation represents the inertia of the moving elements including the effect of the adjacent fluid. The terms on the right hand side represent the external forces due to spring forces, fluid forces, (pressure and fluid drag) and damping.

where:

X = position of the moving element from a reference point (e.g. $X = 0$ corresponds to valve fully closed)

M = total mass of the moving parts

D = valve dimensional characteristics (e.g. I.D.)

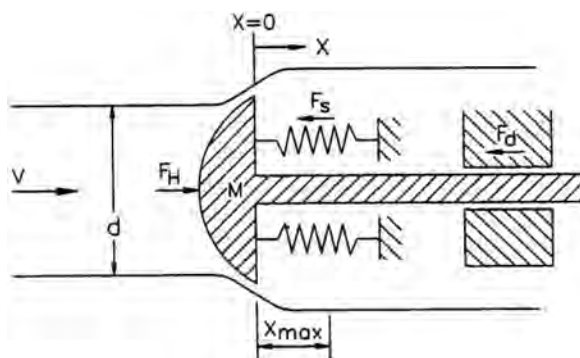


Figure 10-61. A schematic of a piston type check valve.

v = mean flow velocity upstream of the valve
 v_0 = minimum mean flow velocity upstream of the valve enough to open the valve to a fully open position
 F_0 = initial spring loading at $X = 0$
 K = spring stiffness
 K_H = hydrodynamic coefficient, which is function of X and Re
 C_d = damping coefficient
 ρ_f = fluid density
 ρ_d = damping fluid density

Similarly, if the following dimensionless variables are introduced;

$$\xi = \frac{X}{D}, \quad \dot{\xi} = \frac{\dot{X}}{v_0}, \quad \ddot{\xi} = \frac{\ddot{X}D}{v_0^2}, \quad \tau = \frac{tv_0}{D} \quad (10-48)$$

The above equation of motion takes the following dimensionless form:

$$\frac{M}{\rho_f D^3} \ddot{\xi} = \frac{F_0}{\rho_f v_0^2 D^2} - \frac{KD}{\rho_f v_0^2 D^2} \xi + K_H(X) \frac{v}{v_0}^2 - \frac{C_d \rho_d}{\rho_f} \xi \left| \dot{\xi} \right| \quad (10-49)$$

which leads to the following dimensionless numbers:

$$\text{Inertia number } [N_1] = \frac{M}{\rho_f D^3}$$

$$\text{Initial Spring Loading } [N_2] = \frac{F_0}{\rho_f v_0^2 D^2}$$

$$\text{Spring Stiffness number } [N_3] = \left[\frac{KD}{\rho_f v_0^2 D^2} \right]$$

$$\text{Hydrodynamic number } [N_4] = [K_H]$$

$$\text{Deceleration Number } [N_5] = \frac{v}{v_0}$$

$$\text{Damping Number } [N_6] = \frac{C_d \rho_d}{\rho_f}$$

In a steady state case, when the valve is just fully open;

$$X = X_0, \quad \dot{X} = \ddot{X} = 0 \quad \text{and} \quad v = v_0 \quad (10-50)$$

Hence the critical mean flow velocity to maintain the valve fully open is:

$$v_0^2 = \frac{1}{\rho_f D^2 K_H(X_0)} [F_0 + KX_0] \quad (10-51)$$

For geometrically similar valves and for $F_0/KX_0 = \text{constant}$, three of the above similarity numbers (N_2 , N_3 and N_4) become the same, and the solution of the equation of motion

(10-47) depends only on the relative magnitude of the inertia number (N_1), the deceleration parameter, (N_5) and the damping parameter (N_6).

10.4.5 Dynamics of Wafer Type Check Valves

A similar equation of motion can be derived for a dual flapper (bi-fold or wafer) type check valves (see Fig. 10-62) in the following dimensionless form:

$$\left[\frac{I}{\rho_f D^5} \right] \ddot{\theta} = - \left[\frac{T_0}{\rho_f v_0^2 D^3} \right] - \left[\frac{K}{\rho_f v_0^2 D^3} \right] \theta + K_H(\theta) \left[\frac{v}{v_0} \right]^2 - \left[\frac{C_d \rho_d}{\rho_f} \right] \theta |\dot{\theta}| \quad (10-52)$$

where:

θ = wafer angle

I = effective inertia of the moving parts of one flapper and associated attached fluids

D = valve dimensional characteristics (e.g. I.D.)

K = spring tensional stiffness

K_H = hydrodynamic coefficient, which is function of θ and Re

v = mean flow velocity upstream of the valve

v_0 = minimum mean flow velocity upstream of the valve enough to open the valve to a fully open position

T_0 = initial spring torque at $\theta = 0$

C_d = damping coefficient

ρ_f = fluid density

ρ_d = damping fluid density

The hydraulic coefficient (K_H) can be determined from the empirical correlations obtained experimentally as a function of the valve geometry and wafer angle (θ). Six similarity numbers could also be identified similar to those derived for the swing type check valves. Those are:

$$\text{Inertia number } [N_1] = \left[\frac{I}{\rho_f D^5} \right]$$

$$\text{Initial Spring Loading } [N_2] = \left[\frac{T_0}{\rho_f v_0^2 D^3} \right]$$

$$\text{Spring Tensional Stiffness number } [N_3] = \frac{K}{\rho_f v_0^2 D^3}$$

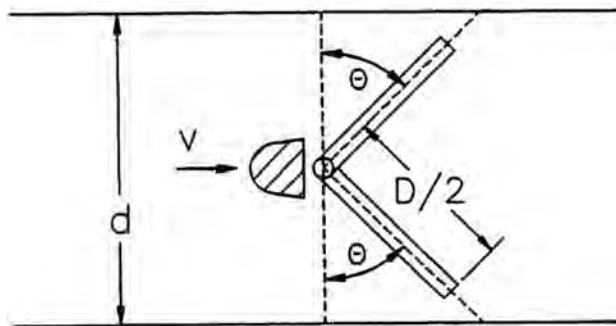


Figure 10-62. A schematic of a wafer type check valve.

Hydrodynamic number $[N_4] = [K_H]$

$$\text{Deceleration Number } [N_5] = \frac{v}{v_0}$$

$$\text{Damping Number } [N_6] = \frac{C_d \rho_d}{\rho_f}$$

In a steady state case, when the valve is just fully open;

$$\theta = \theta_0, \quad \dot{\theta} = \ddot{\theta} = 0 \quad \text{and} \quad v = v_0 \quad (10-53)$$

Hence the critical mean flow velocity to maintain the valve fully open is:

$$v_0^2 = \frac{1}{\rho_f D^3 K_H(\theta_0)} [T_0 + K \alpha_0] \quad (10-54)$$

For geometrically similar valves and for $T_0/K\theta_0 = \text{constant}$, three of the above similarity numbers (N_2 , N_3 and N_4) become the same, and the solution of the equation of motion (10-52) depends only on the relative magnitude of the inertia number (N_1), the deceleration parameter, (N_5) and the damping parameter (N_6).

10.4.6 Effects of Check Valves on Compression Recycle System

It has been shown that the closure behavior of undamped check valves does not influence the flow up to the moment the maximum back flow is reached [43]. Tests have also shown that for these types of valves, the valve almost momentarily closes once the maximum reversed flow corresponding to the flow deceleration is reached [43,47]. Therefore, undamped check valves can be modeled in the following way:

- i) when the mean flow velocity through the valve is positive ($v > 0$), the valve can be modeled as a resistive element with a pressure loss coefficient corresponding to the valve opening position determined from the local mean flow velocity.
- ii) when the flow velocity through the valve is negative, the maximum reverse velocity is first calculated from the DCC curve based on the local mean flow deceleration. The calculated reverse velocity is compared with the maximum reverse velocity characterizing the check valve (e.g. Fig. 10-53). If the former is found to be smaller, the valve is assumed closed (see Fig. 10-52) and flow velocity is set to zero, constituting closed end boundary conditions at the pipe terminals connected to the valve.

The closure behavior of damped check valves is more involved since the assumption that the valve closes momentarily when the maximum reverse velocity is reached cannot hold. Depending on the damping parameter, the valve closure is delayed and the maximum reverse flow (v_r) is larger in magnitude and duration than a corresponding undamped valve [47].

It was mentioned that the most critical point on the ESD path is at the end of phase II (Fig. 10-18). If the time associated with phases I and II combined is long (or the recycle valve size and type limit the magnitude of the perturbations arriving at the compressor to affect an increase in its flow) the end of phase II may cross the surge limit and the compressor will experience a negative flow (surge). Additionally, the point at which the check valve closes depends on the local mean flow velocity and flow deceleration (dv/dt) at the check valve location. It was found to be along phase III or Phase IV for most cases, as will be seen later.

Consider a simple schematic of compressor-recycle system shown in Fig. 10-63. The particulars of this system, its dimensions, operating parameters are given in [11]. The layout shows that the recycle valve and the check valve are located close to the compressor discharge side. This was found to be the best scenario from an ESD point of view following the recycle system investigation in [11]. For a perfect check valve (i.e. one that allows zero reverse flow), the minimum C_g coefficient for the recycle valve of 80 ms pre-stroke delay and 80 ms stroke, is 300. The recycle system resistance line with a $C_g = 300$ recycle valve is shown in Fig. 10-64 to the right of the surge limit of the centrifugal compressor. Recycle system resistance lines with other C_g 's (350 and 400) are also shown in the Fig. 10-64 for comparison, together with the recycle system resistance line with a 37.5% margin from the surge limit as a reference.

A computer simulation of an ESD was conducted on the above simple compression-recycle system where the steady state operating point was initially close to the surge limit (representing a worst case scenario). The check valve dynamic characteristic curve (DCC) was varied according to the following linear characteristics:

$$v_r/v_0 = \frac{D}{v_0^2}(dv/dt) \quad (10-55)$$

where α is a dimensionless constant signifying the slope of the check valve DCC. The value of α was increased systematically (representing slower closing valves) until the compressor

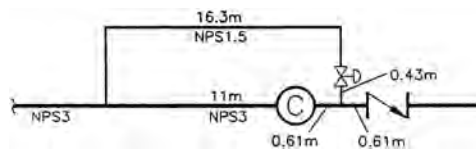


Figure 10-63. A schematic of a typical compression system with a recycle system.

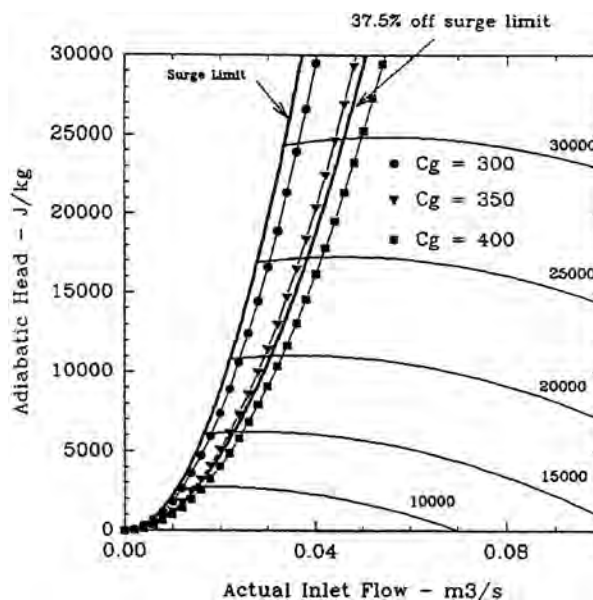


Figure 10-64. Compressor performance characteristics and recycle system flow resistance characteristics [13].

goes into surge at any point during ESD. The maximum value of this parameter α is recorded, which determines the maximum tolerance allowed by the compressor/recycle system for a back flow through the check valve. For the system described above and recycle valve of $C_g = 300$, the maximum value of the parameter α was found to be 1.04. (Note the critical velocity of the swing type check valve used in the air test rig is approximately 40 m/s, and its characteristic diameter D is 0.0766 m).

If the capacity of the recycle valve increases to $C_g = 350$ (representing a recycle resistance line of 30% to the right of the surge limit), the maximum value of α increases to 11.2 – an order of magnitude higher than the previous case. When the capacity of the recycle valve was further increased to $C_g = 400$, representing 48% recycle resistance line (see Fig. 10-64), the maximum permissible value of parameter α increased to 101.5, yet another order of magnitude higher than the previous case. Figure 10-65 shows the simulation results of this case. Notice the higher magnitude of the reverse flow through the valve and yet no sign of compressor surging during this ESD process. This finding suggests that the choice of the check valve and the associated dynamic behavior represented by its dimensionless DCC characteristics should be examined in connection with the recycle system capacity. The higher the recycle system capacity, the more tolerance is allowed for a back flow through the check valve.

The results of the previous three cases are presented on the check valve dynamic plot shown in Fig. 10-66, showing the limiting DCC lines for the various recycle valve C_g . Therefore, proper selection of the check valve should be tied with the cost associated with recycle system capacity. A further consideration for check valves is the incremental fuel cost associated with the pressure loss across the valve. For example, since swing type check valves are generally less expensive than nozzle or piston types up to size NPS 16, a larger capacity recycle valve can be considered provided that the cost of this higher capacity is not offset by the saving in the check valve capital cost and increased compressor fuel cost associated with higher pressure loss. The opposite can be said for check valve sizes greater than NPS 16, where the piston type valves are typically less expensive and where lower reverse flow may allow for the sizing of a lower capacity recycle system resulting in further cost savings.

In summary, increasing the capacity of the recycle system allows for less stringency on the maximum allowable check valve reverse flow (Fig. 10-57).

To put the above results in a dimensionless form, the ratio between C_g/C_{g0} vs. the DCC slope α is plotted in Fig. 10-67. Here, C_{g0} is the reference recycle valve coefficient for hypothetically perfect check valves with very low backflow. The plot shows that C_g/C_{g0} is proportional to the logarithm of α , indicating that a small variation in C_g could have dramatic effects on the maximum permissible value of α . For example, a 15% increase (or decrease) in the recycle valve coefficient C_g could result in values 10 times higher (or lower) than the permissible α coefficient. This elucidates the importance of optimizing the selection of both the check valve and recycle valve to achieve the most cost effective equipment needed.

10.5 RELIEF VALVE DYNAMICS

Pilot-operated safety relief valves are commonly employed in compressor stations. Their design consists of a main valve and a pilot as shown in Fig. 10-68. The pilot controls the pressure at the top (dome) side of the unbalanced piston, while the bottom side of the piston is exposed to the process gas pressure. At pressures below the set point, the pressures on opposite sides of the piston are equal but because of the larger area on the dome side, the net force is in the seat close direction. When the set pressure is reached, the pilot opens, depressurizes the dome and the unbalanced forces on the piston cause it to stroke upward. When the process pressure decreases below the set point, the pilot closes, the dome is repressurized and the valve piston moves downward to the closed position. As an example, in an 8" dual outlet relief valve, the area of the dome side of the piston is 1.4 times larger

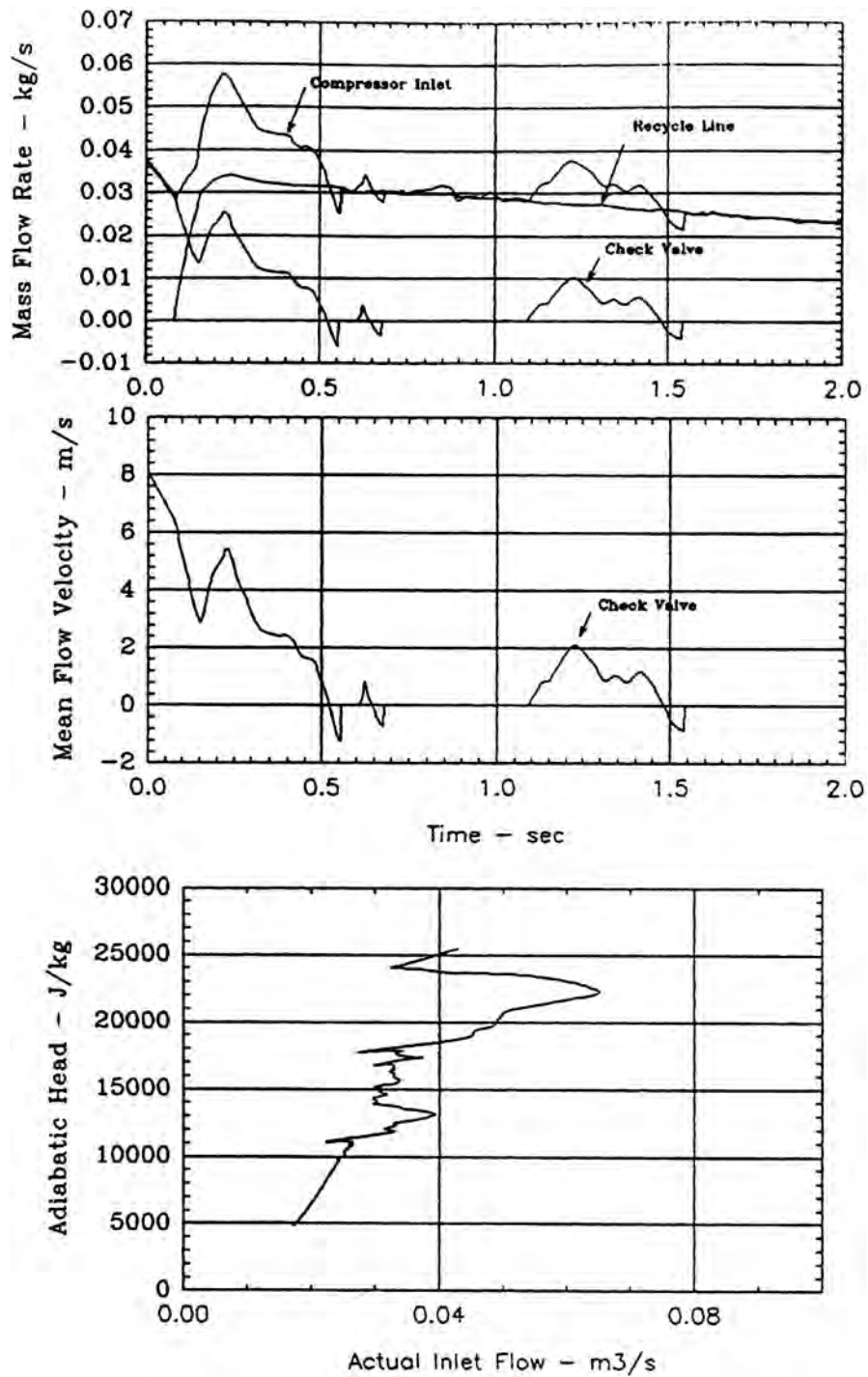


Figure 10-65. Example dynamic simulation results of ESD process of the compression system of Fig. 10-63, for check valve parameter $\alpha = 101.5$ [13].

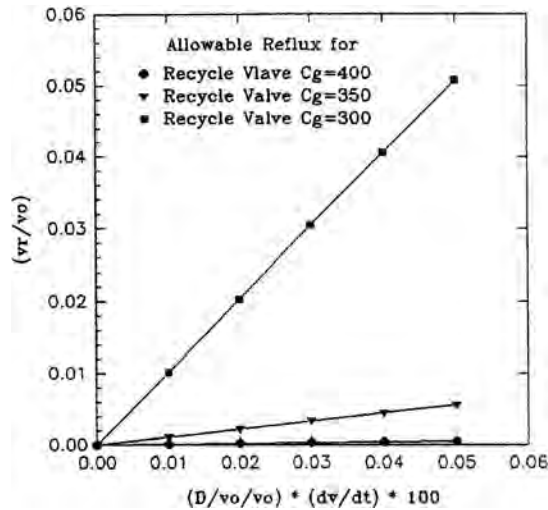


Figure 10-66. Relationship between check valve dynamic characteristics and recycle valve capacity [13].

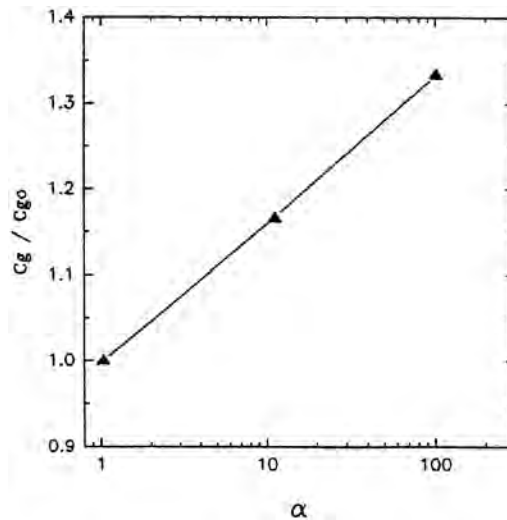


Figure 10-67. Minimum required recycle valve capacity for a given check valve dynamic parameter [13].

than the bottom seating area. Therefore, for the valve to open, the pilot must depressurize the dome to a pressure equal to 71 percent of the process pressure.

10.5.1 Dynamics of Pilot-Operated Relief Valves

The problem of safety relief valve stabilities has been investigated and reported in the literature. Two methods of dealing with this problem have usually been used. Both of the methods deal with the dynamic equations describing the mechanics of the safety valve in connection with the system under consideration. The resulting equations are generally unsolvable by analytical means, and therefore the following two methods have been suggested:

The first applies stability analysis to determine whether a safety valve is dynamically stable or unstable under any set of prevailing conditions. Examples of such analyses are given

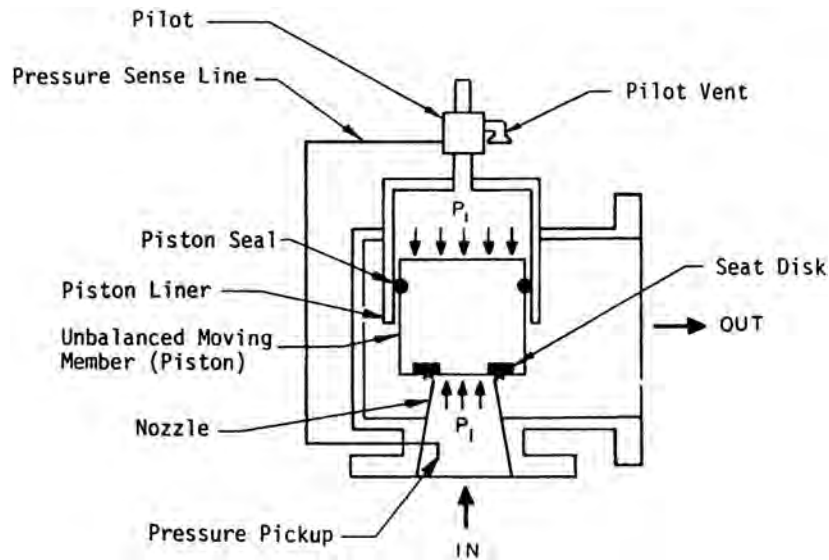


Figure 10-68. Schematic of a typical design of a pilot-operated relief valve.

in [49–53], where frictional forces are generally neglected and fluid inertial forces in the attached piping are considered to be insignificant. These assumptions are appropriate for simple gas-filled systems, such as a pressure vessel and a safety relief valve with a short riser.

The second considers the actual response of the valve piston determined from the solution of the dynamic equations in the time domain [53–56]. Almost all of these reports deal with spring loaded relief type valves. In these analyses, damping can be taken into account in a more rigorous way [54,55]. Additionally, the effects of non-linearity and frequency operation [57]. The first stability study of a pilot-operated relief valve connected to a pressure system through a riser was reported by Emerson [58] and Powell [59]. Here, valve instability was shown to be due to the proximity of the natural frequency of the piston-dome volume system to the acoustic resonance frequency of the riser length. Two riser resonance frequencies were referenced [59], one corresponding to a quarter-wave-length resonance when the valve is closed, and another corresponding to a half-wave-length resonance when the valve is open. Experience reported by Powell [59] has also shown that an operationally unstable valve can be made stable if

$$0.5 > \omega/\omega_n > 2.5 \quad (10-56)$$

where

ω = is the riser acoustic primary resonance frequency

ω_n = is piston natural frequency

Four phases of piston stroking can be identified once the process pressure exceeds the set pressure. The corresponding process and dome pressures are represented schematically in Fig. 10-69 (and also in Fig. 10-70), and the various phases are described as follows:

Phase I: The pilot starts to vent the dome pressure to ambient through a minimum throat area (A_0) in the pilot. This process continues until the dome pressure drops to the threshold level of balanced forces on the piston.

Phase II: The valve piston starts to move upward, relieving process pressure, while the dome pressure continues to drop through dome gas evacuation via the pilot. The main process gas is released to ambient through the single or dual outlets. This

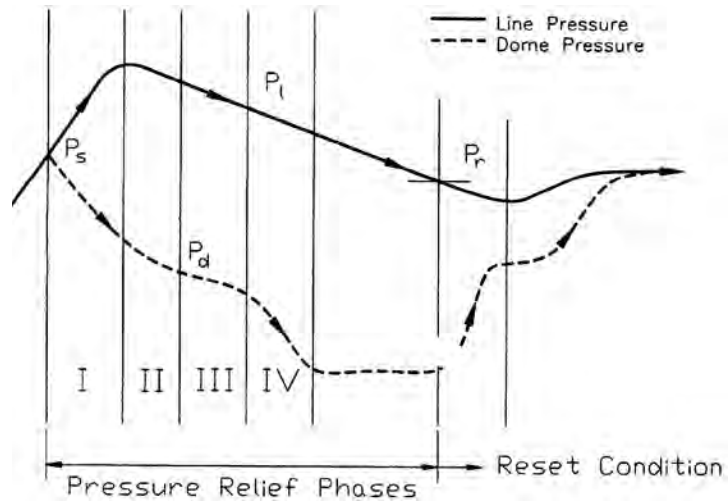


Figure 10-69. Relationship between dome pressure and process gas pressure.

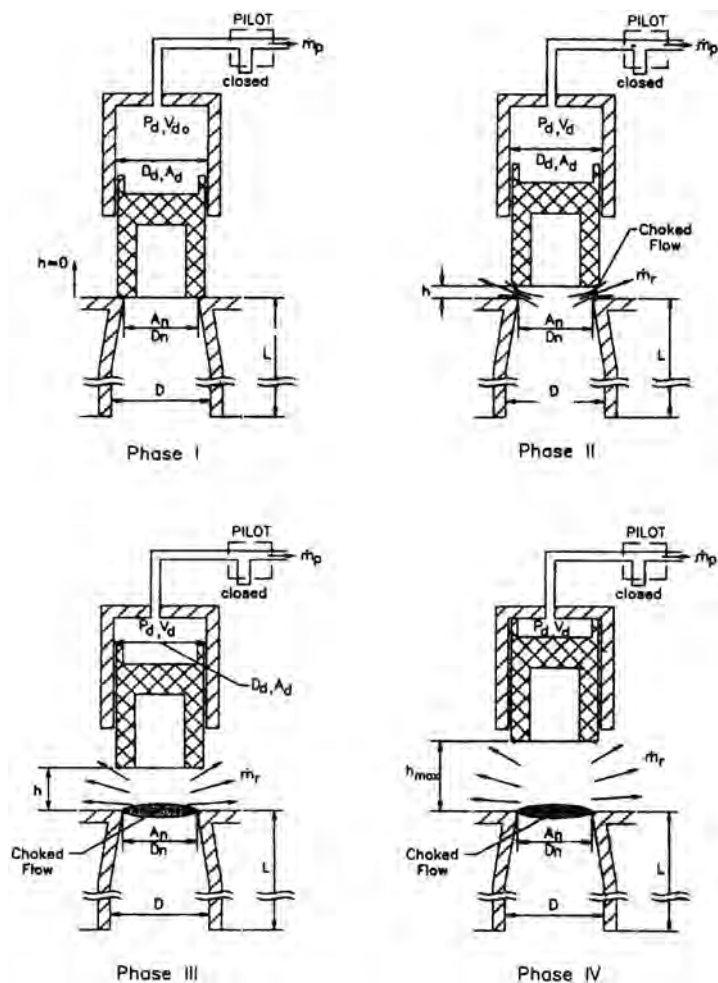


Figure 10-70. Various phases of operation principle of a pilot-operated relief valve.

causes the process gas to reach choked condition at the annulus area produced by the gap between the piston and the riser top (seat). This phase will terminate when the piston is lifted to a position where the process gas will start to choke at the riser nozzle rather than at the annulus gap. This will occur when the annulus' effective area becomes smaller than the nozzle flow area and is defined as "transitional piston height" (h_t). Follmer [60], provided some Mach-Zender-Interferometer pictures of flow through a plane valve choked at the annulus gap.

Phase III: The piston continues to move upward from the transitional height to the top position. The dome gas continues to evacuate to ambient through the pilot, while the piston moves upward, giving rise to a moderate decline in the dome gas pressure. The process gas pressure continues to decline at a rate dictated by the choked flow through the riser nozzle.

Phase IV: Once the piston reaches its top position, the dome gas evacuates at a lower rate; however, its pressure depletes at a much faster rate than the previous phase due to the elimination of the compression action of the piston motion. The process gas pressure continues to relieve through a choked condition at the riser nozzle. This phase ends when the dome pressure reaches ambient pressure. Following this phase, the process gas pressure continues to decline until it reaches a reset pressure, at which time the pilot will reset to charge the dome with process gas to reverse the process.

The governing equations for each of the *above* four phases will be described.

Phase I, shown in Fig. 10-70(I), represents the dome gas evacuation after the line pressure reaches the set pressure. The evacuation mass flow rate is given by:

$$\dot{m}_p = a_d^* \rho_d^* A_0 \times C_d \quad (10-57)$$

Here, C_d is a discharge coefficient for the sonic flow, which can be assumed to be ~ 0.8 , according to Benedict [61], and:

$$\begin{aligned} \dot{m}_p &= \text{pilot vent mass flow rate} \\ a_d^* &= \text{critical speed of sound of the gas in the dome} \\ \rho_d^* &= \text{critical density of the gas in the dome} \\ A_0 &= \text{pilot throat area} \end{aligned}$$

Furthermore, the dome gas expansion caused by the pilot relief is assumed to be isentropic. Hence the associated change in the dome pressure can be determined from:

$$\dot{m}_p dt = V_d \times d\rho_d = V_d \times dP_d / a_d^2 \quad (10-58)$$

where

$$\begin{aligned} V_d &= \text{dome volume} \\ P_d &= \text{dome pressure} \\ a_d &= \text{speed of sound of the gas in the dome} \\ \rho_d &= \text{density of the gas in the dome} \end{aligned}$$

The piston height (h) remains at $h = 0.0$ during this phase, and the process gas release rate is therefore equal to zero.

The Phase II model schematic is shown in Fig. 10-70(II). Here the pilot gas evacuation rate \dot{m}_p , is the same as described by Eq. (10-57) where a_d^* and ρ_d^* are gas properties at the critical condition of the dome gas at the instantaneous pressure and temperature. The

change in the dome gas pressure is related to both gas evacuation and piston motion in the following manner:

$$\begin{aligned}\dot{m}_p dt &= -\rho_d \cdot dV_d - V_d \cdot d\rho_d \\ &= \rho_d A_d dh - (V_d - A_d \cdot h)(dP_d/a_d^2)\end{aligned}\quad (10-59)$$

where A_d is the cross-sectional area of the dome. The process gas release rate is choked at the annulus gap between the valve piston and riser nozzle and can be expressed as:

$$\dot{m}_n = a_n^* \rho_n^* (\pi D_n h) \times C_d \quad (10-60)$$

where subscripts refer to the riser nozzle shown in Fig. 10-70. The term in brackets assumes that the flow area is the full circumferential gap, which may not be true due to the effects of the valve casing. The piston lift (h) from the seating position is determined from the piston equation of motion:

$$M\ddot{h} + C\dot{h} + K_s h = P_n A_n - P_d A_d \quad (10-61)$$

where:

- M = effective mass of the piston/spring
- C = damping coefficient
- K_s = spring stiffness

Here the force acting on the bottom side of the piston is assumed to be uniform and equal to the static pressure at the riser nozzle. A more realistic pressure distribution function would be needed. This pressure is determined from solving the full one-dimensional flow equations of the gas in the riser and associated process system using the method of characteristics described above. The instantaneous flow at the riser nozzle, Eq. (10-60), is used as a boundary condition required for the solution of the hyperbolic P.D.E. representing the flow in the riser and associated process piping system. The upstream boundary conditions for these equations depend on the process piping system. In the present analysis, we assumed that the riser is connected to a large pressurized system (vessel). Hence, the boundary condition at the bottom of the riser is assumed to be an open end and is maintained at a pressure equal to the instantaneous process gas pressure.

Model equations for Phase III depicted schematically in Fig. 10-70(III) are similar to those for Phase II except that the process gas release mass flow rate is equal to:

$$\dot{m}_n = a_n^* \rho_n^* (A_n) \times C_d \quad (10-62)$$

This arose from the fact that the process gas flow is now choked at the riser nozzle rather than at the annulus gap between the piston and riser nozzle. The force distribution is still assumed to result from equal distribution of the riser static pressure at any instant in time.

The Phase IV model equations are the same as those for Phase III, the only difference lying in the thermodynamics of the dome gas. In this phase the piston has reached the top position, Fig. 10-70(IV), and hence the dome gas pressure changes according to the following relation:

$$\dot{m}_p dt = (V_d)_{\min} (dP_d/a_d^2) \quad (10-63)$$

In all of the above phases, the piston equation of motion should be in effect at every time step of the solution procedure in order to allow for piston rebound at either top or bottom positions.

Additionally, the piston natural frequency can be evaluated from the dome gas thermodynamic relation. Assuming isentropic behavior of the dome gas during piston motion, and neglecting gas evacuation through the pilot, the following relation can be written:

$$d(P_d V_d^k) = 0 \quad (10-64)$$

where, k is the isentropic exponent. Hence, the upward incremental force on the piston would be:

$$A_d dP_d = \frac{k P_d A_d^2 dh}{V_d} \quad (10-65)$$

and from the piston equation of motion (10-61), the natural frequency of the piston would be:

$$\omega_n = \sqrt{\frac{k P_d A_d^2}{V_d M} + \frac{K_s}{M}} \quad (10-66)$$

Normally, the second term under the square root is negligible compared to the first term (by at least two orders of magnitude).

Equations of state such as AGA-8 [23] or PR [24] can be used to determine the gas density, the speed of sound and the isentropic exponent at the prevailing local pressure and temperature. Critical conditions are calculated from the stagnation conditions using ideal gas relations with real gas values of isentropic exponents at stagnation conditions. The error associated with this simplification was found to be less than 1 percent for critical pressure, 0.4 percent for critical temperature, 0.2 percent for critical density, and 0.6 percent for speed of sound.

10.5.2 Solution Technique

The above equations pertinent to the pilot's flow, dome volume thermodynamics, piston equation of motion and riser relief flow can be solved simultaneously in a marching-in-time numerical scheme. At any step in time, the above equations form a set of mixed nonlinear algebraic and O.D.E. which form an initial value problem. A standard fourth order Runge-Kutta is used to advance the solution an incremental time step. The time step for the solution of these equations should be at least 1/50th of that required by the method of characteristics applied to the solution of the gas dynamics equations in the attached riser/process system. This was necessary for a stable solution of the O.D.E. system of equations and also for minimizing the resulting higher order truncation errors.

Acoustic Boundary Condition for A Choked Flow. It was mentioned above that in Phases II, III, and IV, the piston has stroked up away from the nozzle allowing the process gas flow to the ambient. Depending on the phase, the gas flow is choked either at the gap between the nozzle and the bottom side of the piston (phase II) or at the nozzle throat (Phases III and IV). There is a need to determine the acoustic boundary condition in order to assess properly the acoustic interaction between the resonance condition in the riser and the piston oscillations, particularly in Phase II. In Phases III and IV, despite the fact that the piston oscillations cannot affect the riser flow condition due to the choke barrier, the opposite can occur in that the oscillating riser pressures affect the piston motion even when the flow is choked.

A one-dimensional treatment of the upstream acoustic boundary condition for choked flows has been given by Bloxsidge [62] in the context of acoustically coupled combustion instability. Study of downstream acoustic boundary conditions of near choked flows at the throat of a converging-diverging nozzle, analytically by Myers and Callegari [63], and numerically by Nayfeh et al. [64], alluded to high acoustic amplitude to incident wave

ratios at the throat when M approaches unity. This indicates that a choked flow resembles acoustically closed end boundary conditions for the upstream field.

To examine this further, consider the schematic of the choked flow boundary condition that is shown in Fig. 10-71; station (1) denotes an upstream location on the riser where flow parameters are (P_1, T_1, ρ_1, U_1) , and cross-sectional area $= A_1$, and station (2) denotes the choked location where flow parameters are $(P_2, T_2, \rho_2, U_2 = a_2)$ and cross-sectional area $= A_2$. If an isentropic perturbation generated at the upstream station (1), is assumed, then

$$\frac{\delta P_1}{P_1} = k_1 \frac{\delta \rho_1}{\rho_1} \quad (10-67)$$

$$\frac{\delta P_1}{P_1} = \frac{k_1}{k_1 - 1} \frac{\delta T_1}{T_1} \quad (10-68)$$

Also, if an isentropic expansion of the gas from station (1) to station (2) where the flow is choked at (2) is assumed, then

$$T_1 \left(1 + \frac{k_1 - 1}{2} M_1^2 \right) = T_2 \left(\frac{k_2 + 1}{2} \right)$$

and in a perturbation form:

$$\delta T_1 \left(1 + \frac{k_1 - 1}{2} M_1^2 \right) + T_1 (k_1 - 1) M_1^2 \frac{\delta U_1}{U_1} = \delta T_2 \frac{k_2 + 1}{2} \quad (10-69)$$

Since perturbations are assumed to be isentropic at station (1) and that the flow between stations (1) and (2) is isentropic, it follows that perturbations at station (2) are also isentropic, and hence:

$$\frac{\delta P_2}{P_2} = k_2 \frac{\delta \rho_2}{\rho_2} \quad (10-70)$$

$$\frac{\delta P_2}{P_2} = \frac{k_2}{k_2 - 1} \frac{\delta T_2}{T_2} \quad (10-71)$$

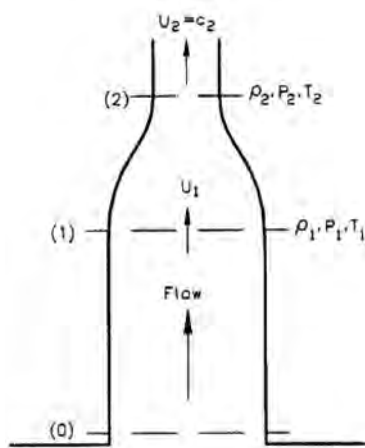


Figure 10-71. Choked flow acoustic resonance model.

As the condition at station (2) is choked, $U_2 = a_2$, and therefore;

$$\frac{\delta v_2}{v_2} = \frac{\delta a_2}{a_2} \quad \text{or, approximately} \quad \frac{\delta v_2}{v_2} = \frac{\delta T_2}{2T_2} \quad (10-72)$$

The continuity equation between stations (1) and (2) yields the following perturbation equation:

$$A_1 v_1 \delta \rho_1 + \rho_1 A_1 \delta v_1 = A_2 v_2 \delta \rho_2 + \rho_2 A_2 \delta v_2 \quad (10-73)$$

Equations (10-67) through (10-73) form a set of seven perturbation equations in eight perturbation quantities (δP_1 , $\delta \rho_1$, δT_1 , δv_1 , δP_2 , $\delta \rho_2$, δT_2 , δv_2), which can be reduced to one equation in the form:

$$\delta P_1 = Z_1 \times \delta v_1 A_1$$

or

$$\delta P_2 = Z_2 \times \delta v_2 \times A_2$$

where,

$$Z_1 = \frac{P_1}{A_1 U_1} \frac{2 k_1 (T_1 - T_2)}{T_1 (k_1 - 1) T_2 (k_2 - 1)} \quad (10-74)$$

and

$$Z_2 = \frac{P_2}{A_2 U_2} \frac{2 k_2}{(k_2 - 1)} \quad (10-75)$$

Z_1 and Z_2 are known as the acoustic impedances at stations (1) and (2), respectively. A sample calculation was performed on a 3.0 m riser containing natural gas at 6000 kPa, and 10°C, and a speed of sound equal to 396 m/s. The impedance at the bottom of the riser is related to Z_1 via the acoustic transfer matrix for the riser pipe between stations (0) and (1) of length = 3.0 m [65]. Consider a numerical case where $v_1 = 60$ m/s and $v_2 = a_2 = 376$ m/s and $k_1 = 1.31$. The fundamental acoustic resonance frequency can be determined from the spectrum of the acoustic impedance at station (0) where Z_0 is at the first minimum. This results in a value of 32 Hz. If, however, a closed boundary condition is assumed at station (2), the acoustic resonance condition would correspond to a quarter-wave resonance yielding a value of 33 Hz which is very close to that determined from the above treatment. Spectra of Z_0 calculated for frequencies up to 200 Hz based on either closed or choked flow boundary conditions were found to be almost the same. It is therefore confirmed that a choked flow can be treated as a closed end boundary condition from an acoustic point of view.

10.5.3 Example

Consider an NPS 8 × 8 dual-outlet pilot-operated relief valve opening following an increase in the line pressure beyond the set pressure. The valve is mounted on an NPS 8 riser. The line pressure was assumed to increase from 6000 kPa to 6010 kPa linearly in 100 ms. The pilot's set pressure was 6010 kPa. The following are other pertinent parameters.

Valve characteristics:

$$D = 0.1937 \text{ m}$$

$$D_n = 0.160 \text{ m}$$

$$L = 3.0 \text{ m}$$

$$h_{\max} = 0.065 \text{ m}$$

$$h_t = 0.04 \text{ m}$$

$$\begin{aligned}
D_d &= 0.189 \text{ m} \\
V_{do} &= 0.002722 \text{ m}^3 \\
V_{d \min} &= 8.98\text{E-}04 \text{ m}^3 \\
A_0 &= 5.47\text{E-}06 \text{ m}^2 \\
M &= 23.289 \text{ kg} \\
K_s &= 7358 \text{ N/m} \\
C_d &= .0.8
\end{aligned}$$

Gas composition:

$$\begin{aligned}
C_1 &= 91.52\%, C_2 = 5.69\%, C_3 = 1.2\%, iC_4 = 0.16\%, nC_4 = 0.22\%, iC_5 = 0.08\%, nC_5 = \\
&0.07\%, N_2 = 0.65\%, CO_2 = 0.50\%
\end{aligned}$$

A laboratory flow test with air was conducted on the pilot to determine the effective flow area when it was forced fully open [66]. The pilot was connected to an air cylinder and the upstream stagnation pressure was varied from 500 to 2500 kPa. Mass flow rate was measured by a calibrated Rockwell turbine meter. The effective throat area of the gas evacuation path through the pilot was found to vary from 4.94 mm² to 5.90 mm² when the stagnation pressure was varied from 500 kPa to 2500 kPa, respectively. Additionally, a simulated laboratory test was conducted on the piston/liner assembly to determine the range of the damping coefficient C . The lowest value of C was found to be around 6000 N/(m/s).

Simulation results are shown in Fig. 10-72 (a through h), which are discussed below.

Piston oscillations (Fig. 10-72a) started as a result of a step change in the net upward force (Fig. 10-72g) due to the initial piston lift, thus exposing a larger piston area at its bottom to the riser gas pressure. Oscillations were then sustained at a slightly increasing net average upward force (Fig. 10-72g). The net upward forces were much larger than the forces caused by the holding spring, or by the piston weight itself.

It took approximately 1.2 s for the valve to stroke to the full open position (Fig. 10-72c) once it started to lift. A period of piston oscillation was observed for 200 ms following the initial lift, with amplitudes decaying in time. The piston oscillations occurred at piston lift (h) below the transitional height ($h_t = 0.04$ m).

During the oscillation period, the riser nozzle static pressure (Fig. 10-72c) was leading the riser flow (Fig. 10-72e) by a 90° phase shift, consistent with an open-end riser bottom from plane wave acoustic theory [65]. The phase angle between the net upward force on the piston (Fig. 10-72g) and piston lift (Fig. 10-72a) is 90° (the piston motion is lagging). This is consistent with the forced vibration theory.

The piston oscillation frequency ω_p was approximately 56 Hz, while ω_n averaged around 60 Hz, and hence ω_d was around 56 Hz ($\xi = 0.37$). This does not mean that $\omega_p = \omega_d$ in general. The relationship between ω_p , ω_n , ω_d and ω will be discussed in more detail later in the section.

The dome pressure (Fig. 10-72d) and pilot's flow (Fig. 10-72f) went through the following phases: a steady decrease while piston was at zero height, an oscillatory phase due to piston oscillation, a constant level due to counter effects of piston moving upward and the pilot's gas evacuation, and finally, a steady decline at a much faster rate once the piston hits its maximum lift h_{\max} .

The import of this simulation's result is that when an improper or low viscosity lubricant is used (hence lower damping coefficient C), the piston oscillations can occur during the opening stroke. This is why valve manufacturers always emphasize the use of specific types of lubricant with certain high shear stresses and viscosity. The C value for such lubricants is at least an order of magnitude higher than the value used in the base case simulation. The reason for using the lower value in the base case simulation was to illustrate this message clearly. In order to substantiate this further, the same simulation was repeated with

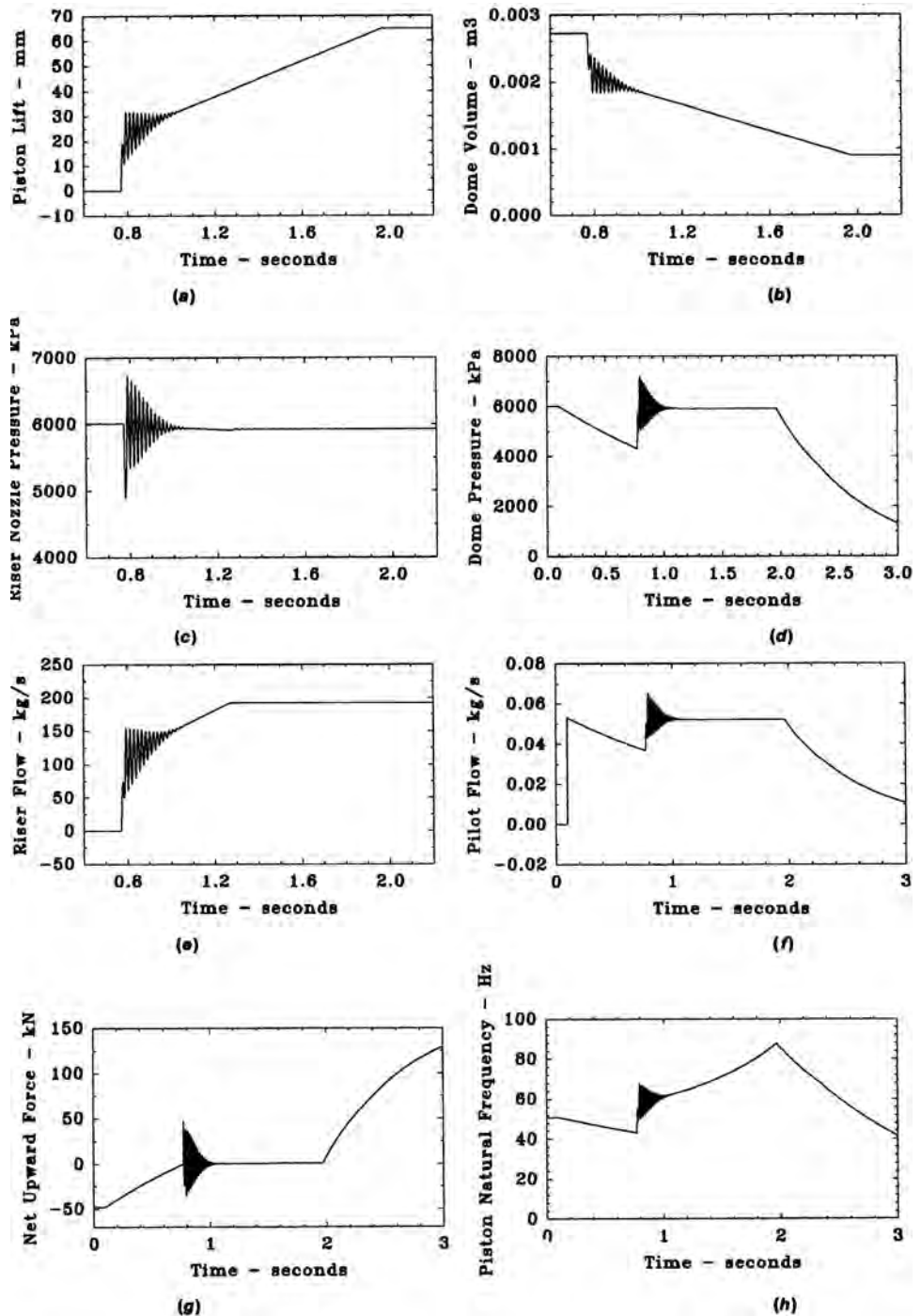


Figure 10-72. Numerical results of relief valve response low damping, ($\xi = 0.37$).

a higher value of C [35,000 N/(m/s)], resulting in $\xi = 2.16$. The result of the piston travel vs. time is shown in Fig. 10-73, indicating substantial suppression of piston oscillations.

The influence of the inlet riser length in the above base case above was also studied numerically [66]. The lower value of C [6000 N/(m/s)] was retained in order to manifest the effect of the riser's dimensionless length (L/D) on both the frequency and amplitude of

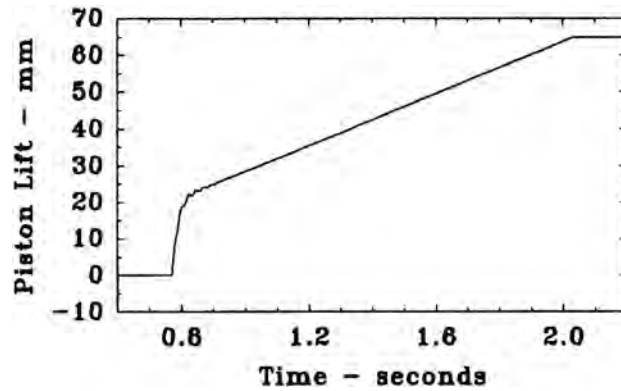


Figure 10-73. Numerical results of relief valve response higher damping, ($\xi = 2.16$).

piston oscillations. Figure 10-74a shows the piston oscillation frequency for various values of L/D . In some cases, two distinct oscillation modes were observed along the piston stroke; the first mode (identified by the symbol \mathbf{X}) was observed first in time, followed by a second mode of different frequency (symbol ℓ). An example of the piston lift-time trace of such behavior is shown in Fig. 10-75, for $L/D = 90$. The riser's acoustic resonance frequency curves corresponding to one quarter wave length (L_1/D) and to odd multiples ($L_{3,5,7,9}/D$) are

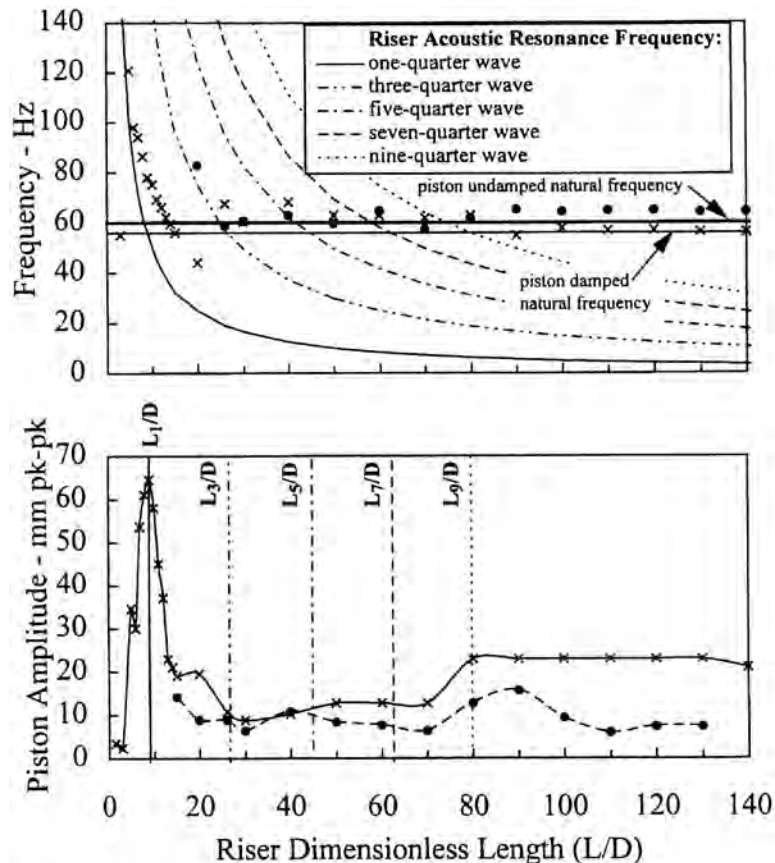


Figure 10-74. Effects of riser length on relieve valve's piston frequency and amplitude.

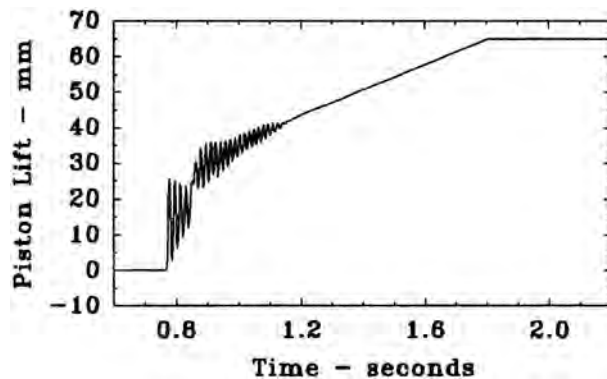


Figure 10-75. Example of two-mode oscillations for $L/D > 20$.

also plotted in Fig. 10-74, along with the piston damped and undamped natural frequencies (ω_d and ω_n). It is observed that the piston oscillation frequency follows the riser's one-quarter wave frequency for lower values of L/D . At $L/D = 20$, the two mode oscillations described above started to emerge with two distinct frequencies. This is perhaps due to the fact that the three-quarter wave resonance in the riser started to approach the piston natural frequency. This two-mode oscillation phenomenon persisted for higher values of L/D up to 140, the maximum considered in the present study, as shown in Fig. 10-74a.

The corresponding piston maximum amplitude (pk-to-pk) is shown in Fig. 10-74b. The various vertical lines correspond to L/D values where the riser's acoustic resonance frequencies are equal to the piston damped natural frequency. Maximum oscillation amplitudes occur at L/D corresponding to $\omega_d = \omega$ (one quarter wave). Amplitudes decreased at lower or higher values of L/D , particularly when L/D approached zero. Interestingly, amplitudes appeared to increase when L/D approached L_5/D and L_9/D but not L_3/D and L_7/D .

The dome depressurization rate was evaluated to determine its effect on piston oscillations. Parametric results obtained by varying the pilot's throat area are shown in Fig. 10-76. Obviously, as the pilot's throat area was increased, the piston oscillations tended to vanish at the cost of higher impact velocity of the piston against the dome end. For example, an increase of the pilot's throat area of 20 times resulted in an increase in the impact velocity from 35 mm/s (Fig. 10-72a) to 700 mm/s (Fig. 10-76). Although valve manufacturers indicate that the current design of relief valves can cope with such an increase in the impact

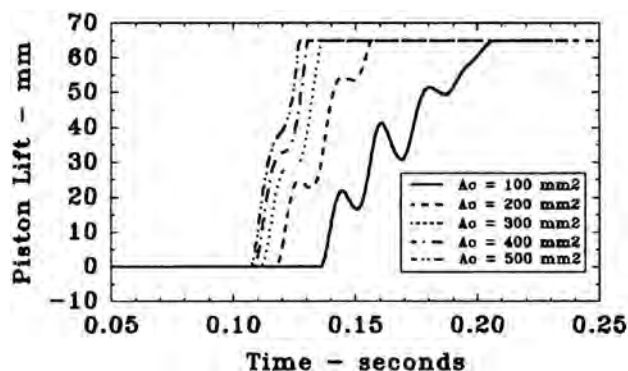


Figure 10-76. Effects of pilot exhaust throat area on piston oscillation during opening.

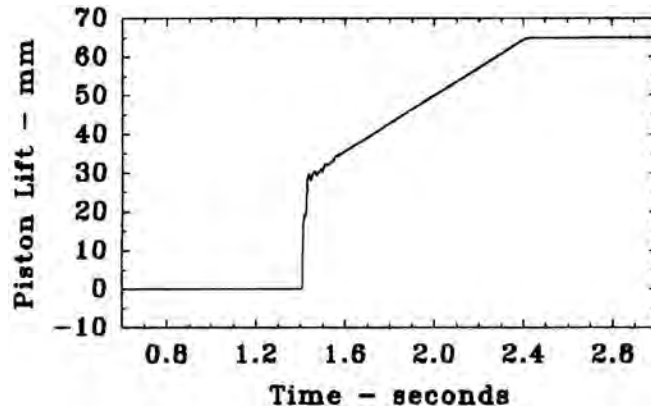


Figure 10-77. Effects of wedge-type ring seal on suppressing piston oscillations.

velocity, a careful optimization should be carried out before deciding on how large a pilot's throat area can be.

Reduction of the piston oscillations was also attempted by a valve manufacturer through a different design of the piston o-ring seals based on a wedge type mechanism. The main purpose of such a mechanism is to increase damping when the piston is moving upward. The device is called a 'pressure-loaded drag wedge seal' since it translates the dome pressure into a radial force via a split wedge ring. By utilizing a free body diagram of the wedge and balancing the axial and radial forces, it is possible to correlate the drag force to the dome pressure. This drag force is only effected during the upward motion of the piston. A wedge case study was simulated for a specific wedge mechanism with the following parameters: wedge angle (75°), radial area ($3,500 \text{ mm}^2$) and friction coefficient (0.2). Other parameters were exactly the same as in the base case in order to permit comparisons. The results are shown in Fig. 10-77, which show a substantial suppression of oscillations (compare to Fig. 10-72a).

10.5.4 Field Tests

Field measurements were taken at TransCanada's Gas Dynamic Test Facility which is part of a compressor station on NOVA's gas Transmission System in Alberta. An NPS 8 8 8 dual-outlet relief valve was mounted on an NPS 8 riser branched off an NPS 30 yard pipe as shown in Fig. 10-78. This setup was supplied with high pressure natural gas from both the NPS 30 and an NPS 42 mainline, operating at 5800 kPa and 23°C . Testing was carried out under ambient temperatures ranging from -25°C to -15°C .

Relief actuation was controlled by a solenoid and manifold arrangement in place of the ordinary pilot. This allowed remote valve triggering and safe isolation. A changeable orifice assembly was used to vary the dome depressurization rate. Measurements were taken with high speed digital data acquisition equipment. The measured parameters included: line pressure immediately below the relief valve, dome pressure, and outlet piping pressure in the valve outlet piping (locations 1, 2 and 3 in Fig. 10-78, respectively). Data was also gathered from existing compressor station temperature, pressure, and flow elements.

Figure 10-79 shows the dome pressure, the riser pressure, and the outlet piping pressure, measured for a pilot equivalent orifice size $\sim 5.48 \text{ mm}^2$. Phase I began at the solenoid (s) trigger (point X) and continued until the piston lifted off and the pressure began to rise in the outlet piping. The dome pressure at the end of Phase I was lower than that predicted from the physical area ratios of the valve. This difference was caused by the increased dampening effected by the wedge seal mechanism as will be in the simulation of this test later.

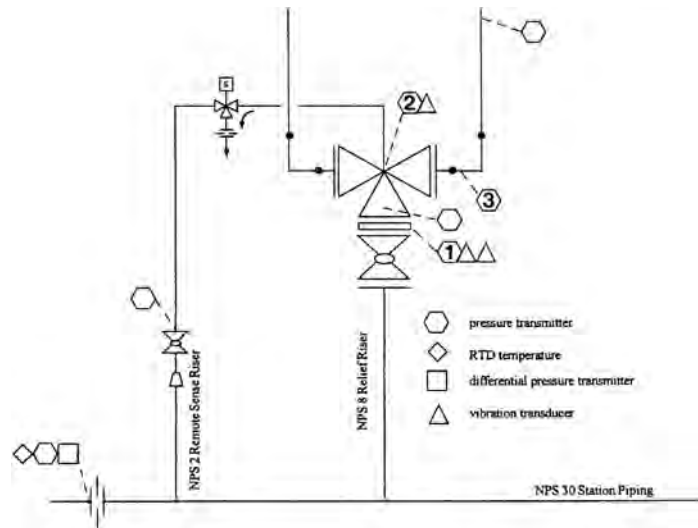


Figure 10-78. Riser-relief valve assembly testes at TransCanada test facility in Alberta, Canada.

Phase II of dome depressurization is characterized by increasing outlet piping pressure and ends when the outlet piping pressure stabilizes. The dome pressure remained relatively constant throughout Phase II. Furthermore, there was no pressure increase at the beginning of this phase nor pressure oscillations, which are indicative of much higher damping likely caused by the extreme cold ambient condition.

The beginning of Phase III is characterized by the outlet piping pressure stabilization, indicating a maximum flow rate, and a transition from a choked piston annulus to a choked valve nozzle. From Fig. 10-79, it is unclear when this Phase ended and phase IV began. The numerical simulation (Fig. 10-72e) clearly displays a transition prior to full piston travel. From this field measurement, however, it can be inferred that the transitional height is close

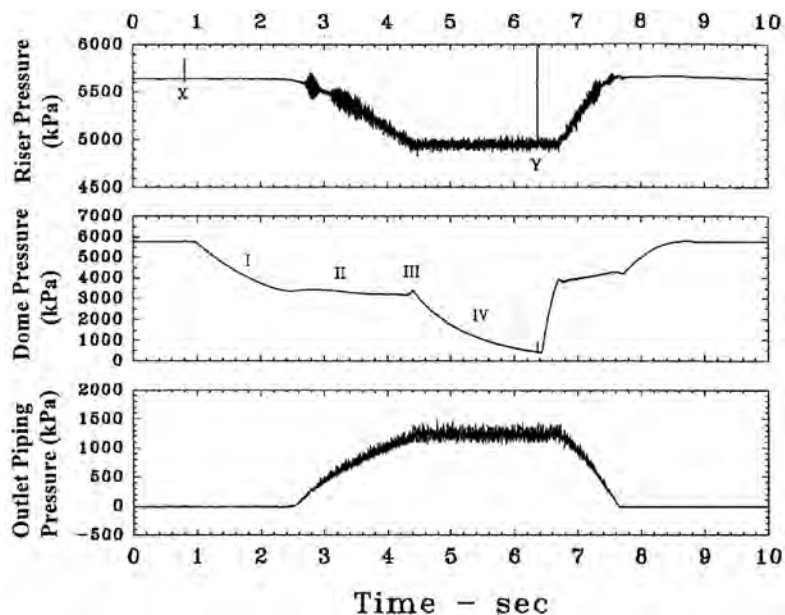


Figure 10-79. Measurements during relief valve opening and closing ($A_0 = 5.48 \text{ mm}^2$).

to the maximum piston lift, indicating that the effective annulus flow area is lower than ($\pi D_n h$). Therefore, Phase III was seen to last for very a short time and was manifested by a small pressure overshoot as shown in Fig. 10-79. Phase IV (maximum piston lift) is indicated by a step change in dome depressurization rate similar to the numerical simulation.

Figure 10-80 shows the measurements for a case without an orifice (dome depressurization was limited by a 1/2" tubing and 9.0-mm² ball valve throat area). Phase I and Phase IV show results similar to the former case, and the higher depressurization rate exhibited in Fig. 10-80 is exactly matching the increase in the throat area.

The relatively constant dome pressure exhibited in Phase II by the former case (Fig. 10-79) is not demonstrated here due to the larger throat area of the dome gas evacuation path. However, the large step change in the outlet piping pressure (indicating a large change in valve flow and, therefore, piston lift) results in a large increase in dome pressure when the valve opens. The kink-shaped dome pressure during this phase can be attributed to the piston being jammed part-way along its upward stroke. This is evident from the constant outlet pressure during this piston jamming period (identified as IIb in Fig. 10-80). The exact cause for this piston jamming during this phase has not been clearly determined. Hence, simulation of this test case was not possible.

The step change in the outlet piping pressure terminating Phase IIb, followed by another pressure stabilization indicate a step change in piston position and an increase in valve flow rate. This reveals that Phase III is of very short duration followed by the normal Phase IV at maximum piston lift.

Additionally, Fig. 10-79 and 10-80 show the dome re-pressurization and re-closing of the valve following the reverse solenoid trigger (points Y). When the piston began to travel to a closed position (indicated by the peak in dome pressure and the drop in outlet piping pressure), the dome pressure required to begin closing the valve correlates very closely to the pressure calculated from the physical area ratios of the valve.

Only the first field test case was simulated using the above numerical analysis method. (Simulation of the second case was not possible as the cause for the apparent piston jamming part-way up was not clearly determined). The damping parameter C had to be increased to

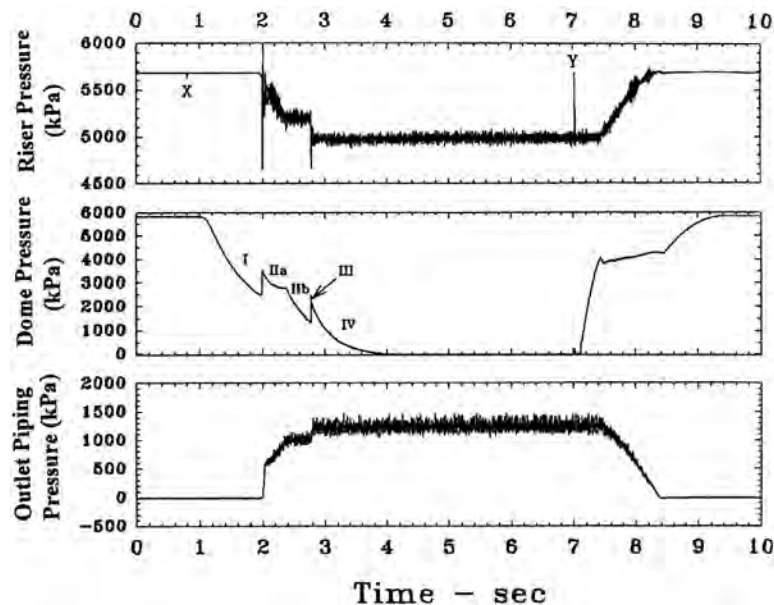


Figure 10-80. Measurements during relief valve opening and closing ($A_0 = 9.0 \text{ mm}^2$).

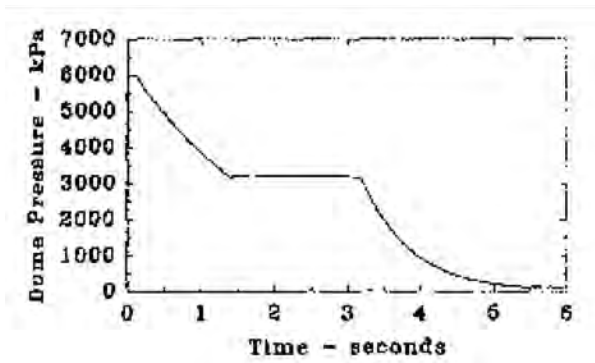


Figure 10-81. Simulation results of the field test case of Fig. 10-78.

a value equal to 90,000 N/(m/s) to correlate with the measurement results. This was not a surprisingly high value of C , considering that severe cold ambient temperature prevailed during the field test. Additionally, the wedge seal model with the specific parameters mentioned earlier was introduced since the relief valve tested was equipped with such a mechanism. The results of this simulation are shown in Fig. 10-81. Clearly, the good agreement between measurement and simulation results with regard to the dome pressure (compare Fig. 10-79 with Fig. 10-81) provides confidence in the modeling and solution techniques employed in the present study. Further analysis to investigate the sticking (jamming) phenomenon, which was apparent in the second field test has been conducted by Botros et al. [67].

10.6 STATION AND GAS PIPELINE BLOWDOWN

Evacuation of a compression station or a gas pipeline occurs during blowdown or after rupture of a pipeline element. In the first case the exit cross-sectional area of the riser is much smaller than that of the main pipe. Consequently, the gas velocity in the pipeline is typically about 10–30 m/s during sonic discharge and the flow can be regarded as quasi-steady. Stagnation pressure at the stack exit, which determines the discharge flux to the atmosphere, is a function of pipeline pressure at the stack entrance and pressure losses in the riser. In case of a rupture, however, the exit area can be as large as the main pipe cross-sectional area and thus flow velocity in the pipe becomes high (about 350 m/s initially at the ruptured section) and varies rapidly with time. The above comparison indicates that the two cases require different physical models and mathematical descriptions for the calculation of pressure time history during evacuation of the pipeline.

The schematic in Fig. 10-82 shows a blowdown riser, where the internal flow during sonic discharge from the stack occurs with low velocity in the main pipe, moderate velocity along L_{s1} , sonic velocity at the valve throat and mostly supersonic velocity along L_{s2} and at the exit. This pattern can be attributed to a typical stack with a plug valve. The geometry of such a stack is characterized by the effective cross-sectional area ratio of the valve throat to the stack being equal to about 0.6 and L_{s2}/D_s being less than 10. After an abrupt enlargement of the duct cross-section downstream of the throat, a supersonic flow with oblique shock waves occurs until the main pipe pressure falls to a level approximately 2.5 times the ambient pressure [68,69]. With further decrease in the main pipe pressure, a subsonic flow is established along L_{s2} , and soon after, the sonic discharge is terminated when the pipe pressure drops approximately below 1.5 times the ambient pressure. Due to the pressure recovery downstream of the throat, the pipe pressure terminating the sonic discharge is lower than that with $L_{s2} = 0$ when no pressure recovery takes place and as a

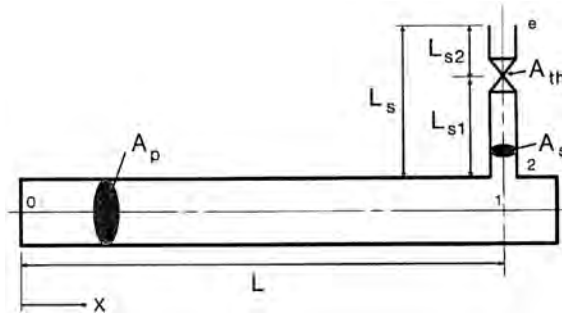


Figure 10-82. Schematic of a blowdown section.

result, the duration of sonic venting is extended. The friction losses along L_{s2} do not affect the flow rate during sonic discharge but slightly raise the pipe pressure at which this phase is terminated. However, during the subsonic discharge obviously these losses decrease the flow rate and hence slow down the discharge process. It seems that these opposite effects, i.e. faster discharge due to extension of sonic venting and slower discharge during the subsonic phase, allow for a simplification to regard the valve throat as an exit to the ambient pressure. Therefore, this simplification was applied to all models and methods of solution discussed in this section.

Generally, the flow pattern along L_{s2} depends on throat/stack area ratio, the pipe pressure and whether (fL_{s2}/D_s) or $(fL_{s2}/D_s)_{\max}$ [25]. These factors determine flow at the exit, M_e or 1. For the stack characterized above, $(fL_{s2}/D_s) < (fL_{s2}/D_s)_{\max}$. However, with abnormally long L_{s2} or different area ratio, the flow may be choked at the exit but not at the valve throat. In that case the downstream friction losses such as those along L_{s1} will decrease the flow rate during the sonic discharge.

Accuracy in predicting the blowdown time is determined by proper description of thermo- and gas dynamic behavior of gas during this unsteady process. Specifically, gas expansion in the pipe and at the throat and precise determination of friction losses in the riser and of throat discharge coefficient, are of particular importance. Pressure losses depend on L/D , L_{s1}/D_s , L_{s2}/D_s , shape of the riser inlet and roughness of the main pipe and the riser. It is expected that stack friction losses can extend the blowdown time by about 5 to 10% [68].

The literature related to blowdown time prediction is rather scarce [70] contrary to many papers dealing with slow [21,71,72] or fast transients [73–76] in gas pipeline systems.

In this Section two physical models are described; the pipeline section is regarded either as a volume with stagnation conditions inside or as a pipe with velocity increasing towards the exit. Solutions of the pertinent equations for each model were obtained analytically for natural gas with some reference gas parameters and numerically taking into account the real gas properties at each time step during blowdown. Effects of friction losses in the riser upstream of the throat were also considered in the numerical methods.

Gas expansion in the main pipe generally is regarded as an isothermal process because the shortest blowdown lasts at least a couple of minutes during which heat transfer to the gas occurs. Thermal capacitance of the pipe and surrounding soil secures sufficient heat flow to prevent much change in the gas temperature. To assess this assumption the gas temperature was measured and calculated during the blowdown of a compressor station piping. The lowest temperature measured was slightly below freezing and the one calculated with a steady heat transfer model was -12°C . Nevertheless, the pressure-time profile calculated for the latter case was very close to that calculated for the isothermal process. In reality, the lowest temperature most probably was below the measured one due to some thermal inertia

of the thermometer housing but above the calculated temperature due to the enhanced heat transfer with a transient temperature distribution in the soil. If contents of the heaviest gas components are not exceeding the specification gas requirements, condensation should not occur above -10°C and therefore it seems that typically there is no need to take it into account. During the isentropic gas expansion at the throat the gas temperature is lowered considerably, but due to the relaxation time condensation should not affect the process of expansion and thus the flow rate.

10.6.1 Volume Model

This model neglects the effects of flow and friction along the main pipe and hence assumes that stagnation conditions prevail inside the whole pipe section under blowdown. Isothermal gas expansion is assumed inside the main pipe and isentropic flow through the stack.

Mass conservation requires that

$$\dot{m}dt = Vd\rho \quad (10-76)$$

The equation of state of the gas has the form:

$$\rho = \rho(P, T) \quad (10-77)$$

where:

- \dot{m} = mass flow rate
- ρ = gas density
- P = pressure
- T = temperature
- R = gas constant
- V = pipeline volume

The procedures describing the analytical and the numerical solutions of these equations are given below.

Analytical Volume Solution: For perfect gas and $T = \text{constant}$, Eq. (10-77) yields

$$d\rho = dP/RT \quad (10-78)$$

and thus Eq. (10-76) can be transformed into

$$\dot{m}RTdt = VdP \quad (10-79)$$

For sonic flow at the valve throat and assuming isentropic expansion from the pipe stagnation conditions, the mass flow rate [25] is:

$$\dot{m}_c = \frac{2}{k+1} \frac{k+1}{2(k-1)} \frac{k}{RT}^{1/2} P \times A_{th} \times C_d \quad (10-80)$$

where:

- \dot{m}_c = mass flow rate through a choked valve
- k = isentropic exponent of the gas
- A_{th} = valve through area
- C_d = discharge coefficient of the valve which depends on the type of the valve

The time constant τ_v is defined as:

$$\tau_v = \frac{V \frac{k+1}{2} \frac{1}{2(k-1)}}{a \times A_{th} \times C_d} \quad (10-81)$$

where a is the speed of sound. Introducing Eqs. (10-80) and (10-81) in the original Eq. (10-79) yields the normalized differential equation:

$$d\bar{t}_c = d\bar{P}/\bar{P} \quad (10-82)$$

where the normalized pressure $\bar{P} = P/P_a$, P_a is the ambient pressure and time $\bar{t} = t/\tau_v$.

After integration from initial pressure \bar{P}_1 to the pressure \bar{P}_c , which terminates sonic flow, one obtains the time of sonic venting as:

$$\bar{t}_c = \ln(\bar{P}_1) - \ln(\bar{P}_c) \quad (10-83)$$

Or taking into account that

$$\bar{P}_c = \frac{k+1}{2} \frac{1}{(k-1)} \quad (10-84)$$

then, the dimensionless time for the sonic venting can be written as;

$$\bar{t}_c = \ln(\bar{P}_1) - \frac{k}{k-1} \ln \frac{k+1}{2} \quad (10-85)$$

Generally, the pressure-time history during sonic venting can be determined from Eq. (10-83) as:

$$P/P_i = e^{-\bar{t}} \quad (10-86)$$

where $0 < \bar{t} < \bar{t}_c$. This indicates that the pressure drop in the main pipe occurs exponentially during sonic venting.

Following the sonic venting is a subsonic discharge where the critical flow pressure corresponding to the line stagnation pressure is less than the ambient pressure P_a . During this period, the mass flow rate can be expressed as:

$$\dot{m}_s = \frac{2}{k-1} \frac{1}{RT} \frac{k}{P} \frac{2}{k} \frac{k+1}{P} \frac{1}{k} \frac{1}{2} P \times A_{th} \times C_d \quad (10-87)$$

Introducing Eq. (10-87) into Eq. (10-79) and following the previous transformations we obtain the differential equations:

$$d\bar{t}_c = \frac{\frac{1}{2^{k-1}(k-1)^{1/2}/(k+1)^{2(k-1)}}}{\bar{P} \bar{P}^{2/k} \bar{P}^{(k+1)/k} \frac{1}{2}} d\bar{P} \quad (10-88)$$

Integration of the above equation from \bar{P}_c to \bar{P}_b (where $\bar{P}_b > 1$) can be carried out to determine the time of subsonic discharge and the blowdown mass flow and line pressure during this time.

Numerical Volume Solution: In the above analytical solution, the gas properties needed for the analysis, namely k and c , were assumed constant for the duration of the blowdown and were calculated at a reference pressure and temperature (averaged throughout the process) from an equation of state. This is rather a necessary assumption if a closed form analytical solution is required. In order to account for variations in gas properties as conditions change in the pipe volume, numerical methods are necessary. An appropriate equation of state, such as the AGA-8 [23] or PR [24] equations, is needed to provide not only the P - ρ - T relation, Eq. (10-77), but also the derived thermodynamic properties required for the numerical computation. The mass conservation equation, Eq. (10-76), is still valid, and the assumptions of isothermal expansion of the gas inside the pipe volume and isentropic flow through the stack (adiabatic flow with no losses) still apply.

For sonic discharge, Eq. (10-76) can be written as:

$$V \frac{d\rho}{dt} = (\rho_{th} \times a_{th} \times A_{th} \times C_d) \quad (10-89)$$

where subscript 'th' refers to blowdown valve throat condition, and

$$\rho_{th} = \rho(P_{th}, T_{th}) \quad \text{and} \quad a_{th} = a(P_{th}, T_{th})$$

are determined from the state equation. The throat pressure and temperature (P_{th} , T_{th}) are related to the pressure and temperature of the gas in the pipe volume (P , T) and can be calculated from the state equation using an iterative procedure for isentropic expansion to sonic conditions. Additionally, the thermodynamic relation:

$$\frac{\partial P}{\partial \rho} \Big|_T = \frac{\partial P}{\partial \rho} \Big|_s / k = a^2 / k \quad (10-90)$$

is used to describe the isothermal expansion of the gas inside the pipe volume, where k is the isentropic exponent of the gas. Hence, Eq. (10-89) can be written as:

$$\frac{kV}{a^2} \frac{dP}{dt} = (\rho_{th} \times a_{th} \times A_{th} \times C_d) \quad (10-91)$$

Equation (10-90) is also used to calculate the speed of sound a from the equation of state.

For subsonic discharge, i.e. when the critical flow pressure is less than the ambient pressure, Eq. (10-91) is replaced by

$$\frac{kV}{a^2} \frac{dP}{dt} = (\rho_{th} \times u_{th} \times A_{th} \times C_d) \quad (10-92)$$

where, $\rho_{th} = \rho(P_a, T_{th})$ and u_{th} is the throat velocity calculated from isentropic expansion from the pipeline volume conditions (P , T) to the ambient pressure P_a , and valve throat to riser area ratio.

This also require an iterative procedure since the R.H.S. of Eq. (10-92) is also a function of the pressure and temperature in the pipe volume. Both Eq. (10-91) and Eq. (10-92) are quasi-linear, ordinary differential equations of the first order which can be solved numerically using the variable order Backward Differentiation Formula (BDF) method known as Gear's method (Harwell Subroutine Library - DC03 Routine, 1988) [77]. The iterative pro-

cedures involved in the isentropic expansion of the gas to the stack throat are quite intensive particularly with the AGA-8 state equation whose coefficients are temperature dependent.

10.6.2 Pipe Model

This model takes into account flow velocity and friction losses along the main pipe section under evacuation. The other assumptions are the same as for the volume model, i.e. isothermal expansion of the gas in the main pipe and isentropic through the stack. The one-dimensional flow along the pipe is described by the continuity equation:

$$\frac{\partial \rho}{\partial t} + \rho \frac{\partial v}{\partial x} + v \frac{\partial \rho}{\partial x} = 0 \quad (10-93)$$

and the momentum equation:

$$\frac{\partial v}{\partial t} + v \frac{\partial v}{\partial x} + \frac{1}{\rho} \frac{\partial p}{\partial x} + \frac{f_{DW}}{2D} v|v| = 0 \quad (10-94)$$

and the gas state equation, Eq. (10-77), where, f_{DW} is Darcy Weisbach friction factor.

This yields a set of non-linear, first-order parabolic partial differential equations for the dependent variables P and v . An Euler implicit finite difference scheme can be used to obtain the solution. This scheme is known to be first-order accurate in time and second-order accurate in space [69]. Alternatively, the method of characteristics can be used as described earlier. The piping system can be divided into elements and nodes, with the previously noted boundary conditions: e.g. zero velocity at closed ends and given mass flow at the blowdown valve throat depending on whether the valve is choked (sonic discharge) or unchoked (subsonic discharge).

If an Euler implicit finite difference scheme is used, for each time step, t , a system of $2n$ (where n is the number of nodes dividing the pipe section) non-linear algebraic equations are formulated from the implicit finite difference scheme. These equations are solved simultaneously using Newton's method. A distinct advantage of this scheme is that the solution is generally stable for all choices of t and x and it is relatively simple to implement. In addition, the formulation of a straight section of a pipeline results, naturally, in a block-tridiagonal system of equations for which the Thomas algorithm described in Rosenberg [78] can be applied quite readily. Note that the blocks in this tridiagonal system are 2×2 since the number of dependent variables is two. In the case of complicated piping networks, this block triangular property is no longer in effect, and a technique based on a sparse variant of Gaussian elimination for sparse systems of equations is used [79].

If the method of characteristics is used, the above hyperbolic partial differential equations are transformed into total differential equations, which lead to a set of algebraic compatibility equations along two characteristic lines and a particle path line as described earlier in this chapter. These compatibility equations, together with the respective characteristic lines are integrated in the time-space domain.

10.6.2.1 Analytical Pipe Model

As in the previous analytical solution for the volume model, a closed form solution is only possible with ideal gas behavior, i.e. $P = \rho RT$. Introduction of the gas flux $Q = \rho v$ as a variable, linearization of the resistive term

$$\frac{f_{DW}}{2D} v|v| = C \propto v \quad (10-95)$$

where C is the attenuation factor, and omission of the inertial terms in Eq. (10-94), and combining the two Eqs. (10-93) and (10-94) yields:

$$\frac{\partial P}{\partial t} = \kappa \frac{\partial^2 p}{\partial x^2} \quad (10-96)$$

where

$$\kappa = \frac{RT}{C} \quad (10-97)$$

The partial differential equation, Eq. (10-96), describing a slowly varying flow in the main pipe, is linear, parabolic and of the second order and is known as the one-dimensional heat conduction equation [80]. This equation can be solved once the boundary and initial conditions for the pipeline are specified. At the closed end, $x = 0$ (Fig. 10-66), $Q = 0$ prevails at all times. At the stack end, $x = L$, and during sonic venting the gas flux is proportional to the pipe pressure, i.e. $Q = EP$, Eq. (10-80), where E is a constant. At the beginning of blowdown the pressure in the entire pipeline is equal to P_i . Botros et al. [81] have given analytical solution for Eq. (10-96) above in terms of an infinite series dependent on geometrical parameters, gas properties and attenuation factor.

10.6.3 Comparison Between Models

Field measurements were taken during blowdown of a gas pipeline section on TransCanada Pipeline system in Alberta, Canada. Particulars of this pipeline section are:

$D_p = 0.203$ m
 $D_s = 0.097$ m
 $A_{th} = 0.00548$ m²
 $L_{s1} = 1.3$ m
 $L_{s2} = 0.7$
 $L = 25523$ m
 $P_i = 4089$ kPa
 $T_i = 302$ K
 Gas composition (Table 10-7)
 $k = 1.298$ at $P = 2000$ kPa, $T = 302$ K
 $a = 420$ m/s at $P = 2000$ kPa, $T = 302$ K

Figure 10-83 shows the measured P - t profile in the main pipe at section 1 (see Fig. 10-82). The valve C_d was estimated to be 0.75, which seems quite reasonable for a plug valve

Table 10-7. Gas composition

	Mole %
C ₁	92.019
C ₂	4.764
C ₃	1.204
iC ₄	0.1393
nC ₄	0.1904
iC ₅	0.0436
nC ₅	0.0342
C ₆ ⁺	0.0452
N ₂	0.696
CO ₂	0.8643
Sum	100
MW	17.578
St. density (kg/m ³)	0.74385

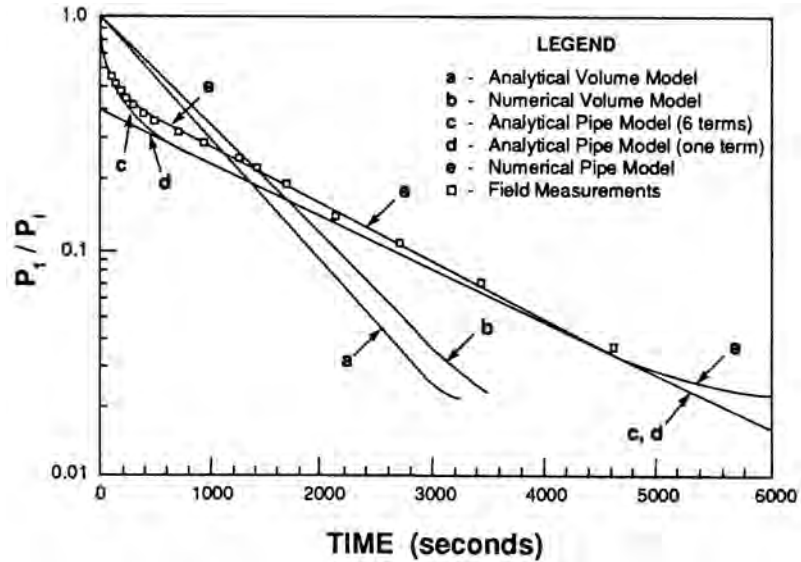


Figure 10-83. Pressure-time profiles based on different models and comparison with field measurements for a pipeline section of $fL/D = 1685$.

when compared to 0.73 for choked sharp-edged orifice with zero velocity of approach [25]. The friction factor was calculated at each time step for each discretized section of the pipe as a function of Reynolds number and relative pipe roughness $= 1.5 \times 10^{-4}$. Entrance and friction losses in the stack are both accounted for in the computation. Notice in particular the sharp pressure decrease at the beginning of the blowdown and the ability of the model to simulate this. This sharp pressure decrease is primarily due to the relatively high $(A_{th}C_d/A_p)$ resulting in a pronounced transient effects immediately after the opening of the blowdown valve.

The same value of $C_d (= 0.75)$ was used in the other models and the respective profiles are also shown in Fig. 10-83. Notice, the large discrepancies in both volume models (analytical and numerical) in estimating the $P-t$ profile. This is mainly due to the fact that for such a large value of $f_{DW}L/D$, the physical model in this case falls short of representing the gas expansion/flow in the pipe. Results of two analytical pipe-models are shown: one considered only one term in the infinite series solution of Eq. (10-96) [81]. It is interesting to see that even with such large discrepancy at $t = 0$, the two pipe model profiles (analytical and numerical) coincide as time elapses, and approach the measured results. Both analytical and numerical volume models did not match the measured profiles. The fact that the volume model solutions generally underpredict the blowdown time is due to the lack of attenuation resulting from friction along the main pipe.

Another field measurement was taken during blowdown of a three-unit compressor station also on TransCanada Pipeline system in Alberta, Canada. Station configuration and dimensions are shown in Fig. 10-84. Other particulars are:

$$\begin{aligned}
 D_s &= 0.2476 \text{ m} \\
 A_{th} &= 0.0301 \text{ m}^2 \\
 P_i &= 6042 \text{ kPa} \\
 T &= 292 \text{ K} \\
 L_{s1} &= 1.829 \text{ m} \\
 L_{s2} &= 1.295 \text{ m} \\
 k &= 1.314 \text{ at } P = 3000 \text{ kPa, } T = 292 \text{ K} \\
 a &= 410 \text{ m/s at } P = 3000 \text{ kPa, } T = 292 \text{ K} \\
 &\text{Gas composition (Table 10-7)}
 \end{aligned}$$

Figure 10-85 shows the measured $P-t$ profile at point 'X' very close to the blowdown stack. Similarly, for best match of the measured profile to that obtained from the numerical pipe model $C_d = 0.87$ was used in the model. The transient flow through the orifice plates, check and globe valves and other elements was accounted for in the simulation but are not discussed here in detail due to space limitation of this paper. In this particular example, the $C_d = 0.87$ is a surprisingly high value probably due to different geometry of the stack valve, and also due to the fact that the system is composed of many throttling elements. These throttling elements were assumed fully open in the simulation, where in reality this may not be the case. As such, error in underestimating local resistances can lead to higher pressure at point 'X', and hence a fictitiously higher C_d value would be required to match the measured $P-t$ profile. The results obtained from all models except the analytical pipe model (which is not possible to obtain due to complexity of the station configuration) are presented for comparison. It is also evident in this case study that the volume (analytical and numerical) models fall short in predicting the blowdown profile and time.

10.6.4 Non-Isothermal Blowdown

In the case of blowdown of gas from above ground piping, vessels and containers such as the Gas Transport Modules (GTM) comprising marine compressed natural gas (CNG), the thermodynamic path taken by the gas contained in the vessel never isothermal because there is neither enough heat input to maintain the isothermal condition nor the required heat-time dependency to maintain isothermal condition cannot be matched by the surrounding sources of heat. In fact, the thermodynamic path could take the other extreme, i.e. along a constant isentropic path if the process is completely adiabatic [82]. The latter will result in extremely low temperatures of the gas, particularly if the initial pressure at the start of the blowdown is relatively high. However, isentropic expansion is not possible either, because when the gas expands to a lower temperature than the pipe or the vessel wall, substantial heat transfer will take place from the wall to the expanding gas, and hence the removal of the '*isentropicity*' of the process. As far as the wall is concerned, there will be four heat transfer processes taking place during blowdown: i) heat transfer by convection (likely natural if we ignore the gas movement in the vessel induced by the blowdown flow); ii) from the wall to the colder gas inside the vessel; iii) reduction in the heat capacity contained in the wall material which acts like a heat source; iv) and heat transfer by convection between the surroundings and the vessel. If the state of the gas inside the vessel at any time during the expansion process of the gas would permit partial condensation, the heat transfer from the wall to the content will further be complicated due to the presence of two phases: vapour and boiling liquid.

Let us consider the general thermodynamics of non-isothermal, non-isentropic blowdown process of gas contained in a vessel of volume V from initial pressure P_i and initial temperature T_i . The first law of thermodynamics can be written as follows (see Fig. 10-86):

$$\dot{Q} = \frac{\partial}{\partial t}(Mu) + \dot{m}h \quad (10-98)$$

where:

\dot{Q} = external heat input rate

\dot{m} = blowdown mass flow rate

u = specific internal energy of the gas remaining in the vessel at any time

h = enthalpy of the gas leaving the vessel at any time

M = mass remained in the vessel at any time

Given the definition of internal energy in terms of the enthalpy as:

$$u = h - Pv \quad (10-99)$$

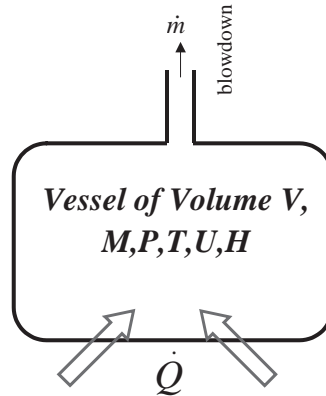


Figure 10-86. A schematic of vessel blowdown with external heat input.

where v is the specific volume of the gas inside the vessel at any time, eq. (10-98) can be manipulated as follows:

$$\dot{Q} = \frac{\partial}{\partial t} [M(h - Pv)] + \dot{m}h \quad (10-100)$$

$$\dot{Q} = \frac{\partial}{\partial t} (Mh) - \frac{\partial}{\partial t} (PV) + \dot{m}h \quad (10-101)$$

$$\frac{\partial Mh}{\partial t} + V \frac{\partial P}{\partial t} \left[1 + \frac{\dot{Q}}{V \frac{\partial P}{\partial t}} \right] = \dot{m}h \quad (10-102)$$

or approximately;

$$M C_p \frac{\partial T}{\partial t} + V \frac{\partial P}{\partial t} \left[1 + \frac{\dot{Q}}{V \frac{\partial P}{\partial t}} \right] = \dot{m}h \quad (10-103)$$

The term between the square bracket can be called the degree of isentropicity or the isentropic coefficient (η_{is}), i.e.

$$\frac{\partial Mh}{\partial t} + V \frac{\partial P}{\partial t} [\eta_{is}] = \dot{m}h \quad (10-104)$$

Three conditions arise from the above expression:

- For an adiabatic blowdown (i.e., $\dot{Q} = 0$), the isentropic coefficient $[\eta_{is}] = 1.0$.
- For a heat input rate such that $\dot{Q} = -V \frac{\partial P}{\partial t}$, the isentropic coefficient will be $[\eta_{is}] = 0.0$, which is isenthalpic.

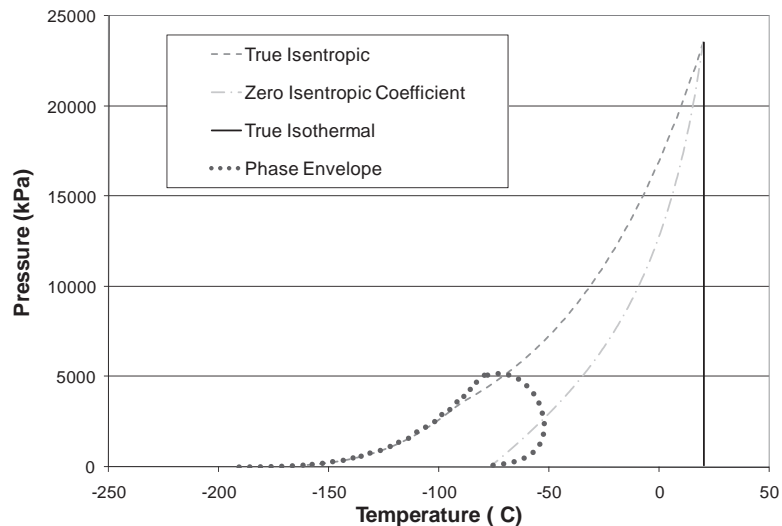
To illustrate the differences between the above processes, consider an example taken from a marine compressed natural gas bank (gang) of 56 GTM's having the characteristics given in Table 10-8.

Table 10-8. Geometrical and initial condition of a marine CNG gang

Model Data		
Initial pressure	23,500	kPa
Initial temperature	20	C
One gang (4 14)	56	GTM
Length of one GTM	22.51	m
D_i	1.02484	m
D_o	1.0668	m
Volume of one GTM	18.57	m ³
Volume of one gang	1,039.70	m ³
Blowdown I.D. diameter (8")	0.17305	m
Discharge coefficient (C_d)	0.9	
Surface area of one GTM	75.43	m ²
Surface area of one gang	4,224.14	m ²
Volume of steel in one GTM	1.55	m ³
Volume of steel in one gang	86.88	m ³
Mass of steel in one gang	677,674	kg
Heat capacity of steel	475	J/kg.C
Heat capacity in gang per 1°C	321,895,024	J/C
Heat capacity in gang per 1°C per 1 m ² of surface area	76,204	J/m ² .C

Blowdown simulations were performed on this system and results of the respective pressure-temperature profiles are plotted on the corresponding mixture phase envelope in Fig. 10-87. The corresponding pressure- and temperature-time profiles are shown in Fig. 10-88. Clearly, the isentropic expansion results in the lowest gas temperature reaching approximately -160°C , as well as potential for condensation in the GTM's. In reality, the gas expansion is neither isentropic (particularly if the vessel is not insulated), nor isothermal (which requires significant amount of heat input and very high heat transfer coefficients). A realistic expansion would be non-isentropic, with isentropic coefficient likely around ± 0.2 , i.e. on either side of the expansion with zero isentropic coefficient.

A more accurate determination of the expansion state (\dot{Q}) in Eq. (10-103). If the temperature gradient across the wall of the vessel is neglected, the following two equations can be written:

**Figure 10-87.** Pressure-temperature profiles of different blowdown expansion processes.

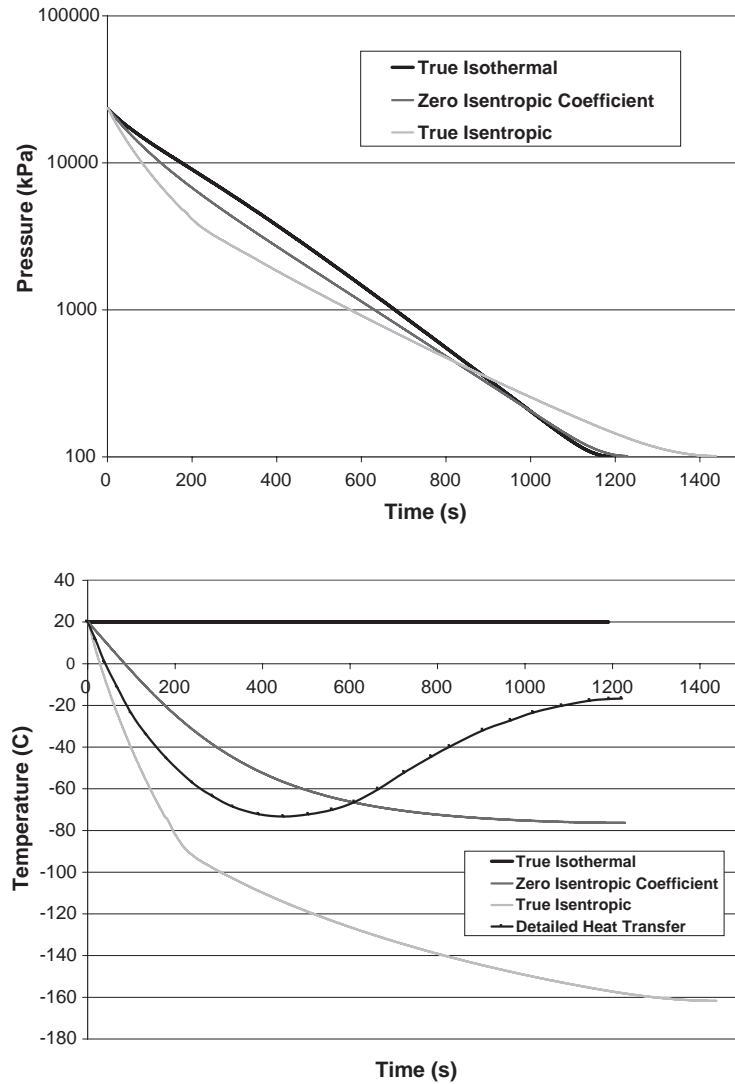


Figure 10-88. Pressure- and temperature-time profiles of different blowdown expansion processes.

Heat transfer from the inner wall to the gas inside the vessel:

$$\dot{Q} = U_i A_i (T_w - T_g) \quad (10-105)$$

Heat balance within the vessel wall material:

$$\dot{Q} = U_0 A_0 (T_0 - T_w) = M_w C \frac{dT_w}{dt} \quad (10-106)$$

where:

A_i = internal wall surface area.

A_0 = external wall surface area.

C = wall material heat capacity per unit mass.

M_w = wall total mass.

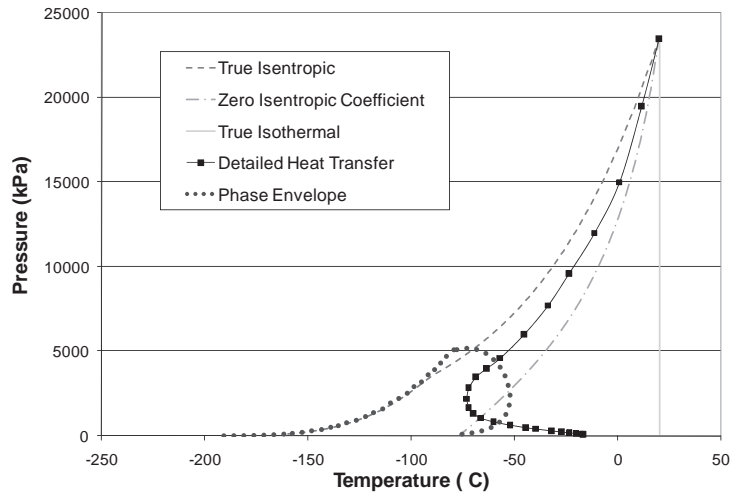


Figure 10-89. Pressure-temperature profile of accounting for detailed heat transfers and comparison to other expansion processes.

U_i = heat transfer coefficient between the internal wall and the gas inside the vessel.

U_o = heat transfer coefficient between the surroundings and the external wall.

T_g = gas temperature.

T_o = surrounding temperature.

T_w = wall temperature.

The above formulation was applied to the marine CNG example given above, and the resulting temperature profile is shown in Fig. 10-88. Note that, initially, the gas expansion is shown to lie between isentropic and non-isentropic behavior, while later in time it tends to asymptote to a temperature higher than the non-isentropic. The deflection trend in the temperature has been observed in the literature [83,84] and the upper trend is attributed to the decreasing mass of the gas remaining in the vessel at the latter stage of the blowdown. Figure 10-89 shows the pressure-temperature expansion profile accounting for detailed heat transfers on the gas phase envelope diagram.

REFERENCES

- [1] Turner, W. J., and Simonson, M. J., 1985. "Compressor Station Transient Flow Modeled," *Oil and Gas Journal*, pp. 79–83, May 20.
- [2] Botros, K. K., 1994. "Transient Phenomena In Compressor Stations During Surge," *37th ASME International Gas Turbine and Aeroengine Congress and Exposition, Cologne, Germany, June 1–4, 1992*, also appeared in the *J. of Eng. for Gas Turbine and Power*, **116**, pp. 133–142, January.
- [3] Botros, K. K., Campbell, P. J., and Mah, D. B., 1991. "Dynamic Simulation of Compressor Station Operation Including Centrifugal Compressor, and Gas Turbine," *ASME Journal of Engineering for Gas Turbines and Power*, **113**, pp. 300–311, April.
- [4] Murphy, K. M. et al., 1992. "On Modelling Centrifugal Compressors For Robust Control Design," *Int. Gas Turbine and Aeroengine Congress and Exposition, Cologne, Germany, 92-GT-231, June 1–4, 1992*.
- [5] Paltovany, D., and Focke, A. B., 1986. "Predictive Surge Control Optimization For A Centrifugal Compressor," *J. Turbomachinery*, **108**, pp. 82–89, July.
- [6] Botros, K. K., Jones, J. B., and Roorda, O., 1996. "Flow Characteristics and Dynamics of Swing Check Valves In Compressible Flow Applications-Part I," *1996 ASME Pressure Vessels and Piping*

- Conference, Symposium on Fluid Structure Interaction*, Montreal, Quebec, Canada, July 21–26, 1996, PVP-Vol. 337, pp. 241–250.
- [7] Wylie, E. B., Streeter, V. L., and Stoner, M. A., 1974. “Unsteady-State Natural Gas Calculations in Complex Pipe Systems,” *Society of Petroleum Engineering Journal*, pp. 35–43, Feb.
 - [8] Al-Nahwi, A. A., and Graf, M. B., 1997. “Modeling of Industrial Pumping System Dynamics,” *ASME Turbo-Expo Conference*, Orlando, Florida, June 2–5, 1997.
 - [9] Botros, K. K., and Richards, D. J., 1995. “Analysis of the Effects Of Centrifugal Compressor’s Performance Characteristics During ESD,” *11th Symposium On Industrial Applications of Gas Turbines*, Canadian Gas Association, Banff, Alberta, Canada, October 11–13, 1995.
 - [10] Botros, K. K., Richards, D. J., Brown, R. J., and Stachniak, D. M., 1993. “Effects of Low Power Turbine/Compressor Rotor Inertia During Shutdown,” Presented at the *1993 Symposium on the Industrial Application of Gas Turbines*, Canadian Gas Association, Banff, Alberta, October 13–15, 1993.
 - [11] Botros, K. K., Jungowski, W. M., and Richards, D. J., 1996. “Compressor Station Recycle System Dynamics During Emergency Shutdown,” *ASME Transactions, J. Eng. for Gas Turbines and Power*, **118**, pp. 641–653, July.
 - [12] Botros, K. K., Jones, B. J., and Richards, D. J., 1996. “Recycle Dynamics During Centrifugal Compressor ESD, Startup and Surge Control,” *International Pipeline Conference (IPC)*, ASME, Calgary, Alberta, Canada, June 9–14, 1996.
 - [13] Botros, K. K., Richards, D. J., and Roorda, O., 1996. “Effect of Check Valve Dynamics on Sizing of Recycle Systems For Centrifugal Compressors,” *41st ASME International Gas Turbine and Aeroengine Congress and Exposition (Turbo-Expo)*, Birmingham, UK, June 10–13, 1996.
 - [14] Greitzer, E. M., 1976. “Surge and Rotating Stall in Axial Flow Compressors,” *J. Eng. Power, Transaction of ASME*, pp. 190–198, April.
 - [15] Moore, K. K., and Greitzer, E. M., 1986. “A Theory of Post Stall Transients in Axial Compression Systems,” *J. Eng. Gas Turbines Power*, **108**, 68–76.
 - [16] Botros, K. K., and Petela, G., 1994. “Use of Method of Characteristics, and Quasi-Steady Approach In Transient Simulation Of Compressor Stations,” *1994 ASME Fluids Engineering Division Summer Meeting-Advances In Computational Methods In Fluid Dynamics*, June 19–23, 1994, Lake Tahoe, Nevada, U.S.A., FED–Vol. 196, pp. 325–338.
 - [17] Cumpsty, N. A., 1989. *Compressor Dynamics*, Longman Scientific, and Technical, New York.
 - [18] Zucrow M. J., and Hoffman J. P., 1976. *Gas Dynamics*, vols. I and II, John Wiley & Sons Inc.
 - [19] Kentfield, J. A. C., 1993. *Non-Steady, One-Dimensional, Internal, Compressible Flows—Theory and Applications*, Oxford Science Publication, 1993.
 - [20] Fox, J. A., 1977. *Hydraulic Analysis of Unsteady Flow In Pipe Networks*, John Wiley & Sons Inc.
 - [21] Osiadacz, A., 1984. “Simulation of Transient Gas Flows In Networks,” *Int. J. for Numerical Methods in Fluids*, **4**, pp. 13–24.
 - [22] Shapiro, A. H., 1983. *The Dynamics and Thermodynamics of Compressible Fluid Flow*-Vol. 2, E. Krieger Publishing Co., Malabar, Florida, pp. 972–973.
 - [23] Starling, K. E., and Savidge, J. L., 1992. “Compressibility Factors for Natural Gas and Other Related Hydrocarbon Gases,” *American Gas Association, Transmission Measurement Committee Report No. 8*.
 - [24] Peng, D. Y., and Robinson, D. B., 1976. “A New Two-Constant Equation of State,” *Industrial and Engineering Chemistry: Fundamentals*, **15**, pp. 58–64.
 - [25] Shapiro, A. H., 1953. *The Dynamics and Thermodynamics of Compressible Fluid Flow*-Vol. 1, John Wiley & Sons.
 - [26] Gas Processors Suppliers Association, 2006. *Engineering Data Book*, Tulsa, Oklahoma.
 - [27] Brown, R. N., 2005. *Compressors, Selection and Sizing*, Elsevier.
 - [28] Audry-Sanchez, J., 1988. “On the Numerical Solution of Differential Algebraic Equations,” *Can. J. Chem. Eng.*, **66**, pp. 1031–1035, Dec.
 - [29] Gear, C. W., 1971. *Numerical Initial Value Problems in Ordinary Differential Equations*, Prentice-Hall, Englewood Cliffs, NJ.

- [30] White, R. C., and Kurz, R., 2006. "Surge Avoidance for Compressor Systems," *Proceedings of the 35th Turbomachinery Symposium*, George R. Brown Convention Centre, Houston, Texas.
- [31] "Axial and Centrifugal Compressors and Expander-compressors for Petroleum, Chemical and Gas Industry Services Downstream Segment," *API Standard 617*, Seventh Edition, July 2002, Amended June 1, 2003.
- [32] Chiu, C., and Kalsi, M. S., 1986. "Plant Availability Improvement by Eliminating Disc Vibrations in Swing Check Valves," *ASME/EEE Power Generation Conference*, Portland, Oregon, 86-JPGC-NE-6, October 19–23, 1986.
- [33] Electrical Producers Research Institute, Application Guidelines for Check Valves in Nuclear Power Plants, 1988. EPRI NP-5479, final report, January.
- [34] Rahmeyer, W. J., 1993. "Sizing Swing Check Valves for Stability and Minimum Velocity Limits," *J. Pressure Vessel Technology*, **115**, pp. 406–410, November.
- [35] Botros, K. K., Jones, J. B., and Roorda, O., 1997. "Effects of Compressibility on Flow Characteristics and Dynamics of Swing Check Valves-Part I," *ASME J. Pressure Vessel Technology*, **119**, pp. 192–198, May.
- [36] Thorley, A. R. D., 1989. "Check Valve Behaviour Under Transient Flow Conditions: A State-of-the-Art Review," *J. Fluids Engineering, Transactions of the ASME*, **111**, pp. 178–183, June.
- [37] Thorley, A. R. D., 1984. "The Dynamic Response of Check Valves," *Chem. Eng.*, **402**, pp. 12–15, April.
- [38] Ellis, J., and Mualla, W., 1986. "Numerical Modelling of Reflux Valve Closure," *J. Pressure Vessel Technology, Transactions of the ASME*, **108**, pp. 92–97, February.
- [39] Hong, H., Svoboda, J. V., and Blach, A. E., 1985. "Design Considerations for Wafer Type Check Valves for Nuclear and Power Plant Services," *International Conference on Developments in Valves, and Actuators for Fluid Control*, Oxford, England, pp. 37–56, September 10–12, 1985.
- [40] Provoost, G. A., 1980. "The Dynamic Behaviour of Non-Return Valves," *3rd International Conference on Pressure Surges*, Canterbury, England, pp. 415–427, March 25–27, 1980.
- [41] Provoost, G. A., 1983. "A Critical Analysis to Determine Dynamic Characteristics of Non-Return Valves," *4th International Conference on Pressure Surges*, Univ. of Bath, England, pp. 275–286, September 21–23, 1983.
- [42] Koetzier, H., Kruisbrink, A. C. H., and Lavooij, C. S. W., 1986. Dynamic Behaviour of Large Non-Return Valves," *5th International Conference on Pressure Surges*, Hannover, Germany, pp. 237–243, September 22–24, 1986.
- [43] Kruisbrink, A. C. H., 1988. "Check Valve Closure Behaviour, Experimental Investigation and Simulation in Waterhammer Computer Programs," *2nd International Conference on Developments in Valves and Actuators for Fluid Control*, Manchester, England, pp. 281–300, March 28–30, 1988.
- [44] Perko, H. D., 1986. "Check Valve Dynamics in Pressure Transient Analysis," *5th International Conference on Pressure Surges*, Hannover, Germany, pp. 229–235, September 2–24, 1986.
- [45] Lee, C. L., Jocson, A. T., and Hsu, S. T., 1992. "On the Dynamic Performance of Large Check Valves," *Unsteady Flow and Fluid Transients Conference*, Durham, U.K., pp. 365–369.
- [46] Andrews, F., and Carrick, H. B., 1983. "Check Valves for Compressor Protection-A User View," *Proceedings of the 12th Turbomachinery Symposium*, College Station, TX, U.S.A., pp. 45–52, November 15–17, 1983.
- [47] Kruisbrink, A. C. H., and Thorley, A. R. D., 1994. "Dynamic Characteristics for Damped Check Valves," *2nd International Conference on Water Pipeline Systems*, BHR Group Ltd., Edinburgh, Scotland, U.K., May 24–26, 1994.
- [48] Botros, K. K., and Roorda, O., 1997. "Effects of Compressibility on Flow Characteristics and Dynamics of Swing Check Valves-Part II," *ASME Journal of Pressure Vessel Technology*, **119**, pp. 199–206, May.
- [49] MacLeod, G., 1985. "Safety Valve Dynamic Instability: An Analysis of Chatter," *J. Pressure Vessel Technology*, **107**, pp. 172–177.
- [50] Krivosheev, A. G., 1988. "Stability of Steady State Operation of Safety Relief Valves," UDC 621.646.4.001.5, Translated from *Khimichskoe*, pp. 81–84.
- [51] D'Netto, W., and Weaver, D. S., 1987. "Divergence and Limit Cycle Oscillations in Valves Operating at Small Openings," *Journal of Fluids and Structures*, **1**, pp. 3–18.

- [52] Thomann, H., 1976. "Oscillations of a Simple Valve Connected to a Pipe-Parts I, II and III," *Journal of Applied Mathematics and Physics (ZAMP)*, **27**.
- [53] Masuda, F., 1985. "Dynamic Response Analysis of a Safety Valve With Transients of a Fluid System," *Transactions of the 8th International Conference on Structural Mechanics in Reactor Technology*, Brussels, F1-(F2), pp. 53–58.
- [54] Watton, J., 1983. "Dynamic Characteristics of a Single Stage Pressure Rate Controlled Relief Valve With Directional Damping," *ASME Winter Annual Meeting*, Paper 83-WA/DSC-40, pp. 1–8.
- [55] Watton, J., 1990. "The Stability and Response of a Two Stage Pressure Rate Controllable Relief Valve," *Journal of Fluid Control*, pp. 50–66.
- [56] Nayfeh, A. H., and Bouguerra H., 1990. "Non-Linear Response of a Fluid Valve," *International Journal of Non-Linear Mechanics*, **25**, pp. 433–449.
- [57] Foy, C. E., Kiel, D. E., and Jungowski, W. J., 1993. "The Effect of Pressure Pulsation and Pilot Setting on the Performance of Pressure Relief Valves," *Society of Petroleum Engineers*, Eastern Regional Meeting, SPE 26907, pp. 183–196.
- [58] Emerson, G. B., 1966. "Safety Valve Operational Stability," Anderson/Greenwood & Co., Internal Report No 2-0089.
- [59] Powell, W. W., 1971. "A Study of Resonant Phenomena in Pilot-Operated Safety Relief Valves," Anderson Greenwood & Co., Internal Report # 2-0175-51.
- [60] Follmer, B., 1980. "Oscillating Functioning of Safety Relief Valves Generated by Their Inlet Geometry," *Flow Visualization 2, Proceedings of the 2nd International Symposium*, September 9–12, New York, pp. 203–208.
- [61] Benedict, R. P., 1971. "Generalized Contraction Coefficient of an Orifice for Subsonic and Supersonic Flows," *Journal of Basic Engineering*, pp. 99–120.
- [62] Bloxsidge, G. J., Dowling A. P., and Langhorne, P. J., 1988. "Reheat buzz: An Acoustically Coupled Combustion Instability-Part 2. Theory," *Journal of Fluid Mech.*, **193**, pp. 445–473.
- [63] Myers, M. K., and Callegari, A. J., 1977. "On the Singular Behavior of Linear Acoustic Theory in Near-Sonic Flows," *Journal of Sound, and Vibration*, **51**(4), pp. 517–531.
- [64] Nayfeh, A. H., Shaker, B. S., and Kaiser, J. E., 1980. "Transmission of Sound Through Non-Uniform Circular Ducts with Compressible Mean Flows," *AIAA Journal*, **18**(5), pp. 515–525.
- [65] Munjal, M. L., 1987. *Acoustics of Ducts and Mufflers*, John Wiley & Sons.
- [66] Botros, K. K., Dunn, G. H., and Hrycyk, J. A., 1997. "Riser – Relief Valve Dynamic Interactions," *ASME Journal of Fluids Engineering*, **119**(3), pp. 671–679, Sept.
- [67] Botros, K. K., Dunn, G. H., and Hrycyk, J. A., 1997. "Riser – Relief Valve Dynamic Interactions (Extension to a Previous Model)," *Advances in Analytical, Experimental and Computational Technologies in Fluids, Structures, Transients and Natural Hazards*, ASME Pressure Vessel and Piping Conference, PVP–Vol. 355, pp. 11–19, Orlando, Florida, USA, July 27–31, 1997.
- [68] Jungowski, W. M., 1968. "Investigation of Flow Pattern Boundary Conditions and Oscillation Mechanism in a Compressible Flow Through Sudden Enlargement of a Duct," *Warsaw Technical University Publication*, No. 3, Mechanika.
- [69] Anderson, J. S., and Meier, G. E. A., 1982. "Steady and Non-Steady Transonic Flow in a Duct with a Sudden Enlargement," *Max-Planck Institute fur Stromungsforschung in Gottingen*, Report 1.
- [70] Gradle, R. J., 1984. "Design of Gas Pipeline Blowdowns," *Energy Processing Canada*, pp. 15–20, January–February.
- [71] Streeter, V. L., and Wylie, E. B., 1970. "Natural Gas Pipeline Transients," *Society of Petroleum Engineering*, SPE Paper No. 2555.
- [72] Rachford, H. H. Jr., and Dupont, T., 1974. "Some Applications of Transient Flow Simulation to Promote Understanding the Performance of Gas Pipeline Systems," *SPE Journal*, pp. 179–186.
- [73] Flatt, R., 1986. "Unsteady Compressible Flow in Long Pipelines Following a Rupture," *Int. Journal for Numerical Methods in Fluids* **6**, pp. 83–100.
- [74] Cronje, J. S., Bishnoi, P. R., and Svrcek, W. Y., 1980. "The Application of the Characteristic Method to Shock Tube Data that Simulate a Gas Pipeline Rupture," *Can. J. Chem. Eng.*, **58**, 289–294.

- [75] Groves, T. K., Bishnoi, P. R., and Wallbridge, J. M. E., 1978. "Decompression Wave Velocities in Natural Gases in Pipe Lines," *Can. J. Chem. Eng.*, **56**, 664–668.
- [76] Picard, D. J., and Bishnoi, P. R., 1988. "The Importance of Real-Fluid Behavior and Non-isentropic Effects in Modeling Decompression Characteristics of Pipeline Fluids for Application in Ductile Fracture Propagation Analysis," *Can. J. Chem. Eng.*, **66**, pp. 3–12.
- [77] Harwell Subroutine Library, 1988. DC03 Routine, Computer Science and Systems Division of AERE, Harwell Laboratory, Oxfordshire, England.
- [78] Von Rosenberg, D. U. "Methods for the Numerical Solution of Partial Differential Equations," American Elsevier Publishing.
- [79] Duff, I. S., 1980. "MA28 – A Set of FORTRAN Subroutines for Sparse Un-symmetric Linear Equations," *Computer Science and Systems Division AERE Harwell*, R.8730, Oxfordshire, England.
- [80] Carslaw, H. S., and Jaeger, J. C., 1959. "Conduction of Heat in Solids," Second Edition, Oxford Press, London.
- [81] Botros, K. K., Jungowski, W. M., and Weiss, M. H., 1989. "Models and Methods of Simulating Gas Pipeline Blowdown," *Canadian Journal of Chemical Engineering*, **67**, August.
- [82] Haque, A., Richardson, S., Saville, G., and Chamberlain G., 1990. "Rapid Depressurization Of Pressure Vessels," *Journal of Loss Prevention in the Process Industries*, **3**(1), pp. 4–7, January.
- [83] Mahgerefteh, H., and Wong, S. M. A., 1999. "A Numerical Blowdown Simulation Incorporating Cubic Equations of State," *Computers, and Chemical Engineering*, **23**(9), pp. 1309–1317, November.
- [84] Botros, K. K., Ruggiero, B. and Ho, C., 2014. "Dynamics of the Recycle Systems of Two Centrifugal Compressors Operating in Series in a Natural Gas Compressor Stations" *Proceedings of the ASME 2014 International Pipeline Conference*, IPC-2014-33022, September 29–October 3, 2014, Calgary, Alberta, Canada.
- [85] Botros, K. K., Hill, S. and Grose, J., 2015. "A New Approach to Designing Centrifugal Compressor Surge Control Systems", *Turbomachinery Symposium, 44th Turbomachinery and 31st Pump Symposium*, Houston, Texas Sept. 14–17, 2015.
- [86] Botros, K. K., Hill, S. and Grose, J., 2016. "Centrifugal Compressor Surge Control Systems - Fundamentals of a Good Design", *ASIA Turbomachinery & Pump Symposium*, Singapore, February 22–25, 2016.

PULSATION AND VIBRATION ANALYSIS OF COMPRESSION AND PUMPING SYSTEMS

11.1 INTRODUCTION

Flow and acoustic phenomena associated with various mechanical components in compressions and pumping systems have been the subject of considerable effort over the past few decades [1–15]. Research efforts concentrated on three main topics: (i) pulsation transmission characteristics of various pipeline elements, such as orifice plate, valves, compressors and branches; (ii) pulsation generation whether it's flow-induced or resulting from reciprocating machines; and (iii) methods to suppress these pulsations by means of passive elements (such as pulsation bottles, mufflers, Helmholtz resonators, or side branch resonators) or actively by active control (e.g., active control of incipient surge in centrifugal compressor). Flow-generated pulsations in pipeline facilities can be broad-band or single-tone with amplitude levels over 20 times [1] higher than the dynamic pressure in main pipe. Such a high level of pulsation disturbs flow measurements [9,10,13] and causes vibration of the piping elements. The latter can result in fatigue and serious accidents.

This chapter briefly presents the current knowledge of technology in this field and the basis of numerical analyses that are often conducted during the design phase of the compression and pumping systems. Examples are taken from meter stations, reciprocating compressor stations, and a pressure-regulating station.

11.2 PULSATION TRANSMISSION THROUGH PIPING ELEMENTS

An incident pressure wave from an external pulsation source is partially reflected and transmitted at every piping element such as orifice plates, valves, any throttling elements, reducers, expanders, etc. In addition to the pure acoustic reflection related to the element geometry, there is also influence of local flow phenomena in these elements, such as flow velocity gradient, flow separation, and shear layers that affect the pulsation transmission through them. In the literature, there are several basic studies dealing with pulsation transmission in internal flow systems or particular piping elements [16–18]. For example, time domain solution for the transmission of intense sound waves through the orifice plate was derived from a fairly simple flow model [16], accounting for the effect of irreversible pressure drop on the wave transmission. Propagation of pressure wave through a sudden pipe enlargement has been solved by the multiplication of a pure acoustic transfer matrix, a matrix related to pressure loss [17] and an adjusted coupling matrix [18].

More recently, and through the efforts of NOVA's research program on the topic, more precise and consistent models of pressure pulsation transmission through various piping elements have been developed [2–4,6,11]. The motivation was to enable the description of the

overall transmission characteristics of an element, despite that it is three-dimensional in nature, by a simple but accurate enough one-dimensional model. This concept was driven from the fact that whatever complex phenomenon takes place within the element, the net effect is a plane wave transmitting both upstream and downstream of it in a one-dimensional mode (if the frequency of propagation is below the cut-off frequency of the pipe). These models are based on the transfer matrix (TM) approach and a concept of accounting for mean flow effects. Some sort of coupling between the pure acoustic transfer matrix (TA) without flow, and another transfer matrix (TP) describing the effects of flow recounted only by the unrecovered pressure drop across the element, is the main feature of these new developments. The manner by which these two matrices are coupled is governed by the type of element under examination. The developed overall TM takes into account interactions between the acoustic field and the highly nonuniform flow within and downstream of an element. The overall TM takes the following form:

$$\begin{bmatrix} P_1 \\ V_1 \end{bmatrix} = \begin{bmatrix} AB \\ CD \end{bmatrix} \begin{bmatrix} P_2 \\ V_2 \end{bmatrix} \quad (11-1)$$

where P and V are the acoustic state vector (pulsation pressure and volume velocity, respectively). Subscripts 1 and 2 refer to upstream and downstream with respect to the direction of pulsation propagation, respectively. In the case of a straight pipe section, this matrix can be obtained analytically by solving the pertinent flow equation in straight pipe. Various models were proposed depending on methods accounting for the damping parameters, which will be briefly described below.

11.2.1 Acoustic Transfer Matrix for a Pipe Element

In the ideal case of a rigid-walled pipe filled with a stationary ideal (inviscid) fluid, and at relatively low frequencies typically encountered in practice, small-amplitude waves travel as plane waves. The acoustic pressure perturbation (p) above the mean fluid pressure (P_0) and flow perturbation velocity (u) above the mean value ($U_0 = 0$) at all points of a cross section are the same. The wave front, defined as a surface at all points of which p and u have the same amplitude and phase, is a plane normal to the direction of wave propagation, which, in the case of a pipe, is the longitudinal axis.

The basic equations for the case are:

Momentum equation:

$$\rho \frac{\partial U}{\partial t} + \frac{\partial P}{\partial x} = 0 \quad (11-2)$$

Continuity equation:

$$\frac{\partial \rho}{\partial t} + \rho \frac{\partial U}{\partial x} = 0 \quad (11-3)$$

Energy (isentropic relation):

$$\left(\frac{\partial P}{\partial \rho} \right)_s = c_0^2 \quad (11-4)$$

where, c_0 is the local speed of sound in the fluid. Using Eq. (11-4) in Eq. (11-3) yields:

Continuity:

$$\frac{\partial P}{\partial t} + \rho c_0^2 \frac{\partial U}{\partial x} = 0 \quad (11-5)$$

If we linearize Eqs. (11-2) and (11-5) by substituting for each variable a sum of its mean value and its fluctuating term in the form:

$$U = U_0 + u(t); \quad P = P_0 + p(t); \quad \rho = \rho_0 + \rho(t)$$

and subtracting similar equations containing only the mean components, it yields the two main equations in the fluctuating components as follows:

Momentum:

$$\rho_0 \frac{\partial u}{\partial t} + \frac{\partial p}{\partial x} = 0 \quad (11-6)$$

Continuity:

$$\frac{\partial p}{\partial t} + \rho_0 c_0^2 \frac{\partial u}{\partial x} = 0 \quad (11-7)$$

Eliminating u from the above two equations yields the one-dimensional wave equation in the form:

$$\frac{\partial^2 p}{\partial t^2} - c_0^2 \frac{\partial^2 p}{\partial x^2} = 0 \quad (11-8)$$

By combining Eqs. (11-6) and (11-7) differently, the wave equation can also be expressed in terms of velocity (u) or density (ρ). The result is that p in Eq. (11-8) may be replaced by either velocity u or density ρ .

The form of solution of the wave equation (Eq. (11-8)) for the perturbation pressure p is a product of a function $X(x)$ that depends only on the axial distance x , and a harmonic function $T(t) = e^{i\omega t}$, (where $i = \sqrt{-1}$ and ω is the frequency in rad/s). Therefore:

$$p(x, t) = X(x) \cdot T(t) = X(x) \cdot e^{i\omega t} \quad (11-9)$$

The solution of the spatial function $X(x)$ can be expressed in the form:

$$X(x) = A \cdot e^{-ik_0 x} + B \cdot e^{+ik_0 x} \quad (11-10)$$

where $k_0 = \frac{\omega}{c_0} = \frac{2\pi f}{c_0}$ is called the wave number and f is the frequency in Hz. Both A and B are constants (complex numbers). Therefore,

$$p(x, t) = [A \cdot e^{-ik_0 x} + B \cdot e^{+ik_0 x}] e^{i\omega t} \quad (11-11)$$

and substituting in Eq. (11-6), we get:

$$u(x, t) = \frac{1}{\rho_0 c_0} [A \cdot e^{-ik_0 x} - B \cdot e^{+ik_0 x}] e^{i\omega t} \quad (11-12)$$

or, in terms of perturbation volume velocity ($v = u \cdot S$), where S is the cross-sectional area of the pipe:

$$v(x, t) = \frac{S}{\rho_0 c_0} [A \cdot e^{-ik_0 x} - B \cdot e^{+ik_0 x}] e^{i\omega t} \quad (11-13)$$

The term $\frac{\rho_0 c_0}{S} = Z_0$ is defined as the acoustic characteristic impedance in the pipe. The acoustic transfer matrix relates acoustic pressure and volume velocity amplitudes at two stations (1) and (2) as shown in Fig. 11-1, in the form of Eq. (11-1). This can be obtained by writing Eq. (11-11) and Eq. (11-13) at the two stations (1) and (2), substituting $x = 0$ at station (1) and $x = L$ at station (2), and solving for A and B in terms of (P_1, V_1) , and (P_2, V_2) . Here, (P_1, V_1) and (P_2, V_2) are the amplitude of pressure and volume velocity oscillations and stations (1) and (2), respectively, i.e.,

$$p_1(x = 0, t) = P_1 e^{i\omega t}; \quad p_2(x = L, t) = P_2 e^{i\omega t} \quad (11-14)$$

and

$$v_1(x = 0, t) = V_1 e^{i\omega t}; \quad v_2(x = L, t) = V_2 e^{i\omega t} \quad (11-15)$$

After some arithmetic manipulation, and replacing the exponential terms by trigonometric functions, we obtain:

$$\begin{bmatrix} P_1 \\ V_1 \end{bmatrix} = \begin{bmatrix} \cos(k_0 L) & iZ_0 \sin(k_0 L) \\ \frac{i}{Z_0} \sin(k_0 L) & \cos(k_0 L) \end{bmatrix} \begin{bmatrix} P_2 \\ V_2 \end{bmatrix} \quad (11-16)$$

The above TM is applicable when the following conditions are met:

- (i) Acoustic variables (p, u) must be small compared to the steady values (as stated in the development of the wave equation).
- (ii) The frequency is below a cutoff value to warrant that the perturbation waves travel as plane waves (for circular pipe, the cut-off frequency is $= 0.586 c_0/D$, where D is the ID of the pipe).

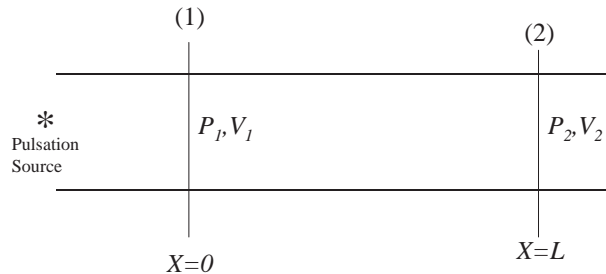


Figure 11-1. Schematic of a pipe element.

11.2.1.1 Effects of Mean Flow on the Acoustic TM for Pipe Element

The above formulations were based on acoustic perturbations traveling up and down the length of a pipe element with no flow and no damping. To account for both, the full momentum and continuity equations should be written with associated terms. These can be written in the form:

Momentum equation:

$$\rho \frac{\partial U}{\partial t} + \rho U \frac{\partial U}{\partial x} + \frac{\partial P}{\partial x} + \zeta \rho U^2 + 2\alpha \rho_0 c_0 U = 0 \quad (11-17)$$

Continuity equation:

$$\frac{\partial \rho}{\partial t} + U \frac{\partial \rho}{\partial x} + \rho \frac{\partial U}{\partial x} = 0 \quad (11-18)$$

Energy (isentropic relation):

$$\left(\frac{\partial P}{\partial \rho} \right)_s = c_0^2 \quad (11-19)$$

Using Eq. (11-19) in Eq. (11-18) yields:

Continuity:

$$\frac{\partial P}{\partial t} + U \frac{\partial P}{\partial x} + \rho c_0^2 \frac{\partial U}{\partial x} = 0 \quad (11-20)$$

If we linearize Eqs. (11-17) and (11-20) by substituting for each variable a sum of its mean value and its fluctuating term in the form:

$$\begin{aligned} U &= U_0 + u(t); & P &= P_0 + p(t); & \rho &= \rho_0 + \rho(t); \\ \zeta &= \zeta_0 + \delta\zeta = \zeta_0 + \frac{\partial \zeta}{\partial U_0} u(t) = \zeta_0 + \zeta_0 \frac{\partial \ln \zeta}{\partial U_0} u(t) \end{aligned} \quad (11-21)$$

and subtracting similar equations containing only the mean components, it yields the two main equations in the fluctuating components as follows:

Momentum:

$$\rho_0 \frac{\partial u}{\partial t} + \rho_0 U_0 \frac{\partial u}{\partial x} + \frac{\partial p}{\partial x} + 2\alpha \rho_0 c_0 u + 2\zeta_0 \rho_0 U_0 u + \zeta_0 U_0^2 \frac{p}{c_0^2} + \rho_0 U_0^2 \zeta_0 \frac{\partial \ln \zeta}{\partial U_0} = 0 \quad (11-22)$$

Continuity:

$$\frac{\partial p}{\partial t} + U_0 \frac{\partial p}{\partial x} + \rho_0 c_0^2 \frac{\partial u}{\partial x} = 0 \quad (11-23)$$

In the above formulation, we have separated the viscothermal drag expressed in the coefficient () in Eq. (11-22) from the wall drag manifested by the friction coefficient (ζ), which is related to Darcy friction Factor F , or the Fanning friction factor FF ,

where:

$$\zeta = \frac{F}{2D} = \frac{2FF}{D} \quad (11-24)$$

Let us consider now the effect of mean flow only (i.e., no damping). The following are reduced forms of both the momentum and continuity equations:

Momentum:

$$\rho_0 \frac{\partial u}{\partial t} + \rho_0 U_0 \frac{\partial u}{\partial x} + \frac{\partial p}{\partial x} = 0 \quad (11-25)$$

Continuity:

$$\frac{\partial p}{\partial t} + U_0 \frac{\partial p}{\partial x} + \rho_0 c_0^2 \frac{\partial u}{\partial x} = 0 \quad (11-26)$$

eliminating (u) from the above equation yields the connective one-dimensional wave equation in the form:

$$\frac{\partial^2 p}{\partial t^2} + 2U_0 \frac{\partial^2 p}{\partial x \partial t} + (U_0^2 - c_0^2) \frac{\partial^2 p}{\partial x^2} = 0 \quad (11-27)$$

Making use of the separation of variables and assessing again a time-dependence function $e^{i\omega t}$, the above wave equation will admit the following general solution:

$$\begin{aligned} p(x, t) &= \left[A e^{\frac{-i\omega x}{c_0 + U_0}} + B e^{\frac{i\omega x}{c_0 - U_0}} \right] e^{i\omega t} \\ &= \left[A e^{\frac{-ik_0 x}{1+M}} + B e^{\frac{ik_0 x}{1-M}} \right] e^{i\omega t} \end{aligned} \quad (11-28)$$

and, hence, from the momentum equation:

$$v(x, t) = \frac{S}{\rho_0 c_0} \left[A e^{\frac{-ik_0 x}{1+M}} - B e^{\frac{ik_0 x}{1-M}} \right] e^{i\omega t} \quad (11-29)$$

Following the same procedure to obtain the acoustic TM relating the acoustic pressure and volume velocity amplitudes at two stations [(1) and (2)], as shown in Fig. 11-1, we obtain:

$$\begin{bmatrix} P_1 \\ V_1 \end{bmatrix} = e^{\frac{-ik_0 LM}{1-M^2}} \begin{bmatrix} \cosh\left(\frac{ik_0 L}{1-M^2}\right) & Z_0 \sinh\left(\frac{ik_0 L}{1-M^2}\right) \\ \frac{1}{Z_0} \sinh\left(\frac{ik_0 L}{1-M^2}\right) & \cosh\left(\frac{ik_0 L}{1-M^2}\right) \end{bmatrix} \begin{bmatrix} P_2 \\ V_2 \end{bmatrix} \quad (11-30)$$

which gives the TM for the pipe element showing the effects of mean flow manifested in the Mach number (M) in the above equation.

11.2.1.2 Effects of Damping (Attenuation)

Damping of pressure pulsation in straight pipe elements with and without flow was considered. Four different acoustic models were found in the literature and are in use in most pulsation analysis and commercial codes such as PULS [19]. These different models are denoted as: Model I [20], Model II [21], Model III [22], and Model IV [23]. These models will be described briefly below.

In Model I [20], damping was introduced by fluid resistance in terms of fluid viscosity. This damping exists whether there is flow or no flow. In essence, it resembles damping of

the acoustic wave propagation offered by the medium itself. The damping factor also contains pipe diameter in the denominator, which suggests indirectly the influence of the pipe wall on damping (the larger the pipe, the lower the damping). In this model, the following equations are written:

Momentum:

$$\rho_0 \frac{\partial u}{\partial t} + \rho_0 U_0 \frac{\partial u}{\partial x} + \frac{\partial P}{\partial x} + 2\alpha \rho_0 c_0 u = 0 \quad (11-31)$$

Continuity:

$$\frac{\partial P}{\partial t} + U_0 \frac{\partial P}{\partial x} + \rho c_0^2 \frac{\partial U}{\partial x} = 0 \quad (11-32)$$

where:

$$\alpha = \frac{2}{c_0 D} \sqrt{\frac{\pi \mu_0 f}{\rho_0}} \quad (11-33)$$

and μ_0 is the dynamic viscosity of the fluid.

Again, following the same procedure to obtain the acoustic TM relating the acoustic pressure and volume velocity amplitudes at two stations [(1) and (2)], as shown in Fig. 11-1, we obtain:

$$\begin{bmatrix} P_1 \\ V_1 \end{bmatrix} = e^{-kLM} \begin{bmatrix} \cosh(kL) & \frac{\rho_0 c_0}{s} \sinh(kL) \\ \frac{s}{\rho_0 c_0} \sinh(kL) & \cosh(kL) \end{bmatrix} \begin{bmatrix} P_2 \\ V_2 \end{bmatrix} \quad (11-34)$$

where the wave number now includes the damping parameter (), as follows:

$$k = (\alpha + ik_0)/(1 - M^2) \quad (11-35)$$

In Model II [21], an additional equation (energy) was used in the derivation of damping effect accounting also for heat transfer. Pipe wall boundary layer and heat transfer coefficient were introduced to formulate the damping coefficient. In short, this model accounts for damping due to fluid viscosity (like in the previous model), pipe wall boundary layer, and heat transfer. In this model, the following equations are written:

Momentum:

$$\rho_0 \frac{\partial u}{\partial t} + \rho_0 U_0 \frac{\partial u}{\partial x} + \frac{\partial P}{\partial x} + 2\alpha \rho_0 c_0 u = 0 \quad (11-36)$$

Continuity:

$$\frac{\partial P}{\partial t} + U_0 \frac{\partial P}{\partial x} + \rho c_0^2 \frac{\partial U}{\partial x} = 0 \quad (11-37)$$

The solution TM, following the above methodology, takes the form:

$$\begin{bmatrix} P_1 \\ V_1 \end{bmatrix} = e^{-kLM} \begin{bmatrix} \cosh(kL) & Z_0 \sinh(kL) \\ Z_0 \sinh(kL) & \cosh(kL) \end{bmatrix} \begin{bmatrix} P_2 \\ V_2 \end{bmatrix} \quad (11-38)$$

where:

$$\begin{aligned}
 k &= \frac{ik_1}{1-M^2} \\
 k_1 &= \frac{\omega^2}{c_0^2} + \frac{2i\omega}{c_0} \left[\alpha_{cl} + (1-i)\alpha_{walls} \right] \\
 \alpha_{walls} &= 2^{-3/2} \sqrt{\frac{\omega\mu_0}{\rho_0 c_0^2}} \left[1 + \frac{(\gamma-1)}{(P_r)^{1/2}} \right] \frac{4}{D} \\
 \alpha_{cl} &= \frac{\omega^2}{c_0^3} \frac{\mu_0}{2\rho_0} \left[\frac{4}{3} + \frac{\gamma-1}{(P_r)} \right]
 \end{aligned} \tag{11-39}$$

and μ_0 is the dynamic viscosity of the fluid, γ is its specific heat ratio, and P_r is its Prandtl number.

In Model III [22], damping was introduced via the friction factor. This can only exist if there is mean flow and is shown to be independent of the wave number. Based on the following equations:

Momentum:

$$\rho_0 \frac{\partial u}{\partial t} + \rho_0 U_0 \frac{\partial u}{\partial x} + \frac{\partial P}{\partial x} + 2\zeta_0 \rho_0 U_0 u + \zeta_0 U_0^2 \frac{P}{c_0^2} + \frac{\partial \ln \zeta}{\partial U_0} = 0 \tag{11-40}$$

Continuity:

$$\frac{\partial P}{\partial t} + U_0 \frac{\partial P}{\partial x} + \rho c_0^2 \frac{\partial U}{\partial x} = 0 \tag{11-41}$$

The TM based on these equations can be derived in the same form:

$$\begin{bmatrix} P_1 \\ V_1 \end{bmatrix} = e^{-kLM} \begin{bmatrix} \cosh(kL) & Z_0 \sinh(kL) \\ Z_0 \sinh(kL) & \cosh(kL) \end{bmatrix} \begin{bmatrix} P_2 \\ V_2 \end{bmatrix} \tag{11-42}$$

where:

$$\begin{aligned}
 k &= (s - ir/\omega) \left(\frac{i\omega}{c_0} \right) \\
 s &= \frac{\zeta U_0}{\omega \tan\left(\frac{\psi}{2}\right)} \\
 r &= \sqrt{\zeta U_0 \omega \tan\left(\frac{\psi}{2}\right)} \\
 \tan(\psi) &= \frac{2\zeta U_0}{\omega \left(1 - \frac{\zeta^2 U_0^4}{4c_0^2 \omega^2} \right)}
 \end{aligned} \tag{11-43}$$

Probably, the most conclusive model of acoustic attenuation in turbulent pipe flow is (IV) [23]. It distinguished damping due to viscothermal effects and damping caused by

turbulence in the presence of mean flow. The former is similar to (model II), while the latter represented by perturbation of the turbulent friction term in the momentum equation, which gives rise to an oscillating friction drag affecting attenuation of the acoustic field. As a result, turbulence damping is not only represented by the friction factor (as in model III) but also by its gradient with respect to mean flow velocity. In this model, we start from the full momentum and continuity equation, as follows:

Momentum:

$$\rho_0 \frac{\partial u}{\partial t} + \rho_0 U_0 \frac{\partial u}{\partial x} + \frac{\partial P}{\partial x} + 2\alpha \rho_0 c_0 u + 2\zeta_0 \rho_0 U_0 u + \rho_0 U_0^2 \zeta_0 \frac{\partial \ln \zeta}{\partial U_0} = 0 \quad (11-44)$$

Continuity:

$$\frac{\partial P}{\partial t} + U_0 \frac{\partial P}{\partial x} + \rho c_0^2 \frac{\partial U}{\partial x} = 0 \quad (11-45)$$

And the solution TM will take the same form as before, i.e.,

$$\begin{bmatrix} P_1 \\ V_1 \end{bmatrix} = e^{-kLM} \begin{bmatrix} \cosh(kL) & Z_0 \sinh(kL) \\ Z_0 \sinh(kL) & \cosh(kL) \end{bmatrix} \begin{bmatrix} P_2 \\ V_2 \end{bmatrix} \quad (11-46)$$

except that the wave number is now defined as:

$$k = \frac{\alpha + \zeta_0 |M| \left(1 + \frac{\text{Re}}{2\text{FF}} \frac{\partial \text{FF}}{\partial \text{Re}} \right) + ik_0}{1 - M^2} \quad (11-47)$$

and the visco-thermal coefficient (α) is defined as:

$$\alpha = \frac{\omega}{c_0} \left[\sqrt{\frac{2\mu_0}{\rho_0 \omega}} + (\gamma - 1) \sqrt{\frac{2K}{\rho_0 \omega C_p}} \right] \quad (11-48)$$

where K is the fluid thermal conductivity and C_p is its specific heat at constant pressure.

Figure 11-2 shows comparison of the above four models when used in evaluating damping in a 381-mm ID anechoic pipe (mean velocity = 10 m/s of natural gas). Attenuation along 500 m is presented in terms of downstream/upstream pulsation pressure ratio versus frequency. It can be seen that attenuation resulting from Model IV greatly exceeds that from Model I.

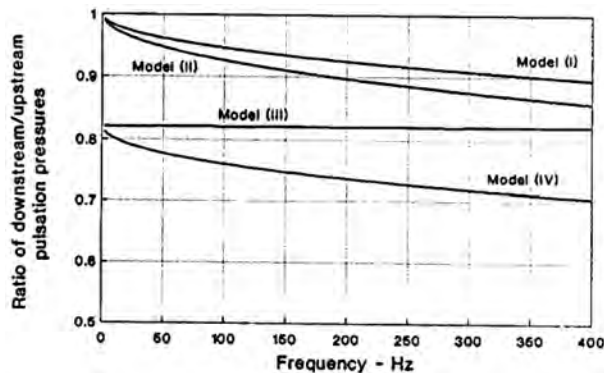


Figure 11-2. Attenuation in 500 m pipe (ID = 381 mm) based on the four TM models for pipe.

11.2.2 Acoustic Transfer Matrix for a Throttle Element

The propagation of pressure waves through a throttling or a pressure drop element such as orifice plates, valves, reducers or expanders, etc., poses some challenges. The main reason is the fact that the plane wave theory, though useful when applied to pulsation propagation in pipe elements, fails to describe the refraction/deflection of acoustic waves at the shear layers caused by flow separation. In the literature, there are several basic studies dealing with pulsation transmission in internal flow systems or particular piping elements [16,24,25]. A time domain solution for the transmission of intense sound waves through the orifice plate was derived from fairly simple flow model [16], accounting for the effect of irreversible pressure drop on the wave transmission. Propagation of pressure wave through a sudden pipe enlargement has been solved by the multiplication of a pure acoustic transfer matrix, a matrix related to pressure loss [24] and an adjusted coupling matrix [25].

Some efforts have been made to develop more precise and consistent models of pressure pulsation transmission through various piping elements [3,6,7]. The motivation was to be able to describe the overall transmission characteristics of an element, despite that it is three-dimensional in nature, by a simple but accurate-enough one-dimensional model. This can conveniently be incorporated into a general tool utilizing the plane wave theory for the entire network of piping. This concept was driven from the fact that whatever complex phenomenon takes place within the element, the net effect is a plane wave transmitting both upstream and downstream of it in a one-dimensional mode (if the frequency of propagation is below the cut-off frequency of the pipe). These models are based on the TM approach and a concept of accounting for mean flow effects. Some sort of coupling between the pure acoustic transfer matrix (TA) without flow, and another transfer matrix (TP), describing the effects of flow recounted only by the unrecovered pressure drop across the element, is the main feature of these new developments.

The manner by which these two matrices are coupled is governed by the type of element under examination. The developed overall TM takes into account interactions between the acoustic field and the highly nonuniform flow downstream of an element where a shear layer, recirculation, flow reattachment and pressure recovery exist. Based on this concept, semi-empirical models of an orifice plate, ball valves and globe valves were developed containing characteristic parameters, which were obtained by flow-acoustic measurements. Experiments were carried out on two facilities with air (90 kPa) and natural gas (6000 kPa) [3]. Basically, the method used in determining experimentally the four components of the TM of a piping element was either the two-load method [24,25] or the two-source method [26]. It is shown that, for relatively geometrically simple elements (such as the orifice plates and the ball valves), separation of the two matrices TA and TP was possible, and the overall TM results from simple multiplication of TA and TP in a proper order [3]. For more geometrically complicated elements, such as the globe valves, the inherent complication of the interaction between local flow phenomena, internal flow passages, wall reflection, and acoustic waves make this separation of the two matrices impossible, as will be discussed later.

The complicated flow through an element of complex geometry can be modeled by a stream tube of varying cross-sectional area following the development of Miles [27]. The pertinent conservation equations describing the flow-acoustic phenomena are as follows:

Momentum equation:

$$\frac{\partial(\rho UA)}{\partial t} + \frac{\partial(\rho U^2 A)}{\partial x} + A \frac{\partial P}{\partial x} + \zeta \rho U^2 = \frac{\lambda_0}{D} \frac{\rho_0 U_0^2}{2} \quad (11-49)$$

Continuity equation:

$$\frac{\partial(\rho A)}{\partial t} + \frac{\partial(\rho UA)}{\partial x} = 0 \quad (11-50)$$

Energy equation:

$$\rho T \frac{ds}{dt} = \frac{\lambda_0}{D} \frac{\rho_0 U_0^3}{2} \quad (11-51)$$

where losses are accounted for by the pressure loss parameter $\lambda_0(x)$. When the above equations are linearized, the set of equations for the perturbations P and U transformed to the frequency domain [16] can be written in the following matrix form:

$$\frac{dY}{dx} = (B_a + B_p)Y \quad (11-52)$$

where

$$Y(x, \omega) = \begin{bmatrix} P(\omega) \\ U(\omega) \end{bmatrix} \quad (11-53)$$

$$B_a = ik \begin{bmatrix} -M & \rho_0 c_0 \\ \frac{1}{\rho_0 c_0} & -M \end{bmatrix}; \quad B_p = G \begin{bmatrix} -M^2 & 2M\rho_0 c_0 \\ 0 & 1 + M^2 \end{bmatrix} \quad (11-54)$$

$$G = \frac{\partial \ln(M)}{\partial x} \left[(1 - M^2) \left(1 + \frac{\gamma - 1}{2} M^2 \right) \right]; \quad k = \frac{k_0}{1 - M^2} \quad (11-55)$$

The matrix B_a above contains the inertial effects, while matrix B_p contains the effects of mean flow parameters and their gradients through the element. In general, it is not possible to retain such a clear separation of these two effects in the integration of Eq. (11-52) since the two matrices B_a and B_p do not commute, i.e., $B_a \cdot B_p \neq B_p \cdot B_a$. Additionally, integration of Eq. (11-52) requires solution of the mean flow parameters $M(x)$, $P(x)$, $\rho(x)$, and $c_0(x)$, which are affected by the complicated geometry of the transmission element (e.g., a globe valve). Flow separation, circulation, and non-uniformities clearly add to the complication. Therefore, a closed form (analytical) solution of Eq. (11-52) is only possible for simple geometry elements such as pipes [16,17] where the two matrices B_a and B_p are constant along x , and also for area discontinuities [3,6].

For geometrically complicated element, a rather heuristic approach is adopted to overcome this problem. The approach stipulates that a general solution of Eq. (11-52) should take the form:

$$Y_1 = T(B_a, B_p) Y_2 \quad (11-56)$$

where $T(B_a, B_p)$ is the transfer matrix, subscripts 1 and 2 are stations at the element boundaries: inlet and outlet (as shown in Fig. 11-3), and B_a and B_p are average representations of the inertial and mean flow effects, respectively. Generally

$$T(B_a, B_p) \neq T(B_p, B_a) \quad (11-57)$$

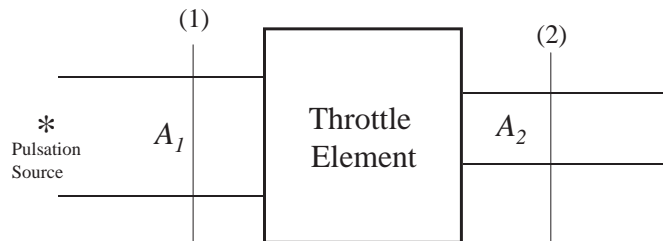


Figure 11-3. Throttle element with different cross-sectional areas upstream and downstream.

However, two limiting cases are obvious:

- (1) No mean flow, $U_0 = 0$ (i.e., pure acoustic);
- (2) With mean flow effects much higher than inertial effects.

In the first case, $T \rightarrow TA = T(B_a)$, while in the second case $T \rightarrow TP = T(B_p)$. The two matrices, TA and TB, are called the acoustic and pressure loss transfer matrices [6], respectively. The first (acoustic) transfer matrix can be obtained by direct measurements utilizing the concept of the two-load [24,25] or two-source methods [26], when there is no flow through the element. Semi-empirical parameters are commonly introduced to fit the data obtained by either method above. The second (pressure loss) matrix is derived from simple considerations based on the compressible flow through the element with known pressure loss coefficient and takes the following form:

$$TP = \begin{bmatrix} T_p^{11} & T_p^{12} \\ T_p^{21} & T_p^{22} \end{bmatrix} \quad (11-58)$$

A closed form expression for each of the four elements the transfer matrix TP is possible, which were derived for incompressible flow by Botros et al. [6] and for compressible flow by Botros [28]. Table 11-1 shows these closed form expressions for the general compressible flow case. The factors (f_1 through f_8) in Table 11-1 are calculated based on mean flow parameters at inlet and outlet of the element (stations 1 and 2). It can be shown that for an element with zero losses (i.e., $\zeta = 0$) and same areas at inlet and outlet (i.e., $A1 = A2$), the pressure loss matrix will be reduced to a unit matrix.

Table 11-1. Pressure drop transfer matrix components for compressible flow through a throttle element [28]

$$\begin{aligned} T_p^{11} &= \frac{f_3 f_6 - f_2 f_7}{f_1 f_6 - f_2 f_7} & T_p^{12} &= \frac{f_1 f_6 - f_2 f_7}{f_1 f_6 - f_2 f_7} \\ T_p^{21} &= \frac{f_2 - f_1 T_p^{11}}{f_1} & T_p^{22} &= \frac{f_4 - f_1 T_p^{12}}{f_1} \\ f_1 &= \frac{1}{\gamma P_1} + \frac{\gamma - 1}{\gamma P_2} \left(\frac{T_1}{T_2} \right) & f_2 &= \alpha^2 - \frac{\alpha U_1^2}{2C_p T_1} + \frac{\beta T_1 P_1 U_2^2}{2P_1 C_p T_2^2} - \xi \frac{U_1^2 P_1}{\gamma P_1} \\ f_3 &= \frac{U_1}{C_p T_2} + \frac{1}{U_1} & f_4 &= \frac{\alpha \gamma P_1 U_1}{(\gamma - 1) C_p T_1} + \frac{\beta \gamma P_2 U_1 U_2^2}{2(\gamma - 1) C_p^2 T_2^2} - \xi \rho_1 U_1 \\ f_5 &= \frac{1}{P_2} & f_6 &= \beta^2 \\ f_7 &= \frac{U_2}{C_p T_2} + \frac{1}{U_2} & f_8 &= \frac{\beta \gamma P_2 U_2}{(\gamma - 1) C_p T_2} + \frac{\beta \gamma P_2 U_2^2}{2(\gamma - 1) C_p^2 T_2^2} \\ \alpha &= \left[1 + \frac{U_1^2}{2C_p T_1} \right]^{\frac{1}{\gamma - 1}} & \beta &= \left[1 + \frac{U_2^2}{2C_p T_2} \right]^{\frac{1}{\gamma - 1}} \end{aligned}$$

The same procedure can be applied to develop the TM for a T-junction. In this case, the TM will have 3×4 elements in the form:

$$\begin{bmatrix} P_1 \\ V_1 \\ P_1 \end{bmatrix} = \begin{bmatrix} T_p^{11} & T_p^{12} & T_p^{13} & T_p^{14} \\ T_p^{21} & T_p^{22} & T_p^{23} & T_p^{24} \\ T_p^{31} & T_p^{32} & T_p^{33} & T_p^{34} \end{bmatrix} \begin{bmatrix} P_2 \\ V_2 \\ P_3 \\ V_3 \end{bmatrix} \quad (11-59)$$

where, subscripts 1, 2, and 3 are referred to the three stations defining the boundaries of a T-junction as shown in the schematic of Fig. 11-4. Expressions for the 3×4 elements of the above TM can be found in [29] in terms of mean flow parameters and pressure loss coefficients in the same manner.

11.2.2.1 Orifice Plate

The propagation of pressure waves through an orifice plate of diameter d_o placed in a circular pipe of internal diameter D has been investigated [6], and the influence of the inertial effects has been described by the so-called equivalent acoustic length l_o . This equivalent length was obtained by the two-load method for cases without flow and is shown in Fig. 11-4 tplot marked ($M = 0$), as a function of the diameter ratio ($\beta = d_o/D$). In the case of wave transmission with flow, separation of the two effects—pure acoustic and influence of flow—was possible, and the overall transmission characteristics can be described by direct multiplication of two TMs: the acoustic TA and the pressure loss TP. The former was found to be dependent on the mean flow Mach number in the main pipe in a manner shown in Fig. 11-5. This dependence most likely delineates the interaction that is taking place between the acoustic field and the highly nonuniform flow downstream of the orifice. The TP matrix was derived from the perturbation formulation described above, as the pressure loss coefficient ζ is known for orifice plates.

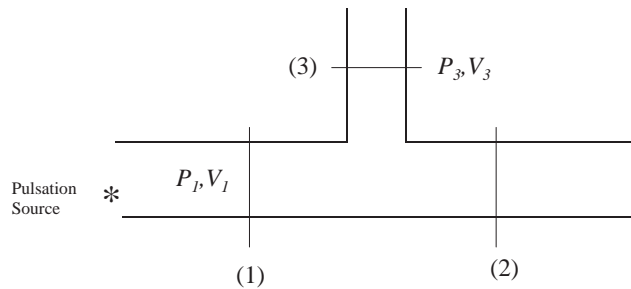


Figure 11-4. Nomenclature for a T-junction element.

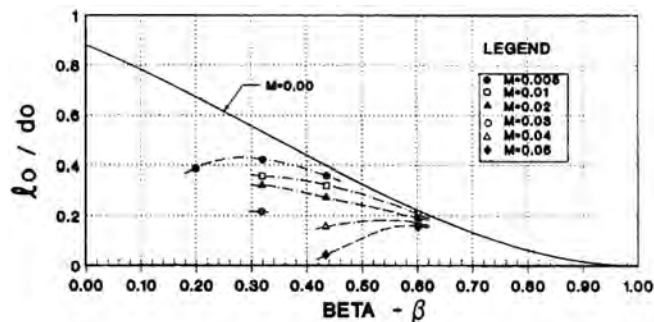


Figure 11-5. Equivalent acoustic length for an orifice plate [6,7,28].

11.2.2.2 Ball Valve

The second example of a separable TM is that for a ball valve. Likewise, the pure acoustic TM was obtained by the two-load method for various valve openings (α). A semi-empirical model was then devised consisting of two orifices of equivalent “ β -ratio” equal to the square root of valve opening area ratio, and a separation of constant area pipe of diameter D and length L determined from fitting the experimental data. The model is depicted in Fig. 11-6, while results of the equivalent length L is shown in Fig. 11-7 [two equivalent lengths are shown, L_A is used for calculating (T_a^{11}, T_a^{12}) and L_B is used for calculating (T_a^{21}, T_a^{22})]. The overall TM for the ball valve with flow was also obtained experimentally using the two-load method and was then compared to the postulated multiplication scheme of the two TMs: TA and TP. Good agreement was obtained and is discussed in more detail in ref. [3].

11.2.2.3 Globe Valve

The multiplication scheme of TA and TP that worked successfully with the above two elements does not apply to globe valve. Even in the case of pure acoustic without flow, it was not possible to construct a basic model with say orifices and straight pipes like in the

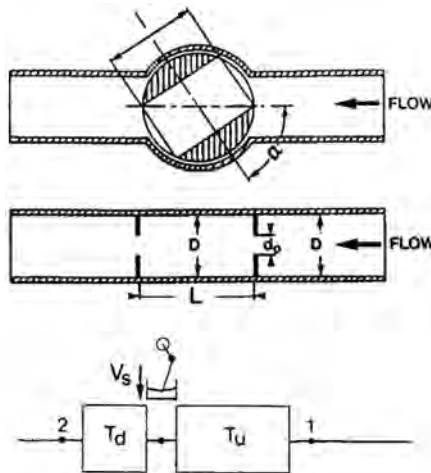


Figure 11-6. Acoustic model for a ball valve [3].

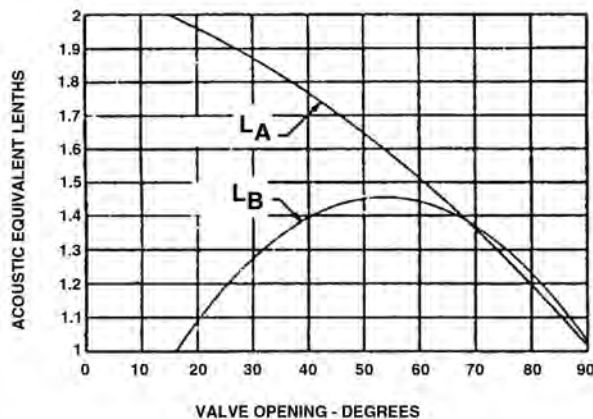


Figure 11-7. Dimensionless acoustic equivalent length (L_A/D) and (L_B/D) for a ball valve [3].

case of a ball valve. Separation of the two effects thus constitutes a rather difficult task and mathematically impossible since the two corresponding matrices B_a and B_p do not commute for such complicated element. It was found that each component of the overall TM is a combination of mixed terms associated with pure acoustic and pressure loss parameters. These two parameters are mixed in a manner that did not permit distinct separation of the two matrices TA and TB as before. From the data measured for a globe valve (100-mm diameter) with varied opening and Mach number, and using the two-load method, it was possible to construct a semi-empirical matrix describing the two effects. The overall TM was thus obtained in the form [28]:

$$TM = \begin{bmatrix} T_p^{11} \cos(kl_0) + ikL_A & T_p^{12} + ikL_B Z_0 \\ \frac{iT_p^{21}}{Z_0} \sin(kl_0) & T_p^{22} \cos(kl_0) + ikL_A \end{bmatrix} \quad (11-60)$$

Figures 11-8, 11-9, and 11-10 present results of the characteristic parameters l_o , L_A , and L_B given in Eq. (11-59) above.

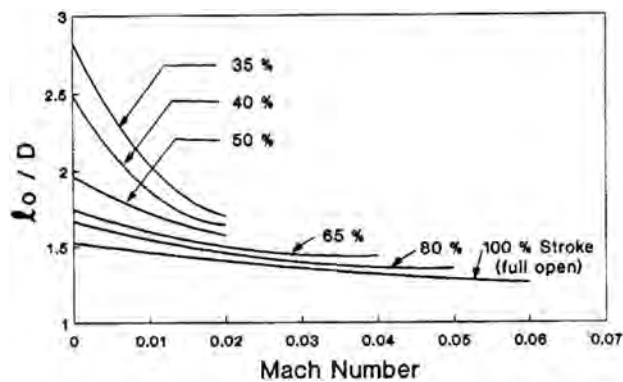


Figure 11-8. Acoustic equivalent length (l_o/D) for a ball valve [28].

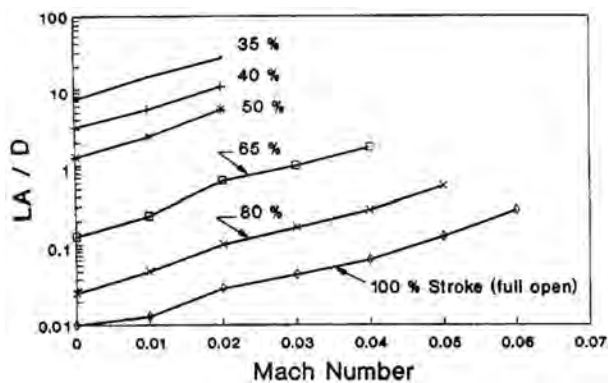


Figure 11-9. Dimensionless acoustic equivalent length (L_A/D) for a ball valve [28].

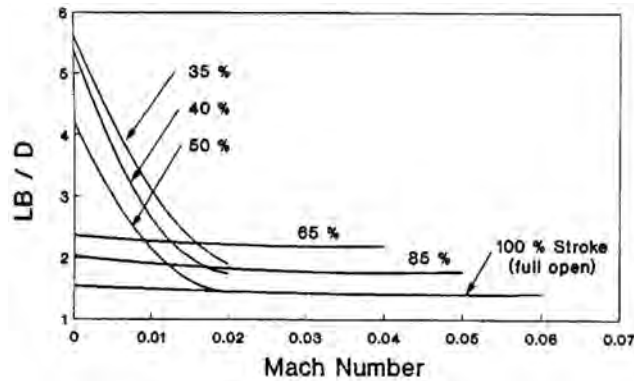


Figure 11-10. Acoustic equivalent length (L_B/D) for a ball valve [28].

11.2.3 Acoustic Transfer Matrix for a Volume Element

Consider the volume element shown in the schematic of Fig. 11-11. Neglecting losses associated with inlet and outlet and considering that pressure perturbations are uniform throughout the volume, and that the perturbations are isentropic in nature, i.e.,

$$\left(\frac{\partial P}{\partial \rho} \right)_s = c_0^2 = \frac{\delta P}{\delta \rho} \quad (11-61)$$

Continuity equation in perturbation parameters ($\delta \dot{m}_1$), ($\delta \dot{m}_2$), ($\delta \rho$):

$$(\delta \dot{m}_1 - \delta \dot{m}_2) = V_0 \frac{\partial \rho}{\partial t} \quad (11-62)$$

or

$$\rho_0(V_1 - V_2) = \frac{V_0}{c_0^2} \frac{\partial P}{\partial t} \quad (11-63)$$

Since the pulsation pressure amplitude $P = e^{i\omega t}$, hence:

$$V_1 - V_2 = \frac{V_0}{\rho_0 c_0^2} (i\omega) \cdot P \quad (11-64)$$

or

$$V_1 = V_2 + \frac{i\omega V_0}{\rho_0 c_0^2} P \quad (11-65)$$

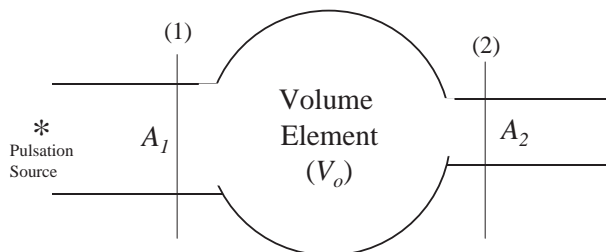


Figure 11-11. Acoustic model for a volume element.

and, from the assumption that pressure perturbations are uniform throughout the volume, i.e.,

$$P_1 = P_2 \quad (11-66)$$

The desired TM for the volume element can be written in the form:

$$\begin{bmatrix} P_1 \\ V_1 \end{bmatrix} = \begin{bmatrix} 1 & 0 \\ \frac{i\omega V_0}{\rho_0 c_0^2} & 1 \end{bmatrix} \begin{bmatrix} P_2 \\ V_2 \end{bmatrix} \quad (11-67)$$

11.2.4 Acoustic Transfer Matrix for a Centrifugal Compressor

Consider the centrifugal compressor element shown in the schematic of Fig. 11-12. The following are the governing equations for the mean variables, assuming the compressor is operating at constant speed:

Continuity:

$$\rho_1 Q_1 = \rho_2 Q_2 \quad (11-68)$$

Head equation:

$$H_a = \frac{ZRT_1}{(k-1)/k} \left[\left(\frac{P_2}{P_1} \right)^{\frac{k-1}{k}} - 1 \right] \quad (11-69)$$

where Q_1 and Q_2 are the actual flow at inlet (station 1) and outlet (station 2) of the compressor. The adiabatic head (H_a) is function of the actual inlet flow Q_1 and the compressor speed (N) and can be expressed, using the Fan laws by the following polynomial:

$$\frac{H_a}{N^2} = a_0 + a_1 \left(\frac{Q_1}{N} \right) + a_2 \left(\frac{Q_1}{N} \right)^2 \quad (11-70)$$

Hence, Eq. (11-69) can be written as follows:

$$a_0 + a_1 \left(\frac{Q_1}{N} \right) + a_2 \left(\frac{Q_1}{N} \right)^2 = \frac{ZRT_1}{\left(\frac{k-1}{k} \right)} \left[\left(\frac{P_2}{P_1} \right)^{\frac{k-1}{k}} - 1 \right] / N^2 \quad (11-71)$$

Together, with the following polytropic relations:

$$\frac{T_2}{T_1} = \left(\frac{P_2}{P_1} \right)^{\frac{n-1}{n}}; \quad \frac{\rho_2}{\rho_1} = \left(\frac{P_2}{P_1} \right)^{\frac{1}{n}} \quad (11-72)$$

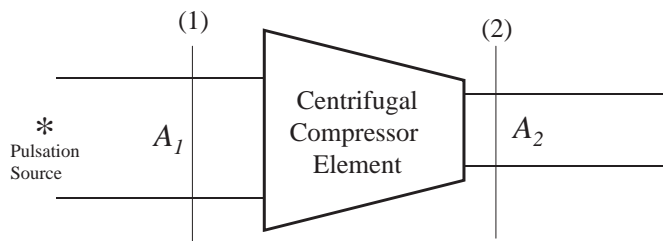


Figure 11-12. Acoustic model for a centrifugal compressor.

where n is the polytropic exponent determined from

$$\left(\frac{n}{n-1} \right) = \left(\frac{k}{k-1} \right) \eta_p \quad (11-73)$$

$$\frac{\delta P_2}{P_2} = \frac{\delta \rho_2}{\rho} + \frac{\delta T_2}{T_2} \quad (11-74)$$

The four Eqs. (11-68), (11-71), (11-72) and (11-74) can be perturbed, which, combined with the following two isentropicity equations:

$$\frac{\delta \rho_1}{\rho_1} = \frac{1}{\gamma} \frac{\delta P_1}{P_1} \quad (11-75)$$

$$\frac{\delta T_1}{T_1} = \left(\frac{\gamma_1 - 1}{\gamma_1} \right) \frac{\delta P_1}{P_1} \quad (11-76)$$

yield six equations in eight variables, namely,

$$\delta P_1, \delta T_1, \delta \rho_1, \delta Q_1 \quad \text{and} \quad \delta P_2, \delta T_2, \delta \rho_2, \delta Q_2 \quad (11-77)$$

which can be reduced to two equations in four variables and hence the formulation of the TM for a centrifugal compressor.

$$\begin{bmatrix} \delta P_1 \\ \delta Q_1 \end{bmatrix} = \begin{bmatrix} A & B \\ C & D \end{bmatrix} \begin{bmatrix} \delta P_2 \\ \delta Q_2 \end{bmatrix} \quad (11-78)$$

11.3 PULSATION GENERATION

11.3.1 Flow-Generated Pulsation from Throttling Elements

Flow going through constriction elements such as orifice plates, valves, and throttling elements can generate pressure perturbations mainly due to the enhanced turbulence, shear layer instability, and reattachment at the pipe wall, both within the element and downstream of it. The resulting perturbations propagate both upstream and downstream and are broadband in nature. To evaluate the source output, the transmission models described above is utilized for the various elements. The distributed sources of pulsation from the non-uniform flow regions within and downstream of the element can be assumed to be localized either immediately downstream or somewhere within the element. Assumed as volume velocity sources, they can be represented by a hypothetical side-branch oscillating piston flush mounted, and in the case of an orifice plate, it is located immediately downstream, as shown in Fig. 11-13. In this case, the overall TM model for the orifice described above (including both TA and TP) is assumed upstream of the source (piston) and is used to evaluate the source strength from the acoustic pressure measurements, both at distances upstream and downstream of the orifice. Experimental evidence showed that the source characteristic versus frequency is almost flat. The piston acoustic volume velocity (V_s , rms) was evaluated at a frequency in the mid range of the spectra from the measured pulsation upstream and downstream. The results are semi-empirically fitted as follows [2]:

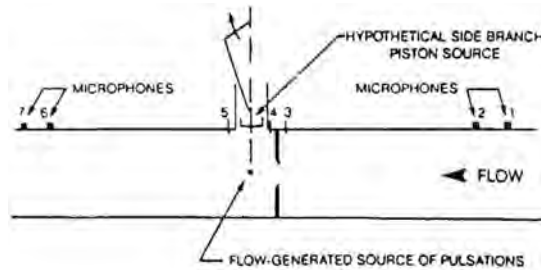


Figure 11-13. Model for flow-generated pulsation at orifice plate.

$$V_s/(Sc) = 225 \times 10^{-3} M(\Delta P/P)^{1.0765} \quad (11-79)$$

where:

- S = cross sectional area of the main pipe
- c = speed of sound in the flowing gas
- M = Mach number of the flow in the main pipe upstream
- P = unrecovered pressure loss
- P = mean static pressure upstream

The same concept of representing the pulsation source by a sidebranch piston is applied to the ball valve but with some adjustment to the overall TM of the valve. It has been found that the pressure loss transfer matrix TP had to be split in a manner shown schematically in Fig. 11-14, so as to maintain continuity of the pulsation pressure at the piston location determined independently from either upstream or downstream pulsation measurements [4]. The split ratio (SR) of TP is shown in Fig. 11-15, and the corresponding value of the source volume velocity (V_s , rms) was fitted as follows [4]:

$$V_s/(Sc) = (0.017 - 0.04)M(\Delta P/P)^{0.9768} \quad (11-80)$$

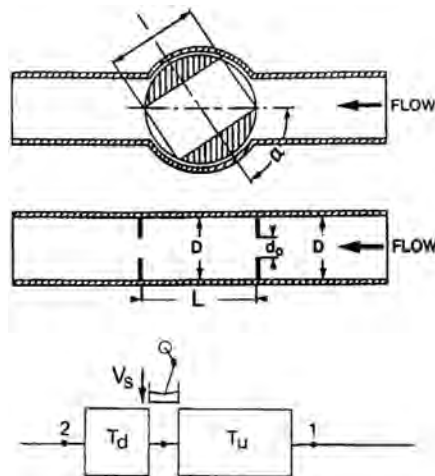


Figure 11-14. Model for flow-generated pulsation at ball valve [4].

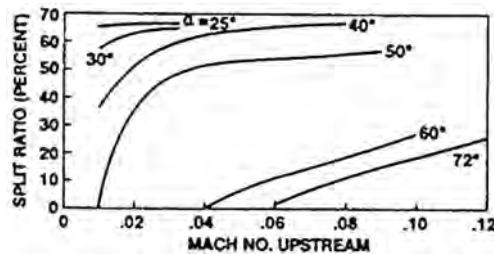


Figure 11-15. Split ratio in use with the acoustic model for flow-generated pulsation at ball valve [4].

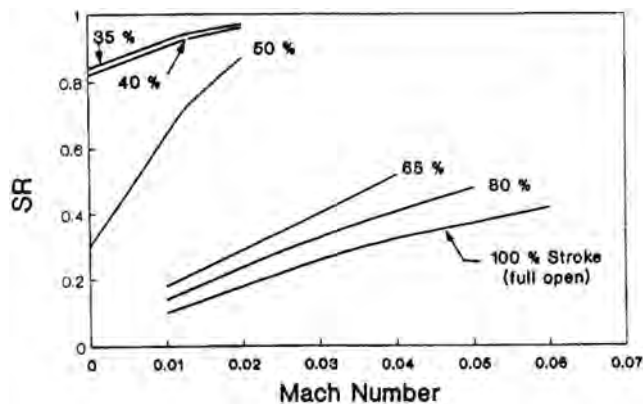


Figure 11-16. Split ratio in use with the acoustic model for flow-generated pulsation at globe valve [7].

The same procedure is applied to the globe valve except that the overall matrix for the valve was split rather than only the TP matrix, as the overall TM for a globe valve was of a non-separable type as discussed earlier. Splitting of the overall TM was necessary to match measured conditions both on the upstream and downstream sides. Since coupling between the two effects (acoustic and pressure loss) in the overall TM is mixed as indicated by Eq. (11-61), a better match was obtained when splitting was applied to all parameters involved in the TM, i.e.; l_o , L_A , L_B , and P . Figure 11-16 gives the result of this SR defined as the ratio of the portion of the parameter contributing to the upstream transfer matrix T_u to the total value of that parameter. The resulting volume velocity characteristic (V_s , rms) is given by [7]:

$$V_s/(Sc) = 1.5 \times 10^{-3} M(\Delta P/P)^{0.4363} \quad (11-81)$$

It was observed from measurements that under the same conditions, the ball valve generates the highest level pulsation followed by the globe valve and then the orifice plate. This can be seen from comparing Eqs. (11-79), (11-80), and (11-81) for the same S , c , M , and P/P . In addition, since P/P is proportional to M^2 , Eqs. (11-79) and (11-80) suggest that both orifice plate and ball valve behave like dipole sources, while the globe valve is more like a monopole source.

11.3.2 Flow-Generated Single-Tone Pulsation from Closed End Side Branch

Flow and acoustic phenomena, associated with various cavities, have been studied for more than 40 years. Numerous data and results have been published, and some extensive

reviews are available (e.g., reference [30]). However, only few studies, e.g., reference [1,8], have concentrated on deep cylindrical cavities (like closed-end sidebranch), which are of relevance to pipeline systems. The main mechanism of pulsations generated, in this case, is that an instability wave in the shear layer is first initiated at the cavity leading (upstream) edge then transformed into a vortex moving over the cavity. This leads to a periodic inward and outward deflection of the shear layer associated with the impingement onto the branch wall below the cavity trailing (downstream) edge and with a vortex shedding from the cavity. Along the shear layer itself, one, two, or three vortices were observed according to different depth modes of oscillation in the cavity. According to the mode number, the oscillation occurs at different values of Strouhal number, St (defined as $St = f \cdot d/U$, where d is the branch diameter and U is mean flow velocity in the main pipe). It was also observed that the onset of the oscillation is not possible below some minimum value of Mach number M , depending on flow and system parameters. The Strouhal numbers (St) resulting from measured tone frequency, approximating quarter wave oscillation in the branch, are plotted versus Mach numbers (M) in Fig. 11-17 [8].

The measurements were taken with a preset M , while the side-branch length was tuned to secure maximum tone amplitude at the closed end. Branch to main pipe diameter ratio (d/D), edge radius (r/d), and mode number had strong effect on the St_m value. The second mode corresponding to two vortices is denoted by a horizontal tail to the symbol and the reflective inlet or outlet by a vertical one. The first mode data were correlated using a least square fit to the following expression for St :

$$St_m = 0.399(1 - r/d)^{0.622}(d/D)^{0.316}(M)^{-0.0831}(\text{Re}/10^6)^{-0.065} \quad (11-82)$$

The measured normalized (w.r.t. main pipe dynamic pressure) tone amplitudes (A_B) at the branch closed end are shown in Fig. 11-18. It was observed that the amplitude is

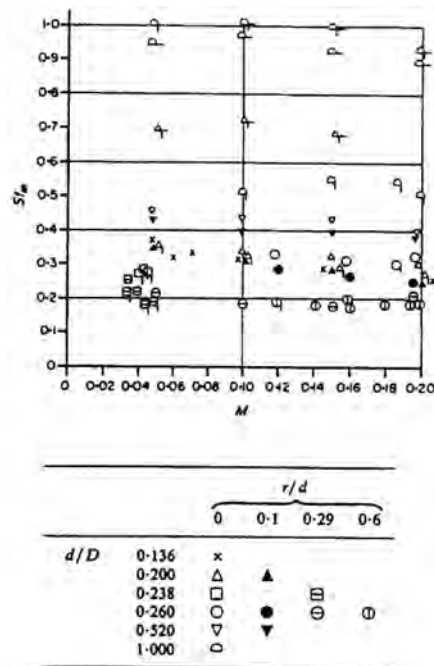


Figure 11-17. Strouhal number for maximum amplitude of pulsation generated at closed end side branch [8].

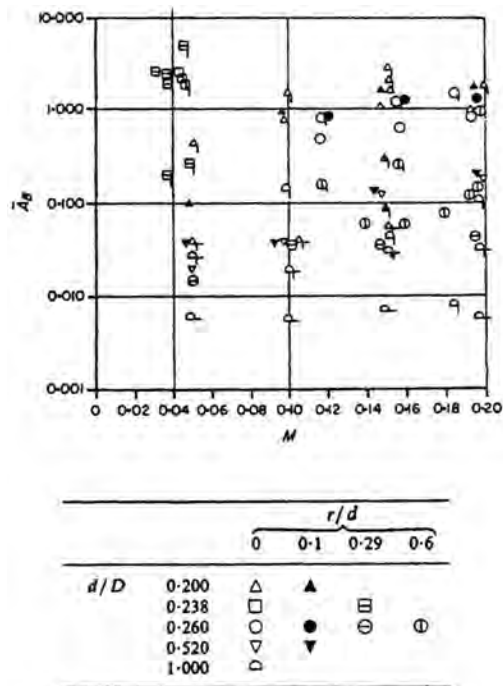


Figure 11-18. Normalized pressure amplitude at the branch end.

higher in the branch than in the main pipe, and that generally, the level rises with higher M , Reynolds number and reflective end on the main pipe. Similar correlation for A_B was obtained fitting the data of Fig. 11-18, but here, a new parameter Z_m had to be added, which is the normalized acoustic impedance at the mouth of the side-branch, normalized w.r.t. main pipe-specific impedance. The following correlation was found:

$$A_B = 0.105(1 - r/d)^{2.091}(d/D)^{-2.757}(M)^{0.1648}(\text{Re}/10^6)^{0.7881}(Z_m)^{1.369} \quad (11-83)$$

The above equation predicts A_B to within +5.6 dB average deviation.

Similar to the broad-band sources, a simple model is developed to enable implementation into a simulation of complex piping system [8]. In this model, the shear layer and branch vortex oscillation, transforming a small fraction of the main flow energy into the

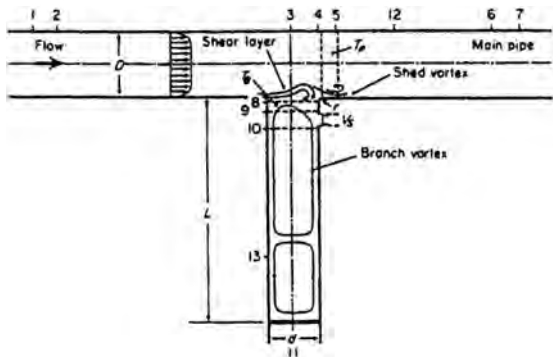


Figure 11-19. Schematic of the side branch, flow pattern, and acoustic source model [8].

acoustic one, were substituted by an oscillatory piston and transfer matrix TB, both located at the mouth of the sidebranch (Fig. 11-19). The effect of vortex shedding in the main pipe was replaced by a transfer matrix TP located at the trailing edge of the branch. Thus, the model is described by three parameters: (V_s , rms) of the hypothetical piston, TB and TP. These parameters were determined from the experimental data and transfer functions between microphones located at points 1, 2, 6, 7, and 11 in Fig. 11-19. The results of (V_s , rms) and the transfer matrices parameters TB and TP can be found in [8].

11.3.3 Pulsation Generated by Reciprocating Compressors and Pumps

Reciprocating compressors and pumps are dealt with as volume velocity sources at the face of the reciprocating piston whether at the head end or the crank end. However, the flow field between the piston face and the connecting piping system on both suction and discharge involves the cylinder volume, which is varying in time; the dynamics of the compressor valves which depends on their types, mass, spring loading, and damping; and on the geometry of the flow passage within the compressor block connecting the two sides of the compressor piston for double acting compressor. The simple model associated with just one side of the piston and neglecting the dynamics of the valve is based on the piston kinematics, which gives the source volume velocity at the piston face as follows:

$$V_s = -AR\omega \sin \theta \left[1 + \frac{R}{L} \frac{\cos \theta}{\sqrt{1 - \left(\frac{R}{L} \sin \theta \right)^2}} \right] \quad (11-84)$$

where:

- A = reciprocating piston effective area
- R = crank radius
- L = connecting rod length
- θ = crank angle from top dead center ($\theta = \omega t$)
- ω = rotational speed (rad/s)

This expression is applicable for both the suction and discharge, which define the limits of θ according to the P-V card of the compressor. These limits depend on the ratio between the suction and discharge pressures, the compression and expansion exponent, and the number of open clearance pockets on both sides of the compressor (i.e., loading condition). Figure 11-20 shows a schematic of an ideal P-V card of the head-end of a reciprocating compressor.

It is apparent that the above volume velocity is periodic, nonsinusoidal (see Fig. 11-21), and therefore, will have a number of harmonics associated with it in the frequency domain. Once decomposed to its harmonics using standard Fourier transform, it is transferred to a location downstream of the valve via a transfer matrix associated with the cylinder space of a volume corresponding to the mean cylinder volume when the corresponding valve is open. Figures 11-22 and 11-23 show an example of the first three harmonics decomposition of the suction and discharge volume velocities at the face of the compressor piston.

The above simple model is only possible when both suction and discharge valves are assumed ideal. Real valve behavior, its dynamics, and the effect of the acoustic response of the connected piping system are quite involved (see, e.g., references [31,32]), and will not be discussed here. When a double-acting compressor is used, the acoustic model should account for the gas passage between the head-end and the crank-end, which connect to compressor suction or discharge nozzle as shown in Fig. 11-24.

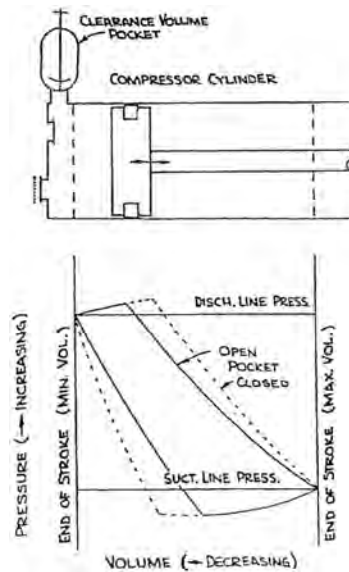


Figure 11-20. Schematic of the P-V card of the head-end of a reciprocating compressor.

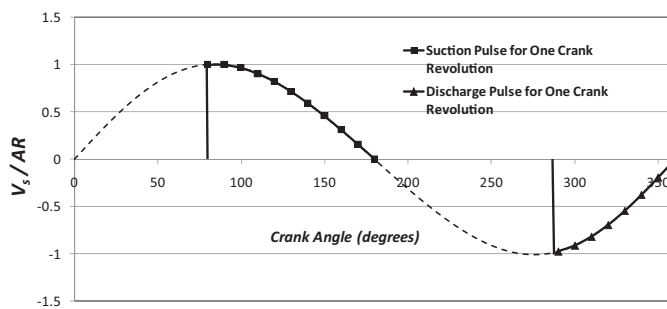


Figure 11-21. Periodic but non-sinusoidal characteristics of the pulsating volume velocity generated by a reciprocating compress.

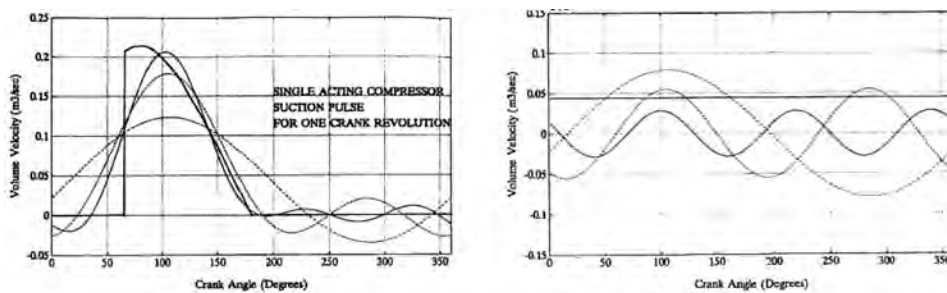


Figure 11-22. Decomposition of the suction pulsating volume velocity to the first three harmonics.

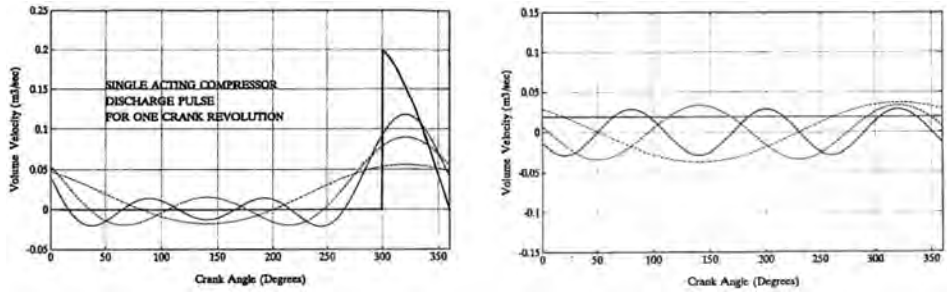


Figure 11-23. Decomposition of the discharge pulsating volume velocity to the first three harmonics.

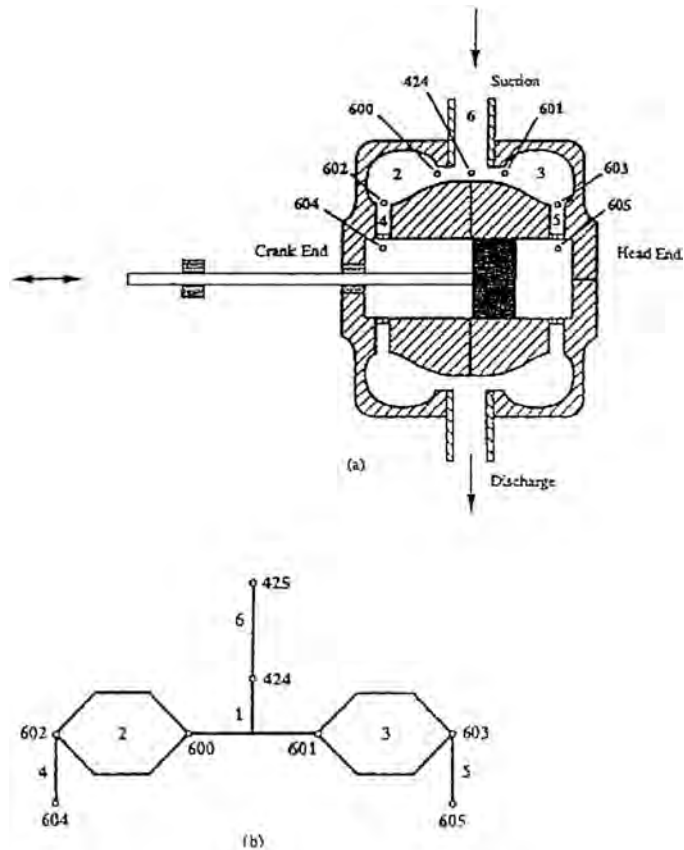


Figure 11-24. Acoustic model for a double acting reciprocating compressor accounting for the internal passage.

11.4 SOLUTION TECHNIQUES

Based on the above formulation of the acoustic transfer matrix for each major piping element and fitting, a digital pipeline acoustic simulation program can be easily developed to analyze the generation and transmission of pressure oscillations in reciprocating and centrifugal compressor installations, as well as any piping configuration and meter and regulating stations. An example is a commercial code “PULS” [19] that is based on the TM approach in

the formulation of the acoustic response of a pipeline system. The program is general enough and contains most elements found in pipeline systems. Special emphasis has been given to flow-generated pressure pulsation and effects of mean flow parameter on the transmission characteristics of various piping elements, as outlined above. The fluid properties are based on one of three state equations, namely, BWRS, Redlich–Kwong–Soave, Peng–Robinson, or user-specified properties. The system geometry is introduced by flexible node numbering system and elements connecting these nodes. Several routines are then called to calculate the transfer matrix for each element at a given frequency. These TMs are then pooled into an overall system matrix, which comprises a system of linear equations in complex numbers. Boundary conditions are then specified to complete the set of equations, which include open end, closed end, anechoic end, reciprocating compressors, or flow-generated source elements such as orifice plates, ball valves and globe valves, or any other known pressure or volume velocity sources. The resulting set of linear algebraic equations is then solved using special sparse matrix computational technique. A preprocessor and post-processor have also been developed to help the user through preparation of the model and analyze the output results.

11.5 ACOUSTIC BOUNDARY CONDITIONS AND RESONANCE

Regardless of the complexity of any piping configuration, the system overall transfer matrix will have the size of $(2N \times 2N)$, where N is the number of nodes between the piping elements comprising the network plus all of the boundary nodes. For example, a network composed of two pipes in series will have total of three nodes: one at the point where the two pipes join, and two boundary nodes. The network example shown in Fig. 11-25 will have 14 nodes: 11 between elements and 3 nodes at the three boundary nodes (1, 5, and 14). In order to determine the amplitude of pulsating pressure and volume velocity at each node, we would need to compose a set of $2N$ equations. The TM for each piping element will provide a set of two equations relating the amplitude of pulsating pressure and volume velocity at the terminal nodes of this element. When the entire TMs for all the elements are written, there will be a less number of equations than the $2N$ equations needed to solve. Each boundary node has to be defined in terms of its acoustic boundary condition. One acoustic equation defining the boundary condition at each of these boundary nodes will close on the system of equations to yield exactly $2N$ equations to be solved simultaneously. Clearly, the magnitude of the amplitude of pulsating pressures and volume velocities at all of the nodes depend on how these boundary conditions are defined.

The acoustic boundary condition at a boundary node can be any one of the following:

1. Closed end, hence, the amplitude of the pulsating volume velocity at this node is zero, i.e., $V = 0$
2. Open end, hence the amplitude of the pulsating pressure at this node is zero, i.e., $P = 0$

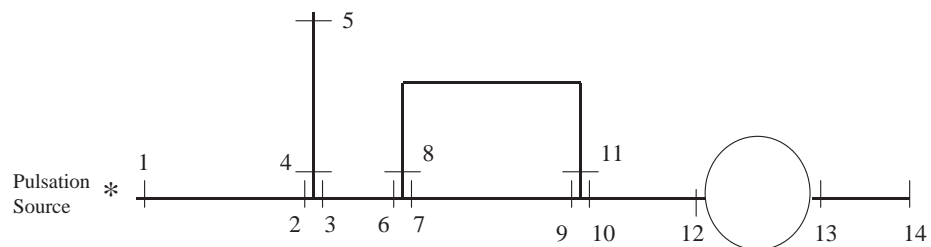


Figure 11-25. Example of a piping network composed of multiple acoustic elements and boundary nodes.

3. An anechoic (non-reflective), like in the case of a long pipe section downstream of this node; in this case, the acoustic impedance at this node is equal to the characteristic impedance of the pipe, i.e.,

$$Z_{\text{anechoic}} = \frac{P}{V} = Z_0 = \frac{\rho c}{S} \quad (11-85)$$

4. A pulsating pressure source of known amplitude (A), i.e., $P = 0$
5. A pulsating volume velocity source of known amplitude (A), i.e., $V = 0$
6. Flow-generated pulsation source from a throttle element (e.g., orifice plate, ball valve, or a globe valve), with known amplitude of pulsating volume velocity [see Eqs. (11-79), (11-80), and (11-81)].
7. Flow-generated pulsation at the mouth of a closed end side branch.
8. Volume velocity source of pulsating generated by a reciprocating compressor [Eq. (11-84)].

Acoustic Resonance Condition of a Piping Network. A piping network could amplify pulsation generated at a source in a system at certain frequencies, dependent on the system geometry, boundary conditions, properties of the fluids, and mean flow parameters. These frequencies are called the resonance frequencies of the system and can be determined by evaluating the impedance at a closed boundary node or at an open boundary node in the system. The resonance frequencies correspond to frequencies at which the acoustic impedance at a closed-end node in the system is maximum, as shown in Fig. 11-26. Similarly, the resonance frequencies correspond to frequencies at which the acoustic impedance at an open-end node in the system is minimum, as shown in Fig. 11-27. If the acoustic source in the system (e.g., reciprocating compressor or closed-end side branch) is generating pulsation at frequencies at or near the system resonance frequencies, pulsation amplitudes will be amplified, which could lead to high shaking forces and severe vibrations. Acoustic simulations are employed during design of a compressor or pump stations to determine if this is the case. Modification of the system geometry is often needed to avoid these resonance conditions, or other means to suppress the source of pulsations would be required, as will be discussed later in this Chapter.

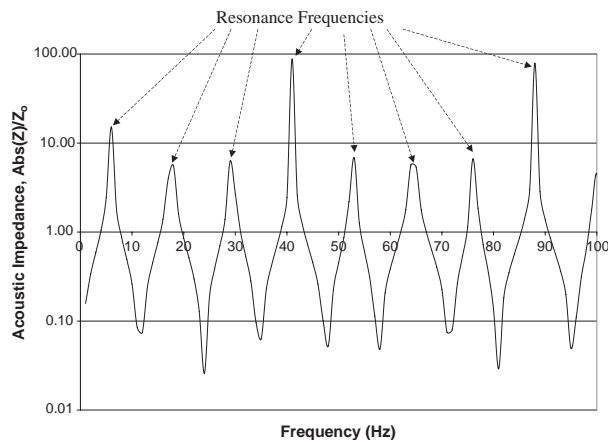


Figure 11-26. Example of acoustic impedance at a closed end node in a system showing the resonance frequencies of that system.

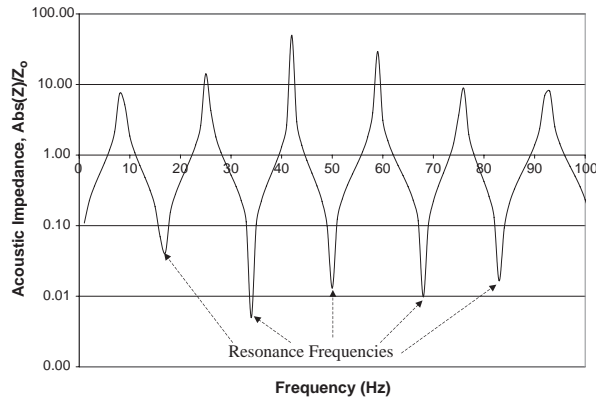


Figure 11-27. Example of acoustic impedance at an open end node in a system showing the resonance frequencies of that system.

11.6 TECHNIQUES FOR PULSATION SUPPRESSION

Pulsation generated by the above elements in natural gas piping systems can be suppressed by three types of devices: (i) reactive silencers (mufflers) whose performance is function of the geometry of their various components; (ii) spoilers, which are used to interfere with the self-sustained oscillations and, hence, suppress pulsations at the source; and (iii) active control, which is based on cancellation of pulsations by means of various electromechanical feed forward and feed back techniques. This latter technique has not been implemented fully into the natural gas application, which is still at the research stage, an example of which is the attempt to suppress oscillations produced by centrifugal compressors' incipient surge [33].

11.6.1 Reactive Silencers

Reactive silencers consist typically of several pipe segments that interconnect with a number of large-diameter chambers. These silencers reduce pulsation levels primarily through the use of cross-sectional discontinuities that reflect the acoustic wave back toward the source. The two parameters used to determine the effectiveness of suppression are the transmission loss (TL) and insertion loss (IL) and are defined in reference [34]. Reactive silencers can be classified as follows:

1. Expansion chambers with and without extended tubes. Fig. 11-28a and b shows examples of these silencers along with the corresponding TL for the dimensions shown [35]. Notice that TL is greater for two chambers than one and also increases as the length of the connecting tube increases.
2. Helmholtz resonators, which consists of a small branch tube (called "neck") and a cavity, as shown in Fig. 11-29. Beranek [35] also gives a good account of sizing and determining the corresponding TL for such silencers. A Helmholtz resonator is most effective at its characteristic frequency, defined as:

$$f_H = \frac{c_0}{2\pi} \sqrt{\frac{A_0}{LV}} \quad (11-86)$$

where, A_0 is the sum of the cross-sectional areas of the connecting tubes, L is the length of the connecting tube, and V is the volume of the vessel.

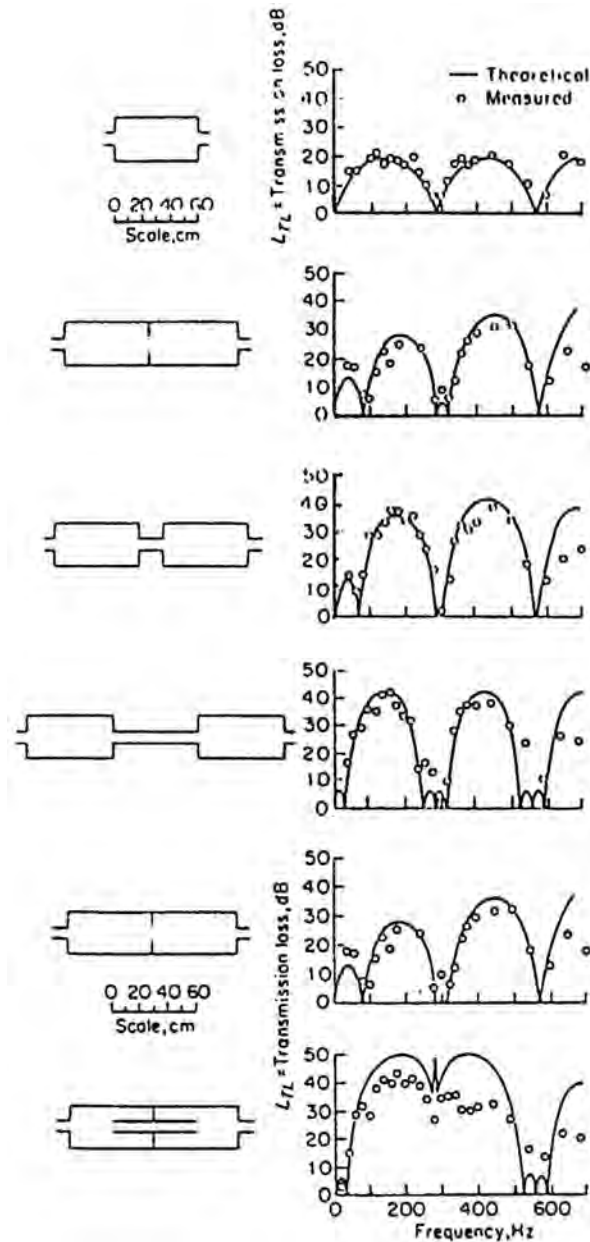


Figure 11-28a. Examples of expansion chambers silencers without extended tubes. TL is greater for two chambers than one and also increases as the length of the connecting tube increases [35].

- Side-branch mufflers, which consist of an annular tubular cavity communicating with the center (propagating pipe) through a number of holes on its periphery, either centered or at one end of the tube as shown in Fig. 11-30. The TL characteristic of such mufflers is shown in Fig. 11-30, which (like the Helmholtz resonators) features a cusp with higher TL than that of the expansion chamber type mufflers which is rather rounded. Therefore, type (2 and 3) mufflers are used when suppression of pulsation is needed for a rather narrow range of frequency, around the cusp frequency, while expansion chambers are used for wider range when frequency is expected to change, e.g., like in the case of a reciprocating compressor.

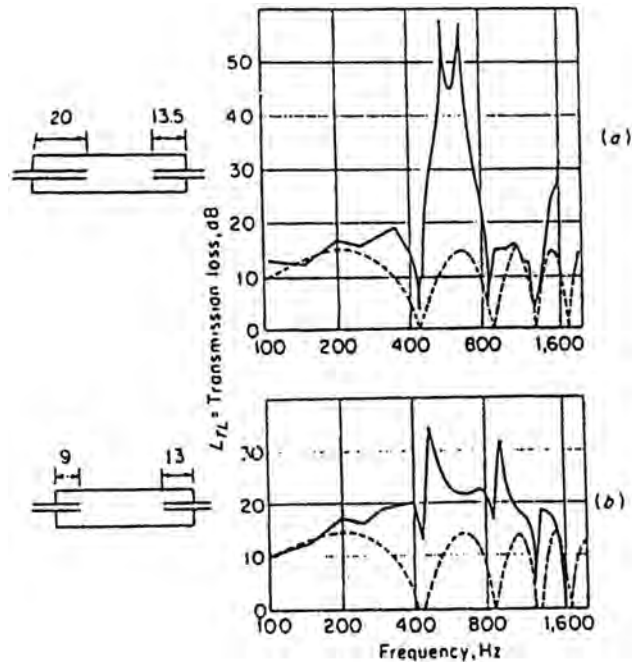


Figure 11-28b. Examples of expansion chambers silencers without extended tubes. TL of an expansion chamber of the same size without extension tubes is shown by dotted lines [35].

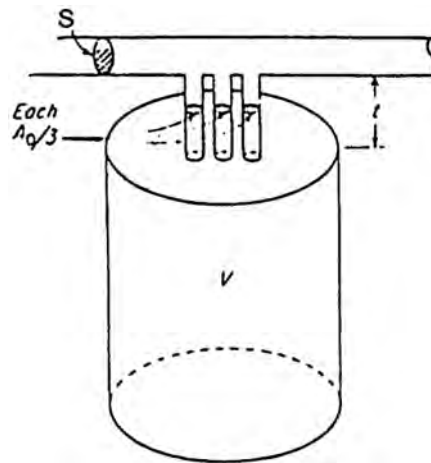


Figure 11-29. Helmholtz resonator.

4. Perforated tube mufflers, which have long been known to be acoustically more efficient than the corresponding simple tubular side branch mufflers. Fig. 11-31 shows three types of these mufflers known as (a) concentric-tube muffler, (b) plug muffler, and (c) three-duct cross-flow muffler. Munjal et al. [41] have developed explicit expressions for the transfer matrices of these mufflers and an example performance is also shown in Fig. 11-31.

The transfer matrices of the above silencers are function of the element geometry, properties of the flow medium, mean flow velocity, and properties of duct liners, if any.

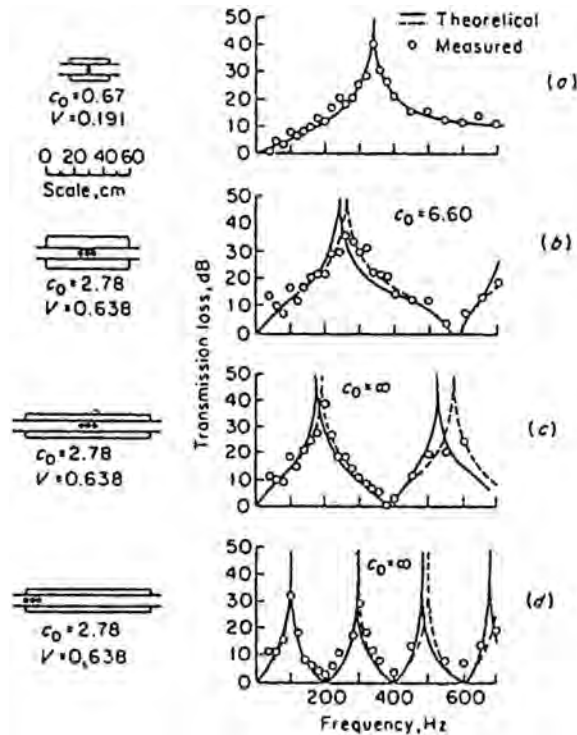


Figure 11-30. Side-branch silencers (c_0 is called conductivity parameter $= A_0/t'$, where, $t' = t + 0.8\sqrt{A_0/n}$) [35].

They are generally composed of sub-matrices of sub-individual components, which can be formulated from the TM's discussed above. The overall matrix for a specific silencer is then used to determine the muffler performance in terms of its TL or in conjunction with the connecting piping system to determine its final performance in terms of the IL parameter.

11.6.2 Spoilers for Pulsation Suppression at Source

Several modifications of the T-junction geometry by means of spoilers for the suppression of single-tone generation have been investigated. Examples of these modifications were reported by Bruggeman et al. [1] and are shown in Fig. 11-32. A reduction in the amplitude level by 20 dB has been achieved by spoilers (a, b) of Fig. 11-32, and a further decrease to more than 30 dB is claimed by using spoilers (c, d) of Fig. 11-32. A different idea was developed by NOVA [36], which also has the effect of disturbing the shear layer at the mouth of a closed-end side-branch, is by means of an insert, shown in Fig. 11-33. The insert can take five different forms as shown in Fig. 11-28. An example of pulsation suppression by these inserts is shown in Fig. 11-33, indicating a reduction in level by more than 40 dB [36].

Another novel technique to suppress pulsation generated by closed end side-branches followed the recent work of Kiel and Foy [12] who discovered that a change in the side branch diameter can reduce significantly the level of pulsation generated. Their results shown in Fig. 11-34 indicate that when the step change in diameter is located closer to the open end and within the first 50% of the equivalent single diameter branch length, pressure amplitudes both at the branch end and in the main pipe are reduced substantially. This

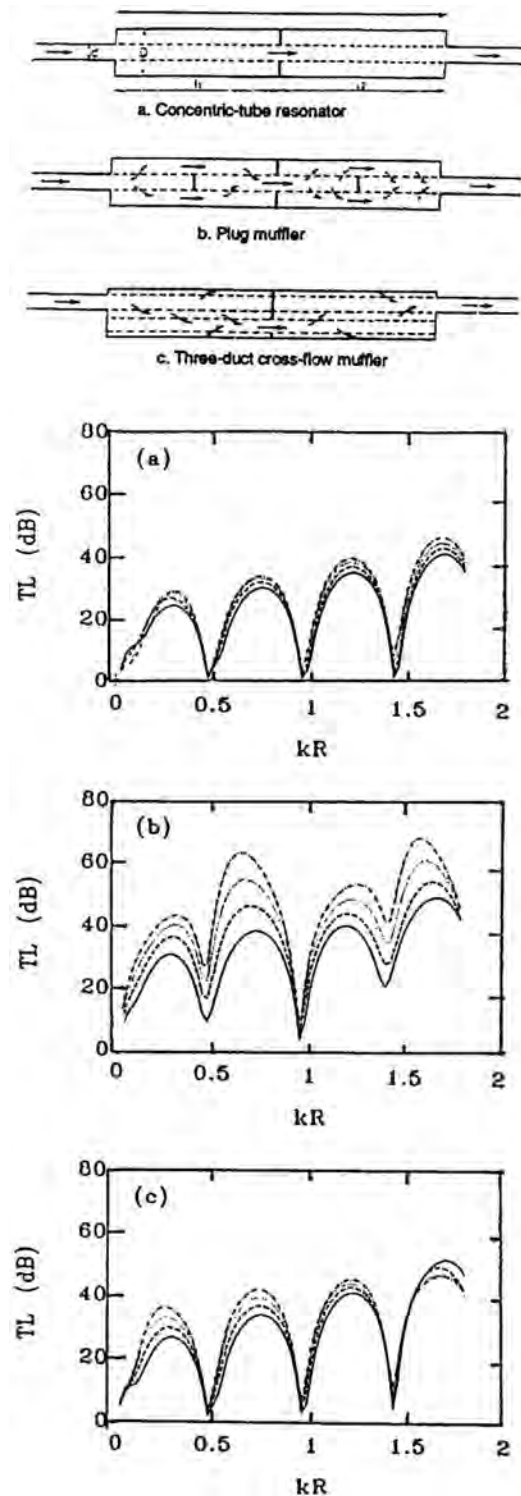


Figure 11-31. Three types of perforated tube mufflers and their corresponding TL performance at different mach numbers [41].

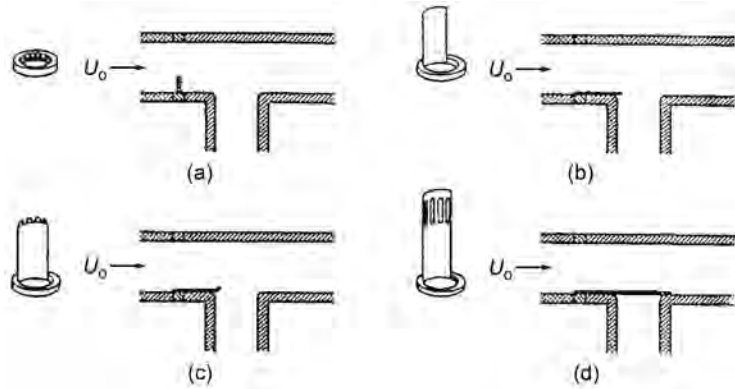


Figure 11-32. Spoilers used to reduce flow-generated pulsations at closed-end side branches [1].

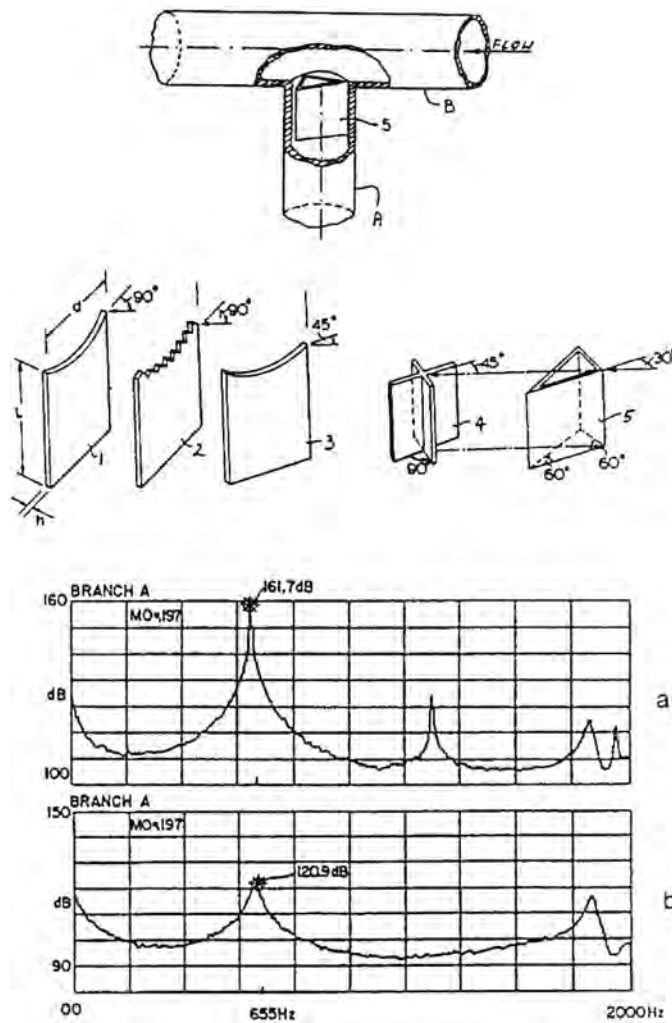


Figure 11-33. Side branch inserts developed by NOVA and example of suppression at $M = 0.197$ (a) without insert, (b) with insert [36].

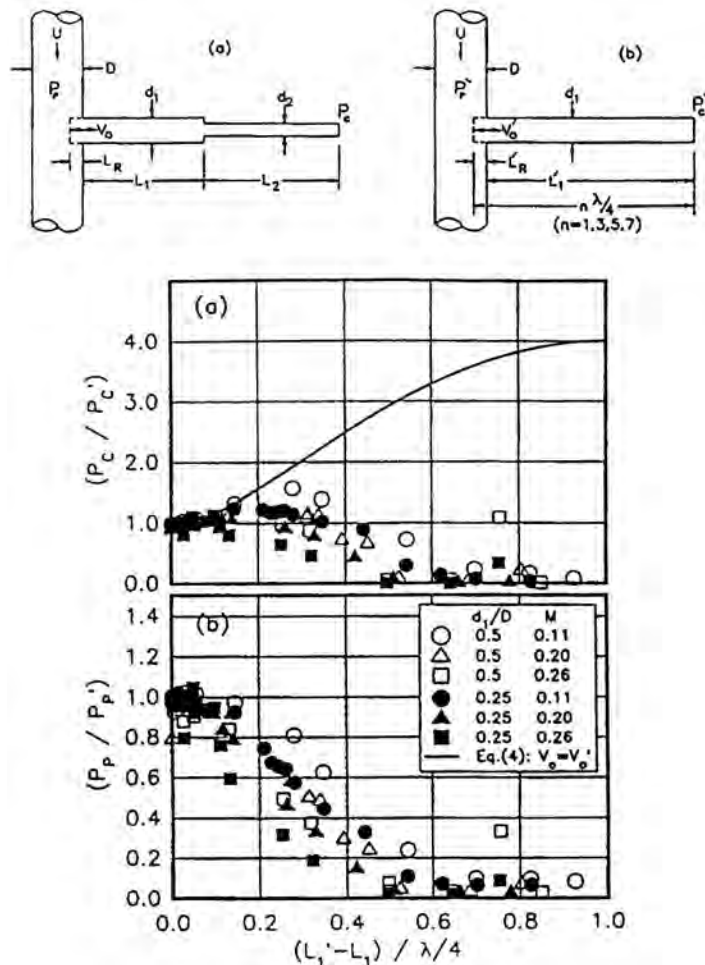


Figure 11-34. Comparison of pulsation pressure amplitudes at the closed end and in the main pipe of two geometry side branches [12].

finding is of importance in certain applications where a step in diameter is required anyway, like in the case of a relief valve stack. In such an application when the reducer is located more toward the base of the stack, significant suppression of pulsation can thus be achieved, according to this result.

11.6.3 Suppression of Noise From Blowdown Stacks

Blowdown of compressor stations involves high flow rate release of a high-pressure natural gas into the atmosphere. Sometimes the pressure in the yard piping reaches 15 MPa. The noise generated by the gas stream blown from the blowdown stack can approach an A-weighted sound level of 150 dB on the largest blowdown stacks and approximately 120 dB on the smaller ones. To minimize noise generation during blowdown, the following recommendations should be implemented.

- The Reynolds numbers of streams flowing through an expansion device should be rather small. This means that characteristic dimensions and velocities must be kept

as small as possible. The pressure-drop coefficients will be high; turbulence, low; and strong flow oscillations, unlikely.

- Avoiding discontinuity regions in the flow is recommended. The instability of these regions leads to various flow oscillations and increased noise production. These include shear layers, stagnation interfaces, reattachment or separation regions, cellular structures, and various shock wave patterns.
- The characteristic dimension responsible for noise generation should be as small as possible. This results in noise of high frequency, which may be less harmful. The higher the frequency, the greater the noise attenuation, with less possibility for resonance; moreover, the sound may be shifted beyond the range of audibility.

Development of the excessive noise suppressors began with multistage nozzles or perforated elements. These devices were insufficiently effective because noise was generated in each intermediate chamber, because of violation of the recommendations, and radiated downstream. Much better results were achieved with noise suppressors, which had only one intermediate chamber between granular layers being cylindrical, conical, or annular [37]. Throttling by a granular layer fulfills all three recommendations. The layer can also absorb some portion of the noise generated upstream. The recommendations have also been satisfied when the fluid flow was forced either through a porous material or through metal discs having expanding passage grooves such as the device shown in Fig. 11-35 [38].

The disks exhibit some tendency to blocking, their fabrication is very expensive, and the disk stacks are large and very heavy. Other typical noise suppressors or mufflers that are used for blowdown noise suppression, such as the one shown in Fig. 11-36 [39], do not prevent noise generation but suppress only noise by absorption. In addition, they also have extremely large dimensions and are expensive.

A novel type of blowdown noise suppressor has recently been developed, as shown in Fig. 11-37 [40]. These noise suppressors can be mounted on a full bore (Fig. 11-37a) or a reduced bore (Fig. 11-37c) stacks, as shown. Proper selection of the granular material,

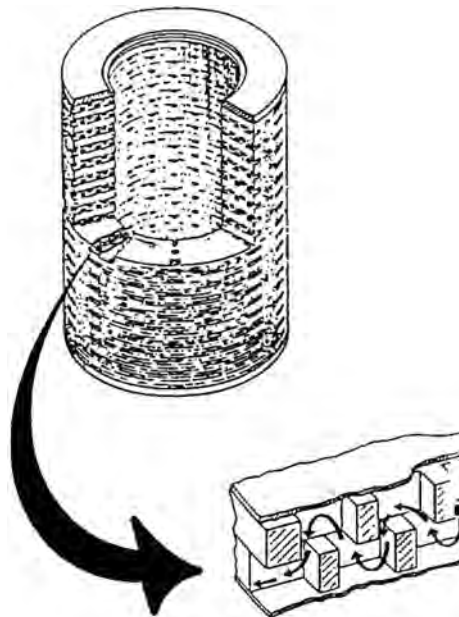


Figure 11-35. Blowdown noise suppressor [38].

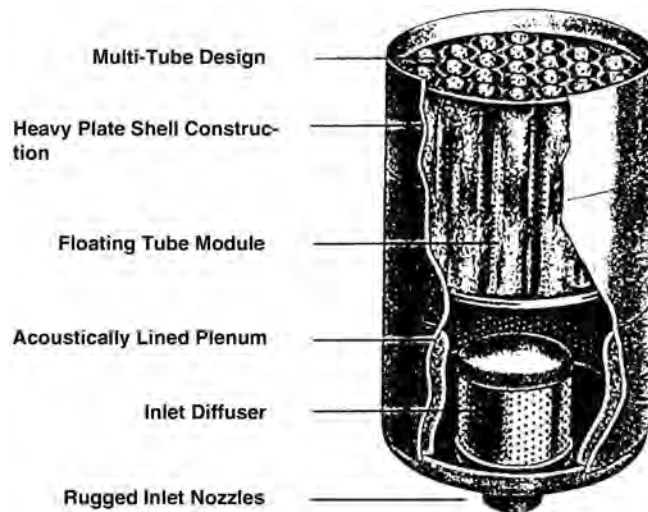


Figure 11-36. Blowdown noise suppressor of absorptive type [39].

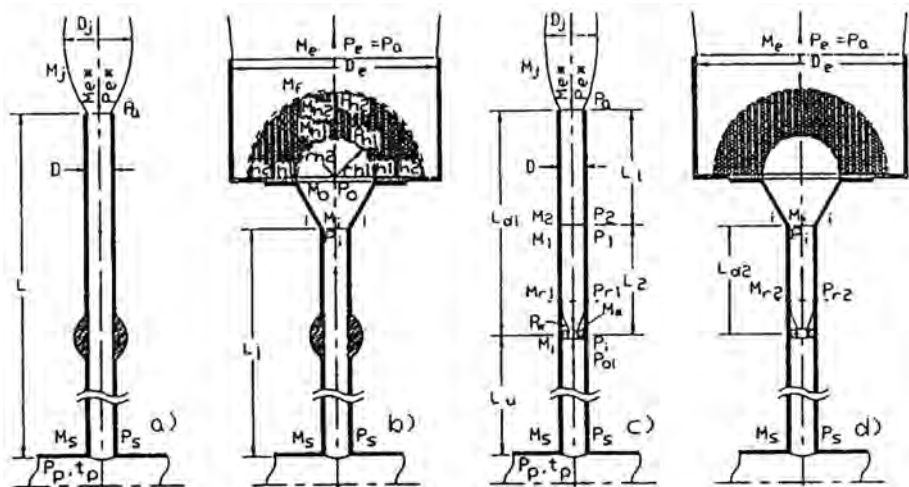


Figure 11-37. Granular-type blowdown noise suppressor [40].

filling the gap between the two perforated hemispheres, will not affect the blowdown time. The small jets exiting from the external hemisphere perforations with Mach number less than 1.0 results in a dramatically reduced noise level and shifts the frequency to a much higher value. The shroud around the device helps in directing the flow from the hemisphere upward and prevents immediate horizontal dispersion of the natural gas, but is not recommended with inert gases or steam. Measurements were carried out at one of TCPL's compressor stations with an NPS 4 stack of the type shown in Fig. 11-37c, without the suppressor, and Fig. 11-37d, with the suppressor. Results are shown in Fig. 11-38, showing a reduction of the order of 33 dB. Simplicity, low cost, and low weight of the suppressor are encouraging.

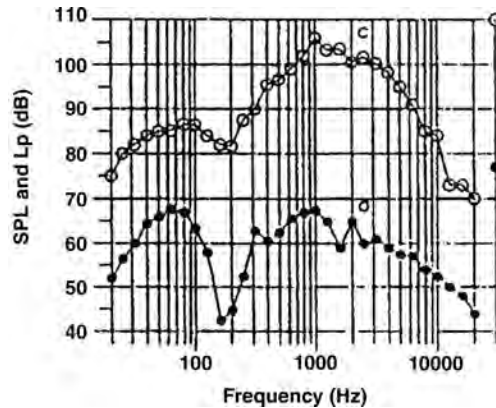


Figure 11-38. One-third octave spectrum measured at 150 m from NPS 4 blowdown stack with and without the granular type suppressor of Fig. 11-32 [40].

11.7 LIQUID VERSUS GAS APPLICATIONS

There are several issues that make liquid systems different from gas systems, such as flashing and cavitation. Systems should however be designed to be flashing and cavitation-free as the analysis of these aspects is almost impossible. In liquid systems, the pressure and temperature have minor effects on the sound speed. New factors come to play in liquid systems, mainly the pipe wall flexibility and amount of air in the liquid. Liquid piping systems can be analyzed using the same formulations for gas systems by considering a modified acoustic velocity that accounts for pipe wall flexibility and air entertainment effects.

Flashing. Flashing is defined as the rapid change of liquid to its vapor due to sudden drop in pressure or increase in temperature. For example, a valve may have a large pressure drop such that downstream pressure is lower than liquid vapor pressure. This will cause part of the downstream liquid to flash till the downstream pressure equalizes the vapor pressure. Pressure fluctuations propagate up and down the line as a sloshing two-phase slug flow. The resultant force reactions can cause severe piping vibrations.

Cavitation. Cavitation is normally caused by pressure waves where the minimum pressure is lower than vapor pressure but the maximum wave pressure is larger than vapor pressure. As the wave traverses a point in the pipe, the negative pulse will cause vapor bubbles to form, but these bubbles will soon collapse after the negative pulse passes. The collapse of the vapor bubbles causes severe local pressure in the order of thousands of g 's. These high-intensity pressures can cause erosion of metal surfaces. Cavitation can occur when low static pressure is combined with high amplitudes of pressure pulsations, as shown in Fig. 11-39.

Speed of Sound in Liquids Piping. The speed of sound in a circular pipe is a function of the bulk modulus of the liquid (K) and its density (ρ), as well as the bulk modulus of elasticity of the pipe material (E) and its diameter to thickness ratio (D/t), by the following relation:

$$c_0 = \sqrt{\frac{1/\rho}{\frac{1}{K} + \frac{1}{E}(D/t)}} \quad (11-87)$$

Table 11-2 gives approximate bulk modulus and density for common liquids, while Table 11-3 gives typical values of the modulus of elasticity of common pipe materials.

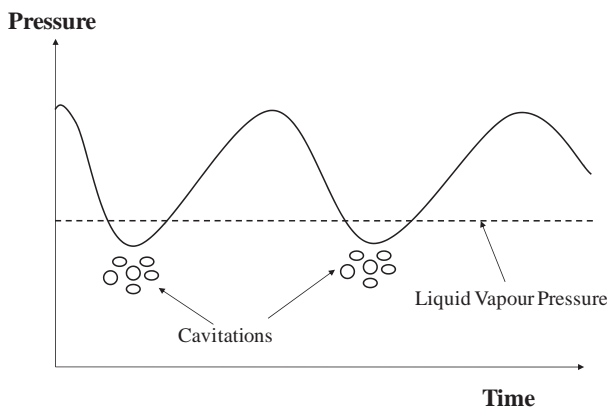


Figure 11-39. Cavitation can occur at low static pressure and high amplitudes of pressure pulsation.

Figure 11-40 shows an example of the speed of sound of water in steel pipe as function of the pipe diameter to wall thickness.

Effects of Vapor Voids in Liquids. The presence of vapor voids in liquids could significantly affect the speed of sound in the piping as it reduces the compressibility of the liquid. Eq. (11-87) is modified to account for the presence of vapor voids as follows:

$$c_0 = \sqrt{\frac{1/\rho}{\frac{1-\alpha}{K} + \frac{\alpha}{kP_{abs}} + \frac{1}{E}(D/t)}} \quad (11-88)$$

where α is the vapor void volume fraction in the liquid, P_{abs} is the static pressure, and k is the vapor polytropic exponent ($k = 1$ for isothermal and $k =$ isentropic exponent for adiabatic flow). Table 11-4 gives the speed of sound for various gas concentrations in a rigid pipe (E is infinite), $k = 1.4$ and $K = 2$ GPa.

Pulsation Filters (Dampeners) in Liquid Systems. Because the acoustic velocity in liquids is several times that in gas, conventional low-pass acoustic filters must often be quite large to provide low cutoff frequency. One approach to minimize the filter sizes is by the use of gas filled side branch elements often referred as snubbers (accumulators or dampeners). Figure 11-41 shows a schematic of a typical snubbers which is similar to a Helmholtz resonator except that the vessel volume is partially filled with gas. Whenever gas appears in a liquid system, it can be converted to an equivalent liquid volume and the same procedures for single fluid would apply. The equivalent liquid volume is:

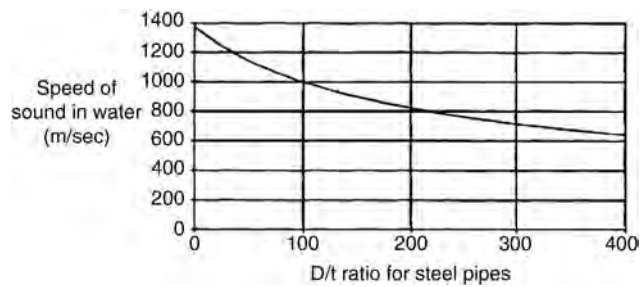
$$V_e = V_g \left(\frac{\rho_L c_L^2}{\rho_g c_g^2} \right) \quad (11-89)$$

Table 11-2. Example of bulk modulus and density for typical liquids

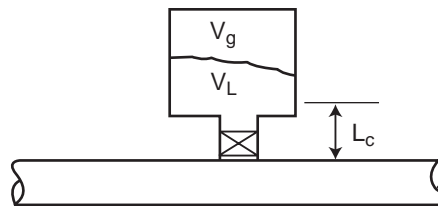
	Modulus of Elasticity K (GPa)	Density (kg/m)	Sound Speed (m/s)
Water at 0°C	1.89	1000	1375
Water at 40°C	2.18	992	1482
Sea water at 0°C	2.04	1028	14083
Petroleum	1.50	835	1340
Oil	1.1–1.6	855–963	855–963

Table 11-3. Modulus of elasticity for typical pipe materials

Pipe Material	Modulus of Elasticity E (GPa)
Steel	200–220
Cast iron	44–120
Copper	120
Glass	5–8
Aluminum	73
Asbestos cement	25
Concrete	20–30
Lead	5–17
Rubber	0.0002–0.0006

**Figure 11-40.** Speed of sound of water in steel pipe as a function of D/t .**Table 11-4.** Effects of vapor voids on the speed of sound of water

Percentage of gas (100°C) α	Sound speed (m/s) at $P_{\text{abs}} = 2 \times 10^6 \text{ Pa}$	Sound speed (m/s) at $P_{\text{abs}} = 2 \times 10^6 \text{ Pa}$
0	1414	1414
0.01	1366	1080
0.1	1081	495
1	498	167
10	175	56

**Figure 11-41.** Schematic of a snubber (accumulator).

The purpose of gas charged snubbers, as in the case of Helmholtz resonators, is to attenuate pulsation at a narrow range of frequency around the characteristics frequency, defined as:

$$f_{\text{snubber}} = \frac{c_L}{2\pi} \sqrt{\frac{A_0}{L(V_e + V_L)}} \quad (11-90)$$

11.8 STANDARDS AND GUIDELINES

11.8.1 API 618 Standard

API Standard 618 5th edition [42] is the recognized specification for users and manufacturers of reciprocating compressors. It defines pulsation and vibration design requirements for reciprocating compressors including high-speed machines. The earlier version (4th edition) was published in 1995. During the past 10 years, the industry has identified many enhancements to this standard. The purpose of API 618 is to establish the minimum requirements, but extra requirements are needed to optimize the compressor design in order to lower total life cycle costs and maximize performance/efficiency. To ensure a global standard, the API 5th edition has been reformatted to harmonized with the ISO requirements. It is anticipated that the next revision will be jointly issued as a merged ISO/API document.

The following points summarize key changes to this new standard:

- a) Pulsation analysis:
 - For cases where the piping design is not available, the pulsation supplier can perform a “pre study” or damper check to calculate bottle sizes. There are consequences to this approach (see below).
 - Unbalanced force guidelines for piping and vessels are defined.
 - Line side pulsation guideline has been updated to account for specific speed of sound of the gas (allows for high pulsations in low density gas and lower pulsations in high density gas).
- b) Mechanical Analysis:
 - The forced response studies (formerly known as M6 and M7 studies) are no longer required on all Design Approach 3 projects. These studies are only required if the pulsation and mechanical natural frequency (MNF) analysis cannot meet the required guidelines. In addition, this new edition provides more specific instructions on how these studies should be performed to ensure accurate results.
 - M8 studies (stress analysis of bottle internals) are no longer required. They become an option for end users.
 - The margin of separation between the MNF and force excitation frequency is 20%. In addition, the minimum MNF must be over 2.4 times maximum run speed.
 - Vibration and stress guidelines have been updated.
 - The end user and packagers are encouraged to exceed these standards to improve efficiency and reduce total life cycle costs.

The new fifth edition of API 618 is written for slow and medium-speed machines but is commonly applied to high-speed units as well. The level of analysis is based on a risk assessment of the compressor and its application. Higher risk requires a higher level of protection, and the study offers higher assurance against problems. Based on the risk assessment, a customer selects one of three Design Approaches.

Design Approach (DA) 1 is a cursory review of the unit and only includes a basic study which determines pulsation bottle designs using simple formulas. No pulsation study is done. A DA 1 is used for very small compressors or simple applications (typically less than 400 hp).

Design Approach 2 involves detailed acoustical modeling, but a very general mechanical review consisting of basic vessel calculations and a review pipe run and anchoring system. Since detailed mechanical analysis is not done, the recommendations tend to be conservative. A DA 2 is for moderate risk applications including units with a narrow range of operating conditions and less than 400 hp/throw. This approach includes the following three components:

- i) Pulsation analysis. The deliverable is a recommended solution to control pulsations. Pulsations are analyzed with acoustic simulation that consists of different approaches depending on the availability of the compressor pipe layout.
- ii) Performance analysis to assess the unit's design and operating conditions, efficiencies, effect of pulsations dynamic pressure drop, capacity, hp, rod loadings, and other factors. The study should include detailed pressure drop reports for all operating conditions.
- iii) Mechanical review using good engineering design practices and basic calculations. However, a thorough calculation of MNFs is not performed.

Design Approach 3 is the most accurate approach and applies to compressors where reliability and availability are important. The additional accuracy provides higher assurance that vibration will be avoided and can avoid unnecessary costs such as bracing and other mechanical supports. A DA 3 is for high-risk applications, larger units, or units with a wide operating envelope. It is more complicated, and a simplified flowchart is provided in Fig. 11-42 to clarify the steps involved in this DA.

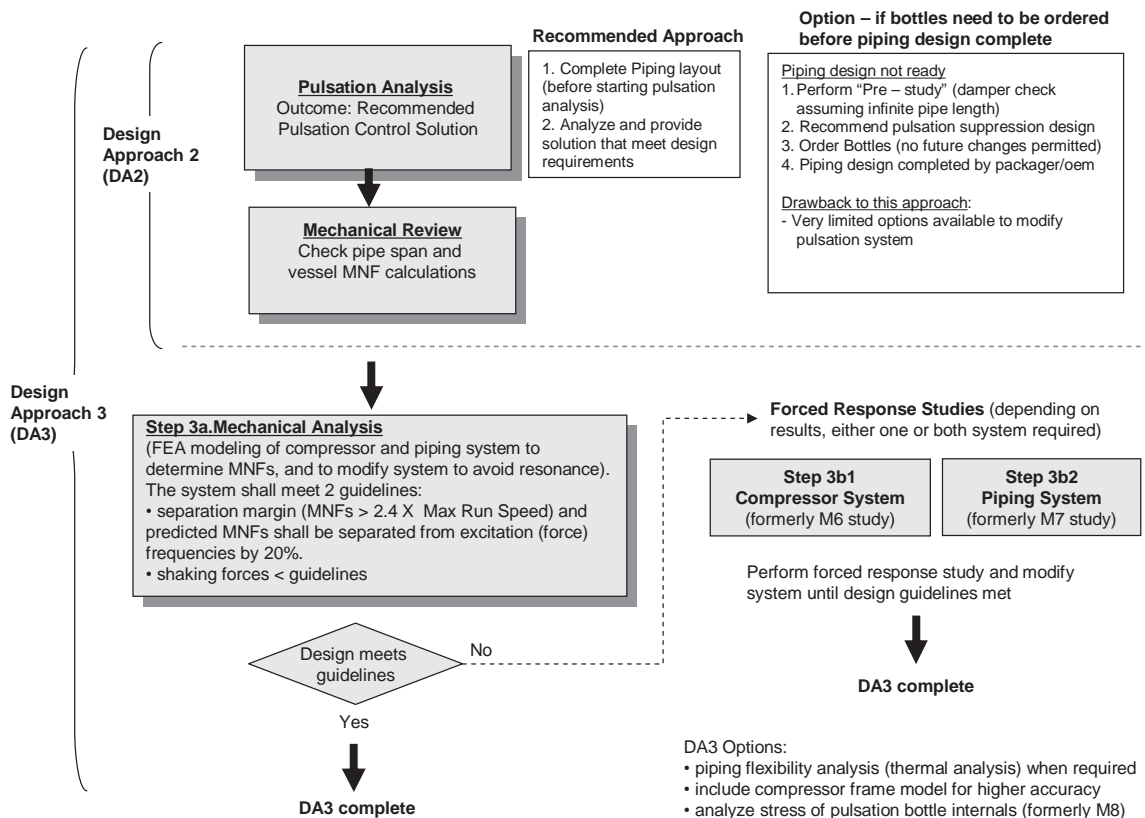


Figure 11-42. Simplified flowchart for DA2 and DA3.

In addition to the pulsation analysis included in DA 2, this approach consists of two possible steps related to mechanical analysis. The first step (Step 3a) analyzes the compressor and piping system to avoid mechanical resonances at frequencies where significant shaking forces exist. The design shall meet two key parameters:

1. *Separation margin* between mechanical natural frequency and the shaking force frequency (also called excitation frequency):
 minimum MNF of any element in the system > 2.4 maximum run speed, AND
 predicted MNF shall be separated from significant excitation frequencies by >20%.
2. *Acoustic shaking forces* shall not exceed the limits based upon the calculated effective static stiffness and the design vibration guideline. API 618 defines a method for estimating the effective stiffness of the piping and the bottle without conducting comprehensive mechanical modeling.

If these design guidelines are met, API 618 DA 3 is complete. If some of the guidelines are not met, a forced response analysis described in the following steps 3b(1) and/or 3b(2) will be required to meet DA 3 requirements:

Step 3b(1). *Compressor mechanical model analysis* applies to the pulsation suppression devices (bottles). If the separation margin or shaking force criteria in step 3a above cannot be met, a forced response analysis of the compressor mechanical model to the pulsation shaking forces and cylinder gas forces must be done.

- This analysis was called the M6 study in the API 618 4th edition.
- The design must meet the allowable cyclic stress criteria (per 7.9.4.2.5.2.5).

The cylinder gas forces (also called frame stretch or cylinder stretch forces) can cause excessive pulsation bottle vibrations even if the pulsation shaking forces meet the standard. API 618 5th edition does not provide any guideline for an acceptable cylinder gas force. Based on industry experience, the Compressor Mechanical Model Analysis is required when:

- hp/cylinder >750 or rod loads exceed 80% rated rod load
- wide speed range operation is required (more than 25% of rated)
- compression ratio is below 1.7
- it is a critical application

Step 3b(2). *Piping system analysis* applies to the piping system. If the separation margin or shaking force criteria in step 3a above cannot be met, a forced response analysis of the piping system to pulsation shaking forces.

- Piping system may include all piping included in the pulsation (acoustic) analysis but it is generally limited to specific areas where the forces exceed the guideline.
- This analysis was formerly called M7 study in the API 618 4th edition.
- The design must meet the allowable cyclic stress criteria (per 7.9.4.2.5.2.5) and vibration limits (per 7.9.4.2.5.2.4).
- Based on current engineering practices, this study is seldom required for standard compressor packages.
- There is a benefit to the packager or end-user for conducting this analysis in specific cases such as:
 - New installations where bottle material has been purchased
 - Existing installation where making pipe layout or support changes are difficult
 - Design optimization studies where analyses have competing requirements. A typical example is the elevated piping around air coolers. The hot discharge

piping requires a flexible design to minimize nozzle loads but the mechanical design for minimum vibration requires a stiff design.

As stated in the new 5th edition, forced response analyses are seldom required. API 618 also has recommendations for torsional vibration analysis which is critical for any new combination of driver and compressor or when operating conditions change for an existing lineup. Other mechanical aspects, such as torsional and thermal analysis, are covered in Chapter 13.

In spite of these improved guidelines, one major issue is that responsibility for deciding the appropriate design studies is ultimately carried by the purchaser, and packagers of reciprocating compressors are less encouraged to include these specialized design studies since they increase their cost. Design studies are usually carried out by an independent third party. The basic design approaches defined in API 618 may not be sufficient and additional studies and services may be desirable.

11.8.1.1 Pulsation Guidelines

In this section, a brief summary of the API 618 Standard is presented. In addition, the methodology of calculating the shaking forces arising from pressure pulsation will be described, which is required to determine the dynamic forces required for performing vibration analysis of the piping structure.

Section 7.9 in API 618 Standard [42] defines three basic means that can be used to control detrimental pulsations and vibrations for reciprocating compressors. These are:

- a) pulsation suppression devices such as pulsation filters and attenuators (including those of proprietary commercial designs based on acoustical suppression techniques), volume bottles without internals, choke tubes, orifice systems, and selected piping configurations;
- b) system design based on studies of the interactive effects of pulsations and the attenuation requirements for satisfactory piping vibration, compressor performance, and valve life;
- c) mechanical restraints such as type, location, and number of pipe hold-downs.

11.8.1.2 General Criteria

Pulsation suppression devices and techniques in accordance with DAs 1, 2, and 3 shall satisfy the following five general criteria:

1. Pulsation-induced vibration and/or mechanically induced vibration shall not cause a cyclic stress level in excess of the endurance limits of materials used for components subject to these cyclical loads. For carbon steel pipe with an operating temperature below 371°C (700°F), the peak-to-peak cyclic stress range shall be less than 179.2 MPa (26,000 psi), considering all stress concentration factors present and with all other stresses within applicable code limits.
Note: Cyclic stresses normally are not calculated for DAs 1 and 2; however, these criteria should still be used as guidelines for DAs 1 and 2.
2. For DA 1 and for initial commercial sizing, pulsation suppression devices shall have minimum suction surge volume and minimum discharge surge volume (not taking into account liquid collection chambers), as determined from the following equations:

$$\text{Suction:} \quad V_s = 8.1PD \left(\frac{kT_s}{M} \right)^{1/4} \quad (11-91)$$

$$\text{Discharge: } V_d = 1.6 \left(\frac{V_s}{R^{1/k}} \right) \quad (11-92)$$

where:

V_s = minimum required suction surge volume in cubic meters.

V_d = minimum required discharge surge volume in cubic meters.

K = isentropic compression exponent at average operating gas pressure and temperature.

T_s = absolute suction temperature, in Kelvin.

M = molecular weight.

PD = total net displaced volume per revolution of all compressor cylinders to be manifolded in the surge volume, in cubic meters per revolution.

R = stage pressure ratio at cylinder flange.

The internal diameter of the surge volume shall be based on the minimum surge volume overall length required to manifold the compressor cylinders. For a single-cylinder surge volume, the ratio of surge volume length to internal diameter shall not exceed a value of 4.0. Note that the above two equations are intended to ensure that reasonably sized pulsation suppression devices are included with the compressor vendor's proposal and should provide satisfactory sizes for most applications. In some instances, however, altering the sizes according to the simulation study employed by DA 2 and 3 will be necessary. Sizing requirements may be substantially influenced by operating parameters, interaction among elements of the overall system, and mechanical characteristics of the compressor manifold system. The magnitude of the effects of these factors cannot be accurately predicted at the outset.

3. Unless other criteria (such as loss of compressor efficiency) are specified, the unfiltered peak-to-peak pulsation level at the compressor cylinder flange, as a percentage of average absolute line pressure, shall be limited to 7% or that percentage determined by the following equation, whichever is lower:

$$P_{cf}(\%) = 3R \quad (11-93)$$

where:

$P_{cf}(\%)$ = maximum allowable unfiltered peak-to-peak pulsation level, as a percentage of average absolute line pressure at the compressor cylinder flange.

4. Unless otherwise specified, the pressure drop based on steady flow through a pulsation suppression device at the manufacturer's rated capacity shall not exceed 0.25% of the average absolute line pressure at the device or the percentage determined by the following Eq. (11-94), whichever is higher.

$$\Delta P(\%) = \frac{1.67(R-1)}{R} \quad (11-94)$$

$P(\%)$ = maximum pressure drop based on steady flow through a pulsation suppression device, as a percentage of the average absolute line pressure at the inlet of the device.

When a moisture separator is an integral part of the pulsation suppression device, the pressure drop based on steady flow through such a device at the manufacturer's rated

capacity shall not exceed 0.33% of the average absolute line pressure at the device or the percentage determined by the following equation, whichever is higher.

$$\Delta P(\%) = \frac{2.17(R-1)}{R} \quad (11-95)$$

5. Operation with alternative gases, alternative conditions of service, or alternative startup conditions shall be specified on the data sheets, and pulsation suppression devices shall be mechanically suitable for all specified conditions and gases. When a compressor is to be operated on two gases of dissimilar molecular weights (e.g., hydrogen and nitrogen), pulsation levels at the cylinder flanges and elsewhere in the entire piping system shall be optimized for the gas on which the unit must operate for the greater length of time. Pulsation levels shall be reviewed for all specified alternative gases, operating conditions, and loading steps to assure that pulsation levels will be acceptable under both operating conditions.

Operating Limits:

The following limits shall apply to the normal operating conditions:

- For DA 1, 2, and 3, allowable pulsations at cylinder flanges shall not exceed the value calculated from Eq. (11-93).
- For DA 1, allowable pulsations at the line side of the suppressor shall not exceed the value calculated from Eq. (11-96).
- For DAs 2 and 3, allowable pulsations in the piping system shall not exceed that allowed by Eq. (11-97).

11.8.1.3 Design Approach 1 Pulsation Limits

Pulsation suppression devices used in accordance with DA 1 shall limit peak-to-peak pulsation levels at the line side of the pulsation suppression device to a value determined by the following equation:

$$P_1(\%) = \frac{4.1}{P_L^{1/3}} \quad (11-96)$$

where:

P_1 (%) = maximum allowable peak-to-peak pulsation level at any discrete frequency, as a percentage of average absolute pressure.

P_L = average absolute line pressure, in bar.

Design Approaches 2 and 3 Pulsation Limits. Acoustical evaluation for DAs 2 and 3 shall be accomplished with proven acoustical simulation techniques that model the compressor cylinders, pulsation suppression devices, piping, and equipment system and that consider dynamic interaction among these elements. Mechanical evaluation for DA 3 shall include an analysis of compressor cylinder manifold and piping systems, including pulsation suppression devices, and the study of the interaction between acoustical and mechanical system responses at specified operating conditions. In addition to the requirements stipulated in the *general criteria*, the following steps are required to accomplish the proper evaluation for DAs 2 and 3:

- a) Determination of the acoustical response of the system, including the amplitude and the spectral frequency distribution of pulsations. This analysis shall ensure minimum degradation of cylinder performance by the effects of dynamic interaction among cylinder, suppression device, and piping.

- b) Determination and control of acoustical unbalanced forces produced within the pulsation suppression devices, piping, heat exchangers, or vessels with internals. Location of inlet and outlet nozzles and internal baffles and choke tubes shall be arranged to minimize these forces.
- c) Determination and control of significant pulsation amplitudes at the compressor cylinder valves. Of particular importance are the frequencies that fall within the range of the mechanical natural frequencies of the valves, generally in the range of 50–100 Hz. Acoustical responses within this range in the valve ports or at the valves have been known to cause valve failures.
- d) For DA 3, determination of the mechanical response of the piping system, including mechanical natural frequencies and mode shapes of the compressor cylinder manifold system. This analysis shall also establish allowable limits for pulsation-induced shaking forces in the piping system based on the cyclic stress levels they can produce.
- e) For DA 3, determination of the required pulsation suppression based on acoustical and mechanical responses and their interactions. To obtain the desired control of vibration and pulsation, selective use should be made of both acoustical and mechanical control techniques. These techniques include the elimination of coincidences between acoustical and mechanical resonant frequencies, acoustical filtering techniques, and changes in mechanical configurations.

Note: When evaluating the need for possible modifications to the piping and/or pulsation suppression devices during an acoustical simulation study, consideration should be given to acoustical-shaking forces and the effect of pulsations on compressor performance. When DA 3 is used, consideration should also be given to mechanical system responses and the use of mechanical vibration control techniques. Pulsation levels (expressed as a percentage of line pressure) should not be used as the sole criterion for making modifications to the piping and/or pulsation suppression devices.

For DAs 2 and 3, based on normal operating conditions, the peak-to-peak pulsation levels in the initial suction, interstage, and final discharge piping systems beyond pulsation suppression devices shall satisfy the requirements of the *General Criteria*. For systems operating at absolute line pressures between 3.5 and 200 bars, this requirement is usually satisfied when the peak-to-peak pulsation level of each individual pulsation component is limited to that calculated by the following equation:

$$P_1(\%) = \sqrt{\frac{c}{350}} \frac{400}{\sqrt{(P_L ID f)}} \quad (11-97)$$

where:

- P_1 (%) = maximum allowable peak-to-peak level of individual pulsation components corresponding to the fundamental and harmonic frequencies, as a percentage of average absolute line pressure.
- c = speed of sound for the gas in m/s.
- P_L = average absolute line pressure, in bar.
- ID = inside diameter of line pipe, in millimeters.
- f = pulsation frequency, in Hz.

For absolute pressures lower than 3.5 bar, use the peak-to-peak levels in bar (not as a percentage) of individual pulsation components calculated for 3.5 bar. For pressures greater than 200 bar, the corresponding calculated cyclic stresses shall be carefully evaluated to assure compliance with the *General Criteria*. Figure 11-43 gives an example of the maximum allowable peak-to-peak level calculated by Eq. (11-97) as for different frequencies and three pipe sizes (line pressure is 60 bars).

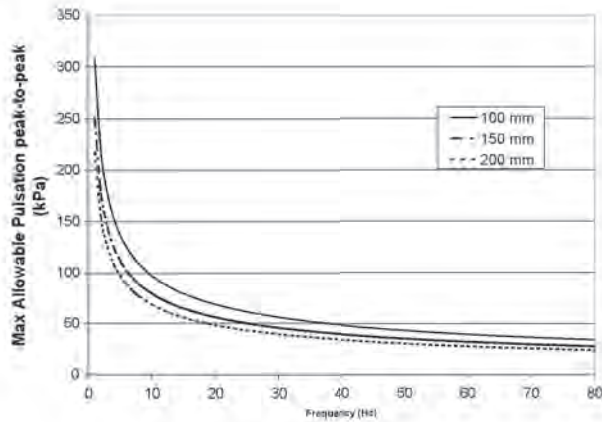


Figure 11-43. Example of API 618 limit peak-to-peak pulsation levels in kPa for various line sizes (line pressure is 60 bars).

11.8.1.4 Maximum Allowable Shaking Forces

The maximum allowable non-resonant shaking force based on the design vibration guideline can be determined from the following equation:

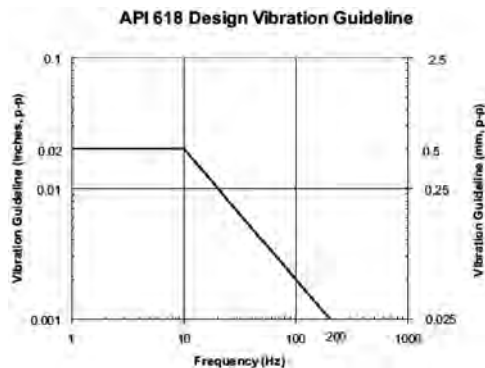
$$SF_k = k_{\text{eff}} \cdot V \quad (11-98)$$

where:

SF_k = the non-resonant shaking peak-to-peak force guideline relative to static structural stiffness in N.

k_{eff} = the effective static stiffness along the piping or pulsation suppression device axis where the shaking force acts in N/mm.

V = the design vibration peak-to-peak guideline in mm, see figure below:



The shaking force guideline (SF_k) applies to non-resonant vibration; therefore, shaking forces near resonance shall be reduced well below the above shaking force guideline. This guideline is simplified from a complex analysis, contains many inherent assumptions, and should be applied with care. See Annex P in API 618 Standards for conventions and a more detailed discussion of the maximum allowable shaking forces.

Various support types provide ranges of support stiffness approximately as follows:

- elevated un-braced tack supports 900–2700 N/mm;
- grade level typical supports and clamps 2700–27,000 N/mm;
- grade level heavy supports and clamps 27,000–45,000 N/mm.

In addition, the API 618 Standard states that maximum allowable piping non-resonant shaking forces shall be the lower of the values calculated from Eq. (11-98) or from the following equation:

$$SF_{pmax} = 45 \cdot NPS \quad (11-99)$$

where:

SF_{pmax} = the maximum piping non-resonant shaking peak-to-peak force guideline based on support strength N .

NPS = the nominal pipe size in mm.

The maximum allowable non-resonant shaking forces for cylinder-mounted pulsation suppression devices shall be the lower of the values calculated from Eq. (11-98) or from Eq. (11-100). For DA 2, since the shaking force levels are not evaluated using Eq. (11-98), the maximum allowable level shall be 10% of Eq. (11-100). For frequencies within $\pm 20\%$ of the calculated pulsation suppression device mechanical natural frequency, the maximum allowable level shall be 1% of Eq. (11-100).

$$SF_{dmax} = 45,000 \quad (11-100)$$

where:

SF_{dmax} = the maximum pulsation suppression device non-resonant shaking peak-to-peak force guideline based on structural strength in N .

Note: The shaking force criteria are intended as design criteria for shaking forces that act along the pulsation suppression device axis. Other shaking forces that can be affected by the pulsation suppression device design such as (but not limited to) those acting parallel to the compressor cylinder nozzles and those acting within the cylinder internal passages must also be evaluated. The evaluation criterion relative to the cylinder varies and should be mutually agreed upon by the purchaser and compressor manufacturer.

11.8.2 API 674 Standard

Similarly, Section 3.6 in API 674 Standard [43] defines three basic means that can be used to control detrimental pulsations and vibrations for positive displacement or reciprocating pumps. These are:

- a) pulsation control devices such as dampeners, accumulators, dampers, preventers, hydraulic isolators, inhibitors, suppressors, stabilizers, acoustic filters, and selected piping configurations;
- b) system design based on studies of the interactive effects of pulsations and the attenuation requirements for satisfactory piping vibration, pump performance, and valve life;
- c) mechanical restraints including such things as type, location, and number of pipe hold-downs.

It also provides two DAs and guidelines for pulsation and vibration control.

Design Approach 1: This approach involves pulsation and vibration control through the use of good piping layout and support/restraint principles, adequate suction pressure (NPSHA), and/or the use of pulsation control devices. DA 1 does not require an acoustical

simulation of the pump and piping system and can be used when experience with similar systems indicates that the likelihood of successful operation is sufficient to justify no acoustical simulation. Cavitation problems in pump systems are significantly influenced by pulsations; therefore, suction-head assessment based on acceleration head calculations, which is a quasi-static method of considering pulsations in piping systems, may not ensure adequate NPSHA.

Design Approach 2: This approach involves pulsation control through the use of pulsation control devices developed using proven acoustical simulation techniques in conjunction with mechanical analysis of pipe runs and support systems (clamp design and spacing) to achieve control of vibrational response. Design Approach 2 is normally applicable to critical pump and piping systems, multiple pumps in parallel, and applications utilizing variable speed, multiple fluids, and variable operating conditions, where safety and reliability are important and where suitability of purpose must be documented. The acoustical characteristics of the entire pump system, including the pump and all important interconnecting piping shall be simulated. The simulation techniques shall be capable of modeling the pulsation-generating mechanisms known to cause pump pulsation and shall be capable of predicting pulsation and shaking force amplitudes throughout the pump and piping system. The simulation techniques shall be capable of evaluating the effectiveness of selected pulsation control devices and/or developing effective acoustical surge volumes, Helmholtz-type acoustic filters, and so forth, if required. Pump valve dynamic effects, such as lag, lift, spring preload and stiffness, and valve areas, may have a significant influence on pulsation amplitudes and, therefore, should be considered in the acoustical simulation.

For the DA 2, the peak-to-peak pulsation levels in the suction and discharge piping systems beyond the pulsation control devices shall not exceed the levels calculated by the following equation, which specifies the allowable peak-to-peak pulsation level of each individual pulsation frequency component.

$$P_1 = \frac{3500}{\sqrt{(IDf)}} \quad (11-101)$$

where:

P_1 = maximum allowable pulsation level in kPa, peak-to-peak of individual pulsation components corresponding to the fundamental and harmonic frequencies.

ID = inside diameter of line pipe, in millimeters.

f = pulsation frequency, in Hz.

Suction and discharge pulsation levels have to be limited to values that will not cause cavitation or relief valve lifting. For this reason, the maximum suction pressure wave amplitude shall not exceed the value calculated using from the following equation:

$$P_2 < 1.5(P_s - P_v) \quad (11-102)$$

where:

P_2 = maximum allowable pulsation level in kPa (amplitude).

P_s = suction pressure in kPa gauge.

P_v = vapour pressure of the fluid in kPa-gauge.

Likewise, the margin of separation between the positive peak of the pulsation amplitude at the relief valve and the relief valve setting shall be 5% of the maximum specified discharge pressure or 165 kPa, whichever is greater, i.e.,

$$P_p \leq (P_R - P_D) - (0.05 \cdot P_D) \text{ or } 165 \text{ kPa, whichever is greater} \quad (11-103)$$

where:

P_p = Positive peak of pulsation amplitude, in kPa.

P_D = The maximum specified value of average discharge pressure, in kPa-gauge.

P_R = Required relief valve setting, in kPa-gauge.

11.8.3 Shaking Forces Arising from Pressure Pulsation

Shaking forces arising from pressure pulsation are dynamic in nature and are caused by the unbalance in dynamic pressure forces acting on the internal surface of a piping structure. These forces can be determined by a simple integration of the pulsating pressure over the internal surface of the structure, taking into account both the amplitude and phase angle variations of this pulsating pressure at different locations of the structure. In general, the following expression is applied:

$$F_{\text{shaking}}(\omega t) = \int P(\omega t + \phi) dA \quad (11-104)$$

where ϕ is the phase angle between the pulsating pressure acting on the internal surface of the structure. For example, consider the pulsation bottle shown in Fig. 11-44. The amplitude of the net unbalanced force in the x direction due to the different pressure pulsations can be calculated as follows:

$$F_{\text{shaking}}(e^{i\omega t + \phi_s}) = A_1 P_1 e^{(i\omega t + \phi_1)} - A_2 P_2 e^{(i\omega t + \phi_2)} + A_3 P_3 e^{(i\omega t + \phi_3)} - A_4 P_4 e^{(i\omega t + \phi_4)} \quad (11-105)$$

where subscripts A_1 through A_4 are the areas identified in the figure, and ϕ_i and ϕ_s are the phase angles of the pulsating pressures and shaking forces, respectively. Note the different sign in front of each term, which defines the direction of the respective force. This shaking force is periodic and can be calculated for each frequency and harmonic generated by the pulsating source.

Another example is shown in Fig. 11-45, where a piping system consisting of two pipe sizes of cross-sectional areas A_1 , has four elbows out-of-plane as shown. The pulsating shaking forces F_1 through F_4 on the four elbows and F_5 on the reducer in the respective direction as indicated can be written as follows:

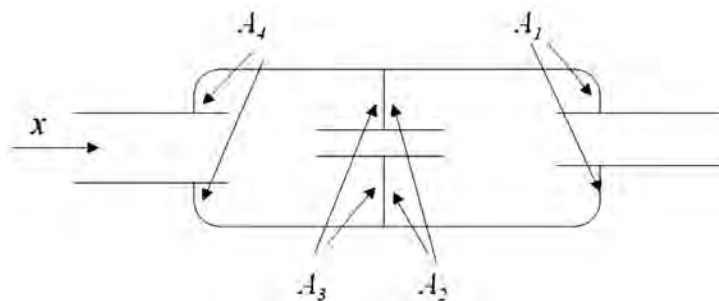


Figure 11-44. Example of the shaking (unbalanced) forces acting on a pulsation bottle due to pressure pulsation.

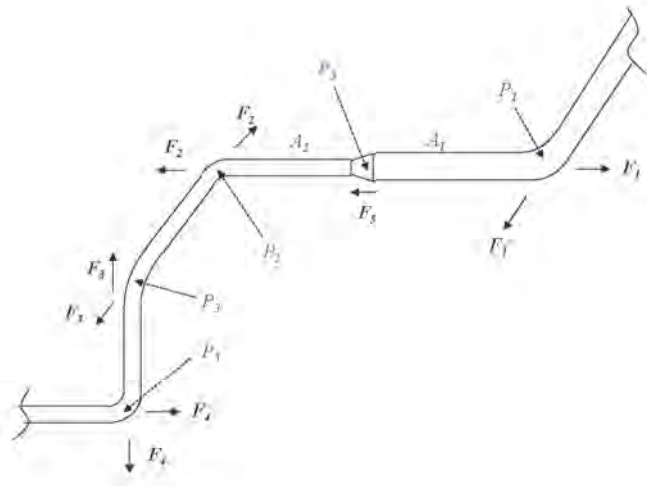


Figure 11-45. Example of the shaking forces arising from the pulsating pressures in a piping systems involving out-of-plane elbows.

$$\begin{aligned}
 F_1(e^{i\omega t + \phi_{s1}}) &= A_1 P_1 e^{(i\omega t + \phi_1)} \\
 F_2(e^{i\omega t + \phi_{s2}}) &= A_2 P_2 e^{(i\omega t + \phi_2)} \\
 F_3(e^{i\omega t + \phi_{s3}}) &= A_2 P_3 e^{(i\omega t + \phi_3)} \\
 F_4(e^{i\omega t + \phi_{s4}}) &= A_2 P_4 e^{(i\omega t + \phi_4)} \\
 F_5(e^{i\omega t + \phi_{s5}}) &= (A_1 - A_2) P_5 e^{(i\omega t + \phi_5)}
 \end{aligned}
 \tag{11-106}$$

The dynamic forces arising from the pulsating velocity and associated change in rate of momentum is generally small compared to that arising from pulsating pressures and often neglected.

Once the shaking force is determined, it is then used in performing mechanical vibration and stress/structural analyses to determine its response of the system in terms of vibration amplitude and stresses at different components of the structure. In terms of vibrations, a simple guideline can be used to determine the seriousness of the vibration level. This is shown in Fig. 11-46 as function of frequency. Five levels of vibration tolerance are identified. The top line indicates that the vibration level is very excessive and is danger to continue to operate the system with the current condition. The second level down “correction” requires attention and correction is needed. The “marginal” level is discretionally and vibration levels should be continuously monitored. The lower two levels are acceptable. Different levels and margins are used by different companies depending on their respective degree of conservatism in their design and operational philosophy.

11.8.4 GMRC Design Guideline for High Speed Reciprocating Compressor Packages for Natural Gas Transmission & Storage Applications

The API 618 standard is most applicable to slow-speed reciprocating compressors, where the compressor frame and driver are mounted directly on a concrete block foundation. While many of the API 618 concepts apply to high speed compressors, the GMRC Design Guideline [44] has additional information regarding high speed compressors which are typically mounted on a steel skid.

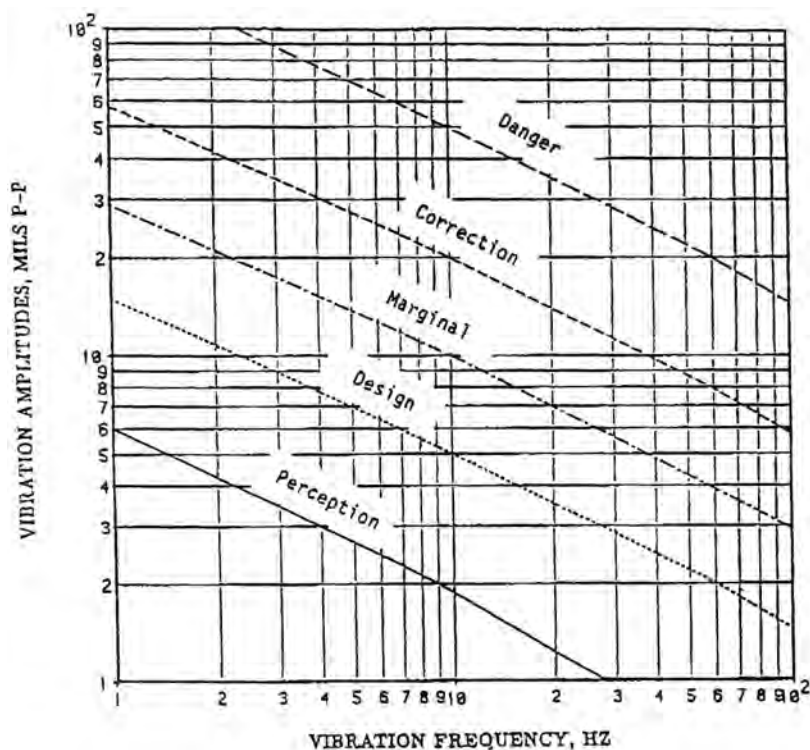


Figure 11-46. Allowable piping vibration levels versus frequency.

One aspect of high speed compressors that could be seen as an advantage is with regards to pulsation bottles that are used to attenuate pulsation. Traditionally for low-speed compressors, initial bottle sizing is based on API 618 requirements. The API 618 method is based on using surge volumes without acoustical filtering, and is most appropriate for low speed, significantly lighter gas (hydrogen) applications. High speed natural gas compressors, due to the high frequency pulsation, can take advantage of volume choke volume low-pass pulsation filter bottle designs. It would be impractical in many slow-speed (300 RPM) applications to consider a low-pass filter since the bottle would have to be very large to achieve a low enough filter frequency. Pulsation filter bottles typically contain choke tubes and baffles, as shown in Fig. 11-47, and have a smaller overall volume than API 618 would require. These types of bottles are required by the GMRC Design Guideline.

The GMRC design guideline also contains design and analysis procedures for steel skid mounted machinery such as is shown in Fig. 11-48. Skids and foundations must be designed to resist the driver dynamic (roll) torque, frame unbalance forces and moments, vertical cross-head forces, time variant gas and inertia forces at each compressor throw and the effects of frame flexibility. The guideline includes, for example, design procedures for designing skid-mounted compressors that are installed on pile foundations, as is often the case in Canada.

Soil dynamic properties are required to achieve an accurate simulation of the skid and foundation system. The critical soil properties to determine are the shear wave velocity, damping, unit weight and Poisson's ratio. Cross-hole seismic testing at the site is the preferred test method in most cases.



Figure 11-47. Acoustic filter pulsation bottle.

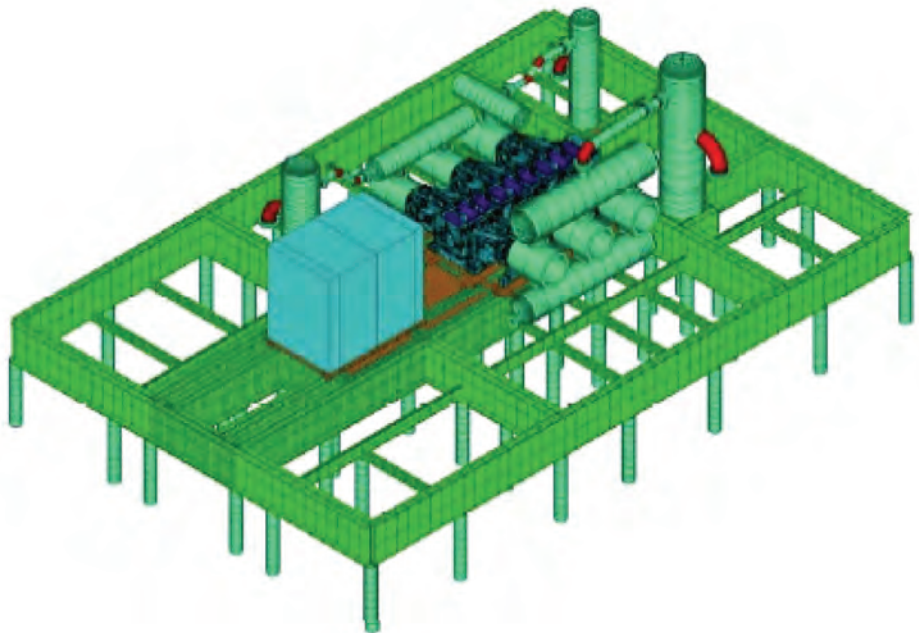


Figure 11-48. Compressor mechanical model including structural steel and piles.

11.8.4.1 API 688 Pulsation and Vibration Control in Positive Displacement Machinery Systems

API 688 [45] is titled “Pulsation and Vibration Control in Positive Displacement Machinery Systems for Petroleum, Petrochemical, and Natural Gas Industry Services”. The first edition was published in 2012 as a Recommended Practice document, and it is a valuable theoretical reference covering many of the same topics as are described in this text. The second edition of the standard will be a normative standard and is scheduled to publish in 2018. The second edition will contain requirements covering API 618 reciprocating compressors, API 674/675 reciprocating pumps, API 619 rotary (screw) compressors, and API 676 rotary (progressive cavity) pumps. The goal is to consolidate requirements regarding pulsation and vibration control into the API 688 document, and later the requirements will be removed from the individual machinery standards.

11.8.5 API 610 and ANSI/HI 9.6.8

Both API 610 and ANSI/HI 9.6.8 [46] apply to centrifugal pumps. The Hydraulic Institute standard specifies three types of dynamic analyses for centrifugal pumps.

- Lateral Rotordynamics
- Torsional Rotordynamics
- Structural Dynamics (Including Reed Critical Frequency)

For each aspect of dynamic analysis, there are 3 levels of analysis described which increase in complexity. Guidance is provided for the appropriate level of analysis for a given application based on experience level and market considerations.

- Level 1. Simple calculations that may be performed using a hand calculator.
- Level 2. Methods employing basic mass elastic modeling using commercially available software tools, such as finite element analysis (FEA) programs.
- Level 3. Computational methods involving multiple specialty programs and complex methodologies.

Structural vibration occurs in both horizontal and vertical pumps. However, vertical structures are particularly vulnerable to mechanical resonance because the natural frequencies of these structures are typically lower and occur near the running speed of the pump.

The first bending mode of vertical pumps is typically referred to as the Reed Critical Frequency (RCF). It is especially important that the RCF does not coincide with the 1st order of run speed, and the half-order of run speed should also be avoided for some applications. The scope of an RCF analysis includes creation of a finite element (FE) model of the pump head from foundation up to and including the motor. A simulation is performed to determine the expected RCF and, if necessary, modifications to shift the RCF. An example of a RCF analysis model is shown in Fig. 11-49.

The Hydraulic Institute Level 3 structural analysis methodology also specifies that forced response analysis also be completed when separation margins cannot be met. One time (IX) synchronous speed excitation due to mechanical and hydraulic excitation should be considered in the forced response analysis. Bearing whirl excitation at approximately 50% running speed should also be included in the structural simulation.

Centrifugal pump lateral rotordynamics are also discussed in both the API 610 and ANSI/HI 9.6.8 standards. API 610 specifies that a lateral analysis is required when the rotor is not classically stiff. A classically stiff rotor is defined as a rotor that has its dry, first bending critical speed at least 20% above the pumps maximum continuous operating speed.

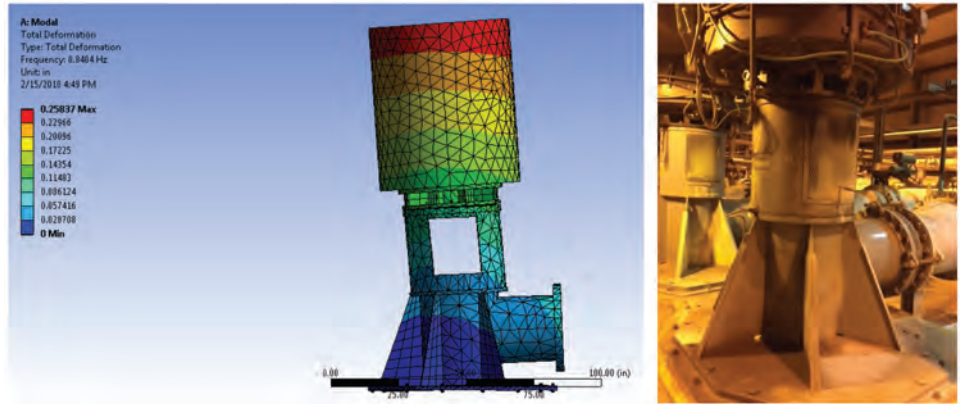


Figure 11-49. Reed Critical Frequency FEA analysis.

API 610 specifies that when lateral rotordynamic analysis is completed, that all of the rotor's damped natural frequencies be calculated for 0 to 2.2 times the maximum continuous operating speed. The stiffness and damping of bearings and seals should be calculated with as-new clearances, and with twice the as-new clearances to take into account worn components. The damping factor versus separation margin should be determined for all modes and compared to the chart shown in Fig. 11-50.

Per API 610, the first assessment of a pump's rotordynamic characteristics is based on damping versus separation, rather than amplification factor versus separation factor as is common with most machinery. If the damping factor is determined to be unacceptable by the criteria in Fig. 11-50, then the rotors damped response to unbalance shall be determined for the modes in question.

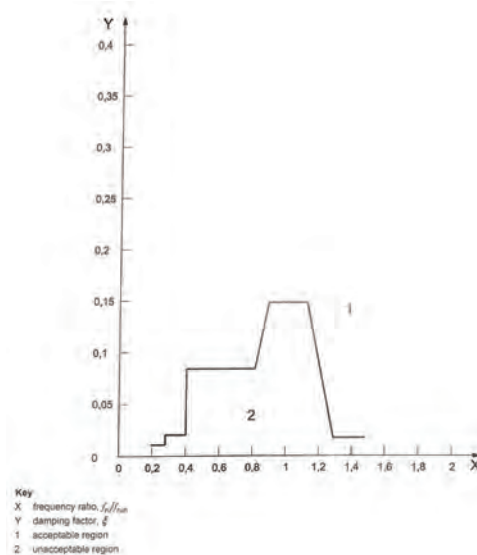


Figure 11-50. API 610 Figure I.1. Damping Factor vs. Frequency Ratio.

11.8.5.1 Case Study, Vertically Suspended Pump

This case study involves a 2800 KW crude oil pipeline pump, operating from 360-720 RPM, as shown in Fig. 11-51. This particular pump had experienced high vibration at 0.5X running speed, a classic indication of oil whirl. The vibration measurement over time is presented in Fig. 11-52. Both a Reed Critical Frequency and Lateral Rotordynamics Analysis per API 610 had been previously completed for this new installation.

The Reed Critical Frequency was measured in the field by completing a modal impact test on the pump and motor assembly. It was determined that the Reed Critical Frequency was at 5 Hz, and generally agreed with the RCF design report. Note that at normal operating speed, the fundamental running speed is 11.8 Hz. Therefore, it was assumed that since the RCF was away from 1X running speed, that vibration would be acceptable. In this case, the RCF was close to the 0.5X, and was being excited by oil whirl of the rotor.

Measurement of the shaft orbit with proximity probes confirmed the presence of a half-speed whirling shaft, as shown in Fig. 11-53.

The lateral rotordynamics design analysis had identified numerous half-speed modes, which is common for vertical pumps due to the extremely lightly loaded journal bearings and numerous seal. However, forced response analysis had indicated that rotor vibration would be acceptable. The rotordynamics simulation did not account for a structural resonance, in this case the RCF mode at half-speed, and therefore did not identify the high vibration levels experienced in the field. This demonstrates the importance of considering 0.5X running speed when completing the RCF analysis. A combined lateral rotordynamics analysis and structural analysis, as recommended in the Hydraulic Institute standard 9.6.8, would have prevented the vibration problem.

The vibration problem was solved by replacing some of the pump bearings, which were just a simple smooth journal bearing design, with the grooved bearing shown in Fig. 11-54. The groove bearing produces less oil whirl cross-coupling, which is responsible for the oil whirl phenomena. The combined oil whirl/reed critical vibration problem did not reoccur after replacement of the bearing.

11.9 CASE STUDY PULSATION EXAMPLES

The following are case studies from actual pipeline installations on the NOVA Gas Transmission System in Alberta, Canada, and a pumping station of water injection into heavy oil reservoir. The first and the second represent cases with flow-induced broadband pulsations from control valves. The third case represents an external source related to reciprocating



Figure 11-51. Crude oil pipeline pump.

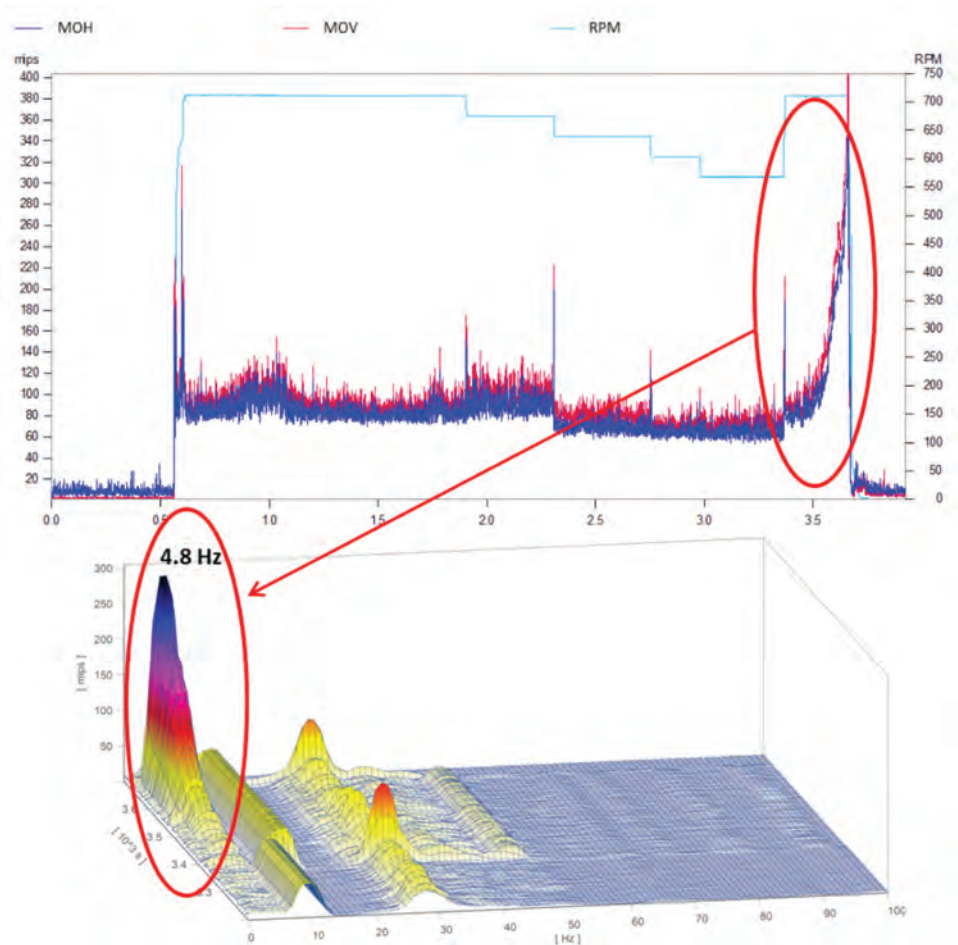


Figure 11-52. Vibration of pump motor.

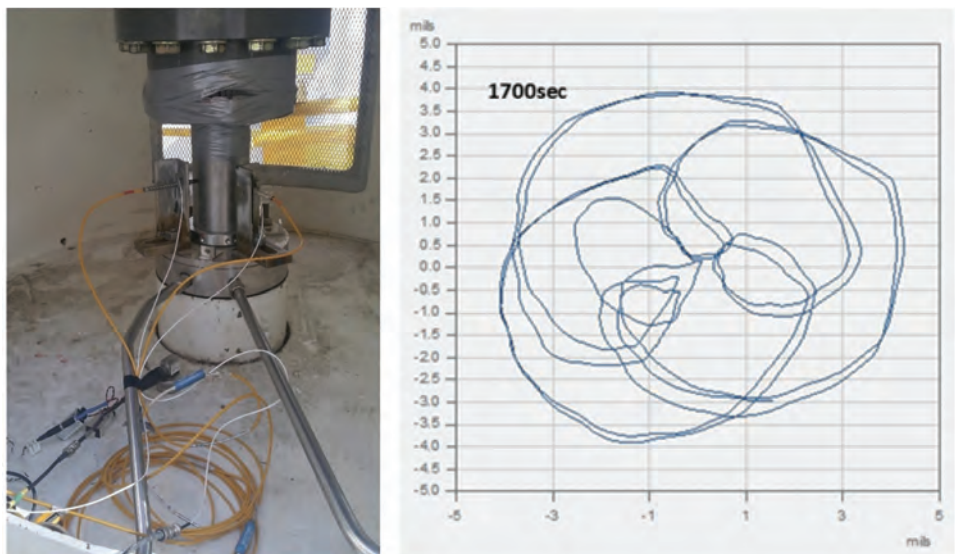


Figure 11-53. Proximity probes and shaft orbit.



Figure 11-54. Replacement groove bearing.

compressor. The fourth case study deals with triplex pumps in parallel with snubbers used on both suction and discharge sides. These case studies were selected in particular to demonstrate the various effects of flow on both transmission and generation of pressure pulsation.

11.9.1 Case Study #1: Single-Source Pulsation

This case study represents pulsation generated by a single throttling valve. Figure 11-55 shows a schematic of a large orifice meter station where a 610-mm-diameter ball valve is used to control the flow through the station and is located 50 m away on the downstream side. Field measurements and pulsation simulation for the station were conducted to assess the associated levels of pulsation at the orifice meter runs. Figure 11-56 shows an example of both results (at node 6 of Fig. 11-55), which seem to be in good agreement in the range of 0–100 Hz. Additionally, both (measured and predicted) data indicate that the level of pulsation is contained below 700 Pa (rms), which amounts to approximately 3.5% to 7.0% of the static differential pressure maintained across the orifice meters.

In order to reduce this level, relocation of the control valve farther downstream of the station was suggested so as to take advantage of pressure wave attenuation. The results

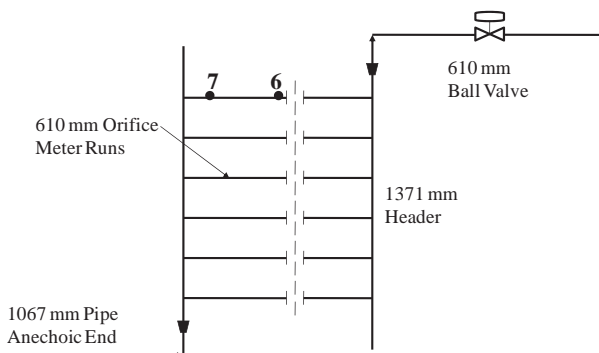


Figure 11-55. Schematic of the meter station of Case Study #1.

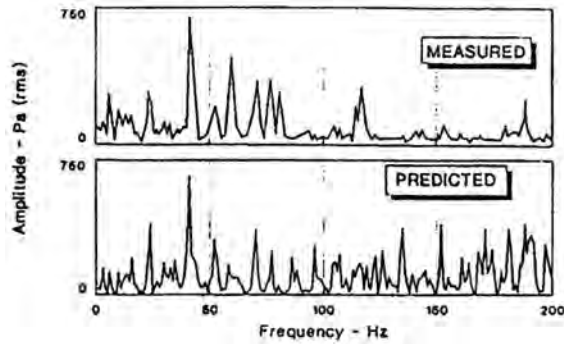


Figure 11-56. Measured and predicted press pulsation at node 6 of Fig. 11-55 before relocating the control valve.

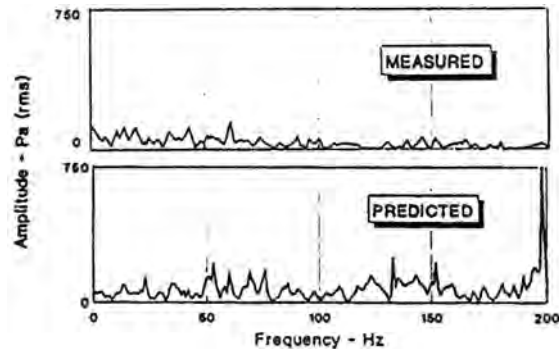


Figure 11-57. Measured and predicted press pulsation at node 6 of Fig. 11-55 before relocating the control valve.

showed that with relocation of the valve 2300 m downstream, pulsation levels would drop down to 200 Pa for the flow conditions encountered. Measurements were taken at the same location (node 6) after the valve was relocated to exactly 2300 m downstream. The measured and predicted results are shown in Fig. 11-57. This case study shows clearly the importance of accounting for flow effects even in modeling the propagation of acoustic waves in constant area pipes.

11.9.2 Case Study #2: Multiple Source Pulsation

Figure 11-58 shows a schematic of a pressure-regulating station consisting of three pressure control valves, namely, 219.1-mm globe valve (top), 323.8-mm globe valve (bottom), and 406.4-mm v-ball valve (middle). The station maximum flow is 50×10^6 m³/day, and differential pressure ranges from 10 to 3800 kPa. At upper limit of the flow, the three valves would be open and, thus, constitute three simultaneous flow-generated pulsation sources. Pulsation monitored at any node in the system would thus be resulting from a vectorial summation (i.e., magnitude and phase) of three pulsation waves generated at each source at any given frequency. At the lowest flow rate, on the other hand, only the 219.1-mm valve would be open, and pulsation seen at any node in the system is single-sourced from that open valve. At intermediate flow rates, two valves can be open fully or partially and, hence, create a double-source system. Three flow conditions systems were thus analyzed. These are:

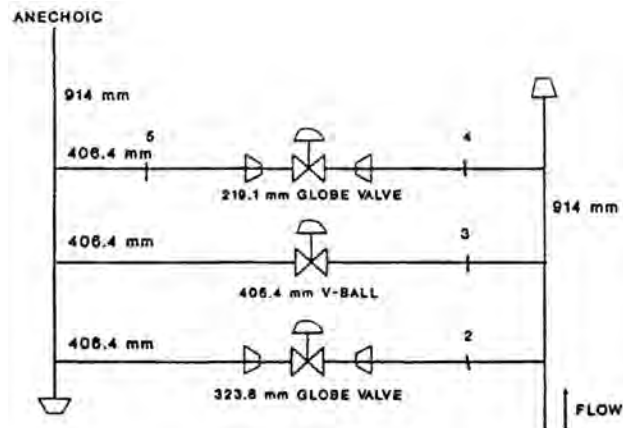


Figure 11-58. Schematic of a pressure regulating station.

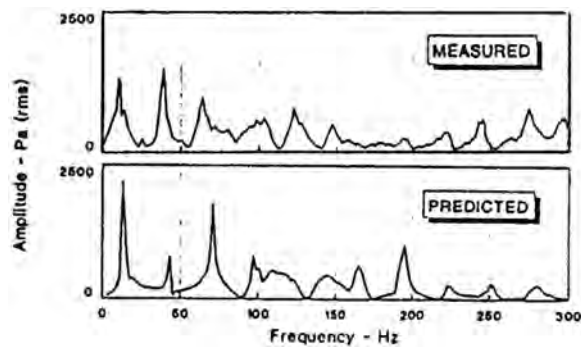


Figure 11-59. Measured and predicted pressure pulsation at node 4 of Fig. 11-58 (only the 219.1-mm valve is open).

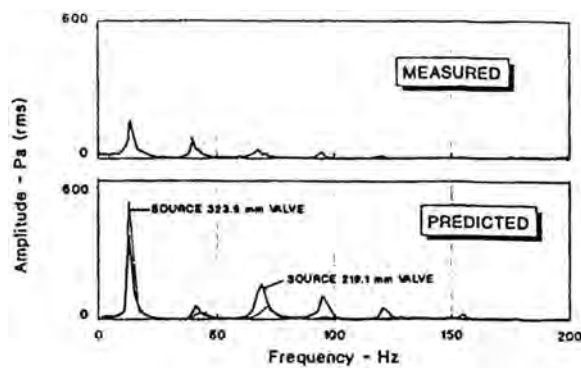


Figure 11-60. Measured and predicted pressure pulsation at node 3 of Fig. 11-58 (both the 219.1 mm and 323.8 mm valves are open).

a) Low-flow case

Here only the 219.1-mm valve was 85% open to allow 9.5×10^6 m³/day flow at 2600 kPa differential pressure. Figure 11-59 shows a comparison of predicted versus measured pulsation at node 4. The agreement of the discrete frequencies is quite remarkable, while the amplitudes are shown to be within +6 dB discrepancy.

b) Intermediate-flow case

In this case, two valves (219.1 mm and 323.8 mm) were fully open to allow 15×10^6 m³/day of flow at 350 kPa differential pressure. Two pulsation sources are recognized, in this case, corresponding to the two valves open. The station was modeled with one source active at a time, and the predicted pulsations at node 3 from each source are plotted in Fig. 11-60. To combine the two results, phase angle information between the two pulsations at this node is needed as function of frequency. This information is not possible to predict. The amplitude, however, should assume a value between two extremes: algebraic addition or subtraction of the levels predicted from each source independently, assuming no acoustic interaction between the two sources. This is indeed the case if one compares the levels of the measured pulsations (overall) to those predicted separately from each source in Fig. 11-60. It is demonstrated here that the measured level lies between the two extremes.

c) High-flow case

The same procedure was followed in analyzing a high-flow case of 50×10^6 m³/day at 60 kPa differential pressure, but with accounting for three simultaneous sources of pulsation related to three open valves. The same findings were also observed, i.e., the measured pulsation lies between two extremes as before.

11.9.3 Case Study #3: Pulsation Generated by a Reciprocating Compressor

A third case study is a reciprocating compressor station. The station consists of two compressor units, 820 kW rating each. Each unit has four double-acting cylinders (203.2 mm bore, 152.4 mm stroke, unloader on the fourth cylinder crank end, speed 600–900 rpm, design flow rate 2163 standard m³/min.). High-level first harmonic pulsation was reported in the suction yard piping and at the scrubber 70 m upstream of the suction pulsation bottles shown in Fig. 11-61. Measurements and simulation of the station suction showed no traces of pulsation at second- and higher-order harmonics indicating that the suction bottles are acoustically efficient for these harmonics but apparently not so for the first. Measurements of pulsation were taken at nodes 1 through 6 of Fig. 11-61 and compared with acoustic simulation at exactly same conditions during the tests. This comparison is shown in Fig. 11-62 for both loaded and unloaded cases at node 5. The illustrated satisfactory agreement between measurements and predictions gave confidence in the modeling variables and allowed subsequent attempts to alleviate the first harmonic pulsation in the yard piping and at the suction scrubber.

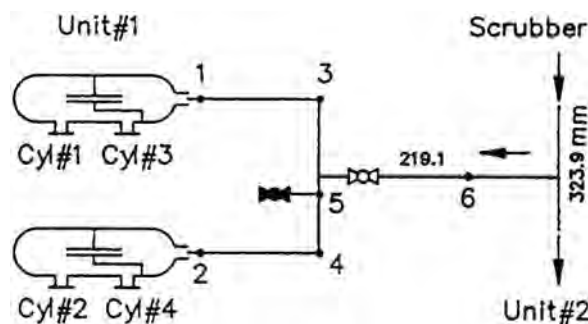


Figure 11-61. Schematic of reciprocating compressor suction piping.

Note: Measured data were acquired without orifice.

A quick and perhaps energy-inefficient method of suppressing this first harmonic pulsation was suggested by placing orifice plates at the two flanges at location 1 and 2 of Fig. 11-61. According to simulation results, 75-mm orifices were sized for enough suppression with reasonable pressure drop and, hence, energy loss in the station suction. This study case is a good example to show the effect of flow on pressure pulsation predictions. If the 75-mm orifices were simulated only acoustically without flow, virtually no suppression was gained and resultant pulsations at node 5 coincide with curves *a* and *c* for both unloaded and loaded conditions, respectively. This is expected because the inertial term in the orifice plate acoustic TM is very small at such low frequency 10–15 Hz (corresponding to first harmonic of 600–900 rpm) [2]. However, when the flow was introduced in the simulation and, hence, an unrecovered pressure drop term is included in the TM, suppression in the order of 7–10 dB was attainable as shown in Fig. 11-62 (curves *b* and *d*). Field observations after placing these 75-mm orifices at locations 1 and 2 indicated remarkable reduction in both pulsation and vibration on the yard piping and at the suction scrubber.

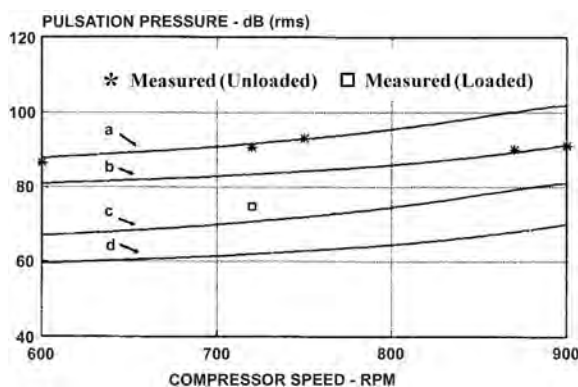


Figure 11-62. First harmonic pulsation pressure in db (reference 1 Pa): a, unloaded condition (without orifice); b, unloaded condition (with 75-mm orifice); c, loaded condition (without orifice); d, loaded condition (with 75-mm orifice).

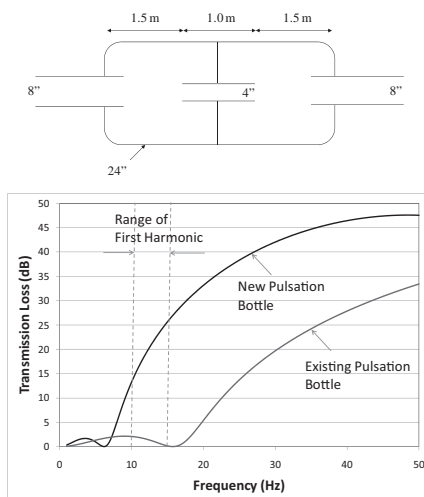


Figure 11-63. Expansion chamber silencer (pulsation bottle) to be located at node 6 of Fig. 11-61 for suppression of first harmonic pulsation.

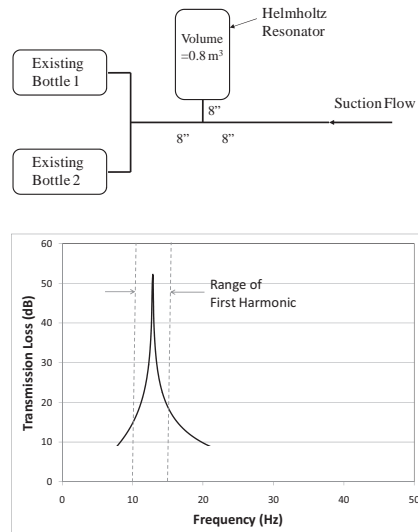


Figure 11-64. Helmholtz resonator to be located at node 6 of Fig. 11-61 for suppression of first harmonic pulsation.

As the orifice plate is an energy-inefficient solution, different silencer techniques were considered to suppress the first harmonic pulsations and to be located at node 6 of Fig. 11-61. The first is of the expansion chamber type with a choke tube joining two chambers. For maximum suppression in the range of 10 to 15 Hz, the size of the silencer would be unreasonably large, and therefore, a compromise is made to reduce the size for still a reasonable suppression. The outcome is the design shown in Fig. 11-63 and the corresponding TL characteristics. Suppression is shown to be in the order of 12 to 25 dB in the first harmonic range. However, the pressure drop of this silencer is comparable to the 75-mm orifice plates. Figure 11-63 shows also the TL characteristic of the existing bottles of Fig. 11-61, which indicate their ineffectiveness in suppressing the first harmonic.

A Helmholtz resonator was also considered, the size of which is shown in Fig. 11-64. Suppression in the order of 17 dB or higher is shown. Notice that the resonator is sized to bring the cusp of the TL characteristic to the middle of the desired frequency range. The pressure drop of this silencer is negligible, but it is like the previous one—rather expensive. The third option, which is less expensive and also offers a negligible pressure drop, is that of a side-branch type, as shown in Fig. 11-65. For a reasonable outer pipe diameter of NPS 14, pulsation suppression of the order of 10 dB and higher is attainable, which is slightly less than the first two options. Notice also the cusp characteristic of the TL plot.

11.10 INSTABILITY CRITERIA OF PRESSURE RELIEF VALVES

Pressure relief valves (PRV) may experience three types of dynamic responses to various flow conditions in the following manner:

- *Cycling*; which is the relatively low frequency (e.g. a few cycles per second to a few seconds per cycle) opening and closing of a relief valve, with relatively small amplitudes.
- *Fluttering*; which occurs when the PRV is open but the dynamics of the system cause abnormal, rapid reciprocating motion of the moveable parts of the PRV.

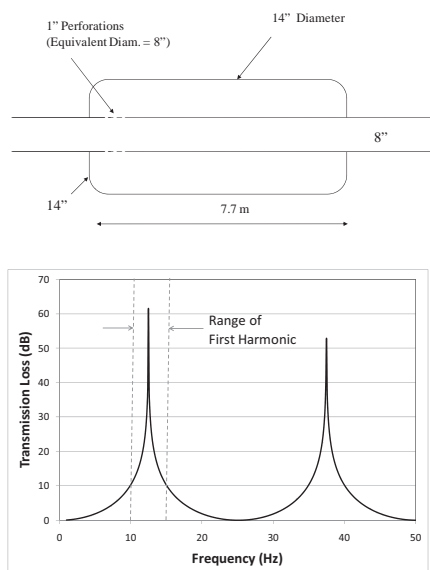


Figure 11-65. Side-branch silencer to be located at node 6 of Fig. 11-61 for suppression of first harmonic pulsation.

During fluttering, the disk does not contact the seat but reciprocates near the natural frequency of the valve.

- *Chattering*; which is a noisy, high-frequency (at the order of the valve's spring/mass system), high-energy oscillation of the valve including persistent impact between the valve and the seat. Spring loaded PRVs and pop-action pilot valves can experience chatter, while modulating pilot-operated or remote sensing pop-action pilot PRVs are less likely to chatter.

All the above instabilities can cause significant mechanical vibrations, and high amplitude upstream pressure waves (especially in liquid systems) that can cause system damage. Furthermore, oscillations can severely restrict the valve's ability to vent at the required flow rate to relieve the over-pressure and may cause wear which compromises pressure-relief events. American petroleum Institute (API 520) standards [47] provides sizing and selection criteria for PRV under steady-state conditions and mention that there can be a number of other factors that may contribute to valve instabilities once it is triggered to open when the system pressure exceeds its set pressure. A typical PRV installation is shown in Fig. 11-66, where the main parameters used in the following instability analysis are indicated. These are:

- V_p, p_r : vessel/reservoir volume and stagnation pressure;
- D_p, A_p, L_p, λ : diameter, cross section area, length and Darcy friction factor of the piping connecting vessel/reservoir to the valve;
- p_e, p_v, p_b : pressure at the pipe inlet ($p_e < p_r$ when valve is open), at the pipe outlet and backpressure (atmospheric or in a relief header), respectively;
- $m_{r,in}, m_{r,out}, m_v$: flow entering the reservoir, flow leaving the reservoir and entering the pipe, and flow through the valve ($m_{r,in} = m_{r,out} = m_v$ in a steady state);
- s, k : spring stiffness and mechanical viscous damping coefficient;
- x_v, x_o : valve lift, valve pre-compression;
- $A_{ft} = Dx_v$: valve discharging area.

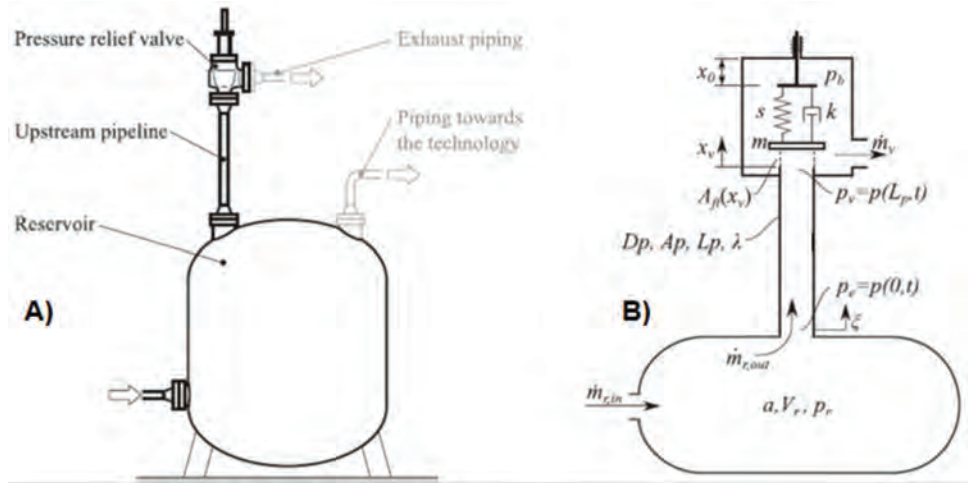


Figure 11-66. Schematic of a PRV connected to a pressure vessel with a riser pipe.

Research and testing indicate that the instability associated with excessive losses in the valve inlet piping during pressure relief may lead to valve cycling, flutter or chattering. The fundamental mechanism of instability triggered by the excessive inlet pressure loss can be explained as follows. Before the valve opens, the pressures at the two ends of the pipe connecting the reservoir to the valve are equal. At the instant at which the valve opens at its set pressure, flow in the pipe builds up, the pressure at the inlet to the PRV valve will then be lower due to the frictional and fittings pressure drop along the pipe leading to the PRV. If this pressure drop is sufficiently high, the valve inlet pressure may fall below the reseating pressure (often called the blowdown pressure, which is typically = 7% of PRV set pressure), the valve will close. At this point, as the vent flow stops, the static pressure builds up again in the pipe above the set pressure level and the valve will open and the whole process is repeated. To avoid this phenomenon, the API-520 [47] recommends limiting the total irreversible pressure drop along the pipe/fittings leading to the PRV to 3% of the set pressure. The rule is based upon the fact that, under steady state conditions, a valve will open at the set pressure and will re-close at the lower reset pressure. The difference between set and re-seating (blowdown) pressure mentioned above. Thus, if the irreversible losses in the piping upstream of the valve, during maximum flow, are always safely lower than 7% of set pressure, (and in the worst scenario equal only to about half of the blowdown), the valve should not re-close and hence would exhibit stable behavior. API 520 makes the exception of this for certain types of thermal relief valves, remotely sensed pilot-operated relief valves and some specific installations.

However, experiments and simulations indicate that inlet pressure loss criterion alone is not sufficient to predict PRV stability, [48–55], because the 3% rule is based on steady state flow conditions. In contrast, valve chatter is typically a high frequency (dynamic) phenomenon, and so is the dynamic response of the valve. These two effects are both a result of the dynamic forces, and the steady state 3% criterion does not reflect these complex non-linear interactions. API 520 acknowledges as well that limiting the inlet pressure drop to a specific value may not be enough to guarantee PRV stability. Thus, the PRV inlet pressure loss criterion has evolved over the years. For decades many companies have accepted PRV inlet losses up to 5% when determining whether modifications to existing installations were warranted. Testing has shown that in many cases PRVs did not chatter when inlet losses exceeded 3% of set pressure while in some tests PRVs chattered when inlet pressure losses were less than 3% [49,55].

Another cause for PRV instabilities is attributed to induced acoustic waves that travel up the pipe and reflect back at the other end. These acoustic waves are always generated during the sudden opening/closure of the PRV, and the resulting pressure oscillations can affect valve stabilities. The valve disc interacts with these acoustic waves which depends, to a large degree, on the degree of the valve opening when it interacts with the reflected wave. If the reflected wave travels long enough that it reaches the valve when it is already fully open, (i.e. if time of the valve opening is shorter than the time needed by the reflected wave to travel back to the valve), the pressure effect of the wave is strong and there is a probability of inducing valve instabilities. However, if the pressure wave returns quickly enough so the valve is still not fully open, then the acoustic effect is weaker and the valve may remain stable. Frommann [51] analyzed the valve chatter induced by pressure waves and concluded that if the valve inlet line is short enough to satisfy 3% pressure loss criterion, the wave will return to the valve before it is fully open, thus the pressure wave effect will be small and can be neglected. Hos et al. [48], on the other hand, proposed that the pressure drop due the reflected acoustic wave should be added to the frictional static losses, and the sum of the static and acoustic losses should be less than 3% of set pressure. The approach given by Darby [52] and developed later by Melhem [49,50] seems to reflect the best API recommendations, which is given below.

Following Darby's [52] and Melhem's [49,50] models of the pressure balance in the valve inlet line, the following criterion is arrived at to prevent PRV instability:

$$p_r - p_{wave} - p_{fr,w} - p_b > p_{close} \quad (11-107)$$

where;

p_{wave} is the pressure drop due to the acoustic wave, $p_{fr,w}$ is the pressure drop due to steady flow irreversible pressure drop and a contribution from the induced acoustic wave, and p_{close} is the pressure at which the valve will close. Expressing reservoir pressure p_r and closing pressure p_{close} as % of the set pressure, the following force balance should be satisfied for a stable operation of a conventional spring loaded PRV:

$$1 + \frac{\%OP}{100} \div p_{set} - p_{wave} - p_{fr,w} - p_b > 1 + \frac{\%BD}{100} \div p_{set} \quad (11-108)$$

or:

$$100 \frac{p_b + p_{wave} + p_{fr,w}}{p_{set}} \div < (\%OP + \%BD) \quad (11-109)$$

where;

$\%OP$, is the over pressure percent at the full open position of the valve, and $\%BD$, is the blowdown percent, both with respect to the set pressure. The following equation is used to determine p_{wave} [48,54]:

$$p_{wave} = \frac{c_o m_v}{A_p} \delta + \frac{m_v^2}{2\rho_o A_p^2} \delta^2 \quad ; \quad \delta = \min \left[1, \frac{t_w}{t_v} \right] \quad (11-110)$$

and;

$$t_w = \frac{2L_p}{c_o} \quad ; \quad t_v = 15 + 20 \frac{\sqrt{2D_v}}{(p_{set}/p_{atm})^{2/3} (1 - p_{atm}/p_{set})^2} \frac{x}{x_{max}} \div \quad (11-111)$$

where;

t_w : wave travel time
 t_v : valve open time (in millisecond)
 L_p : pipe length
 c_o : fluid speed of sound in the pipe
 D_v : valve throat diameter (inches)
 m_v : vent flow rate through the PRV
 ρ_o : fluid density
 x : valve disc actual position
 x_{max} : valve disc maximum position

The following equation is used to determine $p_{fr,w}$:

$$p_{fr,w} = \lambda L_p / D_p \frac{m^2}{2\rho_o A_p^2} \delta^2 \quad (11-112)$$

It is evident that both the pressure drops, from the acoustic reflected wave and due friction, decrease as the length L_p of the valve inlet piping decreases and as its cross-section area p increases.

Finally, the acoustic analysis may not be warranted for the following services because these are lower risk applications [49]:

- Any pilot-operated PRV with a remote sense line connected to the protected equipment because the valve's opening response will be independent of the pressure in the PRV inlet.
- Any modulating pilot-operated relief valve because the response speed of a modulating pilot valve is sufficiently slow to allow for the pressure wave to reflect back in time which would keep the PRV open.
- Thermal relief valves where the relief load is very small and transient.

Table 11-5. Example of PRV stability calculations

PRV Data:			
Set pressure	p_set	3545	kPa-a
Atmospheric pressure	P_atm	100	kPa-a
valve actual lift (0.9 or 1 of x_max)	x	10	mm
valve max lift	x_max	10	mm
sound speed	co	644	m/s
density @ 10% overpressure	ρ	526	kg/m ³
density @ upstream vessel condition	ρ_o	469	kg/m ³
inlet pipe length	Lp	15.862	m
inlet pipe diameter	Dp	0.0779	m
Inlet valve throat diameter	Dv	0.5	in
mass flow rate @ 10% overpressure	m	4.8	kg/s
Back pressure @ relieving conditions	Pb	200	kPa-a
Darcy friction factor		0.012	—
%OP		10	%
%BD		7	%
Calculations:			
t_v		16.962	ms
t_w		49.261	ms
δ		1	
p_{wave}		519.57	kPa
$p_{fr,w}$		2.64	kPa
LHS (Eq. 11-109)		19.81	%
RHS (Eq. 11-109)		17	%

Table 11-5 gives an example calculation on a specific PRV installed on a riser of a given dimension. In this example the valve will be prone to instability for the specified conditions since the L.H.S. > R.H.S. Note that the frictional pressure drop is well below the 3% rule, yet the PRV will be prone to acoustic instability.

REFERENCES

- [1] Bruggeman, J. C., Hirschberg, A., van Dongen, M. E. H., and Goiter, J., 1991. "Self-Sustained Aero-Acoustic Pulsations in Gas Transport Systems: Experimental Study of the Influence of Closed Side Branches," *J. Sound and Vibration*, **150**(3), pp. 371–393.
- [2] Botros, K. K., Jungowski, W. M., Studzinski, W., and Szabo, J. L., 1986. "Pressure Pulsations at Orifice Plates and General Pipeline Flow—Acoustic Simulator," *1986 International Gas Research Conference*, September 8–11, 1986, Toronto, Ontario.
- [3] Jungowski, W. M., Botros, K. K., Studzinski, W., and Szabo, J. L., 1986. "Measuring the Transmission Characteristics of Pulsating Flows Through Orifice Plates and a Ball Valve," *Measuring and Metering of Unsteady Flows - FED-40*, ASME.
- [4] Jungowski, W. M., Botros, K. K., and Studzinski, W., 1987. "Generation and Transmission of Pressure Pulsations at the Ball Valve," *Noise-Co*, n. 87, The Pennsylvania State University, Pennsylvania, June 8–10, 1987.
- [5] Jungowski, W. M., Botros, K. K., Studzinski, W., and Berg, D. H., 1987. "Tone Generation by Flow Past Confined Deep Cylindrical Cavities," *AIAA 11th Aeroacoustics Conference*, October 19–21, 1987, Palo Alto, California.
- [6] Botros, K. K., Jungowski, W. M., and Studzinski, W., 1988. *On the Transfer Matrix of Orifice Plate with Flow*, Noise-Con 88, Purdue University, West Lafayette, Indiana, June 20–22, 1988.
- [7] Botros, K. K., Jungowski, W. M., Studzinski, W., and MacLeod, J., 1988. "Influence of Flow in Pulsation Simulation of Gas Pipeline Installations," *Proceedings of Gas and Liquid Pulsations in Piping Systems—Prediction and Control*, Institute of Mechanical Engineers, London, UK, December 1–2, 1988.
- [8] Jungowski, W. M., Botros, K. K., and Studzinski, W., 1989. "Cylindrical Side-Branch as Tone Generator," *J. Sound and Vibration*, **131**, pp. 265–285.
- [9] Jungowski, W., Studzinski, W., Szabo, J. L., 1990. "Orifice Meter Performance Under Pulsating Flow Conditions," *2nd International Symposium on Fluid Flow Measurement*, Calgary, Alberta, Canada, June 6–8, 1990.
- [10] Jungowski, W., and Petela, G., "Simulation of the Orifice Gauge Line Effect in Pulsating Flow," *Canadian Acoustical Association Conference*, Edmonton, Alberta, Canada, October 9–10, 1991.
- [11] Botros, K. K., 1992. "Transfer Matrices for Piping Elements With Flow," *Second International Congress on Recent Development in Air & Structure-Borne Sound and Vibration*, Auburn University, Auburn, Alabama, March 4–6, 1992.
- [12] Kiel, D. E. and Foy, C. E., 1993. "Tone Generation in Stepped Side Branches," *International Conference on Noise and Vibration Control*, St. Petersburg, Russia, May 31–June 3, 1993.
- [13] Botros, K. K., Jungowski, W. M., and Petela, G., 1992. "Gauge Line Effects and DP Transmitter Response to Flow Pulsation Through Orifice Plate," *Journal of Flow Measurement and Instrumentation*, **3**(3), pp. 130–144, July 1992.
- [14] Foy, C., Kiel, D., Jungowski, W. M., 1993. "The Effect of Pressure Pulsation and Pilot Setting on the Performance of Pressure Relief Valves," *Society of Petroleum Engineers, 1993 Eastern Regional Conference Exhibition*, November 2–4, 1993, Pittsburgh, PA.
- [15] Jungowski, W. M., and Petela, G., 1994. "Excessive Noise Preventor," *Inter-Noise 94*, The 1994 International Congress on Noise Control Engineering, Yokohama, Japan, August 29–31, 1994.
- [16] Cummings, A., and Chang, I. J., 1986. "The Transmission of Intense Transient and Multiple Frequency Sound Waves Through Orifice Plates with Mean Flow," *Rev. Phys. Appl.*, **21**, pp. 151–161.

- [17] Parrott, T., 1973. "Improved Method for Design of Expansion Chamber Mufflers with Application to an Operation Helicopter," *NASA-TND*, p. 7309.
- [18] Lambert, R. F., and Steinbrueck, E. A., 1980. "Acoustic Synthesis of a Flowduct Area Discontinuity," *J. Acoust. Soc. Am.*, **67**(1), pp. 59–64.
- [19] PULS User Manual, *NOVA Corporation of Alberta, Design Engineering*, Calgary, Alberta, Canada, May, 1992.
- [20] Shri Kant Munjal, M. L., and Prassana Rao, D. L., 1974. "Waves in Branched Hydraulic Pipes," *J. Sound Vib.*, **37**(4), pp. 507–519.
- [21] Pierce, A. D., 1981. *Acoustics—An Introduction to its physical principles and applications*, McGraw-Hill, New York, Section 10-5.
- [22] Chen, Y. N., 1967. "Calculation of Gas Vibrations Due To Simultaneous Excitations in Reciprocating Compressor Piping Systems With Allowance For Frictional Effect and Temperature Change in the Flow," *J. Sound Vib.*, **5**(2), pp. 215–256.
- [23] Ingard, V., and Singhal, V. K., 1974. "Sound Attenuation in Turbulent Pipe Flow," *J. Acoust. Soc. Am.*, **55**(3), pp. 535–538.
- [24] To, C. W. S., and Doige, A. G., 1979. "A Transient Testing Technique for the Determination of Matrix Parameters of Acoustic Systems," *J. Sound & Vib.*, **62**, pp. 207–233.
- [25] Lung, T. Y., and Doige, A. G., 1983. "A Time-Averaging Transient Testing Method for Acoustic Properties of Piping Systems and Mufflers with Flow," *J. Acoust. Soc. Am.*, **73**(3), pp. 867–876.
- [26] Doige, A. G., Munjal, M. L., and Alves, H. S., 1988. "An Improved Experimental Method for Determining Transfer Matrices of Pipeline Elements with Flow," *Noise-CON 88*, Purdue University, West Lafayette, Indiana, pp. 481–486, June 20–22, 1988.
- [27] Miles, J. H., 1981. "Acoustic Transmission Matrix of a Variable Area Duct or Nozzle Carrying a Compressible Subsonic Flow," *J. Acoust. Soc. Am.*, **69**(6), pp. 1577–1586, June 1981.
- [28] Botros, K. K., 1992. "Transfer Matrices For Piping Elements With Flow," *Second International Congress on Recent Development in Air- & Structure-Borne Sound and Vibration*, Auburn University, Auburn, Alabama, March 4–6, 1992.
- [29] Botros, K. K., and Rinawi, K., 1996. "Acoustic Transfer Matrix For Tee Elements With Flow," 1996 ASME Fluids Engineering Division Summer Meeting, San Diego, California, FED-237, pp. 395–400, July 7–11, 1996.
- [30] Rockwell, D., and Naudascher, E., 1978. "Review—Self Sustaining Oscillations of Flow Past Cavities," *Journal of Fluids Eng.*, **100**, pp. 152–165.
- [31] Rogers, L. E., 1992. "Design Stage Acoustic Analysis of Natural Gas Piping Systems in Centrifugal Compressor Stations," *J. Eng. Gas Turbines and Power*, **114**, pp. 727–736, October, 1992.
- [32] Rogers, L. E., 1992. "Coupling the Effects of Reciprocating Compressor Valve Dynamics with Piping Acoustic Response," *1992 International Compressor Engineering Conference at Purdue University*, July 14–17, 1992.
- [33] Jungowski, W. M., Weiss, M. H., and Price, G. R., 1994. "Pressure Oscillations Occurring in a Centrifugal Compressor System With and Without Passive and Active Surge Control," *39th International Gas Turbine & Aeroengine Congress & Exposition*, Turbo-Expo, The Hague, Netherlands, June 13–16, 1994.
- [34] Munjal, M. L., 1987. *Acoustics of Ducts and Mufflers*, Wiley, New York.
- [35] Beranek, L. L., 1971. *Noise & Vibration Control*, McGraw-Hill, Chapter 6, 1971.
- [36] Jungowski, W. M., and Studzinski, W., 1989. "Damping Pressure Pulsations in Piping Systems," U.S. Patent Number 4,867,190, September 19, 1989.
- [37] Jungowski, W. M., Selcrowicz, W. C., 1981. "Noise Control Engineering," **17**, p. 86.
- [38] Control Components Inc., 22591 Avenida Empresa, Rancho Santa Margarita, California, 92688.
- [39] American Air Filter, P.O. Box 35690, Louisville, Kentucky 40232–5690.
- [40] Jungowski, W. M., Petela, G., 1985. "Excessive Noise Preventor," *Internoise'94*, Yokohama, Japan, Aug. 29–31, 1994.

- [41] Munjal, M. L., Krishnan, S., and Reddy, M. M., 1993. “Flow-Acoustic Performance of Perforated Element Mufflers with Application to Design,” *Noise Control Engineering Journal*, **40**(1), pp. 159–167, Jan.–Feb., 1993.
- [42] Reciprocating Compressors for Petroleum, Chemical, and Gas Industry Services API Standard 618, Fifth edition, American Petroleum Institute, 1220 L Street, Northwest Washington, D.C. 2005.
- [43] Positive Displacement Pumps-Reciprocating, API STANDARD 674, second edition, June 1995, American Petroleum Institute, 1220 L Street, Northwest, Washington, D.C. 20005.
- [44] GMRC Guideline for High-Speed Reciprocating Compressor Packages for Natural Gas Storage and Transmission Applications, October 2013.
- [45] API 688, 2012. “Pulsation and Vibration Control in Positive Displacement Machinery Systems for Petroleum, Petrochemical, and Natural Gas Industry Services.”
- [46] ANSI/HI 9.6.8, 2014. “Rotodynamic Pumps—Guideline for Dynamics of Pumping Machinery,” 2014 Edition, January 1, 2014.
- [47] American Petroleum Institute API 520, 2014. “Sizing, Selection, and Installation of Pressure-Relieving Devices, Part I - Sizing and Selection,” Ninth Edition, (2014).
- [48] Hos, C. J., et al., 2017. “Dynamic Behaviour of Direct Spring Loaded Pressure Relief Valves Connected to Inlet Piping: IV Review and Recommendations,” *Journal of Loss Prevention in the Process Industries*, **48** (2017), pp. 270–288.
- [49] Melhem, G. A., 2014. “PRV Stability,” *Joint US and European DIERS Users Group Meeting*, June 11, Hamburg, An ioMosaic Corporation White Paper, July 24, 2014.
- [50] Melhem, G. A., 2014. “Analysis of PRV stability in relief systems: part II-screening,” An ioMosaic Corporation White Paper, July 24, 2014.
- [51] Frommann, O. and Friedel, L., 1998. “Analysis of Safety Relief Valve Chatter Induced by Pressure Waves in Gas Flow,” *Journal of Loss Prevention in the Process Industries*, **11** (1998), pp. 279–290.
- [52] Darby, R., 2013. “The Dynamic Response of Pressure Relief Valves in Vapor Or Gas Service, Part I: Mathematical Model,” *Journal of Loss Prevention in the Process Industries*, **26** (2013), pp. 279–290.
- [53] Hos, C. J., et al., 2015. “Dynamic Behaviour of Direct Spring Loaded Pressure Relief Valves in Gas Service: II Reduced Order Modelling,” *Journal of Loss Prevention in the Process Industries*, **36**, (2015), pp. 1–12.
- [54] Cremers, J. et al., 2001. “Validated Sizing Rule Against Chatter of Relief Valves During Gas Service,” *Journal of Loss Prevention in the Process Industries*, **14**, 2001, pp. 261–267
- [55] Izuchi, H., 2011. “Chatter of safety Valve,” PLE Technology Center, Chiyoda Advanced Solutions Corp., Japan, Nov. 2011.

MECHANICAL ANALYSIS

12.1 INTRODUCTION TO MECHANICAL ANALYSIS

Mechanical analysis entails a number of common and related aspects of pumping and compression as they relate to rotating equipment, both drivers and driven equipment, and its interaction with attached piping systems. The various combinations of driver and driven equipment pose unique problems with respect to their rotordynamics that have to be recognized and mitigated by the designer. These include both lateral and torsional rotordynamic effects. In addition, the pumping or compression process may impact the associated piping system, or conversely, the rotating equipment can be adversely affected by piping design. All of these factors, therefore, are important for both the designer and operations and maintenance.

12.2 BASIC ASPECTS OF VIBRATION

12.2.1 General

Vibration is defined as the periodic movement of a body about an equilibrium position. Vibration amplitude is a function of an applied force and the stiffness (or flexibility) at a given frequency:

$$\text{Vibration} = \frac{\text{Dynamic Force}}{\text{Dynamic Stiffness}} = \text{Dynamic Force} \times \text{Dynamic Flexibility} \quad (12-1)$$

In controlling vibration, both aspects of the vibration equation must be considered. To explain vibration, and the units it can be measured in, consider a spring-mass system. The following comments refer to Fig. 12-1.

- A block hanging on a spring will stretch the spring until the upward force of the spring equals the weight of the block.
- If the block is displaced down a distance (e.g., 1.5 in.) and released, the spring will pull the block back to its original position. Momentum will cause the block to continue traveling upwards the same distance (i.e., 1.5 in.) from the original position, where it will stop and start moving back down.
- The time the system takes to complete one full oscillation is the period of oscillation. The number of periods per unit of time is the frequency of the vibration. Typical units of frequency are cycles per minute and cycles per second, which is also known as hertz (Hz).
- In terms of displacement, the peak-to-peak vibration amplitude (or range of motion) is the distance traveled by the block from the highest to lowest position. The peak amplitude of the vibration is the peak to peak distance divided by two. Displacement

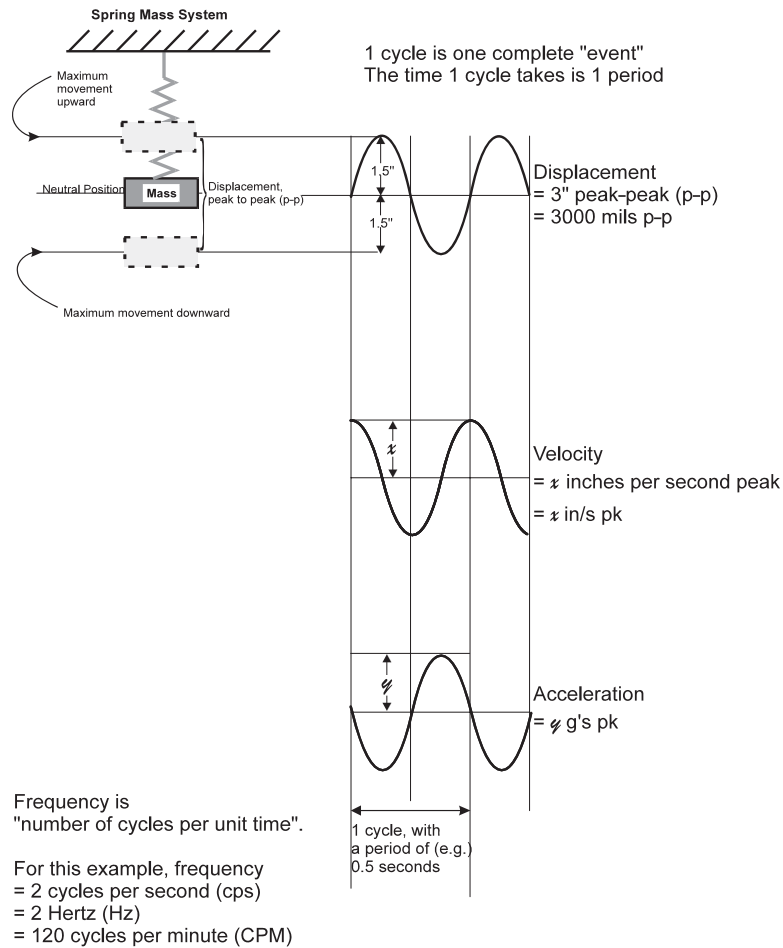


Figure 12-1. Vibration basics (courtesy of Wood.).

amplitudes are typically recorded in mils (1 mil = 1/1000 in.) and must also be defined as peak or peak-to-peak.

- Vibration velocity is the rate at which the block moves. The velocity of the block is maximum when the block passes through the equilibrium position. The velocity is zero when the block is at the highest or lowest displacement. Velocity amplitudes are typically recorded in inches per second (ips) peak.
- Acceleration is the rate of change of the velocity of the block. The acceleration of the block is maximum when the velocity is zero and the block is at the highest or lowest displacement. The block acceleration is zero when the velocity is maximum, and the block passes through the equilibrium position. Typical acceleration amplitudes are recorded in g's peak (where 1 g = 386 ips²).

Vibration measurements can be converted from acceleration, velocity, and displacement, as shown on the graph in Fig. 12-2. It also clarifies that each type of vibration measurement is effective for a range of frequencies.

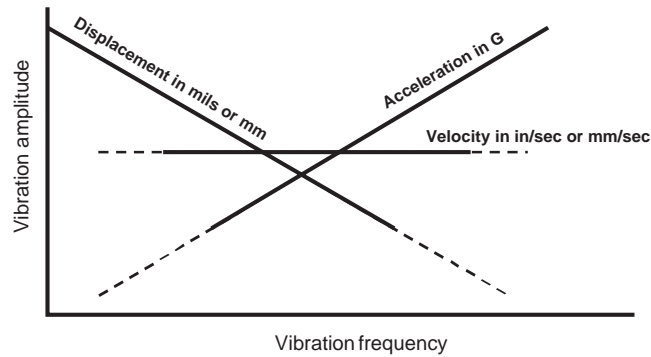


Figure 12-2. Vibration measurement comparison.

12.2.2 Mechanical Natural Frequency and Resonance

The mechanical natural frequency (MNF) of a component is the frequency at which the component vibrates the most in response to a given force. For example, a spring-mass system will oscillate at its natural frequency if the weight is pulled down and then released.

All components or groups of components (piping, pulsation bottles, scrubbers, cylinders, relief valves, etc.) in an installation will have several mechanical natural frequencies. The mechanical natural frequencies of a pipe or piping system depend on lengths, schedules, diameters, elbows, supports, etc. Likewise, the rotor in rotating equipment will exhibit natural frequencies.

A MNF plot shows the frequency at which maximum dynamic flexibility (or minimum dynamic stiffness) occurs in the system. Modifications to the system will shift that peak: increasing mass or decreasing stiffness shifts the peak to the left and increasing stiffness or decreasing mass shifts it to the right.

Mechanical resonance of a component occurs when a forcing function is applied at a frequency coincident with a MNF of the component. When a system, or part of a system, is mechanically resonant, normal (or even low) unbalanced force levels can couple with the system geometry to produce very high vibration levels. Figure 12-3 illustrates the correspondence of forcing frequencies with mechanical frequencies for a fixed speed machine.

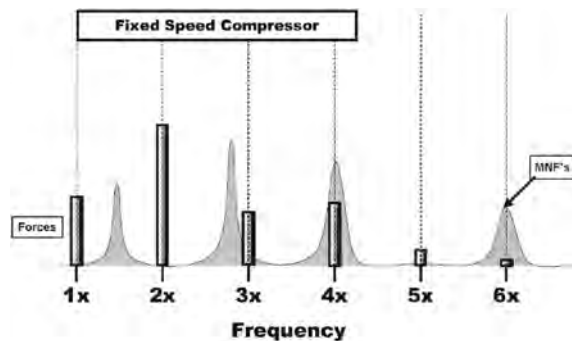


Figure 12-3. Resonance for fixed-speed machine (courtesy of Wood.).

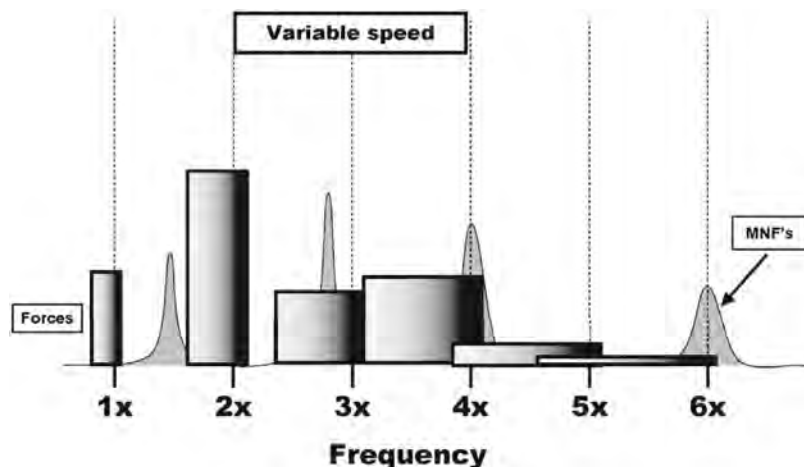


Figure 12-4. Resonance for variable speed machine (courtesy of Wood.).

If an oscillating force of constant amplitude is applied to a system over a range of frequencies, the resulting vibrations of the system will vary. Response will be high at frequencies where the system is flexible and low elsewhere. As seen in Fig. 12-4, this increases the potential overlap and likelihood of resonance.

The shape and the magnitude of the response peak at resonance is a function of the structural damping, or resistance, in the system. The more damping in the system, the broader and lower the peak will be. Structural damping comes from flanged and bolted connections, clamping, material characteristics, etc. In the case of a rotor shaft, it will depend on the flexibility of the shaft.

Unacceptable vibration in a compressor installation at a particular frequency can be the result of high forces, low dynamic stiffness, or a combination of the two. Some common causes of high vibration are the following:

- pressure pulsation-induced unbalanced forces
- unbalanced forces and moments caused by reciprocating parts
- crosshead forces caused by gas pressures and reciprocating inertia
- cylinder stretch (i.e., elongation and shortening of the cylinder assembly due to internal gas forces)
- misalignment between the driver and compressor
- mechanical resonance
- pipe strain (bolt-up)
- thermal strain
- low damping

12.3 MECHANICAL ANALYSIS OF ROTATING EQUIPMENT

12.3.1 General

The reliability of rotating equipment is to a significant extent dependent on managing rotor-dynamics and its interaction with associated components. Much careful engineering goes into the design of drivers and driven equipment to meet requirements specified in industry accepted standards, largely those produced by the American Petroleum Institute (API). An

invaluable aid in understanding rotordynamics aspects of these standards is provided in API 684 [1].

Rotordynamics can be divided into two types: lateral and torsional. Lateral rotordynamics deals with vibration of rotors as measured in the axial and radial directions. Torsional vibration (TV) occurs when there are fluctuations in the rotation of the shaft. Stability refers to the degree in which excitations are dampened, and its analysis is now an important aspect of rotordynamic design considerations.

12.3.2 Lateral Rotordynamics

The primary excitation mechanism for shafts, rotors and couplings in general is the unbalance that always exists to some degree, usually depending on how well they have been balanced during manufacture or maintenance rework. It is, however, not the only source and other mechanisms have to be considered such as:

- misaligned couplings
- improperly installed bearings
- rubs between stationary and rotating components such as seals
- impeller aerodynamics or fouling
- aerodynamic cross-coupling with various types of seals
- electrical forces such as those produced by a Variable Frequency Drive (VFD).

For a real physical system, the simple model of a mass and spring as described earlier has to be enhanced with damping to derive its response. The damped natural frequency is then defined as

$$\omega_d = \sqrt{\frac{k}{m} - \frac{c^2}{4m^2}} \quad (12-2)$$

where:

- ω_d = damped natural frequency of oscillation [rad/s]
- k = stiffness of the elastic element [N/m (lb_f/in)]
- m = mass [kg (lb_m)]
- c = viscous damping coefficient [Ns/m (lb_fs/in)]

For a typical rotor, the force $F(t)$ in N (lbs_f) will be sinusoidal as described by the equation

$$F(t) = A \sin(\omega t) \quad (12-3)$$

and the response will be

$$x(t) = B \sin(\omega t + \theta) \quad (12-4)$$

where

x = displacement [m (in)]

$\frac{B}{A}$ = amplitude ratio

θ = phase angle [rad]

The unbalance force F_U in N (lbs_f) is calculated as

$$F_U = me_u \omega^2 \quad (12-5)$$

The result, which is called a forced response analysis, is shown in Fig. 12-5. Figure 12-5(a) graphs the amplitude ratio against speed (frequency) for different amounts of damping. The maximum amplitude ratio occurs at the natural frequency of the system. The phase difference between the excitation and response can be seen in Fig. 12-5(b). It depends on the degree of damping and shows a phase shift at the natural frequency.

A simplified model of a rotor and bearings is shown in Fig. 12-6. A single rotating mass is supported by a shaft on two identical bearings, each with stiffness and damping. The effective stiffness of the combined rotor and supports will be less than that of the most flexible element. Its response for various degrees of shaft stiffness can be seen in Fig. 12-7. As the shaft stiffness increases, the natural frequency decreases and its amplitude becomes greater. This is because the increase in shaft flexibility decreases the displacement of the shaft in the bearings and thus reduces the damping provided by the bearings. The conclusion is that greater shaft stiffness enhances the damping capability of the bearing.

Real turbomachinery is obviously much more complicated to model, but the basic principles are still followed. This is done by reducing the rotor to a set of lumped masses connected by elastic springs. The supports feature elastic and viscous elements that correspond to the types of bearings and seals being used. Detailed discussion of the modeling

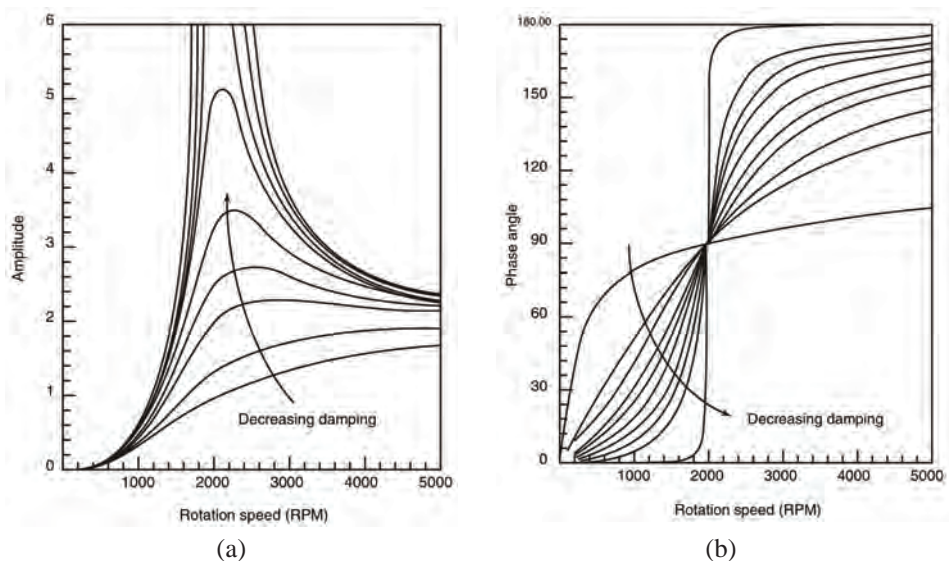


Figure 12-5. Basic rotor response curves. (a) Amplitude ratio versus rotating speed. (b) Phase angle versus rotating speed [1].

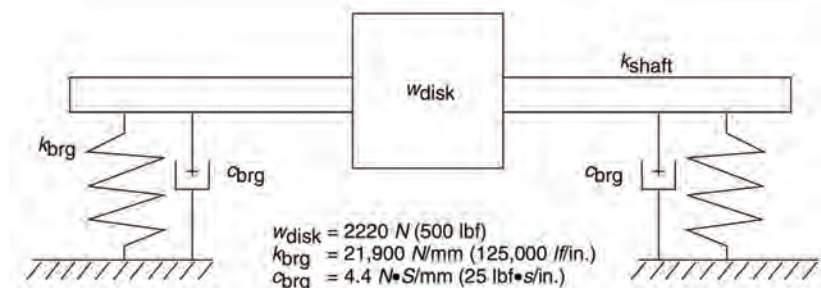


Figure 12-6. Simple model of a rotor and bearings with stiffness and damping [1].

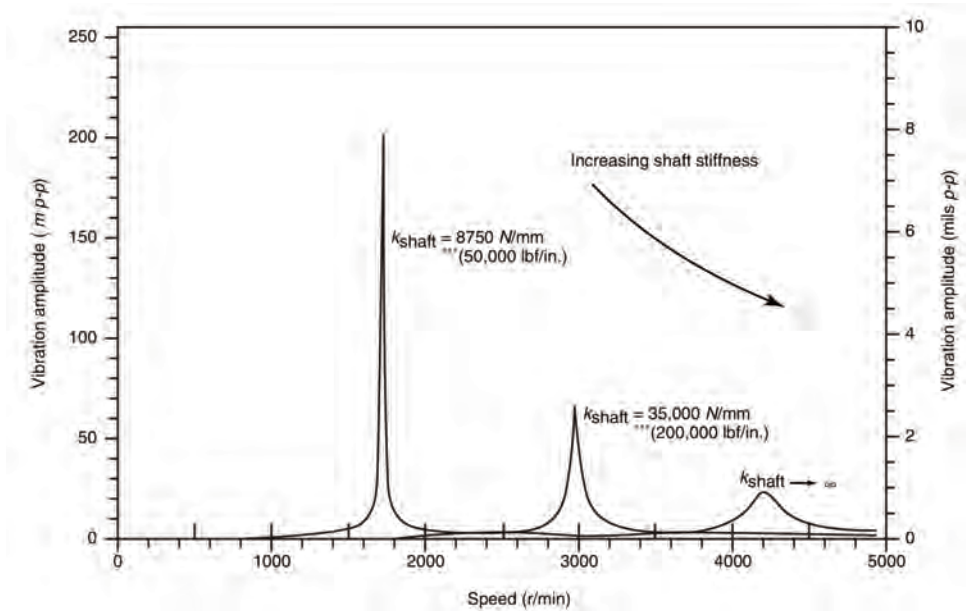


Figure 12-7. Response of simple beam machine for different shaft stiffnesses [1].

required for real rotors, bearings, and seals is provided in Section 2 of API 684 [1] with extensive references.

The mode shapes of a shaft will depend on the stiffness of the bearing supports. If the shaft is relatively stiff relative to the bearing supports, as is the case with shorter and more rigid shafts, the mode shapes are as shown in Fig. 12-8(a). With stiffer bearing supports and a flexible shaft, such as found in longer rotors and trains, the shaft modes are as seen in Fig. 12-8(b).

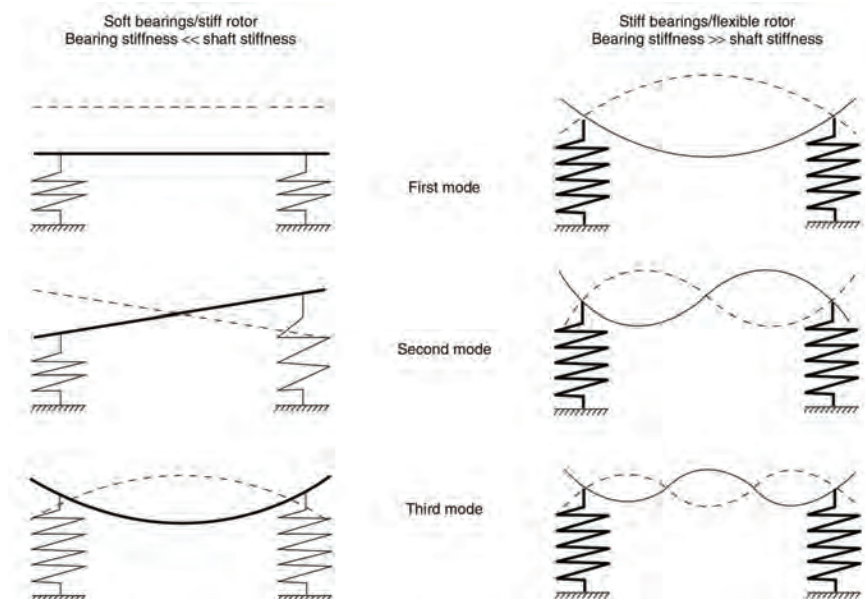


Figure 12-8. Rotor mode shapes. (a) Stiff rotor. (b) Flexible rotor [1].

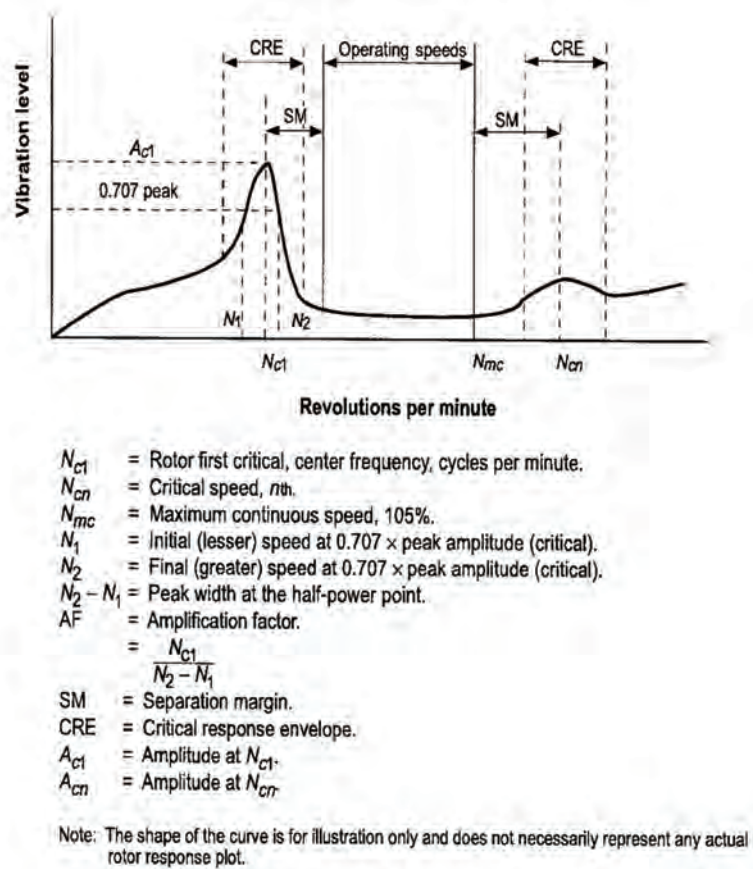


Figure 12-9. General guidelines for measuring rotor response over the operating range [4].

In order to establish whether a design can meet expected vibration levels, a damped response analysis has to be carried out. This is done to ensure that:

- there is an adequate separation margin between critical and operating speeds;
- vibration limits are not exceeded at the maximum allowable residual unbalance; and
- rubbing will not take place up to the limit of the probe vibration.

Figure 12-9 illustrates the response curve normally specified in standards with vibration levels from an operating point of view from startup to maximum allowable speed.

12.3.3 Stability

If a transient or momentary force is applied to the system, it decays over time depending on the amount of damping [see Fig. 12-10(a)]. In this case, the system is stable. In other cases, the response curve increases with time, and the system is unstable as can be seen in Fig. 12-10(b). The type of evaluation is referred to as stability analysis or a damped natural frequency or Eigenvalue analysis. It has now become a standard type of analysis carried out for turbomachinery.

Stability problems with sub-synchronous vibration as larger, high-speed turbomachinery was put into service in the 1960s and 1970s initiated the search for methods to evaluate stability [2]. The complexity is due to the need to include many degrees of freedom and to

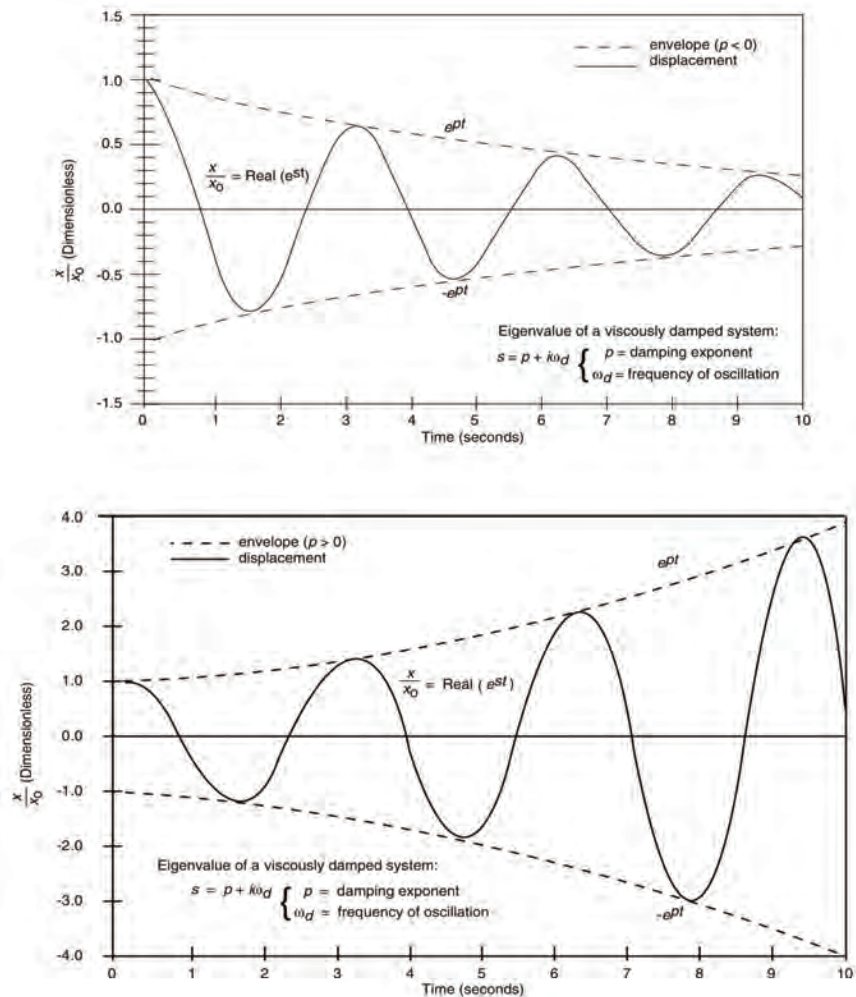


Figure 12-10. Rotor vibration curves for a transient excitation. (a) Stable system. (b) Unstable system [1].

properly model the stiffness and damping coefficients of supports, different types of bearings and seals, aerodynamic forces from impellers, and other factors. Much progress has been made aided by computer-based modeling but controversial issues still remain. A detailed overview of stability analysis is available in Section 3 of API 684 [1]. Recent examples of instability problems with centrifugal compressors can be found in Wilcox and O'Brien [3].

Standards (e.g., API Standard 617 [4]) divide stability analysis into two components: a simplified Level 1 to screen out machines that are clearly far away from instability and a detailed Level 2 for the remaining machines that may exhibit instability problems. Level 2 analyzes second-order effects as well as labyrinth seals, balance piston, and gas path forces and modeling appropriate for the rotor, bearings, seals, and supports.

12.3.4 Torsional Rotordynamics

12.3.4.1 Importance of Torsional Analysis

An additional area of concern in rotordynamics is that of torsional vibration (TV). This is defined as rotational oscillations through deformation of rotating structural elements such

as the shaft and coupling. Similar to lateral rotordynamics, there are torsional natural frequencies (TNF) that can occur in all rotating equipment. When these coincide with forcing functions, either at a constant speed condition or during startup or variable speed operation, excessive TV can occur and cause failure due to low cycle or high cycle fatigue mechanisms. Detailed discussion on torsional rotordynamics can be found in Section 4 of API 684 [1].

Torsional vibration is a unique type of machinery problem because torsional vibration is hard to observe and recognize until it is too late. An exception is the situation where a gearbox is part of the system. If the level of torsional vibration is large enough, the teeth will unload and “gear hammer” will produce an audible noise. The results of excessive torsional vibration however are often catastrophic and expensive.

Torsional design studies can avoid these problems:

- broken or damaged shafts
- broken or damaged couplings
- stalling motors
- failing motor spider welds or rotor bars
- power pollution (fluctuating current, flickering lights, etc.)
- auxiliary equipment failures

Torsional vibration can cause motor shaft failure as in Fig. 12-11. It often occurs in the motor stub shaft where it connects to the coupling since this is usually the point of the highest stress.

Figure 12-12 shows several coupling failures: (a) overtorquing of a flexible coupling, (b) excessive heating in an elastomeric (or soft) coupling, and (c) failure of a disc coupling.

Torsional vibration can cause crankshaft failures as well as excessive displacements in auxiliary equipment driven off a compressor or engine. Dampers typically used in engines to control torsional vibration can cause shaft failures if the fluid in the damper solidifies, something that occurs over time due to heating of the fluid. Design studies will calculate the damper heat load and ensure limits are not exceeded.

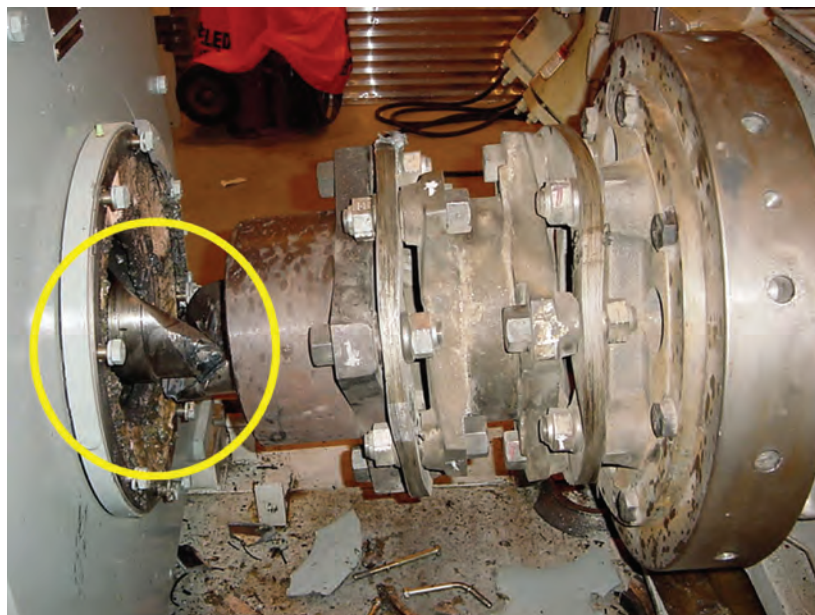


Figure 12-11. Example of a motor shaft failure.

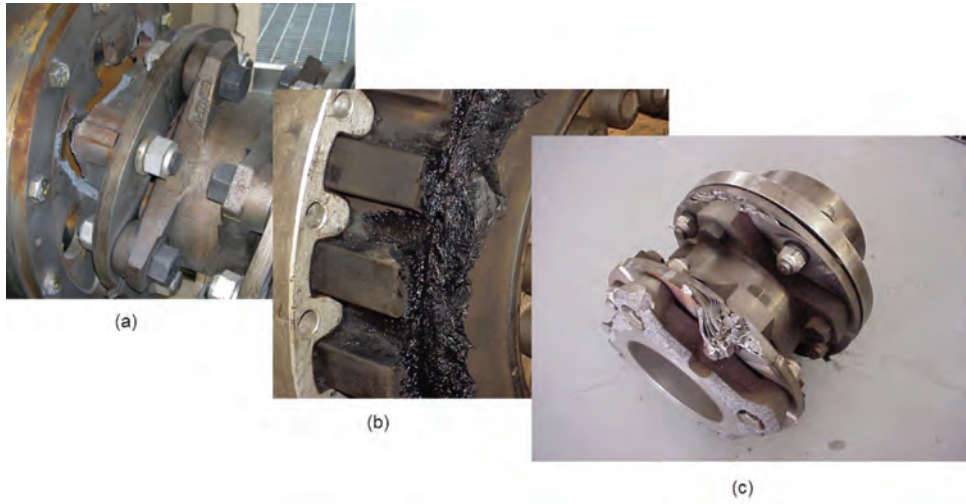


Figure 12-12. Example of coupling damage.

Because of these potential problems, it is important to carry out a design study on critical applications, untested designs, equipment revamp and situations where operating conditions change significantly [5]. These design studies are also recommended by standards such as API 618. Most torsional problems are entirely preventable by proper design studies which are typically done for:

- critical machines (down-time expensive, constant demand, no spares)
- units which need close to 100% reliability
- units going to remote locations, e.g., offshore (repairs are difficult)
- units which will operate over a wide range of conditions
- units with variable speed
- units loaded to over 70% of rated frame load
- motor and engine driven reciprocating machinery

12.3.4.2 Torsional Modeling

The first major step in torsional vibration analysis is to determine the torque effort required by the driven equipment such as reciprocating compressor. If the driver is a constant speed motor, then the compressor is the main source of the vibratory torque. For engines and variable speed motors, this is combined with their torque effort to determine the final torsional response.

The reciprocating compressor provides a continuous alternating torque that is a function of the number of cylinders and gas and inertial forces. The number of cylinders and how they are phased determines the point during the rotation that gas and inertial forces will occur. Throws are typically arranged in pairs for horizontally opposed cylinders with first, second, third, and fourth components due to inertial forces and higher orders possible due to gas forces. For a flat cylinder arrangement, a four throw compressor will typically produce a high second order and a small fourth order. A two throw will produce a high second order and moderate values for the first and third order. Since cylinder sizes (and thus their weight and inertial forces) will vary according to required compressor flow and compression ratio, weights are installed to equalize inertial forces for each pair of cylinders. However, gas forces could well be different and thus the final oscillating forces will vary with operating conditions and cylinder configuration.

Figure 12-13 shows the two major components of the torque effort for a reciprocating compressor: the gas force and the inertial force. The gas force will be the sum of the gas forces from each cylinder, while the inertial force is the result of the reciprocating masses (piston, piston rod, crosshead, and a portion of the connecting rod) and the rotating masses (the crankshaft and the rest of the connecting rod). The torque effort can be analyzed for its frequencies and amplitudes. Figure 12-13 illustrates the torque effort for a two throw reciprocating compressor which exhibits a strong two times frequency.

A reciprocating compressor is modeled as a mass at each throw with a stiffness in between each throw. Other shaft elements such as the compressor stub to which the coupling attached are also modeled as a mass and stiffness. Damping is very low in a reciprocating compressor.

A constant speed induction motor involves oscillations at line and $2 \times$ line frequency if there is an electrical fault or imbalance between the phases. Problems may occur at startup however, and a transient analysis is needed to ensure high stresses do not occur. A synchronous motor has a strong excitation at twice slip frequency at the commencement of startup that must be analyzed. A motor with a variable frequency drive puts out excitations at many orders of running speed, and it is much more difficult to avoid resonance or TNFs.

A motor is modeled as having an inertia and stiffness for each section of the shaft and core (Figure 12-14). A motor with a solid core is considered to have a very high stiffness and one with a spider web as a lower stiffness somewhere between that of a solid core and that of the shaft.

Torsional modeling is concerned with setting up the characteristics of the driver, driven equipment, coupling and any associated flywheels, detuners and dampers needed to perform the torsional analysis. It builds on the torque effort previously determined to enable

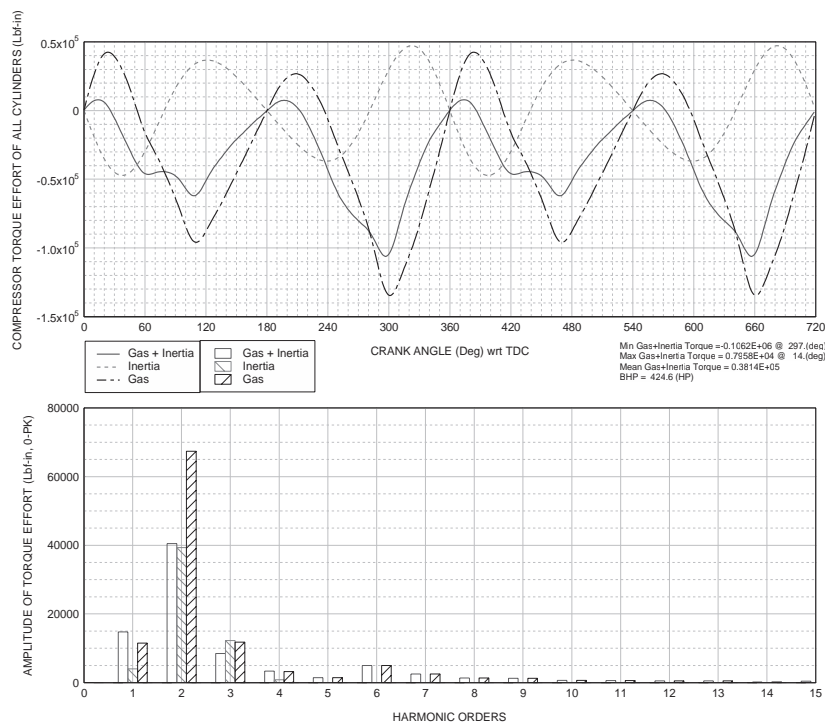


Figure 12-13. The torque effort curve and resultant frequencies for a two throw reciprocating compressor (courtesy of Wood.).

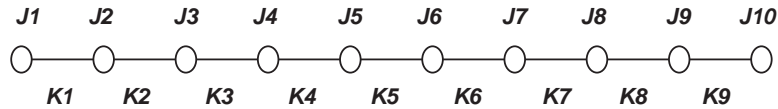


Figure 12-14. Torsional model with inertias (J) and stiffnesses (K) at various nodes.

torsional analysis of the total system. The torsional model usually consists of a model built around a shaft which shows the interconnected inertias and stiffnesses.

An extensive description of modeling of torsional analysis is available in Section 4 of API 684 [1]. The modeling process is somewhat analogous to that for lateral rotordynamics. Comparing a torsional system to a simple spring-mass system, the following are analogous:

- inertia (J) to mass (m)
- rotational stiffness (K) to linear stiffness (Kl)
- angular deflection (θ) to translational deflection (x)

Inertia (J) is essentially a function of density and geometry, and is determined for the system by adding the inertia for each element.

$$J_{\text{system}} = J_{\text{motor}} + J_{\text{coupling}} + J_{\text{compressor}} \quad (12-6)$$

System rotational stiffness is determined from Eq. (12-7), where K is a function of component material, diameter, length, and, in some configurations, loading.

$$\frac{1}{K_{\text{system}}} = \frac{1}{K_{\text{system}}} + \frac{1}{K_{\text{coupling}}} + \frac{1}{K_{\text{compressor}}} \quad (12-7)$$

1-D or one-dimensional torsional modeling techniques are used for most analyses. It is usually not necessary to apply 2-D or 3-D methods to achieve a satisfactory solution.

Holzer's method [6] is the standard method to predict the torsional natural frequencies of a system. In order to follow Holzer's method, a detailed layout of the system with dimensions and mass elastic data must be known.

The Holzer table uses nodes and elements to predict the natural frequencies of a system. The inertias (shown as J) and stiffness (designated as K) of the system are tabulated as nodes and elements respectively in a Holzer table. At each node, the inertias are lumped together and connected to an equivalent stiffness to produce the system model.

The natural frequencies for a simple single one mass system can be calculated from the following relation:

$$\begin{aligned} F &= 1/2\pi \sqrt{K/J} \quad 60 \text{ rpm} \\ &= 9.55 \sqrt{K/J} \text{ rpm} \end{aligned} \quad (12-8)$$

where:

K = stiffness (lb_f-in/rad)

J = inertia (lb_f-in-s²)

Details for setup of a Holzer table for a multi-mass system can be obtained from BICERA. A good explanation with an example is available in ref. [7].

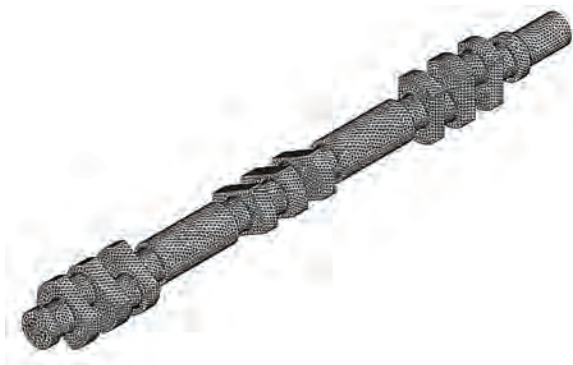


Figure 12-15. Finite element torsional model of a crankshaft (courtesy of Wood.).

Torsional models mostly used for analysis are single branch systems. Some models such as an integrally geared compressor require a multiple branched approach in which case a more complicated method is needed.

The machinery train is divided into segments that represent lumped inertias and torsional stiffness. Care has to be taken with couplings since elastomer couplings have a stiffness that is a non-linear function of applied torque and thus varies with speed. While some geometries are easy to model, others, such as electric motors, have quite complex shapes. For pumps, the inertia of both a dry impeller and a wet one may have to be considered since the inertia of the fluid is considerable, and it does provide an additional level of damping.

For a reciprocating compressor, the Holzer table of a multi-system model consists of the inertia and stiffness of the crankshaft and the inertia of the rotating and reciprocating components. The inertias are lumped at appropriate stations of the compressor crankshaft. These stations represent the nodes in the Holzer table. Finite element analysis is now being applied to calculate the simplified stiffness and inertia of rotating components, particularly for a new crankshaft in a reciprocating compressor as shown in Fig. 12-15.

12.3.4.3 Torsional Analysis

The coupling and driver are modeled in a similar fashion, and the combined machine train is analyzed for the TNFs and the Operating Deflection Shape. An example of an ODS for a motor-driven reciprocating compressor for the first two modes which are normally the most important is shown in Fig. 12-16.

The other important diagram is the interference or Campbell diagram which plots the TNFs against the operating speeds. Several natural frequencies are usually present in the system, and it is important to identify each of them. Figure 12-17 is an example of a constant speed motor running at 1185 rpm with first and second TNFs positioned away from the run speed.

Torsional forced response is a function of both the compressor torque effort and the dynamic amplification ratio [7]. The compressor torque effort is a function of the compressor operating conditions and load steps. Dynamic amplification is a nonlinear function of the system damping, forcing frequency and the TNF, as defined by the system mass-elastic properties. Dynamic amplification is very sensitive to system damping. In fact, at resonance (frequency ratio, $f/f_n=1$), dynamic amplification is limited only by damping. Since the system damping can be very low for a motor driven reciprocating compressor system, the dynamic torsional amplification can be very high. High torsional amplification can result in high shaft stresses, so it is good practice to avoid torsional resonance.

For many trains, damping is quite low so that an undamped natural frequency torsional analysis is able to fairly accurately predict actual natural frequencies within acceptable

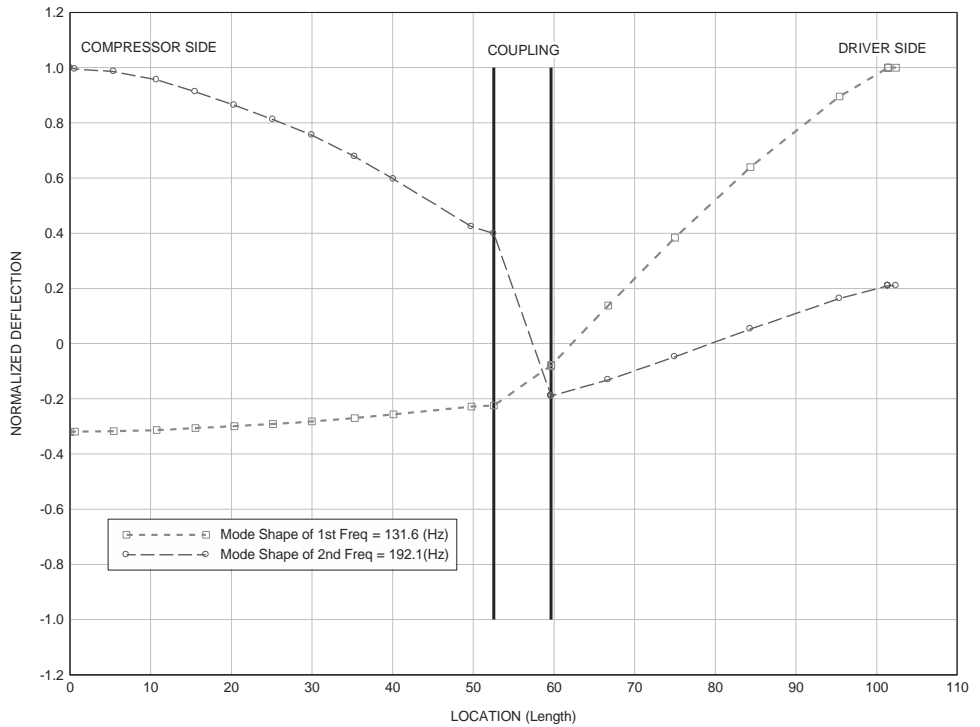


Figure 12-16. Operating deflection shape for a motor-driven reciprocating compressor (courtesy of Wood.).

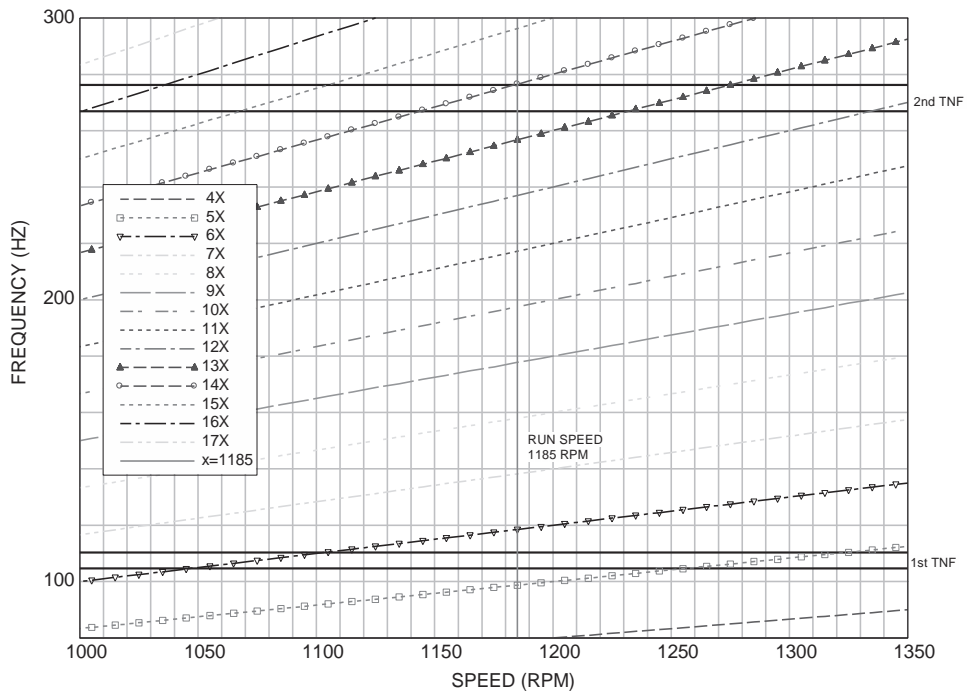


Figure 12-17. Campbell or interference diagram (courtesy of Wood.).

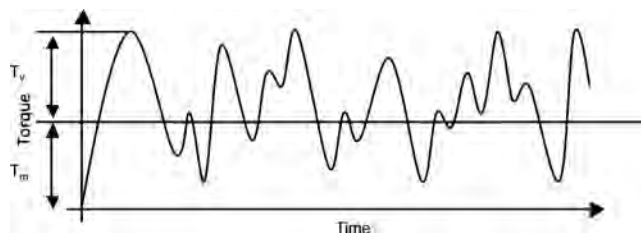


Figure 12-18. Torque definitions.

levels of error. The type of the analysis and the forcing functions that have to be considered vary substantially with the type of rotating machine.

Although torsional resonance can and should be avoided by re-positioning the TNF, it is not entirely obvious where the TNF should be. The compressor torque efforts (i.e., forcing functions) are produced at frequencies corresponding precisely to orders of run speed. Therefore, the TNFs should be positioned as far away from the orders of run speed as possible; positioning the TNFs between orders of run speed typically results in an overall minimum torsional amplification of the torque effort. Although the TNFs should be repositioned midway between orders, there are trade-offs between lowering and raising the system TNFs.

The torsional response could be controlled by raising the first TNF to a frequency at which the torque effort is lower. However, it is usually inconvenient or expensive to make a system torsionally stiffer (i.e., higher TNF). Moreover, dynamic amplification is more difficult to minimize at higher frequencies since the torsional response curves are wider.

To ensure that resonance is avoided, precise calculations are imperative. Moreover, all mass-elastic uncertainties must be quantified, and a TNF “uncertainty band” must be established [8]. All the uncertainties tending toward a high TNF are combined to determine the high limit; all those tending toward a low TNF are combined to determine a low limit. Then, based on experience, a best estimate within those limits is determined.

12.3.4.4 Torsional Solutions

From a physics perspective, mass, stiffness, and damping are the physical parameters that can be adjusted in order to modify the system torsional response. The basic objective of torsional analysis is to avoid correspondence between frequencies generated by the driver and driven equipment and the TNFs (torsional natural frequency) of the system and ultimately to ensure that maximum allowable stress levels are not exceeded. This is done by calculating design factors (DF) of the driven equipment, coupling, and driver for the various operating conditions. High deflections may be damaging to auxiliary equipment such as lube oil pumps which may be installed on the compressor at the non-drive end or a cooler driven from the engine cranknose.

A torsional solution is reached when torsional guidelines and limits are met in accordance with the industry practice and manufacturers data. Experience is critical in making a reasonable judgment besides the given guidelines and limits. A due diligent check on the criticality and sensitivity of a system is also very important in making the final decision.

Since the torque is a fluctuating quantity, there are several possible torque definitions. The nominal torque, T_{KN} is also known as the continuous torque which is the torque that can be continuously transmitted occurring at steady state or stationary services. The nominal torque consists of mean torque, T_m and vibratory torque, T_v .

$$T_{KN} = T_m + T_v \quad (12-9)$$

where:

T_{KN} = nominal Torque

T_m = mean Torque

T_v = vibratory Torque

The maximum torque (Fig. 12-19) or peak overload torque, T_{\max} is the highest torque that occurs during a transient or any abnormal condition such as short circuit, emergency stops, etc. The maximum torque limit has a finite number of cycles.

Manufacturers of compressors, couplings, and drivers have different limits based on these torques so care has to be taken to ensure that their limits are understood and followed.

The guidelines used in the torsional analysis for a shaft type component is called the design factor. There are many different design factor criteria such as Gerber, Soderberg, Goodman, and Bagci. They are used to determine a design factor on which is then based the decision as to whether the torsional design is adequate.

The design factor is what an item is required to be able to withstand. Appropriate design factors are based on several considerations, such as the accuracy of predictions on the imposed loads, strength, wear estimates, and the environmental effects to which the product will be exposed in service. However, the guidelines and limits do not guarantee 100% success. It merely reduces the probability of failure to a minimum based on the existing technique. Likewise, a system that fails to meet guidelines or limits does not mean imminent failure but it does increase the chances of failure.

There are different configurations of driver/coupling/driven equipment, each of which has a unique system torsional response and each of which has options available for satisfying torsional constraints. For compressors, the choice is mainly related to the choice of coupling, flywheels, and detuners. For engines, dampers and flywheels are used to adjust the torsional response.

The first step in determining a torsional solution is to choose the coupling since its torsional response (stiffness and damping) is critical (see Section 8.5 for more details on couplings). Normally a stiff coupling such as a flexible, metal disk coupling is chosen with its size dependent on the torque, power and speed requirements. Although a flexible coupling has some mass, its main contribution is that of stiffness, usually much lower than that of the rest of the system.

A common method of modifying the torsional response is to add a flywheel. A flywheel is a disk that is mounted on or attached to the shaft to provide additional mass. A flywheel is used to attenuate the vibratory torque generated from the compressor or driver from transmitting to the other end of the system. A flywheel is normally installed at the compressor side drive end since the compressor is the main source of the torque effort and it is better able to handle the overhung moment with respect to the bearings. The flywheel may be a separate disk flanged to the compressor hub or inertia may be added to the compressor hub itself as has been done in Fig. 12-20 if a smaller amount is needed. For an engine driven system, a flywheel is typically already installed at the engine side drive end to reduce engine torque variations.

Where the driver is an engine or VFD motor, it is not possible to avoid all of the TNFs and the remaining solution is an elastomeric or “soft” coupling. Soft couplings require regular maintenance to replace the elastomeric elements which deteriorate over time with heating which makes them less desirable from an operating perspective.

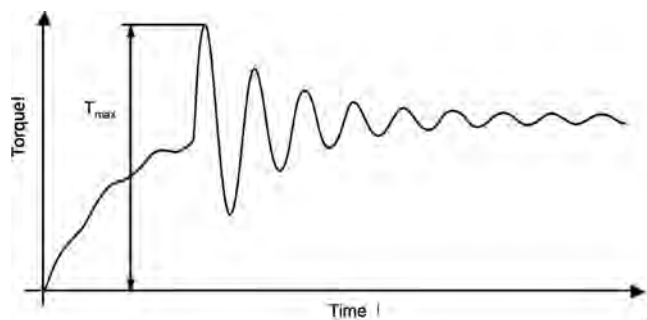


Figure 12-19. Maximum torque.

A screw compressor produces excitations from the gas forces produced by the suction and discharge of the screw. A flooded screw provides sufficient damping to minimize the torsional oscillations and the proper flexible coupling normally suffices.

Sometimes torsional vibration is caused by a source outside of the compressor and driver [9]. A centrifugal compressor driven by electric motor had been modified from its original 450 HP motor to a 600 HP variable frequency drive. Upon startup, the coupling failed (broken bolts) several times. Each of the failures occurred after less than 2 weeks of run time. The coupling was a flexible disk type with a spacer. The compressor manufacturer had done a torsional analysis and had noted that the predicted torsional natural frequency was approximately 38 Hz. They also noted a possible excitation of that natural frequency by a 12th order harmonic from the VFD. An on site test using a digital strain gauge telemetry system was used to measure the actual torque carried by the coupling spacer. What was not expected was that the torsional natural frequency was excited throughout most of the run speed range. Flow induced pulsation caused by vortex shedding of the mean flow past a manway in the suction piping turned out to be the culprit.

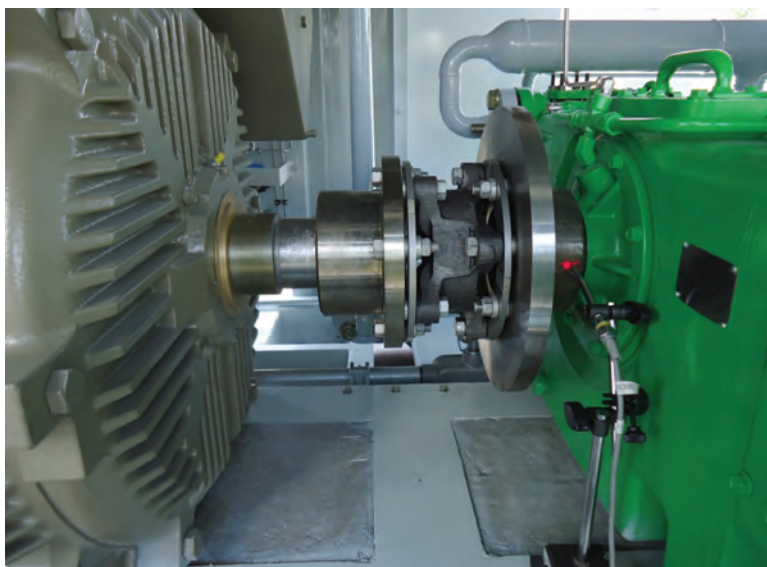
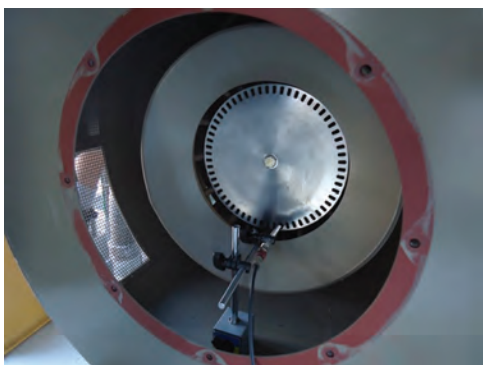


Figure 12-20. Inertia added to a compressor hub (courtesy of Wood.).



(a)



(b)

Figure 12-21. Torsional vibration measurement using (a) an optical pickup or (b) a shaft encoder (courtesy of Wood.).

Although torsional analysis techniques are at a high stage of development, there are uncertainties in both design and actual manufacturing and installation that may justify verification by field testing [10]. A torsional laser vibrometer can be used to measure TNFs and torsional displacements. This can be measured at the coupling as can be seen in Fig. 12-20 or at the non-drive end of a motor such as in Fig. 12-21 using either an optical pickup or a shaft encoder.

There are rare cases where the unexpected happens such as a large compressor installation that experienced rapid crankshaft failures [11]. Field measurements obtained at site identified an unexpected situation where the first two torsional natural frequencies occurred at essentially the same speed. This resulted in a double resonance condition—something very rare in the field of torsional analysis.

12.3.5 Specific Machinery Considerations for Rotordynamics

12.3.5.1 Centrifugal Compressors

Different types of turbomachinery have unique considerations with respect to rotordynamics.

Centrifugal compressors offer some major challenges to designers from a rotordynamics perspective. This is due, first of all, to the fact that the impeller(s) adds less stiffness to the rotor and operation is mainly in the flexible shaft region. Aerodynamic forces are significant due to the higher pressures and rotating speeds. The high pressures make it more difficult to properly model sealing components.

Multi-stage centrifugal compressors usually have a very rigid case to contain the high pressure that results in support stiffness being much higher than that of the bearing. More attention has to be paid to the effects of seals, particularly liquid seals. In contrast, the rotordynamics of single-stage compressors that are overhung are dominated by the weight of the impeller and coupling. The shaft is short however and relatively stiff with short bearing spans. The first two modes therefore result in rigid body motion. Due to the overhung moment, there is an increased likelihood of experiencing synchronous thermal stability or “Morton’s effect” where it couples with asymmetric thermal heating of the bearing journal [7]. It should be noted that this effect is not covered by API standards. The bearing loading is also unique with the journal on the coupling side seeing close to zero load or sometimes even an upward load. The support stiffness may also vary between the impeller side where it is likely to be stiff in contrast with the coupling side bearing may be much less stiff. Careful modeling has to be carried out as a result.

Subsynchronous vibration in a centrifugal compressor is usually assumed to be the result of oil film instability, but as described by Smith and Wachel [8], they can also be the result of forced vibration caused by flow instabilities such as stage stall. The characteristics of self-excited vibration are that:

- vibration usually occurs close to the first critical speed
- it is controlled by the stability of the rotor and oil film
- amplitudes can increase suddenly until stationary parts such as seals and labyrinths are contacted
- whirling of the rotor occurs at subsynchronous frequency in either the forward or backward direction

Forced vibration behaves in the following manner:

- Vibration is caused by flow instabilities that produce pulsation and are influenced by the acoustics of the compressor and its piping.
- Subsynchronous vibration is detected at lower flows near surge and are generally bounded.
- Whirl is in the forward direction.

- Subsynchronous frequency is mostly 5% to 20% of running speed.
- Amplitudes are a function of impeller tip speed and gas density.
- Shaft vibration and pulsation are phase-coherent.
- Pulsations occur on the discharge side unless there is flow distortion in the inlet.
- Excitation is often associated with flow separation in the diffuser or return channel.
- For multi-stage compressors, pulsation normally occurs in the final stages.

12.3.5.2 Reciprocating Compressors

Reciprocating compressors operate at lower speeds where lateral rotordynamic issues are less important than torsional effects. Reciprocating compressors by their very nature undergo significant changes in torque. Two main types of forces act on each throw: inertia and gas load (see Fig. 5-15). If clearance volumes are adjusted, throws may exhibit different torsional behavior due to gas loads. This will also vary with operating conditions [6]. One result may be oil pump failures.

Case Study: Oil Pump Failures. Reciprocating compressor systems often include a lube oil pump driven from the opposite drive end (ODE) of the compressor shaft [9]. This particular system was comprised of:

- six-throw, 3000-hp reciprocating compressor
- squirrel cage induction motor (885 rpm)
- flexible disk coupling

Torsional vibration caused the oil pump drive shaft to fail within 1 hour of service. The compressor torque effort spectrum shown in Fig. 12-22 indicates that the torque effort (input) is primarily concentrated at the third and sixth orders of run speed, with the 3X component much higher.

However, the torsional response curve (Fig. 12-23) is more than 8 times higher at 6X runspeed than at 3X. This difference suggests resonance, and leads to the conclusion that the TNF is close to 6X run speed (88.5 Hz).

Based on measured data and a finite element torsional model, the system's TNF was determined to be approximately 87 Hz (5.9X run speed), too close to the known high-input torque at 6X runspeed. To make matters worse, the pump's drive shaft had a TNF of 93 Hz, or 6.3X runspeed. The combination of all these factors was intolerable.

To reduce the dynamic sixth-order amplification, coincidence of the TNF with the sixth-order torque effort had to be avoided. We added three small donuts (each 4630 lb•in²) to

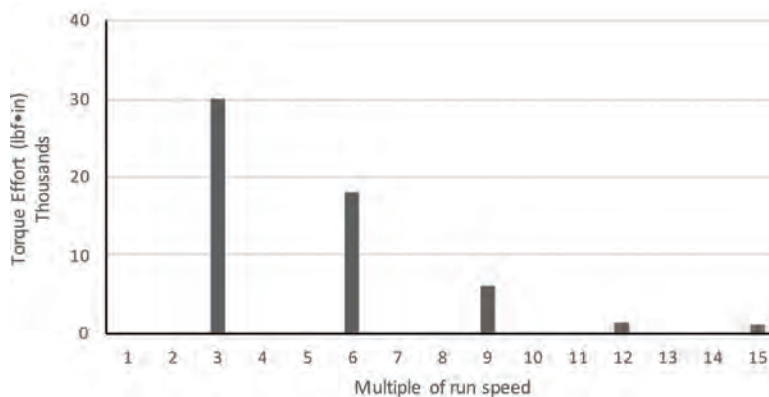


Figure 12-22. Greater torque effort at 3X run speed than at 6X run speed (courtesy of Wood.).

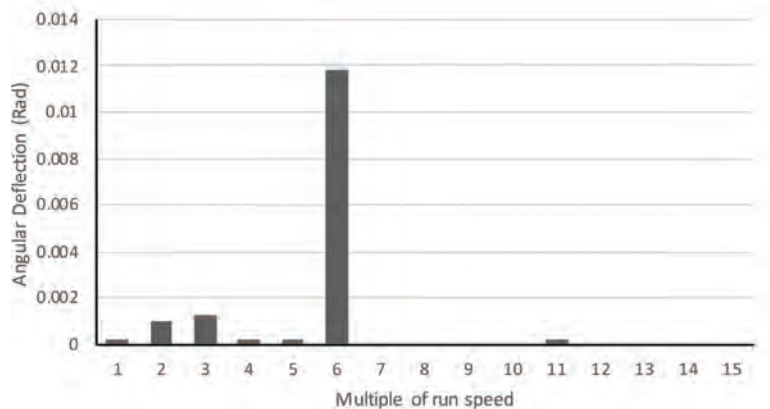


Figure 12-23. Excessive torsional response at compressor ODE for 6X run speed (courtesy of Wood.).

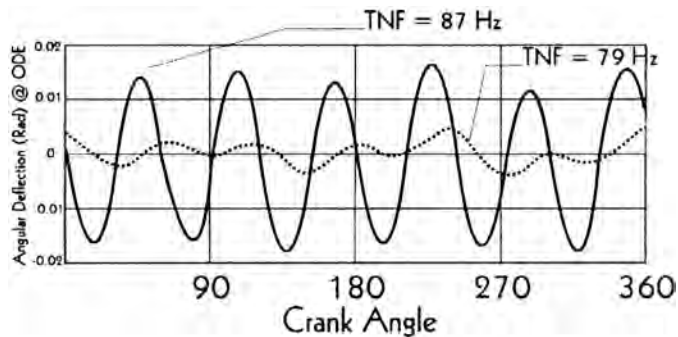


Figure 12-24. Reduced deflection with torsionally soft coupling (courtesy of Wood.).

the compressor shaft. This modification effectively lowered the system's TNF from 87 to 79 Hz which, as shown in Fig. 12-24, reduced the predicted overall angular displacement at the compressor auxiliary drive to 23% of that in the existing system.

12.3.5.3 Centrifugal Pumps

Centrifugal pumps, particularly multi-stage and high-speed types, may see situations where the first or second criticals coincide with the operating speed. The process outlined in API 610 [10] describes the process for deciding whether an analysis is required:

- If a similar or identical pump exists, no analysis is required.
- If the rotor is classically stiff, no analysis is needed (classically stiff is defined as the first dry critical speed being above the maximum continuous speed by 20% for wet running only and 30% for rotors designed to be able to run dry).
- Otherwise, a damped unbalance response analysis is required as agreed by the manufacturer and user.

Pump rotordynamics is affected by impeller clearances at the wear ring, balance drum, and impeller exit. Analysis must take into account that the wear ring clearance will change over time, and this will affect the rotor support stiffness and thus the natural frequency. Operation away from the best efficiency point will increase pulsation-induced forces on the impeller and could cause instability. Various levels of rotordynamic analysis are available

from simple to very sophisticated [11] with much more emphasis placed on this in the latest edition of API 610 [10].

12.3.5.4 Gas Turbines and Power Turbines

Gas turbines normally exhibit a flexible shaft and have complicated rotordynamics. The need to maintain tight tolerances and minimize blade tip wear emphasizes the need to limit startup vibration. An example of the vibration profile during startup for an aeroderivative gas generator is shown in Fig. 12-25. Both the inlet and turbine case vibration show an amplification of more than 3:1, while the response at the center is much less at about 2:1.

Power turbines are somewhat similar to overhung compressors in that the rotor has a large mass at the power turbine end and a smaller mass at the coupling end. In addition, the power turbine and its associated bearing are very hot and experiences thermal growth that may affect alignment. On the coupling side, the bearing may be lightly loaded and may suffer from oil instabilities. Inadequate oil drainage may also cause instabilities. Figure 12-26 illustrates the startup response of a power turbine. It is interesting to note the obvious critical just prior to idle speed seen by the power turbine side bearing and a much lower vibration on the coupling side. The amplification at the critical is not large.

12.3.5.5 Motors

Electric motors may be difficult to model properly because the windings contribute a large mass but little stiffness. The geometry can be challenging. The exciter has to be included and the motor frame stiffness must be accounted for accurate prediction of critical speeds.

An example of the design and testing of a high speed motor [12] illustrates the application of rotordynamic analysis supported by actual testing to verify rotor response. A complete study was performed including lateral and torsional critical speeds, shaft stresses, expected vibration amplitudes, unbalance response analysis, and stability analysis. The requirements of API 541 were to be met in order to meet critical speed separation margins of 20% from running speed and 10% from twice running speed and electrical frequencies.

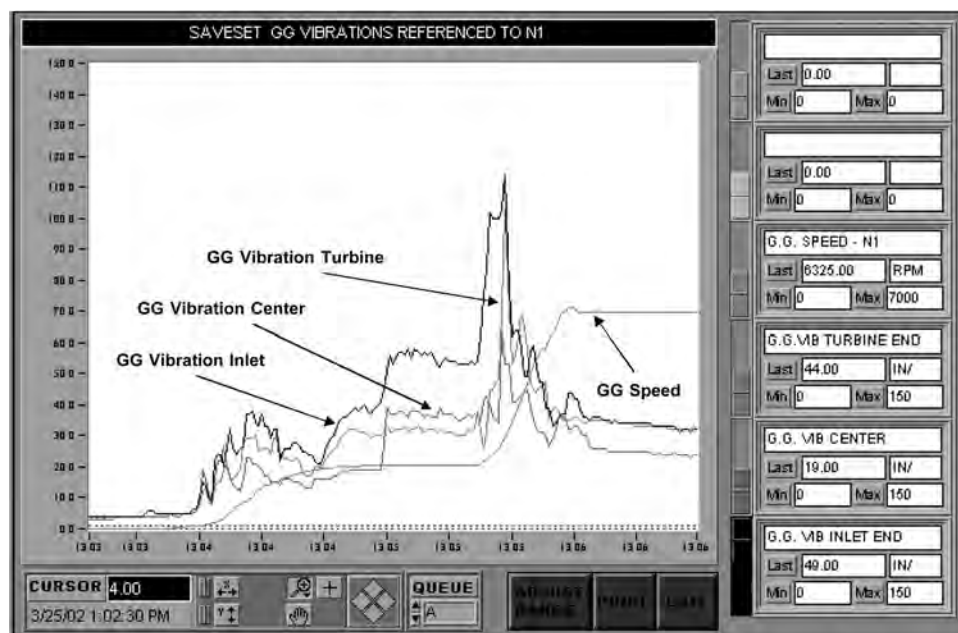


Figure 12-25. Typical power gas generator rotor response curve during startup.

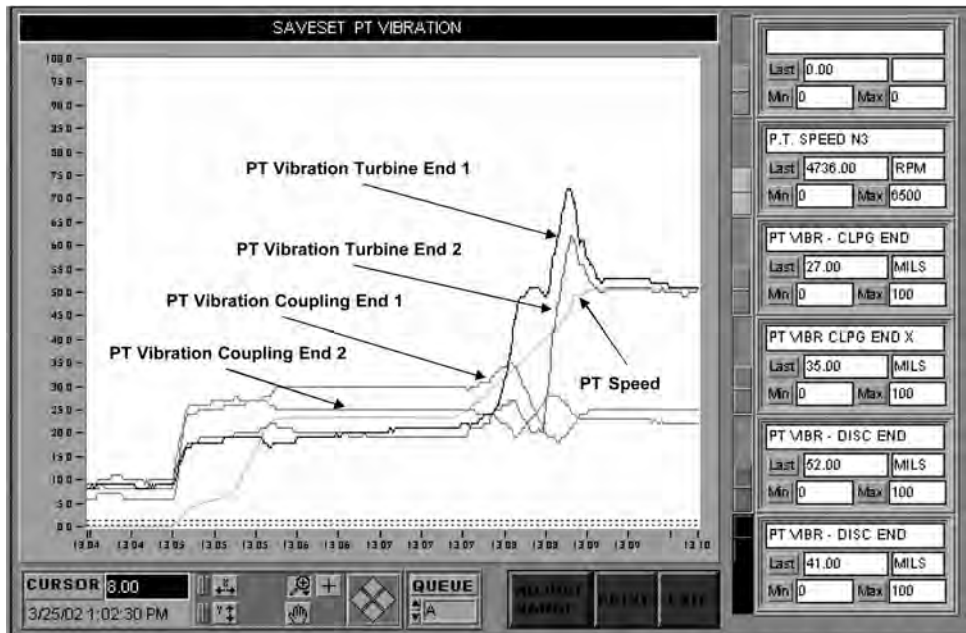


Figure 12-26. Typical power turbine rotor response curve during startup.

Variable speed motors provide a major challenge since the VFD control may interact with the mechanical response of the compressor as shown by the following example [13].

Case Study: Reciprocating Compressors Driven by VFD-Controlled Motors. The system consists of two four-throw pipeline-reciprocating compressors driven by induction motors. Figure 12-27 shows a schematic configuration of one package. There is a large flywheel between the motor and the compressor. One of the compressors is normally started up using the VFD and then switched across the line, delivering the maximum capacity. The second compressor's speed is varied to match the production requirements. Any of the compressors can lead or lag. The VFD manufacturer did not supply the motors.

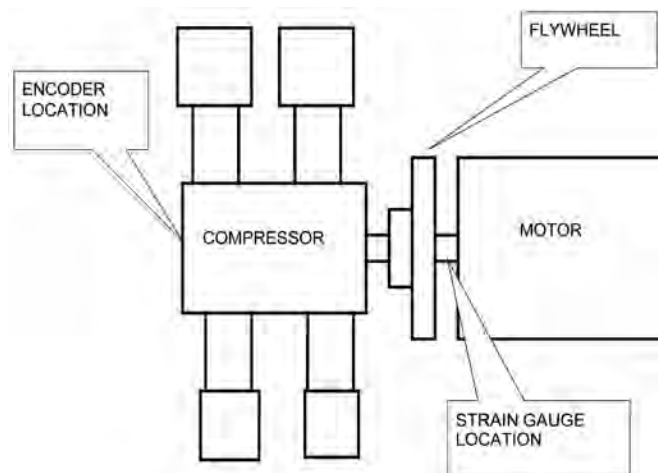


Figure 12-27. Compressor package layout (courtesy of Wood.).

Several motor shaft failures in the stub shaft area occurred, caused by TVs and improper shaft materials. The lateral vibration at the motor drive end and at the compressor drive end were measured using accelerometers oriented parallel to the piston motion (horizontal direction). The TV at the motor shaft was measured using strain gauges and the TV at the compressor auxiliary end was measured using an encoder coupled to a signal demodulator. The lateral vibrations were not high. The spectral analysis at the accelerometer locations showed no evidence of high amplitudes at the frequencies at which the TVs occurred. The pattern of the vibration at the two points measured matched the typical pattern of vibration on a reciprocating compressor package; that pattern consists of amplitudes at multiples of run speed, with the highest amplitudes at 1X and 2X run speed.

Torsional vibrations were measured by analyzing the dynamic component of the torque at the motor shaft and the angular displacement at the auxiliary end of the compressor shaft. The TVs were an issue on the motor side of the flywheel. Torsional vibrations were lower than predicted on the auxiliary end of the compressor. The original symptoms were exhibited in one of the systems. As the speed was increased and the first torsional critical speed was excited, the TVs peaked and then the amplitude of the TV stayed high at the TNF even though the motor speed was still increasing. This speed sweep process is shown in Fig. 12-28. The trend shows two traces: mean torque and dynamic torque. The higher values while operating under VFD control correspond to the dynamic torque caused by TV.

The pattern of high TV was similar for loaded and unloaded conditions. Unit 2 did not exhibit the “lock-in” TV during the initial tests; however, after some changes in VFD parameters, the pattern matched that of Unit 1.

Figure 12-29 shows the waterfall of the dynamic torque spectra during the speed sweep and switching process. Two orders of run speed can be seen clearly: 3X and 4X run speed. These orders increase frequency as the motor is sped up from 700 to 900 rpm. The amplitude at 50 Hz increases significantly when the motor speed reaches 750 rpm and torsional resonance occurs. At higher speeds, the 50-Hz peak reduces its amplitude; however, it is still higher than any other order, despite operating out of resonance.

Several changes were made to different parameters of the VFD software by the VFD manufacturer. We are not privy to the changes made. In some instances, the TV was increased even further. The result of the last set of changes was that the 50 Hz excitation was significantly reduced off-resonance (Fig. 12-30). The two motors then behaved similarly under VFD control. One system showed higher TVs than the other, but the amplitudes

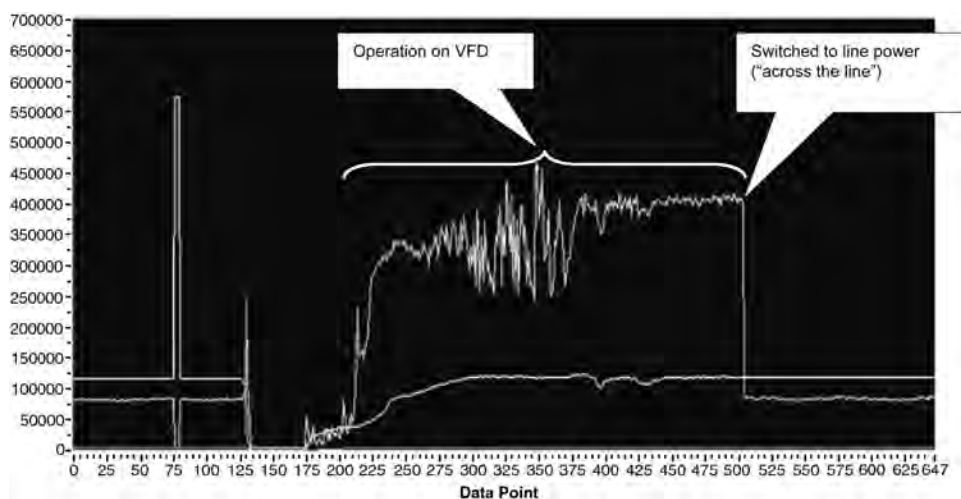


Figure 12-28. Trend showing torque fluctuation (courtesy of Wood.).

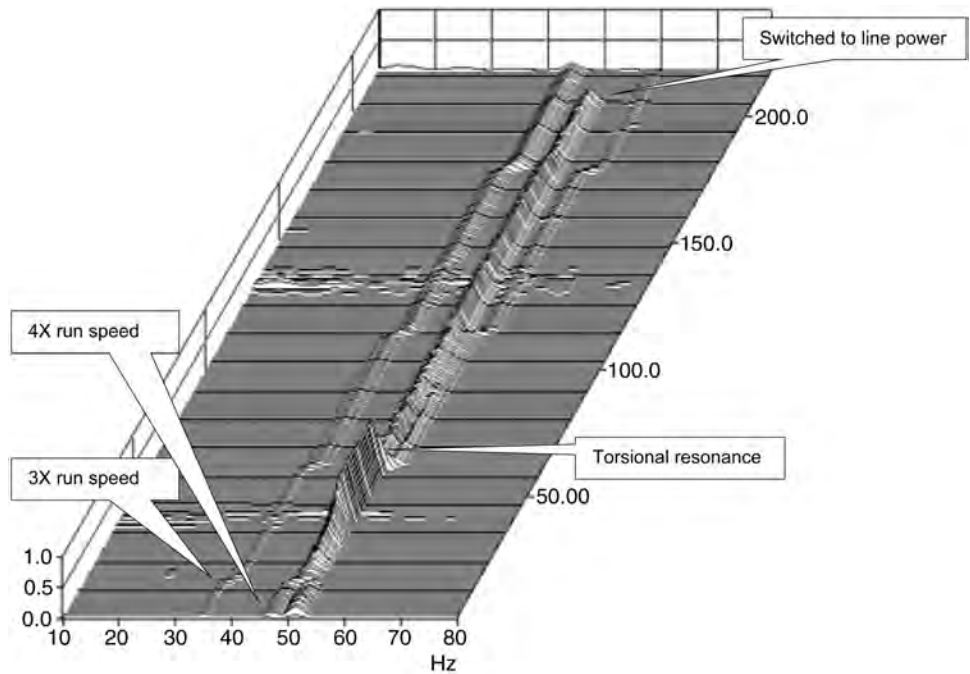


Figure 12-29. Waterfall plot of torque spectra showing high torsional response disappearing when VFD is switched off (courtesy of Wood.).

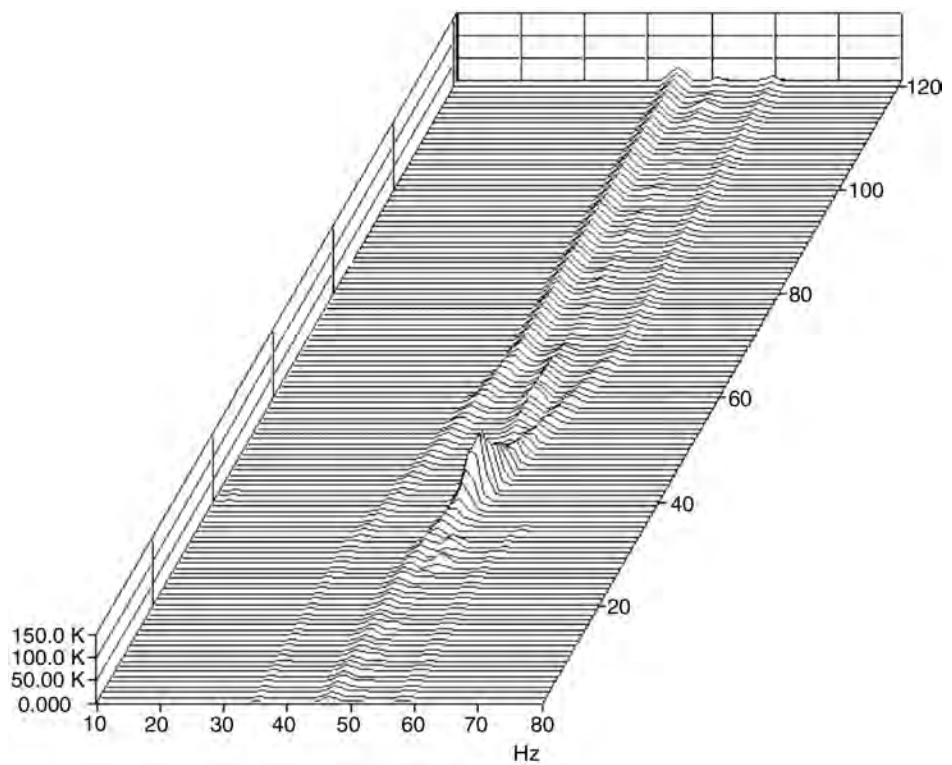


Figure 12-30. Waterfall plot of torque spectra showing normal torsional response after VFD is adjusted (courtesy of Wood.).

were improved from the as found configuration. The lock-in pattern was eliminated, and the TV reduced as the speed moved away from resonance. There was still some remaining TV at 50 Hz while the motor was under VFD control; however, the amplitude was much lower than the 3X or 4X torsional components.

This case study shows that the compressor torque fluctuations can cause speed fluctuations in the motor, which lead to fluctuations in the variables monitored by the VFD. The VFD then changes its output to correct for the deviations from the desired operating conditions. The change in VFD output excites the torsional system, resulting in even larger TV. The flywheel apparently isolates the compressor from the TVs (torque fluctuations) coming from the motor. It was originally installed to isolate the motor from torque fluctuations coming from the compressor.

Designers of torsional systems can only assume that Variable Frequency Drives will not amplify the TVs in a system at this time. In fact, we have seen that amplification does occur. Therefore, the VFD design should consider the torsional oscillation of the motor/compressor system to prevent or eliminate amplification.

12.3.5.6 Gearboxes and Couplings

Gearboxes have interesting characteristics due to their design of multiple shafts and bearings with loading on bearings dominated by radial loads. With transmitted torque varying drastically, high radial loads reduce the tendency for bearing stability at operating speeds while low torque during startup may cause instability.

Couplings form a major component of a torsional analysis, both because they cause problems and also since they can be used to solve torsional issues. Two different types of couplings are normally used: lubricated gear and flexible. The coupling can be seen as several torsional springs in series. Gear couplings have little damping, but flexible couplings can add damping and are often considered to be “soft” since their stiffness is normally lower than that of the remaining train. Damping is especially useful for variable speed or synchronous motors since it reduces the amplification of natural frequencies [14].

Case Study: Coupling Too Stiff for Motor/Compressor Set. The proposed system [9] consisted of a:

- four-throw compressor
- 1250-hp, 1175 rpm squirrel cage electric induction motor, with a shaft designed for a different service
- Flexible disk coupling

Two modifications are discussed:

- addition of a small flywheel (20,000 lb·in²)
- introduction of a “torsionally soft” coupling

Stresses were evaluated against a design factor, which should be greater than 2. As shown in Fig. 12-31, only the system with the torsionally soft coupling met the stress criterion. The calculated TNF of 97 Hz was close to 5X run speed. As shown in Fig. 12-32, there was significant deflection, resulting from interference of the TNF and the torque effort at 5X runspeed.

The flywheel modification reduced the system TNF to about 89 Hz (4.5X runspeed), but as shown in Fig. 12-33, peak deflection is still obvious at 3, 4, and 5X runspeed. These components contributed to the excessive stress indicated in Fig. 12-31. The torsionally soft coupling modification dropped the system TNF to about 10 Hz (0.5X runspeed). As shown in Fig. 12-34, the peak deflection was then minimal.

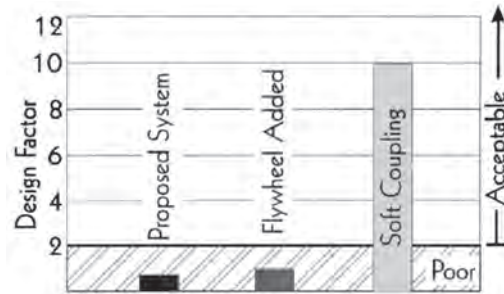


Figure 12-31. Comparison of design factors for proposed system and optional solutions (courtesy of Wood.).

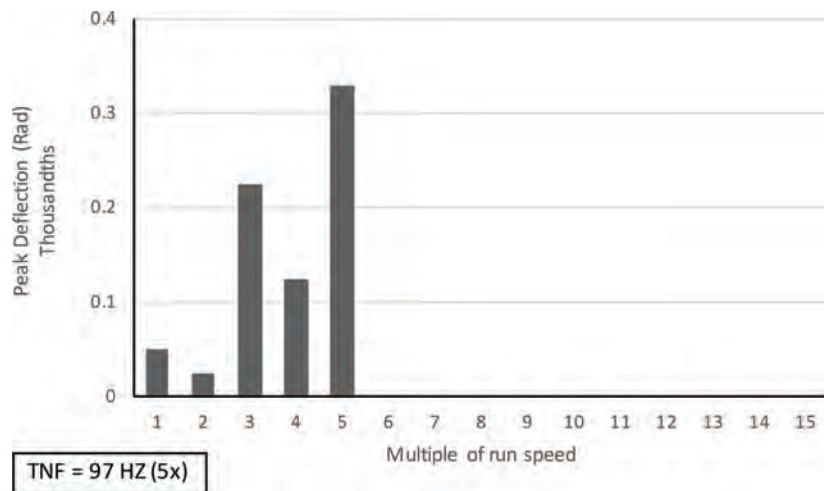


Figure 12-32. Deflection for original system at 1 through 5X run speed (courtesy of Wood.).

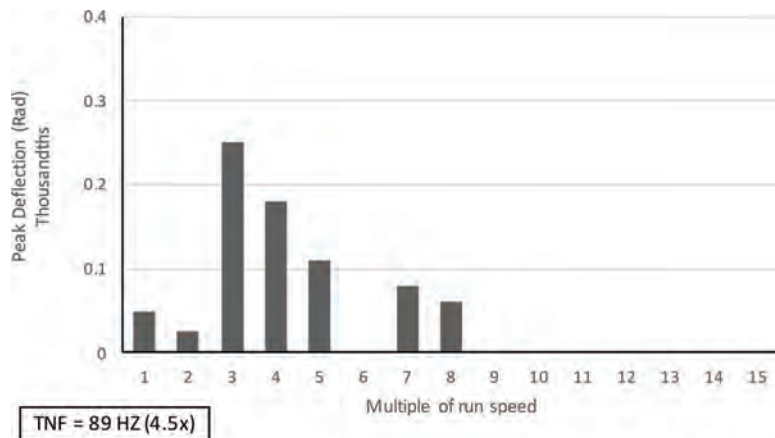


Figure 12-33. Deflection for flywheel option with reduced deflection at 5X but increase at 4X run speed (courtesy of Wood.).

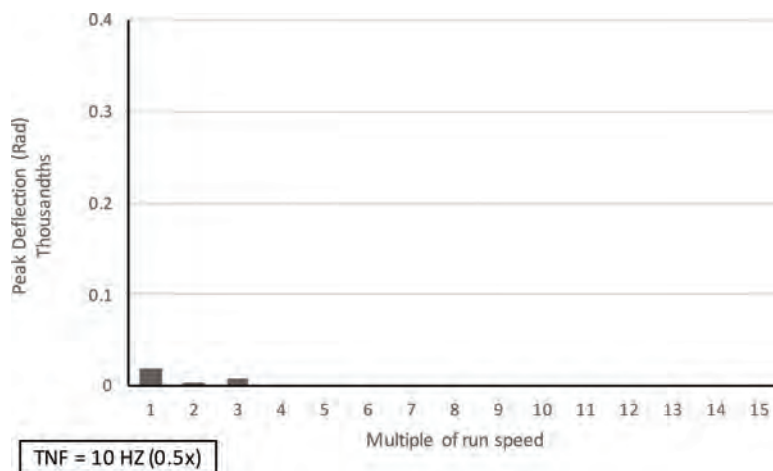


Figure 12-34. Much reduced deflection for torsionally soft coupling (courtesy of Wood.).

12.3.5.7 Active Bearings

A potentially major solution to many of the rotordynamics problems encountered with turbomachinery is the use of bearings that can actively modify rotor response. Two types of bearings offer this capability: pressurized oil bearings and magnetic bearings.

Externally pressurized bearings are an innovation by Bently [15], who has made major contributions to vibration measurement, orbit analysis, and the understanding of rotordynamics. For a long time, conventional wisdom dictated that pressures higher than 25 psig (175 kPa) would lead to bearing instabilities. This has proven to be incorrect and high bearing pressures can be used both to depress or eliminate instabilities and provide diagnostics on rotordynamic problems.

Regular internally-pressurized fluid film bearings operate in a partially flooded mode and depend on the hydrodynamic forces produced by the oil wedge to support and stabilize the rotor. The shaft is positioned in the bearing at moderate to high eccentricity ratios (the ratio of the distance from the bearing center compared to the maximum allowed by the clearance). It is passive and depending on the loading, the bearing stiffness can change. As well, if it is lightly loaded, it can move to a low eccentricity ratio and become more fully flooded. This can lead to fluid instabilities. Various journal bearing designs such as pressure dams, offset half, elliptical, and axial groove solutions have been developed, but they still do not entirely resolve the problem of instability. Tilting pad bearings have largely eliminated instability and are extensively used with turbomachinery because they are mostly impervious to oil fluid instability but this is not universally so.

Externally-pressurized bearings are always fully flooded with pressurized fluid (usually less than 1000 psig or 7000 kPa) supplied through a set of orifices that restrict the flow to pockets that distribute the fluid. The fluid flows axially to the drain between the shaft and the journal. Without additional forces, the shaft is positioned in the center of the bearing. If a force occurs to displace the shaft from the centerline when it is not rotating, the increased flow resistance increases the pressure in the pocket and tends to re-center the shaft. Upon rotation, there is also a pressure wedge that provides additional stiffness so that the overall stiffness is the result of both static and hydrodynamic forces. At higher pressures, the static effects will predominate. Damping is relatively independent of stiffness and can be controlled by oil temperature.

The main advantage of the externally pressurized bearing is that its stiffness can be modified by the supply pressure, either equally to all supply points or to individual ones. This can be done by operator or automatic control. Manual control, however, requires a high

level of understanding of rotordynamics and the potential impact of changes, and this limits this approach. On the other hand, it can be a valuable tool in diagnosing malfunctions such as rubs or misalignment that will act to change the stiffness and resultant rotor response.

Magnetic bearings are the other active control technology available for turbomachinery. It has been applied to turboexpanders and pipeline centrifugal compressors and is becoming a more mature technology as is apparent from the development of ISO standards (ISO 14839-1 [16], ISO 14839-2 [17], and ISO 14839-3 [18]). API 617 [4] does not yet recognize magnetic bearings except for turboexpanders where they are being increasingly applied. However, the development of hermetic compressors where magnetic bearings are standard will encourage recognition of the magnetic bearing as an important bearing technology.

Active control of the magnets placed around the shaft, along with high-speed digital control from position sensors, enables the bearing to apply forces to the shaft and modify its response to misalignment, unbalance, and other forces. The force required from the magnets to keep the shaft centered can be used to mitigate problems and diagnose their causes. From a rotordynamic perspective, static and dynamic forces have to be considered carefully since the magnetic bearing has a limited capacity. The positive aspect is that advanced control algorithms can be applied to dampen rotor response at the critical speeds and reduce unbalance forces [19].

12.3.6 Balancing

Since the major contributor to rotordynamic problems is unbalance, accurate rotor balancing is mandatory for achieving low vibration levels and subsequent reliable operation. This applies not only during initial installation but also after maintenance actions such as rotor repair. There are many reasons for unbalance, including nonhomogeneous material; stacking errors; distortion; a bent shaft; eccentric mounting of components such as couplings; and impeller wear due to erosion, corrosion, or fouling.

Detailed discussion on alignment and balancing can be found in Section 5 of API 684 [1]. API standards require precision balancing that result in low vibration as well as a margin for deterioration such as impeller erosion and fouling, bearing wear, and oil system degradation.

Since the mass of a rotor is never exactly distributed around its geometric centerline, a real rotor prefers to rotate around its center of mass or inertial axis. The resultant displacement is constrained by the bearings so that the center of rotation does not match the center of mass and an unbalance results. For a simple rotor system with static unbalance, the force due to rotation is governed by the equation

$$F = U \cdot 10^{-6} \frac{2\pi N^2}{60} \quad (\text{SI}) \quad (12-10)$$

$$F = U \cdot 1.77 \frac{N^2}{1000} \quad (\text{US Customary})$$

where:

F = unbalance force [N(lb_f)]
 U = unbalance [g-mm (oz-in)]
 N = speed (rpm)

This equation emphasizes that while the force varies directly with the amount of unbalance, it increases as the square of the rotational speed. In other words, an unbalance at 1000 rpm will likely be unacceptable at 4000 rpm since the force will be 16 times higher. The unbalance is measured in the product of a weight and its distance from the center of mass.

This is very useful since it becomes simple to calculate the compensating weight that needs to be added on the opposite side at the available location on the rotor.

Unbalance can be static, couple, or dynamic. With static unbalance (see Fig. 12-35), the rotational axis is offset from the inertial axis in a parallel manner. The unbalance can be corrected by adding a compensating weight opposite the unbalance. Since this is not usually convenient, weights can also be distributed between the ends of the rotor, again 180° from the unbalance. Most rotors have some static unbalance.

A couple unbalance exists if unbalance occurs in opposite directions where the inertial axis intersects the rotational axis (see Fig. 12-36) at the same point as the center of gravity. It is corrected by adding weights opposite each unbalance at the ends of the rotor.

If the intersection of the inertial and rotational axes does not coincide with the center of gravity, dynamic unbalance is produced (Fig. 12-37). This is a combination of static and couple unbalance and is corrected by at least two weights on different planes. It is quite common and requires a more complicated balancing procedure.

The API standard is quite strict compared to the ISO equivalent. The acceptable residual unbalance specified by API is governed by the equation

$$U = 6350 \frac{W}{N} \text{ (SI)} \quad (12-11)$$

$$U = 4 \frac{W}{N} \text{ (US Customary)}$$

where:

U = unbalance [g-mm (oz-in)]

W = weight [kg (lbm)]

N = maximum continuous rotor speed (rpm)

Note that W is the weight at each end, which will be one half of the total rotor weight if it is uniform.

A common standard that is applied is ISO 1940/1 [20]. It defines balancing requirements for rigid rotors using grades to define acceptable residual unbalance. For turbomachinery,

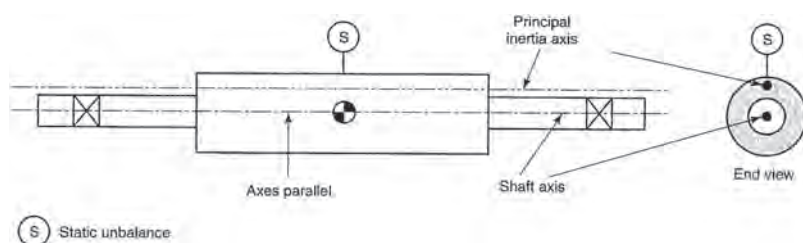


Figure 12-35. Static unbalance [1].

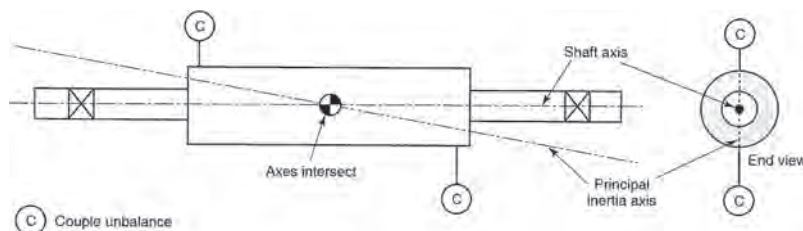


Figure 12-36. Couple unbalance [1].

Engineering Analysis	System	When required
Piping Stress Analysis	All fluids	High temperature/pressure variation
Machinery and Equipment Nozzle Load Analysis	All fluids	Machinery and equipment with low allowable nozzle loads
Small Bore Connection (SBC)	All fluids	All connections not reinforced or braced
Flow Induced Turbulence (FIT)	All fluids	High flow systems with flexible and infrequent supports
Pulsation and Mechanical Analysis	Reciprocating compressor/pump; Screw compressor	High pressure, high power, complex or critical systems
Shell Transverse Acoustical (STA)	All fluids (but gas systems typically)	Thin walled pipe or vessels near compressors and pumps
Flow Induced Vibration (FIV)	Gas systems only	High flow systems with dead legs
Acoustic Induced Vibration (AIV)	Gas systems only	Pressure reducing devices like valves and orifice plates
Compressor Surge Dynamic Simulation	Centrifugal compressor systems	Low inertia, high pressure ratio, complex systems
Cavitation/Flashing	Liquid systems only	Pressure reducing devices like valves and pumps
Transient Vibration Analysis (Gas Systems)	Gas systems only	Blowdown or PSV releasing events, momentum changes
Water hammer	Liquid systems only	Fast acting valves and emergency shutdown events

Figure 12-38. Recommended design requirements for vibration-related piping risks (courtesy of Wood.).

Every piping system has a set of natural frequencies that depend on the distribution of mass and stiffness as determined by pipe dimensions, material properties, wall thickness, location of masses such as valves, fluid density, and support configuration. For each natural frequency, there is a unique deflection shape known as a mode shape that results from the applied excitation and its location relative to the mode shape. The excitation can be tonal at specific frequencies or broadband over a wide range of frequencies and can lead to three possible conditions:

- resonant excitation where a tonal frequency coincides with a natural frequency
- forced excitation where a natural frequency is not excited and vibration occurs due to excitation energy levels being higher than the stiffness of the system
- broadband excitation that will result in some natural frequency related response (but usually lower than the resonant condition) as well as some forced excitation

Failure in pipework will generally be caused by high cycle fatigue of components such as small-bore attachments and failure at weld locations. Detailed survey, screening, and assessment methods can be found in Baker et al. [22].

Where vibration-related risks are high, high reliability can only be achieved if they are addressed during design studies and possible follow-up startup checks and field surveys. Recommended design requirements are summarized in Fig. 12-38.

12.4.2 Vibration and Stress

Ideally, to determine what vibration levels are acceptable, stress levels resulting from the vibration should be considered. When a mechanical system vibrates, it is moved from its normal or equilibrium position. Considering the top section of a piece of pipe, the vibration alternately puts the top of the pipe in tension and compression, causing stresses in the pipe (see Fig. 12-39). Vibration causing large amounts of tension or compression can result in high stresses in piping, which can damage the pipe. Totally eliminating all the vibrations in a given system would not be necessary or practical from a design and/or

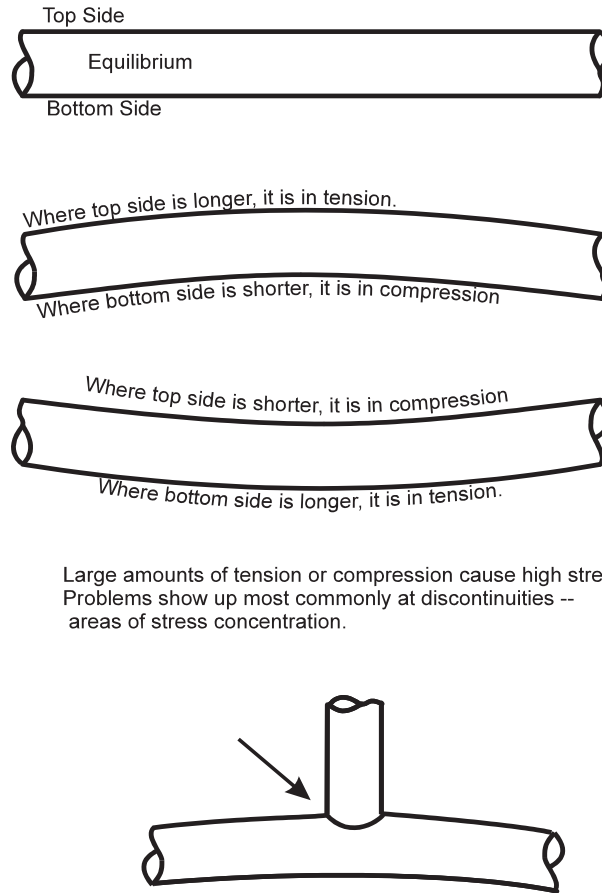


Figure 12-39. Stress in a vibrating pipe (courtesy of Wood.).

economic stand-point. However, it is necessary to reduce vibration to a level where failure will not occur.

It is much easier to measure vibration levels than stress; therefore, vibration limits are commonly used for defining problems. While generating vibration criteria for every possible situation would be next to impossible, vibration limits based on field experience have been established. Vibration limits generally considered industry standard for high speed reciprocating compressors are given in Figs. 12-40 and 12-41. These charts give a guideline limit, as well as other limits, in displacement and velocity. The charts are presented as frequency versus vibration amplitude.

The vibration limit charts do not distinguish between very stiff areas, such as a well-supported discharge bottle, and very flexible areas, such as piping rising to coolers. While following the limits on these charts will be satisfactory for most installations, there is no guarantee that they will be acceptable in all cases.

Acceptable stress and vibration levels depend on many factors, a few of which are:

- material (composition, strength, endurance, etc.)
- geometry (size, quality of manufacturing, stress concentrations such as tee intersections and cutouts, etc.)
- frequency of stress cycle
- amount of residual static stress

Guidelines for Reciprocating Compressors (1800 RPM max)

1. Cylinder guidelines are for axial and vertical directions.
2. Generic frame guideline. Consult OEM for recommended limits.
3. Dashed lines adapted from SwRI.
4. Piping guideline not applicable for <2"NPS.

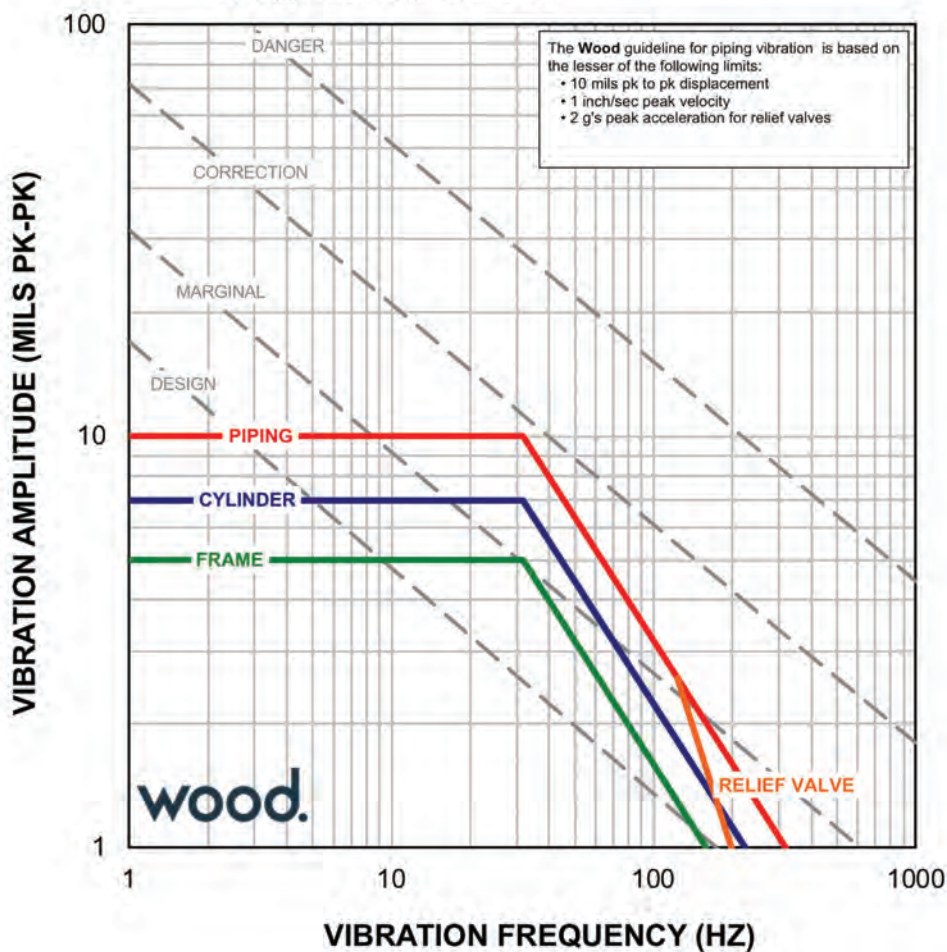


Figure 12-40. Typical guidelines for vibration in displacement (courtesy of Wood.).

12.4.3 Unbalanced Forces

It is important to realize that pulsations as such do not cause vibrations. Rather, the potential for vibration is directly related to how the pulsations couple with the geometry of the compressor and its attached piping.

Unacceptable vibration in a compressor installation at a particular frequency can be the result of high forces, low dynamic stiffness, or a combination of the two. Some common causes of high vibration are:

- pressure pulsation-induced unbalanced forces
- unbalanced forces and moments caused by reciprocating parts
- crosshead forces caused by gas pressures and reciprocating inertia

Guidelines for Reciprocating Compressors (1800 RPM max)

1. Cylinder guidelines are for axial and vertical directions.
2. Generic frame guideline. Consult OEM for recommended limits.
3. Dashed lines adapted from SwRI.
4. Piping guideline not applicable for <2"NPS.

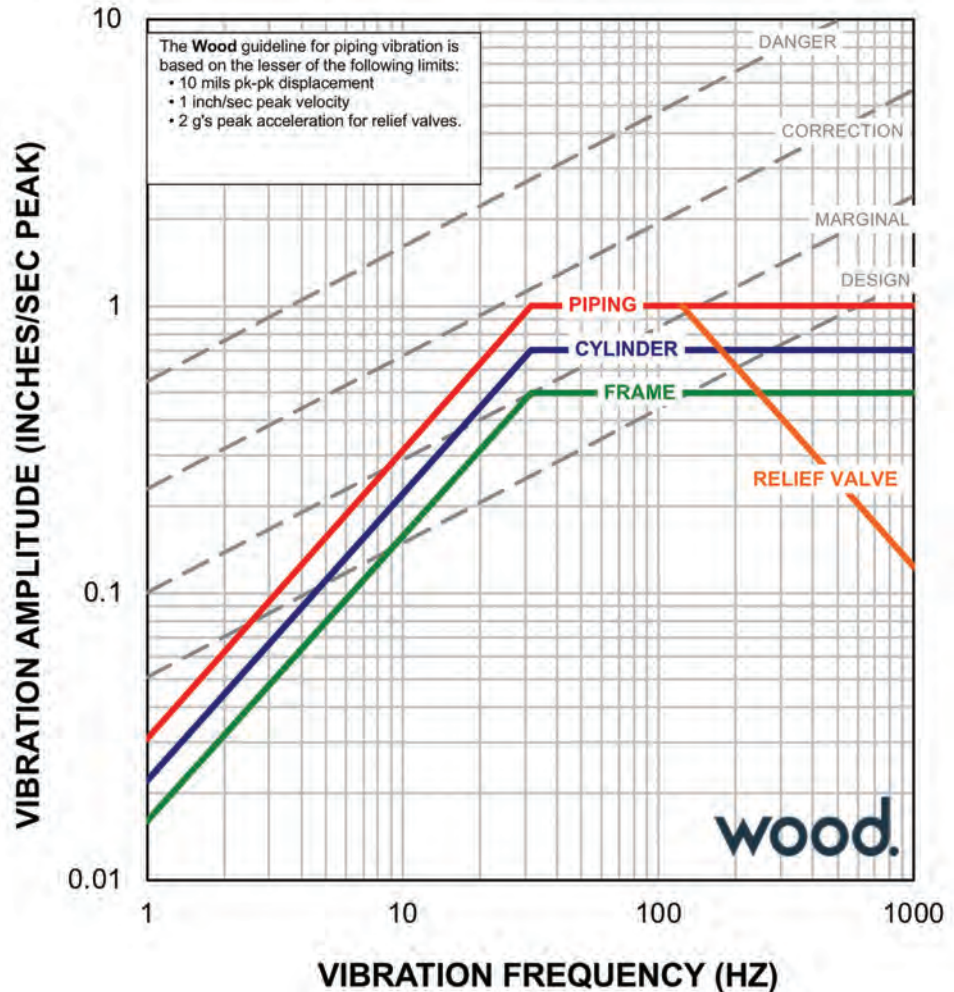


Figure 12-41. Typical guidelines for vibration in velocity (courtesy of Wood.).

- cylinder stretch (i.e., elongation and shortening of the cylinder assembly due to internal gas forces)
- misalignment between the driver and compressor
- mechanical resonance
- pipe strain (bolt-up)
- thermal strain
- low damping

Once a compressor has been operating at a given set of operating conditions for a short period of time, the interaction of the traveling pulses and reflected pulses causes standing

wave patterns. The standing wave pulsation patterns couple with piping geometry to create unbalanced forces. Forces on pipe are dependent on the relationship between pipe length and wavelength. Negligible forces result if the pipe length is much shorter than the wavelength of the pulsation. The highest forces occur when the pipe length is one half of the wavelength.

Unbalanced forces can occur between ends of a header, between bottle ends, between the cylinder and bottle for a reciprocating compressor, or between any two discontinuities in a piping system. Unbalanced forces are best explained with an example, as shown in Fig. 12-42 [23].

Case 1. The header pressure at “A” is at the highest value, and at “B,” the pressure is at the lowest value. At the instant in time when the pressure at “A” is highest and “B” is lowest, the header is being pushed left at “A” with a greater force than it is being pushed right at “B.” At the next instant in time the highest pressure will be at “B” and the lowest at “A.” The net result is that the header has an unbalanced force pushing to the left, then to the right. In this case, the force is equal to the peak-to-peak pulsation times the header area.

Case 2. At one instant in time, the header pressures at “A” and “B” are both at the highest value. At the next instant in time, the pressures at “A” and “B” are at the lowest level.

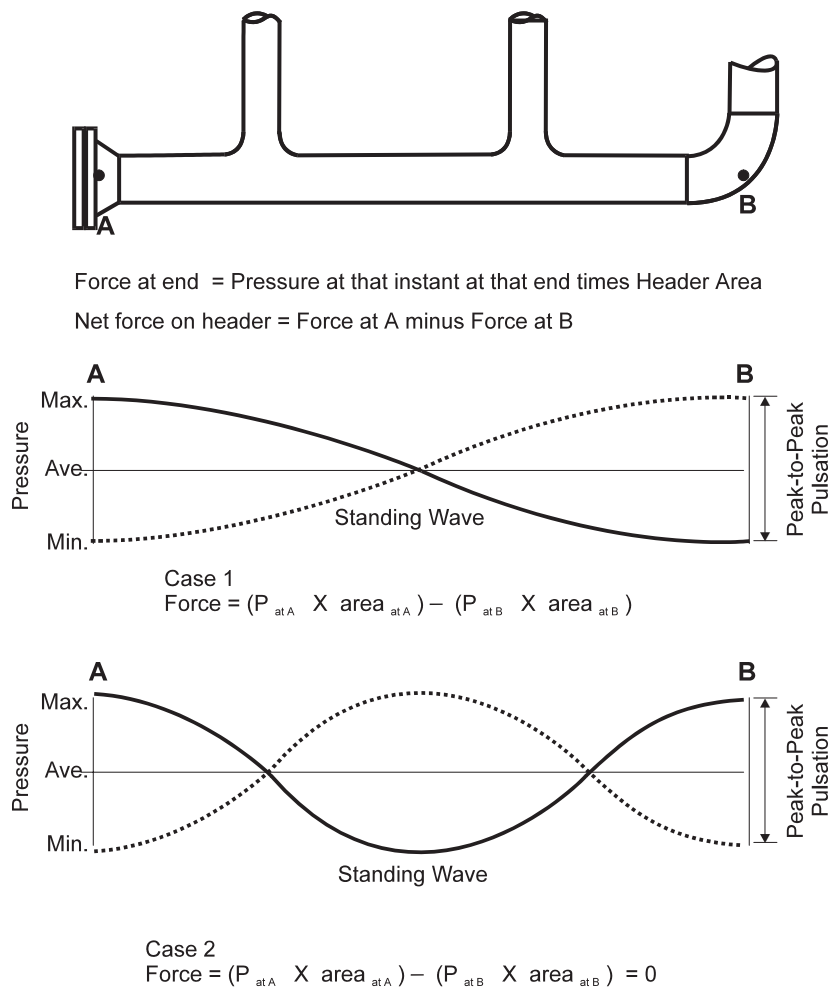


Figure 12-42. Example of forces acting on piping (courtesy of Wood.). (a) Discharge Bottle. (b) Compressor Frame.

The net result is that, at any instant in time, the header has equal forces acting at “A” and “B”; therefore, the unbalanced forces in the header are zero.

12.4.4 Small-Bore Connections

12.4.4.1 General

Small bore connections (SBCs) are a major source of failure on piping systems but are infrequently evaluated during the design phase of a project or during the field commissioning phase. Piping vibration and fatigue can account for up to 20% of hydrocarbon releases, and a large portion of those are due to failure of small bore connections [24]. Hydrocarbon emissions can lead to fire, explosions, injuries, property and environmental damage.

Small bore connections on reciprocating compressor systems cause serious problems with otherwise safe operations when they fail. Costs related to small bore connection failures not only include replacement and lost production costs but also the cost of checking the replacement (vibration checks, dye penetrant check, and/or x-ray checks).

A small bore connection (SBC) is defined as a branched connection on mainline piping that is NPS 2” (DN 50) and smaller, including connections that have a branch pipe to mainline pipe ratio (“branch ratio”) of less than 10%, and excluding connections that have a branch ratio greater than 25% [25]. Note that “mainline piping” could also describe equipment like a vessel or cooler to which the SBC is attached. A chart showing the SBC size definition is shown in Fig. 12-43. The small bore piping that is of most concern is that which contains production fluid at operating pressure. Auxiliary lines, like pneumatic air, crankcase vents, etc., are not as critical.

Small-bore issues should be dealt with in the design stage and during startup of the system. It is better to determine which SBCs are likely to have problems and correct them than to wait for a failure to occur. Two variables that contribute to SBC failure are:

- SBC and SBP design and construction
- vibration of SBC attachment point (base motion)

There are two techniques for screening SBCs for problems: measuring strains and measuring vibrations. When measuring vibrations, there are three issues to consider:

- whether to measure vibration at individual frequencies (frequency domain) or measure overall vibrations (time domain)
- whether to measure vibration velocity or displacement
- whether to measure absolute vibration or relative vibration

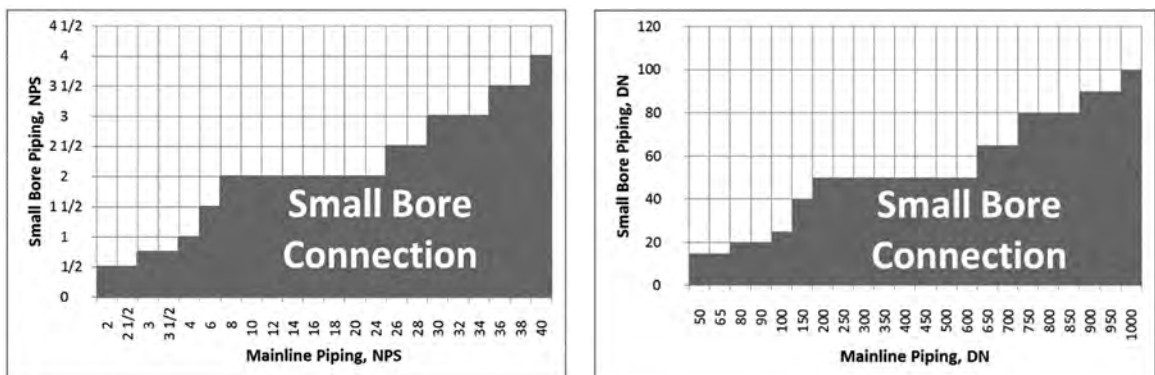


Figure 12-43. Small bore connection definition chart for different pipe sizing [25].

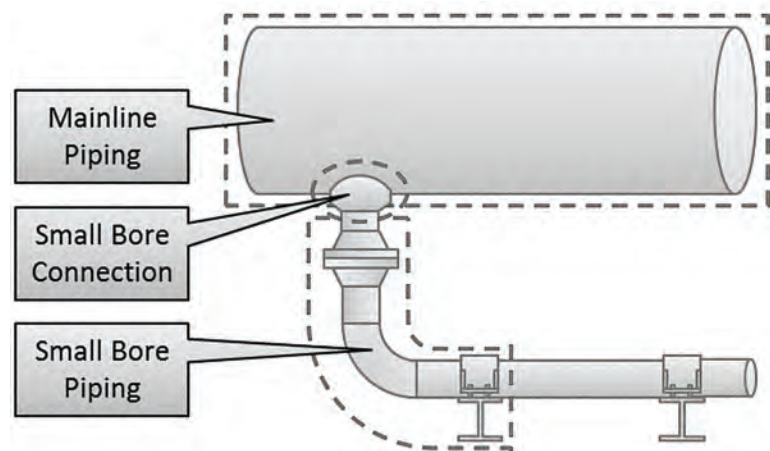


Figure 12-44. Small bore and mainline connection and piping definitions [25].

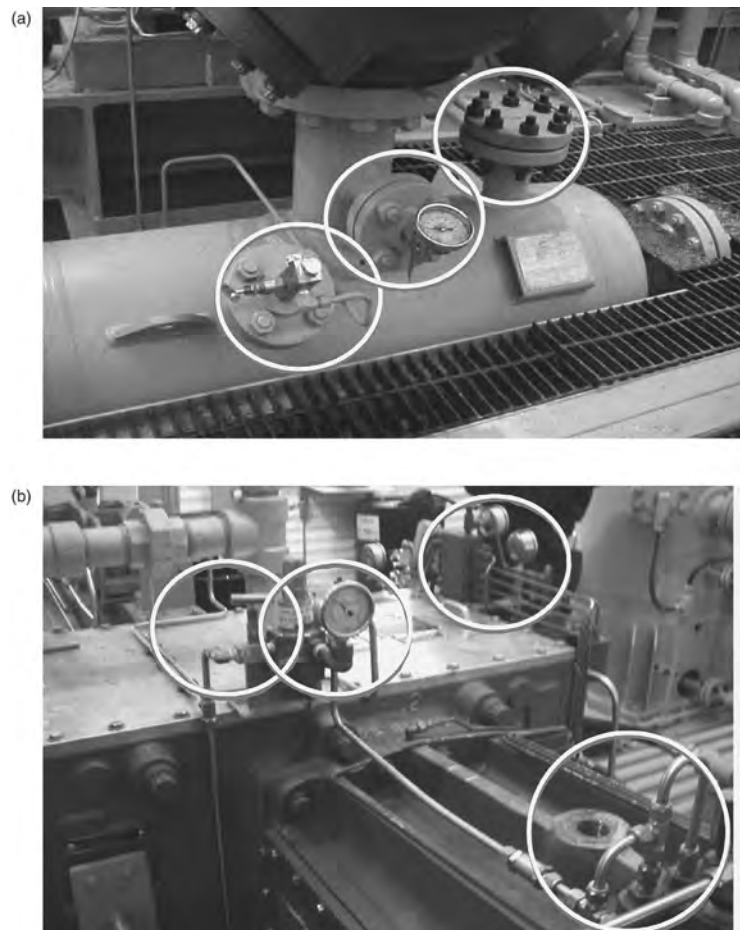


Figure 12-45. Typical small-bore attachments on a reciprocating compressor (courtesy of Wood.).

Figure 12-45 shows some typical SBCs on a pulsation bottle and compressor frame and reinforces how many SBCs are typically found in a reciprocating compressor package. Experience confirms that most small bore problems occur with:

- cantilevered pipe with masses at the end (e.g., flanges, valves)
- long unsupported small-bore piping runs with and without large masses (e.g., valves)

12.4.4.2 Design Best Practices

Good small-bore design can be summarized with three R's [26]:

- removing connections that are not needed
- redesigning connections so they have less cantilevered and unsupported mass
- relocating connections to locations of less base motion

A list of good practices in SBC design [26] is as follows:

- avoid locating SBCs near within about 20' (6m) of rotating machinery, including pulsation bottles and scrubbers on reciprocating compressor manifolds
- avoid mounting SBCs within 10 mainline pipe diameters of pressure reducing devices (e.g., recycle valves, control valves, relief valves, or tight orifice plates) and fittings (e.g., elbows, tees, and reducers)
- SBCs should be located within 2 mainline pipe diameters of pipe clamps and not on long unsupported piping spans. SBCs should be schedule 80 thickness, as a minimum
- heavy valves (including isolation valves, double block and bleed, and gate valves) should not be used on SBCs. Use low profile valves instead, like monoflange valves. If large valves are required, use gussets on the SBC or brace the valve back to the mainline pipe. Other alternatives are to use robust connections like RFLWN or stud-ding outlet connections
- cantilever-type SBP should be as short as possible, and should avoid heavy valves, elbows, and tees

The Energy Institute [24] and Gas Machinery Research Council [27] provide recommendations and screening guidelines for the evaluation of SBCs in vibratory service. There are other screening guidelines available for vibration-induced fatigue failure that contain stress calculations. These guidelines and approaches are useful for screening SBCs but they are not as useful for advanced analysis and field vibration surveys. A more comprehensive approach is provided in [25] and [28].

Failures of SBCs are generally due to alternating stresses caused by vibration at or near the MNF of the SBC (resonance). Designing the MNF of the connection to be well away from the attachment point base motion frequencies will go a long way toward avoiding such failures. In addition, the MNF should not correspond to the MNF of the pipe or vessel to which it is attached because the attachment may act as a vibration absorber.

The orientation of an SBC connected to a system has a significant impact on how much vibration it will exhibit. Orienting an SBC in the direction of compressor cylinder motion is typically better for connections close to a compressor cylinder. Unfortunately, cylinders occasionally vibrate in the vertical direction, so consideration must be given to vibration in that direction as well.

Where an SBC is mounted is also an important consideration. The vibration at the attachment point (base motion) is the driver for the vibration of the connection. The SBC should be located at a point of low vibration. Some examples of better design are:

- installing a pressure tap on a cylinder discharge nozzle instead of putting the same SBC on the discharge bottle
- installing a temperature sensor on the suction scrubber instead of the suction bottle cylinder nozzle
- installing a relief valve on a main piping run near a clamp instead of on an unsupported span or, worse yet, on the discharge bottle itself

Studding outlets should be considered when providing connections for temperature and pressure measurements instead of a cantilevered pair of flanges. Studding outlets have the disadvantage of being somewhat more expensive to buy and having longer delivery than standard flanges. The saving comes in the elimination of potential problem vibration on the appendage and fewer failures.

SBCs can be gusseted down to a repad, but care must be taken not to introduce stress concentration factors near the attachment point. Reference [29] has several figures that show the preferred method of gusseting, where the gusset connects to the main piping (or vessel) several small-bore diameters away from the small-bore appendage attachment point.

Isolating small-bore connections from the base motion is another option that should be considered when controlling base motion is difficult. Typically, this involves remote mounting the appendage and running tubing (or braided hose) to the appendage. The flexibility of the tubing or hose effectively isolates the SBC from the base motion. This will greatly reduce the chance of a failure.

Irrespective of location or design, the amount of dynamic stress that a connection can tolerate will be a function of residual stress in the heat affected zone. If the weld is not stress-relieved, there could be large residual stresses that reduce the endurance limit for the attachment by an unpredictable amount. Use of correct weld procedures can greatly reduce these residual stresses.

After installation and startup of a compressor system, field testing should be performed to ensure that vibrations and stresses are acceptable and to document the baseline conditions for the system. Small-bore appendage failures can happen quickly, so field assessment should be given high priority.

Ideally, guidelines for screening should be derived from a finite element model of the actual geometry of the appendage. This can be done economically by use of parametric models. The goal is to calculate the stress per deflection (psi/mil) at the reference test point (usually the top or a fixed dimension away from the connection point). Divide the allowable stress (endurance limit) by the stress per deflection to get the allowable reference test point deflection. This can be done for every mode shape, but typically, the first-order mode is most important.

For complicated geometry, vibrations as a screening tool will be less accurate. Ultimately, stress estimates from strain gauge readings may be necessary for some locations.

12.4.5 Forced Response Analysis

For rotating machinery and the associated piping systems, traditionally the mechanical analysis design goal is to avoid mechanical resonance. Reciprocating compressors, for example, historically operated at a low speed, such as 300 RPM, and the speed is constant or fixed. Therefore, the design approach to avoid fatigue was a “frequency avoidance” approach. The design philosophy was to design system natural frequencies to be away from 300 RPM. The amount of damping in the system was not considered, and vibration amplitudes are not predicted in this type of modal analysis [30].

However, it is more efficient to operate reciprocating compressors faster, considering the capital cost of the machinery. For example, all things being equal, the compressors can

move twice as much gas if it can run twice as fast. Therefore, compressors are now operating at much higher speeds, up to 1800 RPM, and speeds are increasing. Also, to achieve operational flexibility, these high-speed reciprocating compressors are being operated at variable speeds to control the amount of flow.

For the modern high-speed, variable speed compressors, the traditional “frequency avoidance” design approach is not appropriate. It is often not possible to avoid all overlapping frequencies of excitation, and also it is not necessary to achieve the traditional frequency separation margins. The high-speed compressors will inevitably run at speeds that are at the same as system mechanical natural frequencies, a condition called mechanical resonance. For mechanically resonant systems, a more sophisticated design approach is required to predict vibration levels, and the addition of damping is hugely beneficial.

To predict vibration amplitudes, forced response analysis, sometimes called harmonic response analysis, is required. Also, if forced response analysis is completed, then the amount of damping because of critical importance since the vibration amplitude at resonance is proportional to the amount of system damping (only at resonance). This is analogous to lateral rotordynamics, and the prediction of amplification factors. Vibration amplitudes due to mechanical resonance are technically challenging to predict, requiring accurate boundary conditions and modeling techniques, and bounding of uncertainty regarding the exact resonant frequencies. Following are some guidelines for the accurate application of forced response analysis for machinery and piping systems.

The vibration response is strongly dependent on the precise mechanical natural frequency, and often “identical” units will have significantly different vibration levels when measured in the field due to slight differences of MNFs. Therefore, due to uncertainties in the prediction of mechanical natural frequencies including fabrication tolerances, the vibration response should be predicted assuming mechanical resonance when the mechanical natural frequency is within $\pm 10\%$ of the frequency of the excitation source. This concept is illustrated in Fig. 12-46. The resonant response should be predicted by simulation when 10% separation margin is not met.

Similarly, when comparing vibration that is measured in the field to forced response predictions, it is important to compare vibration at the resonant condition, rather than at a specific frequency. This is due to small uncertainties in MNF predictions combined with a lightly damped “sharp” response peak. With lightly damped systems, very small changes in excitation frequency produce significantly different vibration responses.

Forced response analysis for dynamic machinery should include all sources of vibration. For the reciprocating compressor model shown in Fig. 12-47, sources of vibration include rotating and reciprocating unbalance, cylinder gas rod loads, and pressure pulsation forces.

For reciprocating compressor packages, cylinder gas rod load drives “cylinder stretch” vibration, a significant source of vibration. Since the pressure inside the cylinder does not have a simple sine-wave profile, the Fourier Transform of the gas rod load has components at many harmonics above the fundamental 1x gas rod load. This dynamic force often creates high vibration in mechanically resonant attached pulsation bottles and piping.

Figure 12-48 shows the gas rod load for a typical reciprocating compressor application. The Fourier Transform of the gas rod load is plotted in Fig. 12-49, demonstrating that there are significant force components at many harmonics that could potentially excite attached pulsation bottles and piping.

The cylinder gas load, calculated from the P-V curve, is dependent on the operating condition and load step of the compressor cylinder. Unloading devices such as volume pockets and stepless valve unloaders, in particular, have a significant influence on gas rod loads. Therefore, the cylinder gas rod load should be calculated for all specified operating conditions and load steps to determine the worst-case loads to apply to the compressor system FEA model. This will ensure that the worst-case vibration is predicted when completing the forced response analysis.

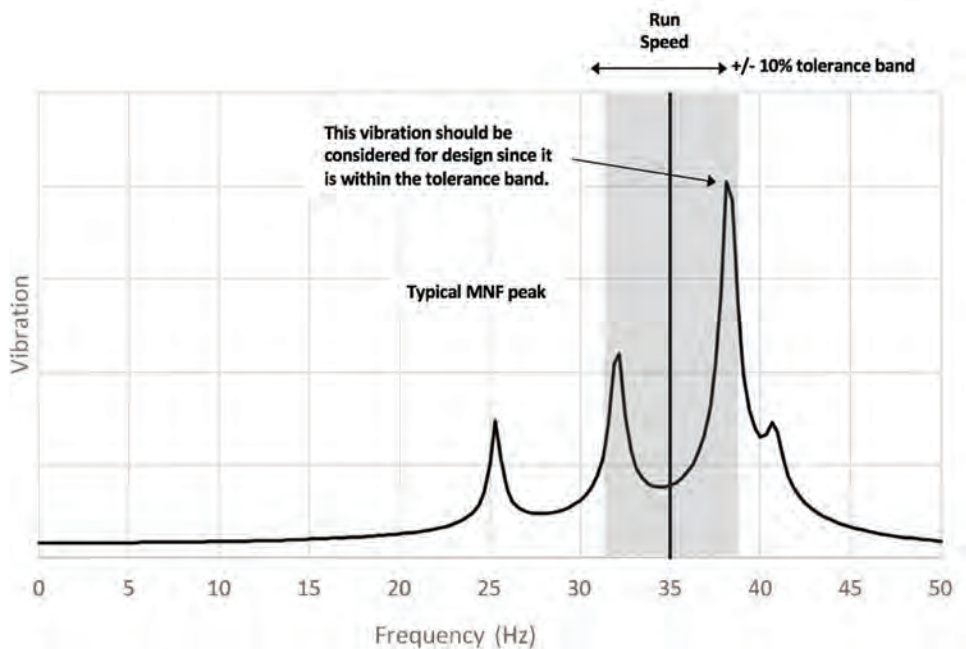


Figure 12-46. Tolerance band to determine maximum vibration when completing forced response analysis (courtesy of Wood.).

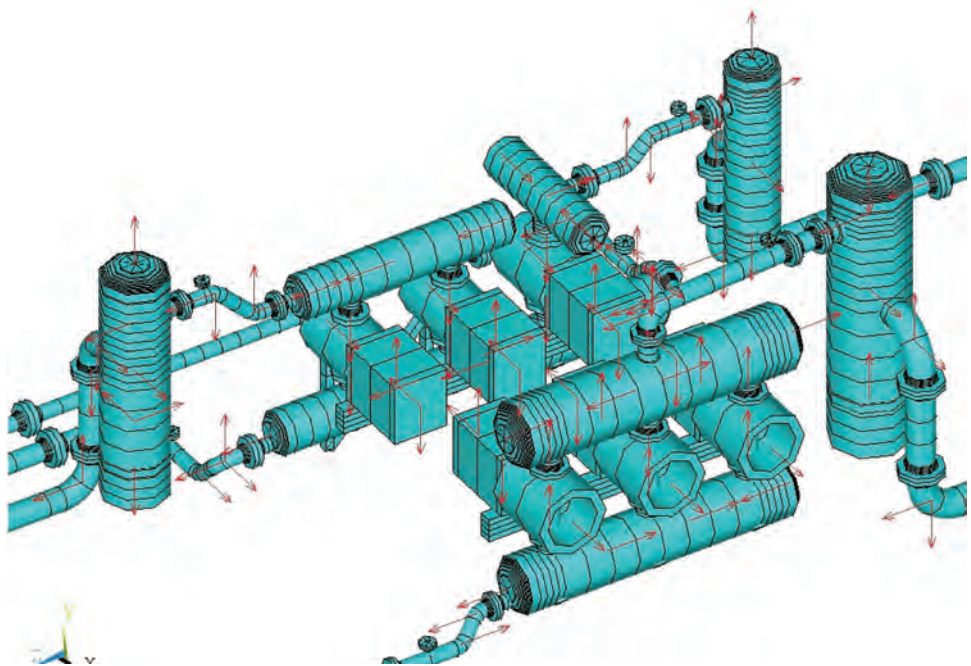


Figure 12-47. Dynamic forces applied to reciprocating compressor finite element model (courtesy of Wood.).

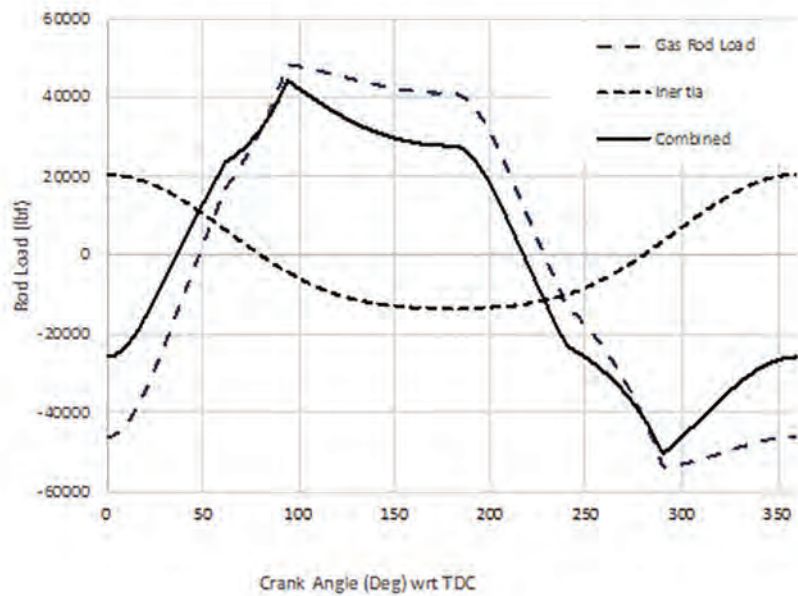


Figure 12-48. Piston rod load due to inertia and internal pressure (courtesy of Wood.).

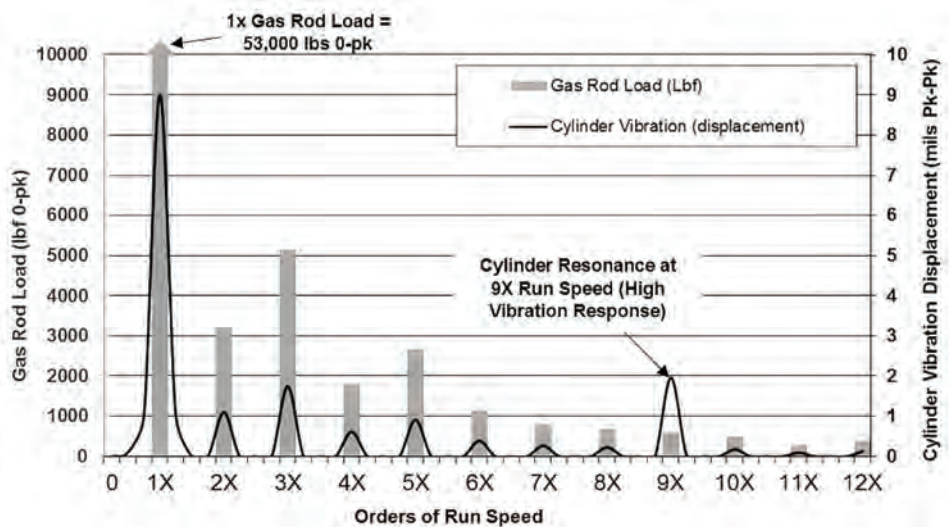


Figure 12-49. Fourier transform of gas rod load and cylinder vibration (courtesy of Wood.).

An example of measured cylinder stretch vibration is shown in Fig. 12-50. The higher frequency components, although lower in amplitude than the fundamental 1x component, are more likely to cause mechanical resonance of pulsation bottles and piping, since these components typically have mechanical natural frequencies in the 30–50 Hz range.

The dynamic forces at 1x compressor speed, including the fundamental gas rod load and rotating unbalance from the drivetrain, are typically much greater than the forces at higher harmonics from pulsation. Accurate forced response analysis at 1x compressor

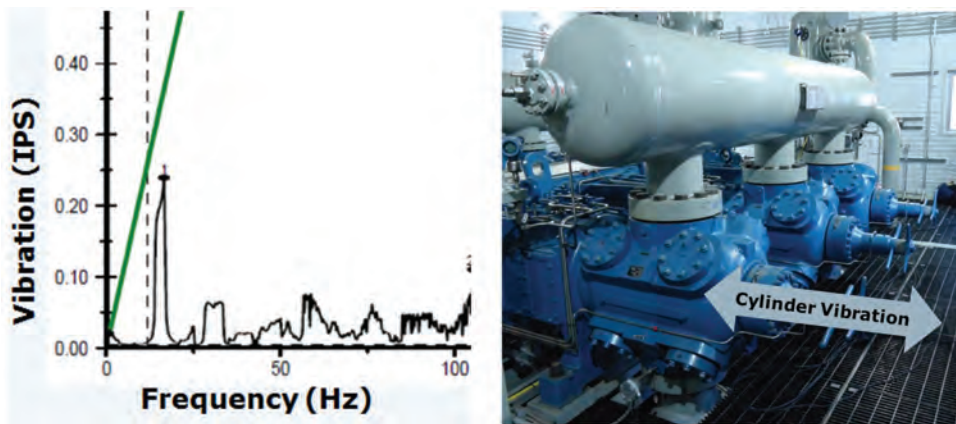


Figure 12-50. Measured reciprocating compressor cylinder stretch vibration compared to Wood vibration guideline (courtesy of Wood.).

running speed requires that the compressor frame, skid and in some cases the foundation be included in the simulation. Figure 12-51 shows an example of a model including the foundation. Often a successful design approach is to design all components to have mechanical natural frequencies above 1x compressor operating speed, and then complete forced response analysis to predict vibration levels at the higher harmonics.

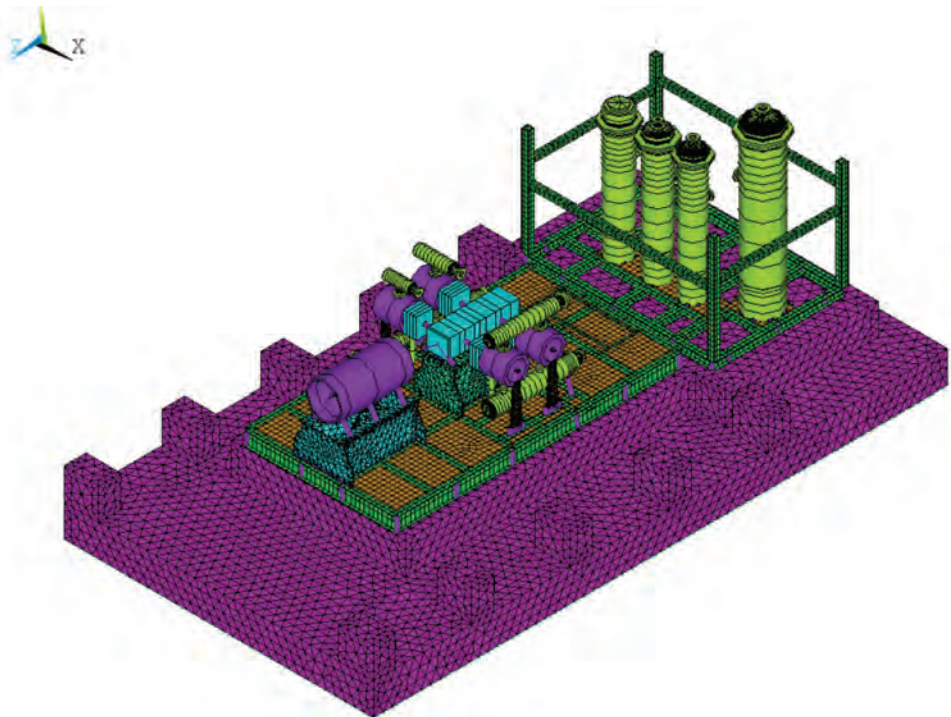


Figure 12-51. Dynamic Finite Element model including reciprocating compressor and concrete foundation (courtesy of Wood.).

12.4.6 Adding Damping to Mechanically Resonant Systems

Field measurements on many problematic machinery and piping systems provided much evidence that the majority of vibration and fatigue problems are due to mechanical resonance and a lack of damping [31]. Whether the source of vibration is from machinery, or acoustically induced or flow induced vibration, forced response analysis is the most accurate design approach to identify mechanically resonant vibration problems, and adding damping is a very effective solution to solve these problems. Since piping systems are typically lightly damped ($\sim 1\%$) and associated vibration problems are due to mechanical resonance, a small increase in damping would serve to eliminate many common vibration problems. An increase in system damping from 1% to 2%, a relatively minor modification, would reduce vibration by 50%, as shown in Fig. 12-52.

For many years damping has been used in industries such as the automotive industry, aerospace, and in commercial appliances. For example, damping materials are why modern automobiles are so quiet. Damping is also used in hand tools to reduce vibration and increase the comfort of the user. Recently there has been an increased use of techniques and products to increase damping in machinery and piping systems, with the goal of reducing vibration and fatigue related failures.

Many mechanisms exist that create damping in mechanical systems. These include friction (Coulomb) and fluid viscosity mechanisms. For the relatively small displacement vibration that is of concern in many machinery and piping systems, “material” or “structural” damping mechanism is most effective. This damping mechanism is a result of internal energy dissipation as materials are cyclically stressed. Viscoelastic materials such as polymers and rubber dissipate significant energy in this way. This mechanism of damping is commonly referred to as hysteretic damping.

The amount of hysteretic damping in this model is quantified by the loss factor η (eta). To gain a general sense of loss factors associated with common materials, refer to Fig. 12-53 by Bhattacharya [30]. As shown, steel has a loss factor of approximately 0.001. For Neoprene rubber, loss factors as high as 2 are possible.

When discussing damping, it is also common to refer to the viscous damping model damping ratio ξ , which is the damping present relative to the “critical” damping. Note that the viscous damping model differs from the hysteretic damping model in that the damping force is proportional to velocity. When comparing these two mathematical models side-by-side, it can be demonstrated that at the system mechanical natural frequency:

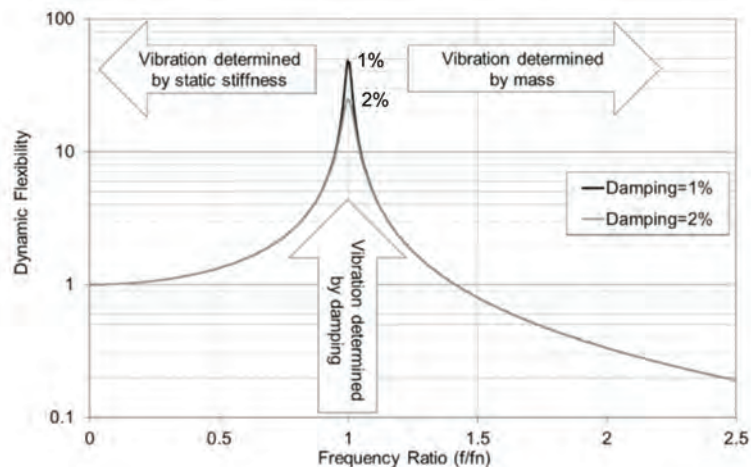


Figure 12-52. Typical frequency response function with different damping (courtesy of Wood.).

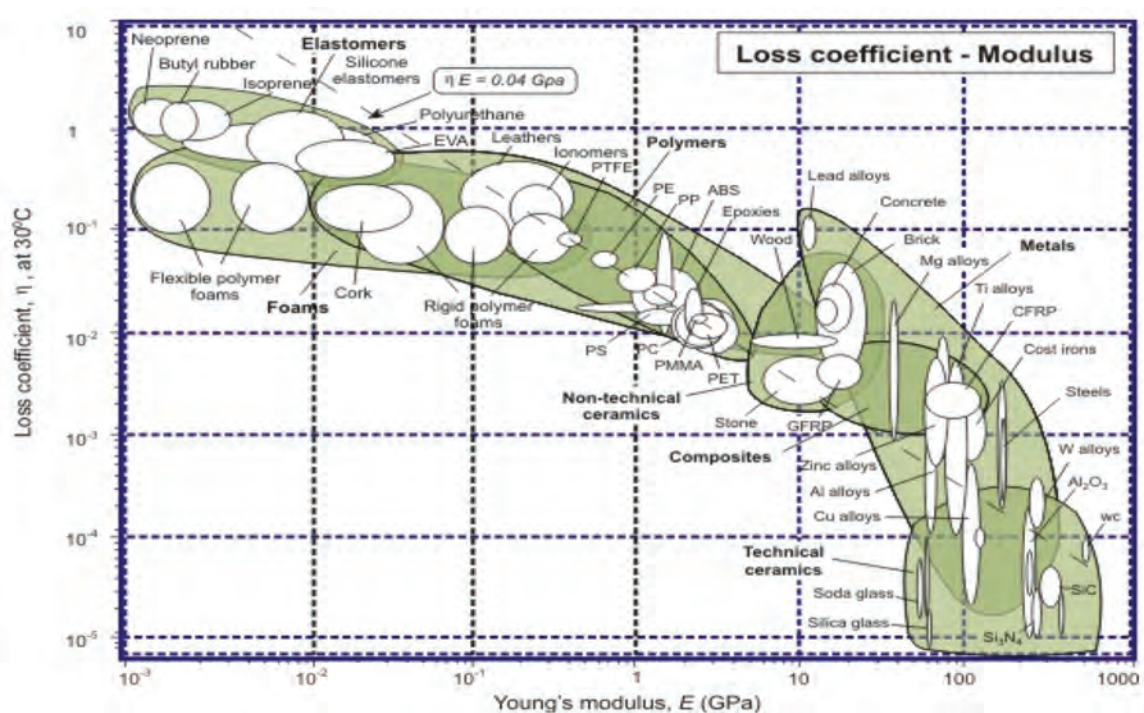


Figure 12-53. Loss factors and Young's modulus of common materials [26].

$$\xi = \eta/2 \quad (12-12)$$

As an example, a loss factor η of 0.1 is equivalent to a damping ratio ξ zeta of 0.05, or it is simply described as having 5% damping. This simple relationship is valid at the system mechanical natural frequency and diverges at other frequencies.

Damping is not commonly utilized in the oil and gas industry to reduce vibration and fatigue. One reason for this is that it is technically challenging to apply damping in an industrial environment. There have been some attempts to utilize damping devices such as automotive shock absorbers or rubber materials, however these devices often result in higher vibration amplitudes over traditional steel supports. In the case of automotive-type shock absorbers or viscous dampers, it is important to realize that the vibration in machinery and piping is characterized by very small amplitudes, a few thousands of an inch. Therefore, a traditional automotive-type shock absorber would not experience enough displacement for the damping mechanism, in this case the flow of hydraulic oil through an orifice, to generate significant damping. Considering rubber mounting materials, similar to rubber engine block mounts, the reduced stiffness of such components when applied to piping systems will result in a significant increase in vibration, not a reduction of vibration. It is true that the damping of the system is increased with the addition of rubber material, however the reduced stiffness defeats any benefit of the increase in damping.

Damping products that utilize industrial viscoelastic materials are best suited to reduce vibration of machinery and piping systems. In addition to having exceptionally high damping factors, these materials have sufficient stiffness to provide damping to the high frequency/low-amplitude vibration that is common in machinery and piping systems. These materials are also extensively tested to ensure longevity and resistance to environmental degradation.

Some examples of damping components added to piping and machinery component are shown in Figs. 12-54 and 12-55. In the case of 12-54, damping braces that utilize

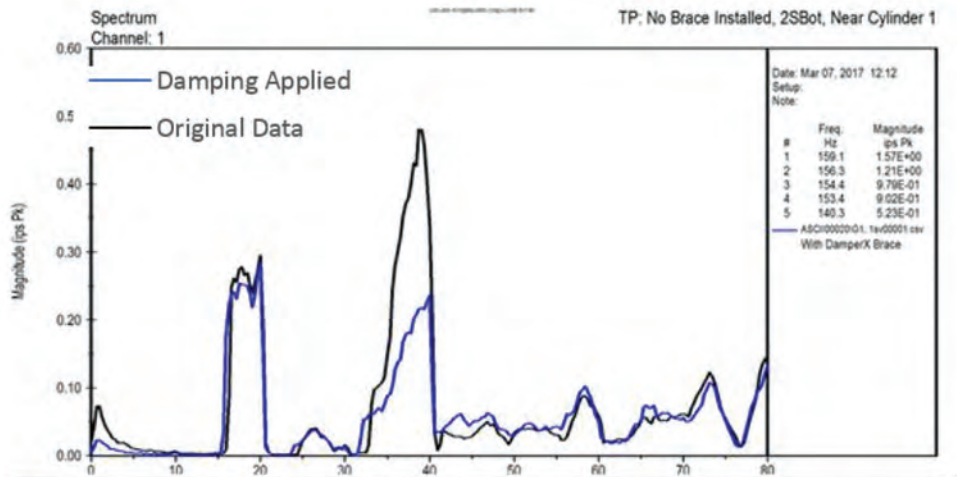


Figure 12-54. Viscoelastic damping braces installed on reciprocating compressor suction bottle (courtesy of Wood.).

viscoelastic material in shear are installed to reduce mechanically resonant vibration on a reciprocating compressor suction bottle. Figure 12-55 shows polymer damping gussets added to a scrubber level switch connection. As is common in the automotive and aerospace industries, the damping materials are intended to be applied using epoxy and can therefore be installed without welding and recertification of piping and pressure vessels. Both of these installations had experienced numerous failures due to mechanically resonant vibration prior to the addition of damping to the systems.

12.4.6.1 Case Study: Damping in Piping Systems

Experimental lab tests, both modal impact tests and shaker vibration tests, were completed by Wood Group for a variety of pipe clamp liners to determine their ability to add damping to piping modes of vibration, and to quantify the corresponding decrease in vibration ampli-

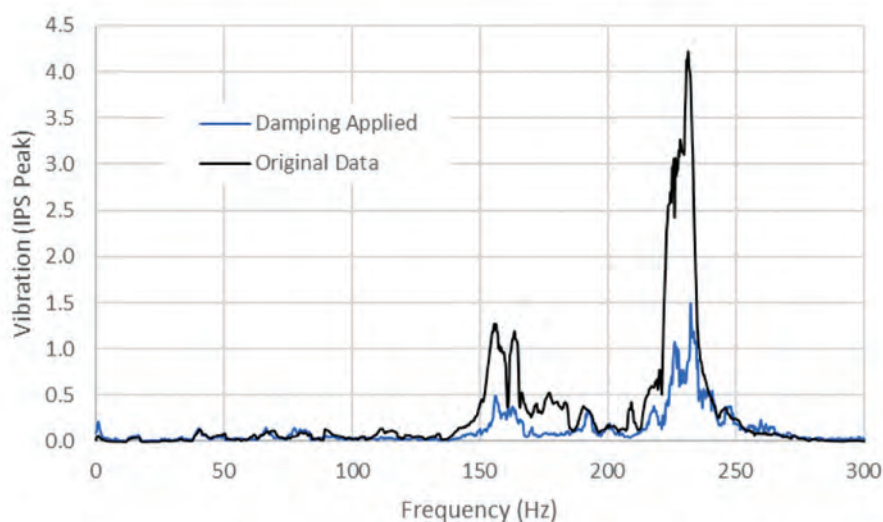


Figure 12-55. Damping material gussets installed on scrubber level switch connection [30].

tude. The tested liners included belting material (elastomeric with fiber reinforcement), silicone rubber, and clamps which have viscoelastic material liners, and a basic steel clamp as a baseline. Only the clamps with viscoelastic liners added significant damping to a test piping span. The clamps with viscoelastic liners were also installed in the discharge line of a reciprocating compressor at a natural gas compressor station, where a reduction of piping vibration amplitudes was measured.

A simple piping system consisting of a span of pipe with 2 clamps was utilized to assess the damping effect of clamp liners, as shown in Fig. 12-56. Wide-flange beams under the pipe

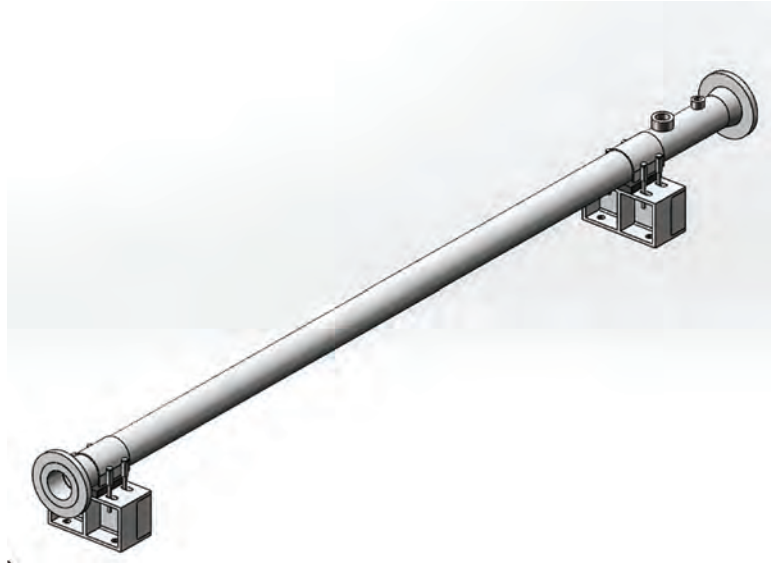


Figure 12-56. Test piping span [30].

clamps were anchored securely to a concrete foundation. An electromagnetic shaker was used to apply a dynamic force to the piping system at the center of the span and create vibration.

Multiple pipe clamp liner materials were evaluated to determine their ability to add damping to the piping system. These are shown in 12-57 and included a basic steel clamp, Teflon, belting material (elastomeric with fiber reinforcement), silicone rubber, and clamps which have viscoelastic material liners.

In all cases the hold-down bolts of the clamps were torqued to 250 in-lb, as is typical for this size pipe clamp. The pipe is 4" XS, and the flanges on the span are ANSI 150# rating. The distance between clamps is 96". This arrangement has the benefits of being easily reproducible for any future testing, and simple to model in any piping analysis software for comparison to the test results.

Two types of tests/measurements were completed to quantify the damping benefits of the various clamps. One test was an impact modal test, also referred to as bump test. The results of this type of test include a frequency response function (FRF), as shown in Fig. 12-58. Analyzer algorithms can process the impact data to calculate an estimation of the amount of modal damping, in this case a "circle-fit" damping calculation.

The tabulated results of the impact tests with the various clamp liners are shown in Fig. 12-59. For the test data presented, the span of pipe was impacted and the vibration response recorded at the center of the span. Modal damping values are listed for both the horizontal (H) and vertical (V) mode directions.



Figure 12-57. Test clamp configurations [30].

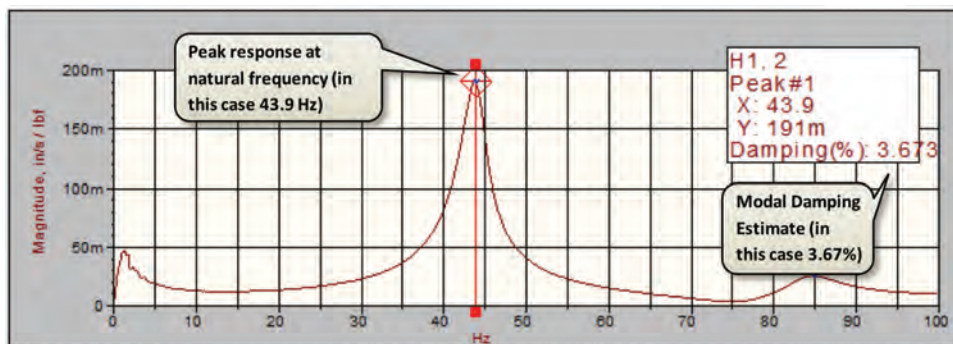


Figure 12-58. Typical impact test FRF results (courtesy of Wood.).

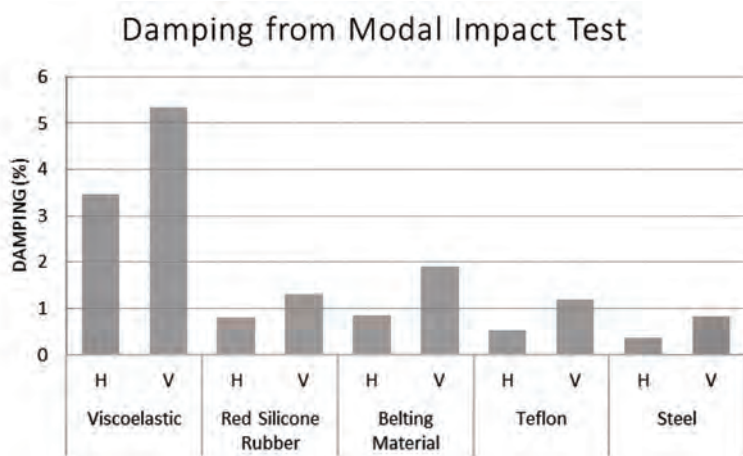


Figure 12-59. Summary of modal impact test (courtesy of Wood.).

Only the clamps with viscoelastic liners significantly increased the damping of the 1st bending mode shape of the piping span. For the liner material to add damping to this mode, the material has to undergo deformation at the clamp location. Previous finite element analysis indicated that since the piping span is nodal (has zero deflection) in the 3 translational directions, the liner material would only add damping to the piping mode if the material was deformed rotationally at the clamp locations.

The next test performed was a running vibration test, where the electromagnetic shaker was used to create vibration in the piping span. The results of this type of test are the actual running vibration amplitude plotted for the entire speed sweep of the test, as shown in Fig. 12-60. The tabulated results of the running tests with the various clamp liners are shown in Fig. 12-61.

Considering the running test and the steel clamps as a baseline, the clamps with viscoelastic liners produced a 77% percent vibration reduction in the horizontal direction, and an 82% reduction in the vertical direction.

The vibration that results with the various clamp liners is a function of liner stiffness, material damping loss factor, coefficient of friction, and the geometry of the pipe clamp relative to the direction of vibration. The silicone rubber liner, for example, has a higher damping loss factor than that of steel. However, the reduction in stiffness results in a higher vibration amplitude.

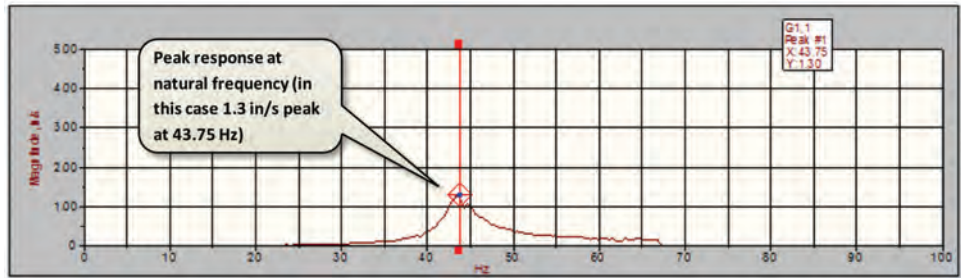


Figure 12-60. Typical speed sweep vibration test (courtesy of Wood.).

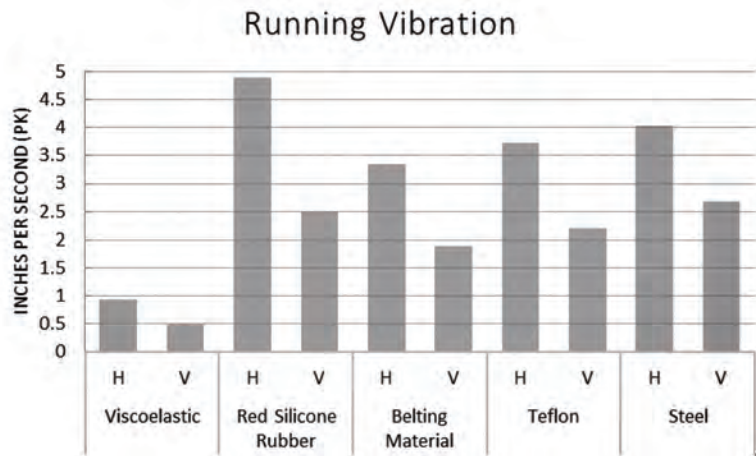


Figure 12-61. Summary of running vibration tests (courtesy of Wood.).

The clamps with viscoelastic liners were also installed in the discharge line of a reciprocating compressor at a natural gas compressor station in Texas. The compressor was a 2-throw single stage unit, operating from 1350–1650 RPM. The installed clamps are shown in Fig. 12-62.

Figure 12-63 is a speed sweep vibration plot at a test point mid-span between supports. The black trace is vibration with the conventional steel pipe supports. The blue trace is vibration after clamps lined with $\frac{1}{2}$ thick viscoelastic liner is installed. The damping was shown to be effective at reducing mechanically resonant vibration considerably.

12.4.7 Thermal Analysis

A thermal analysis may need to be added to determine the stress caused by high and/or fluctuating temperatures. Thermal strain may result from high compression ratios and temperature differentials between suction and discharge conditions and such as those imposed by coolers.

ANSI B31.3 is a typical piping design code for the thermal analysis. Integrating both mechanical dynamic analysis and thermal analysis allows improved efficiency when considering the divergent requirements of the thermal and dynamic designs. A thermal analysis ensures that piping and support stresses due to thermal expansion are acceptable. Thermal load cases have to be selected carefully to ensure that they cover the site conditions and realistic gas temperature possibilities completely. The primary goal is to ensure that the piping



Figure 12-62. Clamps installed with viscoelastic liners [31].

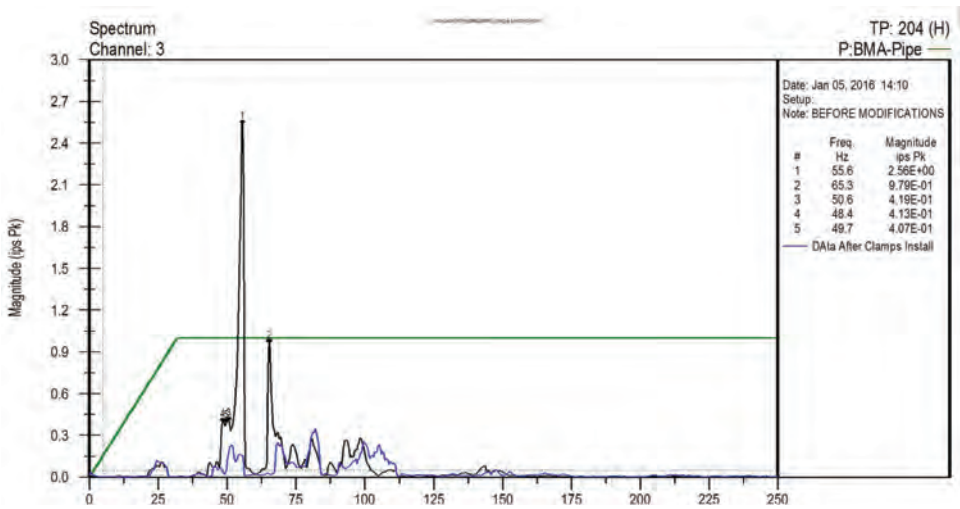


Figure 12-63. Piping vibration [27].

system has the appropriate flexibility in the critical thermal growth directions while being stiff enough in the critical vibration directions to meet the basic mechanical requirements.

12.4.8 Centrifugal Compressors

Centrifugal compressors are not normally associated with piping vibration problems, but numerous problems have been encountered with larger modern designs, particularly high-flow- and low-compression-ratio pipeline compressors. They generate very strong noise that is typically dominated by the blade passing frequency and its higher harmonics.

Various excitation mechanisms of high frequency noise and vibration of piping systems exist [26]. The main sources are usually vortex shedding and/or blade passing frequencies from the impeller or diffuser and typically occur at frequencies higher than 500 Hz. Blade passing frequency will be equal to the product of the number of vanes and the rotational speed. Vortex shedding is more complicated to determine and is a function of the Strouhal number.

Pulsation in reciprocating compressors and positive displacement pumps can generally be described using one-dimensional acoustics. In one-dimensional acoustics, the wavelength of the pulsation is long compared to the pipe diameter and the pressure pulse travels as a plane wave. In a one-dimensional model, the pressure (and flow) properties are assumed to vary only along the length of the pipe and are constant over the cross-sectional area.

However, in large-diameter ducts and piping, the lengths of the waves that propagate can be shorter than the characteristic dimension of the duct or pipe. When this occurs, the wave propagates at an oblique angle relative to the duct or pipe wall, as compared to the plane wave propagation in which the direction of propagation is parallel to the duct wall. As a result, wave interference patterns called cross-wall modes are formed in the duct or pipe. The acoustic pressure across a specific duct cross-section is not constant but varies as a function of the distance across the duct. These acoustical natural frequencies are sometimes referred to as cross-wall or high-order modes.

Several techniques are available to achieve reductions in high-frequency energy [32]. Reduction of vortex shedding energy may be possible by changing the dimensions of the obstruction to discourage vortex shedding or shift its frequency, although piping modifications can be very costly, especially in downtime. Altering the blade-pass frequency requires modification of the compressor internals with potential impact on its performance. Flow splitters, internal bracing, or acoustically absorptive material either inside or outside of the pipe should reduce cross-wall modes, but they may result in other problems such as corrosion or fatigue failures. Acoustic lagging may have to be installed if noise levels are excessive. Testing [33] has revealed that decisions cannot be based on discrete layer testing but have to consider the system as a unit. Air gaps seem to be effective as an intermediate layer.

The high-level noise is not only very disturbing to the people living nearby the installation site but also causes expensive structural failures in the downstream piping. A novel design of Helmholtz array has been developed to address this type of noise problem [34]. Computational studies show that the installation of the Helmholtz array acoustic liner on the compressor diffuser walls is very effective in reducing noise level of the compressor, especially the dominant blade passing frequency noise. The acoustic liner design has been built and tested at an installation site. The data clearly shows that the use of acoustic liners is indeed very effective in the reduction of both the noise and the vibration levels of the machine. Another test resulted in an average reduction in noise levels of about 10 dB for both vaneless and low-solidity diffusers [35] without affecting performance. In another case, however, the solution to a high-frequency piping vibration problem was to remove the diffuser vanes [36]. The following case study provides yet another instance where acceptable shaft and piping vibrations were achieved by redesigning the compressor internals [37].

Case Study: High Shaft and Piping Vibration Levels. Two centrifugal compressors had recently been installed in pipeline service. The compressors were single-stage, 7000 hp with gas turbine drivers, and setup to operate in parallel. The units were equipped with proximity probes to measure shaft motion. Upon startup, high suction and discharge piping vibration was noted. As well, the shaft vibration would periodically exceed alarm levels. Additional supports and clamps were added, which generally reduced the piping vibration levels. However, vibration near the compressors, noise levels in the building, and shaft vibration remained a concern.

An analysis of the two units was conducted. Shaft vibration readings were recorded from the proximity probes (DX and DY at the drive end, and NX and NY at the non-drive end). As well, suction and discharge pulsations and piping vibrations were taken at a number of locations. All measurements were referenced to the once per turn.

The shaft vibration measurements confirmed what the operators were seeing on the panel. The overall readings were spiking intermittently with the DX probe reading often exceeding the alarm level of 2.0 mils peak to peak. The DY probe also spiked and occasion-

ally exceeded the alarm level. The vibration at the non-drive end was considerably lower, but still with the occasional spike in the overall level.

The spectra showed that there was considerable contribution to the overall level from broadband sub-synchronous vibration. Interestingly, the level of vibration did not vary significantly with speed but, rather, with flow.

The suction piping had high vibrations levels also. Vibrations of between 100 and 150 g's were measured on the inlet elbow in the axial direction. The spectra of the vibrations show broad-band excitation centered on the vane pass peak at 2975 Hz.

The discharge piping had even higher vibrations. Overall levels between 175 and 250 g's were measured on the outlet elbow in the axial direction. The spectra of the vibrations again show broad-band excitation centered on the vane pass frequency (see Fig. 12-64). Because of the high frequencies, the actual pipe wall displacements were small, and the piping was not expected to fail. However, there was still concern over fatigue failure of thermowells and small-bore attachments.

The discharge pulsation spectra show a peak pulsation of nearly 50 psi peak to peak (mean pressure was 460 psig) occurring at vane pass frequency. The vibrations and pulsations were definitely due to a flow induced phenomena. The sound level in the compressor building was high, and a major contributor was the sound radiating from the piping at vane pass frequency. Tests were done with the recycle valve opened to allow flow in the recycle line, but that did not result in any improvement.

Considerable discussion took place between the end user, the compressor manufacturer and us. The suction piping layout was seen as a possible cause of turbulent flow at the inlet of the compressor. Redesign of the suction piping would have been prohibitively expensive, so insertion of a flow straightening device was considered to smooth the flow into the compressor inlet. Since the casing had a side inlet, the internal redirection of the flow into the eye of the impellor was also considered a contributor to flow turbulence. In

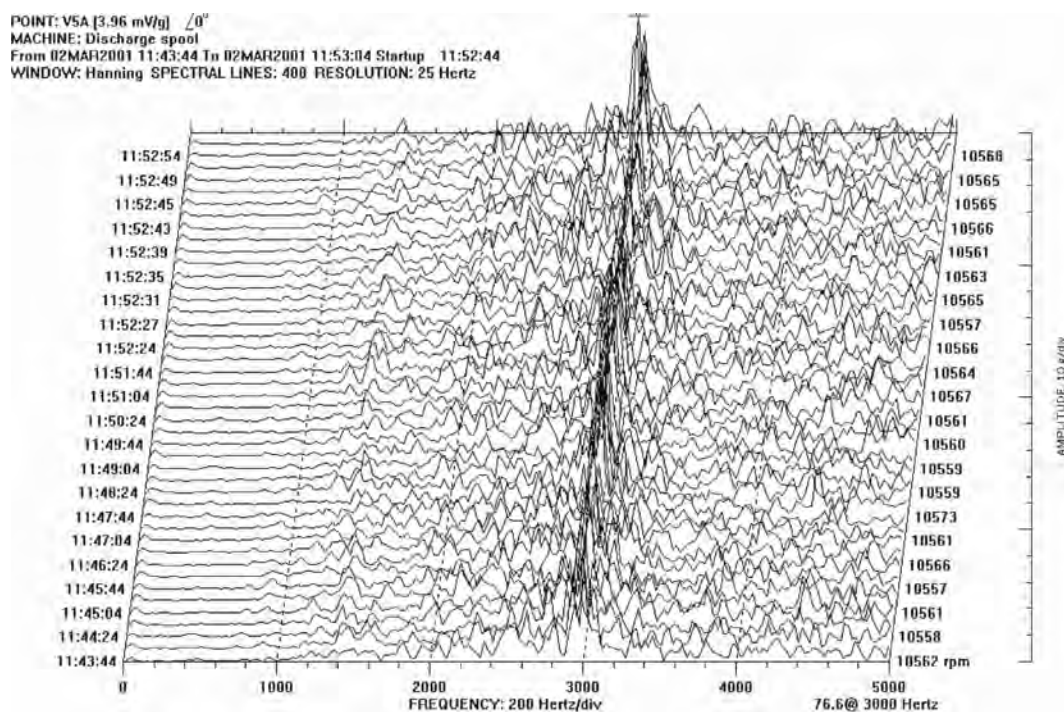


Figure 12-64. Spectra of axial vibration on discharge elbow with dominant component at vane pass frequency (courtesy of Wood.).

any event, there was considerable pulsation energy being generated at vane pass frequencies. The sub-synchronous shaft vibration centered on 100 Hz, which was the compressor rotor natural frequency. The compressor casing had parallel bars that spanned the inlet. The dimensions of the bars and the flow velocities were consistent with a Strouhal vortex shedding frequency near 100 Hz, indicating that the bars were the likely cause of the spiking in the drive end vibration signals.

Because both units failed to meet their head and efficiency guaranties, the vendor agreed to supply new aero-dynamic components (both rotating and stationary). The first of these was installed. Performance testing was conducted on this unit and at the same time vibration and pulsation measurements were taken. With the new aero-dynamic components, the proximity probe readings were generally much lower in magnitude, even at much higher flow rates than in the original testing. As well, the spikiness was much less, and the sub-synchronous components were much lower in magnitude. After the installation of the new aerodynamic components, the most significant component was the synchronous one.

With the new aero-dynamic components, the proximity probe readings were generally much lower in magnitude, even at much higher flow rates than in the original testing. As well the spikiness was much less, and the sub-synchronous components were much lower in magnitude. After the installation of the new aero-dynamic components the most significant component was the synchronous one.

The suction and discharge piping elbow vibrations were significantly lower. The suction piping vibration amplitudes were approximately 1/5 and the discharge amplitudes were approximately 1/3 of those with the original internals. The spectra of the discharge vibrations show that there was still a broadband excitation but at lower amplitude and centered on the new vane pass frequency (Fig. 12-65). Vane pass frequency was only predominant at high flow rates. The discharge pulsations were much lower (again by about two thirds).

Initially, there was some evidence that the piping layout was the main cause of turbulence into the inlet of the compressor; the redesign of the compressor internals reduced the

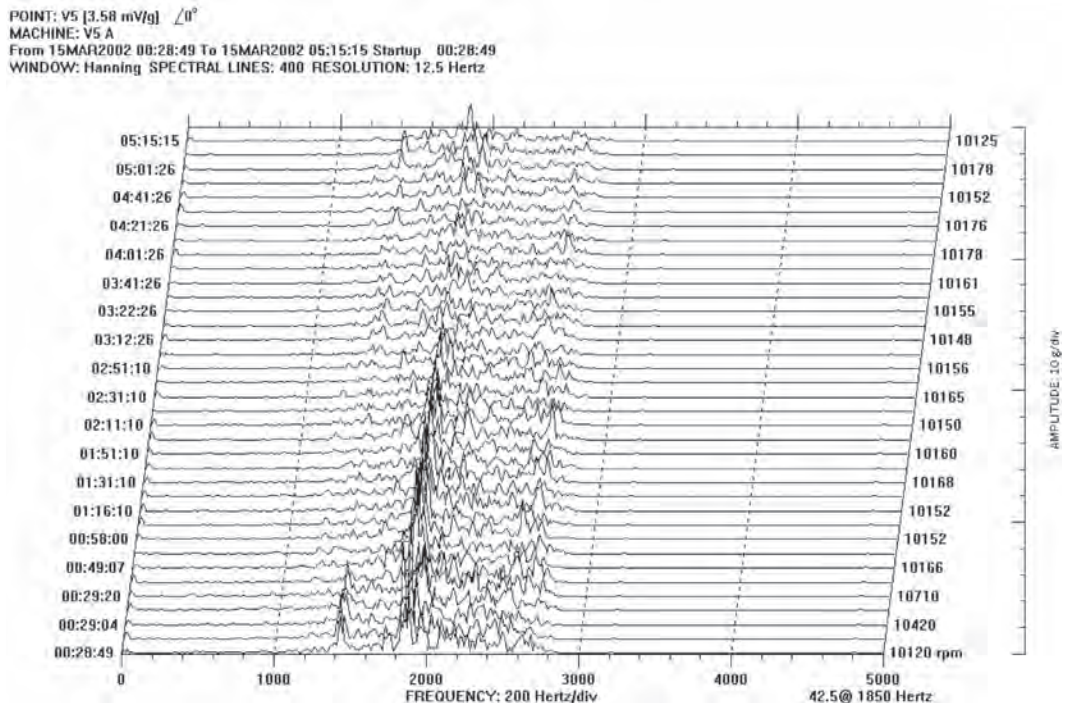


Figure 12-65. Discharge pulsation spectra with new internals (courtesy of Wood.).

pulsation and piping vibration sufficiently. Further recommendations were made to increase the wall thickness of the suction and discharge piping spools immediately upstream and downstream of the compressor. This would alleviate any remaining concerns about possible thermowell fatigue.

The spiking and higher amplitude of the shaft vibration appears to have been caused by the poor aerodynamic performance of the original internals. The redirection of the flow from the side inlet flange to axial for entry into the impeller was a contributor to the turbulence. As well, it is likely that the vortex shedding from the internal bars in the flow passage contributed to the excitation of the shaft critical speed and, hence, the spiking of the shaft vibrations.

REFERENCES

- [1] API Standard 684, 2005. "API Standard Paragraphs Rotordynamic Tutorial: Lateral Critical Speeds, Unbalance Response, Stability, Train Torsionals and Rotor Balancing," *American Petroleum Institute, API Recommended Practice Second Edition*, August 2005, pp. 1–318.
- [2] Mitchell, J. S., 2007. "From Vibration Measurements to Condition Based Maintenance," *Vibration and Sound*, January 2007, pp. 62–78.
- [3] Wilcox, E. and O'Brien, D. P., 2003. "Determining the Root Causes of Subsynchronous Instability Problems in Two Centrifugal Compressors," *Proceedings of the 32nd Turbomachinery Symposium*, Turbomachinery Laboratory, Texas A&M University, College Station, TX, pp. 9–19.
- [4] API Standard 617, 2002. "Axial and Centrifugal Compressors and Expander-compressors for Petroleum," *Chemical and Gas Industry Services, American Petroleum Institute*, Seventh Edition, July 2002, pp. 1–193.
- [5] Murray, B. D., Howes, B. C., Chui, J. and Zacharias, V., 2003. "Sensitivity of Torsional Analyses to Uncertainty in System Mass Elastic Properties," *Beta Machinery Analysis*, pp. 1–8.
- [6] Murray, B. D., Howes, B. C. and Zacharias, V., 1996. "System Torsional Response Over Range of Loading/Operating Conditions," *Beta Machinery Analysis Ltd.*, Nov 1996.
- [7] de Jongh and van der Hoeven, 1998. "Application of a Heat Barrier Sleeve to Prevent Synchronous Rotor Instability," *Proceedings of the 27th Turbomachinery Symposium*, Turbomachinery Laboratory, Texas A&M University, College Station, TX, pp. 17–26.
- [8] Smith, D. R. and Wachel, J. C., 1984. "Experiences with Nonsynchronous Forced Vibration in Centrifugal Compressors," TAMU Instability Workshop, Rotordynamic Instability Problems in High Performance Turbomachinery—1984, Texas A&M University, May 1984, pp. 1–16.
- [9] Murray, B. D., Howes, B. C. and Zacharias, V., 1995. "A Systems Approach to Torsional Analysis," *Gas Machinery Conference*, Corpus Christi, Texas, October 1995, pp. 1–7.
- [10] API Standard 610 (also ISO 13709), 2004. "Centrifugal Pumps for Petroleum, Petrochemical and Natural Gas Industries," *American Petroleum Institute*, 10th Edition, pp. 1–184.
- [11] Marscher, W. D., 2007. "An End-User's Guide to Centrifugal Pump Rotordynamics," *Proceedings of the 23rd Pump Users Symposium*, Turbomachinery Laboratory, Texas A&M University, College Station, TX, pp. 69–93.
- [12] Wood, B. M., Olsen, C. L., Hartzo, G. D., Rama, J. C. and Szenasi, F. R., 1995. "Development of an 11,000 r/min, 3500 hp Induction Motor and Adjustable Speed Drive for Refinery Service," *Petroleum and Chemical Industry Conference*, 1995 Volume, Issue, 11–13 Sep 1995, pp. 55–63.
- [13] De La Roche, L. and Howes, B. C., 2007. "Lateral and Torsional Vibration Problems in Systems Equipped with Variable Frequency Drives," *paper by Beta Machinery Analysis*, pp. 1–18.
- [14] Corcoran, J. and Sakers, C., 2007. "Designing today's couplings," *Turbomachinery International*, Nov/Dec 2007, pp. 38–40.
- [15] Bently, Donald E., 2002. *Fundamentals of Rotating Machinery Diagnostics*, First Edition, Bently Presurized Bearing Press, ISBN 978-0971408104, pp. 1–725.
- [16] ISO 14839-1:2002. "Mechanical vibration—Vibration of Rotating Machinery Equipped With Active Magnetic Bearings—Part 1: Vocabulary," *International Standards Organization*, pp. 1–30.

- [17] ISO 14839-2:2004. "Mechanical vibration—Vibration of Rotating Machinery Equipped With Active Magnetic Bearings—Part 2: Evaluation of Vibration," *International Standards Organization*, pp. 1–40.
- [18] ISO 14839-3:2006. "Mechanical Vibration—Vibration of Rotating Machinery Equipped With Active Magnetic Bearings—Part 3: Evaluation of stability margin," *International Standards Organization*, pp. 1–35.
- [19] Kleynhans, G., Pfrehm, G., Berger H. and Baudelocque, L., 2005. "Hermetically Sealed Oil-free Turbo-compressor Technology," *Proceedings of the 34th Turbomachinery Symposium, Turbomachinery Laboratory*, Texas A&M University, College Station, TX, pp. 63–76.
- [20] ISO Standard 1940-1, 2003. "Mechanical Vibration—Balance Quality Requirements of Rigid Rotors—Part 1: Determination of permissible residual unbalance," *International Standards Organization*, pp. 1–28.
- [21] ISO Standard 11342, 1998. "Mechanical vibration—Methods and Criteria for The Mechanical Balancing of Flexible Rotors," *International Standards Organization*, pp. 1–44.
- [22] Baker, J. R., Skales, W. J. et al., 1999. "Guidelines for the Avoidance of Vibration Induced Fatigue in Process Pipework," *The Marine Technology Directorate Limited (MTD)*, Publication 99/100, pp. 1–120.
- [23] Greenfield, S. D. and de la Roche, L., 2007. "Introduction to Vibration & Pulsation in Reciprocating Compressors," paper by Beta Machinery Analysis, pp. 1–35.
- [24] Guidelines for the Avoidance of Vibration Induced Fatigue Failure in Process Pipework, 2nd Edition, Energy Institute, January 2008.
- [25] Harper, C. B., 2014. "Integrity Evaluation of Small Bore Connections (Branch Connections)," 9th Conference of the EFRC September 10th–12th, 2014, Vienna, 9 pages.
- [26] Howes, B. C. and Harper, C. B., 2003. "Vibration Related Failures of Small-Bore Attachments," Gas Machinery Conference, October 2003, pp. 1–13.
- [27] Design Guideline for Small Diameter Branch Connections, Release 1.0, GMRC/PRCI, March 2011.
- [28] Simons, S., Fierro, F. and White, B., 2016. "Applying the Energy Institute and GMRC/PRCI Guidelines for the Avoidance or Reduction of Vibration Problems in Small Diameter Piping Branch Connections, 45th Turbomachinery & 32nd Pump Symposia, Houston, Texas, Sept. 12–15, 2016, 22 pages.
- [29] Marine Technology Directorate Limited (MTD), 1999. "Guidelines for the Avoidance of Vibration Induced Fatigue in Process Pipework," Publication 99/100.
- [30] Bratek, W., 2015. "Solutions to Mechanical Vibration: Report on Damping Solutions to Address Resonance," Prepared for Gas Machinery Research Council, July 21, 2015, 70 pages.
- [31] Bratek, W. and Shaver, J., 2016. "Damping Components at a Reciprocating Compressor Station – Field Test Results," Presented at Gas Machinery Conference 2016, 15 pages.
- [32] Price, S. and Smith, D. R., 2002. "High-Frequency Piping Vibration and Noise," *Proceedings of International Pipeline Conference*, Calgary, IPC2002-27331, pp. 1–19.
- [33] Schmidt, T. and Motriuk, R. W., 2003. "A Closer Look at the Performance of Acoustical Pipe Lagging," Society of Experimental Mechanics, Presented at IMAC XXI, Kissimmee, FL., Feb. 2, 2003, pp. 1–5.
- [34] Liu, Z., Hill, D. L. and Motriuk, M. W., 2002. "On Reducing Piping Vibration Levels—Attacking the Source," ASME Turbo Expo 2002, Amsterdam, pp. 1–7.
- [35] Liu, Z. and Hill, D. L., 2002. "Centrifugal Compressor Noise Reduction by Using Helmholtz Resonator Arrays," TP052 Dresser-Rand, pp. 1–18.
- [36] Motriuk, R. W. and Harvey, D. P., 1998. "Centrifugal Compressor Modifications and their Effect on High-Frequency Pipe Wall Vibration," *ASME Transaction, Journal of Pressure Vessel Technology*, Vol. 120, pp. 276–282.
- [37] Eckert, W. F. and Howes, B. C., 2002. "A Case Study of Piping and Shaft Vibrations on a Centrifugal Compressor," paper by Beta Machinery Analysis, pp. 1–10.

ENVIRONMENTAL ISSUES RELATED TO COMPRESSOR AND PUMP STATIONS

13.1 INTRODUCTION

Environmental issues are becoming much more prominent for pump and compressor stations with the primary drivers being regulatory requirements and social concerns about their impact on the environment inhabited areas. In spite of the desire by some parts of our society to eliminate fossil fuel pipelines, and by inference pumping and compression, the world economy will be dependent on hydrocarbons for a considerable time, which implies that pump and compressor stations will continue to be a part of the pipeline landscape for a while yet. The rapid increase in shale gas production has accelerated even more the building of pipelines and associated compression. On the consumption side, the conversion from coal to natural for power generation.

Although the large-scale compressor stations generally associated with the major “trunklines” stand out in terms of installed power and throughput capacity, most compressor stations are relatively small-scale operations. For instance, about 75% of all compressor stations in North America have an installed power level below 15 MW [1] and a throughput capacity of less than 28 million m³ per day (1 Bcf per day). The prevalence of smaller scale compressor stations reflects the large number of “grid” type interstate natural gas pipeline systems that operate within established regional markets. Moreover, compressor stations located on grid-type systems tend to be designed with less power because operational line pressures are less, average capacity is lower, and much of the system consists of thinner-walled, smaller-diameter natural gas pipelines. Figure 13-1 shows an example of the huge number of compressor stations installed in the US [1], which speaks to the environmental challenges primarily in terms of noise and emissions and their effect on the populace and the environment.

13.2 ENVIRONMENTAL ISSUES

13.2.1 Summary

Environmental issues for pump and compressor stations mainly revolve around noise and emissions although other issues such as health effects are also sometimes raised. There are regulatory requirements for addressing noise and emissions, but they vary widely based on local and national regulations that continue to change. In particular, there are two major driving forces for these changes. The first one is increasing population pressures that

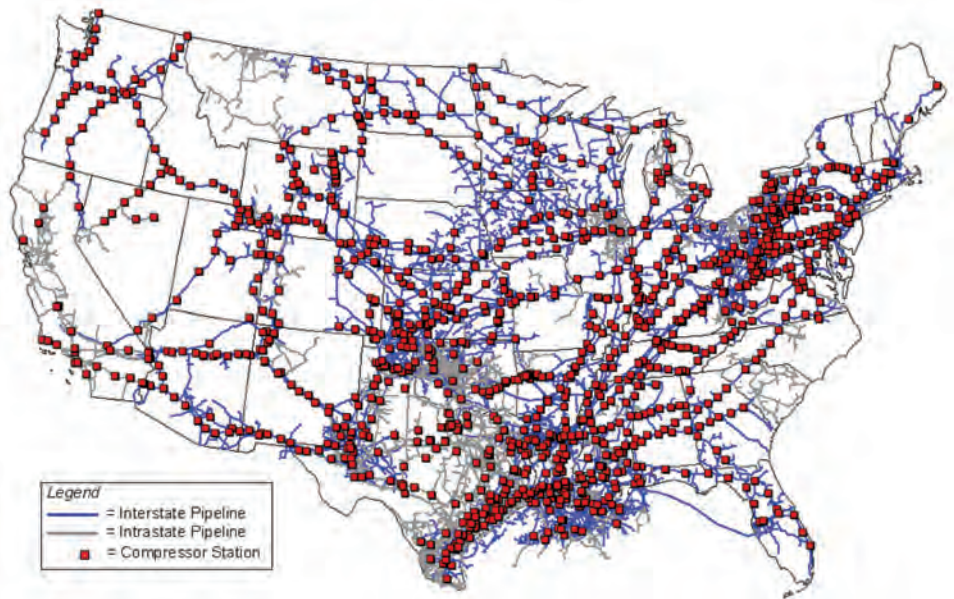


Figure 13-1. US Interstate Natural Gas System Mainline Compressor Stations, 2008 [1].

either increasingly encroach on existing facilities or that make it more difficult to build new pipelines into more densely populated areas where demand is increasing. The second driving force is an increasing focus on addressing climate change with activism to reduce the world's dependence on fossil fuels. This emphasis on climate change as far as pump and compressor stations are concerned is partially concerned with direct emissions from drivers and fugitive emissions from unit and station piping often more targeted at complete elimination of fossil fuels. This chapter will only deal with the former and will leave the latter to other discussions.

Noise has been shown to have dramatic and everlasting effects on people, both from occupational health standpoints, and community annoyance perspectives. Those effects on people that are undesirable are often threatening, induce fatigue, reduce proficiency, modify physiological responses, and harm human systems. At the present time, avoidance of excessive noise exposure is the only assured way to prevent these major hazardous effects.

The practical alternative to complete avoidance is to limit exposures in these environments to those defined as acceptable by appropriate guidelines, standards, and damage risk criteria (DRC). Scientific exposure criteria and guidelines established to curtail these effects are vital parts of comprehensive protection programs of concern to governments, industry, and affected personnel. Most adverse effects of this commonly encountered noise on human systems can be minimized and controlled through engineering and design efforts, conservation programs, personal protective equipment, and administrative actions. Central to these programs and actions are criteria and guidelines that establish acceptable exposure limits.

Noise that is a concern outside the station fence line is mainly produced by gas turbine and engine drivers. Reciprocating compressors by their very nature also produce significant noise while centrifugal compressors are relatively quiet. In addition, piping noise and that of auxiliaries such as aerial and auxiliary coolers contribute to the total noise envelope. Intermittent noise caused by blowdowns or relief venting is also a concern often mentioned by the public.

The first topic related to emissions deals with exhaust emissions from gas turbine and internal combustion engine drivers. These are found primarily at compressor stations since most pump units are driven by electric motors. Gas turbines, due to their high combustion temperatures produce large amounts of nitrogen oxides (NO_x), a pollutant, and carbon dioxide (CO₂), a green house gas (GHG). As is further covered in Chapter 8, section 8.2.9.2, much improvement has been made with reducing NO_x emissions to quite low levels. Section 13.5 describes better monitoring of NO_x emissions using predictive techniques. The same applies to internal combustion engines using natural gas where lean-burn technology is also achieving low emission levels.

Much more emphasis has been placed on the impact of fugitive emissions for methane due to its impact on GHGs although it is often not mentioned that the lasting effect of methane on climate change is much less than that of CO₂. Regulatory requirements for detecting and mitigating fugitive emissions are increasingly being established and best practices have been defined by industry [2].

The environmental impact of a pump station is much less with the primary driver being a non-polluting electric motor and noise levels being quite low. The only significant environmental issue is related to leaks and spills, mostly quite small and most of which are usually contained to the site without impact to the public.

13.2.2 Designing for Environmental Requirements

Past practice for dealing with environmental issues has largely been reactive. The compressor or pump station site is based on land availability and hydraulic design. Major design and equipment decisions are made early without sufficient consideration of the social impact and with mitigative measures only added when pressured by external parties. There has been a tendency for a minimum amount of formal community consultation. The project then has to absorb unplanned schedule and cost changes when the design scope is changed to accommodate social considerations.

Pipeline companies are learning that it is more productive to be proactive by engaging in early and comprehensive formal community consultation by an unbiased third party. Selection of a compressor or pump station site should be based with anticipation of social and environmental concerns. Specific plans need to be made to minimize construction impact. The longer term impact during operation, including future developments around the site, should be considered along with the more temporary impact during maintenance. Unscheduled blowdowns need to be minimized and scheduled ones prior to maintenance widely communicated to the public.

The most important decision is that of the driver to use. Although design measures to minimize noise and emissions can be effective, the easiest solution may be to install an electrically-driven compressor, especially a hermetic compressor that has no emissions or noise concerns. Of course, this solves the local problem but can be seen as transferring these issues to the electric power plant instead.

In the end, the topic of environmental and social concerns around pump and compressor stations comes down to risk and its perception [3]. While it is possible to conduct a formal risk assessment process, usually by experts, the general public depends mostly on intuitive risk judgments with a focus on a “no risk” society. The public and media understandably have difficulties in understanding risk, especially probabilistic processes, with much of their input based on biased media coverage and misleading personal experiences with a focus on worst possible consequences. Disagreements on risk often do not evaporate in the face of evidence. The basic question is how safe is safe enough and what is the balance between risk vs benefits. Observations for experts are generally more based on facts and evidence and a more sophisticated understanding of the context and level of risk but may have similar biases as the public when going beyond available evidence and data.

13.3 NOISE MEASUREMENT

The discussion of noise will start by defining some important parameters that are commonly used in quantifying noise levels, provide a brief exposure limits and noise criteria that are established by most occupational health and safety agencies, and describe some methods and correlations to predict noise emission from typical compressor and pump station facilities.

13.3.1 Noise Level Parameters

A quantity commonly measured in engineering acoustics is *sound intensity*, defined as the continuous flow of power carried by a sound wave through an incrementally small area at a point in space. The units are Watts per square meter (W/m^2). This quantity is important because it is related to the total power radiated into the air by a sound source, and also because it bears at that point a fixed relation to the sound pressure. Sound intensity at a point is directional (a vector) in the sense that the position of the plane of the incrementally small area can vary from being perpendicular to the direction in which the wave is traveling to being parallel to that direction. It has its maximum value, I_{\max} , when its plane is perpendicular to the direction of travel. When parallel, the sound intensity is zero. In an environment in which there are no reflecting surfaces, the sound pressure *at any point in any type of freely traveling* (plane, cylindrical, spherical, etc.) wave is related to the maximum intensity I_{\max} by:

$$P_{\text{rms}}^2 = I_{\max} \cdot \rho_0 c_0 \quad (13-1)$$

where

$$\begin{aligned} P_{\text{rms}} &= \text{root-mean-square (rms) sound pressure, Pa (N/m}^2\text{)} \\ \rho_0 &= \text{density of air, kg/m}^3 \\ c_0 &= \text{speed of sound in air, m/s} \end{aligned}$$

A sound source radiates a measurable amount of power into the surrounding air, called sound power, in watts. If the source is non-directional, it is said to be a spherical sound source. For such a sound source, the measured (maximum) sound intensities at all points on an imaginary spherical surface centered on the acoustic center of the source are equal. Mathematically,

$$W = I_{\max, R} \cdot (4\pi R^2) \quad (13-2)$$

where

$$\begin{aligned} I_{\max, R} &= \text{maximum sound intensity at radius } R \text{ at surface of an imaginary sphere} \\ &\quad \text{surrounding source, W/m}^2; \\ W &= \text{total sound power radiated by source, Watts (N} \cdot \text{m/s)}; \\ R &= \text{distance from acoustical center of source to surface of imaginary sphere, m.} \end{aligned}$$

The sound pressure level (L_p) in decibels (dB) is defined as:

$$L_p = 10 \log_{10} \frac{P_{\text{rms}}^2}{P_{\text{ref}}^2} \quad (13-3)$$

and the sound power level (L_w), also in dB is defined as:

$$L_w = 10 \log_{10} \frac{W}{W_{\text{ref}}} \quad (13-4)$$

where

P_{ref} = reference pressure taken as 20 Pa.

W_{ref} = reference power taken as 10^{-12} W.

From Eqs. (13-1) through (13-4), the following relationship between L_p and L_w can be found:

$$L_p = L_w + 10 \log_{10} \left(\frac{Q}{(4\pi R^2)} \right) + 10 \log_{10} \left(\frac{\rho_0 c_0}{400} \right) \quad (13-5)$$

where R is the radial distance from the source to the receptive location (m), and Q is the directivity index; $Q = 1$ for spherical source, $Q = 2$ for hemispherical source (i.e. source that is emitting from a point on an infinitely large plane), $Q = 4$ for quarter sphere (i.e. source that is emitting from a point at a corner of two perpendicular infinitely large planes), $Q = 8$ for one eighth spherical source, etc.

The above relation [Eq. (13-5)] indicates that if the distance is doubled, the sound pressure (P_{rms}) will be reduced by a factor of 2 and the sound intensity by a factor of 4, and hence the sound pressure level (L_p) will be reduced by 6 dB. If R is increased by a ratio of 10, the sound pressure level will be decreased by 20 dB.

13.3.2 Noise Criteria Limits

Criteria and limits define conditions above which the risk of damage due to an exposure is considered unacceptable. Noise describes exposure characteristics and corresponding undesirable effects such as noise-induced hearing loss, fatigue that cause decreased proficiency and may lead to physiological and psychological adverse impact on people. Damage risk criteria (DRC) have been developed and implemented worldwide. The basic exposure-effects relationships that underlie these criteria are reasonably well understood and are derived from observations and experience as well as good laboratory and field studies. The various criteria contain different limiting values because of variations in interpretations of the basic data and in the rationale used to establish them. The rationale may include practical, legal, and economic considerations as well as humanitarian concerns. It is important that the rationale underlying specific DRC in specific jurisdiction is fully understood by the user to ensure that its application is justified and accurate.

Estimates of noise exposures and of their probable effects on populations are usually expressed in terms of population distribution statistics. These group population effects are not precise descriptors nor are they appropriate for evaluating an individual. Nevertheless, they are adopted by nations and incorporated into national regulations and laws. Many become mandatory requirements included in governmental and industrial activities involving exposure of people to noise and vibration environments.

Permanent hearing loss and its associated problems are clearly the most critical and widespread of the various consequences of excessive noise exposure. The extent of damage to the hearing mechanism caused by noise is related to the amount of acoustical energy reaching the hearing mechanism. Such damage cannot be estimated accurately for an individual because of the variability of the noise and the susceptibility of the exposed ears. The primary factors in noise-induced hearing loss are the level of the noise, the frequency

content or spectrum of the noise, the duration or time course of the noise exposure, and the susceptibility of the ear.

Exposure limits are defined in terms of level, spectrum, and duration of the noise. A-weighted sound energy of an exposure is directly related to noise-induced hearing loss. No other measure of noise exposure provides a better cause-effect relationship with hearing loss. It was agreed that there is no convincing evidence against acceptance of A-weighting measurement of all noises from 20 to 20,000 Hz in determining their permanent threshold shift (noise-induced hearing loss that does not recover to pre-exposure levels after cessation of exposures) hazard except when their unweighted, instantaneous, peak-sound-pressure levels exceed approximately 145 dB. Consequently, exposures are typically described in terms of the average A-weighted levels, or the equivalent continuous A-weighted sound pressure level (L_{eq}), over an average workday. The equivalent continuous sound level (L_{eq}) is the steady sound pressure level which, over a given period of time, has the same total energy as the actual fluctuating noise. The A-weighted equivalent continuous sound level is denoted L_{Aeq} . If the level is normalized to an 8-hour workday, it is denoted $L_{Aeq,8h}$. If it is over a time period of T hours, then it is denoted $L_{Aeq,T}$ and is defined as follows:

$$(L_{Aeq,T}) = 10 \log_{10} \left[\frac{1}{T} \int_0^T \left(\frac{P_A(t)}{P_{ref}} \right)^2 dt \right] \quad \text{dBA} \quad (13-6)$$

Practical measures for the prevention of noise-induced hearing loss are centered in hearing conservation programs. These programs involve definitions of acceptable noise exposure, personal hearing protection, monitoring the hearing of the affected personnel, and appropriate administrative actions to minimize and eliminate identified temporary hearing problems before they become permanent. The basis of a hearing conservation program is the definition of acceptable noise exposure or exposure criteria that specify the acceptable exposure limits and the proportion of the population to be protected. The criteria of various hearing conservation programs and applications differ in their limiting values. The most obvious differences among noise exposure criteria are the sound level at which the implementation occurs and how the duration of the exposure and the sound level of the noise are combined. The duration-sound level relationships are referred to as time-intensity trading rules, which assume that damage to hearing is related to total A-weighted sound level and the duration of exposure time. The permissible A-weighted sound level for an 8-hour exposure ranges from 75 dB(A) for the Environmental Protection Agency (EPA) [4] to 90 dB(A) for the Occupational Safety and Health Administration (OSHA) [5]. In Canada, CSA's Occupational Safety and Health (OHS) specifies 85 dB(A) in most provinces [6]. Table 13-1 provides the allowable exposure limits versus exposure duration per day in US and Canada. The following relationship can be applied to determine the precise exposure limit for any given exposure duration per day.

$$(L_P)_{\text{limit,duration}=T} = (L_P)_{\text{limit,8 hours}} - \frac{R_E}{0.301} \log_{10} \left(\frac{T}{8} \right) \quad \text{dBA} \quad (13-7)$$

where:

R_E = exchange rate (in dBA), that is the decrease in the amount of exposure limit if the exposure time is doubled

T = exposure time in hours

Table 13-1. Exposure noise criteria limits in US and Canada

OSHA (USA)		OHS (Canada)		
Duration Per Day (Hours)	Permissible Exposure "Slow" Response, dBA	Noise Exposure Limits When Criterion Level = 85 dB(A) for 8-Hour Exposure		
		3 dB(A) Exchange Rate	Exposure Time	5 dB(A) Exchange Rate
		Allowable Level dB(A)	(Hours)	Allowable Level
8	90	85	8	85
7	91.0	85.6	7	86.0
6	92.1	86.2	6	87.1
5	93.4	87.0	5	88.4
4	95.0	88.0	4	90.0
3	97.1	89.2	3	92.1
2	100.0	91.0	2	95.0
1.5	102.1	94.0	1	100.0
1	105.0	97.0	0.5	105.0
0.5	110.0	100.0	0.25	110.0
0.25 less	115			

OSHA: Occupational Safety and Health Administration, a federal agency of the United States that regulates workplace safety and health (www.osha.gov)

OHS: refers to www.OHS.CA, the Canadian Occupational Health and Safety standards and activities.

Most criteria utilize the 3-, 4-, or 5-dB exchange rate rule. The 3-dB rule is based on the equal-energy concept and is the most conservative or protective of the three rules. The 4- and 5-dB rules assume that intermittency and interruptions of exposures reduce the risk to less than that expected from the total energy. Consequently, a 50% increase in exposure duration corresponds to sound level decreases of 3 and 5 dB for the respective 3- and 5-dB rules (Table 13-1).

According to OSHA regulations, the daily noise dose (D) in percent is given in terms of slow-response time-average A-weighted sound levels by

$$D = 100 \sum_{i=1}^n \frac{C_i}{T_i} \quad \text{dBA} \quad (13-8)$$

where C_i is the duration of exposure to a specific sound pressure level (SPL) in hours and T_i is the allowable daily duration for exposure to noise at that value of SPL. Under OSHA regulations, noise dosage exceeding 100% is not permitted. Exposure to noise levels above 115 dB(A) is not permitted. Moreover, for exposure to noise having a slow response time-average A-weighted sound level of any value, the instantaneous peak sound pressure level may not exceed 140 dB. It should also be noted that the dosage levels are considered to be attributable to noise that actually reach a worker's station at the ear level. If a worker moves from place to place in the course of his or her occupational assignment, the dosage must be based on the noise exposure and the time spent at each station during the work period.

Example Problem

Monitoring of a noise environment at a location yielded the following time samplings over the course of a normal 8 hours. Compute the dosage and comment on the result.

Exposure Level, dB(A)	Exposure Time (Hours)
85	1.5
90	3
92	2.5
95	0.5
97	0.3
100	0.2

Solution

Applying Eq. (13-1) and using Table 13-1 (OSHA levels), we obtain

$$D = 100 \left(\frac{3}{8} + \frac{2.5}{6} + \frac{0.5}{4} + \frac{0.3}{3} + \frac{0.2}{2} \right) = 112\%$$

This dosage of 112% violates OSHA regulations. However, if this 8-hour workday is cut down by 100/117 to 6.8 hours or less (assuming the noise level distribution is fairly consistent throughout the day), the daily dosage will not exceed 100%. It can also be arranged to move the worker to a region, where the noise level averages 86 dB(A) or less (i.e., below the OSHA noise level range), for 1.16 hours in order to round out 8 hours daily on the job.

The criteria for extended (continuous or steady) noise exposure, noise criteria (NC) curves have been developed Beranek in 1957 [7] which are characterized in octave band levels. In this case, the measured octave band spectrum of the noise is plotted on the family of curves given in Fig. 13-2. The NC index is the value of that curve which lies just above the spectrum of the measured noise. This is called the tangency rule. This approach actually tries to take into account the difference in frequency weighting made by the ear, at different intensity levels. NC values are especially useful when specifying noise in a given environment for control purposes, that is to aid in defining the octave range that is the most culprit and needs to be suppressed.

The NC curves were originally intended primarily for rating air conditioning noise and have been largely superseded by Balanced Noise Criterion (NCB) curves, Fig. 13-3. More detailed information on NCB curves may be found in the standard ANSI S12.2-1995 [8] and in the proposals for its revision by Schomer (1999) [9]. The designation number of an NCB curve is equal to the Speech Interference Level (SIL) of a noise with the same octave band levels as the NCB curve. The SIL of a noise is the arithmetic average of the 500 Hz,

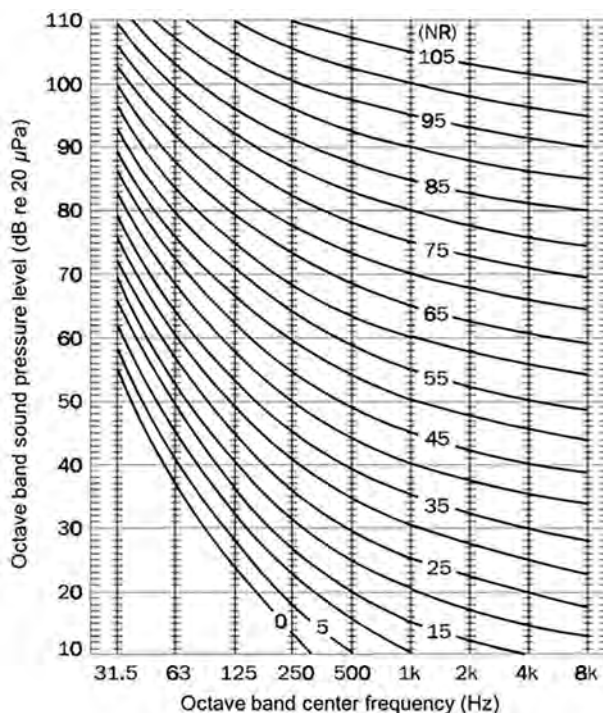


Figure 13-2. Noise criteria (NC) curves.

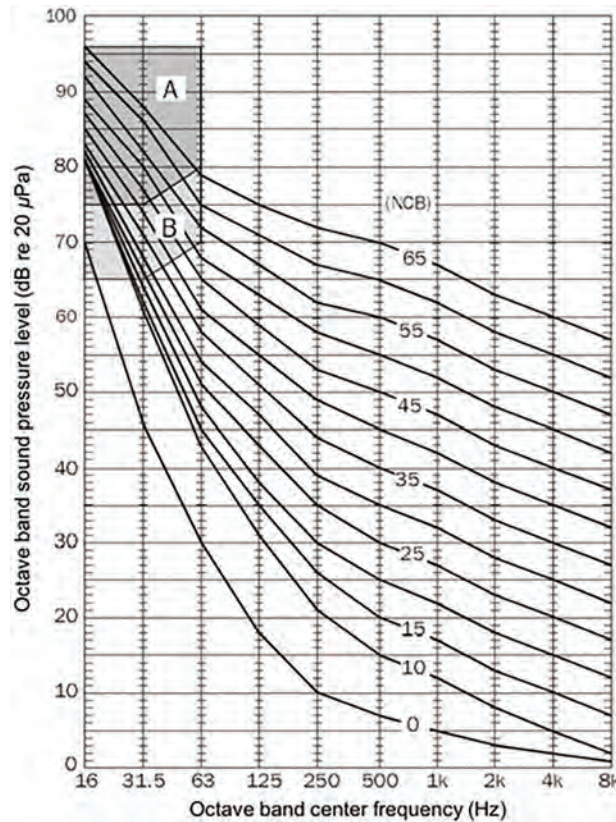


Figure 13-3. Balanced noise criteria (NCB) curves.

1 kHz, 2 kHz, and 4 kHz octave band levels. Note Regions A and B represent the rumbling range (low frequency), where Region A represents exceedance of criteria for readily noticeable vibrations and Region B represents exceedance of criteria for moderately (but not readily) noticeable vibrations. Table 13-2 (Beranek and Ver, 1992) [10] lists the recommended categories of NCB curves for different uses of building interior space.

For community noise assessment, the U.S. Environmental Agency developed the day–night equivalent level (DNL) in order to account for different response of people to noise at night. This equivalent level is defined as:

$$L_{dn} = 10 \log_{10} \left[\frac{15 \left(10^{L_d/10} \right) + 9 \left(10^{(L_n+10)/10} \right)}{24} \right] \text{ dBA} \quad (13-9)$$

where, L_d represents the 15-hour daytime A-weighted equivalent sound level (from 7:00 a.m. to 10:00 p.m.) and L_n is the 9-hour nighttime equivalent A-weighted sound level (from 10 p.m. to 7:00 a.m.). The nighttime value carries a penalty of 10 dB because noise at night is deemed to be much more disturbing than noise generated during the day. The use of the day–night equivalent level as a parameter is increasing in the United States and some nations for evaluating community noise and some cases of airport noise. The U.S. Federal Interagency Committee on Urban Noise (FICUN) [11] adopted DNL as the descriptor of environmental noise that affects residences.

In 2002, the European Union Parliament and Council issued Directive 2002/49/EC in an effort to establish common assessment methods for rating environmental noise in terms

Table 13-2. Recommended NCB curve categories on the basis of interior use and suggested noise criteria range for steady background noise

Type of Space (and Acoustical Requirements)	NCB Curve ^a	Approximate L_A dB
Broadcast and recording studios (distant microphone pickup used)	10	18
Concert halls, opera houses, and recital halls (for listening to faint musical sounds)	10–15	18–25
Large auditoriums, large drama theaters, and large churches (for very good listening conditions)	Not to exceed 20	28
Broadcast, television, and recording studios (close microphone pickup used only)	Not to exceed 25	33
Small auditoriums, small theaters, small churches, music rehearsal rooms, large meeting and conference rooms (for very good listening), or executive offices and conference rooms for 50 people (no amplification)	Not to exceed 30	38
Bedrooms, sleeping quarters, hospitals, residences, apartments, hotels, motels, etc. (for sleeping, resting, relaxing)	25–40	38–48
Private or semiprivate offices, small conference rooms, classrooms, libraries, etc. (for moderately good listening conditions)	30–40	38–48
Living rooms and drawing rooms in dwellings (for conversing or listening to radio and television)	30–40	38–48
Large offices, reception areas, retail shops and stores, cafeterias, restaurants, etc. (for moderately good listening conditions)	35–45	43–53
Lobbies, laboratory work spaces, drafting and engineering rooms, general secretarial areas (for fair listening conditions)	40–50	48–58
Light maintenance shops, industrial plant control rooms, office and computer equipment rooms, kitchens and laundries (for moderately fair listening conditions)	45–55	53–63
Shops, garages, etc. (for just acceptable speech and telephone communication). Levels above NC or NCB 60 are not recommended for any office or communication situation	50–60	58–68
For work spaces where speech or telephone communication is not required, but where there must be <i>no risk</i> of hearing damage.	55–70	63–78

^aSee Figure 13-3.

of harmonized indicators for the determination of noise levels. The concrete figures of any limit values are to be determined by the Member States of the European Union. The common noise indicators adopted are day–evening–night equivalent level L_{den} to assess annoyance and the evening and night equivalent levels, defined as follows:

$$L_{den} = 10 \log_{10} \left[\frac{12 \left(10^{L_d/10} \right) + 4 \left(10^{(L_e+5)/10} \right) + 8 \left(10^{(L_n+10)/10} \right)}{24} \right] \text{ dBA} \quad (13-10)$$

where

L_d = A-weighted average sound level determined over 12-hour day periods of the year

L_e = A-weighted average sound level determined over 4-hour evening periods of the year

L_n = A-weighted average sound level determined over 8-hour night periods of the year

It should be noted that +5 dB(A) and +10 dB(A) penalties have been imposed to reflect the need for quieter periods of evenings and nights, respectively. While the day spans 12 hours, the evening 4 hours, and night, 8 hours, the Member States may shorten the evening period by 1 or 2 hours and lengthen the day and/or the night period, correspondingly, provided the measurements are consistent for all sources and the reporting States provide the European Commission with information on any systematic difference from the default option. The default values of (local) time are 0700–1900 hours for day, 1900–2300 hours for evening, and 2300–0700 hours for night. Use of L_{den} will likely increase in the future for airport noise and other environmental assessments in European Union.

13.3.3 Predictions of Noise Levels from Compressor Stations

There are four major sources that contribute to the overall noise level of a compressor station: the prime mover, whether it is an internal combustion engine or gas turbine; jacket water cooling or high pressure gas fin fan coolers; gas compressors, either reciprocating or centrifugal; and piping and valves including compressor, piping pressure relief, blowdown, and station ESD systems.

Power produced by an internal combustion engine is the result of a spark induced explosion of natural gas and air in the power cylinder. The resultant noise is a function of power, RPM, scavenging means, and type of ignition. Engine noise increases primarily with increase in power. The predominant sources that make up engine noise are air intake, exhaust, and casing noise. Air intake noise is a function of the type of intake whether naturally aspirated, pump scavenged, blower scavenged, exhaust turbocharged, or in some cases a combination. Engine exhaust is the predominant noise source of the internal combustion engine. Naturally aspirated and pump scavenged engines are noisier in the low frequencies. Centrifugal blower scavenged engines develop both low and high frequency noise. Exhaust turbocharged engines develop broad band noise characteristics but are generally less noisy due to the turbocharger absorbing energy from the exhaust system. Casing noise is produced within the engine by minute mechanical component misalignment and slip fittings. The resulting acoustical radiation and vibration migrates to the engine block, cover and accessories.

Gas turbines are generally very noisy due to the high horsepower output and high speed rotating blades. The major sources of gas turbine noise are; intake, exhaust, and casing. Intake noise is created by the interaction of the axial air compressor blades and stator and is a function of pressure increase, number of blades and blade tip speed. The overall level of intake noise is somewhat less than that produced by the exhaust, but its high frequency content sounds much louder than the higher-amplitude, lower frequency exhaust noise. Exhaust from the gas generator/power turbine section is a predominant noise source. Its increase in amplitude and shift to the lower frequencies are due to the combustion process. Casing noise is generated by the high speed misaligned mechanical components within the turbine housing radiating to the outer casing.

Cooling fan noise, whether it is a simple fin fan cooler or a complicated cooling tower design, is produced by the rotating cooling fan blades causing air turbulence. The frequency and amplitude are a function of blade size, pitch, number of blades, and RPM.

Both centrifugal and reciprocating compressors are used to transport gas. They are noise producers but with totally different characteristics. Centrifugal compressor noise is produced primarily by blade-tip turbulence which is a function of power, RPM, mass flow, discharge pressure, number of compression stages, and gas properties. It is primarily a high frequency noise generator. The noise produced by a reciprocating compressor is a function of power, number of cylinders, bore, stroke, RPM, and compression ratio. The reciprocating compressor generates low frequency noise (pulsation).

Safety relief, blowdown, and vent valves are used to relieve pressure in station piping, compressors, vessels such as filter-separators, fuel gas filters, and air starter receivers. When a vent valve is opened, it is typically referred to as a "blowdown." The noise level created by the vent is a function of the upstream pressure, temperature, valve size and type, and downstream piping.

Predictions of noise from the above equipment are often a challenge. However, semi-empirical correlations have been developed to predict both the overall noise levels from these equipment, and in some cases the frequency content. Some of these prediction correlations are given below.

Noise emitted during gas blowdown comes from primarily three sources: a) jet mixing noise, caused by the turbulent mixing of the blowdown jet stream with the ambient medium, b) imperfectly expanded supersonic jets shock-associated noise, produced by the

convection of turbulence through shock cells in the jet, and c) noise generated by the blowdown throttling valve (if it is not a full-bore type valve). The following correlations for these noise sources are based on experimental data obtained and validated by several independent investigators and collated for prediction purposes by the Society of Automotive Engineers [12]. Formulas are given for predicting the free-field radiation from a jet in an ideal acoustic medium. In many applications it will be necessary to modify these predictions to account for atmospheric attenuation and interference caused by reflections from surfaces.

The correlation for jet mixing noise (Fig. 13-4) can be expressed by [12]:

$$(\text{OSPL})_{\text{jet mixing}} = 139.5 + 10 \log_{10} \left(\frac{A}{R^2} \right) + 10 \log_{10} \left[\left(\frac{P_{\text{amb}}}{P_{\text{std}}} \right)^2 \left(\frac{\rho_j}{\rho_{\text{amb}}} \right)^w \right] \quad (13-11)$$

$$+ 10 \log_{10} \left(\frac{M_j^{7.5}}{1 - 0.1 M_j^{2.5} + 0.015 M_j^{4.5}} \right) \quad \text{dB(Lin)}$$

where:

$$w = \frac{3M_j^{3.5}}{0.6 + M_j^{3.5}} - 1$$

and

A = fully expanded jet area (m^2); calculated from [13]:

$$A = \pi / 4 D_j^2; \quad D_j = \alpha D_{\text{exit}}$$

$$\alpha = \left(\frac{P_{\text{exit}}}{P_{\text{amb}}} \right)^{0.4105} \quad (\text{for sonic jet})$$

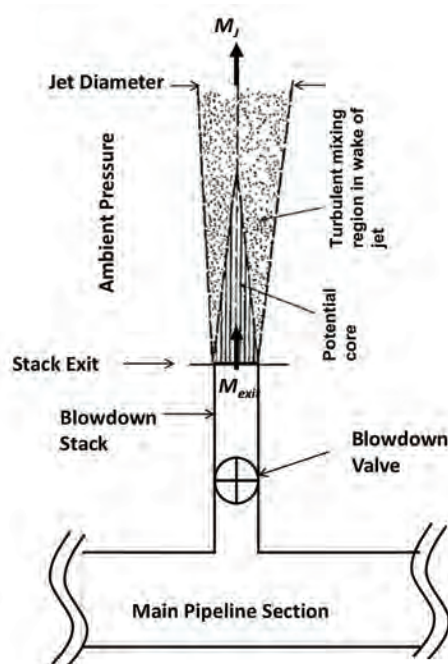


Figure 13-4. Shock-free blowdown gas jet.

$$\alpha = \left(\frac{P_{\text{exit}}}{P_{\text{amb}}} \right)^{0.4878} \quad (\text{for supersonic jet})$$

for subsonic jets, and sonic jets where the exit pressure is equal to the ambient pressure, $A = \pi/4 D_{\text{exit}}^2$ where, D_{exit} , is the stack exit internal diameter.

R = distance from center of the stack exit (m)

P_{amb} = ambient pressure (kPa-a)

P_{std} = standard sea level ambient pressure (=101.325 kPa-a)

ρ_j = expanded jet density calculated at ambient pressure and ambient temperature (kg/m^3)

ρ_{amb} = ambient air density (kg/m^3)

k = gas isentropic exponent at ambient pressure and temperature

M_j = expanded jet Mach number, calculated from [14]:

$$M_j = \left\{ \frac{2}{k-1} \left[\left(\frac{P_0}{P_{\text{amb}}} \right)^{\frac{k-1}{k}} - 1 \right] \right\}^{1/2}$$

P_0 = stagnation pressure of the exit jet, which is approximately equal to the pipeline (reservoir pressure) (kPa-a).

Supersonic, under-expanded, or “choked” jets contain shock cells through which the flow repeatedly expands and contracts (see Fig. 13-5). Seven or more distinct cells are often visible extending up to 10 jet diameters downstream of blowdown stack exit. They are responsible for two additional components of jet noise: *screech* tones and broadband shock-associated noise. Screech is produced by a feedback mechanism in which a disturbance convected in the shear layer generates sound as it traverses the standing system of shock waves. The sound propagates upstream through the ambient atmosphere and causes the release of a new flow disturbance at the stack exit. This is amplified as it convects downstream, and the feedback loop is completed when it encounters the shocks. A notable feature of the screech tones is that the frequencies are independent of the radiation direction. In practice, it is the broadband, shock-associated noise that is important for supersonic jets.

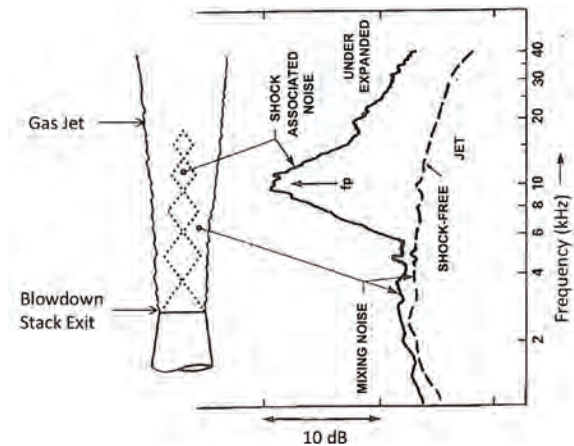


Figure 13-5. Cellular structure within under-expanded blowdown gas jet.

The dominant frequencies are usually higher than the screech tones and can range over several octave bands. For predictive purposes, it is permissible to estimate separately the respective contributions of mixing noise and shock-associated noise to the overall sound power generated by the jet. The overall SPL of shock associated-noise is approximately independent of the radiation direction and may be estimated from [8]:

$$(\text{OSPL})_{\text{jet cellular structure}} = K_0 + 10 \log_{10} \left(\frac{\beta^n A}{R^2} \right) \quad \text{dB(Lin)} \quad (13-12)$$

$$\text{for } \frac{T_j}{T_{\text{amb}}} < 1.1:$$

$$K_0 = 156.5 \text{ dB(Lin)}$$

$$n = 4 \quad (\beta < 1)$$

$$n = 1 \quad (\beta > 1)$$

$$\text{for } \frac{T_j}{T_{\text{amb}}} > 1.1:$$

$$K_0 = 158.5 \text{ dB(Lin)}$$

$$n = 4 \quad (\beta < 1)$$

$$n = 2 \quad (\beta > 1)$$

$$\beta = \sqrt{M_j^2 - 1}$$

where:

R = distance from center of the stack exit (m)

T_j = total pipeline (reservoir) temperature (K)

T_{amb} = ambient temperature (K)

M_j = expanded jet Mach number

Example Problem

Calculate the OSPL from a blowdown stack sonic exit conditions as follows:

Jet exit Mach Number = 1

Jet exit pressure = 6943 kPa a

Jet exit temperature = -42.5°C

Jet exit density = 157.9 kg/m^3

Jet exit speed of sound = 305.9 m/s

Jet exit diameter = 0.2974 m

Gas isentropic exponent = 1.3

Total pipeline (reservoir) pressure = $15,800 \text{ kPa-a}$

Total pipeline (reservoir) temperature = 268 K

Jet exit mass flow rate = 3355 kg/s

Expanded jet conditions:

Expanded jet Mach Number = 3.905

Expanded jet density = 0.7 kg/m^3

Expanded jet diameter = 1.762 m

Expanded jet area = 2.4384 m^2

Ambient conditions:

Ambient pressure = 91 kPa-a

Ambient temperature = 20°C

Ambient density = 1.083 kg/m³

Standard pressure = 101.325 kPa-a

Standard temperature = 15°C

Standard density = 1.227 kg/m³

The jet mixing OSPL is calculated from Eq. (13-11) at 1 m to be 176.2 dB (Lin), and shock related OSPL is calculated at the same distance from Eq. (13-12) to be 166.1 dB (Lin). The combined overall OSPL of both at the same distance = 176.6 dB (Lin).

The noise of gas control or throttling valves may generally be associated with two sources: (a) mechanical vibration of the trim and (b) aerodynamic throttling. Noise generation by these mechanisms rarely occurs simultaneously, but when it does, the cure of one is usually the cure of the other. Investigations of noise-induced pipe failures [15] have enabled maximum safe sound power levels to be established for given pipe sizes and wall thicknesses, as indicated in Fig. 13-6. The sound power levels of choked flow through a throttling valve could be of the order of 130 dBA at 1 m from the pipe wall downstream of the valve. Exceeding this level will most probably lead to piping failure, and a limit of 110 dBA is recommended for safety and to maintain the structural integrity of valve-mounted accessories. The aerodynamic noise is determined by the mechanical stream power W , defined as [16–18]:

$$W = \frac{1}{2} mc^2 \quad (13-13)$$

where

m = mass flow through the valve (kg/s)

c_0 = speed of sound at choked condition (m/s), determined from isentropic expansion of the gas from upstream condition to sonic (choked) condition.

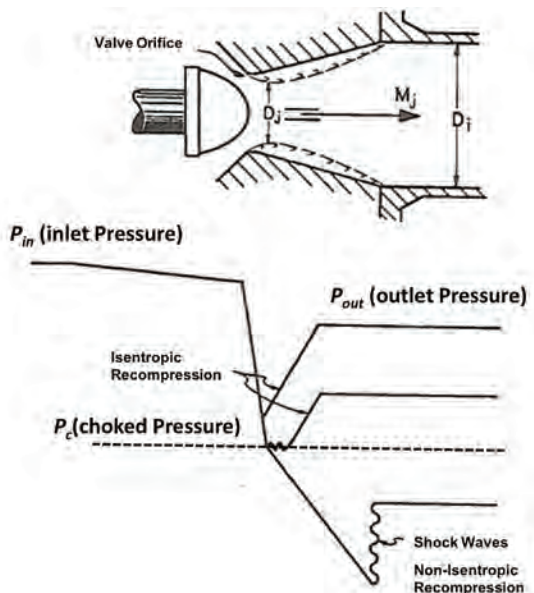


Figure 13-6. Schematic of pressure profiles of throttling valve.

The sound power is equal to ηW , where η is a noise power factor that is a function of the inlet to outlet (recovered) pressure ratio shown in Fig. 13-7 [15–17]. That is:

$$(\text{OPWL}) = 10 \log_{10} \frac{W}{10^{-12}} \quad \text{dB(Lin)} \quad (13-14)$$

Unlike the case of a jet discharging into the atmosphere, the jet from a valve cannot expand freely, and only a fraction of the kinetic energy is converted by turbulence into thermal energy. This is illustrated in Fig. 13-6, which is a schematic view of a throttling valve and associated three pressure profiles depending downstream condition. The sound power or pressure level (L_w or L_p) outside the downstream pipe of the valve suffers from the acoustic transmission loss through the pipe wall and the location of the observer away from the pipe. This transmission loss can be estimated by the following correlation:

$$(\text{TL}) = 10 \log_{10} \left[9 \times 10^6 \frac{R t^2}{D_i^3} \left(\frac{P_{\text{out}}}{P_{\text{amb}}} + 1 \right) \right] \quad \text{dB(Lin)} \quad (13-15)$$

where

- R = distance from center of the stack (m)
- t = stack pipe wall thickness (m)
- D_i = internal diameter of the stack pipe (m)
- P_{out} = internal static pressure downstream of the valve (kPa-a)
- P_{amb} = ambient pressure (kPa-a)

This transmission loss has to be deducted from the estimates of sound power level from Eq. (13-14).

Example Problem

Calculate the *OPWL* from a blowdown valve for the following flow conditions:

- m = mass flow through the valve (kg/s) = 3356
- c_0 = speed of sound at choked condition (m/s) = 305.9
- Ratio of $P_{\text{in}}/P_{\text{out}}$ across the valve = 3.2

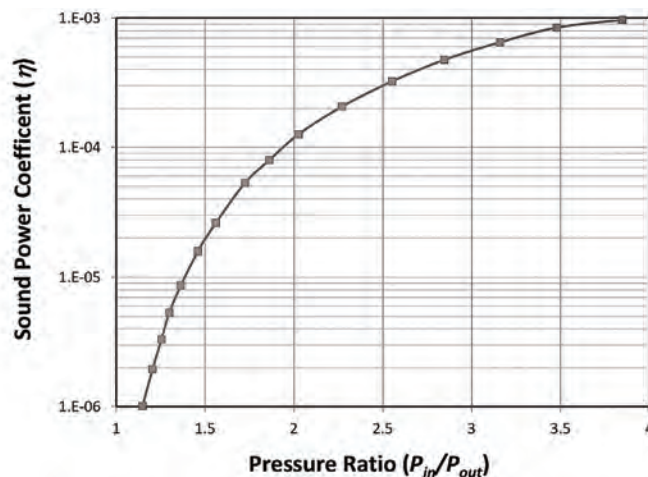


Figure 13-7. Noise power factor for use in Eq. (13-14).

From Fig. 13-7, noise power factor (η) = 7×10^{-4}

The calculated OPWL from the above valve condition = 170.4 dB (Lin).

Assuming the following stack geometry:

R = distance from center of the stack (m) = 1

t = stack pipe wall thickness (m) = 0.021

D_i = internal diameter of the stack pipe (m) = 0.2974

P_{out} = internal static pressure downstream of the valve (kPa-a) = 3930

P_{amb} = ambient pressure (kPa-a) = 101.325

The calculated TL = 67.8 dB (Lin).

Finally, noise generated from gas turbines (driving compressors) is addressed. Noise generated from these engines tends to be predominant at frequencies less than 1 kHz. Combustion processes are a significant component of core noise, both directly in the form of thermal monopole sources and indirectly through the creation of temperature and density inhomogeneities ("entropy spots"), which behave as dipole sources when accelerated in non-uniform flow. The noise prediction correlation given below is based on an analysis of combustion noise of turbojet, turboshaft, and turbofan engines as well as model-scale data. Annular, can-type, and "hybrid" combustors were all included in the validation studies. The overall sound power level (OAPWL, dB) is a function of the operating conditions of the combustor and the turbine temperature extraction and may be estimated from [10]:

$$(\text{OPWL}) = -60.5 + 10 \log_{10} \left(\frac{m c_{\text{ref}}^2}{\Pi_{\text{ref}}} \right) + 20 \log_{10} \left[\frac{(\Delta T/T_i)(P_i/P_{\text{std}})}{(\Delta T_{\text{ref}}/T_{\text{std}})^2} \right] \quad \text{dB(Lin)} \quad (13-16)$$

where

m = combustor mass flow through the combustor (kg/s)

c_{ref} = sea-level speed of sound (340.3 m/s)

Π_{ref} = reference power (10^{-12} W)

T = combustor total temperature rise (K)

T_i = combustor inlet total temperature (K)

P_i = combustor inlet total pressure (kPa-a)

P_{std} = standard sea level ambient pressure (= 101.325 kPa-a)

T_{ref} = reference total temperature extraction by the engine turbines at maximum power output (K)

T_{std} = standard sea level ambient temperature (= 288.15 K)

Example Problem

Calculate the OPWL for a gas turbine engine employed in a compressor station and operating at maximum power of 30.365. The following are the engine parameters at these conditions:

m = combustor mass flow through the combustor (kg/s) = 79

T = combustor total temperature rise (K) = 790

T_i = combustor inlet total temperature (K) = 729

P_i = combustor inlet total pressure (kPa-a) = 2216

T_{ref} = reference total temperature extraction by the engine turbines at maximum power output (K) = 759

The calculated OPWL for the above engine condition = 139.8 dB (Lin).

13.4 NOISE SURVEYS

Noise is generated at compressor and pump stations from a number of sources, including turbomachinery (gas turbines and centrifugal compressors) and reciprocating equipment (engines and reciprocating compressors), air flow through inlet ducts and filters, compressor building ventilation systems, gas scrubbers, exhaust stacks, aerial coolers, yard piping, control valves and auxiliary systems [19–25]. Several techniques are used in noise reduction depending on the source and frequency content of these noise sources. Common to these are close fitting acoustical unit enclosures which provide a significant reduction of casing radiated noise from the gas turbine driver. Acoustical rated compressor buildings can also be used to provide noise reduction not only of the gas turbine unit but also to control noise from other sources such as the compressor casing, interior piping and lube oil cooling skids. The radiated noise contribution from the gas turbine casing as compared to that from the power turbine exhaust usually diminishes at distances greater than 0.5 km away. Then for residences more than 2.0 km away, the exhaust noise is usually the sole remaining contributor [21].

Current computer noise modeling tools utilize three-dimensional topographical and construction/building databases and take into account numerous variables when performing noise calculations and predictions [20]. Among these variables are: equipment sound power levels (SPL), equipment noise source radiation type, equipment noise source elevation and radiation directivity, equipment size, geometric and physical location, building size, geometric and physical location, building wall and roof deck construction, temperature and relative humidity, ground cover, terrain elevations, topographic contours, noise control mitigation, distance dissipation parameter, ground attenuation, atmospheric absorption, barrier attenuation, wind effects, and temperature gradient effects. The output of these tools is commonly presented in isopleths which provide visual maps of potential noise impact or issues of a facility [19]. However, the main challenge with this approach is the degree of confidence in the prediction, given the enormity of the parameters required to perform these simulations and their respective uncertainties [21].

Understanding these noise sources is necessary to ensure that the working conditions on site are safe and that the audible noise at neighboring properties is acceptable (section 13.3). Each noise source has different frequency content, and the overall sound pressure level (OSPL) at any location in the station yard or inside the compressor building is a multiple superposition of these noise sources. A selective detection measurement approach was suggested whereby sound emissions can be allocated to certain emission sources in a nearby plant, and hence allows for identifying cost-effective sound absorbing measures to reduce such noise [22]. Furthermore, the human ear is very good in discerning discrete frequencies, which means that for two noise sources of equal OSPL, the one with significant discrete frequencies is usually considered much more annoying to humans. Therefore, some noise specifications may require that discrete frequencies be attenuated to a level significantly below the average OSPL.

In order to quantify and map the SPL not only as a function of location but, more importantly as a function of the individual frequency content for the purpose of determining the culprit sources and the respective dominant frequency range that contributes the most to the OSPL, the following approach can be followed.

13.4.1 Noise Mapping Methodology

The procedure described here follows a ‘heuristic’ approach in that it focused on a survey of noise sources at a given station employing different numbers and types of compressor/pump units and drivers. The first step primarily involves mapping the noise sources at the station as a first step to understand the nature and the spectral content of the various sound sources

at these stations. The term 'heuristic' is used here because the sound pressure measurements were taken at various locations in the yard and within each of the unit buildings that does not necessarily follow any predetermined pattern, but sporadic enough to cover the entire yard. Figure 13-8 shows an example of a two-unit compressor station and its aerial cooler, while Fig. 13-9 shows the locations of noise measurements taken while the unit is running. Note that a few of the measurements were taken with alternate power unit (APU) running.

The data were collected with a Brüel & Kjær instrument (B&K 7651), which passes the measured sound through a Hanning window and an FFT analyzer to obtain the sound spectra in dBA, which covered a range from 0 Hz to 16,384 Hz, in either 512 or 1024 bins of 32 or 16 Hz, respectively. One such spectrum is shown in Fig. 13-10 as an example. The Hanning window is a function which is multiplied by time signal data before applying FFT to it in order to minimize the spectral leakage from the start and from the end of the signal.

While the sound measurement locations were chosen to capture the noise sources at the compressor station, it resulted in an irregular grid of data. In order to plot the sound contours, the data can be spatially interpolated onto a regular grid. This can be done by the Delaunay triangulation and natural-neighbor interpolation function in matplotlib, a 2D Python plotting library [26,27]. Delaunay triangulation is a technique for connecting unordered points with a set of triangles such that the largest angle in the triangulation is maximized, which avoids producing extremely slender triangles. Any location within the data set is then contained within a single triangle and an interpolated value can be found based on only the three neighboring points. This produces an interpolated sound field that is continuous at all points and has a continuous gradient within each of the Delaunay triangles [28].



Figure 13-8. Example of two-unit compressor station showing the unit air intake and the aerial coolers.

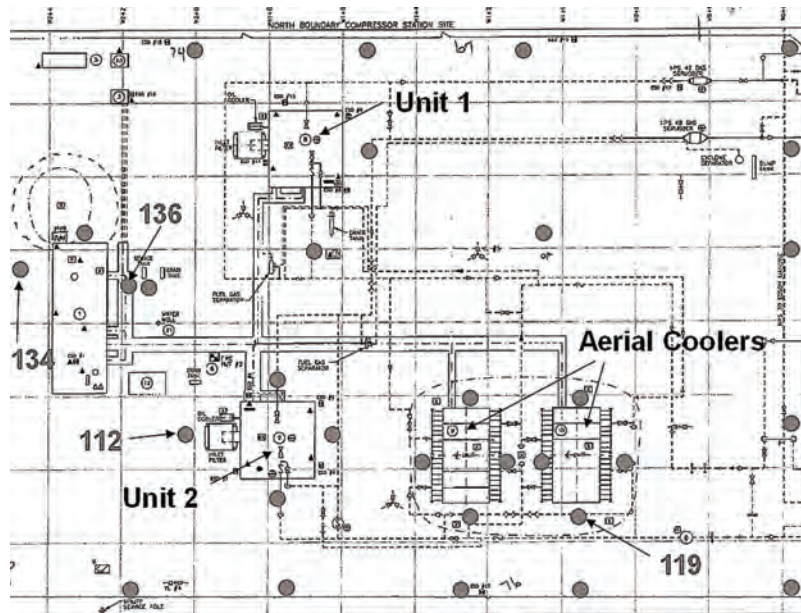


Figure 13-9. Measurement locations at the example compressor station shown in Fig. 13-8. (locations #134 through #136 were taken with the APU running).

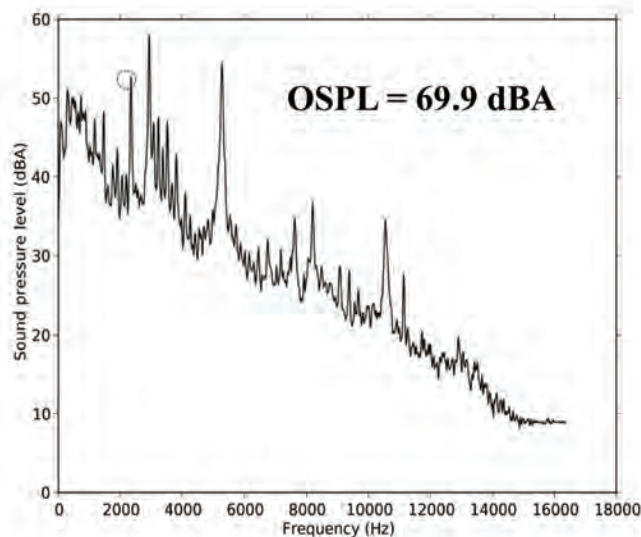


Figure 13-10. Sound pressure spectrum measured at (location 112) with 16 Hz frequency bins.

13.4.2 Example Application on a Compressor Station

The above procedure was applied to the example station of Fig. 13-9, and the results are shown in Fig. 13-11. It shows the OSPL map of the entire station (the black dots are the locations where the individual noise measurements were taken). The most prominent noise sources are the aerial coolers followed by the APU when it is running. On this particular day, one compressor was running and the other was idling. Figure 13-11(a) shows all the data

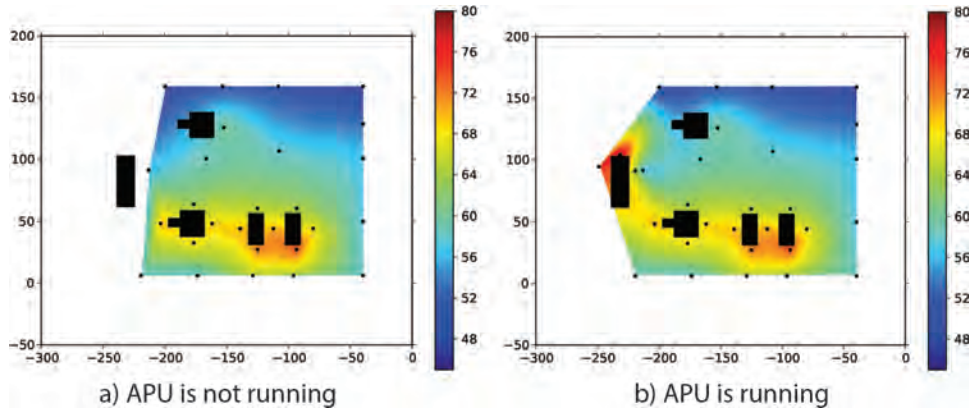


Figure 13-11. Overall sound pressure level (dBA) (axes in meters, OSPL scale is in dBA).

points that were taken without the APU. The contours are determined by the natural-neighbor interpolation, which results in values that are reasonable for much of the yard but which should not be taken literally. For example, the interpolation will never produce a higher SPL than the maximum measured value, even at locations that are closer to the noise source. This is because the interpolation is unaware of the locations or sizes of the noise sources. Figure 13-11(b) is a repeat of the measurements and the procedure but with APU running.

The same Delaunay triangulation and natural-neighbor interpolation techniques can be applied to the noise data at each individual frequency, and the results will be a series of maps at each individual frequency. This can be played in an animation video to allow visual interpretation and analysis of the spectral content of the noise. Figure 13-12 shows an example (screen shot) of this animation of the noise map at noise frequency = 1904 Hz, which is the peak SPL frequency at location 119 near the aerial cooler. Comparing the noise maps at different frequencies allows better distinguishing between the various sources of noise. For example, Fig. 13-11 showed that the strongest noise comes from the aerial coolers, and that the cooler noise was

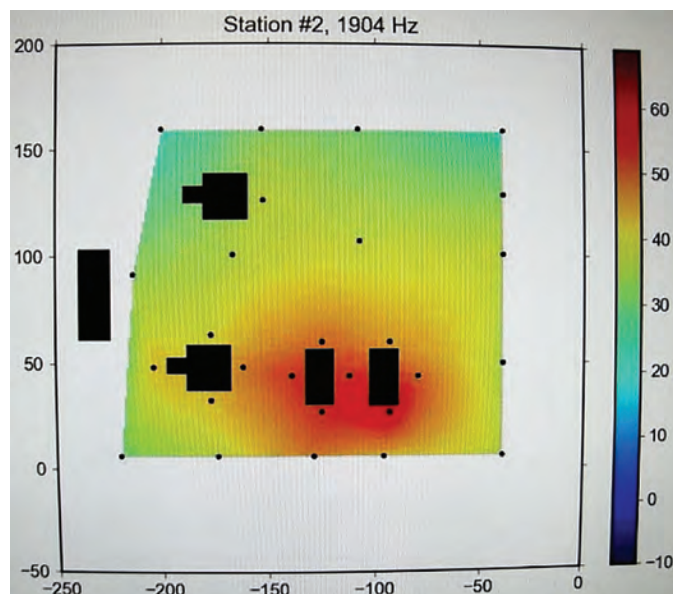


Figure 13-12. SPL animation playing (image captured when noise frequency = 1904 Hz).

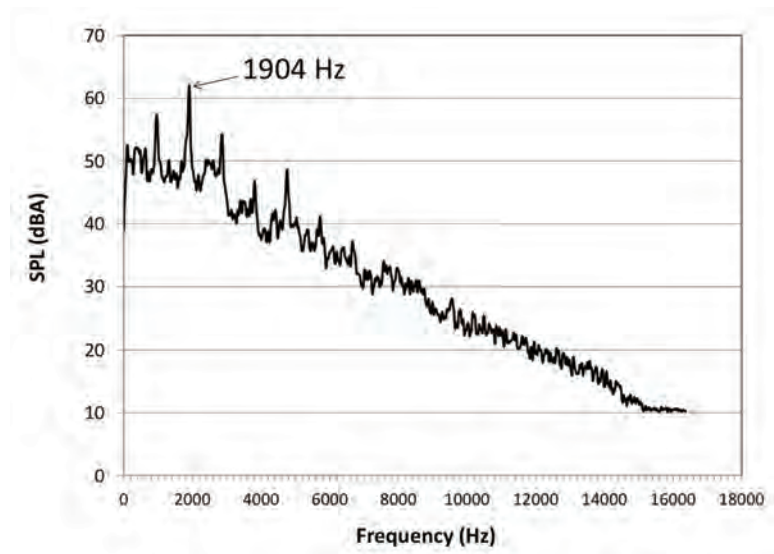


Figure 13-13. SPL spectrum at location 119 (see Fig. 13-9).

most prominent on the south side of the coolers. The aerial coolers have a maximum sound level at 1904 Hz, with several sub- and higher frequency harmonics as shown in Fig. 13-13.

13.5 NO_x EMISSIONS FROM GAS TURBINES

The EPA publishes emission factors for gas turbines in its *Compilation of Air Pollutant Emission Factors, Volume I Stationary Point and Area Sources*, EPA (Environmental Protection Agency) Publication No. AP-42 [29]. The document has been published since 1968 as the primary compilation of EPA's emission factor information. Government regulatory agencies, industry and others use the document to estimate emissions of atmospheric pollutants, a critical step in the development of effective air management strategies.

In Canada, actual NO_x emissions from the pipeline industry are generally not accurately determined since CEM systems are not required on compressor drivers. As an alternate method to quantify the NO_x emission from small-to-medium size gas turbines typically used in pipeline systems, a Predictive Emission Monitoring (PEM) system can be easily developed to provide a better and a credible estimate of NO_x emissions from these engines at all loads and at prevailing ambient conditions. Once integrated on a yearly basis, a PEM system would provide a better estimate of the NO_x emissions from these engines compared to typical estimation methodologies that rely on the AP-42 emissions factors.

Current technologies related to NO_x emissions have advanced rapidly in the past few years to the point that PEM models are now generally accepted for gas turbine applications and are in compliance with CFR Parts 60 and 75 [30,31]. These are shown to offer greater accuracy [32,33] and faster response time (in terms of downtime avoidance) than CEM techniques. They can also provide advance results for a specific set of operating conditions [34–37].

Hung's work on predicting emissions from gas turbines [38] indicates that too much emphasis has been placed on modeling chemical kinetics and not enough on the physical processes of combustion. By and large, NO_x formation was based on finite-rate reaction kinetics and the widely accepted Zeldovich mechanism [37]. Subsequent revisions to the model incorporated a number of features, including the effects of ambient humidity and

temperature, water injection, synthetic coal gas combustion and fuels containing nitrogen in the combustor [40].

Several empirically developed correlations to predict NO_x emissions are listed in [39–41] with combustor pressure, overall fuel-air ratio, combustor inlet temperature, combustor air flow rate and residence time as input variables. These correlations are very useful when applied to specific machines, specific fuels and under specific operating conditions. Recent efforts attempted to improve accuracy of semi-empirical correlations through optimization methods [42–47].

In recent years, emission prediction models have been developed based on an optimized Neural Network (NN) architecture that takes fundamental engine parameters as input variables and predicts NO_x as an output variable. This Section will first describe the model development demonstrated on a GE-LM1600 gas turbine employed in natural gas compressor station. Here, the NN is trained using two sets of actual emission tests conducted on the gas turbine. A total of 387 tests were conducted on two different dates, and at different operating conditions covering the range of the engine operating parameters. This set of data was supplemented by ‘Cycle-Deck’ data generated by a NO_x prediction module developed by GE. The technique is the same as that followed in developing a PEM module for an RR-RB211-24C engine reported in [48] and for a GE-LM2500 reported in [49]. Data from the implemented PEM models on the aforementioned three gas turbines were collected over a period of one year and compared with AP-42 emission factors.

13.5.1 AP-42 Emission Factors

AP-42 Chapter 3.1 [29] uses an emission factor which is a representative value that attempts to relate the quantity of a pollutant released to the atmosphere with an activity associated with the release of that pollutant. For natural gas-fired gas turbines, these factors are usually expressed as the weight of pollutant per unit fuel volume burned or its equivalent heating value (e.g. kg/m³ or kg/GJ). Such factors facilitate estimation of emissions from various sources of air pollution. In most cases, these factors are simply averages of all available data of acceptable quality, and are generally assumed to be representative of long-term averages for all facilities in the source category.

Emission factors in AP-42 Chapter 3.1 have been determined from gas turbines with no add-on control devices (*uncontrolled*) as well as from *controlled* engines. There are three generic types of emission controls in use for gas turbines, wet controls using steam or water injection to reduce combustion temperatures for NO_x control, dry controls using advanced combustor design to suppress NO_x formation and/or promote CO burnout, and post-combustion catalytic control to selectively reduce NO_x and/or oxidize CO emissions from the turbine [29]. Other recently developed technologies promise significantly lower levels of NO_x and CO emissions from diffusion combustion type gas turbines. These technologies have been demonstrated in several installations. Note that the emission factor (EF) of NO_x for an uncontrolled engine is:

All Loads:

EF = 0.127 kg/GJ (0.295 lb/MMBtu)—based on HHV

Loads greater than or equal to 80%:

EF = 0.139 kg/GJ (0.32 lb/MMBtu)—based on HHV

13.5.2 CEM Measurements

Field measurements were taken to determine the variation of emission levels from a GE LM1600 gas turbine used at a natural gas compressor station on the TransCanada Pipeline System in Alberta at various loads, i.e., engine power output. The tests were performed on two different

dates and at different operating conditions covering the range of the engine operating parameters. The levels of NO_x, CO, CO₂, O₂ and moisture in the exhaust stack were measured by CEM [50] using instruments and on-site calibration techniques approved by the U.S. EPA [51], i.e.:

- Carbon Monoxide—EPA Method 10
- Oxides of Nitrogen—EPA Method 7E
- Carbon Dioxide—EPA Method 3A
- Oxygen—EPA Method 3A
- Total Hydrocarbons—EPA Method 25

The moisture content is measured according Alberta Environment Method 4 [52].

In particular, the NO_x measurements were made with an approved chemiluminescent continuous analyzer. These measurements were broken down to total NO_x and NO component, both in ppm by volume (dry and corrected to 15% O₂). The uncertainty in the measurements of NO_x is typically <2% of calibration span of the analyzer.

Pertinent engine performance parameters and ambient conditions at the site were obtained from the station data acquisition system. These parameters were: ambient temperature, the engine shaft speed (N1), air compressor discharge pressure (P3) and fuel gas flow rate (Q_f), i.e., a total of four engine parameters. Gas samples were also taken to determine the composition of the natural gas used for fuel gas.

For each test point, the engine speed was adjusted to reach the desired power output. The engine was allowed to stabilize over a twenty-minute period before the engine condition was changed. The unit load was varied from roughly 33 percent to maximum load to give several operating points on each test date. Emissions in terms of NO_x (in ppm-dry-15% O₂ corrected and in kg/hour) are plotted in Figs. 13-14 and 13-15 versus fuel consumption, respectively. The variations in the NO_x emission for a given fuel consumption is due to variations in the ambient conditions, engine speeds and output shaft power. The overall trend of increasing NO_x with increasing load (and hence Q_f) is due to the higher temperatures in the combustor, which leads to additional NO_x via the thermal mechanism.

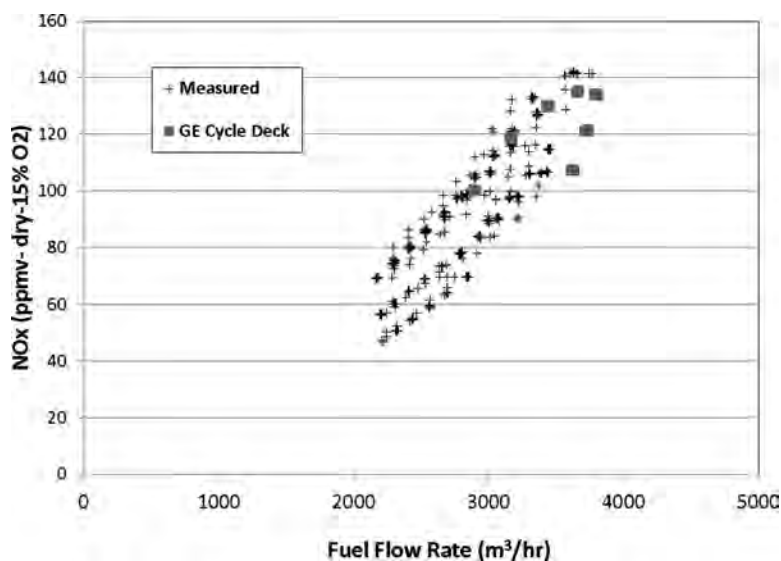


Figure 13-14. Measured and GE cycle-deck NO_x emission data (in terms of ppmv-dry-15% O₂) for a GE LM1600 gas turbine.

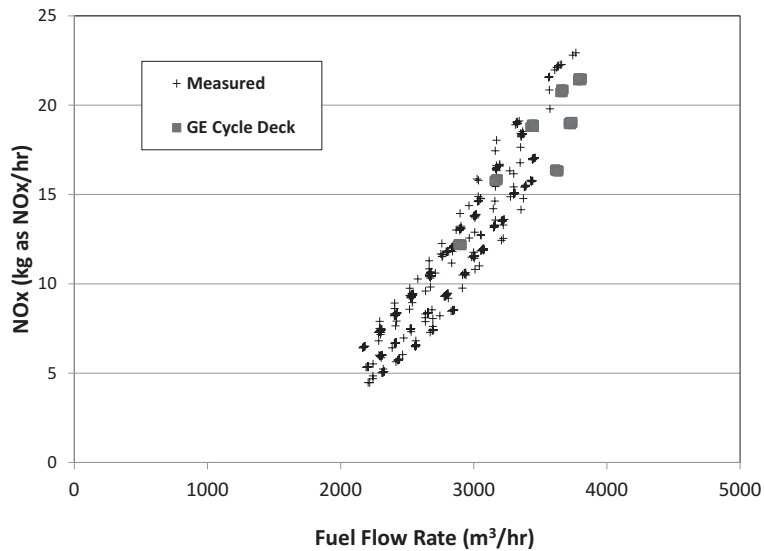


Figure 13-15. Measured and GE cycle-deck NOx emission data (in terms of kg/hour) for a GE LM1600 gas turbine.

These higher combustor temperatures result from higher compressed air temperatures and lower air-to-fuel ratios as the unit load is increased.

The above data were supplemented by a set of data generated by a 'Cycle-Deck' prediction tool developed by GE to cover ambient temperatures outside the range of those of the actual CEM tests. The temperature range considered was from -30°C to $+30^{\circ}\text{C}$ at an increment of 10°C . The generated data are plotted in Figs. 13-14 and 13-15. It is shown that the GE 'Cycle-Deck' generated data are in line with those obtained from the actual CEM tests. A statistical generated noise around these data points of a standard deviation = 0.5% was applied to each of the input and output variables in order to increase the number of data points to match that of the number of measured data point so as to balance the influence of the two sets. Both sets of data, i.e. the CEM measured data set and the 'Cycle-Deck' generated data are then used in the training the NN based PEM model described in the following Section. Training NN is the most crucial and important step in NN-based PEM development and must be conducted with attention to the resulting accuracy and performance of the best or optimized NN architecture.

13.5.3 Neural Network Based PEM models

Neural Network architecture was then developed as a basis for a PEM model. The input parameters are the four engine parameters identified, while only NOx was taken as the output parameter (either in ppmv-dry-15% O_2 , or in kg/hour). Three types of NN architectures were considered and the respective training algorithms were applied to the training set. These were: Multi-Layer Perceptron (MLP), Radial Basis Function (RBF), and Generalized Regression NN (GRNN). These Networks were based on feed forward architectures with back-propagation optimization during training of the network [53]. In the case of MLP, the processing elements, called 'neurons', receive weighted sum of signals from neurons in the layer directly before it and send signals to the neurons in layer following it through a function called the activation function, using the following formulation:

$$Z_{k,i} = \Phi \left[\sum_{j=1}^{M(k-1)} w_{k,i,j} Z_{k-1,j} - B \right] \quad (13-17)$$

where

- k = layer number
- i, j = neuron indices
- $M(k)$ = total number of neurons in layer k
- $Z_{k,i}$ = output of neuron i in layer k
- $w_{k,i,j}$ = weight between neuron j in layer $k - 1$ and neuron i in layer k
- B = a threshold value
- Φ = function to be applied at each neuron

A variety of optimization techniques can be used to find the weights (w), the most common of which are the back propagation, conjugate gradient descent, and quick propagation techniques [55]. Several papers survey the various types of networks, describing their architecture, learning algorithms and applications, e.g., [54,55].

In order to arrive at the optimum NN architecture, several schemes should be tested and the number of neurons in each hidden layer in each of the three structures mentioned earlier varied, and overall normalized error determined for each NN architecture. It was found that the simplest architecture with the least error was of an MLP type with one hidden layer of two neurons as shown in Fig. 13-16. All of the neurons in this architecture are of linear type, which perform a weighted sum of their inputs, biased by a threshold value (see Eq. 13-17). The activation functions are of a hyperbolic type, except for the input layer, consisting of the four neurons corresponding to the four input engine parameters shown, which was linear. The architecture's weights and thresholds constitute the main fitting parameters for implementation in the PEM model.

Sensitivity analysis was then conducted to assess the influence of each of the four input parameters on the output parameter, i.e. the predicted NOx. Table 13-3 shows the results of this analysis in terms of ranking each parameter from highest (rank 1) to the lowest (rank 4). The criterion used in ranking is based on determination of the ratio of the network error if each input is eliminated sequentially to the overall network error when all inputs are present. Ratios close to or less than 1.0 indicate near-irrelevant inputs, while large ratios indicate particularly important input variables. It was found that the fuel flow (Q_f) is the highest sensitive parameter in so far as NOx prediction by this model is concerned.

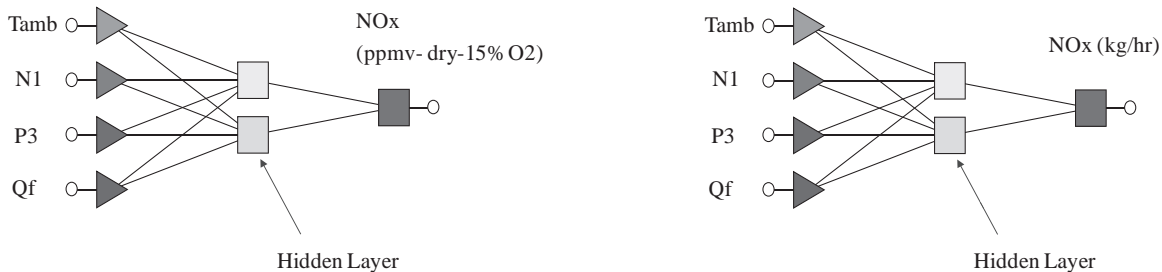


Figure 13-16. MLP architecture for NOx prediction.

Training this network using the 1872 data points resulted in a good fit with a correlation coefficient greater than 0.98 as shown in Table 13-3. The standard deviation of the error in the prediction of NO_x in terms of ppmv-dry-15% O₂ is 3.9 ppmv, and in terms of kg/hour is 0.43 kg/hour. This should not be misconstrued as being the error of NN prediction; it is rather an indication of how well the NN has been trained to match the measured values.

Figures 13-17 and 13-18 show the PEM results after training the NN and comparison with the actual data used in the training. Good agreement is demonstrated based on NO_x in terms of both ppmv and kg/hour). The corresponding error distribution as a function of fuel flow is shown in Figs. 13-19 and 13-20, which show that this error in NO_x is contained within +10 ppmv and +2 kg/hour.

Emission factors in terms of Kg of NO_x per GJ of fuel burned are compared with values set forth by AP-42 of 0.127 kg/GJ (all loads), or 0.139 kg/GJ (for loads greater than 80%), and are shown in Fig. 13-21a. It indicates that for the most part, the actual NO_x

Table 13-3. Training performance and sensitivity of the MLP neural network architecture

NO_x (ppm)

Tamb	Ranking			Correlation Coefficient	Error S.D. (ppm)
	N1	P3	Qf		
2	4	3	1	0.9874	3.9

NO_x (kg/hr)

Tamb	Ranking			Correlation Coefficient	Error S.D. (ppm)
	N1	P3	Qf		
3	2	4	1	0.9948	0.43

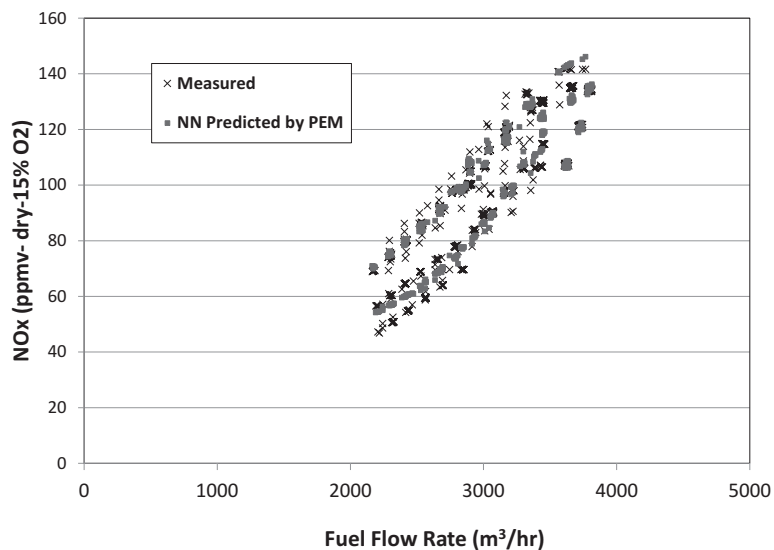


Figure 13-17. Comparison between PEM predicted versus measured and cycle-deck data (in terms of ppmv-dry-15% O₂) for a GE LM1600 gas turbine.

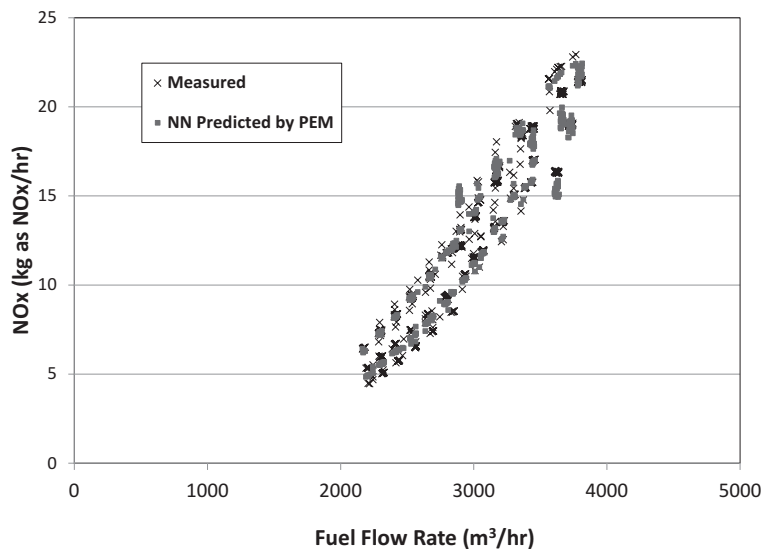


Figure 13-18. Comparison between PEM predicted versus measured and cycle-deck data (in terms of kg/hour) for a GE LM1600 gas turbine.

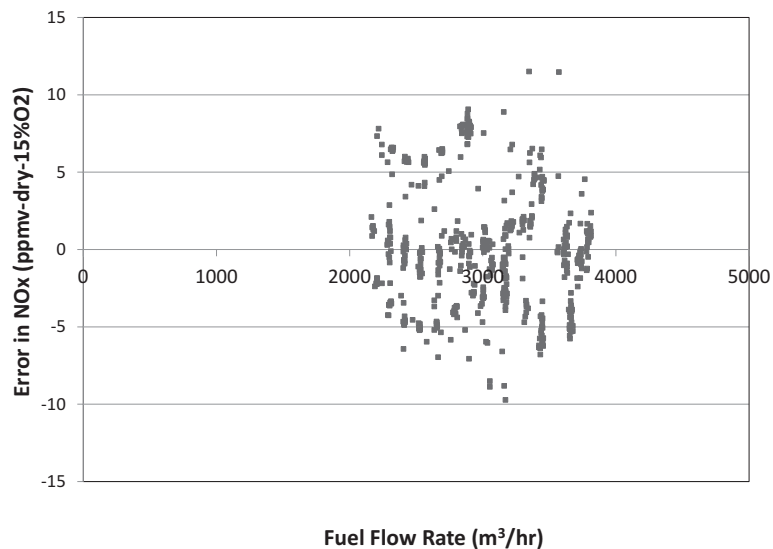


Figure 13-19. Error in PEM prediction (in terms of ppmv-dry-15% O₂) for a GE LM1600 gas turbine.

emission factors are predominantly below AP-42 values. Comparison of the measured NO_x emissions with emission intensity guidelines for stationary combustion turbines published by CCME (Canadian Council of Ministers of the Environment) in 1992 [56] is shown in Fig. 13-21b. It clearly indicates that the LM1600 unit in question for the most part exceeds the emission intensity level according to 1992 CCME guidelines. It should be noted that this unit was installed well before 30 November 1994.

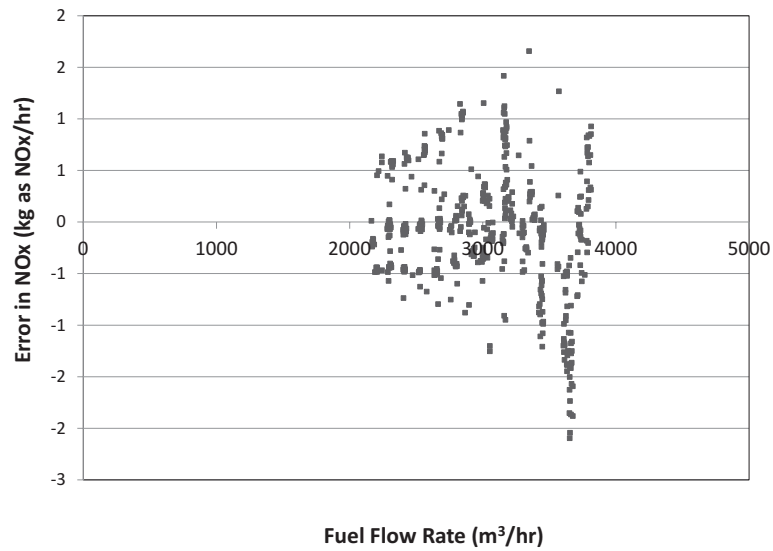


Figure 13-20. Error in PEM prediction (in terms of kg/hour) for a GE LM1600 gas turbine.

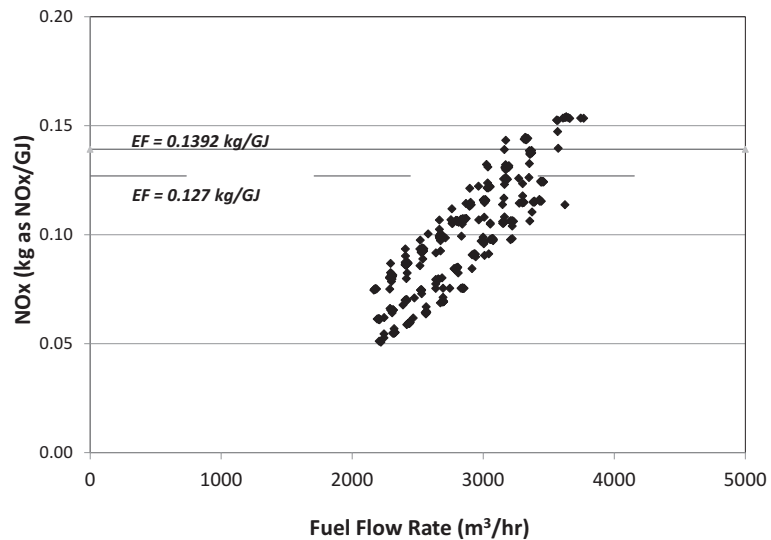


Figure 13-21a. Measured emission factor and comparison with AP42 emission factors (GE LM1600 gas turbine).

Uncertainty analysis was then conducted to assess the error on PEM predictions due to error in measuring any of the four engine parameters. Estimates of error in measuring the engine parameters are as follows:

1. Error in ambient temperature (T_{amb}) = +1°C
2. Error in engine speed (N1) = +1%
3. Error in compressor discharge pressure (P3) = +1%
4. Error in fuel flow (Qf) = +1%

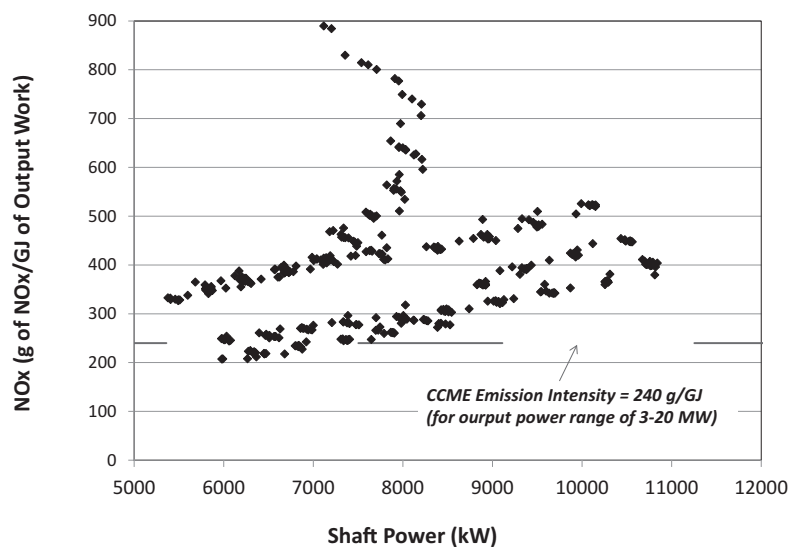


Figure 13-21b. Measured emission factor and comparison with 1992 CCME emission intensity (GE LM1600 gas turbine).

Table 13-4. PEM uncertainty analysis

Uncertainty in	Level of Uncertainty (+ or -)	Error in NOx (ppmv + or - %)	Error in NOx (kgs/h %)
Ambient Air Temperature	1 deg C	0.90%	3.50%
GG Speed (N1)	1%	3.00%	6.00%
Compressor Discharge Pressure (P3)	1%	2.50%	5.30%
Fuel Compressor (Qf)	1%	2.80%	5.90%

The results of this uncertainty analysis are summarized in Table 13-4. It was shown that for uncertainty in the ambient temperature of +1°C, the uncertainty in the NOx prediction is +0.9 to +3.5%. Uncertainties of the order of +1% in the other three input parameters result in uncertainties in NOx predictions in the range of +2.5 to +6%.

13.5.4 PEM Implementation

The above PEM model was implemented in two similar units employed in the station. The implementation was achieved via a module written in C++ and uploaded to the Compressor Equipment Health Monitoring (CEHM) system of the station. Figures 13-22 and 13-23 show collected data from the station CEHM system as a function of fuel flow rates.

Figure 13-24 shows hourly data over one year of emission inventory for both units (#6 and #7), in terms of Kg/GJ of fuel, based on predictions by present PEM model (Units #6 and #7). The two EF values of AP42 are also shown for comparison. It is shown that the predicted emission factors are below the higher AP42 EF value of 0.1392 kg of NOx/GJ of fuel. This led to perform a calculation to determine the total emission inventory for the two units over this one year period using the present PEM model in terms of tonnes of NOx emitted. A comparison is also made with the AP 42 EF values and the 80% load rule.

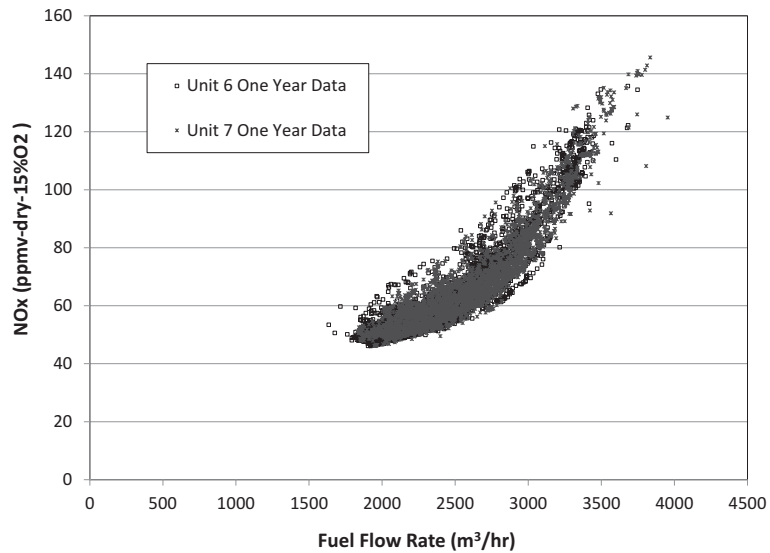


Figure 13-22. Estimate of one year emission inventory (in terms of ppmv-dry-15% O₂) based on predictions by present PEM Model (Units 6 & 7)—GE LM1600 gas turbine.

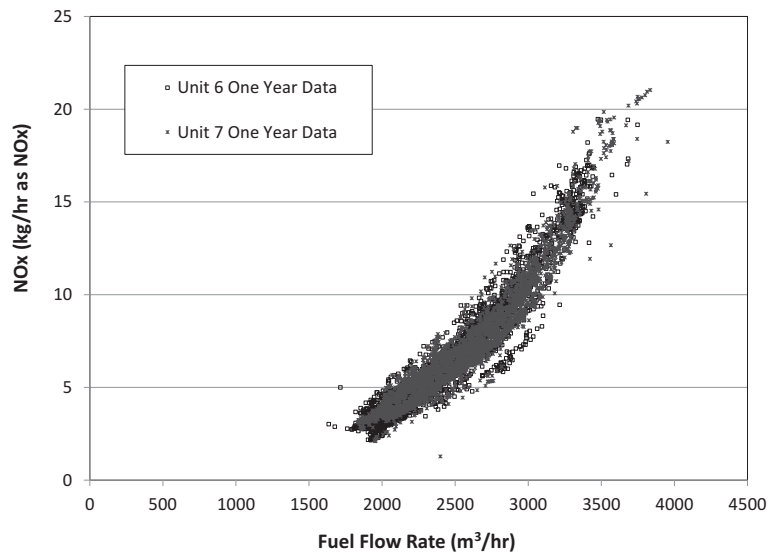


Figure 13-23. Estimate of one year emission inventory (in terms of kg/hour) based on predictions by present PEM Model (Units 6 and 7)—GE LM1600 gas turbine.

The results are shown in Table 13-5, which indicates that Unit #6 actually emitted 20.99 tonnes of NO_x, while if the AP42 EF values and 80% load rule is applied, an estimate of NO_x emission would be 39.31 tonnes, which is nearly double the value predicted by PEM. Similar results are obtained for unit #7 as depicted in Table 13-5.

Finally, based on the measured data obtained for the RB211 [48], GE LM2500 [49], and that for the GE LM1600 engine reported here, comparisons are made between these

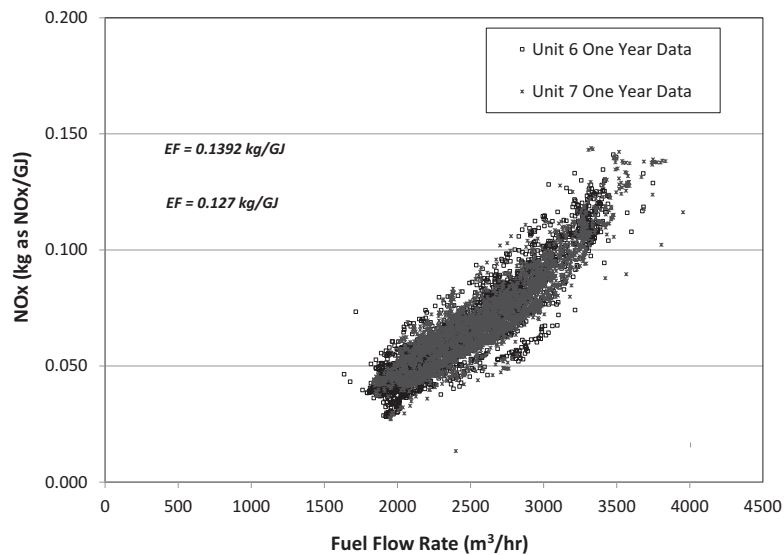


Figure 13-24. Hourly data over one year of emission inventory (in terms of kg/GJ of fuel) based on predictions by present PEM model (Units 6 and 7) and comparison with AP42 emission factors—GE LM1600 gas turbine.

Table 13-5. Comparison of NOx emission inventory from units 6 and 7 over 1 year period, and comparison with AP42 emission factors

		Unit 6	Unit 7
Total Running Time in 1 Year	(hours)	3123	2911
PEM Predicted NOx Emission	(tones of NOx)	20.99	21.41
NOx Emission Based on AP42 Factors	(tones of NOx)	39.31	38.07

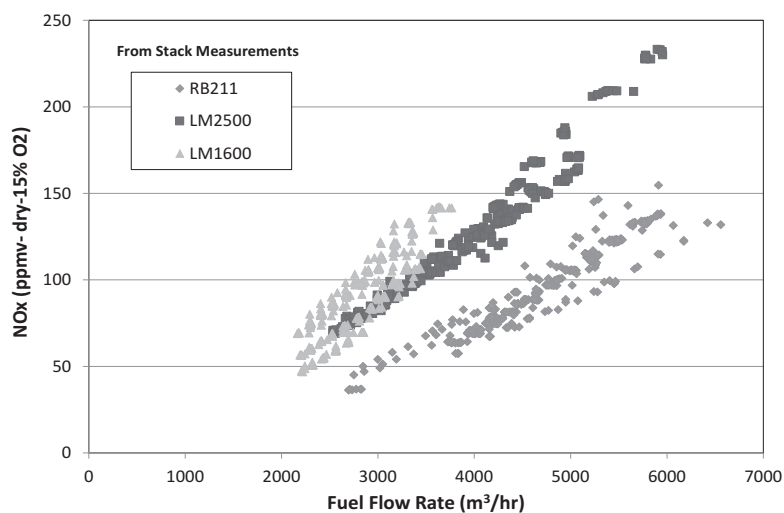


Figure 13-25. Comparison between measured NOx emission (in terms of ppmv-dry-15% O₂) from three different gas turbines employed on natural gas compressor stations.

three engines of the respective NO_x emission. These comparisons are shown in Fig. 13-25 (in terms of NO_x in ppmv-dry-15% O₂) and Fig. 13-26 (in terms of NO_x in kg/hour). It appears that GE LM2500 emissions are higher than the RB211 engines for the same fuel flow rate. NO_x emission from GE LM 1600 engine is slightly higher than GE LM2500 at the same range of fuel gas flow. This is likely due the higher combustion temperature in the LM1600 engines than in the LM2500 (e.g. fuel flow rate of 3500 m³/hour, LM1600 would be close to full load, while LM 2500 would be at 50% load).

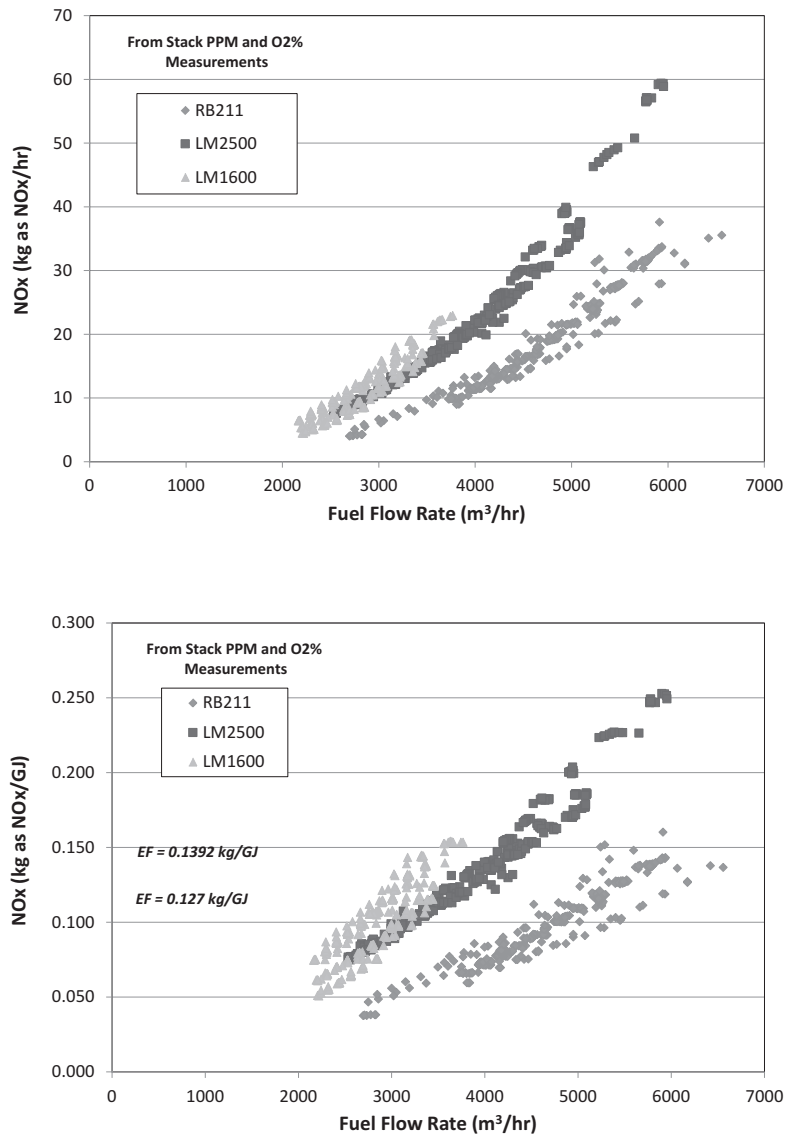


Figure 13-26. Comparison between measured NO_x emission (in terms of kg/hour and kg/GJ) from three different gas turbines employed on natural gas compressor stations.

13.6 INNOVATIONS IN CAPTURING VENT GAS FROM DRY GAS SEALS

Recent developments have been aimed at recovering vent gas loss from dry gas seals through the use of supersonic gas injectors [57]. The main driver for this innovation is to eliminate (or minimize) the environmental impact associated with the vented gas. In the present section, this innovation will be discussed and further explored in more detail.

Supersonic ejectors are well known for their advantage of having no moving parts. No seals, no shafts, no packing, and thus no maintenance are also some of the distinct advantages over mechanical compressors or vacuum pumps, which often require elaborate maintenance programs. Their rugged construction and simplicity of design enables their reliable, maintenance-free use. Although they are considered inefficient in general, they are often used in a wide range of industrial applications such as power plants for the creation of vacuum [58], power and thrust augmentation [59,60], refrigeration and heat pump systems [61–63], gas-vapor recovery from oil storage tanks, transport of solids [64], oil production [65], aero-engine cooling [66], bubble-bed tower reactors and bioreactors [67]. Other applications can be found in reference [64].

A unique application of these ejectors is to capture gas leakage from dry gas seals and re-inject it into a higher-pressure fuel gas stream going to the combustor of the gas turbine driving the gas compressor. This would result in not only saving the leaking gas and utilizing it as a part of the fuel gas, but also eliminating hydrocarbon emissions to the atmosphere. Furthermore, there will be no additional energy requirements to drive this ejector, since its motive gas is basically drawn from the fuel gas line to the gas generator prior to throttling, i.e. line pressure. It is argued that re-injection of the leakage gas into the gas generator fuel gas line is a better option than directing it to a lower pressure utility fuel gas line (e.g. in boilers). This is because boilers typically operate intermittently (on/off), i.e. not always firing while compressor units are running.

The primary challenge to achieve the above lies in the fact that the leakage gas pressures from the first stage dry-gas seals are in the range of 70–340 kPag, while the minimum pressure required downstream of the fuel gas regulator (typically Fisher 310A type) is in the range of 2400–3300 kPag, depending on the gas turbine model. Commercial ejectors typically work either in the subsonic or slightly supersonic regions, which limits the suction pressure with respect to the motive gas pressure. For example, Fletcher [68] documents a discharge pressure calculation curve showing that with motive gas at 7000 kPa-a and suction gas pressure 350 kPa-a; the maximum discharge pressure that can be achieved is approximately 1400 kPa-a. The same curve indicates that for a motive pressure of 7000 kPa-a, and a discharge pressure of 2800 kPa-a, the minimum suction pressure is 900 kPa-a. In the same study it was also shown that for a discharge pressure of 4100 kPa-a and a suction pressure of 1300 kPa-a, the required motive gas pressure would be 10,300 kPa-a. This demonstrates the difficulties associated with meeting both the low suction pressure while discharging to a much higher pressure.

In order to overcome these difficulties, a two-stage supersonic ejector has been developed and tested [69] such that the first stage is highly supersonic (nozzle exit Mach number = 2.54), while the second stage is moderately supersonic (nozzle exit Mach number = 1.72). Several tests were conducted on various configurations of the two stages on natural gas in order to arrive at the optimum design parameter. In the end, the optimum design showed an expansion pressure ratio (motive/suction) in the order of 14.0 and compression pressure ratio (discharge/suction) of around 8.1.

The following describes the optimum configuration arrived at after several iterations of different supersonic expansion nozzles, particularly for the first stage part, and presents the measured performance results of the integrated system that would meet the requirements of capturing

the low pressure, low flow dry gas seal leakage and re-inject it into the fuel gas stream. The operation of the dry gas seal should not be adversely impacted if the dry gas seal vent gas pressure matches the pressure of the suction gas to the first stage ejector, as will be discussed later.

13.6.1 Dry Gas Seal Leakage Rates

A typical dry gas seal is a non-contact end face seal in which the sealing mechanism is comprised of two rings: the first ring with grooves etched in the seal face, which rotates with the shaft, is known as the mating ring, while the second ring has a smooth face and is restrained from movement except along the axis of the shaft. A pair of these seals often co-exists, hence providing a two-stage sealing effect.

For successful operation, it is essential that a steady flow of clean seal gas be supplied to the gaps between the rings. The seal supply gas source must be at a higher pressure than that of the process gas that is being sealed in order for flow to occur. On overhung compressors only one dry gas seal is required, in which case the seal supply gas can be drawn from the compressor discharge, filtered, and supplied in a steady flow to the seal capsule. Most of the seal supply gas re-enters the process cavity, while a small volume (leakage) passes through the seal faces and is vented to atmosphere. The amount of gas leakage depends on the process pressure and rotating shaft diameter. Figure 13-27 gives an example matrix of the order of magnitude of the gas leakage from a typical 1st stage dry gas seal.

The purpose of supersonic ejector development was to provide a means for capturing this gas leakage and re-injecting it into the fuel gas line so that the available energy can be used resulting in fuel savings, in addition to minimizing what would otherwise be greenhouse gas emissions.

13.6.2 Primary Challenges of Supersonic Ejectors

The primary challenge of supersonic ejectors lies in compressing the combined (motive + suction) gas in the supersonic diffuser part of the ejector. In particular, the diffuser throat has to be larger than the nozzle throat to account for stagnation pressure losses through jet entrainment/mixing and at the inlet of the converging supersonic section of the diffuser,

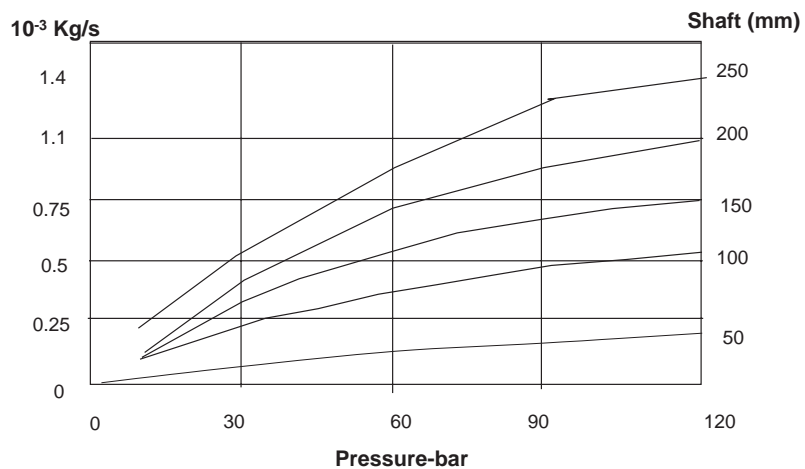


Figure 13-27. Typical dynamic gas leakage rate from the 1st stage dry-gas seal.

otherwise a standing shock would appear inside the nozzle and destroy the desired expansion in the static pressure. One technique to swallow such a shock is to have a variable throat diffuser [70,71], which cannot be implemented here, as it would complicate the design. In order to overcome this challenge, the diffuser throat was made slightly larger than needed, which would keep the standing shock slightly downstream of the diffuser throat, or at best at the throat.

In order to arrive at the optimum design of a fixed-geometry diffuser that could work with different nozzles of different throat areas, a Computational Fluid Dynamics (CFD) analysis was carried out to discern the flow field, accompanied by extensive testing of various configurations. The results of these efforts were presented in ref. [69], along with the methodology to arrive at the optimum configuration. The optimized nozzle/diffuser arrangement showed that the nozzle is clear from a standing shock wave, which is good for suction. It was also shown that the shock wave region in the diffuser section, (which is the region where Mach number drops sharply from supersonic to subsonic, is located at the throat of the diffuser or slightly downstream.

13.6.3 Description of the Two Stages of the Ejector

Based on the above discussion, and in order to satisfy the relatively low suction pressure to match the dry gas seal leakage pressure (~400 kPa-a), an ejector with a highly supersonic exit flow will have to be employed. This would also come with the challenge associated with compression of the same supersonic flow after entraining the dry gas seal leakage gas in a supersonic diffuser. Recognizing the challenge, and in an attempt to optimize a certain design configuration that would minimize the impact of the inevitability of the presence of a shock wave at the throat of the supersonic diffuser, a flexible prototype has been designed and fabricated as shown in Fig. 13-28. This design not only allows for various geometry supersonic nozzles to be tested with a fixed geometry diffuser, but it also allows for fine

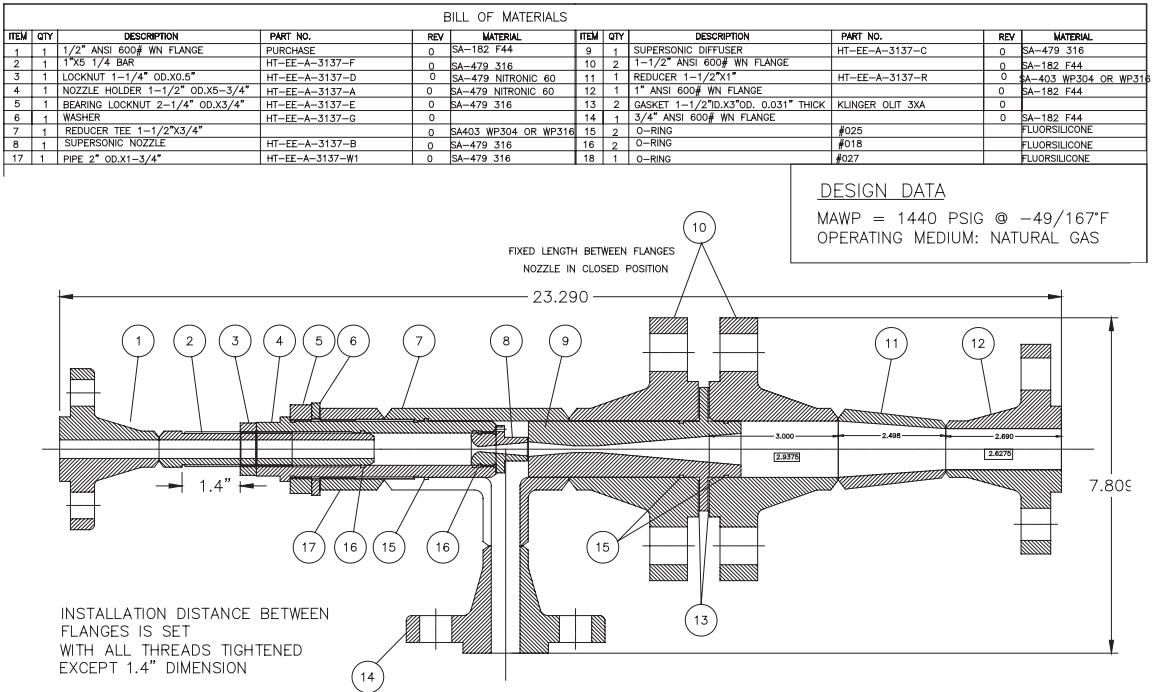


Figure 13-28. Design details of the 1st stage supersonic ejector.

adjustments of the position of the nozzle exit in relation to the diffuser inlet (either positively, i.e. inserted into the diffuser inlet section, or negatively, i.e. retrieved back with a gap in between nozzle exit and diffuser inlet).

The supersonic diffuser has an inlet diameter of 4 mm, a throat diameter of 3.5 mm and length of 8 mm, and an exit diameter of 18 mm. Inlet 1/2 angle of the inlet section is 4.7° , while that of the exit section is 5° . Several supersonic converging/diverging nozzles were fabricated with different throat diameters and exit/throat area ratios. The best performance configuration was obtained with the 1.6 mm (throat) – 2.8 mm (exit) nozzle placed at 20.5 mm inside the supersonic diffuser. Test results of this 1st stage ejector with this nozzle size are shown in Figs. 13-29 and 13-30 in terms of expansion ratio (P_1/P_2), compression ratio (P_3/P_2) and suction to motive gas flow ratio. It is shown that an expansion ratio of 20 and compression ratio of 3.5 has been achieved with motive gas pressure ($P_1 = 5000 \text{ kPa-a}$).

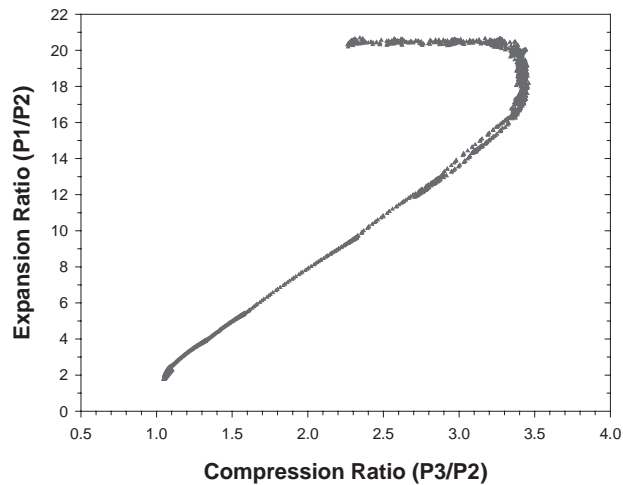


Figure 13-29. Expansion and compression characteristics of the best performing 1st stage ejector.

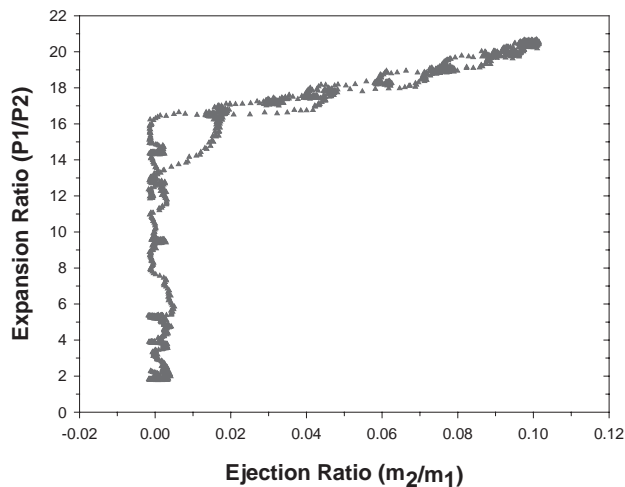


Figure 13-30. Ejection mass ratio of the best performing 1st stage ejector.

The second stage ejector was sized and designed such that it would use the full line gas pressure as motive gas without throttling, and discharge at a pressure (P_{out}) up to 3400 kPa-a (as depicted in Fig. 13-31). The suction flow to this 2nd stage is the exit flow from the 1st stage ejector. Numerical simulation involving a one-dimensional gas dynamics model through the 2nd stage supersonic nozzle was performed to arrive at the nozzle area ratio, from which a nozzle exit to throat area ratio of 1.382 was selected such that the nozzle exit pressure matches the outlet pressure from the 1st stage ejector.

CFD simulations were then utilized to optimize the best supersonic diffuser dimensions (throat, inlet, and outlet diameters, as well as angles) and position of the nozzle with respect to (w.r.t.) diffuser inlet. The optimum design of the 2nd stage is shown in Fig. 13-32.

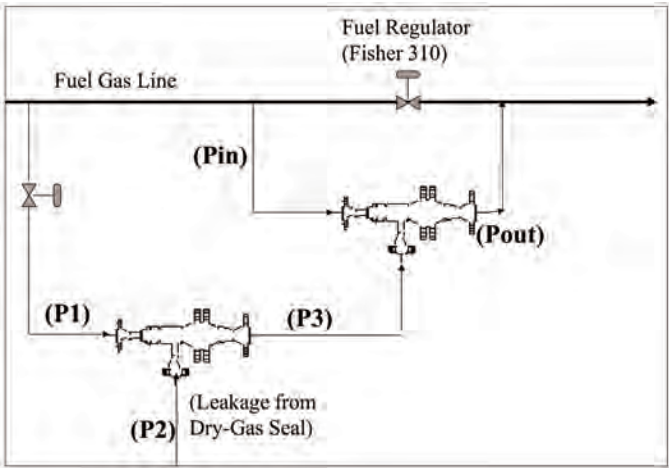


Figure 13-31. Conceptual configuration and design pressures of the two-stage ejector.

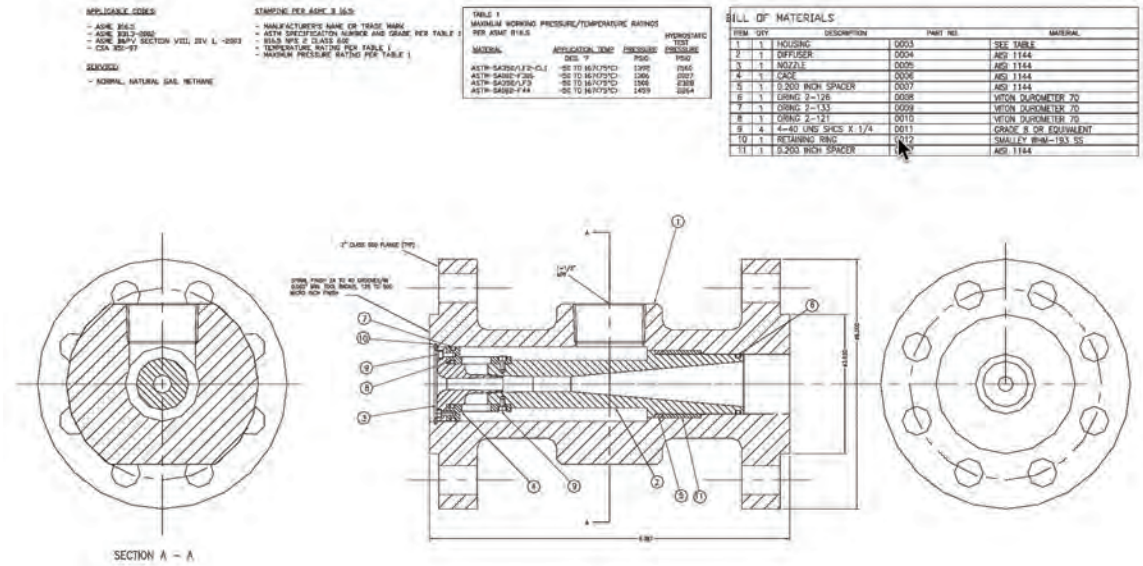


Figure 13-32. Design details of the 2nd stage supersonic ejector.

13.6.4 Performance of the Integrated Two-Stage Supersonic Ejector

Figure 13-33 shows the integrated test rig with all salient components, instrumentations and tubing. Tests were conducted on the 2nd stage ejector alone in order to optimize the position of its supersonic nozzle w.r.t. the diffuser inlet. The best performance was obtained with the position of the nozzle exit at 1.42 mm upstream from the inlet section of the supersonic diffuser in this 2nd stage ejector. Tests were then conducted on the two-stage ejector configuration combined, by varying P_1 to the 1st stage ejector (4600 kPa-a, 5000 kPa-a, and 5500 kPa-a), while maintaining the motive gas pressure (P_{in}) to the 2nd stage ejector at maximum line pressure of approximately 6000 kPa-a.

Figures 13-34 through 13-36 show the results of the integrated two-stage ejector system in terms of the discharge pressure from the 2nd stage ejector (Fig. 13-34), suction flow at the 1st stage (Fig. 13-35), and the intermediate pressure (P_3) for different P_1 (Fig. 13-36). The effects of varying (P_1) are manifested in Fig. 13-34, which indicates that the lower the P_1 the higher the suction flow, but at the expense of the overall discharge pressure (P_{out}).

The optimized configuration is capable of delivering the required discharge pressure (P_{out}) of 3300 kPag with a suction flow of 2–2.5 kg/hour and suction pressure (P_2) of 340 kPag. These values are matching the requirements for this ejector to work with a dry gas leakage and a typical fuel gas line on a typical compressor station. Motive gas flow to the 1st stage is 0.016 kg/s (based on 5000 kPa-a pressure), and to the 2nd stage is 0.464 kg/s (based on 6000 kPa-a pressure).

Recognizing that the motive gas to the 2nd stage ejector is drawn from the compressor discharge side (~6000 kPag), an assessment should be made to the balance-of-plant w.r.t. net energy saved by capturing the vent gas from the dry gas seal. Based on compressor suction pressure of ~5000 kPag, pressure ratio of 1.2, the excess power drawn by the motive gas flow of 0.464 kg/s is 9.3 kW. Assuming a thermal efficiency of the gas turbine/compressor set of 30%, the extra fuel usage due to compressing the motive gas is 31 kW. Now, the gas saving resulting from capturing the dry gas seal vent gas of 9.0 kg/hour amounts to 130 kW

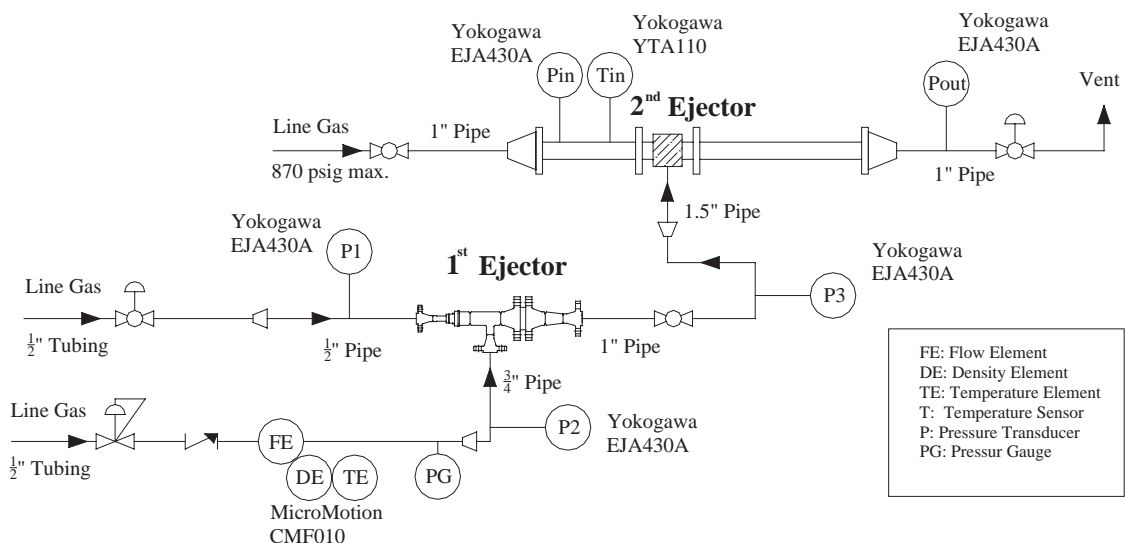


Figure 13-33. Schematic of the two-stage supersonic ejector test rig.

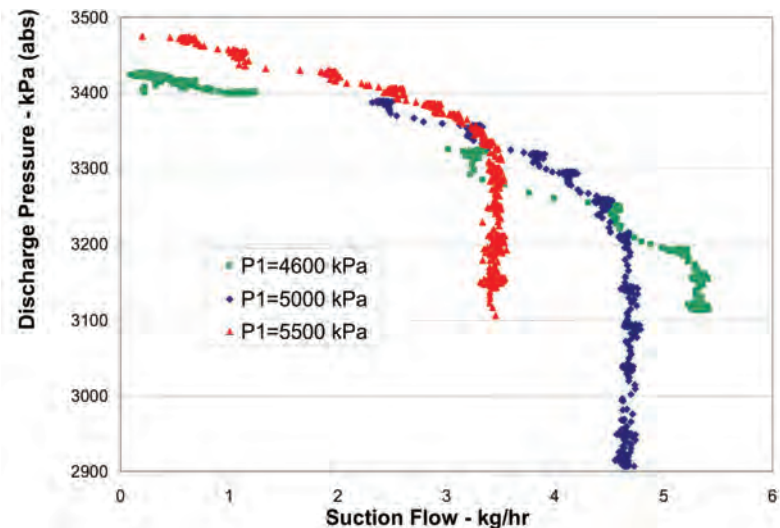


Figure 13-34. Overall performance of the two-stage supersonic ejector (discharge pressure from 2nd stage versus suction flow at 1st stage).

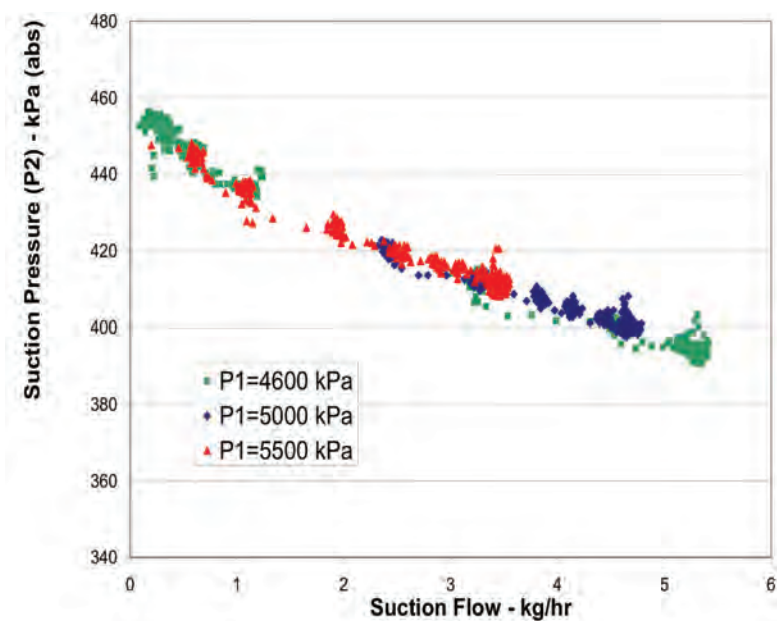


Figure 13-35. Overall performance of the two-stage supersonic ejector (suction pressure versus suction flow at 1st stage).

(based on gas heating value of 39.3 MJ/s.m³). Therefore, the net energy saving in fuel gas would be approximately 99 kW. The more important effect of employing the supersonic ejector is rather the substantial reduction in the GHG as shown by the calculations in Table 13-6. It is demonstrated that the net effect of employing the ejector is approximately a reduction of 1600 tonnes of CO₂-E per year.

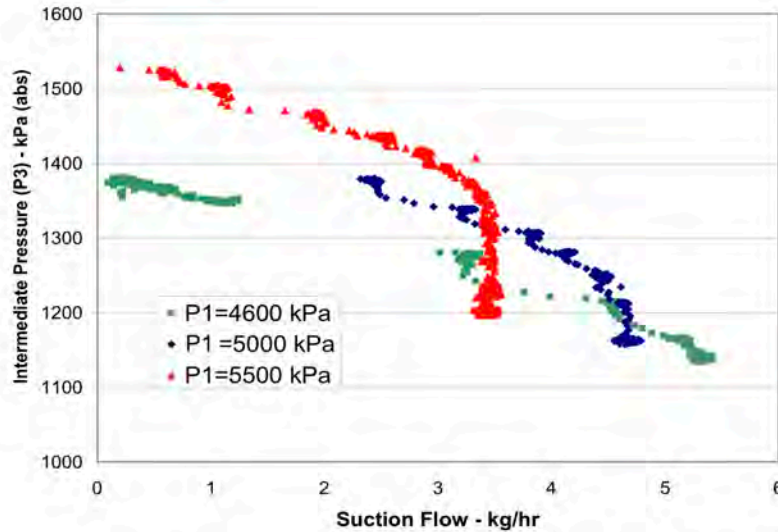


Figure 13-36. Overall performance of the two-stage supersonic ejector (intermediate pressure between the two stages versus suction flow at 1st stage).

Table 13-6. Calculation of the GHG emission benefit of the supersonic ejector

Ejector 2nd stage motive flow	0.4635	kg/s
Motive gas extra power needed	9,300	W
Motive gas turbine extra fuel needed	31,000	W
Fuel heating value	39	MJ/m ³
Fuel heating value	52,000,000	J/kg
Fuel gas burned	0.00059615	kg/s
GHG CO ₂ from above burning	0.00155	kg/s
GHG CO ₂ from above burning	48.8808	tonnes/year
Captured Dry-seal vent gas	9	kg/hr
Captured Dry-seal vent gas	0.0025	kg/s
Heat Energy Equivalent	130,000	W
Heat Energy Saving	99,000	W
GHG CO ₂ -E of the captured gas	0.0525	kg/s
GHG CO ₂ -E of the captured gas	1,656	tonnes/year

13.6.5 Supersonic Ejector in Operation

The present integrated two-stage ejector system has been skid-mounted and installed on a TransCanada compressor station in Alberta, Canada. The centrifugal compressor unit that was selected as a pilot was chosen because of its high utilization hours, so as to test the performance of the ejector system on a wide range of operating conditions and fluctuating loads. One of the other considerations in selecting the compressor unit was the ease of shutting down the unit without interrupting the transmission service to customers. The seal gas leak line currently going to atmospheric vent has a flow meter and a check valve. Table 13-7 gives the compressor operating parameters, Table 13-8 gives the primary gas seal parameters both at the drive-end (DE), and non-drive-end (NDE), and Table 13-9 gives details of the fuel gas system pertaining to the selected compressor unit. The concept of

Table 13-7. Operating parameters of the selected compressor unit for the implementation of the supersonic ejector

Unit #1		
Suction Pressure	4,613.00	kPa-g
Suction Temperature	15.60	C
Discharge Pressure	5,801.00	kPa-g
Discharge Temperature	34.70	C
PT Speed	5,589.00	RPM
Ad. Eff.	79.00	%
Flow	6,715.00	E6M3/d
Flow	58.29	kg/s

Table 13-8. Operating parameters of the DE and NDE of the dry-gas seal on the compressor unit selected for the implementation of the supersonic ejector

Drive End 1st Stage Seal Vent Gas					
Pressure	35	kPa-g	Alarm Pressure	80	kPa-g
Flow	5	SCFM	S/D Pressure	160	kPa-g
Flow	0.002	kg/s	Rupture Disc PSE 1203	700	kPa-g
Non-Drive End 1st Stage Seal Vent Gas					
Pressure	6	kPa-g	Alarm Pressure	80	kPa-g
Flow	2.5	SCFM	S/D Pressure	160	kPa-g
Flow	0.001	kg/s	Rupture Disc PSE 1204	700	kPa-g

Table 13-9. Operating parameters of the fuel gas system on the compressor unit selected for the implementation of the supersonic ejector

Fuel Gas		
Inlet Pressure	4,610.00	kPa-g
Inlet Temperature	15.60	C
Pressure After Heater	4,500.00	kPa-g
Temp After Heater	36.00	C
Pressure After 310	2,700.00	kPa-g
Temp After 310	23.00	C
Flow	135.60	E3M3/d
Flow	1.108	kg/s

the implementation design was based on these two sets of parameters. Figure 13-37 shows that the two primary dry gas leakage lines from the two DE and NDE dry gas seals are connected to form the suction to the first stage ejector. Two check valves are shown to prevent any back flow into the seal area as shown in Fig. 13-37.

The dry gas seal monitoring system was modified slightly by adding backpressure regulators on the seal vents. The back pressure currently at 160 kPag, was increased to 500 kPag. The existing rupture discs rating will remain the same at approximately 700 kPag, while shutdown setpoint was set at 600 kPag. In the event that the ejector could not suck gas from the primary vent, these two regulator valves will vent off the gas to atmosphere so as not to risk the dry gas seal. The rupture discs will continue to provide the same functions if the pressure increases above 700 kPag. The increase in the back pressure on the primary seal from 160 kPag to 500 kPag will not have any adverse impact on the integrity of the dry gas seal. This was reviewed and assured by the specific seal manufacturer of the unit.

For the first stage motive gas, a tie-in line was taken from the outlet of the fuel gas filter and upstream of the Fisher 310 control valve. This pressure varies between 4600 and 5800 kPag. Second stage motive gas was supplied from compressor discharge line downstream of the unit valve, typically 6000–6600 kPag. Using these two motive gas lines, the

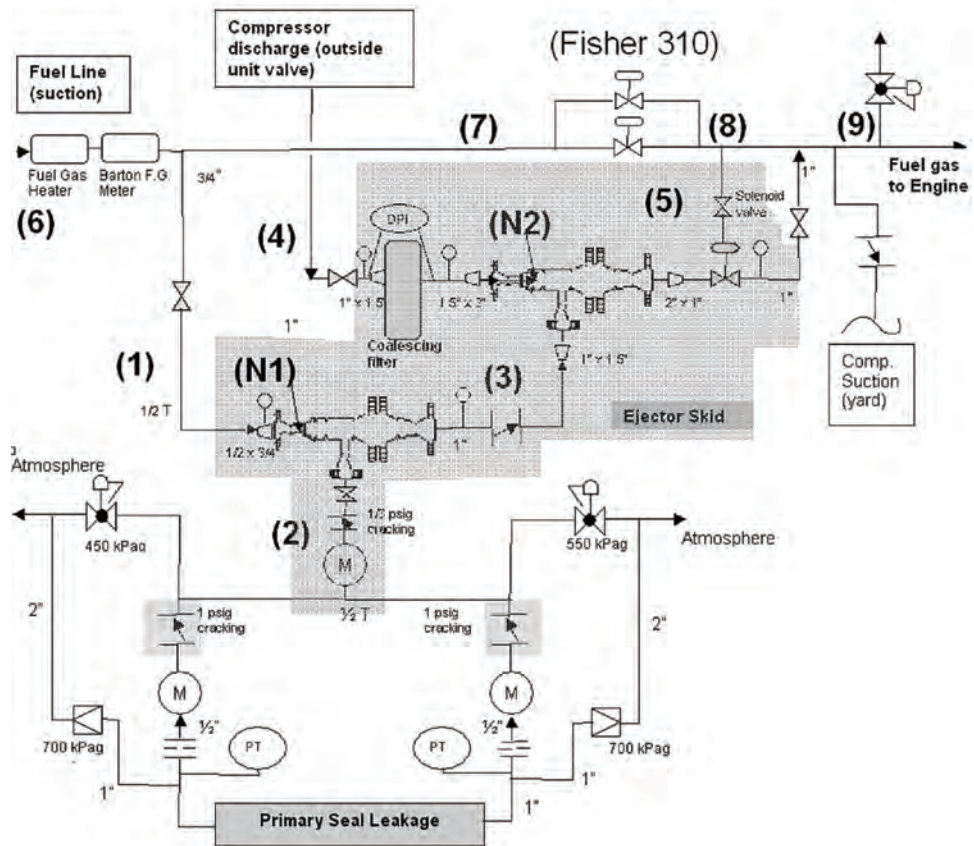


Figure 13-37. Design concept of the two-stage ejector on implementation at a 24 MW compressor/gas turbine unit on the TransCanada system.

two-stage ejector operating parameters (pressures, temperatures and flow rates) at different locations marked with numeric numbers in Fig. 13-37, are given in Table 13-10. It is noted that, due to the supersonic nature of the two stages, the gas expansion through the respective nozzles will result in extremely cold gas temperatures, which correspond to conditions inside the gas two-phase envelope. However, the exit velocity of the gas from the

Table 13-10. Design parameters of the supersonic ejector specific to the compressor unit selected for implementation

Location # (Refer to Fig. 13-37)	P (kPa-a)	T (°C)	Mass Flow (kg/s)
1	4600	35.9	0.016
N1	350	-113.0	0.016
2	350	10.0	0.001
3	1219	12.7	0.017
4	6000	35.0	0.464
N2	1219	-68.0	0.464
5	3260	8.2	0.481
6	4600	35.0	1.177
7	4600	35.0	0.696
8	2500	23.0	0.696
9	2500	18.4	1.777

supersonic section is extremely high, which will not allow for thermodynamic equilibrium. Even if small condensation droplets could form, these will be moved at enormous velocity into the diffuser section of the respective stage and will evaporate due to compression in the diffuser.

A gas coalescer filter is installed on the ejector skid at location 5 (see Fig. 13-37) to filter the final discharge gas from the ejector before entering into the fuel gas line. This is because buffer gas is used to flush the seal chamber of debris or dirty gas and to keep the environment in the seal clean. It is expected that there could be some buffer gas leaking into the primary seal gas system and eventually to the fuel gas through the ejector.

One concern that was raised was in regard to the fact that a higher backpressure on the primary dry gas seal could result in gas migrating to the secondary dry seal, located near to the magnetic bearing cavities. If the purge air fails and this gas migrates into the magnetic bearing cavities, and an ignition source within the magnetic bearing cavities exists, an explosion could result. It was, however, argued that it is highly unlikely for an ignition source to be generated within the magnetic bearing cavities during startup, shutdown, and bearings being de-energized. Additionally, an expert on bearing design ascertained that it would be very difficult for gas to get into the bearing chamber, because there is an outer seal labyrinth on the gas seal that has barrier air going to it, outboard of the secondary vent. Therefore, any gas that gets across the secondary seal will be pushed out to the secondary vent by the barrier air, which should be vented to atmosphere. There is also an air purge to the bearing chambers and they are also vented to atmosphere. Therefore, there is a positive pressure on the bearing housings that should help keep process gas from entering. Additionally, the barrier labyrinth should also help in preventing the combustible gas from migrating into the magnetic bearing chamber. Therefore, as long as the system is working properly, with barrier air flowing, there should not be any process gas getting into the bearing chamber. Furthermore, the magnetic bearing design does not have an ignition source since the whole magnetic bearing assembly is sealed and should be contact-free (rotor and stator) with an air gap that provides the dampening and the magnetic field needed to achieve its function. Finally, there is a differential pressure monitoring device which (if works properly) will trigger a unit to shut down on reversed pressure differential between the magnetic bearing cavities and the secondary dry seal, i.e., purge air and/or the seals fail.

The supersonic ejector skid was installed next to the fuel gas system of the GT unit. Data was collected after successful commissioning and is shown in Table 13-11.

Table 13-11. Actual operating data collected after successful commissioning of the supersonic ejector

Location # (Refer to Fig. 13-37)	P (kPa-a)	T (°C)	Mass Flow (kg/s)	Mass Flow (kg/hr)
1	5090	35.9	0.01770	63.720
DE Seal	506	10.0	0.001607	5.785
NDE Seal	512	10.0	0.001607	5.785
Total Seal Leakage	509	10.0	0.003214	11.570
N1	509	-113.0	0.01770	63.720
2	509	10.0	0.00286	10.285
Vent to Amb	509	10.0	0.00036	1.285
3	1190	12.7	0.021	74.005
4	5990	35.0	0.463	1668.240
N2	1190	-68.0	0.463	1668.240
5	2990	8.2	0.484	1742.245
6	5140	10.0	1.177	4237.500
7	5090	35.9	0.693	2495.255
8	2900	23.0	0.693	2495.255
9	2690	18.4	1.177	4237.500

REFERENCES

- [1] Tobin, J., 2007. "Natural Gas Compressor Stations on the Interstate Pipeline Network: Developments Since 1996," Energy Information Administration, Office of Oil and Gas, November 2007.
- [2] Canadian Energy Pipeline Association, 2016. "Best Management Practice – Fugitive Emissions at Natural Gas Transmission and Storage Facilities," CEPA Working Group on Climate Change and Clearstone Engineering, Sept. 23, 2016, 22 pages.
- [3] Slovic, P., 1987. "Perception of Risk." *Science* 236, 17 April 1987, pp. 280–285.
- [4] Environmental Protection Agency, 1974. "INFORMATION ON LEVELS OF ENVIRONMENTAL NOISE REQUISITE TO PROTECT PUBLIC HEALTH AND WELFARE WITH AN ADEQUATE MARGIN OF SAFETY," U.S. EPA Report No. 550/9-74004, Washington, DC, March 1974.
- [5] US Department of Labor, Occupational Safety and Health Administration, Occupational Noise Exposure, Document No 1910.95.
- [6] Canada Occupational Health and Safety Regulations, http://www.ccohs.ca/oshanswers/phys_agents/exposure_can.html.
- [7] Beranek, L. L., 1957. "Revised Criteria for Noise in Buildings," *Noise Control*, Vol. 3, No. 1, pp. 19–27.
- [8] ANSI S12.2-1995. American National Standard. Criteria for Evaluating Room Noise.
- [9] Schomer, P. D., 1999. "Proposed revisions to room noise criteria," *Noise Control Eng. J.* 48 (4), 85–96, 1999.
- [10] Beranek, L. and Ver., I., 1992. *Noise and Vibration Control Engineering: Principles and Applications*. Wiley- Interscience.
- [11] Federal Interagency Committee on Urban Noise (FICUN), 1980. Guidelines for Considering Noise in Land Use Planning and Control. (U.S. Government Printing Office Report #1981-337-066/8071) Washington, D.C.: FICUN.
- [12] Society of Automotive Engineers, 1985. "Gas Turbine Jet Exhaust Noise Prediction," Report No. SAE ARP 876C, Society of Automotive Engineers, Warrendale, PA.
- [13] Eugene, S., Love, E. S., Grigsby, C. E., Lee, L. P. and Woodling, M. J., 1959. "Experimental and Theoretical Studies of Axisymmetric Free Jets," NASA Report R-6.
- [14] Jungowski, W. and Petela, G., 1994. "Excessive Noise Preventer," Inter-Noise 94, Yokohama, Japan, August 29–31.
- [15] Instrument Society of America, 1985. "Flow Equations for Sizing Control Valves," Standard No. ANSI/ISA S75.01-1985.
- [16] Baumann, H. D., 1984. "Coefficients and Factors Relating to the Aerodynamic Sound Level 'Generated by Throttling Valves,'" *Noise Control Eng. J.* 22, January/February 1984, pp. 1–6.
- [17] Instrument Society of America, 1989. "Control Valve Aerodynamic Valve Noise Prediction," Standard No. ANSI/ISA S75.17.
- [18] Baumann, H. D., 1987. "A Method for Predicting Aerodynamic Valve Noise Based on Modified Free Jet Noise Theories," Paper No. 87-WA/NCA-7, American Society of Mechanical Engineers, New York.
- [19] Frank, L., 2005. "NOISE CONTROL ENGINEERING OBJECTIVES FOR COMPRESSOR STATION TURBO-COMPRESSOR UNITS," Presented at the 16th Symposium on Industrial Application of Gas Turbines (IAGT) Banff, Alberta, Canada, October 12–14, 2005.
- [20] Marks, T., 1999. "NOISE CONTROL AT GAS-FIRED COMPRESSOR STATIONS," Australian Acoustical Society Conference, Melbourne, 24–26 November 1999.
- [21] Liu, Z., Jahnke, B., Marczak, M. and Kiteck, P., 2002. "Reducing Compressor Station Ambient Noise Level by Controlling Compressor Internal Noise Source," *Proceedings Of International Pipeline Conference IPC 2002*, Calgary, Alberta, Canada, September 29–October 3, 2002.
- [22] Zirrig, W. and Schmücker, A., 2001. "Novel Measurement Technique for a Selective Detection of Sources of Sound in Natural Gas Transmission Plant," *Proceedings of the 2001 International Gas Research Conference IGRC*, p. 8, Amsterdam, Netherland, 2001.

- [23] Gužas, D. and Jotautien, E., 1999. "Estimation of sound power of centrifugal machines based on sound intensity measurements," ISSN 1392-2114 ULTRAGARSAS, Nr.1(31). 1999.
- [24] Kudernatsch, G. 2000. "Combustion Turbine Exhaust Systems-Low Frequency Noise Reduction," *Proc. INTER-NOISE 2000*, edited by Didier Cassereau, Noise Control Foundation, Poughkeepsie, New York, 2000.
- [25] Unknown, 2011. "Compressor Station Piping Noise: Noise Mechanisms and Prediction methods," Gas Machinery Research Council and Southwest Research Institute®, February 2011, 41 pages.
- [26] Jones, E., Oliphant, T., Peterson, P., 2001. SciPy—Open source scientific tools for Python, <http://www.scipy.org/>.
- [27] Hunter, J., matplotlib, <http://matplotlib.sourceforge.net/index.html>.
- [28] The matplotlib.mlab.griddata function in the web site provided in ref. 10 above.
- [29] Environmental Protection Agency (EPA)-AP 42, 2000. Fifth Edition, Volume I, Chapter 3.1: Stationary Gas Turbines, April 2000.
- [30] Performance Specification 16 U.S. Code of Federal Regulations, 40 CFR Part 60, Appendix B. Federal Register, 60 FR 40297.
- [31] Alternative Monitoring Systems, U.S. Code of Federal Regulations, 40 CFR Part 75, Subpart E., Federal Register, 60 FR 40297.
- [32] Stambler, I., 1995. "Utilities Testing Predictive Emissions Monitoring as an Alternative to CEM," *Gas Turbine World*, July-August 1995, pp. 20–25.
- [33] Hung, W. S., 1991. "A Predictive NO_x Monitoring System for Gas Turbines," ASME Paper No. 91-GT-306, presented at the International Gas Turbine and Aeroengine Congress and Exposition, Orlando, Florida, June 3–6, 1991.
- [34] Swanson, B. G., 2003. "Demonstration and Certification of A Predictive Emissions Monitoring System Under 40 CFR PART 75, Subpart E Gas Turbine Applications," EPRI CEM User Conference, San Diego, California, 2003.
- [35] Swanson, B. G., 2006. "Predictive Emissions Monitoring (PEMS) for Regulatory Compliance and Emissions Trading Programs," *Proceedings from the 7th International Conference on Emissions Monitoring (CEM 2006)*, CNIT, Paris La Defense, France, pp. 92–104.
- [36] Swanson, B. G., 2008. "A Cost Effective Advanced Emissions Mentoring Solution for Gas Turbines—Statistical Hybrid Predictive System That Accurately Measures Nitrogen Oxides, Carbon Monoxide, Sulfur Dioxide, Hydrocarbon and Carbon Dioxide Mass Emission Rates," ASME Turbo-Expo, Berlin, Germany, June 9–13, 2008.
- [37] Swanson, B. G., and Lawrence, P., 2009. "An Alternative Approach to Continuous Compliance Monitoring and Turbine Plant Optimization using a PEMS (Predictive Emission Monitoring System)," 18th Industrial Application of Gas Turbines (IAGT) Symposium, Banff, Alberta, Canada, October 19–21, 2009.
- [38] Hung, W. S., 1995. "Predictive Emission Monitoring System (PEMS): The Established NO_x Monitoring System for Industrial Gas Turbines," *Air & Waste Management Association Paper No. 95-MP16A.01*, presented at the 88th Annual Meeting & Exhibition, San Antonio, Texas, June 18–23, 1995.
- [39] Lefebvre, A. H., 1995. "The Role of Fuel Preparation in Low-Emission Combustion," *ASME Journal of Engineering for Gas Turbines and Power*, Vol. 117, October 1995, pp. 617–654.
- [40] Lefebvre, A. H., 1983. GAS TURBINE COMBUSTION, Hemisphere Publishing Corp., pp. 33–76, 463–514, and p. 473
- [41] Sullivan, D. A., 1977. "A Simple Gas Turbine Combustor NO_x Correlation Including the Effect of Vitiated Air," *ASME Journal of Engineering for Power*, April 1977, pp. 145–152.
- [42] Botros, K. K., de Boer, M. J., Price, G. R., and Kibrya, G., 1997. "One-dimensional Predictive Emission Monitoring Model for Gas Turbine Combustors," 42nd ASME Gas Turbine and Aeroengine Congress, Exposition, and Users Symposium, Orange County Convention/Civic Center, Orlando, Florida, USA, June 2–5, 1997.
- [43] Syed, K. J., Roden, K. and Martin, P., 2007. "A Novel Approach to Predicting NO_x Emissions From Dry Low Emissions Gas Turbines," *ASME Journal of Engineering for Gas Turbines and Power* 129(3), pp. 672–679.

- [44] Tsague, L., Tsogo, J. and Tatietse, T. T., 2006. "Prediction of the Production of Nitrogen Oxide (NO_x) in Turbojet Engines," *Atmospheric Environment* 40(29), pp. 5727–5733, 2006.
- [45] Box, W. J. and Reinermann, P., 2002. "Predictive Emission Monitoring Systems—An Alternative to Hardware Analyzers for Continuous Monitoring," NPRA Annual Meeting—National Petrochemical and Refiners Association, San Antonio, TX, 2002.
- [46] Jiang, L. and Campbell, I., 2005. "A critical evaluation of NO_x modeling in a model combustor," *ASME Journal of Engineering for Gas Turbines and Power* 127(3), pp. 483–491, 2005.
- [47] Alexander, R., 2004. "Practical Approach to Predictive Emissions Monitoring of Gas Turbine Emissions," *International Gas Research Conference Proceedings*, Vancouver, BC, Canada, 2004.
- [48] Botros, K. K., Selinger, C. and Siarkowski, L., 2009. "Verification of a Neural Network Based Predictive Emission Monitoring Module on a RB211 Gas Turbine," ASME Turbo-Expo 2009, Paper #GT2009–59419, Orlando, Florida, June 8–12, 2009.
- [49] Botros, K. K. and Cheung, M., 2010. "Neural Network Based Predictive Emission Monitoring Module for a GE LM2500 Gas Turbine," *ASME 8th International Pipeline Conference & Exhibition*, TELUS Convention Centre, Calgary, Alberta, Canada, September 27 through October 1, 2010.
- [50] Handbook of Continuous Emissions Monitoring Systems for Non-criteria Pollutants, 1997. Chapter 4, U.S. EPA.
- [51] Nelson, P., 2003. Index to EPA Test Methods, US EPA New England Region 1 Library, Boston, MA USA, revised edition April 2003.
- [52] Alberta Stack Sampling Code, Alberta Environment, <http://environment.gov.ab.ca/info/posting>.
- [53] Bishop, C. M., 1995. *Neural Networks for Pattern Recognition*, Clarendon Press, Oxford.
- [54] Jain, A. K., et al., 1996. "Artificial Neural Networks—A Tutorial," *Computer*, v. 29, n. 3, pp. 31–44.
- [55] Hunt, K. J., Sbarbaro, D., Zbikowski, R. and Gawthrop, P. J., 1992. "Neural Networks for Control Systems—A Survey," *Automatica*, v. 28, n. 6, pp. 1083–1112.
- [56] National Emission Guidelines for Stationary Combustion Turbines, 1992. Canadian Council of Ministers of the Environment, CCME-EPC/AITG-49E, December 1992.
- [57] Botros, K. K., Geerligs, J. and Imran, H., 2012. "Tandem Supersonic Ejectors for The Repressurization of an Off Gas," US Patent No. 8,100,671 B2, January 24, 2012.
- [58] Power, R. B., 1994. "Predicting Unstable-Mode Performance of a Steam Jet Ejector," *Fluid Power Systems Technology*, Collected Papers, ASME, 1994.
- [59] Freeman, B. Z. and Lior, N., 1994. "A Novel High-Temperature Ejector-Topping Power Cycle," *Journal of Engineering for Gas Turbines and Power*, vol. 116, pp. 1–7, January 1994.
- [60] Minardi, J. E., 1982. "Compressible Flow Ejector Analysis with Application to Energy Conversion and Thrust Augmentation," *AIAA 20th Aerospace Sciences Meeting*, Paper #82-0133, Orlando, Florida, January 11–14, 1982.
- [61] Huang, B. J. and Chang, J. M., 1999. "Empirical Correlation for Ejector Design," *International Journal of Refrigeration*, Vol. 22, pp. 379–388, 1999.
- [62] Huang, B. J., Chang, J. M., Wang, J. M. and Petrenko, V. A., 1999. "1-D Analysis of Ejector Performance," *International Journal of Refrigeration*, Vol. 22, pp. 354–364.
- [63] Chen, S. L., Yen, J. Y. and Huang, M. C., 1998. "An Experimental investigation of ejector performance based upon different refrigerants," *ASHRAE Transactions*, vol. 104, no. 2, pp. 153–160, June 1998.
- [64] Sun, Da-Wen and Eames, I. W., 1995. "Recent Developments in the Design Theories and Applications of Ejectors—A Review," *Journal of the Institute of Energy*, vol. 68, no. 475, pp. 65–79, Jun 1995.
- [65] Villa, M., De Ghetto, G., Paone, F., Giachetta, G. and Bevilacqua, M., 1999. "Ejectors for Boosting Low-Pressure Oil Wells," *SPE Production and Facilities*, vol. 14, no. 4, pp. 229–234, Nov 1999.
- [66] Hu, H., Kobayashi, T., Saga, T., Taniguchi, N., Liu, H. and Wu, S., 1999. "Research on the Rectangular Lobed Exhaust Ejector/Mixer Systems," *Transactions of the Japan Society for Aeronautical and Space Sciences*, vol. 41, no. 134, pp. 187–194.
- [67] Zahradnik, J., Fialova, M., Linek, V., Sinkule, J., Reznickova, J. and Kastanek, F., 1997. "Dispersion Efficiency of Ejector-type Gas Distributors in Different Operating Modes," *Chemical Engineering Science*, vol. 52, no. 24, pp. 4499–4510, Dec 1997.

- [68] Fletcher, G. R., 1954. "Gas Jet Compressors," *Petroleum Refiner*, pp. 107–111, February.
- [69] Botros, K. K., Geerligs, J., Imran, H. and Thompson, W., 2006. "Development of a Supersonic Ejector for Capturing Very Low Pressure Vent Gases and Re-injection into a High Pressure Stream," *6th International Pipeline Conference*, Calgary, Alberta, Canada, September 25–29, 2006.
- [70] Shapiro, A. H., 1983. *The Dynamics and Thermodynamics of Compressible Fluid Flow—Vol. 1*, E. Krieger Publishing Co., Malabar, Florida, pp. 972–973.
- [71] Zucrow, M. J. & Hoffman J. P., 1976. *Gas Dynamics, Vol. I*, John Wiley & Sons Inc., 1976.

INDEX

Page numbers followed by f and t indicate figures and tables, respectively.

A

- Acceleration
 - block, 534
 - defined, 534
 - head, 171–172
 - typical, 534
- Accumulator, flow transients of, 344–346, 345f
- Acidity/alkalinity (pH)
 - pump selection and, 23
- Acoustic boundary conditions
 - and resonance, 488–490, 488f–490f
 - acoustic resonance condition of piping network, 488–490, 488f–490f
- Acoustic transfer matrix
 - for centrifugal compressor, 479–480, 479f
 - for pipe element, 464–471, 466f, 471f
 - damping (attenuation) on, 468–471, 471f
 - mean flow on acoustic TM for pipe element, 467–468
 - for throttle element, 472–478, 473f, 474t, 475f, 476f, 477f
 - ball valve, 476, 476f, 477f, 478f
 - globe valve, 476–478
 - orifice plate, 475, 475f
 - for a volume element, 478–479, 478f
- Active bearings, 560–561
- Adaptive control algorithms, 223
- Additives, operational hazards of, 9
- Adiabatic compression, 243, 255
- Adjustments, compressor performance, 272–274
- Aeroderivative gas turbines, 280, 281–282, 291–292
- Affinity laws, 148, 149f
- Aftercooler, defined, 198
- Air compressor surge, 286–287
- Air cooled heat exchanges, 70
- Air coolers, 70
- Air intake system, gas turbines, 286
- Alkalinity
 - pump selection and, 23
- American Gear Manufacturers Association (AGMA), 329–330
- American Petroleum Institute (API), 97
 - API 541, 310
 - API 546, 310
 - API 614, 194, 203, 233, 291
 - API 616, 305
 - API 617, 209, 228, 233, 261
 - API 618, 201, 203, 254
 - API 671, 329
- American Petroleum Institute (API) gravity, SG and, 133–136
- American petroleum Institute (API 520) standards, 526–527
- American Society of Mechanical Engineers (ASME), 97
- Ampliflow™, 218
- Analytical pipe model, 449–450
- Anchor bolts, 183, 184
- Anechoic (non-reflective), acoustic boundary conditions, 489
- ANSI/HI 9.6.8, 516–517
- ANSI pressure limitations, pipeline design and, 21, 34
- Anti-icing systems, 288–289
- AP-42 emission factors, 613
- API, *see* American Petroleum Institute (API)
- API 610, 516–517, 517f
- API 688 document, 516
- API 618 reciprocating compressors, 516
- API 674/675 reciprocating pumps, 516
- API 619 rotary (screw) compressors, 516
- API 676 rotary (progressive cavity) pumps, 516
- API RP 14E recommendations (pipe sizing), 39
- API 618 Standard, 502–510, 503f
 - acoustic shaking forces, 504
 - compressor mechanical model analysis, 504
 - Design Approach 2, 503, 503f
 - Design Approach 3, 503–504
 - Design Approach (DA) 1, 503, 503f
 - Design Approach 1 pulsation limits, 507–509
 - earlier version (4th edition), 502
 - general criteria, 505–507
 - maximum allowable non-resonant shaking forces, 509–510
 - mechanical analysis, 502–503
 - piping system analysis, 504–505
 - pulsation analysis, 502–503
 - pulsation guidelines, 505
 - purpose of, 502
 - separation margin, 504
 - for slow and medium-speed machines, 502
- API 674 Standard, 510–512
- Application torque, calculation, 324
- ASME, *see* American Society of Mechanical Engineers (ASME)

- ASME Power Test Code PTC 10, 228, 261
- Aspects, compressor performance, 237–247
- behavior, 243–244
 - efficiency, 244–245
 - flow, 245
 - gas properties, 237, 238–243
 - compressibility and molecular weight, 238–240
 - EOS, 241–243
 - ideal gas laws, 237, 238
 - ratio of specific heats, 240–241
 - general, 237
 - head, 244
 - nomenclature, 237, 238t
 - power, 245–247
- Asymmetric series compressors with spare unit, 79–80, 81f
- Attenuation
- acoustic transfer matrix for pipe element and, 468–471
- Aude equation, 24
- Automated surge relief installation, 60–61
- Auxiliary system level control, 92
- Axial diffusion coefficient, 46
- Axial-flow compressor, 285
- Axial-flow pumps, 106
- Axial split (casing), 206
- Axial thrust, calculation of, 208, 209
- B**
- Balanced Noise Criterion (NCB) curves, 598
- Balance drum
- defined, 208
 - forces, 208, 209f
- Balance piston
- defined, 208
 - forces, 208, 209f
- Balancing, rotordynamics and, 561–563, 562f–563f
- Ball valves, 44
- acoustic transfer matrix for throttle element, 476, 476f, 477f, 478f
- Barrel-type centrifugal compressors, 203, 204f
- Batch contamination
- in liquid pipelines, 45
- Beam-type compressors, wet seals for, 214
- Bearings
- active, 560–561
 - centrifugal compressors, 209–211
 - externally pressurized, 560
 - gas turbines, 289–291
 - IGCC, 233–234
 - magnetic, 560–561
 - pressurized oil, 560–561
 - reciprocating compressors, 193, 194–196
 - regular internally-pressurized fluid film, 560
 - rotordynamics and, 560–561
- Bed section, of compressor frame, 182–183
- Behavior, compressor, 243–244
- Benedict-Webb-Rubin equations, 228
- Benedict-Webb-Rubin-Starling (BWRS) equation, 242
- Bently Pressurized (orifice) Bearing Company, 211
- Bingham fluids, 21, 22f
- Block acceleration, 534
- Blockage, degradation mechanism, 265
- Blowdown
- noise suppression during, 496–499, 497f–499f
- Blowdown, station and gas pipeline, 444–457, 445f
- comparison between models, 450–453
 - non-isothermal blowdown, 453–457
 - pipe model, 449–450
 - volume model, 446–449
- Booster compression, 6
- Booster pumps, 54
- Boundary conditions, 342–346
- flow transients
 - across other elements, 343–344, 343f–344f
 - of an accumulator, 344–346, 345f
- Bowtie diagrams, 8
- Boyle's law, 238, 243
- Brake horsepower, compressor, 250
- Brayton cycle, 302, 303f
- Broadband shock-associated noise, 603
- Buildings, compressor station, 95
- Bureau of Land Management, 97
- Bypass check valve, 36, 43
- C**
- Canadian Energy Pipeline Association (CEPA), 7
- CAN/CSA Z662 (safety standards), 7
- CAN/CSA Z767-17 (safety standards), 7
- Capacity
- compressors, 245
 - control, reciprocating compressors, 187, 188f, 189f
 - reciprocating compressors, 247–249
- Carbon monoxide (CO), formation, 295
- Cascading effect, 70
- Case studies and examples
- ethylene pump, 365, 367–369, 367f–368f
 - pulsation and vibration analysis
 - multiple source pulsation, 521–523, 522f
 - pulsation generated by a reciprocating compressor, 523–525, 523f–525f
 - single-source pulsation, 520–521, 520f–521f
 - styrene transfer system, 361–365, 361f–362f, 363f, 364f–365f, 366f
- Case study pulsation examples, 518–525
- multiple source pulsation, 521–523, 522f
 - high-flow case, 523
 - intermediate-flow case, 523
 - low-flow case, 523
 - pulsation generated by a reciprocating compressor, 523–525, 523f–525f
 - single-source pulsation, 520–521, 520f–521f
- Casing (axial split), 206

- Causes (bowtie diagram), 8
- Cavitation, 499, 500f
- Cavitation and column separation, 358–361
 - overview, 358–359
 - steam condensation-induced water hammer, 359–361, 360f
- Cavitation in centrifugal pumps, 154–160
 - damage due, 154–155
 - effects of, 155
 - formation, 155, 157f
 - NPSH, 157–158
 - NPSHA, 158, 159f
 - NPSHR, 158–159, 160f
 - phenomenon, 154–155
 - reducing, 155
- CEM measurements, 613–615, 614f, 615f
- Centaur, 281
- Centrifugal booster pumps, 105f
- Centrifugal compression systems
 - blowdown, *see* Blowdown, station and gas pipeline
 - check valve, *see* Check valve dynamics
 - dynamic instabilities, fundamentals of, 372–386
 - complex compression systems, 375–379, 378f, 379f
 - control dynamics, 379–381, 381f
 - simple compression systems, 372–374, 372f–373f, 374f
 - solution techniques, 382–386, 382f–383f, 384f, 385f, 386f
- ESD, *see* Emergency shutdown (ESD)
- overview, 371–372
- relief valve, *see* Relief valve dynamics
- Centrifugal compressors, 203–229
 - acoustic transfer matrix for, 479–480, 479f
 - advantages and disadvantages of, 334
 - bearings, 209–211
 - controls and monitoring, 220–223
 - design(s)
 - general, 203–205, 206f
 - standards, 228–229
 - flow (capacity), 245
 - forced vibration in, 551
 - internals and sealing, 205–209
 - lubrication system, 211, 213
 - mechanical analysis of piping systems, 584–588, 586f, 587f
 - multi-stage, 551
 - performance, 254–267
 - degradation monitoring, 264–266, 267f
 - dynamic performance characteristics, 254–260
 - general, 254
 - mixture composition on, 262–264
 - selection and sizing, 260–261
 - testing, 261–262
 - physical operation, 223–228
 - diffuser, 228
 - fluid properties, effect of, 228
 - impellers, 224–227
 - performance characteristics, 223–224
 - pressure–volume characteristic, 270, 271f
 - rotordynamics and, 551–552
 - sealing system, 213–220
 - dry gas seals, 216–219
 - emerging gas seal technology, 220
 - general, 213–214
 - wet oil seals, 214–215
 - self-excited vibration in, 551
 - subsynchronous vibration in, 551
- Centrifugal impeller design theory, 141–143
- Centrifugal pumps, 104–118; *see also* Pump(s)
 - advantages, 100
 - axial-flow pump, 106
 - centrifugal action, 108
 - components, 108
 - configuration, 107
 - design, 106–109, 110f, 111f
 - impeller, 107–109
 - functioning of, 106–107
 - limits, 163–166
 - minimum flow, 163
 - re-circulation, 164–166
 - temperature rise, 163–164
 - mechanical seals, 109–114, 115f
 - mixed-flow pumps, 106
 - modifications, 150, 151f–153f
 - nozzle loading, 114–118
 - operational hazards of, 9
 - performance of
 - affinity laws, 148, 149f
 - cavitation in, 154–160
 - centrifugal impeller design theory, 141–143
 - coverage chart, 138
 - impeller curve characteristics, 145–147
 - impeller selection, 138–140
 - pipeline-pump operational control, 148–150
 - pump performance curves, 137–138, 139f
 - pump power and, 150
 - radial flow pumps, 105, 106f
 - rotordynamics and, 553–554
 - specific speed, 143–145, 146f
 - system curve, 140, 141f
 - types, 104–106
 - viscous liquids and, 160–163
- Centrifugal pumps, dynamic behavior, 346–353
- dynamic equation, 348, 351–352
- full pump characteristics, 347–348, 349f, 350t–351t
- homologous relations, 347
- pump and motor inertias, 352–353, 352f, 353f
- CEPA, *see* Canadian Energy Pipeline Association (CEPA)
- Characteristic curves, pump, 145–147
- Characteristics
 - centrifugal compressors, dynamic performance, 254–260
 - basic performance curves, 254–257
 - fan laws, 257–258
 - limits, 258–260
 - gas turbine performance, 299, 300, 301, 302f, 303f
 - system, 267–276
 - adjustments, 272–274
 - comparison, 270, 271f
 - curves, 267–270
 - general, 267

- operating considerations, 274–276
- operating limitations, 271–272
- Charles' law, 238
- Chattering, pressure relief valves (PRV), 526
- Check valve dynamics, 411–427
 - compression recycle system and, 425–427, 426f, 428f
 - counterbalance on maximum reverse velocity, 421–422, 422f
 - overview, 411–413
 - piston type check valves, 422–424, 422f
 - swing type check valves
 - description, 411–412, 412f
 - dynamic behavior of, 413–417, 414f, 416f–417f
 - slamming characteristics, 417–421
 - wafer type check valves, 424–425, 424f
- Chip detectors, 292
- Choke, 259, 260, 272
- Circular casing pump, 106
- CleanPac™, 218
- Clearance volume control, 187
- Closed, acoustic boundary conditions, 482–485
- Codes and standards, compressor, 96–97
- Combustion air/lube oil-water cooling, 70
- Combustion engines, internal, 320–323
 - advantages and disadvantages of, 333–334
 - design, 320–322
 - general, 320
 - integral engine/compressors, 322–323
- Compatibility
 - between driver and driven equipment, 331, 332, 333, 334
 - with existing equipment, 331, 332, 334
- Complex compression systems, 375–379, 378f, 379f
- Component matching, defined, 302
- Compressibility
 - correction, 250
 - gases, 238–240
- Compression
 - booster, 6
 - dependability for, 14–15
 - equipment, types, 75–76
 - field, 6
 - gas pipeline and, 5–6, 65
 - gas recovery, 5
 - gas storage, 6
 - ignition engines, 320
 - interchange, 6
 - lateral, 6
 - versus* looping, gas pipelines, 66f, 69–70
 - performance curve, 72f
 - recycle system, check valves
 - effect on, 425–427, 426f, 428f
 - requirements, 85–86
- Compressor Equipment Health Monitoring (CEHM) system, 620
- Compressors
 - centrifugal, *see* Centrifugal compressors
 - classification, 179, 180f
 - cost of operation, 73–74
 - design and operation, *see* Design and operation
 - drivers, *see* Drivers
 - hermetic, 315–317
 - IGCC, 231–234
 - mechanical model analysis, 504, 515f
 - performance, *see* Performance pipeline, overview, 179
 - reciprocating, *see* Reciprocating compressors
 - screw, 229–231
- Compressors arranged in series, recycle system around, 409–410, 409f, 410f–411f
- Compressor stations
 - buildings and weather protection, 95
 - codes and standards, 96–97
 - compression equipment, types, 75–76
 - compressor requirements, 85–86
 - cost of ownership, 74
 - driver requirements, 86–87
 - environmental considerations, 80
 - fire, 9–10
 - layout, 87, 88f
 - NPV analysis (case study), 77–78
 - number of units, 76–77
 - operating considerations, 74–75
 - parallel arrangement, 76
 - pipng layout, 87, 89–90
 - “power” backup, 79
 - predictions of noise levels from, 601–607
 - scrubbers and filters, 90–91
 - series arrangement, 76
 - series-parallel arrangement, 76
 - spacing, 69
 - standby units, 78–80, 81f
 - unit auxiliary systems and, 92
 - unit control systems and, 92–95
 - usage scenario for pipeline stations (case study), 81–85
- Computational Fluid Dynamics (CFD) analysis, 626
- Configuration, pump, *see* Pump configurations
- Consequences (bowtie diagram), 8f, 9
- Constant area pipes, governing equation for, 339–341, 340t–341t
 - assumptions, 339
- Contaminants, in liquid fuels, 293
- Contamination in liquid pipelines, 44–52
 - DNV erosion model, 48, 49f, 49t
 - Zhang et al. erosion model, 48–50
- Control dynamics, 379–381, 381f
- Controlled engines, 613
- Control system
 - centrifugal compressors, 220–223
 - reciprocating compressors, 196
- Conversion factors, for pumps, 175–177
- Coolbrook–White equation, 24
- Cooling requirements, gas pipelines, 70
- Cooper Bessemer GMW family of engines, 322
- Cost
 - of compressor operation, 73–74
 - J-curves graph and, 68

- of ownership, compressor station, 74
- pipeline design and, 21–22
- Counter-swirl position, guide vanes, 273
- Coupling(s), 323–330, 558–560, 559f, 560f
 - connection, 324
 - diaphragm, 325, 326f
 - disc, 325, 326f
 - flexible, 325, 326f
 - fluid, 314, 315f
 - functions, 323
 - gear, 325, 558
 - general purpose, 323
 - lubricated gear, 325
 - much reduced deflection for torsionally soft, 560f
 - selection, 323, 324–325
 - soft
 - elastomeric, 327
 - steel-spring, 327
 - special purpose, 324
 - standards, 329–330
 - too stiff for motor/compressor set, 558
 - torsional analysis, 558
 - torsional vibration problem in reciprocating compressor installation, case study, 327, 328, 329f
- Coverage chart, centrifugal, 138
- Crank end (CE) cycle, 198
- Critical speeds, 272
- Cross-hole seismic testing, 514
- Crude oil, operational hazards of, 9
- Curves
 - performance, centrifugal compressors, 254–257
 - system characteristic, 267–270
- Cycling, pressure relief valves (PRV), 525
- Cyclone scrubber, 91f
- Cylinders, compressor, 183, 185–187
- D**
- Damage risk criteria (DRC), 592, 595
- Dampeners, 413
 - in liquid systems, 500
- Damping
 - acoustic transfer matrix for pipe element and, 468–471, 471f
- Darcy equation, 24–25
- Day–night equivalent level (DNL), 599
- DBB, *see* Double block and bleed capacity (DBB)
- Degradation monitoring, centrifugal compressor performance, 264–266, 267f
- Density, pipeline design and, 21, 22
- Dependability, pipeline system
 - characteristics, interrelationship between, 12
 - concept of, 11–12
 - framework over the life cycle for pipelines, 14f
 - functional and non-functional requirements, 12, 13f
 - for pumping and compression, 14–15
 - RAM models, 15–16, 16f, 17f
 - value of, 12–14
- Design and operation, 179–234
 - centrifugal compressors, 203–229
 - bearings, 209–211
 - controls and monitoring, 220–223
 - diffuser, 228
 - fluid properties, effect of, 228
 - general design, 203–205, 206f
 - impellers, 224–227
 - internals and sealing, 205–209
 - lubrication system, 211, 213
 - performance characteristics, 223–224
 - physical operation, 223–228
 - sealing system, 213–220
 - standards, 228–229
- IGCC, 231–234
 - bearings, seals and gears, 233–234
 - design, 231–233
 - overview, 179, 180f
 - reciprocating compressors, 179–203
 - bearings and lubrication systems, 193, 194–196
 - capacity (flow) control, 187, 188f, 189f
 - considerations, 203
 - control system, 196
 - frame and cylinders, 183–187
 - gas cooling, 198
 - general design, 179–181
 - monitoring system, 197
 - optimization, 200–201
 - packings, 193, 194f
 - physical operation, 198–200
 - rod loading, 201–202
 - running gear, 181, 182–183
 - start-up and shutdown, 197
 - valves, 187, 189–192, 193f
 - screw compressors, 229–231
 - design, 229, 230f
 - operation, 230–231
- Design(s)
 - centrifugal pump, 106–109, 110f, 111f
 - considerations, electric motors, 310, 311f
 - gas turbines, 283–286
 - internal combustion engines, 320–322
 - liquid pipeline systems, 19–28
- Design standards
 - centrifugal compressors, 228–229
 - gas turbines, 305
 - reciprocating compressors, 203
- Diameter, cost of a pipeline and, 1
- Diaphragm coupling, 325, 326f
- Diesel engines, 320
- Differential pressure control, dry gas seals, 217
- Diffuser, centrifugal compressors, 228
- Diffuser pump, 106
- Digital no-flow timer (DNFT) switch, 196
- Dilatant fluids, 21, 22f
- Dilution, 135
- Dimensional analysis, performance of centrifugal compressors, 260
- Dimensionless variables, centrifugal pump, 347
- Direct-acting (steam) pump type, 99
- Disc couplings, 325, 326f

- Discharge piping for reciprocating pumps, 129
 - Discharge temperature
 - centrifugal compressors, 256
 - compressors, 271
 - reciprocating compressors, 251
 - Discharge valve, 187, 189f, 190, 191, 192f
 - DNV erosion model, 48, 49f, 49t
 - DNV Recommended Practice
 - RP-O501, erosion rate and, 50–52
 - Double block and bleed capacity (DBB), 44
 - Double-suction pump, 106
 - Dresser-Rand Datum C hermetic “compact” compressor, 316–317
 - Drip proof, 310
 - Driver and driven equipment unit control, 92
 - Driver operating characteristics, 86–87
 - Drivers, compressor, 279–335
 - couplings, 323–330
 - elastomeric soft, 327
 - flexible, 325, 326f
 - functions, 323
 - gear, 325
 - selection, 323, 324–325
 - standards, 329–330
 - steel-spring soft, 327
 - torsional vibration problem in reciprocating compressor installation, case study, 327, 328, 329f
 - drivers and driven equipment, comparison, 330–335
 - centrifugal compressors, advantages and disadvantages of, 334
 - electric motors, advantages and disadvantages of, 332–333
 - gas turbines, advantages and disadvantages of, 330–332
 - general factors, 330
 - internal combustion engines, advantages and disadvantages of, 333–334
 - reciprocating compressors, advantages and disadvantages of, 335
 - electric motors, 307–319
 - design considerations, 310, 311f
 - economics, 317–319
 - general, 307
 - hermetic compressors, 315–317
 - types, 307–310
 - variable speed drives, 310, 311–315
 - gas turbines, 280–307
 - advantages, 284
 - aeroderivative gas turbine lube oil system, 291–292
 - air compressor surge, 286–287
 - air intake system, 286
 - anti-icing systems, 288–289
 - bearings, 289–291
 - design, 283–286
 - design standard, 305
 - exhaust system, 289
 - fuel system, 292, 293–299
 - industrial gas turbine lube oil system, 292, 293f
 - performance, 299, 300–305
 - types, 280–283
 - variable compressor geometry, 287–288
 - waste heat recovery, 306–307
 - internal combustion engines, 320–323
 - design, 320–322
 - general, 320
 - integral engine/compressors, 322–323
 - overview, 279–280
 - Drivers and driven equipment, comparison, 330–335
 - centrifugal compressors, advantages and disadvantages of, 334
 - electric motors, advantages and disadvantages of, 332–333
 - gas turbines, advantages and disadvantages of, 330–332
 - general factors, 330
 - internal combustion engines, advantages and disadvantages of, 333–334
 - reciprocating compressors, advantages and disadvantages of, 335
 - reciprocating compressors, advantages and disadvantages of, 335
 - Drooping characteristic curve, 146, 147f
 - Dry-gas seals, 216–219
 - leakage rates, 625
 - recovering vent gas loss from, 624–634
 - Dry low emissions (DLE), 296
 - Dry low NOx (DLN), 296–297
 - Dual fuel system, 299, 301f
 - Duplex reciprocating pumps, 122f
 - Dynamic actuator/positioner, 380
 - Dynamic behavior, pumping systems, 339–369
 - boundary conditions, 342–346
 - cavitation and column separation, 358–361
 - centrifugal pumps, *see* Centrifugal pumps
 - examples and case studies, 361–369
 - four quadrant charts, 354–357, 355f, 357f
 - governing equation for constant area pipes, 339–341, 340t–341t
 - overview, 339
 - solution techniques, 341–342, 342f
 - water hammer, 357–358
 - Dynamic Characteristic Curve (DCC), 414
 - Dynamic equation, centrifugal pumps, 348, 351–352
 - Dynamic forces, by reciprocating compressor, 183–184
 - Dynamic performance characteristics, centrifugal compressors, 254–260
 - basic performance curves, 254–257
 - fan laws, 257–258
 - limits, 258–260
 - Dynamic pulsation dampener, 125
- ## E
- Economics, driver, 317–319
 - Effects (bowtie diagram), 8f, 9
 - Efficiencies

- compressor performance, 244–245, 250, 256
- thermal, 331, 332, 334
- VFD, 314
- Elastomeric soft couplings, 327
- Elbow
 - DNV RP O501 erosion model for, 50–52
 - flow distortion and, 41f
- Electric compressor drivers *versus* gas, 69–70
- Electric motors, 307–319
 - advantages and disadvantages of, 332–333
 - design considerations, 310, 311f
 - economics, 317–319
 - general, 307
 - hermetic compressors, 315–317
 - types, 307–310
 - variable speed drives, 310, 311–315
 - fluid coupling, 314, 315f
 - VFD, 310, 311–314
- Elevation profiles, gas pipeline, 72f
- EMD station, 75
- Emergency shutdown (ESD), 94, 95f, 386–410
 - effects of compressor performance characteristics, 389–393, 389f, 390f, 392f–393f
 - inertia number, 405–408, 407f–408f, 407t
 - integrally-gearred compression systems, 402–405, 403f, 403t, 404f–405f
 - recycle system around compressors arranged in series, 409–410, 409f, 410f–411f
 - rotor inertia on, 393, 394f, 395f
- Emerging gas seal technology, 220
- Emission calculations (case study), 84–85
- Emissions
 - exhaust, 331, 332, 334
 - fuel system, 294–297
 - noise, 331, 332, 334
- Enclosures, characteristics, 310
- End cover (radial split), 206
- Energy Institute, 571
- Engine-driven screw compressor, 229, 230f
- Engines
 - capacity curve, 252
 - controlled, 613
 - jacket water cooling, 70
 - uncontrolled, 613
- Engines, internal combustion, 320–323
 - advantages and disadvantages of, 333–334
 - design, 320–322
 - general, 320
 - integral engine/compressors, 322–323
- Enthalpy diagram, for Brayton cycle, 302, 303f
- Entropy diagram, for Brayton cycle, 302, 303f
- “Entropy spots,” 607
- Environmental considerations, compressor station, 80
- Environmental issues, 591–593
 - designing for environmental requirements, 593
- Environmental issues, compressor and pump stations
 - capturing vent gas from dry gas seals, innovations in, 624–634; *see also* Supersonic ejectors
 - noise measurement, 594–607; *see also* Noise, compressor and pump stations
 - noise criteria limits, 595–600, 597t, 598f, 599f, 600t
 - noise level parameters, 594–595
 - predictions of noise levels from compressor stations, 601–607
- NOx emissions from gas turbines, 612–623
 - overview, 591–593
- Environmental Protection Agency, 97
- Equations of state (EOS), gas properties, 241–243
- Erosion, impeller, 261
- Erosion model
 - DNV model, 48, 49f, 49t
 - DNV Recommended Practice RP-O501, 50–52
 - Zhang et al., 48–50
- ESD, *see* Emergency shutdown (ESD)
- Ethylene pump, 365, 367–369, 367f–368f
- Euler’s theory, 142
- Excitation mechanisms
 - mechanical analysis of piping systems, 563–564, 564f
- Exhaust emissions, 331, 332, 334
- Exhaust system, gas turbines, 289
- Expansion chambers, 490–492, 491f, 492f, 524f, 525
- Expenditures, operating, 1
- Explosion proof, 310
- Externally pressurized bearings, 560
- Externally Pressurized Porous (EPP) Gas Bearing Technology, 220
- F**
- Facility Integrity Management Program (FIMP), 7
- Failure modes and effects analysis, 8
- Fan laws, centrifugal compressors, 257–258
- Fast start-up valve positions, 37–38
- Fault tree analysis, 8
- Field compression, 6
- Field tests/testing
 - gas turbine performance, 305
 - relief valve dynamics, 441–444, 442f, 443f–444f
- Filters, compressor station, 90–91
- FIMP, *see* Facility Integrity Management Program (FIMP)
- “Fin-fan” coolers, 70
- 1st stage supersonic ejector, 625–632, 625f, 626f, 627f, 630f, 631f, 632
- Fitting limitations, 34
- Flange–flange coupling connection, 324
- Flange–hub coupling connection, 324
- Flashing, 499

- Flat characteristic curve, 146, 147f
- Flexible couplings, 325, 326f
- Floating ring oil seals, 214
- Flow
 - for compressors, 245
 - reciprocating compressors, 247–249
- Flow control
 - dry gas seals, 217
 - reciprocating compressors, 187, 188f, 189f
- Flow distortion, double-suction pump, 41f
- Flow-generated pulsation from throttling elements, 480–482, 481f–482f
- Flow-generated single-tone pulsation from closed end side branch, 482–485, 483f–484f
- Flow transients
 - across other elements, 343–344, 343f–344f
 - of an accumulator, 344–346, 345f
- Fluid coupling, 314, 315f
- Fluid hammer, 357–358; *see also* Water hammer
- Fluid properties, effect of, 228
- Fluttering, pressure relief valves (PRV), 525–526
- Forced response analysis, 572–576
- Forced vibration, 551
- Force-feed lubrication system, 196
- Fouling, 261, 265
- Foundations, compressor, 183–184
- Four quadrant charts, pump, 354–357, 355f, 357f
- Frame, reciprocating compressors, 183–187
 - integral compressor, 185
 - separable compressor, 184–185
- Free turbine, defined, 283
- Frequency drive, VFD, 310, 311–314
- Friction head
 - liquid pipeline systems, 24
- Fuel system, 292, 293–299
 - dual, 299, 301f
 - emissions, 294–297
 - liquid, 299, 300f
 - LNG, 297
 - natural gas, 297–299
 - types, 292, 293–294
- Fuel usage (case study), 81–84
- Full-scale factory testing, centrifugal compressors, 261–262
- Functional requirements, dependability, 12, 13f
- Functions, coupling, 323
- G**
- Gas coolers, 91, 92f
- Gas cooling, reciprocating compressors, 198
- Gas Machinery Research Council, 571
- Gas pipeline systems, 4–6
 - booster compression, 6
 - buildings and weather protection, 95
 - codes and standards, 96–97
 - components of, 5
 - compression facilities and, 5–6
 - compressor station configuration
 - compression equipment, types, 75–76
 - compressor requirements, 85–86
 - driver requirements, 86–87
 - environmental considerations, 80
 - NPV analysis (case study), 77–78
 - number of units, 76–77
 - operating considerations, 74–75
 - parallel arrangement, 76
 - series arrangement, 76
 - series-parallel arrangement, 76
 - standby units, 78–80, 81f
 - usage scenario for pipeline stations (case study), 81–85
- compressor station spacing, 69
- cooling requirements, 70
- cost of compressor operation, 73–74
- field compression, 6
- gas coolers, 91, 92f
- gas recovery compression, 5
- gas storage compression, 6
- gas *versus* electric compressor drivers, 69–70
- hydraulics, 65, 66f
- hydraulic simulation, 70–73
- hydraulics profile, 71f
- interchange compression, 6
- lateral compression, 6
- looping *versus* compression, 66f, 69–70
- network, 70, 71f
- optimization process, 65–69
 - alternatives, 68–69
 - considerations, 65–66, 69
- pressure regulation methods, 65
- safety systems and environmental controls, 96
- scrubbers and filters, 90–91
- station and unit auxiliary systems, 92
- station and unit control systems, 92–95
- station layout, 87, 88f
- station piping layout, 87, 89–90
- transmission, 6
- Gas properties, for compression performance, 237, 238–243
 - compressibility and molecular weight, 238–240
 - EOS, 241–243
 - ideal gas laws, 237, 238
 - ratio of specific heats, 240–241
- Gas recovery compression, 5
- Gas storage compression, 6
- Gas turbines, 280–307, 554
 - advantages and disadvantages of, 284, 330–332
 - aeroderivative, 280, 281–282, 291–292
 - air compressor surge, 286–287
 - air intake system, 286
 - anti-icing systems, 288–289
 - basic design, 283–286
 - bearings, 289–291
 - design standard, 305
 - exhaust system, 289
 - fuel system, 292, 293–299
 - dual, 299, 301f
 - emissions, 294–297
 - liquid, 299, 300f
 - LNG, 297
 - natural gas, 297–299
 - types, 292, 293–294

- industrial gas turbine lube oil system, 292, 293f
- NOx emissions from, 612–623
- performance, 299, 300–305
 - calculations, 302, 303f, 304–305
 - characteristics, 299, 300, 301, 302f, 303f
 - field testing, 305
- rotordynamics and, 554
- types, 280–283
- variable compressor geometry, 287–288
- waste heat recovery, 306–307
- GasTurb™, 302
- Gearboxes, 558–560, 559f, 560f
- Gear(s)
 - couplings, 325, 558
 - IGCC, 233–234
- General criteria, API 618 Standard, 505–507
- General Electric, 280, 281, 282f
- Geometry, variable compressor, 287–288
- Globe valve
 - acoustic transfer matrix for throttle element, 476–478
- GMRC design guidelines
 - for high-speed reciprocating compressor packages for natural gas transmission & storage applications, 513–516
- Governing equation for
 - constant area pipes, 339–341, 340t–341t
- Groupe Européen de Recherches Gazières (GERG) EOS, 242–243
- Guide vanes
 - centrifugal compressors, 254–255
 - counter-swirl position, 273
 - IGVs, 233, 287, 288
 - pre-swirl position, 273
- H**
- Harmonic filters, 311
- Hazard (bowtie diagram), 8
- Hazard and operability (HAZOP) studies, 8
- Hazardous chemicals, safety regulations, 7
- Hazen–Williams equation, 24
- HAZOP, *see* Hazard and operability (HAZOP) studies
- Head
 - centrifugal performance, 255
 - defined, 244
- Head coefficient, centrifugal pumps, 348, 349f, 350t–351t
- Head curve, liquid pipeline systems, 24–26
- Head end (HE) cycle, 198, 200
- Header piping design, 42–44
- Heat recovery oil heater (HROH), 306, 307
- Helical lobe rotary compressor, 229–231
 - design, 229, 230f
 - operation, 230–231
- Helmholtz free energy, 242–243
- Helmholtz resonators, 463, 490–492, 492f, 500, 502
- Hermetic compressors, 10, 315–317
- Hetzel equation, 24
- High pressure gas cooling, 70
- High-pressure seal oil, 214
- High speed oil free intelligent motorcompressor (HOFIM), 315–316
- History, pump, 100–103
- Homologous relations, centrifugal pumps, 347
- Horizontal pumps, 106, 115–117
- Hub–hub coupling connection, 324
- Hydraulic accumulator, 344–346
- Hydraulics
 - gas pipeline, 65, 66f
 - liquid pipeline, 19, 20f
- Hydraulic simulation, 70–73
 - for assessment, 72–73
- Hydraulics profile, gas pipeline, 71f
- Hydrodynamic bearing, 211, 212f
- I**
- Ideal gas laws, 237, 238
- IEC, *see* International Electrotechnical Commission (IEC)
- IGCC (integrally geared centrifugal compressor), 231–234
 - bearings, seals and gears, 233–234
 - design, 231–233
- IGVs (inlet guide vanes), 233, 287, 288
- Impeller, centrifugal pumps
 - change, 150, 151f
 - curve characteristics, 145–147
 - design, 107–109
 - design theory, 141–143
 - destroyed by cavitation, 154f
 - selection, 138–140
 - specific speed of, 144–145
 - suction specific speed, 165
 - under-filing and over-filing, 150, 152f
 - volute chipping, 150, 153f
 - volute inserts, 150, 153f
- Impeller(s)
 - centrifugal compressors, 206, 224–227
 - erosion, 261
- Implosion, 154
- Incipient surge, defined, 221
- Induction motors, 307–308, 310
- Industrial compression system,
 - dynamic instabilities in, 394, 395–402, 396f, 396t, 397t, 398f, 399f, 400f–401f, 401t, 402f
- Industrial gas turbines, 280, 292, 293f
- Inertia
 - centrifugal pumps, 352–353, 352f, 353f
 - rotor, on ESD, 393, 394f, 395f
- Inertia number, 405–408, 407f–408f, 407t
- Injected seal oil, 214, 215
- Inlet guide vanes (IGVs), 233, 287, 288
- Instrumentation, for centrifugal compressor, 262
- Intake system, air, 286
- Integral engine/compressors, 322–323
- Integrally geared centrifugal compressor (IGCC), 231–234
 - bearings, seals and gears, 233–234
 - design, 231–233

- Integrally-gearred compression systems, 402–405, 403f, 403t, 404f–405f
- Integral reciprocating compressor frame, 185
- running gear, 181, 182f
- Integrated compressor line (ICL), 203, 205f
- Intensifier, defined, 218
- Interchange compression, 6
- Intercooler, defined, 198
- Internal combustion engines, 320–323
- advantages and disadvantages of, 333–334
- design, 320–322
- general, 320
- integral engine/compressors, 322–323
- Internal return rate (IRR), 312, 314
- Internals, centrifugal compressors, 205–209
- International Electrotechnical Commission (IEC), 11, 97
- International Organization for Standardization (ISO), 11, 97
- Inverse reduced temperature, defined, 243
- Isentropic compression, 243, 244, 255, 256, 264
- Isentropic efficiency, 244, 250
- ISO, *see* International Organization for Standardization (ISO)
- Isothermal compression, 244
- J**
- J-curves graph, 68
- Joukowski equation, 55
- Joule-Thompson effect, 294
- K**
- Kinetic pumps
- family of, 101f
- types, 99
- L**
- Labyrinth seals, 206, 214, 217
- Lateral compression, 6
- Lateral rotordynamics, 537–540, 538f–540f
- LCC, *see* Long-term life cycle costing (LCC)
- Length, cost of a pipeline and, 1
- Life Cycle Cost analysis, 314
- Limits in performance, centrifugal compressors, 258–260
- Liquid fuel system, 299, 300f
- Liquid pipeline systems, 2–4
- configuration, 28–37
- contamination in, 44–52
- definitions, 3, 4f
- design, 19–28
- considerations for system curves, 27–28
- curve development example, 26–27
- head curve, 24–26
- hydraulics, 19, 20f
- pipe size and selection, 19–24
- piping system, 34–44
- pressure surges in, 55–61
- pumps for, 99–100
- pump station piping design, *see* Piping design, pump station
- terminal design, 52–61
- unique aspect of, 4
- Liquids
- effects of vapor voids in, 500, 500f
- operational hazards of, 9
- vapor voids in, 500, 501t
- Liquid vs. gas applications, 499–502
- cavitation, 499, 500f
- effects of vapor voids in liquids, 500, 500f
- flashing, 499
- pulsation filters (dampeners) in liquid systems, 500–502
- speed of sound in liquids piping, 499–500, 501f
- Liquified natural gas (LNG), 297
- Loading, rod, 201–202, 271
- London Bridge Waterworks, 103
- Long-term life cycle costing (LCC), 15
- Looping *versus* compression, gas pipelines, 66f, 69–70
- LOPC, *see* Loss of primary containment (LOPC)
- Loss of primary containment (LOPC), 6
- Lower heating value (LHV), 294
- Low-pass filter, 381
- Lube oil cooling, 70
- Lube oil-water cooling, 70
- Lubricated/flooded screw compressor, 229, 230f
- Lubricated gear couplings, 325
- Lubrication regimes, centrifugal pumps, 111, 112f
- Lubrication systems
- centrifugal compressors, 211, 213
- coolers, lube oil, 213
- for gas turbines, 289–292
- aeroderivative, 291–292
- industrial, 292, 293f
- reciprocating compressors, 193, 194–196
- M**
- Mach number, 260
- Magnetic bearings, 211, 212f, 560–561
- MAOP, *see* Maximum allowable operating pressure for the pipeline (MAOP)
- Maps, performance
- centrifugal compressor, 255–257
- reciprocating compressor, 251–254
- Mars, 281
- Matching, component, 302
- Match point, defined, 301
- Materials, for compressor cylinders, 185, 186
- Maximum allowable operating pressure for the pipeline (MAOP), 93
- Maximum allowable shaking forces, API 618 Standard, 509–510
- Maximum Operating Pressure (MOP) limits, 55, 57
- Mean flow
- on acoustic TM for pipe element, 467–468
- Mean time between repairs (MTBR), 314
- Measurement units and conversion factors, 175–177
- Mechanical analysis, 533–588

- API 618 Standard, 502–503, 503f, 504
- centrifugal compressors, 584–588, 586f, 587f
- overview, 533
- of piping systems, 563–588
 - adding damping to mechanically resonant systems, 577–583, 577f, 578f, 579, 580f, 582f
- centrifugal compressors, 584–588, 586f, 587f
- excitation mechanisms, 563–564, 564f
- forced response analysis, 572–576
- small-bore attachments, 569–572
- thermal analysis, 583–584
- unbalanced forces, 566–569, 568f
- vibration and stress, 564–566, 565f, 566f, 567f
- of rotating equipment, 536–563; *see also* Rotordynamics
 - balancing, 561–563, 562f–563f
 - general, 536–537
 - lateral rotordynamics, 537–540, 538f–540f
 - specific machinery considerations for rotordynamics, 551–561
 - stability, 540–541, 541f
 - torsional rotordynamics, 541–551, 542f–544f, 546f, 548f
 - vibration, basic aspects of, 533–536, 534f, 535f
- Mechanical dry seals, 216, 217
- Mechanical efficiency, 250
- Mechanical hazards, 10–11
- Mechanical natural
 - frequency (MNF), 535–536, 535f–536f
- Mechanical resonance
 - mechanical natural frequency and, 535–536, 535f–536f
- Mechanical seals, centrifugal pumps, 109–114, 115f
 - application chart for, 112–113, 115f
 - basic flush plans for, 113
 - equilibrium between forces for, 111, 113f
 - lubrication regimes, 111, 112f
 - materials used, 111, 114f
 - pressure and temperature effect on, 111, 113f
 - pressures apply to, 110
 - pusher type of, 111, 112f
 - tuning, 111
- Metallic element couplings, 325, 326f
- Methane, Wobbe index for, 294
- Metric system, 175
- Minimum flow limits, centrifugal pumps, 163
- Mitigation barriers (bowtie diagram), 8
- Mixed lubrication, 111
- Mixture composition, on centrifugal compressor performance, 262–264
- Molecular weight (MW) of natural gas mixture, 238–240
- Monitoring system
 - centrifugal compressors, 220–223
 - degradation, centrifugal compressor performance, 264–266, 267f
 - reciprocating compressors, 197
- Moody's diagram, 25f
- MOP, *see* Maximum Operating Pressure (MOP) limits
- Motor pipeline compressor (MOPICO), 315–317
- Motors
 - rotordynamics and, 554–558, 556f, 557f
 - VFD-controlled, 555–558
- Multiple source pulsation, 521–523, 522f
- Multi-shaft compressor, 231–234
 - bearings, seals and gears, 233–234
 - design, 231–233
- Multi-stage centrifugal compressors, 551
- Multi-stage pump, 106
- N**
- National Energy Board Regulations SOR/99-294, 7
- Natural gas, 293–294
 - fuel system, 297–299
 - LNG, 297
- Net positive inlet pressure (NPIP) for reciprocating pump, 172
- Net Positive Inlet Pressure Available (NPIPA)
 - for reciprocating pump, 173
- Net Positive Inlet Pressure Required (NPIPR)
 - for reciprocating pump, 173
 - for rotary pump, 170
- Net Positive Suction Head (NPSH), 157–158
 - breakdown curves, 160f
- Net Positive Suction Head Available (NPSHA), 158, 159f
- Net Positive Suction Head Required (NPSHR), 158–159, 160f
- Net present values (NPVs), 74, 210, 312, 314, 318f, 319f
 - analysis (case study), 77–78
- Network, gas pipeline, 70, 71f
- Neural network based PEM models, 615–620, 616f, 617f, 618f, 619f, 620f
- Newtonian fluids, 21
- Newton-Raphson method, 379
- Nitrogen, surge relief valves, 59, 60f
- Nitrogen oxides, formation, 294–295
- Noise, compressor and pump stations
 - noise criteria limits, 595–600, 597t, 598f, 599f, 600t
 - noise level
 - parameters, 594–595
 - predictions, compressor stations, 601–607
 - survey, 608–612
 - noise mapping methodology, 608–610, 609f, 610f
- Noise criteria (NC)
 - index, 595, 598
 - limits, 595–600, 597t, 598f, 599f, 600f, 600t
- Noise emissions, 331, 332, 334
- Noise level parameters, 594–595
- Noise measurement, 594–607
 - noise criteria limits, 595–600, 597t, 598f, 599f, 600t

- noise level parameters, 594–595
- predictions of noise levels from compressor stations, 601–607
- Noise suppression during blow-down, 496–499, 497f–499f
- Noise surveys
 - example application on a compressor station, 610–612
 - noise mapping methodology, 608–610, 609f, 610f
- Nomenclature for compression performance, 237, 238t
- Non-functional requirements, dependability, 12, 13f
- Non-isothermal blowdown, 453–457
- Non-lubricated/dry screw compressor, 229
- Non-Newtonian fluids, 21
- Non-overloading characteristic curve, 147
- NOVA Gas Transmission system, 209
- NOx emissions from gas turbines, 612–623
 - AP-42 emission factors, 613
 - CEM measurements, 613–615, 614f, 615f
 - neural network based PEM models, 615–620, 616f, 617f, 618f, 619f, 620f
 - PEM implementation, 620–623, 621f–623f
- Nozzle loading, centrifugal pump, 114–118
 - horizontal pumps, 115–117
 - vertical inline pumps, 116t, 117–118
- NPIP, *see* Net positive inlet pressure (NPIP)
- NPIPA, *see* Net Positive Inlet Pressure Available (NPIPA)
- NPIPR, *see* Net Positive Inlet Pressure Required (NPIPR)
- NPSH, *see* Net Positive Suction Head (NPSH)
- NPSHA, *see* Net Positive Suction Head Available (NPSHA)
- NPSHR, *see* Net Positive Suction Head Required (NPSHR)
- NPV, *see* Net present value (NPV)
- Number of units
 - compressor station configuration, 76–77
 - liquid pipeline systems, 30–33
- O**
- Occupational Safety and Health Administration (OSHA), 97
- Onsite testing, 228
- Open, acoustic boundary conditions, 488–490
- Operating cost
 - of compressor, 73–74
 - pipelines, 1
- Operating limits, API 618 Standard, 507
- Operational hazards, 9–11
- Operations, compressors
 - centrifugal, 223–228
 - diffuser, 228
 - fluid properties, effect of, 228
 - impellers, 224–227
 - performance characteristics, 223–224
 - considerations, 274–276
 - parallel operation, 276
 - series operation, 275–276
 - shutdown, 276
 - startup, 274–275
 - limitations, 271–272
 - reciprocating, 198–200
 - screw, 230–231
- Optimization, reciprocating compressors, 200–201
- Optimization process, gas pipeline systems, 65–69
 - alternatives, 68–69
 - considerations, 65–66, 69
- Organic Rankine bottoming cycle, 306
- Orifice plate
 - acoustic transfer matrix for throttle element, 475, 475f
- OSHA, *see* Occupational Safety and Health Administration (OSHA)
- OSHA 1910.119 Process safety management, 7
- Over-compression discharge pressure, 231
- Overhung centrifugal compressor, 203, 204f
- Overload, defined, 260
- Overloading characteristic curve, 147
- P**
- Packings, reciprocating compressors, 193, 194f
- Parallel configuration
 - of compressor for gas compression, 76
 - pumping piping, 36, 37f
 - of pumps in liquid pipeline system, 29–30
 - standby unit, 79, 80f
- Parallel operation, compressors, 276
- Particle sizes
 - pump selection and, 23
- PCV, *see* Pressure control valve (PCV)
- PEM implementation, 620–623, 621f–623f
- Peng-Robinson EOS, 241
- Pentane vapor, 307
- Percentage of time, 32
- Perfect gas law, 237, 238
- Perforated tube mufflers, 492, 494f
- Performance, pumps, *see* Pumps, performance of
- Performance correction chart, for viscous liquids, 161, 162f
- Performance modifications, 150, 151f–153f
- Performance(s), compressors, 237–276
 - basic aspects, 237–247
 - behavior, 243–244
 - efficiency, 244–245
 - flow, 245
 - gas properties, 237, 238–243
 - general, 237
 - head, 244
 - nomenclature, 237, 238t
 - power, 245–247
 - centrifugal compressors, 254–267
 - characteristics, 223–224
 - curves, 254–257
 - degradation monitoring, 264–266, 267f

- dynamic performance characteristics, 254–260
- general, 254
- limits, 258–260
- mixture composition on, 262–264
- selection and sizing, 260–261
- testing, 261–262
- gas turbines, 299, 300–305
 - calculations, 302, 303f, 304–305
 - characteristics, 299, 300, 301, 302f, 303f
 - field testing, 305
- overview, 237
- reciprocating compressors, 247–254
 - discharge temperature, 251
 - flow, 247–249
 - general, 247
 - maps, 251–254
 - piston speed, 254
 - power, 249–251
- system characteristics, 267–276
 - adjustments, 272–274
 - comparison, 270, 271f
 - curves, 267–270
 - general, 267
 - operating considerations, 274–276
 - operating limitations, 271–272
- Personnel, operational hazards of, 9
- Physical operation
 - centrifugal compressors, 223–228
 - diffuser, 228
 - fluid properties, effect of, 228
 - impellers, 224–227
 - performance characteristics, 223–224
 - reciprocating compressors, 198–200
- PID controller, 380
- Pilot-operated PRVs, 526
- Pilot-operated relief valves, 429–434, 430f, 431f
- Pipe element
 - acoustic transfer matrix for, 464–471, 466f, 471f
- Pipeline-pump operational control, 148–150
- Pipeline systems
 - advantages, 1
 - gas, 4–6, 5f; *see also* Gas pipeline systems
 - limitations, 1
 - liquid, 2–4, 3f, 4f; *see also* Liquid pipeline systems
 - overview, 1, 2f
 - process safety, 6–11
 - relative transportation cost for petroleum products, 2f
 - safety, 6–17
 - trends in primary energy consumption, 2f
- Pipe model, station and gas pipeline blowdown, 449–450
 - analytical, 449–450
- Pipe size
 - cost and, 21–22
 - liquid pipelines, 19–24
 - piping design and, 39, 41
- Piping design, pump station, 34–44
 - configuration, 34–38
 - fast start-up valve positions, 37–38
 - general station design, 34–38
 - header piping design, 42–44
 - hydraulic considerations, 41–42
 - improvements in, 38–39
 - layout, 39, 40f
 - objectives, 38–39
 - parallel arrangement, 36, 37f
 - physical requirements for, 34
 - pipe sizing, 39, 41
 - series arrangement, 36, 40f
 - series/parallel configuration, 36, 37f
 - valve selection, 44
- Piping system
 - analysis, 504
 - station design for reciprocating pumps, 127, 128f
 - discharge piping, 129
 - suction piping, 127–128
 - suction vessel, 129
- Piping velocity limitations, 34
- Piston, 100
 - pumps, 122–123
 - speed, reciprocating compressors, 254
 - type check valves, dynamics of, 422–424, 422f
- Piston displacement (PD), 247
- Plate valves, 187, 189f, 190f
- Platinum™, 197
- Plunger pumps, 121–122, 123f
- Pneumatic clearance valve, 187, 188f
- Poly-etheretherketone (PEEK), 190
- Polytropic compression, 243–244, 255, 256
- Poppet valves, 187, 189f, 190, 191f
- Positive displacement pumps, 119–129; *see also* Pump(s)
 - overview, 99, 100f
 - performance of
 - net positive pressures, 172–173
 - power and efficiency, 169–170
 - reciprocating pump acceleration head, 171–172
 - reciprocating pump flow characteristics, 171, 172f
 - reciprocating pump selection, 173–175
 - rotary pump performance chart, 167, 168f, 169f
 - rotary pump slips and clearance, 170
 - system head curves and rotary pump curve, 170–171
- pulsation dampeners, 124–126
- reciprocating pumps, 121–124; *see also* Reciprocating pumps
 - rotary pumps, 102f, 119–121, 122f; *see also* Rotary pumps
- Power
 - compressors, 245–247
 - plunger pumps, 124
 - range, 331, 332, 333
 - reciprocating compressors, 249–251
- “Power” backup, compressor station, 79
- Power Test Code (PTC) 10 test, 228, 261
- Power turbines, 554
 - rotordynamics and, 554

- Power usage distribution (case study), 81–83
- Predictive Emission Monitoring (PEM) system
 - implementation, 620–623
- Preheat correction, 251
- Pre-rotation position, for control purposes, 273
- Pressure control valve (PCV), 34, 43–44, 213
 - sudden closure of, 57–58
- Pressure head
 - liquid pipeline systems, 24
- Pressure limitations, pipeline
 - design and, 21, 34
 - MOP and, 55
- Pressure relief, pipeline design and, 34, 58–61
- Pressure relief valves (PRV), 213
 - American petroleum Institute (API 520) standards, 526–527
 - chattering, 526
 - cycling, 525
 - example of PRV stability calculations, 529t
 - fluttering, 525–526
 - instability criteria of, 525–530
 - pilot-operated, 526
 - remote sensing pop-action pilot, 526
 - spring loaded, 526
- Pressure surges in pipelines
 - automated surge relief installation, 60–61
 - causes of, 55
 - nitrogen loaded surge relief valves, 59, 60f
 - pump shutdown and, 56
 - pump startup and, 55–56
 - relief measures, 58–61
 - valve closure and, 56
- Pressure–volume characteristics, of compressors, 270, 271f
- Pressurized oil bearings, 560–561
- Pre-swirl position, guide vanes, 273
- Prevention barriers (bowtie diagram), 8
- Princess Compressor Station (Alberta, Canada),
 - operational hazards, 10
- Probability theory, 30–32
- Process safety, 6–11
 - guidance in API RP1173, 7
 - hazardous chemicals, 7
 - operational hazards, 9–11
- Process Safety Management (PSM), 6–7
 - risk assessment, 7–9
- Process Safety Management (PSM), 6–7
- Pseudo-plastic fluids, 21, 22f
- PSM, *see* Process Safety Management (PSM)
- Pullout torque, defined, 309
- Pulsation analysis, API 618 Standard, 502–504, 503f
- “Pulsation and Vibration Control in Positive Displacement Machinery Systems for Petroleum, Petrochemical, and Natural Gas Industry Services,” 516
- Pulsation attenuation devices, 203
- Pulsation dampeners, 124–126
 - dynamic, 125
 - suction, 125–126
- Pulsation filters (dampeners) in liquid systems, 500–502
- Pulsation generated by a reciprocating compressor, 523–525, 523f–525f
- Pulsation generation, 480–487, 481f–482f, 483f–484f, 486f–487f
 - flow-generated pulsation from throttling elements, 480–482, 481f–482f
 - flow-generated single-tone pulsation from closed end side branch, 482–485, 483f–484f
 - by reciprocating compressors and pumps, 485–487, 486f–487f
- Pulsation guidelines, API 618 Standard, 505
- Pulsation suppression, techniques for, 490–499
 - noise suppression during blow-down, 496–499, 497f–499f
 - reactive silencers, 490–493, 491f–493f
 - spoilers for, 493–496, 494f–496f
- Pulsation transmission, through piping elements, 463–480
 - acoustic transfer matrix
 - for centrifugal compressor, 479–480, 479f
 - for pipe element, 464–471, 466f, 471f
 - for throttle element, 472–478, 473f, 474t, 475f, 476f, 477f
 - for a volume element, 478–479, 478f
 - overview, 463–464
- Pulse width modulation, 311
- Pump configurations
 - centrifugal pumps, 107
 - liquid pipeline systems
 - general, 28–29
 - number of units, 30–33
 - pumps in parallel, 29–30
 - pumps in series, 29
 - pump station configuration, 34–37
- Pump four quadrant charts, 354–357, 355f, 357f
- Pump head capacity (H-Q) curve, 145–147
- Pumping
 - dependability for, 14–15
- Pump(s)
 - centrifugal, 9, 100, 104–118; *see also* Centrifugal pumps
 - energy conversion and, 99
 - family, 99–100
 - history, 100–103
 - chronologically listed events, 103
 - kinetic, 99, 101f
 - for liquid pipeline stations, 99–100
 - performance curves, 137–138, 139f
 - positive displacement, 119–129; *see also* Positive displacement pumps
 - selection for liquid pipeline system, 19–24
- Pumps, performance of, 131–178
 - API gravity and SG, relationship, 133–136
 - centrifugal pumps
 - affinity laws, 148, 149f
 - cavitation in, 154–160

- centrifugal impeller design theory, 141–143
- coverage chart, 138
- impeller curve characteristics, 145–147
- impeller selection, 138–140
- limits, 163–166
- performance modifications, 150, 151f–153f
- pipeline-pump operational control, 148–150
- pump performance curves, 137–138, 139f
- pump power and efficiency, 150
- specific speed, 143–145, 146f
- system curve, 140, 141f
- viscous liquids and, 160–163
- measurement units and conversion factors, 175–177
- overview, 131
- of positive displacement pumps, 167–175
- surge in system operation, 166–167
- system design standards and, 177–178
- system head, 131–133
- vs. pipeline system curve
- Pump shutdown, pressure surge and, 56
- Pump startup, pressure surge and, 55–56
- Pump station configuration
 - general, 28–29
- R**
- Radial flow pumps, 105, 106f
- Radial split (end cover), 206
- RAM models, *see* Reliability, Availability and Maintainability (RAM) models
- Rankine bottoming cycle, organic, 306
- Ratio of specific heats, 240–241
- Reactive silencers for pulsation suppression, 490–493, 491f–493f
- Reciprocating compressors, 179–203
 - advantages and disadvantages of, 335
 - bearings and lubrication systems, 193, 194–196
 - capacity (flow) control, 187, 188f, 189f
 - control system, 196
 - design
 - considerations, 203
 - general, 179–181
 - driven by VFD-controlled motors, 555–558
 - frame and cylinders, 183–187
 - cylinders, 185–187
 - foundations, 183–184
 - integral compressor frame, 185
 - separable compressor, 184–185
 - gas cooling, 198
 - installation, tuning out difficult torsional vibration problem in (case study), 327, 328, 329f
 - integral, 181, 182f, 185
 - monitoring system, 197
 - optimization, 200–201
 - overview, 179
 - packings, 193, 194f
 - performance, 247–254
 - discharge temperature, 251
 - flow (capacity), 245, 247–249
 - general, 247
 - maps, 251–254
 - piston speed, 254
 - power, 249–251
 - physical operation, 198–200
 - pressure–volume characteristic, 270, 271f
 - pulsation generated by, 485–487, 486f–487f, 523–525, 523f–525f
 - rod loading, 201–202
 - rotordynamics and, 552–553, 552f, 553f
 - running gear, 181, 182–183
 - separable, 181, 182f, 183, 184–185
 - start-up and shutdown, 197
 - types, 179–181
 - valves, 187, 189–192, 193f
- Reciprocating pumps, 121–124
 - acceleration head, 171–172
 - disadvantages, 123
 - discharge piping, 129
 - family of, 101f
 - flow characteristics, 171, 172f
 - piston pumps, 122–123
 - plunger pumps, 121–122
 - power plunger pumps, 124
 - pulsation generated by, 485–487, 486f–487f
 - selection
 - charts, 173–174
 - pump power calculations, 174–175
 - theoretical pump volume calculation, 174
 - speed rating, 126–127, 127t
 - station piping design for, 127, 128f
 - suction piping, 127–128
 - suction vessel, 129
 - torque characteristics, 126, 127f
 - type, 99
- Re-circulation in centrifugal pumps, 164–166
- Recycle system around compressors arranged in series, 409–410, 409f, 410f–411f
- Recycling, compressor stations, 93
- Redlich-Kwong EOS, 241
- RefProp, mixture property program, 243, 264
- Regular internally-pressurized fluid film bearings, 560
- Reliability; *see also* Dependability, pipeline system
 - concept, 11
 - standardization, 11
- Reliability, Availability and Maintainability (RAM) models, 15–16, 17f
- Relief valve dynamics, 427, 429–444
 - example, 436–441, 438f–441f
 - field tests, 441–444, 442f, 443f–444f
 - pilot-operated relief valves, 429–434, 430f, 431f
 - solution technique, 434–436
- Remote sensing pop-action pilot PRVs, 526
- Resistance coefficient, 25–26

- Resonance
 for fixed-speed machine, 535f
 for variable speed machine, 536f
 Restaging, 150, 152f
 Rexnord, 325
 Reynolds numbers (Re), 24, 26, 45
 defined, 260
 noise suppression during blow-down, 484, 496–497
 Rising characteristic curve, 146, 147f
 Risk assessment, pipeline system, 7–9
 Rod loading, reciprocating compressors, 201–202, 271
 Rod reversal, defined, 201
 Rolls Royce, 281, 287, 289f, 290
 Rotary compressors, types, 229
 Rotary pumps, 102f, 119–121, 122f
 capability range, 120t
 curve, system head curves and, 170–171
 damage caused by hard contaminant, 121f
 family of, 102f
 flow/capacity control, 121
 inadequate suction conditions correction, 173
 performance chart, 167, 168f, 169f
 power and efficiency, 169–170
 pulsation and pressure relief, 120–121
 slips and clearance, 170
 system configuration, 122f
 types, 99, 119
 Rotating equipments, 536–563
 balancing, 561–563, 562f–563f
 general, 536–537
 lateral rotordynamics, 537–540, 538f–540f
 specific machinery considerations for rotordynamics, 551–561
 stability, 540–541, 541f
 torsional rotordynamics, 541–551, 542f–544f, 546f, 548f
 Rotating stall, *see* Surge
 Rotordynamics
 balancing and, 561–563, 562f–563f
 bearings and, 560–561
 centrifugal compressors and, 551–552
 centrifugal pumps, 553–554
 gas/power turbines, 554
 gearboxes and couplings, 558–560, 559f, 560f
 lateral, 537–540, 538f–540f
 motors, 554–558, 556f, 557f
 reciprocating compressors, 552–553, 552f, 553f
 stability, 540–541, 541f, 561–563
 torsional, 541–551, 542f–544f, 546f, 548f
 Rotors, 285
 inertia, on ESD, 393, 394f, 395f
 Running gear, 181, 182–183
- S**
 Safety, pipeline systems, 6–17
 dependability and, 11–17
 process safety, 6–11
 Safety systems, compressor station, 96
 SCADA, *see* Supervisory control and data acquisition (SCADA) system
 Scavenge pumps, 292
 Screech tones, 603–604
 Screw compressors, 229–231
 design, 229, 230f
 operation, 230–231
 Scrubbers, compressor station, 90–91
 Sealing system, centrifugal compressors, 205–209, 213–220
 dry gas seals, 216–219
 emerging gas seal technology, 220
 general, 213–214
 wet oil seals, 214–215
 Seal-less centrifugal pump type, 99
 Seal(s)
 IGCC, 233–234
 oil, 215
 Selection, performance of centrifugal compressors, 260–261
 Self-excited vibration, 551
 Separable reciprocating compressor
 frame, 184–185
 running gear, 181, 182f, 183
- Series configuration
 of compressor for gas compression, 76
 pumping piping, 36, 40f
 of pumps in liquid pipeline system, 29
 standby unit, 79, 80f
 Series operation, compressors, 275–276
 Series-parallel configuration
 of compressor for gas compression, 76
 pump station piping, 36, 37f
 Service Factor, 324
 SG, *see* Specific gravity (SG)
 Shaft(s)
 arrangements, for gas turbines, 284–285
 centrifugal compressors, 206
 Shaking forces, standards and guidelines, 509–510
 Shared VFDs, 314
 Shear rate, 21, 22f
 Shutdown, 197, 276
 Shutdown control
 ESD, 94, 95f
 SSDL, 94, 95f
 SSDR, 93, 94f
 Shutoff, rise to
 pipeline design and, 23
 Side-branch mufflers, 491
 Siemens, 281
 Simple compression systems, 372–374, 372f–373f, 374f
 Single-source pulsation, 520–521, 520f–521f
 Single-stage pump, 106
 Single-suction pump, 106
 SI units, 175
 Sizing, performance of centrifugal compressors, 260–261
 Slab gate valves, 44
 Small-bore attachments
 mechanical analysis of piping systems and, 569–572
 Small bore connections (SBCs), 569–572
 defined, 569
 definition chart for different pipe sizing, 569f
 design best practices, 571–572
 failures of, 569, 571

- general, 569–571
- guidelines for screening, 572
- isolating, 572
- orientation of, 571
- small bore and mainline connection and piping definitions, 570f
- small-bore attachments on a reciprocating compressor, 570f
- Snubbers, 500–502, 501f
- Soave-Redlich-Kwong EOS, 241
- Soft couplings
 - elastomeric, 327
 - steel-spring, 327
- Solar bearing, 209, 210f
- Solar Centaur, 287, 297
- Solar low NO_x (SoLoNO_x), 296
- Solar Saturn, 281, 282f
- Solar Turbines, 281, 283
- Solids concentrations
 - pump selection and, 23
- Solution techniques, 487–488
 - dynamic instabilities, 382–386, 382f–383f, 384f, 385f, 386f
 - pumping systems, 341–342, 342f
 - relief valve dynamics, 434–436
- Sound
 - intensity, 594–595
 - speed in liquids piping, 499–500, 501f
- Sound pressure level (SPL), 594–597, 608, 611f
- Sour oil, 215
- Spark-ignited engines, 320
- Specific gravity (SG)
 - API gravity and, relationship, 133–136
 - pipeline design and, 22–23
 - pump selection and, 23
 - of some hydrocarbon liquids, 136t
- Specific heat
 - pipeline design and, 21
 - ratio of, 240–241
- Specific speed, efficiency and, 143–145, 146f
- Speech Interference Level (SIL), 598
- Speed drives, variable, 310, 311–315
 - fluid coupling, 314, 315f
 - VFD, 310, 311–314
- Speed of sound in liquids piping, 499–500, 501f
- Speed rating, reciprocating pumps, 126–127
- Spoilers, for pulsation suppression at source, 493–496, 494f–496f
- Spring loaded PRVs, 526
- SSDL, *see* Station shutdown lock-out (SSDL)
- SSDR, *see* Station shutdown restartable (SSDR) mode
- Stability
 - defined, 260
 - rotordynamics, 540–541, 541f, 561–563
- Stable characteristic curve, 147
- Stall, 221–222
- Standards
 - API, *see* American Petroleum Institute (API)
 - compressor, 96–97
 - couplings, 329–330
 - design, *see* Design standards
 - pump and system design, 177–178
- Standards and guidelines, 502–518
 - API 618 Standard, 502–510, 503f
 - API 674 Standard, 510–512
 - shaking forces arising from pressure pulsation, 512–513, 512f–513f
- Standby units, 78–80, 81f
- Startup, 197, 274–275
- Static head
 - liquid pipeline systems, 24
 - velocity and, 25
- Station bypass valve, 34, 35f, 36
- Station check valve, 35f, 36
- Station discharge valves, 34, 35f, 36, 44
- Station isolation valves, 35f, 36
- Station level control, compressor stations, 92
- Station shutdown lockout (SSDL), 94, 95f
- Station shutdown restartable (SSDR) mode, 93, 94f
- Station suction valve, 34, 35f, 36
- Stators, defined, 285
- Steam condensation-induced water hammer, 359–361, 360f
- Steam injection, 296
- Steel-spring soft couplings, 327
- Steep characteristic curve, 146, 147f
- Stonewall, 259, 272
- Stress
 - mechanical analysis of piping systems, 564–566, 565f, 566f, 567f
- Styrene transfer system, 361–365, 361f–362f, 363f, 364f–365f, 366f
- Subsynchronous vibration, 551
- Suction lift, piping design, 34
- Suction piping
 - for reciprocating pumps, 127–128
 - size and design, 34
- Suction pulsation dampeners, 125–126
- Suction specific speed, 165–166
- Suction throttling, 93
- Suction valve, 187, 189f, 190, 191, 192f
- Suction vessel, for reciprocating pumps, 129
- Sump system, 34
- Supercharging, defined, 320
- Supercompressibility, defined, 238
- Supersonic ejectors; *see also* Two-stage supersonic ejectors
 - in operation, 631–634, 632t, 633f, 633t, 634t
 - primary challenges of, 625–626
 - 1st stage, 625–632, 625f, 626f, 627f, 630f, 631f, 632
 - 1st stage supersonic ejector, 625–632, 625f, 626f, 627f, 630f, 631f, 632
 - two stages of ejector, 626–628, 626f–628f
- Supervisory control, compressor stations, 92
- Supervisory control and data acquisition (SCADA) system, 93
- Surge
 - air compressor, 286–287
 - on compressor, 221–222
 - control system, 222–223
 - dynamic compressors, 272

- operating range by, 260
- protection for centrifugal compressors, 270
- relief valves, 59, 60f
- vessel, 59
- Survey
 - noise, compressor and pump stations, 608–610, 609f, 610f, 612–623
- Swing type check valves; *see also* Check valve dynamics
 - description, 411–412, 412f
 - dynamic behavior of, 413–417, 414f, 416f–417f
 - slamming characteristics, 417–421
- Synchronous motors, 308–310
- System characteristics, compressors, 267–276
 - adjustments, 272–274
 - comparison, 270, 271f
 - curves, 267–270
 - general, 267
 - operating considerations, 274–276
 - parallel operation, 276
 - series operation, 275–276
 - shutdown, 276
 - startup, 274–275
 - operating limitations, 271–272
- System curve, centrifugal pumps, 140, 141f
- System head, 131–133
 - vs. specific gravity, pumps delivering the same pressure, 133f
- System head curves
 - of centrifugal pumps, 140, 141f
 - liquid pipeline systems, 24–26
 - pump *versus* pipeline, 132f
- T**
 - “Tail effect,” 45
 - Tangency rule, 598
 - Taurus, 281
 - TB Woods flexible disk couplings, 325
 - TCO, *see* Total cost of ownership (TCO)
 - Technical Committee 56 (TC56), 11
 - Temperature effect, pipeline design, 21
 - Temperature profiles, gas pipeline, 72f
 - Temperature rise in centrifugal pumps, 163–164
 - Terminal, liquid pipeline systems, 4
 - Terminal piping design, 52–61
 - components of, 54
 - layout of, 54
 - pressure surges, 55–56
 - transient analysis, 56–58
 - Testing, performance, centrifugal compressors, 261–262
 - Test tolerances
 - pipeline design and, 23
 - Thermal analysis
 - mechanical analysis of piping systems and, 583–584
 - Thermal efficiency, 331, 332, 334
 - Threats (bowtie diagram), 8
 - Throttle element
 - acoustic transfer matrix for, 472–478, 473f, 474t, 475f, 476f, 477f
 - flow-generated pulsation from, 480–482
 - Throttling, suction and discharge, 272
 - Throttling elements
 - flow-generated pulsation from, 480–482, 481f–482f
 - Thrust force, in two-stage centrifugal compressor, 206, 208f
 - Tilting pad bearings, 209, 210, 211f, 212f
 - Titan, 281
 - Top Event (bowtie diagram), 8
 - Torque characteristics, reciprocating pumps, 126, 127f
 - Torque coefficient, centrifugal pumps, 348, 349f, 350t–351t
 - Torsional analysis, 324, 541–543, 546–548, 547f–548f
 - Torsional modeling, 543–546, 545f, 546f
 - Torsional natural frequencies (TNF)
 - Torsional rotordynamics, 541–551, 542f–544f, 546f, 548f
 - importance of, 541–543
 - torsional analysis, 546–548, 547f–548f
 - torsional modeling, 543–546, 545f, 546f
 - torsional solutions, 548–551, 549f, 550f
 - Torsional solutions, 548–551, 549f, 550f
 - Torsional vibration (TV), 555–556
 - problem in reciprocating compressor installation, case study, 327, 328, 329f
 - Total cost of ownership (TCO), 15
 - Totally enclosed fan-cooled motor cooling, 310, 311f
 - Totally enclosed forced ventilation, 310
 - Totally enclosed water-to-air cooled motor cooling, 310, 311f
 - TransCanada Pipelines, 281
 - Transfer matrix (TM)
 - mean flow on acoustic TM for pipe element, 467–468
 - Transient analysis
 - drawbacks, 57
 - objectives of, 56–57
 - Transmission, 6
 - Turbine inlet temperatures (TITs), 280, 301
 - Turbines
 - gas, 554
 - power, 554
 - Turbocharging, defined, 320
 - Twin-spool gas generator, 285
 - Two-stage supersonic ejectors, 626–628, 626f–628f
 - performance of integrated, 629–632, 629f–631f, 631t
 - Typical acceleration, 534
 - U**
 - Unbalanced forces
 - mechanical analysis of piping systems, 566–569, 568f

- Unburned hydrocarbons (UHC), 295
- Uncontrolled devices, 613
- Uncontrolled engines, 613
- Under-compression discharge pressure, 231
- Unit auxiliary systems, compressor station, 92
- Unit control systems, compressor station, 92–95
- “Universal velocity profile,” 46
- Unloaders, types of, 187, 188f
- Unstable characteristic curve, 147
- U.S. Federal Interagency Committee on Urban Noise (FICUN), 599
- Usage scenario for pipeline stations (case study), 81–85
- V**
- Value
 - of dependability, 12–14
- ValveAlert™, 197
- Valve(s)
 - bleed, 287
 - closure, pressure surge and, 56
 - discharge, 187, 189f, 190, 191, 192f
 - plate, 187, 189f, 190f
 - pneumatic clearance, 187, 188f
 - poppet, 187, 189f, 190, 191f
 - pressure control, 213
 - pressure relief, 213
 - reciprocating compressors, 187, 189–192, 193f
 - selection, piping design, 44
 - suction, 187, 189f, 190, 191, 192f
- Van der Waals mixing rule, 241
- Vaneless diffusers, 261
- Vanes
 - guide, *see* Guide vanes
 - IGVs, 233, 287, 288
 - VSVs, 287–288
- Vapor pressures
 - cavitation and, 155, 156f
 - pump selection and, 23
- Vapor voids in liquids, 500, 501t
- Variable compressor geometry, 287–288
- Variable frequency drive (VFD), 310, 311–314, 315
- Variable speed drives, 310, 311–315
 - fluid coupling, 314, 315f
- VFD, 310, 311–314
- Variable stator vanes (VSVs), 287–288
- Variable volume clearance pocket (VVCP), 186–187, 199–200
- Velocity limitations, piping design, 34
- Vent gas
 - recovering loss from dry gas seals, 624–634
- Vertical booster pump, 104f
- Vertical inline pumps, 116t, 117–118
- Vertical pump (dry pit-type), 106
- Vertical pump types, 99
- Vertically suspended pump, 518
- VFD (variable frequency drive), 310, 311–314, 315
- VFD-controlled motors
 - reciprocating compressors driven by, 555–558
- Vibration, 533–536
 - amplitude, 533
 - basic aspects of, 533–536, 534f, 535f
 - defined, 533
 - forced, 551
 - mechanical analysis of
 - piping systems, 564–566, 565f, 566f, 567f
 - MNF and resonance, 535–536, 535f–536f
 - overview, 533–535, 534f, 535f
 - self-excited, 551
 - subsynchronous, 551
 - torsional, 555–556
- Vibration amplitude, 533
- Vibration velocity, 534
- Viscosity
 - pipeline design and, 21–22, 23f
 - pump selection and, 23–24
- Viscous liquids
 - centrifugal pumps and, 160–163
 - performance correction chart, 161, 162f
- Volume model, station and gas pipeline blowdown, 446–449
 - analytical solution, 446–448
 - numerical solution, 448–449
- Volumetric efficiency (VE), 199, 200, 248–249
- Volute chipping, impeller, 150, 153f
- Volute inserts, impeller, 150, 153f
- Volute pump, 106
- VSVs (variable stator vanes), 287–288
- VVCP (variable volume clearance pocket), 186–187, 199–200
- W**
- Wafer type check valves, dynamics of, 424–425, 424f
- Waste heat recovery, gas turbines, 306–307
- Water cooling, 70
- Water hammer, 357–358
 - steam condensation-induced, 359–361, 360f
- Weather-protected type enclosure, 310
- Weather protection, compressor station, 95
- Wet oil seals, 214–215
- What if/checklists, 8
- Wheel curve, defined, 255
- Wobbe index, 294, 297
- Z**
- Zero emissions seal (ZES), 220